UNIVERSIDADE FEDERAL RURAL DO SEMI-ÁRIDO
CENTRO DE CIÊNCIAS EXATAS E NATURAIS
DEPARTAMENTO DE CIÊNCIAS NATURAIS, MATEMÁTICA E ESTATÍSTICA

ELMER ROLANDO LLANOS VILLARREAL
ENGENHARIA ELÉTRICA, D.SC

MEMORIAL

Apresentado à Universidade Federal Rural do Semi-Árido/ Departamento de Ciências Exatas Naturais, Matemática e Estatística para fins de Progressão da Classe D (Associado) Nível 4 para Classe E (Titular)

Mossoró-RN
Outubro, 2024

Resumo

Villarreal, Elmer Rolando Llanos. **Memorial**. Outubro, 2024. 65 Memorial apresentado à Universidade Federal Rural do Semi-Árido/ Departamento de Ciências Exatas e Naturais para fins de Progressão da Classe D (Associado) Nível 4 para Classe E (Titular).

Apresentação

O presente Memorial, apresentado à Universidade Federal Rural do Semi-Árido/Centro de Ciências Exatas e Naturais/Departamento de Ciências Naturais, Matemática e Estatística, Mossoró, RN, como parte das exigências para Progressão da Classe D (Associado) Nível 4 para Classe E (Titular), contém as atividades desenvolvidas pelo docente Elmer Rolando Llanos Villarreal. Os documentos comprobatorios, apresentados em volumes anexos, recebem a mesma numeração dos itens a que se referem no texto.

Biografia

Elmer Rolando Llanos Villarreal tem 57 anos, nasceu em Huánuco, Peru. Naturalizado Brasileiro na cidade de Mossoró-RN desde o ano 2014. Ele se formou como Bacharel em Ciências em Matemática pela Universidade Nacional de Engenharia de Lima, Peru. Com diploma de graduação revalidado pela Universidade Federal de Santa Carina. Mestre em Engenharia Elétrica (1997) pela Escola Politécnica da Universidade de São Paulo e Doutor em Engenharia Elétrica (2002) pela Universidade Federal de Santa Catarina, Brasil. Pós-doutorado em Engenharia Elétrica pela Universidade Federal Universidade Federal do Rio Grande do Norte (2019). Suas pesquisas estão concentradas em Engenharias 4 com enfase em teoria de controle e Matemática aplicada. É professor da Universidade Federal Rural do Semi-Árido desde 2009.

Agradecimentos

A Deus, por tudo que tenho conseguido até aqui. A minha familia. Venho através desta palavras de agradecimento agradecer todos membros da comunidade professores, servidores da UFERSA por todo o apoio brindado ao longo destes anos no serviço público na cidade de Mossóró. Também desejo agradecer aos professores da comissão especial que fazem avaliação desta defesa de Memorial.

Muito obrigado

Sumário

1 INFORMAÇÕES PESSOAIS 12

1.1 Nome: ELMER ROLANDO LLANOS VILLARREAL 12

1.2 Estado Civil: 12

1.3 Endereço Residencial 12

1.4 Endereço Profissional 12

2 DOCUMENTOS 13

2.1 Cédula de Identidade: 13

2.2 CPF: 13

2.3 Título de Eleitor: 13

2.4 Carteira Profissional: 13

3 FORMAÇÃO ACADÊMICA 14

3.1 Formação Básica 14

3.2 Graduação 14

3.3 Doutorado 15

3.4 Pós-Doutorado 16

4 ATUAÇÃO PROFISSIONAL 17

4.1 Vínculo Institucional: Universidade Federal Rural do Semi-Árido, UFERSA 17

5 ATIVIDADE DIDÁTICA 18

5.1 Exercício no Magistério Superior no Perú 18

5.1.1 Universidad Agraria La Molina-UNALM-Perú 18

5.1.2 Universidad Nacional de Ingeniería-UNI-Perú 18

5.2 Exercício no Magistério Superior no ensino superior particular 18

5.2.1 Unileste-MG 18

5.2.2 IESES-Castelo 19

5.2.3 Associação de Ensino Superior Unificado do Centro Leste 19

5.2.4 Instituto Paulista de Ensino Superior Unificado 19

5.2.5 Fundação Oswaldo Aranha 19

5.3 Exercício no Magistério Superior na UFERSA . . . 19
5.3.1 Professor Adjunto . . . 20
5.3.2 Professor Associado . . . 20
5.4 ATIVIDADES DE ENSINO NA UFERSA . . . 20
5.4.1 Graduação . . . 20
5.4.2 Pós-Graduação . . . 20

6 ATIVIDADE DE PESQUISA . . . 21
6.1 Linhas de Pesquisa . . . 21
6.2 Grupos de Pesquisa . . . 21
6.2.1 CONSTRUIR UM MODELO NO AMBIENTE HFSS PARA USO EM VANTS . . . 21
6.2.2 OBTENÇÃO DE UM SOFTWARE PARA ALGORITMOS DE CONTROLE PID E FUZZY-PID . . . 22
6.2.3 Controle não linear para vant e suas extensões . . . 23
6.2.4 Modelagem Matemática na Região do Semi-árido . . . 23
6.2.5 Plataforma de simulação de Controladores Multiagentes . . . 24
6.3 Produção Bibliográfica . . . 24
6.3.1 Artigos Científicos Completos Publicados em Periódicos . . . 24
6.4 Artigos com publicados em revistas indexadas . . . 25
6.4.1 Energies 2024 . . . 25
6.4.2 Energies 2024 . . . 25
6.4.3 Energies 2024 . . . 25
6.4.4 Sensors 2023 . . . 25
6.4.5 Energies 2022 . . . 26
6.4.6 Energies 2022 . . . 26
6.4.7 IEEE ACCESS 2021 . . . 26
6.4.8 Energies 2021 . . . 26
6.4.9 Energies 2020 . . . 27
6.4.10 PRZEGLAD ELEKTROTECHNICZNY 2019 . . . 27
6.4.11 IEEE ACCESS 2019 . . . 27
6.4.12 SENSORS 2019 . . . 27
6.4.13 IEEE Latin America Transactions . . . 28

6.4.14 International Journal of Artificial Intelligence and Applications 2012 28
6.4.15 COMPUTATIONAL APPLIED MATHEMATICS 2012 28
6.4.16 TEMA 2009 28
6.4.17 IEEE TRANSACTIONS ON AUTOMATIC CONTROL 2003 . . . 29
6.5 Artigos com publicados em anais de congressos internacionais 29
6.5.1 IEEE-CHILE 2022 29
6.5.2 IEEE-CHILE 2021 29
6.5.3 IEEE-CHILE 2021 30
6.5.4 IEEE-CHILE 2021 30
6.5.5 ISMB17 2021 30
6.5.6 ISMB17 2021 31
6.5.7 INTERCON 2020 31
6.5.8 EMI Rio de Janeiro 2017 31
6.5.9 IEEE CONFERENCE PUBLICATIONS México 2015 31
6.5.10 PROCEEDINGS IEEE-ACCA CHILE 2014 32
6.5.11 IFAC IMS2013 2013 32
6.5.12 IFAC IMS2013 2013 32
6.5.13 IFAC IMS2013 2013 32
6.5.14 15th LATINAMERICAN CONTROL CONFERENCE, Lima Perú, 2012 33
6.5.15 15th LATINAMERICAN CONTROL CONFERENCE, Lima Perú, 2012 33
6.5.16 15th LATINAMERICAN CONTROL CONFERENCE, Lima Perú, 2012 33
6.5.17 15th International Conference on Computational Science and Its Applications 2012 34
6.5.18 15th LATINAMERICAN CONTROL CONFERENCE, Lima Perú, 2012 34
6.5.19 15th LATINAMERICAN CONTROL CONFERENCE, Lima Perú, 2012 34
6.5.20 IEEE CESA 2012 34
6.5.21 IFAC Triennial World Congress Barcelona 2002 35
6.5.22 IFAC Triennial World Congress Barcelona 2002 35

6.5.23 IFAC System Structure and Control 2001 . . . 35
6.5.24 8th IEEE MEDITERRANEAN CONFERENCE ON CONTROL AND AUTOMATION, 2000 . . . 35
6.6 Artigos com publicados em anais de congressos nacionais . . . 35
6.6.1 CNMAC 2023 . . . 36
6.6.2 CNMAC 2022 . . . 36
6.6.3 CNMAC 2022 . . . 36
6.6.4 CNMAC 2022 . . . 37
6.6.5 COBEP 2021 . . . 37
6.6.6 CNMAC 2018 . . . 37
6.6.7 CNMAC 2018 . . . 37
6.6.8 CNMAC 2017 . . . 38
6.6.9 CNMAC 2017 . . . 38
6.6.10 DINCON 2017 . . . 38
6.6.11 COBENGE 2016 . . . 38
6.6.12 DINCON 2015 . . . 39
6.6.13 DINCON 2015 . . . 39
6.6.14 CNMAI 2015 . . . 39
6.6.15 COBENGE 2015 . . . 39
6.6.16 COBENGE 2015 . . . 40
6.6.17 DINCON 2013 . . . 40
6.6.18 SBAI 2013 . . . 40
6.6.19 CNMAC 2012 . . . 40
6.6.20 CNMAC Nordeste 2012 . . . 41
6.6.21 DINCON 2011 . . . 41
6.6.22 COBENGE 2011 . . . 41
6.6.23 DINCON 2010 . . . 41
6.6.24 DINCON 2009 . . . 42
6.6.25 CNMAC 2009 . . . 42
6.6.26 CNMAC 2009 . . . 42
6.6.27 CNMAC 2008 . . . 42
6.6.28 CBA 2004 . . . 43
6.6.29 Capítulos de Livro . . . 43

6.6.30 Atena Editora 2022 . . . 43
6.6.31 Livro . . . 43
6.6.32 Editora Conhecimento Livre, 2023 . . . 43
6.6.33 Novas Edições Acadêmicas, 2016 . . . 44
6.6.34 Novas Edições Acadêmicas, 2015 . . . 44

7 ATIVIDADE DE ORIENTAÇÃO E FORMAÇÃO DE PESQUISADORES . . . 45

7.1 Orientações concluídas . . . 45
7.1.1 Dissertações de Mestrado . . . 45
7.1.2 Dissertação, 2017 . . . 45
7.1.3 Dissertação, 2015 . . . 45
7.1.4 Dissertação, 2014 . . . 45
7.1.5 Dissertação, 2014 . . . 45
7.1.6 Dissertação, 2014 . . . 46
7.1.7 Dissertação, 2014 . . . 46
7.1.8 Dissertação, 2013 . . . 46
7.1.9 Dissertação, 2013 . . . 46
7.1.10 Dissertação, 2023 . . . 46
7.1.11 Dissertação, 2018 . . . 47
7.1.12 Dissertação, 2017 . . . 47
7.1.13 Dissertação, 2016 . . . 47
7.1.14 Dissertação, 2016 . . . 47
7.1.15 Dissertação, 2013 . . . 47
7.1.16 Dissertação, 2013 . . . 48
7.1.17 Dissertação, 2013 . . . 48
7.1.18 Orientação de Alunos de Graduação . . . 48
7.1.19 TCC, 2017 . . . 48
7.1.20 TCC, 2017 . . . 48
7.1.21 TCC, 2016 . . . 49
7.1.22 TCC, 2016 . . . 49
7.1.23 TCC, 2013 . . . 49
7.1.24 TCC, 2012 . . . 49

7.1.25 TCC, 2012 . . . 49
7.1.26 TCC, 2011 . . . 49
7.1.27 TCC, 2011 . . . 49
7.1.28 TCC, 2011 . . . 50
7.1.29 Orientação de Alunos Iniciação Científica: . . . 50

8 ATIVIDADE DE EXTENSÃO UNIVERSITÁRIA . . . 54
8.1 Relatoria Ad Hoc . . . 54
8.1.1 International Journal of Systems Science . . . 54
8.1.2 IEEE Latin America Transactions . . . 54
8.1.3 IEEE Access . . . 54
8.1.4 IET Renewable Power Generation . . . 54
8.1.5 Mathematics MDPI . . . 54
8.1.6 Applied Sciences MDPI . . . 54
8.1.7 Energies . . . 54
8.1.8 Electronics MDPI . . . 55
8.1.9 Symmetry-Basel . . . 55
8.1.10 IEEE Transactions on Transportation Eletrification . . . 55
8.1.11 Sensors MDPI . . . 55
8.1.12 Sustainability MDPI . . . 55
8.1.13 Atmosphere . . . 55
8.1.14 Journal of Marine Science and Engineering . . . 55
8.1.15 Aerospace . . . 56
8.1.16 Machines MDPI . . . 56
8.1.17 Axioms MDPI . . . 56
8.2 Atividades de extensão universitária na UFERSA . . . 56
8.2.1 Divulgação de Ações de ensino associadas a Trabalhos desenvolvidos no PROFMAT – UFERSA . . . 56
8.2.2 FÓRUM DE ASSISTÊNCIA ESTUDANTIL DA UNIVERSIDADE FEDERAL RURAL DO SEMI-ÁRIDO . . . 56
8.2.3 Semínários de Pesquisa em Matemática . . . 57
8.2.4 Métodos Diagramáticos em Representação de Álgebras . . . 57
8.2.5 I CONGRESSO DE INOVAÇÃO TECNOLÓGICA DO SEMI-ÁRIDO 57

8.2.6 Simulação de Controladores multiagentes na indústria de petróleo em Mossoró 58

9 ATIVIDADE DE ADMINISTRAÇÃO 59

9.1 Membro de Comissões e Atividades Administrativas 59

9.1.1 CPA,CONSAD. CPPD 59

9.1.2 Participação em Banca de Comissão Julgoradora de Concurso Público (2009-2019) 59

9.1.3 Processo Seletivo para Professor Substituto UFERSA, 2019 59

9.1.4 Processo Seletivo para Professor Substituto UFERSA, 2015 59

9.1.5 Concurso publico professor efetivo edital 007/2014, 2014 59

9.1.6 Concurso público para Professor Efetivo, 2012 59

9.1.7 Concurso Público para professor efetivo, 2009 60

9.1.8 Participação em Bancas de Concurso: Mestrado, Doutorado e Concurso Público 60

9.1.9 Participações em Banca de Mestrado e Doutorado (2010-2024) . . 60

10 PALAVRAS FINAIS 65

1 INFORMAÇÕES PESSOAIS

1.1 Nome: ELMER ROLANDO LLANOS VILLARREAL

Nome em Citações Bibliográficas: VILLARREAL, E. R. L.

Sexo: Masculino

Filiação: Manuel Elmer Llanos Flores e Mery July Villarreal Pasquel

Nascimento: 26 de Março de 1967

Origem : Huánuco-Perú

Naturalidade: Mossoró - RN

Nacionalidade: Brasileiro Naturalizado

1.2 Estado Civil:

Casado

1.3 Endereço Residencial

Av. Francisco Mota 4222, Casa I19 Residencial Ninho CEP 59.626-105 Mossoró, RN - Brasil.

Telefone: (84) 991948432

1.4 Endereço Profissional

Universidade Federal Rural do Semi-Árido – UFERSA

Centro de Ciências Exatas e Naturais -CCEN

Departamento de Ciências Naturais, Matemática e Estatística- DCME.

Av. Francisco Mota, 572 Bairro Costa e Silva

59.625-900 Mossoró-RN - Brasil

Telefone/fax: (84) 3317-8398

E-mail: elmerllanos@ufersa.edu.br

2 DOCUMENTOS

2.1 Cédula de Identidade:

N^o 003571118, Órgão expedidor: ITEP-RN

Data: 09/05/2014

2.2 CPF:

213.060.638-50

2.3 Título de Eleitor:‘

033106131643, zona 033, seção 0333 Local: Mossoró, RN.

Data de emissão: 02-04-2014

2.4 Carteira Profissional:

071126 - série $A01/ES$

3 FORMAÇÃO ACADÊMICA

3.1 Formação Básica

Sou filho de peruanos e natural de Huánuco do Estado do Huánuco no Perú. Meus estudos do ensino médio foi frequentando no Colégio Nacional Leoncio Prado de Huanuco, onde cursei de 1978-1983.

3.2 Graduação

Em março de 1985 ingressei no Curso de bacharel em Matemática na Universidad Nacional de Ingenieria Lima e tive em dezembro de 1993 a conclusão do Curso de Graduação. Diploma Revalidado pela Universidade Federal de Santa Catarina-UFSC 21 de Dezembro de 2000.

Mestrado Inicialmente iniciei o Curso de Pós-graduação em nível de mestrado em Matemática aplicada no IME –USP na Universidade de São Paulo (USP) em agosto de 1994. Em março de 1995 ingressei no Curso de Pós-Graduação em nível de Mestrado em Engenharia Elétrica na Universidade Federal de Santa Catarina (UFSC). Em Março de 1997 apresentei minha Dissertação de Mestrado sob a orientação do Prof. Ph.D. Felipe Miguel Pait e intitulada "Teoria Geométrica de Conjunto Lineares". Durante a realização do Curso de Mestrado fui bolsista do Conselho Nacional de Desenvolvimento Científico e Tecnológico (CNPq) e da Fundação de Amparo à Pesquisa do Estado de São Paulo .

Resumo da Dissertação:

Neste trabalho estudam-se as propriedades topológicas de conjuntos definidos em espaços de importância para a teoria de controle, em especial para controle robusto e adaptativo. A teoria de sistemas dinâmicos beneficia-se do entendimento da geometria dos espaços de estados, o espaço linear no qual o vetor de estados de sistemas assume seus valores. Um exemplo e a abordagem geométrica do controle multivariável, que pode ser estendida para problemas não lineares. Enquanto essa teoria se ocupa principalmente de sistemas invariantes no tempo, o controle adaptativo emprega controladores parametrizados por parâmetros variantes no tempo: a medida em que esses parâmetros variam, os controladores viajam por conjuntos de sistemas lineares. Podemos esperar que o entendimento da geometria desses conjuntos tenham um papel importante em controle adaptativo e em

áreas afins. Duas topologias para espaços de sistemas lineares são comumente usadas. Segundo uma delas, a distância entre dois sistemas é dada pela distância euclideana entre os vetores de coeficientes de suas funções (ou matrizes) de transferência. Esse conceito é usado implicitamente pela teoria de identificação e estimação de parâmetros. Segundo a outra, a chamada topologia do grafo, as vizinhanças relevantes de um processo compreendem aqueles sistemas para os quais estabilidade em malha fechada é preservada.

3.3 Doutorado

Em março de 1998 ingressei no Curso de Pós-Graduação em nível de Doutorado em Engenharia Elétrica na Universidade Federal de Santa Catarina (UFSC) vinculado a Engenharia Elétrica (Departamento de Computação e Automação). Em março de 2002 apresentei minha Tese de Doutorado sob a orientação do Prof. Dr. Eugênio de Bona Castelan Neto. e intitulada "Abordagem Geométrica para Estabilização por Realimentação de Saídas e sua extensão aos Sistemas Descritores". Durante a realização do Curso de Doutorado fui bolsista do Conselho Nacional de Desenvolvimento Científico e Tecnológico (CNPq).

Resumo da Tese:

Este trabalho trata os problemas de estabilização e de posicionamento regional de pólo em sistemas lineares contínuos no tempo usando realimentação estática de saídas. Os resultados apresentados têm como ponto de partida o conceito de subespaços (C,A,B)-invariantes caracterizados algebricamente através de um par de equações acopladas de Sylvester, cuja solução pode ser obtida, para sistemas que verificam a condição de Kimura (m+ p >n), em duas etapas utilizando o algoritmo de Syrmos e Lewis.No caso de sistemas normais, é demonstrado que subespaços (C,A,B)-invariantes estabilizáveis por saídas podem ser caracterizados através de equações acopladas de Lyapunov. Baseada nessas equações, é proposta uma condição necessária e suficiente para a existência de solução do problema de estabilização por realimentação estática de saídas. Para sistemas satisfazendo a condição de Kimura, são propostos dois algoritmos (primal e dual) para solução das equações acopladas de Lyapunov. A técnica de estabilização é então adaptada para tratar o problema de posicionamento regional de pólos. - Durante o período de formação no meu doutoramento na UFSC tive a oportunidade de ter uma boa publicação de artigos

em congressos do IEEE-IFAC e seus respectivos IFAC Proceedings e a publicação de um artigo no IEEE Transactions on Automatic Control.

3.4 Pós-Doutorado

Entre 2007 e 2008 ingressei no Pós-Doutorado como bolsista DCR na cidade de Mossoró, Estado de Rio Grande do Norte (RN), no mestrado em Ciências da Computação da Universidade do Estado do Rio Grande do Norte UERN (RN). Sob a orientação do Prof. Dr. Marcelino Pereira dos Santos Silva desenvolvi durante um ano e a atividades teóricas e aplicações numéricas em Sistemas Multiagentes. Durante a realização do Pós-Doutorado fui contemplado com uma bolsa DCR do Conselho Nacional de Desenvolvimento Científico e Tecnológico (CNPq). Em 2018 e 2019 novamente ingressei no Pós-Doutorado como bolsista pós-doutor na cidade de Natal, no Programa de Pós-graduação em Engenharia Elétrica e Computação (PPGEEC) da Universidade Federal do Rio Grande do Norte UFRN (RN). Sob a orientação do Prof. Dr. Andrés Ortiz Salazar desenvolvi durante um ano atividades teóricas e aplicações numéricas em Controle Preditivo para Redes sem fio usando Markov e LMIs.. Durante a realização do Pós-Doutorado fui contemplado com uma bolsa de pós-doutorado do Conselho Nacional de Desenvolvimento Científico e Tecnológico (CNPq).

4 ATUAÇÃO PROFISSIONAL

4.1 Vínculo Institucional: Universidade Federal Rural do Semi-Árido, UFERSA

Período: 2009 - Atual

Enquadramento funcional: Professor Associado IV

Carga horária: 40 horas semanais

Regime: Dedicação exclusiva

5 ATIVIDADE DIDÁTICA

5.1 Exercício no Magistério Superior no Perú

O Professor Elmer Rolando Llanos Villarreal tem 20 (vinte) anos em sua trajetória docente no Ensino Superior, onde desenvolveu um conjunto quantitativo e qualificado de atividades de ensino, pesquisa e extensão. Do ponto de vista cronológico, minha carreira docente, em termos das progressões, pode ser resumida em:

5.1.1 Universidad Agraria La Molina-UNALM-Perú

– Admissão no Serviço Público Perú– Prof. Colaborador Universidad Agraria La Molina em Lima –Perú com vinculo de 01 de Março de 1994 até 30 de Julho de 1994.

5.1.2 Universidad Nacional de Ingeniería-UNI-Perú

Professor Colaborador em Universidad Nacional de Ingeniería Lima –Perú com vínculo 01 de Abril de 1997 até 28 de Fevereiro de 1998.

5.2 Exercício no Magistério Superior no ensino superior particular

A experiência docente no ensino superior foi averbado com total de 4 anos e seis meses com Carteira de Trabalho e Previdência Social PIS/PASEP 128.47097.12-2 Número 071126 Série A01 (ES).

5.2.1 Unileste-MG

Professsor do Centro Universitário Católica do Leste de Minas Gerais (Unileste) com CNPJ 00.331.801/0006-44 na cidade de Coronel Fabriciano no Estado de Minas Gerais com vinculo de 01 de Agosto de 2002 até 10 de Janeiro de 2003.

5.2.2 IESES-Castelo

Professor do Instituto de Ensino Superior do Espirito Santo com CNPJ 02213188/0001-81 nas cidades de Castelo e Cachoeiro de Itapemirim no estado de Espirito Santo com vinculo de 10 de Fevereiro de 2003 até 09 de Novembro de 2005.

5.2.3 Associação de Ensino Superior Unificado do Centro Leste

Professor da Associação de Ensino Superior Unificado do Centro Leste com CNPJ 02598162/0001-07 na cidade de Serra no estado de Espirito Santo com vinculo de 02 de Fevereiro de 2005 até 09 de Novembro de 2005.

5.2.4 Instituto Paulista de Ensino Superior Unificado

Professor do Instituto Paulista de Ensino Superior Unificado com CNPJ 59622977/0001-93 na cidade de São Carlos no estado de São Paulo com vinculo de 03 de Agosto de 2006 até 29 de Fevereiro de 2006.

5.2.5 Fundação Oswaldo Aranha

02.05.2007- Professor da Fundação Oswaldo Aranha com CNPJ 32504995/0001-14 em Volta Redonda-RJ. Na cidade de Volta Redonda no estado de Rio de Janeiro com vinculo até 30 de Julho de 2007.

A experiência docente no ensino superior foi averbado com total de 4 anos e seis meses com Carteira de Trabalho e Previdência Social PIS/PASEP 128.47097.12-2 Número 071126 Série A01 (ES).

5.3 Exercício no Magistério Superior na UFERSA

Professor Adjunto, Associado no Campus-Mossoro, desde o dia 15 de Janeiro de 2009 até a presente data.

5.3.1 Professor Adjunto

Inicio 15 de Janeiro de 2009.

5.3.2 Professor Associado

Inicio 15 de Janeiro de 2017.

5.4 ATIVIDADES DE ENSINO NA UFERSA

5.4.1 Graduação

No Departamento de Ciências Naturais Matemática e Estatística (DCME) da UFERSA lecionei as seguintes disciplinas: Cálculo I, Cálculo II, Cálculo Numérico, Algebra Linear, Matemática para Gestão, Fundamentos de Matemática.

No Departamento de Ciências Naturais Matemática e Estatística (DCME) da UFERSA participo como docente nas reuniões do Departamento e cada vez que eu sou convocado eu participo.

5.4.2 Pós-Graduação

Programa de Pós-Graduação em Engenharia Elétrica-UFERSA

Participei como docente no Programa de Pós-Graduação em Engenharia Elétrica da UFERSA, desde o ano 2012 até o ano de 2018, onde lecionei as seguintes disciplinas: Sistemas Lineares, Sistemas de Controle Multivariáveis, Modelagem e Simulação de controle, Sistemas de Controle.

Programa de Pós-Graduação em Matemática da UFERSA-PROFMAT Participo desde 2012 como docente no Programa de Pós-Graduação em Matemática da UFERSA onde lecionei as seguintes disciplinas: Geometria I, Números conjuntos e funções elementares, Geometria Analítica, Fundamentos de Cálculo, Matemática e Atualidade, Cálculo Numérico e Resolução de Problemas.

6 ATIVIDADE DE PESQUISA

6.1 Linhas de Pesquisa

- Teoria de Controle e aplicações
- Sistemas descritores e suas extensões
- Controle não linear para vant e suas extensões
- Modelagem Matemática na Região do Semi-árido
- Acionamento de maquinas e automação

6.2 Grupos de Pesquisa

A seguir os grupos de pesquisa.

6.2.1 CONSTRUIR UM MODELO NO AMBIENTE HFSS PARA USO EM VANTS

Descrição: Nos últimos anos, a sociedade tem vivido um processo de avanço tecnológico que atinge diversas áreas de conhecimento, sendo as telecomunicações um domínio que tem atraído a atenção de pesquisadores e indústrias de desenvolvimento tecnológico. Busca-se cada vez mais aumentar a eficiência nos sistemas de telecomunicações em termos de facilidade de uso e rápido estabelecimento da interação entre usuários, além de se buscar formas diversas de se comunicar. Paralelo a isto, veículos aéreos não tripulados (VANTs) têm sido utilizados recentemente, para uma série de aplicações militares, bem como civis. Eles mostram grandes vantagens e importância na busca e salvamento, vigilância em tempo real, operações de reconhecimento, o monitoramento do tráfego e inspeção em locais perigosos. Além disso, os VANTs são adequados para situações que são muito perigosas para o monitoramento humano direto. No entanto, o tipo de missão e a capacidade do VANT que são determinados pela sua forma e construção provoca uma série de problemas de rede . Os VANTs normalmente carregam um grande número de sensores e módulos de comunicação para fins de vigilância e coleta de informações. Ele requer extensas comunicações e transferência de dados entre os sensores, tais como do receptor de GPS e do acelerômetro. Para esta aplicação, a antena se torna uma boa candidata devido à sua geometria simples, perfil baixo e custo barato. O estudo de configurações para circuitos

planares como os de microfita e prototipagem de novos dispositivos é essencial para o desenvolvimento de novos sistemas de comunicação que requerem de seu hardware baixo peso, dimensões reduzidas, baixo custo, facilidade de construção e capacidade de integração com outras tecnologias (incluindo veículos aéreos), além de operação em múltiplas bandas de frequência, com bandas de transmissão mais largas. Através do método WICP pode se determinar a frequência de ressonância, a perda de retorno e largura de banda de antenas de microfita. O WICP (Wave Concept Iterative Procedure) se trata de um método numérico integral para solucionar as equações de propagação da onda eletromagnética. Apresenta a vantagem de que durante sua execução não há inversão de matrizes e inclusão de modos superiores na matriz de espalhamento, reduzindo o esforço computacional e seu tempo de execução. A partir da pesquisa bibliográfica, busca-se compreender os principais conceitos relacionados ao estudo de antenas e da compreensão dos modelos de onda utilizados para fins de comunicação, bem como dominiar o método iterativo baseado no conceito de ondas (WCIP). Através do estudo do método baseado no conceito de ondas (incidentes e refletidas) WCIP usado para projetar antenas e circuitos, pretende-se elaborar um software que expanda o método para uma formulação 3D, haja vista que o que se trabalha atualmente é o modelo em duas dimensões. Intenta-se expandir o método para se trabalhar no domínio do tempo para antenas UWB (Ultra Wid Band). Através do desenvolvimento do estudo do método WCIP, propõe-se implementá-lo de modo a aplicar ao uso na comunicação de VANTs. A simulação e construção do modelo podem ser alcançados pelo método WCIP e são obtidos através de softwares comerciais tais como Ansoft HFSS (o qual implementa o método dos elementos finitos). O programa é muito utilizado para análise de circuitos de alta frequência. Também está a disposição para fins de implementação prática um quadrotor do tipo AR Drone Parrot 1.0. Desenvolvidos em 2016-2018.

6.2.2 OBTENÇÃO DE UM SOFTWARE PARA ALGORITMOS DE CONTROLE PID E FUZZY-PID

Descrição: O controlador Proporcional-Integrativo-Derivativo é bastante utilizado em processos de automação devido sua simplicidade. Sua característica é de possuir três ações ajustáveis: proporcional (P), integral (I) e derivada (D). Ele melhora o seguimento da referência e/ou a rejeição de perturbações. Também melhora a resposta transitória

ou estabilidade relativa. O controlador PID trabalha em um sistema de malha fechada usando o esquemático mostrado abaixo. A variável (e) representa o erro, a diferença entre o valor de entrada desejado (R) e a atual saída (Y). Esse sinal de erro (e) será enviado ao controlador PID, e o controlador calculará tanto o integral quanto o derivativo deste sinal de erro. O sinal (u) que acaba de sair do controlador é agora igual ao ganho proporcional (Kp) vezes a magnitude do erro mais o ganho integral (Ki) vezes a integral do erro mais o ganho derivativo (Kd) vezes o derivativo do erro. Um controlador proporcional (Kp) terá o efeito de reduzir o tempo de subida e reduzirá, mas jamais eliminará, o erro em regime permanente. Um controlador integral (Ki) terá o efeito de eliminar o erro em regime permanente, mas ele deixará pior a resposta transiente. Um controlador derivativo (Kd) terá o efeito de incrementar a estabilidade do sistema, reduzindo o overshoot (o pico de sinal que ultrapassa o valor tolerado), e melhorando a resposta transiente. Efeitos de cada controlador Kp, Kd, e Ki em um sistema de malha fechada estão descritos na tabela a seguir. O algoritmo elaborado no Matlab gerou um programa que pede que o usuário entre com os valores das constantes Kp, Ki e Kd. Também pergunta se o usuário deseja verificar um sistema com malha aberta ou fechada. Utilizando uma função de transferência predeterminada, o programa gera, então, um gráfico da amplitude em função do tempo. Desenvolvidos em 2015-2018.

6.2.3 Controle não linear para vant e suas extensões

Descrição: A interação dos quadrotores com os interesses humanos gera uma relação promissora na inspeção de grandes áreas. Seja na infraestrutura, na agricultura, na pecuária, no monitoramento da poluição ambiental e em todas as áreas que sejam compstas por ambientes hostis que se caracterizam pelo difícil acesso tanto do homem quanto de robores terrestres. Desse modo, o foco principal desse estudo é a aplicação do controle servo visual nos VANT?s, visando o aperfeiçoamento das técnicas de monitoramento e controle de diversos ambientes. Desenvolvidos em 2014-2018.

6.2.4 Modelagem Matemática na Região do Semi-árido

Descrição: O presente projeto tem por objetivo aprofundar o conhecimento científico e técnico do professor de matemática. Fornecer elementos metodológicos aos professores e

alunos, para que eles desenvolvam, em sala de aula, um processo de ensino-aprendizado mais produtivo. Usar a Modelagem Matemática como uma estratégia no ensino-aprendizagem de conceitos matemáticos valorizando-os em um contexto multidisciplinar. Fortalecer e valorizar o conhecimento de cada professor-aluno na construção de modelos de situações reais. Incentivar o trabalho coletivo e solidário do grupo. Articular o Ensino Superior e o Ensino Médio, fazendo com que os professores-alunos se tornem indicadores e agentes das melhorias necessárias ao ensino-aprendizagem da matemática nas escolas na região do semi-árido. Desenvolvidos em 2009-2010.

6.2.5 Plataforma de simulação de Controladores Multiagentes

Descrição: Um dos principais objetivos do projeto é desenvolver algoritmos de controle com uso de agentes que são capazes de determinar uma linha adequada e interpretável através de uma plataforma dentro de um pequeno número de simulações. Assim no presente trabalho tem por objetivo estudar alguns métodos para determinar uma medida fuzzy erro de um sistema dinâmico. O processo de aprendizagem do modelo a ser estudado deve ser dividido em duas fases principais. A primeira fase destina-se a aprender uma primeira o procedimento básico, se não houver conhecimento prévio sobre o sistema que está sendo disponível. A segunda fase deve otimizar as regras, deslocando ou modificando as regras da lógica fuzzy que também devem ser construídas na referida plataforma. Ambas as fases utilizar um erro fuzzy, que deve descrever a qualidade do estado atual do sistema, para aprender ou para otimizar na referida plataforma através de um procedimento básico.Além disso, deve ser possível utilizar o conhecimento prévio para inicializar o processo de aprendizagem, no processo de controle na produção do clinquerer do cimento. Por outro a referida técnica deve usada na Produção de cimento deve ser estendida também aplicar a referida técnica na produção de petróleo, na região do Semi-árido em particular na cidade Mossoró. Desenvolvidos em 2009-2010.

6.3 Produção Bibliográfica

6.3.1 Artigos Científicos Completos Publicados em Periódicos

- Total de artigos: 17

- Total de artigos em periódicos internacionais: 15
- Total de artigos em periódicos nacionais: 2

6.4 Artigos com publicados em revistas indexadas

6.4.1 Energies 2024

Valberio Gonzaga de Araujo Aziz Oloroun-Shola Bissiriou Juan Moises Mauricio Villanueva Elmer Rolando Llanos Villarreal Andres Ortiz Salazar Rodrigo de Andrade Teixeira and Diego Antonio de Moura Fonseca Monitoring and Diagnosing Faults in Induction Motors' Three-Phase Systems Using NARX Neural Network. Energies , v. 17(18), p. 4609-4609(40), 2024.

6.4.2 Energies 2024

DANTAS NETO, JOSÉ RAIMUNDO ; LOPES, JOSÉ SOARES BATISTA ; FONSÊCA, DIEGO ANTONIO DE MOURA ; GARCIA, ANTONIO RONALDO GOMES ; FERREIRA, JOSSANA MARIA DE SOUZA ; Villarreal, Elmer Rolando Llanos ; SALAZAR, ANDRÉS ORTIZ . Artificial Intelligence for the Control of Speed of the Bearing Motor with Winding Split Using DSP. Energies , v. 17, p. 1029-1029(28), 2024.

6.4.3 Energies 2024

TEIXEIRA, RODRIGO DE ANDRADE ; DA SILVA, WERBET LUIZ ALMEIDA ; AMARAL, ADSON EMANUEL SANTOS ; RODRIGUES, WALTER MARTINS ; SALAZAR, ANDRÉS ORTIZ ; Villarreal, Elmer Rolando Llanos . Application of Active Disturbance Rejection in a Bearingless Machine with Split-Winding. Energies , v. 16, p. 3100, 2023.

6.4.4 Sensors 2023

ECHAIZ ESPINOZA, GERMAN ALBERTO ; OLIVEIRA, GABRIEL PEREIRA DE ; LIMA, VERIVAN SANTOS ; FONSECA, DIEGO ANTONIO DE MOURA ; SILVA,

WERBET LUIZ ALMEIDA DA ; MAITELLI, CARLA WILZA SOUZA DE PAULA ; Villarreal, Elmer Rolando Llanos ; SALAZAR, ANDRÉS ORTIZ . Thermal Profiles in Water Injection Wells: Reduction in the Systematic Error of Flow Measurements during the Transient Regime. SENSORS , v. 23, p. 9465, 2023.

6.4.5 Energies 2022

DO NASCIMENTO, THIAGO F. ; NUNES, EVANDRO A. D. F. ; VILLARREAL, ELMER R. L. ; PINHEIRO, RICARDO F. ; SALAZAR, ANDRÉS O. . Performance Analysis of an Electromagnetic Frequency Regulator under Parametric Variations for Wind System Applications. Energies , v. 15, p. 2873-1-27, 2022.

6.4.6 Energies 2022

CRISÓSTOMO, DANIEL C. C. ; DO NASCIMENTO, THIAGO F. DO ; NUNES, EVANDRO A. D. F. ; VILLARREAL, ELMER ; PINHEIRO, RICARDO ; SALAZAR, ANDRÉS . Fuzzy Control Strategy Applied to an Electromagnetic Frequency Regulator in Wind Generation Systems. Energies , v. 15, p. 7011-7011(21), 2022.

6.4.7 IEEE ACCESS 2021

FONSECA, DIEGO ANTONIO DE MOURA ; SALAZAR, ANDRES ORTIZ ; Villarreal, Elmer Rolando Llanos ; ESPINOZA, GERMAN ALBERTO ECHAIZ ; LEITE, ALAN CASSIO QUEIROZ BEZERRA . Downhole Telemetry Systems to Monitor Electric Submersible Pumps Parameters in Oil Well. IEEE Access , v. 9, p. 1-1, 2021.

6.4.8 Energies 2021

CARVALHO SOUZA, FRANCISCO ELVIS ; SILVA, WERBET ; ORTIZ SALAZAR, ANDRÉS ; PAIVA, JOSÉ ; MOURA, DIEGO ; Villarreal, Elmer Rolando Llanos . A Novel Driving Scheme for Three-Phase Bearingless Induction Machine with Split Winding. Energies , v. 14, p. 4930-4930 (1-15), 2021.

6.4.9 Energies 2020

TEIXEIRA, RODRIGO DE A. ; SILVA, WERBET L. A. ; PESSOA, GUILHERME A. P. DE C. A. ; NETO, JOAO T. CARVALHO ; VILLARREAL, ELMER R. L. ; SALAZAR, ANDRÉS O. ; LOCK, ALBERTO S. . One Cycle Control of a PWM Rectifier a New Approach. Energies , v. 13, p. 5523-5546, 2020.

6.4.10 PRZEGLAD ELEKTROTECHNICZNY 2019

FONSECA, D. ; SALAZAR, A. ; GONCALVES, T. ; ELMER VILLARREAL . Electrical modelling of an electrical submersible pump system three-phase power cable used in power line communication. PRZEGLAD ELEKTROTECHNICZNY , v. 10, p. 22-26, 2019.

6.4.11 IEEE ACCESS 2019

DE FREITAS NUNES, EVANDRO AILSON ; SALAZAR, ANDRES ORTIZ ; Villarreal, Elmer Rolando Llanos ; SOUZA, FRANCISCO ELVIS CARVALHO ; JUNIOR, LUCIANO PEREIRA DOS SANTOS ; LOPES, JOSE SOARES BATISTA ; LUQUE, JUAN CARLOS CUTIPA . Proposal of a Fuzzy Controller for Radial Position in a Bearingless Induction Motor. IEEE Access , v. 7, p. 114808-114816, 2019.

6.4.12 SENSORS 2019

DA SILVA, FABRICIO ROOSEVELT MELO ; FONSÊCA, DIEGO ANTONIO DE MOURA ; DA SILVA, WERBET LUIZ ALMEIDA ; Villarreal, Elmer Rolando Llanos ; ECHAIZ ESPINOZA, GERMAN ALBERTO ; SALAZAR, ANDRÉS ORTIZ . System of Sensors and Actuators for the Production of Water Used in the Manufacture of Medicines. SENSORS , v. 19, p. 4488-4488/22, 2019.

6.3.1.12 Xiankleber Benjamim ; Felipe O. S. Gama; Rodrigo S. Semente; Elmer R. L. Villarreal and Andrés O. Salazar Development and Analysis of a Cryptographic Algorithm

for Genetically Optimized Wireless Sensor. PRZEGLAD ELEKTROTECHNICZNY , v. 1, p. 81-86, 2018.

6.4.13 IEEE Latin America Transactions

REGIS MELO, REUBER ; CARATTI FILHO, EGMIDIO ; SIMONE SILVA CASILLO, DANIELLE ; ROLANDO LLANOS VILLARREAL, ELMER . Benchmark of a PI Controller Implemented in Java and Native Code on the Android- Platform Embedded on ARM. IEEE Latin America Transactions , v. 13, p. 2488-2494, 2015.

6.4.14 International Journal of Artificial Intelligence and Applications 2012

VARGAS, J. A. R. ; Vargas, Josek A. R ; VILLARREAL, E. R. L. ; HEMERLY, E. M. . Stability Analysis of A Neuro-Identification Scheme with Asymptotic Convergence. International Journal of Artificial Intelligence and Applications, v. 3, p. 35-50, 2012.

6.4.15 COMPUTATIONAL APPLIED MATHEMATICS 2012

LIMA, JOÃO D. ; SILVA, FRANCISCO M. ; VILLAREAL, ELMER R.L. . A new approach for data transmission system on topological surfaces. COMPUTATIONAL APPLIED MATHEMATICS , v. 31, p. 143-168, 2012.

6.4.16 TEMA 2009

VILLARREAL, E. R. L.; J. A. R. Vargas ; Elder M. Hemerly . Static Output Feedback Stabilization using Invariant Subspaces and Sylvester Equations. TEMA. Tendências em Matemática Aplicada e Computacional, v. 1, p. 99-110, 2009.

6.4.17 IEEE TRANSACTIONS ON AUTOMATIC CONTROL 2003

CASTELAN, E.B. ; HENNET, J.-C. ; VILLARREAL, E.R.L. . Quadratic characterization and use of output stabilizable subspaces. IEEE TRANSACTIONS ON AUTOMATIC CONTROL , v. 48, p. 654-660, 2003.

6.5 Artigos com publicados em anais de congressos internacionais

Os artigos internacionais foram publicados em eventos de qualidade na área de Controle de Processos e concentram-se nos seguintes eventos:

- Conference on Decision and Control (CDC)
- American Control Conference (ACC)
- World Congress of the International Federation of Automatic Control (IFAC)
- IFAC Conference on Advances in PID Control
- IFAC Symposium on Advances in Control Education
- IEEE International Conference on Control Applications

6.5.1 IEEE-CHILE 2022

SALAZAR, ANDRES O. ; CRISOSTOMO, DANIEL C. C. ; MANICOBA, GLAUCO G. C. ; NUNES, EVANDRO A. D. F. ; VILLARREAL, ELMER R. L. . Analysis and Modeling of an Electromagnetic Speed Regulator for Wind Energy Conversion Systems. In: 2022 IEEE International Conference on Automation/XXV Congress of the Chilean Association of Automatic Control (ICAACCA), 2022, Curicó. 2022 IEEE International Conference on Automation/XXV Congress of the Chilean Association of Automatic Control (ICA-ACCA). Curicó, Chile: IEEE, 2022. v. 1. p. 1-6.

6.5.2 IEEE-CHILE 2021

Villarreal, Elmer Rolando Llanos; SALAZAR, A. O. ; DA SILVA, WERBET LUIZ ALMEIDA ; PEREIRA I, V. M. S. . Impulse elimination for singular second-order system : approach. In: IEEE IFAC Internacional Conference on Automation, 2021, Santiago Chile.

IEEE IFAC Internacional Conference on Automation / XXIV Congreso de la Asociación Chilena de Control Automático. Santiago Chile: USACH, 2021. v. 1. p. 1-6.

6.5.3 IEEE-CHILE 2021

Elmer R. L. Villarreal; SALAZAR, A. O. ; VIEIRA, P. V. F. . Approach to partial eigenvalue assignment using Sylvester equation in system-second order. In: IEEE IFAC International Conference on Automation, XXIV Congreso de la Asociación Chilena de Control Automático, 2021, Santiago Chile. IEEE IFAC International Conference on Automation, XXIV Congreso de la Asociación Chilena de Control Automático. Santiago Chile: USACH, 2021. v. 1. p. 7-12.

6.5.4 IEEE-CHILE 2021

DA SILVA, WERBET LUIZ ALMEIDA ; SALAZAR, A. O. ; Elmer R. L. Villarreal ; VIEIRA, P. V. F. ; JACOME, M. C. . Radial Position Control of a Bearingless Machine with Active Disturbance Rejection Control Fuzzy an approach. In: IEEE IFAC International Conference on Automation, XXIV Congreso de la Asociación Chilena de Control Automático, 2021, Santiago Chile. IEEE IFAC International Conference on Automation, XXIV Congreso de la Asociación Chilena de Control Automático. Santiago Chile: USACH, 2021. v. 1. p. 13-18.

6.5.5 ISMB17 2021

SILVA, WERBET L. A. ; Villarreal, Elmer Rolando Llanos ; FERREIRA, J. M. S. ; PAIVA, J. A. ; SALAZAR, A. O. ; MAITELLI, A. L. . Application of Active Disturbance Rejection Control (ADRC) in the Radial Position Control of a Bearingless Induction Machine With Split Winding. In: The International Symposium on Magnetic Bearings ISMB17 RIO JANEIRO, 2021, RIO JANEIRO. The International Symposium on Magnetic Bearings ISMB17 RIO JANEIRO (Virtual Conference). Rio de Janeiro: ISMB17, 2021. v. 1. p. 1-13.

6.5.6 ISMB17 2021

PAIVA, J. A. ; SILVA, WERBET L. A. ; FERREIRA, J. M. S. ; MAITELLI, A. L. ; SALAZAR, A. O. ; VILLARREAL, ELMER R. L. . REVIEW ABOUT CONTROL AND ESTIMATION STRATEGIES APPLIED TO BEARINGLESS MACHINES. In: The International Symposium on Magnetic Bearings ISMB17 RIO JANEIRO (Virtual Conference), 2021, RIO JANEIRO. The International Symposium on Magnetic Bearings ISMB17 RIO JANEIRO (Virtual Conference). Rio de Janeiro: ISMB17, 2021. v. 1. p. 14-27.

6.5.7 INTERCON 2020

S SILVA, WERBET L. A. ; SALAZAR, ANDRES O. ; CABRAL NETO, RONALDO JOSE N. ; VILLARREAL, ELMER R. L. . Radial Position Control of a Bearingless Machine with Active Disturbance Rejection Control. In: 2020 IEEE XXVII International Conference on Electronics, Electrical Engineering and Computing (INTERCON), 2020, Lima. 2020 IEEE XXVII International Conference on Electronics, Electrical Engineering and Computing (INTERCON), 2020. v. 1. p. 1-4.

6.5.8 EMI Rio de Janeiro 2017

JACOME, M. C. ; E. R. L. Villarreal . Proposed of active suspension with fuzzy control. In: 2017 EMI International Conference, 2017, Rio de Janeiro. 2017 EMI International Conference. Rio de Janeiro: 2017 EMI International Conference, 2017. v. 1. p. 1-5.

6.5.9 IEEE CONFERENCE PUBLICATIONS México 2015

FERNANDES, A. ; BRANDAO, A. S. ; VILLARREAL, E. R. L. . A Comparative Study of Altitude and Yaw Controllers for Rotorcraft UAV. In: 2015 Workshop on Research, Education and Development of Unmanned Aerial Systems (RED-UAS), 2015, CANCUN MEXICO. Proceedings of the 2015 IEEE 3rd International Workshop on Research, Education and Development of Unmanned Aerial Systems to be held in

Cancun Mexico. CANCUN MEXICO: IEEE CONFERENCE PUBLICATIONS, 2015. v. 1. p. 411-418.

6.5.10 PROCEEDINGS IEEE-ACCA CHILE 2014

SENA, F. C. B. ; SILVA, J. P. ; MOURA, A. A. F. ; VILLARREAL, E. R. L. ; DANTAS, E. R. M. . FUZZY PITCH CONTROLLER APPLIED TO VARIABLE-SPEED WIND TURBINE. In: ACCA 2014 CHILE, 2014, Santiago Chile. PROCEEDINGS ACCA 2014 CHILE. santiago de chile: publications Federação Internacional de Controle Automático, 2014. v. 1. p. 1-6.

6.5.11 IFAC IMS2013 2013

TEIXEIRA JUNIOR, C. A. ; VILLARREAL, E. R. L. ; CINTRA, M. E. ; LIMA, N. W. B. . Proposal of a Fuzzy Control System for the Management of Traffic Lights. In: 11th IFAC Workshop on Intelligent Manufacturing Systems (IMS?13), 2013, São Paulo. Proceedings 11th IFAC Workshop on Intelligent Manufacturing Systems (IMS13),. São Paulo-SP Brasil: Intelligent Manufacturing Systems International Federation of Automatic Control, 2013. v. 11. p. 456-461.

6.5.12 IFAC IMS2013 2013

Clayton, Oliveira ; VILLARREAL, E. R. L. ; REUBER REGIS DE MELO . Solution of Equations of State and Output Feedback for a Line Transmission Via Invariant Subspaces. In: 11th IFAC Workshop on Intelligent Manufacturing Systems (IMS?13), 2013, São Paulo. Proceedings 11th IFAC Workshop on Intelligent Manufacturing Systems (IMS?13). São Paulo SP Brasil: Intelligent Manufacturing Systems, 2013. v. 46. p. 288-293.

6.5.13 IFAC IMS2013 2013

REUBER REGIS DE MELO ; CARATTI FILHO, E. ; CASILLO, D. S. S. ; VILLARREAL, E. R. L. . New Approach in Building Supervision Systems, Automation

and Control Based on ARM. In: 11th IFAC Workshop on Intelligent Manufacturing Systems (IMS?13), 2013, São Paulo. Procedings 11th IFAC Workshop on Intelligent Manufacturing Systems (IMS?13). São Paulo SP Brasil: Proceedings Intelligent Manufacturing Systems International Federation of Automatic Control, 2013. v. 11. p. 128-132.

6.5.14 15th LATINAMERICAN CONTROL CONFERENCE, Lima Perú, 2012

VILLARREAL, E. R. L.; Walter Martins Rodrigues ; João de Deus Lima ; J. A. R. Vargas . APPROACH ON SOLUTION TO SYLVESTER EQUATION STABILIZATION IN SINGULAR SYSTEM. In: 15th LATINAMERICAN CONTROL CONFERENCE, 2012, Lima Perú. Proceedings 15th LATINAMERICAN CONTROL CONFERENCE. Lima-Perú: Tarea Associación Gráfica Educativa, 2012. v. 11. p. 24-27.

6.5.15 15th LATINAMERICAN CONTROL CONFERENCE, Lima Perú, 2012

C. M. MEDEIROS DE AZEVEDO ; VILLARREAL, E. R. L. ; Antonio Ronaldo Gomes Garcia . MODELING OF MECHANICAL SYSTEM: OUTPUT FEEDBACK AND DERIVATIVE FEEDBACK. In: 15th LATINAMERICAN CONTROL CONFERENCE, 2012, Lima Perú. PROCEEDINGS 15th LATINAMERICAN CONTROL CONFERENCE. Lima: Tarea Associación Gráfica Educativa, 2012. v. 1. p. 8-13.

6.5.16 15th LATINAMERICAN CONTROL CONFERENCE, Lima Perú, 2012

CARATTI FILHO, E. ; VILLARREAL, E. R. L. ; CASILLO, D. S. S. ; PAVAO, A. C. ; REUBER REGIS DE MELO . LINEAR SYSTEMS APPLIED IN SUSPENDED WEIGHT OF OIL RIGS. In: Proceedings 15th LATINAMERICAN CONTROL CONFERENCE, 2012, Lima Perú. Proceedings 15th LATINAMERICAN CONTROL CONFERENCE. Lima: Tarea Associación Gráfica Educativa, 2012. v. 1. p. 134-138.

.

6.5.17 15th International Conference on Computational Science and Its Applications 2012

DE AZEVEDO, CLAUDIO MARCIO MEDEIROS ; Villarreal, Elmer Rolando Llanos . Stabilization: Algorithms for Mechanical System Using Output Feedback and State Feedback. In: 2012 12th International Conference on Computational Science and Its Applications, 2012, Salvador. 2012 12th International Conference on Computational Science and Its Applications. v. 1. p. 97-102.

6.5.18 15th LATINAMERICAN CONTROL CONFERENCE, Lima Perú, 2012

LIMA, N. W. B. ; SILVA, R. D. ; VILLARREAL, E. R. L. ; Walter Martins Rodrigues . Applied in Fuzzy Logic Controller in Smart Structures. In: 15th Latinamerican Control Conference CLCA 2012, 2012, Lima. Proceedings 15th Latinamerican Control Conference CLCA 2012. Lima: CD CLCA 2012 Lima, 2012. v. 1. p. 1-5.

6.5.19 15th LATINAMERICAN CONTROL CONFERENCE, Lima Perú, 2012

MORAIS, F. A. ; VILLARREAL, E. R. L. ; GURGEL, D. P. ; Walter Martins Rodrigues . New Approach in pH Neutralization Process Using Fuzzy Controller. In: Proceedings 15th Latinamerican Control Conference CLCA 2012, 2012, Lima Perú. Proceedings 15th Latinamerican Control Conference CLCA 2012. Lima PERU: CLCA 2012 PERU, 2012. v. 1. p. 1-6.

6.5.20 IEEE CESA 2012

C. M. MEDEIROS DE AZEVEDO ; VILLARREAL, E. R. L. . Mechanical System Modelling Output Feedback and State Feedback. In: IEEE CESA 2012 Conference on Computational Engineering in Systems Applications, 2012, Santiago Chile. Proceedings IEEE CESA 2012 Conference on Computational Engineering in Systems Applications. Santiago de Chile: Proceedings IEEE CESA 2012, 2012. v. 1. p. 229-233

6.5.21 IFAC Triennial World Congress Barcelona 2002

CASTELAN NETO, E. B. ; AGUINALDO S. SILVA. ; VILLARREAL, E. R. L. ; SOPHIE TARBOURIECH. REGIONAL POLE PLACEMENT BY OUTPUT FEEDBACK FOR A CLASS OF DESCRIPTOR SYSTEMS. IFAC Triennial World Congress Barcelona 2002. vol 1. p.101-106.

6.5.22 IFAC Triennial World Congress Barcelona 2002

CASTELAN NETO, E. B. ; VILLARREAL, E. R. L. ; HENNET, J. C. OUTPUT FEEDBACK DESIGN BY COUPLED LYAPUNOV -LIKE EQUATIONS. IFAC Triennial World Congress Barcelona 2002. vol 1. p.207-212.

6.5.23 IFAC System Structure and Control 2001

CASTELAN NETO, E. B. ; VILLARREAL, E. R. L. ; SOPHIE TARBOURIECH. QUADRATIC CHARACTERIZATION AND USE OF OUTPUT STABILIZABLE FOR DESCRIPTOR SYSTEMS. IFAC System Structure and Control 2001. vol 1. p.255-260.

6.5.24 8th IEEE MEDITERRANEAN CONFERENCE ON CONTROL AND AUTOMATION, 2000

CASTELAN NETO, E. B. ; VILLARREAL, E. R. L. ; HENNET, J. C. . QUADRATIC CHARACTERIZATION AND USE OF OUTPUT STABILIZABLE. In: 8th IEEE MEDITERRANEAN CONFERENCE ON CONTROL AND AUTOMATION, 2000, PATRAS. PROCEEDINGS , 2000: 8th IEEE MEDITERRANEAN CONFERENCE ON CONTROL AND AUTOMATION, 2000. v. 1. p. 1-6.

6.6 Artigos com publicados em anais de congressos nacionais

Os artigos nacionais foram publicados em eventos de qualidade na área de Controle se concentram-se nos seguintes eventos:

- Congresso Nacional de Matemática Aplicada e Computacional(CNMAC)

- Congresso Brasileiro de Automática (CBA)
- Simpósio Brasileiro de Automação Inteligente (SBAI)
- Congresso Brasileiro de Educação em Engenharia (COBENGE)
- Conferência Brasileira de Dinâmica, Controle e Aplicações (DINCON)

6.6.1 CNMAC 2023

SILVA, LUCAS D. DA ; RODRIGUES, WALTER M. ; SILVA, NATHAN R. DA ; JÁCOME, MAXWELL C. ; SALAZAR, ANDRES O. ; VILLARREAL, ELMER R. L. . Tuning Method in the Implementation Fuzzy ADRC Controllers for a Mass-Spring-Damper System: An approach. In: v. 10 n. 1 (2023): CNMAC 2023, 2023, BONITO/ MS. São Carlos SP: CNMAC 2023, 2023. v. 10.

6.6.2 CNMAC 2022

Villarreal, Elmer Rolando Llanos; SALAZAR, ANDRÉS ORTIZ ; NASCIMENTO, T. F. ; SILVA, L. D. ; Walter Martins Rodrigues . An Approach to Partial Quadratic Eigenvalue Assignment of Vibration Systems Using Sylvester equations. In: XLI Congresso Nacional de Matemática Aplicada e Computacional (CNMAC 2022), 2022, Campinas/SP. Proceeding Series of the Brazilian Society of Computational and Applied Mathematics. São Carlos/SP: SBMAC - Sociedade de Matemática Aplicada e Computacional, 2022.

6.6.3 CNMAC 2022

VILLARREAL, ELMER R. L.; SALAZAR, ANDRES O. ; NASCIMENTO, THIAGO F. DO ; SILVA, LUCAS D. DA ; RODRIGUES, WALTER M. . Eigenvalue Assignment in Second order systems Using Sylvester equations: Approach. In: CNMAC 2022 XLI Congresso Nacional de Matemática Aplicada e Computacional, 2022, Campinas/SP, 2022.

6.6.4 CNMAC 2022

JACOME, M. C. ; SILVA, L. D. ; SALAZAR, ANDRÉS ORTIZ ; Walter Martins Rodrigues ; Villarreal, Elmer Rolando Llanos . Stabilization in semiactive systems using Sylvester equations: Approach. In: XLI Congresso Nacional de Matemática Aplicada e Computacional (CNMAC 2022), 2022, Campinas/SP. Proceeding Series of the Brazilian Society of Computational and Applied Mathematics. São Carlos/SP: SBMAC - Sociedade de Matemática Aplicada e Computacional, 2022.

6.6.5 COBEP 2021

S TEIXEIRA, RODRIGO DE A. ; ORTIZ SALAZAR, ANDRÉS ; Villarreal, Elmer Rolando Llanos ; SILVA, W. L. A. ; CARVALHO NETO, J. T. . ONE CYCLE CONTROL APPLIED TO A THREE-PHASE PWM RECTIFIER. In: 16 Brazilian Power Electronics Conferences COBEP 2021, 2021, João Pessoa. 16 Brazilian Power Electronics Conferences COBEP 2021. João Pessoa: CEAR UFPB João Pessoa, 2021. v. 1. p. 1-6.

6.6.6 CNMAC 2018

S VILLARREAL, E. R. L.; REGO, R. C. B. ; BENJAMIM, X. C ; SALAZAR, A. O. ; LOCK, A. S. ; DIONISIO, C. R. P. . Controle MPC com Atrasos e Perdas de Pacotes. In: XXXVIII Congresso Nacional de Matemática Aplicada e Computacional CNMAC 2018, 2018, CAMPINAS SP. Controle MPC com Atrasos e Perdas de Pacotes. CAMPINAS SP: SBMAC, 2018. v. 1. p. 1-7.

6.6.7 CNMAC 2018

VILLARREAL, E. R. L.; SALAZAR, A. O. ; LOCK, A. S. ; RODRIGUES, W. M. . Output Feedback Control in Descriptor System Admissible. In: Proceeding Series of the Brazilian Society of Computational and Applied Mathematics, 2018, CAMPINAS SP. Output Feedback Control in Descriptor System Admissible. CAMPINAS: Proceeding

Series of the Brazilian Society of Computational and Applied Mathematics, 2018. v. 1. p. 7-13.

6.6.8 CNMAC 2017

E R L Villarreal; JACOME, M. C. ; MORAIS, E. R. ; QUEIROZ, J. V. ; RODRIGUES, W. M. . Optimization Based Output Feedback Control Design in Descriptor Systems. In: CNMAC 2017(Congresso Nacional de Matemática Aplicada e Computacional), 2017, São Jose dos Campos. Optimization Based Output Feedback Control Design in Descriptor Systems. São José dos Campos SP: CNMAC 2017, 2017. v. 1. p. 1-7.

6.6.9 CNMAC 2017

E. R. L. Villarreal; JACOME, M. C. ; MORAIS, E. R. ; QUEIROZ, J. V. ; Walter Martins Rodrigues . Aplicação da equação diferencial de Sylvester. In: CNMAC2017 (Congresso Nacional de Matemática Aplicada e Computacional), 2017, São José dos Campos. Aplicação da equação diferencial de Sylvester. Sao Jose dos Campos: CNMAC 2017, 2017. v. 1. p. 8-14.

6.6.10 DINCON 2017

JACOME, M. C. ; REBOUCAS, I. O. ; MENDES, N. E. C. ; Elmer R. L. Villarreal ; Walter Martins Rodrigues . Suspensão Semi-ativa com Controlador Fuzzy. In: CONFERÊNCIA BRASILEIRA DE DINÂMICA, CONTROLE E APLICAÇÕES, 2017, São José Rio Preto. DINCON 2017 CONFERÊNCIA BRASILEIRA DE DINÂMICA, CONTROLE E APLICAÇÕES. São José Rio Preto: Proceddings DINCON 2017, 2017. v. 1. p. 1-7.

6.6.11 COBENGE 2016

JACOME, M. C. ; MENDES, N. E. C. ; VILLARREAL, E. R. L. . Uso do Simulink para simulação de um sistema dinâmico descito por equaões diferenciais. In: XLIV Congresso Brasileiro de Educação em Engenharia (COBENGE), 2016, Natal RN.

Uso do Simulink para simulação de um sistema dinâmico descito por equaões diferenciais. COBENGE 2016 NATAL: COBENGE 2016 NATAL, 2016. v. 1. p. 1-5.

6.6.12 DINCON 2015

BEZERRA FILHO, F. A. ; JACOME, M. C. ; VILLARREAL, E. R. L. . Aplicação do Controle Servo Visual em um Quadrirrotor. In: Conferência Brasileira de Dinâmica Controle e aplicações DINCON 2015, 2015, Natal. Conferência Brasileira de Dinâmica Controle e aplicações DINCON 2015, 2015. v. 1. p. 1-6.

6.6.13 DINCON 2015

VILLARREAL, E. R. L.; BRANDAO, A. S. ; MORAIS, E. R. ; COLACA, C. F. . Modeling and Stabilization of a Quadrotor using Output Feedback. In: Conferência Brasileira de Dinâmica Controle e Aplicações DINCON 2015, 2015, Natal. Conferência Brasileira de Dinâmica Controle e Aplicações DINCON 2015. Natal: Dincon 2015, 2015. v. 1. p. 7-11.

6.6.14 CNMAI 2015

VILLARREAL, E. R. L.; BRANDAO, A. S. ; SILVA, A. S. A. . Modeling and Control Output Feedback of a VANT. In: II Congresso Nacional de Matemática aplicada à Industria CNMAI2015, 2015, Fortaleza. II Congresso Nacional de Matemática aplicada à Industria CNMAI 2015, 2015. v. 1. p. 1-7.

6.6.15 COBENGE 2015

VILLARREAL, E. R. L.; BEZERRA FILHO, F. A. ; ANDRADE, L. C. ; JACOME, M. C. . Aplicação dos quadrirrotores como objeto de estudo de diversas áreas de engenharia. In: XLIII CONGRESSO BRASILEIRO DE EDUCAÇÃO EM ENGENHARIA COBENGE 2015, 2015, São Bernardo do Campo. XLIII CONGRESSO BRASILEIRO DE EDUCAÇÃO EM ENGENHARIA COBENGE 2015, 2015. v. 1. p. 1-6.

6.6.16 COBENGE 2015

ALVES, C. C. ; GONCALVES, T. M. P. ; VILLARREAL, E. R. L. . DESENVOLVER UM CONTROLADOR FUZZY-PID PARA UM VEICULO ÁEREO NÃO TRIPULADO VANT. In: XLIII CONGRESSO BRASILEIRO DE EDUCAÇÃO EM ENGENHARIA COBENGE 2015, 2015, São Bernardo do Campo SP. XLIII CONGRESSO BRASILEIRO DE EDUCAÇÃO EM ENGENHARIA COBENGE 2015. São Bernardo do Campo: COBENGE 2015, 2015. v. 1. p. 8-13.

6.6.17 DINCON 2013

Villarreal, Elmer Rolando Llanos; SILVA, ALEX SANDRO DE ARAUJO ; OLIVEIRA, SAMEQUE FARIAS CUNHA DE . Approach in nonlinear descriptor system using output feedback. In: DINCON 2013 - Conferência Brasileira de Dinâmica, Controle e Aplicações, 2013, Fortaleza. Fortaleza: Dincon /fortaleza, 2013. v. 1.

6.6.18 SBAI 2013

LIMA, A. M. ; OLIVEIRA, S. F. C. ; FARIAS, M. S. ; VILLARREAL, E. R. L. . APPLICATION THE CONTROL IN TANKS USING FUZZY THEORY. In: Simpósio Brasileiro de Automação Inteligente SBAI 2013, 2013, Fortaleza. Proceedings Simpósio Brasileiro de Automação Inteligente SBAI 2013. Fortaleza-CE: Departamento de Engenharia Elétrica da Universidade Federal do Ceará (UFC)., 2013. p. 1-5.

6.6.19 CNMAC 2012

VILLARREAL, E. R. L.; João de Deus Lima ; Walter Martins Rodrigues ; BORJAS, S. D. M. . ALGORITHM FOR STABILIZATION BY REGIONAL POLE REGIONAL. In: 34 CONGRESSO NACIONAL DE MATEMATICA APLICADA E COMPUTACIONAL, 2012, AGUAS DE LINDOIA. 34 CONGRESSO NACIONAL DE MATEMATICA APLICADA E COMPUTACIONAL. AGUAS DE LINDOIA: CNMAC2012, 2012. v. 1. p. 243-249.

6.6.20 CNMAC Nordeste 2012

LIMA, N. W. B. ; SILVA, R. D. ; VILLARREAL, E. R. L. ; Walter Martins Rodrigues ; REUBER REGIS DE MELO . Equação diferencial, Lógica fuzzy em estruturas inteligentes. In: Congresso de Matemática Aplicada e Computacional CMAC Nordeste 2012, 2012, Natal. ANAIS DO CONGRESSO DE MATEMATICA COMPUTACIONAL CMAC-Nordeste 2012. Natal: ANAIS CMAC-Nordeste Natal, 2012. v. 1. p. 53-56.

6.6.21 DINCON 2011

VILLARREAL, E. R. L.; Walter Martins Rodrigues ; Samara Jéssica Monte Bezerra ; J. A. R. Vargas . STABILIZATION BY OUTPUT FEEDBACK IN REGIONAL POLE PLACEMENT. In: X Conferência Brasileira de Dinâmica, Controle e Aplicações, 2011, Aguas de Lindoia. Proceedings Dincon 2011 X Conferência Brasileira de Dinâmica, Controle e Aplicações. Aguas de Lindoia São Paulo: Proceedings DINCON 2011, 2011. v. 1. p. 786-789.

6.6.22 COBENGE 2011

Alexandre Henrique Soares de Oliveira ; Isau Macedo Balbino ; VILLARREAL, E. R. L. . CONTROLE PID PARA VÁZÃO, UMA AULA DIDÁTICA USANDO SIMULAÇÃO NA UFERSA. In: XXXIX CONGRESSO BRASILEIRO DE EDUCAÇÃO EM ENGENHARIA, 2011, BLUMENAU. XXXIX CONGRESSO BRASILEIRO DE EDUCAÇÃO EM ENGENHARIA. BLUMENAU: 2011 - XXXIX COBENGE: FURB - Blumenau/SC, 2011. v. 1. p. 1-6.

6.6.23 DINCON 2010

VILLARREAL, E. R. L.; BORJAS, S. D. M. ; Walter Martins Rodrigues ; J. A. R. Vargas . Sufficient conditions for stabilization by ouput feedback in descriptor systems. In: 9th Brazilian Conference on Dynamics, Control and Their Applications, 2010, Serra Negra/SP. 9th Brazilian Conference on Dynamics, Control and Their Applications. Serra

Negra/ São Paulo Brasil: Proceedings 9th Brazilian Conference on Dynamics, Control and Their Applications, 2010. v. 1. p. 934-939.

6.6.24 DINCON 2009

VILLARREAL, E. R. L.. Approach for stabilization by output feedback, invariant subspace, Sylvester Equations, and Ricatti Equations. In: DINCON'09 - 8th Brazilian Conference on Dynamics, Control and Applications, 2009, Bauru. DINCON'09 - 8th Brazilian Conference on Dynamics, Control and Applications, 2009.

6.6.25 CNMAC 2009

VILLARREAL, E. R. L.. Aspect algorithm for stabilization by output feedback, Lyapunov Equations, and Ricatti Equations for class descriptor system. In: CNMAC 2009, 2009, CUIABA MT. XXXII CNMAC ? Congresso Nacional de Matemática Aplicada e Computacional. CUIABA: CNMAC 2009, 2009. v. 1. p. 1-4.

6.6.26 CNMAC 2009

VILLARREAL, E.R.L.. Approach for stabilization by output feedback, invariant subspace, Lyapunov equations and Riccati equations. In: Anais XXXII CNMAC ? Congresso Nacional de Matemática Aplicada e Computacional, 2009, Cuiabá. Approach for stabilization by output feedback, invariant subspace, Lyapunov Equations and Riccati Equations for class descriptor system. Cuiaba: CNMAC 2009, 2009. p. 1-4.

6.6.27 CNMAC 2008

VILLARREAL, E. R. L.; João de Deus Lima . Approach For Stabilization by Output Feedback, Invariant Subspaces and Sylvester Equations. In: 31 Congresso Nacional de Matemática Aplicada e Computacional (CNMAC 2008), 2008, Belém-PA. 31 Congresso Nacional de Matemática Aplicada e Computacional (CNMAC 2008). BELEM/PA: SBMAC, 2008. v. 1. p. 262-268.

6.6.28 CBA 2004

CASTELAN NETO, E. B. ; VILLARREAL, E. R. L. . Estabilização de Sistemas Descritores por Realimentação de Saídas via subespaços invariantes (artigo 660). In: Congresso brasileiro de Automatica (CBA2004), 2004, Gramado Rio Grande do Sul. Anais do XV Congresso brasileiro de Automatica, 2004. v. v1. p. 1-6.

6.6.29 Capítulos de Livro

Os seguintes capítulos de livro foram publicados:

6.6.30 Atena Editora 2022

VILLARREAL, E. R. LL.; JACOME, M. C. ; MORAIS, E. R. ; QUEIROZ, J. V. ; Walter Martins Rodrigues . Collection: Applied computer engineering. In: Lilian Coelho de Freitas. (Org.). Optimization Based Output Feedback Control Design in Descriptor Systems. 1ed.Ponta Grossa PR: Atena Editora, 2022, v. 1, p. 218-224.

6.6.31 Livro

Tive os livros publicados

6.6.32 Editora Conhecimento Livre, 2023

RODRIGUES, WALTER MARTINS ; Villarreal, Elmer Rolando Llanos . História da Matemática e estratégias interdisciplinares no ensino de Logaritmos. 1. ed. Piracanjuba-GO: Editora Conhecimento Livre, 2023. v. 1. 151p

6.6.33 Novas Edições Acadêmicas, 2016

CONFESSOR, S. L. M. ; VILLARREAL, E. R. L. . Análise comparativa de controladores MPPT em um sistema fotovoltaico. 1. ed. alemanha: Novas Edições Acadêmicas (2016-04-28), 2016. v. 1. 76p .

6.6.34 Novas Edições Acadêmicas, 2015

VILLARREAL, E. R. L.. Abordagem Geométrica para Estabilização por Realimentação de Saída. 1. ed. ALEMANHA: NOVAS EDIÇÔES ACADEMICAS, 2015. v. 1. 140p .

7 ATIVIDADE DE ORIENTAÇÃO E FORMAÇÃO DE PESQUISADORES

7.1 Orientações concluídas

7.1.1 Dissertações de Mestrado

No Programa de Pós-Graduação em Engenharia Elétrica da UFERSA orientei o seguinte alunos:

7.1.2 Dissertação, 2017

EDPO RODRIGUES DE MORAIS. DESENVOLVIMENTO DE UM CONTROLADOR HÍBRIDO FUZZY-PID PARA ESTABILIZAÇÃO DE VANT DO TIPO QUADRIRROTOR NA REALIZAÇÃO DE UM VOO AUTÔNOMO VERTICAL. 2017. Dissertação (Mestrado em Engenharia Elétrica).

7.1.3 Dissertação, 2015

Sameque Farias Cunha de Oliveira. Estabilização da atitude de um quadrimotor utilizando o controle Fuzzy-PID. 2015. Dissertação (Mestrado em Engenharia Elétrica).

7.1.4 Dissertação, 2014

Clayton Antonio de Miranda Oliveira. Projeto de Observadores de Estado utilizando Algoritmos Genéticos. 2014. Dissertação (Mestrado em Engenharia Elétrica).

7.1.5 Dissertação, 2014

Carlos Alberto Teixeira Junior. Análise comparativa entre os controladores Fuzzy PD+I e PID Convencional. 2014. Dissertação (Mestrado em Engenharia Elétrica).

7.1.6 Dissertação, 2014

Danilo de Santana Pena. Avaliação de estratégias de controle adaptativo do gerador síncrono de íma permanente aplicado em sistema de energia eólica. 2014. Dissertação (Mestrado em Engenharia Elétrica).

7.1.7 Dissertação, 2014

Sâmya Lorena de Medeiros Confessor. ANÁLISE COMPARATIVA CONTROLADORES MPPT APLICADOS A UM SISTEMA FOTOVOLTAICO. 2014. Dissertação (Mestrado em Engenharia Elétrica).

7.1.8 Dissertação, 2013

Cláudio Márcio Medeiros de Azevedo. Um modelo matemático para controle de um sistema ativo de suspensão automotiva. 2013. Dissertação (Mestrado em Engenharia Elétrica).

7.1.9 Dissertação, 2013

Reuber Regis de Melo. Uma abordagem no desenvolvimento de sistemas de automação industrial e controle utilizando um microcontrolador ARM. 2013. Dissertação (Mestrado em Engenharia Elétrica) .

No Programa de Pós-Graduação em Matemática (PROFMAT) da UFERSA orientei o seguinte alunos:

7.1.10 Dissertação, 2023

Rogério da Silva Costa. RECOMPOSIÇÃO DA APRENDIZAGEM MATEMÁTICA: UMA ABORDAGEM ATRAVÉS DAS OPERAÇÕES BÁSICAS NA ESCOLA DOMINGOS COSTA TEOBALDO EM ARACATI CEARÁ PÓS PANDEMIA COVID-19. 2023. Dissertação (Mestrado em PROFMAT Polo Mossoró).

7.1.11 Dissertação, 2018

MAYKEL SAMUEL MARINHO CÂMARA. UMA PROPOSTA DE ABORDAGEM DA TRIGONOMETRIA APRESENTANDO A FUNÇÃO DE EULER NO ESPAÇO COM O SOFTWARE GEOGEBRA. 2018. Dissertação (Mestrado em PROFMAT Polo Mossoró).

7.1.12 Dissertação, 2017

HILDEBERTO FERNANDO DE FREITAS REGIS. O USO DE QUEBRA-CABEÇAS PARA ESTIMULAR O APRENDIZADO DE POLIGONOS NA DISCIPLINA DE MATEMATICA NO ENSINO FUNDAMENTAL. 2017. Dissertação (Mestrado em PROFMAT Polo Mossoró).

7.1.13 Dissertação, 2016

HUGO ARNAUD MENDES. A INTERDISCIPLINARIDADE NO AUXÍLIO DO CONHECIMENTO DOS TERMOS MATEMÁTICOS NO SEXTO DO ENSINO FUNDAMENTAL. 2016. Dissertação (Mestrado em PROFMAT Polo Mossoró).

7.1.14 Dissertação, 2016

FRANCISCO RAFAEL DE FREITAS CAVALCANTE. ENSINO DE GEOMETRIA ESPACIAL: UMA PROPOSTA GEOGEBRA DE ATIVIDADES COM O USO DO GEOGEBRA. 2016. Dissertação (Mestrado em PROFMAT Polo Mossoró).

7.1.15 Dissertação, 2013

Antônio Carlos de Queiroz Silveira. A HISTÓRIA DA MATEMÁTICA COMO ELEMENTO MOTIVADOR NO ENSINO DE MATEMÁTICA. 2013. Dissertação (Mestrado em Mestrado em Matemática).

7.1.16 Dissertação, 2013

João Dehon de Sousa. OS JOGOS COMO RECURSOS DIDÁTICOS PARA A MELHORIA DA APRENDIZAGEM DOS APRENDENTES NAS AULAS DE MATEMÁTICA. 2013. Dissertação (Mestrado em Mestrado em Matemática).

7.1.17 Dissertação, 2013

Jozildes Vieira Lima. APLICAÇÕES DAS FUNÇÕES SENO E COSSENO ATRAVÉS DO MOVIMENTO DAS MARÉS E ONDAS SONORAS.. 2013. Dissertação (Mestrado em Mestrado em Matemática).

7.1.18 Orientação de Alunos de Graduação

Tive vários alunos com orientações de Iniciação Científica, Trabalho de Conclusão de Curso na UFERSA. . A seguir, apresenta-se apenas os resultados quantitativos:

- Trabalho de Conclusão de Curso: 10

7.1.19 TCC, 2017

Luiz Felipe Nunes de Oliveira. ESTUDO DAS SEÇÕES CÔNICAS: PROPRIEDADES REFLETORAS E SUAS APLICAÇÕES TECNOLÓGICAS. 2017.

7.1.20 TCC, 2017

Valmir Pereira Bezerra Júnior. ANÁLISE DE CONTROLE E ESTABILIDADE DO PÊNDULO INVERTIDO EM UM PLANO INCLINADO UTILIZANDO CONTROLADORES PID E FUZZY. 2017.

7.1.21 TCC, 2016

MAXWELL CAVALCANTE JÀCOME. Proposta de suspensão ativa com controlador fuzzy?. 2016.

7.1.22 TCC, 2016

Rafael Helano Soares de Paiva. DESENVOLVIMENTO DE UM CONTROLADOR PID E SUAS APLICAÇÔES.

7.1.23 TCC, 2013

JOSE BERNARDO DO NASCIMENTO. DISCALCULIA: PROBLEMÁTICA DO ENSINO FUNDAMENTAL NAS ESCOLAS DE AREIA BRANCA. 2013.

7.1.24 TCC, 2012

Yago Felipe da Costa. Controle de Nivel usando Lógica Fuzzy. 2012.

7.1.25 TCC, 2012

Francisco Aldo de Morais. CONTROLE FUZZY DE UM PROCESSO DE NEUTRALIZAÇÃO DE PH. 2012.

7.1.26 TCC, 2011

FRANCISCO DE ASSIS MONTEIRO DE SOUZA. Análise de Bombas e Controlador Fuzzy para sistemas Hidráulicos. 2011.

7.1.27 TCC, 2011

DIEGO GURGEL PIRES. Lógica Fuzzy e aplicação no MATLAB em sistemas de controle. 2011.

7.1.28 TCC, 2011

ERIC MURILO CORREIA DE MACEDO. MODELAGEM MATEMÁTICA E RECURSOS HÍDRICOS: UMA REVISÃO DE LITERATURA. 2011.

7.1.29 Orientação de Alunos Iniciação Científica:

A seguir a relação dos 26 alunos de iniciação científica.

1. João Victor De Oliveira Dantas. controle ADRC e sua relação com equação de segunda ordem. 2023. Iniciação Científica. (Graduando em Ciência e tecnologia) - Universidade Federal Rural do Semi-Árido, Conselho Nacional de Desenvolvimento Científico e Tecnológico.
2. NATHAN RODRIGUES DA SILVA. Controle por Rejeição Ativa de Distúrbios e suas aplicações. 2022. Iniciação Científica. (Graduando em Engenharia Elétrica) - Universidade Federal Rural do Semi-Árido, Conselho Nacional de Desenvolvimento Científico e Tecnológico.
3. Lucas Dantas Da Silva. Controle por Rejeição Ativa de Distúrbios e suas aplicações. 2021. Iniciação Científica. (Graduando em Engenharia Mecânica) - Universidade Federal Rural do Semi-Árido, Coordenação de Aperfeiçoamento de Pessoal de Nível Superior.
4. PAULO VICTOR FERNANDES VIEIRA. Estabilidade condicionamento em problemas de Engenharia com uso do Scilab. 2020. Iniciação Científica. (Graduando em Interdisciplinar em Ciência e Tecnologia UFERSA Mossoró) - Universidade Federal Rural do Semi-Árido, Conselho Nacional de Desenvolvimento Científico e Tecnológico.
5. MATHEUS MORAIS FERREIRA GOMES. ESTUDO DO COMPORTAMENTO MECÂNICO DE MATERIAIS COMPÓSITOS UTILIZANDO O MÉTODO DOS ELEMENTOS FINITOS. 2018. Iniciação Científica. (Graduando em Ciência e Tecnologia) - Universidade Federal Rural do Semi-Árido, Conselho Nacional de Desenvolvimento Científico e Tecnológico.
6. MAXWELL CAVALCANTE JÁCOME. OBTENÇÃO DE UM SOFTWARE PARA ALGORITMOS DE CONTROLE PID E FUZZY-PID DE UM CONTROLADOR

DE ALTITUDE DE VANT. 2016. Iniciação Científica. (Graduando em Ciência e Tecnologia) - Universidade Federal Rural do Semi-Árido, Conselho Nacional de Desenvolvimento Científico e Tecnológico. Orientador: Elmer Rolando Llanos Villarreal.

7. NATANAEL EXPEDITO DE CARVALHO MENDES. DESENVOLVER UM CONTROLADOR FUZZY PARA UMA VANT E SUAS EXTENSÕES. 2016. Iniciação Científica. (Graduando em Ciência e Tecnologia) - Universidade Federal Rural do Semi-Árido, Conselho Nacional de Desenvolvimento Científico e Tecnológico.
8. VALMIR PEREIRA BEZERRA JUNIOR. DESENVOLVER UM CONTROLADOR PI PARA UMA VANT E SUAS EXTENSÕES. 2016. Iniciação Científica. (Graduando em Ciência e Tecnologia) - Universidade Federal Rural do Semi-Árido, Conselho Nacional de Desenvolvimento Científico e Tecnológico.
9. THIAGO FERREIRA DE CARVALHO. DESENVOLVER UM CONTROLADOR PID PARA UMA VANT E SUAS EXTENSÕES. 2016. Iniciação Científica. (Graduando em Ciência e Tecnologia) - Universidade Federal Rural do Semi-Árido.
10. THIAGO DIAS DE CARVALHO QUARESMA GAMA. MATERIAL COMPÓSITO DE VEÍCULOS AÉREOS NÃO TRIPULADOS E SUAS TÉCNICAS. 2016. Iniciação Científica. (Graduando em Ciência e Tecnologia) - Universidade Federal Rural do Semi-Árido.
11. LUANA CARLA DE ANDRADE. DESENVOLVER UM CONTROLADOR DE ALTITUDE PARA UMA VANT USANDO CONTROLADOR PID-FUZZY. 2016. Iniciação Científica. (Graduando em Engenharia Mecânica) - Universidade Federal Rural do Semi-Árido.
12. PAULO ISRAEL OLIVEIRA BEZERRA. Simulação computacional da estrutura de uma asa de um VANT. 2016. Iniciação Científica. (Graduando em Ciência e Tecnologia) - Universidade Federal Rural do Semi-Árido, Coordenação de Aperfeiçoamento de Pessoal de Nível Superior. Orientador: Elmer Rolando Llanos Villarreal.
13. CIRO SIMÃO DE MEDEIROS. O método FDTD em Antenas e suas aplicações. 2016. Iniciação Científica. (Graduando em Ciência e Tecnologia) - Universidade Federal Rural do Semi-Árido, Conselho Nacional de Desenvolvimento Científico e Tecnológico.
14. CAUÊ COELHO ALVES. DESENVOLVER UM CONTROLADOR FUZZY PARA UMA VANT. 2015. Iniciação Científica. (Graduando em Bacharelado em Ciência

e Tecnologia) - Universidade Federal Rural do Semi-Árido, Conselho Nacional de Desenvolvimento Científico e Tecnológico.

15. Tiago Mateus Pereira Gonçalves. DESENVOLVER UM CONTROLADOR PID PARA UMA VANT. 2015. Iniciação Científica. (Graduando em Bacharelado em Ciência e Tecnologia) - Universidade Federal Rural do Semi-Árido, Conselho Nacional de Desenvolvimento Científico e Tecnológico.
16. Maxwell Cavalcante Jácome. DESENVOLVER UM CONTROLADOR PI PARA UMA VANT. 2015. Iniciação Científica. (Graduando em Bacharelado em Ciência e Tecnologia) - Universidade Federal Rural do Semi-Árido.
17. Flávio de Abreu Bezerra Filho. CONTROLADOR SERVO VISUAL BASEADO EM POSIÇÃO DE VANT. 2015. Iniciação Científica. (Graduando em Bacharelado em Ciência e Tecnologia) - Universidade Federal Rural do Semi-Árido, Conselho Nacional de Desenvolvimento Científico e Tecnológico.
18. Katia Nascimento de Souza. Analise, Controle e Aerodinâmica de um quadrotor. 2014. Iniciação Científica. (Graduando em Engenharia Mecânica) - Universidade Federal Rural do Semi-Árido, Conselho Nacional de Desenvolvimento Científico e Tecnológico.
19. Francisco Aldo de Morais. Controle Fuzzy de processo de neutralização de pH. 2013. Iniciação Científica. (Graduando em Ciência e Tecnologia) - Universidade Federal Rural do Semi-Árido, Conselho Nacional de Desenvolvimento Científico e Tecnológico.
20. Nataniel Wontoon Barbosa Lima. Controle Fuzzy e Estruturas Inteligentes. 2013. Iniciação Científica. (Graduando em Ciência e Tecnologia) - Universidade Federal Rural do Semi-Árido, Conselho Nacional de Desenvolvimento Científico e Tecnológico.
21. HIAN DE FREITAS MACEDO. Controlador Fuzzy e aplicações. 2013. Iniciação Científica. (Graduando em Bacharelado em Ciência e Tecnologia) - Universidade Federal Rural do Semi-Árido, Conselho Nacional de Desenvolvimento Científico e Tecnológico.
22. BRUNA MONALLIZE DUARTE MOURA. Controlador Fuzzy e aplicações. 2013. Iniciação Científica. (Graduando em Bacharelado em Ciência e Tecnologia) - Universidade Federal Rural do Semi-Árido. Orientador: Elmer Rolando Llanos Villarreal.

23. FERNANDA LIGIA DOS SANTOS DE OLIVEIRA. Controlador Fuzzy e aplicações. 2013. Iniciação Científica. (Graduando em Bacharelado em Ciência e Tecnologia) - Universidade Federal Rural do Semi-Árido.
24. FRANCISCA JOYCE DOS SANTOS BANDEIRA. Controlador Fuzzy e aplicações. 2013. Iniciação Científica. (Graduando em Bacharelado em Ciência e Tecnologia) - Universidade Federal Rural do Semi-Árido.
25. Samara Jessica Monte Bezerra. Sistemas de Controle e Aplicações. 2012. Iniciação Científica. (Graduando em Ciência e Tecnologia) - Universidade Federal Rural do Semi-Árido.
26. SAMARA JÉSSICA MONTE BEZERRA. CONTROLE POR REALIMENTAÇÃO DE SAÍDA E SUAS APLICAÇÕES. 2010. Iniciação Científica. (Graduando em Bacharelado em Ciência e Tecnologia) - Universidade Federal Rural do Semi-Árido.

8 ATIVIDADE DE EXTENSÃO UNIVERSITÁRIA

8.1 Relatoria Ad Hoc

8.1.1 International Journal of Systems Science

Revisor ad hoc da Revista: International Journal of Systems Science a partir de 2010.

8.1.2 IEEE Latin America Transactions

Revisor ad hoc da Revista: : IEEE Latin America Transactions a partir de 2016.

8.1.3 IEEE Access

Revisor ad hoc da Revista: IEEE Access a partir de 2021.

8.1.4 IET Renewable Power Generation

Revisor ad hoc da Revista: IET Renewable Power Generation a partir de 2021.

8.1.5 Mathematics MDPI

Revisor ad hoc da Revista: Mathematics MDPI a partir de 2020.

8.1.6 Applied Sciences MDPI

Revisor ad hoc da Revista: Applied Sciences MDPI a partir de 2019.

8.1.7 Energies

Revisor ad hoc da Revista: Energies MDPI a partir de 2019.

8.1.8 Electronics MDPI

Revisor ad hoc da Revista: Electronics MDPI a partir de 2021.

8.1.9 Symmetry-Basel

Revisor ad hoc da Revista: Symmetry-Basel a partir de 2021.

8.1.10 IEEE Transactions on Transportation Eletrification

Revisor ad hoc da Revista: IEEE Transactions on Transportation Eletrification a partir de 2021.

8.1.11 Sensors MDPI

Revisor ad hoc da Revista: Sensors MDPI a partir de 2021.

8.1.12 Sustainability MDPI

Revisor ad hoc da Revista: Sustainability a partir de 2020.

8.1.13 Atmosphere

Revisor ad hoc da Revista: Atmosphere a partir de 2022.

8.1.14 Journal of Marine Science and Engineering

Revisor ad hoc da Revista: Journal of Marine Science and Engineering a partir de 2022.

8.1.15 Aerospace

Revisor ad hoc da Revista: Aerospace a partir de 2021.

8.1.16 Machines MDPI

Revisor ad hoc da Revista: Machines a partir de 2020.

8.1.17 Axioms MDPI

Revisor ad hoc da Revista: Axioms a partir de 2021.

8.2 Atividades de extensão universitária na UFERSA

8.2.1 Divulgação de Ações de ensino associadas a Trabalhos desenvolvidos no PROFMAT – UFERSA

Integrantes: Elmer Rolando Llanos Villarreal - Integrante / Walter Martins Rodrigues - Coordenador / Antonio Ronaldo Gomes Garcia - Integrante. Desenvolvido em 2021-2021.

8.2.2 FÓRUM DE ASSISTÊNCIA ESTUDANTIL DA UNIVERSIDADE FEDERAL RURAL DO SEMI-ÁRIDO

Descrição: I FÓRUM DE ASSISTÊNCIA ESTUDANTIL DA UNIVERSIDADE FEDERAL RURAL DO SEMI-ÁRIDO como membro da comissão organizadora do Evento de Extensão I FÓRUM DE ASSISTÊNCIA ESTUDANTIL DA UNIVERSIDADE FEDERAL RURAL DO SEMI-ÁRIDO - UFERSA, com 4 hora(s) de atividades desenvolvidas em 28 de Agosto de 2017, no âmbito da Universidade Federal Rural do Semi-Árido. Desenvolvido em 2017-2017. Integrantes: Elmer Rolando Llanos Villarreal - Coordenador / Júlio César Rodrigues de Sousa - Integrante.

8.2.3 Semínários de Pesquisa em Matemática

Projeto certificado pelo(a) coordenador(a) Walter Martins em 25/09/2021.

Descrição: Semínários de Pesquisa em Matemática vice-coordenador do Projeto de Extensão SEMÍNÁRIOS DE PESQUISA EM MATEMÁTICA, com 36 hora(s) de atividades desenvolvidas no período de 3 de Agosto de 2017 a 15 de Dezembro de 2017, no âmbito da Universidade Federal Rural do Semi-Árido.Desenvolvido em 2017-2017. Integrantes: Elmer Rolando Llanos Villarreal - Integrante / Walter Martins Rodrigues - Coordenador / Antonio Ronaldo Gomes Garcia - Integrante.

8.2.4 Métodos Diagramáticos em Representação de Álgebras

Descrição: Trataremos de um estudo de Representações de Álgebras por métodos diagramáticos no estudo de anéis artinianos. Buscando a classificação por tipos de representações (mansa, finito ou selvagem), e particular o estudo de categorias de módulo com seqüências de Auslander-Reiter no estudo de representações de aljavas e/ou conjuntos parcialmente ordenados/algebra de incidência. Objetivando apresentar a passagem do tratamento desta problemática em categorias derivadas. O projeto também visa trabalhar os conceitos de análise algébrico na solução de sistemas lineares com aplicações na teoria de controles e física matemática. Desta forma a representação da álgebra e do conhecimento da categoria de módulos finitamente gerados associada a ela pode-se generalizar soluções de equações diferenciais ordinárias e de equações diferenciais parciais. Desenvolvidos em 2017-2018. Integrantes: Elmer Rolando Llanos Villarreal - Integrante / Walter Martins Rodrigues - Coordenador / Antonio Ronaldo Gomes Garcia - Integrante / Ivan Mezzomo - Integrante / Nir Cohen - Integrante.

8.2.5 I CONGRESSO DE INOVAÇÃO TECNOLÓGICA DO SEMI-ÁRIDO

Descrição: I CONGRESSO DE INOVAÇÃO TECNOLÓGICA DO SEMI-ÁRIDO 22/09/2016 – 24/09/2016. Integrantes: Elmer Rolando Llanos Villarreal - Coordenador / integrantes: Walter Martins Rodrigues / Antonio Ronaldo Gomes Garcia.

8.2.6 Simulação de Controladores multiagentes na indústria de petróleo em Mossoró

Descrição: Estudos de uma possivel implementacao de um processo de controle de temperatura e nível em um reservatório com o objetivo de analisar o desempenho do simulador e a possibilidade de aplicação de algoritmos de controle com usa da logica Fuzzyo. Para efetuar simulações associadas sera usada uma programação de algoritmos valendo-se do software MATLAB. Desenvolvido em 2009-2012. Integrantes: Elmer Rolando Llanos Villarreal - Coordenador / Integrantes: Walter Martins Rodrigues/ Antonio Ronaldo Gomes Garcia / Fábio Francisco da Costa Fontes.

9 ATIVIDADE DE ADMINISTRAÇÃO

9.1 Membro de Comissões e Atividades Administrativas

9.1.1 CPA,CONSAD. CPPD

Membro suplente CPA, Membro titular CONSAD E Membro suplente CPPD na UFERSA. Fui membro suplente ativo da CPA em 2011 e 2012. Em 2024 fui eleito membro titular do CONSAD com previsão de 2025. Em 2024 fui eleito membro suplente do CPPD onde fui convocado duas vezes.

9.1.2 Participação em Banca de Comissão Julgoradora de Concurso Público (2009-2019)

9.1.3 Processo Seletivo para Professor Substituto UFERSA, 2019

Walter Martins Rodrigues; MAIA, M. B.; NORIEGA, T. K.; Villarreal, Elmer Rolando Llanos. Processo Seletivo para Professor Substituto UFERSA. 2019. Departamento de Ciências Exatas Naturais, Matemática e Estatística DCME.

9.1.4 Processo Seletivo para Professor Substituto UFERSA, 2015

VILLARREAL, E. R. L.; MEDEIROS, S. K.; MARTINEZ, M. Z.. Processo Seletivo para Professor Substituto da UFERSA Edital 060/2014. 2015. Universidade Federal Rural do Semi-Árido.

9.1.5 Concurso publico professor efetivo edital 007/2014, 2014

MEZZOMO , I.; VILLARREAL, E. R. L.; LEITE, F. E. A.. concurso publico professor efetivo edital 007/2014. 2014. Universidade Federal Rural do Semi-Árido.

9.1.6 Concurso público para Professor Efetivo, 2012

SILVA, G. G.; SANTOS, E. C.; VILLARREAL, E. R. L.. Concurso público para Professor Efetivo. 2012. Universidade Federal Rural do Semi-Árido.

9.1.7 Concurso Público para professor efetivo, 2009

Francisco Aldo de Morais; Antonio Ronaldo Gomes Garcia; VILLARREAL, E. R. L.. Concurso Público para professor efetivo. 2009. Universidade Federal Rural do Semi-Árido.

9.1.8 Participação em Bancas de Concurso: Mestrado, Doutorado e Concurso Público

O Professor Elmer Rolando Llanos Villarreal participou durante a sua vida acadêmica de várias bancas internas externa na UFERSA nos níveis de mestrado, doutorado, exame de qualificação de doutorado e de concurso público. Entretanto, ênfase é atribuída somente aos últimos anos, ou seja, compreendendo o período de 2010-2024.

9.1.9 Participações em Banca de Mestrado e Doutorado (2010-2024)

Teses de doutorado-UFRN , UNB

1. SALAZAR, A. O.; SOUSA JUNIOR, V. A.; SILVEIRA, L. F. Q.; VILLARREAL, E.R.L.; FERNANDES, J. D.; SEMENTE, R. S.. Participação em banca de FELIPE OLIVEIRA SIMÕES GAMA. DESENVOLVIMENTO DE SISTEMAS DE COMUNICAÇÕES CODIFICADOS POR WAVELETS E BASEADOS NO PADRÃO IEEE 802.15.4 PARA SISTEMAS DE CONTROLE POR REDES DE SENSORES SEM FIO INDUSTRIAL. 2021. Tese (Doutorado em PROGRAMA DE PÓS-GRADUAÇÃO EM ENGENHARIA ELÉTRICA E DE COMPUTAÇÃO) - Universidade Federal do Rio Grande do Norte.
2. VARGAS, J. A. R.; TOGNETTI, E. S.; VILLARREAL, E. R. LL.; TORRICO, B. C.. Participação em banca de Kevin Herman Muraro Gularte. CONTROL OF CHAOTIC AND HYPERCHAOTIC SYSTEMS USING LYAPUNOV STABILITY THEORY. 2021. Tese (Doutorado em ENGENHARIA DE SISTEMAS ELETRÔNICOS E DE AUTOMAÇÃO) - Universidade de Brasília.
3. SALAZAR, A. O.; MAITELLI, A. L.; E R L Villarreal; FERNANDES, J. D.; GABRIEL FILHO, O.. Participação em banca de Gustavo Fernandes de Lima. Proposta de controle de velocidade de Ferramenta de Inspeção de Dutos utilizando

válvula de Desvio e Microletronica. 2019. Tese (Doutorado em Ciência e Engenharia de Petróleo) - Universidade Federal do Rio Grande do Norte.

4. SALAZAR, A. O.; MAITELLI, A. L.; Elmer R. Llanos Villareal; VILLANUEVA, J. M. M.; SEMENTE, R. S.. Participação em banca de XIANKLEBER CAVALCANTE BENJAMIM. Utilização de Técnica Preditiva em uma malha de controle em Sensores sem Fio. 2018. Tese (Doutorado em PROGRAMA DE PÓS-GRADUAÇÃO EM ENGENHARIA ELÉTRICA E DE COMPUTAÇÃO) - Universidade Federal do Rio Grande do Norte.

Qualificações de Doutorado UFRN-UNB

1. J. A. R. Vargas; TOGNETTI, E. S.; BESTARD, G. A.; VILLARREAL, E. R. L.. Participação em banca de JUAN CARLOS GONZÁLEZ GÓMEZ. SINCRONIZAÇÃO DE UMA CLASSE GENÉRICA DE SISTEMAS CAÓTICOS SUBATUADOS COM APLICAÇÕES PARA SEGURANÇA DA INFORMAÇÃO. 2021. Exame de qualificação (Doutorando em ENGENHARIA DE SISTEMAS ELETRÔNICOS E DE AUTOMAÇÃO) - Universidade de Brasília.
2. VARGAS, J. A. R.; TOGNETTI, E. S.; BESTARD, G. A.; Villarreal, Elmer Rolando Llanos. Participação em banca de Kevin Herman Muraro Gularte. CONTROL OF CHAOTIC AND HYPERCHAOTIC SYSTEMS USING LYAPUNOV STABILITY THEORY. 2020. Exame de qualificação (Doutorando em ENGENHARIA DE SISTEMAS ELETRÔNICOS E DE AUTOMAÇÃO) - Universidade de Brasília.
3. VARGAS, J. A. R.; BESTARD, G. A.; ISHIHARA, J. Y.; E R L Villarreal. Participação em banca de WILLIAN ARVEY MOLANO GABALÁN. ESQUEMAS BASEADOS EM CAOS E NA TEORIA DE ESTABILIDADE DE LYAPUNOV PARA A TELECOMUNICAÇÃO SEGURA. 2019. Exame de qualificação (Doutorando em Pós-graduação em Sistemas Mecatrônicos) - Universidade de Brasília.
4. SALAZAR, A. O.; MAITELLI, A. L.; PAIVA, J. A.; Elmer R. L. Villarreal. Participação em banca de Werbet Luiz Almeida da Silva. Implementação da técnica ADRC (Active Disturbance Rejection Control) no Controle de Posição Radial de Uma Máquina de Indução Sem Mancal Com Bobinado Dividido.. 2019. Exame de qualificação (Doutorando em Programa de Engenharia Eletrica e de Computação) - Departamento de Engenharia de ComputaÃ§Ã£o e AutomaÃ§Ã£o.

5. SALAZAR, A. O.; SILVEIRA, L. F. Q.; SOUSA JUNIOR, V. A.; Elmer R. L. Villareal; FERNANDES, J. D.. Participação em banca de FELIPE OLIVEIRA SIMÕES GAMA. Desenvolvimento de Sistemas de Comunicações Codificados por Wavelets e Baseados no Padrão IEEE 802.15.4 para Sistemas de Controle por Redes de Sensores Sem Fio Industrial. 2018. Exame de qualificação (Doutorando em Engenharia Elétrica) - Universidade Federal do Rio Grande do Norte.

MESTRADO

1. ARAUJO, F. R. C. D.; FREIRE, E. N.; Walter Martins Rodrigues; Villarreal, Elmer Rolando Llanos. Participação em banca de Rogério da Silva Costa. RECOMPOSIÇÃO DA APRENDIZAGEM MATEMÁTICA: UMA ABORDAGEM ATRAVÉS DAS OPERAÇÕES BÁSICAS NA ESCOLA DOMINGOS COSTA TEOBALDO EM ARACATI CEARÁ PÓS PANDEMIA COVID-19.. 2023. Dissertação (Mestrado em PROFMAT Polo Mossoró) - Universidade Federal Rural do Semi-Árido.
2. VILLARREAL, E. R. L.; RODRIGUES, W. M.; COSTA, C. M.. Participação em banca de MAYKEL SAMUEL MARINHO CÂMARA. UMA PROPOSTA DE ABORDAGEM DA TRIGONOMETRIA APRESENTANDO A FUNÇÃO DE EULER NO ESPAÇO COM O SOFTWARE GEOGEBRA. 2018. Dissertação (Mestrado em PROFMAT Polo Mossoró) - Universidade Federal Rural do Semi-Árido.
3. NUNES, A. G.; RODRIGUES, W. M.; VILLARREAL, E. R. L.. Participação em banca de HILDEBERTO FERNANDO DE FREITAS REGIS. O USO DE QUEBRA-CABEÇAS PARA ESTIMULAR O APRENDIZADO DE POLIGONOS NA DISCIPLINA DE MATEMÁTICA NO ENSINO FUNDAMENTAL. 2017. Dissertação (Mestrado em PROFMAT Polo Mossoró) - Universidade Federal Rural do Semi-Árido.
4. VILLARREAL, E. R. L.; FERNANDES NETO, A. P.; LAURA, T. L.; SOUSA NETO, M. P.. Participação em banca de EDPO RODRIGUES DE MORAIS. DESENVOLVIMENTO DE UM CONTROLADOR HÍBRIDO FUZZYPID PARA ESTABILIZAÇÃO DE UM VANT DO TIPO QUADRIRROTOR NA REALIZAÇÃO DE UM VOO AUTÔNOMO VERTICAL. 2017. Dissertação (Mestrado em Engenharia Elétrica) - Universidade Federal Rural do Semi-Árido.
5. GARCIA, A. R. G.; VILLARREAL, E. R. L.; RODRIGUES, W. M.; DANTAS, A. S.. Participação em banca de HUGO ARNAUD MENDES. A INTERDISCIPLINA-

RIDADE NO AUXÍLIO DO CONHECIMENTO DOS TERMOS MATEMÁTICOS NO SEXTO DO ENSINO FUNDAMENTAL. 2016. Dissertação (Mestrado em PROFMAT Polo Mossoró) - Universidade Federal Rural do Semi-Árido.

6. GARCIA, A. R. G.; CAMACHO, R. G. V.; VILLARREAL, E. R. L.. Participação em banca de FRUTUOSO GOMES TOMAZ. TEORIA DOS CONJUNTOS E TAXONOMIA BIOLÓGICA: Um estudo Interdisciplinar. 2016. Dissertação (Mestrado em PROFMAT Polo Mossoró) - Universidade Federal Rural do Semi-Árido.
7. MARTINEZ, M. Z.; DANTAS, A. S.; VILLARREAL, E. R. L.. Participação em banca de RAFAEL DO NASCIMENTO TOMÉ RIBEIRO. PROBABILIDADES E ESTATÍSTICA APLICADAS AO ESPORTE. 2016. Dissertação (Mestrado em PROFMAT Polo Mossoró) - Universidade Federal Rural do Semi-Árido.
8. VILLARREAL, E. R. L.; RODRIGUES, W. M.; BRANDAO, M. C. M.. Participação em banca de FRANCISCO RAFAEL DE FREITAS CAVALCANTE. ENSINO DE GEOMETRIA ESPACIAL: UMA PROPOSTA DE ATIVIDADES COM O USO DO GEOGEBRA. 2016. Dissertação (Mestrado em PROFMAT Polo Mossoró) - Universidade Federal Rural do Semi-Árido.
9. MARTINEZ, M. Z.; DANTAS, D. J.; VILLARREAL, E. R. L.. Participação em banca de COSME WEDSON BEZERRA FERNANDES. O ENSINO DE ANÁLISE COMBINATÓRIA ATRAVÉS DA RESOLUÇÃO DE PROBLEMAS. 2016. Dissertação (Mestrado em PROFMAT Polo Mossoró) - Universidade Federal Rural do Semi-Árido.
10. VILLARREAL, E. R. L.; SILVA, A. S. A.; Walter Martins Rodrigues; SOUSA NETO, M. P.. Participação em banca de Sameque Farias Cunha de Oliveira. Estabilização da atitude de um quadrimotor utilizando o controle Fuzzy-PID. 2015. Dissertação (Mestrado em Engenharia Elétrica) - Universidade Federal Rural do Semi-Árido.
11. SILVA, J. P.; MOURA, A. A. F.; SOUSA NETO, M. P.; VILLARREAL, E. R. L.. Participação em banca de FRANCISCO DAS CHAGAS BARBOSA DE SENA. CONTROLE FUZZY APLICADO A OTIMIZAÇÃO DE UM SISTEMA EÓLICO DE VELOCIDADE VARIÁVEL. 2015. Dissertação (Mestrado em Engenharia Elétrica) - Universidade Federal Rural do Semi-Árido.
12. VILLARREAL, E. R. L.; SILVA, J. P.; DIAS, S. M.; SILVA, A. S. A.. Participação em banca de Clayton Antonio de Miranda Oliveira. Projeto de Observadores de

Estado utilizando Algoritmos Genéticos. 2014. Dissertação (Mestrado em Engenharia Elétrica) - Universidade Federal Rural do Semi-Árido.

13. VILLARREAL, E. R. L.; SILVA, A. S. A.; VARGAS, J. A. R.; BRANDAO, A. S.; DIAS, S. M.. Participação em banca de DANILO DE SANTANA PENA. AVALIAÇÃO DE ESTRATEGIAS DE CONTROLE ADAPTATIVO DO GERADOR SÌNCRONO DE ÍMA PERMANENTE APLICADO EM SISTEMA DE ENERGIA EÓLICA. 2014. Dissertação (Mestrado em Engenharia Elétrica) - Universidade Federal Rural do Semi-Árido.
14. VILLARREAL, E. R. L.; QUEIROZ JUNIOR, I. S.; SILVA, A. S. A.; BRANDAO, A. S.; VARGAS, J. A. R.. Participação em banca de Carlos Alberto Teixeira Junior. ANÁLISE COMPARATIVA ENTRE OS CONTROLADORES FUZZY PD+I E PID CONVENCIONAL. 2014. Dissertação (Mestrado em Engenharia Elétrica) - Universidade Federal Rural do Semi-Árido.
15. VILLARREAL, E. R. L.; FERNANDES NETO, A. P.; SILVA, A. S. A.; BRANDAO, A. S.; VARGAS, J. A. R.. Participação em banca de AUGUSTO CESAR DE SOUSA. Proposta de um quadrotor PID-Neural para estabilização em voo pairado de um quadrotor. 2014. Dissertação (Mestrado em Engenharia Elétrica) - Universidade Federal Rural do Semi-Árido.
16. SILVA, J. P.; FONSECA, I. E.; SANTOS, M. D.; VILLARREAL, E. R. L.. Participação em banca de TARCISIO DA SILVA BARRETO. ANÁLISE DE TAXA DE BLOQUEIO EM CONEXÕES POR ALGORITMOS DE CAMINHOS MÍNIMOS: ALGORITMO GENÉTICO E ALGORITMO DE YEN. 2014. Dissertação (Mestrado em Engenharia Elétrica) - Universidade Federal Rural do Semi-Árido.
17. VILLARREAL, E. R. L.; FERNANDES NETO, A. P.; Walter Martins Rodrigues; SOUSA NETO, M. P.. Participação em banca de Sâmya Lorena de Medeiros Confessor. ANÁLISE COMPARATIVA ENTRE CONTROLADORES MPPT APLICADOS A UM SISTEMA SOLAR FOTOVOLTAICO. 2014. Dissertação (Mestrado em Engenharia Elétrica) - Universidade Federal Rural do Semi-Árido.
18. VILLARREAL, E. R. L.; GARCIA, .. A. R. G.; RODRIGUES, W. M.; CUNHA, C. A. R.. Participação em banca de A HISTÓRIA DA MATEMÁTICA COMO ELEMENTO MOTIVADOR NO ENSINO. A HISTÓRIA DA MATEMÁTICA COMO ELEMENTO MOTIVADOR NO ENSINO DE MATEMÁTICA. 2013. Dissertação (Mestrado em Matemática) - Universidade Federal Rural do Semi-Árido.

10 PALAVRAS FINAIS

Palavras de agradecimento aos membros da comunidade professores, servidores por todo o apoio brindado ao longo destes anos e na esperança de continuar o trabalho com mais anos no serviço público.

Mossoró, RN, Outubro de 2024.

Professor Dr. Elmer Rolando Llanos Villarreal

ESTADO DO RIO GRANDE DO NORTE

SECRETARIA DE ESTADO DA SEGURANÇA PÚBLICA E DA DEFESA SOCIAL

INSTITUTO TÉCNICO-CIENTÍFICO DE PERÍCIA

INSTITUTO DE IDENTIFICAÇÃO - II

NOME

ELMER ROLANDO LLANOS VILLARREAL

FILIAÇÃO

MANUEL ELMER LLANOS FLORES

MERY JULY VILLARREAL VASQUEZ

DATA NASCIMENTO: 26/03/1967

NATURALIDADE: HUANUCO

FOTO Nº: *

ÓRGÃO EXPEDIDOR: ITEP/RN

OBSERVAÇÃO: 2ª VIA

ASSINATURA DO TITULAR

LEI Nº 7.116, DE 29 DE AGOSTO DE 1983

CPF 213.060.638-50 DNI *

REGISTRO GERAL 3.571.118 DATA DE EXPEDIÇÃO 16/03/2023

REGISTRO CIVIL: CERT. CAS. Nº0000695 - LIV.00003 - FLS.189 - CARTORIO 2º MOSSORO RN

T. ELEITOR CTPS SÉRIE UF

* * * *

NIS/PIS/PASEP IDENTIDADE PROFISSIONAL

* *

CERT. MILITAR

*

CNH CNS

* *

POLEGAR DIREITO

Marcela Aurila Ferreira Caldas

ASSINATURA DO DIRETOR

VALIDA EM TODO O TERRITORIO NACIONAL

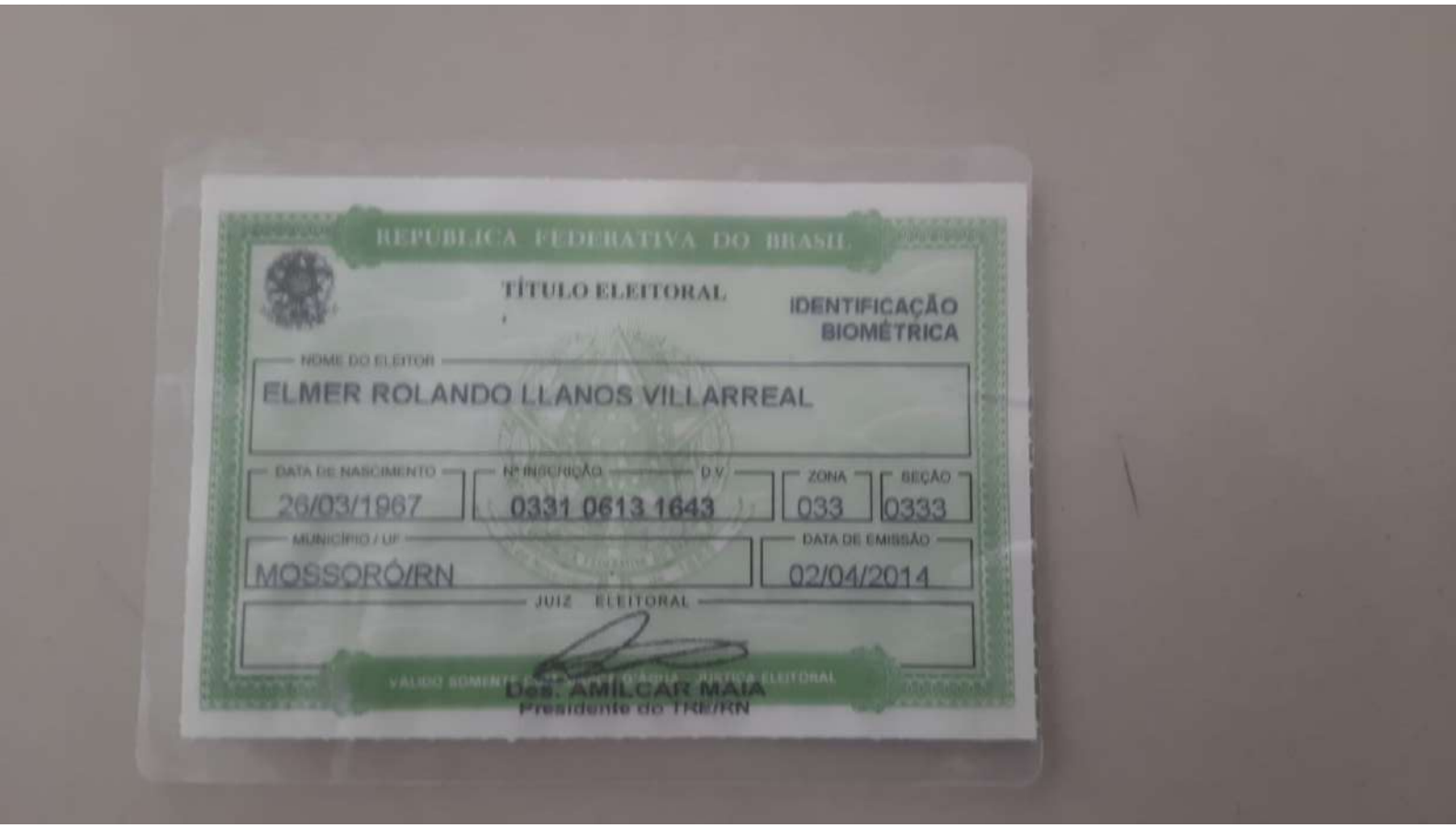

REPUBLICA FEDERATIVA DO BRASIL

TÍTULO ELEITORAL

IDENTIFICAÇÃO BIOMÉTRICA

NOME DO ELEITOR

ELMER ROLANDO LLANOS VILLARREAL

DATA DE NASCIMENTO	Nº INSCRIÇÃO	D.V.	ZONA	SEÇÃO
26/03/1967	0331 0613 1643		033	0333

MUNICÍPIO / UF	DATA DE EMISSÃO
MOSSORÓ/RN	02/04/2014

JUIZ ELEITORAL

VÁLIDO SOMENTE COM A ASSINATURA DO JUIZ ELEITORAL

Des. AMILCAR MAIA
Presidente do TRE/RN

REPÚBLICA FEDERATIVA DO BRASIL
MINISTÉRIO DAS CIDADES
DEPARTAMENTO NACIONAL DE TRÂNSITO
CARTEIRA NACIONAL DE HABILITAÇÃO
RN
NOME
ELMER ROLANDO LLANOS VILLARREAL
DOC. IDENTIDADE / ÓRG. EMISSOR / UF
3571118 SSP RN
CPF
213.060.638-50
DATA NASCIMENTO
26/03/1967
FILIAÇÃO
MANUEL ELMER LLANOS FLORES
MERYJULY VILLARREAL PASQUEL
PERMISSÃO
ACC
CAT. HAB.
B
Nº REGISTRO
05152974533
VALIDADE
20/08/2023
1ª HABILITAÇÃO
25/02/2011
VÁLIDA EM TODO O TERRITÓRIO NACIONAL
16793215555

REPUBLICA DEL PERU

A NOMBRE DE LA NACION

EL RECTOR DE LA UNIVERSIDAD NACIONAL DE INGENIERIA

POR CUANTO:
EL CONSEJO UNIVERSITARIO, VISTO QUE HAN SIDO CUMPLIDOS LOS REQUISITOS ESTABLECIDOS EN LA FACULTAD DE CIENCIAS,

HA OTORGADO CON FECHA 26 DE ENERO DE 1994
EL GRADO ACADEMICO DE BACHILLER EN CIENCIAS CON MENCION EN:
MATEMATICAS

A DON

ELMER ROLANDO LLANOS VILLARREAL

POR TANTO:
EXPIDE EL PRESENTE DIPLOMA PARA QUE SE LE RECONOZCA COMO TAL
DADO EN LIMA A 01 DE FEBRERO DE 1994

Secretario General | Decano de la Facultad | Rector de la Universidad

REGISTRADO A FOJAS 209 DEL TOMO 05 RESPECTIVO

CORREGEDORIA GERAL DA JUSTIÇA - RJ
SELO DE FISCALIZAÇÃO
AUTENTICAÇÃO
ELU
1 ATO
EHN94259

CARTÓRIO DO OFÍCIO ÚNICO
TEL.: 3356-2811
PINHEIRAL - RJ

CART. DO OFÍCIO ÚNICO - PINHEIRAL RJ
Coronel Joaquim F. Ribeiro, 1004 - Loja 1, Centro, Tel 356.28.11
AUTENTICAÇÃO
Certifico e dou fé que a presente cópia é a reprodução fiel do original que me foi apresentado (Tabs. 7-4,1-5,1-9)
Pinheiral-RJ, 28/08/07 R$ 4,44
Raphael de Almeida Fagundes Silva - Substituto

Nº 16912-B

REPUBLICA DEL PERU
MINISTERIO DE EDUCACION
SECRETARIA GENERAL
OFICINA DE TRAMITE DOCUMENTARIO
En la fecha se legaliza la firma que antecede sin juzgar el contenido del Documento.
Nº 05080
Lima, 07 MAR. 2000
BERTHA SARDINAS ALVAREZ
LEGALIZACIONES

SECRETARIA GENERAL
TRAMITE DOCUMENTARIO
Revisado Conforme
25 FEB. 2000
Nº 410R

Lima, 29 de Febrero del 2000
El Secretario General de la Universidad Nacional de Ingeniería, CERTIFICA; la autenticidad de las firmas precedentes las mismas que pertenecen, al Sr. Victor Javier Adelo Nadal Asesor Alcalde Secretario General Dr. Rafael Muñoz Cota de esta Casa de Estudios.

Dr. RAFAEL MUÑOZ COTO
Secretario General

SELO DE RELACIONES EXTERIORES DEL PERU
DIRECCION GENERAL DE ASUNTOS CONSULARES
LEGALIZACIONES
No. 1023379
Se legaliza la firma que antecede de:
Bertha Cardenas A.
Nota: SE LEGALIZA LA FIRMA SIN JUZGAR EL CONTENIDO DEL DOCUMENTO.
Lima, 09 MAR. 2000
FUNCIONARIO AUTORIZADO
DIRECCION DE TRAMITES CONSULARES
LEGALIZACIONES

EMBAIXADA DO BRASIL EM LIMA, PERU
Serviço Consular
Recomheço verdadeira por semelhança, assinatura do Sr. Antonio Barrionuevo Arenas, Funcionário do Ministério das Relações Exteriores do Perú
E, para constar onde convier, mandei passar o presente, que assinei e fiz selar com o selo desta Embaixada, Dispensada a legalização da assinatura consular de acordo com o artigo 3º, do Decreto 34451, de 31/01/50.
Lima, 10 de março de 2000
MARA FERREIRA CHIES
Vice-Cônsul
SELO CONSULAR
REAIS-CUZCO

APOSTILA
Revalidado o diploma nos termos do processo nº. 23080.018364/2000-15 de acordo com a resolução nº. 03 de 10/06/85 do CFE e Parecer nº 30/CEG/2000 da Câmara de Ensino e Graduação da UFSC 2000
Universidade Federal de Santa Catarina, em Florianópolis, 21 de 12 de 2000

Universidade Federal de Santa Catarina
Pró-Reitoria de Ensino de Graduação
Departamento de Administração Escolar-DAE
Divisão de Programação, Registro e Controle Acadêmico DPRCA
Serv. de Exped. e de Reg. de Diplomas-SERD
DIPLOMA Registrado sob nº. 432
livro L-39 folhas 111 em 21/12/2000
Processo nº. 23080.018364/2000-15
nos termos do artigo 48 da Lei nº. 9.394, de 20 de dezembro de 1996.
Florianópolis, 21/12/2000
Elizabete F. do Espírito Santo
Chefe do SERD
Luiz Carlos Podestá
Diretor da DPRCA-DAE
VISTO Nair C. da Cunha
Nair Cardoso da Cunha
Diretora do Depto. Adm. Escolar-DAE
Delegação do Reitor Port. nº. 1328/GR/96

Cartório do Ofício Único
Pinheiral - R.J.
AUTENTICAÇÃO NO VERSO

República Federativa do Brasil
Universidade de São Paulo

O Reitor da Universidade de São Paulo confere a

ELMER ROLANDO LLANOS VILLARREAL

peruano, natural do Peru

nascido a 26 de março de 1967, R.N.E.: V156570-E - SP,

o presente diploma de ***Mestre em Engenharia Elétrica***

Área de concentração: ***Engenharia de Sistemas***

tendo em vista que, em 10.03.1997, satisfez todas as exigências pertinentes a este grau, estabelecidas no Regulamento dos Cursos de Pós-Graduação da

Escola Politécnica

para que possa gozar de todos os direitos e prerrogativas concedidas pela legislação vigente.

Reitoria da Universidade de São Paulo, aos 06 de abril de 1999.

Prof. Dr. Jacques Marcovitch Reitor	Prof. Dr. Héctor Francisco Terenzi Pró-Reitor	Profa. Dra. Lor Cury Secretária Geral

Curso Reconhecido
de acordo com o disposto
na Portaria MEC n.º 132
de 02.02.99, DOU de
03.02.99.

UNIVERSIDADE DE SÃO PAULO
Secretaria Geral
Divisão de Registros Acadêmicos

Diploma registrado sob n.º 030554

Processo n.º 98.5.648.3.1,

nos termos do Artigo 48 da Lei 9394/96.

São Paulo, 24 de maio de 1999

LUIS CARLOS PASTUR
Técnico Acadêmico

De acordo..

Profa. Dra. LOR CURY
Secretária Geral

REPÚBLICA FEDERATIVA DO BRASIL
MINISTÉRIO DA EDUCAÇÃO E DO DESPORTO

A **UNIVERSIDADE FEDERAL DE SANTA CATARINA**

confere o presente

DIPLOMA

a

Elmer Rolando Llanos Villarreal

de nacionalidade ***peruana***, cédula de identidade registro geral nº ***06443693-G/Peru***, nascido a ***26 de março de 1967***, natural ***de Huanuco/Peru***, pela conclusão do ***Curso de Pós-Graduação e Defesa Pública de Tese de Doutorado***, realizada em ***15 de março de 2002***, outorgando-lhe o grau de

DOUTOR em **ENGENHARIA ELÉTRICA**,

na Área de Concentração **Sistemas de Informação** para que possa gozar de todos os direitos, prerrogativas e honras inerentes ao Título.

Florianópolis, 11 de junho de 2002.

Prof. Edson Roberto De Pieri,Dr.
Coordenador

Elmer Rolando Llanos Villarreal
Titulado

Prof. Rodolfo Joaquim Pinto da Luz
Reitor

Curso reconhecido pelo Portaria/Federal nº. 132 - de 2/2/99, publicada no Diário Oficial da União de 3/2/99

Universidade Federal de Santa Catarina
Pró-Reitoria de Ensino de Graduação
Depto. de Administração Escolar - DAE
Divisão de Programação, Registro e Controle Acadêmico/DPRCA

Serv. de Exped. e de Reg. de Diplomas - SERD
DIPLOMA Registrado sob nº. 7.82
livro PG-7 folhas 196 V. em 23/09/02
Processo nº. 23080.013169/2002-52
nos termos do artigo 48 da Lei nº. 9.394, de 20 de dezembro de 1996.
Florianópolis, 23/09/02

Elizabete Fermiano do E. Santo
Chefe do SERD

Luiz Carlos Podestá
Diretor da DPRCA - DAE

VISTO

Nair Cardoso da Cunha
Diretora do Depto. Adm. Escolar - DAE
Delegação do Reitor Port. nº. 1328/99/96

UFRN
Portal do Coordenador Stricto

UNIVERSIDADE FEDERAL DO RIO GRANDE DO NORTE
SISTEMA INTEGRADO DE GESTÃO DE ATIVIDADES ACADÊMICAS

EMITIDO EM 02/05/2019 11:21

sinfo

DECLARAÇÃO

Declaramos que o Prof. Dr. ELMER ROLANDO LLANOS VILLAREAL, CPF 213.060.638-50, participou como Examinador Externo à Instituição da Comissão Examinadora de Defesa de Tese de Doutorado do(a) pós-graduando(a) GUSTAVO FERNANDES DE LIMA, intitulada:

PROPOSTA DE CONTROLE DE VELOCIDADE DE FERRAMENTA DE INSPEÇÃO DE DUTOS UTILIZANDO VÁLVULA DE DESVIO E MICROELETRÔNICA

no PROGRAMA DE PÓS-GRADUAÇÃO EM CIÊNCIA E ENGENHARIA DE PETRÓLEO do CENTRO DE CIÊNCIAS EXATAS E DA TERRA da UNIVERSIDADE FEDERAL DO RIO GRANDE DO NORTE , em sessão pública realizada no dia 14 de Junho de 2019 às 09:00.

Membros da Banca

ANDRES ORTIZ SALAZAR (UFRN - Presidente) - ORIENTADOR
ANDRÉ LAURINDO MAITELLI (UFRN - Examinador Interno)
ELMER ROLANDO LLANOS VILLAREAL (UFERSA - Examinador Externo à Instituição)
JEFFERSON DOOLAN FERNANDES (IFRN - Examinador Externo à Instituição)
OSCAR GABRIEL FILHO (PETROBRAS - Examinador Externo à Instituição)

Prof(a). Dr. CARLOS ALBERTO MARTINEZ HUITLE
Coordenador(a) do PROGRAMA DE PÓS-GRADUAÇÃO EM CIÊNCIA E ENGENHARIA DE PETRÓLEO- UFRN

Número do Documento: 1468763
Código de Verificação: 55cd1d9803

ATENÇÃO

Para verificar a autenticidade deste documento acesse **https://sigaa.ufrn.br/sigaa/documentos/** e utilize o link *Ensino >> Declaração de Participação como Membro de Banca de Pós-Graduação Stricto Sensu*, informando o número do documento, a data de emissão e o código de verificação.

SIGAA | Superintendência de Informática - (84) 3215-3148 | Copyright © 2006-2019 - UFRN - sigaa08-producao.info.ufrn.br.sigaa08-producao

Universidade Federal do Rio Grande do Norte
Centro de Ciências Exatas e da Terra
Departamento de Informática e Matemática Aplicada

PARECER

O projeto "Abordagem Empírica Cognitiva para a Construção de um Protótipo de Simulação para Ambientes Automatizados" coordenado pelo professor **Elmer Rolando Llanos Villarreal**, foi submetido à Universidade Estadual do Rio Grande do Norte, UERN, com o intuito de atender um dos requisitos para concessão de bolsa de Desenvolvimento Científico Regional do CNPq. Através de contato com o professor Francisco Chagas de Lima Jr. dessa instituição, se me pediu para dar um parecer de mérito do referido projeto o qual faço a seguir:

O projeto tem por objetivo descrever uma modelagem e simulação híbrida para ambientes automatizados, utilizando-se dos princípios e ferramentas de sistemas multi-agentes cognitivos. Para isto deverá ser construído um protótipo de simulação baseada em sistemas multi-agentes, voltado à modelagem empírica em ambientes automatizados.

Sistemas multi-agentes é uma área muito usada hoje em dia na construção de sistemas inteligentes para situações complexas e que pelo mesmo tem tido muitas aplicações nas mais diversas áreas de conhecimento. O processo de simulação proposto reduziria os custos de analises de viabilidade de um projeto de software complexo. Por tanto acredito que este projeto venha ser de importante para a consolidação do novo programa de mestrado da UERN assim como o desenvolvimento da industria de software da região. Assim, sou de parecer favorável enquanto ao mérito do projeto.

Natal, 30 de julho de 2007

Prof. Benjamin René Callejas Bedregal
Depto. de Informática e Matemática Aplicada - DIMAp
Universidade Federal do Rio Grande do Norte - UFRN
Matrícula SIAPE: 2313115

UNIVERSIDAD NACIONAL AGRARIA LA MOLINA
FACULTAD DE CIENCIAS

UNIVERSIDAD NACIONAL AGRARIA
DPTO. DE MATEMATICA
04 ABR. 1994
Hora de Ingreso N°

La Molina, 1994 abril 18
TR.No. 1796/94-FC-UNALM

Señor
[illegible]
Presente.-

Con fecha 14 del presente se ha expedido la siguiente Resolución.

RESOLUCION FC-1796/94.- La Molina, 1994 abril 14.

CONSIDERANDO:

- Las comunicación DM-0600-069/94 en la cual solicita la contratación del Bach. Elmer Rolando Llanos Villarreal, como Jefe de Prácticas a D.E., a partir del 8 de abril de 1994 y hasta la culminación del Semestre I-94, de acuerdo al Art. 298° del Reglamento General de la UNALM;

- El Informe favorable CED-403/94 de la Comisión de Evaluación de Docentes de la Facultad de Ciencias, concorde con el Art 287° del Reglamento General de la UNALM.

Estando a lo acordado en la sesión ordinaria del Consejo de Facultad de fecha 14 de abril de 1994.

SE RESUELVE:

1. Proponer la contratación del Bach. ELMER ROLANDO LLANOS VILLARREAL, como Jefe de Prácticas a D.E., a partir del 8 de abril de 1994 y hasta la culminación del Semestre I-94 en el Departamento de Matemática en la plaza de la Ing. Ana Arana.

2. Elévese al Consejo Universitario para su ratificación.

Regístrese y Comuníquese.- Fdo. M.Sc. César Guerrero Flores.- Decano.- Decano.- Sello del Decanato.- Fdo. Ing. Sandro Alencastre Calderón.- Secretario.- Sello de la Secretaría.

Lo que cumplo con poner en su conocimiento.

Atentamente,

Ing. Sandro Alencastre Calderón
SECRETARIO

UNIVERSIDAD NACIONAL AGRARIA
FACULTAD DE CIENCIAS
SECRETARIA
LA MOLINA

c.c. Secretaría General
Oficina de Personal
Dpto. de Matemática

unilesteMG
CENTRO UNIVERSITÁRIO DO LESTE DE MINAS GERAIS

DECLARAÇÃO

Declaramos para os devidos fins, que Elmer Rolando Llanos Villarreal, portador do RNE-V156570E-SP, ministrou no 2º semestre de 2002, as disciplinas Álgebra Linear II e Controle Não Linear no Curso de Engenharia Elétrica do Centro Universitário do Leste de Minas Gerais – Unileste-MG.

Por ser verdade, firmo a presente declaração.

Coronel Fabriciano, 12 de dezembro de 2002.

Ramon da Cunha Lopes
Coordenador do Curso de Engenharia Elétrica

UNIVERSIDADE FEDERAL RURAL DO SEMI-ÁRIDO
CONFERE COM O ORIGINAL
Mossoró(RN) 23/10/08
Membro - CPPS

CENTRO UNIVERSITÁRIO DO LESTE DE MINAS GERAIS
✆ GERAL 31 3846-7900
FAX 31 3842-6482
Av. Presidente Tancredo Neves, 3500 - Bairro Universitário
CEP 35.170-056 - Coronel Fabriciano - Minas Gerais
INTERNET: www.unilestemg.br
E-MAIL: unilestemg@unilestemg.br

UCL
ENSINO SUPERIOR

FACULDADE DO CENTRO LESTE – UCL – UCL

Serra - ES, 19 de novembro de 2005.

Declaração

A UCL - ENSINO SUPERIOR, inscrita no CNPJ sob o número 02.598.162/0001-07, declara para os devidos fins que **Elmer Rolando Llanos Villarreal,** inscrito no CPF sob o número 021.360.338-60, foi professor desta instituição de Ensino Superior no período de 02/02/2005 a 06/11/2005, ministrando na graduação as disciplinas de **Controle Automático I** e **Controle Automático III** no **Primeiro Semestre de 2005** e as disciplinas de **Controle Automático I** e **Controle Automático II** no **Segundo Semestre de 2005**.

Ministrou também no Curso de pós-graduação "*Especialização em Engenharia Mecatrônica – Controle de Processos*" a disciplina de **Modelagem e Simulação** no período de **17 de setembro a 29 de outubro de 2005**.

Sendo só para o presente.

Colocamo-nos a inteira disposição para informações adicionais através do telefone 3328-2828 ou do e-mail: ucl@ucl.br.

Atenciosamente

UCL - Ensino Superior
Ronaldo Alvarenga Alves
Setor de Pessoal

Ronaldo Alvarenga Alves
Setor de Pessoal

IFADISC
Faculdades Integradas de São Carlos

INSTITUTO PAULISTA DE ENSINO SUPERIOR UNIFICADO - IPESU
Inscrição Estadual: Isento
CNPJ: 59.622.977/0001-93
Rua Dr. Marino da Costa Terra, n.º 786 • CXP 195 • CEP: 13560-970 • São Carlos - SP
Fone: (16) 3362-4300 / Fax: (16) 3362-4316 • http://www.fadisc.edu.br • e-mail: fadisc@fadisc.edu.br

DECLARAÇÃO

Declaramos para os devidos fins que **ELMER ROLANDO LLANOS VILLARREAL**, portador da Carteira Profissional nº 071126 serie nº A01-ES, faz parte do quadro de funcionários desta Instituição desde 03/08/2006, onde exerce as funções de Professor Titular dos cursos de Engenharia Civil e Produção.

Para maior clareza e efeitos legais, firmamos a presente.

São Carlos, 10 de agosto de 2006.

IPESU - Instituto Paulista de Ensino Superior Unificado

Carlota Cristina Miceli Marra
Enc. Depto. Recursos Humanos

DECLARAÇÃO

Declaramos para os devidos fins, que o Sr. **Elmer Rolando Llanos Villarreal**, matrícula 03807, portador da CTPS 071126 série 865-RJ, foi funcionário desta Instituição de Ensino desde 05 de fevereiro de 2007 até 30 de Julho de 2007, exercendo a função de Professor Responsável Diretor, e que o mesmo lecionava nas disciplinas, conforme segue:

Curso Engenharia Elétrica

- Vetores e Geometria Analítica – 3h/A – (Turma Betha)
- Computação Aplicada – 3h/A – (2º Período)

Curso Engenharia Mecânica

- Vetores e Geometria Analítica – 3h/A – (Turma Alpha)
- Vetores e Geometria Analítica – 3h/A – (Turma Omega)

Por ser verdade firmamos a presente.

Volta Redonda, 07 de Agosto 2007.

32504996/0001-14
FUNDAÇÃO OSWALDO ARANHA

Av. Paulo Erlei Alves Abrantes, 1325
Três Poços - CEP 27251-970
Volta Redonda - RJ

MINISTÉRIO DO TRABALHO

SECRETARIA DE POLÍTICAS DE EMPREGO E SALÁRIO

CARTEIRA DE TRABALHO E PREVIDÊNCIA SOCIAL

PIS/PASEP

128.47097.12-2

NÚMERO	SÉRIE	UF
071126	A01	ES

ASSINATURA DO TITULAR

POLEGAR DIREITO

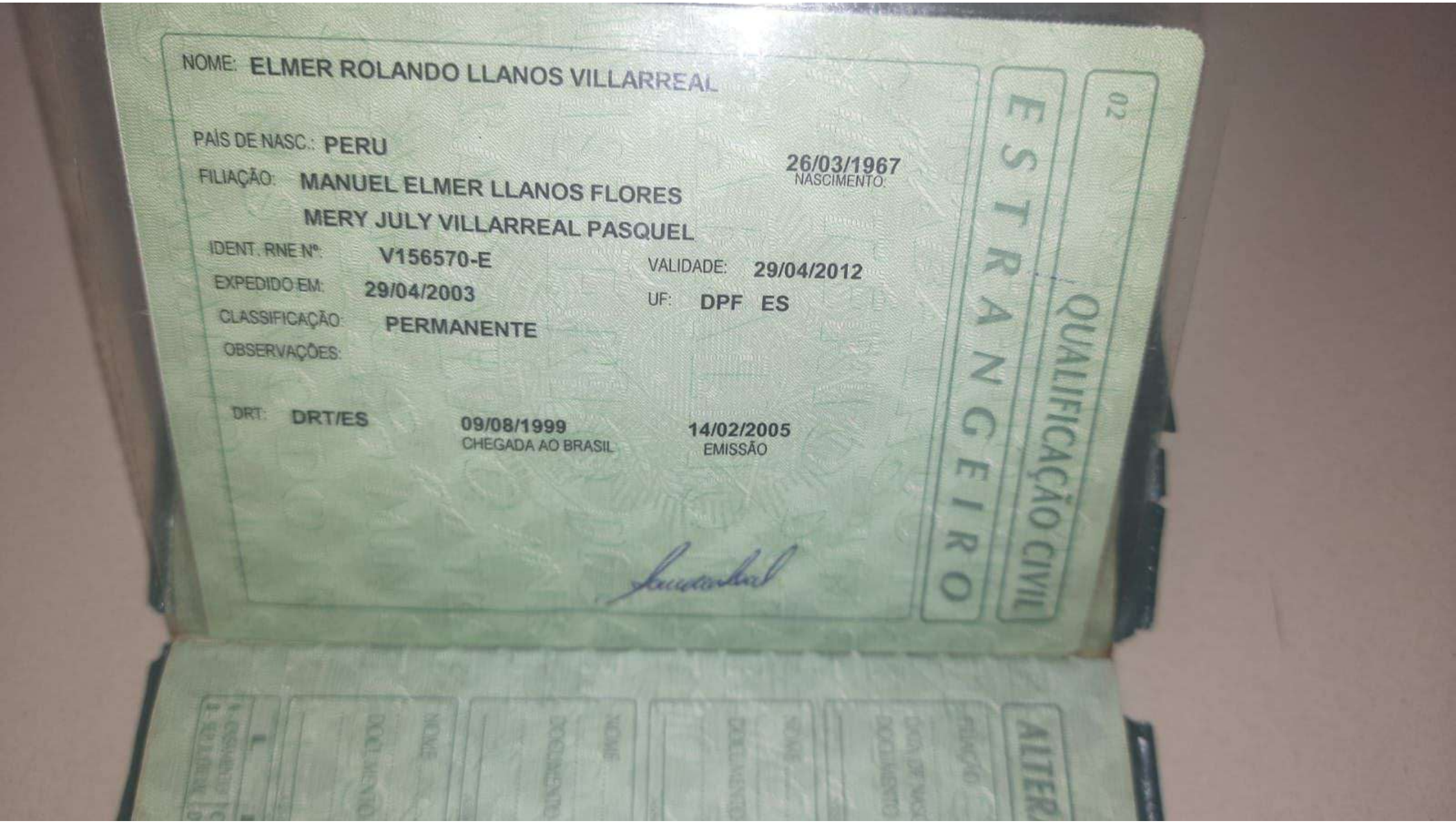

02

QUALIFICAÇÃO CIVIL

ESTRANGEIRO

NOME: ELMER ROLANDO LLANOS VILLARREAL

PAÍS DE NASC.: PERU

26/03/1967
NASCIMENTO:

FILIAÇÃO: MANUEL ELMER LLANOS FLORES

MERY JULY VILLARREAL PASQUEL

IDENT. RNE Nº: V156570-E

VALIDADE: 29/04/2012

EXPEDIDO EM: 29/04/2003

UF: DPF ES

CLASSIFICAÇÃO: PERMANENTE

OBSERVAÇÕES:

DRT: DRT/ES

09/08/1999
CHEGADA AO BRASIL

14/02/2005
EMISSÃO

ALTERAÇÕES

08

CONTRATO DE TRABALHO

02.598.162/0001-07

EMPREGADOR U.C.L. Assoc. Est. de Ensino Superior

ENDEREÇO Rua [illegible] 17 - Centro

MUNICÍPIO [illegible] Santa UF ES

ESP. DO ESTABELECIMENTO [illegible]

CARGO professor DJL

CBO Nº [illegible]

DATA DE ADMISSÃO 02 DE fevereiro DE 2005

REGISTRO Nº livro 03 FLS/FICHA 42

REMUNERAÇÃO ESPECIFICADA 27,25 + 15% planejamento

(vinte sete e vinte e cinco centavos) p/hora

UCL Ensino Superior

Bruno Loyola Del Caro

DATA DE SAÍDA 04 DE novembro DE 2005

UCL Ensino Superior

Bruno Loyola Del Caro

COM. DISPENSA CD Nº [illegible]

FGTS Nº DA CONTA [illegible]

09

CONTRATO DE TRABALHO

EMPREGADOR INSTITUTO DE ENSINO SUPERIOR DO ESPIRITO SANTO

COG/CPF/CEI 02213 169/0001-81

ENDEREÇO RUA LUIZ CEOTTO, 57

CENTRO

MUNICÍPIO CASTELO UF ES

ESP. DO ESTABELECIMENTO ENS. SUPERIOR

CARGO PROFESSOR

CBO Nº [illegible]

DATA DE ADMISSÃO 10 DE FEVEREIRO DE 2003

REGISTRO Nº LIVRO 02 FLS/FICHA FOLHA 26

REMUNERAÇÃO ESPECIFICADA R$ 30,24 (TRINTA REAIS E VINTE E QUATRO CENTAVOS) H/A

INSTITUTO DE ENSINO SUPERIOR DO ESPÍRITO SANTO

DATA DE SAÍDA 09 DE NOVEMBRO DE 2005

INSTITUTO DE ENSINO SUPERIOR DO ESPÍRITO SANTO

COM. DISPENSA CD Nº [illegible]

FGTS Nº DA CONTA [illegible]

10

CONTRATO DE TRABALHO

Empresa: INST PAUL ENS SUP UNIF IPESU

CNPJ/CEI/CPF: 59622977000193
ESP ESTAB: ESTABELECIMENTO DE ENSINO
ROD WASHINGTON LUIZ KM 00231

SAO CARLOS/SP
DATA DE ADMISSAO: 03/08/2006
CARGO: PROF TT- C ENG PROD
CBO: 234310
REGISTRO:
Remuneração Especificada: 21,17 POR HORA
VINTE E UM REAIS E DEZESSETE CENTAVOS **
****

IPESU - Instituto Paulista de Ensino Superior Unificado

Fábio Pereira Honda
Vice - Presidente

27

IPESU - Instituto Paulista de Ensino Superior Unificado

Fábio Pereira Honda
Vice - Presidente

11

CONTRATO DE TRABALHO

32504995/0001-14

FUNDAÇÃO OSWALDO ARANHA

Av. Paulo Erial Alves Abrantes, 1325
Três Poços - CEP 27251-970
Volta Redonda - RJ

Professor

05 de Fevereiro de 2007

0380 2

R$ 27,24 (Vinte e sete reais e vinte e quatro centavos) Hora/AVP

30 de Junho de 2007

SERVIÇO PÚBLICO FEDERAL
MINISTÉRIO DA EDUCAÇÃO
UNIVERSIDADE FEDERAL RURAL DO SEMI-ÁRIDO
PRÓ-REITORIA DE RECURSOS HUMANOS

DECLARAÇÃO

Declaramos para os fins que se fizerem necessários que o Professor **Elmer Rolando Llanos Villarreal**, é servidor do Quadro Permanente desta Universidade, ocupante do cargo de Professor Adjunto, admitido em 14 de janeiro de 2009.

Mossoró, 08 de julho de 2009.

Marcelo José Matos Herculano
Pró-Reitor Substituto

24.529.265/0001-40
MINISTÉRIO DA EDUCAÇÃO
Universidade Federal Rural do Semi-Árido
BR-110 - KM 47 - CX. POSTAL 137
PRES. COSTA E SILVA
CEP: 59625-900
MOSSORÓ - RN

TERCEIRO OFÍCIO DE NOTAS

AUTENTICAÇÃO: Certifico que esta é a reprodução fiel do original que me foi apresentado e qual autentico. Dou fé.
Mossoró/Rn, 8 de Julho de 2009.
Sarah Tieianne Nunes Lopes
Oficial

Válido somente com o selo de autenticidade Nº AGU 042478

Portal do Docente

Universidade Federal Rural do Semi-Árido
Sistema Integrado de Gestão de Atividades Acadêmicas

Emitido em

Pró-Reitoria de Graduação

Declaração de Disciplinas Ministradas

Declaramos para os devidos fins que o Docente ELMER ROLANDO LLANOS VILLARREAL, Matrícula SIAPE de número 1673887, ministrou nesta instituição os seguintes componentes curriculares, em seus respectivos períodos letivos:

Turmas Presenciais

2024.1	**Nível**	**Qtd. Al. Mat.**
GEOMETRIA ANALÍTICA - 60 h	PÓS-GRADUAÇÃO	19
2023.2	**Nível**	**Qtd. Al. Mat.**
FUNDAMENTOS DE MATEMATICA (1200470) - 60 h	GRADUAÇÃO	47
MATEMÁTICA PARA GESTÃO - 60 h	GRADUAÇÃO	46
2023.1	**Nível**	**Qtd. Al. Mat.**
FUNDAMENTOS DE MATEMATICA (1200470) - 60 h	GRADUAÇÃO	50
MATEMÁTICA PARA GESTÃO - 60 h	GRADUAÇÃO	49
GEOMETRIA I - 120 h	PÓS-GRADUAÇÃO	2
RESOLUÇÃO DE PROBLEMAS - 60 h	PÓS-GRADUAÇÃO	22
2022.2	**Nível**	**Qtd. Al. Mat.**
CÁLCULO I - 16 h	GRADUAÇÃO	24
FUNDAMENTOS DE MATEMATICA (1200470) - 60 h	GRADUAÇÃO	52
MATEMÁTICA PARA GESTÃO - 60 h	GRADUAÇÃO	49

FUNDAMENTOS DE CÁLCULO - 60 h	PÓS-GRADUAÇÃO	4
2022.1	**Nível**	**Qtd. Al. Mat.**
FUNDAMENTOS DE MATEMATICA (1200470) - 60 h	GRADUAÇÃO	50
2021.2	**Nível**	**Qtd. Al. Mat.**
CÁLCULO II - 10 h	GRADUAÇÃO	26
CALCULO II (1200008) - 60 h	GRADUAÇÃO	57
FUNDAMENTOS DE MATEMATICA (1200470) - 60 h	GRADUAÇÃO	56
MATEMÁTICA PARA GESTÃO - 60 h	GRADUAÇÃO	53
2021.1	**Nível**	**Qtd. Al. Mat.**
CALCULO II (1200008) - 60 h	GRADUAÇÃO	64
FUNDAMENTOS DE MATEMATICA (1200470) - 60 h	GRADUAÇÃO	43
MATEMÁTICA PARA GESTÃO - 60 h	GRADUAÇÃO	53
2020.3	**Nível**	**Qtd. Al. Mat.**
FUNDAMENTOS DE MATEMATICA (1200470) - 60 h	GRADUAÇÃO	53
MATEMÁTICA PARA GESTÃO - 60 h	GRADUAÇÃO	49
2020.2	**Nível**	**Qtd. Al. Mat.**
CALCULO II (1200008) - 60 h	GRADUAÇÃO	52
FUNDAMENTOS DE MATEMATICA (1200470) - 60 h	GRADUAÇÃO	45
MATEMÁTICA PARA GESTÃO - 60 h	GRADUAÇÃO	53
2020.1	**Nível**	**Qtd. Al. Mat.**
CALCULO II (1200008) - 60 h	GRADUAÇÃO	51
FUNDAMENTOS DE MATEMATICA (1200470) - 60 h	GRADUAÇÃO	33
MATEMÁTICA PARA GESTÃO - 60 h	GRADUAÇÃO	40
2019.2	**Nível**	**Qtd. Al. Mat.**

FUNDAMENTOS DE MATEMATICA (1200470) - 40 h	GRADUAÇÃO	40
MATEMÁTICA PARA GESTÃO - 40 h	GRADUAÇÃO	47
2018.2	**Nível**	**Qtd. Al. Mat.**
FUNDAMENTOS DE MATEMATICA (1200470) - 20 h	GRADUAÇÃO	43
MATEMÁTICA PARA GESTÃO - 20 h	GRADUAÇÃO	47
2018.1	**Nível**	**Qtd. Al. Mat.**
CALCULO I (1200003) - 60 h	GRADUAÇÃO	48
FUNDAMENTOS DE MATEMATICA (1200470) - 60 h	GRADUAÇÃO	52
MATEMÁTICA PARA GESTÃO - 60 h	GRADUAÇÃO	51
SISTEMAS LINEARES - 60 h	PÓS-GRADUAÇÃO	1
2017.2	**Nível**	**Qtd. Al. Mat.**
ALGEBRA LINEAR (1200260) - 60 h	GRADUAÇÃO	56
ALGEBRA LINEAR (1200260) - 60 h	GRADUAÇÃO	53
ALGEBRA LINEAR (1200260) - 60 h	GRADUAÇÃO	55
SISTEMAS LINEARES - 60 h	PÓS-GRADUAÇÃO	1
2017.1	**Nível**	**Qtd. Al. Mat.**
CALCULO II (1200008) - 60 h	GRADUAÇÃO	26
CALCULO II (1200008) - 60 h	GRADUAÇÃO	55
CALCULO II (1200008) - 60 h	GRADUAÇÃO	48
RESOLUÇÃO DE PROBLEMAS - 60 h	PÓS-GRADUAÇÃO	15
SISTEMAS DE CONTROLE MULTIVARIÁVEIS - 60 h	PÓS-GRADUAÇÃO	2
2016.2	**Nível**	**Qtd. Al. Mat.**
CALCULO II (1200008) - 20 h	GRADUAÇÃO	40
CALCULO II (1200008) - 20 h	GRADUAÇÃO	41

CALCULO II (1200008) - 20 h	GRADUAÇÃO	52
CALCULO NUMERICO - 30 h	GRADUAÇÃO	4
CALCULO NUMERICO (1200128) - 60 h	GRADUAÇÃO	42
CALCULO NUMERICO (1200128) - 30 h	GRADUAÇÃO	49
CÁLCULO NUMÉRICO - 120 h	PÓS-GRADUAÇÃO	11
SISTEMAS LINEARES - 60 h	PÓS-GRADUAÇÃO	1
2016.1	**Nível**	**Qtd. Al. Mat.**
CALCULO NUMERICO - 60 h	GRADUAÇÃO	11
CALCULO NUMERICO (1200128) - 60 h	GRADUAÇÃO	55
CALCULO NUMERICO (1200128) - 60 h	GRADUAÇÃO	39
CALCULO NUMERICO (1200128) - 60 h	GRADUAÇÃO	58
MATEMÁTICA E ATUALIDADE - 120 h	PÓS-GRADUAÇÃO	3
MODELAGEM MATEMÁTICA - 120 h	PÓS-GRADUAÇÃO	4
SISTEMAS DE CONTROLE MULTIVARIÁVEIS - 60 h	PÓS-GRADUAÇÃO	1
2015.2	**Nível**	**Qtd. Al. Mat.**
CALCULO NUMERICO - 60 h	GRADUAÇÃO	7
CALCULO NUMERICO (1200128) - 60 h	GRADUAÇÃO	62
CALCULO NUMERICO (1200128) - 60 h	GRADUAÇÃO	59
CALCULO NUMERICO (1200128) - 60 h	GRADUAÇÃO	48
FUNDAMENTOS DE CÁLCULO - 120 h	PÓS-GRADUAÇÃO	1
MODELAGEM E SIMULAÇÃO DE CONTROLE - 60 h	PÓS-GRADUAÇÃO	3
SISTEMAS LINEARES - 60 h	PÓS-GRADUAÇÃO	6
2015.1	**Nível**	**Qtd. Al. Mat.**

CALCULO II (1200008) - 60 h	GRADUAÇÃO	56
CALCULO II (1200008) - 60 h	GRADUAÇÃO	51
CALCULO II (1200008) - 60 h	GRADUAÇÃO	59
SISTEMAS DE CONTROLE MULTIVARIÁVEIS - 60 h	PÓS-GRADUAÇÃO	5
2014.2	**Nível**	**Qtd. Al. Mat.**
CALCULO II (1200008) - 60 h	GRADUAÇÃO	80
CALCULO II (1200008) - 60 h	GRADUAÇÃO	61
CALCULO II (1200008) - 60 h	GRADUAÇÃO	68
GEOMETRIA ANALÍTICA - 60 h	PÓS-GRADUAÇÃO	18
SISTEMAS LINEARES - 60 h	PÓS-GRADUAÇÃO	11
2014.1	**Nível**	**Qtd. Al. Mat.**
CALCULO II (1200008) - 60 h	GRADUAÇÃO	58
CALCULO II (1200008) - 60 h	GRADUAÇÃO	60
CALCULO II (1200008) - 60 h	GRADUAÇÃO	44
SISTEMAS DE CONTROLE MULTIVARIÁVEIS - 60 h	PÓS-GRADUAÇÃO	2
2013.2	**Nível**	**Qtd. Al. Mat.**
CALCULO I (1200003) - 60 h	GRADUAÇÃO	65
CALCULO I (1200003) - 60 h	GRADUAÇÃO	53
CALCULO I (1200003) - 60 h	GRADUAÇÃO	57
GEOMETRIA ANALÍTICA - 60 h	PÓS-GRADUAÇÃO	17
SISTEMAS LINEARES - 60 h	PÓS-GRADUAÇÃO	11
2013.1	**Nível**	**Qtd. Al. Mat.**
CALCULO I (1200003) - 60 h	GRADUAÇÃO	51
CALCULO I (1200003) - 60 h	GRADUAÇÃO	55

CALCULO I (1200003) - 60 h	GRADUAÇÃO	56
FUNDAMENTOS DE MATEMATICA (1200470) - 20 h	GRADUAÇÃO	42
SISTEMAS DE CONTROLE MULTIVARIÁVEIS - 60 h	PÓS-GRADUAÇÃO	8
2012.3	**Nível**	**Qtd. Al. Mat.**
CALCULO NUMERICO (1200128) - 60 h	GRADUAÇÃO	58
CALCULO NUMERICO (1200128) - 60 h	GRADUAÇÃO	1
2012.2	**Nível**	**Qtd. Al. Mat.**
ALGEBRA LINEAR (1200260) - 60 h	GRADUAÇÃO	37
CALCULO I (1200003) - 60 h	GRADUAÇÃO	44
CALCULO I (1200003) - 60 h	GRADUAÇÃO	44
GEOMETRIA ANALÍTICA - 60 h	PÓS-GRADUAÇÃO	22
SISTEMAS LINEARES - 60 h	PÓS-GRADUAÇÃO	4
2012.1	**Nível**	**Qtd. Al. Mat.**
FUNDAMENTOS DE MATEMATICA (1200470) - 60 h	GRADUAÇÃO	57
FUNDAMENTOS DE MATEMATICA (1200470) - 60 h	GRADUAÇÃO	46
GEOMETRIA ANALITICA (1200255) - 60 h	GRADUAÇÃO	52
PRATICA DE ENSINO VI - EPISTEMOLOGIA DA MATEMATICA - 75 h	GRADUAÇÃO	12
NÚMEROS, CONJUNTOS E FUNÇÕES ELEMENTARES - 60 h	PÓS-GRADUAÇÃO	25
SISTEMAS DE CONTROLE - 30 h	PÓS-GRADUAÇÃO	7
SISTEMAS DE CONTROLE MULTIVARIÁVEIS - 60 h	PÓS-GRADUAÇÃO	4
2011.3	**Nível**	**Qtd. Al. Mat.**
CALCULO NUMERICO (1200128) - 60 h	GRADUAÇÃO	24
2011.2	**Nível**	**Qtd. Al. Mat.**

CALCULO NUMERICO - 60 h	GRADUAÇÃO	6
CALCULO NUMERICO (1200128) - 60 h	GRADUAÇÃO	42
CALCULO NUMERICO (1200128) - 60 h	GRADUAÇÃO	32
CALCULO NUMERICO (1200128) - 60 h	GRADUAÇÃO	16
CALCULO NUMERICO (1200128) - 60 h	GRADUAÇÃO	19
GEOMETRIA I - 60 h	PÓS-GRADUAÇÃO	24
SISTEMAS LINEARES - 60 h	PÓS-GRADUAÇÃO	10
2011.1	**Nível**	**Qtd. Al. Mat.**
CALCULO I (1200003) - 60 h	GRADUAÇÃO	42
CALCULO NUMERICO (1200128) - 60 h	GRADUAÇÃO	44
CALCULO NUMERICO (1200128) - 60 h	GRADUAÇÃO	28
CALCULO NUMERICO (1200128) - 60 h	GRADUAÇÃO	20
ESTATISTICA (1104001) - 60 h	GRADUAÇÃO	13
2010.3	**Nível**	**Qtd. Al. Mat.**
CALCULO II (1200008) - 60 h	GRADUAÇÃO	46
2010.2	**Nível**	**Qtd. Al. Mat.**
CALCULO NUMERICO (1200128) - 60 h	GRADUAÇÃO	49
CALCULO NUMERICO (1200128) - 60 h	GRADUAÇÃO	51
CALCULO NUMERICO (1200128) - 60 h	GRADUAÇÃO	36
CALCULO NUMERICO (1200128) - 60 h	GRADUAÇÃO	0
CÁLCULO NUMÉRICO (1200128) - 60 h	GRADUAÇÃO	2
2010.1	**Nível**	**Qtd. Al. Mat.**
CÁLCULO II - 60 h	GRADUAÇÃO	15
CALCULO NUMERICO - 60 h	GRADUAÇÃO	1

CALCULO NUMERICO (1200128) - 60 h	GRADUAÇÃO	38
CALCULO NUMERICO (1200128) - 60 h	GRADUAÇÃO	45
CALCULO NUMERICO (1200128) - 60 h	GRADUAÇÃO	29
2008.2	**Nível**	**Qtd. Al. Mat.**
ALGEBRA LINEAR (1200260) - 60 h	GRADUAÇÃO	44
2008.1	**Nível**	**Qtd. Al. Mat.**
CALCULO I (1200003) - 60 h	GRADUAÇÃO	46

MOSSORÓ, 28 de Agosto de 2024

Código de Verificação:
d75d07448e

Para verificar a autenticidade deste documento acesse **https://sigaa.ufersa.edu.br/sigaa/documentos/**, informando a Matrícula do SIAPE , data de emissão do documento e o código de verificação.

SIGAA | Superintendência de Tecnologia da Informação e Comunicação

UNIVERSIDADE FEDERAL RURAL DO SEMI-ÁRIDO
PRÓ-REITORIA DE PESQUISA E PÓS-GRADUAÇÃO

CGC: 24.529.265/0001-40
Av. Francisco Mota, 572 - Costa e Silva, CEP: 59625-900
(084) 3317-8295 - Fax: (084) 3317-8228 - e-mail: proppg@ufersa.edu.br

DECLARAÇÃO

Declaramos que o(a) professor(a) ELMER ROLANDO LLANOS VILLARREAL, portador(a) do CPF 213.060.638-50, matrícula SIAPE nº 1673887, atuou como Coordenador no projeto de pesquisa PIC20015-2019 - CONJUNTOS INVARIANTES DE SEGUNDA ORDEM E SUAS APLICAÇÕES, com carga horária semanal de 30h, no período de 1 de Dezembro de 2019 até a presente data.

Mossoró, 27 de Setembro de 2024.

Liana Holanda Nepomuceno Nobre
Pró-Reitor de Pesquisa

Alexsandra Fernandes Pereira
Pró-Reitor Adjunto de Pesquisa

Código de verificação:
fa09c56f34

Para verificar a autenticidade deste documento acesse **https://sigaa.ufersa.edu.br/sigaa/documentos/**, informando a matrícula, data de emissão do documento e o código de verificação.

UNIVERSIDADE FEDERAL RURAL DO SEMI-ÁRIDO
PRÓ-REITORIA DE PESQUISA E PÓS-GRADUAÇÃO

CGC: 24.529.265/0001-40
Av. Francisco Mota, 572 - Costa e Silva, CEP: 59625-900
(084) 3317-8295 - Fax: (084) 3317-8228 - e-mail: proppg@ufersa.edu.br

DECLARAÇÃO

Declaramos que o(a) professor(a) ELMER ROLANDO LLANOS VILLARREAL, portador(a) do CPF 213.060.638-50, matrícula SIAPE nº 1673887, atuou como Coordenador no projeto de pesquisa PIC20004-2020 - Estabilidade condicionamento e fatoração LU em problemas de Engenharias e suas aplicações com uso do Scilab, com carga horária semanal de 30h, no período de 1 de Agosto de 2020 até a presente data.

Mossoró, 27 de Setembro de 2024.

Liana Holanda Nepomuceno Nobre
Pró-Reitor de Pesquisa

Alexsandra Fernandes Pereira
Pró-Reitor Adjunto de Pesquisa

Código de verificação:
20c8f82ca0

Para verificar a autenticidade deste documento acesse **https://sigaa.ufersa.edu.br/sigaa/documentos/**, informando a matrícula, data de emissão do documento e o código de verificação.

UNIVERSIDADE FEDERAL RURAL DO SEMI-ÁRIDO
PRÓ-REITORIA DE PESQUISA E PÓS-GRADUAÇÃO

CGC: 24.529.265/0001-40
Av. Francisco Mota, 572 - Costa e Silva, CEP: 59625-900
(084) 3317-8295 - Fax: (084) 3317-8228 - e-mail: proppg@ufersa.edu.br

DECLARAÇÃO

Declaramos que o(a) professor(a) ELMER ROLANDO LLANOS VILLARREAL, portador(a) do CPF 213.060.638-50, matrícula SIAPE nº 1673887, atuou como Coordenador no projeto de pesquisa PIC20001-2021 - Controle por Rejeição Ativa de Distúrbios e suas aplicações, com carga horária semanal de 30h, no período de 4 de Fevereiro de 2021 até a presente data.

Mossoró, 27 de Setembro de 2024.

Liana Holanda Nepomuceno Nobre
Pró-Reitor de Pesquisa

Alexsandra Fernandes Pereira
Pró-Reitor Adjunto de Pesquisa

Código de verificação:
c1d1c4e603

Para verificar a autenticidade deste documento acesse **https://sigaa.ufersa.edu.br/sigaa/documentos/**, informando a matrícula, data de emissão do documento e o código de verificação.

UNIVERSIDADE FEDERAL RURAL DO SEMI-ÁRIDO
PRÓ-REITORIA DE PESQUISA E PÓS-GRADUAÇÃO

CGC: 24.529.265/0001-40
Av. Francisco Mota, 572 - Costa e Silva, CEP: 59625-900
(084) 3317-8295 - Fax: (084) 3317-8228 - e-mail: proppg@ufersa.edu.br

DECLARAÇÃO

Declaramos que o(a) professor(a) ELMER ROLANDO LLANOS VILLARREAL, portador(a) do CPF 213.060.638-50, matrícula SIAPE nº 1673887, atuou como Coordenador no projeto de pesquisa PIC20013-2024 - Ensino em Matemática: Aprendizagem e avaliação nas escolas, com carga horária semanal de 20h, no período de 1 de Agosto de 2024 até a presente data.

Mossoró, 27 de Setembro de 2024.

Liana Holanda Nepomuceno Nobre
Pró-Reitor de Pesquisa

Alexsandra Fernandes Pereira
Pró-Reitor Adjunto de Pesquisa

Código de verificação:
2b48396578

Para verificar a autenticidade deste documento acesse **https://sigaa.ufersa.edu.br/sigaa/documentos/**, informando a matrícula, data de emissão do documento e o código de verificação.

UNIVERSIDADE FEDERAL RURAL DO SEMI-ÁRIDO
PRÓ-REITORIA DE PESQUISA E PÓS-GRADUAÇÃO

CGC: 24.529.265/0001-40
Av. Francisco Mota, 572 - Costa e Silva, CEP: 59625-900
(084) 3317-8295 - Fax: (084) 3317-8228 - e-mail: proppg@ufersa.edu.br

DECLARAÇÃO

Declaramos que o(a) professor(a) ELMER ROLANDO LLANOS VILLARREAL, portador(a) do CPF 213.060.638-50, matrícula SIAPE nº 1673887, atuou como Coordenador no projeto de pesquisa PIC20006-2024 - Controle por Rejeição Ativa de Distúrbios e suas aplicações, com carga horária semanal de 20h, no período de 1 de Setembro de 2024 até a presente data.

Mossoró, 27 de Setembro de 2024.

Liana Holanda Nepomuceno Nobre
Pró-Reitor de Pesquisa

Alexsandra Fernandes Pereira
Pró-Reitor Adjunto de Pesquisa

Código de verificação:
48f8737a77

Para verificar a autenticidade deste documento acesse **https://sigaa.ufersa.edu.br/sigaa/documentos/**, informando a matrícula, data de emissão do documento e o código de verificação.

UNIVERSIDADE FEDERAL RURAL DO SEMI-ÁRIDO
PRÓ-REITORIA DE PESQUISA E PÓS-GRADUAÇÃO

CGC: 24.529.265/0001-40
Av. Francisco Mota, 572 - Costa e Silva, CEP: 59625-900
(084) 3317-8295 - Fax: (084) 3317-8228 - e-mail: proppg@ufersa.edu.br

DECLARAÇÃO

Declaramos que o(a) professor(a) ELMER ROLANDO LLANOS VILLARREAL, portador(a) do CPF 213.060.638-50, matrícula SIAPE nº 1673887, atuou como Coordenador no projeto de pesquisa PEC00002-2014 - Desenvolvimento de sensores para posicionamento e
mobilidade de ve culos n~ao-tripulados, com carga horária semanal de 10h, no período de 1 de Setembro de 2014 a 30 de Junho de 2019.

Mossoró, 27 de Setembro de 2024.

Liana Holanda Nepomuceno Nobre
Pró-Reitor de Pesquisa

Alexsandra Fernandes Pereira
Pró-Reitor Adjunto de Pesquisa

Código de verificação:
8c04b13f36

Para verificar a autenticidade deste documento acesse **https://sigaa.ufersa.edu.br/sigaa/documentos/**, informando a matrícula, data de emissão do documento e o código de verificação.

UNIVERSIDADE FEDERAL RURAL DO SEMI-ÁRIDO
PRÓ-REITORIA DE PESQUISA E PÓS-GRADUAÇÃO

CGC: 24.529.265/0001-40
Av. Francisco Mota, 572 - Costa e Silva, CEP: 59625-900
(084) 3317-8295 - Fax: (084) 3317-8228 - e-mail: proppg@ufersa.edu.br

DECLARAÇÃO

Declaramos que o(a) professor(a) ELMER ROLANDO LLANOS VILLARREAL, portador(a) do CPF 213.060.638-50, matrícula SIAPE nº 1673887, atuou como Coordenador no projeto de pesquisa PIC20017-2018 - OTIMIZAÇÃO DE ASAS DE MATERIAL COMPÓSITO DE VEÍCULOS AÉREOS NÃO TRIPULADOS USANDO ELEMENTOS FINITOS, com carga horária semanal de 10h, no período de 2 de Julho de 2018 a 31 de Julho de 2021.

Mossoró, 27 de Setembro de 2024.

Liana Holanda Nepomuceno Nobre
Pró-Reitor de Pesquisa

Alexsandra Fernandes Pereira
Pró-Reitor Adjunto de Pesquisa

Código de verificação:
b8e1f3b9b8

Para verificar a autenticidade deste documento acesse **https://sigaa.ufersa.edu.br/sigaa/documentos/**, informando a matrícula, data de emissão do documento e o código de verificação.

MINISTÉRIO DA EDUCAÇÃO
UNIVERSIDADE FEDERAL RURAL DO SEMI-ÁRIDO
PRÓ-REITORIA DE PESQUISA E PÓS-GRADUAÇÃO
Av. Francisco Mota, 572 – C. Postal 137 – Bairro Pres. Costa e Silva – Mossoró – RN – CEP: 59.625-900 - Tel.: (84)3317-8296 – E.mail: proppg@ufersa.edu.br

D E C L A R A Ç Ã O

Declaro, para os fins que se fizerem necessários, que **Elmer Rolando Llanos Vilarreal**, professor/pesquisador desta IFES, foi **membro** dos projetos cadastrados nesta Pró-Reitoria de Pesquisa e Pós-Graduação, abaixo relacionados:

Título do Projeto	Coordenador	Tipo	Período de Execução
PI1416B-152 Projeto, fabricação, e testes de um novo VANT hibrido com aplicação no controle de fitopatologias	Alex Sandro de Araújo Silva	Interno	01-08-2014/ 30-07-2016
PI1617C-84 Construções de jogos computacionais e desenvolvimento de modelos de controles elementares	Walter Martins Rodrigues		02-06-2016/ 05-06-2017

Mossoró (RN), 30 de outubro de 2018.

Jean Berg Alves da Silva
Pró-Reitor de Pesquisa e Pós-graduação

Av. Francisco Mota, 572 – C. Postal 137 – Bairro Pres. Costa e Silva – Mossoró – RN – CEP: 59.625-900 - Tel.: (84)3317-8296 – E.mail: proppg@ufersa.edu.br

Departamento de Ciências Exatas e Naturais - DCEN

Última atualização em 22/07/2016

Legenda:

	Coordenador(a) do Projeto
1	Pesquisador
2	Aluno(a) de Pós-Graduação
3	Aluno de graduação
PI	Projeto Interno

CÓDIGO: PI1113C-41
TÍTULO DO PROJETO: UFERSA Virtual- Campus virtual inteligente para navegação e integração de serviços acadêmicos.
EQUIPE: Angélica Félix de Castro, Daniel Faustino Lacerda de Souza[1], Marcelo Roberto Bastos Guerra Vale[1], Alexandro Lima Damasceno[3], Paulo Robson[3], Juliana Lima Ferreira[3], Adriana Mara Guimarães de Farias[3], Hugo Wendell Maia.
VIGÊNCIA: 07-2011/ 07-2016

CÓDIGO: PI1317C-55
TÍTULO DO PROJETO: Grupo de Estudos e Desenvolvimento em Energia e Automação - GEDEA.
EQUIPE: Danielle Simone da Silva Casillo, José Patrocínio da Silva, Egmidio Caratti Filho, Emmanuel Ramon Marques Dantas, Reuber Regis de Melo, Cláudio Márcio Medeiros de Azevedo, Ádller de Oliveira Guimarães.
VIGÊNCIA: 02-2013 / 12-2017

CÓDIGO: PI1317C-60
TÍTULO DO PROJETO: Grupo de estudos utilizando Arduíno em pesquisa com tecnologias da informação - GRAPETI.
EQUIPE: Leonardo Augusto Casillo, Danielle Simone da Silva Casillo, Lázaro Luiz Lima de Sousa, Marcelo Roberto Bastos Guerra Vale, Danniel Cavalcante Lopes, Amanda Gondim de Oliveira, João Phellipe de Freitas Pinto, Alessandro Muras de Oliveira Pino, Ronnison Reges Vidal, Maurício dos Santos Lima, Fausto Blanco Diniz Leal de Souza, Talles Amony Alves de Santana, Jefferson Costa Conceição Silva, Samanta Mesquita de Holanda.
VIGÊNCIA: 01-12-2013/ 31-12-2017

CÓDIGO: PI1416C-62
TÍTULO DO PROJETO: Compartilhamento de dados multimídia em sistemas móveis - Parte II.

Av. Francisco Mota, 572 – C. Postal 137 – Bairro Pres. Costa e Silva – Mossoró – RN – CEP: 59.625-900 - Tel.: (84)3317-8296 – E.mail: proppg@ufersa.edu.br

EQUIPE: Angélica Félix de Castro, Daniel Faustino Lacerda de Souza,Hélcio Wagner da Silva, Gerlan Stanley de Lima Gonçalves.
VIGÊNCIA: 05-2014/ 07-2016

CÓDIGO: PI1416C-64
TÍTULO DO PROJETO: Estudo ab initio de sistemas cristalinos, moleculares e nanoestruturadas .
EQUIPE: Francisco Franciné Maia Júnior, Roner Ferreira da Costa, José Júnior Alves da Silva, Erlânia Lima de Oliveira, Geovani Ferraira Barbosa, Francisco Odolberto de Araújo, Valder Nogueira Freire, Ewerton Wagner Santos Caetano.
VIGÊNCIA: 01-08-2014/ 31-07-2016

CÓDIGO: PI1417C-65
TÍTULO DO PROJETO: Controle não linear para vant e suas extensões.
EQUIPE: Elmer Rolando Llanos Villarreal, Alex Sandro de Araújo Silva.
VIGÊNCIA: 01-08-2014/ 31-07-2017

CÓDIGO: PI1416C-66
TÍTULO DO PROJETO: Geração de Bases de Conhecimento Fuzzy utilizando o Paradigma Genético
EQUIPE: Marcos Evandro Cintra, Karla Raphaela Cardoso, Alex Lima Silva, Hugo Wendell Maia
VIGÊNCIA: 01-08-2014/ 31-07-2016

CÓDIGO: PI1516C-71
TÍTULO DO PROJETO: Computação ubíqua aplicada à educação
EQUIPE: Bruno de Sousa Monteiro, Paulo Gabriel Gadelha Queiroz, Leonardo Augusto Casillo
VIGÊNCIA: 24-08-2015/24-07-2016

CÓDIGO: PI1517C-72
TÍTULO DO PROJETO: Desenvolvimento de um controlador de altitude fuzzy-pid para um vant
EQUIPE: Elmer Rolando Llanos Villareal, Alexandre Santos Brandão, Edpo Rodrigues de Morais, Maxwell Cavalcante Jacomé
VIGÊNCIA: 01-08-2015/31-07-2017

CÓDIGO: PI1517C-73
TÍTULO DO PROJETO: Otimização de asas de material compósito de veículos áereos não tripulados usando elementos finitos

Av. Francisco Mota, 572 – C. Postal 137 – Bairro Pres. Costa e Silva – Mossoró – RN – CEP: 59.625-900 - Tel.: (84)3317-8296 – E.mail: proppg@ufersa.edu.br

EQUIPE: Elmer Rolando Llanos Villarreal, João Vitor de Queiroz, Maxwell Cavalcante Jacomé
VIGÊNCIA: 01-08-2015/31-07-2017

CÓDIGO: PI1517C-74
TÍTULO DO PROJETO: Controle, modelagem matemática, linearização e simulação no processo GMAW
EQUIPE: Elmer Rolando Llanos Villarreal
VIGÊNCIA: 01-03-2015/28-02-2017

CÓDIGO: PI1517C-75
TÍTULO DO PROJETO: Aplicação de learning analytics para avaliação do desempenho de tutores no âmbito da educação à distância
EQUIPE: Francisco Milton Mendes Neto, Rafael Castro de Souza, Laysa Mabel de Oliveira Fontes, Ricardo Alexsandro de Medeiros Valentim, Efraim Naasson Helem Dantas Rodrigues
VIGÊNCIA: 01-08-2015/01-08-2017

CÓDIGO: PI1517C-76
TÍTULO DO PROJETO: Desenvolvimento de um ambiente virtual de aprendizagem 3D multiagente para o ensino de música utilizando a metodologia de aprendizagem baseada em problemas
EQUIPE: Francisco Milton Mendes Neto, Giann Mendes Ribeiro, Alisson de Oliveira Maurício, Ana Thaise Barbosa da Costa, Artur Afonso Amaro Araújo, Humberto Lima de Castro Saraiva
VIGÊNCIA: 01-08-2015/01-08-2017

CÓDIGO: PI1517C-77
TÍTULO DO PROJETO: DocTraining: um ambiente 3D multiagente com suporte ao treinamento de estudantes de medicina
EQUIPE: Francisco Milton Mendes Neto, Araken de Medeiros Santos, Rodrigo Monteiro de Lima, Ademar França de Sousa Neto, Felipe César Pinheiro Leão, Fernando Henrique Alves, Francisco Tailânio de Macedo, Maria Luzia Silva de Carvalho
VIGÊNCIA: 01-08-2015/01-08-2017

CÓDIGO: PI1517C-78
TÍTULO DO PROJETO: Mobilehealth: um ambiente de apoio à saúde 2.0
EQUIPE: Francisco Milton Mendes Neto, Bruno Elvis Costa Rodrigues da Silva
VIGÊNCIA: 01-08-2015/01-08-2017

CÓDIGO: PI1517C-79
TÍTULO DO PROJETO: Um jogo adaptativo para auxiliar crianças com transtorno do desenvolvimento cognitivo
EQUIPE: Francisco Milton Mendes Neto, Karla Rosane do Amaral Demoly, Mariza de Souza Moura, Rafael de Almeida Rodrigues, Everton Jales de Oliveira, Danilo Gomes Carlos
VIGÊNCIA: 01-08-2015/01-08-2017

CÓDIGO: PI1517C-80
TÍTULO DO PROJETO: Estudos das propriedades eletrônicas em heteroestruturas semicondutoras de baixa dimensionalidade
EQUIPE: Jusciane da Costa e Silva, Subênia Karine de Medeiros, Ana Tereza Abreu de Lima, Samuel Alves, Jonathan Marcelino de Lima, Ricardo Hugo Medeiros Filho
VIGÊNCIA: 29-05-2015/28-05-2017

CÓDIGO: PI1517C-81
TÍTULO DO PROJETO: Construção de linhas de produto de sistemas embarcados críticos e suas aplicações
EQUIPE: Paulo Gabriel Gadelha Queiroz, Silvio Roberto Fernandes de Araújo, Leonardo Augusto Casillo
VIGÊNCIA: 01-08-2015/01-08-2017

CÓDIGO: PI1517C-82
TÍTULO DO PROJETO: Colaborative road maps: sociedade e autoridades de segurança unidas em prol da paz nas estradas
EQUIPE: Francisco Milton Mendes Neto, Aliathar Gibson Tavares de Lira, Kleber Jacinto
VIGÊNCIA: 01-07-2015/01-07-2017

CÓDIGO: PI1618C-83
TÍTULO DO PROJETO: Criação de um motor didático para o desenvolvimento de jogos
EQUIPE: Judson Santos Santiago, Helcio Wagner da Silva (VC), André Vitor de Souza e Silva
VIGÊNCIA: 01-02-2016/01-02-2018

CÓDIGO: PI1617C-84
TÍTULO DO PROJETO: Construções de jogos computacionais e desenvolvimento de modelos de controles elementares
EQUIPE: Walter Martins Rodrigues, Paulo César Linhares da Silva (VC), Aleksander Saraiva Dantas, Kézia Vianna, Valdemar Siqueira, Samuel Azevedo, Franceliza Monteiro, Elmer Rolando Llanos Villareal, Hugo Luiz Moura, Antônio Ronaldo Gomes Garcia, Daniel Alves Bezerra

Av. Francisco Mota, 572 – C. Postal 137 – Bairro Pres. Costa e Silva – Mossoró – RN – CEP: 59.625-900 - Tel.: (84)3317-8296 – E.mail: proppg@ufersa.edu.br

VIGÊNCIA: 02-06-2016/05-06-2017

CÓDIGO: PI1618C-85
TÍTULO DO PROJETO: Métodos numéricos em antenas
EQUIPE: Elmer Rolando Llanos Villarreal, Maxwell Cavalcante Jácome, Ciro Simão Medeiros
VIGÊNCIA: 01-08-2016/31-07-2018

energies

MDPI

Article

Artificial Intelligence for the Control of Speed of the Bearing Motor with Winding Split Using DSP

José Raimundo Dantas Neto [1,†], José Soares Batista Lopes [2,†], Diego Antonio De Moura Fonsêca [1,†], Antonio Ronaldo Gomes Garcia [3,†], Jossana Maria de Souza Ferreira [4,†], Elmer Rolando Llanos Villarreal [3,*,†] and Andrés Ortiz Salazar [1,†]

[1] Department of Computer Engineering and Automation, Federal University of Rio Grande do Norte (DCA-UFRN), Natal 59072-970, Brazil; jose.raimundo@ifce.edu.br (J.R.D.N.); diegomoura@dca.ufrn.br (D.A.D.M.F.); andres@dca.ufrn.br (A.O.S.)
[2] Federal Institute of Education, Science and Technology of Rio Grande do Norte (IFRN), Natal 59015-300, Brazil; jose.soares@ifrn.edu.br
[3] Department of Natural Sciences, Mathematics, and Statistics, Federal Rural University of Semi-Arid (DCME-UFERSA), Mossoró 59625-900, Brazil; ronaldogarcia@ufersa.edu.br
[4] School of Science & Technology, Federal University of Rio Grande do Norte (ECT-UFRN), Natal 59072-970, Brazil; jossana.ferreira@ufrn.br
* Correspondence: elmerllanos@ufersa.edu.br
† These authors contributed equally to this work.

Abstract: This article describes the study and digital implementation of a system onboard a TMS 3208F28335 ® DSP for vector control of the bearing motor speed with four poles split winding with 250 W of power. Smart techniques: ANFIS and Neural Networks were investigated and computationally implemented to evaluate the bearing motor performance under the following conditions: operating as an estimator of uncertain parameters and as a speed controller. Therefore, the MATLAB program and its toolbox were used for the simulations and the parameter adjustments involving the structure ANFIS (Adaptive-Network-Based Fuzzy Inference System) and simulations with the Neural Network. The simulated results showed a good performance for the two techniques applied differently: the estimator and a speed controller using both a model of the induction motor operating as a bearing motor. The experimental part for velocity vector control uses three control loops: current, radial position, and speed, where the configurations of the peripherals, that is, the interfaces or drivers for driving the bearing motor.

Keywords: bearingless; DSP; induction motor; radial position control

check for updates

Citation: Dantas Neto, J.R.; Lopes, J.S.B.; Fonseca, D.A.D.M.; Garcia, A.R.G.; Ferreira, J.M.d.S.; Villarreal, E.R.L.; Salazar, A.O. Artificial Intelligence for the Control of Speed of the Bearing Motor with Winding Split Using DSP. *Energies* **2024**, *17*, 1029. https://doi.org/10.3390/en17051029

Academic Editors: Zbigniew Hanzelka, Daniel Morinigo-Sotelo, Grzegorz Sieklucki and Tomasz Drabek

Received: 20 December 2023
Revised: 16 January 2024
Accepted: 12 February 2024
Published: 22 February 2024

Copyright: © 2024 by the authors. Licensee MDPI, Basel, Switzerland. This article is an open access article distributed under the terms and conditions of the Creative Commons Attribution (CC BY) license (https://creativecommons.org/licenses/by/4.0/).

1. Introduction

Victor in [1] analyzed the feasibility of using a conventional induction machine as a split-winding bearingless motor. He performed position and current control of the machine; however, he observed that radial position control was not satisfactory for speeds below the rated limit. In recent years, Ref. [2] studied the replacement of PID controllers for radial position control with controllers based on fuzzy logic. Noting the strong nonlinear and parameter-varying characteristics of induction motor bearings, he analyzed the contribution of Fuzzy controllers on transient and permanent regime performance. In order to reduce the number of equipment needed for machine control, Ref. [3] optimized the structure of the motor bearing by proposing a new way to connect the coils in the machine stator. In [4], the machine's performance operation with a conventional state estimator and a neural state estimator was compared.

Speed control operating with the bearing motor was studied by [5,6]. The Artificial Neural Networks (ANN) technique was chosen. The ANFIS technique was investigated and studied by [7–9]. The adaptive neuro-fuzzy in motor studied by [10,11]. The speed control

operating with the bearing motor was evaluated by comparing the implementation of classic PI control with an artificial intelligence technique. Thus, the Artificial Neural Networks (ANN) technique was chosen to replace the classic PI control technique. The first step in implementing ANN was choosing the data set, the ANN input data are the mechanical speed and the mechanical speed error. The ANN output data is the torque current.

This work aimed to study and implement the artificial intelligence technique applied to vector speed control for the split wound type bearing motor based on the induction motor. The aim was to investigate and simulate the intelligent ANFIS techniques and Neural Networks to evaluate the performance of the motor-bearing in the following conditions: operating as an estimator and as a speed controller. In the experimental part, the TMS3208F28335 DSP was used to integrate the control algorithm with the current, position, and speed interfaces, by composing a cascade system. The intelligent technique implemented was the Neural Network, which acted as a speed controller. The position and mechanical speed results were compared with the PI speed controller and the Neural Controller. The control algorithm implemented in the TMS320F28335 DSP was developed in ANSI C programming language. The motor-bearing system is located in the Computer and Automation Engineering Laboratory (LECA) at UFRN.

On the other hand, we have the following articles. In [12], it is presented that crack is a common fault of rotor systems. The research on crack fault detection methods is mainly divided into numerical and experimental studies. In [13], the article classifies the dynamic response of rolling bearings in terms of radial internal clearance values. The value of the radial internal clearance in rolling-element bearings cannot be described in a deterministic manner, which shows the challenge of its detection through the analysis of the bearing's dynamics. In [14], it is presented that traditional machine learning prediction methods usually only predict input parameters through a single model, so the problem of low prediction accuracy is common.

The article describes the implementation details of controllers that provide the operation of the bearing motor. The system is made up of current, radial rotor position, and speed, which operate in a cascade. Control loop implementations started with the loop from the innermost (fastest) control to the outermost (slowest) loop, following the sequence: current control, position control, and speed control. Speed and position controllers are responsible for the generation of reference currents for current control. Other articles dealing with the topic of Bearingless Induction Motor are listed below [15–20].

The article has the following sections: In Section 1, the introduction is presented. In Section 2, simulations of the techniques of Artificial Intelligence are presented. In Section 3, the design and analysis of the ANFIS System is presented. In Section 4, neural controller design and analysis are presented. In Section 5, the Experimental Arrangement is presented. In Section 6, the control structure in the bearing motor cascade is presented. In Section 7, position control is presented. In Section 8, radial forces generation is presented. In Section 9, experimental results are presented. Finally, in Section 10, it is presented conclusions.

2. Simulations of the Techniques of Artificial Intelligence

This section introduces vector modeling of the induction machine working as a bearing motor. The characteristics have detailed the design of the Neuro-Fuzzy Estimator and the Neural Controller. The results showed a good performance for the two applied techniques: as an estimator and as a speed controller, both of them are models of the induction motor operating as a bearing motor.

The evaluation of artificial intelligence techniques uses the diagram of blocks of Figure 1. The neural controller replaced the green block represented by the Proportional-Integral, and the estimator conventional represented by the orange block by ANFIS.

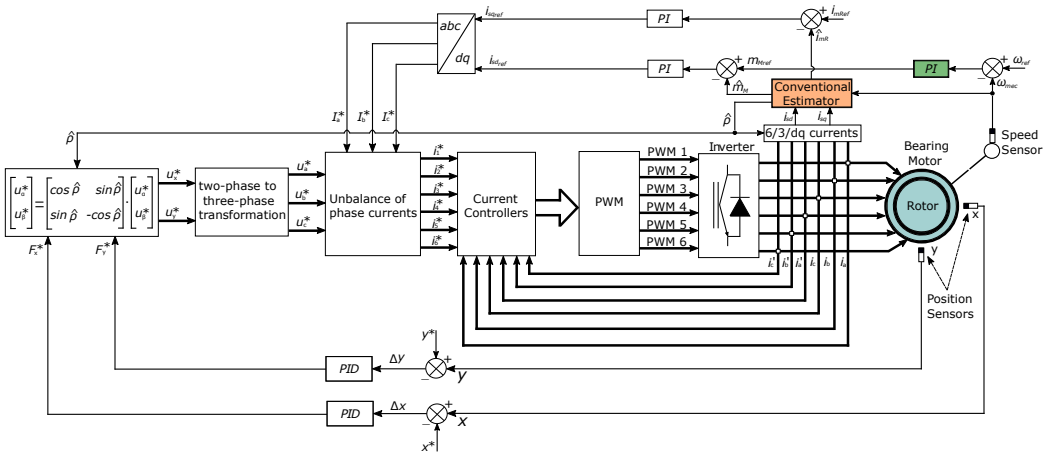

Figure 1. Block diagram of the proposed simulated system.

The block diagram in Figure 1 presents the system's complete structure adopted in the computer simulation stage. The modeling described in the next section and the other topics describe the main parts, requirements, and restrictions for the system to function as a bearing motor (blue block).

2.1. Three-Phase Induction Bearing Motor with Coil Divided

The proper operation of a bearingless machine requires control of the position, rotation, and torque of the rotor shaft. Table 1 presents some parameters obtained through tests performed in the laboratory [1] and adopted in this work for the simulations and obtaining the results.

Table 1. Motor Parameters and Characteristics.

Symbols	Description	Values
Pnom	Rated power	3.70 kW
Wmec	Rated Speed	1715 RPM
Tnom	Rated voltage	380 V
Np	Pole Pair Number	2
R1	Stator Resistance	1.182 Ω
R2	Rotor Resistance	1.42 Ω
J	Inertia moment	0.00995 kg·m^2
Ls	Stator Inductance	6.56 mH
Lr	Rotor Inductance	6.56 mH
Lm	Magnetization Inductance	0.14 H
r_{fe}	Core loss	891.2 Ω
g_0	Gap size	0.25 mm

The machine's structure adopted as a reference in this work has three phases, four poles, and utilizes the squirrel cage rotor; the coils are connected in series to form a phase group, and each phase group has two diametrically opposite coils, according to Figure 2. Figure 2 shows the distribution of the coils in the stator and the currents in each half group of the winding for the bearing motor used in the research. Figure 2 shows the stator winding distribution, where there is a 120° phase shift angle between each phase group axis. Figure 2 below describes the unbalance of the currents for the position control. In order to reduce the system's complexity, it was considered that the rotor be centered for the simulations. Note that i_{a1} is the stator current, and i'_{a1} represents the rotor current.

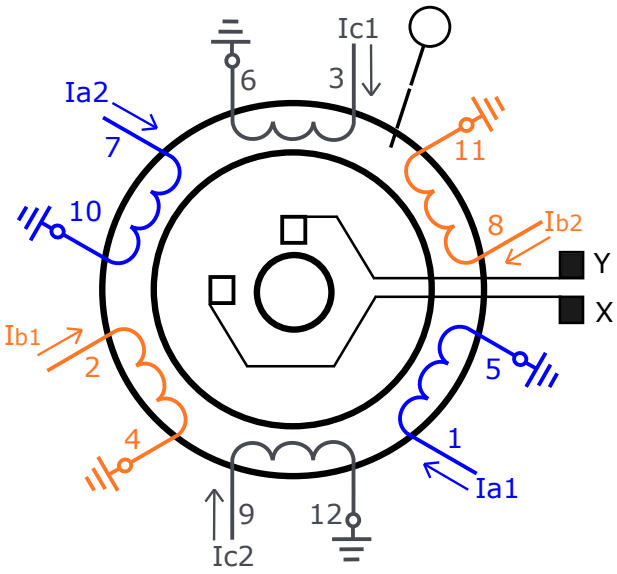

Figure 2. Stator coil layout.

2.2. Description of Artificial Intelligence Techniques Applied to the Bearing Motor

The implementation of artificial intelligence techniques took into account consideration of some criteria for the simulation. Use MATLAB for the implementation of the proposed system in Figure 1.

2.3. ANFIS Estimator

The conventional estimator adopted in the simulations was compared with the ANFIS estimator, and the training process using a 60-s training time interval, and variations of parameters were imposed considering the following criteria:

- Successive ascending and descending steps were applied between 0 and 2000 rpm (reference speed ranges);
- Variation of rotor time constant (every 2 s, so random values ranging from 0–20% concerning the nominal value of the constant);
- Every 5 s, increasing and decreasing variations were applied load of 0.05 N·m (load torque variation); This criterion was based in [21].

2.4. Neural Controller

The Neural Controller replaces the PI Speed controller in Figure 1. The data collection for training the neural network followed some criteria:

- The training process used a training time interval 60 s;
- Successive ascending and descending steps were applied between 600 and 1900 rpm (random variations of reference speeds);

3. Design and Analysis of the ANFIS System

The structures adopted in the Neuro-Fuzzy estimator were based on two estimators, one for estimating the magnetizing current and the other for estimating the rotor flux. The ANFIS 1 estimator uses the following inputs: the direct field current i_{Sd} and the delayed magnetizing current, and as output, the magnetization current. The ANFIS 2 uses the following inputs: mechanical velocity quadrature current i_{Sq} angular velocity as output estimated after discretization $d\hat{\rho}$.

In order to find the best configuration, it was performed several training with different parameters to obtain better criteria for the simulations according to Tables 2 and 3.

Table 2. ANFIS 1 Parameters.

Pertinence Functions	Epoach	Training Error	Validation Error
2	50	0.0558002	0.00813261
3	150	0.0488926	0.00815185
3	300	0.0409925	0.01109080
5	500	0.00175787	0.00781050

Table 3. ANFIS 2 Parameters.

Pertinence Functions	Epoach	Training Error	Validation Error
2	50	0.00406290	0.00489893
3	150	0.00533958	0.7491140
3	300	0.00448118	0.3522810
5	400	0.00359959	0.3302490

The criteria adopted in both estimators were 300 times for training and zero-tolerance error.

Figure 3A illustrates the Fuzzy surface obtained as a result of quadrature and magnetization current training. It is deduced that the linear result obtained is due to the centered rotor. Figure 3B illustrates the Fuzzy nonlinear surface obtained due to speed training mechanics and quadrature current.

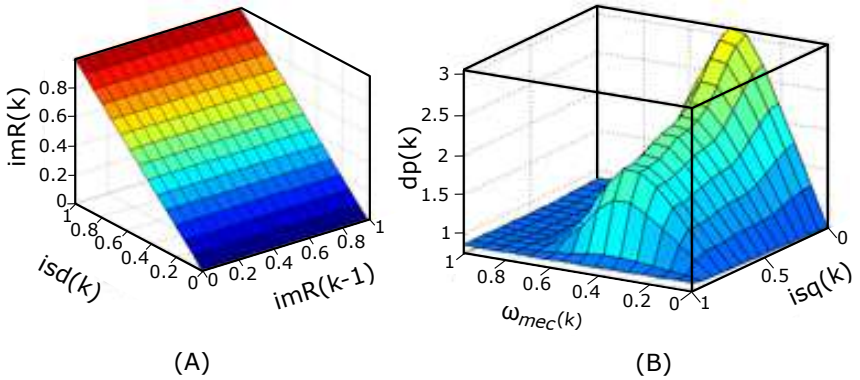

Figure 3. (**A**)—Fuzzy Sugeno Surface—ANFIS 1 and (**B**)—ANFIS 2.

Figure 4 illustrates the behavior before and after training to adjust the memberships: i_{Sq} and i_{mR} the curves [blue, green and red] represent the rules generated by ANFIS and {in1mf1, in1mf2 and in1mf3} are the memberships generated by ANFIS 1 and by ANFIS 2 are {in2mf1, in2mf2 and in2mf3}.

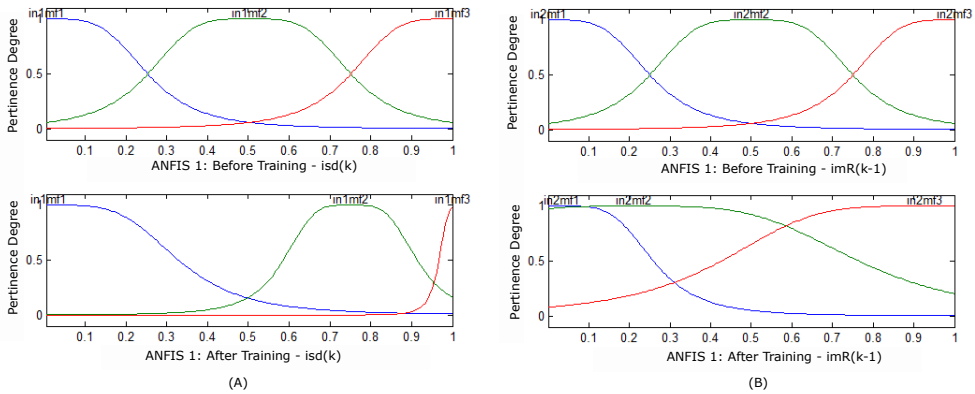

Figure 4. (**A**) Pertinences before training and after $-i_{Sd}(k)$; (**B**) Pertinences before training and after $i_{mR}(k-1)$.

It is observed that after the end of the training, the pertinence functions of Figure 5 were adjusted for each input of estimator 1 of Figure 3A. With the result of the training of the ANFIS 2 estimator, the membership settings for the entries were obtained. Figure 5 illustrates the behavior before and after mechanical speed training.

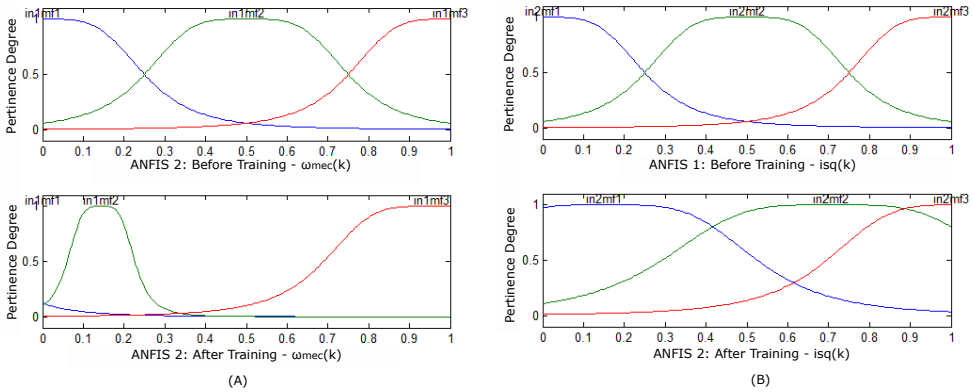

Figure 5. (**A**) Pertinences before training and after $-\omega_{mec}(k)$; (**B**) Pertinences before training and after $i_{Sq}(k)$.

Figure 5A shows the cancellation of membership already in Figure 5B there was no cancellation of membership, but a distribution of the same. These elimination and distribution results are pertinent to the Neuro-Fuzzy training.

Results of Simulations with the ANFIS Estimator

The simulations were run in the range of 0 to 20 s. The result shown in Figure 6 shows the mechanical speed of the motor simulated subject to the following reference changes 680, 1800, and 900 rpm, and then a perturbation at the instant 10 s is applied. The disturbance was an application of a load torque with a nominal value of 5.4 N·m.

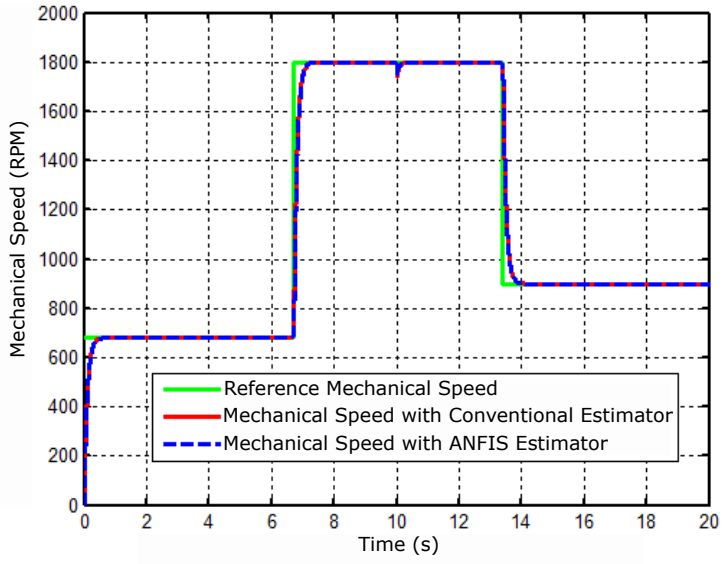

Figure 6. Comparative result of mechanical speed with estimators.

Figure 7 shows the behavior of the electrical torque in the conditions imposed in the simulation with conventional estimators and with the Neuro-Fuzzy estimator.

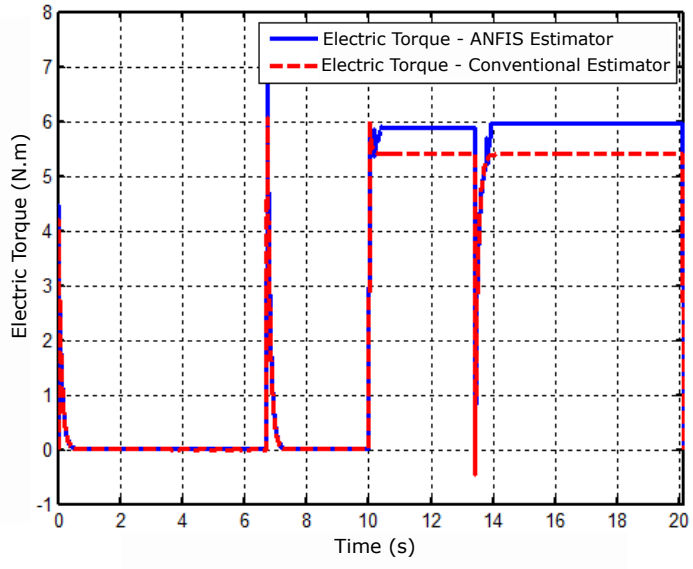

Figure 7. Electrical torque response operating under simulation conditions.

Figure 8 shows the behavior of the angular position with a zoom in an operating range of 0 to 0.2 s, which is observed in these results from the $\rho(k)$ timing for the estimators.

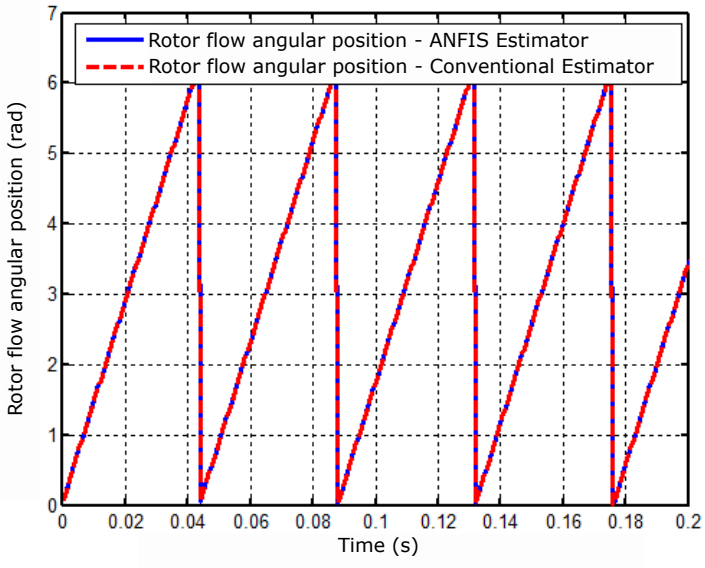

Figure 8. Angular position result of the rotor flux.

4. Neural Controller Design and Analysis

The neural structure used the three inputs: mechanical speed—wmec(k), error(k) current error; and the previous error (k-1) and as an output torque reference (nM_{ref}) for the torque controller. The process of training was carried out in offline mode, and its collection used 12,000 points for the input and output pairs, with a mechanical speed variation of 600 to 2000 rpm, randomly. Table 4 presents the parameters structures of the Neural Network, in which the convergence of the training process occurred in 841 epochs.

The topology in Table 4 was chosen after several performance tests with a different number of layers and neurons per layer, the algorithm of chosen training was the Levenberg–Marquardt. Figure 9 shows the error curve obtained with network training neural.

Table 4. Neural Network Parameters.

Network Architecture	Multilayer Perceptron
Training type	Supervised-offline
Layers number	3
Input layer neurons	3
1st hidden layer neurons	10
Output layer neurons	1
Training algorithm	Levenberg–Marquardt backpropagation
Learning rate	5×10^{-2}
Epochs number	841
Training error	9.4197×10^{-7}
Hidden layer activation function	Hyperbolic tangent
Output layer activation function	Linear

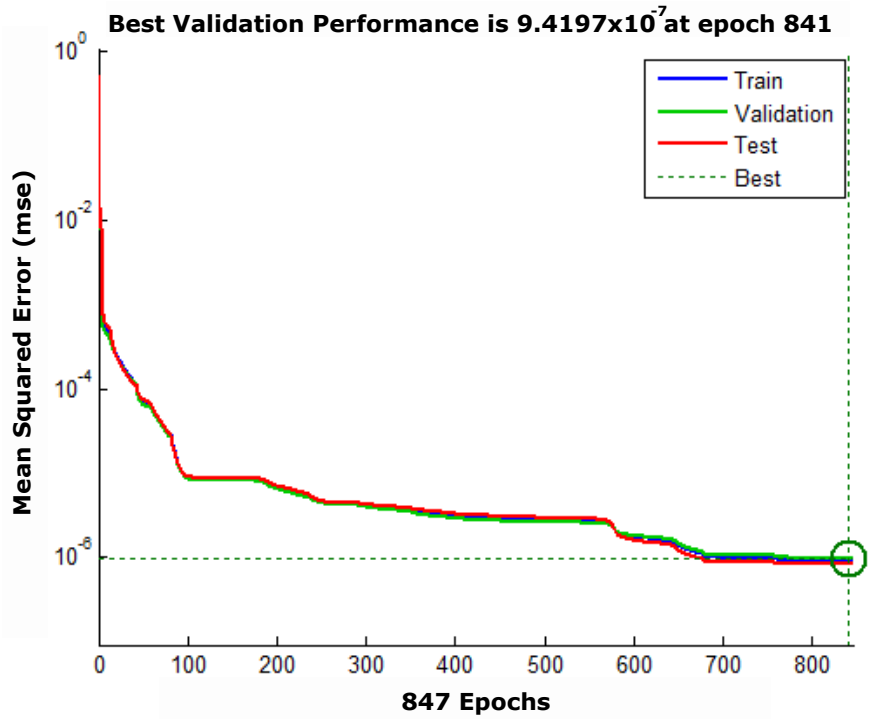

Figure 9. Mean squared error for training (9.4197×10^{-7}) with 847 epochs.

Figure 10 shows the performance of training, validation, and assessed tests resulting from the training.

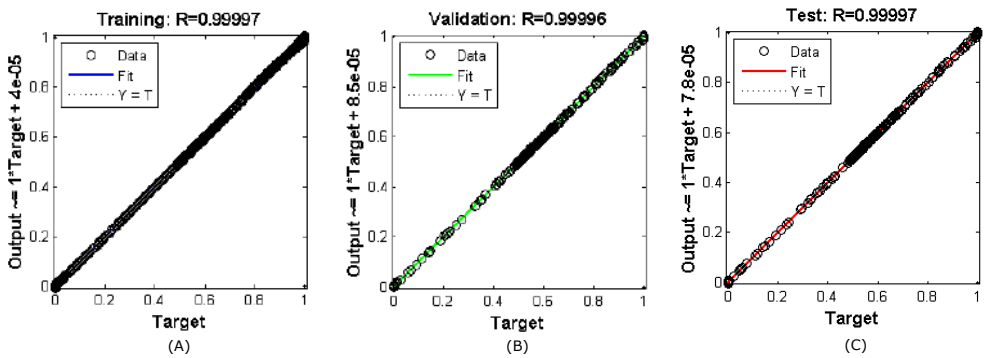

Figure 10. Results of training (**A**); validation (**B**); and Neural Network tests (**C**).

Figure 10 shows the R parameter at the top. This parameter indicates the relationship between the output and the target, varying between 0 and 1. The closer to 1, the better the prediction. After training, the weights were adjusted, and the neural network simulation replaced the PI control in Figure 1.

Results Neural Network Simulations

The simulations were run from 0 to 10 s. The results shown in Figure 11 show the mechanical speed of the motor simulated subject to the following reference changes: 1200, 1800, and 1500 rpm.

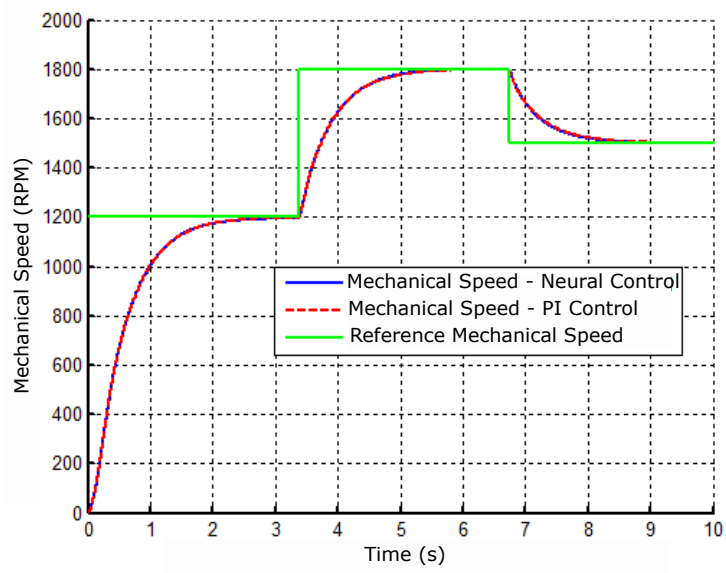

Figure 11. Comparative result of the mechanical speed with the controllers: neural and PI.

Figure 12 shows the behavior of the angular position with a zoom-in operating range from 0 to 0.4 s. It is observed in these results that the $\rho(k)$ timing for the estimators.

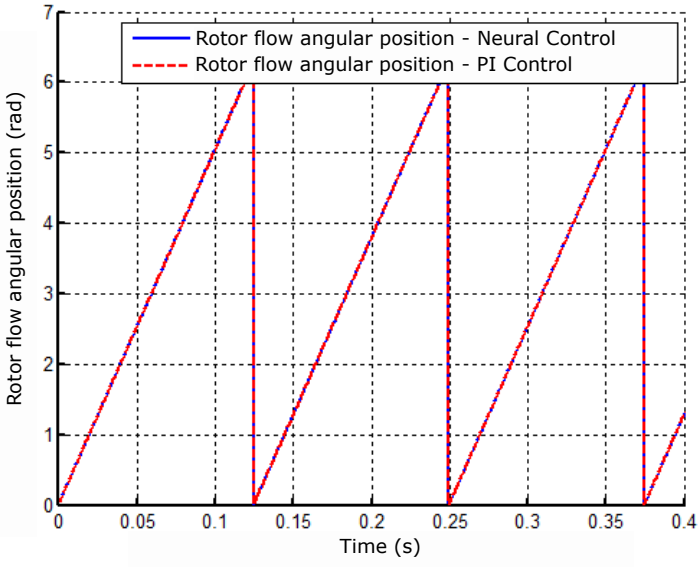

Figure 12. Angular position result of the rotor flux with the neural controller and PI of velocity.

5. Experimental Arrangement

The 3.7 kVA three-phase induction motor received modifications to operate a bearing motor; for example: the configuration of the double star coils and the removal of one of the bearings from one end of the rotor shaft. This last modification caused problems in the work of [1], according to which the problem of eccentricities of the motor-bearing shaft caused when there is displacement of the rotor made it difficult to adjust the position controller gains. The orbits were designed by rotating the shaft manually and then translating it through the periphery of the air gap. According to [1], after installing the self-aligning bearing, the shaft started to produce several orbits when peripherally displaced. Figure 13 shows three possible orbits designed by moving the shaft peripherally in the housing box of the top bearing.

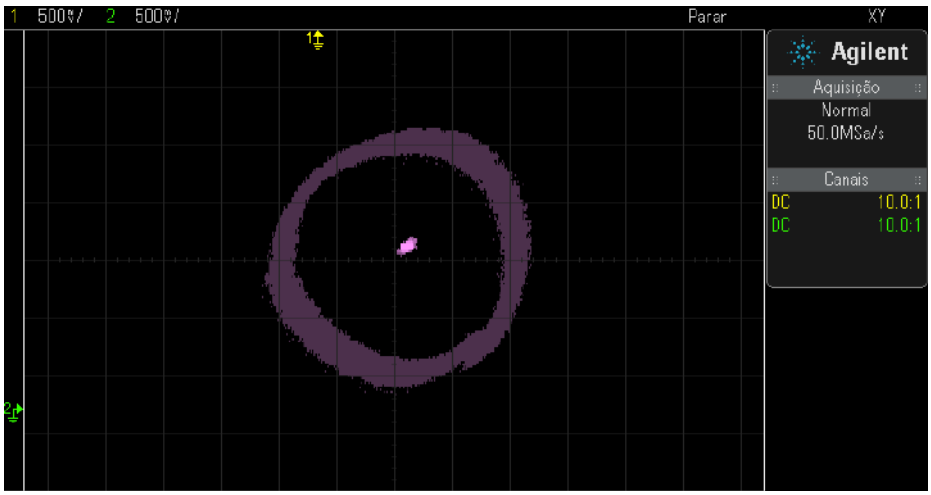

Figure 13. Motor-bearing shaft eccentricities.

After replacing DSP 2812 with DSP 28335, the empirical tuning of the Position PD controller was a difficult task. In order to correct the imbalance, the induction motor was disassembled, and the rotor shaft composed of the bearings and the disc was positioned in the lathe to perform roughing on the disc. In order to increase accuracy, the clock was used in thinning.

However, the eccentricity problem persisted, decreasing only the number of orbits. With the correction of the unbalance of the shaft in the lathe, the number of orbits went from three to two. This phenomenon made it difficult to tune in to the position controller. The solution found was the replacement of the conventional induction motor modified by the prototype of the bearing motor used, which was located in the Laboratory of Computer Engineering and Automation (LECA) at UFRN.

The bearing motor is a conventional induction machine adapted to operate without its mechanical bearings, having its radial positioning controlled by magnetic fields. The data used as parameters for the control of the machine were from the Table 5.

Table 5. Motor prototype parameters.

Parameters	Values
Rated power	1 Hp
Frequency	60 Hz
Poles numbers	4
Rated voltage	220/380 V
Rated current	3.02/1.75 A
Empty current	1.90 A
No load power	160.00 W
Resistance	7.38 Ohms
Stator Resistance per Phase	0.73 Ohms

After the replacement of the motor, it was necessary to configure the connection of the electric motor. For this, the coils and they were respective phases, because, the stator coils suffered some changes, they were divided in half as a strategy to carry out of control. In Figure 14, the location and identification of the groups of coils.

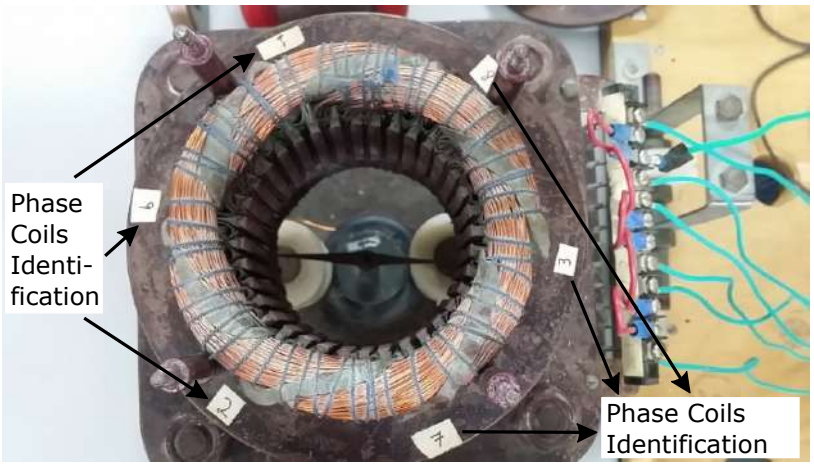

Figure 14. Coverless bearing motor with identification of the coil groups.

Based on the experiments, Figure 15 shows the arrangement of connections of these windings for operation as a bearing-less machine of the split coiled.

In order to facilitate the identification of phases and coil groups for name the *X* and *Y* axes for position control, it was necessary to perform two experiments with the aid of a compass. It is possible to check the compass orientation indicating the *Y* direction, shown in the Figure 16.

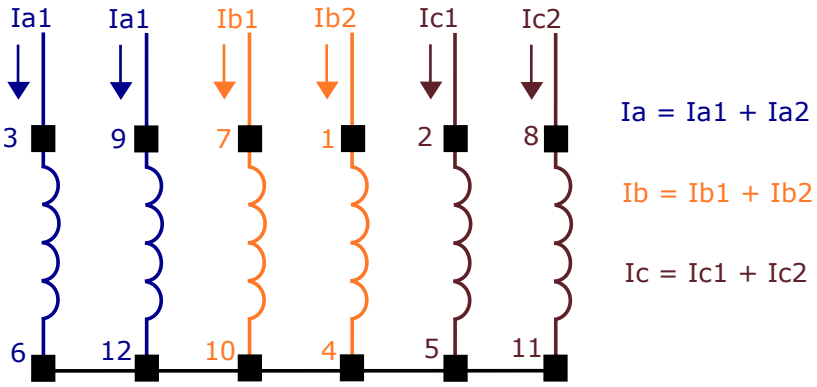

Figure 15. Motor-bearing winding connection arrangement.

The results of Figure 16 identified each coil group according to the sequence of Figure 15. For this, each group of coils was excited with continuous tensions.

However, it was necessary to adjust the position and speed of the related peripheral to allow effective control under the conditions imposed on the bearing motor. These modifications are presented in the following sections.

5.1. Radial Position Sensors

The radial position control for a bearing motor consists of making the rotor float; that is, without mechanical contact with the stator. Another advantage identified in replacing the bearing motor was the increase in the air gap, which went from 0.3 mm to 0.5 mm, which allows a larger range for empirical tuning of position control.

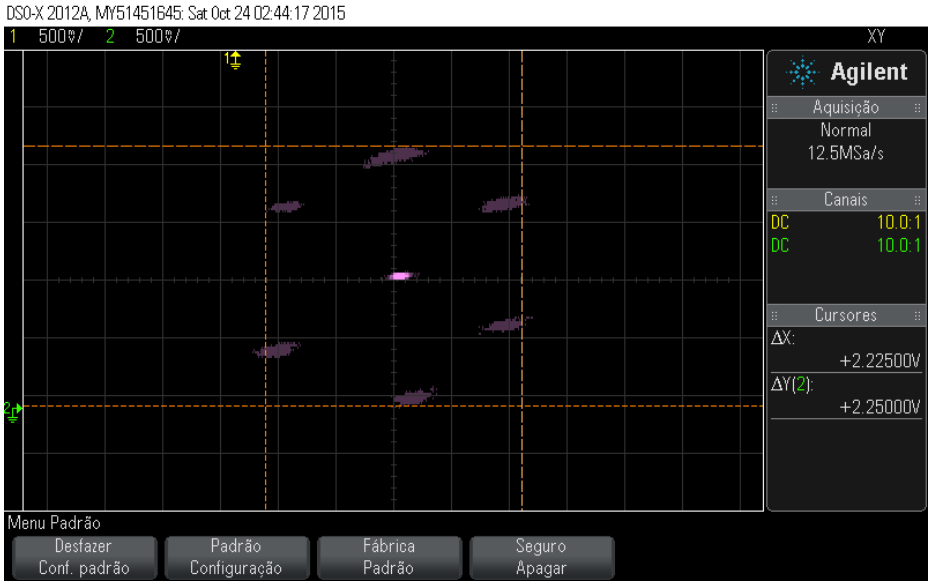

Figure 16. Bearing motor winding connection arrangement. The result identified each coil group according to the sequence of Figure 15.

5.2. Rotation Sensors

A rotating machine, when subjected to a torque on the shaft, in addition to needing more current in the coils, it also undergoes a variation in rotation. Thus, it is essential to know the rotation in real-time and the currents in the coils to implement a control machine rotation. In order to measure the rotation on the axis of the bearing motor, an encoder consisting of a disc was adopted uniformly perforated, a receiving transistor, and a light-transmitting LED structured infrared.

Among the peripherals that make up the bearing motor, such as those that were used in [1].

5.3. Complete System

The modulation of current in frequency inverters is performed through signals from the DSP control system. The current produced generates both torque and radial forces from rotor positioning. The mechatronic system, including each of the elements composed by the system and other components such as interfaces, sensors, and command devices, can be seen in Figure 17.

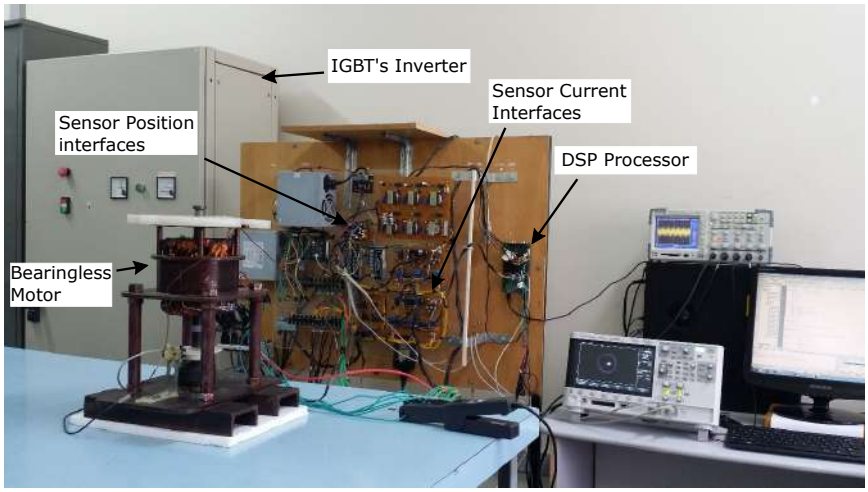

Figure 17. Mechatronic system with interfaces and the bearing motor.

This section dealt with the details of the changes made to the interfaces with the bearing motor. Basically, there were changes in the position and velocity sensors, and after adjustments, the system was able to implement the control structure and obtain the experimental results, which are exposed in the following section.

6. Control Structure in Bearing Motor Cascade

The following text describes the implementation details of the controllers that provide the operation of the bearing motor. The complete system comprises the current, position, and speed controllers, which operate in a cascade. The implementations of the control loops were started with the loop. from the innermost (fast) control to the outermost (slower) loop, following the sequence: current control, position control, and speed control. The speed and position controllers generate reference currents for current control. So after the action of controlling the currents of each coil is applied to the motor-bearing windings, the scalar PWM outputs are generated for the two three-phase inverters.

Current Control

The high performance in the drive of electrical machines depends mainly of the control technology implemented, being employed control techniques with current feedback in all applications. These techniques require fast response, high accuracy, and a performance high level. Current sensors, as well as other sensors used in the machine are important for the control in real-time, can impose changes necessary for the correct functioning of the machine. Current controllers must be of the Proportional-Integrative type (PI), they are simple to implement and manage to eliminate errors in regime [1]. The structure used for the control of current in this work was based on the module implemented by Texas (C28x Solar Library [22]). This module has the following characteristics: programmed output saturation; adjustment of independent weights on actions proportional and derivative; reset in anti-windup integrator; and a filter Programmable for a derivative action. However, the derivative action was annulled for this control, acting only on the proportional and integral actions.

The equation of the PID controller before saturation is described as Equation (1):

$$v_1(k) = K_p[u_p(k) + u_i(k) + u_d(k)] \tag{1}$$

Each term can be written as follows: Proportional term:

$$u_p(k) = K_r r(k) - y(k) \tag{2}$$

Integral term:

$$u_i(k) = u_i(k-1)K_i[r(k) - y(k)] \tag{3}$$

Derivative term with filter:

$$u_d(k) = K_d[c_2 u_i(k-1) + c_1 e(k) + c_1 e(k-1)] \tag{4}$$

Finally, the output with saturation is defined:

$$u(k) = \begin{cases} U_{max} : v_1(k) > U_{max} \\ U_{min} : v_1(k) < U_{min} \\ v_1(k) : U_{min} < v_1(k) < U_{max} \end{cases} \tag{5}$$

In these, $r(k)$ a reference; $y(k)$ a control variable; $u_d(k)$ term derivative; $u_i(k)$ integrative term; $u_p(k)$ proportional term; K_r, the weight referring to reference; K_p the proportional gain; K_d the derivative gain; c_1 the derivative filter coefficient 1; c_2 the coefficient of derivative filter 2; U_{max}, the maximum saturation limit; U_{min}, minimum saturation limit.

The control laws of Equations (1)–(5) were implemented in DSP 28335. The implementation is obtained from Texas Instruments, [22]. Six PI controllers operate in a closed loop inside the DSP interrupt to control the bearing motor current.

7. Position Control

For the implementation of position control, you must take into consideration the study by [1,21]. These works demonstrate the rotor positioning model and identify that the model is unstable in open mesh due to the presence of two poles, one in each semi-plane. The solution found for the system to become stable was the implementation of the Proportional-Derivative (PD) controller, which adds a zero which is positioned to attract the place of the closed-loop roots to the left half-plane. The control law implemented for position control was based on [1].

8. Radial Forces Generation

Signals u_α, u_β come from the position control. Then, they undergo a rotational transformation to the static orthogonal system and transform into u_x, u_y and lastly there is a coordinate transformation biphasic to triphasic, resulting in u_a, u_b u_c, observed, that the controller signals u_a, u_b u_c, after the transformations, they have added to the phase current references or subtracted in each half group of coils from phases A, B, and C, respectively, to control the restoring forces of the rotor position, (Equation (6)).

$$\begin{aligned} I_1^* &= I_a^* + u_a \\ I_2^* &= I_a^* - u_a \\ I_3^* &= I_b^* + u_b \\ I_4^* &= I_b^* - u_b \\ I_5^* &= I_c^* + u_c \\ I_6^* &= I_c^* - u_c \end{aligned} \tag{6}$$

In these equations, I_a^*, I_b^*, and I_c^*, are the imposed phase reference currents and I_1^*, I_2^*, I_3^*, I_4^*, I_5^*, I_6^*, are the reference currents for position control. Due to the nonlinearity of the system, the tuning of the controllers becomes difficult to obtain; however, the parameters of the controllers were determined empirically.

Vector Speed Control

The speed controller used is a PI (Proportional-Integral) with anti-windup, the feature that interrupts the integration process when output has already reached a maximum saturation value [23]. For the implementation of velocity vector control; initially, the structure of control of Figure 18 using flow estimator. The big advantage of this structure using this estimator is the presence of a small number of equations, minimizing the computational effort [24].

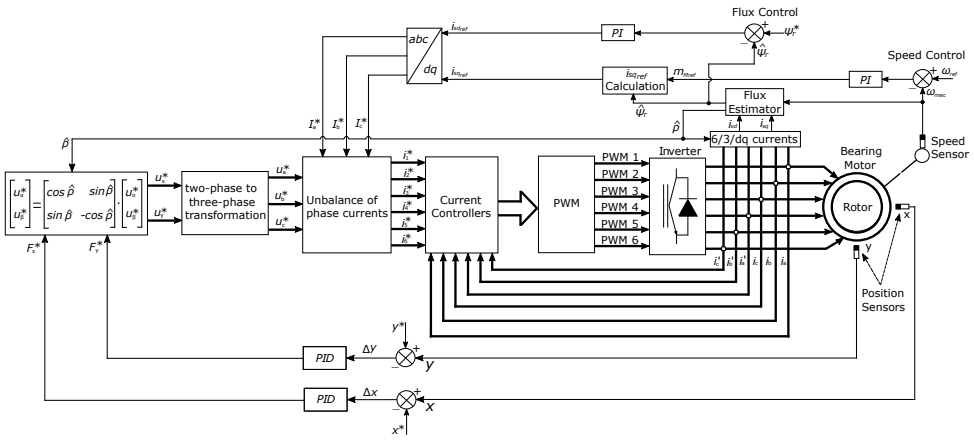

Figure 18. Control structure with flux estimator.

The flux estimator used in [24] is given by:

$$\hat{\lambda}_{est} = L_m i_{sd} \tag{7}$$

In this, $hat\lambda_{est}$, L_m the estimated flux; i_{sd} the mutual inductance.; i_{sd} the field current. Equation (7) is calculated from the field current i_{sd} and the inductance mutual L_m. Thus, the calculation of the torque current (i_{sq}) obtained from the Equation (8).

$$nM_{ref} = \frac{PL_m}{L_r}\lambda_r i_{sq} \tag{8}$$

here, nM_{ref} reference torque; L_r the inductance of the rotor; λ_r, the flux reference rotor; and P, the number of pole pairs. However, this structure was chosen for the following reasons: the difficulty of tuning in empirically the control loops, which consumed more time, and the fact of not having the necessary machine parameters to be used in Equations (7) and (8).

However, it was thought to obtain the parameters from laboratory tests, which were discarded due to the following disadvantages: A delay in the digital implementation of the control structure may be a physical problem with the engine, generating more time for its solution or maintenance. Therefore, the control system implemented for the vector control of speed of Figure 19 took into account two simplifications: impose a reference field current to not implement flow control and eliminate the current torque calculation, causing the control output go straight into Park, and Clarke's inverse transforms as torque investigation will not be taken into account. The structure of Figure 19 has three loops, the outermost being the Proportional-integral (PI) speed control, which controls the rotor shaft speed from the sensed feedback and whose output is the torque current isq_{ref} the Proportional-Derivative Integral (PID) controller for the positions referring to the x and y coordinates of the rotor, since, in practice, the added integral action should decrease the regime error. Position control is classified as a regulator, unlike the current control system, which is classified as a follower. Therefore, the last control loop is the current one, the innermost one, and quick response, with PI controllers for the six stator windings.

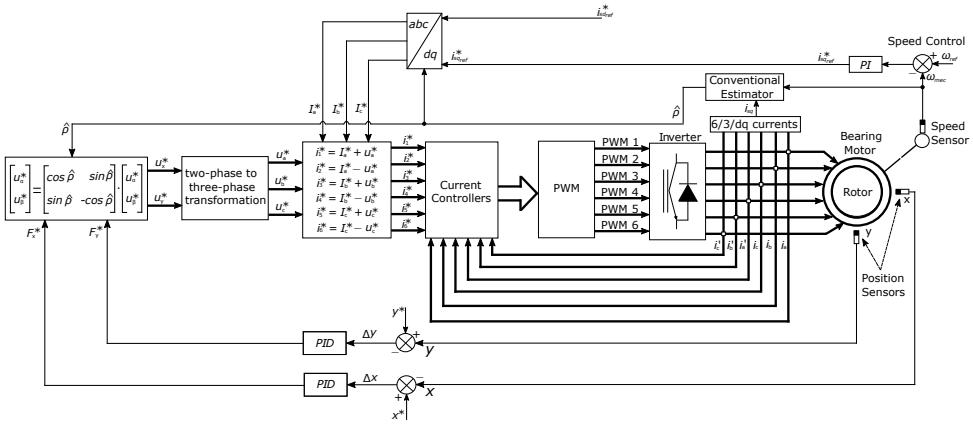

Figure 19. Bearing motor cascade control diagram.

This section allowed us to deduce the simplified control diagram and function for implementing velocity vector control. The choice is to discuss the current position and speed controllers that helped to define the chosen strategy. The next section presents the experimental results of each step of the cascade control loop of the bearing motor.

9. Experimental Results

The experimental results were obtained with the digital implementation of the control system in the motor-bearing using the DSP 28335. An artificial intelligence approach was implemented in the results of speed vector control. In addition, a comparison of the Proportional-integral velocity vector control with the neural controller.

9.1. Stator Currents

To validate the digital implementation of the current control, some experiments with the centralized rotor with the current PI control. The procedure followed the block diagram sequence in Figure 20, based on the block structure of Figure 19.

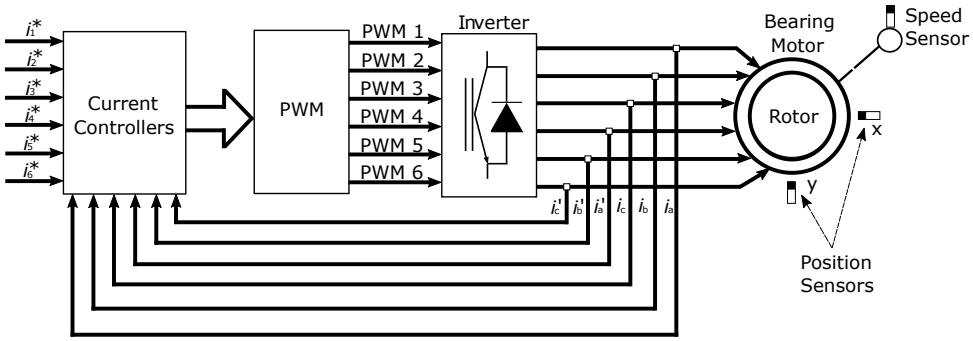

Figure 20. Motor-bearing current control.

Some experiments were carried out to validate the performance of the current PI controller. The first one was the response to several steps in the reference imposed on coil i_1 according to Figure 21. The PI controller parameters of current $K_p = 200$ and $K_i = 1.464844 \times 10^{-6}$ were empirically adjusted for obtaining the results and other experiments.

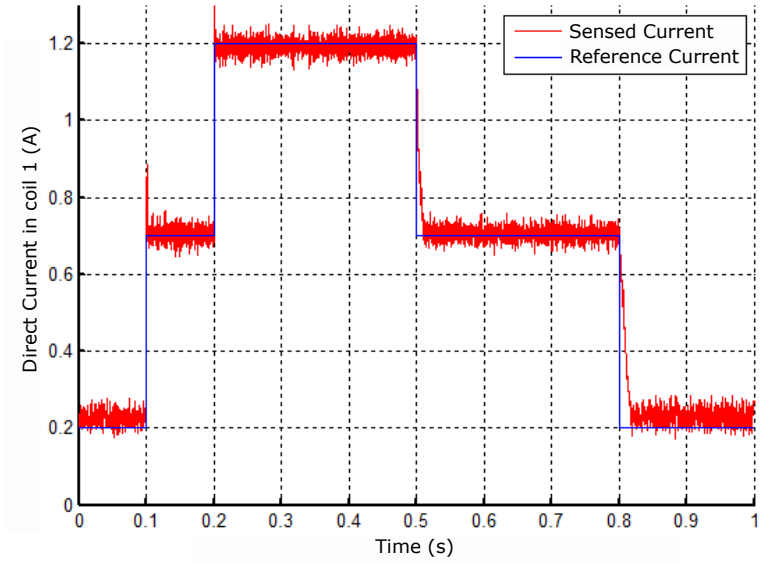

Figure 21. Response to the reference change in coil 1.

For this experiment, continuous currents were imposed with reference changes over 1 s interval of execution. Another result obtained was the current of sinusoidal reference, and we alternated it at a frequency of 60 Hz and with an amplitude equal to 1.5 according to Figure 22.

The experiments were carried out by changing the frequency and the reference range. Figure 23 shows the experiment obtained when the engine works at 15 Hz frequency with equal reference amplitude (Imax) to 0.8 A.

To evaluate the behavior of the bearingless machine operating as a induction and activating the six coils, it was necessary to perform two procedures: (1) fix the rotor shaft in the center so that it does not influence the dynamics of the experiment and operate with the rotor centered; (2) generate six streams of 120° offset references to generate the rotating field Equation (9).

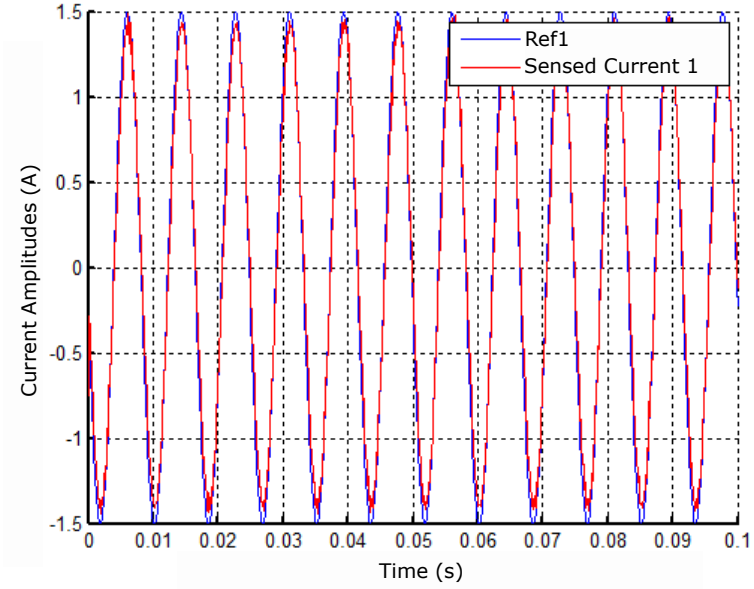

Figure 22. Response to sinusoidal reference in coil 1.

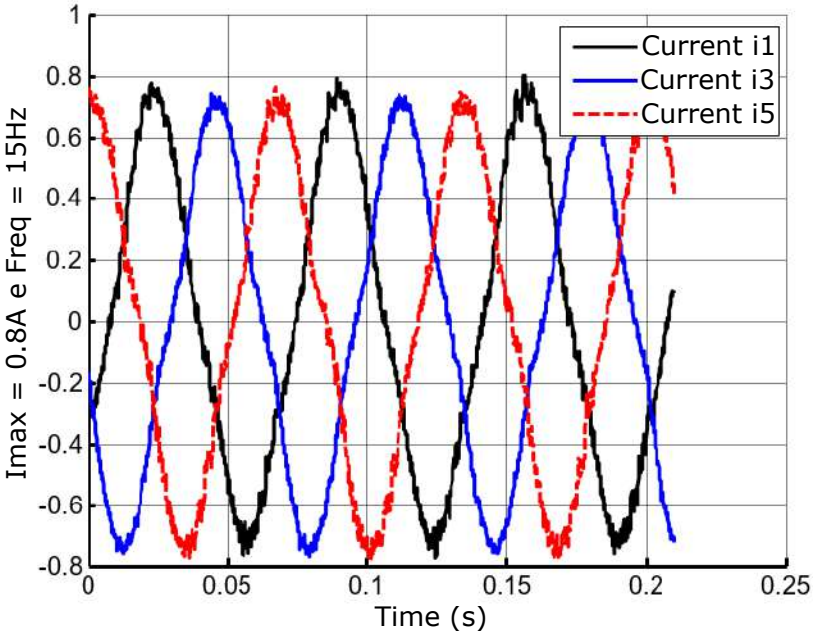

Figure 23. Lagged currents at 15 Hz frequency and 0.8 A amplitude.

$$\begin{aligned} i_1^* &= Imax * sin(wt + 0) \\ i_2^* &= Imax * sin(wt + 0) \\ i_3^* &= Imax * sin(wt - \frac{2\pi}{3}) \\ i_4^* &= Imax * sin(wt - \frac{2\pi}{3}) \\ i_5^* &= Imax * sin(wt + \frac{2\pi}{3}) \\ i_6^* &= Imax * sin(wt + \frac{2\pi}{3}) \end{aligned} \tag{9}$$

9.2. Radial Rotor Position

The results presented below were obtained with the control Proportional-Derivative-Integrative (PID) from some experiments. The results used the block diagram strategy of Figure 24 based on Figure 19.

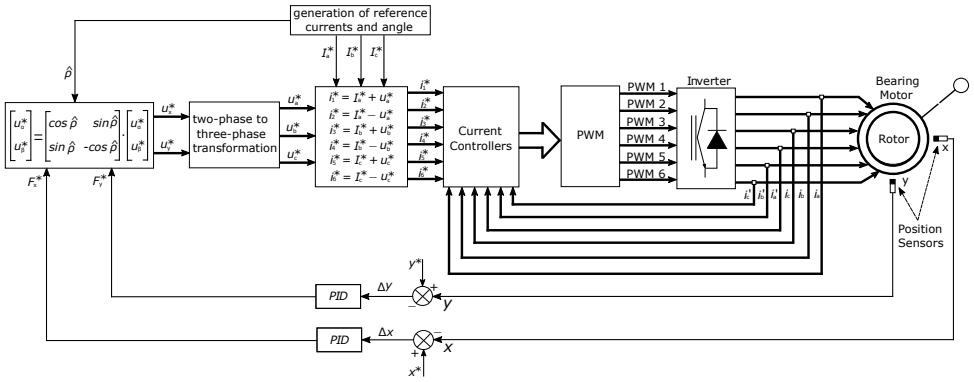

Figure 24. Cascade position control with motor-bearing current control.

After some empirical adjustments on the controller parameters, the gains obtained were: $K_{px} = 0.0005$, $K_{dx} = 0.028$, $K_{ix} = 1 \times 10^{-8}$, $K_y = 0.0005$, $K_{dx} = 0.06$, $K_{py} = 1 \times 10^{-8}$. An experiment was carried out with the controls of position acting independently, evaluating the behaviors of the X-axis and Y-axis. Figure 25 shows the response to a step variation for the position control along the X-axis.

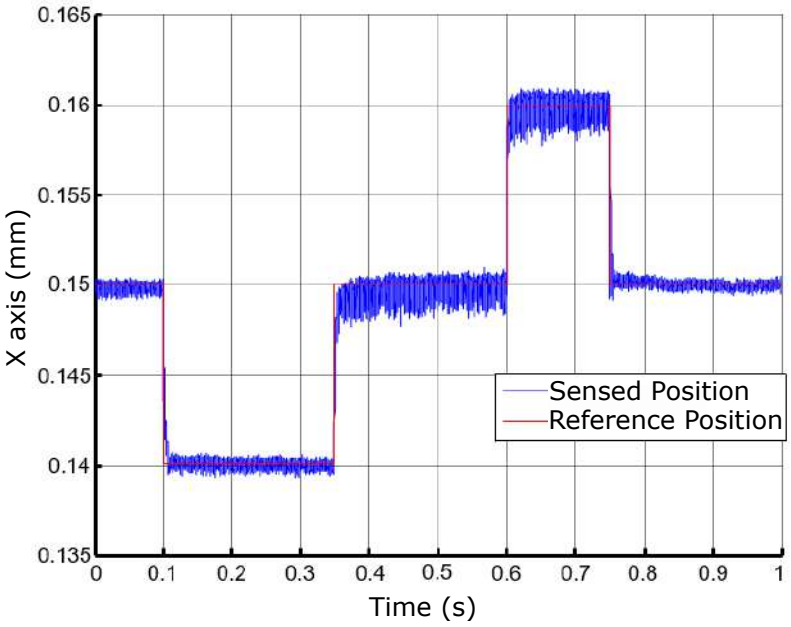

Figure 25. Position control results for the X axis.

Figure 26 shows the response to a step change for the control of position along the Y axis.

The results were collected in a steady state. The experiment performed operated at the frequency of 60 Hz according to Figure 27. The spot in the center of the figures represents the positions that the rotor has assumed in a given moment: the oscilloscope is in trace persistence mode.

In order to illustrate the dynamics of cascading control, the results considered an equal time window for the position controllers and the current operating at a frequency of 60 Hz. Figures 28–30 show the results of the cascading current and position controllers accordingly with the block diagram of Figure 24. The graphic of Figure 28A shows the reference currents, that is, the imposed currents I_a^*, I_b^*, and I_c^* for control of position, collected at an interval of 0.08 s.

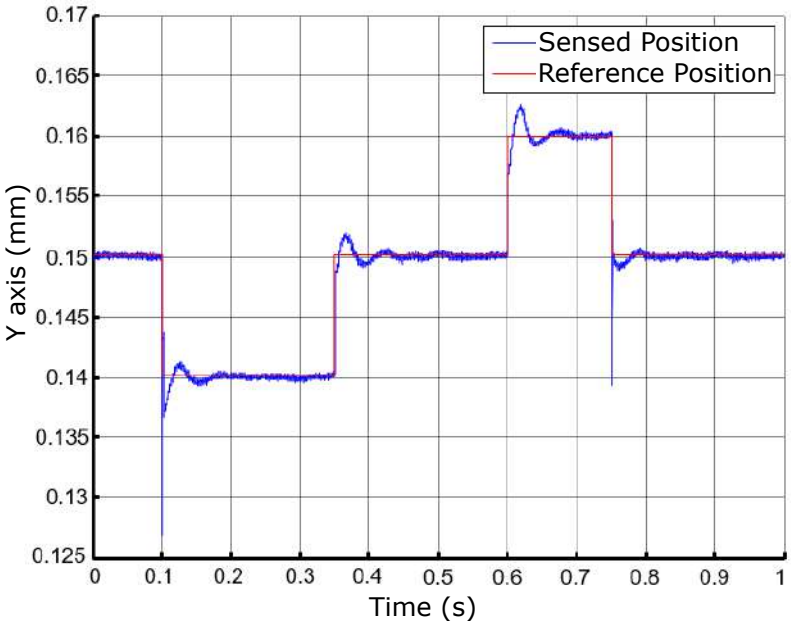

Figure 26. Position control results for the Y axis.

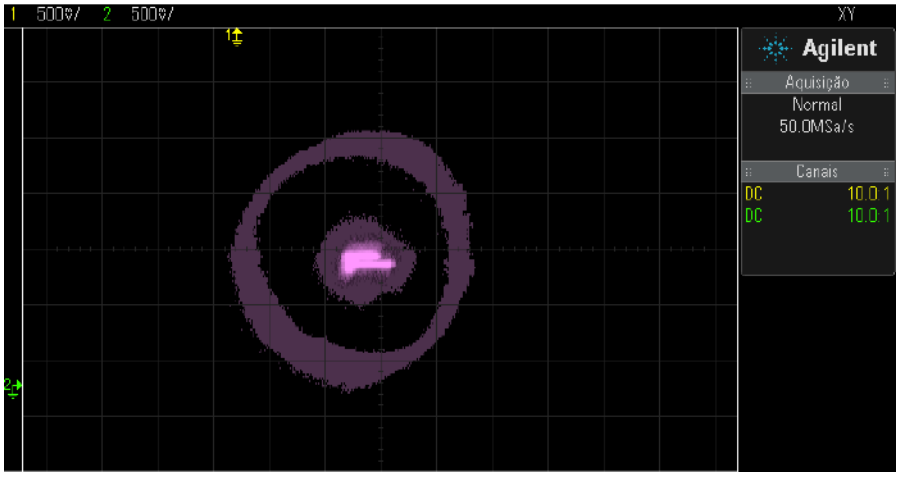

Figure 27. Position control results with a rotor scatter area for activation at 60 Hz.

The graph in Figure 28B, identified by the subtitles Ref1, Ref2 and Ref3, represents the composition of the reference currents I_a^*, I_b^*, and I_c^* with the signs from position controllers u_a^*, u_b^*, and u_c^*. Finally, the graph in Figure 28C represents the equivalent sensed currents in each phase. Figures 29 and 30 show the responses of the X and Y positions with their respective reading errors associated and control signals. There is a small change in the behavior of the sensed currents in Figure 28 at times close to 0.02 s, for example. This change is due to the control adjustment of the position of Figures 29 and 30 and observed in the control signals for the X and Y positions.

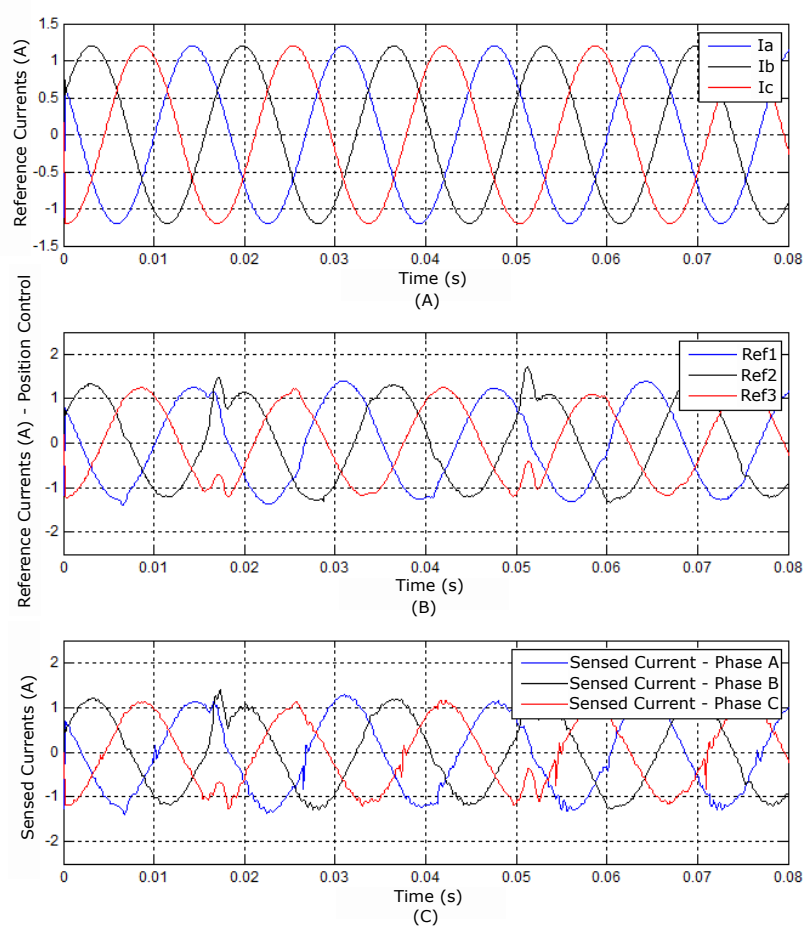

Figure 28. Results referring to (**A**) imposed, (**B**) controlled, and (**C**) sensed currents.

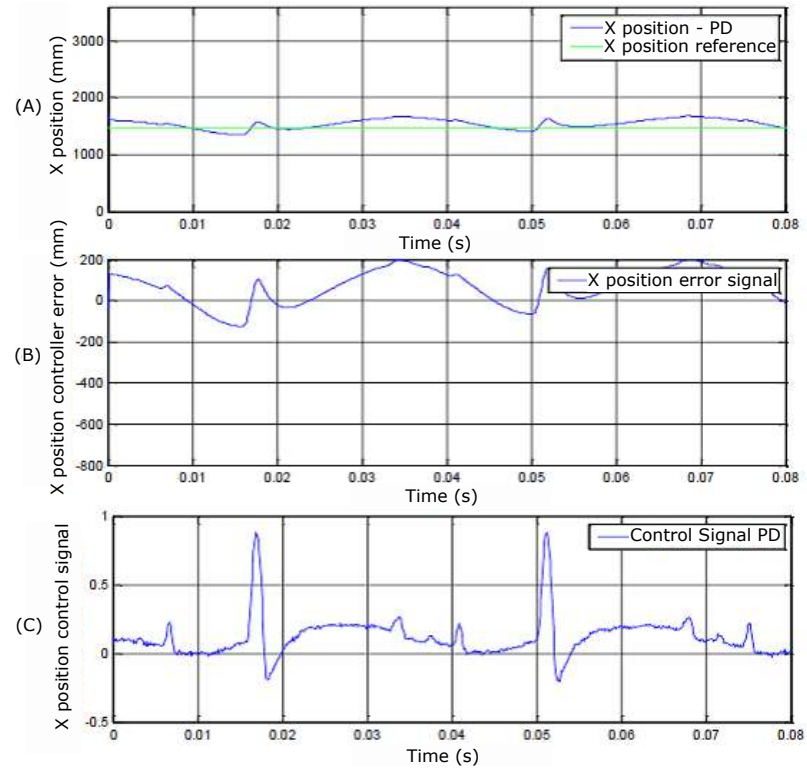

Figure 29. (**A**) *X* position, (**B**) controller error, and (**C**) control signals.

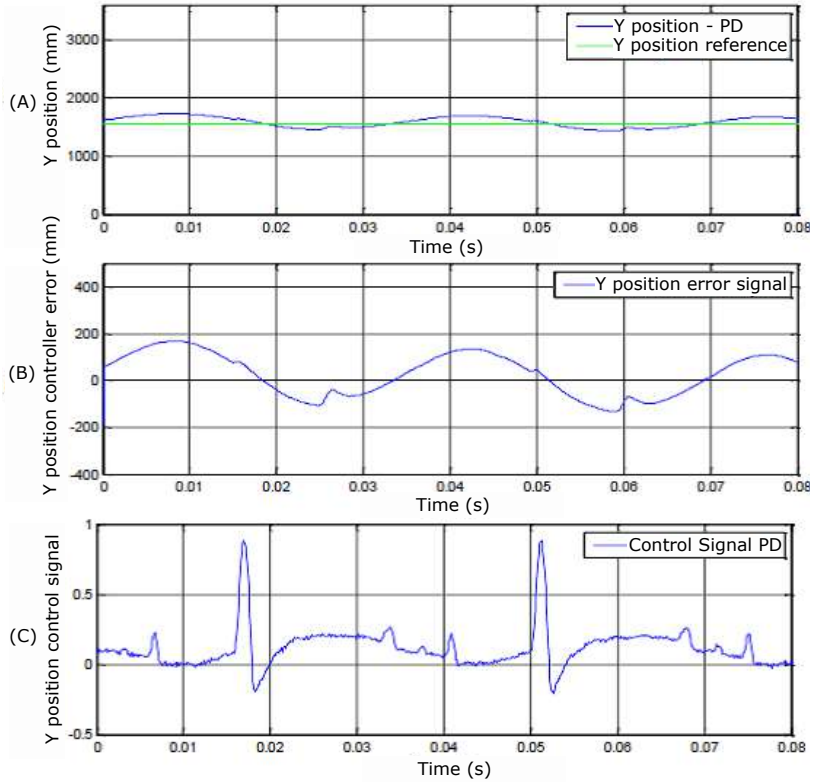

Figure 30. (**A**) *Y* position; (**B**) controller error; and (**C**) control signals.

9.3. Speed Control

The speed control operating with the bearing motor was evaluated by comparing the implementation of classic PI control with an artificial intelligence technique. The technique chosen was the Artificial Neural Networks (RNA) to replace the classic PI control. The ANFIS technique was investigated. However, due to the computational cost of its implementation, it was discarded.

The first step in implementing the ANN was choosing the data set for training and validation. The inputs are the mechanical speed (W_{mec}) the mechanical speed error $((Error_w))$ and the output is the current (Isq_{ref}). The input and output data pairs are used to adjust the internal parameters of ANN according to [25]. The RNA was configured fully connected. The database was developed with 20,200 samples, of which 70% of the data were used in training and 30% for validation. The training process was carried out in offline mode, and its collection used the input data with a variety of mechanical speeds randomly from 1% to 5% overrated speed 1800 rpm. Table 6 presents the structural parameters of the Neural Network, in which the convergence of the training process occurred in 104 epochs.

Table 6. New Neural Network Parameters.

New Network Architecture	New Multilayer Perceptron
Type of training	Supervised-offline
Number of layers	3
Input layer neurons	2
1st hidden layer neurons	10
Output layer neurons	1
Training algorithm	Levenberg–Marquardt backpropagation
Learning rate	5×10^{-2}
Epoch number	104
Training error	1.3909×10^{-5}
Hidden layer activation function	Hyperbolic tangent
Output layer activation function	Linear

The training algorithm chosen was the Levenberg–Marquardt, used in the Matlab toolbox for better accuracy; the topology Table 6 was chosen after several performance tests with a different number of layers and neurons per layer. The final choice led to considering the digital implementation and evaluating the processing time of the DSP. The more layers and neurons, the longer the processing time increases. Thus, the implemented structure analyzed the computational cost. Figure 31 shows the training performances, validation, and the evaluated test resulting from the training.

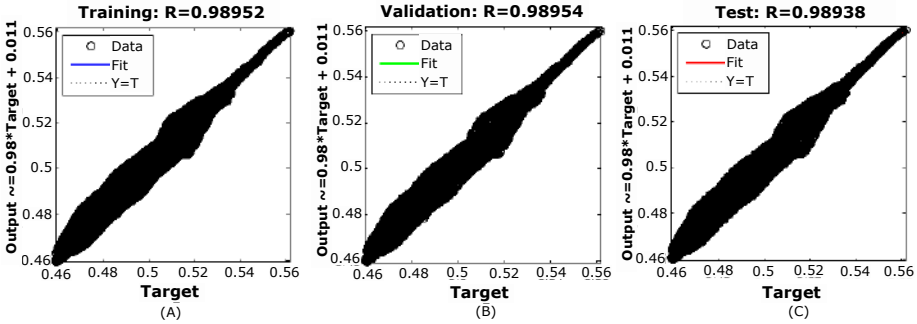

Figure 31. Result of training, validation, and testing of the Neural Network.

Figure 31 shows the R parameter at the top. This parameter indicates the relationship between the output and target, varying between 0 and 1. The more close to 1, the better the prediction. Figure 32 shows the training graph with the Mean Square Error (MSE).

After training, the weights and carried out two experiments to evaluate the functioning of the bearing motor operating with PI speed control with gains $K_{pw} = 0.01$ and $k_{pi} = 7.5 \times 10^{-5}$ and with the neural structure. The two case studies used the same RNA structure implemented.

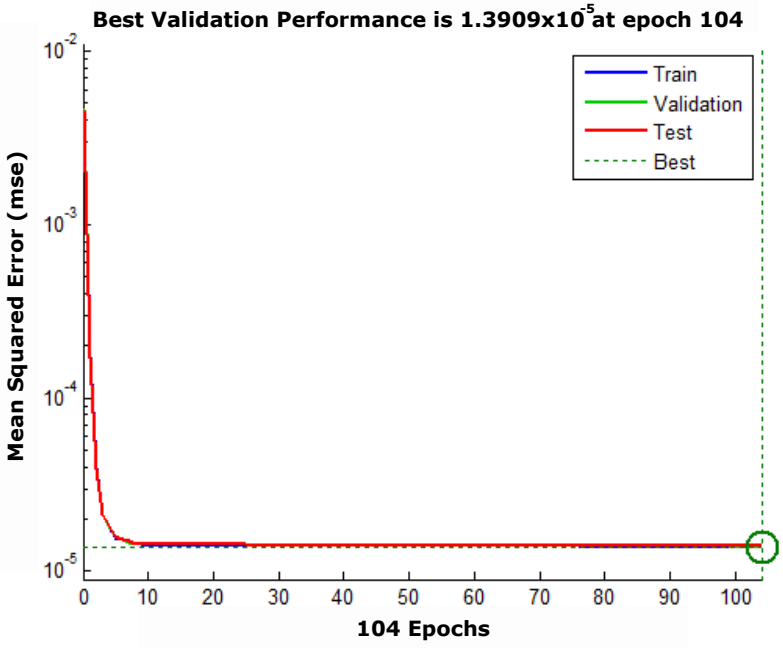

Figure 32. Mean squared error for training (1.3909×10^{-5}) with 104 epochs.

9.3.1. Case Study I—Ramp

The first experiment presents the system's behavior when being powered from rest to a rated speed of 1800 rpm. Figure 33 shows the mechanical velocity dynamics and the X and Y positions, respectively, in the function of time operating with the two controllers.

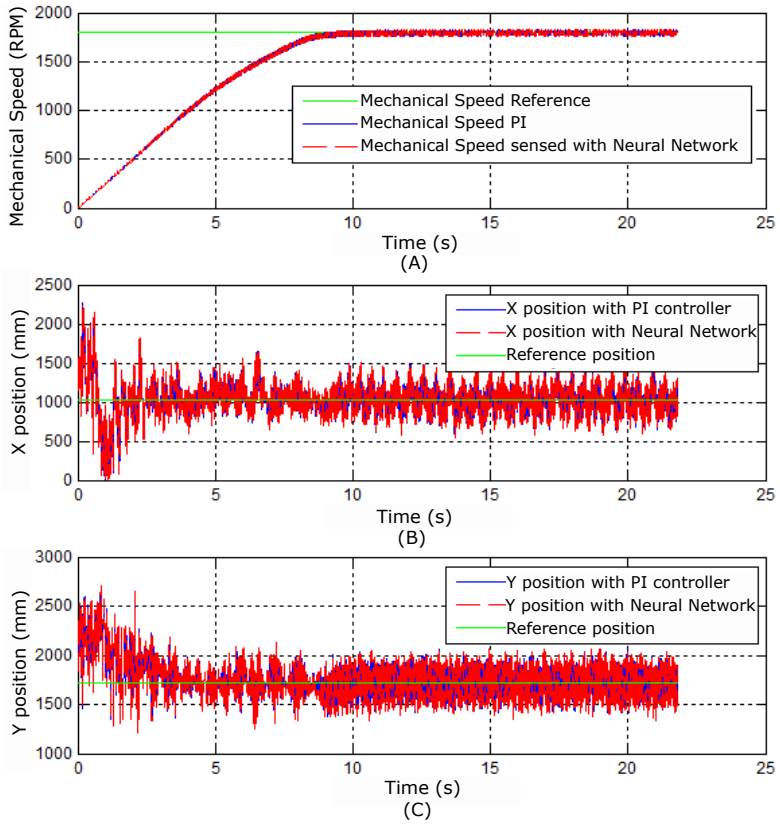

Figure 33. Mechanical speeds and X and Y positions for step speed reference constant.

The legends of the graphs in the experiments present, respectively, the references and the responses with the PI control and with control identified by the colors green, blue, and red. Figure 34 shows the control signal behavior for the implemented controllers.

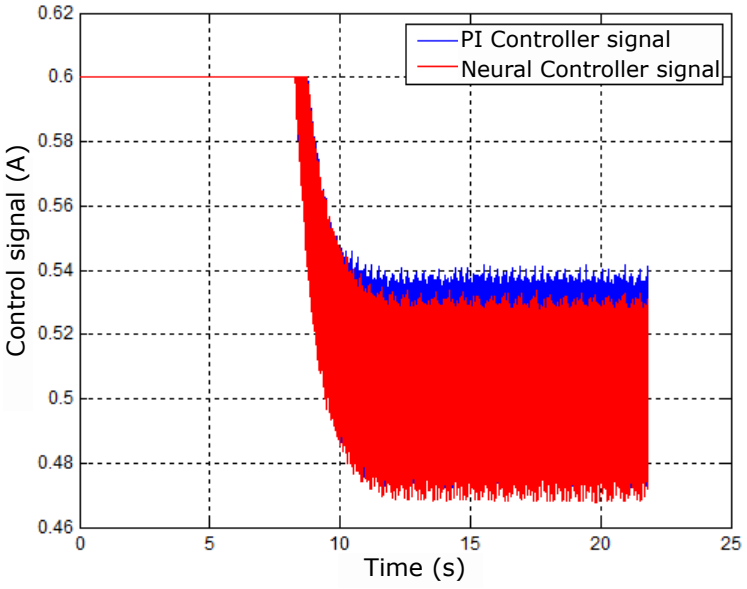

Figure 34. PI and neural control signals for step speed reference.

Figure 34 shows that the control signals are limited due to the motor constraints on the amplitude of 0.6 A, that is, a constraint on the speed control signal for bearing motor operation.

9.3.2. Case Study II—Step Variation

The second experiment presents the system behavior operating at the nominal speed of 1800 rpm with a variation of 5%, that is, operating at 1710 rpm and 1890 rpm. Figure 35 shows the behavior of the mechanical speed and the X and Y positions referring to the rotor position.

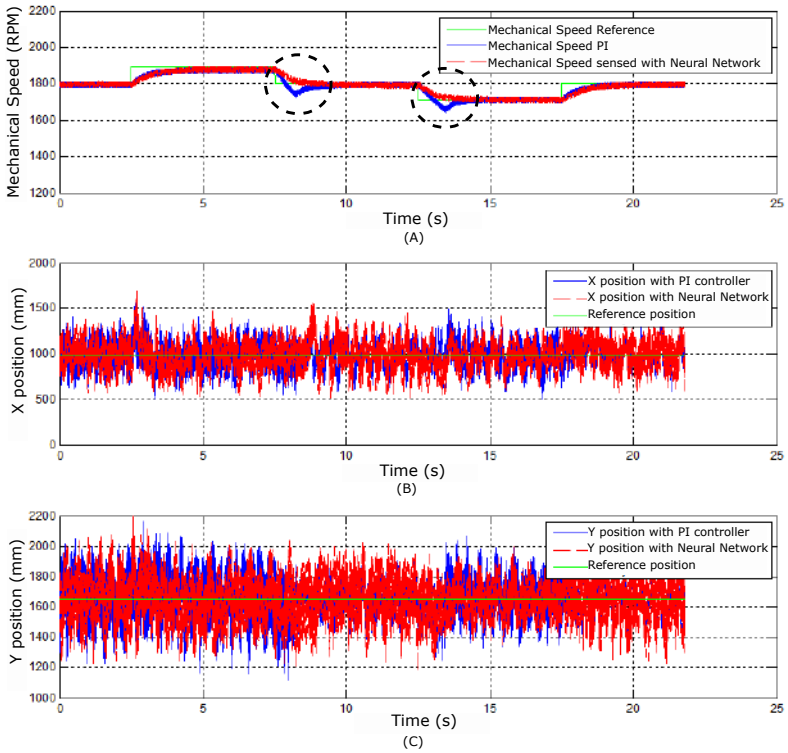

Figure 35. Mechanical speed and X and Y positions for step speed reference.

In this case, the presence of overshoots in the performance of the The PI controller was identified with dashed circles, which did not occur with the neural controller. This behavior can be seen in Figure 35 because there were higher amplitudes in the PI control signal compared to the neural control. Despite the variations of the control signal in Figure 36, it can be seen that the position control performed well because the X and Y signs did not suffer variation.

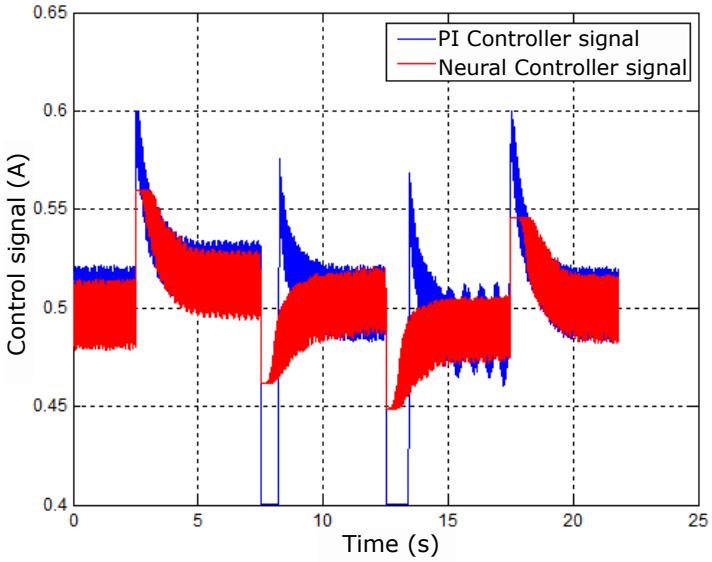

Figure 36. Control signals for step speed reference.

Figure 37 shows the errors of the controllers being acted on by the PI and neural controllers. There is also a difference in amplitude between the controllers due to the effect shown in Figure 35; the responses are also different.

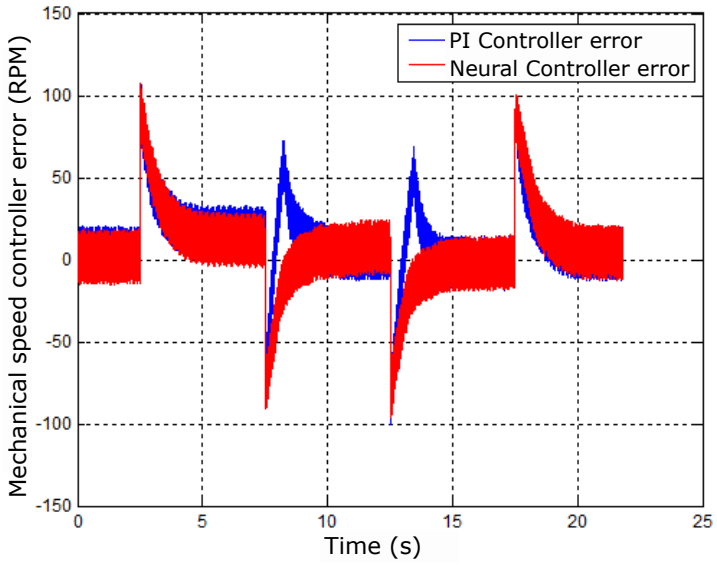

Figure 37. Control error signals for step speed reference.

Thus, even with variations or changes in references in the speed control, Figure 38 shows the dispersion of *XY* signals concentrated, as these variations did not disturb the position control.

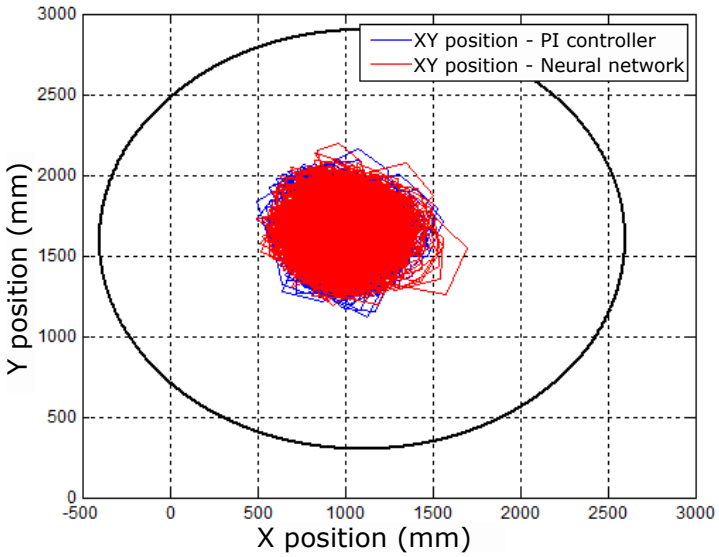

Figure 38. Radial positioning diagrams for step speed reference.

A model DT-2234*B* digital tachometer was used to validate and check the mechanical speed of the rotor operating at 1800 RPM and using the PI and neural controllers. Figure 39 shows the mechanical speed results under regime permanent in Figure 39A working with the PI controller and Figure 39B with the controller neural.

(A) (B)

Figure 39. Mechanical velocity measurement (**A**) PI control and (**B**) neural control.

10. Conclusions

The purpose of this article was to present the study and implementation of artificial intelligence techniques for motor-bearing speed control with a split coil. ANFIS Smart Techniques and Neural Networks were investigated and computationally implemented for the evaluation of the motor-bearing performance. The simulated results showed a good performance for the two techniques: as an estimator and as a speed controller, using both an induction motor model operating as a bearing motor. The experimental implementation required adjustments in the interfaces of position, in the speed sensor, and in the replacement of the DSP TMS 3220*F*2812 by the DSP TMS 3220*F*28335, moving from fixed-point floating-point implementation. With the implementation of the motor-bearing system and the analysis of obtained results, some conclusions were possible: the use of DSP 28335 helped in the implementation of the cascade control; the tuning of the current, position, and speed controller, in the experimental results implemented in the DSP *F*28335, was carried out empirically through the trial and error method, whose adjustment is difficult and laborious; current control results were investigated with DC and AC currents, validating the controller tuning in the bearing motor; the position control result has been implemented and tuned to the frequency of 60 Hz, but it presented the best results at the frequencies of 15 Hz, 30 Hz and 45 Hz; the speed control operating conditions were synchronized with the position control, so the motor-bearing system operated properly with current control; the operation of cascaded meshes requires a synchronism between the position control and the speed control because, if it does not occur, the controllers will not achieve stabilization; the speed PI controller had overshoots, and the neural controller system did not present them, demonstrating the ability to learn and generalization of Neural Networks.

Author Contributions: J.R.D.N., J.S.B.L. and A.O.S. conceived and designed the study; J.S.B.L. and D.A.D.M.F., methodology; J.R.D.N. and D.A.D.M.F. performed the simulations and experiments; E.R.L.V., A.R.G.G., J.M.d.S.F. and A.O.S. reviewed the manuscript and provided valuable suggestions; E.R.L.V., J.S.B.L., D.A.D.M.F. and A.R.G.G. wrote the paper; supervision, A.O.S. and J.M.d.S.F. All authors have read and agreed to the published version of the manuscript.

Funding: This research was funded in part by the Coordenação de Aperfeiçoamento de Pessoal de Nível Superior Brasil (CAPES) Finance Code 001 and Conselho Nacional de Desenvolvimento Científico e Tecnológico (CNPq).

Data Availability Statement: The original contributions presented in the study are included in the article, further inquiries can be directed to the corresponding author.

Conflicts of Interest: The authors declare no conflicts of interest.

Abbreviations

The following abbreviations are used in this manuscript:

PWM	Pulse-Width Modulation
DSP	Digital Signal Processor
PI	Proportional Integral
PD	Proportional-Derivative
PID	Proportional Derivative Integral
MSE	Mean Square Error
AEC 5505-04	Sensors
DC	Direct Current

References

1. Victor, V.F.; Quintaes, F.O.; Lopes, J.S.B.; Junior, L.d.S.; Lock, A.S.; Salazar, A.O. Analysis and study of a bearingless AC motor type divided winding, based on a conventional squirrel cage induction motor. *IEEE Trans. Magn.* **2012**, *48*, 3571–3574. [CrossRef]
2. Nunes, E.A.D.F.; Salazar, A.O.; Villarreal, E.R.L.; Souza, F.E.C.; Dos Santos Júnior, L.P.; Lopes, J.S.B.; Luque, J.C.C. Proposal of a fuzzy controller for radial position in a bearingless induction motor. *IEEE Access* **2019**, *7*, 114808–114816. [CrossRef]
3. Carvalho Souza, F.E.; Silva, W.; Ortiz Salazar, A.; Paiva, J.; Moura, D.; Villarreal, E.R.L. A Novel Driving Scheme for Three-Phase Bearingless Induction Machine with Split Winding. *Energies* **2021**, *14*, 4930. [CrossRef]
4. Teixeira, R.d.A.; da Silva, W.L.A.; Amaral, A.E.S.; Rodrigues, W.M.; Salazar, A.O.; Villarreal, E.R.L. Application of Active Disturbance Rejection in a Bearingless Machine with Split-Winding. *Energies* **2023**, *16*, 3100. [CrossRef]
5. Buro, N.G. Magnetic bearings and non-stationary dynamics of rotors. In Proceedings of the Forth International Symposium on Magnectic Bearings, Zurich, Switzerland, 24–26 August 1994.
6. Bu, W.; Li, Z.; Wang, X.; Li, X. A control method of bearingless induction motor based on neural network. In Proceedings of the 2015 IEEE International Conference on Information and Automation, Lijiang, China, 8–10 August 2015; pp. 2252–2257.
7. Depari, A.; Flammini, A.; Marioli, D.; Taroni, A. Application of an ANFIS Algorithm to Sensor Data Processing. *IEEE Trans. Instrum. Meas.* **2007**, *56*, 75–79. [CrossRef]
8. Ding, W.; Liang, D. Modeling of a 6/4 Switched Reluctance Motor Using Adaptive Neural Fuzzy Inference System. *IEEE Trans. Magn.* **2008**, *44*, 1796–1804. [CrossRef]
9. Zhi-xiang, H.; He-qing, L. Nonlinear system identification based on adaptive neural fuzzy inference system. In Proceedings of the International Conference on Communications, Circuits and Systems, Guilin, China, 25–28 June 2006.
10. Vasudevn, M.; Arumugam, R.; Paramasivam, S. Adaptive neuro-fuzzy inference system modeling of an induction motor. In Proceedings of the International Conference on Power Electronics and Drive Systems, 5, Singapore, 19–24 February 2003.
11. Wang, Z.; Liu, X.X. Nonlinear Internal Model Control for Bearingless Induction Motor Based on Neural Network Inversion. *Acta Autom. Sin.* **2013**, *39*, 433–439. [CrossRef]
12. Wang, C.; Zheng, Z.; Guo, D.; Liu, T.; Xie, Y.; Zhang, D. An Experimental Setup to Detect the Crack Fault of Asymmetric Rotors Based on a Deep Learning Method. *Appl. Sci.* **2023**, *13*, 1327. [CrossRef]
13. Ambrożkiewicz, B.; Syta, A.; Georgiadis, A.; Gassner, A.; Litak, G.; Meier, N. Intelligent Diagnostics of Radial Internal Clearance in Ball Bearings with Machine Learning Methods. *Sensors* **2023**, *23*, 5875. [CrossRef] [PubMed]
14. Fu, Z.; Zhou, Z.; Zhu, J.; Yuan, Y. Condition Monitoring Method for the Gearboxes of Offshore Wind Turbines Based on Oil Temperature Prediction. *Energies* **2023**, *16*, 6275. [CrossRef]
15. Yang, Z.; Ding, Q.; Sun, X.; Lu, C. Design and Analysis of a Three-Speed Wound Bearingless Induction Motor. *IEEE Trans. Ind. Electron.* **2022**, *69*, 12529–12539. [CrossRef]
16. Chen, J.; Fujii, Y.; Johnson, M.W.; Farhan, A.; Severson, E.L. Optimal Design of the Bearingless Induction Motor. *IEEE Trans. Ind. Appl.* **2021**, *57*, 1375–1388. [CrossRef]
17. Zhu, H.; Yang, Z.; Sun, X.; Wang, D.; Chen, X. Rotor Vibration Control of a Bearingless Induction Motor Based on Unbalanced Force Feed-Forward Compensation and Current Compensation. *IEEE Access* **2020**, *8*, 12988–12998. [CrossRef]
18. Bian, Y.; Yang, Z.; Sun, X.; Wang, X. Speed Sensorless Control of a Bearingless Induction Motor Based on Modified Robust Kalman Filter. *J. Electr. Eng. Technol.* **2023**, *1*. [CrossRef]

19. Ahn, H.J.; Vo, N.V.; Jin, S. Three-Phase Coil Configurations for the Radial Suspension of a Bearingless Slice Motor. *Int. J. Precis. Eng. Manuf.* **2023**, *24*, 95–102. [CrossRef]
20. Falkowski, K.; Kurnyta-Mazurek, P.; Szolc, T.; Henzel, M. Radial Magnetic Bearings for Rotor-Shaft Support in Electric Jet Engine. *Energies* **2022**, *15*, 3339. [CrossRef]
21. Paiva, J.A. Speed Vector Control of an Induction Machine without Three-Phase Bearings with Split Winding Using Neural Estimation Flux. Ph.D. Thesis, Universidade Federal do Rio Grande do Norte, Natal, Brazil, 2007.
22. *C28x Solar Library: Module User's Guide*; Texas Instruments: Dallas, TX, USA, 2014; v1.2.
23. Gomes, R.R. Bearing Motor with Control Implemented in a DSP. Master's Thesis, UFRJ, Rio de Janeiro, Brazil, 2007.
24. Silva, P.V. Electromagnetic Frequency Regulator Applied in the Wind Generator Speed Control. Ph.D. Thesis, Universidade Federal do Rio Grande do Norte, Natal, Brazil, 2015.
25. Santos, T.H.D. Estimador neural da velocidade do mit acionado por um driver com controle vetorial orientado pelo fluxo do estator. In Proceedings of the XII Simpósio Brasileiro de Automação Inteligente (SBAI), Natal, Brazil, 25–29 October 2015.

Disclaimer/Publisher's Note: The statements, opinions and data contained in all publications are solely those of the individual author(s) and contributor(s) and not of MDPI and/or the editor(s). MDPI and/or the editor(s) disclaim responsibility for any injury to people or property resulting from any ideas, methods, instructions or products referred to in the content.

energies

MDPI

Article

Monitoring and Diagnosing Faults in Induction Motors' Three-Phase Systems Using NARX Neural Network

Valbério Gonzaga de Araújo [1,†], Aziz Oloroun-Shola Bissiriou [2,†], Juan Moises Mauricio Villanueva [3,†], Elmer Rolando Llanos Villarreal [4,†], Andrés Ortiz Salazar [2,*,†], Rodrigo de Andrade Teixeira [2,†] and Diego Antonio de Moura Fonsêca [2,†]

1 Federal Institute of Education, Science and Technology of Rio Grande do Norte (IFRN), Canguaretama 59190-000, RN, Brazil; valberio.araujo@ifrn.edu.br
2 Department of Computer Engineering and Automation, Federal University of Rio Grande do Norte (DCA-UFRN), Natal 59072-970, RN, Brazil; aziz.bissiriou.b07@ufrn.edu.br (A.O.-S.B.); rodrigoandradeteixeira@gmail.com (R.d.A.T.); diegomoura@dca.ufrn.br (D.A.d.M.F.)
3 Department of Electrical Engineering, Center for Alternative and Renewable Energies—CEAR, Federal University of Paraíba (CEAR-UFPB), João Pessoa 58051-900, PB, Brazil; jmauricio@cear.ufpb.br
4 Department of Natural Sciences, Mathematics, and Statistics, Federal Rural University of Semi-Arid (DCME-UFERSA), Mossoró 59625-900, RN, Brazil; elmerllanos@ufersa.edu.br
* Correspondence: andres@dca.ufrn.br
† These authors contributed equally to this work.

Abstract: Three-phase induction motors play a key role in industrial operations. However, their failure can result in serious operational problems. This study focuses on the early identification of faults through the accurate diagnosis and classification of faults in three-phase induction motors using artificial intelligence techniques by analyzing current, temperature, and vibration signals. Experiments were conducted on a test bench, simulating real operating conditions, including stator phase unbalance, bearing damage, and shaft unbalance. To classify the faults, an Auto-Regressive Neural Network with Exogenous Inputs (NARX) was developed. The parameters of this network were determined through a process of selecting the best network by using the scanning method with multiple training and validation iterations with the introduction of new data. The results of these tests showed that the network exhibited excellent generalization across all evaluated situations, achieving the following accuracy rates: motor without fault = 94.2%, unbalanced fault = 95%, bearings with fault = 98%, and stator with fault = 95%.

Keywords: artificial intelligence; failure classification; induction motor; artificial neural network

check for updates

Citation: Araújo, V.G.d.; Bissiriou, A.O.-S.; Villanueva, J.M.M.; Villarreal, E.R.L.; Salazar, A.O.; Teixeira, R.d.A.; Fonsêca, D.A.d.M. Monitoring and Diagnosing Faults in Induction Motors' Three-Phase Systems Using NARX Neural Network. *Energies* **2024**, *17*, 4609. https://doi.org/10.3390/en17184609

Academic Editor: K. T. Chau

Received: 18 June 2024
Revised: 19 July 2024
Accepted: 24 July 2024
Published: 13 September 2024

Copyright: © 2024 by the authors. Licensee MDPI, Basel, Switzerland. This article is an open access article distributed under the terms and conditions of the Creative Commons Attribution (CC BY) license (https://creativecommons.org/licenses/by/4.0/).

1. Introduction

Three-phase induction motors (TIMs) are widely used as the driving force in various industrial applications, ranging from clean environments, such as in the food industry, to more challenging or aggressive environments in heavy installations, such as the petrochemical and metal-processing industries. They are preferred due to several advantageous characteristics, including low cost, robustness, high reliability, and constructive simplicity. Many studies focus on improving the design, dynamic performance, and these machines' efficiency [1]. Three-phase induction motors are electromechanical energy converters that transform electrical input power from the power supply into mechanical output power delivered to the load, and despite inherent losses in the process, they remain highly efficient. In Brazil, the industrial sector demands 31.6% of the domestic electricity supply, with electric motors consuming 68% of this energy, highlighting the significant potential for energy savings [2].

Motors are subject to unavoidable stresses in practice. Environmental, thermal, mechanical, magnetic, and electrical variations can cause certain faults in motors. These faults,

if not detected and eliminated in time, can lead to an unexpected breakdown and stoppage of the motor and, consequently, a reduction in the industry's efficiency and possible damage to equipment or people nearby [3].

According to the work in [4], approximately 40–50% of induction motor failures are related to mechanical defects. These failures can be classified into two main categories: (i) rolling element bearing damage and (ii) eccentricity. Bearing failures can manifest as defects in the outer race, inner race, balls, or rollers. Factors such as vibrations, internal stresses, inherent eccentricity, and bearing currents significantly influence the development of these failures. Furthermore, temperature is a significant contributing factor to bearing failure. It is therefore recommended that the temperature does not exceed the predetermined limits under nominal load conditions. As stated in reference [5], it is crucial not to neglect voltage imbalance in the power supply. This imbalance leads to a significant increase in stator currents, causing copper losses and constituting one of the main sources of temperature rise. Conventional induction motors are designed to operate in ambient temperatures of up to 40 °C. Therefore, temperatures exceeding this standard limit can result in thermal stress.

Fault diagnosis can be carried out using traditional noninvasive techniques. These strategies generally involve analyzing parameters such as vibration, voltage, current, torque, and speed [6].

Since the installation of several backup motor units is not economical, monitoring induction machines is essential to ensure safe operation and maintain product quality. Therefore, the monitoring, detection, classification, and diagnosis of faults are crucial for keeping equipment in good operating condition. There are two main categories of techniques for identifying machine faults: invasive and noninvasive, with noninvasive techniques generally being preferred. Artificial intelligence (AI) systems have been proposed for the noninvasive detection of machine faults [7].

Among the conventional methods widely used in the literature, the Time–Frequency Domain Analysis (TFDA) method stands out for the detection of faults in induction motors. For instance, in [8], an approach based on the Fast Fourier Transform (FFT) is reported, which aims to analyze the motor's vibration and current signature for fault detection. This approach proposes to detect both mechanical faults, such as bearing damage, and electrical faults, such as unbalanced voltage supply or single-phase conditions. In this context, the authors employ Fourier spectral analysis via the FFT to extract features sensitive to the presence of faults. Mechanical and electrical faults imprint specific frequency characteristics on the current and vibration spectrum, which can be used for fault detection by comparing the amplitude of certain frequency components under normal and faulty conditions. Also, a discrete wavelet transform is employed in [9] for the detection of inter-turn short-circuit (ITSC) faults in induction motor stators. However, these Time–Frequency-Domain-based methods can be highly sensitive to noise in the measured signals, as high-frequency noise can mask actual faults, complicating accurate detection.

Fault-diagnosis methods using computational intelligence, through techniques based on Artificial Neural Networks (ANNs), Fuzzy Inference Systems (FISs), and Genetic Algorithms (GAs), have shown promising results in detecting and identifying faults in three-phase induction motors.

The objective of this work is to use artificial intelligence techniques to diagnose and classify faults related to shaft imbalance, stator damage, and bearing damage in three-phase induction motors. This will be performed by monitoring current, vibration, and temperature signals. The main aim is to achieve greater precision in the diagnosis of these mechanical and electrical faults, harnessing the power of artificial intelligence to analyze data and identify patterns, which can result in more assertive and effective interventions in the preventive and corrective maintenance of the equipment. This paper proposes to explain four distinct test scenarios that are important for identifying the motor operating conditions. These scenarios are fundamental because they allow for the collection of engine signal readings in different situations, which is essential for validating the proposed method.

This paper is organized as follows. Section 1 presents the introduction. Section 2 presents the preliminaries. The theoretical background is presented in Section 3. Section 4 describes the materials and methods used. Section 5 presents the results obtained. Section 6 shows the discussions, and Section 7 concludes this paper.

2. Preliminaries

Monitoring faults in three-phase induction motors has aroused the interest of many researchers, resulting in a growing number of papers on the subject. This section presents some of these studies.

In [10], observing the low dynamic processing capacity as the main limitation of modeling methods based on feed-forward neural networks for detecting turn faults in the stator winding of an induction motor, the authors implemented a diagonal recurrent neural network based on an online turn fault-detection approach. In this case, two diagonal recurrent neural networks were used, one to estimate the severity of the fault and the other to determine the exact number of times it occurs. To make the network more accurate, an adaptive dynamic backpropagation algorithm was used. The results demonstrated that the diagnostic model based on a diagonal recurrent neural network accurately determines shorted turns and is more effective than the diagnostic model based on a direct neural network.

In [11], a support vector machine algorithm based on artificial immunity for diagnosing faults in induction motors was proposed. In this paper, the stator and rotor faults in an induction motor were detected using the three-phase motor currents. The healthy and faulty motor conditions were classified in combined phase space using an immunity-based SVM algorithm. The optimal SVM parameters are obtained using a clonal selection algorithm. Besides, the motor currents were taken in a real experimental setup, and successful results were obtained.

In [12], an approach to the problem of fault detection and isolation in three-phase induction motors using recurrent neural networks and dynamic Bayesian modeling was presented. The idea was to create a neural model to emulate the system's normal behavior and additional models to emulate various fault conditions. The neural models are placed in parallel with the system to be monitored, and fault detection is achieved by comparing the outputs of the neural models with the actual outputs of the system. The neural network was trained using the stochastic simultaneous perturbation approximation (SPSA). Fault classification was based on a simple threshold test of the residuals, which were formed by subtracting each neural model output from the corresponding real system output. A hybrid system that used data collected by vibration and current sensors for the early and efficient detection of incipient faults in three-phase induction motors was used. The system employed advanced vibration and current analysis techniques, including multiresolution analysis with wavelet, Fourier transform, and fuzzy logic for fault classification.

In [13], an approach for monitoring the operating conditions of three-phase induction motors based on extracting the characteristics of a vibration signal obtained with a MEMS accelerometer is investigated. The authors extracted data from the decomposition of the vibration signal by the Haar transform and through the fractal dimension, which were employed to train an ELM Neural Network.

In [14], strategies were introduced for diagnosing and predicting faults and failures in induction motors as an alternative tool to traditional models for detecting short-circuit faults between stator turns, rotor bar breakage, and bearings under normal operating conditions using Artificial Neural Networks with a radial basis function. The current signals of a three-phase induction motor under various fault conditions were treated and processed using synchronous axis transforms. These signals were classified using the RBF network, indicating the samples referring to the signals without faults and with the three types of faults. It was found that the network presented 1.33% error for loads of 1 Nm, 2 Nm, and 3 Nm and zero error for loads of 4 Nm and 5 Nm. The experimental results demonstrated that the employed methodology successfully classified the signals.

In [15], a proposal for a three-phase induction motor signature analysis technique to diagnose faults between stator turns was considered. This technique employs a wavelet transform and a support vector machine as a classification tool. The proposed technique was based on the stator current analysis under healthy and faulty conditions. The wavelet decomposition, based on a lifting algorithm, was implemented in the system with an ARM processor to reduce implementation costs.

In [16], a study was presented on fault-diagnosis techniques for three-phase induction motors, focusing on industrial applications. In this paper, various methods were explored, including current signature analysis, mechanical vibration, acoustic vibration, energy efficiency, and air gap torque. The authors also employed the Fast Fourier Transform and the multiresolution analysis with a wavelet. Mechanical faults were effectively diagnosed using vibration analysis and sound analysis of the noise emitted by the motor. MRA analysis proved to be efficient for practically all types of faults associated with various types of failure. The torque spectral analysis in the air gap and sound acquisition by MRA proved to be excellent alternatives for detecting broken bars. For bearing fault detection, spectral analysis combined with MRA analysis for vibration signals proved to be the most suitable approach. The mechanical vibration fault diagnosis via spectral analysis also proved to be the best option for unbalancing for different applied loads.

In [17], an alternative method for detecting faults in the bearings of three-phase induction motors directly connected to the mains was proposed. This method utilizes the amplitudes of voltage and current magnitudes in the time domain, eliminating the need for signal manipulation and transformation. Experimental data collected in the laboratory facilitated the establishment of an ANN topology capable of better interpreting the signals used as input. This approach obtained satisfactory results with over 99% accuracy for cross-validation and around 97% for validation with data acquired from machines not used in the training process. The proposed network was the Multilayer Perceptron (MLP), consisting of two hidden layers with seven neurons each, plus the output layer with two neurons for classification. Supervised training was also applied with the backpropagation method plus the Levenberg–Maquardt (LM) algorithm, stipulating the Mean Square Error (MSE) as the stopping criterion.

In [18], a comprehensive review of AI algorithms for diagnosing faults in rotating machines is presented from both a theoretical and an industrial application standpoint. The methods presented include k-nearest neighbor, Naïve Bayes, support vector machine, Artificial Neural Network, and deep learning, which are discussed as potential approaches for fault diagnosis. As AI techniques continue to mature, it is anticipated that they will remain a valuable and powerful tool for diagnosing faults in rotating machinery.

In [19], continual learning is introduced as a promising technique that allows intelligent motor fault-diagnosis models to extend new diagnosable fault classes without costly training from scratch.

In [20], a two-step approach for fault detection and classification in electric motor drives used in wind turbine pitch systems is presented. The proposed methodology is suitable for application in offshore wind farms, both for electrical pitch systems driven by induction motors and by permanent magnet synchronous motors. The adopted strategy involved measuring the three-phase current signal of the motors in the pitch drives, using these measurements to detect faults and feed a classifier based on support vector machines (SVMs). The proposed method was validated in an internal test environment of the pitch drive system. The SVM classifier demonstrated an overall accuracy of 98% in predicting fault classes in the training set and 96.5% in predicting fault classes in the test set.

Despite the reliability generally associated with three-phase induction motors, they are still susceptible to a variety of faults from both mechanical and electrical sources during motor operation. This scenario presents a significant challenge for the industry, requiring the ongoing development of techniques capable of monitoring and diagnosing these faults at an early stage.

Several approaches have been proposed to detect these issues, all with the clear objective of contributing to more effective maintenance and, consequently, reducing production losses. In many investigations, artificial intelligence has been highlighted by various authors as a crucial tool in systems modeling. Among the various artificial intelligence techniques, machine learning stands out in the development of fault-classification systems, as corroborated by the works cited.

It can be concluded that the topic has not yet reached its full maturity, presenting numerous opportunities for exploration, particularly in the field of deep learning through Artificial Neural Networks. Ongoing research and development in this area are crucial for enhancing the reliability and efficiency of three-phase induction motors. This, in turn, will contribute to the safer and more economical operation of these essential systems across various industrial applications.

3. Theoretical Background

This section presents fundamental concepts and theoretical aspects related to the development of this work. It includes an overview of three-phase induction motors, a discussion of typical faults in these motors, and a brief description of AI techniques applied to fault detection in motors.

3.1. Three-Phase Induction Motors

An electric motor is a machine designed to transform electrical energy into mechanical energy. Among the various types of motors, the induction motor is the most widely used as it offers a combination of advantages when it comes to the use of electrical energy. The main advantages of induction motors are their low cost, ease of transportation, cleanliness, and simplicity of control. These advantages are derived from the simple construction, low cost, and great versatility in adapting to loads of the most diverse types, as well as better efficiency yields [21]. A large proportion of the industrial sector consists of electric motors, including both direct current (DC) and alternating current (AC) motors. These motors are essential for the functioning of industrial processes [22].

The induction machine mainly functions as a motor and can be categorized as either three phase or single phase (two phase). Single-phase models use specialized devices to achieve the starting torque. A key feature is its independence from a DC source, making it robust, versatile, and cost-effective. These motors come in various power capacities, from large-scale to fractional power applications. Furthermore, the lack of brushes reduces the need for maintenance.

Figure 1 shows the main components of a TIM.

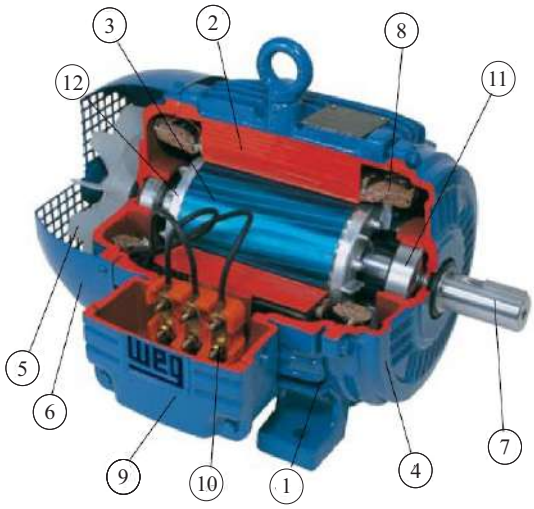

Figure 1. TIM components.

Estator:

- Housing (1)—the supporting structure of the assembly; it is made by employing robust construction with cast iron, steel, or injected aluminum and is corrosion-resistant and has fins.
- Core plates (2)—the plates are made of magnetic steel and are heat-treated to reduce losses of iron to a minimum.
- Three-phase winding (8)—Three equal sets of coils, one for each phase. These coils form a three-phase system and are connected to the three-phase supply network.

Rotor:

- Shaft (7)—Transmits the mechanical power developed by the engine. They are heat-treated to avoid problems such as warping and fatigue.
- Core plates (3)—the plates have the same characteristics as the stator plates.
- Short-circuit bars and rings (12)—made of aluminum die cast in a single piece.

Other parts of the TIM:

- Cover (4).
- Fan (5).
- Deflector cover (6).
- Junction box (9).
- Terminals (10).
- Bearings (11).

3.1.1. Working Principle

Induction motors, available in single-phase or three-phase configurations, are named after the power transfer principle from the stator's primary winding to the rotor. This transfer happens due to the relative movement between the magnetic field generated by the stator winding and the rotor conductors, inducing a voltage in the rotor. This principle underlies the fundamental dynamics behind the efficient and versatile operation of induction motors, which are crucial in many industrial and commercial applications [23].

3.1.2. Synchronous Speed

The motor synchronous speed is defined by the rotational speed of the motor rotating field, which depends on the number of poles (p) of the motor and the frequency (f) of the network, in hertz. Windings can be constructed with one or more pairs of poles, which are distributed alternately (north and south) along the periphery of the magnetic core. The rotating field travels through a pair of poles (p) each cycle. Thus, as the winding has poles or p pairs of poles, the field speed will be:

$$n_s = \frac{120 \cdot f}{p} \quad (1)$$

n_s — speed (rpm) under nominal conditions.
f — frequency of the electrical supply voltage (Hz).
p — total number of poles per phase.

3.1.3. Slip

The induction motor is also referred to as an asynchronous motor, given that the operational speed of the shaft is slightly below the synchronous speed. This small difference occurs because the rotor speed is slightly lower than the speed of the rotating magnetic field. This difference, called slip, increases with each rise in the mechanical load on the shaft.

Slip is the difference between the motor speed n and the synchronous speed ns, which can be expressed in rpm as a fraction of the synchronous speed or as a percentage of it:

$$S_{rpm} = n_s - n \quad (2)$$

$$S = \frac{(n_s - n)}{n_s} \times 100 \quad (3)$$

S — slip.
n_s — rotating magnetic field speed (rpm).
n — nominal speed (rpm). - nominal speed (rpm).

3.1.4. Rated Speed

The nominal speed of the motor (n) operating at nominal power under nominal voltage and frequency, depends on the slip and the synchronous speed. Therefore, the nominal speed in rpm is calculated by:

$$n_{rpm} = n_s \cdot \left(1 - \frac{S}{100}\right) \quad (4)$$

3.2. Typical Engine Failures

The presence of a fault, even if incipient, can have a significant impact on the machine's performance, resulting in losses to the production process. Unscheduled downtime represents major challenges in the industrial sector, increasing maintenance costs and production losses. The monitoring and diagnosis of a three-phase induction machine (TIM) is based on information extracted from the equipment. This information is properly processed to ensure that its characteristics allow for a reliable analysis [22]. The ongoing search for optimizing efficiency and productivity extends beyond merely adopting new technologies to replace manual work. Today, it also involves generating and analyzing large amounts of data related to the maintenance and operating conditions of production line components [24]. A fault detection and diagnosis system can be a crucial tool for the maintenance sector in various industries. One of its main advantages is the ability to identify failures at early stages, which not only facilitates the implementation of predictive maintenance but can also prevent unscheduled machine downtime.

Figure 2 shows the fault-classification tree in a TIM divided into two classes: electrical faults and mechanical faults. The percentages of failures in three-phase induction motors can be distributed as follows: bearing-related failures: 40%, stator winding failures: 38%, rotor-related failures: 10%, other failures: 10% [4].

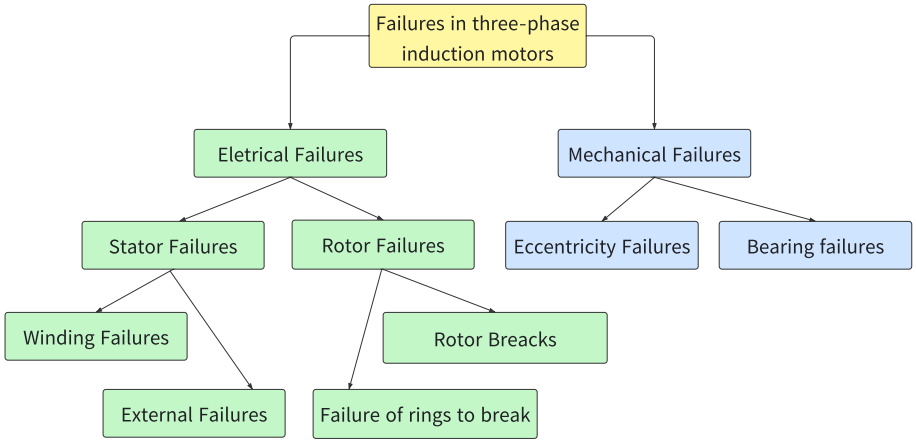

Figure 2. Failure tree.

3.3. AI Techniques Applied to Engine Fault Detection

One of the most interesting topics in the field of science is the concept of intelligence. Since the dawn of civilization, both philosophical thinkers and scientists have dedicated themselves to understanding the intelligence of nature and how it manifests itself in living organisms. With technological advances, especially with the introduction of digital

computing systems in the 20th century, questions arose about the possibility of computers being capable of demonstrating behaviors that could be considered intelligent [25].

The implementation of artificial intelligence techniques in fault detection allows real-time monitoring to be carried out using computers, requiring minimal interaction with the user. In several situations, these technologies are capable of diagnosing faults without the need for intervention from maintenance specialists [26].

Condition monitoring in induction motors is a process divided into several phases. This includes information collection, predictive analysis, feature extraction, and fault identification using machine learning (ML) algorithms. To develop a classifier with ML algorithms, intelligence-based fault-identification systems must undergo data extraction algorithms. Several strategies are employed for function identification and classification, including evolutionary algorithms, angular improvement, and data extraction. Machine learning algorithms, such as k-nearest neighbors, Artificial Neural Networks, support vector machines, random forests, Bayesian classification algorithms, Naïve Bayes, and intelligent systems, have been successfully used to build intelligence methods. Recently, researchers have been exploring supervised learning for fault identification [27].

Artificial Neural Networks (ANNs) represent a powerful tool for the accurate diagnosis of faults in induction motors (IMs). These networks are effective pattern classifiers, which makes them capable of solving a wide range of problems, especially those that involve the recognition of variables that cannot be fully described or predicted, as is the case with failures in MIs. Thus, by creating a neural network, we can successfully address pattern classification issues, which proves to be fundamental in the detection and accurate diagnosis of faults in induction motors [28].

3.4. Recurrent Neural Networks

Recurrent neural networks (RNNs) are characterized by their ability to retain information by feeding back the outputs of one or more neurons. This mechanism allows recurrent networks to maintain internal states that evolve dynamically, incorporating both new inputs and weights from previous states. This characteristic gives RNNs a structure that resembles a memory, where relevant information is preserved and used for subsequent processing. A dynamic neural network can be characterized as one that contains synaptic feedback connections between layers and delays that enable the transmission of the dynamics of a phenomenon through neurons from different layers, as illustrated in Figure 3. In this way, recurrence can be defined as a type of short-term memory, which allows for the network process of retrieving information from the recent past.

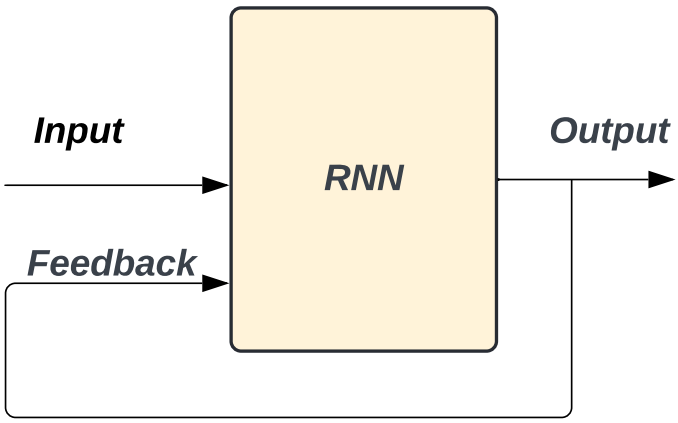

Figure 3. Topology of a recurrent neural network.

The NARX model is a form of recurrent Artificial Neural Network with feedback mechanisms, especially suitable for the nonlinear modeling of systems, focusing on time series, where past data are used to predict future values [29]. NARX networks are an efficient alternative to recurrent networks, offering similar computational efficiency. The

NARX model integrates both the initial input data and the output data generated after training. In this way, the network can improve its capacity for continuous learning [30].

Figure 4 shows the topology of a NARX neural network, where u represents the external input, y denotes the previous response, and $y(k)$ is the estimated output. The blue boxes indicate the network's delays, while the numbered circles represent the neurons in the hidden layer.

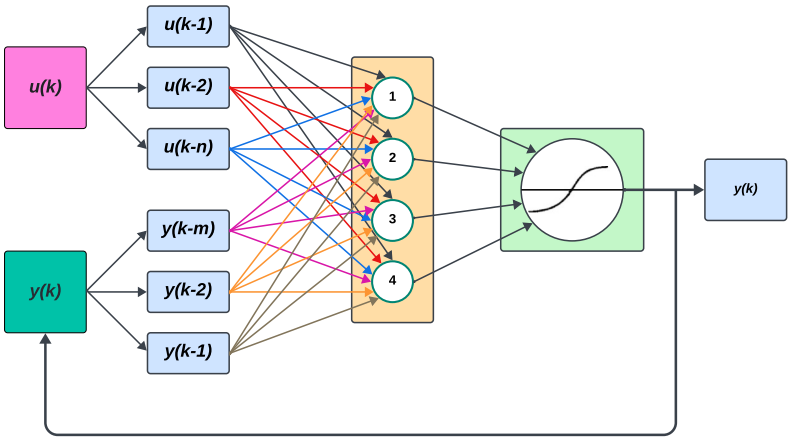

Figure 4. Topology of a NARX neural network.

The equation that defines the NARX model is

$$y(k) = f(u(k-1), u(k-n), \ldots, y(k-m), y(k-1)) \quad (5)$$

where
u_k—the input feature vector for the network.
y_k—the output vector for the network.
n—the index of the nth coefficient in $u(k)$.
m—the index of the nth coefficient in $y(k)$.

3.5. Evaluation Metrics for Classification in Machine Learning

The machine-performance-evaluation learning algorithm on a specific dataset is carried out by measuring how well the predictions generated by the adjusted model reflect the observed values for the variable of interest.

Classification is based on predicting the category of a given observation. Some of the applications of ANNs are related to pattern classification. In these applications, the neural network is trained to distinguish an unknown pattern among several classes or categories. Thus, when faced with an unknown pattern, the neural network must assign it to one of the existing classes. To evaluate the classifier's performance with new patterns (patterns different from those used in training), it is necessary to carry out a testing or practical application phase. During this phase, we evaluate the number of hits made by the classifier on a set of patterns whose classes are known. It is important to highlight that none of the patterns in this set must have been used during the training of the classifier [31].

3.5.1. Predicted Data Classes: TP, TN, FP, and FN

In a classification problem, there are two possible solutions: right or wrong. However, for a binary classification problem, there are still two other possible classes that are called positive and negative classes.

True positive (TP): when the method says that the class is positive and, when checking the answer, it can be seen that the class was positive.

True negative (TN): when the method says the class is negative and, when checking the answer, it is seen that the class was negative.

False positive (FP): when the method says that the class is positive, but instead when you check the answer, you see that the class was negative.

False negative (FN): when the method says that the class is negative, but when checking the answer, it is seen that the class was positive.

3.5.2. Evaluation Metrics

In contexts where the number of classes exceeds the binary paradigm, the complexity of the problem increases, making it prone to mistakes in the implementation of multiclass classifiers. Therefore, several parameters are used to evaluate the effectiveness of a classifier in artificial intelligence systems [32].

The main metrics that can be used to evaluate the quality of a classifier are the following:

Accuracy: The proportion of correct predictions about the total number of predictions. The accuracy metric is commonly used as one of the main criteria in the evaluation of classifiers in artificial intelligence. This is due to its effectiveness and its conceptually simple nature, which facilitates its understanding [32]:

$$\text{Accuracy} = \frac{\text{Correct predictions}}{\text{Total predictions}} \tag{6}$$

Precision: Calculates the proportion of true positives about all examples classified as positive. Precision seeks to answer the following question: what percentage of predicted true positives is correct? It represents the proportion of true positives in all classified positive values (true positives plus false positives). When the number of false positives is high, accuracy decreases significantly. It is generally used when false positives have a potentially more harmful impact than false negatives [32]:

$$\text{Precision} = \frac{TP}{TP + FP} \tag{7}$$

Recall: Also referred to as recall or "sensitivity", this metric seeks to answer the following question: what percentage of all true positives were predicted correctly? It is calculated as the ratio of true positives to the sum of true positives and false negatives. This metric is commonly applied in situations where false negatives are potentially more concerning than false positives. It evaluates the rate of true positives that the model can predict, allowing for an analysis of the classifier's ability to identify false negatives [32]:

$$\text{Recall:} = \frac{TP}{TP + FN} \tag{8}$$

F1 score: The score (or simply F1-Score for true values) combines two essential metrics in binary machine learning classifiers: accuracy and recall. It is calculated as the harmonic mean of these metrics. A low F1 score indicates that both precision and recall are below optimal levels, suggesting the need for adjustments in the classifier. The F1 score is a machine learning model performance metric that assigns equal weight to accuracy and recall. The results provided by this metric offer high-level, reliable insights into the classifier' output [32]:

$$\text{F1} - \text{Score} = 2 \cdot \frac{\text{Accuracy} \cdot \text{Recall}}{\text{Precision} + \text{Recall}} \tag{9}$$

ROC Curve: Within the analysis of the performance of classification models, there are a variety of statistical estimators used. One of the most common is the ROC curve (Receiver Operating Characteristic), which offers a graphical representation of a model's performance in relation to its sensitivity (the fraction of true positives) and its specificity (the fraction of false positives) at different cutoff points. On the X-axis (horizontal), we have the false positive rate (Specificity: $1 -$ specificity), and on the Y-axis (vertical), we have the true positive rate (sensitivity). The Figure 5 show examples of ROC curves represented in green, orange, and blue. The closer the sensitivity and specificity values are to 100%, the

higher the accuracy of the test. The ROC curve demonstrates how sensitivity and specificity vary as different cutoff values are considered [33].

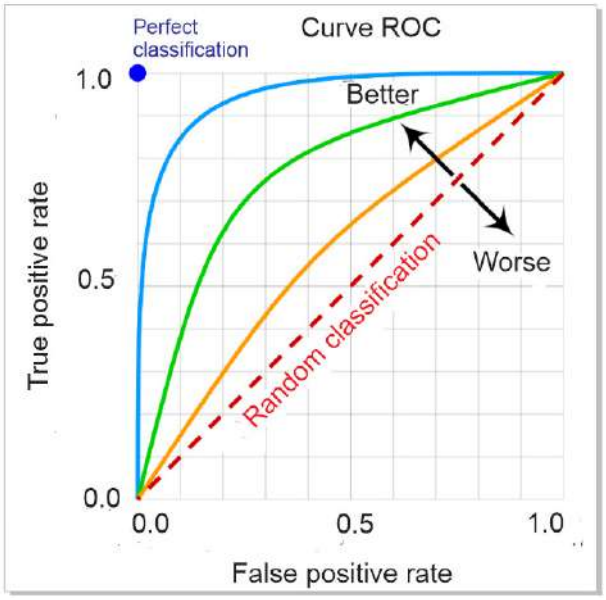

Figure 5. ROC curve.

Confusion matrix: The confusion matrix is a technique widely used in evaluating classification algorithms. Also referred to as an error matrix, it consists of a table that simplifies the analysis of the performance of such algorithms. The data contained in this matrix are essential for the mathematical formulation of various classification metrics. It is made up of the number of true positives (TPs), true negatives (TNs), false positives (FPs), and false negatives (FNs).

$$\text{Accuracy} = \frac{TP + TN}{TP + FN + TN + FP} \tag{10}$$

The multiclass confusion matrix illustrated in Figure 6 can be interpreted as follows: the main diagonal, colored green, represents the true positives (TPs); above the main diagonal are the false positives (FPs); and below the main diagonal are the false negatives (FNs).

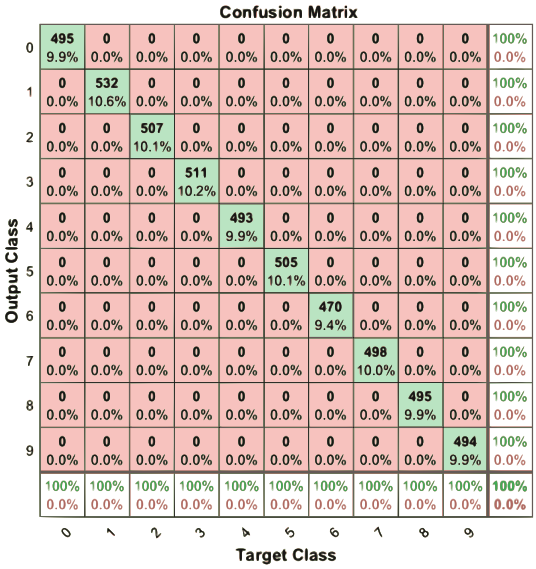

Figure 6. Confusion matrix for multiclass classification.

3.6. Remarks

The good performance of the three-phase induction motor is due to its simple and efficient construction. Due to this simplicity, associated with robustness and low cost, the three-phase induction motor is placed on the list of the most used motors in industries.

The cost of equipment maintenance is still considerably high in the industry. Therefore, developing systems that enable the monitoring and diagnosis of possible failures can reduce this cost. To develop these systems, various techniques have emerged.

One of the most used techniques has been artificial intelligence. This technique has been very important for solving complex problems. Artificial intelligence makes it possible to detect faults that may occur in the three-phase induction motor more quickly and accurately. Two important areas of artificial intelligence are presented: machine learning and deep learning.

There are several evaluation metrics commonly used in machine learning, each with its specific purpose and interpretation. Choosing the appropriate metrics depends on the type of problem we are addressing and the objectives of the model.

4. Materials and Methods

This section covers a detailed description of the methodology adopted in the development of the monitoring and fault-diagnosis system for three-phase induction motors. The experiments were carried out on an experimental bench installed in the machine laboratory of the Federal University of Rio Grande do Norte (UFRN). The experimental bench used in this research emulates a real engine operation application. Two categories of failures were diagnosed: mechanical failures (unbalanced shaft and defective bearings), which are identified through vibration and temperature analysis, and electrical failure (defective stator), identified through winding current and temperature signals. These current, vibration, and temperature signals were used to build a dataset to feed the input to the NARX neural network. The tests were conducted under normal operating conditions, as well as in simulated failure situations, including stator voltage unbalance, shaft unbalance, and bearing defects. The subsequent sections aim to detail the procedures, materials, and methods used in signal acquisition, as well as explain how the faults were emulated.

Figure 7 show the block diagram used to implement the proposed methodology. The diagram is organized into five main blocks. Block 1 corresponds to the test bench, where faults will be simulated in the installed motor. Block 2 is responsible for data collection, performed through the reading of signals captured by vibration, current, and temperature sensors. In Block 3, the collected signals are processed using LabVIEW software, where both time-domain and frequency-domain graphs are generated. Block 4 performs fault classification using the NARX neural network. Finally, in Block 5, the classified fault results are presented.

The subsequent sections aim to detail the procedures, materials, and methods used in the signal acquisition, as well as explain how the faults were identified.

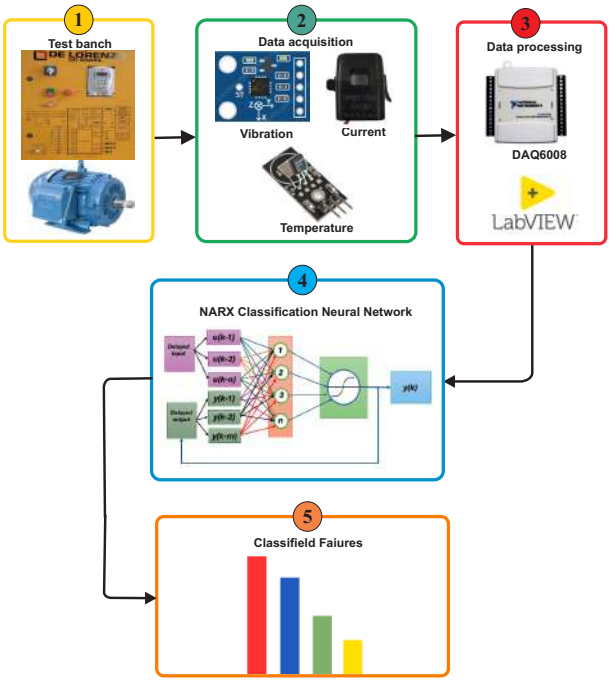

Figure 7. Process flowchart.

4.1. Materials—Test Bench

The bench used to carry out the experiments is the DLB MAQ-RN, manufactured by the company De Lorenzo of Brazil. This bench is equipped with the necessary resources for the execution of signal acquisition procedures and the identification of faults in an efficient and precise manner, enabling reliability in results and consisting of a WEG of Brazil brand frequency inverter model CFW-09 with power 1.5 CV and current 10A and a cage-type induction motor.

Figure 8 shows the complete bench, Figure 9 shows the three-phase induction motor, and Table 1 shows the characteristics of the motor.

Figure 8. Test bench.

Figure 9. Three-phase induction motor.

Table 1. Characteristics of the three-phase induction motor.

Features	Data
Power	1.1 HP
Speed	1720 RPM
Frequency	60 Hz
FS	1.5
Ip/In	7.8 A
Voltage	220/380 V
Current	4.43/2.56 A

4.2. Materials—Data Collection

Data collection was carried out using five sensors, strategically installed in the engine. These include three current sensors distributed across the three phases that power the motor, providing a comprehensive analysis of its electrical performance. Furthermore, a temperature sensor was positioned to monitor thermal variations, while an accelerometer-type vibration sensor was used to evaluate the mechanical oscillations of the system. This variety of sensors allows for comprehensive data collection, offering valuable insights into many aspects of engine operation.

4.2.1. Current Measurement

To measure three-phase currents in the stator, noninvasive current sensors based on the Hall effect were used, specifically the 5A/2V model - OPCT 10AL.

Figure 10 shows the noninvasive current sensor, and Table 2 shows its characteristics.

Figure 10. Current sensor.

Table 2. Characteristics of the current sensor.

Features	Technical Data
Rated Input	5 A (AC)
Rated Output	5 V (DC)
Accuracy error	0.5%
Linearity	0.5%

Converting AC Voltage Signal to DC

The sensor was calibrated to measure the maximum alternating current of 5A AC. This 5A value is the RMS value, which is also called the effective value. The RMS value is equal to the maximum value that the current can reach (peak current) divided by the square root of two. At the sensor output, the induced current signal is similar to that in Figure 11.

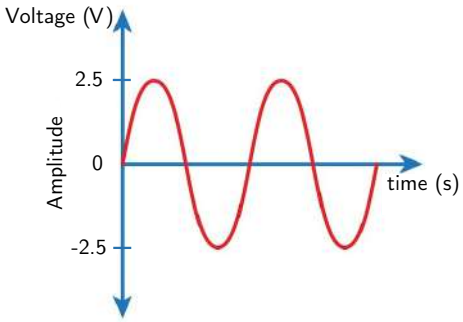

Figure 11. Signal at the output of the sensor.

In Figure 11, an alternating voltage signal oscillating between positive 2.5 V and negative 2.5 V is shown. However, the DAQ-6008 interface device, being powered by a, is capable of measuring signals within the range of 0 to 5 V. Therefore, it is necessary to adjust the signal so that the signal variation is in the range of 0 V to 5 V. To achieve this adjustment, initially, a voltage divider was implemented using the 5 V power supply provided by the DAQ-6008 device. In this context, we chose to configure resistors R1 and R2 with the same value, both 10 kΩ.

Figure 12 shows the signal conditioning circuit, and Figure 13 shows the conditioning board.

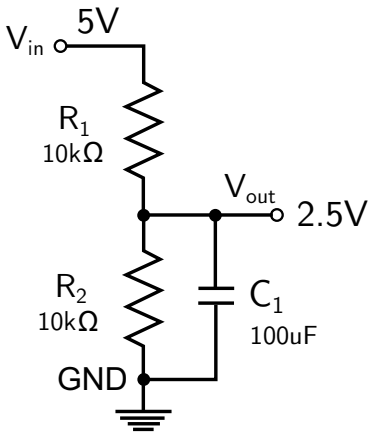

Figure 12. Current conditioning circuit.

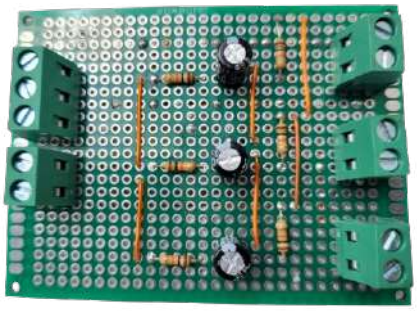

Figure 13. Current conditioning board.

This choice guarantees that the voltage across them is equal, as the 5 V coming from the device will be distributed evenly between them, as can be seen in Figure 14.

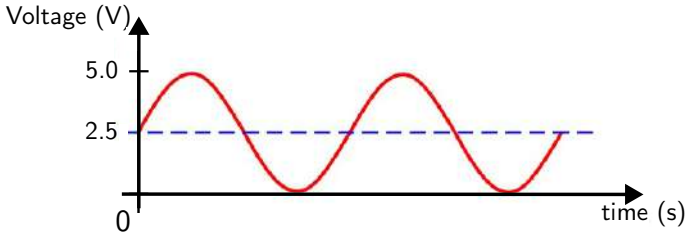

Figure 14. Sinusoidal waveform with offset value.

4.2.2. Vibration Sensor

The GY-61 DXL335 3-axis accelerometer module is an advanced sensor that utilizes the ADXL335 integrated circuit. This triaxial accelerometer offers an exceptional performance, characterized by a very low level of noise and energy consumption. With a full detection range of ±3 g, the sensor is capable of measuring both static accelerations due to gravity, in tilt sensing applications, and dynamic acceleration resulting from movement, impact, or vibration.

Figure 15 shows the vibration sensor, and Table 3 shows the characteristics.

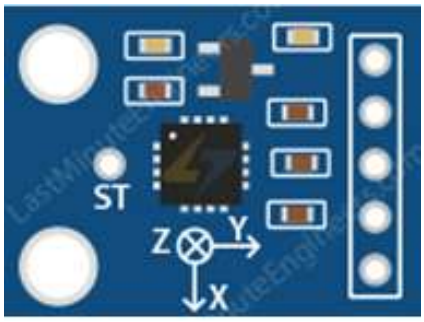

Figure 15. Vibration accelerometer sensor.

Table 3. Characteristics of the vibration sensor.

Features	Technical Data
Sensor Chip	ADLX335
Operating voltage range	3 to 5 V (DC)
Supply current	400 µA
Scale range	±3 g
Operating temperature	−40 °C to +85 °C
Sensitivity	300 mV/g
Accuracy	±10%

4.2.3. Temperature Measurement

To measure the engine temperature, the LM35DZ temperature sensor module was used. The LM35DZ temperature sensor consists of a high-precision integrated circuit, whose output voltage varies linearly about the temperature in degrees Celsius. The LM35DZ device eliminates the need for external calibration or adjustments, providing remarkable accuracies of $\pm\frac{1}{4}$ °C at room temperature and $\pm\frac{1}{4}$ °C over a wide thermal range, ranging from −55 °C to 150 °C.

Figure 16 shows the temperature sensor module, and Table 4 shows its characteristics.

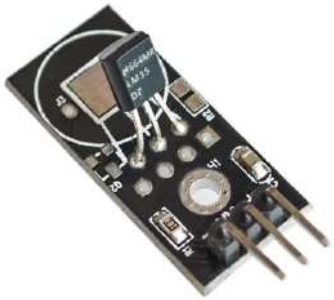

Figure 16. Temperature sensor.

Table 4. Characteristics of the temperature sensor.

Features	Technical Data
Operating voltage	4 to 30 V
Drain current	<60 µA
Measuring range	−55 to 150 °C
Sensitivity	10 mV/°C
Accuracy	0.5 °C (at 25 °C)

4.3. Data Processing

During the data collection stage, the sensors were connected to the DAQ—USB-6008 interface board, manufactured by National Instruments, to capture the signals, which were later read in the LabVIEW software. ADAQ—USB-6008 is an affordable and user-friendly solution for interfacing input and output signals with a personal computer. Connectable via a simple USB cable, this board offers a direct and efficient connection to the PC.

Figure 17 shows the voltage sensor module, and Table 5 shows its characteristics.

Figure 17. NI USB 6008.

Table 5. Characteristics of the NI USB-6008.

Features	Technical Data
Supply voltage	5VDC
Analog inputs 12/14 bits	8
Analog outputs 12 bits	2
32-bit	5 Mhz counter
Sampling Rate	1 KHz
Acquisition Mode	Continuous Samples
Recommended Software	LabVIEW

LabVIEW Block Diagram Code

Programming on the LabVIEW platform was carried out through a graphical interface in the block diagram, where each block represents a specific LabVIEW function. In the case of the vibration-, current-, voltage-, and temperature-monitoring program, the analyses are

continuous, and therefore it is necessary to implement a loop (while) to execute in cycles. This loop is interrupted when a stop condition is reached, such as pressing the stop button.

The graphs are generated according to the selected quantity. In this process, the graphics block identifies one of the signals given in its input and applies a Fast Fourier Transform (FFT) to the signal. Subsequently, the data are presented in both the time and frequency domains, allowing for visualization in the corresponding graphs. In addition to the graphical representation, the data are exported to Excel, where they are compiled into a database. This database is essential to feed the artificial intelligence algorithms used later.

Figure 18 shows the block diagram developed in LabVIEW software to perform signal processing. The diagram is divided into five blocks: block 1, DAQ assistant, is responsible for configuring the ports on the data acquisition board; block 2 is responsible for configuring the reading of the vibration signal for the three axes of the accelerometer and generating graphs to display these signals in both time and frequency; block 3 has the same function as block 2, but for the current signal, generating similar graphs; block 4 is responsible for configuring the temperature signal reading and displaying this signal through a graph; and in block 5, the while loop time and the determination of the stopping criteria are configured.

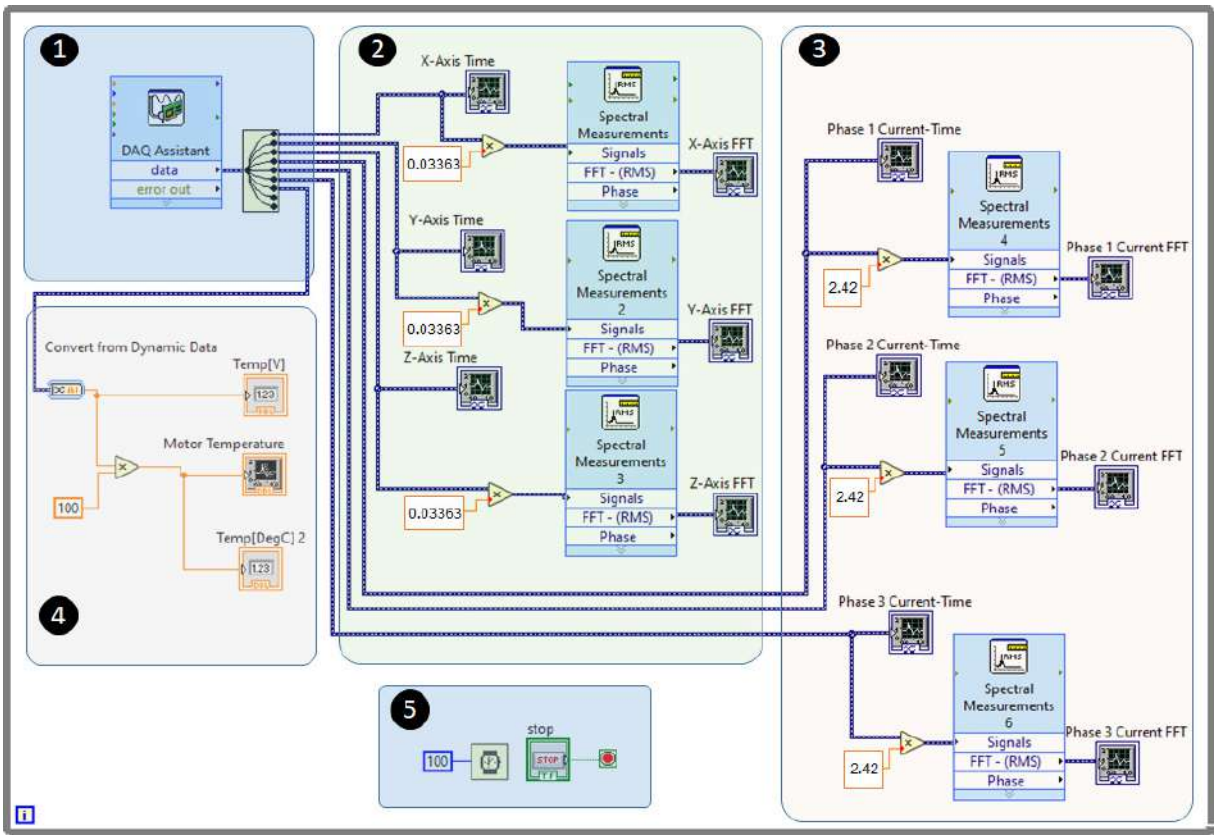

Figure 18. LabVIEW block diagram.

4.4. Methodology of the Fault-Detection Process

This section describes the methodology adopted to build the database from the signals collected in the engine, as well as the process of normalizing these data and the development of the fault-classification algorithms addressed in this work.

For training, validation, and testing of the neural network, a set of data was constructed from the signals collected by the sensors installed in the engine, having a csv table format with columns referring to the network's input and output data. The dataset, in turn, was subdivided into three sets, one for training, another for validation, and another for testing, following the proportions 70%, 15%, and 15%, respectively.

After creating the datasets, they were normalized. Normalization is a process by which data are adjusted to a scale with a range between zero and one. This practice is crucial, as neural network models tend to perform optimally when inputs are in this range. Equation (11) shows the formula used to calculate the normalized value of input X:

$$\mathbf{X}_{standardized.} = \frac{X - X_{min}}{X_{max} - X_{min}} \tag{11}$$

NARX Neural Network for Classification

The NARX (Nonlinear AutoRegressive with Exogenous inputs) neural network is a powerful architecture for modeling nonlinear dynamical systems, enabling accurate predictions and adaptation to changing operating conditions. This work explores significant modifications to network parameters, such as the cross-entropy loss function and the use of the softmax activation function at the output, specifically aimed at diagnosing faults in three-phase induction motors.

Changes in the parameters of the NARX neural network open up significant opportunities for its application in categorical multiclass fault-classification tasks. Although the original NARX framework is widely used for time series forecasting and modeling, these modifications allow it to be adapted for classification problems, especially where temporal characteristics are essential for identifying fault patterns and characteristics.

One of the main advantages of this approach is the ability to use the architecture of neural networks to extract and learn complex representations of input data, including past temporal information. With modifications to the parameters, the network can focus on identifying patterns and characteristics relevant to classifying faults.

Furthermore, adopting a NARX network for categorical multiclass classification enables the use of specific evaluation techniques and metrics for classification problems, such as precision, recall, F1 score, and confusion matrix. This allows for a more accurate assessment of network performance in identifying and classifying different types of faults.

Another significant advantage is the flexibility of this approach. By using a modified neural network structure, it is possible to easily tune the network architecture, experiment with different configurations of hidden layers, activation functions, and training methods, optimizing the network performance for the specific fault-classification problem.

In summary, when using a NARX network in the categorical multiclass classification of faults, benefits such as the ability to extract relevant temporal information, the use of specific classification techniques, and the flexibility to adjust the network architecture are obtained, better meeting the needs of the problem in question.

Figure 19 shows the topology of the NARX neural network for categorical multiclass classification.

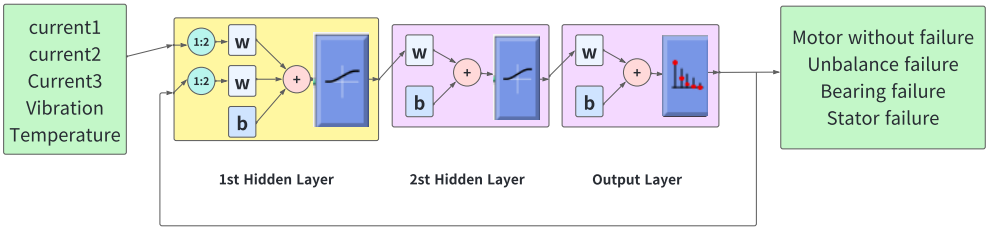

Figure 19. NARX neural network.

5. Results

Next, the results obtained from the proposed methodology application will be presented, which aim to evaluate the performance of the NARX neural network through comparisons of dynamic response and efficiency. These results were obtained through tests conducted on the experimental bench in the Automation and Control Laboratory of the Federal University of Rio Grande do Norte. Four scenarios were established for data

collection, which will be described below. Then, the NARX neural network will be trained, validated, and tested based on this collected data.

5.1. Scenarios for Data Collection

The programmed failure test followed a script with the development of five scenarios for case studies, aiming to identify failures in the electric motor through signal analysis. The scenarios were developed to represent various engine operating conditions, including normal operating situations and simulated failures, such as shaft unbalance, bearing damage, and stator current unbalance. The tests were carried out at three speeds: 900 RPM, 1200 RPM, and 1800 RPM. For this article, only data for the 1800 RPM speed are presented.

5.1.1. Scenario 1: Collecting Data from the Engine in Good Operating Conditions

This scenario serves as a reference point, representing normal engine operation under ideal conditions. Vibration, electrical current in the phases, and temperature signals were collected. Figure 20 shows the engine with the sensors installed. Figures 21 and 22, respectively, show the signals in the time domain for vibration and current signals, while Figures 23 and 24 illustrate the signals in the frequency for the same signals. Figure 25 shows the temperature in ideal engine conditions.

Figure 20. Sensors installed in the motor.

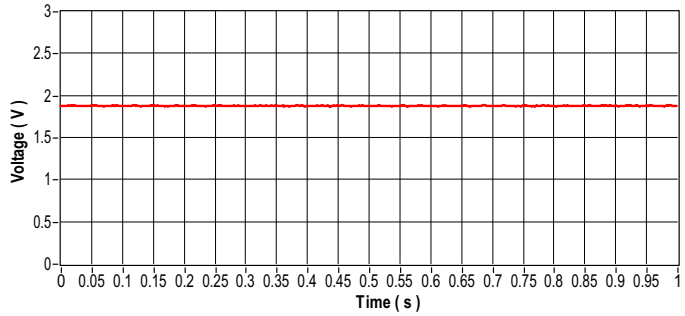

Figure 21. Vibration signal in the time domain.

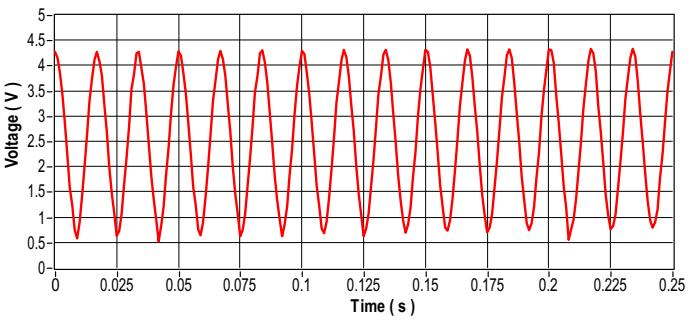

Figure 22. Current signal in the time domain.

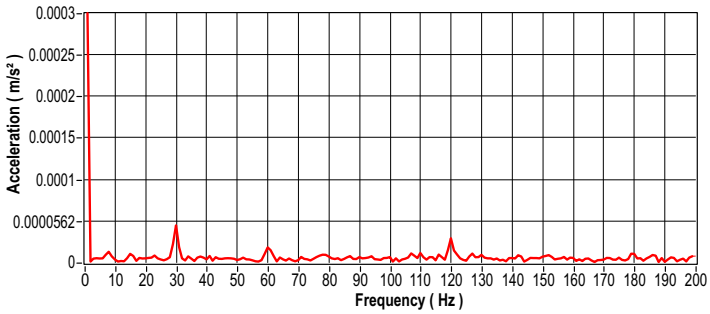

Figure 23. Vibration signal in the frequency domain.

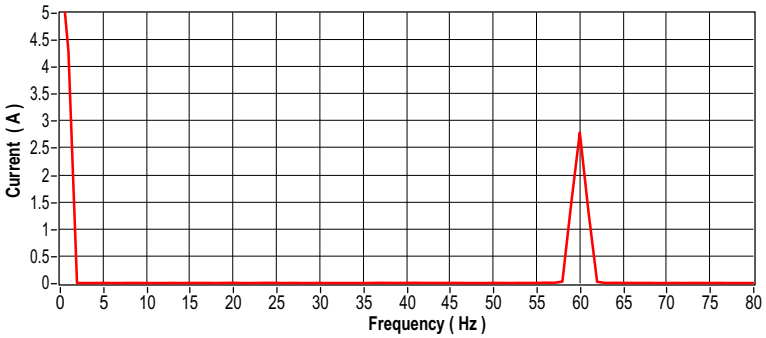

Figure 24. Current signal in the frequency domain.

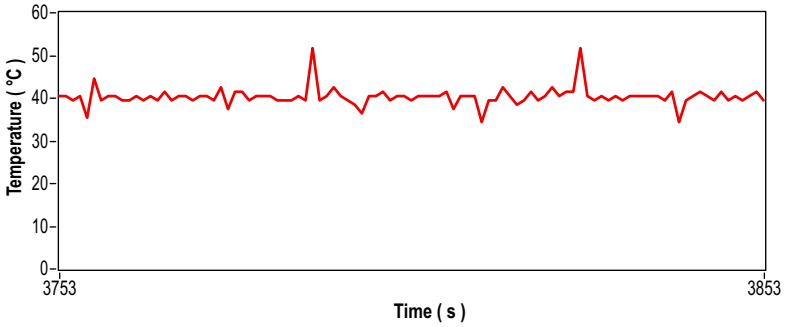

Figure 25. Signal of motor temperature under good operating conditions.

5.1.2. Scenario 2: Motor Data Collection with Shaft Unbalance

Engine unbalance is characterized by the uneven distribution of mass around the axis of rotation of the engine shaft. Due to this imbalance, the centripetal forces generated during the operation increase bearing wear. The phenomenon is typically observed in all rotating machines and is identified by an amplitude peak at the shaft rotation frequency, shown in the frequency spectrum.

To create a dynamic eccentricity that corresponds to an unbalance in the motor shaft for this scenario, a mass weighing 28 g was used. Figure 26 shows its fixation on a disc coupled to the motor shaft. The vibration signal that results from the induced unbalance is shown in Figure 27. The vibration signal for this case presents a sinusoidal pattern, as is typical of an unbalance. Figure 28 shows the frequency domain analysis, showing an amplitude peak at the shaft rotation frequency that corresponds to 30 mechanical Hz for a speed of 1800 RPM. The current signal in the time and frequency domains is shown in Figures 29 and 30, respectively, and the motor temperature variations are shown in Figure 31. These graphs provide more information about the behavior of the motor with the shaft unbalanced. Comparing the current signal with the unbalanced shaft and the current signal with the motor in ideal conditions, it can be seen that the current underwent a small change, changing from 2.8 A to 3 A. The temperature remained within the same variation range.

Figure 26. Installation of mass for unbalancing.

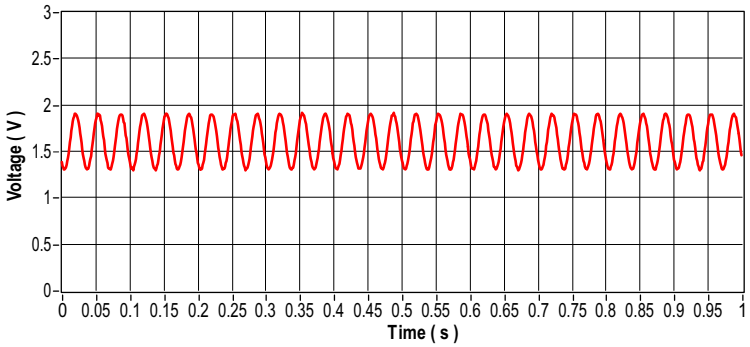

Figure 27. Vibration signal in the time domain.

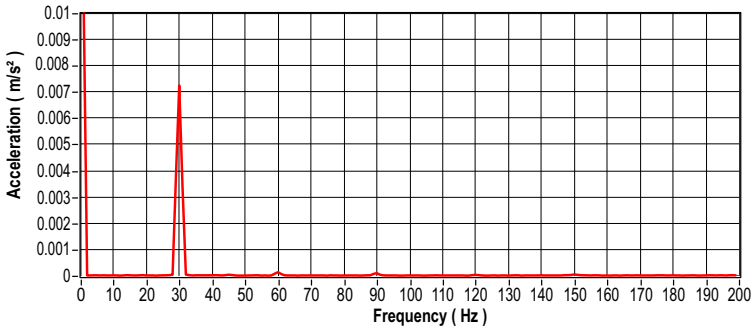

Figure 28. Vibration signal in the frequency domain.

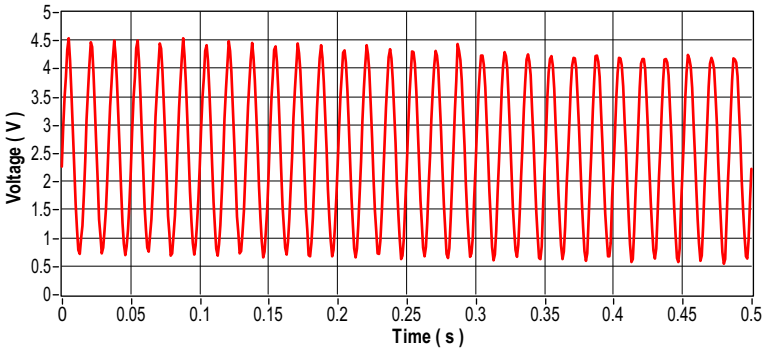

Figure 29. Current signal in the time domain.

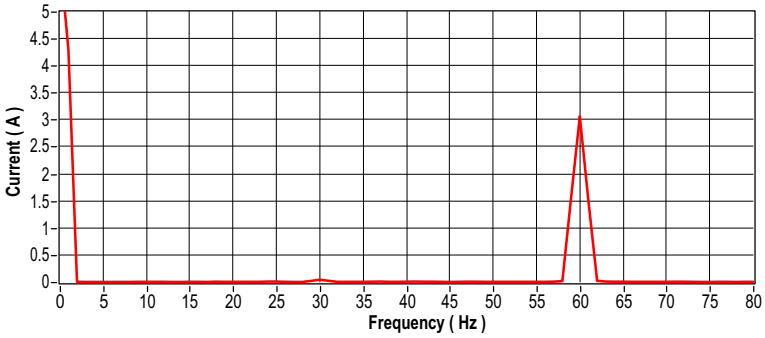

Figure 30. Current signal in the frequency domain.

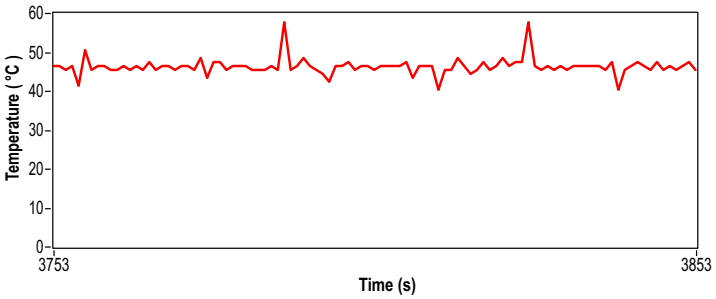

Figure 31. Temperature signal for the unbalanced motor.

5.1.3. Scenario 3: Data Collection from the Engine with Failed Bearings

Bearings consist of inner and outer rings, rolling elements (such as balls or rollers), and a cage. This component is widely recognized as one of the most frequent causes of failures in rotating machines. The premature emergence of failures is generally associated with inadequate operating conditions. Among the main factors that contribute to early bearing failures are dirt and water contamination, bearing overload, lack of lubrication, and inadequate procedures during assembly of the bearing assembly. The most common bearing failures tend to occur in the inner and outer races, and in the balls or rollers. Fault detection is usually performed by transforming the signal from the time domain to the frequency domain. This approach is adopted for several reasons. Firstly, machine faults are identified in the signal spectrum through peaks at characteristic frequencies, as each component or fault emits a unique frequency vibration. The intensity of the characteristic harmonic indicates the presence or severity of such a fault [34].

There are four basic frequencies generated by bearing defects:

- BPFI defect. Internal ring passage frequency.
- BPFO defect. Ring outer pass frequency.
- BSF defect. Rolling element passing frequency.
- FFT defect. Fundamental frequency (cage frequency).

On the SKF website, one of the main bearing manufacturers, a valuable online tool is available for calculating rotational and over-rolling frequencies. This calculator allows for the determination of bearing frequencies based on manual input of bearing geometric data. For comparison purposes with the data obtained from vibration signal analysis to identify defective bearings, calculations were carried out for the frequency of 30 mechanical Hz or 1800 RPM for the 6203–2z and 6204–2z bearings.

Figures 32 and 33 show the calculated rolling frequencies. Figure 34 shows the damaged 6403–2z and 6404–2z bearings used in this test scenario. The vibration signal is shown in Figure 35 in the time domain and Figure 36 in the frequency domain. The current signal is shown in Figure 37 in the time domain and Figure 38 in the frequency domain. The engine temperature for this scenario is illustrated in Figure 39.

Frequency Results

SKF	Rotational frequency				Frequency of over-rolling		
Designation	Inner ring	Outer ring	Rolling element set & cage	Rolling element about its axis	Point on inner ring	Point on outer ring	Rolling element
	f_i (Hz)	f_o (Hz)	f_c (Hz)	f_r (Hz)	f_{ip} (Hz)	f_{op} (Hz)	f_{rp} (Hz)
■ 6203-2Z	30	0	11.449	59.81	148.408	91.592	119.621

Figure 32. Failure occurrence frequencies for bearings 6203–2z.

Frequency Results

SKF	Rotational frequency				Frequency of over-rolling		
Designation	Inner ring	Outer ring	Rolling element set & cage	Rolling element about its axis	Point on inner ring	Point on outer ring	Rolling element
	f_i (Hz)	f_o (Hz)	f_c (Hz)	f_r (Hz)	f_{ip} (Hz)	f_{op} (Hz)	f_{rp} (Hz)
■ 6204-2Z	30	0	11.446	59.749	148.435	91.565	119.498

Figure 33. Failure occurrence frequencies for bearings 6204–2z.

Figure 34. Bearings with defects 6203–2z/6204–2z.

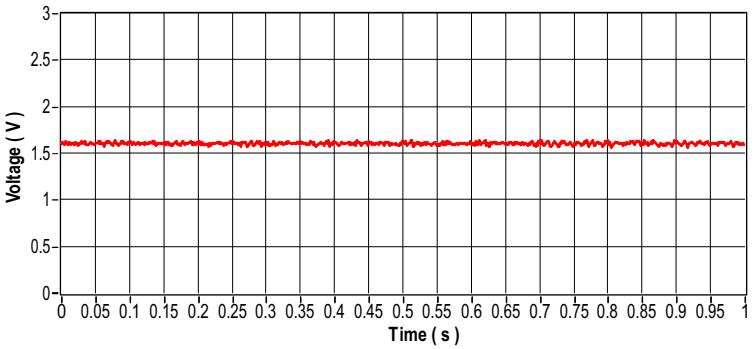

Figure 35. Vibration signal in the time domain.

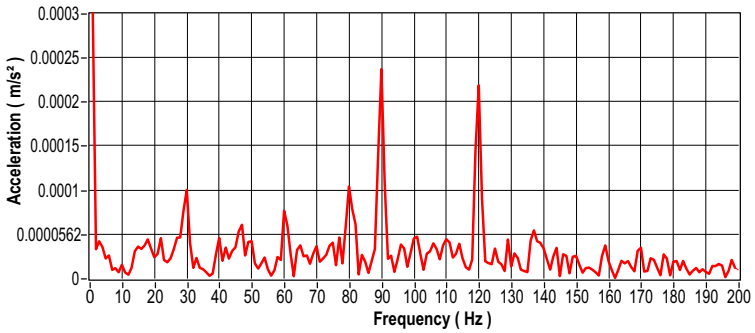

Figure 36. Vibration signal in the frequency domain.

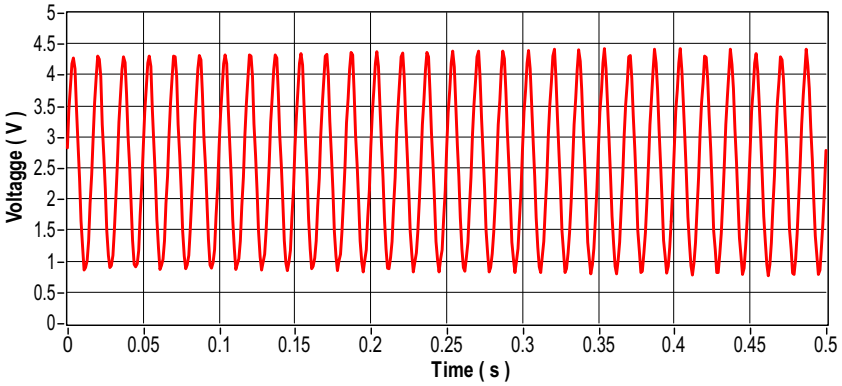

Figure 37. Current signal in the time domain.

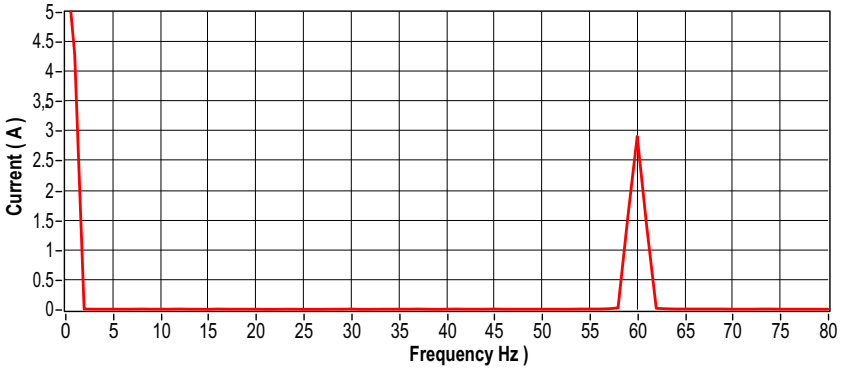

Figure 38. Current signal in the frequency domain.

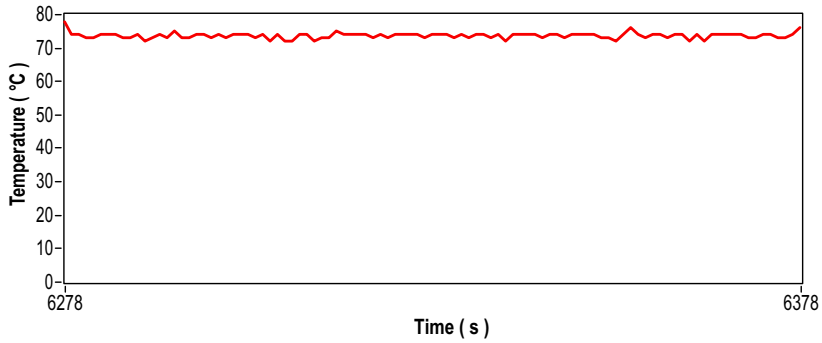

Figure 39. Temperature signal of motor bearing with defect.

5.1.4. Scenario 4: Motor Data Collection with Stator Current Imbalance

When the stator currents in an electric motor become unbalanced, several problems can arise, including overheating, excessive vibration, decreased efficiency, and premature wear. To investigate these phenomena, an approach was adopted: a bank of resistors with an ohmic load of 83.5 Ω was connected in series with one of the stator coils to cause variations in currents. Figure 40 shows the arrangement of the resistor bank used to induce such variations. Figure 41 (in the time domain) and Figure 42 (in the frequency domain) show the vibration signals recorded for this scenario. Figures 43–48 show the current readings, both in the time and frequency domains, corresponding to the three phases of the system. Finally, Figure 49 shows the temperature behavior for this same experimental scenario.

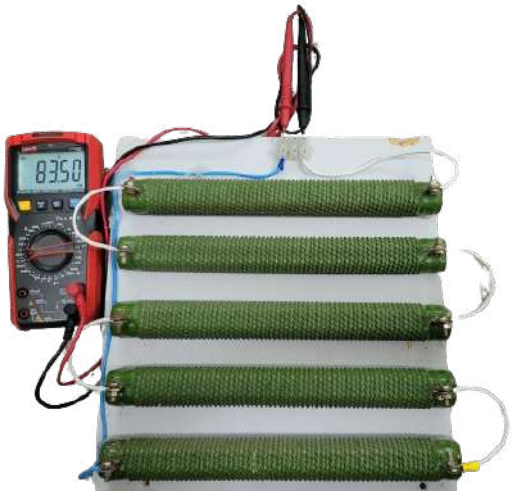

Figure 40. Bank of resistors for current unbalance.

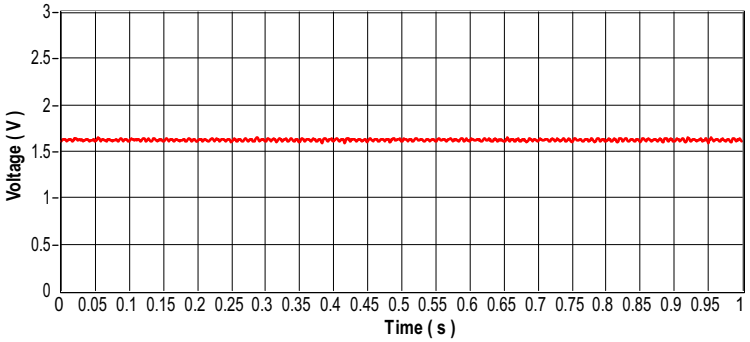

Figure 41. Vibration signal in the time domain.

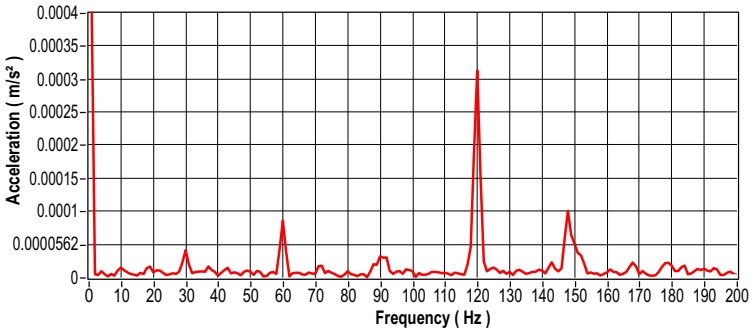

Figure 42. Vibration signal in the frequency domain.

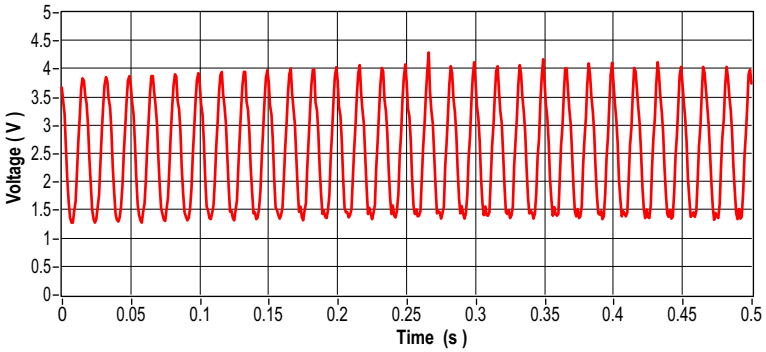

Figure 43. Current signal in the time domain—Phase 1.

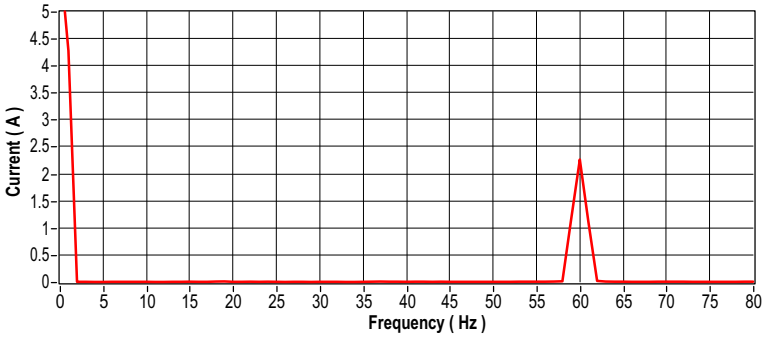

Figure 44. Current signal in the frequency domain—Phase 1.

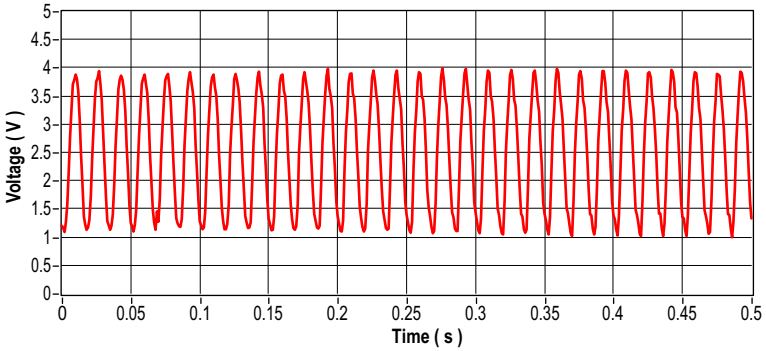

Figure 45. Current signal in the time domain—Phase 2.

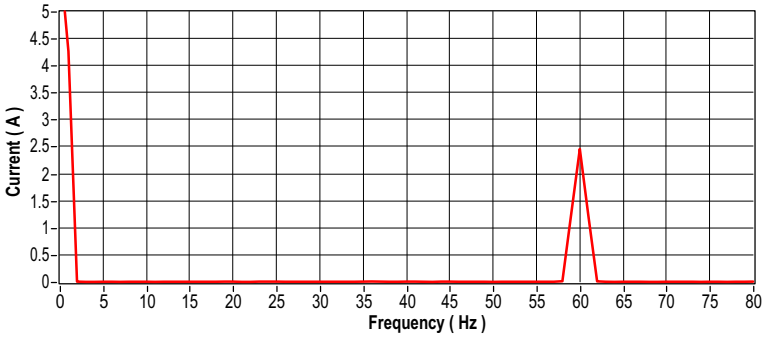

Figure 46. Current signal in the frequency domain—Phase 2.

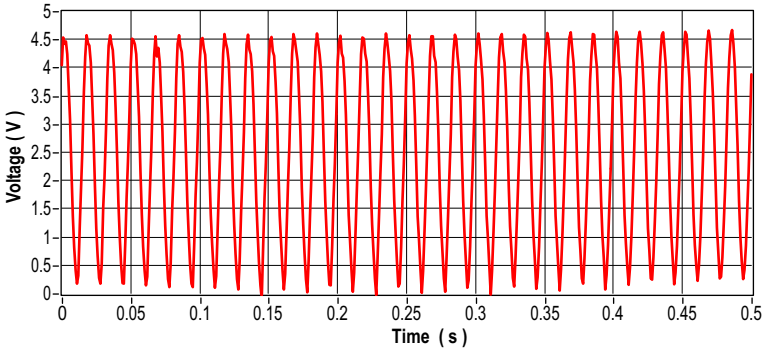

Figure 47. Current signal in the time domain—Phase 3.

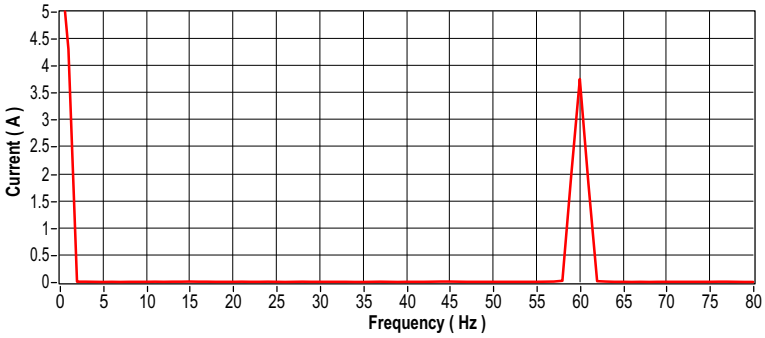

Figure 48. Current signal in the frequency domain—Phase 3.

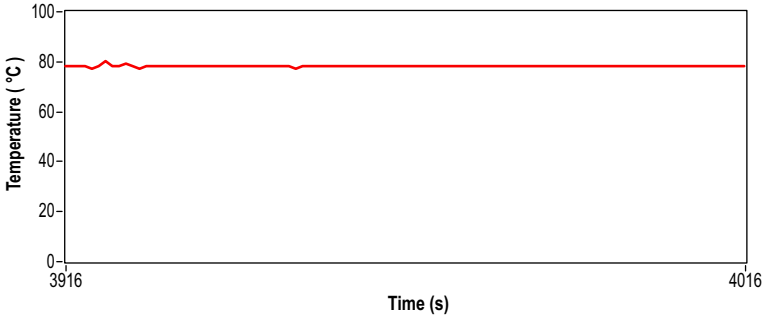

Figure 49. Temperature signal for phase unbalanced motor.

5.2. NARX Neural Network Training

The NARX network stands out for its use of recurrence and temporal delays in both inputs and feedback. During project development, it is essential to define the amount of delays and adjust other network-specific parameters, such as the number of neurons in each layer, the activation function of each neuron, and the learning algorithm used.

To obtain the best results, the NARX neural network was subjected to multiple trainings in a scan loop to determine the optimal number of neurons in the two hidden layers and the delays at both inputs and output. The training was carried out with datasets of 50 thousand events, collected from the four previously mentioned scenarios, using Matlab® software in offline mode. After training, the best network configuration was identified and subjected to testing and validation to evaluate its generalization capacity. Four different types of network outputs were examined, corresponding to different engine operating conditions: faultless motor, unbalanced defect, defective bearings, and defective stator.

During the optimization process, the following parameters were adjusted between 1 and 30 to find the optimal network configuration:

- Delay = delay steps for the input data.
- Feedback = output feedback delay steps.
- Neurons–H1 = number of neurons in the first hidden layer.
- Neurons–H2 = number of neurons in the second hidden layer.

To achieve the best network performance, the following parameter settings were determined:

- TrainFcn = 'trainscg'—"Scaled Conjugate Gradient" (SCG).
- TrainParam.epochs = 500—maximum number of training epochs.
- PerformFcn = 'crossentropy'—categorical cross-entropy cost function.
- layers1.transferFcn = 'logsig'—logistic sigmoid function first hidden layer.
- layers2.transferFcn = 'logsig'—logistic sigmoid function second hidden layer.
- layersend.transferFcn = 'softmax'—output activation function.

To train the network, a balanced dataset was used, ensuring that the number of examples of each type of failure was equal. After several training cycles, the optimal network configuration was identified, as illustrated in Table 6. Figure 50, the ROC curve,

and Figure 51, the confusion matrix, show the network's performance for the test set. Figure 52 shows the class graph showing the number of faults classified, and Table 7 presents the performance metrics of the trained network.

Table 6. Best parameters found from the trained network.

Delay	Feedback	Neurons-H1	Neurons-H2
3	4	10	10

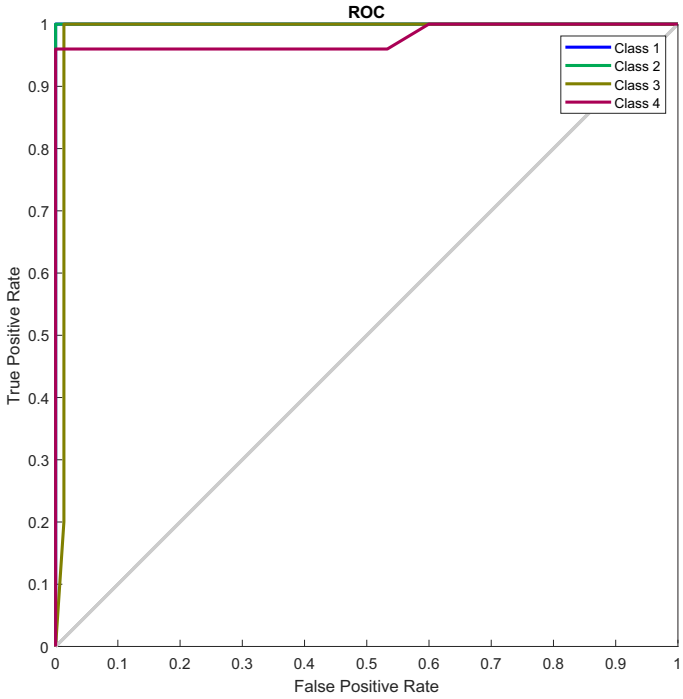

Figure 50. Standard training ROC curve.

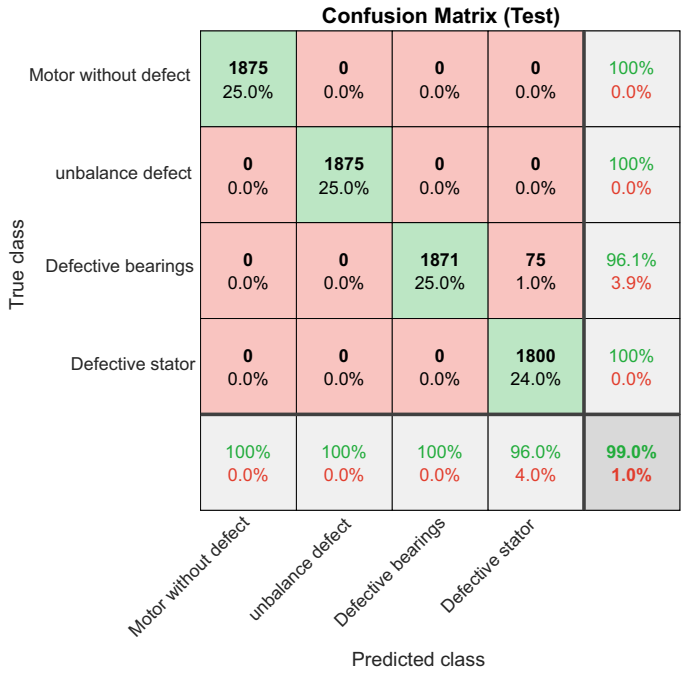

Figure 51. Standard training confusion matrix.

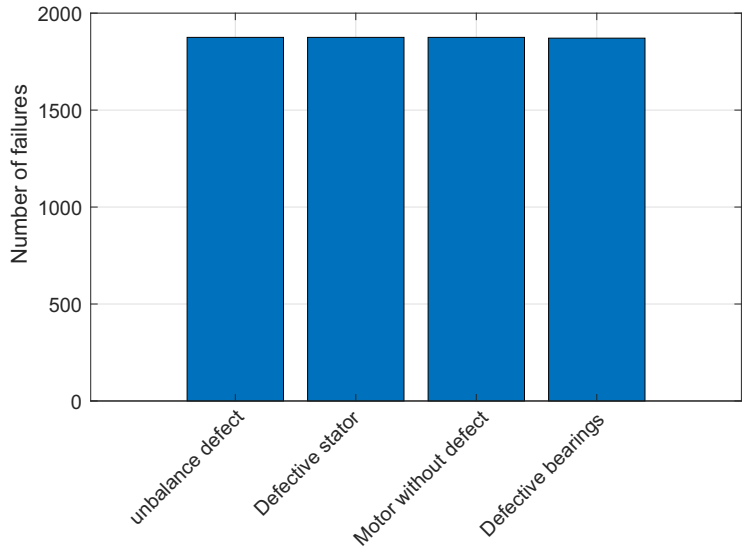

Figure 52. Failures classified in standard training.

Table 7. Performance of the trained NARX neural network.

Accuracy	Precision Total	Recall	F1 Score
0.99	1.0	0.99	0.99

Once the best network was obtained, it was necessary to validate it with new data from the engine signals. The tests described below aim to validate the NARX network implemented and trained previously to identify the four faults described in previous sections.

5.2.1. Case 1: Network Test—Motor without Failures

For this first network-validation scenario, a new dataset made up of signals collected from the engine in good operating conditions was inserted into the inputs of the NARX neural network. For this type of failure, the network responded well, achieving a performance of 94.2%. Figures 53–55 and Table 8 illustrate the network's overall performance.

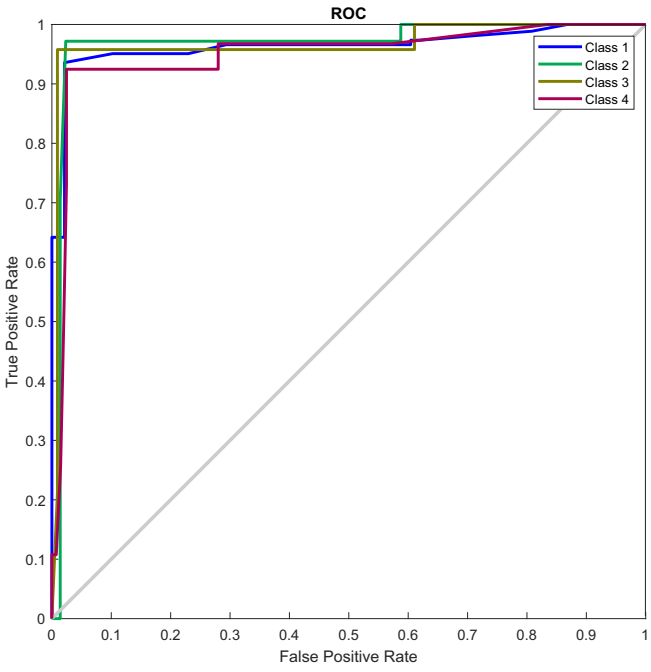

Figure 53. ROC curve of the motor without defect test set.

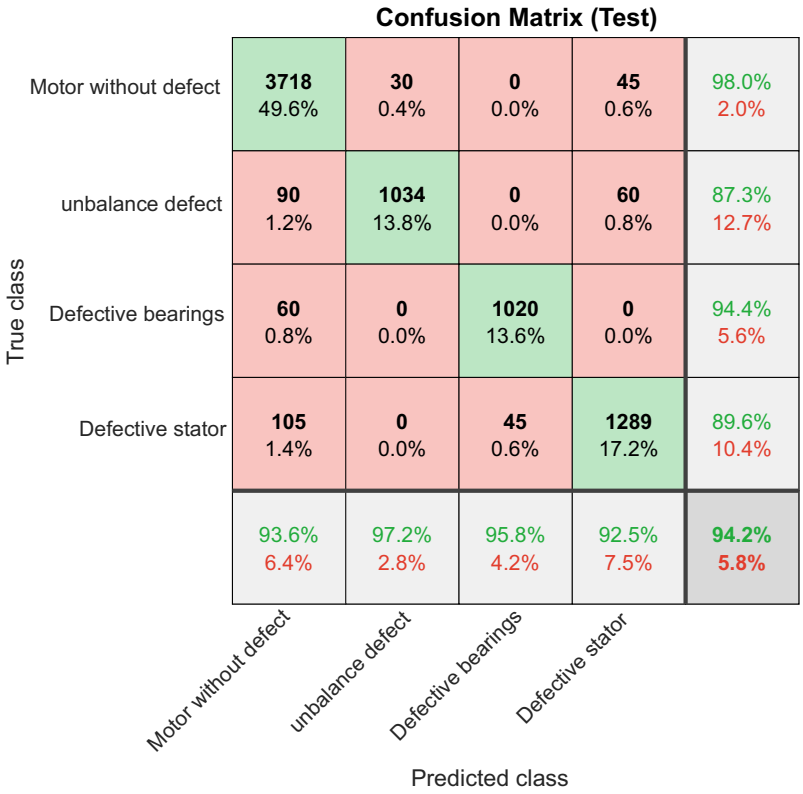

Figure 54. Confusion matrix of the 'Motor without defect' test set.

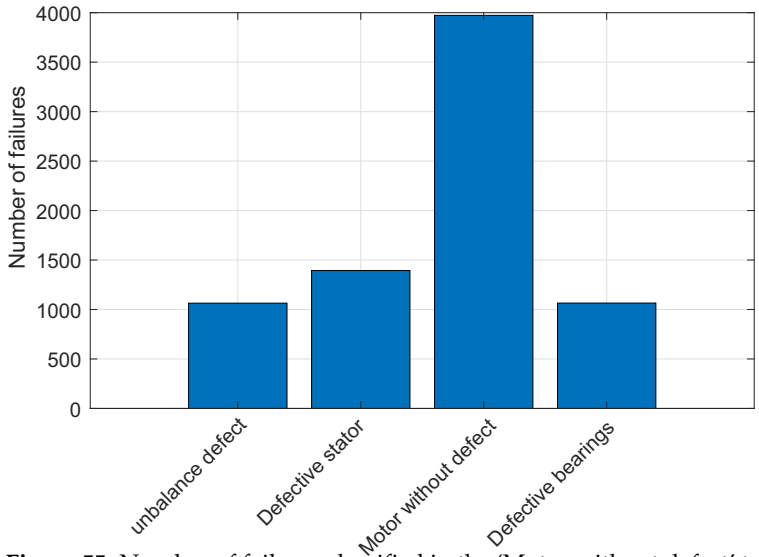

Figure 55. Number of failures classified in the 'Motor without defect' test set.

Table 8. Performance of NARX neural network for imbalance defect.

Accuracy	Precision Total	Recall	F1 Score
0.94	0.96	0.98	0.97

5.2.2. Scenario 2—Validation of the NARX Network—Unbalanced Fault

For this second network-validation scenario, a new dataset made up of signals collected from the motor with an unbalanced shaft was inserted into the inputs of the NARX neural network. For this type of fault, the network responded well, achieving a performance of 95%. Figures 56–58 and Table 9.

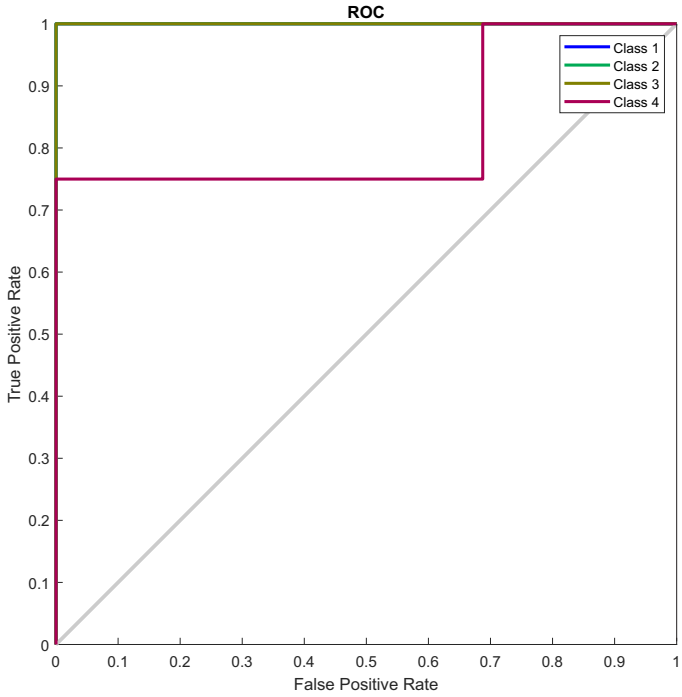

Figure 56. ROC curve of the defect unbalanced test set.

Figure 57. Confusion matrix of the 'Defect unbalance' test set.

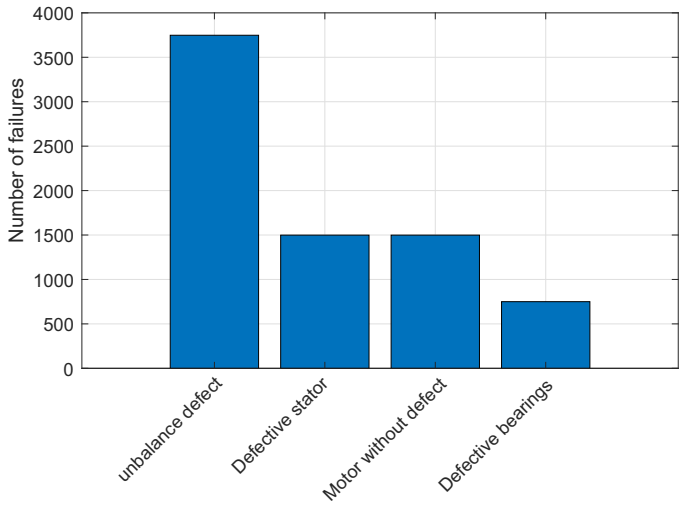

Figure 58. Number of failures classified in the 'Defect unbalance' test set.

Table 9. Performance of NARX neural network for imbalance defect.

Accuracy	Precision Total	Recall	F1 Score
0.95	1.0	0.95	0.97

5.2.3. Scenario 3—Validation of the NARX Network—Defective Bearings

For this third network-validation scenario, a new dataset made up of signals collected from the engine with damaged bearings was inserted into the NARX neural network inputs. For this type of fault, the network responded well, achieving a performance of 95%. Figures 59–61 and Table 10.

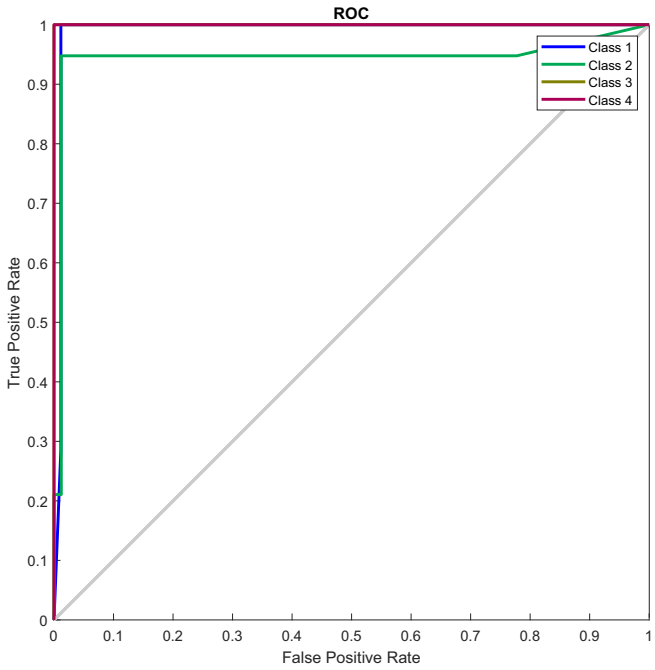

Figure 59. ROC curve of the faulty bearings test set.

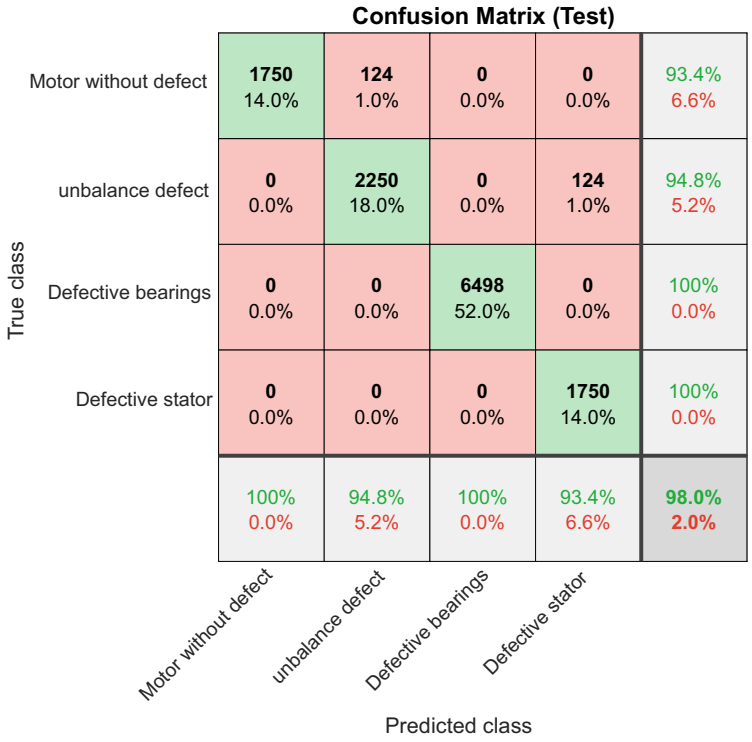

Figure 60. Confusion matrix for defective bearings.

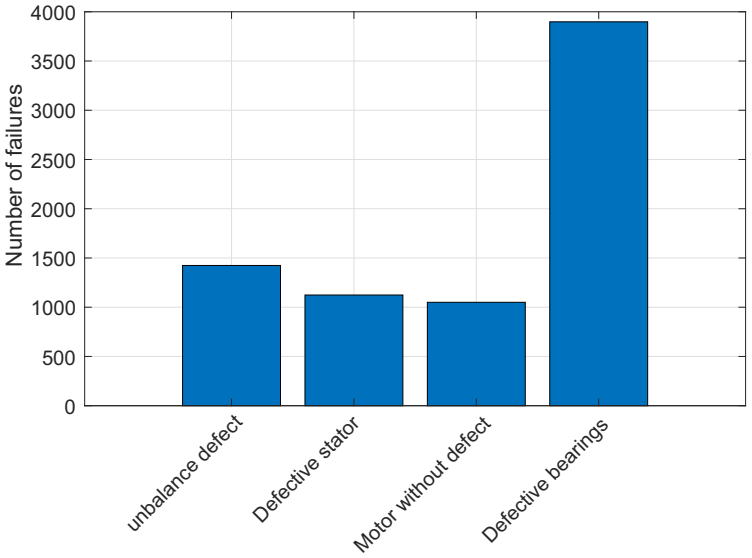

Figure 61. Classified failures for defective bearings.

Table 10. NARX neural network performance for defective bearings.

Accuracy	Precision Total	Recall	F1 Score
0.98	1.0	0.98	0.99

5.2.4. Scenario 4—Validation of the NARX Network—Faulty Stator

For this fourth network-validation scenario, a new dataset made up of signals collected from the motor with unbalanced stator phases was inserted into the inputs of the NARX neural network. For this type of fault, the network responded well, achieving a performance of 98%. Figures 62–64 and Table 11.

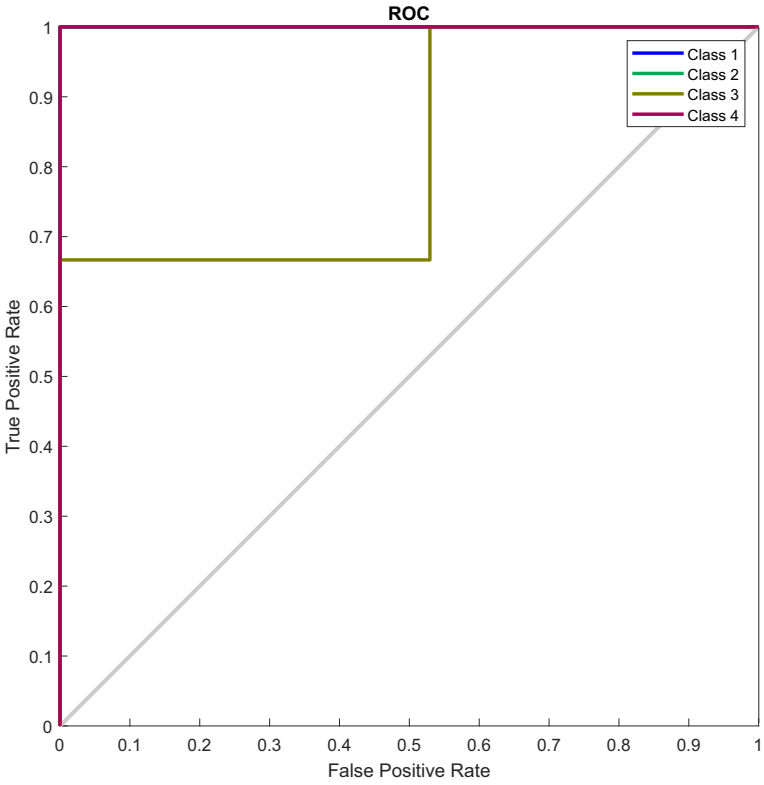

Figure 62. ROC curve for defective stator.

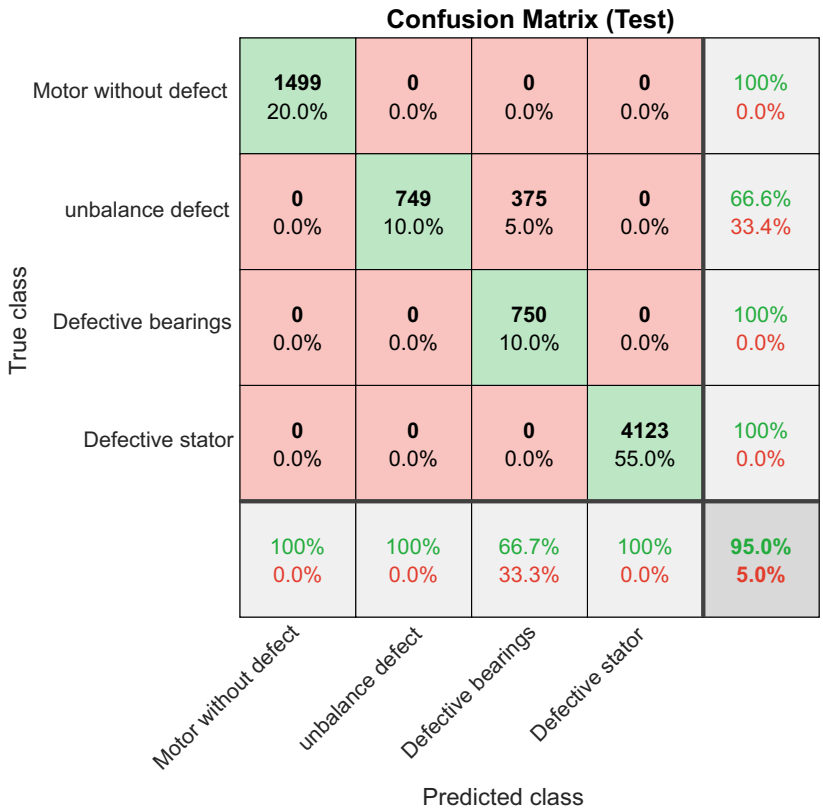

Figure 63. Confusion matrix for the defective stator.

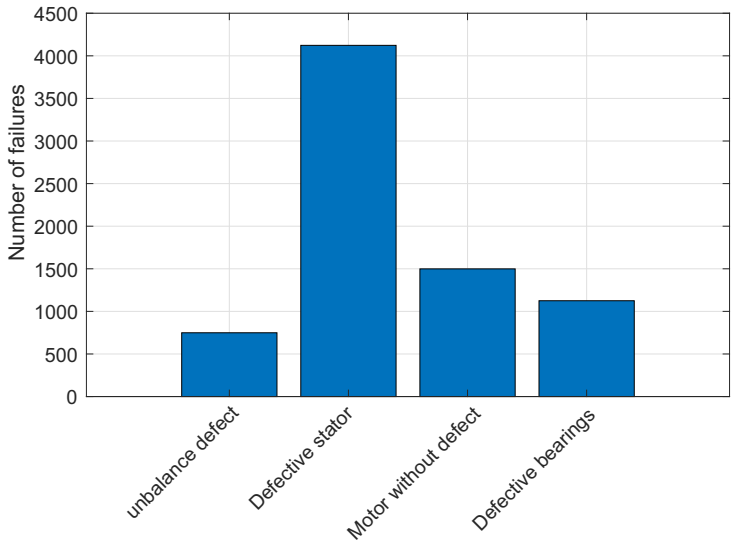

Figure 64. Faults classified for defective stator.

Table 11. Performance of NARX neural network for defective stator.

Accuracy	Precision Total	Recall	F1 Score
0.95	1.0	0.95	0.97

6. Discussion

The NARX model was used as a viable tool for diagnosing and classifying faults in three-phase induction motors. After a scanning process to find the best network, with the ideal number of neurons for the two hidden layers and the delays for the inputs and outputs, the selected network was subjected to a series of validation tests. The results of these tests showed that the network has an excellent generalization capacity in all the situations evaluated. The data obtained prove the network's excellent performance in classifying faults, even when new data are presented. Table 12 shows the hit rate for each engine condition in the four test scenarios discussed in Section 5.2.

Table 12. Performance of the NARX neural network for each type of fault classified.

Motor without Defect	Unbalanced Defect	Defective Bearings	Defective Stator
94.2%	95%	98%	95%

Comparing the Results

Various studies have investigated the application of machine learning algorithms for fault diagnosis in induction motors, presenting variations in their methodologies and results. The Multilayer Perceptron Neural Network (MLP) proposed by [17] for classifying faults in three-phase induction motors achieved an accuracy of 97%. Conversely, the SVM method used by [20] for detecting and classifying faults in three-phase induction motors within wind turbine pitch control systems achieved an overall accuracy of 98% on the training set and 96.5% on the test set.

In this context, the present study developed a Nonlinear Autoregressive Network with Exogenous Inputs (NARX) for classifying faults in three-phase induction motors, achieving an accuracy of 99% on the training set and 98% on the test set. The applied methodology included a rigorous validation process using a diverse dataset, which strengthens the reliability of the obtained results.

When comparing the results of previous studies with those of the present work, it is evident that the NARX neural network demonstrated superior performance. This increase in accuracy can be attributed to various factors such as the network structure, the quantity and diversity of the data used, and the validation process adopted. While the work of [17] demonstrated the effectiveness of the MLP and [20] evidenced the capability of the SVM, the present study highlights the superiority of the NARX neural network in the specific task of classifying faults in three-phase induction motors, and the incorporation of highly nonlinear relationships between electrical and mechanical quantities in NARX networks facilitates the classification of faults.

These quantities selected as input parameters in the NARX network define the dynamic and operational behavior of the motors, such as the engine power, temperature rise affecting the stator windings, and efficiency.

7. Conclusions

Three-phase induction motors play a crucial role in industrial processes. The proper functioning of this equipment is essential to ensure the good performance of the machines on the production line. The identification and classification of initial failures in these engines are vital to increasing efficiency, safety, reliability, and durability, thus ensuring quality production. Therefore, developing effective techniques for obtaining data and diagnosing faults in three-phase induction motors is essential. This paper focuses on the early identification of faults through the accurate diagnosis and classification of faults in three-phase induction motors using a neural network through the analysis of current, temperature, and vibration signals. The development and use of an Exogenous AutoRegressive Neural Network (NARX) for fault classification obtained satisfactory results, validating the effectiveness of the proposed method. The case study showed that the proposed method for developing a classification model using a neural network is very efficient in identifying failures in TIMs. Among the faults classified with greater accuracy, the proposed model stood out in detecting defective bearings, achieving an accuracy of 98% for new data. In this research, the neural network was developed in the Matlab® environment, which demonstrated an excellent performance. However, for future research, it is important to consider the need to adapt the code to a language that can be incorporated into embedded systems for real-time detection.

The main differences of the NARX neural network are the following:

Dynamical Systems Modeling: The NARX network is designed to model dynamical systems, where the future state of the system depends not only on current inputs but also on previous states. This characteristic is particularly important in engine analysis, where operating conditions may vary over time and failures may develop gradually. The ability to consider the history of engine states allows the NARX network to identify complex temporal patterns that other neural networks may not capture.

Inclusion of Exogenous Inputs: The NARX network can incorporate exogenous inputs, such as environmental or operational variables, that can influence engine performance. For example, ambient temperature, applied load, and other external conditions can be included in the model, providing a more holistic and accurate analysis of engine conditions.

Robustness in Prediction and Diagnosis: Due to its autoregressive structure, the NARX network is more robust in predicting and diagnosing failures, even in situations where the data are noisy or incomplete. The ability to make predictions based on historical data helps in the early identification of anomalies, enabling corrective actions before failures become critical.

Versatility and Adaptability: The NARX network can be trained for different engine types and operating conditions, making it a versatile and adaptable tool. Its flexibility allows it to be applied to a wide range of fault-diagnosis scenarios, from induction motors to direct current motors and synchronous motors.

The use of a NARX neural network in engine fault classification offers significant advantages in terms of accuracy, robustness, and dynamic systems' modeling capabili-

ties. Its ability to incorporate exogenous inputs and consider historical states makes it a powerful tool for predictive maintenance and the efficient management of electric motors. Adopting this technology can result in better fault detection, reduced maintenance costs, and increased operational reliability.

An innovative aspect of this work is the application of the NARX neural network as a multiclass classifier for failures in three-phase induction motors. NARX networks are typically used for time series forecasting, so their application in this context is relatively rare in the scientific literature. Thus, this paper makes a significant contribution to technical and scientific advancements in this field.

Author Contributions: V.G.d.A., J.M.M.V., and A.O.-S.B. conceived and designed the study; V.G.d.A., J.M.M.V., A.O.S. and D.A.d.M.F. were responsible for the methodology; V.G.d.A., A.O.-S.B., R.d.A.T., and D.A.d.M.F. performed the simulations and experiments; V.G.d.A., A.O.-S.B., J.M.M.V., E.R.L.V., R.d.A.T. and D.A.d.M.F. reviewed the manuscript and provided valuable suggestions; V.G.d.A., J.M.M.V., E.R.L.V., R.d.A.T., and D.A.d.M.F. wrote the paper; J.M.M.V. and A.O.-S.B. were responsible for supervision. All authors have read and agreed to the published version of the manuscript.

Funding: This research was funded and supported by the Coordenação de Aperfeiçoamento de Pessoal de Nível Superior—Brasil (CAPES)—Finance and Conselho Nacional de Desenvolvimento Científico e Tecnológico (CNPq).

Conflicts of Interest: The authors declare no conflicts of interest.

Abbreviations

The following abbreviations are used in this manuscript:

ANN	Artificial Neural Network
DC	Direct current
FFT	Fast Fourier Transform
FIS	Fuzzy Inference System
GA	Genetic Algorithm
IM	Induction motor
LM	Levenberg–Maquardt
ML	Machine learning
MLP	Multilayer Perceptron
MSE	Mean Square Error
NARX	Nonlinear AutoRegressive Exogenous inputs
RNN	Recurrent neural network
SVM	Support vector machine
TIM	Three-phase induction motor

References

1. Graciola, C.L.; Goedtel, A.; Castoldi, M.F.; Gentil, M.G.; Souza, W.A.; Vitor, A.L.O. An Efficiency Study of a Three-Phase Induction Motor Through Predictive Control Strategies. In Proceedings of the 2023 15th IEEE International Conference on Industry Applications (INDUSCON), São Bernardo do Campo, Brazil, 22–24 November 2023; pp. 899–905. [CrossRef]
2. Santos, M.S.; Paz, E.H.; Aguiar, V.B.; Pontes, R.T. Non-invasive monitoring system for analysis of energy efficiency of three-phase induction motors. In Proceedings of the 2022 Workshop on Communication Networks and Power Systems (WCNPS), Fortaleza, Brazil, 17–18 November 2022; pp. 1–6. [CrossRef]
3. Ojaghi, M.; Mohammadi, M. Modeling eccentricity faults with axial asymmetry in three-phase induction motors. In Proceedings of the IECON 2016—42nd Annual Conference of the IEEE Industrial Electronics Society, Florence, Italy, 23–26 October 2016; pp. 1524–1529. [CrossRef]
4. Alsaedi, M.A. Fault diagnosis of three-phase induction motor: A review. *Optics* **2015**, *4*, 1–8. [CrossRef]
5. Sheikh, A.; Bakhsh, S.; Irfan, M.; Nor, N.; Nowakowski, G. A Review to Diagnose Faults Related to Three-Phase Industrial Induction Motors. *J. Fail. Anal. Prev.* **2022**, *22*, 1546–1557. [CrossRef]
6. Broniera, P.J.; Gongora, W.S.; Goedtel, A.; Godoy, W.F. Diagnosis of stator winding inter-turn short circuit in three-phase induction motors by using artificial neural networks. In Proceedings of the 2013 9th IEEE International Symposium on Diagnostics for Electric Machines, Power Electronics and Drives (SDEMPED), Valencia, Spain, 27–30 August 2013; pp. 281–287. [CrossRef]

7. Okpo, E.E.; Le Roux, P.F.; Nnachi, A.F. Induction Motor Fault Identification using Support Vector Machine. In Proceedings of the 2023 6th International Conference on Renewable Energy and Power Engineering (REPE), Beijing, China, 15–17 September 2023; pp. 168–174. [CrossRef]
8. Narwade, S.; Kulkarni, P.; Partil, C. Fault detection of induction motor using current and vibration monitoring. *Int. J. Adv. Comput. Res.* **2013**, *3*, 272.
9. Almounajjed, A.; Sahoo, A.K.; Kumar, M.K. Diagnosis of stator fault severity in induction motor based on discrete wavelet analysis. *Measurement* **2021**, *182*, 109780. [CrossRef]
10. Xuhong, W.; Yigang, H. Diagonal recurrent neural network based on-line stator winding turn fault detection for induction motors. In Proceedings of the 2005 International Conference on Electrical Machines and Systems, Nanjing, China, 27–29 September 2005; Volume 3, pp. 2266–2269.
11. Aydin, I.; Karakose, M.; Akin, E. Artificial immune based support vector machine algorithm for fault diagnosis of induction motors. In Proceedings of the 2007 International Aegean Conference on Electrical Machines and Power Electronics, Bodrum, Turkey, 10–12 September 2007; pp. 217–221.
12. Cho, H.C.; Knowles, J.; Fadali, M.S.; Lee, K.S. Fault detection and isolation of induction motors using recurrent neural networks and dynamic Bayesian modeling. *IEEE Trans. Control. Syst. Technol.* **2009**, *18*, 430–437. [CrossRef]
13. Ramalho, G.L.B.; Pereira, A.H.; Rebouças Filho, P.P.; Medeiros, C.M.d.S. Detecção de falhas em motores elétricos através da classificação de padrões de vibração utilizando uma rede neural ELM. *Holos* **2014**, *4*, 185–194. [CrossRef]
14. Vitor, A.L.O.; Oliveira, F.M.; Ronqui, L.A.; Goedtel, A.; Scalassara, P.R.; Silva, S.A.O.; Vallim, M.B.R. Detecção de falhas elétricas em motores de indução utilizando rede radial basis function. *An. Congr. Bras. Automá Tican* **2014**, *46*, 37–42.
15. Jagadanand, G.; Dias, F.L. ARM based induction motor fault detection using wavelet and support vector machine. In Proceedings of the 2015 IEEE International Conference on Signal Processing, Informatics, Communication and Energy Systems (SPICES), Kozhikode, India, 19–21 February 2015; pp. 1–4.
16. Sobrinho, C.A.N.; Lima Filho, A.C.; de Sena, A.P.C.; Brito, J.N.; da Silva, J.F.; Mafaldo, M. Wavelet Transform for detecting broken bars in Three-Phase Induction Motors. *Principia Mag. IFPB Sci. Technol. Dissem.* **2018**, *42*, 72–83.
17. Gongora, W.S.; Goedtel, A.; da Silva, S.A.O.; Graciola, C.L. Neural approach to fault detection in three-phase induction motors. *IEEE Lat. Am. Trans.* **2016**, *14*, 1279–1288. [CrossRef]
18. Liu, R.; Yang, B.; Zio, E.; Chen, X. Artificial intelligence for fault diagnosis of rotating machinery: A review. *Mech. Syst. Signal Process.* **2018**, *108*, 33–47. [CrossRef]
19. Ding, A.; Yi, X.; Qin, Y.; Wang, B. Self-driven continual learning for class-added motor fault diagnosis based on unseen fault detector and propensity distillation. *Eng. Appl. Artif. Intell.* **2024**, *127*, 107382. [CrossRef]
20. Kandukuri, S.T.; Senanyaka, J.S.L.; Robbersmyr, K.G. A two-stage fault detection and classification scheme for electrical pitch drives in offshore wind farms using support vector machine. *IEEE Trans. Ind. Appl.* **2019**, *55*, 5109–5118. [CrossRef]
21. WEG Specification Guide: Electric Motors. In Portuguese Language. 2023.
22. Guedes, J.J.; Goedtel, A.; Castoldi, M.F.; Sanches, D.S.; Serni, P.J.A.; Rezende, A.F.F.; Bazan, G.H.; de Souza, W.A. Three-phase induction motor fault identification using optimization algorithms and intelligent systems. In *Soft Computing*; Springer: Berlin/Heidelberg, Germany, 2024; pp. 1–16.
23. Silva, M.A.; Lucena-Junior, J.A.; da Silva, J.C.; Belo, F.A.; Lima-Filho, A.C.; Ramos, J.G.G.d.S.; Camara, R.; Brito, A. Sensorless Speed Estimation of Induction Motors through Signal Analysis Based on Chaos Using Density of Maxima. *Entropy* **2024**, *26*, 361. [CrossRef] [PubMed]
24. Lucas, G.B.; de Castro, B.A.; Rocha, M.A.; Andreoli, A.L. Three-phase induction motor loading estimation based on Wavelet Transform and low-cost piezoelectric sensors, Measurement. *Measurement* **2020**, *164*, 107956. [CrossRef]
25. Oliveira, R.F. *Artificial Intelligence in Portuguese*; Educational Publisher and Distributor S.A.: Londrina, Brazil, 2018.
26. Santos, G.R.; Brito, J.N.; Santana, C.; Lara, H. Monitoring of three-phase motors through artificial intelligence. In *Anais do XVIII Congresso Nacional de Engenharia Mecânica e Industrial*; Embra Embra Serviços em Tecnologia Ltda EPP: Campinas, Brazil, 2018; Volume 2.
27. Preethi, I.; Suryaprakash, S.; Mathankumar, M. A State-of-Art Approach on Fault Detection in Three Phase Induction Motor using AI Techniques. In Proceedings of the 2021 5th International Conference on Computing Methodologies and Communication (ICCMC), Erode, India, 8–10 April 2021; pp. 567–573. [CrossRef]
28. Mohamed, M.; Mohamed, E.; Mohamed, A.A.; Abdel-Nasser, M.; Hassan, M.M. Detection of Inter Turn Short Circuit Faults in Induction Motor using Artificial Neural Network. In Proceedings of the 2020 26th Conference of Open Innovations Association (FRUCT), Yaroslavl, Russia, 20–24 April 2020; pp. 297–304. [CrossRef]
29. Aquize, R.; Cajahuaringa, A.; Machuca, J.; Mauricio, D.; Mauricio Villanueva, J.M. System Identification Methodology of a Gas Turbine Based on Artificial Recurrent Neural Networks. *Sensors* **2023**, *23*, 2231. [CrossRef] [PubMed]
30. Khaled, S.; Fakhry, M.; Mubarak, A.S. Classification of pcg signals using a nonlinear autoregressive network with exogenous inputs (narx). In Proceedings of the 2020 International Conference on Innovative Trends in Communication and Computer Engineering (ITCE), Aswan, Egypt, 8–9 February 2020; pp. 98–102.
31. de Pádua Braga, A.; de Leon Ferreira, A.C.P.; Ludermir, T.B. *Artificial Neural Networks: Theory and Applications*; LTC Publisher: Hong Kong, China, 2007. (In Portuguese)

32. Junior, G.B.V.; Lima, B.N.; Pereira, A.A.; Rodrigues, M.F.; Oliveira, J.R.L.; Silio, L.F.; Carvalho, A.S.; Ferreira, H.R.; Passos, R.P. Métricas utilizadas para avaliar a eficiência de classificadores em algoritmos inteligentes. *Rev. Cpaqv-Centro Pesqui. Avançadas Qual. Vida* **2022**, *14*, 2.
33. Polo, T.C.F.; Miot, H.A. Applications of the ROC curve in clinical and experimental studies. *J. Vasc. Bras.* **2020**, 1–4.
34. César da Silva, J.; Lima, T.L.d.V.; Lucena Júnior, J.A.d.; Lyra, G.J.; Souto, F.V.; Pimentel, H.d.S.; Belo, F.A.; Lima Filho, A.C. Non-Invasive Method for In-Service Induction Motor Efficiency Estimation Based on Sound Acquisition. *Appl. Sci.* **2020**, *10*, 3757. [CrossRef]

Disclaimer/Publisher's Note: The statements, opinions and data contained in all publications are solely those of the individual author(s) and contributor(s) and not of MDPI and/or the editor(s). MDPI and/or the editor(s) disclaim responsibility for any injury to people or property resulting from any ideas, methods, instructions or products referred to in the content.

energies

MDPI

Article

Application of Active Disturbance Rejection in a Bearingless Machine with Split-Winding

Rodrigo de Andrade Teixeira [1,†], Werbet Luiz Almeida da Silva [1,†], Adson Emanuel Santos Amaral [2,†], Walter Martins Rodrigues [3,†], Andrés Ortiz Salazar [1,†] and Elmer Rolando Llanos Villarreal [3,*,†]

1 Department of Computer Engineering and Automation, Federal University of Rio Grande do Norte (DCA-UFRN), Natal 59072-970, Brazil
2 School of Science and Technology, University of Rio Grande do Norte (UFRN), Natal 59072-970, Brazil
3 Department of Natural Sciences, Mathematics, and Statistics, Federal Rural University of Semi-Arid (DCME-UFERSA), Mossoró 59625-900, Brazil
* Correspondence: elmerllanos@ufersa.edu.br
† These authors contributed equally to this work.

Abstract: In this paper it is proposed the displacement control of a bearingless induction machine (BIM) with split winding and optimized drive structure using Active Disturbance Rejection Control (ADRC). Considering that the BIM is a multivariable, nonlinear, and time-varying system with coupled variables, advanced control techniques can be useful in order to make the system operate efficiently and with good dynamic performance. The ADRC considers the total disturbance, composed of unmodeled dynamics, nonlinearities, uncertainties, and load variations, as an extended state and estimates it in real-time through a state observer. This increases the overall robustness of the control system to disturbances of different natures. The application of the ADRC technique on the radial position control of the BIM used in this work showed that a Linear version of ADRC is not able to compensate for radial load disturbances but this drawback can be solved by the use of a nonlinear observer in the ADRC structure. Besides that, both control versions of the ADRC were able to make stable the naturally unstable radial displacement of the machine's rotor.

Keywords: ADRC control; induction machine; radial position control

check for updates

Citation: Teixeira, R.d.A.; da Silva, W.L.A.; Amaral, A.E.S.; Rodrigues, W.M.; Salazar, A.O.; Villarreal, E.R.L. Application of Active Disturbance Rejection in a Bearingless Machine with Split-Winding. *Energies* **2023**, *16*, 3100. https://doi.org/10.3390/en16073100

Academic Editors: Jin-Woo Ahn, Jang-Young Choi and Jaehyuk Kim

Received: 28 February 2023
Revised: 24 March 2023
Accepted: 27 March 2023
Published: 29 March 2023

Copyright: © 2023 by the authors. Licensee MDPI, Basel, Switzerland. This article is an open access article distributed under the terms and conditions of the Creative Commons Attribution (CC BY) license (https://creativecommons.org/licenses/by/4.0/).

1. Introduction

Magnetically suspended induction machines meet a specific industry demand for less noisy motors that can reach higher speeds and do not cause product contamination in situations where the machine directly handles the process. The induction motor is a multivariable, nonlinear system [1] that has a strong coupling between variables. When used in bearingless systems, the degree of control complexity is even greater, especially when placed in situations with shaft load application. In these cases, linear controllers may not achieve a sufficiently fast and stable response for adequate suspension and control of the other system parameters. The emergence of microprocessor devices and power electronics has provided conditions for the application of advanced control theories such as predictive controllers, sliding mode controllers, neural and artificial network-based controllers, Fuzzy controllers, and others [2].

In recent years, the ADRC technique has been used for the control of various types of systems [3–8]. ADRC is a robust control technique that uses state observers in order to estimate in real time the disturbances and uncertainties involved in the controlled process, and from this estimation obtains a good capacity to reject disturbances [9]. ADRC Control is a controller originally based on nonlinear functions, composed of three main blocks: Tracking Differentiator (TD), Extended State Observer (ESO), and the block corresponding to the control law that has received different contributions over the years. The tracking

differentiator provides a smoothed version of the input signal and its derivatives. The extended state observer processes the control signal and the system output to estimate the states variables of the process.

As a fundamental step in the acceptance process of a new control technique in industrial systems, the ADRC is being tested in many different systems. Experimental runs are creating information about the applicability of this control technique, and its potential and limitations are being discovered. Furthermore, the characteristics of the bearingless machine with split-winding with optimized drive structure, such as the natural unstable behavior of radial displacement outputs and complexities of the electrical machine itself makes the process of extending the results obtained by other systems to the BIM complex.

This work investigated the application of ADRC controllers to the position control of a bearingless split-winding induction machine, aiming to understand the limitations of applying this type of controller to the motor-bearing system and to explore the benefits that a technique with active disturbance rejection can bring to radial position control. Keeping the linear structure of the ADRC fixed, this paper analyzed two extended state observer structures. The first structure uses a linear observer and the second structure uses a nonlinear extended state observer, which makes it possible to observe the influence of the addition of nonlinearities on the dynamic performance of the system.

The remainder of the article is structured as follows: Section 2 shows the electrical structure of the BIM with a split-winding and optimized driving system. Section 3 shows the structure of the ADRC controller, the structure of the LADRC controller, and the control structures using linear and nonlinear observer. Section 4 describes the experimental bench used and the control algorithm implemented. Section 5 shows and discusses the experimental results and Section 6 reports the conclusion of the work.

In [10,11] investigates the application of the Active Disturbance Rejection Control (ADRC) technique on the stabilization and control of the rotor radial position of a bearingless induction machine with split winding.

2. Split-Winding Bearingless Motor

The first split-winding bearing motor was proposed by Salazar & Stephan [12]. They built a 4-pole two-phase motor that used the motor's torque coils for radial force generation. In this topology, only one of the phases was responsible for radial position control and both phases were used for torque generation. The two-phase motor proposed by [12] was the starting point for the work of [13], who proposed a three-phase motor in which the coils of each phase were divided into two. In this topology, the three phases were used in the generation of radial force and torque. In [14], the speed vector control of the three-phase motor-mancal was done using neural networks for rotor flux estimation. In this work, the performance of the machine operating with a conventional state estimator and with a neural state estimator was compared. In [15], analyzed the feasibility of using a conventional induction machine as a split-winding bearingless motor. He performed position and current control of the machine, however, he observed that radial position control was not satisfactory for speeds below rated. Ref. [16] studied the replacement of PID controllers for radial position control with controllers based on Fuzzy logic. Noting the strong nonlinear and parameter-varying characteristics of induction motor bearings, he analyzed the contribution of Fuzzy controllers on transient and permanent regime performance. In order to reduce the number of equipment needed for machine control, Ref. [17] optimized the structure of the motor bearing by proposing a new way to connect the coils in the machine stator. In [17] investigated the spatial distribution of the machine's coils and realized that it was possible to generate the radial position control components using only two phases. In this topology, the coils of one of the machine phases are connected directly to the center point of the inverter's DC bus. In this way, only two phases are controlled and the drive structure is optimized.

In this paper, the ADRC control technique is applied with two different structures to the control of a bearingless induction machine, the first structure uses linear estimation

while the second uses nonlinear estimation. The results obtained show the dynamic behavior of the system output and states for the two versions.

Operation Principle

In the bearingless split-winding induction machine, the electric currents in the stator and rotor coils generate magnetic fields that interact with each other. As a result of this interaction, forces arise that act on the rotor, promoting its rotation and radial positioning. In the stator of the three-phase bearing motor, there are three divided groups of windings, where each phase is displaced by 120° relative to the others. With this distribution, it is possible to control the radial positioning of the rotor in all directions from the composition of the radial forces generated. Figure 1 shows the position of the windings relative to the X and Y axes.

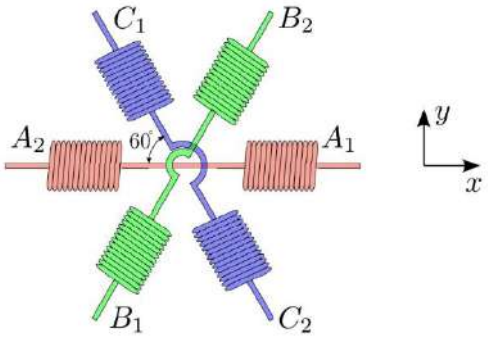

Figure 1. Spatial arrangement of the stator windings of a bearingless induction motor with split winding.

In the optimization proposal by Ref. [17], the coil connection arrangement was modified to the structure shown in Figure 2. This modification reduced the number of control and drive components for the currents in each phase.

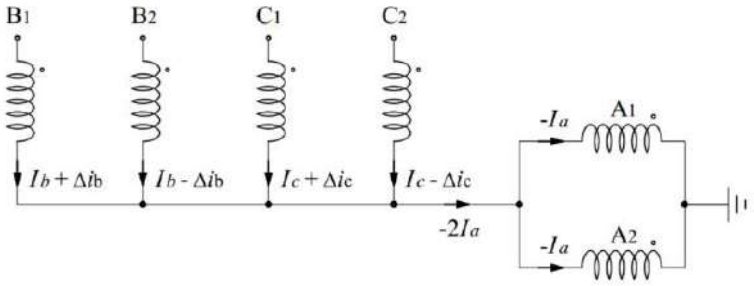

Figure 2. Connection of the coils for two-phase position control.

Considering the currents I_b and I_c are given respectively by:

$$I_b = I_m cos(\omega t - \frac{2\pi}{3}) \qquad (1)$$
$$I_c = I_m cos(\omega t + \frac{2\pi}{3})$$

The sum of these currents, for the circuit in Figure 2 results in:

$$I_b + I_c = I_m cos(\omega t) \qquad (2)$$

Since $I_b + I_c = -I_a$, it can be seen that for the modification performed by Ref. [17], the characteristics of the coil currents of phase A have been preserved.

We will illustrate the behavior of the currents per phase in the split-wound three-phase induction machine driven by a 4-arm inverter. Figure 3 shows the waveforms of the currents in each phase for the situation where the rotor is centered on the air gap. When

the rotor is centered, the modulation components are zero, therefore the phase currents have the same modulus $I_a = I_b = I_c$.

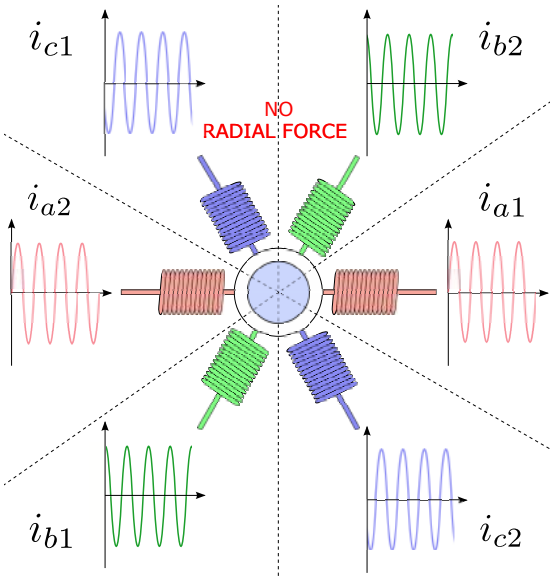

Figure 3. Stator of the bearingless induction motor with split winding.

When unbalance occurs in one of the modulation components or disturbances that tend to move the rotor radially, the phase currents are altered by the control system in order to generate radial forces that bring the rotor back to the center of the stator.

Figure 4 shows the behavior of the currents during radial force generation to the right. To move the rotor shaft in the indicated direction, the control system must increase the currents of coils B_1 and C_2, and reduce the currents of coils B_2 and C_1.

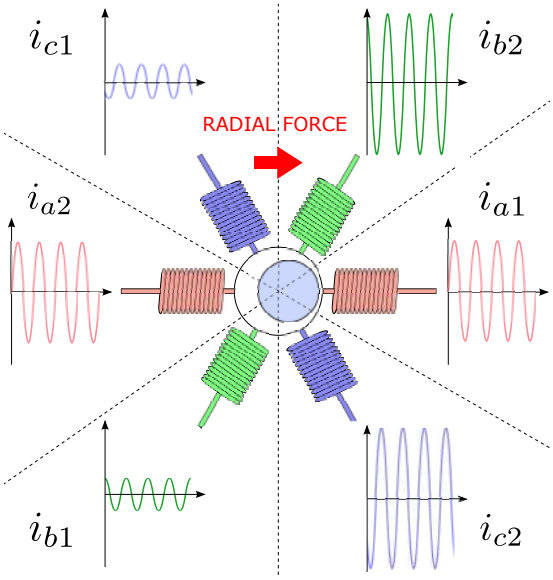

Figure 4. Stator of the bearingless induction motor with split-winding subjected to right-side radial force.

3. ADRC Control

Modern control theory is focused on the time domain and can be applied to systems with multiple inputs and outputs, linear and nonlinear systems, and time-varying and time-invariant systems. One of the difficulties of modern state feedback control systems is that some variables are not accessible by measurement. In this sense, the concept of

a state observer becomes very useful to reconstruct non-measurable state variables from measurable variables. The Active Disturbance Rejection Control technique uses state observers to estimate in real-time the disturbances involved in the controlled process and then uses this information to obtain a good disturbance rejection capability [9].

The structure of an ADRC controller is implemented based on three blocks: a reference generator, controller, and estimator. Figure 5 shows the general idea of a generic process controlled by an ADRC structure. The reference generator block provides a smoothed version of the input signal and its derivatives. The estimator processes the control signal and the system output to estimate the state variables of the process. As will be shown soon in this section, the ADRC structure includes an additional state on the estimator that lump all system uncertainties and disturbances. As the estimator provides a numeric value to the additional state, its effect is removed from the control loop by means of an internal feed-forward loop. This mechanism simplifies the natural plant dynamic from the controller block point of view. This way the controller only needs to deal with an emulated and simpler plant.

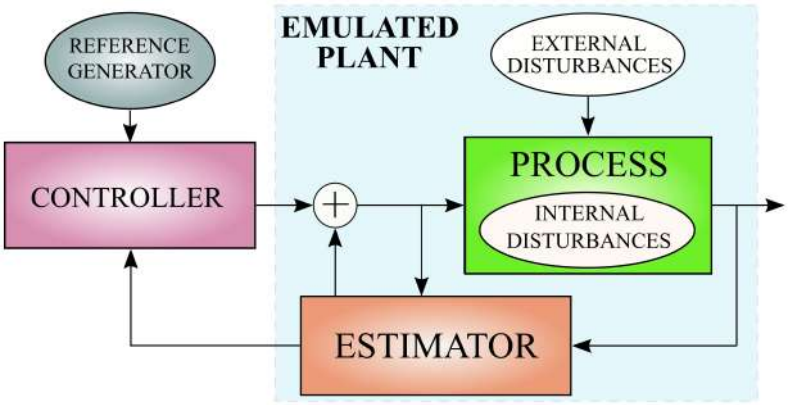

Figure 5. General idea of the ADRC controller.

To provide a mathematical approach to the general idea of an ADRC controller, let us consider a generic second-order process given by:

$$\ddot{y} = -a\dot{y} - by + w + bu \tag{3}$$

where y is the output; u is the input; w represents an external disturbance; a and b are system parameters. By the control systems literature, the parameter b is equivalent to the system input gain. Considering that the numeric value of b is not available, it is possible to consider that $b \approx b_0$ and the difference between the real and the approximated value can be included to the system dynamic in Equation (3) by:

$$\ddot{y} = -a\dot{y} - by + w + (b - b_0)u + b_0u \tag{4}$$

The term $b - b_0$ is part of the uncertainty in the system model. Consider that all unknown terms of Equation (3) can be grouped and a unique variable is used instead them:

$$\ddot{y} = f + b_0u \tag{5}$$

This way, $f = -a\dot{y} - by + w + (b - b_0)u$. The variable f is named in the ADRC technique as generalized disturbance and its value is equivalent to the combined effect of dynamic uncertainties, external, internal, and time-varying disturbances, nonlinearities,

and internal parameter variations. Assuming $x_1 = y$ and $x_2 = \dot{x}_1$, the state space form of Equation (5) is given by:

$$\begin{aligned} \dot{x}_1 &= x_2 \\ \dot{x}_2 &= f + b_0 u \\ y &= x_1 \end{aligned} \tag{6}$$

The key point of the ADRC technique is to use an estimated numeric value of the generalized disturbance f to remove its effect from the dynamics of the controlled process (6) using a simple algebraic operation such as:

$$u = \frac{u_0 - f}{b_0} \tag{7}$$

This operation changes the original dynamic of Equation (6) to a simpler emulated second order dynamic such as:

$$\begin{aligned} \dot{x}_1 &= x_2 \\ \dot{x}_2 &= u_0 \\ y &= x_1 \end{aligned} \tag{8}$$

The block diagram of the ADRC control of the process represented by Equation (5) is represented in Figure 6, in which the additional state given by the Estimator block is equal to the generalized disturbance variable f.

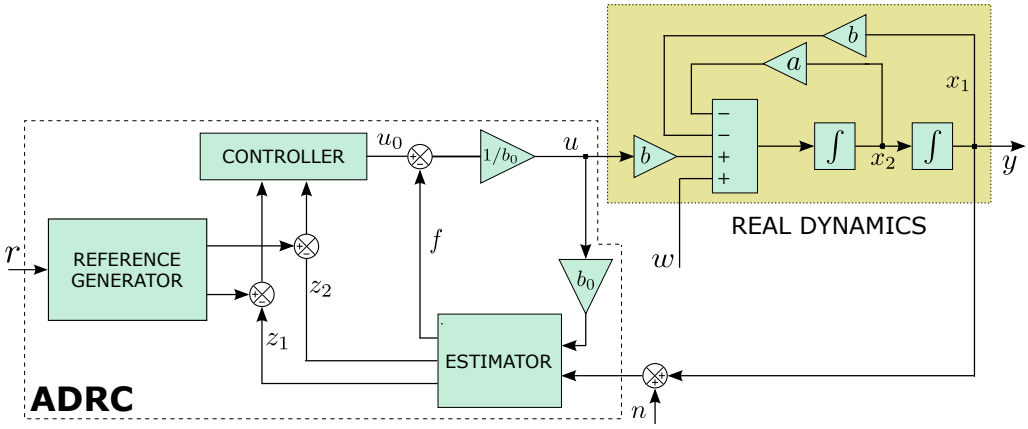

Figure 6. ADRC block diagram of a generic second order plant.

The disturbance rejection mechanism given by the estimation of the general disturbance and the algebraic operation (7) makes the controller see the real dynamics as a more simple plant. This way, the block diagram of Figure 6 is virtually reduced to the diagram of Figure 7.

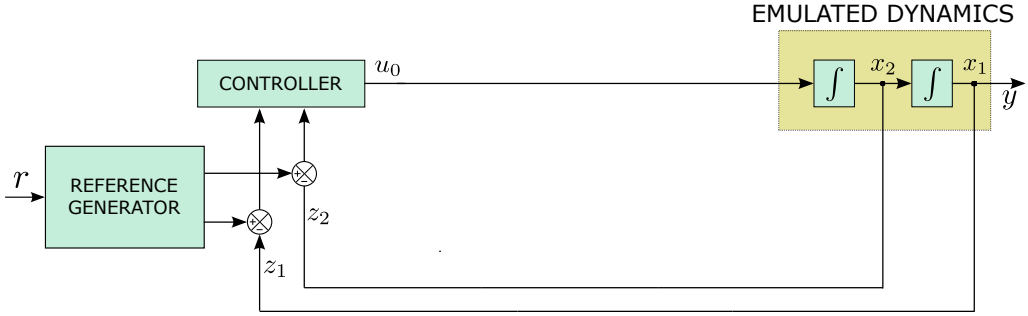

Figure 7. Equivalent block diagram.

The generalized disturbance is capable of encompassing a wide range of uncertainties and effects, such as: external and time-varying disturbances, unmodeled internal dynamics, nonlinearities, and internal parameter variations. ADRC groups these uncertainties and effects and uses this information to remove the effects of this information from the process control.

In Gao [18] a linear structure for ADRC applied to second-order systems was proposed, in which the controller and estimator (called the Linear Extended State Observer—LESO) are fully linear functions. Furthermore, this structure does not use the reference generator block. The block diagram in Figure 8 shows the application of linear ADRC to a second-order G_p system.

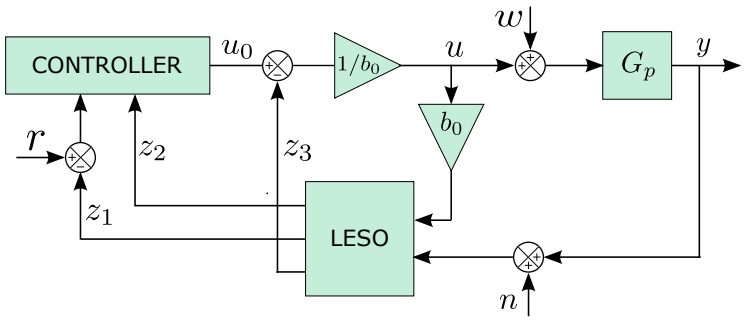

Figure 8. LADRC block diagram.

The output y is controlled by a LADRC from the application of input r. The states estimated by the linear extended state observer (LESO) are given by z_1, z_2, and z_3. The estimated state z_3 is equal to the generalized disturbance f of the Equation (5). The parameter b_0 is a tuning parameter. The external disturbances are represented by: w (input disturbance) and n (measurement noise).

Using the linear ADRC structure proposed in [18] this paper analyzed the application of two extended state observer structures. The first structure uses a linear observer with a saturator at the output, as shown in Figure 9a.

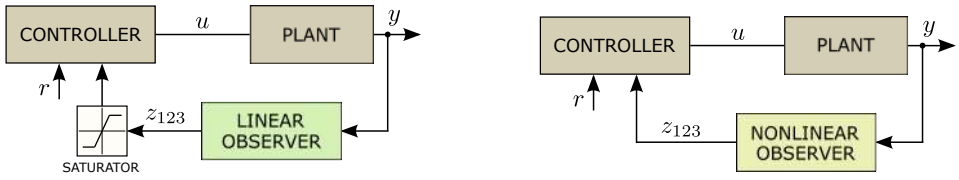

(**a**) (**b**)

Figure 9. Block diagrams of the implemented controllers. (**a**) Linear ADRC. (**b**) Nonlinear ADRC.

The saturator block in the LADRC structure was necessary because the effect of peak phenomenon [19] impossible the stabilization of the radial displacement outputs due to the synchronous disturbances that are present in this type of system, as described in the work [20]. The second structure uses a nonlinear extended state observer as shown in Figure 9b. This structure makes it possible to observe the influence of adding the nonlinearities on the dynamic performance of the system.

4. Description of the System

4.1. System Overview

Figure 10 provides an overview of the bench. The equipment has been grouped into the following blocks: monitoring and control, power supply circuit, and bearingless machine.

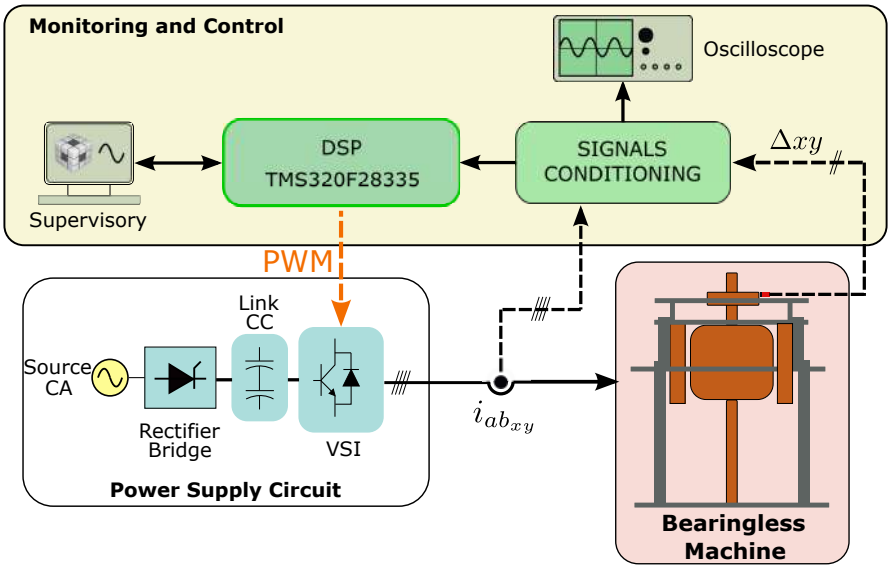

Figure 10. Overview of the components of the experimental bench.

The bearingless machine block consists of the bearingless electric induction machine on which the tests were performed. The power supply circuit block comprises the entire infrastructure of electronic components and equipment responsible for providing the power supply at the appropriate levels to control the machine variables. This is achieved by a three-phase Voltage Source Inverter (VSI). The monitoring and control block consists of the electronic circuits, Digital Signal processor (DSP), and monitoring devices that were necessary to implement the system's control and supervision routines. The variable i_{abxy} represents the four-phase electrical connections that allow the drive block to supply controlled electrical currents to the bearing motor. Figure 10 also indicates the reading of these i_{abxy} currents performed by the monitoring and control block. The variable Δ_{xy} represents the signals corresponding to the radial positions of the x and y axes of the bearing motor read by the monitoring and control block. Finally, the orange arrow named PWM indicates the signals sent by the monitoring and control block to the drive block.

Figure 11 shows a real image of the experimental bench. This structure is located in the Laboratory in the Computer and Automation Engineering Department at UFRN.

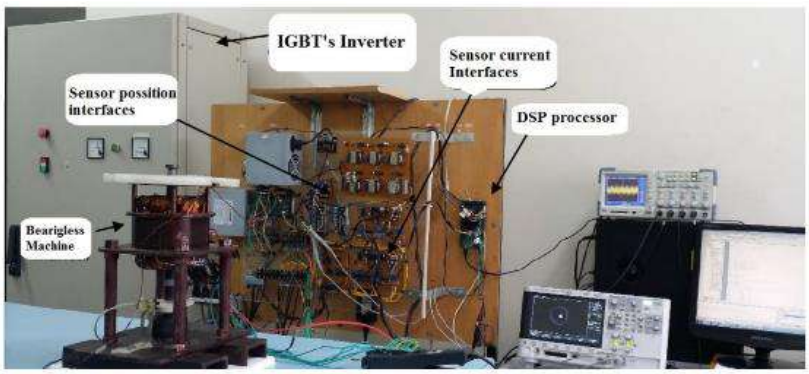

Figure 11. Experimental bench.

4.2. Split-Winding Bearingless Machine

The prototype used works vertically with the goal of simplifying radial position control. The machine's rotor is supported in the axial position by a mechanical bearing that is also responsible for fixing the machine's lower end. Figure 12 shows the prototype.

Figure 12. Split-winding bearing machine prototype.

The electrical data of the machine is detailed in Table 1.

Table 1. Machine parameters.

Parameters	Values
Frequency	60 Hz
Poles number	4
Supply voltage	220/380 V
Current	3.02/1.75 A
No-load current	1.9 A
No-load power	160 W
Stator resistance per phase	0.63 Ohm

4.3. DSP TMS320F28335

The *DSP TMS*320*F*28335 is a digital signal controller that has the characteristics of a conventional processor because it contains in its structure circuits capable of executing programs stored in memories and also has additional circuits for digital signal processing, which includes hardware with special architecture and instructions for mathematical calculations and are able to perform real-time operations. In addition, the *TMS*320*F*28335 has in its structure memory and programmable input and output components, which also makes the *TMS*320*F*28335 a microcontroller.

4.4. Control Algorithm Implementation

The block diagram in Figure 13 shows the blocks needed for the practical experiments with the system. With the exception of the inverter block, all other blocks were implemented in *C* language in the *DSP* programming interface.

The general idea of the control algorithm is the existence of two cascaded control loops: the current control loop, with fast dynamic response and with the objective of making the currents in the controlled phases follow the specified reference; and the position control loop, which has slower dynamics than the current control loop and operates in a more external way, generating the references for the current control loop. The position control loop aims to maintain the radial position at the reference values Y_{ref} and X_{ref}, for this, the position control signals are added to the magnetization currents I_m to generate the necessary currents for the positioning of the rotor radial.

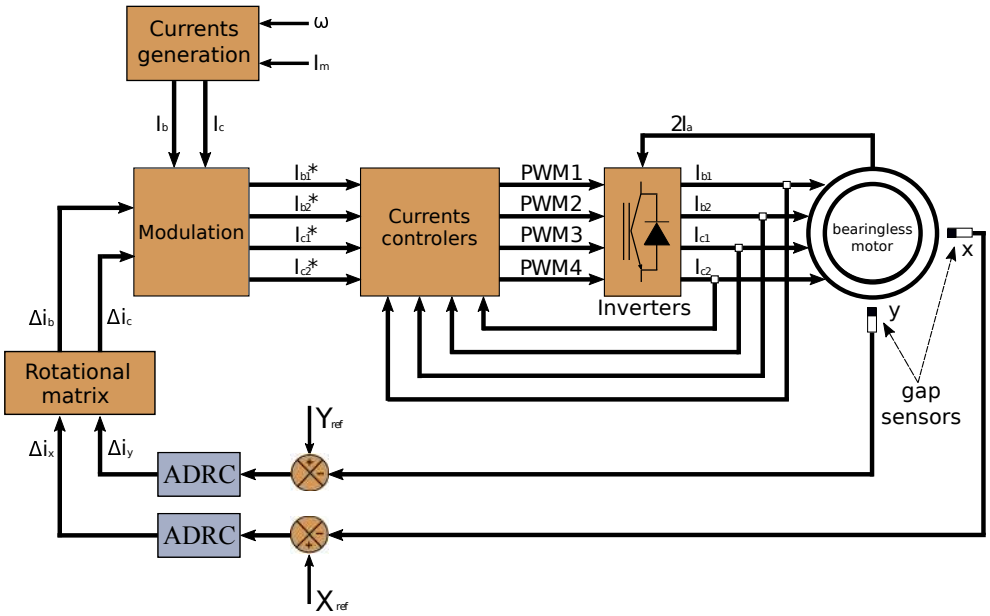

Figure 13. Control system diagram.

The bias current block is responsible for generating via software the magnetizing currents of the machine. This block implements Equations (1) and its arguments are the angular velocity and the peak value of the magnetizing currents. In the control algorithm, there are two ADRC blocks, one for each radial positioning axis of the machine. These blocks implement all the blocks required in the structure of the ADRC technique. These blocks receive the error calculated from subtracting the radial positions of the rotor by its references Y_{ref} and X_{ref} and perform the necessary operations to generate the correction signal $\Delta_i y$ and $\Delta_i x$. The rotational transformation block converts the control signals calculated in the x–y positioning referential to b–c corresponding to the spatial alignment of the controlled motor-manifold coils. The function of the modulation block is to perform the composition of the rotation currents I_b and I_c with the control signals $\Delta_i b$ and Δ_{ic} and thus generate the references I^*_{b1}, I^*_{b2}, I^*_{c1} and I^*_{c2}. Finally, the current control block implements four digital PI controllers, which monitor the machine currents and generate the PWM control signals for driving the inverters.

5. Experimental Results and Discussion

Two versions of ADRC controllers have been implemented in the DSP TMS320F28335. The first one used the linear form proposed by Gao in [18] for the extended observer and the PD controller. The other version used fal-type nonlinearities in the observer structure. The results in three dimensions for the two implemented controllers can be seen in Figure 14.

Figure 14a shows the behavior of positions X and Y in steady state for the first version of the controller. A mean error of -1.17% with a standard deviation of 0.03 mm was obtained for the X axis. As for the Y-axis, an average error of 0.76% with a standard deviation of 0.05 mm was obtained. Figure 14b shows the behavior of the X and Y positions in a steady state for the version with nonlinearities. The mean error for the X-axis was -0.09% with a standard deviation of 0.07 mm. For the Y axis, the mean error was -0.05% with a standard deviation also of 0.05 mm. The results indicate the effect of adding non-linearity on the observer's structure. It was possible to improve the regime error with the non-linear versions, but the variation around the reference became more evident, indicating an increase in the aggressiveness of the controller response.

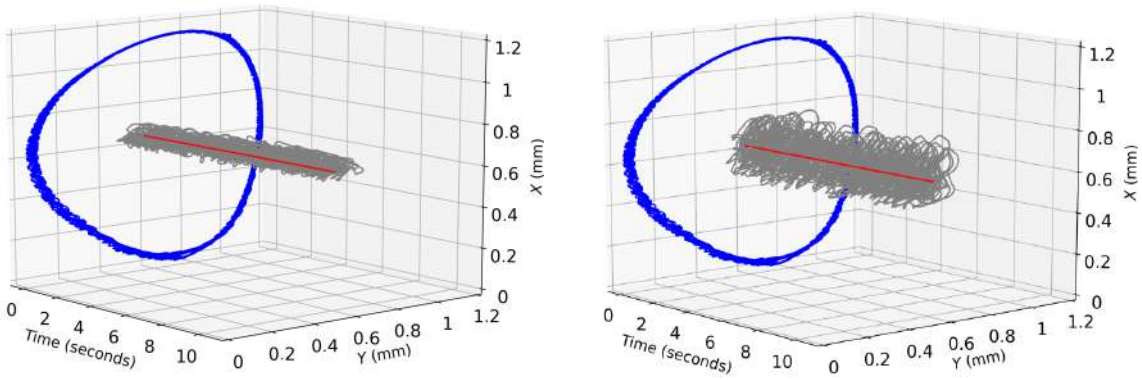

(**a**) (**b**)

Figure 14. Steady state response of radial position control for the linear and nonlinear controllers in 3D. (**a**) Linear ADRC. (**b**) Nonlinear ADRC.

Figure 15a,b shows the behavior of the radial position signals when there are step-type reference variations in the *X*-axis only, keeping the *Y*- axis reference fixed, and Figure 15c,d when step-type variations occur in *Y*, keeping the *X*-axis reference is fixed.

The results in Figure 15 show that step variations in one of the axes do not result in a significant influence on the dynamic behavior of the opposite axis. The same test was performed to the controller with a nonlinear observer; the results are shown in Figure 16. The results obtained indicate that there is a decoupling in the dynamic behavior of the radial position between the two axes.

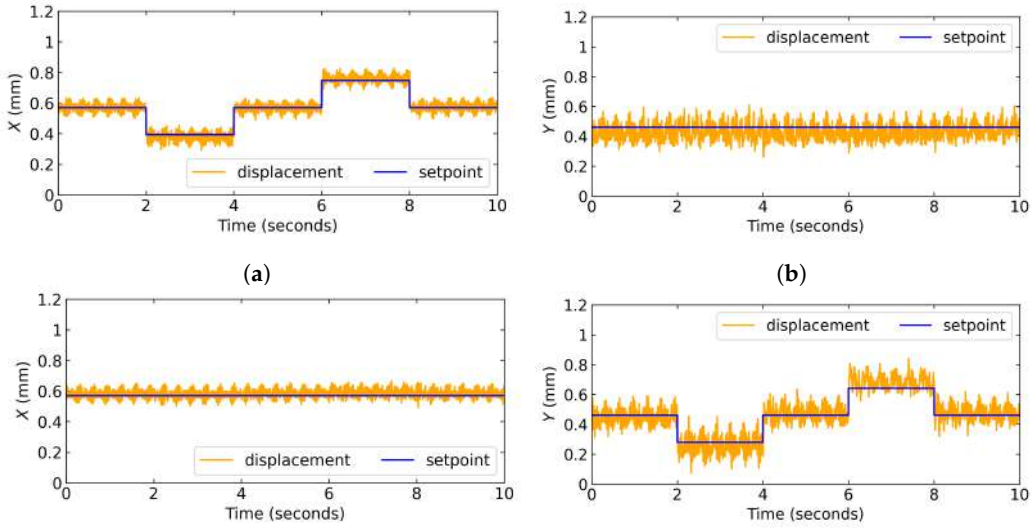

(**a**) (**b**)

(**c**) (**d**)

Figure 15. Response of radial position control under step setpoint changes for Linear ADRC. (**a**) *X*-axis behavior with step setpoint changes applied. (**b**) *Y*-axis behavior with step setpoint changes applied to *X*-axis. (**c**) *X*-axis behavior with step setpoint changes applied to *Y*-axis. (**d**) *Y*-axis behavior with step setpoint changes applied.

The addition of a radial load to the machine shaft in operation is an important analysis since this load is seen by the position controllers as an external disturbance in the form of a step. Therefore, it is a simple way to impose a perturbation and analyze the robustness of the controller in situations such as this. For this analysis, an apparatus that allowed the addition of a radial load aligned with the *X*-axis was used. Figure 17 illustrates how the device was used to add the radial disturbance.

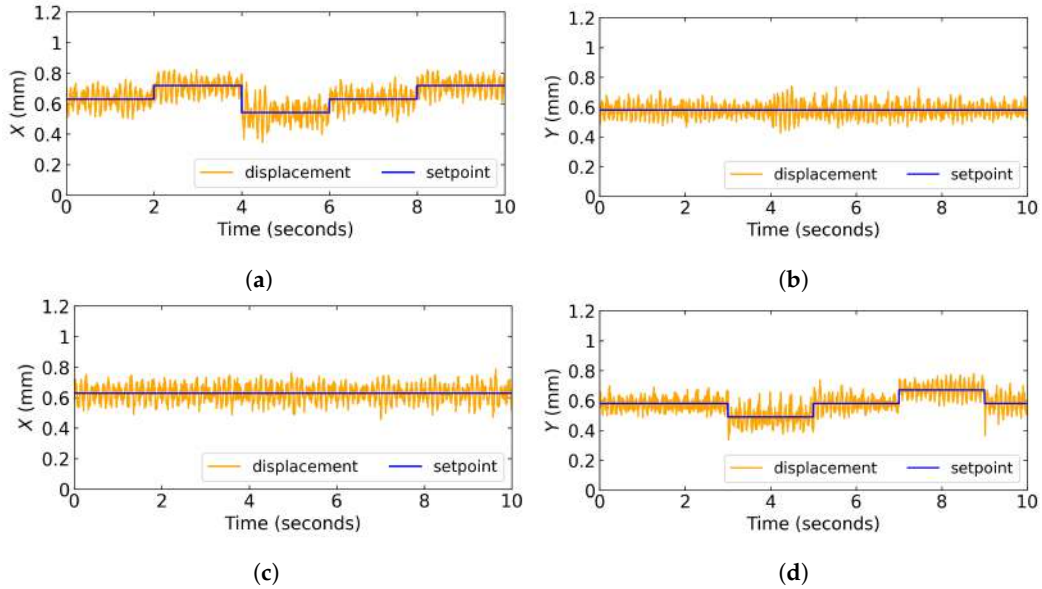

Figure 16. Response of radial position control under step setpoint changes for Nonlinear ADRC. (**a**) X-axis behavior with step setpoint changes applied. (**b**) Y-axis behavior with step setpoint changes applied to X-axis. (**c**) X-axis behavior with step setpoint changes applied to Y-axis. (**d**) Y-axis behavior with step setpoint changes applied.

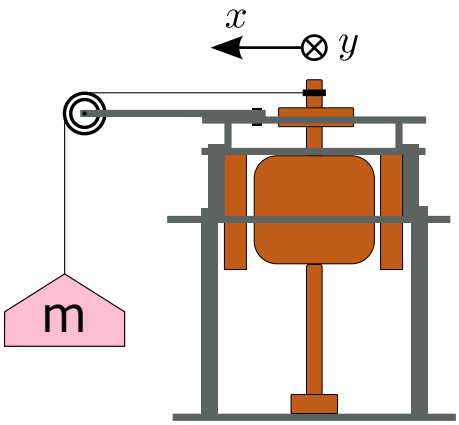

Figure 17. Illustrative image of the machine subjected to load addition.

For each controller, the z_1, z_2, and z_3 states of the X and Y axes were collected in a time interval that allowed detecting the exact instant of addition of the radial load to the machine axis. Figures 18 and 19 show the behavior of the states of the X and Y axes for the two implemented controllers. In each graph, a green dashed vertical line was inserted to indicate the instant the application of 150 g of radial load aligned to the X-axis. This load was inserted in such a way that the radial load tends to move the radial position in the positive direction of the axis. Figure 18a,b show the state behavior of the linear controller. Visually, it is possible to state that there was a certain degree of rejection of the radial disturbance, but it is evident that the regime error of the X-axis increased after the moment of application of the load. The Y-axis remained stable. It is not possible to perceive variations in the z_3 state on the scale used because the linear controller was implemented with saturators at the observers' output in order to avoid the Peak phenomenon.

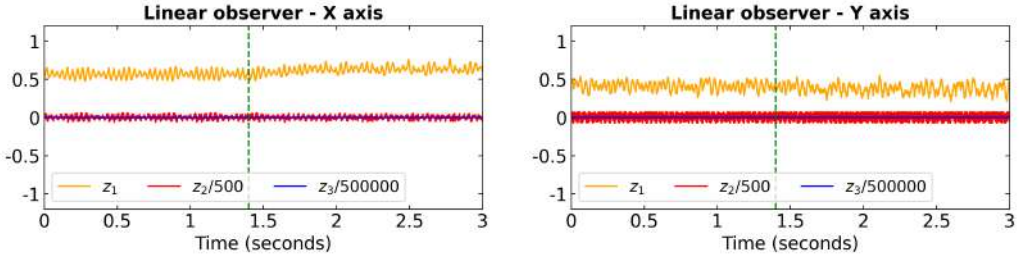

(**a**) (**b**)

Figure 18. Estimated states behavior for linear ADRC under radial load application. (**a**) Linear ADRC—*X*-axis states. (**b**) Linear ADRC—*Y*-axis states.

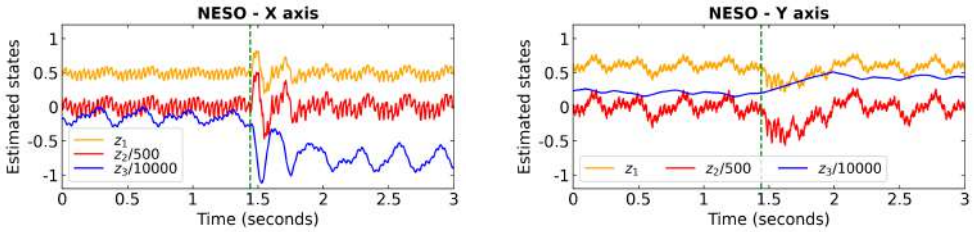

(**a**) (**b**)

Figure 19. Estimated states behavior for nonlinear ADRC under radial load application. (**a**) Nonlinear ADRC—*X*-axis states. (**b**) Nonlinear ADRC—*Y*-axis states.

Through the analysis of the z_1 states of Figure 19a,b. it is possible to conclude that the ADRC controller with NESO was less influenced by the application of the radial load in the steady state since qualitatively the response was very similar for the intervals before and after the addition of the disturbance. The behavior of the states indicated an aggressive reaction of the controller in the transient regime, resulting in high values of z_2 during this region of the collection. The change in the mean value observed for the z_3 state indicates that this variable was able to identify the addition of the external disturbance. The good rejection of the observed perturbation may be a result of this. Quantitatively, the results of Figures 18 and 19 can be summarized according to Table 2. Table 2 shows the average values in a steady state of the observed states.

Table 2. Mean values of the states estimated by the linear and nonlinear ESO before and after the radial load application.

Controller	**State z_1**		**State z_2**		**State z_3**	
Load Application	**Before**	**After**	**Before**	**After**	**Before**	**After**
Linear ESO	0.57	0.64	−0.32	−0.33	1.64	−7
Nonlinear ESO	0.48	0.48	−1.34	−2.6	−1522	−7909

The value of the z_1 state for the linear controller indicates that there was a displacement of the mean value of the output after applying the load. This is a limitation of the linear observer as its states the need to read limited amplitude to avoid peak phenomenon and guarantee stability. As indicated by the value of z_3 after applying the load, it was blocked in the imposed saturation. The saturation of state outputs impairs the ability to reject disturbances. The mean value of the z_1 state of the non-linear indicates that it was able to reject the load addition. Furthermore, the significant change in the value of z_3 shows that it was able to identify the disturbance.

The value of z_3 in Table 2 becomes more negative after adding the load because the control loop error is given by:

$$Error = pos - ref \tag{9}$$

that is, when the radial position is displaced from the reference value in the sense of increasing the error value, the control signal must increase in order to restore the equilibrium position close to the reference. Knowing that the control signal is calculated by:

$$u = \frac{u_0 - z_3}{b_0} \tag{10}$$

it means that the more negative the value of z_3, the greater the values of the control signals and the greater the control effort in the sense of rejecting the action of the disturbance in the system output. The more positive the displacement value is in relation to the reference, the greater the control signal must be.

Finally, to analyze the relationship between the value of z_3 and the intensity of the radial disturbance applied to the motor shaft and also to verify to what extent the system could reject the radial load, masses of 32 g were added one by one in the application support of the load. This test was performed with the NESO-based controller only. In the first step, the radial load support was aligned on the X-axis and then on the Y-axis. For each added mass, the regime errors of the X and Y positions were calculated and the z_3 states were collected. The results are shown in Figures 20 and 21. Figure 20 shows the results for the radial load bearing aligned with the X-axis.

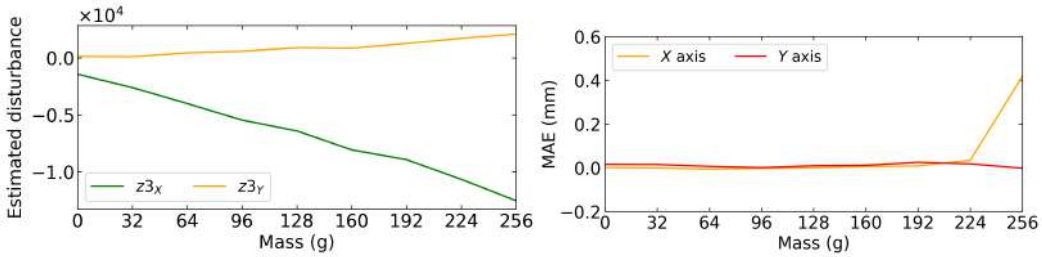

(**a**) (**b**)

Figure 20. Generalized disturbance estimation and mean steady state error for X and Y axes to different values of radial load aligned with the X-axis. (**a**) Generalized disturbance estimation (z_3). (**b**) Mean absolute error for X and Y axes.

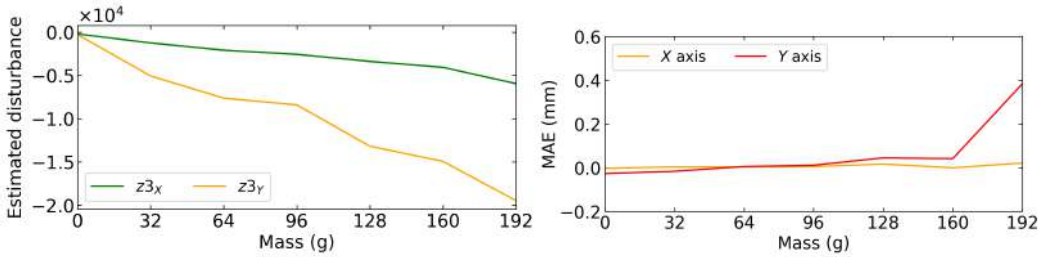

(**a**) (**b**)

Figure 21. Generalized disturbance estimation and mean steady state error for X and Y axes to different values of radial load aligned with the Y-axis. (**a**) Generalized disturbance estimation (z_3). (**b**) Mean absolute error for X and Y axes.

Figure 20b shows that the regime error remained close to zero for loads of up to 224 g. When the radial load increased to 256 g, the position control in the X-axis became unstable but remained stable on the Y-axis. Figure 20a shows the estimation of generalized disturbances for the X and Y axes increase in load and the z_3 state of the X-axis. This variable becomes more negative as the load increases, as expected. Figure 20a also shows that the load added in the X direction also influenced the z_3 state of the Y axis. This indicates that the load support was not perfectly aligned with the desired axis, or that the X and Y sensors could not have been perfectly spaced 90 degrees apart.

Figure 21 shows the analysis of radial load disturbance for the radial load added in the positive direction of Y. The Y axis showed a lower radial disturbance rejection capacity since it only managed to keep the regime error close to zero up to 160 g of load. The Y-axis control became unstable for the 192-g load, while the X-axis remained stable for all analyzed loads. Figure 21a indicates that there is also an approximately linear relationship between the value of z_3 and the value of the added charge. Likewise, there was a smaller scale detection of radial disturbance by the z_3 state of the X-axis. In this test, the influence on the cross-axis was greater. The results of the load curve for both axes showed that there is a linear relationship between the perturbation and the z_3 state. This relationship is fundamental to the success of the strategy and indicates that the extended state observers are capable of detecting external disturbances without the need for physical sensors installed in the process.

6. Conclusions

This paper examined the ADRC active disturbance rejection technique applied to a bearingless induction machine. Two structures were employed in the laboratory testing for the extended state estimator, one linear and the other nonlinear. For both versions, the step reference variation results exhibit a satisfactory level of dynamic decoupling between the radial displacements in the X and Y axes. The test with load imposition showed that both observers were able to detect the generalized disturbance, however, only the nonlinear observer was able to maintain the same average system output value before and after load application. The results obtained show the success of the ADRC technique in the active estimation and rejection of disturbances in the radial positioning process of a split rotor bearingless machine. The results also show the higher active rejection capability of the technique applied with a nonlinear observer since with this type of observer disturbances of this nature are estimated and compensated.

Author Contributions: R.d.A.T., W.L.A.d.S. and A.O.S. conceived and designed the study; R.d.A.T., A.E.S.A. and W.L.A.d.S., methodology; R.d.A.T., A.E.S.A. and W.L.A.d.S. performed the simulations and experiments; E.R.L.V., W.M.R. and A.O.S. reviewed the manuscript and provided valuable suggestions; E.R.L.V., R.d.A.T., W.L.A.d.S. and W.M.R. wrote the paper; supervision, A.O.S. and W.M.R. All authors have read and agreed to the published version of the manuscript.

Funding: This research was funded in part by the Coordenação de Aperfeiçoamento de Pessoal de Nível Superior—Brasil (CAPES)—Finance Code 001 and Conselho Nacional de Desenvolvimento Científico e Tecnológico (CNPq).

Conflicts of Interest: The authors declare no conflicts of interest.

Abbreviations

The following abbreviations are used in this manuscript:

BIM	Bearingless Induction Machine
ADRC	Active Disturbance Rejection Control
LADRC	Linear Active Disturbance Rejection Control
ESO	Extended State Observer
LESO	Linear Extended State Observer
NESO	Nonlinear Extended State Observer
TD	Tracking Differentiator
DSP	Digital Signal Processing
PID	Proportional-Integral-Derivative
PD	Proportional-Derivative
PI	Proportional-Integral
PWM	Pulse Width Modulation
DC	Direct Current
VSI	Voltage Source Inverter

References

1. Yang, Z.; Jia, J.; Sun, X.; Xu, T. An enhanced linear adrc strategy for a bearingless induction motor. *IEEE Trans. Transp. Electrif.* **2021**, *8*, 1255–1266. [CrossRef]
2. Yang, Z.; Ji, J.; Sun, X.; Zhu, H.; Zhao, Q.Q. Active Disturbance Rejection Control for Bearingless Induction Motor Based on Hyperbolic Tangent Tracking Differentiator. *IEEE J. Emerg. Sel. Top. Power Electron.* **2020**, *8*, 2623–2633. [CrossRef]
3. Li, J.; Zhang, L.; Li, S.; Mao, Q.; Mao, Y. Active Disturbance Rejection Control for Piezoelectric Smart Structures: A Review. *Machines* **2023**, *11*, 174. [CrossRef]
4. Heidary, J.; Gheisarnejad, M.; Khooban, M.H. Stability Enhancement and Energy Management of AC-DC Microgrid based on Active Disturbance Rejection Control. *Electr. Power Syst. Res.* **2023**, *217*, 109105. [CrossRef]
5. Huang, C.; Zhao, H. Error-Based Active Disturbance Rejection Control for Wind Turbine Output Power Regulation. *IEEE Trans. Sustain. Energy* **2023**, *1*, 1–10. [CrossRef]
6. Zhou, Z.; Li, X.; Tuo, W.; Wang, F. Design of active disturbance rejection control with noise observer for an optical reference unit. *Control Eng. Pract.* **2023**, *132*, 105427. [CrossRef]
7. Shao, X.; Fan, Y.; Shao, J.; Sun, G. Improved active disturbance rejection control with the optimization algorithm for the leg joint control of a hydraulic quadruped robot. *Meas. Control* **2023**, *1*. [CrossRef]
8. Li, J.; Liu, J.; Huangfu, S.; Guoyan Cao, G.; Yu, D. Leader-follower formation of light-weight UAVs with novel active disturbance rejection control. *Appl. Math. Model.* **2023**, *117*, 577–591. [CrossRef]
9. Zhu, L.; Zhang, G.; Jing, R.; Bi, G.; Xiang, R.; Wang, G.; Xu, D. Nonlinear active disturbance rejection control strategy for permanent magnet synchronous motor drives. *IEEE Trans. Energy Convers.* **2022**, *37*, 2119–2129. [CrossRef]
10. Silva, W.L.A.; Salazar, A.O.; Cabral Neto, R.J.N.; Villarreal, E.R.L. Radial Position Control of a Bearingless Machine with Active Disturbance Rejection Control. In *2020 IEEE XXVII International Conference on Electronics*; Electrical Engineering and Computing (INTERCON): Lima, Perú, 2020; pp. 1–5.
11. Silva, W.L.A.; Salazar, A.O.; Vieira, P.V.F.; Jácome, M.C.; Villarreal, E.R.L. Radial Position Control of a Bearingless Machine with Active Disturbance Rejection Control Fuzzy an approach. In Proceedings of the 2021 IEEE International Conference on Automation/XXIV Congress of the Chilean Association of Automatic Control (ICA-ACCA), Online, 22–26 March 2021; pp. 1–5.
12. Salazar, A.O.; Stephan, R.M. A bearingless method for induction machines. *IEEE Trans. Magn.* **1993**, *29*, 2965–2967. [CrossRef]
13. Ferreira, J.M.S.; Salazar, A.O. Máquina de Indução Sem Mancais: Modelo e Acionamento. *Eletrônica de Potência* **2007**, *12*, 2509–2521.
14. De Paiva, J.A.; Salazar, A.O.; Maitelli, A.L. Review of Control Strategies and Model Estimation Techiniques Applied to Bearingless Induction Machine with Divided Winding. In Proceedings of the 1st Brazilian Workshop on Magnetic Bearings, Rio de Janeiro, Brazil, 25–26 October 2013; Volume 1, pp. 1–6.
15. Victor, V.F.; Quintaes, F.O.; Lopes, J.S.B.; Santos Junior, L.D.; Lock, A.S.; Salazar, A.O. Analysis and Study of a Bearingless AC Motor Type Divided Winding, Based on a Conventional Squirrel Cage Induction Motor. *IEEE Trans. Magn.* **2012**, *48*, 3571–3574. [CrossRef]
16. Nunes, E.A.D.F.; Salazar, A.O.; Villarreal, E.R.L.; Souza, F.E.C.; Dos Santos Júnior, L.P.; Lopes, J.S.B.; Luque, J.C.C. Proposal of a fuzzy controller for radial position in a bearingless induction motor. *IEEE Access* **2019**, *7*, 114808–114816. [CrossRef]
17. Carvalho Souza, F.E.; Silva, W.; Ortiz Salazar, A.; Paiva, J.; Moura, D.; Villarreal, E.R.L. A Novel Driving Scheme for Three-Phase Bearingless Induction Machine with Split Winding. *Energies* **2021**, *14*, 4930. [CrossRef]
18. Gao, Z. Scaling and bandwidth-parameterization based controller tuning. In Proceedings of the 2003 American Control Conference, Denver, CO, USA, 4–6 June 2003; Volume 6, pp. 4989–4996.
19. Maopeng, R.; Li, J.; Xie, L. A new extended state observer for uncertain nonlinear systems. *Automatica* **2021**, *131*, 109772.
20. Mota, A.I.P.; Silva, W.L.A.; Souza, F.E.C.; Salazar, A.O. Synchronous disturbance suppression in bearingless machines with active disturbance rejection controller. In Proceedings of the 2021 Brazilian Power Electronics Conference (COBEP), João Pessoa, PB, Brazil, 7–10 November 2021; pp. 1–5.

Disclaimer/Publisher's Note: The statements, opinions and data contained in all publications are solely those of the individual author(s) and contributor(s) and not of MDPI and/or the editor(s). MDPI and/or the editor(s) disclaim responsibility for any injury to people or property resulting from any ideas, methods, instructions or products referred to in the content.

sensors

MDPI

Article

Thermal Profiles in Water Injection Wells: Reduction in the Systematic Error of Flow Measurements during the Transient Regime

German Alberto Echaiz Espinoza [1,†], Gabriel Pereira de Oliveira [2,†], Verivan Santos Lima [2,†], Diego Antonio de Moura Fonseca [2,†], Werbet Luiz Almeida da Silva [2,†], Carla Wilza Souza de Paula Maitelli [3,†], Elmer Rolando Llanos Villarreal [4,*,†] and Andrés Ortiz Salazar [2,†]

[1] Department of Electronics Engineering, Universidad Nacional de San Agustin de Arequipa, Arequipa 04002, Peru; gechaiz@unsa.edu.pe
[2] Department of Computer Engineering and Automation, Federal University of Rio Grande do Norte (DCA-UFRN), Natal 59072-970, RN, Brazil; gabrpereira20@gmail.com (G.P.d.O.); verivan@petrobras.com.br (V.S.L.); diegomoura@dca.ufrn.br (D.A.d.M.F.); werbethluizz@hotmail.com (W.L.A.d.S.); andres@dca.ufrn.br (A.O.S.)
[3] Department of Petroleum Engineering, Federal University of Rio Grande do Norte (DPET-UFRN), Natal 59072-970, RN, Brazil; carla.maitelli@ufrn.br
[4] Department of Natural Sciences, Mathematics, and Statistics, Federal Rural University of Semi-Arid (DCME-UFERSA), Mossoró 59625-900, RN, Brazil
* Correspondence: elmerllanos@ufersa.edu.br
† These authors contributed equally to this work.

Abstract: This article presents an analytical solution for calculating the flow rate in water injection wells based on the established thermal profile along the tubing. The intent is to minimize the intrinsic systematic error of classic quasi-static methodologies, which assume that all thermal transience on well completion has passed. When these techniques are applied during the initial hours of injection well operation, it can result in errors higher than 20%. To solve this limitation, the first law of thermodynamics was used to define a mathematical model and a thermal profile was established in the injection fluid, captured by using distributed temperature systems (DTSs) installed inside the tubing. The geothermal profile was also established naturally by a thermal source in the earth to determine the thermal gradient. A computational simulation of the injection well was developed to validate the mathematical solution. The simulation intended to generate the fluid's thermal profile, for which data were not available for the desired time period. As a result, at the cost of greater complexity, the systematic error dropped to values below 1% in the first two hours of well operation, as seen throughout this document. The code was developed in Phyton, version 1.7.0., from Anaconda Navigator.

Keywords: oil reservoir; thermal profile; geothermal profile; flow rate injection

check for updates

Citation: Echaiz Espinoza, G.A.; Oliveira, G.P.d.; Lima, V.S.; Fonseca, D.A.d.M.; Silva, W.L.A.d.; Maitelli, C.W.S.d.P.; Villarreal, E.R.L.; Salazar, A.O. Thermal Profiles in Water Injection Wells: Reduction in the Systematic Error of Flow Measurements during the Transient Regime. *Sensors* **2023**, *23*, 9465. https://doi.org/10.3390/s23239465

Academic Editors: Flavio Esposito, Davide Astolfi, Stefania Campopiano and Agostino Iadicicco

Received: 16 September 2023
Revised: 25 October 2023
Accepted: 20 November 2023
Published: 28 November 2023

Copyright: © 2023 by the authors. Licensee MDPI, Basel, Switzerland. This article is an open access article distributed under the terms and conditions of the Creative Commons Attribution (CC BY) license (https://creativecommons.org/licenses/by/4.0/).

1. Introduction

When working with water injection in an oil production field, knowing the injected flow rate is crucial. Deviations from the designed flow rates can result in lost oil production and damage to the reservoir in the worst case. In the case of multiple injection zones, where fluid is injected simultaneously in several sections along the injection well, the quality of the flow rate value is more critical due to the risk of greater flow deviations between zones, where a problem in one injection zone can completely change the flow rate being injected in another zone.

Currently, the flow rate is measured at the surface near the well. Typically, an orifice plate takes the measurement [1]. Another method could be used. To measure the flow below the surface using well tubing, it is necessary to shut down the well to install and use

specialized instrumentation (e.g., flow meters and radioactive tracers). The measurement is not continuous. It is executed at a single point in time, which makes these methods very expensive and not suitable for continuous well production. For wells with only one injection zone, this is sufficient. However, for wells with multiple zones, the proportion of the flow in each zone is estimated from the surface flow. The estimate is based on the pressure applied to mechanical flow regulators, which are installed in the injection zone. This approach normally leads to an incorrect injection flow rate.

To overcome these difficulties and limitations, several measurement techniques are being developed based on the thermal profile in the injection column obtained by so-called distributed temperature sensors (DTSs). In this technique, an enriched fiber at predetermined points provides, in real-time, the temperature along the production column through the intensity of the reflected light wave. From this thermal profile, it is possible to derive the flow rate transported inside the tube and, consequently, the injection flow [2].

As a result of the small radii of well completions ($<$1 m) compared to the radius of the formation, which is assumed to have infinite extension ($>>$1 m), all previous researchers have ignored the transient heat flow in the well completion (tubing, annulus, casing, and cementation). Ramey was one of them. He proposed the first practical and consistent work to predict the fluid's thermal profile in the tubing. Since heat flow is a very slow process, the heat transient in well completion is still significant during the initial hours of well operation. This implies a significant systemic error inherent in the methodology.

Motivated by the need to reduce the systematic error in the calculation of the flow rate inside the tubing during the first hours of well operation and originally inspired by the work of Ramey, this paper proposes a solution that takes into account the effect of the transient heat flow in well completion on the prediction of the thermal profile of the fluid and, consequently, the flow rate, the desired variable.

2. Preliminaries

Consider an injection well with the standard completion shown in Figure 1. Furthermore, assume that the well is in an idle state in thermal equilibrium with the formation. Under this condition, the temperatures of the well, completions, and formations are equal to the geothermal temperature, $T_g(z)$, which increases linearly with depth, given by:

$$T_g(z) = az + b \tag{1}$$

where z is the vertical coordinate (depth), a is the geothermal gradient, and b is the surface temperature. The geothermal temperature is the temperature naturally established in the formation and wellbore by heat flow from the earth's center. It is a very slow process compared to the thermal processes involved in well completion.

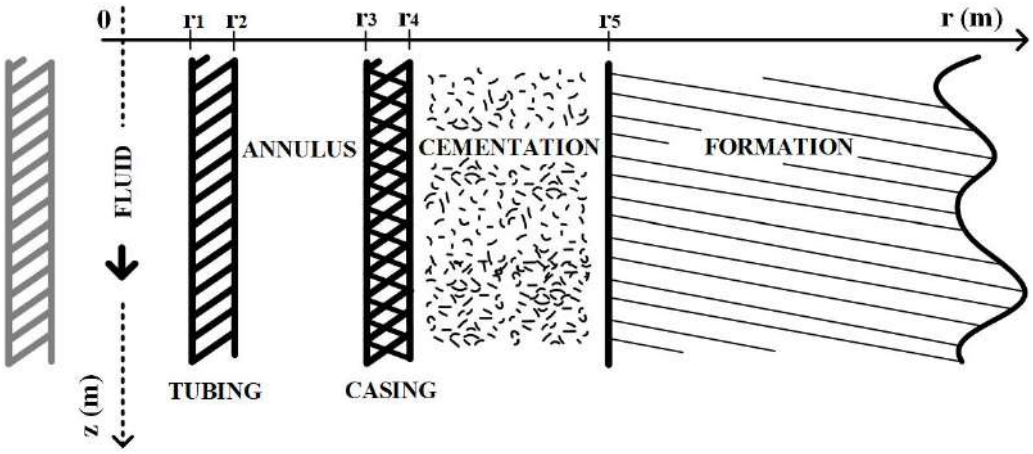

Figure 1. Standard well schematic.

Assume that a new injection process starts at $t = 0$. Furthermore, assume that the injection fluid has no phase change, is incompressible, and is colder than the reservoir. Under these conditions, as the fluid moves through the tubing, it gains thermal energy from its surroundings, and its temperature increases, creating a thermal profile along the tubing. The profile created is directly related to the flow rate in the tubing.

To calculate the flow rate for $t > 0$, consider the application of the energy and mass conservation principle to the control volume (CV) highlighted in Figure 2. In this figure, $\dot{m}$ is the forced mass flow in the tubing, $\dot{Q}_1$, and $\dot{Q}_2$ are the heat flows entering the control volume by convection at the upper and lower surfaces, and $\delta\dot{Q}_3$ is the heat flow entering the control volume by convection at the inner tubing surface of size δz.

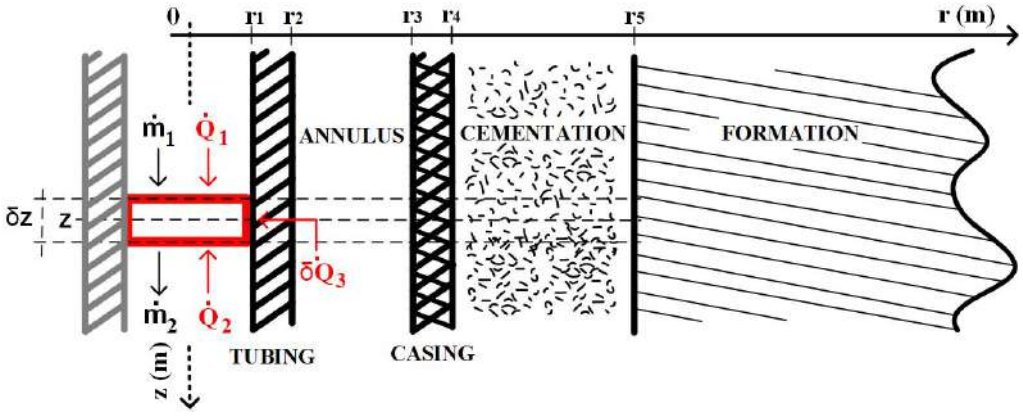

Figure 2. Control volumes and conservation of energy.

Assume that the flow rate is constant and the flow pattern is turbulent. As a result of this last characteristic, the fluid can be treated as an agglomerated system, in which the transience of the heat transfer in the fluid can be neglected because of the slowness of the transfer mechanisms in its environment. Consider also that the thermal properties are isotropic, homogeneous, and invariant with time and that there is no heat generation due to the fluid viscosity.

In this context, applying the principles of conservation of energy and mass to the CV, we have:

$$\dot{E}_{\dot{m}_1}(z - \frac{\delta z}{2}, t) - \dot{E}_{\dot{m}_2}(z + \frac{\delta z}{2}, t) + \dot{Q}_1(z - \frac{\delta z}{2}, t) + \dot{Q}_2(z + \frac{\delta z}{2}, t) + \delta\dot{Q}_3(r_1, z, t) = \frac{\partial E_{CV}(z,t)}{\partial t} \quad (2)$$

where $\dot{E}_{\dot{m}}$ is the energy flow (thermal, kinetic, gravitational, and hydraulic potential energy) associated with the mass flow entering or leaving the control volume (CV). $\dot{E}_{\dot{C}V}$ is the total energy within the CV.

Since the vertical heat flows $\dot{Q}_1$ and $\dot{Q}_2$ are a negligible fraction of the heat transported by the mass flow, they are assumed to be zero in this paper. As a result, the mass flow inside the tubing is given by [3,4]:

$$\dot{m} \cong \frac{2\pi r_1 U(z,t)}{c}\left[T_g(z) - T_f(z,t)\right] \Big/ \frac{\partial T_f(z,t)}{\partial z} - \pi(r_1)^2 \rho \frac{\partial T_f(z,t)}{\partial t} \Big/ \frac{\partial T_f(z,t)}{\partial z} \quad (3)$$

where c is the specific thermal capacity of the fluid, ρ is the specific volume of the fluid, $T_f(z,t)$ is the temperature of the fluid at the center of tubing ($r = 0$), and $U(z,t)$ is the global heat transfer coefficient, with $r = r_1$ as the reference. The coefficient $U(z,t)$ includes all thermal resistance to heat propagation, from convection at the inner surface of the tubing

at $r = r_1$ to the radial limit of thermal disturbance caused by transporting the fluid at a colder temperature. For example, if the thermal disturbance is beyond the cementation, this coefficient includes the following resistances: tubing conduction, natural convection in the annulus, casing conduction, cementation conduction, and finally, formation conduction from $r = r_5$ to the thermal disturbance inside the formation. It is defined by [5]:

$$U(z,t) = \frac{\delta \dot{Q}_3(z,t)}{2\pi r_1 \delta z [T_g(z) - T_f(z,t)]} \tag{4}$$

The calculation of the flow rate, $\dot{m}$, as can be deduced from Equation (3), depends on the value of $U(z,t)$, which in turn depends on the convection coefficient on the inner surface of the tubing, which depends on the desired flow rate. In other words, to determine the value of the flow rate, it is necessary to solve the following system of nonlinear equations:

$$Pr = \frac{\mu c}{k} \tag{5}$$

$$Re = \frac{\rho v_{med}(2r_1)}{\mu} \tag{6}$$

$$f = [0.79 \ln(Re) - 1.64]^{-2} \tag{7}$$

$$h = \frac{(f/8)(Re - 1000)Pr}{1 + 12.7(f/8)^{0.5}(Pr^{2/3} - 1)} \frac{k}{2r_1} \tag{8}$$

$$\widetilde{U} \cong U(\tilde{z},t) \tag{9}$$

$$\dot{m} \cong \frac{2\pi r_1 \widetilde{U}}{c} \frac{\int_{z_1}^{z_2} [T_g(z) - T_f(z,t)]dz}{T_f(z_2,t) - T_f(z_1,t)} - \pi (r_1)^2 \rho \frac{\int_{z_1}^{z_2} [\partial T_f(z,t)/\partial t]dz}{T_f(z_2,t) - T_f(z_1,t)} \tag{10}$$

where Pr is the Prandtl number, Re is the Reynolds number, f is the friction factor, h is the convection coefficient, $U(\tilde{z},t)$ is the global average heat transfer coefficient in the interval [z_1,z_2], and $\dot{m}$ is the desired mass flow rate. The variables μ, c, k, and ρ are the absolute viscosity, specific heat capacity, thermal conductivity, and specific mass, respectively, all relative to the fluid in flow.

Equation (7) corresponds to Petukhov's first explicit equation for calculating the friction factor in smooth tubes. It is valid for $3 \times 10^3 < Re < 5 \times 10^6$ [6].

Equation (8) is the Gnielinski equation for calculating the convection coefficient for a forced turbulent flow moving in a tube. It is valid for $0.5 \leq Pr \leq 2 \times 10^3$ and $3 \times 10^3 < Re < 5 \times 10^6$ [6].

The system resulting from Equations (5) to (10) can be solved, among other methods in the literature, by executing the algorithm shown in Figure 3.

The approach chosen for calculating $\widetilde{U}$ will define its applicability and the intensity of the corresponding systematic error. This article presents two approaches: (a) the quasi-static approach, which assumes that the thermal processes are already slow enough to be considered in thermal equilibrium, and (b) the purely analytical approach, which seeks the solution by solving the differential heat transfer equations.

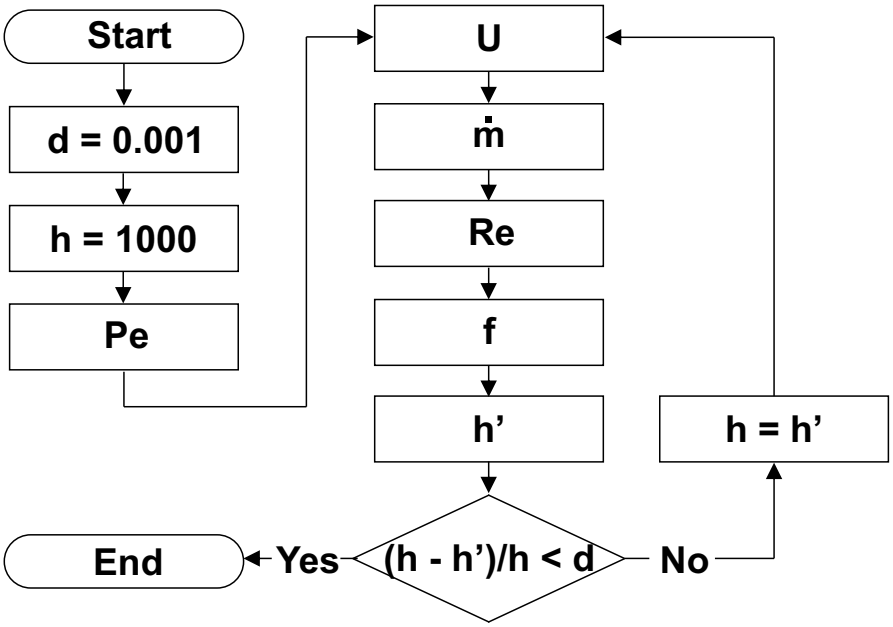

Figure 3. Algorithm for solving the equation system.

3. Quasi-Static Approach

As a result of the small radius of the completion compared to the formation ($r >> r_5$), which corresponds to the radius of the outer cementation surface ($r = r_5$ in Figure 2), the quasi-static solutions ignore all thermal transients in the fluid and completion (tubing, annulus, casing, and cementing). As a result, still taking Figure 2 as a reference, the global heat transfer coefficient and the mass flow will be given by:

$$\widetilde{U} \cong \left[\frac{1}{h} + \frac{r_1}{k_{tub}}\ln(\frac{r_2}{r_1}) + \frac{r_1}{r_2}\frac{1}{h_{comb}} + \frac{r_1}{k_{rev}}\ln(\frac{r_4}{r_3}) + \frac{r_1}{k_{cim}}\ln(\frac{r_5}{r_4}) + \frac{r_1 f(t)}{k_{for}}\right]^{-1} \tag{11}$$

$$\dot{m} \cong \frac{2\pi r_1 \widetilde{U}}{c}\frac{\int_{z_1}^{z_2}\left[T_g(z) - T_f(z,t)\right]dz}{T_f(z_2,t) - T_f(z_1,t)} \tag{12}$$

where k_{tub}, k_{rev}, k_{cim}, and k_{for}, are the thermal conductivity of tubing, casing, cementation, and formation, respectively. r_1, r_2 are the tubing's inner radius and external radius in m, respectively, r_3 and r_4 are the casing's inner and outer radius, respectively, r_5 is the cementation's external radius, h_{comb} is the combined heat transfer coefficient, and $f(t)$ is the transient function for heat propagation in the formation up to the thermal perturbation limit [5]. This function encompasses the entire time dependence of heat propagation in the formation. It is the primary variable to be determined in this methodology. It is defined by:

$$f(t) = \frac{2\pi k_{for}\left[T(r_5,z,t) - T_g(z)\right]\Delta z}{\Delta\dot{Q}(r_5,z,t)} \tag{13}$$

In Equation (13), $T(r_5,z,t)$ is the temperature at the interface with the formation, $T_g(z)$ is the geothermal temperature at depth z, and $\Delta\dot{Q}(r_5,z,t)$ is the heat rate transferred to the formation by the depth element Δz [5].

In 1962, Ramey proposed the following approximation for times longer than a week [5]:

$$f(t) \cong -\ln\frac{r_5}{2\sqrt{\alpha t}} - 0.290 \tag{14}$$

with α being the thermal diffusivity of the formation and t being the time measured in days.

In 1967, Matthews and Russell, assuming that the fluid inside the tubing could be considered a linear geometric heat source (line source) and given the small radius of the

tubing compared to the radius of the formation, came up with the following approximation for the transient function [7]:

$$f(\tau) \cong \frac{1}{2}\int_{\frac{1}{4\tau}}^{\infty} \frac{e^{-u}}{u} du \tag{15}$$

where τ corresponds to the dimensionless Fourier time for formation, i.e.,

$$\tau = \frac{k_{for} t}{\rho_{for} c_{for} {r_5}^2} \tag{16}$$

where c_{for} is the specific heat of formation and ρ_{for} is the mass density of the formation.

In 1994, Hasan and Kabir proposed the following approximation for the transient function referring to the condition of constant heat flow at the interface with the formation in r_1 [8,9]:

$$\tau \leq 1.5 \rightarrow f(\tau) = 1.1281\sqrt{\tau}(1 - 0.3\sqrt{\tau}) \tag{17}$$

$$\tau > 1.5 \rightarrow f(\tau) = [0.4063 + 0.5\ln(\tau)](1 + \frac{0.6}{\tau}) \tag{18}$$

In 2004, Hagoort proposed an approximate function for the constant temperature boundary condition at the internal interface of the formation. This is [10]:

$$\tau < 1 \rightarrow f(\tau) = \frac{1}{\frac{1}{\pi\tau} + 0.5 - 0.2\sqrt{\tau/\pi}} \tag{19}$$

$$1 < \tau < 10^5 \rightarrow f(\tau) = -0.0012[\ln(\tau)]^3 + 0.0249[\ln(\tau)]^2 + 0.3083\ln(\tau) + 1.0504 \tag{20}$$

$$\tau > 10^5 \rightarrow f(\tau) = 0.5\ln(\frac{\tau}{0.447}) \tag{21}$$

In general, the transient functions for boundary conditions of the "constant temperature at r_1", "constant flow at r_1", and "fluid with constant temperature and convection boundary condition at r_1" types are given, respectively, by

$$f(\tau) = 1/\mathcal{L}_{s\rightarrow\tau}^{-1}\left\{\frac{K_1(\sqrt{s})}{\sqrt{s}K_0(\sqrt{s})}\right\} \tag{22}$$

$$f(\tau) = \mathcal{L}_{s\rightarrow\tau}^{-1}\left\{\frac{K_0(\sqrt{s})}{s\sqrt{s}K_1(\sqrt{s})}\right\} \tag{23}$$

$$f(\tau) = \mathcal{L}_{s\rightarrow\tau}^{-1}\left\{\frac{1}{s}\frac{K_0(\sqrt{s})}{K_0(\sqrt{s}) + \frac{\sqrt{s}}{\beta_{for}}K_1(\sqrt{s})}\right\} \Big/ \mathcal{L}_{s\rightarrow\tau}^{-1}\left\{\frac{1}{\sqrt{s}}\frac{K_1(\sqrt{s})}{K_0(\sqrt{s}) + \frac{\sqrt{s}}{\beta_{for}}K_1(\sqrt{s})}\right\} \tag{24}$$

where $\mathcal{L}_{s\rightarrow\tau}^{-1}\{-\}$ is the inverse Laplace transformation from s to τ, K_0 and K_1 are the Bessel functions of the second kind and order 0 and 1, respectively, and β_{for} is the Biot number for the formation [6], i.e.,

$$\beta_{for} = \frac{r_1 U_{for}}{k_{for}} \tag{25}$$

where U_{for} is the global heat transfer coefficient up to the interface with the formation, given by:

$$U_{for} = \left[\frac{1}{h} + \frac{r_1}{k_{tub}}\ln(\frac{r_2}{r_1}) + \frac{r_1}{r_2}\frac{1}{h_{comb}} + \frac{r_1}{k_{rev}}\ln(\frac{r_4}{r_3}) + \frac{r_1}{k_{cim}}ln(\frac{r_5}{r_4})\right]^{-1} \tag{26}$$

The derivation of the listed equations, i.e., the solution of the system of differential equations for the mentioned boundary conditions, can be found in the work of Lima [4].

4. Analitical Approach

Wu and Pruess in 1990 [3], Assmann [11] in 1993, and Haggort in 2004 [10] presented analytical solutions for calculating the temperature of the fluid inside the tubing. Using the concept of the global heat transfer coefficient to synthesize the thermal resistances up to the formation, they all disregarded the transience in the completion. In addition, the work by Wu and Pruess presented data on the relationship between vertical and radial gradients, justifying the assumption of a zero vertical heat flow.

Although the solutions obtained by Wu and Pruess, Assmann, and Hagoort, among others, show good results after the well has been in operation for less than two weeks, like Ramey's solution, disregarding the transience of the heat transfer in the completion, as well as the variation in the internal energy of the fluid (second part of Equation (10)), makes it impossible to obtain better results for times around the transit time of the fluid in the tubing.

Consider the simplified completion shown in Figure 4, where the annulus has been ignored to illustrate the methodology. The layers of the well have been numbered to facilitate the naming of properties and variables. Furthermore, in the same figure, the chosen positions (z_1 and z_2) to calculate the integrals of Equation (10) are shown.

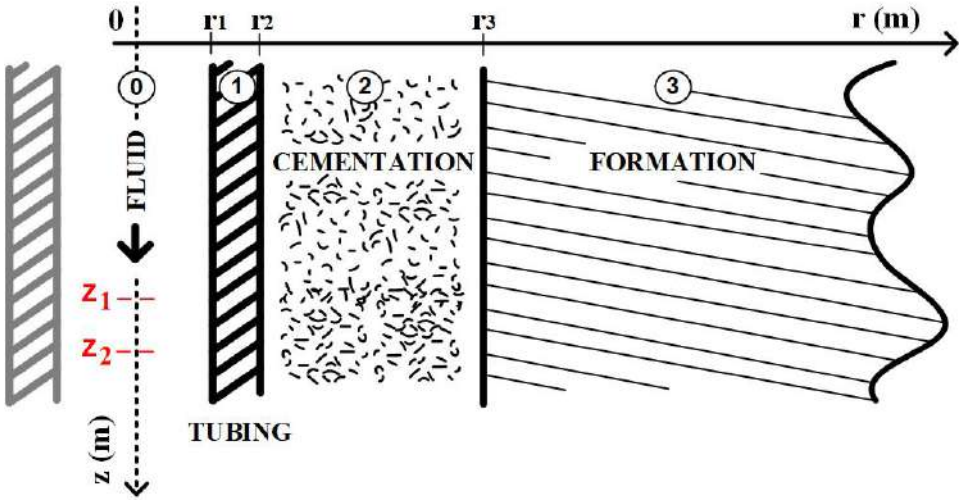

Figure 4. New control volumes and conservation of energy.

As we have seen so far, calculating the flow rate depends on knowing the value of the overall heat transfer coefficient, which in turn depends on the convection coefficient, the fluid temperature, the geothermal temperature, and the temperature of the internal tubing interface. Consider the following dimensionless temperatures for the fluid and the internal tubing interface:

$$\theta_f(z,t) = \frac{T_f(z,t) - T_g(z)}{T_g(z)} \tag{27}$$

$$\theta_1(z,t) = \frac{T(r_1,z,t) - T_g(z)}{T_g(z)} \tag{28}$$

with θ_f being the injection fluid temperature and θ_1 being the temperature of medium 1.

Since the heat flow by convection at the internal interface of the tubing must be equal to the heat flow at the same interface due to the use of the global heat coefficient, we have:

$$U(z,t) = h\frac{T_f(z,t) - T(r_1,z,t)}{T_f(z,t) - T_g(z)} \tag{29}$$

and, consequently:

$$U(z,t) = h - \frac{\theta_1(z,t)}{\theta_f(z,t)}h \tag{30}$$

Considering that the vertical thermal gradient, and consequently the heat flow in the same direction, is only significant when compared to the intensity of the radial flow at the thermal disturbance front, which occurs during the fluid's transit time in the tubing, it will be disregarded in this analysis [3]. Thus, excluding the vertical heat flow, assuming that the flow regime inside the tubing is turbulent, and applying the principles of conservation of energy and mass, we have the system of partial differential equations described in Table 1. The deduction of the equations and the solution can be found in Appendix A of the work by Lima [4].

Table 1. System of differential equations—simplified completion.

	Description	Equation
Formation ($r_3 \leq r \leq \infty$)	General Equation	$\frac{\partial^2 T(r,z,t)}{\partial r^2} + \frac{1}{r}\frac{\partial T(r,z,t)}{\partial r} = \frac{1}{\alpha_3}\frac{\partial T(r,z,t)}{\partial t}, \quad \alpha_3 = \frac{k_3}{\rho_3 c_3}$
	Initial Condition	$T(r,z,0) = T_g(z)$
	Boundary Condition (∞)	$\lim_{r\to\infty} T(r,z,t) = T_g(z)$
	Boundary Condition (r_3)	(a) $k_2\frac{\partial T(r_3^-,z,t)}{\partial r} = k_3\frac{\partial T(r_3^+,z,t)}{\partial r}$ (b) $T(r_3^-,z,t) = T(r_3^+,z,t)$
Cementation ($r_2 \leq r \leq r_3$)	General Equation	$\frac{\partial^2 T(r,z,t)}{\partial r^2} + \frac{1}{r}\frac{\partial T(r,z,t)}{\partial r} = \frac{1}{\alpha_2}\frac{\partial T(r,z,t)}{\partial t}, \quad \alpha_2 = \frac{k_2}{\rho_2 c_2}$
	Initial Condition	$T(r,z,0) = T_g(z)$
	Boundary Condition (r_3)	(a) $k_2\frac{\partial T(r_3^-,z,t)}{\partial r} = k_3\frac{\partial T(r_3^+,z,t)}{\partial r}$ (b) $T(r_3^-,z,t) = T(r_3^+,z,t)$
	Boundary Condition (r_2)	(a) $k_1\frac{\partial T(r_2^-,z,t)}{\partial r} = k_2\frac{\partial T(r_2^+,z,t)}{\partial r}$ (b) $T(r_2^-,z,t) = T(r_2^+,z,t)$
Tubing ($r_1 \leq r \leq r_2$)	General Equation	$\frac{\partial^2 T(r,z,t)}{\partial r^2} + \frac{1}{r}\frac{\partial T(r,z,t)}{\partial r} = \frac{1}{\alpha_1}\frac{\partial T(r,z,t)}{\partial t}, \quad \alpha_1 = \frac{k_1}{\rho_1 c_1}$
	Initial Condition	$T(r,z,0) = T_g(z)$
	Boundary Condition (r_2)	(a) $k_1\frac{\partial T(r_2^-,z,t)}{\partial r} = k_2\frac{\partial T(r_2^+,z,t)}{\partial r}$ (b) $T(r_2^-,z,t) = T(r_2^+,z,t)$
	Boundary Condition (r_1)	(a) $-r_1^+\frac{\partial T(r_1^+,z,t)}{\partial r} = \beta_1[T_f(z,t) - T(r_1^-,z,t)], \quad \beta_1 = \frac{r_1 h}{k_1}$ (b) $T(r_1^-,z,t) = T(r_1^+,z,t)$
Fluid ($0 \leq r \leq r_1$)	General Equation	$\frac{\partial T_f(z,t)}{\partial t} + v_{med}\frac{\partial T_f(z,t)}{\partial z} = \frac{2h}{r_1\rho_0 c_0}[T(r_1,z,t) - T_f(z,t)]$
	Initial Condition	$T_f(z,0) = T_g(z)$
	Boundary Condition (z_0)	$T_f(0,t) = T_{f0}$
	Boundary Condition (r_1)	(a) $-r_1^+\frac{\partial T(r_1^+,z,t)}{\partial r} = \beta_1[T_f(z,t) - T(r_1^-,z,t)], \quad \beta_1 = \frac{r_1 h}{k_1}$ (b) $T(r_1^-,z,t) = T(r_1^+,z,t)$

As a result, the dimensionless temperature of fluid in the center of the tubing at $r = 0$ and the dimensionless temperature at $r = r_1$ are given by:

$$\theta_f(w,\tau) = \frac{1}{T_g(w)}\Big[- a_w\mathcal{L}_{s\to\tau}^{-1}\Big\{\frac{1-e^{-g(s)w}}{sg(s)}\Big\} + b_w\theta_{f0}\mathcal{L}_{s\to\tau}^{-1}\Big\{\frac{e^{-g(s)w}}{s}\Big\}\Big] \tag{31}$$

and

$$\theta_1(w,\tau) = \frac{1}{T_g(w)}\Big[- a_w\mathcal{L}_{s\to\tau}^{-1}\Big\{\bar{\bar{\theta}}_1(w,s)\frac{1-e^{-g(s)w}}{sg(s)}\Big\} + b_w\theta_{f0}\mathcal{L}_{s\to\tau}^{-1}\Big\{\bar{\bar{\theta}}_1(w,s)\frac{e^{-g(s)w}}{s}\Big\}\Big] \tag{32}$$

where

$$g(s) = 2\alpha_1\beta_1[1 - \bar{\bar{\theta}}_1(w,s)] + s \tag{33}$$

$$\bar{\bar{\theta}}_1(w,s) = \bar{c}_{11} I_o(\sqrt{s}) - \bar{c}_{12} K_o(\sqrt{s}) \tag{34}$$

such that:

$$\bar{\theta}_1(w,s) = \bar{\bar{\theta}}_1(w,s)\bar{\theta}_f(w,s) \tag{35}$$

For Equations (31)–(35), ω is a dimensionless vertical coordinate, a_ω is the angular coefficient of geothermal temperature with respect to ω, b_ω is the linear coefficient of geothermal temperature with respect to ω, $\bar{\theta}_1$ is the dimensionless temperature of medium 1 in the Laplace domain, α_1 is the thermal diffusivity of medium 1, and β_1 is the Biot number relative to medium 1.

The function $g(s)$ is used to simplify the notation. The functions $I_0(\sqrt{s})$ and $K_0(\sqrt{s})$ are known in the literature as modified Bessel functions of the first and second kind, respectively, both of zero order. The variables $\bar{c}_{11}$ and $\bar{c}_{12}$ are functions in the Laplace domain, independent of the radial coordinate, r, and related to the *mean 1* of the completion under study, taken as a reference in the process of dimensioning the variables. Their values are given by a system of linear functions in the Laplace domain, which is a consequence of the boundary conditions of the problem. See [4] for more information.

In Equations (31) and (32), τ is the dimensionless time, w is the dimensionless vertical coordinate, θ_{f0} is the dimensionless temperature of the fluid at $w = 0$, a_w is the geothermal gradient related to the dimensionless coordinate w, and b_w is the linear coefficient of the dimensionless geothermal temperature. The values of τ , w, a_w, and b_w are given, respectively, by:

$$\tau = \frac{k_1}{\rho_1 c_1 {r_1}^2} t \tag{36}$$

$$w = \frac{k_1}{v_{med}\rho_1 c_1 {r_1}^2} z \tag{37}$$

$$a_w = \frac{v_{med}\rho_1 c_1 {r_1}^2}{k_1} a_z \tag{38}$$

$$b_w = T_g(0) \tag{39}$$

where k_1 is the thermal conductivity, ρ_1 is the mass density, c_1 is the specific heat related to medium 1, v_{med} is the average velocity of the fluid velocity profile, and a_z is the geothermal gradient related to independent variable z.

The dimensionless variables represented by Equations (27), (28), (36), and (37) are consequences of the algebraic manipulations that attempt to reduce the mathematical complexity of the system of partial differential equations. Among them, the dimensionless time variable (τ) is known in the literature as the dimensionless Fourier time.

Thus, in addition to Equation (30), the global heat coefficient can be rewritten as:

$$U(\tilde{z},t) = h - \frac{-a_w \mathcal{L}^{-1}_{s\to\tau}\left\{\bar{\bar{\theta}}_1(w,s)\frac{1-e^{-g(s)w}}{sg(s)}\right\} + b_w\theta_{f0}\mathcal{L}^{-1}_{s\to\tau}\left\{\bar{\bar{\theta}}_1(w,s)\frac{e^{-g(s)w}}{s}\right\}}{-a_w \mathcal{L}^{-1}_{s\to\tau}\left\{\frac{1-e^{-g(s)w}}{sg(s)}\right\} + b_w\theta_{f0}\mathcal{L}^{-1}_{s\to\tau}\left\{\frac{e^{-g(s)w}}{s}\right\}} h \tag{40}$$

and, finally, the mass flow can be calculated by Equation (10), where the integral limits, z_1 and z_2, can be chosen in the interval belonging to the transport part of the tubing under analysis. $\tilde{z}$ can be assumed as an average of z_1 and z_2. In other words,

$$\tilde{z} \cong \frac{z_1 + z_2}{2} \tag{41}$$

The inverse Laplace transforms of Equation (40) can be calculated numerically using the Gaver–Stehfest algorithm [12,13], which was adopted in this article, or other methods available in the literature.

As seen, it is possible to use a standard script for both approaches by continuing to use the global heat transfer coefficient as the basis for calculating the flow rate. However, unlike the previous quasi-static approach, the calculation of the global coefficient given by Equation (40) also considers the thermal transience in the layers of the well.

5. Computer Simulations

Given the very specific operating conditions regarding data collection and storage in the first moments of injection in a reservoir with the original initial conditions, the possibility of the existence of real, unmotivated data from the operation of a well in production under these specific conditions has proven unfeasible up to the point of the completion of this article, making it considerably difficult to evaluate the proposed analytical solution.

As a countermeasure to the lack of data for validation, a computerized well simulator was designed and developed to generate the temporal evolution of the thermal profile of the injection fluid along the tubing.

Due to its widespread use in the scientific community, the finite difference method, specifically the explicit Euler method, was used as a numerical tool in the simulator code development. In this method, the central idea is to replace the differential equations with algebraic equations, exchanging the derivatives for difference approximations and applying the resulting equations to each subdivision of the problem domain, referred to in this article as the control volume (CV). The result is an algebraic equation for each subdivision, making up a system of linear equations [6].

The code was developed in Phyton, version 3.9.13, from Anaconda Navigator, version 2.3.1. The code and packets used can be found in the work of Lima [4].

6. Results

Two computer simulations were carried out to evaluate the proposed method. The first simulation aimed to verify the alignment of the proposed solution with the classical quasi-static solutions proposed by Ramey and their successors. To this end, a schematic of a well without completion was adopted, aligning it with the reference model used to calculate the transient functions. The second simulation aimed to verify the proposed analytical solution in a well with simplified completion (tubing and cementing) and compare its performance with quasi-static solutions.

6.1. Simulation 1: Well without Completion

In this first analysis, the data generated in the simulation of a well without completion were processed, as shown in Figure 5. This configuration is a good representation of the prototype well installed at UFRN [14]. Although the prototype has tubing, its high thermal conductivity means that its presence does not make a noticeable difference to the fluid temperature evolution, as will be seen below.

Once the oil industry has no wells without completions, the well shown in Figure 5 cannot be used as a real-world model. However, by processing the fluid temperature evolution for this configuration, it is possible to evaluate the contribution of the transient functions to the flow measurement since these functions were derived from a similar schematic of the well. Furthermore, since water injection wells operate for months, sometimes years, heat conduction in the formation is the dominant thermal process in flow measurements. Under these conditions, after the first two weeks of operation, any thermal transient in the completion that could influence the flow inference becomes insignificant [5]. In this way, a simulation without completion provides indications and trends for the behavior of the flow to be measured.

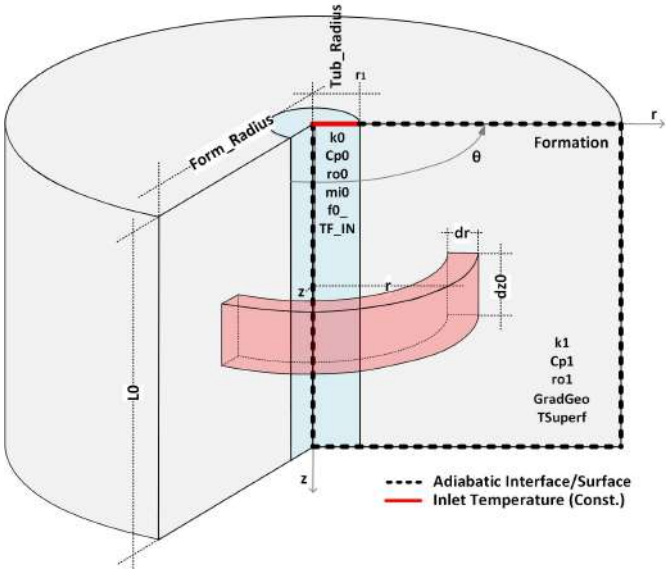

Figure 5. Well without completion—details of the problem.

6.2. Simulation 1: Simulation Data

Table 2 shows the variables and values used in the simulation of the well shown in Figure 5. The other variables used in the simulation are functions of the values shown in the table.

Table 2. Well without completion—data used in the simulation (L = 10 m).

	Variable	Value	Description
General data	dt0	0.25 s	Time step
	dz0	0.1 m	Space step in the z direction (longitudinal)
	tsimu	6 h	Simulation time
	p_samples_z	0.1 m	Sampling period in the "z" direction
	p_samples_t	15 s	Time sampling period
	TAmb	35 °C	Environment temperature
	TgeoType	1	Geothermal temperature type (0 = constant; 1 = linear)
	ThermalSource	0	0 = Adiabatic boundary; 1 = Thermal source equal to Tgeo
Geometric	L0	10 m	Longitudinal length of the well to be simulated
	Tub_Radius	0.0254 m	[r1] tubing inner radius
	Reserv_Radius	1 m	[r2] Reservoir external radius
	DIV0	1	Number of region radial divisions 0
	DIV1	40	Number of region radial divisions 1
Fluid	k0	0.636 W/(m·K)	Water thermal conductivity
	Cp0	4184 J/(kg·K)	Water-specific thermal capacity
	ro0	1000 kg/m^3	Water-specific mass
	mi0	0.0006 N·s/m^2	Absolute viscosity
	f0_	0.0003 m^3/s	Volume flow
	TF_IN	20 °C	Inlet fluid temperature
Formation	k1	2.42 W/(m·K)	Reservoir thermal conductivity
	Cp1	1500 J/(kg·K)	Reservoir-specific thermal capacity
	ro1	2100 kg/m^3	Reservoir-specific mass
	GradGeo	0.365 °C/m	Geothermal gradient in the "z" dimension
	TSurf	TAmb	Surface temperature

6.3. Simulation 1: General Results

Figure 6 shows the time evolution of the fluid temperature along the tubing. The curve for "$t \leq 0$ s" corresponds to the geothermal temperature. It is the initial condition used

in solving the system of nonlinear equations. The curve for "$t = 1$ min" corresponds to the temperature profile established after a transit time, which is the time required for the fluid to travel the total simulated 10 m. It can be seen that the dynamic change in the curve slows down as the operating time increases. In particular, the curve for 2 h differs little from the curve for 6 h.

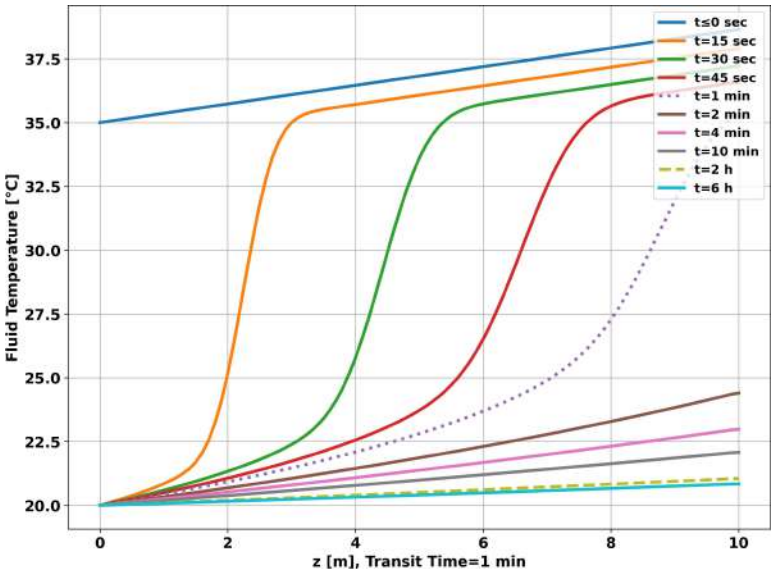

Figure 6. Well without completion—longitudinal temperature evolution.

Figure 7 shows the time evolution of the radial temperature at a depth of 5 m. As can be seen in the graph, after 6 h, the thermal disturbance was approximately restricted to a distance of 50 cm from the center of the tubing, validating the external radius of the reservoir used in the simulation (1 m). Given the simulation time considered (6 h), using a small value for the outer radius of the reservoir (Reserv_Radius) would result in overheating/undercooling of the well, saturating the simulation and making the generated data unrepresentative of the real situation.

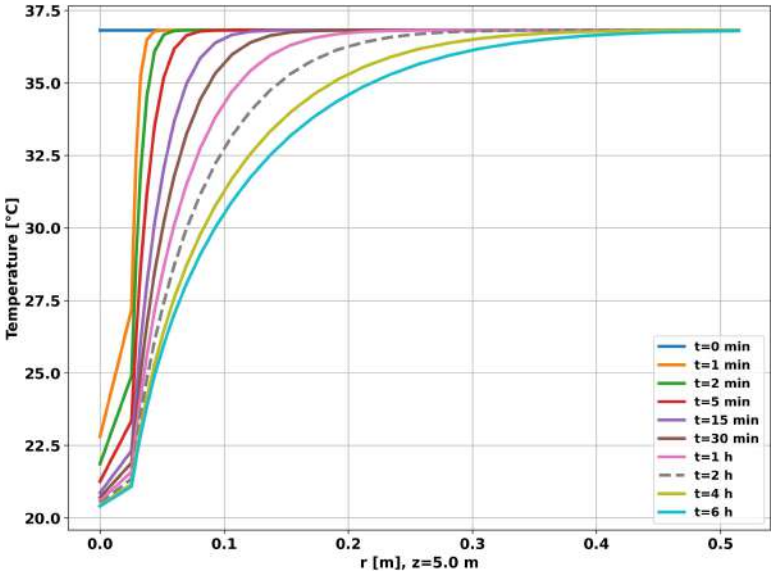

Figure 7. Well without completion—radial temperature evolution.

Therefore, for the prototype installed at UFRN, which has an outer radius of approximately 30 cm, we recommend adopting 2 h as the maximum operating time. After this time, the prototype will overheat, and the generated data will no longer be valid.

6.4. Simulation 1: Inferred Flow

The graph in Figure 8 shows the evolution of the flow measurement for the methods and functions presented in this work. As can be seen, all the methods tend to converge to the reference flow used in the simulation (0.3×10^{-3} (m^3/s)). However, the methods derived from the constant temperature assumption show better results, i.e., a constant temperature at r_1 (curve Constant Temp), a constant fluid temperature with convection conditions at r_1 (curve Convection Condition) and the Hagoort approximations (curve Hagoort). This greater accuracy of the constant temperature methods is a consequence of the short transit time of the fluid in the tubing, equal to 1 min, which means that the fluid temperature at the measurement point has a small time variation compared to the time variation of the heat flow.

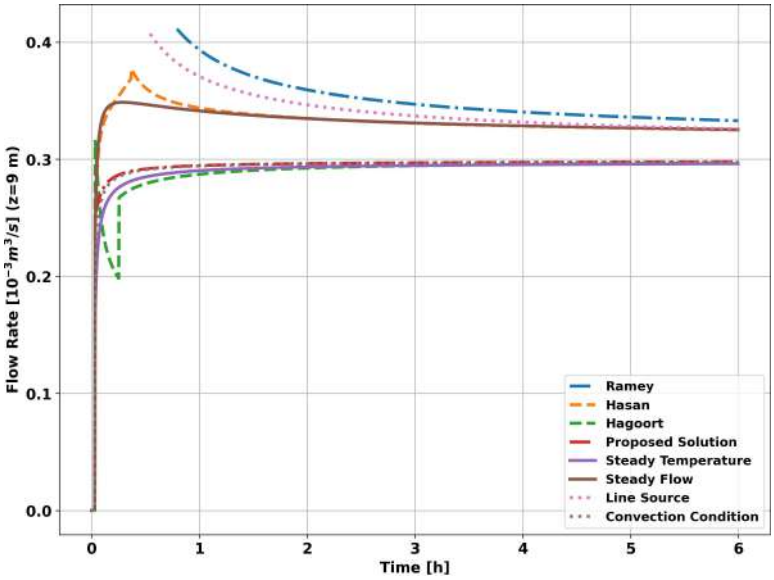

Figure 8. Well without completion—measurement at 9 m.

The graph in Figure 9 shows the evolution of the flow measurement error. As expected, the choice of transient function will result in a greater or lesser systematic error. Applying the proposed analytical solution results in a significantly lower systematic error for the entire simulated operating time.

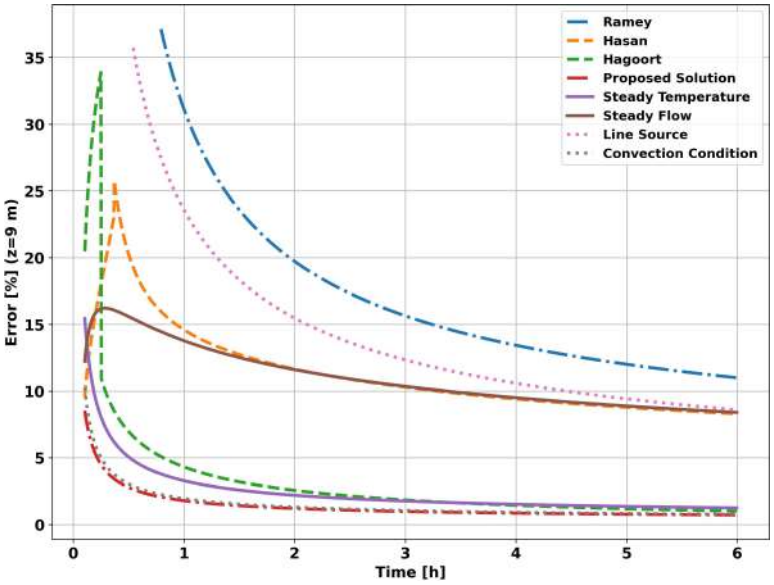

Figure 9. Well without completion—measurement error at 9 m.

6.5. Simulation 2: Well with Simplified Completion

This second simulation aims to verify the impact of transient heat transfer in the well completion on the inference of flow rate using the methods and formulations outlined in this article. To achieve this, consider the well completion represented in Figure 10. This completion technique, which involves only tubing and cementation, is widely utilized in real injector and producer wells.

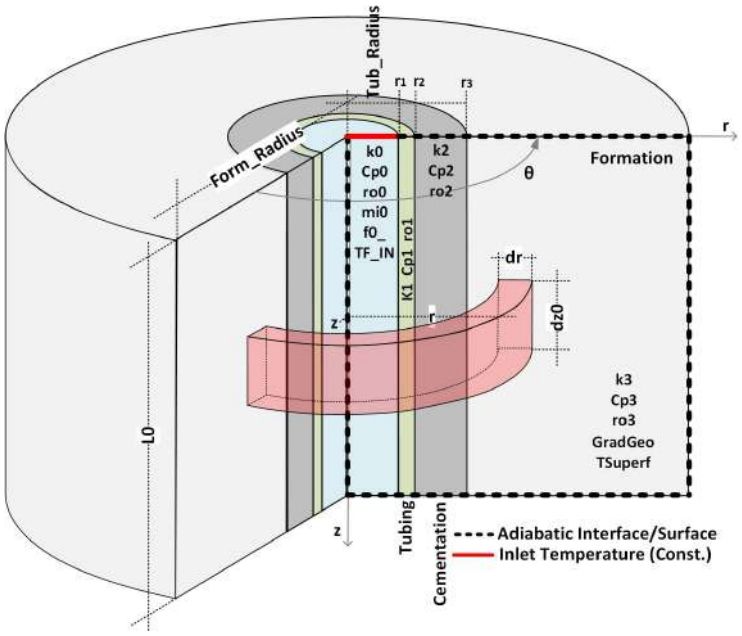

Figure 10. Completion with two layers—details of the problem.

As in the previous simulation, adiabatic boundaries were used at the edges of the simulated well, making it easy to detect saturation. A constant temperature was also used at the inlet of the injection column (tubing).

6.6. Simulation 2: Simulation Data

Table 3 shows the variables and values used in this simulation. Following the same approach as the previous simulation, the other variables used are functions of the values presented.

Table 3. Completion with two layers—data used in the simulation.

	Variable	Value	Description
General data	dt0	0.25 s	Time step
	dz0	0.1 m	Space step in the z direction (longitudinal)
	tsimu	6 h	Simulation time
	p_samples_z	0.1 m	Sampling period in the "z" direction
	p_samples_t	15 s	Time sampling period
	TAmb	35 °C	Environment Temperature
	TgeoType	1	Geothermal temperature type (0 = constant; 1 = linear)
	ThermalSource	0	0 = Adiabatic boundary; 1 = Thermal source equal to Tgeo
Geometric	L0	10 m	Longitudinal length of the well to be simulated
	Tub_Radius	0.0254 m	[r1] Longitudinal length of the well to be simulated
	Reserv_Radius	1 m	[r4] Reservoir external radius
	DIV0	1	Number of region radial divisions 0
	DIV1	3	Number of region radial divisions 1
	DIV2	10	Number of region radial divisions 2
	DIV3	30	Number of region radial divisions 3

Table 3. *Cont.*

	Variable	Value	Description
Fluid	k0	0.636 W/(m·K)	Water thermal conductivity
	Cp0	4184 J/(kg·K)	Water-specific heat capacity
	ro0	1000 kg/m^3	Water-specific mass
	mi0	0.0006 N·s/m^2	Absolute viscosity
	f0_	0.0003 m^3/s	Volume flow
	TF_IN	20 °C	Inlet fluid temperature
Tub	k1	14 W/(m·K)	Reservoir thermal conductivity
	Cp1	502 J/(kg·K)	Reservoir-specific thermal capacity
	ro1	8000 kg/m^3	Reservoir-specific mass
	Tub_Thickness	0.635 cm	Tubing thickness
Cement	k2	0.9 W/(m·K)	Reservoir thermal conductivity
	Cp2	900 J/(kg·K)	Reservoir-specific thermal capacity
	ro2	2400 kg/m^3	Reservoir-specific mass
	Cim_Thickness	5.08 cm	Cementation thickness
Formation	k3	2.42 W/(m·K)	Reservoir thermal capacity
	Cp3	1500 J/(kg·K)	Reservoir-specific thermal capacity
	ro3	2100 kg/m^3	Reservoir-specific mass
	GradGeo	0.365 °C/m	Geothermal gradient in the "z" dimension
	TSurf	TAmb	Surface temperature

6.7. Simulation 2: General Results

The graph in Figure 11 shows the time evolution of the fluid temperature along the tubing. As in the previous simulation, the curve for "$t \leq 0$ s" corresponds to the geothermal temperature. It is the initial condition used in solving the system of nonlinear equations. It can be seen, as before, that the dynamics of the change in the curve lose speed as time progresses, but with less intensity, resulting in higher temperatures at the end of each measurement time. As observed in the previous simulation, the fluid temperature curve for 2 h of operation differs little from the curve for 6 h.

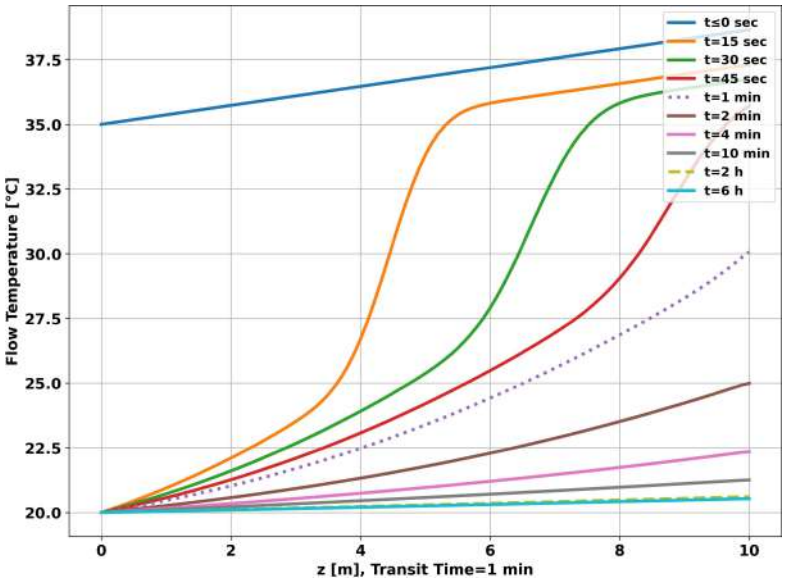

Figure 11. Completion with two layers—longitudinal temperature evolution.

The graph in Figure 12 shows the time evolution of the radial temperature at a depth of 5 m, half the length of the tubing. After 6 h, the thermal disturbance was restricted to a distance of 50 cm from the center of the tubing, which shows that the simulation was not saturated for the time considered.

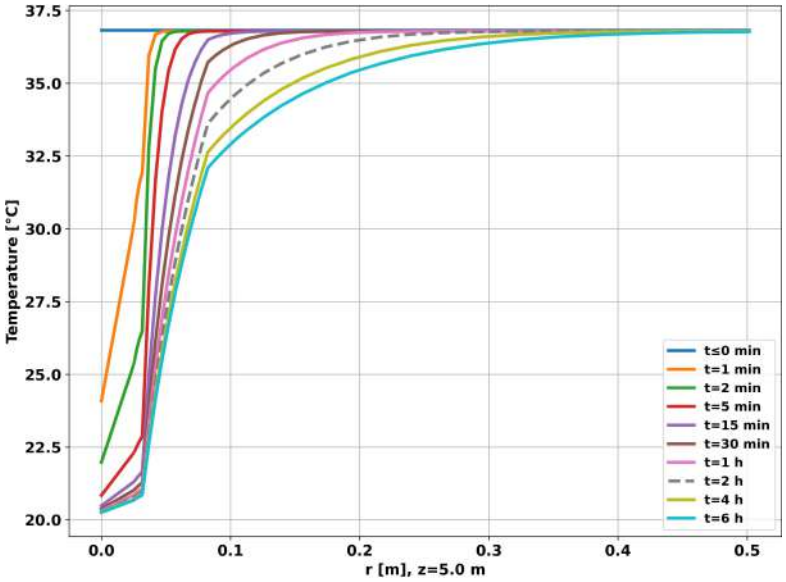

Figure 12. Completion with two layers—radial temperature evolution.

6.8. Simulation 2: Inferred Flow

When the flow is measured using the classical methods, simplifications are made in calculating the global heat transfer coefficient, i.e., the transient heat transfer through the completion (tubing and cementing) is not considered. When measured using the proposed analytical method, only the transient effects of the tubing are ignored due to its high thermal conductivity when compared to the other layers of the well (cementing and formation). The graph in Figure 13 shows the evolution of flow measurement for the methods and transient functions presented in this article.

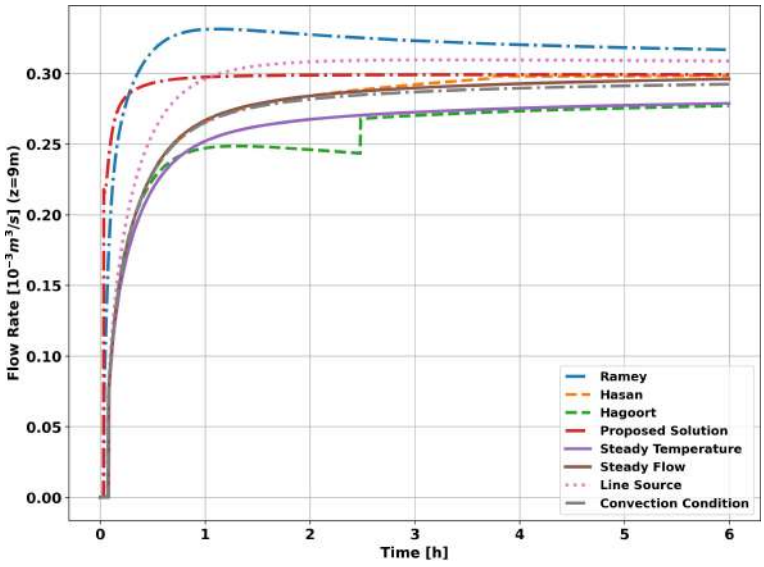

Figure 13. Completion with two layers—measured at 9 m.

As can be seen in Figure 13, as in the previous simulation, all the methods tended to converge to the reference flow rate (0.3×10^{-3} (m^3/s)). However, unlike the previous simulation, the methods derived from the assumption of a constant heat flow, i.e., constant heat flow at r_1 (Constant Flow curve) and the Hasan and Kabir approximations (Hasan curve), showed better results. The method based on applying the convection boundary condition in conjunction with the assumption of a constant fluid temperature (Convection Condition curve) showed good results in both simulations, given its flexibility in dealing with heat flow into the reservoir. In the same sense, the proposed analytical solution

(Proposed Solution curve) enabled flexibility in the fluid temperature and showed visibly better results than all the other methods studied.

The graph in Figure 13 shows the evolution of the systematic error in flow measurements. The systematic error resulting from applying the proposed analytical method (Proposed Solution curve) tends to be less than 1% in the initial moments of the simulation, unlike the other methods, which require hours or days of operation. The graph in Figure 14 shows the evolution of the systematic error in flow measurement. The systematic error in the initial instants of the analytical approach is a consequence of neglecting the heat flow in the vertical direction, which is significant in the initial moments in the vicinity of the well, and of not taking into account the effects of the tubing on heat propagation in the system as a whole.

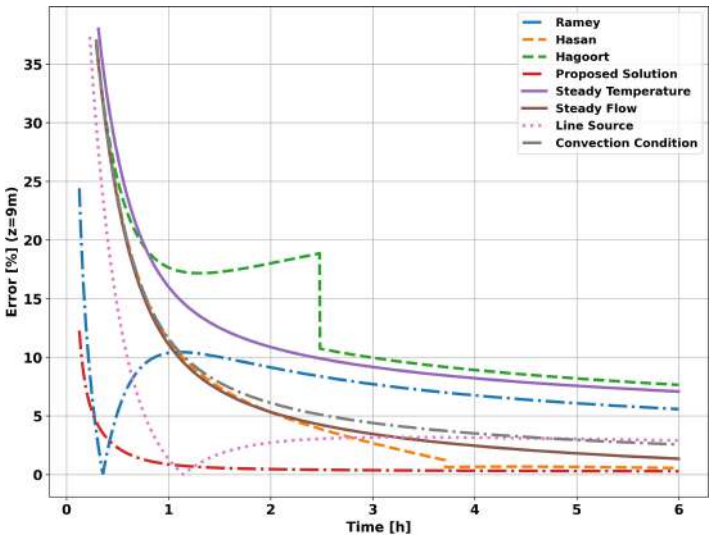

Figure 14. Completion with two layers—measurement error at 9 m.

7. Conclusions

This work proposed an analytical solution to predict the thermal profile of the fluid inside an injection well during the initial hours of well operation, a period not covered in the reviewed articles. The intention was to calculate the flow rate inside the tubing, crucial information for the success of an injection plan, and avoid damage to the oil reservoir. Unlike other studies, the transient heat flow in the well completion was addressed to achieve this, resulting in a complex system of partial differential equations.

Due to the absence of real data to evaluate the proposed solution, a computer simulation was conducted to predict the evolution of the thermal profile of the fluid inside the tubing. Two simulations were performed. The first, without any completion, was intended to verify the concordance of the proposed analytical solution with the solutions of Ramey and other researchers. The second, with a well-completion composed of tubing and cementation, was intended to verify the superiority of the proposed analytical solution.

Based on the data from the first simulation, it was observed that the proposed analytical solution is consistent with the quasi-static solution and shows slightly better results than the other studied solution over the six hours simulated. The error in the calculated flow rate was 1.8% after one hour and 1.2% after two hours of well operation. The average errors of the other solution studied were 13.2% and 9.2% after one and two hours, respectively. In the same way, using the data from the second simulation, the proposed analytical approach exhibits an error of 0.9% after one hour and an error of 0.5% after the first two hours, much less than the other solutions studied, which present an average error of 11.4% and 8.3% after one and two hours, respectively.

In summary, the proposed analytical solution has shown better results compared to the other solutions studied. Since the proposed solution considers the transient behavior of the heat flow in well completion, which, as was seen, is significant in the initial hours of

well operation, these results were expected. However, the solution is more complex and more difficult to implement.

Author Contributions: V.S.L., C.W.S.d.P.M. and A.O.S. conceived and designed the study; V.S.L., C.W.S.d.P.M., W.L.A.d.S. and G.A.E.E. were responsible for the methodology; V.S.L., G.P.d.O. W.L.A.d.S. and D.A.d.M.F. performed the simulations and experiments; V.S.L., E.R.L.V., G.P.d.O. and D.A.d.M.F. reviewed the manuscript and provided valuable suggestions; V.S.L., E.R.L.V., G.P.d.O. and D.A.d.M.F. wrote the paper; G.A.E.E., C.W.S.d.P.M. and A.O.S. were responsible for supervision. All authors have read and agreed to the published version of the manuscript.

Funding: This research was funded in part by Universidad Nacional de San Agustin de Arequipa (UNSA), and supported by the Coordenação de Aperfeiçoamento de Pessoal de Nível Superior—Brasil (CAPES)—Finance Code 001 and Conselho Nacional de Desenvolvimento Científico e Tecnológico (CNPq).

Data Availability Statement: Data are contained within the article.

Conflicts of Interest: The authors declare no conflict of interest.

Abbreviations

The following abbreviations are used in this manuscript:

α	Thermal diffusivity (m^2/s)
α_1	Thermal diffusivity of medium 1 (m^2/s)
α_2	Thermal diffusivity of medium 2 (m^2/s)
α_3	Thermal diffusivity of medium 3 (m^2/s)
β_1	Biot number relative to the medium 1
β_{for}	Relative Biot number of the formation
μ	Absolute viscosity ($N{\cdot}s/m^2$)
θ_1	Dimensionless temperature of the medium 1
$\bar{\theta}_1$	Dimensionless temperature of medium 1 in the Laplace domain
θ_f	Dimensionless injection fluid temperature
$\bar{\theta}_f$	Dimensionless temperature of the injection fluid in the Laplace domain
rho ρ	Mass density (kg/m^3)
ρ_0	Mass density of the medium 0 (kg/m^3)
ρ_1	Mass density of the medium 1 (kg/m^3)
ρ_2	Mass density of the medium 2 (kg/m^3)
ρ_3	Mass density of the medium 3 (kg/m^3)
ρ_{for}	Mass density of the formation (kg/m^3)
τ	Shear stress (N/m^2)
τ	Dimensionless Fourier time
a_w	Angular coefficient of geothermal temperature with respect to w (°C)
b_w	Linear coefficient of geothermal temperature with respect to w (°C)
c	Specific heat ($J/(kg{\cdot}K)$)
c_0	Specific heat of the medium 0 ($J/(kg{\cdot}K)$)
c_1	Specific heat of the medium 1 ($J/(kg{\cdot}K)$)
c_2	Specific heat of the medium 2 ($J/(kg{\cdot}K)$)
c_3	Specific heat of the medium 3 ($J/(kg{\cdot}K)$)
c_{for}	Specific heat of formation ($J/(kg{\cdot}K)$)
f	Friction factor
$f(t)$	Transient formation function
h	Heat convection coefficient ($W/(m^2{\cdot}K)$)
h_{comb}	Combined heat transfer coefficient ($W/(m^2{\cdot}K)$)
I_0	Modified Bessel function of first type and order 0

k	Thermal conductivity (W/(m·K))
k_0	Thermal conductivity of the medium 0 (W/(m·K))
k_1	Thermal conductivity of the medium 1 (W/(m·K))
k_2	Thermal conductivity of the medium 2 (W/(m·K))
k_3	Thermal conductivity of the medium 3 (W/(m·K))
k_{cim}	Thermal conductivity of cementation (W/(m·K))
k_{for}	Thermal conductivity of the formation (W/(m·K))
k_{tub}	tubing thermal conductivity (W/(m·K))
k_{rev}	Casing thermal conductivity (W/(m·K))
K_0	Modified Bessel function of second type and order 0
L	Length (depth) of the well (m)
$\dot{m}$	Mass flow (kg/s)
r	Radial coordinate (m)
r_1	tubing inner radius (m)
r_2	tubing external radius (m)
r_3	Casing inner radius (m)
r_4	Casing outer radius (m)
r_5	Cimentation external radius (m)
Re	Dimensionless Reynolds number
Pr	Prandtl dimensionless number
$\dot{Q}$	Heat transfer rate (W)
s	Transformation variable for the Laplace domain
t	Time (s)
T	Temperature (°C)
T_f	Average fluid temperature (°C)
T_g	Geothermal temperature (°C)
U	Overall heat transfer coefficient (W/(m^2·K))
$\widetilde{U}$	Average overall heat transfer coefficient (W/(m^2·K))
v_{med}	Average velocity of the fluid velocity profile (m/s)
w	Dimensionless vertical coordinate
z	Vertical coordinate (m)
z_1	Initial vertical coordinate of the region under analysis (m)
z_2	Final vertical coordinate of the region under analysis (m)
$\tilde{z}$	Average vertical coordinate (m)

References

1. Thomas, J.E. (Organizador); *Fundamentos de Engenharia de Petróleo*, 2nd ed.; Interciência: Rio de Janeiro, Brazil, 2001. (In Portuguese)
2. Reges, J.E.O.; Salazar, A.O.; Maitelli, C.W.S.P.; Carvalho, L.G.; Britto, U.J.B. Flow Rates Measurement and Uncertainty Analysis in Multiple-Zone Water-Injection Wells from Fluid Temperature Profiles. *Sensors* **2016**, *16*, 1077. [CrossRef]
3. Wu, Y.S.; Pruess, K. An analytical solution for wellbore heat transmission in layered formations. *SPE Reserv. Eng.* **1990**, *5*, 531–538. [CrossRef]
4. Lima, V.S. Perfis téRmicos em Poços Injetores d'água: Redução do Erro Sistemático na Medição de Vazão Durante o Regime Transitório. Ph.D. Thesis, UFRN University, Natal, Brazil, 2019. (In Portuguese)
5. Ramey, H., Jr.; Henry, J. Wellbore heat transmission. *J. Pet. Technol.* **1962**, *14*, 427–435. [CrossRef]
6. Çengel, Y.A.; Ghajar, A.J. *Tranferência de Calor e Massa: Uma Abordagem Prática*, 4th ed.; AMGH: Porto Alegre, Brazil, 2012; Volume XXII, 904p. (In Portuguese)
7. Matthews, C.S.; Russell, D.G. *Pressure Buildup and Flow Tests in Wells*; Henry L. Doherty Memorial Fund of AIME New York: New York, NY, USA, 1967; Volume 1.
8. Hasan, A.R.; Jang, M. An analytic model for computing the countercurrent flow of heat in tubing and annulus system and its application: Jet pump. *J. Pet. Sci. Eng.* **2021**, *203*, 108492. [CrossRef]
9. Hasan, A.R. ; Kabir, C.S. Aspects of wellbore heat transfer during two-phase flow. *SPE Prod. Facil.* **1994**, *9*, 211–216. [CrossRef]
10. Hagoort, J. Ramey's wellbore heat transmission revisited. *SPE J. Soc. Pet. Eng.* **2004**, *9*, 465–474. [CrossRef]
11. Assmann, B.W. *Previsão do Comportamento de Pressão e Temperatura Transitorios em Poços de Petroleo e Oleodutos*; Dissertação (Mestrado)—Universidade Estadual de Campinas, UNICAMP: Campinas, Brazil, 1993; Volume XII, 128p. (In Portuguese)
12. Jacquot, R.; Steadman, J.; Rhodine, C. The gaver-stehfest algorithm for approximate inversion of laplace transforms. *IEEE Circuits Syst. Mag.* **1983**, *5*, 4–8. [CrossRef]

13. Mu, L.; Zhang, Q.; Li, Q.; Zeng, F. A Comparison of Thermal Models for Temperature Profiles in Gas-Lift Wells. *Energies* **2018**, *11*, 489. [CrossRef]
14. Silva, W.L.A. ; Lima, V.S.; Fonseca, D.A.M.; Salazar, A.O.; Maitelli, C.W.S.P. ; Echaiz, E.G.A. Study of Flow Rate Measurements Derived from Temperature Profiles of an Emulated Well by a Laboratory Prototype. *Sensors* **2019**, *19*, 1498. [CrossRef] [PubMed]

Disclaimer/Publisher's Note: The statements, opinions and data contained in all publications are solely those of the individual author(s) and contributor(s) and not of MDPI and/or the editor(s). MDPI and/or the editor(s) disclaim responsibility for any injury to people or property resulting from any ideas, methods, instructions or products referred to in the content.

energies

MDPI

Article

Fuzzy Control Strategy Applied to an Electromagnetic Frequency Regulator in Wind Generation Systems

Daniel C. C. Crisóstomo [1], Thiago F. do Nascimento [2], Evandro A. D. F. Nunes [3], Elmer Villarreal [4,*], Ricardo Pinheiro [2] and Andrés Salazar [2]

[1] Department of Sciences and Technology, Federal Rural University of Semi-Arid (DCT-UFERSA), Caraúbas 59780-000, Brazil
[2] Department of Computer Engineering and Automation, Federal University of Rio Grande do Norte (DCA-UFRN), Natal 59072-970, Brazil
[3] The Federal Institute of Education, Science and Technology of Bahia (IFBA), Salvador 40301-015, Brazil
[4] Department of Natural Sciences, Mathematics and Statistics, Federal Rural University of Semi-Arid (DCME-UFERSA), Mossoró 59625-900, Brazil
* Correspondence: elmerllanos@ufersa.edu.br

Abstract: This paper presents the implementation of a fuzzy control strategy for speed regulation of an electromagnetic frequency regulator (EFR) prototype, aiming to eliminate the dependence on knowledge of physical parameters in the most diverse operating conditions. Speed multiplication is one of the most important steps in wind power generation. Gearboxes are generally used for this purpose. However, they have a reduced lifespan and a high failure rate, and are still noise sources. The search for new ways to match the speed (and torque) between the turbine and the generator is an important research area to increase the energy, financial, and environmental efficiency of wind systems. The EFR device is an example of an alternative technology that this team of researchers has proposed. It considers the main advantages of an induction machine with the rotor in a squirrel cage positively. In the first studies, the EFR control strategy consisted of the conventional PID controllers, which have several limitations that are widely discussed in the literature. This strategy also limits the EFR's performance, considering its entire operating range. The simulation program was developed using the Matlab/Simulink platform, while the experimental results were obtained in the laboratory emulating the EFR-based system. The EFR prototype has 2 poles, a nominal power of 2.2 kW, and a nominal frequency of 60 Hz. Experimental results were presented to validate the efficiency of the proposed control strategy.

Keywords: speed control; fuzzy controller; electromagnetic frequency regulator; wind energy; photovoltaics

check for updates

Citation: Crisostomo, D.C.C.; do Nascimento, T.F.; Nunes, E.A.D.F.; Villarreal, E.; Pinheiro, R.; Salazar, A. Fuzzy Control Strategy Applied to an Electromagnetic Frequency Regulator in Wind Generation Systems. *Energies* **2022**, *15*, 7011. https://doi.org/10.3390/en15197011

Academic Editor: Xiangwu Yan

Received: 17 June 2022
Accepted: 15 September 2022
Published: 24 September 2022

Publisher's Note: MDPI stays neutral with regard to jurisdictional claims in published maps and institutional affiliations.

Copyright: © 2022 by the authors. Licensee MDPI, Basel, Switzerland. This article is an open access article distributed under the terms and conditions of the Creative Commons Attribution (CC BY) license (https://creativecommons.org/licenses/by/4.0/).

1. Introduction

Due to environmental issues, electricity generation systems using wind energy have increased rapidly all over the world. However, the variation in wind speed is the main problem for this type of system. Considering the wide range of wind variations and taking into account that turbine torque and power are very sensitive to such variations (torque varies as the square and power as the cube of wind speed), wind turbines are oversized concerning the energy they actually produce over time, which is characterized by the capacity factor. In addition, the need to expand generation capacity has led to turbines with increasingly larger diameters, which increases the torque produced on the turbine shaft and reduces the permissible speed at the blade tip. Thus, a speed multiplier is used in many of the technologies to match the wind turbine and the electric generator speeds [1].

Currently, speed multipliers are the main cause of noise in wind turbines. In addition, they are the equipment that most require maintenance and replacement in a wind power system [2–4] and have a very short lifespan when compared to other elements of a wind

generation system [5,6]. On the other hand, conventional wind systems are connected to the electrical power system (EPS) through power electronic devices, which can contribute to the increase of voltage and current harmonic distortion at the point of common coupling (PCC) of the system AC, whose intensity needs to be limited [7]. In order to overcome these limitations, the line of research that deals with the EFR stand out, which is defined as a device consisting of an induction machine with adaptations [8]. Among the main objectives of the EFR are:

- Contribute to the reduction of mechanical impacts that shorten the useful life of the speed multiplier;
- Reduce disturbances in active and reactive power and harmonics caused by connecting electronic converters in the interconnection of wind turbines, photovoltaic systems, or other forms of generation with the electrical grid;
- Provide an alternative for the hybridization of renewable, intermittent energy sources, whose synergy, under adequate dimensioning, allows the generation of firm energy, regardless of the climatic conditions of each moment;
- Enable distributed generation systems from intermittent renewable sources, which can operate in isolation from the electricity grid, ensuring full service to demand with a high level concerning the quality of the energy supplied.

In recent years, some works related to the application and control of the EFR device have been proposed in the literature [8–14]. In order to increase the reliability and efficiency of the wind generation system, the replacement of the speed multiplied by the EFR was proposed in [8–10]. In these works, it was installed between the wind turbine and a synchronous generator connected to the electrical grid. In this case, the main objective was to ensure that the EFR's rotor shaft, which was mechanically coupled to the rotor shaft of the synchronous generator, had the necessary rotation speed so that the frequency of the voltage generated was compatible with the electrical grid frequency, regardless of the variation in wind speed. The EFR-based system presented a satisfactory performance for a small range of speeds. However, it did not obtain the same performance in more abrupt variations of the speed reference values. In addition, the system behavior for low values of armature speed, in which wind turbines are usually affected (6–20 rpm), was also not evaluated. In [11], a method was proposed to track the maximum wind power extraction point through the control structure associated with the EFR. In this work, unlike the applications found in the literature, the EFR device was used to drive a squirrel-cage induction generator connected to the electrical network. The system presented a satisfactory performance for large variations in wind speed. Furthermore, as the converter has no connection to the grid, this topology proved to be more effective at withstanding a severe short circuit at the induction generator terminals than a conventional doubly-fed induction generator (DFIG) topology. Subsequently, a power quality analysis applied to the wind generation topology discussed in [11] was proposed by [12]. The authors concluded that the high-frequency components of the voltage generated in an EFR-based system are naturally attenuated by the inertia inherent in the EFR-SCIG mechanical system, which results in an advantage compared to DFIG wind generation and permanent magnet synchronous generator (PMSG) topologies.

One application of EFR would be for low-power wind farms. As for the application in small/large systems, it is possible that in particular situations, the use of small systems may dispense with the speed multiplier. Large systems, due to the very high torque and low speed transmitted by the turbine and, on the other hand, the high speed and low torque required by the generator, make the speed multiplier essential; however, there exist operational and useful life advantages.

The control strategy adopted in the works mentioned above was based on a vector control technique that consists of two cascaded control loops, as discussed in [13]. In addition, the control framework employs standard PI-type controllers. However, the controller design was not presented in these works, making it difficult to adjust the control gains to achieve a desired dynamic response. Thus, a design methodology for a vector control

strategy applied to EFR was proposed in [14]. The system controllers were designed using the root locus method (RLM) and presented dynamic performance compatible with the desired transient response specifications. However, the controller's performance was not evaluated for parametric variation of the system. Thus, a system dynamic analysis considering variations in the EFR's parameters was proposed in [15]. The analysis based on transient and steady-state response specifications showed the varying influence of the EFR device parameters on its dynamic behavior. The authors concluded that large parametric variations could result in degradation in the transient response of the system controllers. Consequently, it is necessary to evaluate the dynamic behavior of the EFR operating with more robust control strategies with parametric variations and system disturbances.

2. System Description

Figure 1 presents the EFR-based system block diagram employed for conducting performance studies. In this configuration, a DC motor is responsible for emulating the kinect energy stored in turbine blades of a wind power system which is then transmitted through the low-speed shaft. DC motor is mechanically coupled to EFR's armature, and along this connection it is possible to access its armature phases by slip rings that is fed by means of a three-phase voltage source inverter (VSI) with L-filter. The EFR is the speed conversion stage main device and allows torque transmission to the synchronous generator that supplies energy to a three-phase resistive load.

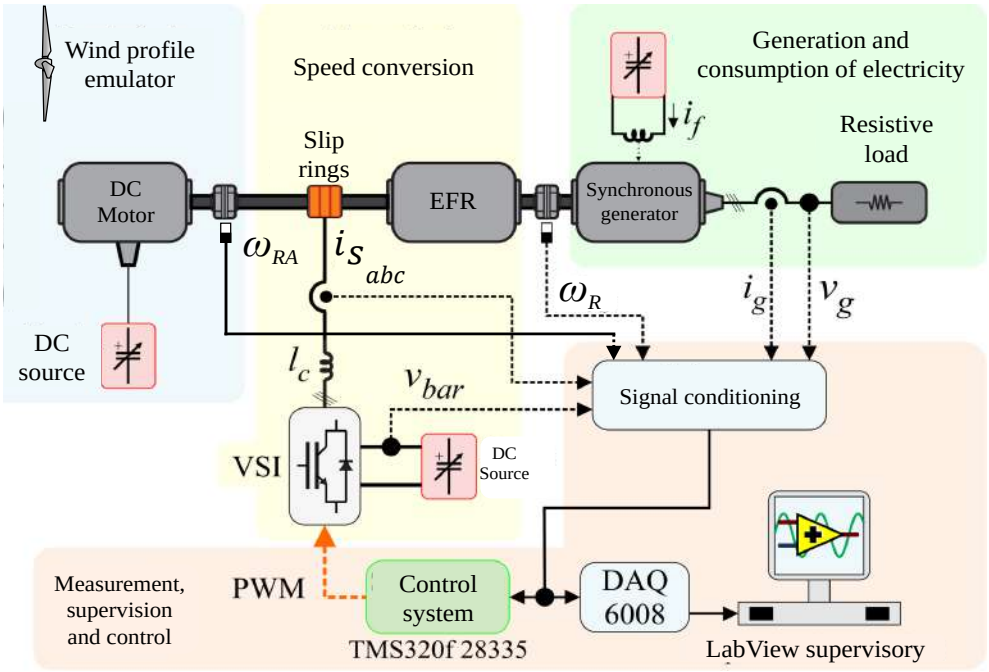

Figure 1. Block Diagram of EFR Based-Wind Power System.

The measurement, supervision and control stage deals with the main system variables such as DC-link voltage (v_{bar}), EFR's armature currents ($i_{S_{abc}}$), DC motor (ω_{RA}) and EFR's rotor speed (ω_R), and a single-phase voltage (v_g) and current (i_g) absorbed by the resistive load. These data are sent to a LabView supervisory through a digital acquisition device DAQ 6008 and to the control system that is performed by a Texas Instruments TMS320f28335 which runs the control strategy. In the Tables 1–3, we present the main specifications of the EFR Based system in Figure 1.

A summary of the most important system parameters is given in Tables 1–3.

Table 1. DC Motor Nominal Parameters.

Parameters	Value
Power	1.5 cv
Velocity	1800 rpm
Voltage	180 V
Current	6.0 A

Table 2. EFR Nominal Parameters.

Parameters	Value
Nominal Power	3.0 cv
Nominal Speed	3600 rpm
Number of poles	2
Voltage	180 V
Resistance of rotor and armature	2.3 and 2.8 Ohm
rotor and armature reactance	3.7 and 3.9 Ohm
Mutual Inductance	220 mH

Table 3. Synchronous Generator Nominal Parameters.

Paramaters	Value
Power	1.0 kW
Velocity	1800 rpm
Number of poles	4
Voltage	180 V
Resistance of rotor and armature	1.7 and 4.1 Ohm
Field Resistance and Reactance	1.1 and 2.8 Ohm
Mutual Inductance	300 mH

The EFR constructive aspect is depicted in Figure 2. The armature consists of a conventional induction machine stator with adaptations that enables its rotation by a prime mover, represented, in this work, by the DC motor rotor shaft. The electrical contact at coils of this rotor is carried out by means of slip rings, which allow injection and monitoring of the flowing currents through the EFR armature windings. The rotor consists of a squirrel-cage rotor and its rotation is the EFR's output speed, which in turn drives the synchronous-machine-rotor shaft. The junction and the support of the EFR's rotor with the synchronous generator rotor are carried out using a coupler and mechanical bearing, respectively. Thus, the rotor is responsible for maintaining the voltage and frequency stability of the power supplied to the resistive load. More information about EFR features are found in [9,10,15].

The armature is powered by a frequency inverter that produces currents that determine the speed of the rotating field, in relation to the fixed reference "F", presented in Figure 3 as $\overrightarrow{\omega^{F}_{f_A}}$, which, added to the turbine speed (ω_v) results in a rotor speed (ω_r), subtracting the value of the slip (S), following the vector of the rotating field of the synchronous rotor $\overrightarrow{\omega^{F}_{f_R}}$, in the value of the desired synchronous speed in the generator shaft. If the wind speed is equal to zero, the diagram resembles the operation of a conventional induction machine in [10].

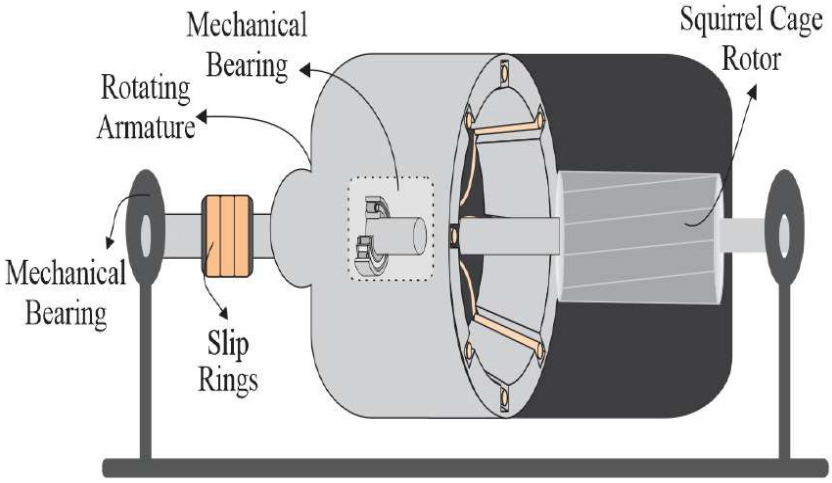

Figure 2. Constructive Aspect of the EFR.

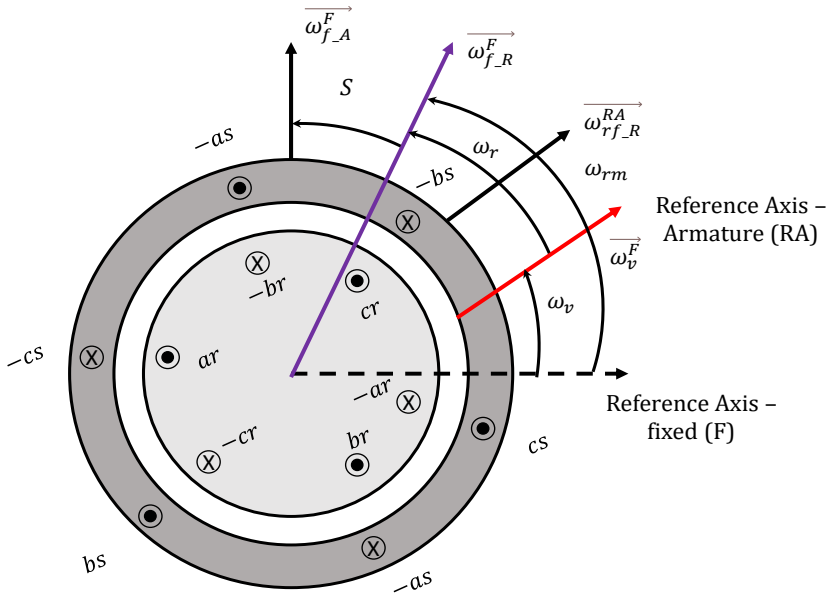

Figure 3. Schematic diagram illustrating the fixed fields in the synchronous and asynchronous rotors and velocities involved.

When adding the turbine speed (ω_v) to the fixed reference axis (F), the armature is displaced, resulting in a new reference axis (RA), rotating at the same speed as the turbine. The vector of the rotating field velocity of the currents injected by the inverter concerning the axis of the asynchronous rotor is called $\overrightarrow{\omega^{RA}_{rf_RA}}$, also illustrated in Figure 3. Although the reference system between the armature and the rotor remains equivalent to that of a conventional induction machine, the relative positioning between the rotor and the fixed reference axis becomes different as the armature undergoes a vector displacement called $\overrightarrow{\omega^{f}_{v}}$. In this way, it can be observed that the stationary fields between the armature and the rotor are maintained, which is an essential condition for maintaining the electromagnetic torque that moves the synchronous rotor. Analyzing Equation (1), it can be seen that, for zero wind speed, there is the traditional reference system, with the field vector of the asynchronous rotor rotating with speed equal to the vector of the rotating field of the

currents injected into it. Thus, the field speed of the asynchronous rotor is equal to the speed of the synchronous rotor.

$$\overrightarrow{\omega_{f_R}^{F}} = \overrightarrow{\omega_{rf_R}^{RA}} + \overrightarrow{\omega_{v}^{f}} \quad (1)$$

3. Efr Modeling and Simulation

In this Section 3 the EFR's model is described, as is a simulation by numerical computation software for later validation.

3.1. Efr'S Dynamic Model

The dynamic model of the EFR device is based on the model of a squirrel-cage rotor induction machine given by:

$$v_{sd} = R_s i_{sd} + \frac{d\lambda_{sd}}{dt} - \omega_s \lambda_q \quad (2)$$

$$v_{sq} = R_s i_{sq} + \frac{d\lambda_{sq}}{dt} - \omega_s \lambda_d \quad (3)$$

$$\lambda_{sd} = L_s i_{sd} + L_m i_{rd} \quad (4)$$

$$\lambda_{sq} = L_s i_{sq} + L_m i_{rq} \quad (5)$$

$$v_{rd} = R_r i_{rd} + \frac{d\lambda_{rd}}{dt} - (\omega_s - \omega_r)\lambda_{rq} \quad (6)$$

$$v_{rq} = R_r i_{rq} + \frac{d\lambda_{rq}}{dt} - (\omega_s - \omega_r)\lambda_{rd} \quad (7)$$

$$\lambda_{rd} = L_r i_{rd} + L_m i_{sd} \quad (8)$$

$$\lambda_{rq} = L_r i_{rq} + L_m i_{sq} \quad (9)$$

The electromagnetic torque is the variable that works as the connecting link between the electrical and mechanical system of the EFR and can be described by the Equation (10). In this Equation (10) can be seen that if i_{sd} is kept at zero, the entire electromagnetic torque can only be obtained by regulating i_{sq}.

$$T_{EFR} = p_{efr}(\lambda_{sd} \cdot i_{sq} - \lambda_{sq} \cdot i_{sd}) \quad (10)$$

The Equation (11) describes the EFR's mechanical behavior, with J_m, F_m, T_m, ω_r being the moment of inertia of the entire mass connected to the rotor, the friction coefficient of the rotor, the resistant torque of the load coupled to the motor shaft and the angular speed of the rotor.

$$J_m \frac{d\omega_r}{dt} = T_{EFR} - T_m - F_m \omega_r \quad (11)$$

From the prototype constructive aspect with the EFR, it is known that the armature is free to rotate favorably to the movement of the mechanical driving force emulated by the DC motor. Thus, this movement also has a mechanical behavior, as shown in Equation (12).

$$J_a \frac{d\omega_{ra}}{dt} = T_v - T_{EFR} - F_a \omega_{ra} \quad (12)$$

where J_a, F_a, T_v, ω_{ra} represent the inertia moment in the entire connected mass to the armature, the friction coefficient of armature, conjugate imposed by the wind emulation, and the angular velocity of armature. The Equations (11) and (12) demonstrate that T_{EFR} performs as the intermediate between the speeds of rotor and armature.

3.2. Model Simulation Validation

For validation through simulation, the Simulink/Matlab software is used. Initially, the induction machine model is implemented traditionally by the Equations (2) to (11). However, incorporating the mechanical behavior of the armature into the model generates an alteration that deserves to be mentioned. The synchronous speed depends only on the frequency of the voltages applied to the machine armature. Thus, the armature angular speed perturbs this variable, increasing or decreasing the rotor's liquid field. So, for this effect to be perceived by the rotor, the block diagram, illustrated in Figure 4, is inserted in the induction machine model code. Another change concerns the Equations (2), (3), (6) and (7), which instead of receiving ω_s directly, now get ω_{sa} on input of its blocks, which represents the angular speed resulting from the sum of ω_{ra} and ω_s.

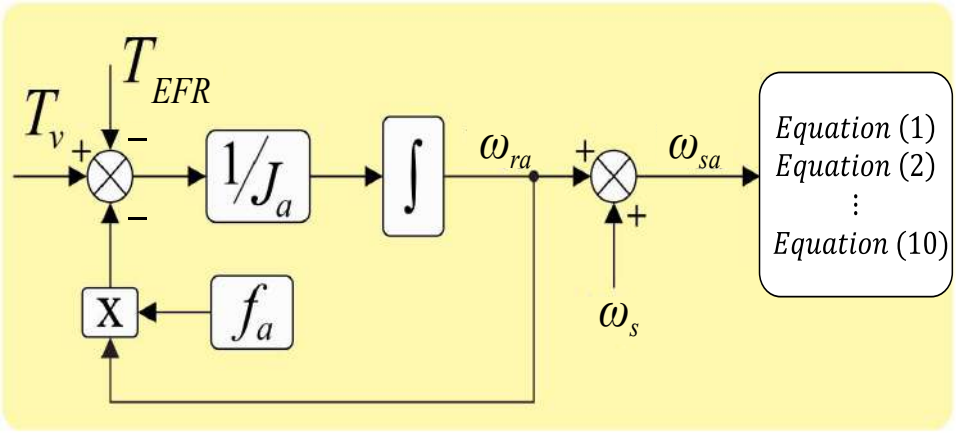

Figure 4. Block diagram of armature speed influence.

Thus, in order to approximate the simulation to the real scenario with the EFR, an induction machine with the same rated power as the EFR and with similar dimensions is used. The main simulation specifications are summarized in Table 4.

Table 4. Specifications for the simulation of the EFR elementary model.

Parameter	Value
Poles number (P_{efr})	2
Rotor resistance (R_r)	6 Ω
Armature resistance (R_s)	6 Ω
Armature inductance (L_s)	30 mH
Rotor inductance (L_r)	30 mH
Mutual coupling inductance (L_m)	500 mH
Nominal Power (P)	2.0 kW
Nominal Voltage (V_L)	380 V
Nominal Current (I_f)	2.8 A
Nominal frequency	60 Hz
Nominal Velocity	1740 rpm
Inertia Moment (Rotor+Generator) (J_m)	0.02 kg·m
Inertia Moment (Armature+Turbine) (J_a)	0.978 kg·m
Friction coefficient (Rotor+Generator) (F_m)	0.003 N·m/rad·s
Friction coefficient (Rotor+Turbine) (F_a)	9.0 N·m/rad·s

The test for the elementary model validation consists of a direct start of the machine for an analysis period of 5 s, and the results is shown in Figure 5. There is no velocity regulation in this simulated scenario. The rotor speed reaches the nominal value after 0.7 s has elapsed, as illustrated in Figure 5a, while no torque value T_v is imposed on the model, as shown in to Figure 5b. Under these conditions, the EFR's model behaves like

a traditional induction motor, with armature inrush currents that reach almost five times the rated current value and with reduced rotor currents for the nominal slip at no load, as shown in Figure 5c,d.

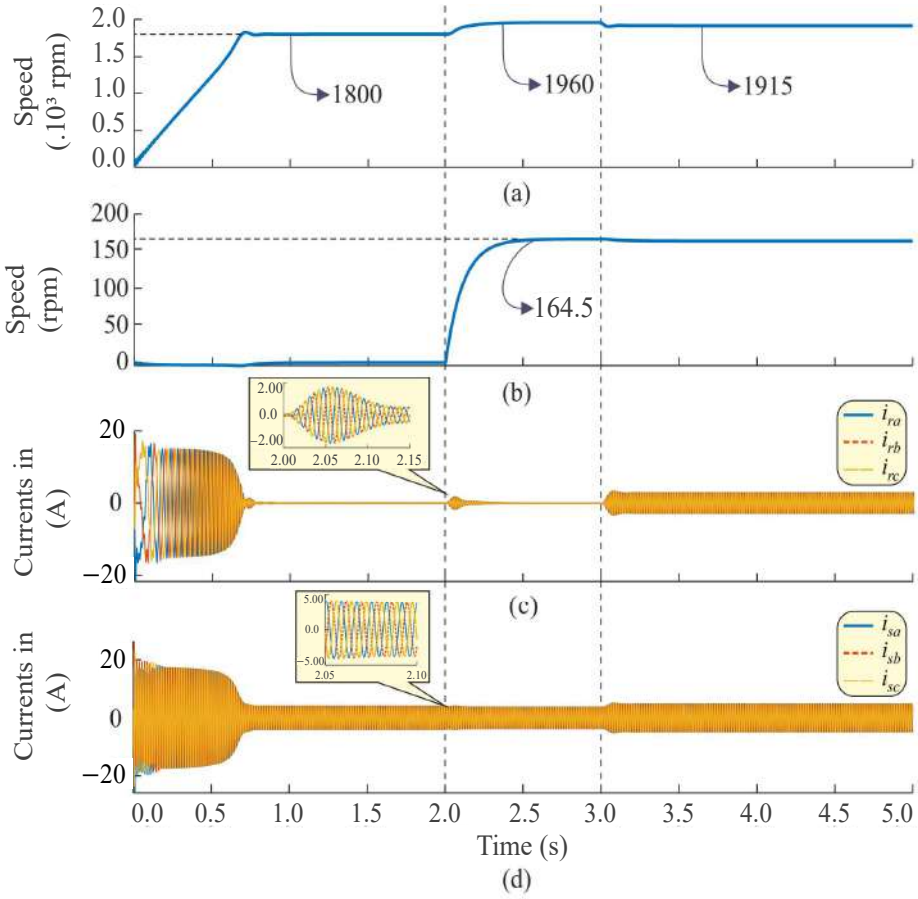

Figure 5. Simulation analysis for the EFR elementary model of EFR (**a**) Rotor speed, (**b**) Armature speed, (**c**) Rotor currents, (**d**) Armature currents.

After 2.0 s, the wind emulator starts with a torque T_v equivalent to 300 N. Under these conditions, the resulting armature speed reaches 164.5 rpm. This velocity is transferred to the rotor motion, even with the main frequency maintained at 60 Hz. Another interesting outcome is the effective reduction in current consumed by the armature from 2.819 A to 2.653 A, as illustrated in Figure 5d. Meanwhile, the rotor suffers from the synchronous speed increase and the speed of the armature, as the amplitude of the current signals of rotor. Here, it is possible to manage the system's power flow with EFR. As of 3.0 s, a constant torque load equivalent to 5 N·m is entered in the rotor. With this disturbance in the system, it is possible to see that the model remains functional, as it manages to overcome the resistant conjugate with the increase of currents from rotor and armature. There is also a reduction in rotor speed at 45 rpm, which causes an increase in the EFR's slip.

4. Control Strategy

In section is presented aspects related to the EFR-based system control, together with the detailing of the main contribution to speed regulation.

4.1. Rotor Flux Oriented Control (Foc)

The control strategy initially proposed by [9] consists of an adaptation of the FOC and is illustrated in Figure 6. The estimation of the rotor flux is important to obtain the rotor angle (ρ) that is necessary for the decoupling of the variables that influence the rotor flux (i_{sd}) and also the conjugate (i_{sq}). From these variables, current controllers R_{id}(s) and

R_{iq}(s) were used, which initially employ PI-type controllers. These controllers determine the reference voltages ($v^*_{f\,abc}$) that should be applied to the VSI via PWM modulation.

With the measurement of mechanical velocity (ω), it is possible to elaborate a control loop responsible for determining the reference torque from the quadrature-axis current ($i^*_{sq_{efr}}$), which is necessary for the system energy balance, which is guaranteed using a speed regulator (R_ω) of the PI controller. Due to its direct relationship with the quadrature-axis current, as already determined by [13], the reference current ($i^*_{sq_{efr}}$) plays an important role in the transmission of energy by the EFR through the conjugate (T_{EFR}) see in Equation (10).

It is necessary to adopt a suitable rotor flux for system operation without considerable vibrations and minimal heating losses. This flux regulation is performed by a PI controller R_ϕ(s) that acts on the direct-axis current ($i^*_{sd\,efr}$). The dimensioning of controller gains used for the conventional regulation follows the procedures proposed in [13].

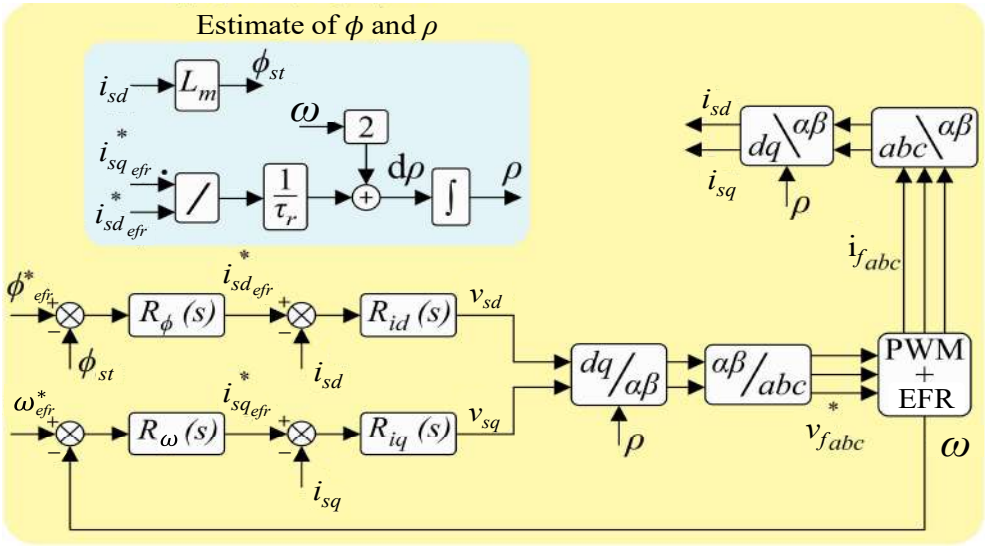

Figure 6. Rotor-flux-oriented control with conventional speed regulation.

4.2. Fuzzy Control Implementation

An essential contribution of this article is the regulation of speed and torque through a Sugeno model Fuzzy-PI controller replacing the PI controller, adopted by [9]. The schematic diagram of the proposed fuzzy speed control is illustrated in Figure 7. A fuzzy controller requires knowledge of the error signal and also the error variation to determine the control signal, which must be integrated to represent the reference stream ($i^*_{sq_{efr}}$).

The gains tuning associated with the fuzzy controller was performed according to the procedures available in the works of [16,17]. This controller considered three triangular membership functions for the error signal with the following linguistic variables: Negative Error—EN; Zero Error—EZ; Positive Error—EP. In Figure 8, the literal intervals of relevance function to the speed error as a function of its respective universe of discourse. In the figure on screen, the axis that represents the discourse universe is not on a linear scale. For the error derivative, were used three triangular membership functions with the following nomenclatures: Negative Derivative—DN; Derivative Zero—DZ; and Positive Derivative—DP, because in the analysis of the derivative, it is only necessary to evaluate if it increases, remains constant or decreases and, with that, know if the signal is moving away from or approaching the reference. Figure 9 illustrates the ranges of membership functions for the derivative of the velocity error. Once again, the axis that represents the discourse universe is not on a linear scale.

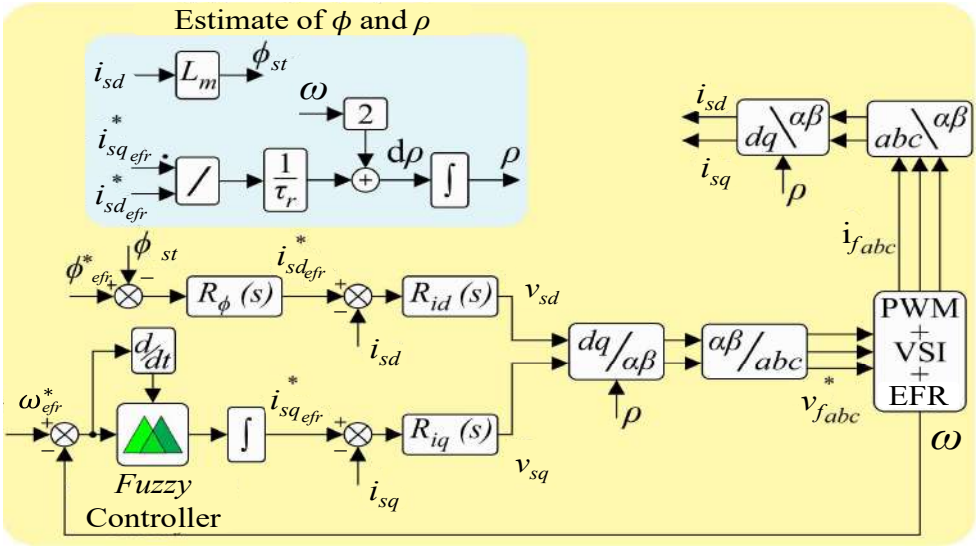

Figure 7. Rotor-flux-oriented control with fuzzy speed regulation.

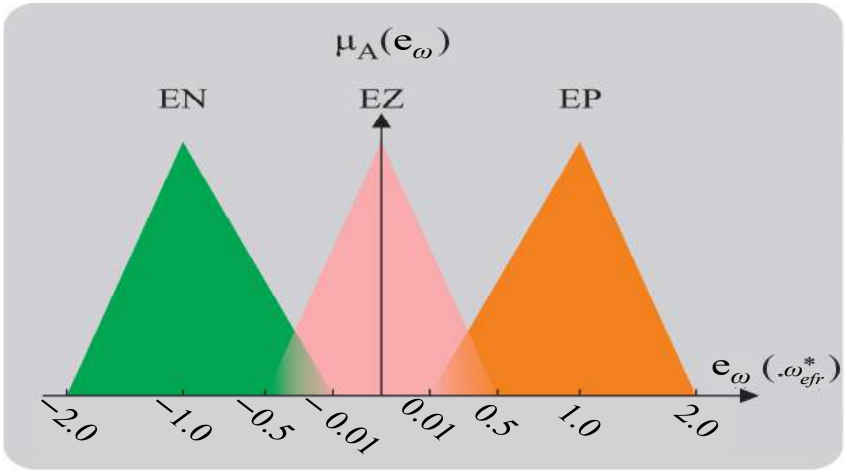

Figure 8. Membership functions associated with the speed error signal.

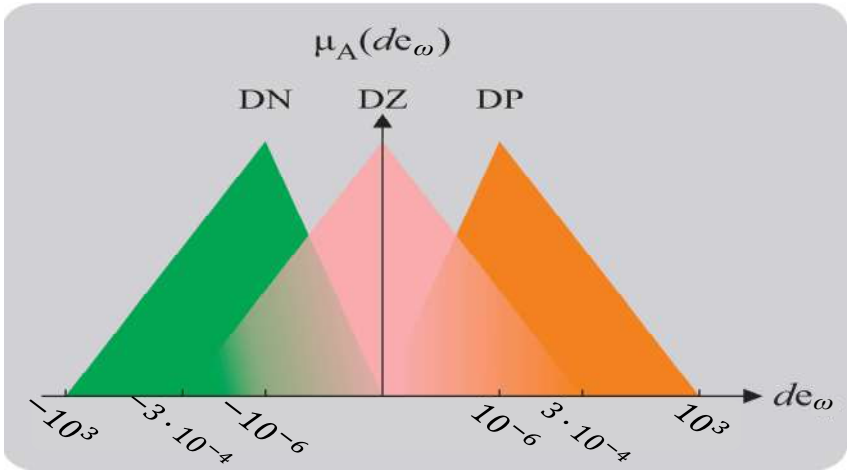

Figure 9. Membership functions associated with the sign of the speed error derivative.

The range used for error signals depends on the imposed reference value to speed control and may consider the possibility of the EFRs operating in both rotation directions with nominal values. As for the error variation of velocity, the polarity of the variation

measured by the acquisition system was considered data. Based on this organization, the ranges of membership functions are summarized in the Table 5.

Table 5. Parameters of Membership Functions e_w and de_w.

FP	Parameter	Value	Parameter	Value	Parameter	Value
EN	a_1	$-2\omega^*_{efr}$	b_1	$-\omega^*_{efr}$	c_1	$-0.01\omega^*_{efr}$
EP	a_2	$-0.01\omega^*_{efr}$	b_2	ω^*_{efr}	c_2	$2\omega^*_{efr}$
EZ	a_3	$-0.5\omega^*_{efr}$	b_3	0.0	c_3	$0.5\omega^*_{efr}$
DN	a_4	-1000	b_4	-0.00001	c_4	0.0
DP	a_5	0.0	b_5	0.00001	c_5	1000
DZ	a_6	-0.0003	b_6	0.0	c_6	0.0003

After implementing the controller inputs, it was necessary to design the functions output suggestion for each of the angles, as illustrated in the Table 6. The rules of inference implemented follow the Equation (13), with $n = 1, 2, \ldots, 9$:

$$S_n = K_{pn} \cdot de_w + K_{in} \cdot e_w + H_0 \tag{13}$$

where H_0 is a homopolar component that can be inserted into the control to compensate for offset values, with $H_0 = 0$. Thus, the rules of inference implemented follow the Equation (14), with $n = 1, 2, \ldots, 9$:

$$S_n = K_{pn} \cdot de_\omega + K_{in} \cdot e_\omega \tag{14}$$

Based on Table 5 and the Equation (13) were obtained $S_1, S_2, S_3, S_4, S_5, S_6, S_7, S_8$ and S_9 described in the Table 6. Thus, the fuzzification process is represented by the two inputs (e_w and de_w) and respective rules and the defuzzification process is represented by the output with the values obtained in $S_1, S_2, S_3, S_4, S_5, S_6, S_7, S_8$ and S_9.

Table 6. Fuzzy rules framework for EFR speed regulation.

de_ω \ e_ω	EN	EZ	EP
DN	S_1	S_2	S_3
DZ	S_4	S_5	S_6
DP	S_7	S_8	S_9

In this Section 4, the control characteristics of the generation prototype of wind energy developed in laboratory elucidate the application of the fuzzy controller in the system speed regulation. In addition, the tuning procedure was described in the above-mentioned controller.

5. Experimental Results

The EFR-based system prototype evaluation using the control strategies described in the section is based on the transient and steady-state performance analysis for different operating scenarios. In this section, the details of the tests carried out are described. In addition, the experimental results for each oprational scenario are discussed and a comparative analysis between employed control strategies is presented.

5.1. Description of Operation Scenarios

In this work, the operating scenarios are characterized by synchronous generator mode traction, which can be both no-load and loaded. Both discuss the main differences in performance based on the control strategy adopted. In the first scenario, the generator electrical terminals are disconnected from any element that consumes electrical energy and, therefore, there is no relevant value of current or power electrical system that requires

evaluation. In this scenario, power is expressive only during start-up, as the drive system must overcome the inertia of an equivalent mass to the sum of the EFR's rotor and the synchronous generator rotor individual masses. In the EFR's rotor and the synchronous generator rotor individual masses scenario, two resistors are connected in parallel to each phase of the synchronous generator so that the power to be consumed can exceed 200 W per phase, depending on the field winding excitation circuit. In addition, the equivalent mass of the rotating parts together with the resistive load connected to the synchronous generator terminals gives rise to a counter-conjugate, proportional to the excitation current I_f in the synchronous generator rotor shaft, which must be compensated for by the EFR's drive system. For this study, the load is kept constant throughout all scenarios operating under load.

The set of technical specifications for the operating conditions of the EFR-based system prototype analyzed in this EFR-based system is summarized in Table 7.

Table 7. Technical specifications for the operating scenarios.

Parameter	Value
DC motor power range	$v_{cc} = 0$–50 V, $i_{cc} = 0$–6 A
VSI DC bus voltage	$v_{bar} = 100$ V
DC-link capacitors	$C = 4700$ µF
Filter inductors L	$l_c = 500$ µF
EFR magnetizing inductance	$l_m = 0.22$ H
Voltage in the generator field winding	$v_f = 0$–7.0 V
Current in the generator field winding	$i_f = 0$–4.5 A
DAQ—electrical signal sampling	1 kHz
DAQ—mechanical velocity signal sampling	5 Hz
Resistive load per phase	$P_r = 200$ ohms per phase

5.2. Empty Synchronous Generator Traction

5.2.1. Open-Loop Speed Regulation

The open-loop system dynamic performance is presented in Figure 10. Initially, a reference voltage with a frequency equal to 15 Hz is imposed on the EFR's armature terminals causing its rotor to reach a speed of approximately 932 rpm at t = 4 s as shown in Figure 10a. At instant τ_1, the synchronous generator field circuit is supplied with v_f = 7.0 V and i_f = 4.5 A, which results in rms empty voltages equal to 105 V per phase, as illustrated in Figure 10b. In this case, since the synchronous generator has 4 poles, the empty voltages frequency is equal to approximately 31 Hz, which represents half of its nominal value. Due to the counter-conjugate generated after powering the generator field winding, EFR's rotor speed is subjected to a small deceleration, as illustrated in Figure 10a. At the instant τ_2, the DC motor is gradually activated to reach a speed equal to 310.4 rpm. This speed is imposed on the EFR's armature mass as illustrated in Figure 10c, which results in the EFR's rotor speed increasing to 1224 rpm.

After stabilizing the armature speed at a value close to 30% of rotor speed, the voltages available at the synchronous generator terminals have a value effective and electrical frequency equivalent to 138 V and 40.8 Hz, respectively, which represent an increase of 21% and 31.6%, respectively, with the initial performance. Thus, the increase in rotor speed is proportional to the speed imposed on the armature mass. This essay describes the operation principle of the EFR device, since the amplitude and frequency of the generated voltage depend both on the voltage at the armature terminals and on the rotation speed of the armature mass. However, due to the amplitude and frequency variation of the voltage at the synchronous generator output terminals, the operation of the EFR-based system in open-loop is not feasible in practice, since the electrical loads connected to the generator as well as the power grid, requires a voltage with constant amplitude and frequency.

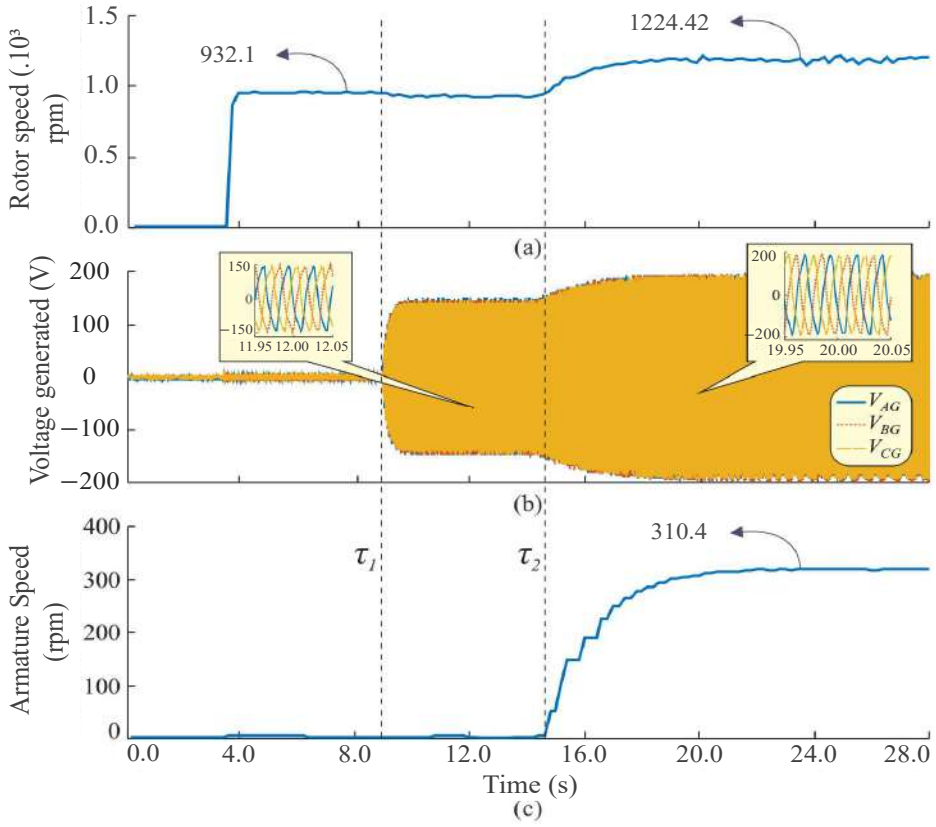

Figure 10. Open-loop speed gain analysis with illustration of the performance of the (**a**) rotor speed, (**b**) the generator output voltages and (**c**) armature speed.

5.2.2. Speed Regulation by Foc Control

The amplitude and frequency stability of the synchronous generator output voltage is only possible by regulating the EFR's rotor speed. For this purpose, rotor-flux-oriented control is performed as discussed in the Section 4. The controller gains employed in the current, flux and speed control loops are summarized in Tables 8–10 respectively. The criteria adopted for generator traction at no load were a settling time (T_s 2%) less than or equal to 15 s and a percent overshoot (μ_p) less than or equal to 5%. The dimensioning of the controller gains goes through a process of fine-tuning to compensate the nonlinearities and non-modeled dynamic of the system.

Table 8. Current regulator parameters in the synchronous reference $R_{idq}(s)$.

Parameters $R_{idq}(s)$			
$k_{p_{id}}$	25.0	$k_{p_{iq}}$	60.0
$k_{i_{id}}$	20.0	$k_{i_{iq}}$	25.0

Table 9. Rotor flux regulator parameters $R_\phi(s)$.

Parameters $R_\phi(s)$	
ϕ^*_{efr}	0.8 W_b
k_{p_ϕ}	3.0
k_{i_ϕ}	3.5

Table 10. Speed regulation parameters $R_\omega(s)$.

Parameters $R_\omega(s)$	
ω^*_{efr}	1800 rpm
k_{p_ω}	1.3
k_{i_ω}	2.0

Figure 11 shows the rotor-flux-oriented control based speed regulation dynamic performance. According to Figure 11a, a 1800 rpm step-type reference signal results to a speed controller transient response with settling time and percent overshoot approximately equal to 23 s and 7.53%, respectively, which corresponds to a peak value approximately equal to 1935.5 rpm. On the other hand, steady-state error is equal to 0.078%, which can be considered null. Therefore, despite the rotor speed accurately tracking its reference value, the transient response does not match the desired performance criteria. This can be explained by the PI controller negative phase contribution characteristic, which tends to degrade the system transient response. The speed controller transient performance is reflected in the dynamic behavior of voltages at the synchronous generator output terminals, as shown in Figure 11b, which can damage the electrical loads connected to the generator. Figure 11c shows a DC motor speed variation that drives the EFR's armature. For the evaluated period, two speed profiles with 400 and 800 rpm are imposed on the armature. The rotor-flux-oriented control based speed regulation keeps the EFR's rotor speed constant during armature speed variations, which contributes to steady-state stability of the synchronous generator output voltage.

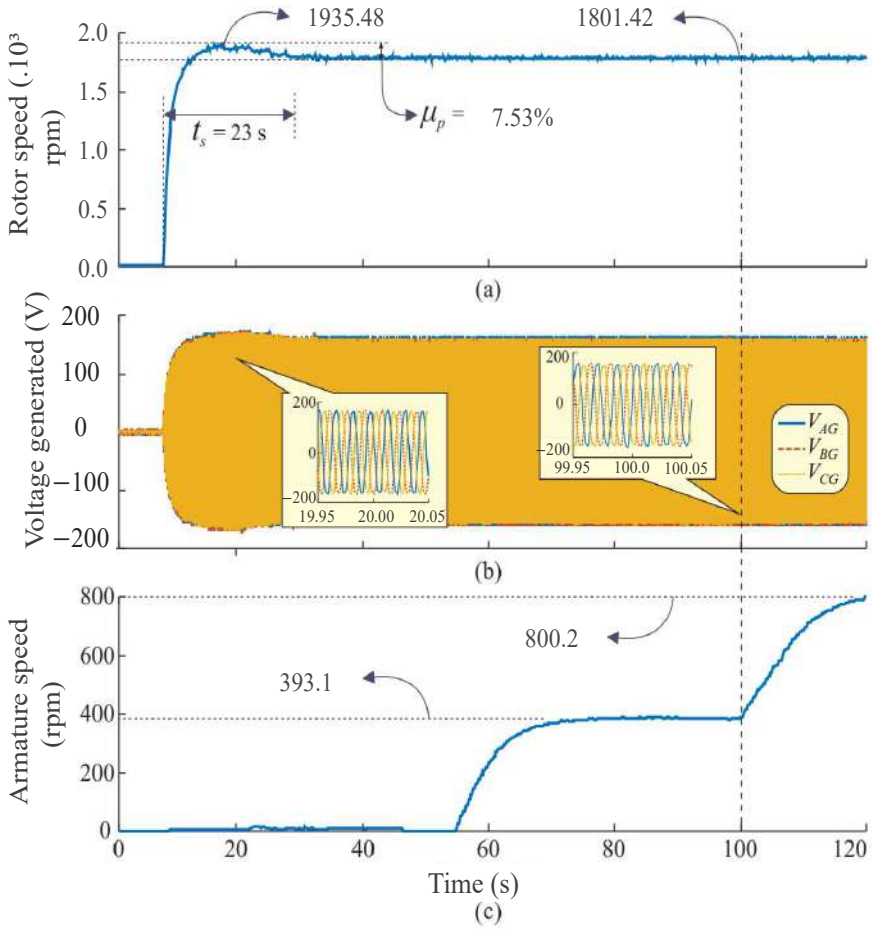

Figure 11. Rotor-flux-oriented control based speed regulation dynamic performance (**a**) rotor speed, (**b**) the generator output voltages, (**c**) speed armature.

5.2.3. Speed Regulation by Fuzzy Control

The experimental validation of the Fuzzy controller dynamic performance is performed using a test similar to the applied to rotor-flux-oriented control.The desired performance criteria are also the same, that is, $\mu_p \leq 5\%$ and $T_s 2\% \leq 15$ s. In this experiment, the field circuit of the synchronous generator is fed with v_f = 5.9 V and i_f = 3.6 A. The gains associated with the inference rules defined in (14) are summarized in the Table 11, with $H_0 = 0$. Although tuning the fuzzy controller need not take taking into account specific parameters of the system model, the speed controller gains employed in the rotor-flux-oriented control based speed regulation were used as a starting point for the adjustment of the fuzzy controller gains. After some initial tests, it was empirically found that much smaller gains than those employed in the rotor flow-oriented control strategy were sufficient to achieve the desired dynamic performance. Therefore, the tuning of the fuzzy controller was performed with these smaller gains listed in Table 11.

Figure 12 shows the fuzzy control based speed regulation dynamic performance. According to Figure 12a, for the same speed step of 1800 rpm, the speed control transient response presents settling time approximately equal to 4 s, which meets the desired performance criterion. Contrary to what is expected for a reduction of ts with speed regulation based on a PI controller, the transient response of the speed regulation using the fuzzy controller does not present a percent overshoot and stabilizes at an average value of 1794.2 rpm, which results in a negligible steady-state error of 0.32%. The absence of percent overshoot in the fuzzy based rotor speed control makes the EFR start-up smooth, which contributes to synchronous generator terminal voltages without any level of transient over voltage, as shown in Figure 12b. Furthermore, according to Figure 12a, the Fuzzy controller was able to keep the rotor speed constant during EFR's armature speed variations illustrated in Figure 12c.

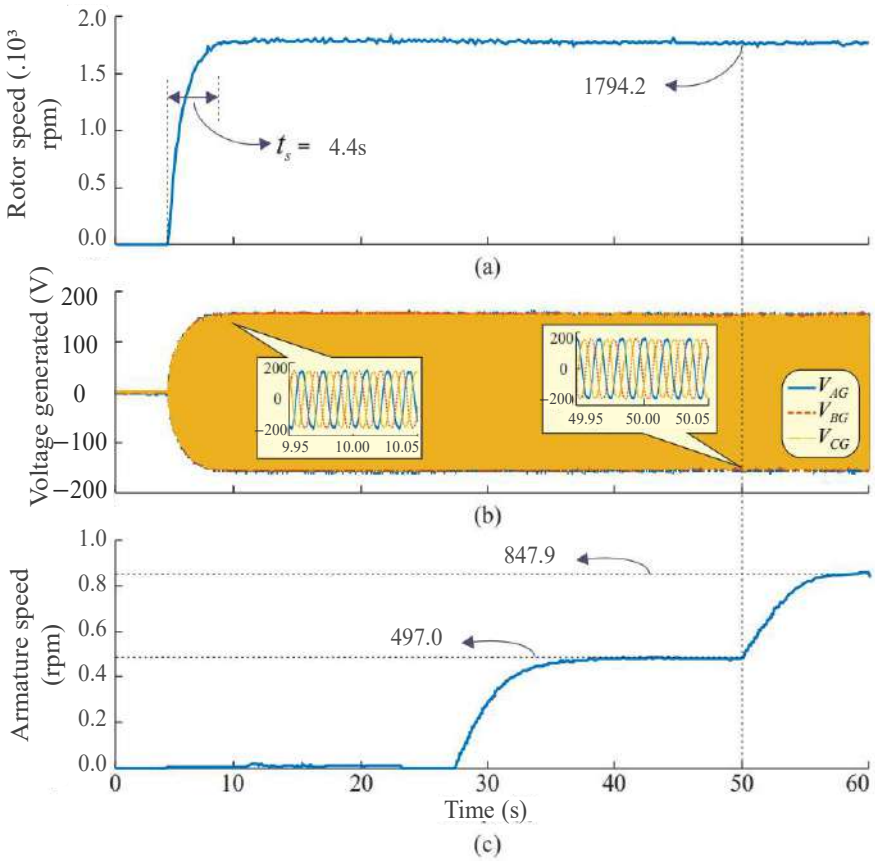

Figure 12. Analysis of speed gain by Fuzzy regulation with illustration performance of (**a**) rotor speed, (**b**) the generator output voltages and (**c**) armature speed.

Table 11. Fuzzy controller gains after empirical adequacy.

$K_{p_{1,2,3}}$	0.2	$K_{p_{4,5,6}}$	0.7	K_{p_7}	2.5	K_{p_8}	2.9	K_{p_9}	2.5
$K_{i_{1,2,3}}$	0.5	$K_{i_{4,5,6}}$	1.1	K_{i_7}	8.0	K_{i_8}	12.5	K_{i_9}	4.0

5.2.4. Performance Indices

According to [18], the performance index is a measure quantitative performance of the system and chosen in such a way that it emphasizes specifications system important. In [18] propose the use of the performance index is the integral absolute error *IAE*, Integral of the Absolute magnitude of the Error), which is defined by:

$$IAE = \int_0^T |e(t)|dt \tag{15}$$

To avoid the influence of a large input error signal during systems with a step reference. In [18] propose the use of the index of the integral time multiplied by absolute error (*ITAE*) defined by:

$$ITAE = \int_0^T t|e(t)|dt \tag{16}$$

The *ITAE* provides better selectivity of performance indices, as the value minimum of the integral is easily distinguished while the system parameters are changed.

5.2.5. Comparison of Control Strategies through Performance Indicators

For the graphical analysis and the analysis of transient regime parameters, the indices controller performance are evaluated in accordance with Equations (15) and (16) in Section 5.2.4. The indices values calculated in the synchronous generator traction empty scenario, with both closed-loop control strategies, are summarized in Table 12.

Table 12. Comparison of performance indicators for control strategies.

Indicator	Conventional	Fuzzy	Reduction (%)
IAE	9.5084×10^4	5.8363×10^4	38.60
ITAE	7.4050×10^5	4.2112×10^5	43.13

According to Table 12, the conventional speed regulation obtained higher values for the accumulated error and for the error in relation to the time when compared to fuzzy regulation indices. The absence of overshoot, together with the reduced T_s due to fuzzy control, causes a reduction average of 43.13% of the performance indicators in relation to the conventional control.

5.3. Synchronous Generator Traction under Load

For evaluating the power flow of the power generation prototype based on the EFR, the two closed-loop control strategies are used for the traction of the synchronous generator when it supplies constant power to the resistive load of 200 W per phase. Under these conditions, the field circuit of the synchronous generator is driven with v_f = 3.15 V and i_f = 1.79 A. The operating point chosen for the analysis had to change. Based on a test build, the operating speed of the synchronous generator has been reduced to 1200 rpm. Furthermore, for the purposes of this analysis, only the steady-state will be considered for the following calculations. In these operating scenarios, the influences of the armature speed variation through driving force were emulated by the DC motor.

5.3.1. Velocity Regulation by Foc Control

For the evaluation of the electrical power transfer performance of the prototype with conventional rotor speed regulation, a test of 280 s is illustrated in Figure 13. The controller gains are the same as used in Section 5.2.2. The armature speed variation is performed in

four distinct sectors identified by A, B, C and D, with values of 300, 580, 860 and 1080 rpm, respectively, and can be observed in Figure 13a. A detailed exploration of sector A is carried out based on the Figure 13b–g. The voltages and electrical currents supplied by the VSI to the EFR can be observed in Figure 13b,c, respectively. The profile of voltages and currents supplied by the synchronous generator to the resistive load can be analyzed in Figure 13d,e, respectively. Again, with operation at a speed value far from the rated value, the maximum voltages generated are also lower than expected for the rated performance of the synchronous generator, with maximum values, on average, of 100 V per phase. With the objective of mitigating the influences of oscillations arising from the speed variation imposed on the armature, the evaluation of the power flow is carried out in a period of 10 s, as illustrated in Figure 13f. In this figure, there are the active power curves involved in the system elements. Throughout the analysis, it is possible to observe an average power of approximately 1.0 kW consumed by the EFR, from 600 W by the resistive load, while the DC motor provides something over 300 W to armature. It is worth noting that the active power consumed by the EFR is measured at the output of the three-phase VSI and therefore does not represent the mechanical power available at the tip of the rotor axis. For power flow assessment, the two driving forces emulated by the DC motor and the VSI that powers the EFR are considered positive power flow. On the other hand, resistive load consumption is defined as a negative power flow in the energy balance equation.

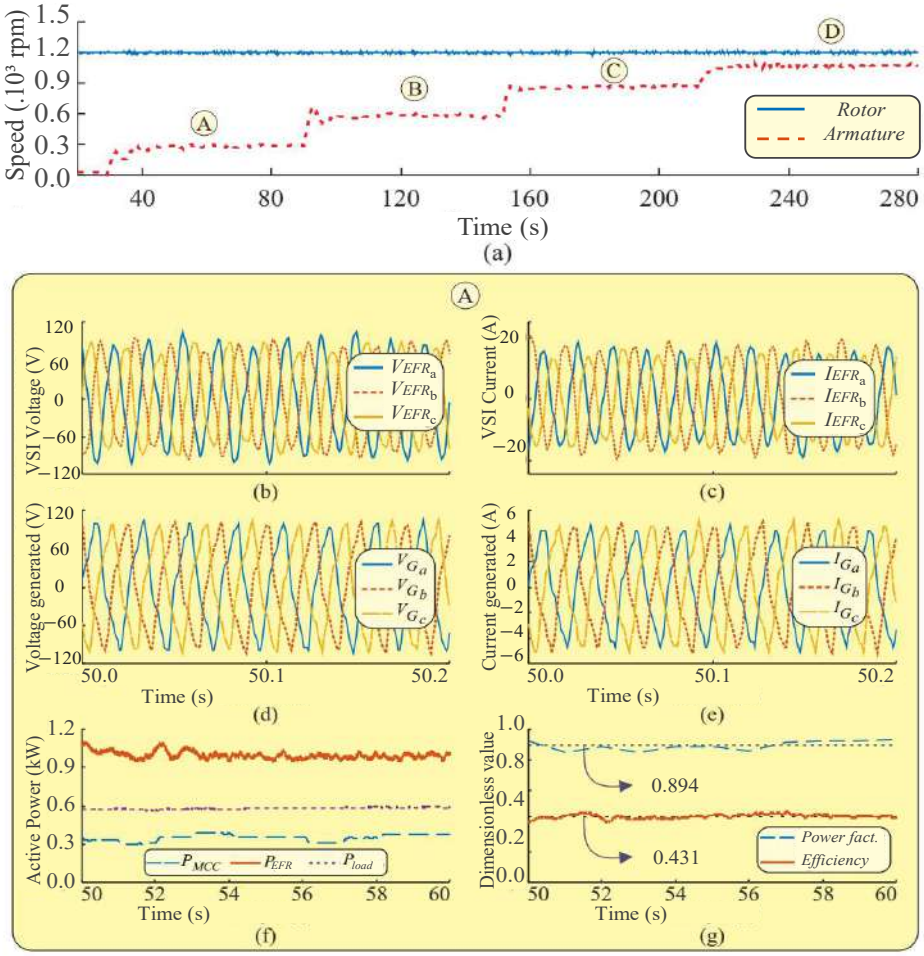

Figure 13. Power flow analysis with conventional speed regulation with illustration of (**a**) rotor and armature profiles, (**b**) voltages and (**c**) currents consumed by EFR, (**d**) voltages, (**e**) currents consumed by the resistive load, (**f**) electrical power of the devices and (**g**) EFR power factor and prototype global efficiency.

System efficiency is estimated based on the percentage of available power at the system's output in relation to the amount of input power and is illustrated in Figure 13f with the EFR power factor in the same period considered for Figure 13g. The system efficiency reaches an average value of 43.1% in the evaluated period, while the power factor reaches a value of 0.894 inductive. Therefore, the existence of a factor more powerless than unity occurs due to the EFR synchronous field maintenance.

5.3.2. Power Flow Analysis with Fuzzy Speed Regulation

For the evaluation of the electrical power transfer performance of the prototype with rotor speed Fuzzy regulation, a slightly shorter test is analyzed, totalling 120 s, and is illustrated in Figure 14. The associated gains of the Fuzzy controller are the same as those used in the Section 5.2.3, and the generator excitation circuit synchronous remains unchanged. For this test, the armature speed variation follows the same sectoral profile defined previously and can be seen in Figure 14a, with a specific detail of sector A that is illustrated in the Figure 14b–g. The voltages and electrical currents supplied by the VSI to the EFR can be observed in the Figure 14b,c, respectively. Due to the constructive aspects of the EFR, an average RMS value per voltage phase and current of 58.0 V and 13.0 A were reported, respectively, which are very similar values to those obtained for conventional speed regulation. The profile of voltages and currents supplied by the synchronous generator to the resistive load can be analyzed in Figure 14d,e, respectively. For the operation of EFR's rotor with a speed value lower than the rated value, the maximum voltages generated are also lower than expected for the nominal performance of the synchronous generator, with maximum values, on average, of 99 V per phase. With the objective of mitigating the influences of oscillations arising from the speed variation imposed on the armature, the evaluation of the power flow is carried out in a period of consecutive 5 s, as illustrated in Figure 14f. Over the evaluation time, it is possible to observe an average power slightly less than 1.0 kW consumed by the EFR, of 600 W by the resistive load, while the DC motor provides, on average, 330 W to the armature. The efficiency of the system is illustrated in Figure 14g together with the power factor of the EFR in the same period considered for the analysis of the individual powers of Figure 14f.

The system efficiency reaches an average value of 44.0% in the evaluated period, while the power factor reaches the value of 0.877 inductive. Thus, there is an increase in 0.9% concerning the average efficiency obtained by conventional speed regulation and a reduction in the magnitude of the power factor, still inductive, by 0.017.

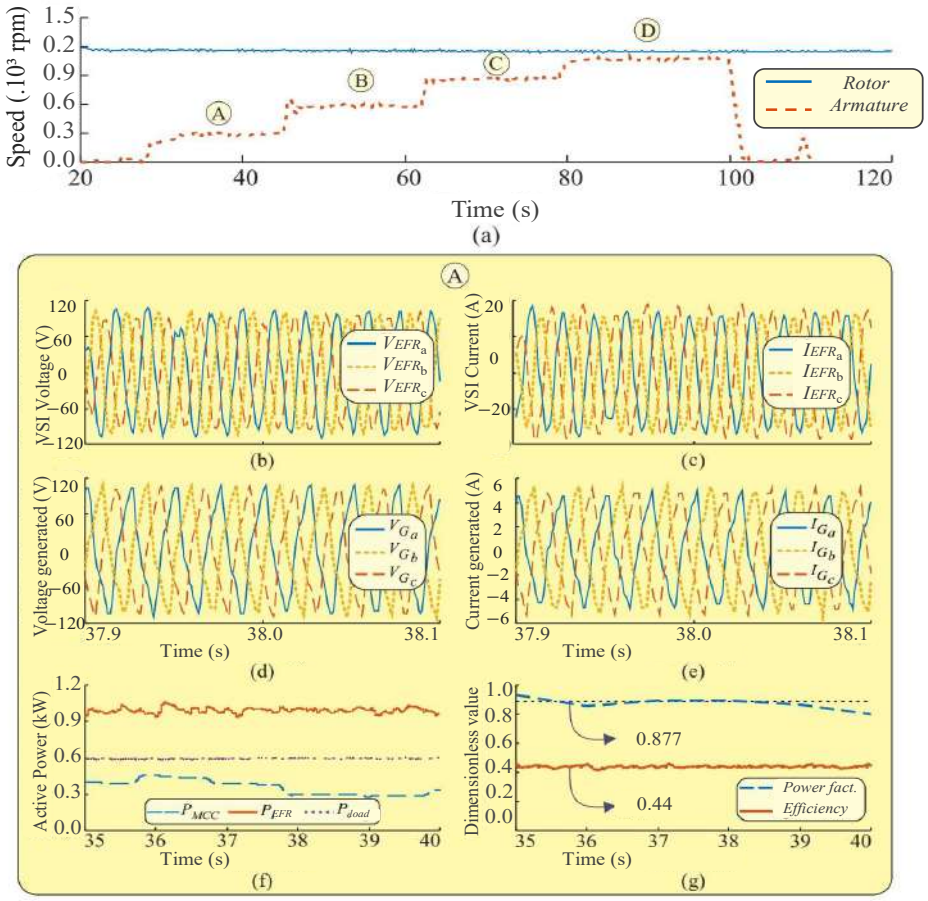

Figure 14. Power flow analysis with fuzzy speed regulation with illustration of the (**a**) rotor and armature profiles, (**b**) Voltage and (**c**) currents consumed by the EFR, (**d**) Voltage, (**e**) currents drawn by the resistive load, (**f**) electrical power of devices a, and (**g**) EFR power factor and overall prototype efficiency.

6. Conclusions

This article proposed new contributions to the control strategy applied to the power generation prototype based on EFR. Computer simulations were proposed using the models of induction machines, which are widely known in the scientific community. To better identify the operating ranges of the prototype, several tests were undertaken with load variation on the synchronous generator and wind emulation. In the experimental scenarios, the fuzzy controller was compared with the conventional controller, proposed together with the creation of the EFR. In scenarios where the generator is idle, the speed regulation by the fuzzy controller presents the best performance in the transient regime compared to the conventional regulation. The gains associated with the fuzzy controller to obtain better performance are lower than those imposed by conventional regulation based on the PI controller. The fuzzy controller presented a regime error four times higher than the PI controllers for steady state. However, this is not a dissadvantage the fuzzy due to the magnitudes of the errors obtained. An error of 0.32% can be considered zero for this application. Furthermore, for evaluating the controllers, there was a significant reduction in the *IAE* and *ITAE* indicators for fuzzy speed regulation. Thus, fuzzy regulation presents better applicability to the prototype concerning the current speed regulation. From the power flow point of view, the prototype's efficiency presents a tendency for efficiencies to decrease as the armature and rotor speed match. However, for the tests evaluated, the fuzzy regulation presented the advantage of providing a less accentuated reduction, characterizing robustness with the velocity multiplication compared to the conventional controller.

Based on the results obtained in this study and on the limitations found in the prototype generation with the EFR, the following proposals for future works are suggested: (1) Undertaking studies in the sizing of machines to obtain an optimization via the good choice of the numbers of poles of the EFR and the generator; (2) Making a new generation prototype based on the new version of the EFR, with the necessary mechanical corrections; (3) Improvement of the fuzzy controller used, with greater quantity and profiles of membership functions being applied; (4) Implementing a flux-slip-based control strategies rotor; (5) Implementing control strategies that guarantee operation with a factor of the EFR's nominal power.

Author Contributions: E.A.D.F.N., R.P. and A.S. conceived and designed the study; D.C.C.C., T.F.d.N. and R.P., methodology; R.P., T.F.d.N. and E.A.D.F.N. performed the simulations and experiments; E.V., D.C.C.C., R.P. and A.S. reviewed the manuscript and provided valuable suggestions; D.C.C.C., T.F.d.N., R.P. and E.A.D.F.N. wrote the paper; supervision, A.S. All authors have read and agreed to the published version of the manuscript.

Funding: This research was funded in part by the Coordenação de Aperfeiçoamento de Pessoal de Nível Superior—Brasil (CAPES)—Finance Code 001 and Conselho Nacional de Desenvolvimento Científico e Tecnológico (CNPq).

Conflicts of Interest: The authors declare no conflict of interest.

Abbreviations

The following abbreviations are used in this manuscript:

PCC	Point of Common Coupling
DC	Direct Current
DFIG	Doubly-Fed Induction Generator
DTC	Direct Torque Control
EFR	Electromagnetic Frequency Regulator
EPS	Electrical Power System
FOC	Field Oriented Control
IAE	Integral of the Absolute magnitude of the Error
ITAE	Integral of Time multiplied by the Absolute Error
PI	Proportional-Integral
PID	Proportional-Integral-Derivative
PMSG	Permanent Magnet Synchronous Generator
RES	Renewable Energy Sources
RLM	Root Locus Method
V/F	Voltage-Frequency
VSI	Voltage Source Inverter

References

1. Polinder, H.; Ferreira, J.A.; Jensen, B.B.; Abrahamsen, A.B.; Atallah, K.; Mcmahon, R.A. Trends in wind turbine generator systems. *IEEE J. Emerging Sel. Top. Power Electron.* **2013**, *1*, 174–185. [CrossRef]
2. Mckenna, R.; vd Leye, P.O.; Fichtner, W. Key challenges and prospects for large wind turbines. *Renew. Sustain. Energy Rev.* **2016**, *53*, 1212–1221. [CrossRef]
3. Alhmoud, L.; Wang, B. A review of the state-of-the-art in wind-energy reliability analysis. *Renew. Sustain. Energy Rev.* **2018**, *81*, 1643–1651. [CrossRef]
4. Azevedo, H.D.M.; Araújo, A.M.; Bouchonneau, N. A review of wind turbine bearing condition monitoring: State of the art and challenges. *Renew. Sustain. Energy Rev.* **2016**, *56*, 368–379. [CrossRef]
5. Ribrant, J.; Bertling, L.M. Survey of Failures in Wind Power Systems with Focus on Swedish Wind Power Plants During 1997–2005. *IEEE Trans. Energy Convers.* **2007**, *22*, 167–173. [CrossRef]
6. Perez, J.M.P.; Marquez, F.P.G.; Tobias, A.; Papaelias, M. Wind turbine reliability analysis. *Renew. Sustain. Energy Rev.* **2013**, *23*, 463–472. [CrossRef]
7. *IEEE Std 1547-2018 (Revision of IEEE Std 1547-2003)*; IEEE Standard for Interconnection and Interoperability of Distributed Energy Resources with Associated Electric Power Systems Interfaces. IEEE: New York, NY, USA, 2018; pp. 1–138. [CrossRef]

8. Vitor Silva, P.; Ferreira Pinheiro, R.; Ortiz Salazar, A.; Pereira do Santos Junior, L.; Cesar de Azevedo, C. A Proposal for a New Wind Turbine Topology Using an Electromagnetic Frequency Regulator. *IEEE Lat. Am. Trans.* **2015**, *13*, 989–997. [CrossRef]
9. Silva, P.V.; Pinheiro, R.F.; Salazar, A.O.; Fernandes, J.D. Performance analysis of a new system for speed control in wind turbines. *Renew. Energy Power Qual. J.* **2015**, *1*, 455–460. [CrossRef]
10. Silva, P.V.; Pinheiro, R.F.; Salazar, A.O.; Júnior, L.P.S.; Fernandes, J.D. A New System for Speed Control in Wind Turbines using the Electromagnetic Frequency Regulator. *EletrôNica PotêNcia* **2015**, *20*, 254–262. [CrossRef]
11. Ramos, T.; Júnior, M.M.; Pinheiro, R.; Medeiros, A. Slip Control of a Squirrel Cage Induction Generator Driven by an Electromagnetic Frequency Regulator to Achieve the Maximum Power Point Tracking. *Energies* **2019**, *12*, 2100. [CrossRef]
12. Da Silva, J.C.L.; Ramos, T.; Junior, M.F.M. Modeling and Harmonic Impact Mitigation of Grid-Connected SCIG Driven by an Electromagnetic Frequency Regulator. *Energies* **2021**, *14*, 4524. [CrossRef]
13. Jacobina, C.B.; Lima, A.M.N. Estratégias de Controle Para Sistemas de Acionamento Com Máquina Assíncrona. *SBA Controle Automação* **1996**, *7*, 15–28.
14. Do Nascimento, T.F.; Nunes, E.A.F.; Salazar, A.O. Modeling and Controllers Design for an Electromagnetic Frequency Regulator Applied to Wind Systems. In Proceedings of the 2021 Brazilian Power Electronics Conference (COBEP), João Pessoa, Brazil, 7–10 November 2021; pp. 1–8.
15. Do Nascimento, T.F.; Nunes, E.A.F.; Villarreal, E.R.L.; Pinheiro, R.F.; Salazar, A.O. Performance Analysis of an Electromagnetic Frequency Regulator under Parametric Variations for Wind System Applications. *Energies* **2022**, *15*, 2873. [CrossRef]
16. Simoes, M.G.; Shaw, I.S. *Controle e Modelagem Fuzzy*; Blusher: São Paulo, Brazil, 2007.
17. Araújo, F.M.U.; Cavalcante, M.S.F.F.; de Vasconcellos, B.S.; Mendes, W.R. Comparison of fuzzy type-2 and conventional fuzzy controllers tuned by ant colony optimization. In Proceedings of the 24th ABCM International Congress of Mechanical Engineering, Curitiba, Brazil, 3–8 December 2017; p. 9.
18. Nise, N.S. *Control Systems Engineering*, 8th ed.; Wiley: Hoboken, NJ, USA, 2019; ISBN: 978-1-119-47422-7.

energies

MDPI

Article

Performance Analysis of an Electromagnetic Frequency Regulator under Parametric Variations for Wind System Applications

Thiago F. do Nascimento [1,†], Evandro A. D. F. Nunes [2,†], Elmer R. L. Villarreal [3,*,†], Ricardo F. Pinheiro [1,†] and Andrés O. Salazar [1,†]

[1] Department of Computer Engineering and Automation, Federal University of Rio Grande do Norte (DCA-UFRN), Natal 59072-970, Brazil; thiago.figueiredo@ufrn.br (T.F.d.N.); ricardo.pinheiro@ufrn.br (R.F.P.); andres@dca.ufrn.br (A.O.S.)
[2] The Federal Institute of Education, Science and Technology of Bahia (IFBA), Salvador 40301-015, Brazil; evandro.nunes@ifba.edu.br
[3] Department of Natural Sciences, Mathematics and Statistics, Federal Rural University of Semi-Arid (DCME-UFERSA), Mossoró 59625-900, Brazil
* Correspondence: elmerllanos@ufersa.edu.br
† These authors contributed equally to this work.

Abstract: The electromagnetic frequency regulator (EFR) device has proven to be an attractive solution for driving grid-connected electrical generators in distributed generation (DG) systems based on renewable energy sources (RES). However, the dynamic characteristic of the EFR has not yet been discussed for cases where its parameters vary from the nominal values. To evaluate this issue, this paper proposes a method for transient and steady-state performance analysis applied to the EFR device considering parametric variations. To perform this analysis, a dynamic model of the EFR device is derived, and its dynamic characteristics are discussed. Based on this model, the system's controller gains are designed by using the root-locus method (RLM) to obtain the desired dynamic performance. Then, a sensitivity analysis of the closed-loop poles under the effect of parameters variation is performed. In addition, the paper also presents an analysis of the EFR-based system operating with the designed controllers. The proposed theoretical analysis is assessed using simulation and experimental results. The simulation program was developed using a Matlab/Simulink platform, while the experimental results were obtained through a laboratory setup emulating the EFR-based system.

Keywords: electromagnetic frequency regulator; distributed generation; renewable energy sources; root-locus method; performance analysis

check for updates

Citation: do Nascimento, T.F.; Nunes, E.A.D.F.; Villarreal, E.R.L.; Pinheiro, R.F.; Salazar, A.O. Performance Analysis of an Electromagnetic Frequency Regulator under Parametric Variations for Wind System Applications. *Energies* **2022**, *15*, 2873. https://doi.org/10.3390/en15082873

Academic Editors: Seyed Morteza Alizadeh and Akhtar Kalam

Received: 26 February 2022
Accepted: 30 March 2022
Published: 14 April 2022

Publisher's Note: MDPI stays neutral with regard to jurisdictional claims in published maps and institutional affiliations.

Copyright: © 2022 by the authors. Licensee MDPI, Basel, Switzerland. This article is an open access article distributed under the terms and conditions of the Creative Commons Attribution (CC BY) license (https://creativecommons.org/licenses/by/4.0/).

1. Introduction

The increased penetration level of DG systems provides greater robustness and operational reliability in modern electrical networks. In addition, RES-based DG systems reduce environmental impact and ties into global concern with sustainability [1]. In this scenario, the implementation of wind and photovoltaic systems has become increasingly common in modern energy systems [2]. The electricity generated through these energy sources has grown sharply in recent years, with an emphasis on wind generation, which has presented faster growth than other emerging RES [3]. However, RES-based generation still presents several challenges related to intermittency of power, stability and power quality issues [4]. Thus, the development of new technologies to improve the reliability and efficiency of these generation systems has been the objective of many researchers worldwide.

One of the most important wind generation system stages is speed multiplication that suits the angular speeds of both the slow-rotating shaft and the fast-rotating shaft. This functionality is performed by gearboxes [5] that are intently studied and improved [6–8] but

still remain a source of reliability problem to wind systems due to their high maintenance cost [9] and reduced lifespan [10]. In addition, RES-based generation systems are usually connected to the grid through power converters, which can contribute to the increase of harmonic components in the voltages and currents generated. In order to overcome these problems, the use of an electromagnetic frequency regulator (EFR) to drive grid-connect electrical generators was proposed in the literature [11–16]. The EFR device consists of a modified induction machine, whose conventional armature mass can rotate, powered by a wind turbine or any other system that can impose a mechanical torque on its axis, as illustrated in Figure 1. In addition, the EFR device has a squirrel-cage rotor, which can be coupled to an electrical generator. Thus, the main function of the EFR is to convert a variable turbine speed imposed on the armature axis (ω_{am}) and provide a desired speed to the rotor axis (ω_{rm}) through a suitable control strategy. In addition, the EFR device enables mechanical decoupling between the wind turbine and the grid-connected generator.

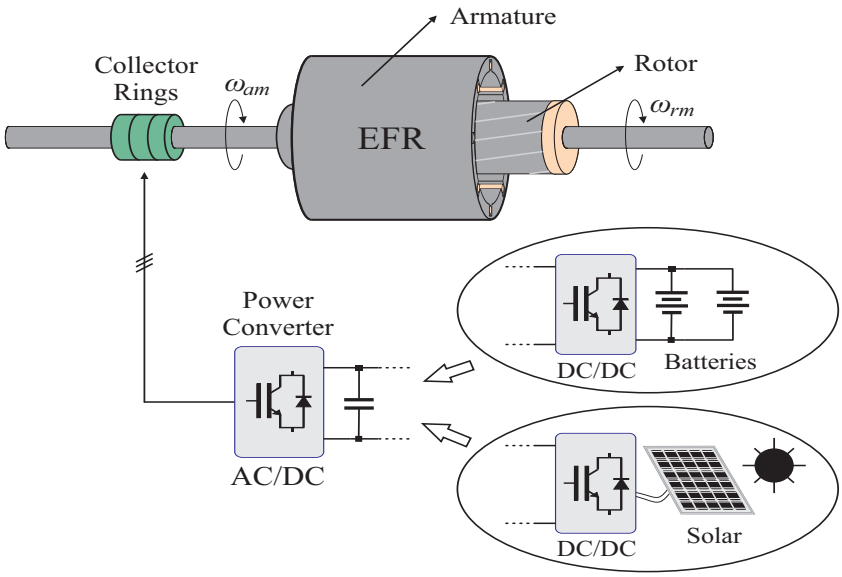

Figure 1. EFR's construction characteristics.

As seen in Figure 1, the EFR's armature windings are connected to the output of a three-phase power converter through collector rings, which allows implementation of a system control strategy. EFR-based systems prevent electronic power devices from being connected directly to the power grid. In addition, the EFR device also makes it possible to implement a hybrid distributed generation system, since a secondary source such as a solar energy source and/or an energy storage system can be connected to the DC bus of the power converter as depicted in Figure 1, which allows power-sharing in the system.

In [11–13], an EFR device was employed in the driving of a synchronous generator connected to the power grid. The authors proposed replacing the wind system gearbox with the EFR device in order to increase reliability and efficiency. The EFR's dynamic behavior was described by a similar mathematical model to applied for a conventional induction machine, and a field orientation control strategy was implemented to regulate rotor speed and flux as well as armature currents using PI controllers. However, the results obtained demonstrate the adequate operational behavior of the EFR only for a small range of armature speeds. In addition, the controllers' design can contribute to the system achieving the desired dynamic response in cases of abrupt speed and load variations, however, it was not discussed in this work. Subsequently, in [14], the EFR was employed in the driving of a squirrel-cage induction generator (SCIG) connected to the grid. In this work, the conjugate corresponding to the maximum wind power extraction was used to define the reference value of the EFR's rotor speed control loop. The EFR's dynamic behavior was described by a more realistic dynamic modeling in which the armature mechanical speed influences on all equations of the model. Once again, a field orientation control strategy

was applied to EFR using PI controllers. The EFR-based system showed a satisfactory performance for large variations in wind speed. In addition, because the converter has no connection to the grid, this topology proved to be more effective in riding through a severe short-circuit at the induction generator terminals compared to a doubly-fed induction generator (DFIG) topology. The power quality issues are essential for the integration of distributed energy resources to the grid. However, they were not adequately discussed in this work. Further, the control gain adjustment method was also not presented.

In [15], the proposal was to perform a power-quality analysis applied to the topology proposed in [14]. The analysis was based on the steady-state harmonic model of the EFR-driven generation system developed in the stationary frame. Based on this model, a study of the harmonic disturbances in the electrical and mechanical variables due to the PWM converter of the EFR's armature voltage was performed. The authors conclude that the EFR-based system has more efficient power-quality performance compared to conventional wind generation topologies such as DFIG and permanent magnetic synchronous generator (PMSG), since the high-frequency components due to converter switching are naturally attenuated by the inherent inertia of the mechanical system. However, the controller's design was again not presented in this work. Consequently, a design method is still needed to adjust controller gains to achieve desired dynamic performance in EFR-based systems. Thus, a controller design method based on a detailed modeling of the EFR device is proposed in [16]. The controllers' design considered desired specifications for transient response using RLM. In addition, the closed-loop poles behavior for EFR's impedance and inertia moments parameters variations was evaluated. The system's controllers presented the desired performance with the proposed design method. However, the system dynamic analysis was performed without considering large parametric variations, which can result in degradation of the system controllers' dynamic performance.

A dynamic analysis assuming large parametric variations can contribute to the suitable design of system controllers. Therefore, this paper proposes a complete performance analysis applied to EFR-based systems. This analysis is based on a mathematical model considering the EFR's dynamic characteristics and the dynamic response specifications for system controllers. Thus, the EFR's control parameters can be designed accurately in order to achieve the desired dynamic response and minimize performance degradation resulting from variations in system parameters. In addition, the proposed analysis contributes to the implementation of more robust control strategies with regard to perturbations since knowledge of the effect of parameter uncertainty can contribute to the adjustment of control gain. Simulation and experimental results verify the proposed performance analysis. This paper is organized as follows: Section 2 presents the system description and control strategy. Dynamic modeling of the EFR device is presented in detail in Section 3. System dynamic analysis is presented in Section 4. Controller design and sensitivity analysis are presented in Sections 5 and 6, respectively. Simulation and experimental results for the controller performance analysis are presented in Section 7, while Section 8 concludes this paper.

2. System Description and Control Strategy

Figure 2 shows the topology and control scheme of the wind systems employed in this study. A wind turbine is mechanically coupled to the EFR's armature axis using a gearbox (GB), since its speed is significantly lower than the rotating field speed needed to generate voltage at the grid frequency. A three-phase voltage-source converter (VSC) is employed to regulate the EFR's armature current and provide a desired angular speed to the synchronous generator (SG) rotor despite the variable angular speed of the wind turbine. Due to the rotational motion of the EFR's armature axis, collector rings are employed to connect the VSC to the armature windings terminals. The primary source of the EFR-connected converter (i.e., photovoltaic system with energy storage) is emulated by a DC voltage source. The SG stator windings are connected to the point of common coupling (PCC) through a three-phase transformer to adjust the generated voltage values to the power grid voltages. An ideal three-phase voltage source represents the power grid interconnected to

the PCC through an equivalent grid impedance composed of series-connected inductor L_g and resistor R_g.

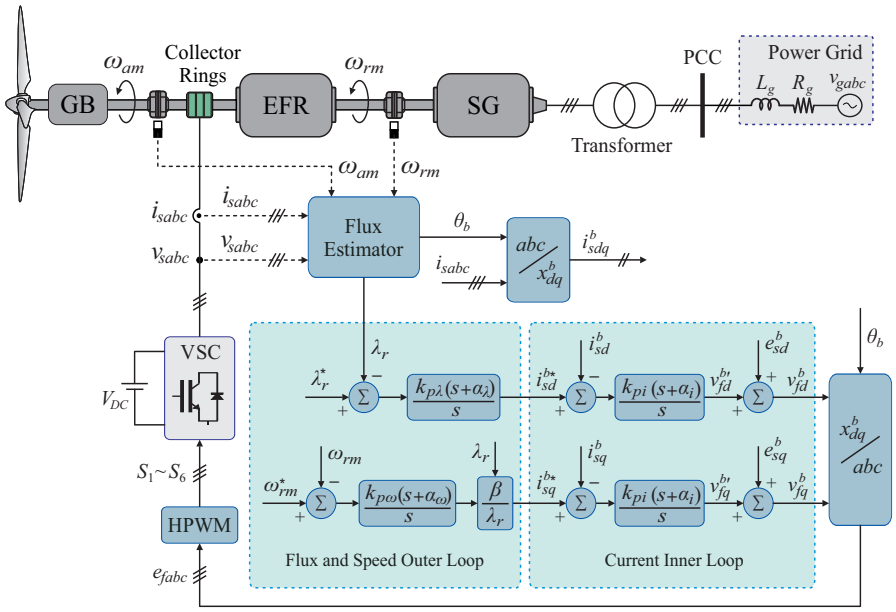

Figure 2. Topology of the wind system with EFR and its control strategy.

As shown in Figure 2, the rotor flux field orientation control strategy implemented in this work consists of an outer control loop that regulates the EFR's rotor flux and speed in cascade with an inner control loop to the EFR's armature currents. In this control strategy, the system's dynamic performance is assessed by tuning standard PI controllers. The orthogonal transformations from the *abc* natural reference frame to the *dq* field-oriented reference frame employ the phase-angle θ_b provided by a flux estimator, which also determines the EFR rotor flux instantaneous value for feedback in the flux loop. In this work, the reference value ω^*_{rm} can be determined according to the maximum power-point tracking (MPPT) operation of the wind turbine as discussed in [14]. The flux controller output determines the reference value i^*_{sd} for *d*-axis armature current control, while the reference value i^*_{sq} used in *q*-axis armature current control is adjusted by the speed controller output. The reference voltages e_{fabc} determined by the inner loop is applied via the hybrid pulse width modulation (HPWM) technique [17], which determines the drive signals of power converter $S_1 \sim S_6$.

3. EFR Slip and Dynamic Modeling

3.1. EFR Slip

As mentioned earlier, the EFR device consists of an induction machine with a squirrel-cage rotor and a rotating armature. In this case, the armature windings current produces a rotating field with an absolute angular speed ω_{sm} in mechanical radians per second given by:

$$\omega_{sm} = \omega_{am} + \frac{2}{P_{efr}}\omega_i, \tag{1}$$

where ω_{am} and ω_i represent the EFR's armature angular speed imposed by the wind turbine and the angular frequency of the current in the EFR's armature windings, respectively. The P_{efr} term represents the EFR poles number. Thus, when the rotor is rotating with a constant speed ω_{rm} in mechanical radians per second, the relative speed per unit or slip between the rotor and the armature rotating field is defined as:

$$s_{efr} = \frac{\omega_{sm} - \omega_{rm}}{\omega_{sm}} = \frac{\omega_{am} + \frac{2}{P_{efr}}\omega_i - \omega_{rm}}{\omega_{am} + \frac{2}{P_{efr}}\omega_i}. \tag{2}$$

On the other hand, the induced voltages in the rotor windings due to the armature rotating field have an angular frequency equal to the slip speed in mechanical radians per second given by:

$$s_{efr}\omega_{sm} = s_{efr}\left(\omega_{am} + \frac{2}{P_{efr}}\omega_i\right). \tag{3}$$

Since the rotor windings are short-circuited, the induced voltages will cause currents to flow in the rotor circuit with an amplitude proportional to the induced voltage amplitude and rotor-windings impedance at the slip frequency. Similar to armature currents, rotor currents will establish their rotating field with speed $s_{efr}\omega_{sm}$ relative to the rotor. Since the rotor itself is rotating with speed ω_{rm}, the absolute speed of the rotor rotating field is defined as:

$$\omega_{rm} + s\omega_{sm} = \omega_{rm} + \left(\frac{\omega_{sm} - \omega_{rm}}{\omega_{sm}}\right)\omega_{sm} = \omega_{sm}. \tag{4}$$

According to (4), the rotating fields related to the EFR's armature and rotor rotate with the same absolute speed, which is similar to conventional induction machines.

3.2. EFR Dynamic Modeling

Figure 3 shows the armature and rotor *abc* variables in a natural reference frame and *dq* variables in an arbitrary reference frame. L_s and L_r represent the self-inductances of the armature and rotor windings, respectively, which also have intrinsic resistances equal to R_s and R_r.

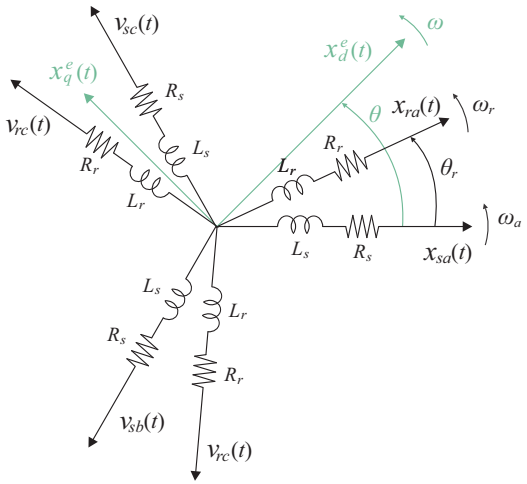

Figure 3. Relationship between *abc* and *dq* variables.

According to Figure 3, θ represents the angular difference between the *d*-axis of the arbitrary reference frame and the *a*-axis of the armature windings, which is expressed as:

$$\theta = \int_0^t (\omega - \omega_a)dt, \tag{5}$$

where ω represents the rotation speed of the arbitrary *d*-axis, while ω_a represents the armature rotating speed in electrical radians per second.

On the other hand, θ_r is the angular difference between the *a*-axes of the armature and rotor windings, which is given by:

$$\theta_r = \int_0^t (\omega_r - \omega_a)dt, \tag{6}$$

in which ω_r represents the rotor's rotational speed in electrical radians per second. The θ and θ_r angles described in (5) and (6) are used to obtain the armature and rotor *dq* variables.

Considering the EFR device a symmetrical induction machine, without magnetic saturation and with flux sinusoidal distribution, and then applying Kirchhoff's voltage law to the three-phase circuit composed by the armature and rotor windings, it is possible to obtain its characteristic equations given by:

$$\vec{v}_s^e = R_s\vec{i}_s^e + \frac{d\vec{\lambda}_s^e}{dt} + j(\omega - \omega_a)\vec{\lambda}_s^e, \tag{7}$$

$$0 = R_r\vec{i}_s^e + \frac{d\vec{\lambda}_r^e}{dt} + j(\omega - \omega_r)\vec{\lambda}_r^e, \tag{8}$$

in which

$$\vec{\lambda}_s^e = (L_s - L_{sm})\vec{i}_s^e + \frac{3}{2}L_{sr}\vec{i}_r^e, \tag{9}$$

$$\vec{\lambda}_r^e = (L_r - L_{rm})\vec{i}_r^e + \frac{3}{2}L_{sr}\vec{i}_s^e, \tag{10}$$

represent the armature and rotor dq flux linkages, respectively. The superscript e denotes the arbitrary dq reference frame, while any variable $\vec{x}$ in these equations represents vectors expressed as:

$$\vec{x} = \frac{1}{\sqrt{2}}(x_d + jx_q). \tag{11}$$

The L_{sm} and L_{rm} terms represent the mutual inductance between two windings in the armature and the mutual inductance between two windings in the rotor, respectively, while L_{sr} is mutual inductance between the stator and rotor windings. The electromagnetic conjugate of the EFR device can be computed as:

$$T_{em} = \frac{3PL_{sr}}{2}\left(\vec{i}_r^e \times \vec{i}_s^e\right), \tag{12}$$

where the $\times$ operator represents the vector product between $\vec{i}_r^e$ and $\vec{i}_s^e$ current vectors.

The mechanical motion related to the EFR's armature can be described by the swing equation given by:

$$T_{am} - T_{em} = J_a\frac{d\omega_{am}}{dt} + f_{am}\omega_{am}, \tag{13}$$

in which J_a is the total inertia of the wind turbine coupled to the rotating armature on the high-speed side of the gearbox and f_{am} is the armature friction factor. The swing equation for the EFR rotor's mechanical motion is given by:

$$T_{em} - T_{rm} = J_r\frac{d\omega_{rm}}{dt} + f_{rm}\omega_{rm}, \tag{14}$$

where J_r is the sum of the inertia of the EFR rotor with the SG rotor, and f_{rm} is the rotor friction factor. The T_{am} term represents the wind turbine mechanical conjugate at the high-speed side of the gearbox, while T_{rm} represents the mechanical conjugate applied to the EFR rotor.

The referential frame for the dq quantities in (7)–(12) is chosen according to the control technique implemented. For the rotor-flux-field-orientation method employed in this work, the arbitrary d-axis is aligned with the rotor-flux-vector axis, which results in decoupling between the flux and conjugate loops [18,19]. Thus, considering the rotor-flux-field-orientation reference frame, it is possible to obtain the transfer functions which will be used in the design and performance analysis of the system controllers.

3.2.1. Armature Current Model

The mathematical model employed to evaluate the dynamic behavior of EFR's armature current can be obtained from (7)–(10), which results in the equations:

$$v_{sd}^{e} = R_{sr} i_{sd}^{e} + \sigma \frac{di_{sd}^{e}}{dt} + e_{sd}^{e}, \tag{15}$$

$$v_{sq}^{e} = R_{sr} i_{sq}^{e} + \sigma \frac{di_{sq}^{e}}{dt} + e_{sq}^{e}, \tag{16}$$

in which

$$e_{sd}^{e} = -(\omega - \omega_a)\sigma i_{sq}^{e} - (\omega_r - \omega_a)\left(\frac{1.5L_{sr}}{L_r - L_{rm}}\right)\lambda_{rq}^{e} - \frac{1.5L_{sr}R_r}{(L_r - L_{rm})^2}\lambda_{rd}^{e}. \tag{17}$$

$$e_{sq}^{e}(t) = (\omega - \omega_a)\sigma i_{sd}^{e}(t) + (\omega_r - \omega_a)\left(\frac{1.5L_{sr}}{L_r - L_{rm}}\right)\lambda_{rd}^{e}(t) - \frac{1.5L_{sr}R_r}{(L_r - L_{rm})^2}\lambda_{rq}^{e}(t), \tag{18}$$

represents disturbances to be compensated for at the current-controller output as illustrated in Figure 2. The σ and R_{sr} terms are constants given by:

$$R_{sr} = R_s + R_r\left(\frac{1.5L_{sr}}{L_r - L_{rm}}\right)^2, \tag{19}$$

$$\sigma = L_s - L_{sm} - \frac{2.25L_{sr}^2}{L_r - L_{rm}}. \tag{20}$$

Assuming the rotor-flux-field-orientation reference frame defined by $\lambda_{rd}^{b} = \lambda_r$, $\lambda_{rq}^{b} = 0$ and $\omega = \omega_b$ [18], (15) and (16) can be rewritten as:

$$v_{sd}^{b} = R_{sr} i_{sd}^{b} + \sigma \frac{di_{sd}^{b}}{dt} + e_{sd}^{b}, \tag{21}$$

$$v_{sq}^{b} = R_{sr} i_{sq}^{b} + \sigma \frac{di_{sq}^{b}}{dt} + e_{sq}^{b}, \tag{22}$$

in which

$$e_{sd}^{b} = -(\omega_b - \omega_a)\sigma i_{sq}^{b} - \frac{1.5L_{sr}R_r}{(L_r - L_{rm})^2}\lambda_r, \tag{23}$$

$$e_{sq}^{b} = (\omega_b - \omega_a)\sigma i_{sd}^{b} + (\omega_r - \omega_a)\left(\frac{1.5L_{sr}}{L_r - L_{rm}}\right)\lambda_r. \tag{24}$$

The superscript b denotes the rotor-flux-field-orientation reference frame. Assuming $v_{sd}^{b'} = v_{sd}^{b} - e_{sd}^{b}$ and $v_{sq}^{b'} = v_{sq}^{b} - e_{sq}^{b}$, and then applying Laplace transformation in (21) and (22), it is possible to obtain a transfer function defined as:

$$G_i(s) = \frac{I_{sdq}^{b}(s)}{V_{sdq}^{b'}(s)} = \frac{1}{\sigma s + R_{sr}}. \tag{25}$$

The transfer function given in (25) describes the dynamic relationship between the armature current and voltage in the rotor-flux-field-orientation reference frame.

3.2.2. Rotor Flux Model

Similarly, the model employed to evaluate the dynamic behavior of EFR's rotor flux can also be obtained from (7)–(10), which results in the expression given by:

$$\frac{1.5L_{sr}}{\tau_r} i_{sd}^{e} = \frac{1}{\tau_r}\lambda_{rd}^{e} + \frac{d\lambda_{rd}^{e}}{dt} - (\omega - \omega_r)\lambda_{rq}^{e}, \tag{26}$$

in which

$$\tau_r = \frac{L_r - L_{rm}}{R_r}. \tag{27}$$

Assuming the rotor-flux-field-orientation reference frame, i.e., $\lambda_{rd}^b = \lambda_r$, $\lambda_{rq}^b = 0$ and $\omega = \omega_b$, (26) can be rewritten as:

$$\frac{1.5L_{sr}}{\tau_r} i_{sd}^b = \frac{1}{\tau_r}\lambda_r + \frac{d\lambda_r}{dt}. \tag{28}$$

Applying Laplace transformation in (28), it is possible to obtain the transfer function, defined as:

$$G_{\lambda_r}(s) = \frac{\Lambda_r(s)}{I_{sd}^b(s)} = \frac{1.5L_{sr}}{\tau_r s + 1}, \tag{29}$$

which correlates the d-axis armature current with the rotor flux.

3.2.3. Rotor Speed Model

From (10) and (12), the electromagnetic conjugate can be expressed as follows:

$$T_{em} = P_{efr}\frac{1.5L_{sr}}{L_r - L_{rm}}\left(\lambda_{rd}^e i_{sq}^e - \lambda_{rq}^e i_{sd}^e\right), \tag{30}$$

in which adopting the rotor-flux-field-orientation reference frame results in the following expression:

$$T_{em} = P_{efr}\frac{1.5L_{sr}}{L_r - L_{rm}}\lambda_r i_{sq}^b = \frac{1}{\beta}\lambda_r i_{sq}^b, \tag{31}$$

in which

$$\beta = \frac{(L_r - L_{rm})}{1.5P_{efr}L_{sr}}. \tag{32}$$

Since the d-axis armature current is directly related to the rotor flux and the q-axis armature current is directly related to the electromagnetic conjugate as expressed in (28) and (31), respectively, it is possible to obtain decoupling between the flux and conjugate control loops of the EFR device.

From (14), it is possible to obtain a dynamic relationship between the electromagnetic conjugate and the rotor speed. Thus, substituting (31) in (14), and assuming the mechanical conjugate T_{rm} as a disturbance to the control action, results in the following expression:

$$\frac{\lambda_r}{\beta} i_{sq}^b = J_r\frac{d\omega_{rm}}{dt} + f_{rm}\omega_{rm}. \tag{33}$$

Considering rotor flux magnitude constant, i.e., $\lambda_r \approx \lambda_{rn}$, and then applying the Laplace transformation in (33), it is possible obtain the following transfer function:

$$G_{\omega_r}(s) = \frac{\Omega_{rm}(s)}{I_{sq}^b(s)} = \frac{\lambda_{rn}}{\beta(J_r s + f_{rm})}, \tag{34}$$

in which λ_{rn} represents the EFR's rated rotor flux.

The model given in (34) describes the dynamic relationship between rotor speed and q-axis armature current, which in turn is directly related to the electromagnetic conjugate.

4. EFR's Dynamic Analysis

The dynamic analysis implements the current, flux and speed models obtained in the previous section in order to obtain the dynamic behavior of the EFR device under parametric variations. This analysis employs the parameters listed in Table 1.

Table 1. EFR's parameters.

	Parameter	Value
EFR device	Poles number (P_{efr})	2
	Armature inductance (L_s)	242 mH
	Rotor inductance (L_r)	242 mH
	Armature resistance (R_s)	5.795 Ω
	Rotor resistance (R_r)	5.795 Ω
	Armature mutual inductance (L_{sm})	121 mH
	Rotor mutual inductance (L_{rm})	121 mH
	Armature-to-rotor inductance (L_{sr})	265 mH
	Rotor inertia moment (J_r)	0.02 kg·m^2
	Rotor friction factor (f_{rm})	0.003 N·m/rad·s^{-1}

4.1. Transient Response Analysis

4.1.1. Current Transient Response

Since the transfer function given in (25) is a first-order system, the armature current transient response can be evaluated by specifying settling time ($T_{s2\%}$), defined as [20]:

$$T_{s2\%} = \frac{4}{a} = \frac{4\sigma}{R_{sr}}, \tag{35}$$

where $a = R_{sr}/\sigma$ represents the open-loop system pole. According to (35), the settling time value depends on the armature and rotor windings impedance of the EFR.

Figure 4 shows the settling time assuming variations in the inductance and resistance of the EFR armature. In this case, armature inductance and resistance were increased with an increment rate of 20% around their values defined in Table 1. According to Figure 4a, when L_s armature inductance increases from 260 to 480 mH, the settling time increases from 15 to 95 ms, approximately, which represents a degradation to armature current transient performance. On the other hand, according to Figure 4b, when R_s armature resistance increases from 5.6 to 10.4 Ω, the settling time decreases from 140 to 35 ms, approximately, which may represent an improvement on the transient performance. Therefore, armature current transient behavior is influenced by EFR's parameters.

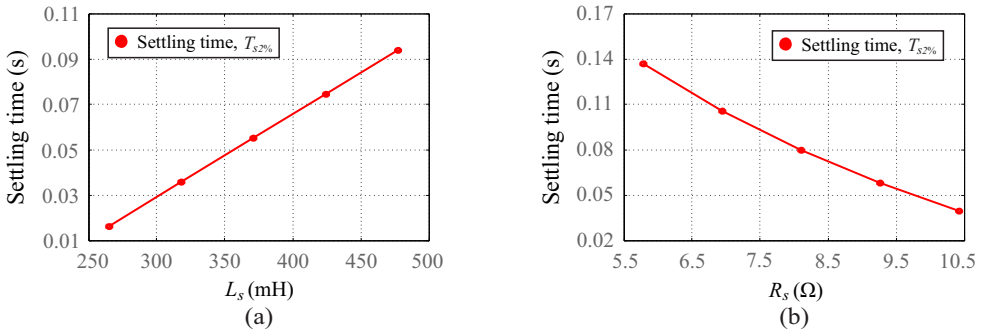

Figure 4. Settling time for variations in the (**a**) L_s armature inductance (**b**) R_s armature resistance.

4.1.2. Flux Transient Response

According to the rotor flux field orientation method, the rotor flux loop is nested to the *d*-axis armature current loop. Thus, from (25) and (29), it is possible to obtain a direct relationship between rotor flux and *d*-axis armature voltage expressed by the following transfer functions:

$$G_{\lambda i}(s) = G_{\lambda_r}(s)G_i(s) = \frac{\Lambda_r(s)}{V_{sd}^{b\prime}(s)} = \frac{\frac{1.5L_{sr}}{\tau_r\sigma}}{s^2 + \left(\frac{\tau_r R_{sr}+\sigma}{\tau_r\sigma}\right)s + \frac{R_{sr}}{\tau_r\sigma}}. \tag{36}$$

The model described by (36) represents a second-order system in which pole locations vary as a function of the armature and rotor impedance parameters of the EFR. Thus, by matching the dynamic model $G_{\lambda i}(s)$ to the typical second-order transfer function, natural frequency ($\omega_{\lambda i}$) and the damping ratio ($\xi_{\lambda i}$) related to this model can be calculated as follows:

$$\omega_{\lambda i} = \sqrt{\frac{R_{sr}}{\tau_r \sigma}}, \tag{37}$$

$$\xi_{\lambda i} = \frac{\tau_r R_{sr} + \sigma}{2\sqrt{\tau_r \sigma R_{sr}}}. \tag{38}$$

In this case, the system parameters' influence on EFR rotor flux transient response can be evaluated by specifications defined as rise time ($T_{r0-100\%}$), peak time (T_p), percent overshoot (%OS) and settling time ($T_{s2\%}$). Their values are computed by the following expressions [20]:

$$\begin{aligned} T_{r0-100\%} &= \frac{\pi - cos^{-1}(\xi_{\lambda i})}{\omega_{\lambda i}\sqrt{1-\xi_{\lambda i}^2}} \\ &= 2\tau_r\sigma\left[\frac{\pi - cos^{-1}\left(\frac{\tau_r R_{sr}+\sigma}{2\sqrt{\tau_r\sigma R_{sr}}}\right)}{\sqrt{(\sigma-\tau_r R_{sr})(\tau_r R_{sr}-\sigma)}}\right], \end{aligned} \tag{39}$$

$$T_p = \frac{\pi}{\omega_{\lambda i}\sqrt{1-\xi_{\lambda i}^2}} = \frac{2\pi\tau_r\sigma}{\sqrt{(\sigma-\tau_r R_{sr})(\tau_r R_{sr}-\sigma)}}, \tag{40}$$

$$\begin{aligned} \%OS &= e^{-\left(\xi_{\lambda i}\pi/\sqrt{1-\xi_{\lambda i}^2}\right)} \times 100 \\ &= e^{-\left[\frac{(\tau_r R_{sr}+\sigma)\pi}{\sqrt{(\sigma-\tau_r R_{sr})(\tau_r R_{sr}-\sigma)}}\right]} \times 100, \end{aligned} \tag{41}$$

$$T_{s2\%} = \frac{4}{\xi_{\lambda i}\omega_{\lambda i}} = \frac{8\tau_r\sigma}{\tau_r R_{sr}+\sigma}. \tag{42}$$

According to (39)–(42), similar to the case of the current model, the transient response specification values for the flux model also depend on the impedance of the EFR windings. Figure 5 shows the rise time, peak time, percent overshoot and settling time for different armature inductance and resistance values of the EFR. According to Figure 5a,b, when L_s armature inductance increases from 260 to 480 mH, the rise time, peak time and settling time increase, approximately, from 10 to 90 ms, from 0.025 to 0.225 s and from 0.03 to 0.14 s, respectively, which can represent a degradation in transient performance. On the other hand, percent overshoot decreases from 3% to 0.2%, approximately, which may represent an improvement in rotor flux transient performance. According to Figure 5c,d, when R_s armature resistance increases from 5.6 to 10.4 Ω, the peak time and settling time decrease, approximately, from 27 to 18 ms and from 0.31 to 0.22 s, respectively, which may represent an improvement in rotor flux transient performance. On the other hand, the percent overshoot and rise time increase from 2.9% to 3.25% and from 6.5 to 9.2 ms, respectively, which can represent a degradation in transient performance. Therefore, rotor flux transient behavior can be greatly influenced by EFR parameters.

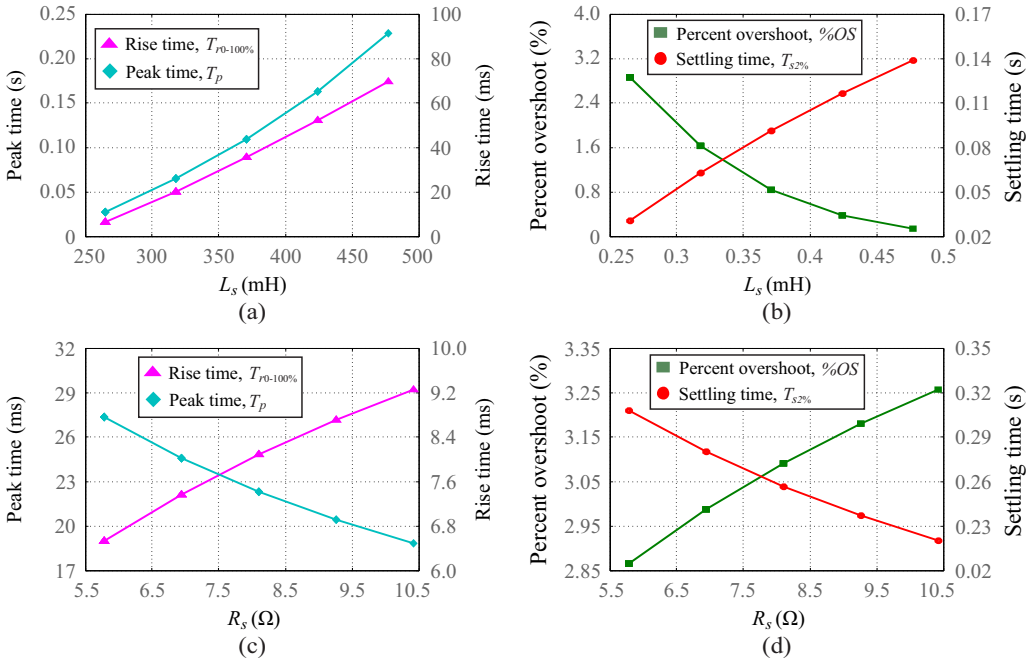

Figure 5. Flux transient response specifications for armature winding parameter variations. (**a**) Rise time and peak time for L_s variations. (**b**) Percent overshoot and settling time for L_s variations. (**c**) Rise time and peak time for R_s variations (**d**) Percent overshoot and settling time for R_s variations.

4.1.3. Speed Transient Response

By using a similar procedure, since the rotor speed loop is nested to the q-axis armature current loop, from (25) and (34) it is possible to obtain a transfer function that describes the direct relationship between rotor speed and q-axis armature voltage given by:

$$G_{\omega i}(s) = G_{\omega_r}(s)G_i(s) = \frac{\Omega_r(s)}{V_{sq}^{b\prime}(s)} = \frac{\frac{\lambda_{rn}}{J_r\sigma\beta}}{s^2 + \left(\frac{J_rR_{sr}+f_{rm}\sigma}{J_r\sigma}\right)s + \frac{f_{rm}R_{sr}}{J_r\sigma}}, \tag{43}$$

which results in a natural frequency ($\omega_{\omega i}$) and damping ratio ($\xi_{\omega i}$) related to this model given by:

$$\omega_{\omega i} = \sqrt{\frac{f_{rm}R_{sr}}{J_r\sigma}}, \tag{44}$$

$$\xi_{\omega i} = \frac{J_rR_{sr} + f_{rm}\sigma}{2\sqrt{J_r\sigma f_{rm}R_{sr}}}. \tag{45}$$

In this case, the transient response specifications of the EFR's rotor speed can be computed as follows:

$$\begin{aligned} T_{r0-100\%} &= \frac{\pi - cos^{-1}(\xi_{\omega i})}{\omega_{\omega i}\sqrt{1-\xi_{\omega i}^2}} \\ &= 2J_r\sigma\left[\frac{\pi - cos^{-1}\left(\frac{J_rR_{sr}+f_{rm}\sigma}{2\sqrt{J_r\sigma f_{rm}R_{sr}}}\right)}{\sqrt{(f_{rm}\sigma - J_rR_{sr})(J_rR_{sr} - f_{rm}\sigma)}}\right], \end{aligned} \tag{46}$$

$$T_p = \frac{\pi}{\omega_{\omega i}\sqrt{1-\xi_{\omega i}^2}} = \frac{2\pi J_r\sigma}{\sqrt{(f_{rm}\sigma - J_rR_{sr})(J_rR_{sr} - f_{rm}\sigma)}}, \tag{47}$$

$$\begin{aligned} \%OS &= e^{-\left(\xi_{\omega i}\pi/\sqrt{1-\xi_{\omega i}^2}\right)} \times 100 \\ &= e^{-\left[\frac{(J_r R_{sr}+f_{rm}\sigma)\pi}{\sqrt{(f_{rm}\sigma-J_r R_{sr})(J_r R_{sr}-f_{rm}\sigma)}}\right]} \times 100, \end{aligned} \tag{48}$$

$$T_{s2\%} = \frac{4}{\xi_{\omega i}\omega_{\omega i}} = \frac{8J_r\sigma}{J_r R_{sr}+f_{rm}\sigma}. \tag{49}$$

According to (46)–(49), the transient response specifications for the rotor speed depend on the EFR windings impedance parameters as well as on its parameters of inertia moments and friction factors. Figure 6 shows the behavior of these specifications assuming variations in the inductance and resistance values of the EFR armature. According to Figure 6a,b, when L_s increases from 260 to 480 mH, the rise time, peak time and settling time increase, approximately, from 8 to 44 ms, from 25 to 145 ms and from 30 to 195 ms, respectively, while the percent overshoot decreases from 4.31% to 4.25%, approximately. On the other hand, according to Figure 6c,d, when R_s increases from 5.6 to 10.4 Ω, the rise time, peak time and settling time decrease from 24 to 16 ms, from 26 to 18 ms and from 33 to 23 ms, respectively, while the percent overshoot increases from 4.309% to 4.313%, approximately. Therefore, lower values for the L_s/R_s ratio result in higher percent overshoot; however, their values were little affected by variations in the armature parameters. On the other hand, the values of the other transient specifications can be greatly influenced by these parameters.

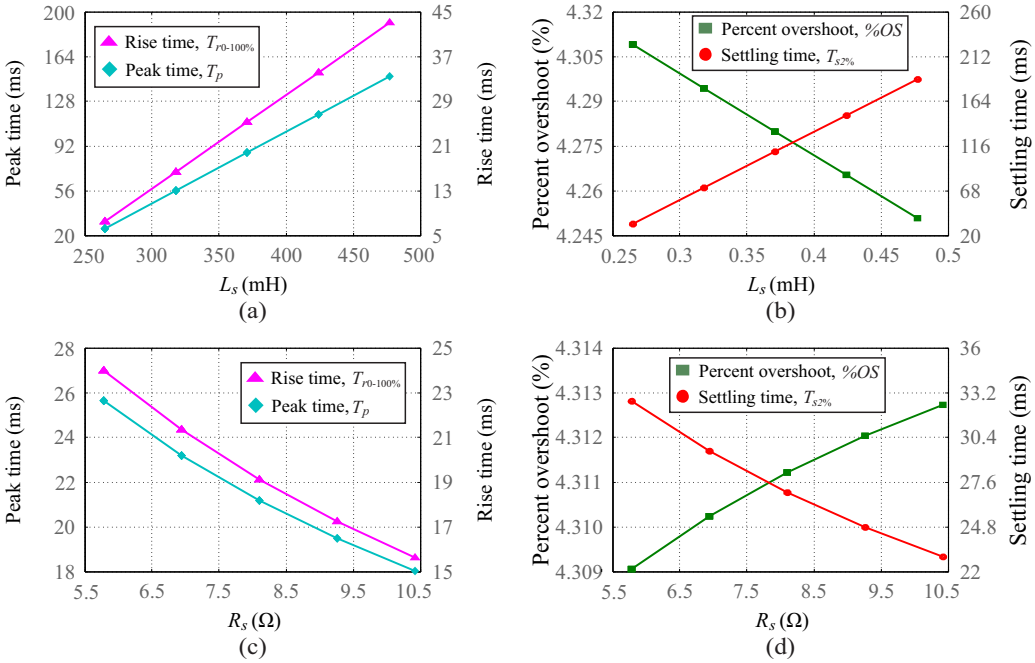

Figure 6. Speed transient response specifications for armature winding parameter variations. (**a**) Rise time and peak time for L_s variations. (**b**) Percent overshoot and settling time for L_s variations. (**c**) Rise time and peak time for R_s variations. (**d**) Percent overshoot and settling time for R_s variations.

4.2. Steady-State Response Analysis

The steady-state response analysis for models describing the EFR device can be performed by evaluating error specifications for unity feedback systems. For a stable closed-loop system, these specifications can be obtained by the final value theorem [20].

4.2.1. Current Steady-State Response

Considering the model described in (25) and assuming a step input, the steady-state error values for armature current can be defined as:

$$e_i(\infty) = \frac{1}{1+\lim_{s\to 0} G_i(s)} = \frac{R_{sr}}{R_{sr}+1}, \tag{50}$$

where the $\lim_{s\to 0} G_i(s)$ term represents static gains computed as:

$$\lim_{s\to 0} G_i(s) = \frac{1}{R_{sr}}. \tag{51}$$

According to (50), the steady-state error value of current does not depend on the armature inductance, since it depends only on the parameter R_{sr} described in (19). Figure 7 shows the current steady-state error values for different L_r and R_s parameter values. According to Figure 7a, the error value decreases from 0.916 to 0.888 approximately, when L_r increases from 260 to 480 mH. On the other hand, for variations to R_s between 5.6 to 10.4 Ω, the error value increases from 0.916 to 0.94, as shown in Figure 7b. Therefore, variations in rotor inductance and armature resistance can modify the armature current steady-state response.

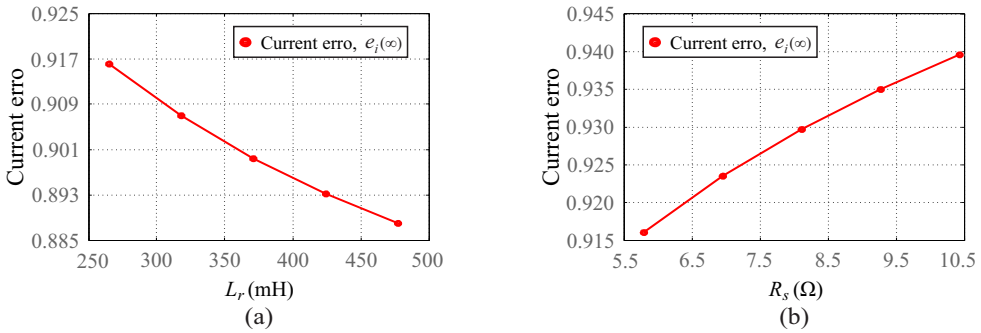

Figure 7. Armature current error values for (**a**) L_r variations and (**b**) R_s variations.

4.2.2. Flux and Speed Steady-State Response

The flux and speed steady-state response can be evaluated using the models described in (29) and (34). Thus, assuming these systems have unitary feedback and step inputs, their steady-state error values are defined as:

$$e_{\lambda i}(\infty) = \frac{1}{1+\lim_{s\to 0} G_{\lambda i}(s)} = \frac{R_{sr}}{R_{sr}+1.5L_{sr}}, \tag{52}$$

$$e_{\omega i}(\infty) = \frac{1}{1+\lim_{s\to 0} G_{\omega i}(s)} = \frac{f_{rm}R_{sr}\beta}{f_{rm}R_{sr}\beta+\lambda_{rn}}, \tag{53}$$

in which

$$\lim_{s\to 0} G_{\lambda i}(s) = \frac{1.5L_{sr}}{R_{sr}}, \tag{54}$$

$$\lim_{s\to 0} G_{\omega i}(s) = \frac{\lambda_{rn}}{f_{rm}R_{sr}\beta}. \tag{55}$$

Figure 8 shows the flux and speed steady-state error values for variations of L_r and R_s. According to Figure 8a, for variations of L_r between 260 to 480 mH, the flux error value decreases from 0.968 to 0.956, while the speed error value increases from 0.014 to 0.016, approximately. For variations of R_s between 5.6 to 10.4 Ω, the flux and speed error values increase from 0.968 to 0.977 and 0.014 to 0.02, respectively, as shown in Figure 8b. Therefore, similar to the current error, variations in rotor inductance and armature resistance can also modify the steady-state response of the rotor flux and speed.

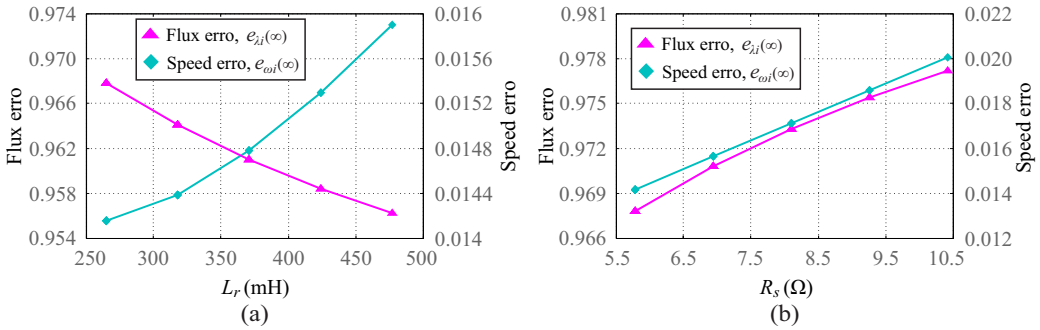

Figure 8. Flux and speed error values for (**a**) L_r variations and (**b**) R_s variations.

5. EFR Controller Design

In this section, the EFR controllers are designed by using the RLM and the parameters described in Table 1.

5.1. Current Controller Design

The control strategy employs standard PI controllers for regulating the *dq* components of the EFR armature current (see Figure 2), whose transfer function given by (25) describes its dynamic behavior. Thus, the EFR current control has an open-loop transfer function described as:

$$H_i(s) = k_{pi} T_i(s) = \frac{k_{pi}(s + \alpha_i)}{s(\sigma s + R_{sr})}, \tag{56}$$

where k_{pi} and α_i represent the current PI controller gains.

Since the EFR controllers compose a multi-loop control scheme, the design requirements for the inner control loop are chosen so as not to affect the dynamic performance of the outer control loop [21]. Based on this idea, a percent overshoot (%OS) less than or equal to 5% and a settling time ($T_{s2\%}$) less than or equal to 0.08 s are used in the design of the current PI controllers. Based on these performance requirements, the minimum value of the natural frequency (ω_i) and damping ratio (ξ_i) for the closed-loop current control are calculated as follows [20]:

$$\xi_i \geqslant \frac{-ln(\%OS/100)}{\sqrt{\pi^2 + ln^2(\%OS/100)}} = \frac{-ln(0.05)}{\sqrt{\pi^2 + ln^2(0.05)}} \approx 0.7, \tag{57}$$

$$\omega_i \geqslant \frac{4}{\xi_i T_{s2\%}} = \frac{4}{0.7 \times 0.08} \approx 71.43 \text{ rad/s}, \tag{58}$$

and correspond to the desired region for the closed-loop poles illustrated in Figure 9.

According to the RLM, the controller zero can be chosen to allow all poles of the closed-loop system to be allocated within the desired region. In this case, this is achieved by setting $\alpha_i = 280$, which results in the controller zero shown in Figure 9. Then, the k_{pi} gain can be calculated by the module restriction given by the following expression [20]:

$$k_{pi} = \frac{1}{|T_i(s_d)|}. \tag{59}$$

The s_d term represents the desired closed-loop pole. In this case, its is allocated in the break-in point on the real axis, which results in $s_d = -380$. Therefore, substituting the value of s_d in (59) results in a controller gain computed as $k_{pi} = 22.965$. Figure 9 shows the root locus for the $H_i(s)$ open-loop system. The closed-loop system has two real and equal poles corresponding to s_d, which results in a transient response without percent overshoot.

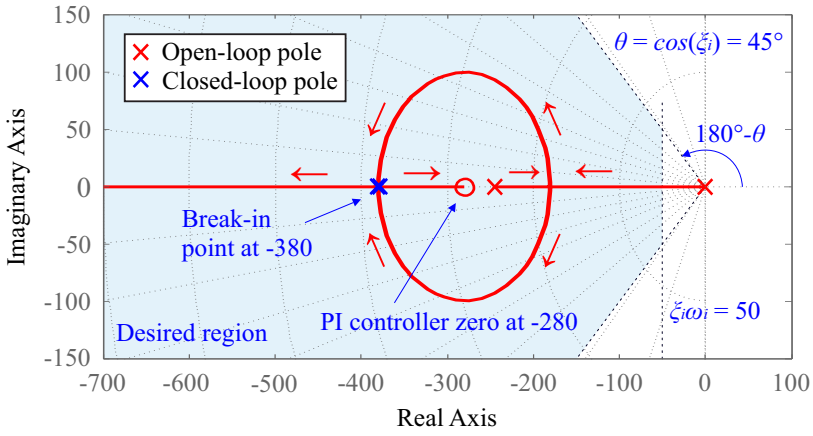

Figure 9. Root locus for current control loop.

5.2. Flux Controller Design

The flux control loop is in cascade with the d-axis armature current control loop as shown in Figure 2. Therefore, considering the dynamic model described in (29) and inner current controller dynamics, it is possible to obtain the open-loop transfer function for flux control as follows:

$$\begin{aligned} H_\lambda(s) &= k_{p\lambda} T_\lambda(s) \\ &= \frac{1.5 L_{sr} k_{pi} k_{p\lambda} (s+\alpha_i)(s+\alpha_\lambda)}{s(\tau_r s+1)\left(\sigma s^2 + \left(R_{sr}+k_{pi}\right)s + k_{pi}\alpha_i\right)}, \end{aligned} \tag{60}$$

in which $k_{p\lambda}$ and α_λ represent the flux controller gains.

For guaranteeing the proper performance of the multi-loop scheme composed of the flux controller and the d-axis current controller, the design requirements can be chosen so that the control action of the flux outer loop is slower than that of the current inner loop [21]. Thus, assuming $\%OS \leqslant 5\%$ and $T_{s2\%} \leqslant 1$ s, which results in $\xi_\lambda \geqslant 0.7$ and $\omega_\lambda \geqslant 5.714$ rad/s as design criteria, it is possible to obtain the desired region illustrated in Figure 10. In order to allocate all closed-loop poles within this desired region, the zero of the flux PI controller is chosen by setting $\alpha_\lambda = 20$. The $k_{p\lambda}$ gain can be determined by:

$$k_{p\lambda} = \frac{1}{|T_\lambda(s_d)|}. \tag{61}$$

Therefore, assuming $s_d = -30.4$ results in a control gain computed as $k_{p\lambda} = 7.845$. Figure 10 shows the root locus for the $H_\lambda(s)$ open-loop system. The closed-loop system has two real and equal dominant poles that correspond to the s_d adopted and two complex non-dominant poles located furthest from the imaginary axis. In this case, the allocation of non-dominant poles depends on the design requirements adopted for the current inner controller.

5.3. Speed Controller Design

According to Figure 2, the speed control loop is in cascade with the q-axis armature current control loop. Thus, considering the dynamic model given by (34) and closed-loop current control, it is possible to obtain an open-loop transfer function defined as:

$$\begin{aligned} H_\omega(s) &= k_{p\omega} T_\omega(s) \\ &= \frac{k_{p\omega} k_{pi} (s+\alpha_i)(s+\alpha_\omega)}{s(J_r s + f_{rm})\left(\sigma s^2 + \left(R_{sr}+k_{pi}\right)s + k_{pi}\alpha_i\right)}, \end{aligned} \tag{62}$$

where $k_{p\omega}$ and α_ω represent the speed controller gains.

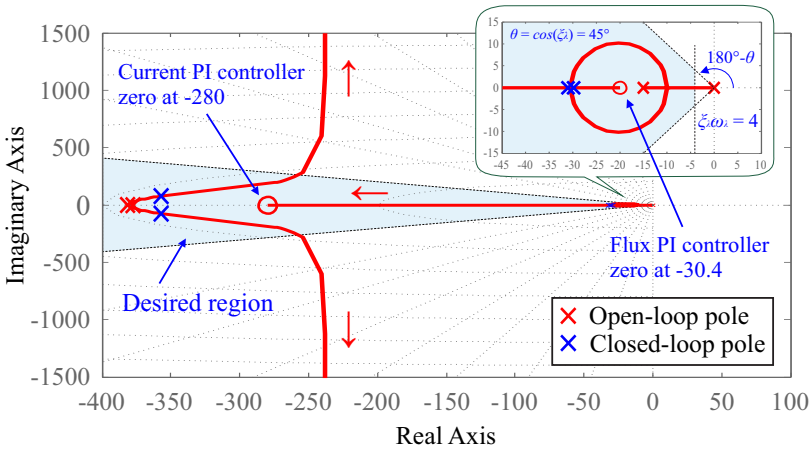

Figure 10. Root locus for flux control loop.

In this case, the performance requirements applied to the speed controller are $\%OS \leqslant 5\%$ and $T_{s2\%} \leqslant 4$ s, which results in $\xi_s \geqslant 0.7$ and $\omega_s \geqslant 1.43$ rad/s. The desired region corresponding to these requirements is shown in Figure 11. Thus, assuming the same procedure employed in the design of flux and current controllers, the speed controller zero is defined by $\alpha_\omega = 0.75$, while the $k_{p\lambda}$ gain can be computed by:

$$k_{p\omega} = \frac{1}{|T_\omega(s_d)|}, \tag{63}$$

in which, assuming $s_d = -1.44$, the controller gain is calculated as $k_{p\omega} = 0.0327$. Figure 11 presents the resulting root locus for the speed control loop. According to Figure 11, all closed-loop poles are located within the desired region. In this case, the closed-loop system has two real and equal non-dominant poles that correspond to the closed-loop poles of the current inner loop and are located further from the imaginary axis. In addition, the closed-loop system also has two real and equal dominant poles that are allocated closer to the origin and correspond to the desired pole s_d.

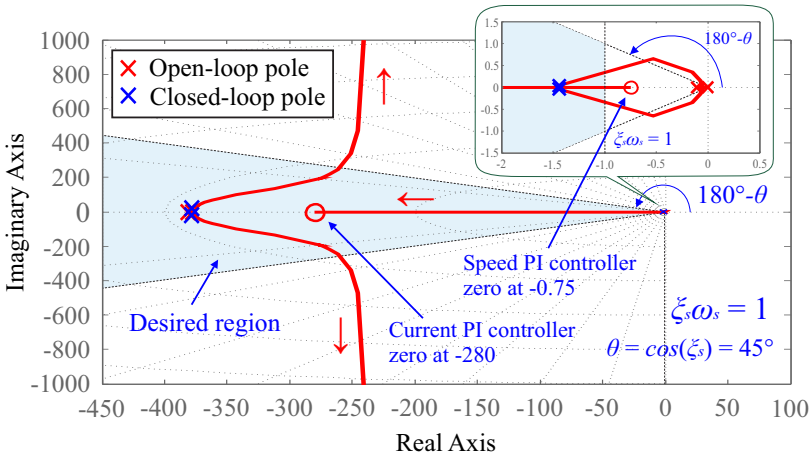

Figure 11. Root locus for speed control loop.

6. Closed-Loop Poles Sensitivity Analysis

In this section, a sensitivity analysis is performed in order to compare the dynamic performance of the system's controllers assuming variations in the EFR parameters listed in Table 1. This analysis employs the control gains designed in the previous section and summarized in Table 2.

Table 2. Parameter design for system controllers.

	Parameter	Value
Current Controller	Proportional gain (k_{pi}) Gain (α_i)	22.965 280
Flux Controller	Proportional gain ($k_{p\lambda}$) Gain (α_λ)	7.845 20
Speed Controller	Proportional gain ($k_{p\omega}$) Gain (α_ω)	0.0327 0.75

6.1. Current Inner Loop

From the dynamic model given in (56) and assuming systems with unitary feedback, it is possible to obtain the closed-loop transfer function for current control given by:

$$H_{icl}(s) = \frac{H_i(s)}{1 + H_i(s)} = \frac{\frac{k_{pi}}{\sigma}(s + \alpha_i)}{s^2 + \left(\frac{R_{sr} + k_{pi}}{\sigma}\right)s + \frac{k_{pi}\alpha_i}{\sigma}}. \tag{64}$$

According to (64), the closed-loop current control has two poles whose location depends on the EFR parameters. Figure 12 shows the closed-loop poles' behavior when L_s and R_s parameters vary. According to Figure 12a, when L_s is increasing, the closed-loop poles are closer to the imaginary axis, which corresponds to a decrease in the system stability margin. In addition, large variations in armature inductance can move the closed-loop poles outside the desired region, which results in degradation of the controller performance. The R_s variation effect in the location of the closed-loop poles is presented in Figure 12b. While R_s is increasing, the complex closed-loop poles are closer to the real axis, which can result in a more dampened transient response. Furthermore, during the variation of R_s, the closed-loop poles are allocated within the desired region, which demonstrates the low influence of this parameter on the performance of current controllers.

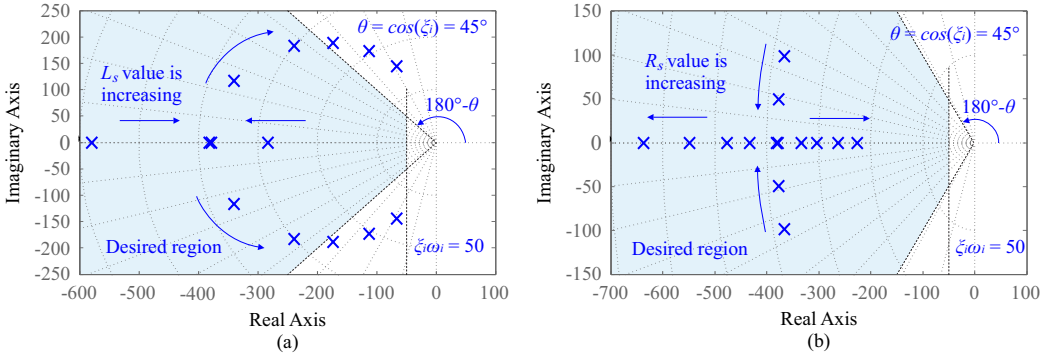

Figure 12. Closed-loop poles for current control when (**a**) L_s varies and (**b**) R_s varies.

6.2. Flux and Speed Outer Loop

From (60), it is possible to obtain a closed-loop transfer function which describes the flux dynamic behavior, given by:

$$H_{\lambda cl}(s) = \frac{H_\lambda(s)}{1 + H_\lambda(s)} = \frac{\frac{1{,}5L_{sr}k_{pi}k_{p\lambda}}{\tau_r\sigma}\left(s^2 + (\alpha_i + \alpha_\lambda)s + \alpha_i\alpha_\lambda\right)}{s^4 + a_3s^3 + a_2s^2 + a_1s + a_0}, \tag{65}$$

in which

$$a_3 = \frac{\tau_r\left(R_{sr} + k_{pi}\right) + \sigma}{\tau_r\sigma}, \tag{66}$$

$$a_2 = \frac{k_{pi}\left(1.5L_{sr}k_{p\lambda} + \tau_r\alpha_i + 1\right) + R_{sr}}{\tau_r\sigma}, \tag{67}$$

$$a_1 = \frac{1.5L_{sr}k_{pi}k_{p\lambda}(\alpha_i + \alpha_\lambda) + k_{pi}\alpha_i}{\tau_r\sigma}, \tag{68}$$

$$a_0 = \frac{1.5L_{sr}k_{pi}k_{p\lambda}\alpha_i\alpha_\lambda}{\tau_r\sigma}. \tag{69}$$

According to (65), the closed-loop system has four poles whose localization depends on the EFR parameters. Figure 13a,b shows the effect of L_r and R_r parameter variation in the position of the closed-loop poles for flux control. According to Figure 13a, when L_r is increasing, the non-dominant and dominant poles are closer to the imaginary axis, which corresponds to a decrease in the system stability margin. In addition, large variations in the rotor inductance move the closed-loop poles outside the desired region, which results in degradation of the desired dynamic response. On the other hand, according to Figure 13b, while R_r is increasing, the non-dominant and dominant poles are closer to the real axis, which can result in a less oscillatory transient response. Furthermore, during variation of R_r, the closed-loop poles are allocated within the desired region, which demonstrates its low influence on flux controller performance.

Similarly, considering the system described in (62), the closed-loop transfer function for speed control is given by:

$$H_{\omega cl}(s) = \frac{H_\omega(s)}{1 + H_\omega(s)} = \frac{\frac{k_{pi}k_{p\omega}}{J_r\sigma}\left(s^2 + (\alpha_i + \alpha_\omega)s + \alpha_i\alpha_\omega\right)}{s^4 + b_3s^3 + b_2s^2 + b_1s + b_0}, \tag{70}$$

in which

$$b_3 = \frac{J_r\left(R_{sr} + k_{pi}\right) + f_{rm}\sigma}{J_r\sigma}, \tag{71}$$

$$b_2 = \frac{k_{pi}\left(k_{p\omega} + J_r\alpha_i + f_{rm}\right) + f_{rm}R_{sr}}{J_r\sigma}, \tag{72}$$

$$b_1 = \frac{k_{pi}k_{p\omega}(\alpha_i + \alpha_\omega) + f_{rm}k_{pi}\alpha_i}{J_r\sigma}, \tag{73}$$

$$b_0 = \frac{k_{pi}k_{p\omega}\alpha_i\alpha_\omega}{J_r\sigma}. \tag{74}$$

Figure 13c,d show the closed-loop pole behavior of the speed control during variations in J_r and f_{rm}. According to Figure 13c, when J_r is increasing, the non-dominant poles are closer to the real axis, while the dominant poles are place outside the desired region and closer to the imaginary axis, which can result in a more oscillatory transient response and a decrease in the system stability margin. On the other hand, according to Figure 13d, when f_{rm} is increasing, the location of the non-dominant poles has negligible change, while the dominant poles are closer to the real axis, which can result in a more dampened transient response. However, the dominant poles are allocated within the desired region, which demonstrates the low influence of f_{rm} parameter variation on the speed controller performance.

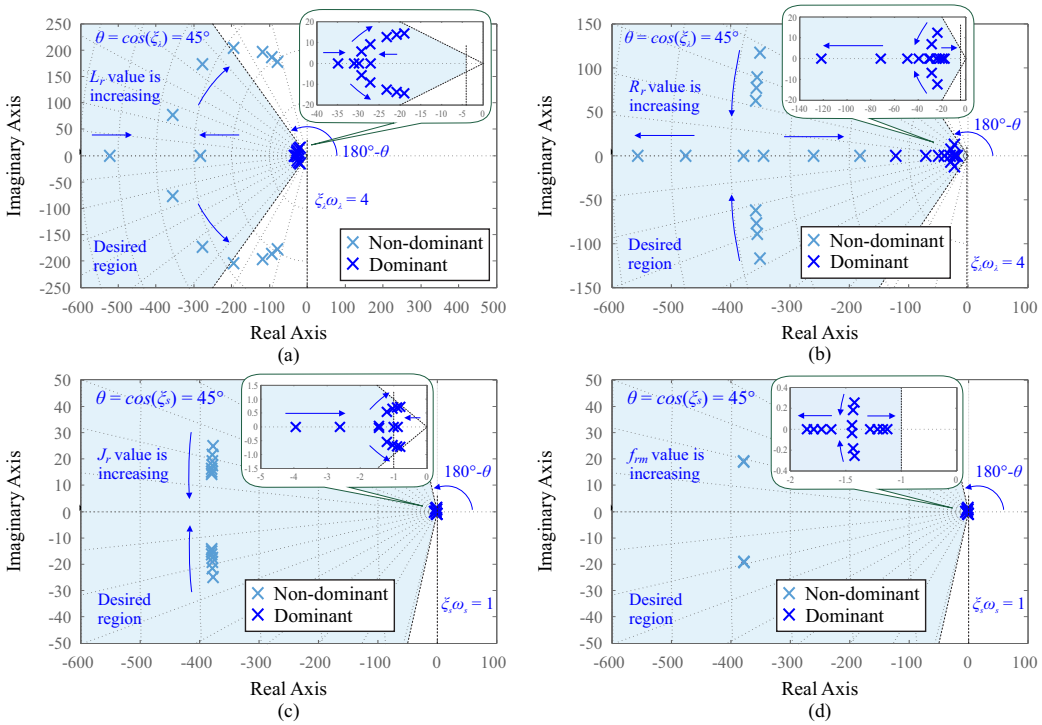

Figure 13. Closed-loop poles for (**a**) flux control when L_r varies, (**b**) flux control when R_r varies, (**c**) speed control when J_r varies and (**d**) speed control when f_{rm} varies.

7. Simulation and Experimental Results

The EFR-based system parameters for the simulation and experimental study are shown in Tables 1–3. The wind turbine parameters used for the simulation and experimental assays were taken from [22]. However, the turbine blade radius and the rated wind speed were adjusted to match the rated turbine and EFR power ratings.

Table 3. EFR-based system's parameters.

	Parameter	Value
Wind Turbine	Rated power	1.5 kW
	Blade radius	2 m
	Rated wind speed	8 m/s
	Air density	1.225 kg·m^3
	Power coefficient	0.411
	Inertia moment (J_a)	0.2 kg·m^2
	Friction factor (f_{am})	1.0 N·m/rad·s^{-1}
EFR and SG	Rated power	1.5 kW
	SG Poles number	4
	Rated voltage	380 V_{rms}
	Rated frequency	2π60 rad/s
VSC	DC-Link voltage (V_{DC})	900 V
	Switching frequency (f_s)	10 kHz

7.1. Simulation Results

To verify the effectiveness of the proposed performance analysis applied to the EFR-based system, the simulation of the system topology shown in Figure 2 has been carried out using the MATLAB/Simulink software.

7.1.1. Performance Analysis of the EFR Controllers

Figure 14 shows the dynamic response of the EFR controllers. According to Figure 14a, when the reference signal for the rotor flux changes from 0 to 1.2 Wb at 0 s, the instantaneous rotor flux tracks this reference value without steady-state error with settling time equal to 0.95 s, approximately. Then, Figure 14b shows that quickly, in approximately 0.075 s, the d-axis armature current reaches its reference value. Instantly at $t = 3.0$ s, a step from 0 to 188.5 rad/s is applied to the rotor-speed reference as depicted in Figure 14c. At this speed, as the synchronous generator has 4 poles, the voltage generated presents a frequency of 60 Hz. According to Figure 14c, the rotor speed reaches its reference value accurately in approximately 3.8 s without percent overshoot. This transition results in the application of an electromagnetic torque to the rotor proportional to the reference value for the q-axis armature current shown in Figure 14d. In this case, similar to the d-axis armature current, the q-axis armature current quickly tracks its reference value. Therefore, in relation to the adopted design criteria, the dynamic performance of the EFR controllers is within the desired limits.

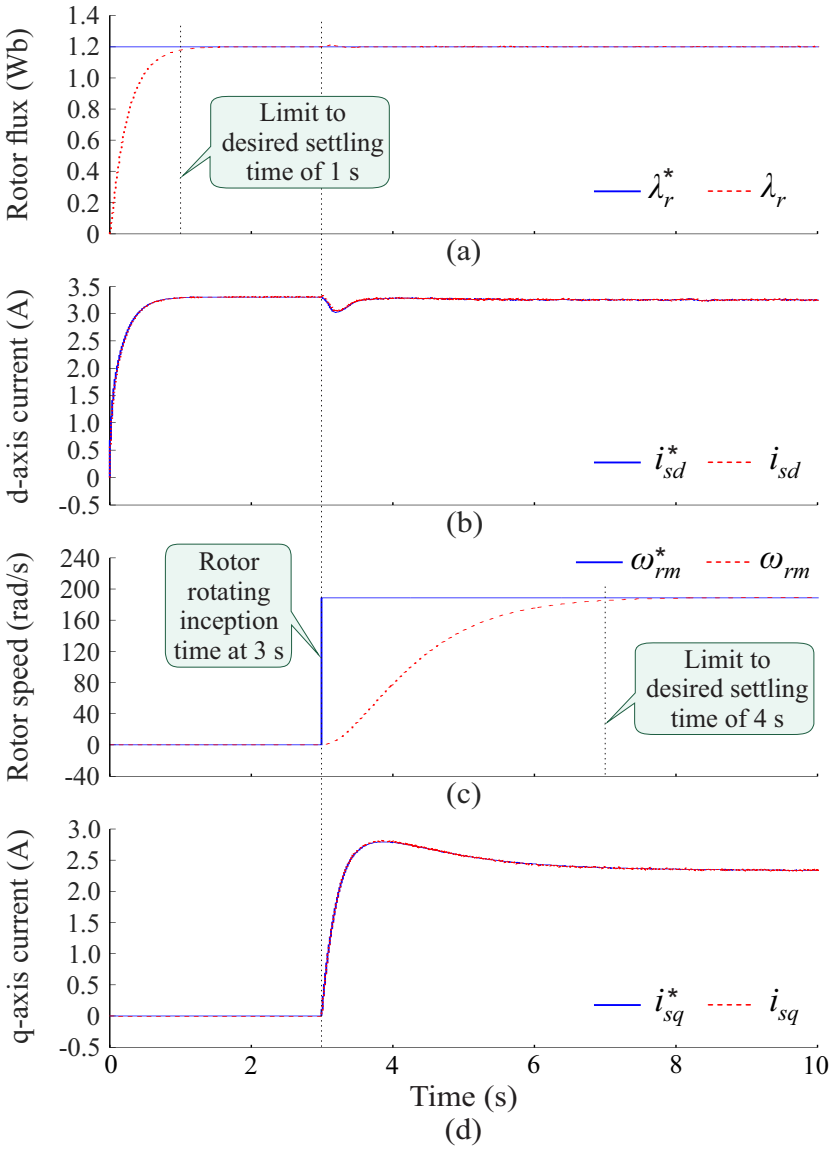

Figure 14. Dynamic responses from system's controllers (**a**) rotor flux controller, (**b**) d-axis armature current controller, (**c**) rotor speed controller and (**d**) q-axis armature current controller.

Figure 15 shows the speed controller dynamic response assuming variations in the J_r and f_{rm} parameters around their nominal values listed in Table 1. According to Figure 15a, adopting a 40% lower value for J_r, the rise time is reduced, while the settling time and percent overshoot do not change. On the other hand, adopting an 80% higher value for J_r, the speed controller transient response presents a higher rise time, settling time and percent overshoot. Then, Figure 15b illustrates the speed controller dynamic performance considering similar variations in f_{rm}. In this case, the effect of the variation in f_{rm} was small, since the controller transient responses were almost identical. Therefore, the speed controller dynamic performance assuming variation in J_r and f_{rm} is in accordance with the sensitivity analysis performed in the previous section.

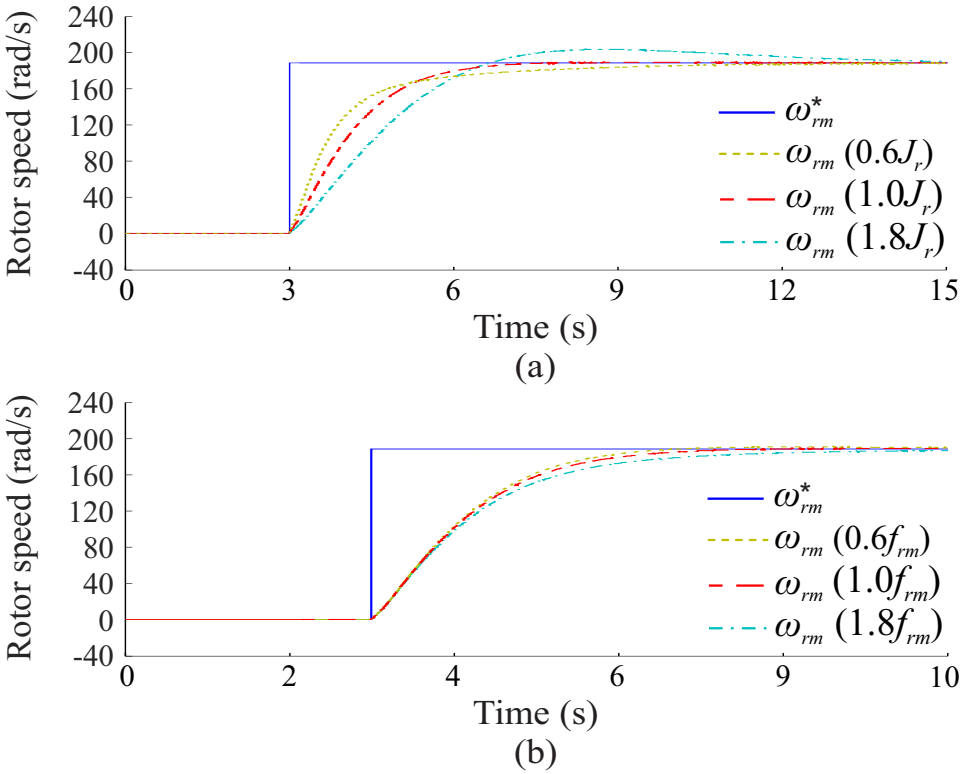

Figure 15. Dynamic response of the speed controller to (**a**) J_r variations and (**b**) f_{rm} variations.

7.1.2. System Performance Analysis Assuming Variations in Armature Speed

Figure 16 shows the effect of armature speed variation on rotor speed dynamic behavior. In addition, the relationship between armature speed and angular frequency of the armature and rotor currents is also presented. According to Figure 16a, the variations in the mechanical speed of the EFR armature shown in Figure 16b result in small oscillations in rotor speed. However, these oscillations quickly converge to the reference value, so that rotor speed remains constant during system operation. As indicated in Figure 16b,c, a change in the mechanical speed of the EFR armature results in a proportional change in the frequency of the armature currents, so that the absolute angular speed of the armature rotating field given in (1) always remains constant. In this case, the frequency of the rotor currents, which corresponds to the slip speed described in (2), also remains constant during variations in the armature rotating speed, as shown in Figure 16d.

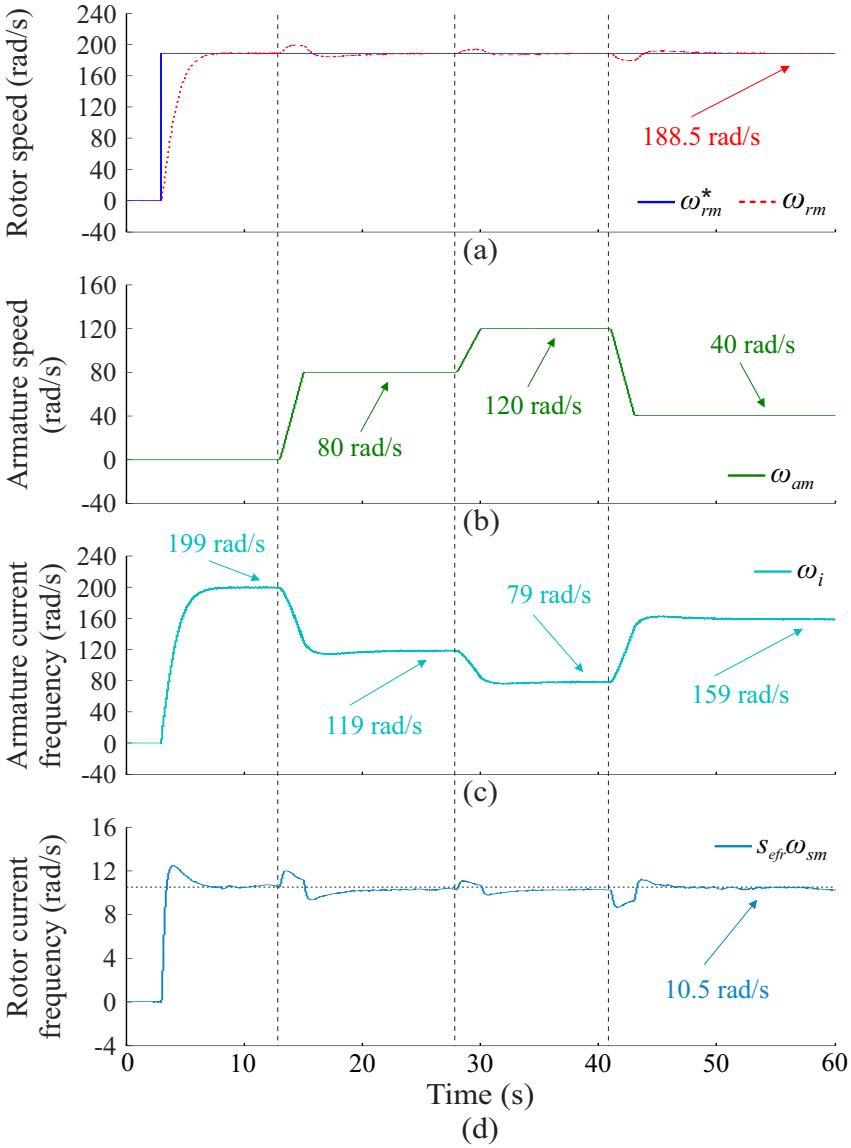

Figure 16. Relationship between mechanical speed and angular frequency in the EFR device: (**a**) EFR rotor speed, (**b**) EFR armature speed, (**c**) armature current frequency and (**d**) Rotor current frequency.

7.1.3. System Power-Sharing Analysis

Figure 17 shows power-sharing in the EFR-based system during armature speed variations. According to Figure 17a, in the interval from 3 to 13 s, the EFR rotor operates at a speed equal to 188.5 rad/s, while the armature shaft is in repose. In this interval, the power supplied by the primary source of the VSC is equal to the generated power of 1 kW (100%), as shown in Figure 17b,d, while the power supplied by the wind turbine is equal to zero (0%) as shown in Figure 17c. In the interval of 13 to 28 s, the armature speed reaches 80 rad/s, which results in the reduction of the power supplied by the VSC to 0.6 kW (60%) and in increasing the power supplied by the wind turbine to 0.4 kW (40%), as shown in Figure 17b,c, respectively. When the armature speed reaches 120 rad/s, which occurs in the interval of 28 to 41 s, the power supplied by the VSC and the wind turbine are 0.4 kW (40%) and 0.6 kW (60%), respectively. Finally, for $t > 41$ s, the armature speed decreases to 40 rad/s, which corresponds to a power supplied by the VSC of 0.8 kW (80%) and a power supplied by the wind turbine of 0.2 kW (20%). Based on these results, it is possible to share between the power supplied by the VSC and the wind turbine so that the power generated is always constant, as shown in Figure 17d. Therefore, the EFR-based system allows for

implementation of a hybrid generation system with two energy sources providing the resulting power to the power grid or to an isolated load.

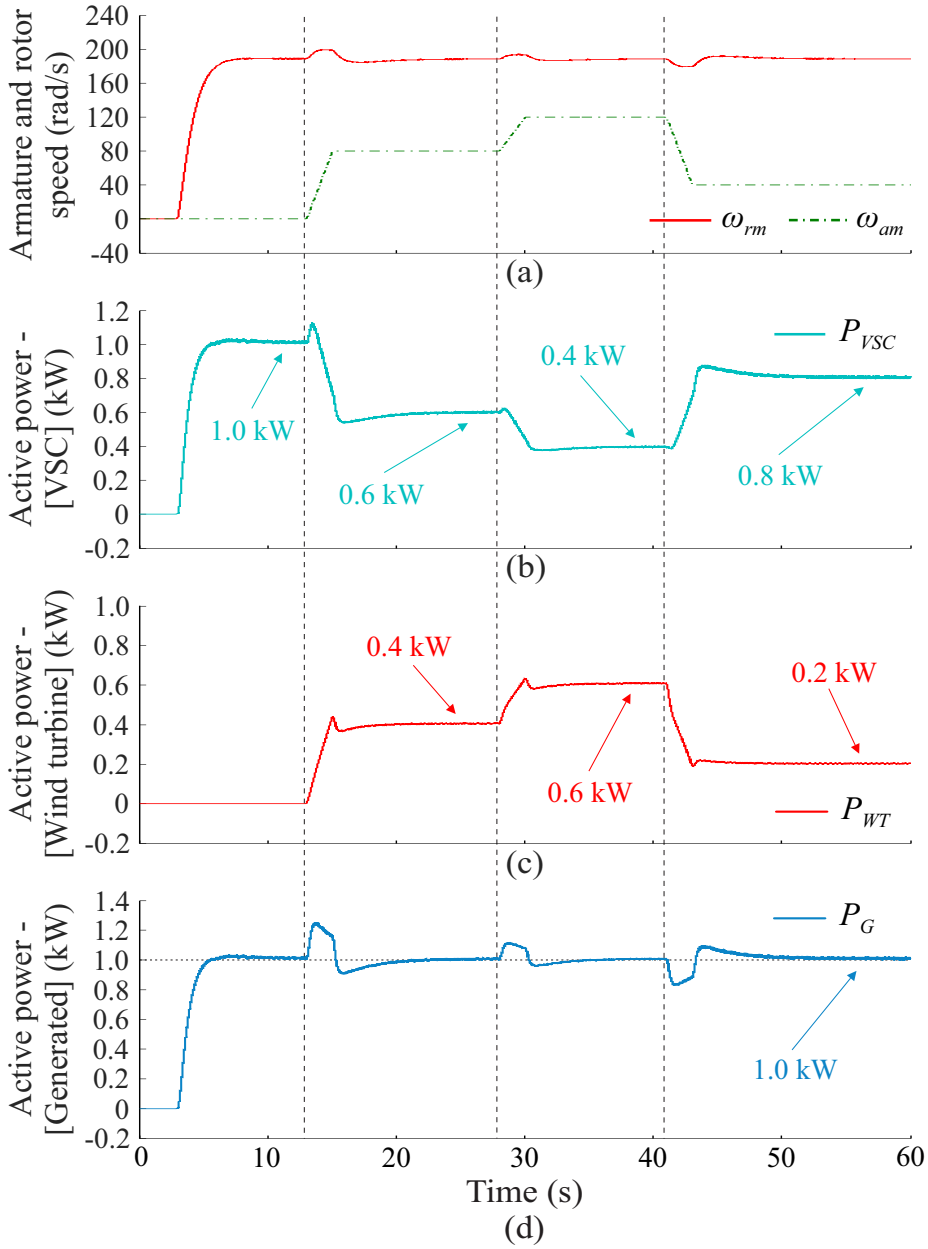

Figure 17. Power-sharing in the EFR-based system: (**a**) armature end rotor speed, (**b**) VSC active power, (**c**) wind turbine active power and (**d**) generated active power.

7.2. Experimental Results

To demonstrate the validity of the proposed performance analysis, experimental results were obtained using a laboratory setup to emulate the EFR-based system, as shown in Figure 18. In the experimental platform, a DC motor was used to emulate wind turbine behavior, as indicated in Figure 18c. Furthermore, the control algorithm was executed using a fast prototyping system DSP-TMS320f28335 with a sampling time of 100 µs. The measurement of instantaneous voltage and current values was performed using hall-effect sensors LV20-P and LAH25-NP, respectively.

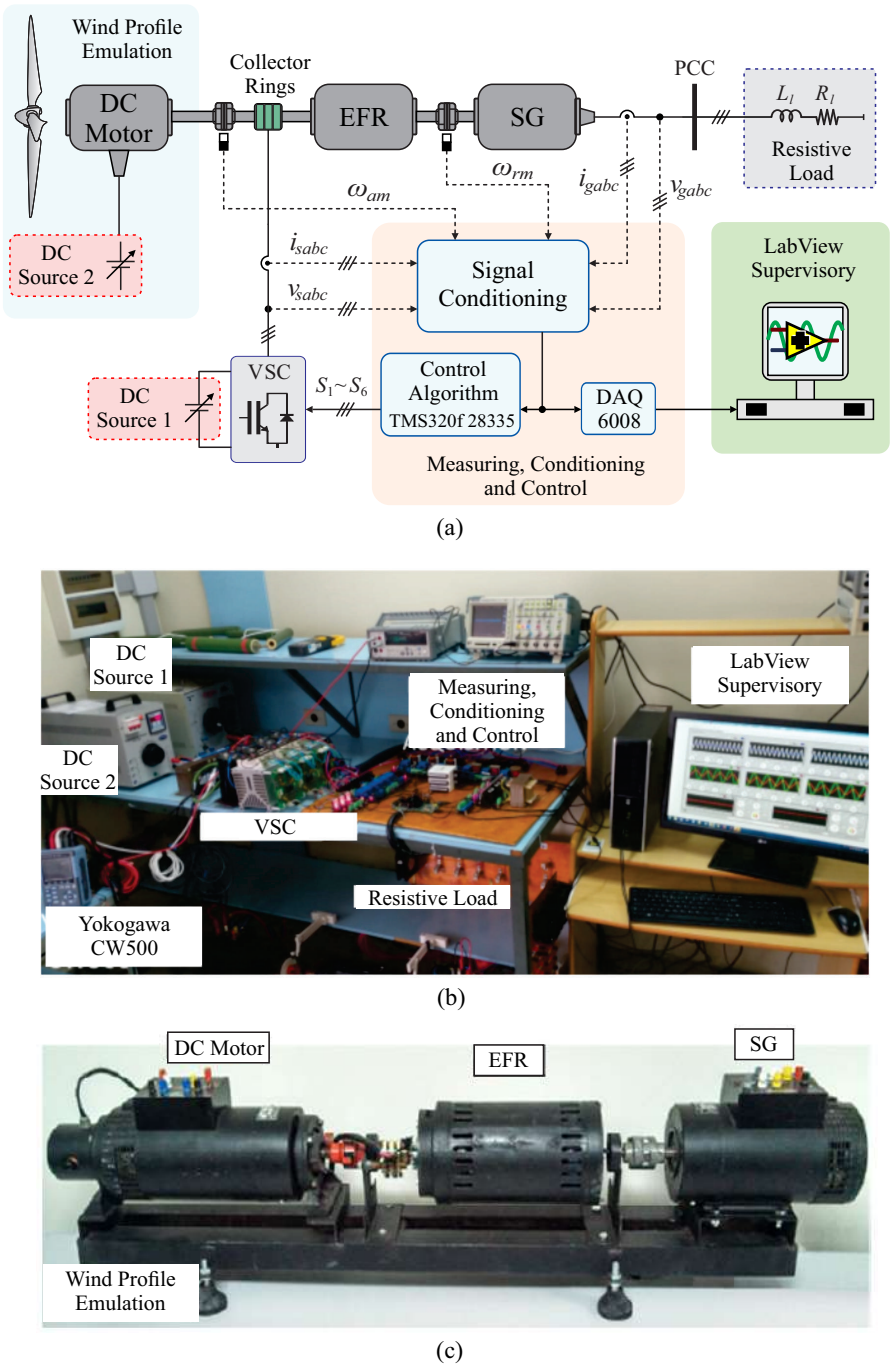

Figure 18. Experimental platform: (**a**) block diagram, (**b**) layout of laboratory equipment and (**c**) prototype machinery.

The experimental assays employed the same reference values for flux and speed control used in the simulation assays, which correspond to 1.2 Wb and 188.5 rad/s, respectively. Figure 19 shows the speed controller dynamic response. In addition, the generator a-phase armature voltage is also presented. According to Figure 19a, the rotor speed converges to the reference value without percent overshoot and with a transient response compatible with the design criteria adopted for the speed controller, as shown in Table 4. At $t = 28$ s, the rotational movement of the EFR armature is started. In this case, the DC motor that emulates the wind turbine is driven in order to establish an armature rotation speed equal to 50 rad/s (Figure 19a), approximately. According to Figure 19b, the amplitude and frequency of the voltage delivered to the resistive load remains constant different armature speeds, which is desired during system operation.

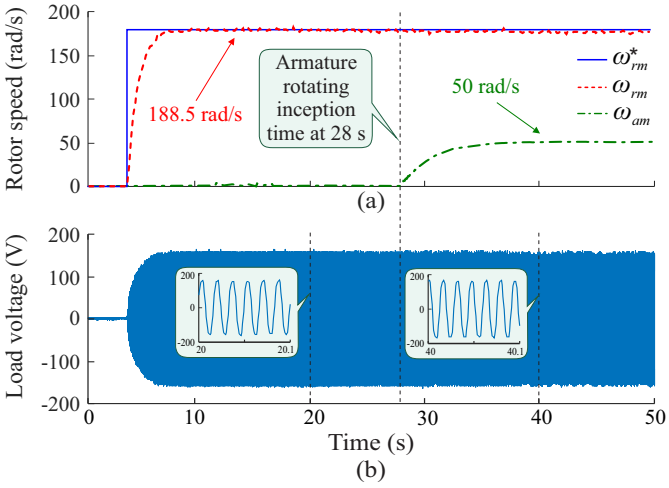

Figure 19. Experimental results for performance analysis of the EFR-based system: (**a**) rotor and armature speed and (**b**) load voltage.

Table 4. Comparison between simulation and experimental results.

		Simulation	Experimental
	Design Criteria	**Values Obtained**	**Values Obtained**
Speed Controller	Settling time $T_{s2\%} \leqslant 4$ s	3.8 s	4 s
	Percent overshoot $\%OS \leqslant 5\%$	0	0

8. Conclusions

This paper presented a performance analysis applied to an electromagnetic frequency regulator employed in distributed generation systems based on wind sources. Analyzes based on transient and steady-state response specifications indicated the influence of the variation of electromagnetic frequency regulator device parameters on its dynamic behavior. The paper also presented the design methodology of the system's controllers and a sensitivity analysis of the closed-loop poles which were validated through simulation and experimental results. This work serves as a complement to the previous related works and contributes to the proper operation of the electromagnetic frequency regulator device in distributed generation systems, since the control strategy has a great influence on the system dynamic performance. In addition, the electromagnetic frequency regulator device also allows the implementation of a hybrid generation system with the integration of photovoltaic energy to supply the power converter. Future work is needed to evaluate the electromagnetic frequency regulator dynamic behavior operating with more robust control strategies in relation to parametric variations and perturbations.

Author Contributions: T.F.d.N. and A.O.S. conceived and designed the study; T.F.d.N. and R.F.P., methodology; R.F.P., T.F.d.N. and E.A.D.F.N. performed the simulations and experiments; E.R.L.V., R.F.P. and A.O.S. reviewed the manuscript and provided valuable suggestions; T.F.d.N., R.F.P. and E.A.D.F.N. wrote the paper; A.O.S. supervised. All authors have read and agreed to the published version of the manuscript.

Funding: This research was funded in part by the Coordenação de Aperfeiçoamento de Pessoal de Nível Superior—Brasil (CAPES)—Finance Code 001 and Conselho Nacional de Desenvolvimento Científico e Tecnológico (CNPq).

Conflicts of Interest: The authors declare no conflict of interest.

Abbreviations

The following abbreviations are used in this manuscript:

DG	Distributed Generation
DC	Direct Current
DFIG	Doubly Fed Induction Generator
EFR	Electromagnetic Frequency Regulator
GB	Gearbox
HPWM	Hybrid Pulse Width Modulation
MPPT	Maximum Power Point Tracking
PCC	Point of Common Coupling
PI	Proportional-Integral
PMSG	Permanent Magnetic Synchronous Generator
RES	Renewable Energy Sources
RLM	Root-locus Method
SG	Synchronous Generator
SCIG	Squirrel Cage Induction Generator
VSC	Voltage-Source Converter

References

1. Akella, A.K.; Saini, R.P.; Sharma, M.P. Social, economical and environmental impacts of renewable energy systems. *Renew. Energy* **2009**, *34*, 390–396. [CrossRef]
2. Duan, Y.; Harley, R.G. Present and future trends in wind turbine generator designs. *IEEE Power Electron. Mach. Wind Appl.* **2009**, *1*, 1–6.
3. Global Wind Energy Council. Global Wind Report 2021. 2021. Available online: https://gwec.net/global-wind-report-2021/ (accessed on 4 May 2021).
4. Alhmoud, L.; Wang, B. A review of the state-of-the-art in wind-energy reliability analysis. *Renew. Sustain. Energy Rev.* **2018**, *81*, 1643–1651. [CrossRef]
5. Polinder, H.; Pijl, F.F.A.V.D.; Vilder, G.D.; Tavner, P.J. Comparison of direct-drive and geared generator concepts for wind turbines. *IEEE Trans. Energy Convers.* **2006**, *21*, 725–733. [CrossRef]
6. Herbet, G.J.; Iniyan, S.; Sreevalsan, E.; Rajapandian, S. A review of wind energy technologies. *Renew. Sustain. Energy Rev.* **2007**, *11*, 1117–1145. [CrossRef]
7. Thresher, R.; Robinson, M.; Veers, P. To capture the wind. *IEEE Power Energy Mag.* **2007**, *5*, 34–46. [CrossRef]
8. Yaramasu, V.; Wu, B.; Sen, P.C.; Kouro, S.; Narimani, M. High-power wind energy conversion systems: State-of-the-art and emerging technologies. *Proc. IEEE* **2015**, *103*, 740–788. [CrossRef]
9. Perez, J.M.P.; Marquez, F.P.G.; Tobias, A.; Papaelias, M. Wind turbine reliability analysis. *Renew. Sustain. Energy Rev.* **2013**, *23*, 463–472. [CrossRef]
10. Mckenna, R.; Leye, P.O.V.D.; Fichtner, W. Key challenges and prospects for large wind turbines. *Renew. Sustain. Energy Rev.* **2016**, *53*, 1212–1221. [CrossRef]
11. Vitor Silva, P.; Ferreira Pinheiro, R.; Ortiz Salazar, A.; do Santos Junior, L.P.; de Azevedo, C.C. A Proposal for a New Wind Turbine Topology Using an Electromagnetic Frequency Regulator. *IEEE Lat. Am. Trans.* **2015**, *13*, 989–997. [CrossRef]
12. Silva, P. V.; Pinheiro, R.F.; Salazar, A.O.; Fernandes, J.D. Performance analysis of a new system for speed control in wind turbines. *Renew. Energy Power Qual. J.* **2015**, *1*, 455–460. [CrossRef]
13. Silva, P.V.; Pinheiro, R.F.; Salazar, A.O.; Júnior, L.P.S.; Fernandes, J.D. A New System for Speed Control in Wind Turbines using the Electromagnetic Frequency Regulator. *Eletrônica Potência* **2015**, *20*, 254–262. [CrossRef]
14. Ramos, T.; Júnior, M.M.; Pinheiro, R.; Medeiros, A. Slip Control of a Squirrel Cage Induction Generator Driven by an Electromagnetic Frequency Regulator to Achieve the Maximum Power Point Tracking. *Energies* **2019**, *12*, 2100. [CrossRef]
15. Da Silva, J.C.L.; Ramos, T.; Júnior, M.F.M. Modeling and Harmonic Impact Mitigation of Grid-Connected SCIG Driven by an Electromagnetic Frequency Regulator. *Energies* **2021**, *14*, 4524. [CrossRef]
16. Do Nascimento, T.F.; Nunes, E.A.F.; Salazar, A.O. Modeling and Controllers Design for an Electromagnetic Frequency Regulator Applied to Wind Systems. In Proceedings of the 2021 Brazilian Power Electronics Conference (COBEP), João Pessoa, Brazil, 7–10 November 2021; pp. 1–8.
17. Blasko, V. Analysis of a hybrid PWM based on modified space-vector and triangle-comparison methods. *IEEE Trans. Ind. Appl.* **1997**, *33*, 756–764. [CrossRef]
18. De Doncker, R.W.; Novotny, D.W. The universal field oriented controller. *IEEE Trans. Ind. Appl.* **1994**, *30*, 92–100. [CrossRef]
19. Jacobina, C.B. ; Lima, A.M.N. Estratégias de Controle Para Sistemas de Acionamento Com Máquina Assíncrona. *SBA Controle Automação* **1996**, *7*, 15–28.
20. Nise, N.S. *Control Systems Engineering*, 6th ed.; John Wiley & Sons, Inc.: Hoboken, NJ, USA, 2011.

21. Li, Y.W. Control and Resonance Damping of Voltage-Source and Current-Source Converters with *LC* Filters. *IEEE Trans. Ind. Electron.* **2009**, *56*, 1511–1521.
22. Kim, K.; Van, T.L.; Lee, D.; Song, S.; Kim, E. Maximum Output Power Tracking Control in Variable-Speed Wind Turbine Systems Considering Rotor Inertial Power. *IEEE Trans. Ind. Electron.* **2013**, *60*, 3207–3217. [CrossRef]

energies

MDPI

Article

A Novel Driving Scheme for Three-Phase Bearingless Induction Machine with Split Winding

Francisco Elvis Carvalho Souza [1,†], Werbet Silva [2,†], Andrés Ortiz Salazar [2,†], José Paiva [1,†], Diego Moura [2,†] and Elmer Rolando Llanos Villarreal [3,*,†]

1 The Federal Institute of Education, Science and Technology of Rio Grande do Norte (IFRN), Natal 59015-000, Brazil; elvis.carvalho@ifrn.edu.br (F.E.C.S.); alvaro.paiva@ifrn.edu.br (J.P.)
2 Department of Computer Engineering and Automation, Federal University of Rio Grande do Norte (DCA-UFRN), Natal 59072-970, Brazil; werbethluizz@hotmail.com (W.S.); andres@dca.ufrn.br (A.O.S.); diegomoura@dca.ufrn.br (D.M.)
3 Department of Natural Sciences, Mathematics, and Statistics, Federal Rural University of Semi-Arid (DCME-UFERSA), Mossoró 59625-900, Brazil
* Correspondence: elmerllanos@ufersa.edu.br
† These authors contributed equally to this work.

Abstract: In order to reduce the costs of implementing the radial position control system of a three-phase bearingless machine with split winding, this article proposes a driving method that uses only two phases of the system instead of the three-phase traditional one. It reduces from six to four the number of inverter legs, drivers, sensors, and current controllers necessary to drive and control the system. To justify the proposal, this new power and control configuration was applied to a 250 W machine controlled by a digital signal processor (DSP). The results obtained demonstrated that it is possible to carry out the radial position control through two phases, without loss of performance in relation to the conventional three-phase drive and control system.

Keywords: bearingless; DSP; induction motor; radial position control

check for updates

Citation: Carvalho Souza, F.E.; Silva, W.; Ortiz Salazar, A.; Paiva, J.; Moura, D.; Villarreal, E.R.L. A Novel Driving Scheme for Three-Phase Bearingless Induction Machine with Split Winding. *Energies* **2021**, *14*, 4930. https://doi.org/10.3390/en14164930

Academic Editor: Mohamed Benbouzid

Received: 5 July 2021
Accepted: 6 August 2021
Published: 12 August 2021

Publisher's Note: MDPI stays neutral with regard to jurisdictional claims in published maps and institutional affiliations.

Copyright: © 2021 by the authors. Licensee MDPI, Basel, Switzerland. This article is an open access article distributed under the terms and conditions of the Creative Commons Attribution (CC BY) license (https://creativecommons.org/licenses/by/4.0/).

1. Introduction

Bearingless machines use magnetic forces to support the rotor shaft, reducing losses, and maintenance due to mechanical wear [1].

Among the topologies of bearingless machines developed in recent years, three-phase bearingless induction machines. In these machines, there are two windings in the stator, a 4-pole winding for torque production and an additional 2-pole winding to promote magnetic bearing of the rotor [2–5]. In these works, both windings are three-phase and, therefore, driven by three-phase inverters, one inverter for each winding, this increases the complexity and cost of the drive. An important variant of this machine is the three-phase induction bearingless motor with split winding. In this type of machine, there is only one winding in the stator responsible for simultaneously producing the torque and promoting the magnetic support of the rotor [6–9]. These works have the advantage of reducing the space required for the windings, making the machine more compact and, therefore, lighter. However, the coils of each phase are divided into two groups so that the current in each group is individually controlled. This results in the need to separately control six currents leading to a relatively more complex and costly drive structure as a six-legged voltage inverter, six current sensors, two-position sensors, and other auxiliary components as power sources are required. power supply, signal conditioning boards, and digital signal processors.

In order to reduce this drive structure and consequently costs, this work proposes a driving scheme that uses only two-phase currents to control the radial position of the rotor. The current of the third phase necessary for the operation of the machine is obtained by

the composition of the two controlled currents. This approach reduces from six to four the number of inverter legs, drivers, and current sensors.

There are other proposals to reduce the costs of starting driving and controlling a bearingless motor without a bearing as in [10,11]. However, they are special motors (disk shape) intended for specific applications. Induction motors are robust, low cost, widely used in industry, and extremely reliable [12,13].

The driving of three-phase loads using only two phases is nothing new, Refs. [14,15] show studies that confirm the possibility of this type of drive, Ref. [16] presents the two-phase drive of a conventional three-phase motor. Applying the two-phase driving scheme in a three-phase bearingless induction machine with split winding is a new and challenging study once in this system, the control signal for radial position control is superimposed on the current signals produce torque.

This work sought to validate the reduced drive structure as a new way to drive motors without split winding bearings. In this way, the results presented in this text cover the addition of the current control in the machine coils and the radial position control. This is an intermediate step for a more complete analysis of the dynamic performance of the studied motor, which paves the way for the complete dynamics of the system, including the torque and speed control loops, to be studied in future works.

The proposed technique was implemented in a three-phase induction bearingless machine whose radial rotor position is actively controlled with two degrees of freedom. For that, the digital signal processor (DSP) TMS320F28335® from Texas Instruments was used. The experimental results without demonstrated the strategy's viability loss of performance of the prototype [17].

2. Radial Forces Generation

Figure 1 shows the process of generating radial position forces on the rotor shaft of a bearingless machine with split windings. For simplicity, only the phase$-A$ group of windings are represented.

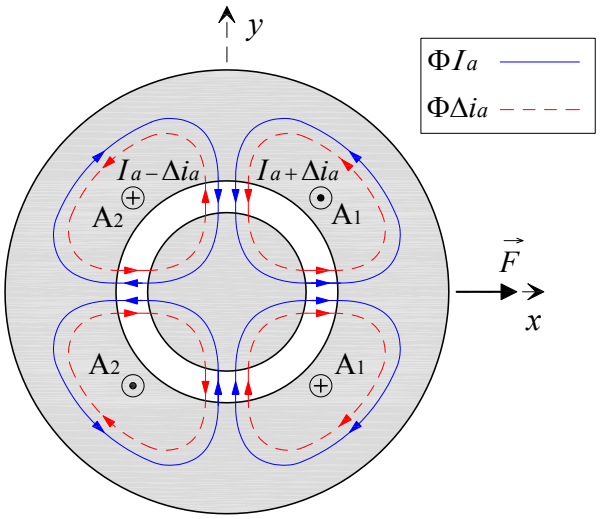

Figure 1. Magnetic flux produced by coils A_1 and A_2. Where ΦI_a and $\Phi \Delta i_a$ are the magnetic fluxes generated by currents I_a and Δi_a, respectively.

By feeding coils A_1 and A_2 with the same current I_a, a magnetic flux ΦI_a is created as shown by the continuous blue lines in the Figure 1. When the rotor is centralized on the center of the stator, the magnetic flux densities in both air gaps along the x-axis are equal and, therefore, there is no net radial force acting on the rotor.

Suppose a value of Δi_a is added to the current of coil A_1 and this same value is simultaneously subtracted from the coil A_2, an additional magnetic flux $\Phi \Delta i_a$, represented by red dashed lines, appears through the magnetic circuit of the Figure 1. The direction of

the incremental magnetic flux generated by Δi_a is such that it flows in the same direction of the flux of A_1 and in the opposite direction of the flux of A_2. This effect makes the total magnetic flux unbalanced and then produces a radial magnetic force in the positive direction of the x-axis of the rotor. In the vertical direction, the additional flux is canceled and, consequently, there are no resultant forces in this direction.

By means of the differential action on the currents that flow through the two coils, forces can be generated to centralize the position of the rotor in the center. This effect is the same in all pairs of opposing coils, and the force obtained acts along the axis that passes through the center of them. Therefore, in a three-phase machine, positioning forces can be controlled in any direction of the transverse plane, superimposing the effects along the three actuation axes formed by the coil pairs, as shown in Figure 2.

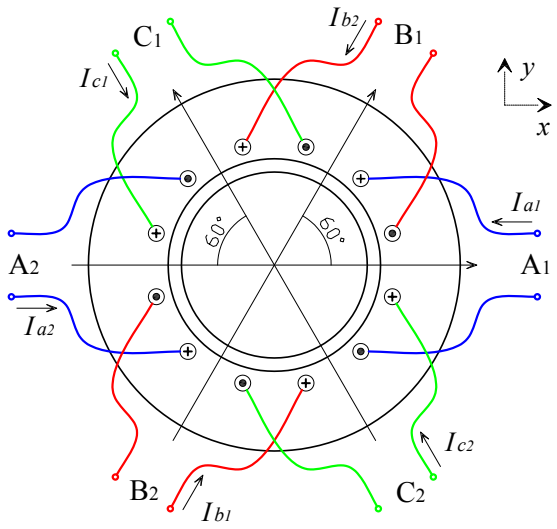

Figure 2. Arrangement of the windings in the stator.

3. The Drive System

Independent of the control system used (conventional three-phase or two-phase), the bearingless machine with split winding must be fed on its 06 (six) coils to ensure radial positioning and the desired torque. The difference between the systems mentioned is essentially in the number of switches to be controlled. The use of the three-phase drive system requires a drive structure with 12 (twelve) static switches of the IGBT type. Choosing the two-phase system to perform the same task, it will be necessary to control only 08 (eight) keys of the same model, resulting in benefits such as the reduction in costs and dimensions of the power driver, in addition to reducing the computational load on the DSP. In this context, the DSP is the device responsible for all system control steps including: PID type radial position control algorithms and PI type current control algorithms, in addition to generating the pulse width modulation (PWM) signals responsible for the drive static switches (IGBTs). PWM signals are generated by comparing reference currents, with a triangular 10 kHz frequency carrier. After the comparison, the generated PWM signals are made available on the microcontroller's digital outputs. As the signals supplied by the DSP operate at voltages from 0 to 3.3 Volts, an interface circuit is used to convert them to voltages from −8 to 15 V in order to meet the IGBTs driver specifications. The composition of the PWM signals applied to the static switches allows the flux of currents originating from the DC bus available in the DC–AC converter to the machine's winding. Thus, the main difference between the three-phase conventional and two-phase drive systems is in the number of controlled coils. In the three-phase system, 06 (six) reference currents are needed to obtain the desired radial position control, as shown in Figure 3. So that phase A current is a vector composition of the controlled currents of phases B and C, as shown in Figure 4. Using the proposed two-phase system, one of the phases is put to operate in the configuration shown in Figure 5.

3.1. Conventional Driving Technique

The stator winding comprises six groups of equal coils, two per phase, as shown in Figure 2. In order to implement position control, the currents of each group of coils must be controlled separately. For this, a drive circuit is used, composed of six single-phase inverters, as shown in Figure 3. Each inverter controls the current of a coil group.

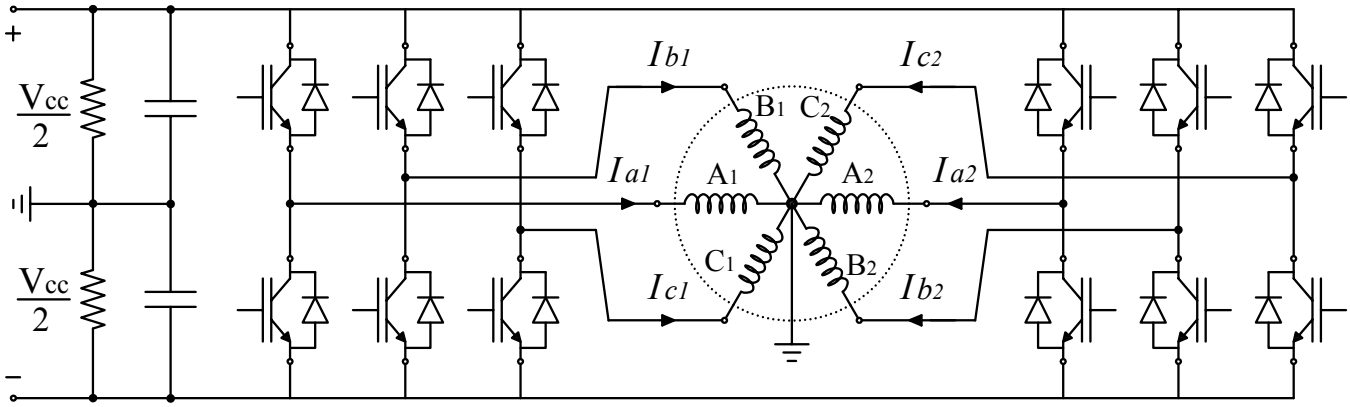

Figure 3. Conventional drive circuit.

In order to guarantee the rotating magnetic field integrity, two coil groups of the same pair (same phase) must be fed by currents of the same phase but 120° out of phase with the other pairs' currents.

3.2. Winding Currents Composition

Traditionally, the bearingless induction motor with split winding is controlled by six currents generated from the three-phase currents I_a, I_b, and I_c, which are modulated by the radial positioning components, Δi_a, Δi_b, and Δi_c as shown in the set of Equation (1).

$$\begin{aligned} I_{a1} &= I_a + \Delta i_a \\ I_{a2} &= I_a - \Delta i_a \\ I_{b1} &= I_b + \Delta i_b \\ I_{b2} &= I_b - \Delta i_b \\ I_{c1} &= I_c + \Delta i_c \\ I_{c2} &= I_c - \Delta i_c \end{aligned} \tag{1}$$

The positioning components Δi_a, Δi_b, and Δi_c are obtained through the vector transformation (2) of the orthogonal position control signals Δi_x and Δi_y.

$$\begin{bmatrix} \Delta i_a \\ \Delta i_b \\ \Delta i_c \end{bmatrix} = \mathbf{T} \begin{bmatrix} sin(\omega t) & -cos(\omega t) \\ -cos(\omega t) & -sin(\omega t) \end{bmatrix} \begin{bmatrix} \Delta i_x \\ \Delta i_y \end{bmatrix} \tag{2}$$

where:

$$\mathbf{T} = \begin{bmatrix} 1 & 0 \\ \frac{1}{2} & \frac{\sqrt{3}}{2} \\ -\frac{1}{2} & \frac{\sqrt{3}}{2} \end{bmatrix} \tag{3}$$

The differential application of the positioning components in (1) prevents them from interfering with conjugate [7]. The following analysis can verify this: for example, if the increase in current Δi_b in coil B_1 (Figure 2) causes an increase in torque, subtracting the same value in the current from B_2 will decrease the torque in the same proportion,

maintaining the contribution of phase B conjugate invariant concerning Δi_b. The same behavior occurs in the coil pairs of phases A and C.

3.3. Proposed Driving Technique

The driving technique proposed in this work makes it possible to control the rotor's radial position by controlling only two of the machine's three-phase currents. It can be seen in Figure 2 that the coils of phases B and C are aligned to no-orthogonal axes. These axes, represented in Figure 4 as b-axis and c-axis, form a system of non-orthogonal coordinates capable of composing forces in any direction of the plane. Thus, the radial position's control can be obtained by adding control actions only in phases B and C, leaving the current of phase A free from control.

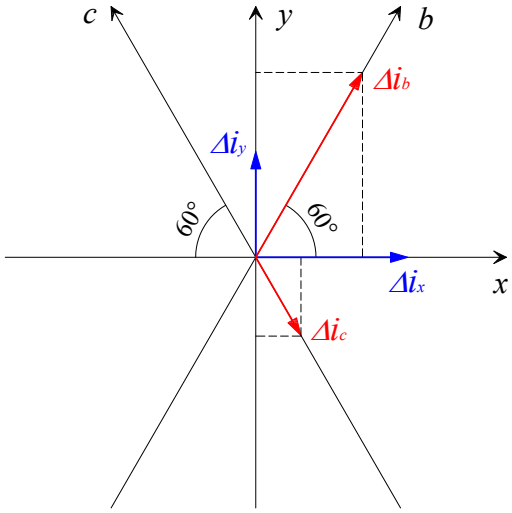

Figure 4. Transformation of coordinates.

In prototype, the position sensors are arranged in orthogonal directions. Therefore, it is necessary to transform the control actions of the x-axis and y-axis system (orthogonal) to the b-axis and c-axis system. From Figure 4 it obtain:

In the prototype, the position sensors are arranged in orthogonal directions. Therefore, it is necessary to transform the x-axis and y-axis system's control actions (orthogonal) to the b-axis and c-axis system. From Figure 4, it obtains:

$$\begin{bmatrix} \Delta i_b \\ \Delta i_c \end{bmatrix} = \begin{bmatrix} 1 & \frac{\sqrt{3}}{3} \\ -1 & \frac{\sqrt{3}}{3} \end{bmatrix} \begin{bmatrix} \Delta i_x \\ \Delta i_y \end{bmatrix} \tag{4}$$

3.4. Obtaining the Winding Currents

Modulating the polarization currents I_b and I_c with the respective position control components Δi_b and Δi_c generate the currents of the B_1, B_2, C_1, and C_2 coils. The following set of equations achieves the modulation:

$$\begin{aligned} I_{b1} &= (I_m + \Delta i_b)cos(\omega t - \frac{2\pi}{3}) \\ I_{b2} &= (I_m - \Delta i_b)cos(\omega t - \frac{2\pi}{3}) \\ I_{c1} &= (I_m + \Delta i_c)cos(\omega t + \frac{2\pi}{3}) \\ I_{c2} &= (I_m - \Delta i_c)cos(\omega t + \frac{2\pi}{3}) \end{aligned} \tag{5}$$

where I_m is the amplitude of the currents in Amperes, ω is the angular frequency in rad/s, and t is time in seconds.

For the drive, the circuit of Figure 5 obtained by modifying the conventional drive circuit was proposed. Two two-phase inverters were used. Each inverter has 2 IGBT SKM 75GB 176 DN modules. The scalar PWM modulation technique was used, in which the sinusoidal references are generated by the processor. The PWM signals are sent switches through SKHI 23/17 drivers.

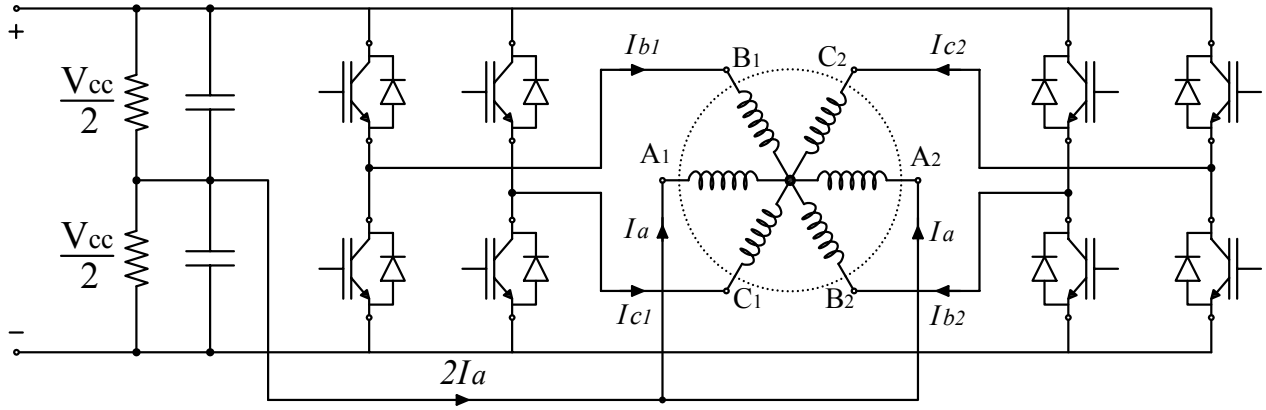

Figure 5. Proposed driving circuit.

The phase A currents can be determined from the circuit analysis in Figure 5 as follows:

$$I_a + I_a + I_{b1} + I_{b2} + I_{c1} + I_{c2} = 0 \quad (6)$$

$$2I_a = -(I_{b1} + I_{b2} + I_{c1} + I_{c2}) \quad (7)$$

Replacing the currents I_{b1}, I_{b2}, I_{c1} and I_{c2} with the values presented in Equation (5) it is obtained:

$$2I_a = 2I_m cos(\omega t) \quad (8)$$

$$I_a = I_m cos(\omega t) \quad (9)$$

It is important to note that current I_a is 120° out of phase with other currents, thus composing a three-phase set of currents. Furthermore, the current I_a is not affected by the modulation components Δi_b and Δi_c.

For experimental validation of the drive structure, control of system variables, and collection of results obtained from a DSP from The Texas Instruments model TMS320F28335. This processor is part of the C2000 processor family. It is a 32-bit microcontroller with Havard-modified architecture in which the instruction bus is separate from the data bus. The CPU performs floating point operations and the hardware has a specific AD converter and PWM generation module for driving and controlling machines.

4. Control Diagram

To acquire data from the system, we used a tool embedded on the DSP: an interface that allows loading data and transfer to Matlab in which we fill vectors with data and hold them in the Matlab workspace to display them. Furthermore, the rotor position in mm was determined from the measurement of the air gap length. Then, this value was related to the digital information generated by the DSP AD converter from the response curve of the position sensors.

As it is shown in the Figure 6 the control scheme is composed of two loops: an external one for radial position control of the rotor on the axes X and Y and an internal one that controls the current on the machine windings. Displacement sensors by eddy currents model PU-05, coupled to an AEC-55 signal converter detect the radial position of the rotor in the xy plane. Then these signals are compared with the X_{ref} and Y_{ref} position references, and the error signals feed PID controllers to calculate the orthogonal control signals Δi_x and

Δi_y. These values are transformed by (4) to obtain the components Δi_b and Δi_c. Then, the components are added to the currents I_b and I_c to generate the references I^*_{b1}, I^*_{b2}, I^*_{c1} and I^*_{c2} to current controllers. The current control is performed by four identical and independent PI controllers. Position control is performed by two identical PID controllers.

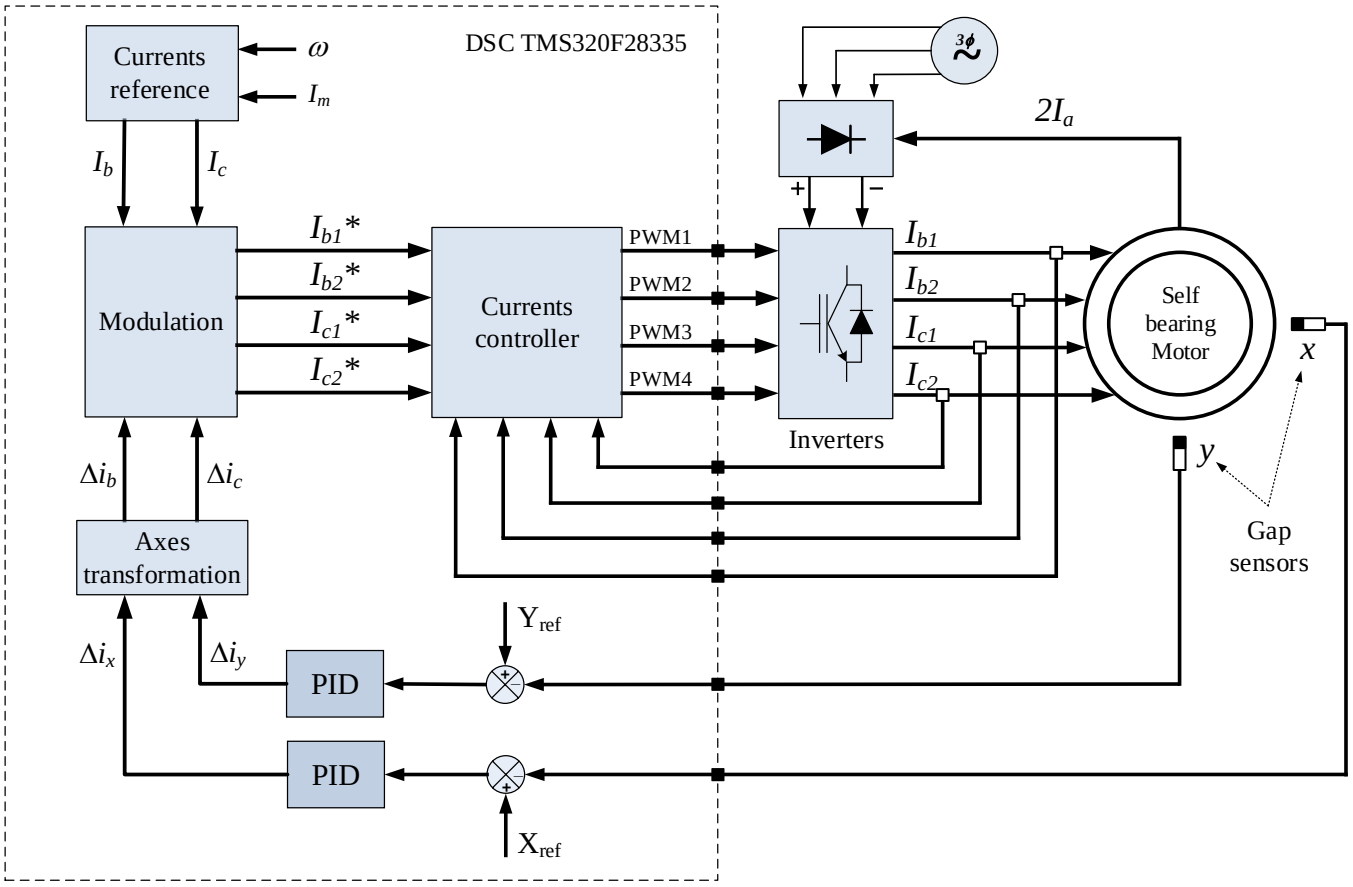

Figure 6. Control diagram.

Control is performed by a digital signal processor (DSP), the TMS320F28335® from Texas Instruments®. It was chosen 10 kHz as inverter's switching frequency. This same frequency was used to sample the signals.

This first part of the research focused only on the control rotor radial position, so the torque and speed control loops were not included.

5. Prototype Description

The bearingless machine used in the experiments is a three-phase induction machine with four active and consequent poles. The stator winding consists of six groups of coils (two groups per phase) with three coils in each group. The machine core is made of laminated ferrosilicon. Table 1 shows the main parameters of the bearing used motor.

A wound rotor with a ferrosilicon laminated core was used Figure 7. It is structural electrical is composed by four coils groups in a four-pole arrangement.

The bearingless machine operates in a vertical position and without radial bearings on the upper shaft end and a pivot bearing on the lower end. There is only one bearing at the bottom end to allow pivoting movement. Figure 8 shows a cross-section of the machine with mechanical details and its dimensions. Figure 9 shows a real image of the prototype used in the experiments.

Table 1. Bearingless Induction Machine Parameters.

Parameter	Description	Values
P_n	Rater power	250 W
L	Average windings inductance	16.5 mH
R	Average windings resistance	1.1 Ω
V_n	Rated voltage	115 V
I_n	Rated current	2.5 A
N_p	Number of stator and rotor poles	4
N	Number of turns	120 Spirals
N_{ss}	Number of stator slots	36
N_{rs}	Number of rotor slots	48
I_r	Transversal inertia moment	0.1454 kg·m^2
W_r	Rotor weight	3.5 kg

Figure 7. Rotor image.

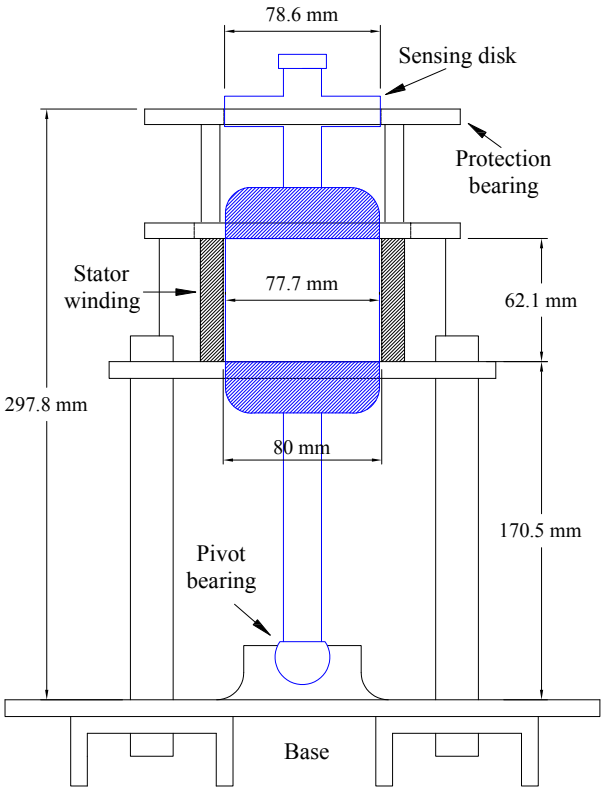

Figure 8. The cross-section view of the bearingless motor.

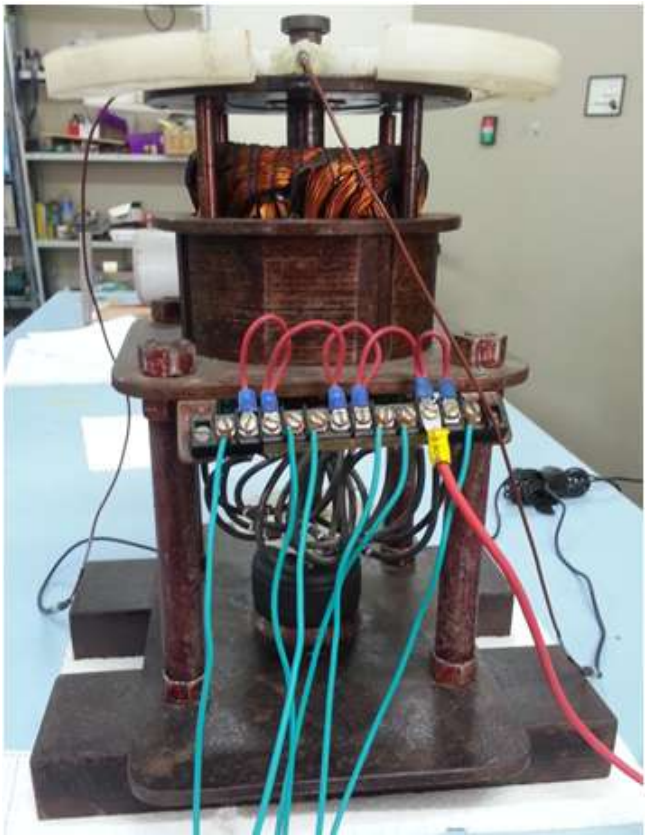

Figure 9. Image of the prototype of the bearing motor.

6. Experimental Results

As described in Section 4 and shown in the control diagram in Figure 6, the control system is formed by two loops, an internal one to control the currents, and an external one that controls the radial position of the rotor. In this study, speed and torque control was not contemplated, so the speed was in an open loop. The speed control study is ongoing, and its results will be published as soon as they are completed. The current control was performed by proportional integrative (PI) controllers tuned by empirical adjustments. For this, the rotor axis was fixed in the center of the stator to avoid its radial displacement and the consequent variation in the winding inductances. The radial position controller was disabled so as not to interfere with the tuning of the current controllers.

Two sinusoidal signals, free of position control modulation, with 60 Hz frequency and 1 A amplitude, 120° out of phase, were applied as current references to the controllers.

After a series of tests and empirical adjustments, the parameters obtained for each current controller are shown in the Table 2. Table 2 shows the parameters of all controllers implemented in this study. To define the Yref and Xref values, we measure the maximum gap length and positioned the rotor radially at the center of the gap.

Table 2. Implemented controllers parameters .

Controller Name	Two-Phase Driving			Three-Phase Driving		
Parameters	k_p	k_i	k_d	k_p	k_i	k_d
Current Control (PI)	150	1500	–	150	1500	–
Position Control (PID)	6×10^{-4}	4×10^{-3}	9×10^{-6}	8×10^{-4}	3×10^{-3}	15×10^{-6}

The dynamic behavior of the radial position control depends on the performance of the current control system applied to the currents of phases B and C. Thus, before presenting the results regarding the radial position control, it is important to check the response of the current controllers.

Figure 10 shows the phase-A (I_{a1} and I_{a2}), phase-B (I_{b1} and I_{b2}), and phase-C (I_{c1} and I_{c2}) with their respective references (dashed lines).

Despite some distortion level, Figure 10 indicates that the controlled currents of phases B and C are sinusoidal and follow the references satisfactorily. It is also possible to see that the uncontrolled current of phase A has the same behavior. This is an important result since it shows that the proposed drive technique is suitable for the application.

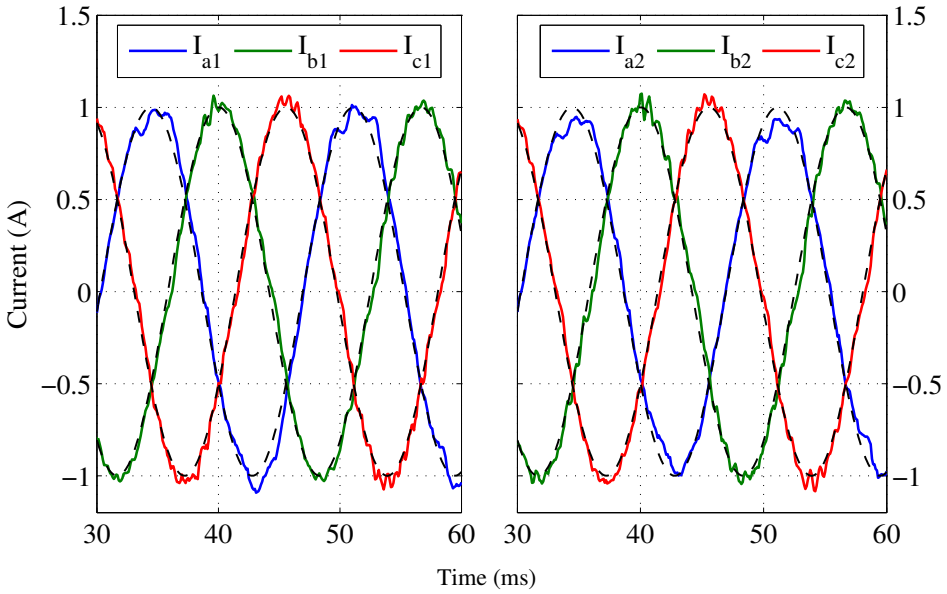

Figure 10. Current controllers output to sinusoidal reference inputs. The currents I_{b1}, I_{b2}, I_{c1}, and I_{c2}, have a closed-loop controller, and the currents I_{a1} and I_{a2} are obtained by the other ones' composition.

6.1. Radial Positioning Control

Aiming to evaluate the radial position control's performance with the two-phase driving technique, its dynamical behavior was compared to the traditional three-phase one under different conditions. Three experiments were performed:

6.1.1. Experiment 1

The machine was supplied at three different frequencies: 50 Hz, 60 Hz, and 70 Hz. The response of the position control is shown on the two-dimensional XY plane in Figure 11. The dispersion area (blue region) in the center of the figure is the position of the rotor during the tests that lasted 10 s (each test). The circle curve in the surroundings indicates the maximum limits allowed for rotor displacement. Figure 11 shows that the biphasic control, despite presenting more dispersion, remained stable and with little variation in the face of frequency changes, while the three-phase control system worsened the dispersion operating at 70 Hz.

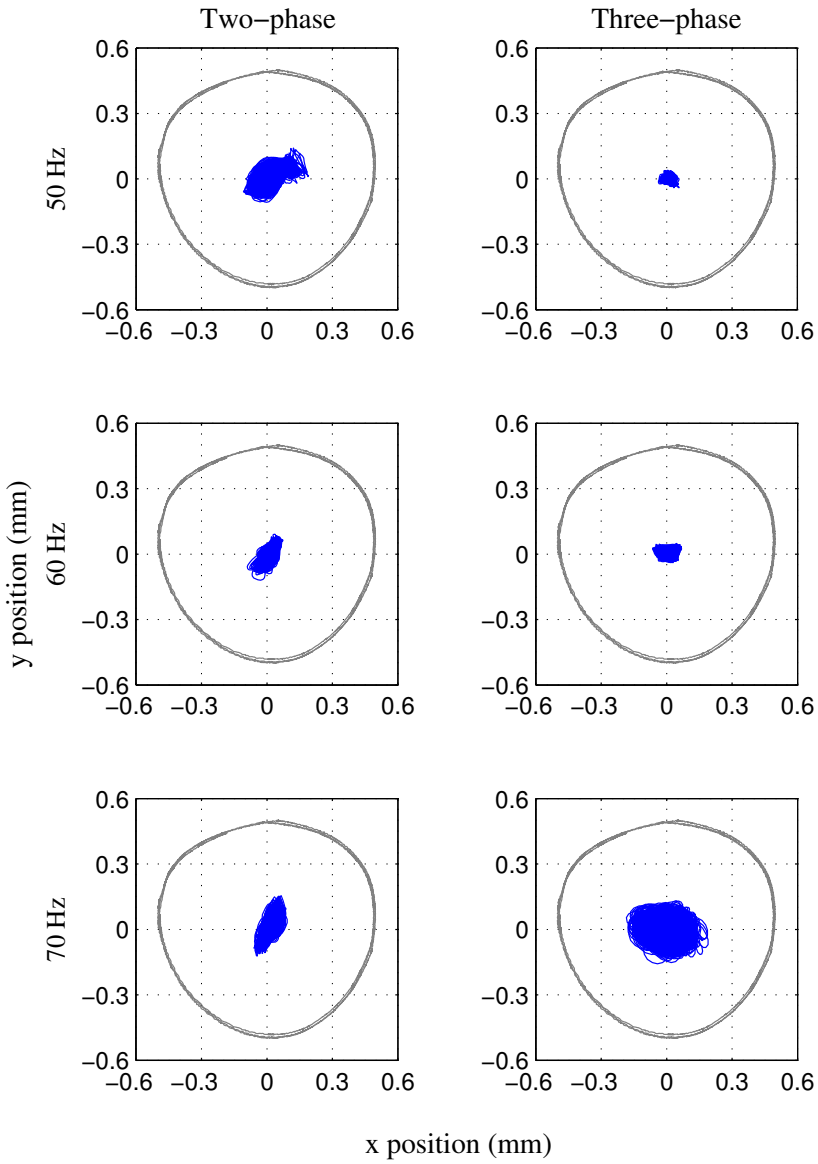

Figure 11. Responses of the proposed two-phase and conventional three-phase radial position controllers for different supply frequencies.

6.1.2. Experiment 2

To observe the position control transitory behavior, we applied step reference changes to the X and Y axes controllers. The machine was powered with currents at 60 Hz. Figure 12 shows the output for the two-phase system. The position control system followed the reference changes with low overshoot without steady-state error and a suitable speed. Step changes in the Y direction do not disturb the X-direction position and vice-versa, which indicates the independence in each axis's control.

Figure 13 shows the position response for the traditional three-phase system. These results show a similar behavior if compared to the two-phase system in Figure 12.

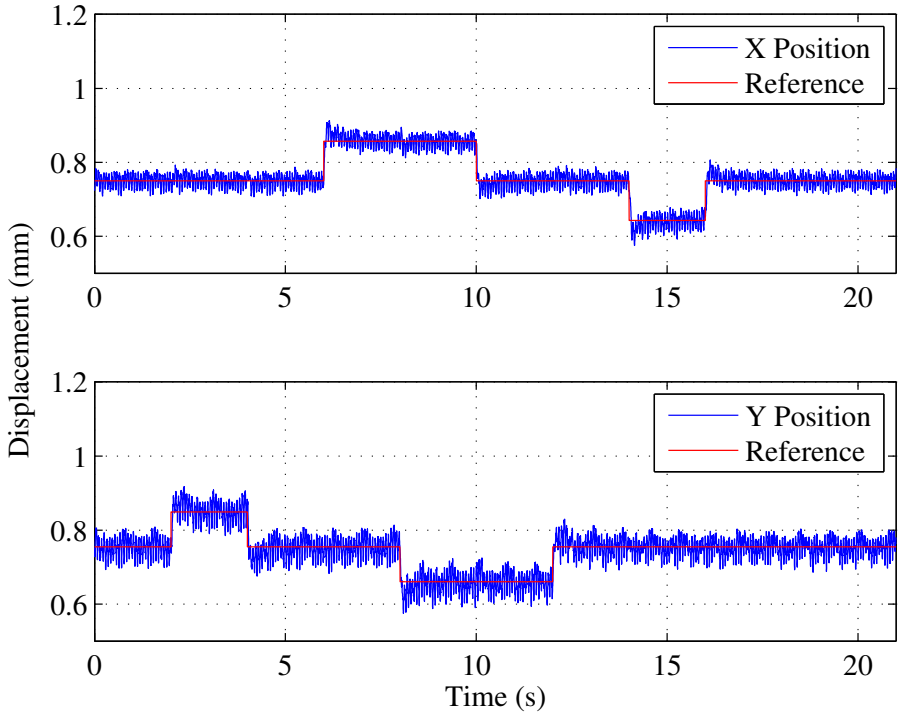

Figure 12. Position controllers output for step input references changes—two-phase system with a radial load.

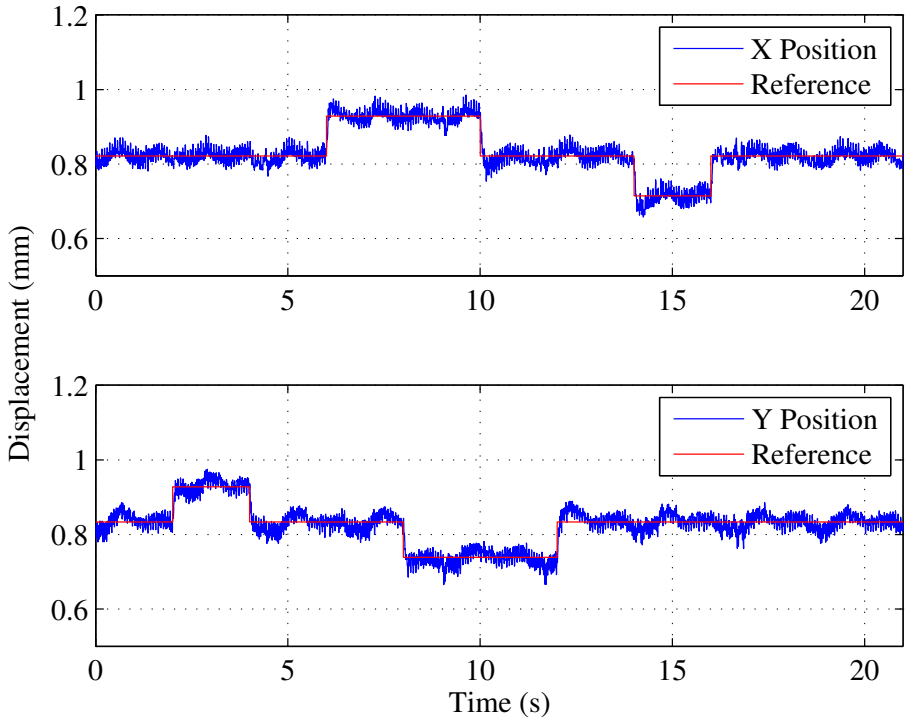

Figure 13. Position controllers' output for step input references changes—a three-phase system with a radial load.

6.1.3. Experiment 3

This test assesses the position control's response to an abrupt change in the radial load applied to the rotor. The motor is again powered at 60 Hz. With the machine running in a steady-state and with the load applied to the rotor, the x and y positions' sampling begins. In approximately $t = 7$ s, the load was removed, and about 7 s later it was applied again.

Figure 14 shows the result for the proposed two-phase drive system. The changes in the radial load produced rotor displacements on the x and y axes that the position controllers quickly recovered. Figure 15 shows the results of the three-phase system. The system is more robust to load variations than the two-phase approach.

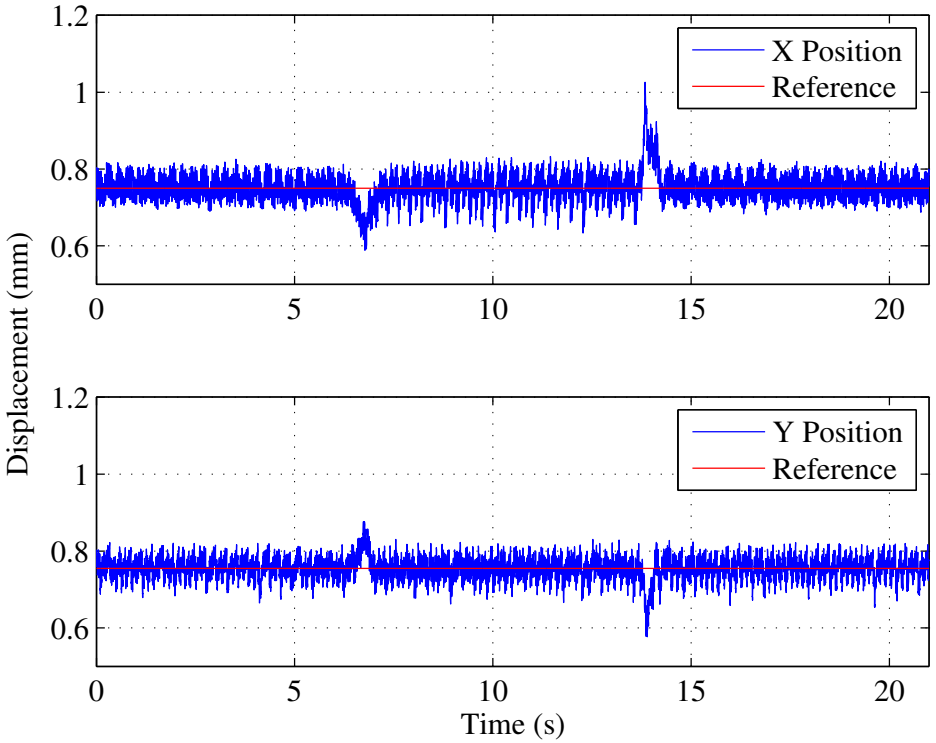

Figure 14. Two-phase system position response for load changes.

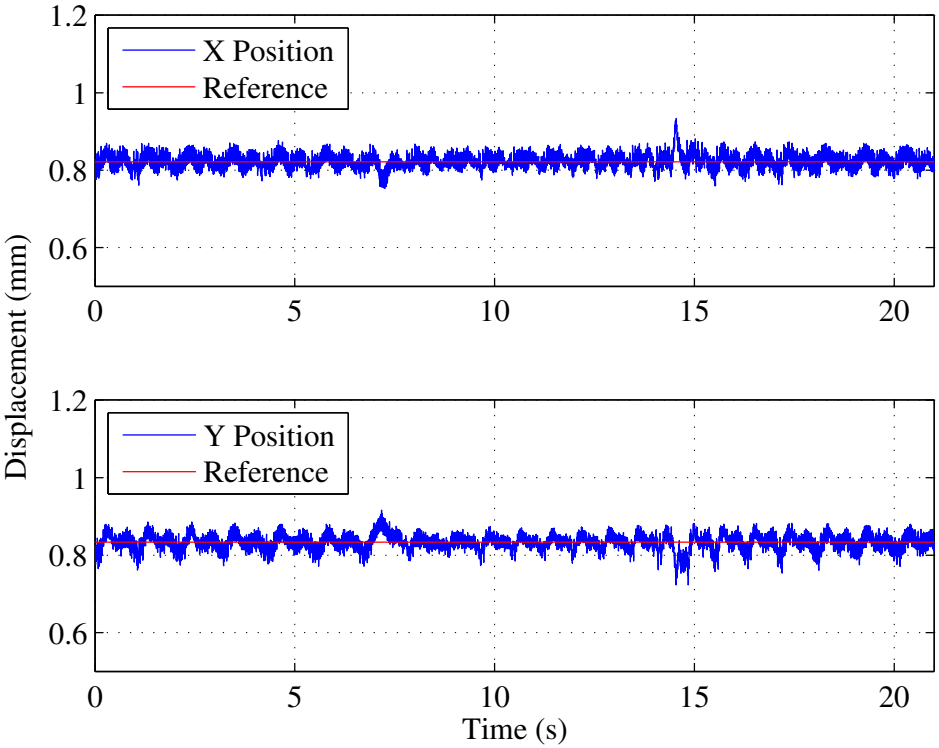

Figure 15. Three-phase system position response for load changes.

Table 3 shows a comparative chart of the two drive techniques with six and four legs, showing a similar behavior, making the four-legs system more efficient due to having fewer semiconductor devices in the drive.

Table 3. Comparative chart of the two techniques (in nominal conditions).

	Type of Inverter Six Legs Inverter	Four Legs Inverter
Response time (ms)	1.5	1.6
Precision (%)	2.3	3.1
Efficiency (%)	85	91
Distortion (%)	18	21

Figure 16 shows the three-phase current forms of the system: (a) for the six-leg system and (b) for the four-leg system. Figure 16 is linked to the results in Table 3.

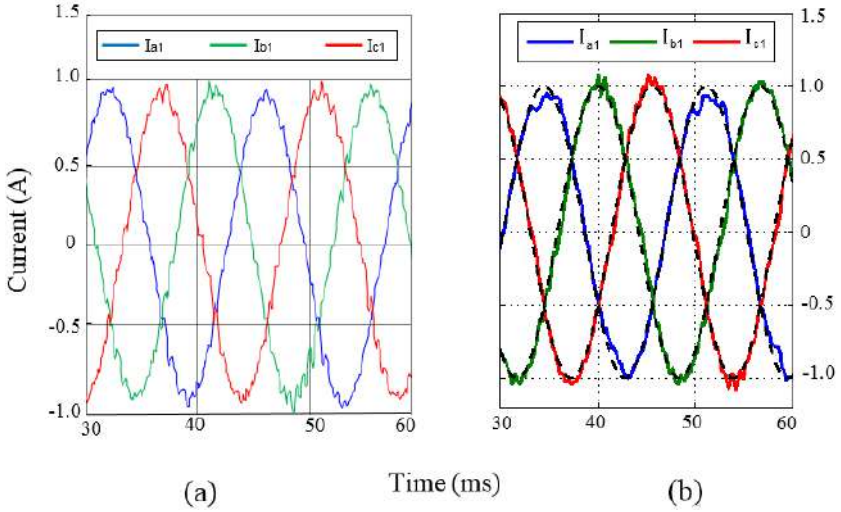

Figure 16. The three-phase current of the system: (**a**) for the six-leg inverter and (**b**) for the four-leg inverter.

7. Conclusions

This work proposed a two-phase approach to drive and control a three-phase induction machine with split winding. In order to evaluate the proposed driving technique's performance, experimental tests were carried out for different radial loads applied to the machine's rotor.

The results were compared to the traditional three-phase approach. It was possible to observe that, despite some low mismatches, the systems dynamical behavior was similar for all tests performed. This similarity was confirmed through statistical studies, in which there were some dynamic characteristics such as: precision, efficiency, and distortion. In this way, the two-phase driving techniques seem to be an interesting way to drive the split winding induction machine system once it uses fewer components and is cheaper than the traditional one.

Author Contributions: F.E.C.S. and A.O.S. conceived and designed the study; F.E.C.S. and W.S.; methodology; J.P., D.M. and W.S. performed the simulations and experiments; E.R.L.V. and A.O.S. reviewed the manuscript and provided valuable suggestions; J.P., E.R.L.V., and F.E.C.S. wrote the paper; supervision, A.O.S. All authors have read and agreed to the published version of the manuscript.

Funding: This research was funded in part by the Coordenação de Aperfeiçoamento de Pessoal de Nível Superior—Brasil (CAPES)—Finance Code 001 and Conselho Nacional de Desenvolvimento Científico e Tecnológico (CNPq).

Conflicts of Interest: The authors declare no conflict of interest.

Abbreviations

The following abbreviations are used in this manuscript:

DSP	Digital signal processor
PI	Proportional integrative
PID	Proportional integrative derivative
FSTPI	Four-switch three-phase inverter

References

1. Ferreira, J.M.S.; Salazar, A.O. Máquina de Indução Sem Mancais: Modelo e Acionamento. *Eletrônica Potência* **2007**, *12*, 2509–2521.
2. Chiba, A.; Power, D.T.; Rahman, M.A. Characteristics of a bearingless induction motor. *IEEE Trans. Magn.* **1991**, *27*, 5199–5201. [CrossRef]
3. Nomura, S.; Chiba, A.; Nakamura, F.K.; Ikeda, K.; Fukao, T.; Rahman, M.A. A radial position control of induction type bearingless motor considering phase delay caused by the rotor squirrel cage. In Proceedings of the Conference Record of the Power Conversion Conference—Yokohama 1993, Yokohama, Japan, 19–21 April 1993; Volume 1, pp. 438–443.
4. Chiba, A.; Deido, T.; Fukao, T.; Rahman, M.A. An analysis of bearingless AC motors. *IEEE Trans. Energy Convers.* **1994**, *9*, 61–68. [CrossRef]
5. Chiba, A.; Power, D.T.; Rahman, M.A. Analysis of No-Load Characteristics of a Bearingless Induction Motor. *IEEE Trans. Ind. Appl.* **1995**, *31*, 77–83. [CrossRef]
6. Victor, V.F.; Quintaes, F.O.; Lopes, J.S.B.; Santos Junior, L.D.; Lock, A.S.; Salazar, A.O. Analysis and Study of a Bearingless AC Motor Type Divided Winding, Based on a Conventional Squirrel Cage Induction Motor. *IEEE Trans. Magn.* **2012**, *48*, 3571–3574. [CrossRef]
7. Ferreira, J.M.S.; De Paiva, J.A.; Salazar, A.O.; Castro, F.E.F.; Lisboa, S.N.D. DSP utilization in radial positioning control of bearingless machine. In Proceedings of the 2003 IEEE International Symposium on Industrial Electronics, Rio de Janeiro, Brazil, 9–11 June 2003; Volume 1, pp. 312–317.
8. Nunes, E.A.D.F.; Salazar, A.O.; Villarreal, E.R.L.; Souza, F.E.C.; Dos Santos Júnior, L.P.; Lopes, J.S.B.; Luque, J.C.C. Proposal of a fuzzy controller for radial position in a bearingless induction motor. *IEEE Access* **2019**, *7*, 114808–114816. [CrossRef]
9. De Paiva, J.A.; Salazar, A.O.; Maitelli, A.L. Review of Control Strategies and Model Estimation Techiniques Applied to Bearingless Induction Machine with Divided Winding. In Proceedings of the 1st Brazilian Workshop on Magnetic Bearings, Rio de Janeiro, Brazil, 25–26 October 2013; Volume 1, pp. 1–6.
10. Asama, J.; Oi, T.; Oiwa, T.; Chiba, A. Simple Driving Method for a 2-DOF Controlled Bearingless Motor Using One Three-Phase Inverter. *IEEE Trans. Ind. Appl.* **2018**, *54*, 4365–4376. [CrossRef]
11. Bartholet, M.T.; Nussbaumer, T.; Silber, S.; Kolar, J.W. Comparative Evaluation of Polyphase Bearingless Slice Motors for Fluid-Handling Applications. *IEEE Trans. Ind. Appl.* **2009**, *45*, 1821–1830. [CrossRef]
12. Chen, J.; Severson, E.L. Design and Modeling of the Bearingless Induction Motor. In Proceedings of the 2019 IEEE International Electric Machines & Drives Conference (IEMDC), San Diego, CA, USA, 12–15 May 2019; pp. 343–350.
13. Ye, X.; Yang, Z.; Zhu, J.; Guo, Y. Modeling and operation of a bearingless fixed-pole rotor induction motor. *IEEE Trans. Appl. Supercond.* **2019**, *29*, 1–4. [CrossRef]
14. Jacobina, C.B.; Da Silva, E.R.C.; Lima, A.M.N.; Ribeiro, R.L.A. Vector and scalar control of a four switch three phase inverter. In Proceedings of the 1995 IEEE Industry Applications Conference Thirtieth IAS Annual Meeting, St. Louis, MO, USA, 12–15 October 1998; Volume 3, pp. 2422–2429.
15. Kim, D.; Jang, D.; Yoon, D. Comparative analysis of CBPWM methods for two-phase three-leg inverters using zero sequence concept. *J. Power Electron.* **2020**, *20*, 948–957. [CrossRef]
16. Jangjaempradit, S.; Morimoto, M. Two Phase Inverter Drive of Three Phase Motor. In Proceedings of the 2007 7th International Conference on Power Electronics and Drive Systems, Bangkok, Thailand, 27–30 November 2007; Volume 1, pp. 1492–1499.
17. Souza, F.E.C.; Salazar, A.O.; Silva, C.Y.; Da Silva, W.L.A.; Ferreira, J.M.S.; De Carvalho Neto, J.T. Optimization of self bearing induction motor drive. In Proceedings of the IECON 2018 44th Annual Conference of the IEEE Industrial Electronics Society, Washington, DC, USA, 21–23 October 2018; Volume 1, pp. 1–5.

IEEE Access
Multidisciplinary | Rapid Review | Open Access Journal

Received December 3, 2020, accepted December 28, 2020, date of publication January 4, 2021, date of current version January 22, 2021.

Digital Object Identifier 10.1109/ACCESS.2020.3049116

Downhole Telemetry Systems to Monitor Electric Submersible Pumps Parameters in Oil Well

DIEGO ANTONIO DE MOURA FONSÊCA[1], ANDRÉS ORTIZ SALAZAR[1], (Member, IEEE), ELMER ROLANDO LLANOS VILLARREAL[2], (Member, IEEE), GERMAN ALBERTO ECHAIZ ESPINOZA,[3], AND ALAN CÁSSIO QUEIROZ BEZERRA LEITE[4]

[1]Department of Computer Engineering and Automation, Federal University of Rio Grande do Norte (DCA-UFRN), Natal 59072-970, Brazil.
[2]Department of Natural Sciences, Mathematics and Statistics, Federal Rural University of the Semi-Arid (DCME-UFERSA), Mossoró 59625900, Brazil
[3]Department of Electronics Engineering, Universidad Nacional de San Agustin de Arequipa, Arequipa 04001, Peru
[4]Renewable Energy Department, Federal University of Ceará (CCTSSER-IFCE), Juazeiro do Norte 63040-540, Brazil

Corresponding author: Elmer Rolando Llanos Villarreal (elmerllanos@ufersa.edu.br)

This work was supported in part by the Comissão de Aperfeiçoamento de Pessoal do Nível Superior (CAPES), in part by the Conselho Nacional de Desenvolvimento Científico e Tecnológico (CNPq), and in part by the Universidad Nacional de San Agustin de Arequipa (UNSA) Investiga under Grant IAI-019-2018-UNSA.

ABSTRACT The electrical submersible pump (ESP) is widely used in the oil industry as an artificial lift method in deep wells, and its primary application of ESP is to increase the oil flow rate. Information such as the pump intake and discharge pressure, the oil reservoir and motor winding temperature, etc., provide critical data necessary to ensure proper ESP system operation and optimize production. In this article, an ESP downhole parameter monitoring system is proposed. Potentiometers are used to generates analog signals, emulating the analog sensors. The information is sent up to the surface based on the current loop through the same power cable by DC signals overlapping to AC signals in the proposed design. The article details the construction of the communication protocol and electronic circuits used in telemetry. The tests were carried out in an oil-producing company to validate the proposed telemetry system's reliability and accuracy. The good results of the robust design demonstrated it to be a promising downhole sensor for industrial applications.

INDEX TERMS Electrical submersible pump, downhole monitoring tool, submersible motor, power line communications, current loop.

I. INTRODUCTION

Information such as downhole pressure and temperature are valuable in order to optimize production and also help in identifying or avoiding problems that may lead to an undesired shut-down of an oil well [1].

As important artificial lifting equipment, electric submersible pump perform an irreplaceable role in the secondary and tertiary oil recovery, which puts forward higher requirements for the application reliability of electric submersible pump [2]. The electric submersible pump (ESP) has been widely used in oil fields [3] for its advantages of high lift, large displacement, and convenience for management [4].

The total number of oil wells worldwide utilizing some method of artificial lifting is around 95%, the most common being the Mechanical Pump (BM), with 74% of the total number of these facilities, followed by the ESP [5]–[7], with an amount ranging from 150 to 200 thousand wells in operation [8]. Despite the second position in terms of facilities, ESP is the system with the highest sales, 54% of the artificial elevation market representing in 2014 43% of the global annual expenditure in that market. [5]. Considered the best choice when high production volumes are required, ESP is typically used in wells with a production of 200 to 20,000 barrels of oil per day, although it is a high-cost method. [5], [9]–[11].

In low price season, it is indisputable that producing wells operate efficiently to provide at a lower cost per barrel. Information such as downhole pressure and temperature are valuable in order to optimize production and also help in identifying or avoiding problems that may lead to an undesired shut-down of an oil well. Observation of the operating

The associate editor coordinating the review of this manuscript and approving it for publication was Mauro Fadda.

This work is licensed under a Creative Commons Attribution 4.0 License. For more information, see https://creativecommons.org/licenses/by/4.0/

conditions of downhole equipment, such as the motor and pump, is carried out by installing a set of sensors close to the downhole. Thus, parameters such as pump intake and discharge pressure, motor temperature, produced oil temperature, vibration, contamination of the engine insulating oil, and current leakage are collected by the set of sensors at the bottom of the well and transmitted to the surface through a communication system to be processed. Through the use of these ESP operating parameters, it is also possible to understand the behavior well and ESP as a system. Such understanding leads to better system design and a continuous improvement process based on measured data known. Onshore ESP wells can achieve a depths from 500 to 4,000 meters [10], [12]. It is impracticable to lay an extra cable for powering the measurement system due to costs with extra materials and human resources. Besides, exist the chance of increasing the failure of the component [12], [13]. The most natural alternative in this situation is to use the three-phase cable itself that feeds the ESP motor as the physical medium to transmit the data to the surface [12], [13].

The data obtained from the downhole sensor will allow obtaining a direct measurement of ESP and evaluate the ESP system's performance trends, including the production field. These trends alert experts to the occurrence of possible problems with surface and subsurface equipment in advance, in time to take corrective measures [14], preventing the premature system failure. A forced shut down due to a failure that requires the replacement of one of the constituent components of the ESP system can cost from U$ 15,000 to U$ 40,000 [15]. Also, the production stoppage results in a loss of revenue, which is often more expensive than the amount spent on the equipment and services associated with its replacement [16]. Also, Operators can use a downhole sensor to determine operating parameters in completions with ESP pumps and increase pump lifting efficiency while controlling the pump operating time. Therefore, it is of great significance to carry out the research on the theory and technology for fault diagnosis of the ESP [4].

The most used downhole monitoring tool design in the field downhole utilizes a DC communication signal transmitted over the three phases of the downhole main power cable. The structure conceived in served as a basis for the development of several telemetry systems that either used the structure initially proposed or suggested a new topology with small basic structure changes [17], [18]. Another communication strategy is through modulating high-frequency signals to transmit information from the motor/pump system at the bottom of the well. This method has higher transmission rates and tolerance to SLG (single-line-to-ground) faults compared to the dc communication scheme [13]. Despite the high transfer rates and mitigating the SLG problem, this technique has a current limitation of the system's constructive character. The impedance imposed by the physical environment and the harmonic filter (installed in VSDs in ESP systems) will cause a strong attenuation in the high-frequency signals. As a consequence, the signals will be uncharacterized, and, therefore, their transfer will be compromised.

Aiming to overcome major drawbacks and limitations of the two existing downhole monitoring tool design methods in 2015 [13] proposed a phase-to-phase communication scheme using power-line communication technique known as a ''two-way automatic communication system (TWACS)'' for the downhole monitoring tool design. On that occasion, two case studies are conducted using a real ESP system under normal and single-line-to-ground fault conditions. Following the same idea, in 2017 [12], suggested a downhole tool design method using a phase-to-neutral communication scheme in which an effective signal communication path is formed by external impedance on the wellhead connecting one phase to the ground combined with a controlled thyristor at downhole connecting the neutral of an electrical submersible motor to the ground. The performance of the method is evaluated using simulation through the case and sensitivity studies.

In this article, it is implemented a downhole telemetry system's complete solution uses a DC signal (digital pulses) over three phases of the main power cable to transmit data between the downhole module and the surface monitoring electronics unit. It is proposed a new communication protocol, based on the Manchester coding, which guarantees the data from the parameters measured at the bottom of the well reach the surface module to be read. The protocol transfer rate was established based on impedance analysis of the three-phase cable that powers the motor. Details of the construction of the protocol, as well as the telemetry system, are presented. The validation of the proposed protocol, implemented in the telemetry system's transmission and reception modules, was performed through tests in an oil well using the ESP elevation method. At the time, the performance of the proposed solution was evaluated for different values of motor frequency.

II. MATERIALS AND METHODS

A. ESP EXPERIMENTAL SETUP

The experimental setup reproduces the electric drives and controllers project system of the ESP artificial lifting method. The main components in the proposed setup include a variable speed drive (VSD) and a three-phase wye-connected choke, both as surface electronic devices. Besides, a three-phase power cable feeding main AC power to the motor and an ESP motor makes up the subsurface units. The Figure 1 shows a snapshot of the experimental setup.

The field tests were planned in a pilot well with ESP installation. The well where the tests will be carried out has a depth of 30 meters with a diameter of the 13.5/8″. However, from the well, the subsurface modules (cable and motor) were not used. In other words, a 2036 m motor power cable and an ESP motor, both on the surface, were used. In this way, it was possible to connect our bottom sensor to that motor on the surface. Regarding our surface module, it was connected directly to the well surface filter. Its surface unit has a set of four protection and monitoring modules, in addition to the Human Machine Interface (HMI). On the subsurface, is the

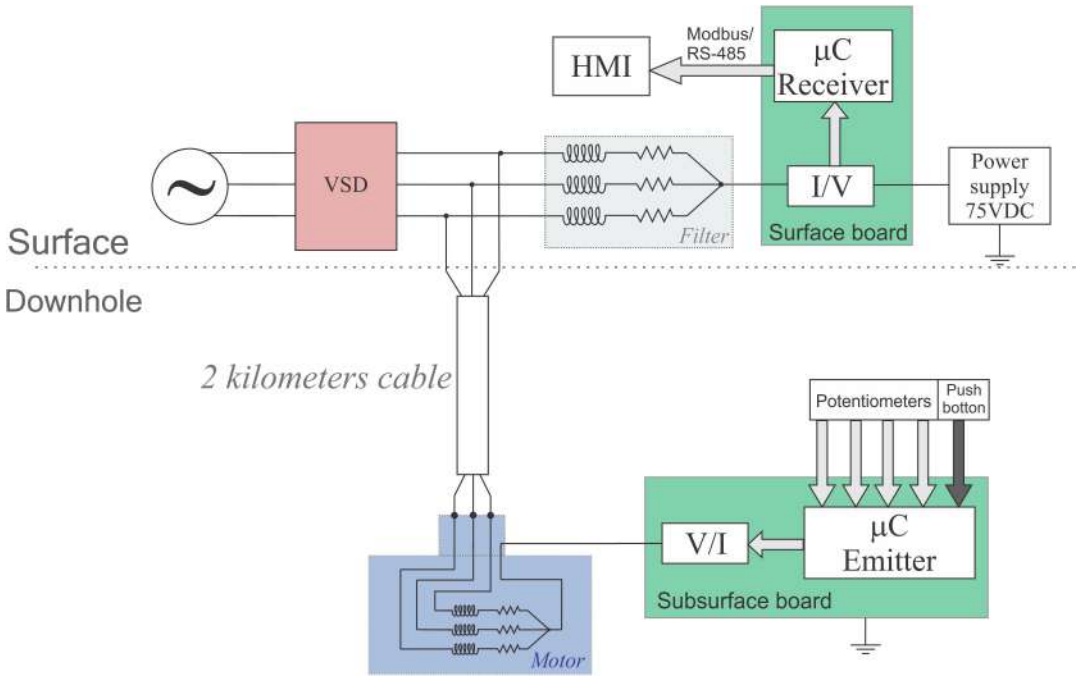

FIGURE 1. The structure of the communication system.

the motor. The Table 1 presents the characteristics of the equipment used in the tests. This basic well structure makes it possible to evaluate the ESP system for several different conditions, that is, the use of different inverters, as well as cables of different sizes, diameters, and shapes (flat or round).

TABLE 1. Units for Magnetic Properties

Equipment	Parameter
Transformer	Dry Type, Power Rating 125 kVA, Primary Voltage 420-480 V, Secondary Voltage 900-1400 V
Power cable	AWG#2, 5 kV, round construction, 2,236 m
ESP Motor	80 HP, 440 V, 101 A a 60 Hz
Variable speed drive	150 kVA, active filter, nominal current 242 A, switching frequency 2 kHz
Variable speed drive (no active filter)	110 kVA, 440 V, nominal current 124 A, switching frequency 4 kHz

The power cable connects the variable frequency drive to the AC motor to transmits the required surface power to it. In [19] was presented the modeling of the 2036 m ESP power cable used in field tests. The electrical parameters of the cable, such as impedance, phase, inductance, and capacitance, were obtained through the Keysight impedance analyzer E4990A. Five hundred points were collected with the following information: frequency, absolute value, and phase, which served to characterize and model the cable.

A VSD can control the submersible electrical motor at a speed that the well produces with the greatest efficiency and keeps the ESP within its best efficiency range [8]. The VSDs also offer soft motor starting for ESP systems and reduce the impact to power grid during the motor start-up [20]. The drive allows the pump to be operated continuously or intermittently or be shut off in the event of a significant operational problem. The direct speed control afforded by the VSD increases system efficiency and the run life of the ESP system while reducing the incidence of downtime [8]. The main advantage of the VSD is that it allows the operator to change the speed of the ESP to account for uncertainty in the productivity index of the well or changing well conditions. The VSD works as a power supply, generating frequency and resonance values according to the curve that relates frequency and output voltage.

The surface induction power is a set of three-phase inductors in star connection ungrounded system. Also known as choke panel, it is the interface between the ESP power system and the surface electronics equipment, filtering the digital communication signal from the AC power line [21]. The purpose of the surface choke is to allow the ESP Gauge Interface to provide power to and communicate with the downhole tool, in the later case creating a virtual ground via WYE point for direct connection for downhole communication.

The schematic diagram of the surface filter is shown in Figures 2, 3:

The artificial star point is constructed by a three-phase electric reactor with the same three-phase winding parameters as the downhole motor, which supplies power for the downhole monitoring circuit based on the principle of star point equipotential [2]. The electronic surface unit connects to the downhole tool via the motor power cable through the choke. This electronic module is connected to the choke wye point and the wellhead ground. Likewise, the downhole

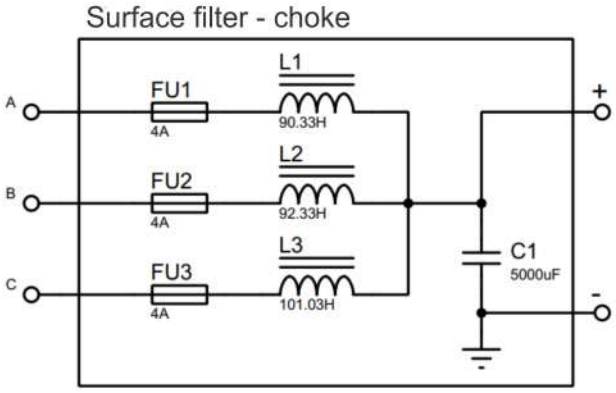

FIGURE 2. The three-phase inductors at the surface: Choke diagram.

FIGURE 3. The three-phase inductors at the surface: Real choke.

electronic module connects to the neutral of the ESP motor and the downhole system's ground through the well casing. The neutrals of the choke and the ESP motor are ungrounded. Meanwhile, a loop for current signal transmission was established, eliminating the need for an extra communication cable [22], [23]. The downhole sensor sends the data as a train of current pulses to the surface. In this way, the downhole unit is equivalent to a current source under the control of the uphole group in series with a resistance [11]. The current loop shows strong anti-interference and high reliability because the influence of line impedance, cable length, voltage drop as well as noise interference is negligible when transmitting data in this way. Therefore, the current loop is suitable for long-distance data transmission [24].

The Figures 3–6 provide a panoramic view of the test system together with the proposed electronic modules.

B. PROPOSED TELEMETRY SYSTEM

The telemetry system consists of five electronic modules. These modules collect information from the sensors installed in the subsurface equipment, located at the bottom of the well, processing them and sending them to the surface. On the surface, the data will be made available for monitoring and analysis. The block diagram illustrated in Figure 7 shows the layout of these modules and how they are interconnected.

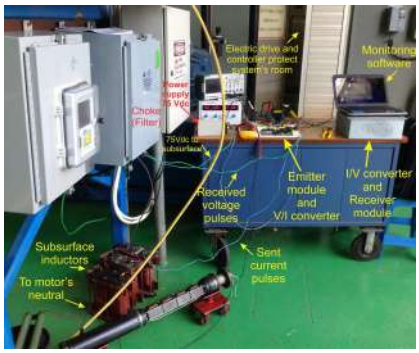

FIGURE 4. The experimental setup overview.

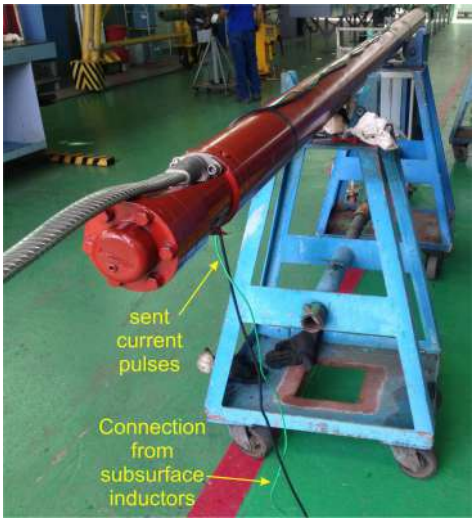

FIGURE 5. ESP components: Motor-pump assembly installed horizontally.

FIGURE 6. ESP components: Three-phase power cable.

1) AUXILIARY POWER SUPPLY

The three-phase wye-connected choke on the wellhead and the motor are linked in parallel, as shown in Figure 8. This feature ensures that both neutrals point (choke and motor) are kept at the same relative potential.

The artificial star point is constructed by a three-phase electric reactor with the same three-phase winding parameters as the downhole motor, which supplies power for the downhole monitoring circuit based on the principle of star

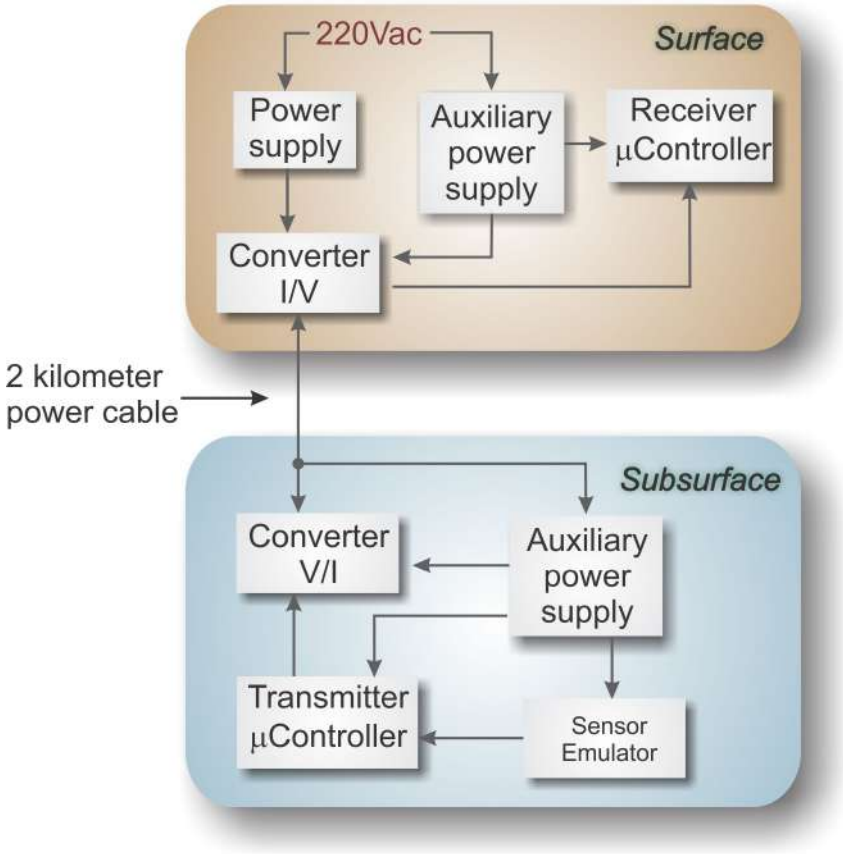

FIGURE 7. The block diagram of the proposed system.

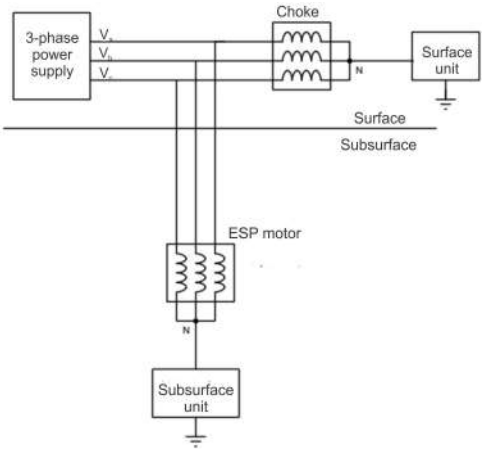

FIGURE 8. Schematic diagram of energization of subsurface electronics.

point equipotential. At the surface, the electronics module includes a 75 V_{dc} power supply that provides DC voltage to the downhole electronics module. The surface electronics unit is connected to the neutral of the choke. This way, the 75 V_{dc} reaches the upper end of the power cable and, consequently, the motor's neutral. The motor's neutral wire is connected to the voltage regulator circuit that supplies DC voltage levels of 5 V_{dc} and 15 V_{dc} to the electronic subsurface modules. Such operation characterizes the circuit as a subsurface source, terminology that will be used throughout the article. The Figure 9 depicts the power source circuit diagram.

For protection measures and to prevent that alternating motor current may cause communication interference between downhole and uphole unit, the source circuit is connected to the motor neutral via a large inductor, which can reach the value of 120 H [23]. Therefore, the alternating current flowing from the surface through the ESP power cable and the motor is filtered by this inductor so that the data signals can be transmitted without any alternating current influence. In the testbed used for the experiments, three inductors in series with an equivalent inductance of $L_eq = 53.4\ H$ represent the mentioned inductance.

2) TRANSMITTER DEVICE

The data acquisition and transmission circuit collects data from the sensors installed in the subsurface equipment, analyze, process, and send the acquired data to the receiver module, on the surface. For practical purposes, the analog and digital signals related to downhole sensors will be generated by potentiometers and an on-off switch in this research. The Figure 7, at the bottom of the well, shows a block diagram illustrating how the transmitting circuit is associated with the other components. The Microchip PIC 18F4550

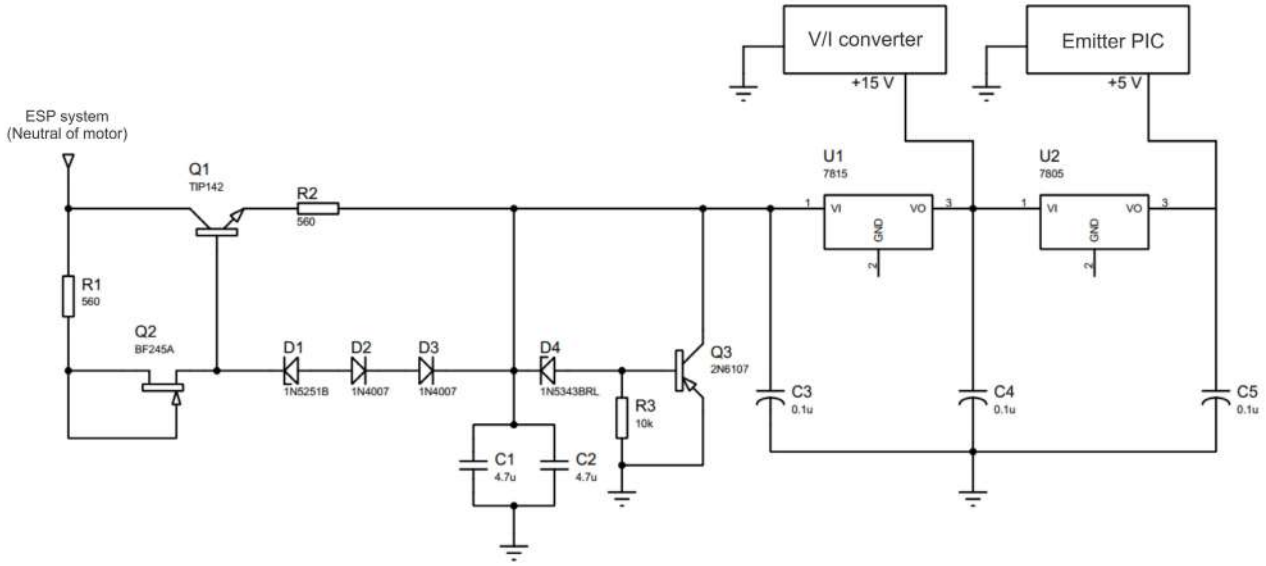

FIGURE 9. Circuit diagram of the auxiliary power supply.

microcontroller was chosen because it has technical requirements that meet the application. Among the elements is compatibility with the SPI communication protocol, the quantity of analog and digital inputs, in addition to the low cost.

An ESP well running with a downhole monitoring tool, the downhole parameters usually monitored include: pump intake pressure and temperature, motor oil or motor winding temperature, pump discharge pressure. Some modern downhole monitoring tools have inputs for vibration and electric current leakage signals, which allows cable degradation to be determined.

Another critical parameter is the contamination of insulating oil in the motor applied to the electrical submersible pump which indirectly protects the induction motor associated with that system [25]. The seal with the continuous work causes the onset of motor oil contamination, which leads to the loss of its insulating property. The statistics show that the induction motor has the highest failure rate by oil contamination. This contamination causes problems to the induction motor due to short-circuiting.

The data acquisition process begins when the information from the potentiometers arrives at the microcontroller ADC pins. The pic microcontroller 18F4550 has an inbuilt 10-bit resolution ADC. The temperature and pressure data are stored in the internal microcontroller RAM. However, due to data volume generated by the vibration sensor (x and y axes) was necessary an external RAM. On the contrary, the contamination sensor signal is sent to a digital input indicating whether or not the insulating oil is contaminated.

a: COMMUNICATION PROTOCOL

The physical topology of the proposed telemetry system is point-to-point. The three-phase motor power cable and the downhole sensor ground (or well casing) constitute the current loop, i.e., the physical medium. The transmission is unidirectional (or simplex) so that only the sender device sends the data.

Due to the impossibility of using an external clock, we opted for the use of a self-synchronized signal, which includes synchronism information in the transmitted data. Guaranteed transitions each bit period, even in the event of long sequences of 1s or 0s, enables straightforward recovery of the clock and data signal by the receiver. Another relevant factor in digital communication is the DC components, that is, if the data has a long sequence of zeros and the average signal strength becomes distorted. Thereby, the receiver may have trouble distinguishing between a bit zero and bit one.

The polar line coding (NRZ, RZ, Bi-phase Manchester, and differential Manchester) have characteristics that meet the needs imposed by the scenario found in the ESP system. In this case, it was decided to use the bi-phase Manchester encoding to implement the protocol. There is always at least one transition per bit period to enable clock recovery by the receiver. Figure 10 illustrates the behavior of a bit sequence sent by the Manchester method. In this application, low-to-high transitions are received as binary ones, high-to-low transitions as zeros. Figure 10 shows that each bit has a positive and negative contribution in terms of voltage, eliminating the DC components. However, The Figure 10 also demonstrates a disadvantage of Manchester encoding: it is necessary a transition for every bit, which means two Manchester logic states are used to convey one standard logic state. Thus, twice as much bandwidth is needed to transfer data at the same rate. However, compared to the benefits obtained with the encoding Manchester, this limitation does not compromise the protocol's performance.

The protocol provides two different frame types. The first, called "regular sensors", encapsulates information from

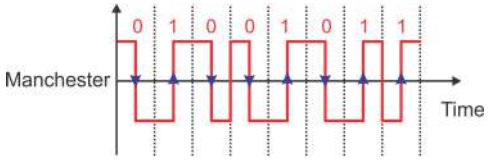

FIGURE 10. Manchester encoding.

four analog variables (for example, two temperatures and two pressures) and one digital variable (insulating oil contamination). The second frame, denominated ''special sensors'', encapsulates the data generated by the accelerometers. The frame size is variable, depends on the number of installed instruments. The minimum frame size is 42 bits, sending data from a single sensor, and 117 bits considering the five sensors. Figure 11 shows how the fields are organized in the table that encapsulates the data.

FIGURE 11. Frame format for pressure, temperature and contamination variables.

In addition to the fields referring to the values of the variables, the structure has the following control fields:

startBit: 1 bit signals the start of the frame

varCount: 3 bits indicating the number of variables to be sent.

data: the size varies from 19 to 95 bits, according to the number of sensors read.

CRC: 16 bits that indicate the value of the CRC (cyclic redundancy check) used to detect transmission errors.

stoptBit: 2 bits signal the end of frame transmission.

Figures 12 and 13 exemplify the data frame format to send one and two variables, respectively. The first one is an illustration of the data field for one sensor. The first 3 bits to identify the sensor and 16 bits to store the value read from it. The Figure 13 depicts the case of reading two sensors. In this respect, the first 19 bits refer to the first sensor, and the following 19 bits relating to the second one. Both data field are with the identification field, followed by the read value field.

FIGURE 12. Frame structure for sending regular sensor information. Organization of the data field for sending values from: one regular sensor.

The second frame, denominated ''special sensors'', encapsulates the data generated by the accelerometers. The frame has a fixed size of 69 bits. It was modified to suit the content of the information to be sent. The vibration massage is transmitted simultaneously on both the X and Y-axis. The control field is 22 bits wide, as in the regular sensor's frame. The difference from that is the number of bits in the data: 19 up to 95 for regular sensors against 47 for the special one. The format of a vibration data frame is shown in Figure 14

where,

startBit: 1 bit that signals the start of the frame

varCount: 3 bits indicating the number of variables to be sent.

data: it is divided into smaller fields and has a size fixed at 47 bits, of which 3 bits define the sensor, 12 bits identify the packet, and the remaining 32 bits store the read values, 16 for each coordinate.

CRC: 16 bits that indicate the value of the CRC (cyclic redundancy check) used to detect transmission errors.

stoptBit: 2 bits signal the end of frame transmission.

The data field in the described frame has that structure because it is needed to store 4 thousand vibration points acquired data in 1 second for each coordinate. The microcontroller is limited in memory to send this volume at once. In this case, the acquired data is fragmented to fit into the data field, and in each packet sent, a piece of vibration information is transported. For the purpose of providing sequence control, each packet is given a 12 bits sequence number. Since this field is just 12 bits long, it identifies 4096 frames. The 12 bits id field provides a mechanism for the receiver to reassemble the complete vibration message. Figure 15 shows the described field.

b: DOWNHOLE SENSOR INFORMATION - ESP

Each downhole equipment will have a unique serial number. From that information, it will be possible to track it through data such as location, operating time, and category to which it belongs. The class indicates which and quantity of sensors in the equipment. The possible sensors are temperature, pressure, contamination, and vibration. Therefore, when in operation, the sender's first action is to transmit this information to the receiver and then start the sensor data acquisition process. As there is no bidirectional communication between the communication modules, which would allow a request in case of an error in the received package, this information is sent twice in a row at the beginning and specific periods.

c: ACQUISITION AND PROCESSING OF ANALOG AND DIGITAL PARAMETERS

The data acquisition process begins after sending the identification information to the surface microcontroller. Electrical signals from the temperature and pressure sensors are fed into a 10-bit built-in ADC converter, which digitizes these analog signals into their computer-compatible equivalent. There is no signal conditioning circuit because the potentiometers used to emulate the sensors generate signals from 0 to 5 V. The downhole module will be located in an environment subject to noise, mechanical vibration, and high temperatures. Thus, for each sensor, a certain number of acquisitions is performed, and the arithmetic mean is calculated. The number of readings is defined by the number of unused bits after the A/D conversion. In other words, the 10 bits resulting from the

FIGURE 13. Frame structure for sending regular sensor information. Organization of the data field for sending values from: two regular sensors.

FIGURE 14. Frame structure for vibration data.

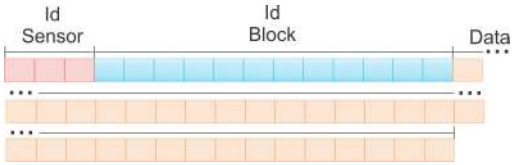

FIGURE 15. Organization of the data field for sending vibration values.

A/D conversion are stored in a 16-bit variable, thus leaving 6 ''free'' bits, which allows the sum of 64 readings of that sensor. In the end, this sum is divided by 64 to obtain an average of 10 bits.

A 10-point moving average filter is responsible for smoothing the acquired values, and therefore to reduce the noise effect. The moving average filter is a simple Low Pass FIR (Finite Impulse Response) filter commonly used for regulating an array of sampled data/signals. It is optimal for reducing random noise while retaining a sharp step response. In this application moving average filter takes ten samples of the previously calculated values in the arithmetic average at a time and takes the average of those to produce a single output point. Each provided point is stored in the array called ''data vector''. Once filled, the content of the data vector is copied to the data field of the data frame, and together with the control fields, will form the vector that will carry the data to the surface. The Figure 16 represents the acquisition and processing steps.

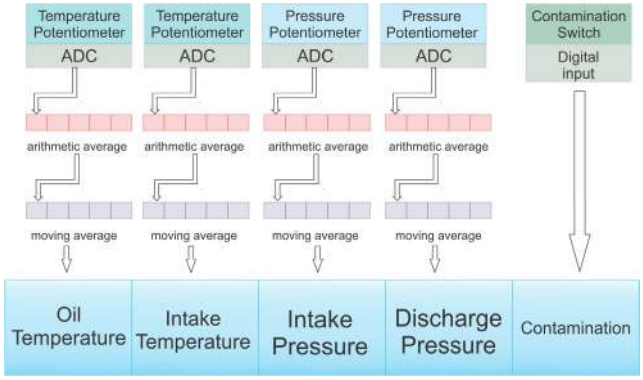

FIGURE 16. Data frame assembly steps.

The acquire information regarding the vibration frequencies process follows the same steps as the analog data acquisition process. The differences in the forms of acquisition are the volume and speed at which the vibration data is read. Two potentiometers emulate the accelerometers, one for the x-axis and one for the y-axis. From each of these 4,000 points will be obtained in 1 second. Although each potentiometer is connected to a channel, the microcontroller has a single A/D converter. Therefore, the reading of each analog input is done through a switch, whose frequency is fast enough so that there is no loss of information read. The conversion process ends only when it reaches 8 thousand points. The MCU does not have enough RAM to store a large amount of vibration data at the same time. The solution was incorporating an external memory chip. The Microchip 23K256, with 256 Kbits (32 KBytes) of memory, provides storage for the application. The module is connected to the microcontroller board through the serial interface. The option for serial communication was due to the pin limitation of the microcontroller. However, the serial writing time in memory could be seen as a complicator in the process of acquiring the vibration data. This possible limitation was overcome with using a 32 MHz quartz crystal, thus providing resources for the configuration of the A/D converter and the writing process of 8 thousand points within 1 second.

The points of the X and Y coordinates are stored in RAM as follows: the four thousand points referring to the X coordinate occupy the first eight thousand positions (0000h to 1F3Fh) and the other four thousand referring to the Y-axis, the following eight thousand locations (1F40h to 3E7Fh). The writing in memory occurs sequentially and not in batch, so, after reading a point X, a point Y is read, and then writing occurs. This process repeats up to acquiring the 8 thousand points.

After the data storage generated by the accelerometers is completed, the data treatment step to send them to the receiver begins. The protocol frame is a series of bits composed of information from a single pair of XY coordinates. Therefore, it is necessary to assemble 4,000 frames to send a 1-second acquiring of the vibration variable. The 12-bit identifier (4096 identifiers) allows the correct reassembly of the segments to ensure that the packages are assembled to form the original information.

The sending of the vibration frames alternates with the frames of conventional sensors. Once the sending of the vibration data is complete, a new cycle of data acquisition and treatment begins, repeating the entire process.

The data transfer rate of such systems is limited by the electrical impedance of the motor windings and the power cable.

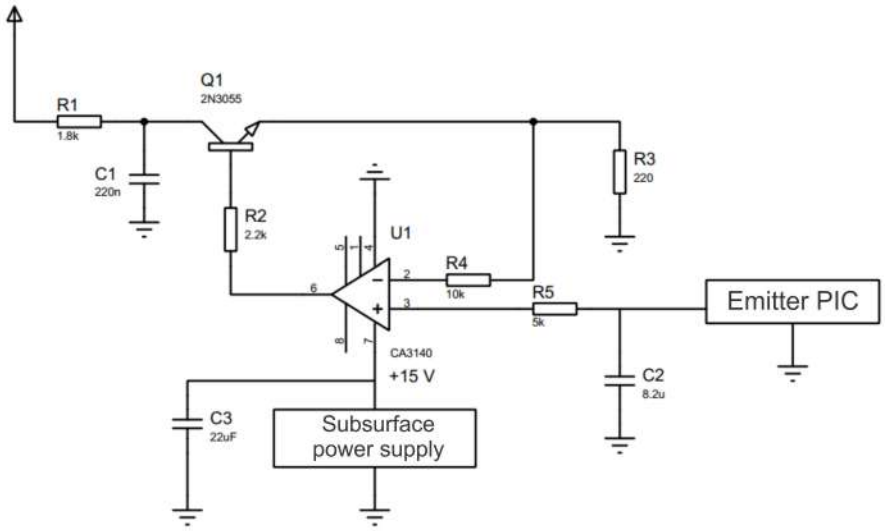

FIGURE 17. Circuit diagram of voltage to current converter.

3) SUBSURFACE COUPLING

As described in section about choke, the system ground will serve as the signal return path to the surface. The data packages are sent to the surface as a current signal, whereas the cable length for the ESP wells can reach 4000 m [10], [12]. Under these conditions, the voltage signals would have attenuated due to the cable length. Alternatively, the current signal does not present any loss considering the same scenario, in addition to having low sensitivity to electrical noise and not having its accuracy affected by the voltage drop in interconnections. However, the power cable lenght and the electrical impedance of the motor windings limite data transfer rate of the such system. A more precise analysis of the physical layer, in which only the three-phase cable was considered. The cable length was 2036 meters, three-phase 4 AWG, and a flat profile. The analysis showed that the cable acts as a low-pass filter with a cutoff frequency of 10Hz [19].

4) VOLTAGE TO CURRENT CONVERTER (V/I)

The emitting module's micro-controller generates a square voltage signal whose amplitude is $5V_{dc}$, and the baud rate is 10 bps. The voltage-to-current converter shown in Figure 17 converts the voltage signal generated by the PIC into a square current signal with approximately $500mA$ amplitude and the same frequency as the voltage signal.

The circuit works as follows: the emitting microcontroller, connected to the non-inverting input of the operational amplifier, sends a voltage signal (pulse) of 5 V_{dc}. The rising edge of the pulse causes a positive variation, which is amplified, causing a voltage V_o. Thus, the voltage on the resistor R_4 increases proportionally, making the power difference between the inputs of the opamp tend to zero again. In the case of the falling edge of the pulse, the reverse occurs.

5) SURFACE COUPLING

The reception of data on the surface is executed by the coupling circuit, which can be divided into two stages. The first is the filtering of signals at the fundamental frequency (50/60 Hz) to extract the DC current signal with the information of the parameters read. The DC current signal then passes through the current-voltage converter circuit, and its output provides a sign with the same amplitude and frequency as the signal emitted by the sub-surface microcontroller. The following topics detail each of these steps.

6) CURRENT TO VOLTAGE CONVERTER (I/V)

After removing the fundamental frequency, the modulated signal is converted back into a voltage output. The proposed I/V converter circuit consists of three stages (Figure 18). In the first, a closed-loop current transducer using the Hall effect technology, the LA 50-p / SP55, provides an output voltage proportional to the current flowing through the sensor. The operational amplifiers U_1, U_2 and U_3 remove the DC offset signal from the previous step. The sign is amplified (opamp U_4) and sent to a comparator (Schmidt Trigger - CI 4093), which saturates the signals at the high and low levels. The comparator output, which is the output of the I/V converter, delivers the signals with their original properties to the receiving microcontroller.

C. RECEIVER DEVICE

The defined receiver module has one microcontroller unit (MCU) responsible for making the information from downhole parameters available in a Modbus bus network to industrial systems such as PLC (Programmable Logic Controller).

The main components of the receiver module are the PIC 18F4550 microcontroller, which implements the Tx-Rx and

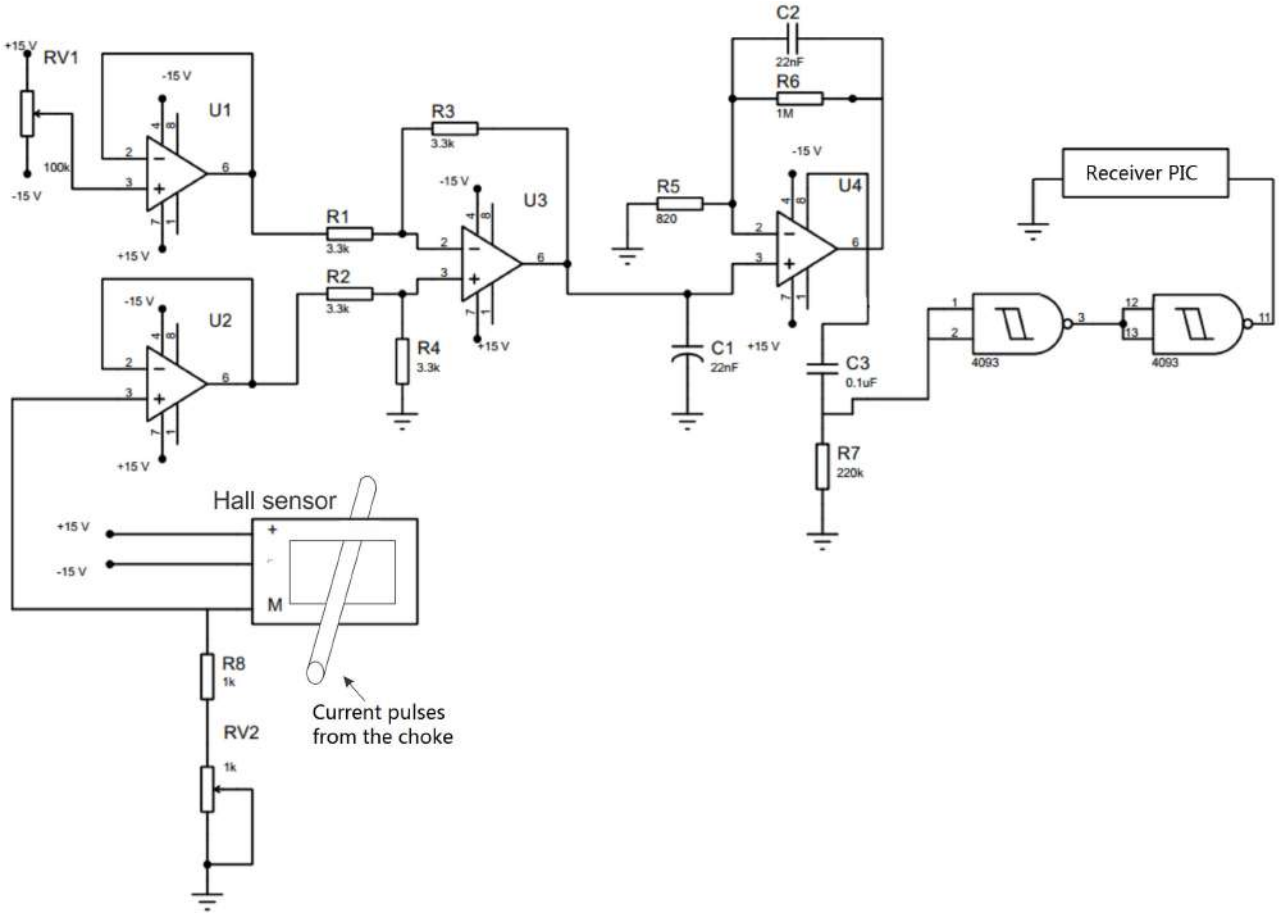

FIGURE 18. Circuit diagram for current to voltage converter.

FIGURE 19. Sharing memory between the writing and reading stage.

Rx-PLC logics, an SRAM serial memory for sensor data storage, a MAX485 transceiver as an interface to the RS-485 standard, a MAX232 transceiver and various components such as capacitors, resistors, and terminals.

The receiver is configuring to attend two main tasks: the first one deals with the communication with the transmitter module, called Rx-Tx, and the second task, referred to as Rx-PLC, is responsible for the connection with the industrial devices. These two demands were implemented in order to share a single memory space, where Rx-Tx records the sensor data in that space, and the Rx-PLC part accesses them to make them available, as shown in Figure 19.

The availability of the data collected for industrial equipment is in charge of the receiver's Rx-PLC segment, which implements the Modbus-RTU protocol with physical layer RS-485. The memory map to be accessed by industrial equipment is organized according to the Figure 20, where positions 0 to 3.999 are samples of the X-axis, 4.000 to 7.999 of the Y-axis, position 8000 indicates the number of sets of 4 thousand points (X; Y) that have already been made available and from 8.001 to 8.016 is used to store data from up to 16 regular sensors. In Figure 20, sensors of the special type represent accelerometers, while regular sensors correspond to pressure, temperature, and contamination.

The implemented Modbus protocol is configurated as follows:

- Operation mode: slave;
- Slave address: 1;
- Data structure type: holding register;
- Transmission mode: serial RTU;
- Inter character timeout: 70 ms;
- Baud rate: 9600 bps;
- Parity: none;
- Stop bit: 1;
- Data bits: 8;
- RTC/CTS: none.

The slave address and baud rate can be configured through a dedicated interface. All other configuration properties can be modified, however, only modifying and compiling the source code. Because the Modbus data structure that stores the sensor data is of the holding register type, the PLC must execute read requests with function code 0×03. Due to protocol limitations, up to 127 memory locations can be requested at a time. In this application, the Modbus protocol uses the data structure of the holding register type to store the sensor data. Therefore, the PLC must execute reading requests using the function code 0×03. Due to protocol limitations, up to 127 memory locations can be requested at a time. Figure 20 shows the memory addresses available for reading the PLC. In this way, the requests for readings of the regular sensors by the PLC must obey the structure of the Figure 21. The previous Figure depicts an example of requesting the regular sensor stored at address 8.001.

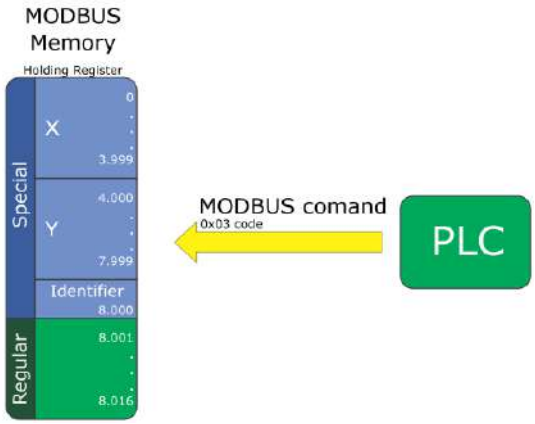

FIGURE 20. Modbus memory map.

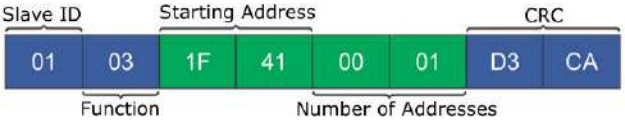

FIGURE 21. Example of modbus request for regular sensors.

Considering the special sensors, the PLC must monitor address 8.000 (identifier) to detect changes in its value. The identifier acts as a counter for how many sets of 4 thousand points have already been made available for reading. Therefore, the increase in this field means that a new set of 4 thousand points is available to be read. Figure 22 exemplifies a request for reading the first 100 samples of the X-axis.

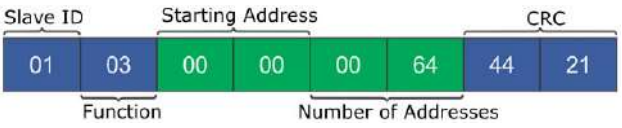

FIGURE 22. Example of modbus request for special sensors.

MEMORY ORGANIZATION

The memory described here deals only with information related to the sensors, having no relation to aspects of the source code of the device. Considering that information from special sensors requires 4 thousand samples per axis and only one is necessary for regulars, the memory was ordered according to Figure 23.

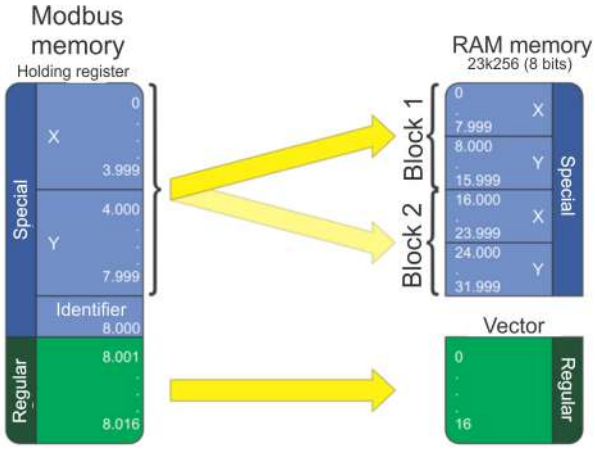

FIGURE 23. Memory organization.

The mapping of 8 thousand Modbus addresses to 16 thousand addresses in the SRAM memory results from the fact that the Modbus addresses have 16 bits and those of the SRAM memory only 8 bits. Therefore, two memory locations are required for each Modbus position. As for regular sensors, the mapping is done directly, since both structures use 16 bits. The creation of two blocks allows us to read the sensor data at the same time that the new ones are stored. This way, while the PLC is reading a set of 4,000 points in one block, the receiver module is storing a new set of 4,000 points in the other block. When filling a block, the receiver increments the identifier, which indicates which block is ready for reading and begins the process of filling in the next. Thus, the reading and writing processes continue to alternate between blocks 1 and 2.

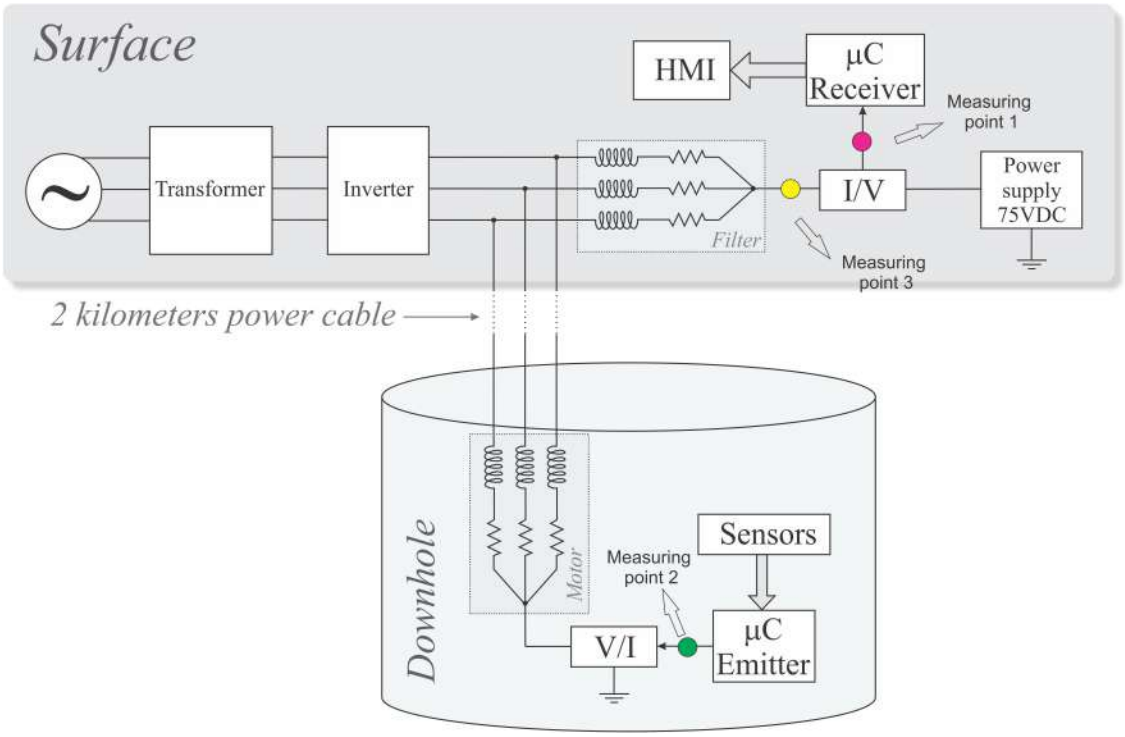

FIGURE 24. Panoramic view of the ESP structure used in the tests and the measurements points.

III. RESULTS

In this section, in order to validate the developed telemetry system, the experimental results are now exposed. The testing consisted primarily of transmitting information of three analog sensors and a digital sensor. In the experiments, the behavior of the signal during the sending of data for different motor speeds is evaluated.

A. FIELD DATA TRANSFER TEST WITH ESP SYSTEM IN OPERATION

In order to verify the behavior of the current signal sent by the emitter module along the three-phase cable and in an environment without noise, at the first moment, a test was performed with the system de-energized. Due to the simplicity of this first test and the possibility to monitor possible causes of communication failure, it was decided not to use the well structure, but to work with the ESP motor-pump assembly horizontally, connected to the 2,236-meter long cable still wound on the coil and connected to the surface filter.

The equipment used was: prototype of the transmitter module, three protection inductors connected in series, ESP pump and motor, three-phase cable with 2,236 meters, choke and receiver module. The Figure 24, which will serve as the basis for the following tests, gives a panoramic view of how the ESP equipment is arranged and the measurements points.

The points shown in Figure 24 highlight the locations for monitoring the signals. Therefore, prototypes are evaluated based on the analysis of the behavior of the signals sent and received and the voltage in the motor neutral. The result of this test (Figure 25) showed the expected behavior, which is the reproduction on the surface of the signal sent by the bottom module, verifying that the functionality of the developed equipment was proven. It is observed that in this case, both signals have no signs of noise that could compromise the sending of information. These characteristics are due to the fact that the ESP system is not connected to the three-phase supply.

FIGURE 25. The signals of the sent and received data, and the voltage at the motor neutral for the inverter de-energized. In green is the sent signal, the pink is the received one and the yellow refer to the voltage value in the motor neutral.

Around 50 packages of regular variables (pressure, temperature and vibration) were sent, all being monitored by the Hercules SETUP tool. Figure 26 displays a terminal screen where information such as frame size, values of received variables, number of packets received with and without error, Modbus registers, among others, are presented.

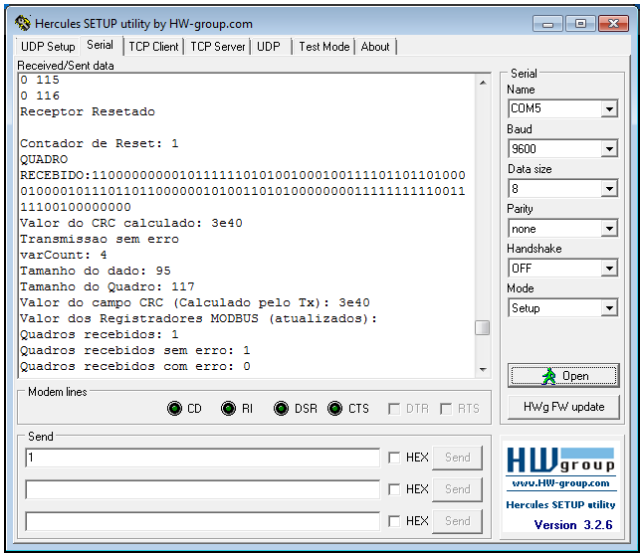

FIGURE 26. Monitoring of the received data.

The experimental arrangement of the previous step was coupled with the ESP power stages: step-down transformer, frequency inverter, and step-up transformer. The present test reproduces the previous experiment, considering the ESP system energized, however not operating. The purpose is to verify the influence of the three-phase network on the communication channel. All packets sent were received without error.

The motor is from Baker Hughes company, model FMHXG with a power of 62 HP and voltage of 1170 V. The pump also manufactured by Baker Hughes, model P4 PMXSSD 400 series with 70 stages. The cable is Prysmian, model EPDM / LEAD / GSTA, 2,236 meters long, 2 AWG (33,6 mm^2), and flat configurations. The purpose of this test is to evaluate the behavior of the communication modules with the ESP system in operation and subjected to a variation of the motor's operating frequency. Therefore, the emitter and receiver were only started after the ESP motor was launched at a frequency of 10 Hz. The transition between the frequency values occurred dynamically, that is, with the system in operation, ranging from 10 to 59.8 Hz.

The Figures 27 and 28 show screenshots of the oscilloscope of the test described for 30 Hz and 60 Hz. Channel 4 of the oscilloscope, in green, represents the signal at the transmitter, the pink wave the sign at the receiver, and the yellow wave reproduces the behavior of the voltage at the motor neutral. The idea of monitoring this voltage is to protect the electronic boards and prevent accidents, as an imbalance in the motor phases would produce a relatively high voltage. It can be seen in the image that the scale of this wave is at 100V per division.

The result shows a voltage oscillations in the motor neutral. However, despite this voltage variation, the digital signals referring to the sent and received data did not present any noise effects. The test lasted 30 minutes, and the results achieved showed no transmission error for any frequency value.

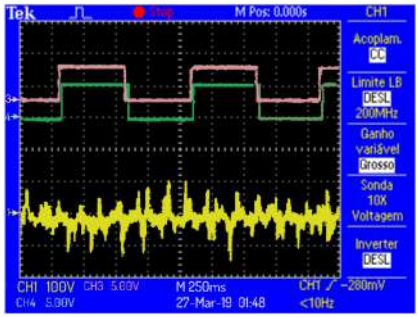

FIGURE 27. The six pulse VSD operating at 30 Hz. waveform using the baker hughes 6-pulse inverter®. VSD operating at 30 Hz.In green is the sent signal, the pink is the received one and the yellow refer to the voltage value in the motor neutral.

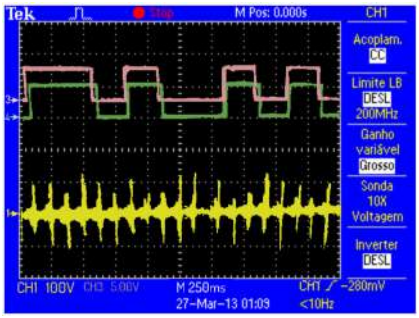

FIGURE 28. The six pulse VSD operating at 60 Hz. waveform using the baker hughes 6-pulse inverter®. VSD operating at 60 Hz.In green is the sent signal, the pink is the received one and the yellow refer to the voltage value in the motor neutral.

Following the same profile, the fourth test considered the same structure, except the frequency inverter. The experimental setup utilizes now a VSD manufactured by Schneider Electric ®, Altivar 61 model, PWM type, which provides the motor with a supply voltage closer to the sinusoidal. Compared to the 6-pulse converter, PWM has, among other advantages, the ability to inject less noise into the network. An active filter, Schneider Electric ®, is also integrated into the same drive panel as the Schneider Electric inverter Accusine model. Despite the existence of this tool that would reduce the disturbances caused by the inverter, it was decided in a first step to leaving it decoupled, to evaluate only the influence of the PWM converter.

This test provides, as well as the previous one, to evaluate the behavior of the signals involved in the transmission, considering an increase of the motor rotation frequency. The motor was started at a low frequency of 30 Hz and was it increased from 5 Hz to 5 Hz until reaching 60 Hz. The packet sending process started after the engine started at low frequency. The test lasted 2 hours, with 120 data packets being sent. Figures 29 and 30 illustrate parts of the signals being sent and received for the frequencies of 30 Hz and 60 Hz, respectively. The signal captured at the transmitter is green, the pink signal refers to the receiver and the yellow signal to the neutral voltage.

As seen in Figures 29 and 30, the monitored signals have virtually no interference from noise. This behavior is mainly

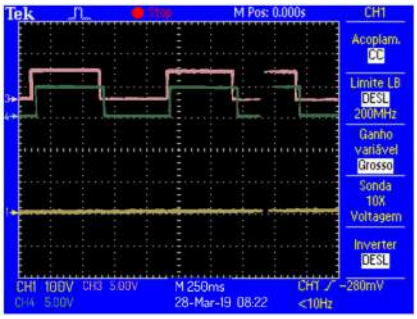

FIGURE 29. Waveform obtained using the PWM inverter *Schneider* ®: VSD operating at 30 Hz. In green is the sent signal, the pink is the received one and the yellow refer to the voltage value in the motor neutral.

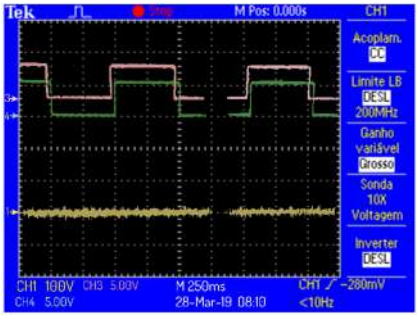

FIGURE 30. Waveform obtained using the PWM inverter *Schneider* ®: VSD operating at 60 Hz. In green is the sent signal, the pink is the received one and the yellow refer to the voltage value in the motor neutral.

due to the PWM inverter quality, which injects less noise into the motor supply line and the cable shield. The increment of the noise of motors supplied from PWM controlled inverters compared with the same one supplied from a sinusoidal supply is relatively small. The engine shutdown caused the generation of a high amplitude impulsive noise (from -300 to 300 V) at the neutral point. The cause for noise with impulsive and short-lived characteristics is due to the instantaneous unbalance of the voltage in the motor winding. Despite the high voltage amplitude in the neutral, the printed circuit boards have not been damaged. Figure 31 highlights this event.

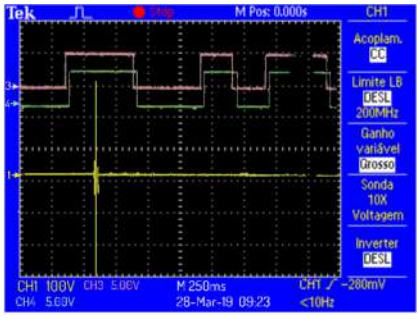

FIGURE 31. Peak voltage in neutral after switching off the PWM inverter.

Finally, the prototypes were subjected to the starting conditions of the well with ESP. The structure of the previous test

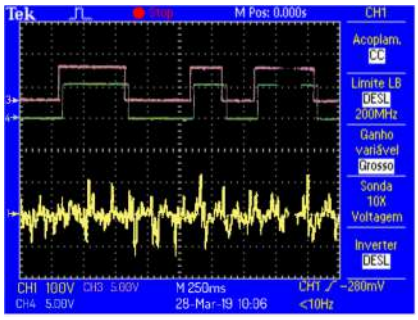

FIGURE 32. The signals of the sent and received data, and the voltage at the motor neutral at low frequencies during ESP startup with Accusine active filter. In green is the sent signal, the pink is the received one and the yellow refer to the voltage value in the motor neutral.

was maintained. However, added the Accusine active filter from Schneider Electric ®. This test aims to analyze how the signals behave during the transient of the activation, in which the channel presents as a very noisy characteristic behavior. Also lasting 40 minutes, the test showed no error in any of the packets sent, including at the critical moment of activation. In Figure 32 it is possible to see the behavior of the neutral voltage in the motor and of the signals sent and received for a frequency of 6.3 Hz during the startup of the ESP system.

IV. CONCLUSION

The favorable results achieved allowed the evaluation of the prototypes' performance under the conditions found in an ESP well. The equipment installed in the ESP wells provided a favorable channel for data transfer. The inductance of the motor winding acts as a filter for high frequencies, eliminating the noise associated with it but leaving only the medium and low AC frequency. The shielded cable, built especially for the ESP protects, or as the name suggests, shields the channel against the effects of electromagnetic interference. In the absence of extra protection, cables can act both as a source, conducting noise to other equipment, as well as a receiver or antenna, capturing radiated EMI from other sources. The active filter installed for each phase at the inverter output is characterized as a low-pass filter and has a cutoff frequency between the output AC frequency and the PWM frequency of the inverter. Therefore, an active filter provides a channel free of harmonic currents caused by non-linear loads. Also, as could be observed in the test that considered the filter active, the voltage in the neutral had a low oscillation, which is due to the ability of the filter to balance the voltage values that reach the motor.

The proposed communication protocol ensure determinism and reliability during the data transfer between the sending and receiving devices. The implementation of two frames of different sizes made it possible to send regular variables (pressure, temperature, and contamination) and vibration data. Manchester encoding enabled synchronization between the bottom and surface modules, and the CRC error detection

method, typically used in digital networks, was used to verify the integrity of the packets.

One of the main contributions of this article is to present a hardware and software solution for monitoring the subsurface parameters of the ESP artificial lift method. In summary, the evaluation results for the first tests showed the reliability and robustness of the proposed telemetry system. The transfer rate of 5 to 10 bps, considered low compared to other telemetry/communication systems, is sufficient for applications such as reading sensors to adjust production and collecting information for predictive maintenance, considering the slow dynamics of ESP.

REFERENCES

[1] S. Quintero, S. Figueiredo, V. Takahashi, R. Llerena, and A. Braga, "Passive downhole pressure sensor based on surface acoustic wave technology," *Sensors*, vol. 17, no. 7, p. 1635, Jul. 2017.
[2] N. Song, M. Wang, B. Dang, S. Liu, and Z. Ren, "Real-time monitoring system of leakage current for electric submersible pump," *IOP Conf. Ser., Mater. Sci. Eng.*, vol. 799, May 2020, Art. no. 012008.
[3] J. Han and Q. Gao, "Research on downhole multi-parameters monitoring system," in *Proc. 7th Int. Power Electron. Motion Control Conf.*, Jun. 2012, pp. 2765–2768.
[4] L. Li, C. Hua, and X. Xu, "Condition monitoring and fault diagnosis of electric submersible pump based on wellhead electrical parameters and production parameters," *Syst. Sci. Control Eng.*, vol. 6, no. 3, pp. 253–261, Sep. 2018.
[5] M. Hackworth and S. Williams, "Real-time decision making for ESP management and optimization," presented at the SPE North Amer. Artif. Lift Conf. Exhib., The Woodlands, TX, USA, Oct. 2016, doi: 10.2118/181219-MS.
[6] S. Spagnolo, S. Pilone, and L. Corti, "Fully retrievable ESP: A new artificial lift concept," in *Proc. Int. Petroleum Technol. Conf.*, Beijing, China: SPE, China, 2013, p. 350.
[7] R. Bates, C. Cosad, L. Fielder, A. Kosmala, S. Hudson, G. Romero, and V. Shanmugam, "Taking the pulse of production wells—ESP surveilanc," *Oilfield Rev.*, vol. 16, no. 2, pp. 16–25, 2004.
[8] R. Flatern, *The Defining Series: Electrical Submersible Pumps*. Houston, TX, USA: Schlumberger, 2015.
[9] X. Liang and E. Fleming, "Electrical submersible pump systems: Evaluating their power consumption," *IEEE Ind. Appl. Mag.*, vol. 19, no. 6, pp. 46–55, Nov. 2013.
[10] X. Liang, J. He, and L. Du, "Electrical submersible pump system grounding: Current practice and future trend," *IEEE Trans. Ind. Appl.*, vol. 51, no. 6, pp. 5030–5037, Nov. 2015.
[11] X. Liang and W. Xu, "Downhole monitoring tool design using power line disturbances," in *Proc. IEEE/IAS 51st Ind. Commercial Power Syst. Tech. Conf. (I&CPS)*, May 2015, pp. 1–11.
[12] X. Liang, O. Ghoreishi, and W. Xu, "Downhole tool design for conditional monitoring of electrical submersible motors in oil field facilities," *IEEE Trans. Ind. Appl.*, vol. 53, no. 3, pp. 3164–3174, May 2017.
[13] O. Ghoreishi, X. Liang, and W. Xu, "Phase-to-phase communication scheme for downhole monitoring tool design in electrical submersible pump systems," *IEEE Trans. Ind. Appl.*, vol. 52, no. 3, pp. 2077–2087, May 2016.
[14] C. Bremner, G. Harris, A. Kosmala, B. Nicholson, A. Ollre, M. Pearcy, C. Salmas, and S. Solanki, "Evolving technologies: Electrical submersible pumps," *Oilfield Rev.*, vol. 18, no. 4, pp. 30–43, 2006.
[15] T. R. Brinner, J. D. Atkins, and M. O. Durham, "Electric submersible pump grounding," *IEEE Trans. Ind. Appl.*, vol. 40, no. 5, pp. 1418–1426, Sep. 2004.
[16] T. R. Brinner and R. A. Durham, "Transient-voltage aspects of grounding," *IEEE Trans. Ind. Appl.*, vol. 46, no. 5, pp. 1796–1804, Sep. 2010.
[17] J. Miaoxin, G. Qiang, and X. Dianguo, "A downhole multi-parameter monitoring system," in *Proc. 3rd Int. Conf. Instrum., Meas., Comput., Commun. Control*, Sep. 2013, pp. 1660–1663.
[18] Y. Qureshi, G. P. P. Gunarathne, and K. Christidis, "Dynamic impedance matching of transmission cables for downhole tools," in *Proc. IEE Seminar Online Monit. Techn. Off-Shore Ind.*, Aberdeen, U.K., 1999, pp. 12/1–12/5, doi: 10:1049=ic:19990731.
[19] D. Fonsêca, A. Salazar, T. Gonçalves, and E. Villarreal, "Electrical modelling of an electrical submersible pump system three-phase power cable used in power line communication," *Przeglad Elektrotechniczny*, vol. 10, no. 3, pp. 22–26, 2019.
[20] X. Liang, N. C. Kar, and J. Liu, "Load filter design method for medium-voltage drive applications in electrical submersible pump systems," *IEEE Trans. Ind. Appl.*, vol. 51, no. 3, pp. 2017–2029, May 2015.
[21] N. K. Mitra, *Principles of Artificial Lift*, 1st ed. Bengaluru, India: Allied Publishers Pvt, 2012. Accessed: Nov. 20, 2020. [Online]. Available: https://books.google.com.br/books?id=6NokTvD4mjoC
[22] J. Miaoxin, Z. Wei, G. Qiang, and X. Dianguo, "An ESP downhole parameters monitoring system based on current loop transmission method," in *Proc. Int. Power Electron. Conf. (IPEC-Hiroshima - ECCE ASIA)*, May 2014, pp. 3050–3054.
[23] Y. Lv, Q. Gao, and D. Xu, "Study on downhole multi-sensor monitoring and data transmission of electric submersible pump," in *Proc. 1st Int. Conf. Instrum., Meas., Comput., Commun. Control*, Oct. 2011, pp. 70–73.
[24] P. Zhang, Q. Gao, L. Cheng, and D. Xu, "Research on downhole multi-parameter comprehensive measurement of ESP," in *Proc. 4th Int. Conf. Instrum. Meas., Comput., Commun. Control*, Sep. 2014, pp. 346–350.
[25] F. Quintaes, A. O. Salazar, A. L. Maitelli, F. Fontes, M. A. A. Vieira, and T. Eslley, "Magnetic sensor used to detect contamination of insulating oil in motors applied to electrical submersible pump," *IEEE Trans. Magn.*, vol. 47, no. 10, pp. 3756–3759, Oct. 2011.

DIEGO ANTONIO DE MOURA FONSÊCA was born in Natal, Rio Grande do Norte, Brazil. He received the degree in computer engineering from the Federal University of Rio Grande do Norte, in 2007, and the master's degree in electrical and computer engineering from the Federal University of Rio Grande do Norte, in 2011. He is currently a Computer Engineer with the Federal University of Rio Grande do Norte. His current research interests include computer engineering, with emphasis on electronic automation of industrial processes, acting mainly on the following themes: instrumentation, industrial automation, and programming.

ANDRÉS ORTIZ SALAZAR (Member, IEEE) was born in Lima, Peru. He received the degree in electronic engineering from the National University of Engineering, Lima, and the master's degree in electric engineering and the Ph.D. degree in electric engineering from the Federal University of Rio de Janeiro, Brazil, in 1989 and 1994, respectively. He held a postdoctoral position in electric engineering with the Tokyo University of Science, SUT, Japan, in 2000. He has been a Teacher with the Federal University of Rio Grande do Norte, since 1994, where teaches instrumentation, industrial automation, power electronics, machine activation, and automation. His researches are concentrated on the Electronic Automation of Electrical and Industrial Processes.

ELMER ROLANDO LLANOS VILLARREAL (Member, IEEE) was born in Huánuco, Peru. He received the B.Sc. degree in mathematics from the National University of Engineering, Lima, Peru, the master's degree in electric engineering from the Polytechnic School University of Sao Paulo, in 1997, and the Ph.D. degree in electric engineering from the Federal University of Santa Catarina, Brazil, in 2002. In 2019, he held a postdoctoral position in electric engineering with the Federal University of Rio Grande do Norte. Since 2009, he has been a Teacher with the Federal Rural University of the Semi-Arid, where teaches linear algebra, linear systems, and numerical calculus. His researches are concentrated on the Mathematical Modeling and control system.

GERMAN ALBERTO ECHAIZ ESPINOZA was born Arequipa, Peru. He received the degree in electronic engineering from the National University of Engineering, Lima, Peru, the master's degree in instrumentation and control, and the Ph.D. degree in energy engineering from the Universidad Nacional de San Agustin de Arequipa, Arequipa, Peru. He is currently the Director of the Academic Department of Electronic Engineering, Universidad Nacional de San Agustin de Arequipa.

ALAN CÁSSIO QUEIROZ BEZERRA LEITE was born in Mossoró, Rio Grande do Norte, Brazil. He received the degree in electrical engineering from the Federal University of Rio Grande do Norte. He was a Technician in electrotechnics from the Federal Institute of Rio Grande do Norte. He was also a Substitute Professor of higher teaching with the School of Sciences and Technologies, Federal University of Rio Grande do Norte, and also with the Department of Communications Engineering. Has to experience in electrical engineering, with emphasis on automation of electrical systems and photovoltaic energy.

energies

MDPI

Article

One Cycle Control of a PWM Rectifier a New Approach

Rodrigo De A. Teixeira [1,†], Werbet L. A. Silva [1,†], Guilherme A. P. De C. A. Pessoa [1,†], Joao T. Carvalho Neto [2,†], Elmer R. L. Villarreal [3,†], Andrés O. Salazar [1,*,†] and Alberto S. Lock [4,†]

1 Department of Computer Engineering and Automation, Federal University of Rio Grande do Norte (DCA-UFRN), Natal 59072-970, Brazil; rodrigoandradeteixeira@gmail.com (R.D.A.T.) ; werbethluizz@hotmail.com (W.L.A.S.); guilhermepillon@hotmail.com (G.A.P.D.C.A.P.)
2 The Federal Institute of Education, Science and Technology of Rio Grande do Norte (IFRN), Natal 59015-000, Brazil; joao.teixeira@ifrn.edu.br
3 Department of Natural Sciences, Mathematics, and Statistics, Federal Rural University of Semi-arid (DCME-UFERSA), Mossoro 59625-900, Brazil; elmerllanos@ufersa.edu.br
4 Renewable and Alternative Energy Center (CEAR-UFPB), João Pessoa, PB 58051-900, Brazil; aslock@cear.ufpb.br
* Correspondence: andres@dca.ufrn.br
† These authors contributed equally to this work.

Received: 1 September 2020; Accepted: 3 October 2020; Published: 21 October 2020

Abstract: This paper analyzes a Digital Signal Processor (DSP) based One Cycle Control (OCC) strategy for a Power Factor Corrector (PFC) rectifier with Common-mode Voltage (CMV) immunity. It is proposed a strategy that utilizes an emulated-resistance-controller in closed-loop configuration to set the dc-link voltage to achieve unity power factor (UPF). It is shown that if the PFC can achieve UPF condition and if the phase voltage is only affected by CMV, then phase current is free from CMV, as well as a lead-lag compensator (LLC) to average phase current.

Keywords: power factor corrector; one cycle control; common-mode voltage; common-mode current

1. Introduction

One-Cycle Control (OCC)is a nonlinear control theory proposed by [1] able to control switching converters with only one switching cycle. The controller achieves instantaneous dynamic control of an average value of the switching variables after a transient. The most important feature of OCC is the control of the carrier amplitude, in contrast to Pulse Width Modulation, which controls the variable. The OCC technique provides: low complexity, low-cost implementation, disturbance rejection, robustness, good stability and fast dynamic response. OCC based controllers have been widely used to control power factor correction and it has been applied in modular multilevel converters [2], grid-tied single-stage buck-boost DC-AC micro-inverters [3], Vienna Rectifiers [4], novel multi-converter-based unified power quality conditioners (MCB-UPQC) [5] and analysis of harmonics, energy consumption and power quality of light-emitting diode lamps equipped in building lighting systems [6]. The literature also presents a novel, two-stage and hybrid approach based on variational mode decomposition (VMD) and the deep stochastic configuration network (DSCN) for power quality (PQ) disturbances detection and classification in power systems [7]. In the field of power quality, two of the most significant concerns are harmonic currents and power factor (PF) caused by nonlinear loads. While the former may cause false triggering of protection devices and bad functioning of motors and transformers, the later reduces available active power at the utility grid. The past few decades have witnessed extensive studies on power quality, mainly to satisfy specific standards, i.e., IEEE 519-1992 [8], which recommend limiting harmonics distortion. In order to solve these issues

for end-consumer, a PWM rectifier can be used to substitute each nonlinear load by an active resistance seen from the utility grid [9]. Hence, this rectifier always tries to achieve unity power factor. If the grid voltage is sinusoidal, then the current drawn by the rectifier must be sinusoidal and in phase with the voltage, avoiding any current harmonics. Several methods have been proposed to achieve UPF in PWM rectifiers based on the enhanced control-loops concept [10], such as: inner current loop, instantaneous power loop and outer voltage loop. To force the phase-current to follow voltage loop reference it is necessary to sense three-phase voltages, a DC-link voltage, three-phase currents [11] and in some cases, the use of a phase-locked loop (PLL) to guarantee voltage and current synchronization [12]. The control techniques based on this concept use space vector modulation (SVM), Park/Clarke transformations and control coupled terms such as: voltage oriented control (VOC) [13], direct power control (DPC) [14], model predictive control (MPC) [15], deadbeat control [16], fuzzy control [17] and neural networks [18]. Nevertheless, these methods are time-consuming, as they rely on system parameters, requiring complicated online calculation. Resistance-emulation is another technique employed in PWM rectifiers, generally using average value and PWM modulators. In this technique is always assumed that UPF is already achieved. There are two main methods based on open-loop and closed-loop controls [9]. Open-loop methods control the estimated emulated-resistance assuming a fixed value [19] while closed-loop methods adjust the emulated-resistance value by feedback [20]. Although these techniques were proposed for single-phase boost converters with diode rectifiers, they are complicated to implement as they employ the four arithmetical operations.

The One Cycle Control is a kind of open-loop method, originally proposed as a hardware technique [21] (Figure 1a) implemented either by a few commercials ICs or just a single chip as a cost-effective solution. It uses a variable sawtooth-carrier-amplitude (Figure 1b) and only adding and subtracting operations, contributing to its arithmetic simplicity and performing its control tasks in the only one switching cycle, therein the name OCC, despite this technique was also proposed for three-phase, six power-switches boost-converter. The OCC technique does not use neither phase-locked-loop (PLL) nor Park/Clarke transformations, which allows a fast dynamic system response while satisfying the UPF condition. Moreover, it eliminates the need of three grid-voltage sensors, which adds control and hardware simplicity. Although this technique was applied several times in active power filters (APF) [22,23], in flexible ac transmission systems (FACTs) [24] and in photovoltaic grid-connected inverters (GCI) [25–27], the OCC has presented such serious instability problems [21,28,29]. To solve these issues it was necessary to add extra circuitry sacrificing control and hardware simplicity.

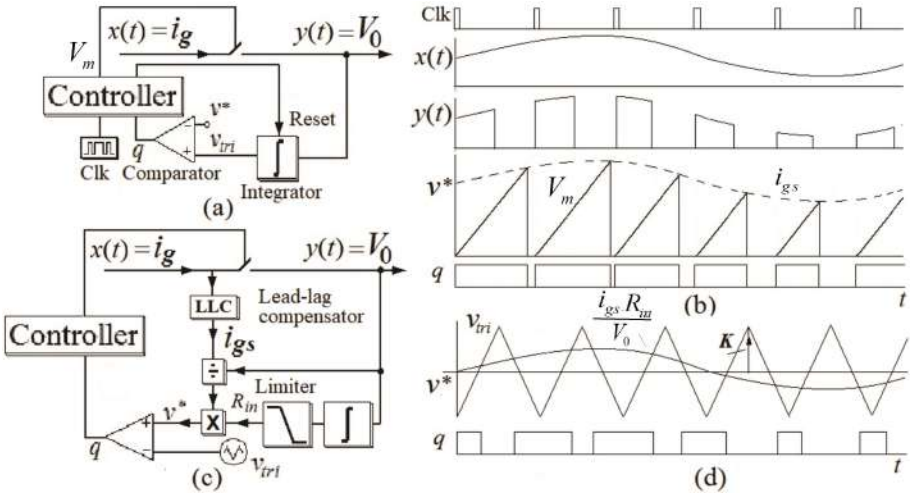

Figure 1. (**a**) Hardware OCC. (**b**) Associate waveforms. (**c**) Software-OCC. (**d**) Associate waveforms.

In order to preserve the control and hardware simplicity, the OCC was emulated in a DSP system. A DSP-based software-OCC was proposed in [30] based on the scheme shown on the Figure 1c.

This version enhances OCC with DSP calculation capability and uses closed-loop resistance emulation. Then, the software offers more possibilities to apply the OCC to the most complex control issues than those of hardware [31–33]. Besides, unlike enhanced-loops methods mentioned above, [11–18] The software-OCC does not use PLL, Park/Clarke transformations or online parameter calculations, therefore, it achieves some control simplicity. However, it was not reported any further analysis, in spite DSPs have already applicated to OCC as a control core, i.e., for motor drivers [34,35] and photovoltaics [27], while OCC runs as a sort of auxiliary circuit. Previous treatments to solve stability problems at no-load have sacrificed OCC simplicity once they use an additional bulky resistor at DC-link [21,29]. Instead, in order to decrease current distortion, an artificial phase-current was created [36–38]. However, despite the efforts, instability remains when load current falls below a certain limit [24,39,40]. On the other side, due to a lack of PLL synchronization, OCC has experienced PF derating at high-load [21,29,37–39]. To avoid this, OCC has sacrificed its simplicity again as they use input voltage multiplexers, and other additional analog and logic circuits [23,24,39–41], requiring the knowledge of 600 angular sectors and to select positive and negative peak voltages as reference current vectors. In [28,42], it was also necessary to sacrifice OCC simplicity by adding a few analog multipliers and heavy and bulky inductors (10 mH), but sacrificing the cost-effectiveness of OCC solution. Hence, despite all the efforts, it is apparent that, to date, OCC has been not able, whatsoever, to solve its own problems fully. Above all, even though a few hardware methods have solve partially OCC stability issues at no-load [21,36–38,42] and at high-load [28,39–41], they were never reported working together over a wide load range. Thus, one of the paper's major contributions is to present a simple and stable DSP based OCC system working at no-load and high-load considering that the proposed digital implementation presents improvements relationed to hardware-OCC systems. Thus, one of the paper's major contributions is to present a simple and stable OCC system working at no-load and high-load.

In this paper, analysis, simulation, and experimental results prove, based on the resistance-emulated controller [30], that software-OCC does not possess instability issues and preserves OCC simplicity and dynamical response, also satisfying UPF condition. The paper is organized as follows: Section 2 presents a review of software-OCC fundamentals. Section 3 shows OCC issues and discusses software-OCC solving method. Section 4 depicts DSP implementation and discusses the cost-effectiveness of software-OCC. Simulation and experimental results are shown in Section 5. Conclusions are shown in Section 6 .

2. Fundamentals of Software-OCC

Software-OCC is a PWM, where an average phase-current compares to carrier and control system is integrated into the modulator, similar to hardware-OCC of (Figure 1c) [21]. Nevertheless, unlike hardware-OCC, this version is not a circuit, but a software. Hence, software-OCC implements OCC features by programming embedded DSP devices and using just a few equations. However, a high-performance OCC system is obtained, as using a high-frequency DSP, the one switching-cycle control can be guaranteed. (Figure 2) displays a three-phase, IGBT PWM rectifier. As in hardware-OCC, it is assumed that,

- The switching frequency f_C is much higher than line frequency f, hence the switching period T_C is much lower than the line period T, so $f_C >> f$ and $T_C << T$.
- The switches in each leg operate in a complementary fashion, i.e., the duty cycle for the upper and bottom switch is d_g and $d_{gn} = (1 - d_g)$, respectively $(g = a, b, c)$, $0 < d_g < 1$.
- Input impedance seen from the grid is a resistance, similar to the resistance emulation concept in [9]. Besides, software-OCC, (Figure 1c), presents the following differences from hardware-OCC.

(i) Multipliers and dividers presence, as they are not much DSP time-consuming [43].
(ii) The average method, i.e., a LLC (Figure 1c) decreases the delay response caused by the lagging part, using a leading constant.

(iii) Carrier generation uses a triangular waveshape, (Figure 1d), instead of a sawtooth carrier in the hardware OCC.
(iv) Fixed amplitude carrier due of a software DSP limitation.
(v) Closed-loop emulated resistance-control, guaranteeing UPF by feedback.
(vi) Use of limiters at resistance control output.

Except for the item (iv), these differences result of the superior software-DSP-calculation capability over hardware technique.

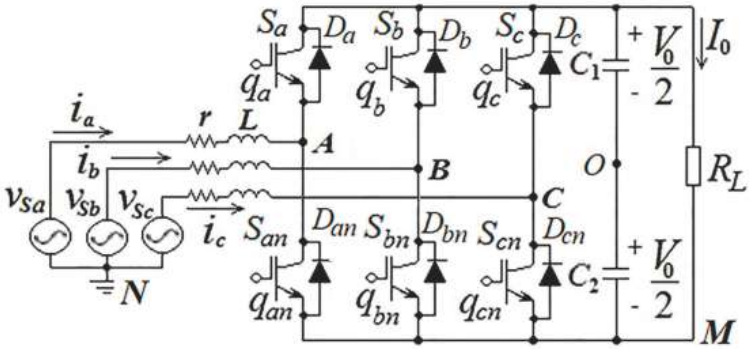

Figure 2. Three phase, PWM rectifier.

Applying Kirchhoff voltage law to the $r-L$ branch in the Figure 2, where r is inductor resistance, L is inductor inductance; v_{Sg} and i_g are grid voltage and phase current, respectively; v_{GN} is pole voltage $(G = A, B, C)$, O is the middle point of dc-link capacitors C_1 and C_2, v_{NO} is the voltage between neutral of the utility grid and middle point O of dc-link voltage, and V_0 and I_0 are load voltage and current respectively.

$$\begin{aligned} v_{Sa} - ri_a - L\frac{di_a}{dt} &= v_{AN} + v_{NO} \\ v_{Sb} - ri_b - L\frac{di_b}{dt} &= v_{BN} + v_{NO} \\ v_{Sc} - ri_c - L\frac{di_c}{dt} &= v_{CN} + v_{NO} \end{aligned} \tag{1}$$

Analysis of Voltage v_{NO}

The expressions given by (1), it is apparent that to obtain an exact expression for phase-current, it is necessary to find an analytical expression for voltage v_{NO}. However, although some previous works indicate that this voltage does not depend on grid frequency [13,44], the mathematical proof is missing. It is always possible to bypass the problem by assuming some control strategy, as it allows additional simplifications [45,46]. Hence, considering a balanced system:

$$\begin{aligned} v_{Sa} + v_{Sb} + v_{Sc} &= 0 \\ i_a + i_b + i_c &= 0 \end{aligned} \tag{2}$$

Grid voltages are given by:

$$\begin{aligned} v_{Sa} &= V_p cos\omega t \\ v_{Sb} &= V_p cos(\omega t - \frac{2\pi}{3}) \\ v_{Sc} &= V_p cos(\omega t + \frac{2\pi}{3}) \end{aligned} \tag{3}$$

where V_p is voltage amplitude, $V_p > 0$. Although OCC does not use references [21,40], for mathematical purposes, it could be useful to admit grid voltage (3), as a virtual phase-current reference, as phase-current has the same waveshape and in phase with of the grid voltages. In addition, considering a balanced system, given by (2), and manipulating (1):

$$v_{NO} = \frac{-1}{3}(v_{AN} + v_{BN} + v_{CN}) \tag{4}$$

The Equation (4) says that voltage v_{NO} is related to pole voltage. In this way, finding an analytical expression for v_{NO} could be long and tedious as in a PWM modulator, pole voltage depends on Bessel functions and Fourier series [47]. From the Equation (4), the average v_{N0} is:

$$\frac{1}{T_C}\int_0^{T_C} v_{NO}dt = \frac{-1}{3T_C}(\int_0^{T_C} v_{AN}dt + \int_0^{T_C} v_{BN}dt + \int_0^{T_C} v_{CN}dt) \tag{5}$$

To find the average pole voltage (Figure 2) it should be noted that:

$$\frac{1}{T_C}\int_0^{T_C} v_{GN}dt = \frac{1}{T_C}\int_0^{T_C} v_{GM}dt - \frac{V_0}{2} \tag{6}$$

Since average value of pole voltage v_{GN} over switching period is given by (see Figure 3):

$$\frac{1}{T_C}\int_0^{T_C} v_{GN}dt = \frac{1}{T_C}[\int_0^{t_{gn}} V_0 dt + \int_{t_{gn}}^{T_C} 0dt] = V_0 d_{gn} \tag{7}$$

where $t_{gn} = d_{gn}T_C$. Hence, combining (6) and (7):

$$\frac{1}{T_C}\int_0^{T_C} v_{GN}dt = \frac{V_0}{2}(1 - 2d_{gn}) \tag{8}$$

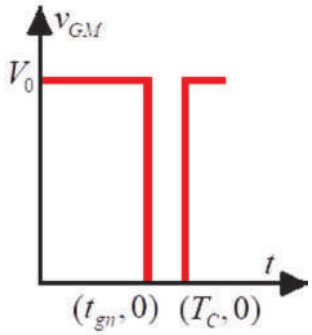

Figure 3. Pole voltage, v_{GM}.

Moreover, as duty cycle in a PWM modulator is proportional to its reference (3), provided that $f_C >> f$ [47]:

$$d_{gn} = D_p cos(\omega t + \phi) \tag{9}$$

where $0 < D_p < 1$, ϕ is such that, $\phi = 0$ for $g = a, \phi = \frac{-2\pi}{3}$ for $g = b$ and $\phi = \frac{2\pi}{3}$ for $g = c$. Then, combining (5), (8) and (9) yields:

$$\frac{1}{T_C}\int_0^{T_C} v_{NO}dt = \frac{-V_0}{2} \tag{10}$$

A common assumption in hardware OCC is that the current ripple is small and that inductor current works in current continuous mode, (CCM) [21], so phase-current is proportional to its average value. Thereby, using this assumption in software-OCC, phase-current can be written as:

$$i_g = \frac{K}{T_C}\int_0^{T_C} i_g(\gamma)d\gamma \tag{11}$$

where K is proportionality constant. Then, for $t > 0$,

$$t di_g(t) = K\int_0^{t} i_g(\gamma)d\gamma \tag{12}$$

differentiating former equation:

$$t\frac{di_g}{dt} = (K-1)i_g \tag{13}$$

combining (1) and (13):

$$v_{Sg} - ri_g - \frac{L}{t}(K-1)i_g = v_{GN} - v_{NO} \tag{14}$$

As input impedance seen from the utility grid is assumed a resistance (condition c):

$$v_{Sg} = R_{in}^0 i_g \tag{15}$$

where R_{in}^0 is assumed input resistance seen from the grid. This resistance is based on loss-free resistor concept [48], since it transfers all energy from the input to the output port and does not dissipate active power. Denoting $r' = (K-1)\frac{L}{t}$, where K is a constant ($K > 1$), and combining (14) and (15):

$$R_{in} i_g = v_{GN} - v_{NO} \tag{16}$$

$$R_{in} = R_{in}^0 - (r + r') \tag{17}$$

Likewise, resistance R_{in} is input resistance seen from the grid. Nonetheless, this is the final resistance which is controlled by software-OCC (21) [30,32]. Averaging Equation (16), it leads to:

$$R_{in}\frac{1}{T_C}\int_0^{T_C} i_g dt = \frac{1}{T_C}\int_0^{T_C} v_{GN}dt - \frac{1}{T_C}\int_0^{T_C} v_{NO}dt \tag{18}$$

Combining the Equations (8), (10) and (18):

$$R_{in} i_{gs} = -V_0(1 - d_{gn}) \tag{19}$$

where i_{gs} is average phase-current. The right term of the former equation is the variable amplitude of the hardware-OCC carrier. The negative signal means that the carrier comes from $-V_0$ to 0 ($d_{gn} = 1$).

The former equation is consistent to emulated resistance concept, as that resistance was assumed since operation beginning [9]. Furthermore, this constitutes a classical OCC equation as it achieves the same level of OCC simplicity, i.e., it uses a sawtooth carrier and does not employ coupled terms, nor Park/Clarke transformations [21,40]. In addition, emulated resistance R_{in} satisfies:

$$v_{Sg} = R_{in} i_g \tag{20}$$

In order to ensure that resistance is seen from the grid, satisfying condition c, R_{in} can become a V_0 voltage controller. So if R_{in} is a V_0 controller, it also controls active power P as it depends on V_0, since $P = V_0 I_0$, where I_0 is load current, Figure 2. Resistance R_{in} also controls power factor indirectly,

since active power (P), reactive power (Q) and apparent power (S) are related by the expression $S = \sqrt{P^2 + Q^2}$. In this sense, as S is fixed, if power P is set to a relatively high value (close to S), reactive power Q should be close to zero:

$$R_{in} = K_p(V_0^* - V_0) + K_I \int (V_0^* - V_0)dt \tag{21}$$

where V_0^* is load voltage reference, K_p, K_I are proportional and integrative PI constants, respectively. PI constants are positive $K_p > 0$, $K_I > 0$, to guarantee that $R_{in} > 0$, when $V_0^* > V_0$. R_{in} controller, name as emulated resistance controller, leads to a resistive impedance seen from the grid. Moreover, in frequency domain R_{in} controller can be expressed as a function of load voltage error $(V_0^* - V_0)$:

$$R_{in} = (V_0^* - V_0)(K_{p1} + \frac{K_{I1}}{s}) \tag{22}$$

According to Equation (19), the average current multiplied by R_{in} is compared to variable amplitude carrier, $V_0 A_{tri}(t)$, where carrier $A_{tri}(t) = -(1 - d_g)$. This could be the essence of the OCC method when implemented by hardware since a variable carrier amplitude s a hardware-OCC characteristic [21,36]. However, as the goal of the system is a software implementation, therefore, DSP characteristics must be included. In this order, it would be useful to modify classical software-OCC modulator, (19) to:

$$q_{gn} = \begin{cases} 1, & when\ i_{gs}.R_{in} \geq V_0.A_{tri}(t) \\ 0, & otherwise \end{cases} \tag{23}$$

where q_{gn} is the logical state at the gate of lower switch of power converter shown in Figure 1a. Yet, as DC-link voltage is positive, $V_0 > 0$, former relation can be modified as:

$$q_{gn} = \begin{cases} 1, & when\ \frac{(i_{gs}R_{in})}{V_0} \geq A_{tri}(t) \\ 0, & otherwise \end{cases} \tag{24}$$

The relationships (23) and (24) are equivalent, once generate the same firing pulses. The relationship represents OCC variable-amplitude carrier Figure 4a while the former is adequate for DSP manipulation, as we willl see later in Section 4. Besides, it resembles a PWM modulator with zero-sequence injection producing Space Vector PWM, (SVPWM [49]), or phase-clamping [50], but without phase-current distortion.

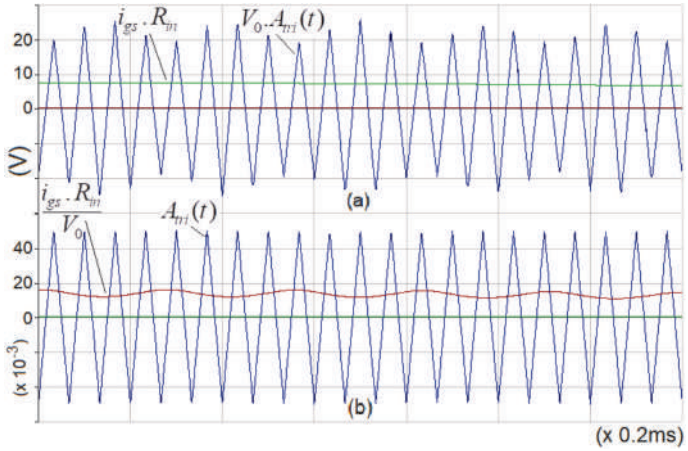

Figure 4. Software-OCC waveforms to $f_C = 15$ kHz and $f = 60$ Hz, it was considered $V_0 = 450 + 67.5sin(2\pi f_2 t)V$, where $f_2 = 3.6$ kHz and $R_{in} = 1\ \Omega$. (**a**) Classical modulator Equation (23). (**b**) Modified modulator Equation (24).

3. Occ Stability Analysis

There is no simple method to analyze hardware-OCC stability by conventional control theory, as this technique is all except conventional, once control and hardware are integrated, while in software-OCC control and hardware are implemented and integrated by software. There are two main stability issues reported in hardware-OCC, at no-load [21,29,36], and high-load [28]. This situations were adressed using a hardware analysis instead of traditional control theory once the OCC instability is provoked by over modulation [21] and hardware limitations and not by poles or zeros misplacement. Stability issues in hardware-OCC can be solved by using an emulated-resistance controller R_{in} of software-OCC [30] and maximum and minimum limiters (Figure 5). The next subsection presents a model based on emulated-resistance control, which explains the hardware-OCC instability and software-OCC solutions to the problem.

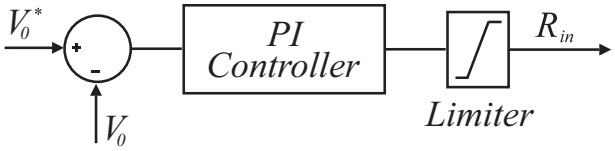

Figure 5. R_{in} controller and its maximum R_{in-max} and minimum R_{in-min} limits.

3.1. Hardware-OCC Theoretical Background

In hardware-OCC, voltage V_m is a PI controller of DC voltage, given by [21]:

$$V_m = (V_0^* - V_0)(K_{p1} + \frac{K_{I1}}{s}) \tag{25}$$

where V_m is the carrier amplitude controller, in frequency domain, V_m is defined by [21]:

$$V_m = \frac{K_1 R_s V_0}{R_{in1}} \tag{26}$$

where K_1 is a parameter, $(\frac{V_{Sg}}{V_0} < K_1 < 1 + \frac{V_{Sg}}{V_0})$; R_S is current sensor resistance $(R_S = 1\ \Omega)$ and R_{in1} is emulated resistance [21]. In addition, as in hardware-OCC firing pulses can be defined as:

$$q_{gnh} = \begin{cases} 1, & when\ i_{gs} \geq v_m.A_{tri}(t) \\ 0, & otherwise \end{cases} \tag{27}$$

where q_{gnh} is the logical state at the gate of lower switch of power converter, A_{trih} is fixed carrier amplitude. The former equation represents the hardware-OCC modulator since modulating wave is compared to a variable-amplitude carrier, controlled by V_m (25). Note that this carrier leads to a multiplication operation, despite OCC arithmetic simplicity. Besides, as for a PWM rectifier, as shown in (Figure 2), average dc voltage V_0 has a voltage ripple V_{0r} related to its peak value V_{0p} [51], (see Figure 5). Hence

$$V_0 = V_{0p} - \frac{I_0}{8C} T_{SW} \tag{28}$$

where $V_{0r} = \frac{-I_0}{8C}$, I_0 is the DC-link current; R_L is dc-link load; $I_0 = \frac{V_0}{R_L}$; C the DC-link equivalent capacitor, $C = \frac{C_1 C_2}{(C_1 + C_2)}$, T_{SW} is switching time period, $T_{SW} = 2T_0$, T_0 is time period between peaks of voltage ripple. Although dc-link capacitor C is assumed large that voltage ripple is neglected and hence average and peak DC-link values are the same [51]. Yet, for practical values of capacitance, only Equation (28) is valid.

3.2. Hardware-OCC Issues

In principle the control technique with hardware-OCC offers a simple solution in terms of hardware, control and arithmetic, however, every system connected to the network needs synchronization, and the lack of synchronization may result in instability and power factor reduction. In order to overcome this situation, the carrier with variable amplitude was created, but at the cost of instability in the system without load.

Stability at no-load: in general in a PWM rectifier the output power P_0 equals input power P_T minus power losses, P_L, ($P_0 = P_T - P_L$). Then, admitting a proportionality factor (K_3) between power losses and input power:

$$P_0 = K_3 P_T \tag{29}$$

In addition, assuming UPF, input power is given by:

$$P_T = 3 V_{Sg} I_g \tag{30}$$

where V_{Sg} and I_g denotes grid voltage and phase current in frequency domain, respectively, while the output is:

$$P_0 = V_0 I_0 \tag{31}$$

Then, combining Equations (29)–(31), it yields:

$$I_g = K_4 I_0 \tag{32}$$

where $(K_4 = \frac{V_0}{(3K_3 V_{Sg})})$ and I_0 is the DC current. The former equation says that phase-current I_g is proportional to I_0. Yet, Equation (32) has practical limits given by the sensitivity of the technique. A small phase-current could exist when I_0 is null, or lower than a threshold value, I_{0th}, causing phase-current distortion when I_g is greater than amplitude V_m, as reported in [21,24,29,36–40]. In order to explain this phenomenon from an emulated-resistance approach, the Equation (26) can be rewritten as:

$$R_{in1} = \frac{K_1 V_0}{V_m} \tag{33}$$

Which leads to a virtual input resistance R_{in1}, as a sort of V_0 controller. Besides, as in OCC, phase-current varies according to [52]:

$$I_g = \frac{V_{Sg}}{R_e + sL} \tag{34}$$

where R_e denotes the OCC input resistance in frequency domain. Hence, by making $R_e = R_{in1}$ and combining Equations (25), (33) and (34):

$$m_a = \frac{I_g}{V_m} = \frac{V_{Sg}}{K_1 V_0 + L(V_0^* - V_0)(sK_{P1} + K_{I1})} \tag{35}$$

The Equation (35) denotes the modulation index m_a, as I_g is the phase current in the frequency domain and V_m is carrier amplitude [21]. Applying the final value theorem to Equation (35), for a unit step response $(\frac{1}{s})$:

$$m_a = lim_{S \to 0} \frac{1}{S} S \frac{I_g}{V_m} = \frac{V_{Sg}}{K_1 V_0 + L K_I (V_0^* - V_0)} \tag{36}$$

Due to the increase of V_0 without load, it tends to its reference V_0^*, while $V_0^* - V_0$ approaches zero. In this case, Equation (36) becomes:

$$m_a = \frac{V_{Sg}}{K_1 V_0} \tag{37}$$

The overmodulation occurs when $m_a > 1$ Equation (37) as $\frac{V_p}{V_0} > K_1 > 0$, once $(V_{Sg} = V_p cos\omega t)$, Equation (3), $m_a > 0$, $K_1 = 0.25\frac{V_p}{V_0}$, $m_a = 4$, $V_p > 0$, $V_0 > 0$. The Equation (37) can explain why previous works did not suppress fully the overmodulation by growing or falling the I_g [24,36–40], once K_1 cannot be controlled [21]. The Figure 6 illustrates this by ploting m_a vs. K_1, Equation (37), for $0.67 > K_1 > 0.19$, $V_p = 155.56$ V, $V_0 = 467$ V, when I_g grows 20%(A) and when I_g falls 20% (C). Notice that when $K_1 \leq 0.25$, the method does not work, as $m_a > 1$.

As was mentioned earlier, PF derating occurs through a lack of grid synchronization. However, this can not be predicted by an open-loop resistance-emulator value, r_e [12,21] as in frequency domain it leads to $R_e = \frac{r_e}{s}$, which combined to Equation (34), it gives $I_g = s\frac{V_{Sg}}{(r_e + s^2 L)}$, leading to an admittance angle $\phi_v = arctan(\frac{I_g}{V_{Sg}}) = \frac{\pi}{2}$. However, a better prediction can be obtained by combining Equations (25) and (35):

$$\frac{I_g}{V_{Sg}} = \frac{(V_0^* - V_0)(sK_{P1} + K_{I1})}{[sK_{P1}L(V_0^* - V_0) + K_{I1}L(V_0^* - V_0) + K_1 V_0]s} \tag{38}$$

Therefore, the phase angle ϕ_v is given by:

$$\phi_v = \phi_1 - arctan[\frac{\omega L K_{P1}(8C(V_0^* - V_{0p}) + I_0 T_{SW})}{LK_{I1}(8C(V_0^* - V_{0p}) + I_0 T_{SW}) + K_1(8CV_{0p} + I_0 T_{SW})}] \tag{39}$$

$$\frac{\partial \phi}{\partial I_0} = \frac{8\omega L C T_{SW} K_{P1} K_1 V_0^*}{(LK_{I1} I_0 T_{SW} + K_1(8CV_{0p} - I_0 T_{SW}))^2 + (\omega L K_{P1} I_0 T_{SW})^2} \tag{40}$$

It can be noticed that the former equation predicts PF derating because admittance angle ϕ_v is a decreasing function. It matches the results of previous works [29,37–39]. The Figure 7 shows Equation (39), $V_p = 155.56$ V, $V_{0p} = V_0^* = 467$ V, $K_1 = 1$, $K_{p1} = 1$, $K_{I1} = 1$. The figure confirms that ϕ_v is decreasing when I_0 increases, from $I_0 = 10$A (P) to $I_0 = 20$A (N) and $I_0 = 30$A (M).

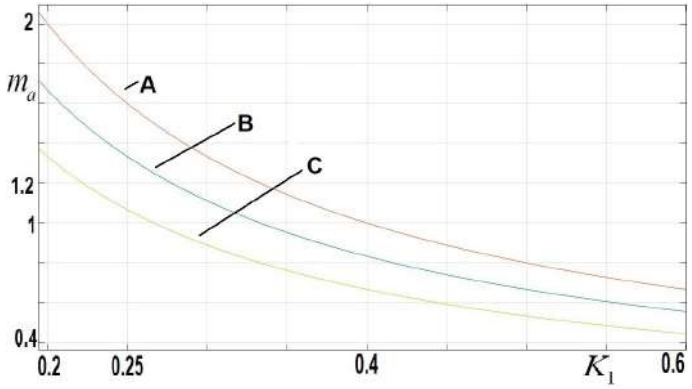

Figure 6. Hardware-OCC. *ma* vs. K_1, Equation (37), The curve denoted by A: I_g grows 20%, The curve denoted by B: Without correction C: I_g falls 20%.

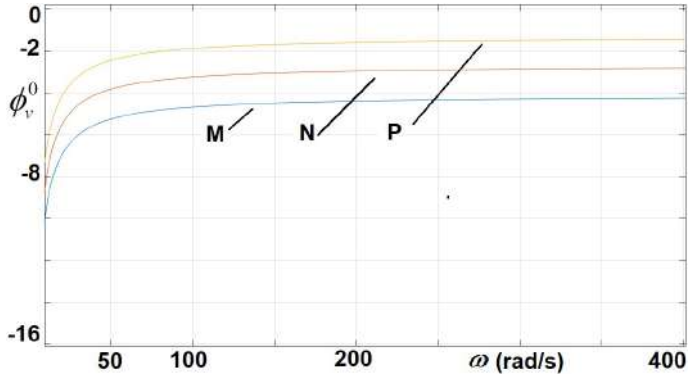

Figure 7. Hardware-OCC. Angle ϕ_v (0.1^0/div) vs. angular frequency (rad/s) as a function of the dc current I_0, $V_0^* = V_{0p} = 467$ V, $T_{sw} = 8.33$ ms, $C = 1000$ µF, L = 1 mH, $K_{p1} = K_{I1} = K_I = 1$.

3.3. Software-OCC Solutions

Although subtle, the main difference between Hardware-OCC and Software-OCC is in bus voltage control, in the hardware version this controller is called V_m and controls the amplitude of the carrier Equations (25) and (27), in the software version this controller is called R_{in} and controls modulation. However, only R_{in} allows the OCC to solve instability problems and power factor decrease.

As was mentioned earlier, phase-current is proportional to DC current, Equation (32), but only under practical limits, through the sensitivity of OCC modulator. Since a small distorted phase-current could appear when DC current is less than the threshold current, I_{0th}. In order to avoid this effect in software-OCC, maximum the controller limiter R_{in-max} could be calibrated to set up minimum phase-current I_{gmin}, since $I_g = \frac{V_{Sg}}{R_{in}}$, Equation (20). Then, as voltage V_{Sg} is fixed, minimum phase-current I_{gmin} occurs when the resistance R_{inmax} is reached, as $I_g R_{in} = V_{Sg}$ is a hyperbolic curve working at first quadrant, $I_g > 0$, $R_{in} > 0$. That is:

$$I_{gmin} = \frac{V_{Sg}}{R_{inmax}} \tag{41}$$

Thereby, to avoid phase-current distortion at no-load, R_{inmax} must be set up to achieve a minimum phase-current I_{gmin} when DC current is less than I_{0th} . Thus:

$$I_g = \begin{cases} I_{gmin}, & when\ I_0 < I_{0th} \\ K_4 I_0, & when\ I_0 \geq I_{0th} \end{cases} \tag{42}$$

Figure 8 shows a plot of I_g vs. I_0, Equation (32), when $I_{gmin} = 1.4$ A, $I_{0th} = 0.5$ A, $v_{Sg} = 110$ V, $R_{inmax} = 78.01\ \Omega$. Unlike hardware-OCC, a tiny DC controller value does not provoke overmodulation, so the current distortion becomes simpler to avoid. As at no-load, there is no current distortion, it would be necessary to check if at no-load PF derating could be generated. In this sense, no-load and high-load cases must be analyzed for PF derating. Thus, substituting $R_e = R_{in}$ in Equation (34):

$$I_g = \frac{V_{Sg}}{R_{in} + sL} \tag{43}$$

Note that in the former equation if denominator left term is much greater than the right one, $(R_{in} >> sL)$ on this way, the last equation becomes equivalent to Equation (20). However, to achieve UPF, another expression can be found by combining Equations (22) and (43), and relation $(R_{in} >> sL)$:

$$I_g = \frac{V_{Sg}}{(V_0^* - V_0)(K_P + \frac{K_I}{s})} \tag{44}$$

The Relation ($R_{in} >> sL$) can be forced by setting resistance lower limit $R_{in_min} = 10\omega L$, as showed in Figure 5, since in practice this relation implies ($R_{in} \geq 10\omega L$ $R_{in} \geq 10\omega L$). Besides, from the Expression (44), admittance angle ($\phi = arctan(\frac{I_g}{V_{Sg}})$) is given by:

$$\phi_v = \frac{\pi}{2} - arctan(\frac{\omega K_P}{K_I}) \quad (45)$$

It can be noticed that this angle does not depend on the DC current, nor dc voltage. Figure 9 shows a plot of admittance angle ϕ_v vs. ω, for the software-OCC, Equation (45), when $K_P = 1$ and $K_I = 1$. This plot does not depend on the DC current.

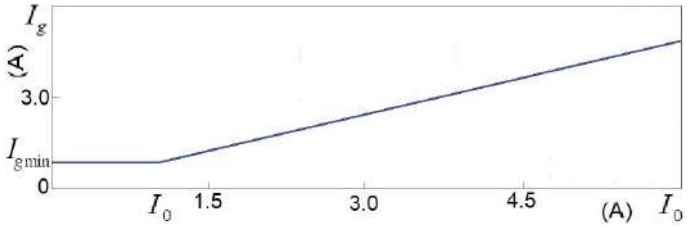

Figure 8. Software-OCC, I_g vs. I_0, Equation (34), with a minimum value, $I_{gmin} = 1$, $V_{Sg} = 110$ V and $V_0^* = 467$ V.

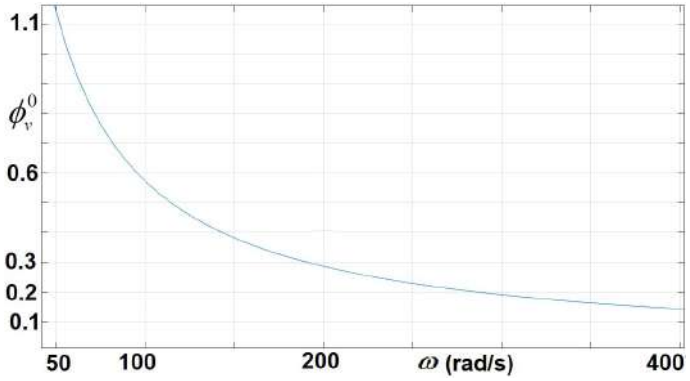

Figure 9. Software-OCC. Angle ϕ_v(0.10/div) vs. angular frequency (rad/s) as a function of dc current I_0, $V_0^* = V_{0p} = 467$ V, $T_{SW} = 8.33$ ms, $C = 1000$ µF, $L = 1$ mH and $K_{p1} = K_{I1} = K_I = 1$.

4. DSP Implementation

As can be observed in Figure 10a, Software-OCC controller employs embedded DSP devices like PWM modulators, analog to digital converters and the arithmetic-logic unit, blocks to perform all its tasks digitally, arithmetic and logic operations (including multiplication and division), digital comparators, digital inverters, PI controllers, output limiters and lead-lag compensators (LLC). Yet, it is necessary a phase-current conditioner. As observed in the Figure 10b, it is necessary a phase-current conditioner consisting of a Hall-effect current-sensor [53], some operational amplifiers, OP-AMPs, and a few resistors to change phase-current over dc voltage and then transforms it into digital, through A/D converter.

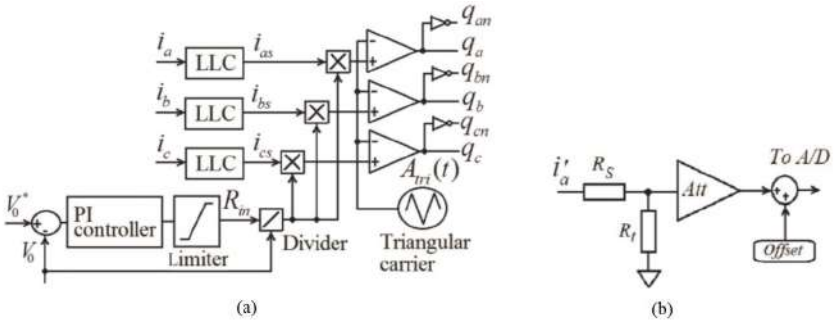

Figure 10. (**a**) Software-OCC. (**b**) Phase-current conditioner.

Hence, a proportionality between analog and digital is guaranteed for DSP to perform OCC control operations, once a scale factor K_S (bits /A) is maintained for all currents. For hardware-OCC, something similar occurs, but now the scale factor is a resistance R_S (V/A), since a current-sensor resistor is generally used in hardware systems. Anyway, for the sake of simplicity, to establish an equivalency between hardware and software-OCC, it is defined in the later, resistor R_S as unity, $R_S = 1\ \Omega$, denoting that phase-current corresponds to the digital value adopted in DSP control operations. After the digitalizing process, phase-current pass through the software implemented LLC, which averages phase-current according to:

$$F(s) = G_0 \frac{(1 + s\tau_1)}{(1 + s\tau_2)} \tag{46}$$

where $(F(s) = \frac{I_{gs}(s)}{I_g(s)})$, and $I_{gs}(s)$ and $I_g(s)$ correspond in the frequency domain to the phase current and its average respectively , in the time domain G_0 is the gain, and τ_1 , τ_2 are lead and lag compensator constants. The main idea of the former equation is to average the phase-current i_g without unwanted delay on phase angle, from the manipulation of τ_1 and τ_2 values. A further analysis of LLC on software-OCC is performed in [32]. On the other hand, for DSP, carrier waveshape (a sawtooth or a symmetrical triangle) is a choice of DSP-PWM modulator. Thus, in software-OCC, a triangle carrier is chosen since, for a sinusoidal modulating wave, it produces less current harmonics than those in a sawtooth carrier [54]. Another DSP choice is produced when carrier slope (rising or falling) intercepts current, generating an inherent delay related to the inverse of the carrier frequency. This does not jeopardize the time control algorithm, as DSP operations are performed between the interceptions. Yet, in software-OCC, a variation in carrier amplitude also involves a variation in carrier frequency, as shown in Table 1 [55]. Then, there is no direct method to change carrier amplitude without vary carrier frequency also. However, in order to solve this issue, focusing on generating the same firing pulses, the OCC modulator (Equation (23)) is modified as in the Equation (24), which becomes the most suitable expression for DSP implementation as it considers a fixed carrier amplitude. In fact, the software-OCC controller is based on Equations (21) and (24), as observed in Figure 10 .

Table 1. Carrier Amplitude and frequency for DSP TMS3020F335.

Carrier Amplitude (A)	f_C (kHz)
3750	20
5000	15
7500	10

Cost-Effectiveness Software-OCC Discussion

Although the solution with Hardware-OCC is a cost effective solution [21], it presented serious stability problems, which was not practical for applications like APF [56] and photovoltaic systems [27].

Later instability solutions performed by hardware at no-load were reported, but there was always current distortion when dc current falls below a certain level [24,36–40], except when a bulky resistor was placed at dc-link [21,29] and at high-load where complex circuits [23,24,39–41], or costly systems were used [28,42]. Thereby, despite these works represent a nice try to solve specific problems, they do not provide a definitive solution, even sacrificing hardware simplicity, or cost-effectiveness of OCC [21,29]. Furthermore, any of the above-mentioned reported works were capable of operating both at no-load and at high-load. Thus, to compare the fair cost-effectiveness of existing hardware-OCC works with present software-OCC, it would be necessary to compare reported works of the same performance, that is, OCC rectifiers operating at a wide range of load. Otherwise, it is like comparing a calculator with a computer. Above all, although the present work was implemented by using a TMS 320*F*28335 evaluation board in a laboratory prototype, a pretty cost-effective solution could be found acquiring a DSP chip and its accessories separately, or by using a simpler DSP, or a microcontroller chip, i.e., a PIC. In any case, the present proposal results in a cost-effective solution on a full range of load, at least, for lack of another option.

5. Simulation and Experimental Results

The performance of software-OCC has been verified by simulation by using MATLAB and PSCAD/EMTDC and by experimental runs using DSP TMS320F28335. The experiments were performed in a three-phase rectifier similar to the one shown on the Figure 11. The simulation results from PSCAD software are shown in the Figures 12–14. The MATLAB ones are shown in the Figures 7 and 9. From the Figures 15–25 we show the experimental results.

Parameter values are in Table 2. In Figures 21 and 26, V_{grms} = 110 V and $V_0^* = 100$ V, but in Figures 15–20, due to technical problems, V_{grms} = 21 V and $V_0^* = 100$ V. Figure 12 presents a simulation result only with hardware-OCC evidencing its instability, while the Figure 26 presents a simulation result on stability at no-load and high-load conditions for software-OCC. It can be observed that at no-load, it does not present hardware-OCC stability issues, like overmodulation [21] (current distortion), nor present PF derating. This result verify Equation (43) when $K_{P1} >> K_{I1}$.

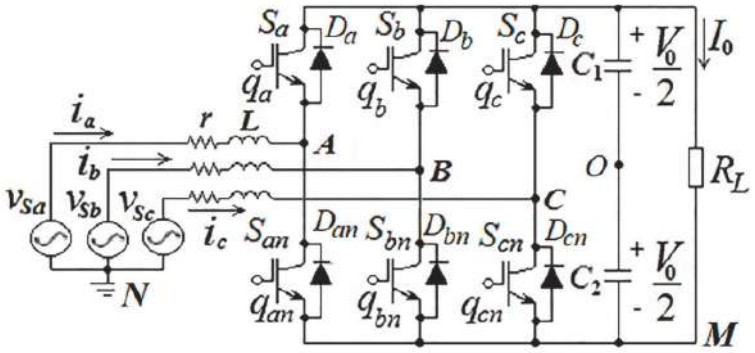

Figure 11. Electrical diagram of the PWM rectifier used on the experimental setup.

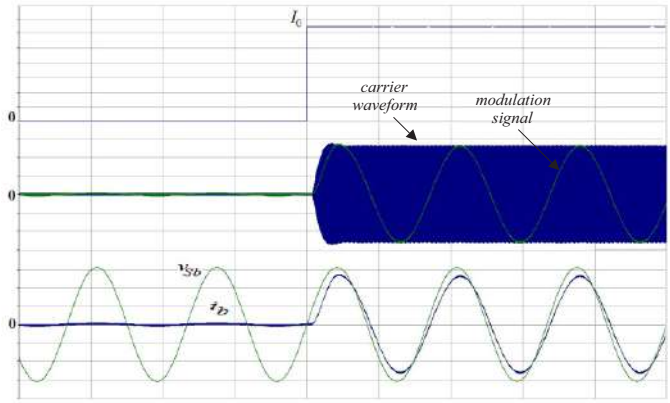

Figure 12. Hardware-OCC. Overmodulation at no-load. Transitory from no-load to high-load (10 ms/div). Upper: DC current I_0 (5 A/div). Middle: waveform carrier and modulation signal (2 V/div). Down: Grid voltage (50 V/div) and phase current (5 A/div).

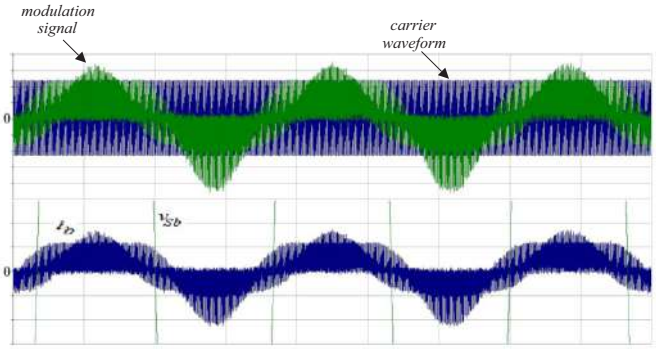

Figure 13. Overmodulation at no-load (5 ms/div). Detailed view. Upper: waveform carrier and modulation signal (0.05 V/div). Down: Grid voltage (2.5 V/div) and phase current (2.5 A/div).

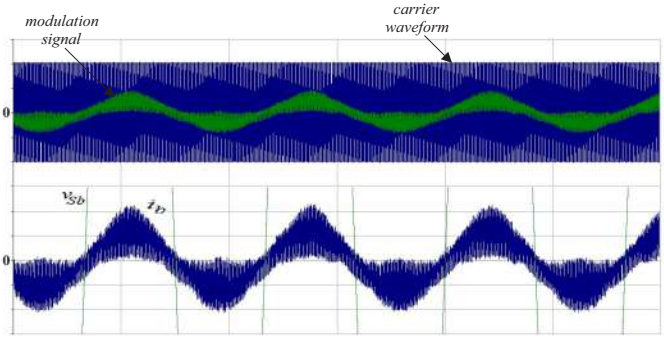

Figure 14. No overmodulation (5 ms/div). Detailed view. Upper: waveform carrier and modulation signal (0.05 V/div). Down: Grid voltage (2.5 V/div) and phase current (2.5 A/div).

Experimental results in Figures 15–24 are dedicated to confirm former result, or enhance it. Figure 26 shows software-OCC behavior at start-up at no-load, verifying that there is no current distortion, unlike [21], nor even in smaller amount [36–38]. This is because to avoid current distortion, software-OCC can define minimum current when load current is null, by using R_{in}. Figure 15 illustrates dc-link voltage response to a current step, from no-load to high-load, showing a relatively fast-software-OCC dynamic-response considering dc-link capacitors size, thus complementing the Figures 12–14. Figure 16 is the enlargement of Figure 15 highlighting the rapid dynamics of the system. Figure 15 shows the dynamics of the emulated resistor R_{in} due to load variation in the rectifier circuit.

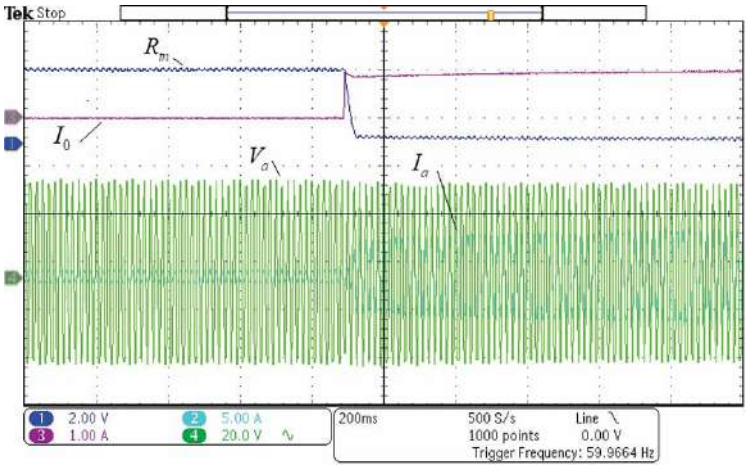

Figure 15. R_{in} controller (5 Ω/V) (2 V/div), dc-link current (1 A/div), grid voltage (20 V/div) and phase current (5 A/div) for PWM rectifier transient from no -load to high -load. Hor. 40 ms/div.

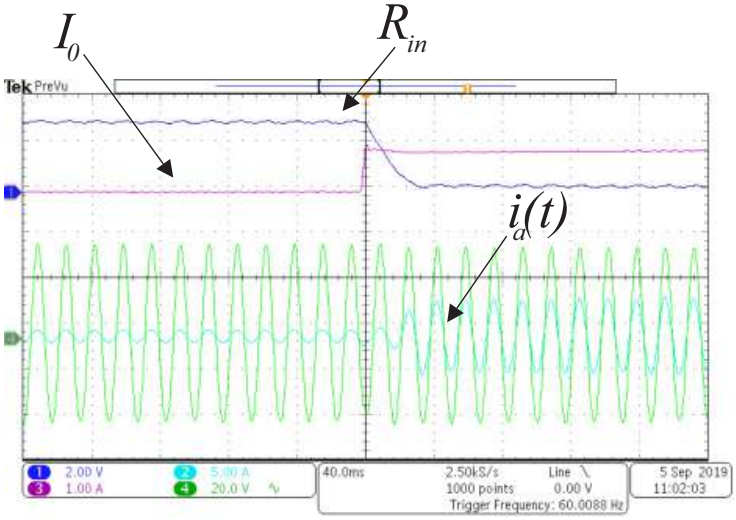

Figure 16. R_{in} controller (5 Ω/V) (2 V/div), DC-link current (1 A/div), grid voltage (20 V/div) and phase current (5 A/div) for PWM rectifier transient from no-load to high-load. Hor. 40 ms/div.

It can be noticed in the Figure 26, that at no-load, when $I_0 = 0$, phase-current is small, but it does not exhibit current distortion, as it could be expected considering power balancing in Equation (41), but instead, regarding a minimum phase-current, according to Equation (42), see Figures 16, 17 and 19. Also, it can be observed that there is no power factor derating, as occurs in conventional hardware-OCC [21], (see Figures 18 and 20), and to preserve power factor, it is not necessary to use bulky inductors, unlike [28,42], as observed in Table. 2. Thus, also confirming the Figure 26.

Table 2. Parameters on simulation and experimentals.

Parameter	R (Ω)	ω (r/s)	L (mH)	C_1 (μF)	C_2 (μF)	v_{Sg} (V)	τ_1 (ms)	τ_2 (ms)	f_C (kHz)
Simulation	1	377	1	670	670	110	1	0.15	20
Experimental	1	377	1	2200	2200	110	1	0.15	25

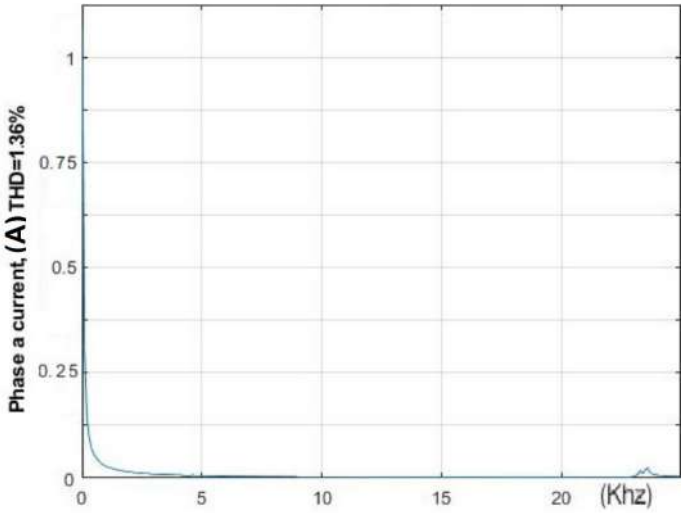

Figure 17. Harmonic spectrum. Phase a current, at no = load. $f_C = 24$ kHz. THD = 1.36%.

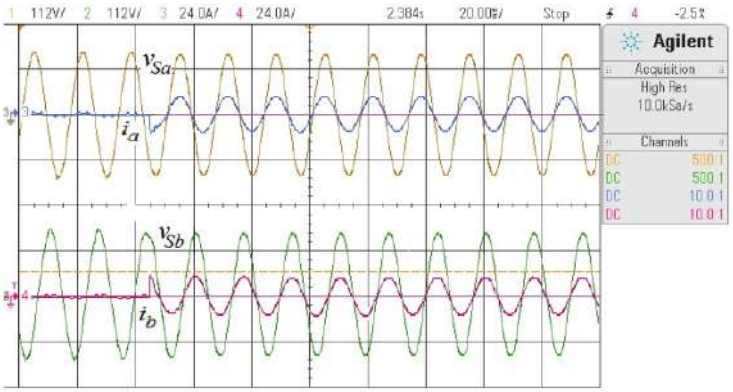

Figure 18. (20 ms/div). Grid voltage (2 V/div) and phase-current (1 A/div) at high-load, f_C = 24 kHz. Phase A.

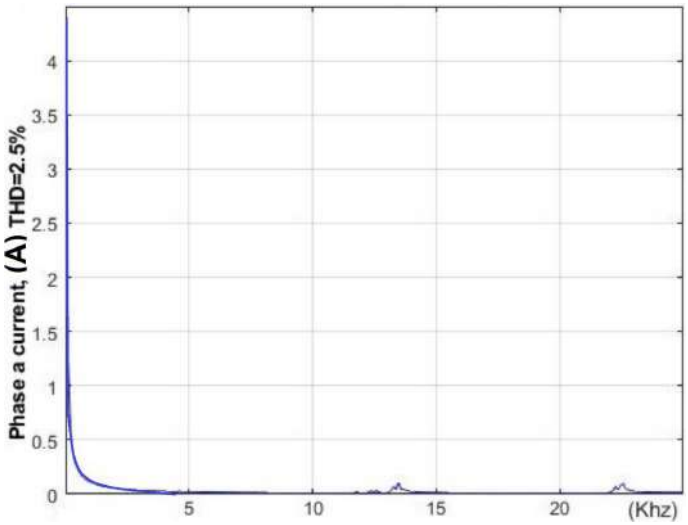

Figure 19. Phase A current at a high-load situation with $f_C = 24$ kHz and $THD = 2.5\%$.

From Figures 17 and 19, it can be deduced that the present proposal satisfies IEEE Std 519-1992 [8], as current distortion is small. The Figure 18 shows the proposed controller start-up when the load is

high. It illustrates a high dynamic response of software-OCC at high-load and that in such conditions there is no PF derating. This result could substitute Figures 16 and 23 results, once these figures do not achieve high-load results. On the other hand, the Figure 20 shows PF derating vs. phase current at different load conditions. Figure 20 demonstrates that there is a tiny variation when phase currents change. Figures 21 and 22 illustrate DC-link voltage response to a current step, from high-load to no-load, showing a relatively fast software-OCC dynamic-response due to DC-link capacitors size, thus complementing the Figure 26. Figure 23 illustrate the current variation at the output of the rectifier I_0 and the resistance R_{in}.

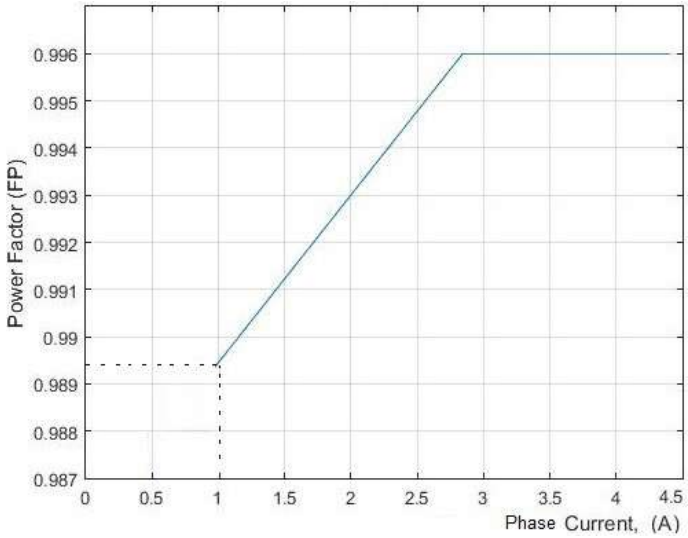

Figure 20. Power factor vs. phase current.

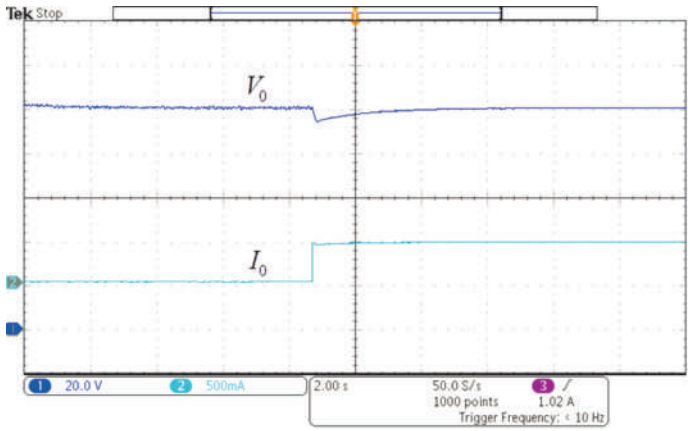

Figure 21. DC-link voltage V_0 (20 V/div) and DC-link current I_0 (0.5 A/div), for the PWM rectifier transient from no-load to high-load. V_{grms} = 21 V and 2 s/div.

Figure 24 illustrates the dynamic response of software PWM-OCC (switching frequency: 24 kHz, R_L: 100 Ω) as well as the charging capacitor of the dc-link voltage. It spends approximately 0.55 s, which is consistent with C = 1100 µF, Table 2, and R_L. The time constant $\tau = R_L C$ and charging capacitor should last 3τ approx. Although OCC systems usually have a high dynamic response, for DC-link capacitor charging, this response depends on the capacitor value. In the present case, the capacitor value could not be changed due to the physical stability of the Semikron board and laboratory facilities setup Figure 25.

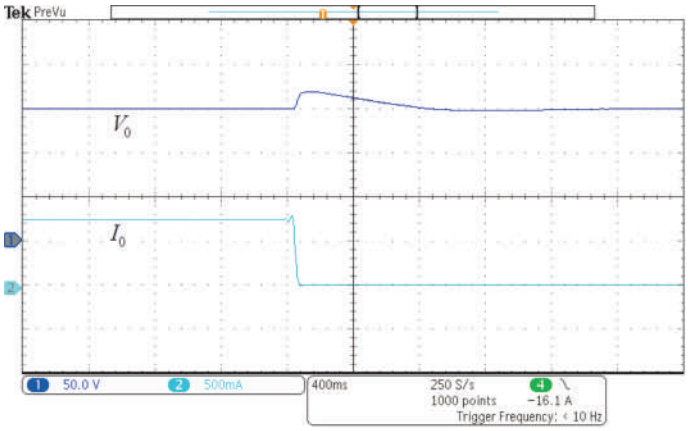

Figure 22. PWM rectifier transient from high-load to no-load. DC-link voltage (50 V/div) and dc-link current (2A/div). $V_{grms} = 21$ V. Hor 0.4 s/div.

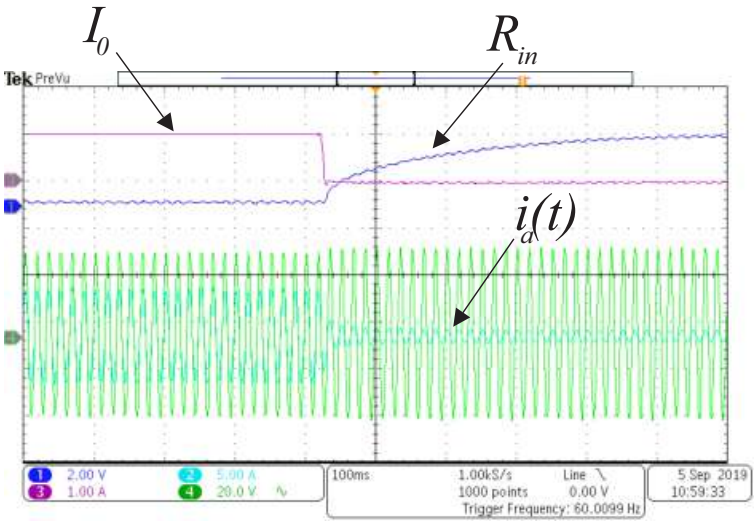

Figure 23. R_{in} controller (5 Ω/V) (2 V/div), DC-link current (1 A/div), grid voltage (20 V/div) and phase current (5 A/div) for the PWM rectifier transient from high-load to no-load. Hor 40 ms/div.

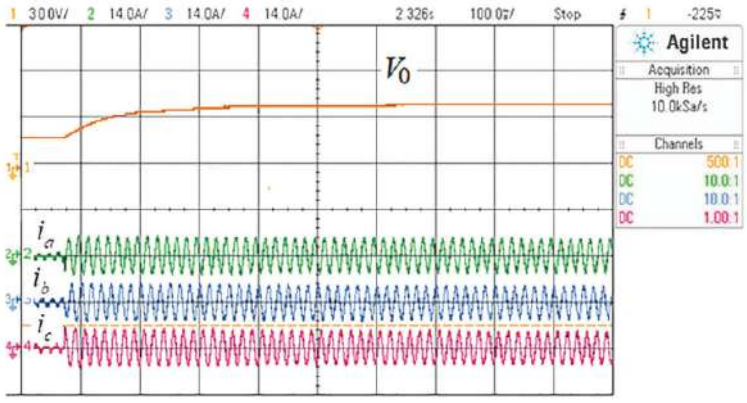

Figure 24. DC-link voltage V_0 (300 V/div) and phase currents i_a, i_b and i_c (14 A/div), $V_0^* = 390$ V and $V_{grms} = 110$ V. Hor 100 ms/div.

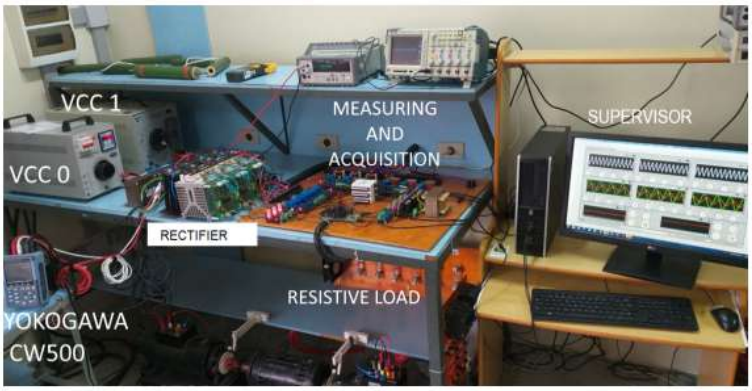

Figure 25. Experimental set-up.

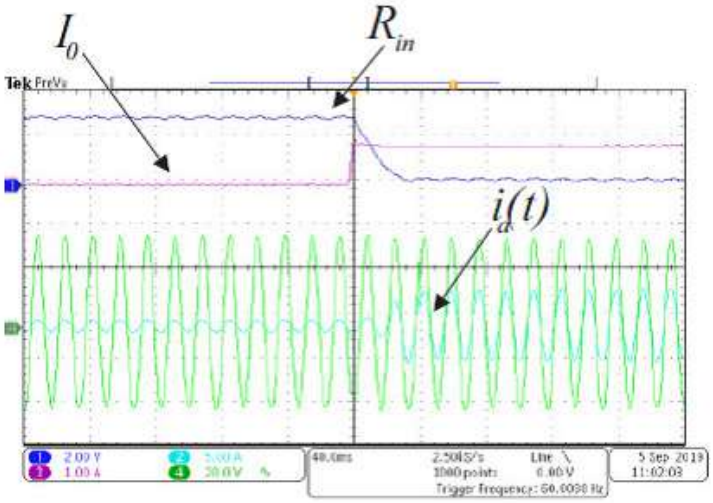

Figure 26. Software-OCC. Transitory from no-load to high-load (10 ms/div). DC current I_0 (5 A/div). waveform carrier and modulation signal (0.1 u/div). Grid voltage (50 V/div) and phase currents (5Ω/div).

6. Conclusions

Despite the stability problems, the hardware-OCC contributions to power quality like hardware and control simplicity and high dynamic response are well known. Somehow, software-OCC raises as a solution to these problems and as a way to enhance and increase OCC contributions. The DSP can not emulate variable-carrier amplitude OCC in this software version, since switching frequency depends on the carrier amplitude and vice versa. However, using a mathematical equivalency, the firing gate pulses of the software-OCC and the hardware-OCC are equivalent. This allows the resistance controller limiters to solve stability issues.

From the stability analysis of the emulated-resistance controller for a PWM rectifier, it has stated that: despite, several authors provided solutions to hardware-OCC instability at no-load, or at high-load separately; any of these provide a full-load solution, at no-load and at high-load at the same time. The Software-OCC does not present Hardware-OCC problems, even over a wide load range, and presents a cost-effective solution, once DSP and its components were acquired separately, or a simpler DSP or a PIC was acquired. The Software-OCC also provided fast dynamic-response in comparison to the researches in this field, eliminating power factor derating and minimizing current distortion caused by overmodulation.

Author Contributions: A.O.S. and A.S.L. conceived and designed the study; J.T.C.N., methodology ; R.D.A.T., G.A.P.D.C.A.P. and W.L.A.S. performed the simulations and experiments; J.T.C.N. and A.S.L. reviewed the manuscript and provided valuable suggestions; E.R.L.V. and A.L. wrote the paper; supervision, A.O.S. All authors have read and agreed to the published version of the manuscript.

Funding: This research was funded in part by the Coordenacao de Aperfeicoamento de Pessoal de Nivel Superior-Brasil (CAPES)-Finance Code 001 and Conselho Nacional de Desenvolvimento Cientifico e Tecnologico (CNPq).

Conflicts of Interest: The authors declare no conflict of interest.

Abbreviations

The following abbreviations are used in this manuscript:

DSP	Digital Signal Processor
OCC	One Cycle Control
CMV	Common-mode Voltage
LLC	lead-lag compensator
UPF	unity power factor
APF	active power filters
FACTs	flexible ac transmission systems
GCI	photo-voltaic grid-connected inverters.

References

1. Smedley, K.M.; Cuk, S. One-cycle control of switching converte. In Proceedings of 22nd Annual IEEE Power Electronics Specialists Conference (PESC '91), Cambridge, UK, 24–27 June 1991; pp. 888–896.
2. Zhao, B.; Huangfu, Y.; Abramovitz, A. Derivation of OCC Modulator for Grid-Tied Single-Stage Buck-Boost Inverter Operating in the Discontinuous Conduction Mode. *Energies* **2020** , *13*, 3168.
3. Tian, X.; Ma, Y.; Yu, J.; Wang, C.; Cheng, H. A Modified One-Cycle-Control Method for Modular Multilevel Converters. *Energies* **2019**, *12*, 157.
4. Wang, C.; Liu, J.; Cheng, H.; Zhuang, Y.; Zhao, Z. A Modified One-Cycle Control for Vienna Rectifiers with Functionality of Input Power Factor Regulation and Input Current Distortion Mitigation. *Energies* **2019**, *12*, 3375.
5. Yang, B.; Liu, K.; Zhang, S.; Zhao, J. Design and Implementation of Novel Multi-Converter-Based Unified Power Quality Conditioner for Low-Voltage High-Current Distribution System. *Energies* **2018**, *11*, 3150.
6. Phannil, N.; Jettanasen, C.; Ngaopitakkul, A. Harmonics and Reduction of Energy Consumption in Lighting Systems by Using LED Lamps. *Energies* **2018**, *11*, 3169.
7. Cai, K. ; Alalibo, B.P. ; Cao, W.; Liu, Z.; Wang, Z.; Li, G. Hybrid Approach for Detecting and Classifying Power Quality Disturbances Based on the Variational Mode Decomposition and Deep Stochastic Configuration Network. *Energies* **2018**, *11*, 3040.
8. IEEE. *Recommended Practice and Requirements for Harmonic Control in Electric Power Systems*; IEEE Standard 519-1992; IEEE: Piscataway, NJ, USA, 1992.
9. Erickson, R.W. *Fundamentals of Power Electronics*; Kluwer Academic Publishers: Dordrecht, The Netherlands, 2000.
10. Rodriguez, J.R.; Dixon, J.W. ; Espinoza, J.R.; Pontt, J.; Lezana, P. PWM regenerative rectifiers: state of the art. *IEEE Trans. Ind. Electron.* **2005**, *52*, 5–22.
11. Hartman, M.; Ertl, H.; Kolar, J.W. Current control of three phase rectifier system using three independent current controllers. *IEEE Trans. Power Electron.* **2013**, *28*, 2088–3000.
12. Chung, S.K. Phase-locked loop for grid-connected three-phase power conversion systems. *IEE Proc.-Electr. Power Appl.* **2000**, *147*, 213–219.
13. Kazmierkowski, M.; Malesani, L. Current control techniques for three-phase voltage-source PWM converters: A survey. *IEEE Trans. Ind. Electron.* **1998**, *45*, 691–703.
14. Monfared, M.; Rastegar, H.; Kojabadi, H.M. High performance direct instantaneous power control of PWM rectifiers. *Energy Convers. Manag.* **2010**, *51*, 947–954.

15. Bouafia, A.; Gaubert, J.; Krim, F. Design and implementation of predictive current control of three-phase PWM rectifier using space-vector modulation (SVM). *Energy Convers. Manag.* **2010**, *51*, 2473–2481.
16. Malesani, L.; Mattavelli, P.; Buso, S. Robust dead-beat current control for PWM rectifier and active filters. *IEEE Trans. Ind. Appl.* **1999**, *35*, 613–620.
17. Dixon, J.; Contardo, J.; Moran, L. A Fuzzy-Controlled Active Front-End Rectifier with Current Harmonic Filtering Characteristics and Minimum Sensing Variables. *IEEE Trans. Power Electron.* **1999**, *14*, 724–729.
18. Coteli, R.; Acikgoz, H.; Ucar, F.; Dandil, B. Design and implementation of Type-2 fuzzy neural system controller for PWM rectifiers. *Int. J. Hydrog. Energy* **2017**,*42*, 20759–20771.
19. Chattopadhyay, S.; Ramanarayanan, V. Digital Implementation of a Line Current Shaping Algorithm for Three Phase High Power Factor Boost Rectifier Without Input Voltage Sensing. *IEEE Trans. Power Electron.* **2004**, *19*, 709–711.
20. Maksimovic, D.; Jang, Y.; Erickson, R.W. Nonlinear-carrier control for high-power-factor boost rectifiers. *IEEE Trans. Power Electron.* **1996**, *11*, 578–584.
21. Qiao, C.; Smedley, K.M. Unified constant-frequency integration control of three-phase standard bridge boost rectifiers with power-factor correction. *IEEE Trans. Ind. Electron.* **2003**, *50*,100–107.
22. Qiao, C.; Smedley, K.M. Three-Phase Bipolar Mode Active Power Filters. *IEEE Trans. Ind. Appl.* **2002** *38*, 149–158.
23. Qiao, C.; Jin, T.; Smedley, K.M. One-cycle control of three-phase active power filter with vector operation. *IEEE Trans. Ind. Electron.* **2004** *51*, 455–463.
24. Jin, T.; Li, L.; Smedley, K.M. A Universal Vector Controller for Four-Quadrant Three-Phase Power Converters. *IEEE Trans. Circuits Syst. Regul. Pap.* **2007**, *54*, 377–390.
25. Chen, Y.; Smedley, K.M. A cost-effective single-stage inverter with maximum power point tracking. *IEEE Trans. Power Electron.* **2004**, *45*, 1289–1294.
26. Chen, Y.; Smedley, K.M. Three-Phase Boost-Type Grid-Connected Inverter. *IEEE Trans. Power Electron.* **2008**, *23*, 2301–2309.
27. Fortunato, M.; Giustiniani, A.; Petrone, G.; Spagnuolo, G.; Vitelli, M. Maximum Power Point Tracking in a One-Cycle-Controlled Single-Stage Photovoltaic Inverter. *IEEE Trans. Ind. Electron.* **2008**, *55*, 2684–2693.
28. Ghodke, D.V.; Sreeraj, E.S.; Chatterjee, K.; Fernandes, B.G. One-Cycle-Controlled Bidirectional AC-to-DC Converter with Constant Power Factor. *IEEE Trans. Ind. Electron.* **2009**, *56*, 1499–1519.
29. Smedley, K.; Zhou, L.; Qiao, C. Unified constant-frequency integration control of active power filters-steady-state and dynamics. *IEEE Trans. Power Electron.* **2001**, *16*, 428–436.
30. Lock, A.S.; Da Silva, E.R.C.; Elbuluk, M.E.; Fernandes, D.A. A hybrid current control for a controlled rectifier. In Proceedings of the IEEE Energy Conversion Congress and Exposition (ECCE), Atlanta, GA, USA, 12–16 September 2010; pp. 920–926.
31. Lock, A.S.; Da Silva, E.R.C.; Elbuluk, M.E.; Fernandes, D.A. Torque control of induction motor drives based on One-Cycle Control method. In Proceedings of the 2012 IEEE Industry Applications Society Annual Meeting, Las Vegas, NV, USA, 7–11 October 2012; pp. 1–8.
32. Lock, A.S.; Da Silva, E.R.C.; Elbuluk, M.E.; Fernandes, D.A. An -OCC strategy for common-mode current rejection. *IEEE Trans. Ind. Appl.* **2016**, **52**, 4935–4945.
33. Bento, A.M. ; Lock, A.S.; Da Silva, E.R.C.; Fernandes, D.A. Hybrid one-cycle control technique for three-phase power factor Control. *IET Power Electron.* **2018**, *11*,484–490.
34. Primavera, S.; Rella, G.; Maddaleno, F.; Smedley, K.; Abramovitz, A. One-cycle controlled three-phase electronic load. *IET Power Electron.* **2012**, *5*, 827–832.
35. Niasar, A.H. ; Moghbeli, H. ; Kashani, E.B. A Low-Cost Sensorless BLDC Motor Drive using One-Cycle Current Control Strategy. In Proceedings of the 2014 22nd Iranian Conference on Electrical Engineering (ICEE), Tehran, Iran, 20–22 May 2014; pp. 659–664.
36. Vamanan, N.; John, V. Dual comparison One Cycle Control for single phase AC to DC converters. *IEEE Trans. Ind. Appl.* **2016** *52*, 3267–3278.
37. Ghodke, D.V.; Chatterjee, K.; Fernandes, B.G. Modified One-Cycle Controlled Bidirectional High-Power-Factor AC-to-DC Converter. *IEEE Trans. Ind. Electron.* **2008**, *55*, 2459–2472.
38. Chatterjee, K.; Ghodke, D.V.; Chandra, A.; Al-Haddad, K. Modified one cycle controlled load compensator. *IET Power Electron.* **2011**, *4*, 481–490.

39. Chen, Y.; Smedley, K.M. Parallel operation of one-cycle controlled three-phase PFC rectifiers. *IEEE Trans. Ind. Electron.* **2007**, *54*, 3217–3224.
40. Chen, G.; Smedley, K.M. Steady-State and Dynamic Study of One-Cycle-Controlled Three-Phase Power-Factor Correction. *IEEE Trans. Ind. Electron.* **2005**, *52*, 355–362.
41. Jin, T.; Li, L.; Smedley, K. A universal vector controller for three-phase PFC, APF, STATCOM, and grid-connected inverter. In Proceedings of the Nineteenth Annual IEEE Applied Power Electronics Conference and Exposition, APEC '04, Anaheim, CA, USA, 22–26 February 2004; pp. 594–600.
42. Ghodke, A.A.; Chatterjee, K. One-cycle-controlled bidirectional three-phase unity power factor *ac*/*dc* converter without having voltage sensors. *IET Power Electron.* **2005**, *5*, 1944–1955.
43. Texas Instruments (2012) SPRS439M: TMS320F28335 Data Manual. Available online: http://www.ti.com (accessed on 29 July 2020).
44. Hava, A.M.; Un, E. Performance Analysis of Reduced Common-Mode Voltage PWM Methods and Comparison with Standard PWM Methods for Three-Phase Voltage-Source Inverters. *IEEE Trans. Power Electron.* **2009**, *45*, 782–793.
45. Lai, R.; Wang, F.; Burgos, R.; Boroyevich, D.; Jiang, D.; Zhang, D. Average Modeling and Control Design for VIENNA-Type Rectifers Considering the DC-Link Voltage Balance. *IEEE Trans. Power Electron.* **2009**, *24*, 2509–2521.
46. Lee, D. ; Lim, D. AC Voltage and Current Sensorless Control of Three-Phase PWM Rectifiers. *IEEE Trans. Power Electron.* **2002**, *17*, 883–890.
47. Holmes, D.G.; Lipo, T.A. *Pulse Width Modulation for Power Converters*; Wiley: New York, NY, USA, 2003.
48. Singer, S.; Smilovitz, D. Transmission line-based loss free resistor. *IEEE Trans. Circuits Syst. Fundam. Theory Appl.* **1994**, *41*, 120–126.
49. Blasko, V. A hybrid PWM strategy combining modified space vector and triangle comparison methods. In Proceedings of the PESC Record. 27th Annual IEEE Power Electronics Specialists Conference, Baveno, Italy, 23–27 June 1996; pp. 872–1878.
50. Hava, A.M.; Kerkman, R.J.; Lipo, T.A. Simple analytical and graphical methods for carrier-based PWM-VSI drives. *IEEE Trans. Power Electron.* **1999**, *14*,49–61.
51. Mohan, N. ; Undeland, T.M. ; Robbins, W.P. *Power Electronics Converters, Applications, and Design*, 3rd ed.; John Wiley & Sons: Hoboken, NJ, USA, 2002.
52. Ben-Yaakov, S. ; Zeltser, I. The dynamics of a PWM boost converter with resistive input. *IEEE Trans. Ind. Appl.* **1999**, *46*, 613–619.
53. LEM, Current Sensor LA25-NP. Available online: https://uk.rs-online.com/web/p/current-transducers/0286311/ (accessed on 29 July 2020).
54. Sun, J. *Pulse-width Modulation in Dynamics and Control of Switched Electronic Systems*; Springer: London, UK, 2012.
55. Texas Instruments, Inc. Using PWM Output as a Digital-to-Analog Converter on a TMS320F28X, Dallas, TX, USA, Appl. Rep. SPAA88A. (2008). Available online: http://www.ti.com (accessed on 29 July 2020).
56. Qasim, M. ; Kanjiya, P. ; Khadkikar, V. Artificial-neural-network-based phase-locking scheme for active power filters. *IEEE Trans. Ind. Electron.* **2014**, *61*, 3857–3866.

Publisher's Note: MDPI stays neutral with regard to jurisdictional claims in published maps and institutional affiliations.

© 2020 by the authors. Licensee MDPI, Basel, Switzerland. This article is an open access article distributed under the terms and conditions of the Creative Commons Attribution (CC BY) license (http://creativecommons.org/licenses/by/4.0/).

Diego FONSÊCA[1], Andres SALAZAR[1], Tomaz GONÇALVES[1], Elmer VILLARREAL[2]

Federal University of Rio Grande do Norte (1), Federal University of the Semi-Arid (2), Brazil

doi:10.15199/48.2019.10.04

Electrical modelling of an electrical submersible pump system three-phase power cable used in power line communication

***Abstract**. In this paper, an analysis of electrical parameters of a 2036 m ESP three-phase power cable and round profile has been carried out. This analysis will provide subsidies to electrically model the channel through which the data will be transmitted from downhole to the surface. A printed circuit board was developed through the correct grouping of passive electronic components to represent the same impedance and phase behavior of the measured ESP power cable for a frequency range from 20 Hz to 200 kHz.*

Streszczenie.** W artykule nalizowany jest system komunikacji w zanurzeniowej pompie zasilanej napieciem trójfazowy za pośrednictwem kabla. Ten sam kabel jest też wykorzystywany do przesyłania sygnałów z czujników. **Model elektryczny pompy zanurzeniowej w której kabel zasilający wykorzystywany jest do komunikacji.

Keywords: electrical submersible pump, three-phase power cable, artificial lift, impedance analysis.
Słowa kluczowe: pompa zaniurzenmiowa, kabel zasilahjący, przesyłanie danych.

Introduction

Electrical submersible pumps (ESPs) are commonly used artificial lift method in deep wells in oil industry. ESPs are typically installed in oil wells ranging from a few hundred to a few thousand feet deep [1].

In the ESP artificial lift method the electric energy is transmitted to the bottom of the well through a cable, where it is transformed into mechanical energy by a subsurface motor. This motor is connected to a centrifugal pump, which transmits the energy to the fluid in the form of pressure, lifting it to the surface. Fig. 1 shows the structure of a ESP well with its main components.

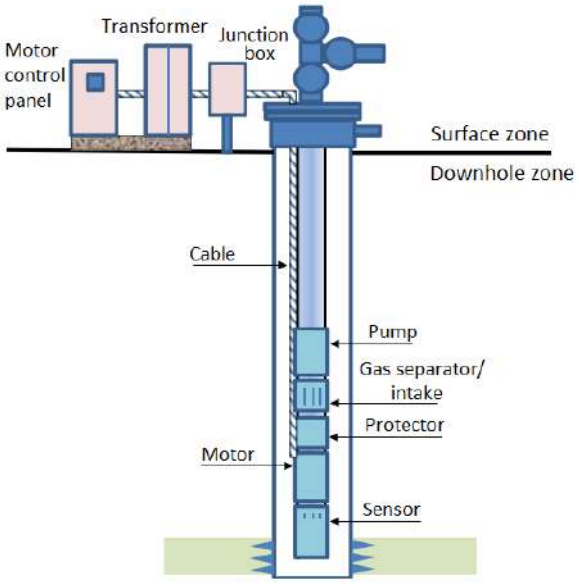

Fig.1. Typical Electrical Submersible Pump system and main components.

To assist in optimizing production, gathering equipment lifetime data gathering and to ensure optimal ESP performance, operators may install downhole sensors that continuously acquire real-time system measurements such as pump intake and discharge pressures and temperatures, vibration, current leakage rate [1, 2, 3] and contamination of insulating oil in motors [4, 5]

The downhole monitoring tools are used to transmit the read data to the surface. They are connected to the neutral of the electrical submersible motor at the bottom of the ESP string and send signals through the main power cable to the surface read out unit.

One comon downhole monitoring tool design used in the field is to utilize a modulated DC loop current over the three-phase power cables to transmit data between the downhole sensors and the surface monitoring electronics unit. The downhole tool is connected to the Y-point of the ESP motor and to the ground of the downhole system [5, 6].

In this dc communication scheme, the surface electronic device provides DC power to the downhole sensor circuitry over the main power cable with the ground serving as the return path. The main power cable and surface electronic device are separated through a DC choke [1, 3].

Downhole sensors, designed in the form of a current sink, retrieve the dc power from the neutral-point of the submersible motor and modulate the current signal. The surface electronic devices determine downhole conditions by detecting and measuring the modulated current signal [1, 3].

In this paper an electrical model is proposed that accurately reproduces the electrical impedance and phase behavior of a ESP cable 2,036 m long for a specific frequency range. The model will allow a more thorough analysis of the channel in order to obtain points of low impedance and, make it possible an increase in the transmission rates of the data to the surface.

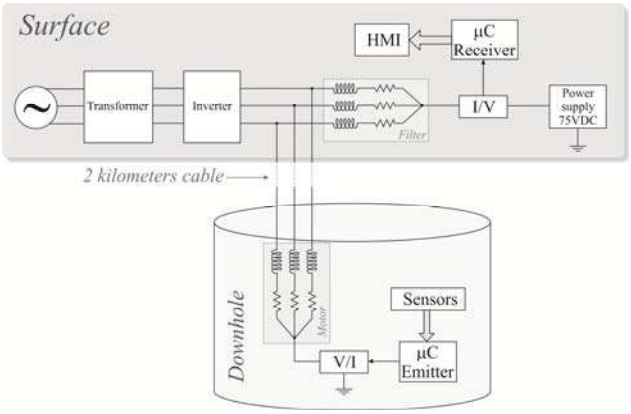

Fig.2. Overview of ESP communication modules.

ESP System Configuration With the Proposed Communication Channel and Electrical Modules

The collected data will be sent to the surface through a communication system as showed in Fig. 2. The downhole sensor, formed by the sensors, microcontroller emitter and voltage-current converter *(V/I)*, is connected to the neutral of the motor. At this point a DC (Direct Current) current signal is inserted by the downhole sensor, which will flow over the three phases of the electrical supply cable. On the surface, a three-phase Y connection inductive filter acts as an interface for withdrawing the DC current signal, as well as removing signals at the fundamental frequency. The current signal is available to the surface module formed by the current-voltage converter (*I/V*), the microcontroller receiver and the 75 V_{DC}, power supply, which is responsible for powering the electronics on the downhole sensor.

Impedance of three-phase ESP power cable

The data transmission rate on the ESP systems varies from 5 to 10 bits/s [7]. This data transfer rate is adopted due to the physical layer provided by the ESP system, which acts as a low-pass filter with a cutoff frequency of 10 Hz.

In this sense, a more accurate analysis of the channel, which is the three-phase cable itself, is required. However, given the difficulty of access to ESP equipment as a cable and motor, the proposal is to design an electronic circuit that reproduce the same electrical behavior (impedance and phase as a function of frequency) of a ESP cable. In this paper, was focused only in the modeling of the power cable. The Impedance measurements was carried out for a low votlage power cable. The cable length was 2036 meters, three-phase 4 AWG and flat profile. The cable was measured in the following signal couplings: L_1 e L_2. The input impedance was measured when the L_1 and L_2 ends was short-circuited and when they were open, the signal being injected into L_1 and returned by L_2. The measured frequency band was 20 Hz – 10 MHz and a linear frequency sweep was applied. The impedance analyser Keysight E4990A stored 500 data points (frequency, absolute value and phase) for each measurement.

The impedance measurement with signal coupling $L_1 - L_2$ and cable end short-circuited is illustrated in Fig. 3.

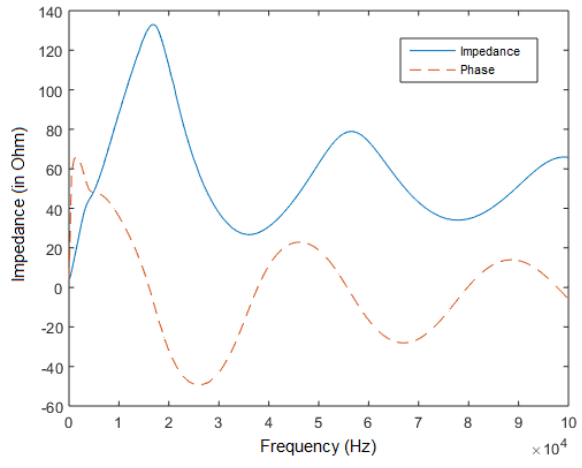

Fig.3. Input impedance (continuous line) and phase (dashed line) as a function of frequency for the low voltage power cable with signal coupling $L_1 - L_2$ and cable end short-circuited.

Fig. 3 shows the repetition of peaks and slopes in the impedance curve. At the impedance peak, the cable behaves as a parallel resonant circuit and at the point of slope presents the characteristic of a series resonant circuit.

In case of no losses in the cable the input impedance of the circuit would be infinite when it was in parallel resonant. The input resistance, in this case, should have a very high value (infinity) for the current to flow into the capacitive and inductive components without loss of energy by resistive components, resulting in the desired resonance. The same goes for the series resonant circuit. Thus, to have a perfect resonance between the inductors and capacitors, the input impedance value should be zero for the current to flow to the resonant components without losing power. Therefore, if the load and discharge of the capacitor occur without losses, the cycle would occur for infinite time. As a consequence a sinusoidal signal would be generated and it frequency would depend on the values of the capacitor and the inductor. In practice, however, the inductor leads and circuit resistors represent a resistance that absorbs energy. Thus, the oscillation that occurs is cushioned until it disappears.

Influence of parasitic elements

All real components have their frequency-dependent values due to the existence of parasitic elements. However, not all parasitic elements affect measurements, but some more prominent determine the frequency response of the component. The prominent parasitic elements will be dominant when the impedance value of the primary element is no longer the same [7]. According to [8], in relation to capacitors, the inductive parasite series (L_S) is the main cause of the frequency response. At low frequencies, the impedance phase angle (q) is about *-90°*, thus, the reactance is capacitive.

The capacitor frequency response has a minimum impedance point at a self-resonance frequency (SRF), which is determined from the capacitance and parasitic inductance of a series equivalent circuit model for the capacitor [7]. At the self-resonance frequency, the capacitive and inductive reactance values are the same, according to equation 1.

$$\frac{1}{\omega \times C} = \omega \times L_S \tag{1}$$

where: ω – Angular frequency, C – capacitance, L – series parasitic inductance.

As a result, the phase angle is $0°$ and the device is resistive. After the resonant frequency, the phase angle changes to a positive value around $+90°$ and, therefore, the reactance becomes inductive due to the parasitic inductance being predominant.

Capacitors behave as inductive devices at frequencies above the SRF and as a result can not be used as capacitors at these particular frequencies [7]. Likewise, about the inductors, the parasitic capacitance causes a typical frequency response. Due to the parasitic capacitance (C_P), the inductor has a maximum impedance point at the SRF, where

$$\omega \times L = \frac{1}{\omega \times C_P} \tag{2}$$

where: ω – Angular frequency, C – parallel parasitic capacitance, L –inductance.

In the low frequency region (below the SRF), the reactance is inductive. After the self-resonance frequency, the parasitic capacitance becomes dominant and the reactance becomes capacitive. The SRF determines the maximum usable frequency of capacitors and inductors.

At frequencies above the SRF, a negative inductance value is displayed because the measured inductance value (L_m) is calculated from a capacitive reactance vector, which is te opposit of the inductive vector. The same happens for the measured capacitance values (C_m) when they pick frequencies above the SRF, since these are now calculated from an inductive reactance vector. Therefore, analyzing the obtained data, can be see that at resonance frequency, the values of inductances are negative, then it means that the parasite capacitance predominates in relation to the inductance.

As it can be seen in Fig. 3 the phase tends to become negative as it approaches the respective resonant frequencies. It is known that the phase is zero in the resonant frequency, however soon after this frequency, the value tends to be negative, showing again that the parasite capacitance predominates. In addition, it is noted that after the frequency starts to approach the resonance frequency of a series circuit (in this case, 36 kHz), the phase value starts to increase again and becomes positive, indicating that the inductance is predominating. And so the cycle repeats itself by going through all the resonance points. The inductor together with the parasitic capacitor in parallel, form the peaks of the impedance curves and the capacitor together as series parasitic inductor, form the slopes of the impedance curves.

Electrical model of ESP three-phase power cable

The methodology used to find the capacitance, inductance and resistance values was to fix an inductance value that represents the same inductance value of the ESP cable, and then find the value of the parasite capacitance.

However, the L_S data obtained from the impedance analyzer indicated that the inductance varies greatly according to frequency. This behavior is due to the fact that: the higher the frequency and the closer to the (parallel) resonance frequency, the lower the influence of the inductor and the greater the influence of the parasitic components (in this case, C_P). The inductor has an initial fixed value, however when the frequency is increasing its inductance becomes smaller Therefore, to find a fixed inductance value representing the first impedance curve, the mean of all L_S values until the exact moment before the first resonance (16.52 kHz), since after this ferquency L_S becomes negative. The same method was used for the second impedance curve and the mean of all L_S positive values at the exact moment before the second resonance (56.51 kHz) The inductance values calculated were 1 mH for the first resonance frequency and 0.44 μF. On the basis of these values it was possible to calculate the values (from Equation 3) of the parasitic capacitances associated to each inductance, referred to in the Table 1.

$$f_r = \frac{1}{\sqrt{L \times C} \times 2\pi} \quad (3)$$

where: f_r – resonant frequency, L – inductance, C – capacitance.

Table 1. Inductance and parasitic capacitance values for resonant frequencies

Resonant frequency (f_r)	Parasitic capacitance (C_P)	Inductance (L)
16.51 kHz	0.0930 μF	1 mH
56.52 kHz	0.1803 μF	0.44 μH

After obtaining the values of the components for each resonant frequency, the circuit representing the three-phase cable was implemented at first in a simulation software (see Fig. 4).

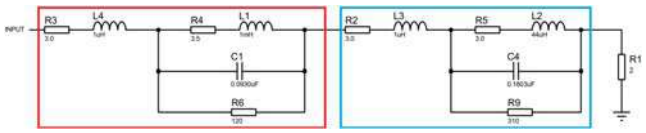

Fig.4. Electrical model of three-phase cable in simulation software.

The red and blue meshes represent, respectively, the electrical models for the resonance frequencies in the first and second curve in Fig. 3.

The 3 Ω resistances at the beginning of each meshe were placed to simulate the low resistive value presented by the evaluated ESP cable. The 1 μH inductance in series with the resistors represent parasitic inductances read from the data collected from the impedance analyzer. For low resistance values the series parasitic inductances arise as the frequency increases. If the resistance had a high value, a parasitic capacitance would appear in parallel with this resistance [8]

The parasitic resistances values in series with the inductance (3.5 Ω e 3.0 Ω), provided by the impedance analyzer, represent the minimum impedance and they are determined by the winding resistance (R_S). At the lower frequencies, the inductive reactance (ωL) decreases so that inductive winding resistance will be the inductance value [8].

The parasitic parallel resistances (R_P) with the inductance and capacitance (120 Ω e 310 Ω), provided by the impedance analyzer, represent the magnetic loss of the inductor core.

The resistance value connected to earth was chosen with a low value (2 Ω) simulates a shortcut to ground.

Once the data and graphs of the simulation software were obtained, a printed circuit was produced by combining resistors, inductors and capacitors of commercial values to reproduce the results of the simulation. As the components are manufactured with already defined values, it was necessary to group them in order to find the closest possible values of the previously calculated values as shown in Fig 5.

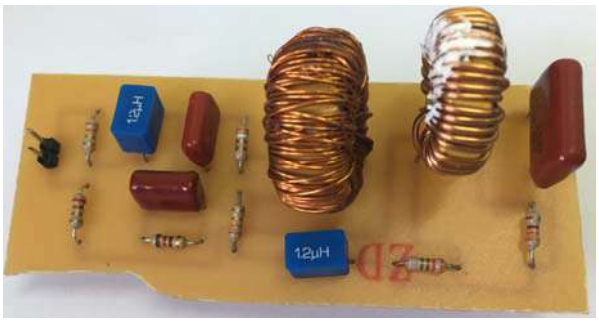

Fig.5. Printed circuit board (PCB) used for representing the electrical modelo f the ESP cable

The electronic components assembled on the PCB had commercial values closer to those found for the model were used. In the circuit of Fig. 6 present the value of each component.

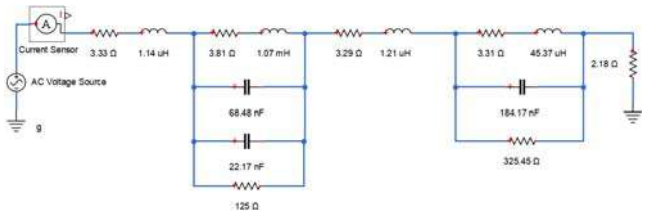

Fig.6. Schematic circuit with the real measured values of the components

Results

For an initial analysis of the proposed model, simulations were carried out in the same frequency range used to measure the actual cable parameters, from 20 Hz a 10 MHz. However, it was observed that from 200 kHz there was no other resonance frequency. This value was therefore used as the maximum frequency. Fig. 7 shows the result obtained.

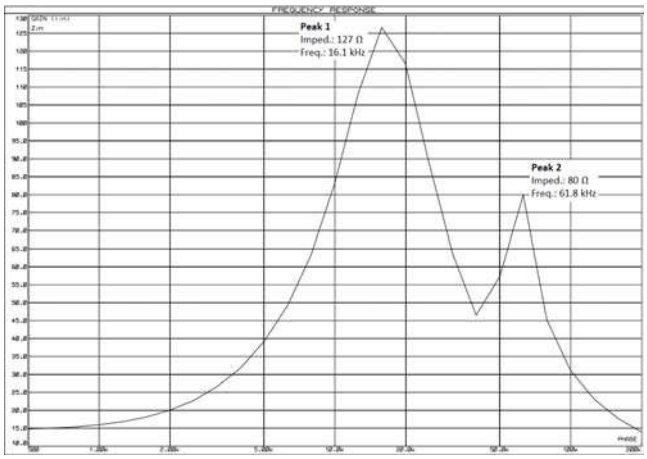

Fig.7. Impedance curve from the simulated circuit for a frequency of 20 Hz to 200 kHz.

A printed circuit board has been designed to reproduce the same impedance behavior of the ESP cable. Its implementation has been based on the data provided by the impedance analyzer and simulation results. Fig. 8 shows the behavior of the impedance obtained with the printed circuit board.

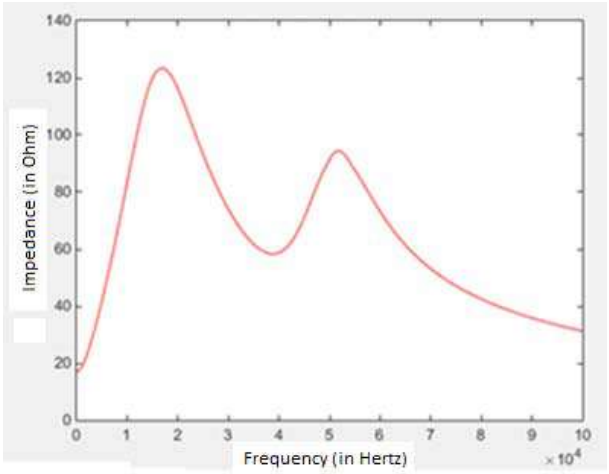

Fig.8. Impedance behavior measured on the printed circuit board at a frequency range from 20 Hz to 10 MHz.

Analyzing the characteristic impedance curve, it was verified that there is a similarity in the behavior of this parameter for the cable, the simulation and the proposed electric model.

Despite presenting similar impedance values, small deviations have been observed. These differences are due to the use of commercial components as well as the sensitivity of the resonance frequency to any difference in the inductance and capacitance values. At the first resonance peak the calculated real values (1.07 mH e 90.65 nF) were close to the calculated theoretical values (1 mH e 93 nF). However, as observed in Fig. 8, the values of the components responsible for the second peak curve (45.37 μH e 184.17 nF) would result in a resonance frequency around 54.8 kHz (according to Eq.01). So we can say that the second peak curve achieve the expected values.

Table 2 presents a comparison between the impedance vaues (Z) at the resonance frequencies (f_r) for the ESP cable, the simulation and the PCB. Table 3 shows the relative percent errors for the resonance frequency and inductance indicated in Table 2.

Table 2. Comparison between the resonance frequency and the impedance for the ESP cable, simulation and printed circuit board.

f_r cable [kHz]	Z cable [Ω]	f_r simul. [kHz]	Z simul. [Ω]	f_r circuit [kHz]	Z circuit [Ω]
16.51	133	16.1	126	17.02	123.5
56.52	79	61.8	80	52.01	92.77

Table 3. Relative percent errors for the resonance frequency and impedance referring to Table 2.

Error f_r simul. [%]	Error Z simul. [%]	Error f_r circuit. [%]	Error Z circuit [%]
2.48	5.26	3.09	7.14
9.34	1.26	7.97	17.43

According to Table 3 it is possible to observe that in some situations the errors have approached to and even passed the 10% mark. In the case of the simulation, the output should match the values found for the cable. This difference is due to the fact that the inductance and capacitance values are calculated from the average of the points collected up to a point before the resonance frequency, not precisely a single point.

The errors presented by the printed circuit are due to the inaccuracies of the electronic components used. In situations that did not have a component with the correct value, either an approximate value was used, or an association that provided the value close to the appropriate value.

Conclusions

It is possible to represent a three-phase cable for Electrical Submersible Pump through the appropriate association of inductors, capacitors and resistors.

The methods used to calculate the values of the passive components were correctly applied because the results obtained in both the simulation and the cable emulator circuit were acceptable.

For cables whose length is significant, it is more feasible to analyze electrical parameters through a current signal instead of voltage signal. Because, due to the cable size, the signal will have a voltage drop along it and the analysis will be faulty.

***Authors**: Eng. PhD. Diego A. M. Fonsêca, prof. PhD. Andres O. Salazar, Eng. Tomaz R. Gonçalves, Department of Computer Engineering and Automation, Federal University of Rio Grande do Norte, Natal/RN, Brazil, ZIP 59072-970, e-mail diegomoura@dca.ufrn.br, andres@dca.ufrn.br, tomazrochag@gmail.com; prof. PhD. Elmer R. L. Villarreal, Exact and Natural Sciences Center, Federal University of the Semi-Arid, Mossoró/RN, Brazil, ZIP 59625-900, e-mail elmerllanos@ufersa.edu.br*.

REFERENCES

[1] O. Ghoreishi, X. Liang and W. Xu, "Phase-to-Phase Communication Scheme for Downhole Monitoring Tool Design in Electrical Submersible Pump Systems", *IEEE Transactions on Industry Applications*, vol. 52, no. 3, pp. 2077-2087, 2016. Available: 10.1109/tia.2016.2527724

[2] Flatern, R., The Defining Series: ElectricalSubmersible Pumps (2015).

[3] F. Quintaes, A. O. Salazar, A. L. Maitelli, F. Fontes, M. A. A. Vieira, T. Eslley, "Magnetic sensor used to detect contamination of inulating oil in motors applied to electrical submersible pump*",IEEE Transactions on Magnetics*, vol. 47, no. 10, pp. 3756-3759, Oct. 2011. Available: 10.1109/TMAG.2011.2154359

[4] A. O. Salazar, D. A. M. Fonsêca, A. L. Martelli, F. Fontes and F. de Oliveira Quintaes, "Instrumentation to detect contamination of insulating oil in motors applied to electrical submersible pump", *2014 11th IEEE/IAS International Conference on Industry Applications, Juiz de Fora, 2014, pp. 1-7*.Available: 10.1109/INDUSCON.2014.7059440

[5] X. Liang, O. Ghoreishi and W. Xu, "Downhole Tool Design for Conditional Monitoring of Electrical Submersible Motors in Oil Field Facilities", *IEEE Transactions on Industry Applications*, vol. 53, no. 3, pp. 3164-3174, 2017. Available: 10.1109/tia.2016.2613984

[6] X. Liang, and W. Xu, "Downhole Tool Design for Conditional Monitoring of Electrical Submersible Motors in Oil Field Facilities", *IEEE/IAS 51st Industrial & Commercial Power Systems Technical Conference (I&CPS)*, 2015. Available: 10.1109/ICPS.2015.7266427

[7] D. Fonsêca, "Implementação de Sistema de Transmissão de Dados Através da Linha de Potência dos Poços com o Método de Elevação Bombeio Centrífugo Submerso", *master's thesis,* Federal University of Rio Grande do Norte, Aug 2018

[8] Keysight Technologies, *Impedance Measurement Handbook - A guide to measurement technology and techniques*, 6. ed. Santa Rosa, CA, 2016. Available in: <http://literature.cdn.keysight.com/litweb/pdf/5950-3000.pdf?id=1000075407:epsg:dow>. [Accessed 18 August 2017]

IEEE Access
Multidisciplinary | Rapid Review | Open Access Journal

Received July 9, 2019, accepted July 29, 2019, date of publication August 12, 2019, date of current version August 29, 2019.

Digital Object Identifier 10.1109/ACCESS.2019.2934820

Proposal of a Fuzzy Controller for Radial Position in a Bearingless Induction Motor

EVANDRO AILSON DE FREITAS NUNES[1], ANDRÉS ORTIZ SALAZAR[1], (Member, IEEE), ELMER ROLANDO LLANOS VILLARREAL[2], (Member, IEEE), FRANCISCO ELVIS CARVALHO SOUZA[3], LUCIANO PEREIRA DOS SANTOS JÚNIOR[3], JOSÉ SOARES BATISTA LOPES[3], AND JUAN CARLOS CUTIPA LUQUE[4], (Member, IEEE)

[1]Department of Computer Engineering and Automation, Federal University of Rio Grande do Norte, Natal 59072-970, Brazil
[2]Department of Natural Sciences, Mathematics and Statistics, Federal Rural University of Semi-arid, Mossoró 59625900, Brazil
[3]Federal Institute of Education, Science and Technology of Rio Grande do Norte, Natal, Brazil
[4]Department of Electronics Engineering, Universidad Nacional de San Agustin de Arequipa, Arequipa 04001, Peru

Corresponding author: Elmer Rolando Llanos Villarreal (elmerllanos@ufersa.edu.br)

This work was suported in part by the Comissão de Aperfeiçoamento de Pessoal do Nível Superior (CAPES), in part by the Conselho Nacional de Desenvolvimento Científico e Tecnológico (CNPq), and in part by the UNSA Investiga under Grant IAI-019-2018-UNSA.

ABSTRACT In this paper, a radial position control approach of a bearingless induction motor is proposed. The rotor is supported by magnetic forces, which is complex to model. Generally, simplifications are adopted to determine a linearized model that hinders classical controllers' performance. On the other hand, fuzzy controllers have non-linear characteristics and do not require precise mathematical models. Instead, it uses the experience and knowledge of human operators to build a knowledge base to be used on the control. The prototype under study is a three-phase induction motor without a rated power of 1 HP, 4-pole, 220/380V and rated current 3/1.75A. It operates on a vertical axis, so there is no need to compensate for the rotor weight. The paper proposes the implementation of a Mamdani Fuzzy PD controller in order to control the rotor radial position of a three-phase induction motor by means of a Texas Instruments TMS320F28335 Digital Signal Processor (DSP). We present experimental results that validate the good performance of the fuzzy controller.

INDEX TERMS Fuzzy controller, DSP, bearingless induction motor, split windings machine.

I. INTRODUCTION

There are several applications involving electric machines wherein maintenance becomes a challenge due to the working conditions of them, e.g., motors under great depths, high temperatures, or in impermeable environments [1]. One of the engine components that require a lot of maintenance is the mechanical bearings, due to the natural wear and tear. This fact led researchers in the 1970s to study the magnetic suspension applied to rotorless non-contact rotor systems, the so-called magnetic bearings [2]. This device solves the wear problem of the mechanical bearings but increases the size of the machine [3]–[6]. A solution to overcome the drawbacks of magnetic machines are the bearingless machines that avail their own windings to produce magnetic forces that keep the machine rotor centralized. These bearings, as well as magnetic bearings, do not require lubrication, have a no-noise operation and are suitable for applications with an unusual rotational speed (above 3600 rpm) [7].

There are basically two structures for bearingless induction machines: two winding systems and split winding systems. The first one was proposed by [8] and consists of adding an extra set of windings that enables flux distribution changing through the magnetic overlap to produce radial positioning forces, and torque aiming mechanical rotation. The second one proposed in [9] spatially divides the stator windings into coil groups that are responsible for regulating flux distributions through the current imbalance among them. The first work with this type of system employed a biphasic four-pole motor, in which the winding of one of the phases is divided into four groups arranged symmetrically and orthogonally to each other [10].

Then, it was proposed the implementation of a three-phase motor with four poles, wherein each phase is divided into pairs of opposing groups, for a total of six coils in the stator [11]. The mentioned proposal had its successful

The associate editor coordinating the review of this article and approving it for publication was Jinpeng Yu.

This work is licensed under a Creative Commons Attribution 4.0 License. For more information, see http://creativecommons.org/licenses/by/4.0/

implementation and became object of several other studies that explored all the classical techniques (PID) to control the rotor radial position [1], [7], [12], [13] and [14]. In [15], Chiba *et al.* employ PID controllers to regulate the radial position of a bearingless induction motor. However, when the radial electromagnetic force follows the radial force reference signals a phase delay generates a coupling between the so-called alpha-beta axes. As a solution, the authors implemented lead-lag compensators that maintain an average change of 50 um in radial position. This solution makes the strategy implementation more complex and highly sensitive to parametric variations.

In [16], Rodriguez and Santisteban also employ a PID control in radial position regulation and emphasize the need for identifying motor electrical parameters for a good controllers' performance. In the experimental results, the authors realize that the median values on the y-axis reach almost 10 times the median values observed in the x-axis and suggest an automatic angular correction for the y-axis that acts directly on the reference signals of the radial position controllers. However, these controllers are tuned to a certain operating point, and if it suffers a considerable variation, the controller decreases performance or even stability margin. In addition, electric machines are nonlinear systems with parameters susceptible to uncertainties that may hamper the performance of classical controllers. Furthermore, due to the current difficulty in modeling suspension forces, many simplifications are required to determine a representative linear model [1], [7], [17].

In order to overcome classical PID limitations, several other strategies have been proposed like genetic-algorithms [18]–[27] and artificial intelligence [28], [29], with special attention given to a fuzzy controller [18].

Fuzzy systems allow the analysis of a problem from a humanlike point of view by using linguistic variables. It also allows for a gradual transition between sets. Thus, fuzzy control systems can be modeled to emulate strategies that humans use to solve problems, and due to this feature is considered an intelligent system. These systems provide a formal method of translating verbal, vague, imprecise, and qualitative expressions, usual in human communication, into numerical values [18]. The basic structure of a rule-based fuzzy controller consists of three steps: Fuzzification, Inference, and defuzzification. In fuzzification, the input data are coded or converted into fuzzy values, that is, qualitative or linguistic values understandable by the inference mechanism.

The fuzzification process occurs through the application of membership functions in the input variables. The inference is responsible for the application of rules and fuzzy operations in order to map input linguistic values to output linguistic values. In defuzzification, fuzzy values resulting from inference are converted into crisp values, that is, numerical quantities by means of membership functions in the output variable [19].

With these considerations, it is proposed the application of a controller based on fuzzy logic in order to keep a machine rotor centralized even if lacking some variable specifications.

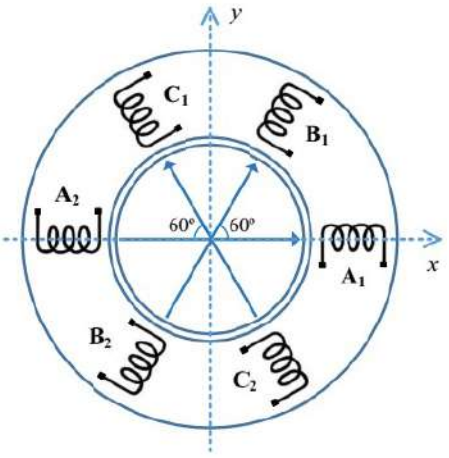

FIGURE 1. Stator winding arrangement.

This type of controller has non-linear characteristics and does not require precise mathematical models. Instead, it uses the experience and knowledge of human operators to build a knowledge base necessary for control [18]. Diffuse logic proved to be a powerful and effective tool in motor drive and control applications [20]–[23]. However, applications in magnetic suspension systems, especially in bearingless motors, are incipient. In [24], He *et al.* present an adaptive fuzzy PID controller to control the radial rotor position of a non-rolling switched reluctance motor. In the case of bearingless induction motors [25], the fuzzy control is applied to the angular speed loop, but no fuzzy control applications were found in the radial positioning of the rotor of these machines. The purpose of this paper is to implement a fuzzy PD controller to regulate the rotor radial position of a three-phase induction machine with split windings embedded in a Texas Instruments TMS320F28335 Digital Signal Processor (DSP).

The next sections of this paper will be organized as follows: in section II is presented the preliminary concepts. In section III is presented the system description. In section IV is presented the control strategy. In section V is presented the fuzzy controller. In section VI is presented the experimental results. Finally, in section VII are presented the conclusions of this paper.

II. PRELIMINARY CONCEPTS

A. OBTAINING RADIAL FORCES

To understand the configuration of radial forces acting on the rotor, it is necessary to visualize the internal distribution of the magnetic flux and the arrangement of the windings within the stator from a cross-section of the machine depicted in Fig. 1.

The magnetic flux configuration due to feeding A_1 and A_2 coils is depicted in Fig. 2. Feeding these coils with the same electric current results in a magnetic flux configuration represented in the left side of Fig. 2. Assuming the rotor is in the center of the stator, the magnetic flux density in both sides along the x-axis are equal, so there is no resulting horizontal force acting on the rotor.

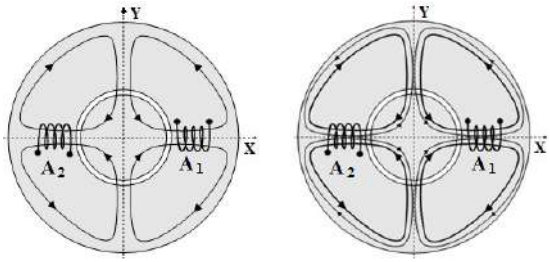

FIGURE 2. Configuration of the magnetic flux produced by coils A_1 and A_2. Additional magnetic flux caused by the differential variation of the currents of A_1 and A_2 (right).

By increasing the current value, Δi_a in the winding A_1 and simultaneously decreasing the same value in the flux of the winding A_2, an additional magnetic flow arises as shown in the right side of Fig. 2 through the thinner lines. This additional flux joins the flux of A_1 and opposes the flux of A_2, originating magnetic flux imbalance which generates a radial magnetic force on the rotor in the positive direction of $x-$axis. Through this differential action on the currents flowing through the two remaining coils, the forces are generated and modify the rotor position. This is valid for any pair of opposing coils, and the force obtained acts along the axis passing through the center [7]. In this way, the positioning forces are controlled in any transverse plane direction, overlapping the effects along the three actuation axes, as shown in Fig. 1, by the arrows drawn inside the rotor.

III. SYSTEM DESCRIPTION

The prototype under study is a 1HP, fourpoles, 220/380V and nominal current 3/1.75A three-phase induction motor. The motor shaft is orthogonally positioned in relation to the prototype base in order to mitigate the rotor weight effects. Both the rotor and the stator have undergone changes in their structure, as described below, and these modifications do not disfigure the induction machine configuration.

A. ROTOR CONFIGURATION

The traditional squirrel cage rotor does not present a satisfactory response to the radial positioning control, due to the appearance of induced currents with the same stator frequency content in the rotor. The existence of bipolar flux control components in the rotor is not desirable, because they would cause a delay in the response of the controller [17]. This problem is overcome by employing a four-pole winding rotor. This configuration ensures that only four-pole fields belonging to the feed frequency of the machine are induced. It prevents bipolar magnetic fluxes from being generated due to the modulated control components in the stator currents [7] and [17].

B. STATOR CONFIGURATION

The stator winding consists of six groups of coils, two per phase. Fig. 3 shows how the six groups are connected to start

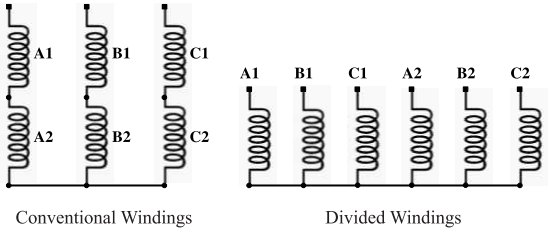

FIGURE 3. Difference between conventional and divided winding.

the engine. In that sense, the only difference compared to a conventional motor is that the pairs of opposing groups are not connected in series. Instead, they are divided into pairs, making it possible to feed each of them independently.

The feeder currents should produce the required torque and generate restoring forces to regulate the rotor radial position. Thus, the stator currents are divided into the three-phase reference currents I_a, I_b and I_c responsible for the torque, and the positioning components Δi_a, Δi_b and Δi_c are calculated by the position controllers. Therefore, the currents of the six groups of windings are determined by equation (1).

$$\begin{aligned} I_{a1} &= I_a + \Delta i_a \\ I_{a2} &= I_a - \Delta i_a \\ I_{b1} &= I_b + \Delta i_b \\ I_{b2} &= I_b - \Delta i_b \\ I_{c1} &= I_c + \Delta i_c \\ I_{c2} &= I_c - \Delta i_c \end{aligned} \tag{1}$$

C. ACTIVATION

The developed bearingless motor drive structure is depicted in Fig. 4. It consists of two-stage conversion. The first one employs a non-controlled diode-based rectifier responsible for delivering energy to dc-link electrolytic capacitors. The second stage performs DC-AC conversion by means of two three-phase Voltage Source Inverters (VSIs). Each of the six arms employs an IGBT SEMIKRON module and is responsible for feeding the motor bearing coils individually.

IV. CONTROL STRATEGY

The block diagram of Fig. 5 shows the system control strategy scheme. It consists of two control loops. The first one is responsible for regulating the stator currents and the second one is responsible for regulating the rotor radial position. The speed regulation is performed by an open loop strategy.

A. POSITION CONTROL

The control strategy is depicted in Fig.5; wherein two orthogonally positioned sensors acquire xy axes radial position signals. These signals are compared to the position references, and position error signals Δi_x and Δi_y, respectively, and then converted to the stationary reference frame by means of Clark transform ($2\phi/3\phi$ block). The imbalance of the currents is

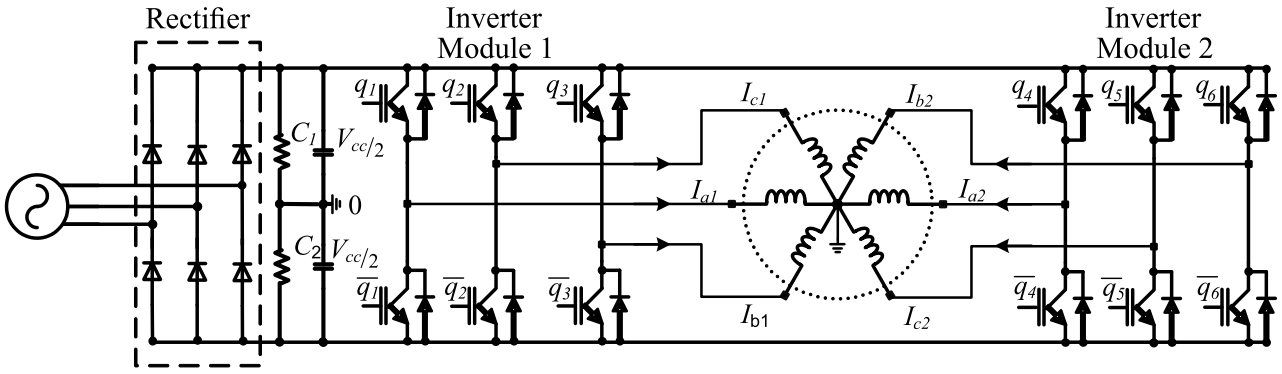

FIGURE 4. Drive structure of the bearingless motor.

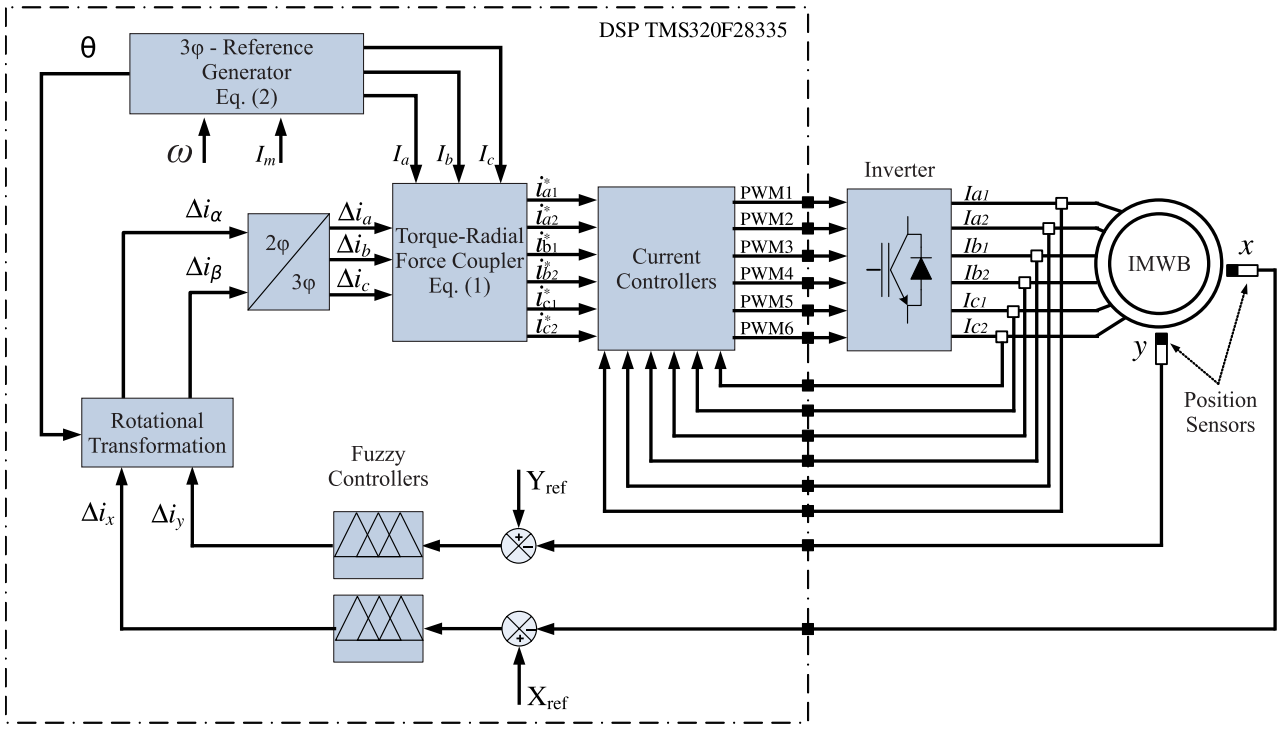

FIGURE 5. Block diagram of the control system.

performed by applying equation (1), resulting in six reference values for the stator current controllers.

B. CURRENT CONTROL

Current control is performed by six identical and independent proportional-integral (PI) digital controllers, one for each stator coil. These controllers compare current references produced by equation (1) with the currents read directly from the current sensors and thus generate the control signals to be applied to the coils through the VSIs. The three-phase reference currents are digitally generated in DSP by:

$$\begin{aligned} I_a &= I_m sin(\omega t) \\ I_b &= I_m sin(\omega t - \frac{2\pi}{3}) \\ I_c &= I_m sin(\omega t + \frac{2\pi}{3}) \end{aligned} \tag{2}$$

wherein ω is the angular frequency and I_m maximum current amplitude. The current controller design can be found in [7], however the tuning was performed empirically.

V. FUZZY CONTROLLER

According to [9]–[14], the radial position model of a split winding bearingless three-phase machine is open-loop unstable due to a right half-plane pole for each direction axis. This pole existence hampers a PD strategy implementation that adds a zero on the left half-plane to ensure that the feedback loop is stable. In addition, system tuning becomes more complex and highly sensitive to parametric variations. In this work, a fuzzy controller with traditional PD features and able to deal with model imperfections replaces the controller adopted in [9]. In order to control the radial position of the rotor, two independent fuzzy PD controllers of the Mamdani

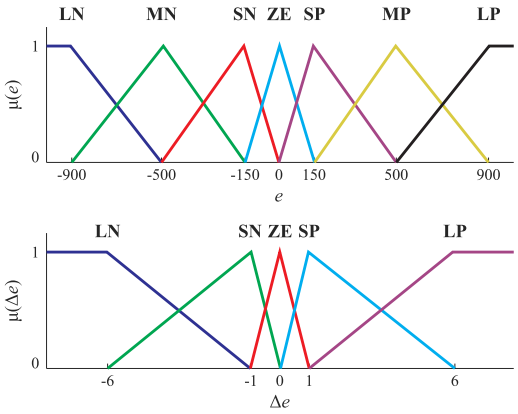

FIGURE 6. Membership functions of input variables.

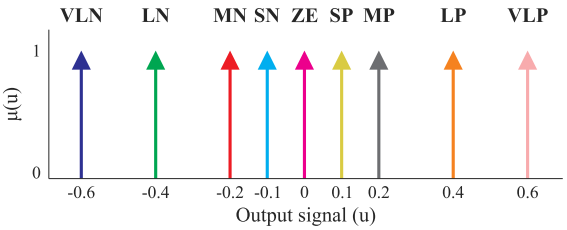

FIGURE 7. Membership functions of output variables.

type were implemented, one for the x-axis and one for the y-axis, according to the diagram in Fig. 5.

The basic structure of a rules-based fuzzy controller consists of three stages: fuzzification, inference and defuzzification [18]. In the fuzzification, input data are converted into fuzzy values, i.e., qualitative values comprehensible by the inference mechanism.

A. MEMBERSHIP FUNCTIONS

For each controller, five triangular and two rectangular membership functions were defined for the error variable and three triangular and two rectangular membership functions for the change in the error variable, according to Fig. 6. For generating the output, nine singleton functions were chosen, as depicted in Fig. 7. With these functions, the defuzzification is done simply by the formula:

$$\Delta_i = \frac{\sum_{i=1}^{N} u_i \sum_{i=1}^{N} \mu_{out}(u_i)}{\sum_{i=1}^{N} \sum_{i=1}^{N} \mu_{out}(u_i)} \tag{3}$$

wherein u_i is the i^{th} membership function, $\mu_{out}(u_i)$ represents its degree of membership and N the number of employed functions [18].

Through experiments with the machine, we defined the speech universes of the input and output variables [26]. Otherwise, it determined the range from -1500 to 1500, for a range variation of -10 to $+10$. (These numbers are not in physical units, they are called directly from the A/D of the DSP).

With respect to the output variable Δ_i (control signal), the speech universe was defined based on previous knowledge obtained from previous experiments with another controller [14]. Thus, the proposed speech universe Δ_i was the range of -0.6 to $+0.6$.

TABLE 1. Linguistic labels adopted to describe fuzzy sets.

Label	Signification
VLN	Very Large Negative
LN	Large Negative
MN	Medium Negative
SN	Small Negative
ZE	Zero
SP	Small Positive
MP	Medium Positive
LP	Large Positive
VLP	Very Large Positive

Initially, membership functions were distributed evenly in the speech universe. Afterward, adjustments were performed experimentally by changing functions closer to the zero function to achieve higher precision and better performance of the controllers. They were used as membership functions in both axes.

B. RULES BASIS

Defining the rule sets is directly related to the aim of the control. Since the bearingless motor aims to keep the rotor centralized, the main task is to minimize the position tracking error. The higher the error, the higher the control input. However, a change in error also affects the value of the control input. Consequently, the error and change in error are used in the control rules as the linguistic variables. These are defined as:

$$\begin{aligned} e &= error = P_{ref} - P_{meas} \\ \Delta_e &= change\ in\ error = e[k] - e[k-1] \end{aligned} \tag{4}$$

wherein e is the error signal, P_{ref} is the position reference, P_{meas} is the axis position measured by the acquisition device, $e[k]$ is the actual error and $e[k-1]$ the error calculated in the previous sample of k.

The rules of fuzzy controller are of the form:

$$\begin{aligned} &If\ error\ = A\ and\ change\ in\ error = B \\ &Then\ u = C \end{aligned} \tag{5}$$

The memberships functions are named by linguistic labels that are summarized in Table (1). The rule base is summarized into a table in which the columns represent the error variable and the lines represent the change in error. The x-axis rand y-axis rule bases are summarized in Table (2) and Table (3), respectively. The a, b, c and d mean Δ_{e_x}, e_x, Δ_{e_y} and e_y, respectively.

An initial rule base was developed using prior knowledge of the system. Then adjustments were made based on the behavior of the system during the experiments. The rules were changed until they could no longer improve the response, so the membership functions were adjusted. The adjustments of the rules were intercalated with the adjustments of the membership functions, never both at the

TABLE 2. Rules for *x*-axis fuzzy controller.

a \ b	LN	MN	SN	ZE	SP	MP	LP
LP	VLN	VLN	VLN	VLN	LN	SN	SN
SP	VLN	LN	MN	ZE	SP	LP	LP
ZE	LN	SN	SN	SP	MP	LP	VLP
SN	VLN	LN	MN	ZE	SP	LP	LP
LN	SP	LP	LP	LP	SP	VLP	VLP

TABLE 3. Rules for *y*-axis fuzzy controller.

c \ d	LN	MN	LN	ZE	SP	MP	LP
LP	VLN	VLN	VLN	LN	MN	MN	SN
SP	VLN	MN	MN	MN	ZE	SP	SP
ZE	LN	MN	ZE	ZE	SP	MP	LP
SN	SN	SN	SP	SP	MP	LP	VLP
LN	SP	MP	LP	LP	LP	VLP	VLP

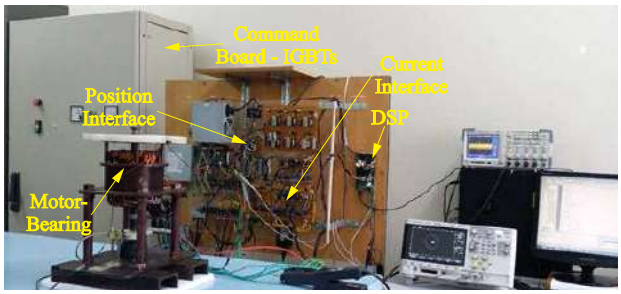

FIGURE 8. Experimental setup of the system.

same time. The adjustments originated the error and change in error membership functions illustrated in Fig. 6 and the output membership functions depicted in Fig. 7 and the rules summarized in Table (2).

VI. EXPERIMENTAL RESULTS

The experimental setup of the bearingless motor control is depicted in Fig. 8 according to the Fig. 4. The control is performed by Texas instruments DSP TMS320F28335, incorporated into the Spectrum Digital $eZdsp^{TM}$ kit. The period adopted for sampling the signals is $100\mu s$ in order to reduce switching losses and improve the prototype efficiency [30].

In order to verify the performance of the controller, experimental tests were carried out. The stator cross-section center corresponding to the coordinate system point (x,y)=(0,0) was adopted as the reference radial position. It is the position that the rotor must operate. Fig. 9 shows the steady-state behavior of the system, when the rotor speed reaches 1774 rpm and oscillates around the reference position with an average error of -0.000206mm (0.052%) and -0.000743mm (0.186%) in the x and y directions, respectively. The dynamics of the two axes is slightly different, so there is also a low-frequency oscillation on the *y*-axis.

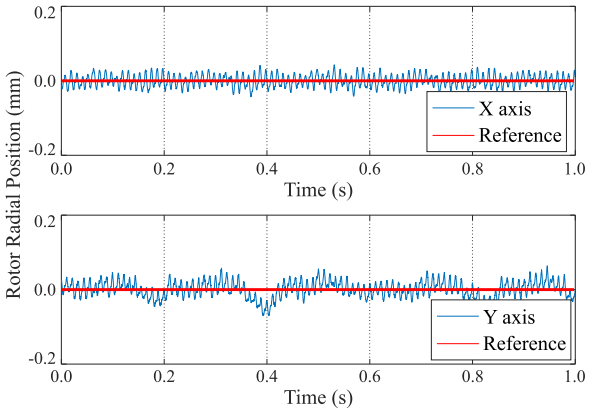

FIGURE 9. Radial position at steady state.

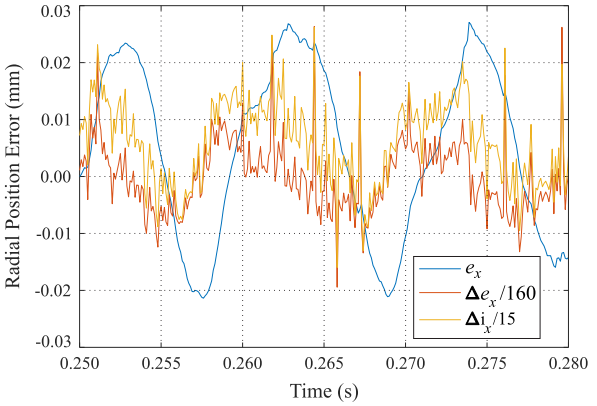

FIGURE 10. Position error, change in error and control signal on *x*-axis.

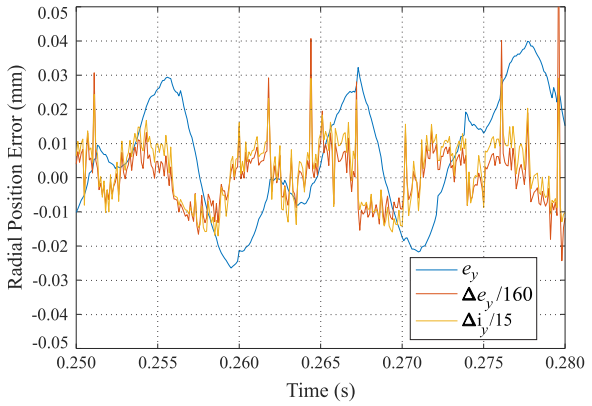

FIGURE 11. Position error, change in error and control signal on *y*-axis.

The amplitude of the rotor oscillation around the reference can be seen in Fig. 10 and Fig. 11. These figures show the position error (which coincides with the position, since the reference is zero) to the error variation and the control signals Δi_x and Δi_y of both controllers (x and y axes). The scale of the error variations was reduced by a factor of 160 when scaling the control signals by a factor of 15, so that they can be visualized along with the error signal.

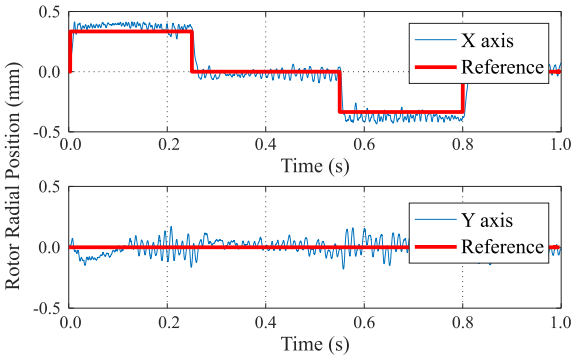

FIGURE 12. System behavior under step disturbance applied on *x*-axis.

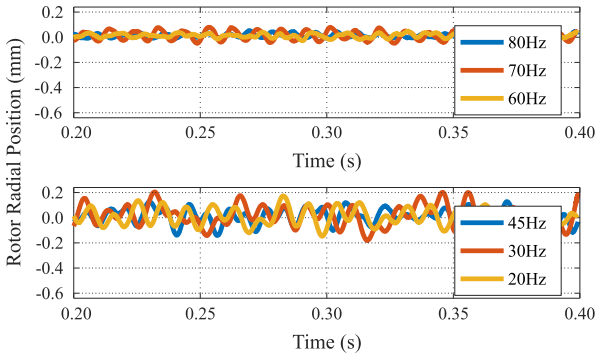

FIGURE 13. Controller response at different frequencies (*x*-axis).

It is observed in Fig. 10 and Fig. 11 that the control signal is proportional to the change in error. It is expected behavior in controllers equipped with derivative gain necessary to stabilize unstable systems as well as the proposed system. Also, it can be seen that there are error variations peaks that are responsible for control spikes. This behavior is due to the roughness on the disk used to measure the radial position.

A slight difference between *xy* axes signals is evident. It occurs due to the radial position reference adopted in this paper, depicted in Fig. 1. The regulation in *x*-axis is performed by phase A and contributions from phase B and C through its coils. On the other hand, there is a decoupling between the x and y reference axis due to the orthogonality between them. So the regulation in the *y*-axis is only performed by the contribution of phases B and C. As a consequence, there is less magnetic flux able to produce magnetic force and regulate the *y*-axis position. This behavior is observed in the error and change in error signals. This leads to larger control signals produced by this position controller.

The controller response to reference value step changes which magnitude varies between $\pm 0.33mm$ is depicted in Fig. 12. The rotor position, when the reference is at $x = 0$, shows a mean error of less than $0.022mm$. Facing the applied steps (0.33 and -0.33) the mean error is $0.047mm$. The existence of a steady-state error is acceptable since the controller is a fuzzy PD [18]. The reference steps were applied only on the *x*-axis, but similar results were also observed when applied on the *y*-axis. The disturbance observed on the *y*-axis is due to a coupling between the axes, caused mainly by the gyroscope effect. Thus, when there are changes of references in the *x*-axis, the *y*-axis is disturbed.

The fuzzy controller is set to operate at a frequency of $60Hz$. However, in order to verify its robustness, the motor is excited with other frequencies, and the results are depicted in Fig. 13. It was verified that it maintains the same performance for frequencies above $60Hz$. At frequencies lower than $60Hz$, the system remains stable but shows the increased amplitude of the oscillations. Similar results were observed on the *y*-axis.

The system performance during motor start-up is depicted in Fig. 14. The positions of each axis as a function of time can be observed in Fig. 14(a). It illustrates the movement towards the reference point, including the acceleration until reaching steady-state behavior, in approximately 14 seconds. The upper waveforms describe *x*-axis position behavior, while the

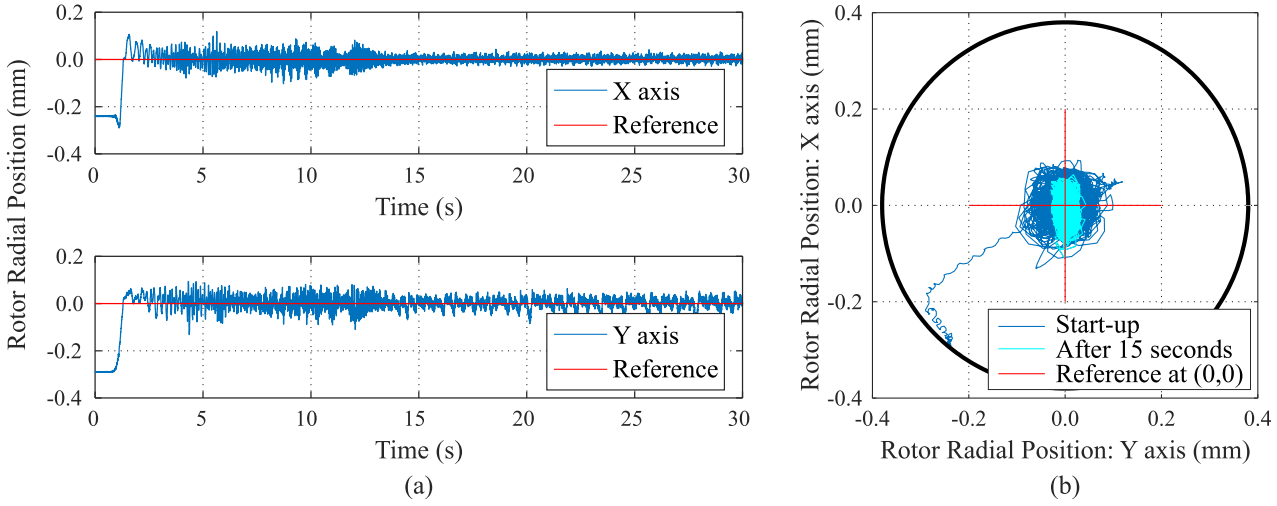

FIGURE 14. System behavior during engine startup for (a) *x* and *y* positions as functions of time and (b) rotor position in the *xy* plane.

lower ones describe *y*-axis position behavior. In Fig. 14(b) the same result is presented in the XY plane, in which the whole behavior is analyzed: rotor displacement for reference, acceleration, and steady-state. The steady-state period is highlighted in the cyano color in the center of Fig. 14(b), we note the small variation of the position on the *x*-axis, and a slightly larger oscillation on the *y*-axis.

VII. CONCLUSIONS

This article aimed to study and implement a fuzzy controller with PD features in the rotor positioning of a bearingless induction motor. The experimental results confirmed the good performance of the implemented fuzzy controller, both at the operating point, as well as at a reference away from it, which shows a certain degree of robustness. The good performance was guaranteed even not knowing the motor nonlinearities and lacking the traditional parameter generally required for tuning classical controllers. Robustness can also be verified with excitation frequencies above 60 Hz. Although performance at the lower frequencies is unsatisfactory, system stability is still maintained. The contribution of this paper is to provide a non-linear control for a system that, depending on the operating conditions, can reveal significant nonlinearities. Previous research has addressed classical control techniques that are limited to systems with linear characteristics. For future work prospects, an optimization of fuzzy controller and new control methods i.e., Neuro-Fuzzy strategies, are planned. In addition, there will be an improvement in the system for disturbance analysis in rotor shaft radial directions, either by an external force or by a torque on the axis.

REFERENCES

[1] J. M. S. Ferreira and A. O. Salazar, "Máquina de indução sem mancais: Modelo e acionamento," *Eletrônica de Potência*, vol. 12, no. 3, pp. 217–222, Nov. 2007.

[2] P. Studer, "A practical magnetic bearing," *IEEE Trans. Magn.*, vol. 13, no. 5, pp. 1155–1157, Sep. 1977.

[3] L. Zhuchong, L. Kun, and Z. Wei, "Inertially stabilized platform for airborne remote sensing using magnetic bearings," *IEEE/ASME Trans. Mechatronics*, vol. 21, no. 1, pp. 288–301, Feb. 2016.

[4] S. Ghiringhelli, F. Braghin, F. Castelli-Dezza, M. S. Carmeli, M. Mauri, and M. Rossi, "New large airgap active magnetic bearings: Modeling and experimental validation," in *Proc. Int. Symp. Power Electron., Elect. Drives, Automat. Motion (SPEEDAM)*, Anacapri, Italy, Jun. 2016, pp. 546–551.

[5] A. Chiba, D. T. Power, and M. A. Rahman, "Characteristics of a bearingless induction motor," *IEEE Trans. Magn.*, vol. 27, no. 6, pp. 5199–5201, Nov. 1991.

[6] A. Chiba, T. Deido, T. Fukao, and M. A. Rahman, "An analysis of bearingless AC motors," *IEEE Trans. Energy Convers.*, vol. 9, no. 1, pp. 61–68, Mar. 1994.

[7] F. E. F. Castro, "Three phase induction bearingless motor with divided winding: Optimization of the radial positioning system," M.S. thesis, UFRN, Natal, Brazil, 2004, p. 105.

[8] A. Chiba, D. T. Power, and M. A. Rahman, "No load characteristics of a bearingless induction motor," in *Proc. IEEE Ind. Appl. Soc. Annu. Meeting*, Dearborn, MI, USA, vol. 1, Sep./Oct. 1991, pp. 126–132.

[9] A. O. Salazar and R. M. Stephan, "A bearingless method for induction machines," *IEEE Trans. Magn.*, vol. 29, no. 6, pp. 2965–2967, Nov. 1993.

[10] A. O. Salazar, R. M. Stephan, and W. Dunford, "An efficient bearingless induction machine," in *Proc. COBEP*, vol. 1, 1993, pp. 419–424.

[11] J. M. S. Ferreira, M. Zucca, A. O. Salazar, and L. Donadio, "Analysis of a bearingless machine with divided windings," *IEEE Trans. Magn.*, vol. 41, no. 10, pp. 3931–3933, Oct. 2005.

[12] V. F. Victor, J. Á. de Paiva, A. O. Salazar, and A. L. Maitelli, "Performance analysis of a neural flux observer for a bearingless induction machine with divided windings," *Revista de Eletrônica de Potência*, vol. 15, pp. 107–114, 2010.

[13] V. F. Victor, F. O. Quintaes, J. S. B. Lopes, L. D. S. Junior, A. S. Lock, and A. O. Salazar, "Analysis and study of a bearingless AC motor type divided winding, based on a conventional squirrel cage induction motor," *IEEE Trans. Magn.*, vol. 48, no. 11, pp. 3571–3574, Nov. 2012.

[14] J. S. B. Lopes, L. P. dos Santos, J. Á. de Paiva, V. F. Victor, A. L. Maitelli, and A. O. Salazar, "Application of neuro-fuzzy estimation for rotor flux in speed vector control of bearingless induction motor," *J. Energy Power Eng.*, vol. 9, pp. 192–198, Apr. 2015.

[15] S. Nomura, A. Chiba, F. Nakamura, K. Ikeda, T. Fukao, and M. A. Rahman, "A radial position control of induction type bearingless motor considering phase delay caused by the rotor squirrel cage," in *Proc. Conf. Rec. Power Convers. Conf.*, Yokohama, Japan, Apr. 1993, pp. 438–443.

[16] E. F. Rodriguez and J. A. Santisteban, "An improved control system for a split winding bearingless induction motor," *IEEE Trans. Ind. Electron.*, vol. 58, no. 8, pp. 3401–3408, Aug. 2011.

[17] A. Chiba, T. Fukao, O. Ichikawa, M. Oshima, M. Takemoto, and D. G. Dorrell, *Magnetic Bearings and Bearingless Drives*, 1st ed. Burlington, VT, USA: Elsevier, 2005.

[18] M. G. Simoes and I. S. Shaw, *Fuzzy Control and Modeling*. 2007.

[19] G. J. Klir and B. Yuan, *Fuzzy Sets and Fuzzy Logic: Theory and Applications*. Upper Saddle River, NJ, USA: Prentice-Hall, 1995.

[20] J. L. P. Azcue and E. Ruppert, "Three-phase induction motor DTC-SVM scheme with self-tuning PI-type fuzzy controller," in *Proc. 7th Int. Conf. Fuzzy Syst. Knowl. Discovery*, Yantai, China, 2010, pp. 757–762.

[21] S. Pati, M. Patnaik, and A. Panda, "Comparative performance analysis of fuzzy PI, PD and PID controllers used in a scalar controlled induction motor drive," in *Proc. Int. Conf. Circuits, Power Comput. Technol. (ICCPCT)*, Nagercoil, India, Mar. 2014, pp. 910–915.

[22] S. Gdaim, A. Mtibaa, and M. F. Mimouni, "Design and experimental implementation of DTC of an induction machine based on fuzzy logic control on FPGA," *IEEE Trans. Fuzzy Syst.*, vol. 23, no. 3, pp. 644–655, Jun. 2015.

[23] H. Sudheer, S. Kodad, and B. Sarvesh, "Direct torque and flux control of induction machine using fuzzy logic controller," in *Proc. 2nd Int. Conf. Adv. Elect., Electron., Inf., Commun. Bio-Inform. (AEEICB)*, Chennai, India, Feb. 2016, pp. 193–197.

[24] Y. He, Y. Tang, D.-H. Lee, and J.-W. Ahn, "Suspending control method of BLSRM based on adaptive Fuzzy PID controller," in *Proc. IEEE Transp. Electrific. Conf. Expo, Asia–Pacific (ITEC Asia–Pacific)*, Busan, South Korea, Jun. 2016, pp. 755–760.

[25] X. Liu, B. Zhu, J. Zheng, and Z. Wang, "Air-gap-flux oriented optimized control of bearingless induction motor," in *Proc. 30th Chin. Control Conf.*, Jul. 2011, pp. 3549–3553.

[26] L. P. S. Junior, "Implementation of an intelligent radial position control system applied to an induction machine as divided winding-type drive motor," M.S. thesis, Federal Univ. Rio Grande do Norte, Natal, Brazil, 2017.

[27] S. Haffner, L. A. Pereira, and L. F. A. Pereira, "A method for optimization of five-phase induction machines based on genetic algorithms," *J. Control, Automat. Elect. Syst.*, vol. 26, no. 5, pp. 521–534, 2015.

[28] N. El Ouanjli, S. Motahhir, A. Derouich, A. El Ghzizal, A. Chebabhi, and M. Taoussi, "Improved DTC strategy of doubly fed induction motor using fuzzy logic controller," *Energy Rep.*, vol. 5, pp. 271–279, Nov. 2019.

[29] C. M. R. Osorio, J. L. A. Puma, D. B. Luque, J. A. T. A. Carcasi, and A. J. Sguarezi Filho, "Controle das potências do aerogerador de Indução com Rotor Bobinado com emprego de controladores PI e fuzzy tipo Mamdani," in *Proc. XII Simpósio Brasileiro de Automação Inteligente (XII SBAI)*, Santo André, Brazil, 2015.

[30] O. Oñederra, I. Kortabarria, I. M. de Alegría, J. Andreu, and J. I. Gárate, "Three-phase VSI optimal switching loss reduction using variable switching frequency," *IEEE Trans. Power Electron.*, vol. 32, no. 8, pp. 6570–6576, Aug. 2017.

EVANDRO AILSON DE FREITAS NUNES was born in Natal, Brazil. He is graduated in electric engineering from the Federal University of Rio Grande do Norte, the master's degree in electric engineering from the Federal University of Rio Grande do Norte, in 2017, and the Ph.D. degree in electric engineering, in 2018. He has been a Teacher with the Federal Institute of Bahia, IFBA, since 2018, where teaches contents of electrical systems analysis, electric machine drives, and electric machines theory. His current research interests include renewable energy generation, process automation, and the distribution of electric power.

ANDRÉS ORTIZ SALAZAR (M'11) was born in Lima, Peru. He is graduated in electronic engineering from the National University of Engineering, Lima, and the master's degree in electric engineering and the Ph.D. degree in electric engineering from the Federal University of Rio de Janeiro, Brazil, in 1989 and 1994, respectively. He held a postdoctoral position in electric engineering with the Tokyo University of Science, SUT, Japan, in 2000. He has been a Teacher with the Federal University of Rio Grande do Norte, since 1994, where teaches instrumentation, industrial automation, power electronics, machine activation, and automation. His current research interest includes the electronic automation of electrical and industrial processes.

ELMER ROLANDO LLANOS VILLARREAL (M'19) was born in Huánuco Peru. He received the B.Sc. degree in mathematics from the National University of Engineering, Lima, Peru, the master's degree in electric engineering from the Polytechnic School University of Sao Paulo, in 1997, and the Ph.D. degree in electric engineering from the Federal University of Santa Catarina, Brazil, in 2002. He held a postdoctoral position in electric engineering with the Federal University of Rio Grande do Norte, in 2019. He has been a Teacher with the Federal Rural University of Semi-arid, since 2009, where teaches linear algebra, linear systems, and numerical calculus. His current research interests include mathematical modeling and control systems.

FRANCISCO ELVIS CARVALHO SOUZA was born in Apodi Rio Grande do Norte, Brazil. He is graduated and received the master's and Ph.D. degrees in electric engineering from the Federal University of Rio Grande do Norte, in 2004, 2006, and 2011, respectively. He is currently a Professor with the Federal Institute of Education, Science and Technology of Rio Grande do (IFRN), Mossoró, Brazil. His research interests include electric machines, power electronics, power systems control, and nebulous logic applied to control.

LUCIANO PEREIRA DOS SANTOS JÚNIOR was born in Aracaju, Brazil. He is graduated in electric engineering by University Pio Decimo, in 2004, and received the master's and Ph.D. degrees in electric engineering from the Federal University of Rio Grande do Norte, in 2009 and 2017, respectively. He is currently a Professor with the Federal Institute of Education, Science and Technology of Rio Grande do Norte (IFRN), Natal, Brazil. His current research interests include electrical engineering, with emphasis on power electronics, working mainly in the following topics: three-phase PWM converters, PFCs, inverters, machines, microcontrollers, and processors applied in electronic power.

JOSÉ SOARES BATISTA LOPES was born in Natal, Brazil, in 1980. He received the B.S. degree in computing engineering from Potiguar University (UnP), Brazil, in 2004, and the M.Sc. and D.Sc. degrees in electrical engineering from the Federal University of Rio Grande do Norte (UFRN), in 2011 and 2016, respectively. He is currently a Professor with the Federal Institute of Education, Science, and Technology of Rio Grande do Norte Federal. His current research interests include automation, intelligent systems, and educational robots.

JUAN CARLOS CUTIPA LUQUE (M'15) was born in Arequipa, Peru. He is graduated in electronic engineering from the Universidad Nacional de San Agustin de Arequipa, Peru, in 2004, and the M.Sc. and Ph.D. degrees in mechanical engineering from the University of São Paulo, Brazil, in 2007 and 2012, respectively. He is currently a Professor with the Electronic Engineering Department, Universidad Nacional de San Agustin de Arequipa, Peru. His research interests include advanced control systems for autonomous underwater vehicles (AUVs), remote-operated submersible vehicles (ROVs), unmanned surface vehicles (USV), and electric vehicles.

sensors

MDPI

Article

System of Sensors and Actuators for the Production of Water Used in the Manufacture of Medicines

Fabricio Roosevelt Melo da Silva [1], Diego Antonio de Moura Fonsêca [1], Werbet Luiz Almeida da Silva [1], Elmer Rolando Llanos Villarreal [2,*], German Alberto Echaiz Espinoza [3] and Andrés Ortiz Salazar [1]

1 Department of Computer Engineering and Automation, Federal University of Rio Grande do Norte (DCA-UFRN), Natal 59072-970, Brazil; fabricio@dca.ufrn.br (F.R.M.d.S.); diegomoura@dca.ufrn.br (D.A.d.M.F.); werbethluizz@hotmail.com (W.L.A.d.S.); andres@dca.ufrn.br (A.O.S.)

2 Department of Natural Sciences, Mathematics, and Statistics, Federal Rural University of Semi-arid (DCME-UFERSA), Mossoró 59625-900, Brazil

3 Automation and Control Department, School of Electronical Engineering, National University of San Agustín de Arequipa (UNSA), Arequipa 04002, Peru; gechaiz@unsa.edu.pe

* Correspondence: elmerllanos@ufersa.edu.br; Tel.: +55-084-99194-8432

Received: 4 September 2019; Accepted: 12 October 2019; Published: 16 October 2019

Abstract: This paper presents the development and implementation of a centralized industrial network for an automatic purified water production system used in the pharmaceutical industry. This implementation is part of a project to adapt an industrial plant to cope with advances in industrial technology to achieve the level of Industry 4.0. The adequacy of the instruments and the interconnection of the controllers made it possible to monitor the process steps by transforming a manual plant, with discontinuous production into an automated plant, improving the efficiency and quality of the produced water. The development of a supervisory system provides the operator with a panoramic view of the process, informing in real-time the behavior of the variables in the process steps, as well as storing data, event history and alarms. This system also prevented the collection of erroneous or manipulated data, making the process more transparent and reliable. Accordingly, we have been able to tailor this water treatment plant to operate within the minimum requirements required by the regulator.

Keywords: automation; conductivity; MODBUS; purified water; sensors; SCADA; medicines manufacturing

1. Introduction

Water is one of the major commodities used by the pharmaceutical industry [1], and is the raw material most widely used in the manufacture of pharmaceutical products [2].

Water has unique chemical properties due to its polarity and hydrogen bonds. This means it can dissolve, absorb, adsorb, or suspend many different compounds, including contaminants [3].

Thus, it needs to be of high purity, and it is of great importance that its composition analysis is carried out to identify contaminants that may interfere with its quality, thus compromising the efficacy and quality of the produced medicines [2].

In the pharmaceutical industry, water can be used as a reagent, ingredient, or vehicle. However, there are formulas in which water is part of the composition of the product, such as injectables, eye drops, ophthalmic solutions, syrups, and suspensions, making it essential that the quality meets the specifications of use [4,5].

In this sense, water quality control plays an important role, as it is an essential tool that ensures the production of medicines meeting required specifications [6]. Therefore, the quality of the water used

in the industry should follow standards according to its application [2]. According to [7], water for pharmaceutical use is classified into three categories: purified water (PW), Highly purified water (HPW) and water for injection (WFI), as shown in Table 1.

Table 1. Types and main parameters of pure water.

Types of Water	Conductivity (µS/cm)	TOC(CFU)
Purified water	Up to 1.3	Up to 100
Water for Injectables	Up to 0.7	Up to 50
Highly Purified Water	Up to 0.1	Up to 10

Given the importance of water in the drug production process, the Agência Nacional de Vigilância Sanitária (ANVISA) ("National Sanitary Vigilance Agency") the regulatory agency responsible for medicines manufactured/marketed in Brazil, has determined rules and standards for Good Manufacturing Practices (GMP) for water for pharmaceutical use. These are found in [8] and [7], which set out, respectively, Good Manufacturing Practices and water quality requirements for Pharmaceuticals.

A water treatment system for pharmaceutical purposes consists of a pretreatment unit, treatment unit, water storage and distribution structure, process monitoring, and control devices and chemical cleaning and sanitation systems. Associated with these segments, the validation and qualification of water purification, storage, and distribution systems are a fundamental part of GMP and form an integral part of the GMP inspection [3,9].

Validation and qualification of water purification, storage, and distribution systems, as well as continuous production and a computerized system for monitoring and storing system data, are fundamental parts of GMP and are the requirements inspected by the regulatory agency. The latter being recently inserted, as the standards are updated continuously.

The Water Treatment Station (WTS) of the Núcleo de Pesquisa em Alimentos e Medicamentos (NUPLAM) ("Food and Drug Research Center"), located at the Federal University of Rio Grande do Norte, needed to changes, because it had treatment phases isolated from each other, with a totally discontinuous production, necessity of the present operator constant, and has no type of data storage system.

Given this problem, the main objective was to elaborate a project to adapt and update this treatment plant following the standards required by ANVISA. The project was divided into two stages. The first step (the focus of this article) is the implementation of an industrial network to establish a link among controllers, sensors, and actuators as a solution to enhance the connectivity of the legacy Water Treatment Station. This stage also contemplates the development of a SCADA (Supervisory Control and Data Acquisition) system with the particularity required by ANVISA reaching the minimum requirements for this WTS to operate within the legislation. However, the proposed project should consider adequacy only with existing equipment. This has become a challenge due to equipment from different manufacturers.

The second stage, expected to be implemented in another phase of the project, is the implementation of the paradigms that underlie Industry 4.0, such as the internet of things and data storage in clouds , as well as upgrading or replacing equipment (controllers, sensors, and actuators) that meets these characteristics. Therefore, in this last step, all these devices will be interconnected in a virtual repository where all information about each production data will be stored. New services derived from analyzing this stored data will be added, preparing the industry to enter Industry 4.0 or IIoT (Industrial Internet of Things) [10,11].

Using the latest software, we will be able to identify trends and patterns for specific processes and devise strategies to increase industry performance and efficiency throughout the production cycle. As well as provide feedback through corrective actions in the functional system that has remote access and control through advanced terminals and WebService outside the factory environment [12,13].

This article has been divided into five sections. In the first section, we had a brief introduction showing the importance of water in the pharmaceutical industry, the steps of this entire project, and the focus of our work on adapting a water treatment plant through automation. In Section 2, we will show the operation of the purified water treatment station, object of study, with its steps, functions, equipment, and characteristics. In Section 3, we show the proposed system with the implementations and modifications made in the plant. In Section 4, we will show some results and case studies on atypical days (maintenance or sanitization days) at WTS after the deployed system. Finally, in Section 5, we will make a brief conclusion about this work and future challenges of this project.

2. Materials and Methods

Before approaching the proposed automation solution to meet the requirements imposed by ANVISA, it is necessary to include, as a starting point, a general description of the Water Treatment Station (WTS). The WTS is the NUPLAM sector responsible for producing purified water that will be used in other factory sectors that need this product. Nowadays, the produced purified water is being used for cleaning and sanitizing materials, instruments, and surfaces, although it has the quality to be used in synthesizing drugs, in formulations and production of medicines.

In the process of producing purified water, the combination of two or more techniques to remove all types of contaminants is required [14]. Any purification methodology is permissible provided that the quality requirements for use are achieved. Purified water is commonly produced by ion exchange, reverse osmosis, ultrafiltration and/or electro-deionization processes and distillation [3]. Each of the purification technologies must be used in an appropriate sequence to optimize their particular removal capabilities.

A typical purified water system consists of various stages, depending on the methodology. In the WTS, four units compose the plant: pretreatment, treatment, water storage, distribution and loop structure, and chemical cleaning and sanitation systems. The treatment unit is subdivided into two stages: deionization and reverse osmosis. All units have automation elements such as metering pumps, sensors, actuators, controllers, etc. The tasks of each unit are now explained:

The schematic below shows the water purification system at WTS designed to produce purified water.

2.1. Pretreatment

The first step is pretreatment equipment specifically designed to remove contaminants in the feed water. Pretreatment removes contaminants that may affect purification equipment located downstream, especially reverse osmosis (RO) systems [15].

Pretreatment includes the addition of chlorine to control the growth of bacteria in pipes and tanks and a stage that incorporates sand filtration, which helps solids settle to the bottom of a storage tank. The first stage of the process starts before the water reaches WTS, with chlorine injection through a metering pump, still in the water tank, outside the factory (Figure 1).

Chlorinated water flows to the WTS through a 2″ PVC line. At the WTS, this water passes through a chlorine sensor that sends a 4–20 mA signal to the chlorine analyzer, which according to the established reference value (2 ppm), sends the command to the metering pump to inject or no chlorine in the water. Chlorinated water remains temporarily stored in a closed 500 L tank before being transferred to the next step, the deionization. The main instruments involved in the pretreatment step are the chlorine sensor, the HMI (Human-Machine Interface) chlorine analyzer/controller and the chlorine metering pump. The most relevant information to be measured at this stage is the amount of chlorine present in the water. Figure 1 illustrates this first stage.

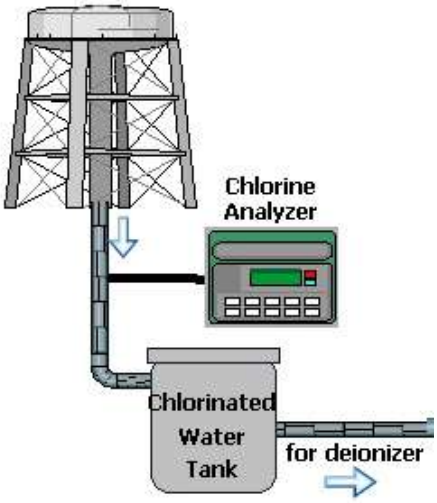

Figure 1. Pre-treatment system.

2.2. Deionizer

The deionization process consists of the removal of cations and anions that are dissolved in water [16] by synthetic ionic resins in series. Initially, the cationic-exchange resin is followed by anionic-exchange, generating the replacement of ions by cations and anions present as impurities [17]. The cation-exchange resin captures ions such as calcium, magnesium, and sodium, resulting in an uptake of cations by the spatially fixed resin and release of hydrogen ions (H^+) in exchange. In the anion-exchange resin, as anions are acquired by the anion-exchange, hydroxyl ions (OH^-) are liberated. The cationic and anionic resins are regenerated with acids and bases, respectively [7]. This technique alone does not produce high purity water; for this reason, it is widely used in water pretreatment together with other processes, as it is effective in removing dissolved ions [8]. This process eliminates ions and non-organic matter, so it is easily contaminated [18,19].

At the WTS, the deionization process begins when chlorinated water stored in the tank is transferred to the deionizer system through a centrifugal pump. At the outlet tank, a metering pump injects a sodium metabisulfite solution in order to eliminate residual chlorine present in water, as it is a strong reducing agent used for removing chlorine and chloramines from water [7]. The metabisulfite injection is regulated by an ORP analyzer (indirect measure) that acts according to the ORP (Oxidation Reduction Potencial) sensor installed inline. The residual chlorine is eliminated to avoid the saturation of ionic resins prematurely.

The process begins by opening the V-03 valve for four minutes to discard water present in the piping and deionizer system. At the end of this period, the V-03 valve is closed, and the V-04 valve opens so that the water coming from the pretreatment circulates through the deionizer system for 6 min. Both periods can be modified by the operator via the PLC (Programmable Logic Controller) HMI. At the end of this time, the conductivity sensor installed at the output of the second (cationic) resin verifies the conductivity of the water. At this point, the water conductivity should begin to decrease below the setpoint value of 25 µS/cm, configured on the conductivity analyzer. If the conductivity value does not decrease as expected, it is indicative that the resins are saturated and ionic exchanges cannot be carried out. In this situation, the deionization system automatically begins the resin regeneration process, which consists of replacing the resin particles, cations, and anions uptake during normal operation with H^+ and OH^- ions, respectively. Once the regeneration process is completed, the system begins a new deionization cycle, this time ensuring ionic exchange during the passage of water through the resins. When the water conductivity reaches the setpoint value, the conductivity analyzer sends a signal to the PLC to close valve V-04 and to open the valve V-05. This action releases the flow of water to the deionized water tank, which will serve as a buffer tank to supply the next stage of

the process, reverse osmosis. The storage tank has a capacity of 2000 L and is made of 316 L stainless steel (Figure 2).

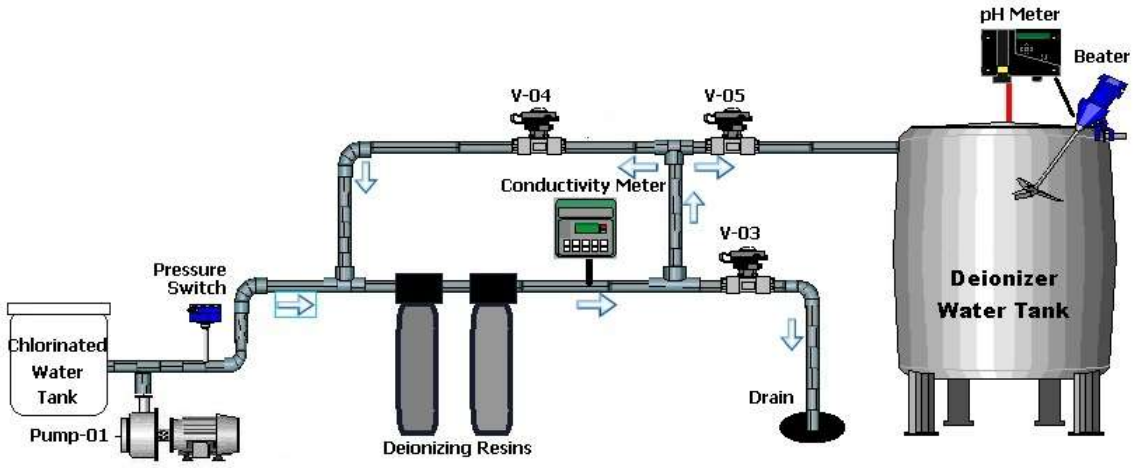

Figure 2. Deionization system.

A Delta PLC (model DVP-PS02) controls, through dedicated software, the deionization process by detecting the conductivity and opening/closing valves. The whole process can be easily managed through an HMI panel on the side. In this deionization step, the primary variable analyzed is water conductivity.

2.3. Reverse Osmosis

Reverse osmosis (RO) is a representative demineralization process for which a semipermeable membrane is adopted to remove the dissolved substances from a solution. Liquid and only the marginal portion of some ions can pass to the permeate side through a semipermeable membrane, but the majority of the dissolved materials are rejected [20]. Reverse osmosis is the primary method used in the final treatment stage for the production of purified water [8].

RO membranes push water molecules from saline water to the less saline area by applying a hydraulic pressure greater than the osmotic pressure across a semipermeable membrane [21]. This semipermeable membrane inhibits the majority of dissolved impurities from passing through to the pure water side (Figure 3). The number of impurities carried over depends on the type and condition of the membrane (i.e., age and cleanliness) and the amount of pressure applied (energy) to the process [22].

The RO system produces one purified water stream called permeate and a second stream called concentrate, brine, or reject [22,23]. The permeable membranes permit the desalinated product water while inhibiting the passage of dissolved salts to pass through [24,25].

Due to the aromatic chain that makes up the membrane, the rejection rate of contaminants ranges from 90 to 99% [20,26–28].

In some RO system, two-stage membrane (or double passes) configuration is adopted for better solute rejection [29]. In the double pass reverse osmosis, the water produced by the 1st membrane group feeds a 2nd membrane group, duplicating the purification process. The 2nd group rejects are returned entirely to the storage tank.

Water from the deionizer system can contain chlorides and volatile organic compounds. Because these contaminants have a smaller physical size than water, the semi-permeable membranes used in the process are not able to retain them [8]. Membranes should, therefore, be adequately controlled as to deposition/scaling of calcium, magnesium and other salts, and biofilm, a critical source of microbial and endotoxin contamination [7,26]. In addition, different factors can significantly influence the separation of particles of impurities from water, such as pH, membrane differential pressure,

and temperature. These factors may compromise process efficiency if there are no control methods for the water pretreatment that feeds the system [7].

A pH sensor inside the tank can provide a feedback signal to a metering pump inject acid or basic reagent and to a portable mixer, also installed in the tank, in order to homogenize the solution, and therefore, to maintain the pH within acceptable limits. Some types of RO membranes are sensitive to feed water pH and can become damaged if the pH is outside the recommended range of 5–8 pH.

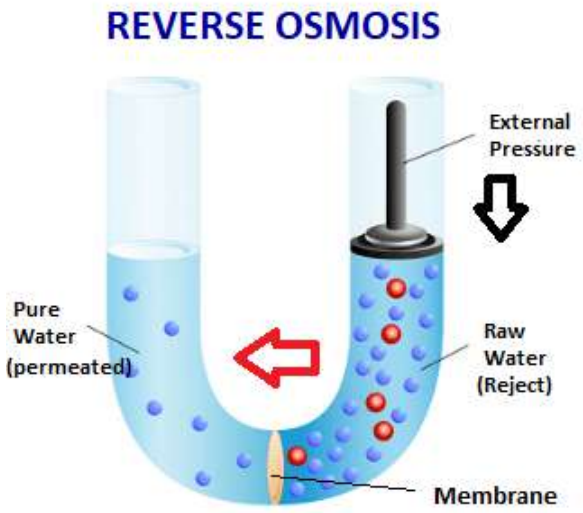

Figure 3. Reverse Osmosis.

Once the pH condition has been achieved, the water flows through a chiller heat exchanger to lower its temperature in order to achieve both criteria:

- Water conductivity is directly proportional to temperature. Therefore, the lower the temperature, the lower its conductivity.
- Reverse osmosis membranes have higher efficiency in feedwater below 20 °C (Increased feedwater temperature also results in lower salt rejection or higher salt passage).

The RO high-pressure centrifugal pump is typically multistage that continuously feeds the membrane system. Within the membrane system, the feedwater is divided into two streams according to the conductivity value indicated by the sensor installed at the second pass outlet, as illustrated in Figure 4. The low conductivity stream, called permeate, flows to the purified water tank through valve V-08 in case the conductivity value is lower than the setpoint value (0.7 µS/cm). The high conductivity flux, called concentrate, which values are greater than 0.7 µS/cm, returns to the deionized water tank for further processing. PLC controls the RO process by receiving information from the conductivity analyzer at the second pass outlet and commands the opening and closing of these valves (V-08 and V-07) according to the setpoint. System protection against high pressure or low pressures it is ensured by four pressure switches distributed throughout the reverse osmosis system.

2.4. Storage, Distribution and Loop

The storage and distribution system should be considered as a key part of the whole system and should be designed to be fully integrated with the water purification components of the system [3]. Once the water has been purified, it can either be used directly or, more frequently, it will be fed into a storage vessel for subsequent distribution to points of use [3]. The purified water distribution system is responsible for supplying all manufacturing areas that need water directly or indirectly, either in the manufacture or cleaning of the equipment used for this purpose [1,8,30].

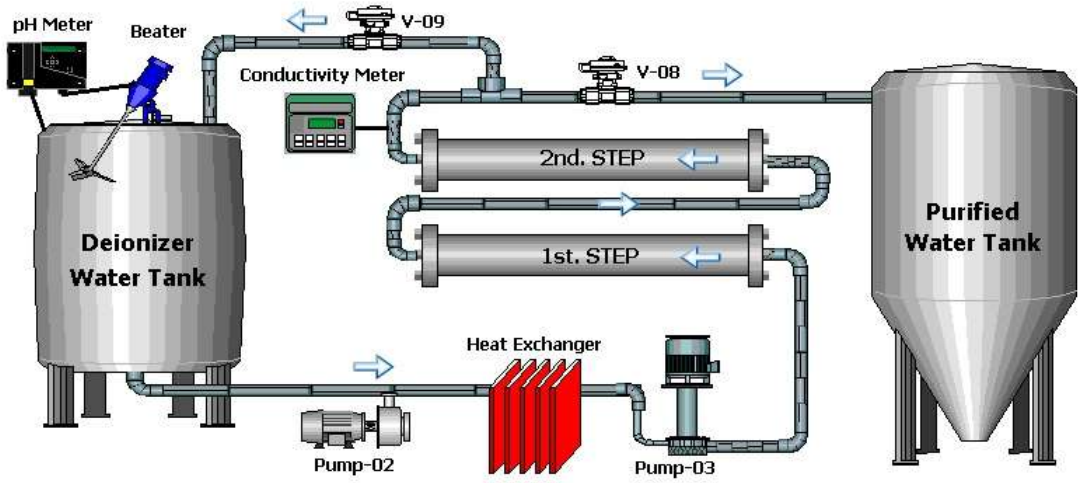

Figure 4. Reverse osmosis system.

The distribution of PW, HPW, and WFI should be accomplished using a continuously circulating pipework loop. The proliferation of contaminants within the storage tank and distribution loop should be controlled [1]. It should be subjected to a combination of online and off-line monitoring to ensure that the appropriate water specification is maintained [3]. Good justification for using a non-recirculating one-way system should be provided [1].

The PW water previously stored in the tank must supply the factory daily consumption points through a sanitary centrifugal pump. The PW storage should be designed to provide adequate protection, therefore, avoiding the water recontamination after treatment [8]. The higher the water purification quality, the faster the water tends to be contaminated in [7].

The distribution loop must be sized to meet the daily and peak usage demands for purified water during the reverse osmosis process. Maintainance of continuous turbulent flow circulation within the water distribution system reduces microbial contamination and biofilm formation [8,31].

The WTS's storage, distribution, and loop system is composed by: a 316 L stainless steel insulated vessel (PW tank) with capacity of 2000 L, a heat exchange for bringing down the temperature (and reduce the risk of microbial growth), a circulation pump (with sanitary design and appropriate seals that prevent contamination of the system) to deliver purified water to a 316 L stainless steel circulation loop. A UV (ultraviolet) lamp is installed at the beginning of the loop to reduce the microbial load. A TOC (Total Organic Carbon) meter is installed at the return of the loop It measures both conductivity and Total Organic Carbon [32]. A temperature and level sensors monitor in real-time the current water temperature and PW tank level.

The centrifugal pump is applied in sending the water stored in the PW tank to a pure water circulation system, i.e., a closed-loop circulation system that uses a dedicated water pipe, with 11 consumption points, which loops throughout the factory, ending either at the pure water tank or the buffer tank. However, before return to the PW or buffer tank, the not consumed water passes through an inline TOC meter to measure the level of Total Organic Carbon. The heat exchanger reduces the circulating pure water temperature to around 19 °C.

Figure 5 presents the idea of the process of storage, internal distribution and return of water through the loop.

The recycle valve (V-11), which is an on/off valve, installed in the return line to buffer tank controls the volume of water that returns to the PW tank according to its level measured by a radar level sensor. Therefore, if the PW tank exceeds the pre-set maximum level, the water flows to the buffer tank. At the moment that the PW tank level reaches half of the maximum set point level, the PLC sends a command to close the valve (V-11). So, the level will rise again until it up to reaches the maximum level, starting then a new cycle.

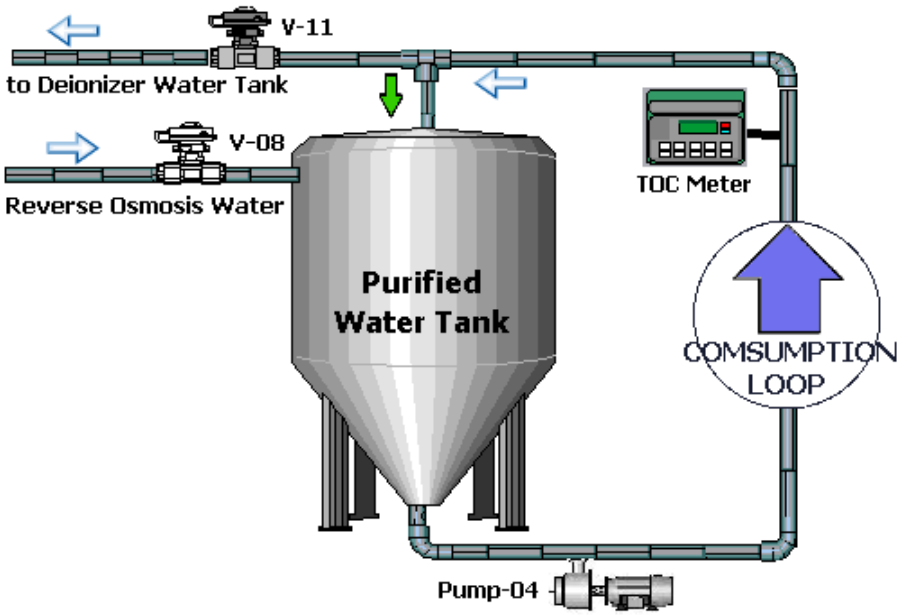

Figure 5. System: storage, distribution and loop.

The Storage, distribution, and loop process is controlled by a Siemens S7-1200 PLC. A Siemens TP-700 Confort HMI associated with the PLC provides information such as temperature, TOC, level in the storage tank and conductivity.

However, although the water purification process plant consists of the four required steps for the treatment, some adjustments must be made regarding the process in order to reach the new standards imposed by ANVISA.

3. Proposed Architecture

Considering the need to adapt WTS to ANVISA standards, improvements have been implemented, such as integrating the automation of each stage through an industrial serial digital communication network and the development of a supervisory system [33]. As already mentioned in the introduction, this initial implementation will make WTS meet the minimum operating requirements within current legislation.

Thus, a new hardware and software architecture based on Fieldbus class architectures is proposed to establish communication between the steps of the purified water production process. This proposal allows for dealing with the interoperability and integration of the controllers, sensors, and instruments involved in the automation system. The proposed architecture comprises the first three levels of the automation pyramid. Figure 6 (automation pyramid) illustrates this three-level topology implemented for vertical integration.

At the lowest layer are the sensors and actuators responsible for data acquisition, monitoring and alarm emission, actuation, and information provision at the top level. These instruments are connected directly to the controllers and, when endowed with intelligence, are integrated into the bus to which the controllers are also connected.

In the next layer or field layer, the main command unit is the PLC. These computational units are responsible for process control, processing and data provision to operators and gathering information about unit production, use of raw materials, energy and inputs and transfer to the higher level [34,35].

In the third tier, which covers supervisory, control, and monitoring system functions, the SCADA system is responsible for performing some functions in a manufacturing environment. Among these functions, we can highlight: operator communication with the various process steps, collection, storage

and transfer of logical and analogical information about the system state, and can also generate control signals so that the controlled variable behaves according to presets setpoints.

In the future (at the end of the entire project) field devices and the cloud can communicate directly [36,37]. Thus, the new industrial communication hierarchy can be considered flat: services are available to any automation system participant [38,39]. For [40] and [41], one of the crucial points of industrial automation is communication, where there are a multitude of industrial communication systems adapted to data exchange, especially in the lower layers of the system.

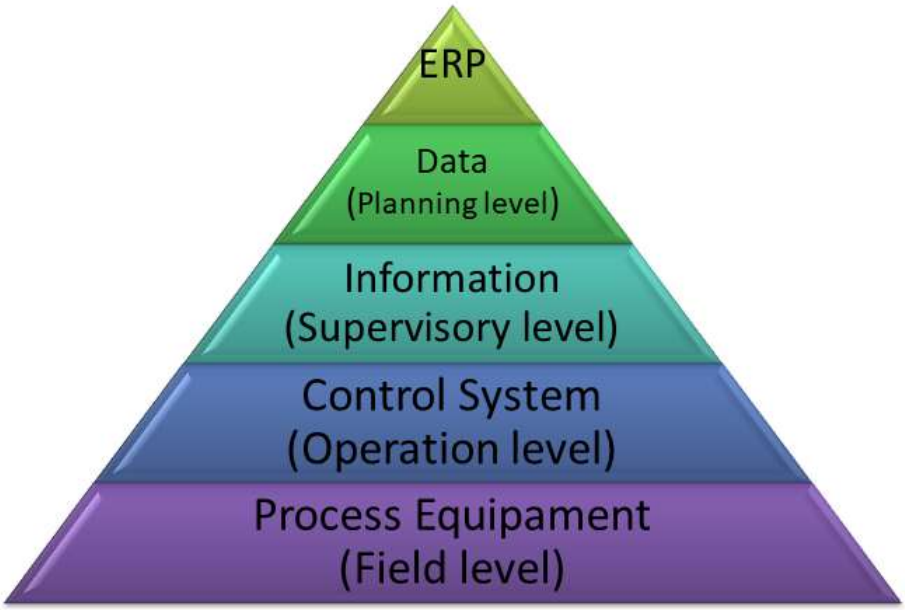

Figure 6. Automation pyramid.

All steps described in Section 3 except pretreatment include a PLC for performing tasks. A computer located in the control room gives the operator/user access to the supervisory application, from which it is possible to monitor and adjust process step parameters.

The integration between the PLCs of each process step, actuators and sensors were done through the MODBUS/RTU protocol in a standard RS-485 network that has a master-slave architecture [42]. The choice of this type of communication occurred because most of the equipment and instruments have in their structure the interface for this communication protocol. Instruments that did not have this type of communication, such as the chlorine analyzer, were connected to the analog inputs of the master PLC. The PLC chosen as the network master was the last step (storage, distribution, and loop) because it has more processing capacity, inputs, and outputs available. It also has two types of communication interfaces, Profinet (Ethernet standard) and RS-485, conditioning it to interconnect data between slave PLCs, peripheral instruments and SCADA. Table 2 shows the leading equipment present in the station, with its main functions and characteristics.

For the communication between Elipse SCADA and the PLC, the application manufacturer has developed a communication driver, called Driver M-Prot; it allows communication using ISO/TCP protocol, or ISO over TCP [43]. This protocol is message-oriented, that is, it informs the length and end of the message, unlike TCP that has a deterministic network, it is data flow-oriented, where the message recipient is not aware of the size and where the message ends [44]. Thus, the distribution of the industrial communication network of the plant in WTS, shown in Figure 7, was as follows:

- Digital inputs and outputs: from the master PLC to inputs and outputs that use Boolean digital logic (0 and 1) or simply the signal on and off, such as buttons, relays, LEDs, lights indicators, etc.

- Analog inputs: between the master PLC and sensors and instruments that do not have RS-485 communication and use current signals (4 to 20 mA);
- Ethernet communication standard: it makes a connection between the master PLC, the HMI and the computer(PC) where the SCADA is installed;
- MODBUS communication (RS-485 standard): from master PLC to slave PLCs and equipment with RS-485 communication interface [45];

The master PLC is programmed through its manufacturer's software. This PLC previously configured only with the control logic of the distribution, storage and loop step of the plant is now also responsible for centralizing the automation network. New commands have been implemented in their programming logic, adding new functions blocks responsible for the communication of the master PLC with the slave equipment. New data blocks have also been added, these for new addressing and storing data from slaves in the master PLC [46].

Table 2. Leading Equipment.

Equipament	Location	Model	Main Features	Current Function
Delta PLC	Deionizer System	DVP-SS2	8-Digital Inputs, 6-Digital Outputs, Communication RS-232 and RS-485	Controls deionizer system logic
Logo PLC	RO System	Siemens-Logo	4-Digital Inputs, 8-Digital Outputs (with additional module)	Controls RO system
Siemens PLC	Loop System	S7-1200	8-Digital Inputs, 6-Digital Outputs, 6-Analog Inputs (2-Internal and 4-Auxiliary Module), Communication Ethernet and Communication RS-485 (Auxiliary Module)	Master PLC
HMI	Loop System	Siemens-TP700 Comfort	2-Communication Ethernet	Internal HMI in the Station
SCADA CPU	Supervisor's Room	Desktop HP Intel Dual Core	Communication Ethernet	SCADA System
Peripheral Analyzers	In every plant	Miscellaneous Models	Communication RS-485 and use current signals (4 to 20 mA)	Analyser Chlorine, pH, Level Sensor, TOC, Conductivity meters

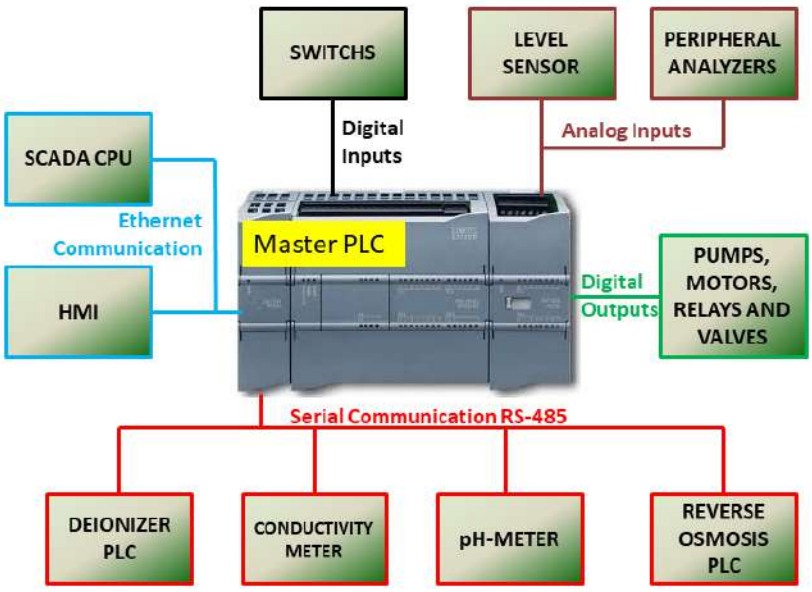

Figure 7. Automation system after interconnection of equipment.

The digital inputs and outputs of the PLC use voltage signals to define the boolean levels (0 and 24 Vdc), to represent levels 0 and 1, respectively. The analog inputs connected to the instruments receive a current signal, in the PLC this signal is converted into a term of 16 bits (word), which varies from 0 to 27,648, where 0 represents the lowest level of 4 mA, while 27,648 is the highest level of 20 mA [46]. Then for the master PLC to demonstrate the correct value read by the sensor, Is used the normalization and scheduling technique in its programming, according to Figure 8.

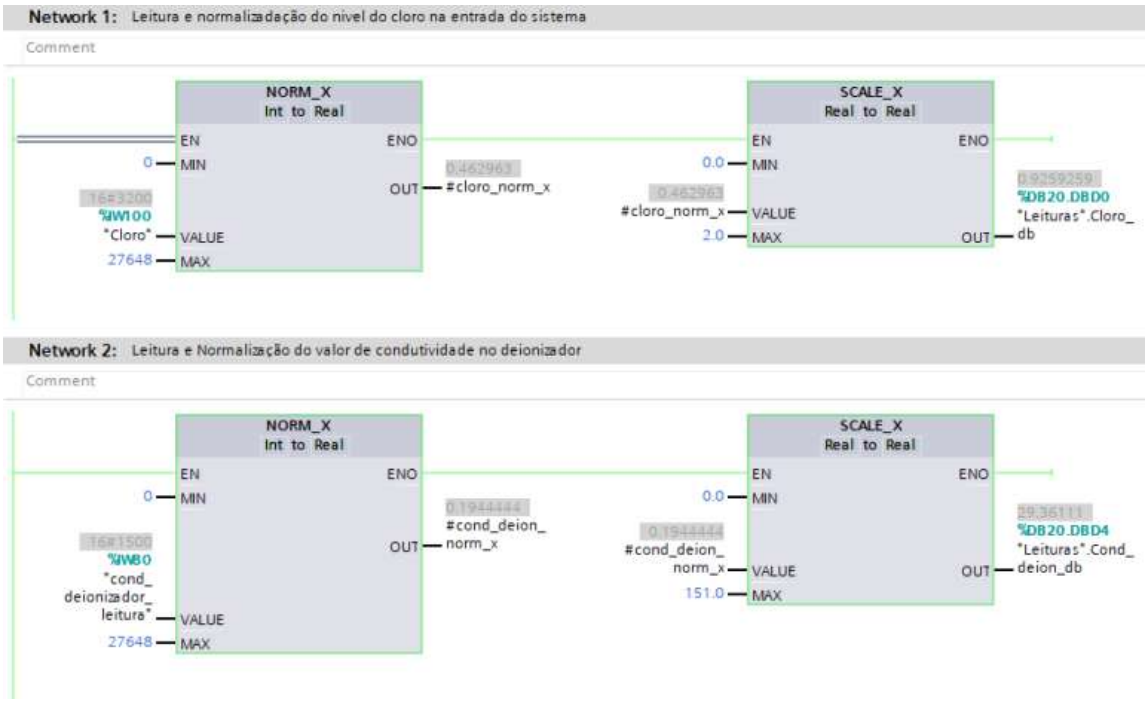

Figure 8. Configuration of the TIA Portal software to include the block diagram for normalization of the reading values of the variables.

According to the master/slave architecture of the MODBUS protocol, it was done a sequencing in the PLC configuration application. Thus, the master writes or reads in a slave, waits for his answer (one second at most, otherwise he jumps to the next in the queue), and continues the sequence, by reading ou write on to the next slave. This sequencing is cyclic, that is, after the response of the last configured slave returns to the first, and a new cycle begins. It is essential to configure three basic items (Figure 9), for correct reading the slave data in the master PLC: the slave address (MB_ADDR), the initial data memory address (DATA_ADDR) and the word length (DATA_LEN) [47].

The addressing (MB_ADDR) was done sequentially, from slave one (PLC Deionizer) to four (pHmetro). The initial address of the data memory (DATA_ADDR) changes from slave to slave and depends on the type of equipment. In the case of analysis and measurement equipment, they generally use a certain memory position fixed to express reading values. In PLCs, the amount of data is much greater: inputs, outputs, memory locations, internal keys, timers, among others. First, we verify the data that will be used in the SCADA, collecting them and configuring only those that are indispensable to the supervisor's needs.

The word length (DATA_LEN) will be the number of memory locations to be read or written from the starting address, just as in the initial address they have fixed numbers, a boolean, a byte, an integer, etc., and can vary according to the need [47]. For example, to read the status of input X0 of slave 1. So MB_ADDR = 1 (Deionizer System PLC), this PLC has specific addresses for each type of variable to be collected, ie, there is one memory address (DATA_ADDR) for the inputs, another for the outputs, and so on. To read only the status of the input X0, set DATA_ADDR = 11,025 and DATA_LEN = 1. If it needs to read all physical inputs, from X0 to X7, the DATA_ADDR will be the

same (11,025) and change the DATA_LEN to eight positions:$(X0, X1, X2, \ldots, X7)$. Another important configuration parameter in the function block is the DATA_PTR, which serves as a pointer to a block of data or bit memory from which data is to be written or read. This data is stored in a data block (DB) in the master PLC, and this DB block is available for reading or writing.

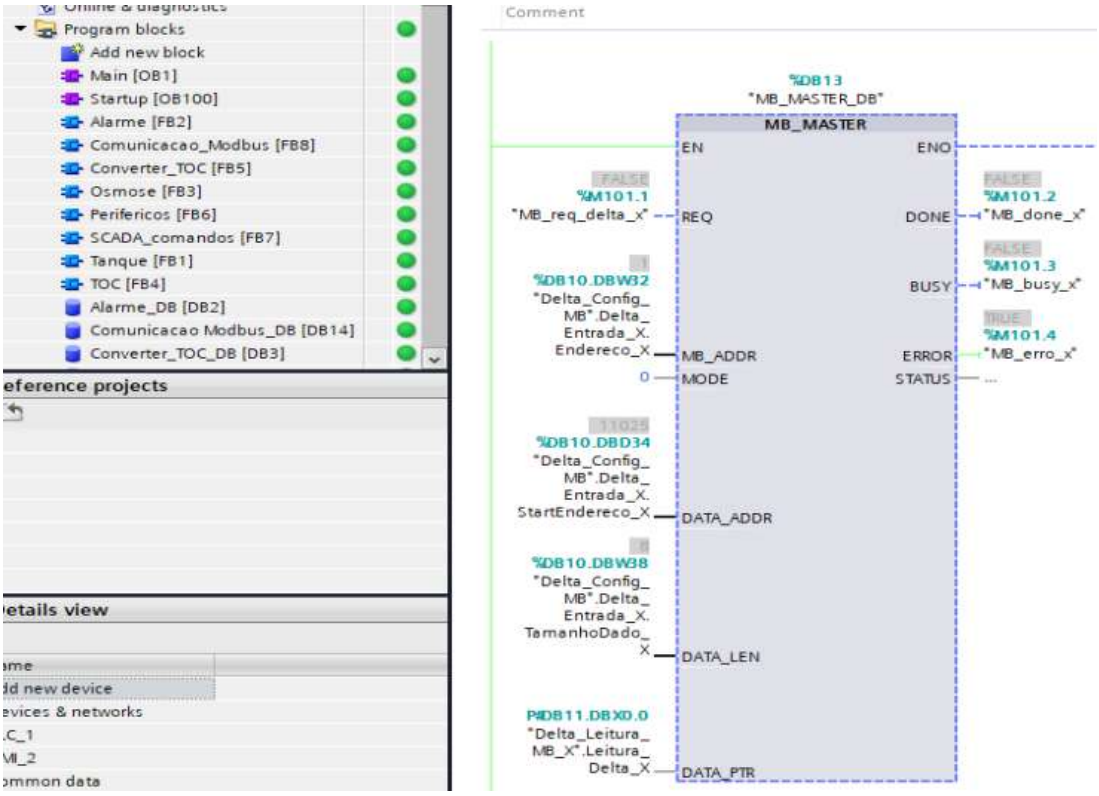

Figure 9. TIA Portal software configuration to add the block diagram of the slave equipment configuration in the new automation network.

For the correct interaction between the PLC master and SCADA, the M-Prot driver is required to be installed and configured; it uses the ISO/TCP protocol to communicate with the PLC master [43]. The main parameters to be configured in the driver are a local address, rack, and slot where the PLC, it is physically located, the type of communication (Ethernet) and its IP address. After these settings, TAGs, are added, in the SCADA, and then their connectivity is tested with the PLC. All TAGs used in SCADA must also, be configured in the driver. This configuration will be the main point of connection between the PLC data and SCADA [48]. For a successful connection, four fields need to be configured: N1, N2, N3, and N4, which have the following characteristics:

1. N1 is the address of the PLC; there is only one PLC in the automation network communicating with SCADA, then N1 = 1 [43].
2. N2 is the reported data type; In this case, the data provided by the application manufacturer [46] is used, these values are multiplied by 100. For example, if N2 = 206, a byte data ($2 \times 100 = 200$) is accessed at the digital inputs (200 + 6 = 206) [43].
3. N3 is filled only if the area to be read or written is in a datablock (DB) of the PLC; otherwise, it can be zeroed (N3 = 0) [43].
4. N4 is the offset address of the chosen DB; it will only be filled if a DB is used in the previous item (N3); otherwise, N4 = 0. For example, if N3 = 3 and N4 = 4, it means that we will be reading or writing one data in offset 4 of the DB3 of the PLC [43].

SCADA

The developed system has features for generation and visualization of reports, necessary mainly during the validation process of the system. The Water Treatment Station Supervisory System (called SISETA, Sistema Supervisório da Estação de Tratamento de Água) also has user administration, event signaling, reporting and alarms feature [48]. For better interactivity with the user, this SCADA was developed in three different screens: the main screen, deionizer system, and reverse osmosis system, each one with its peculiarities. Figure 10 shows the first screen, called the main screen, where the user has a broad view of the WTS structure with the central monitoring and control parameters. On this screen there are the readings of the PW tank variables and setpoints, the main plant measuring instruments, the system status, if the loop pump is turned on or off, if the loop recycling valve is open or closed, besides the alarms.

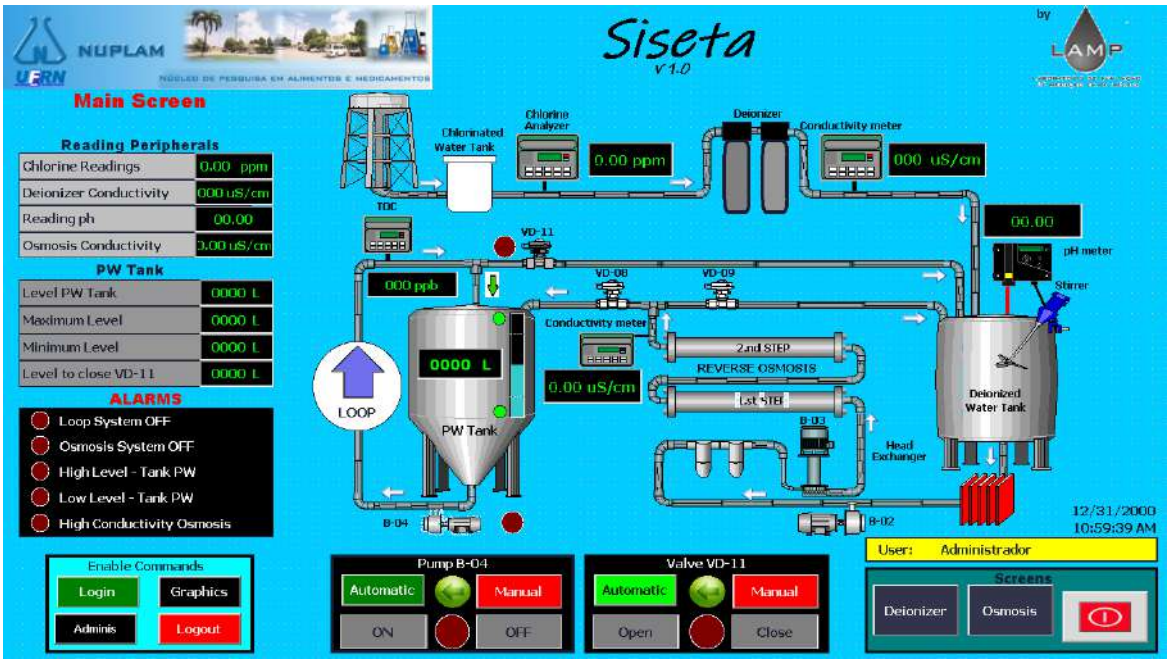

Figure 10. Main Screen of the Supervisory System (SISETA).

Figure 11 shows the second screen, called Deionizer, showing the step of the same name, showing the state and the times of the internal processes, the readings of the measuring instruments of this stage, besides the alarms. As in the first screen, the reading variables can be seen in the side panel and the plant illustration.

Figure 12 shows the third screen, reverse osmosis, with a view of the PW tank level, the conductivity of this stage, and its alarms. All screens have commands to enable and disable their systems, but they will only be accessible if the logged-in user has permission to do so; otherwise, they will only be able to view the screens and will not be able to execute any commands. On all screens, there are viewing and printing commands, which allow you to access the daily reports of the main variables of the system.

There are other technical requirements to be met by a SCADA system for the production of purified water in the pharmaceutical industry in Brazil, the main ones (implemented in SISETA) listed in Table 3. By way of comparison, the requirements commonly implemented in a supervisory system for a water and sewage treatment plant were listed.

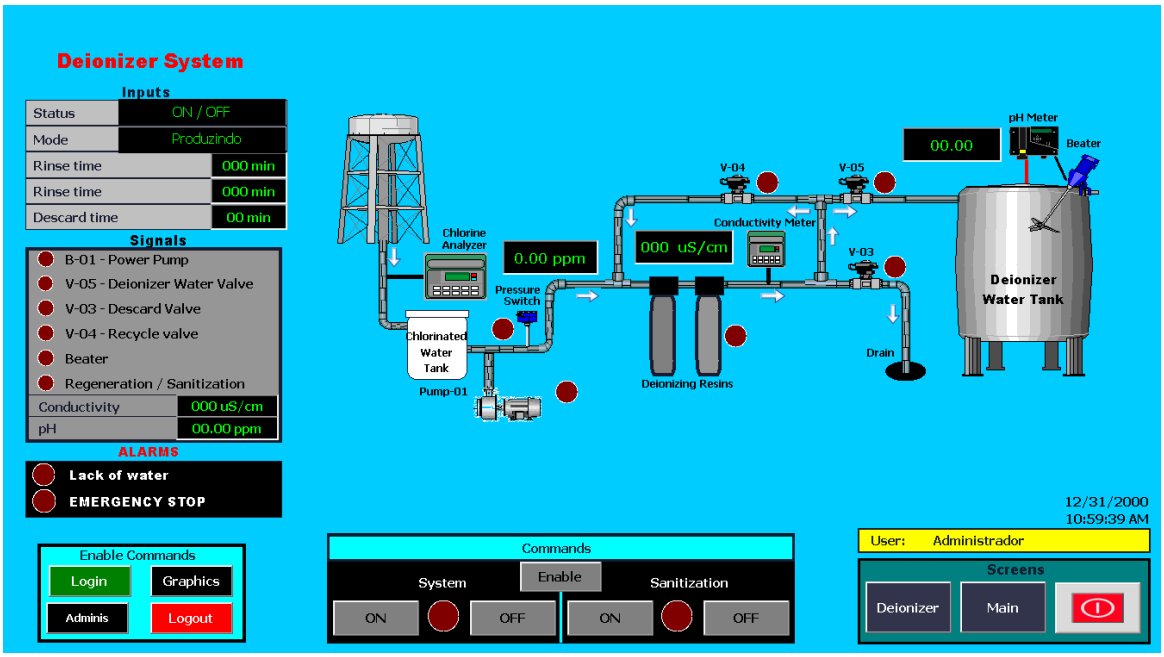

Figure 11. Deionizer System Screen (SISETA).

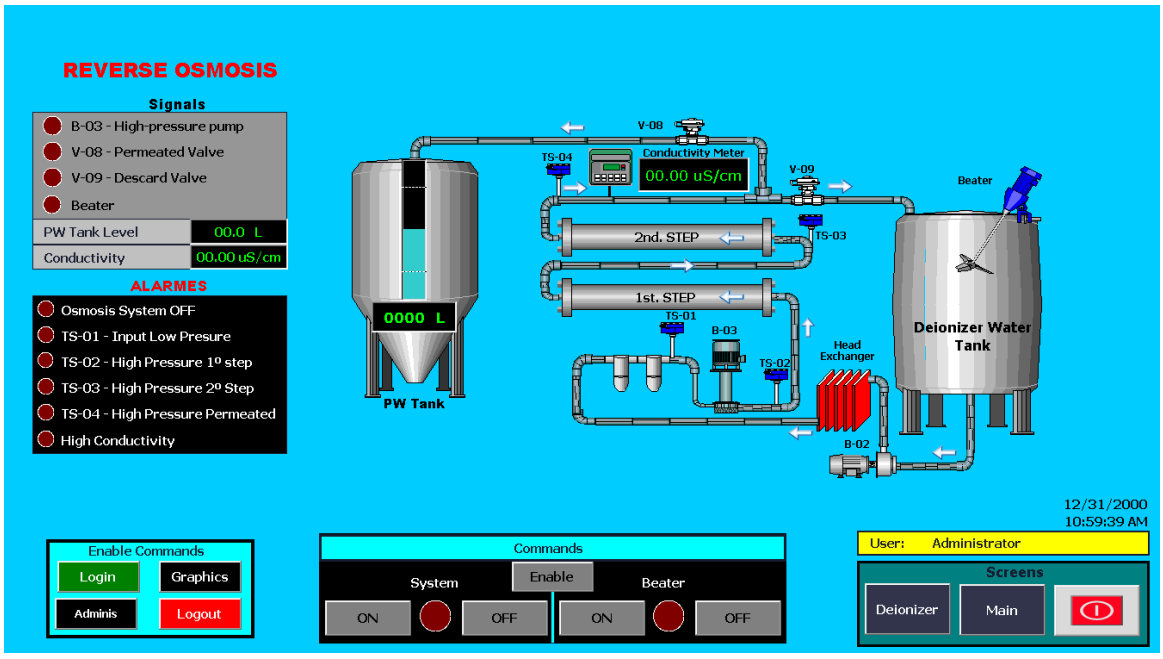

Figure 12. Screen of reverse osmosis system (SISETA).

Table 3. Main requirements for the validation of the supervisory system (ANVISA).

SISETA	SCADA for Wastewater Treatment Plants
Controlled access to the supervisory application	Automation of emergency procedures
Automatic user logoff	Monitoring and control of the system
Versioning of the application with electronic signature	Graphic display of all informations
Presentation of encrypted data in a readable format	Diagnostic and security management
Redundant recording of electronic records	Alarm management, notification and optimization
Encryption of Electronic Data Records	Data elaboration in real time, trend and reports for offline data analisys
Audit Trail occurrence records	
Detection of improper alteration of electronic records	
Alarm configuration and control with notification	
Display of sensor values in real-time	

4. Results and Discussions

The integration of water production phases into a single PLC facilitated the collection of variable data. Figure 13 illustrates the architecture of the plant before the intervention, totally decentralized, and without any communication between the stages of production. However, after the intervention, with the PLC of the last stage becoming the master and brain of this new architecture, according to as seen in Figure 7, we have a unified and centralized system.

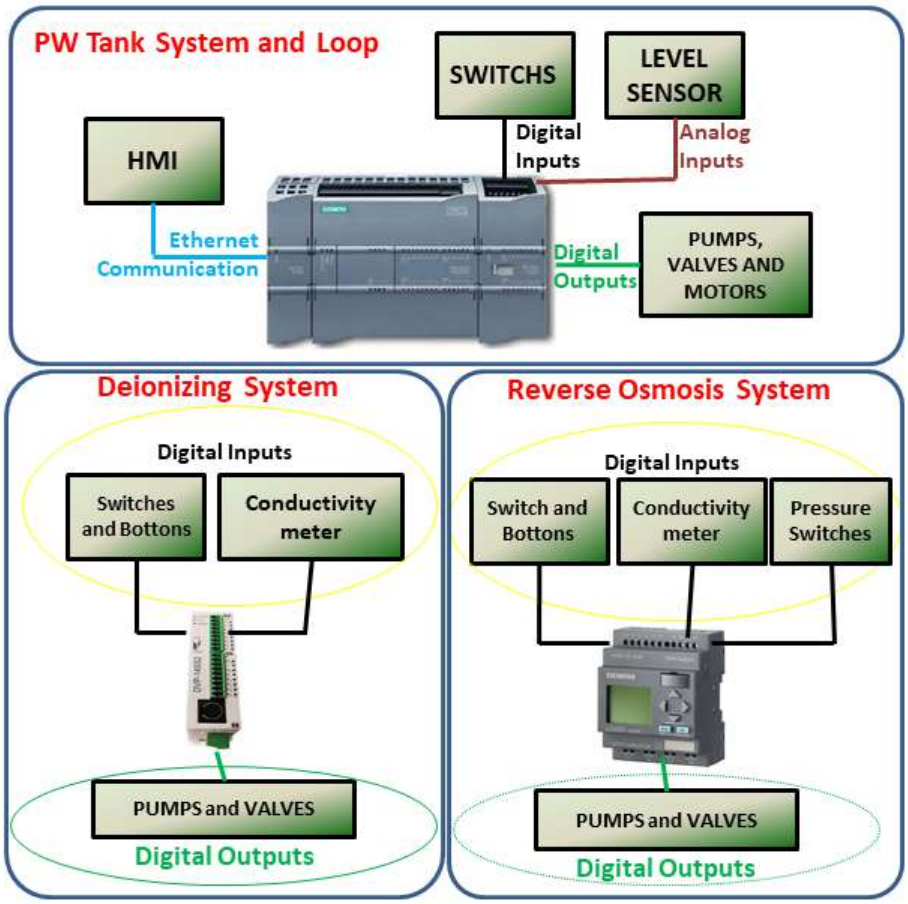

Figure 13. Decentralized systems before intervention.

After deploying SCADA in conjunction with this new network architecture, users can monitor and control the WTS of the supervisory room, managing, and interacting with the process, making it an important process tool. The system assists the operators in any intervention, achieving an increase in the efficiency and reliability of the process operation. The values of the variables correspond to those read in the instruments in real-time, and the reports are being generated and archived daily in a safe place, avoiding manipulation of data. Concerning reports, the system generates and stores to disk on the supervisory PC.

Figure 14 illustrates part of a report generated. This report aims to prove the performance of the system over the days and, consequently, in the months in which it is in the validation period, imposed by ANVISA [7]. Before the implementation of the system, these data were collected manually, which gave rise to error or even data manipulation, thus having no legal value for validating these values to the regulator.

PROCESS DATA REPORT						
Date	Hour	Chlorine (PPM)	Conductivity (µS/CM)	pH	PW Tank Level (L)	TOC (CFU)
13/10/2018	00:04	0.00	1.32	7.62	490.23	112.71
13/10/2018	00:09	0.00	1.37	7.61	488.83	112.73
13/10/2018	00:14	0.00	1.35	7.64	498.00	112.68
13/10/2018	00:19	0.00	1.29	7.63	493.03	112.73
13/10/2018	00:24	0.00	1.36	7.61	490.77	112.80
13/10/2018	00:29	0.00	1.32	7.64	492.79	112.86
13/10/2018	00:34	0.00	1.38	7.68	492.72	112.80
13/10/2018	00:39	0.00	1.36	7.61	491.55	112.87
13/10/2018	00:44	0.00	1.35	7.62	492.17	112.79
13/10/2018	00:49	0.00	1.32	7.65	494.66	112.81
13/10/2018	00:54	0.00	1.34	7.65	492.33	112.80
13/10/2018	00:59	0.00	1.35	7.64	496.45	112.88
13/10/2018	01:04	0.00	1.35	7.60	494.97	112.76
13/10/2018	01:09	0.00	1.32	7.63	495.51	112.75
13/10/2018	01:14	0.00	1.33	7.60	495.44	112.76
13/10/2018	01:19	0.00	1.38	7.62	494.50	112.67
13/10/2018	01:24	0.00	1.36	7.60	489.84	112.74
13/10/2018	01:29	0.00	1.37	7.60	493.88	112.82
13/10/2018	01:34	0.00	1.35	7.62	497.84	112.82

Figure 14. Daily report of the system stored in the SCADA PC.

Therefore, with this data stored, it can, if necessary, create performance graphs and verify if there were any system abnormalities during the day, week, month, or year. It can verify anomalies for a specific period or even the behavior of the system after some operator procedure, such as cleaning and sanitizing the system.

Figure 15 illustrates the graphical of the PW tank level in its regular operation, you can see well the increase and decrease the water level in the PW tank, it is seen that the maximum setpoint it is set to 1200 L, and o the closing level of the recycle valve is 600 L, half the maximum setpoint defined to the operator.

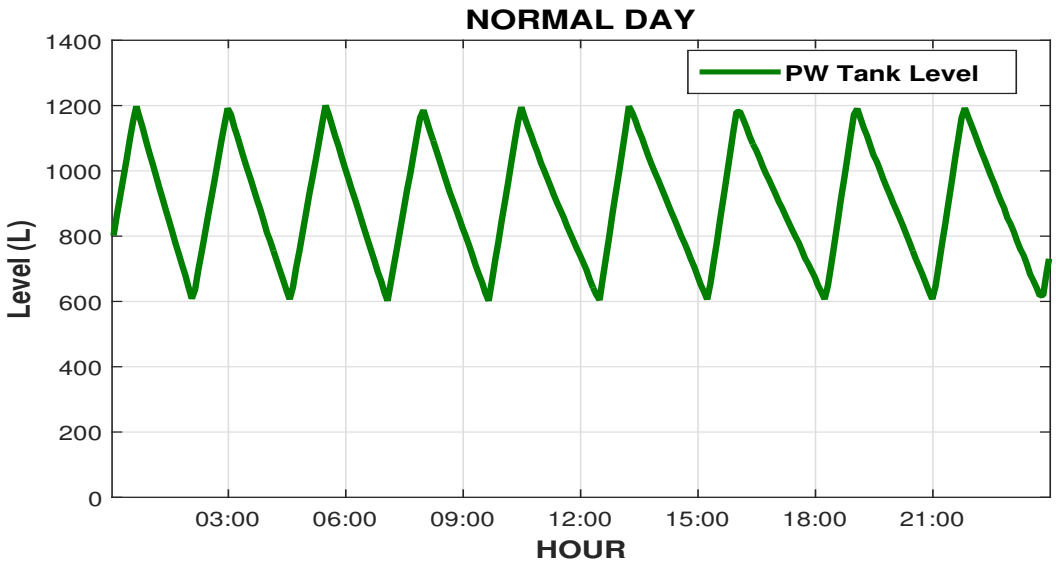

Figure 15. Sketch of the PW tank level reading graph.

To better exemplify supervision and control of the system by the automation network in conjunction with the sensors and the SCADA system, we chose atypical days of the system. These days are usually days when the system goes through some intervention and/or maintenance; then we made the graphs with the data stored.

This maintenance occurred due to the significant increase in conductivity in the osmosis system output, as well as a significant variation in ph values, as shown in Figure 16, where these setpoints, its usually set at 0.7 µS/cm and 7.5, respectively. After brief maintenance on the system it is observed that around 12 hs A.M., the conductivity decreased and was below the setpoint, a sign that the sanitization of the RO had been satisfactory, but the pH (which this measured in the tank before

RO) still had a wide variation, based on these data, operators see the need also to sanitize the deionizer system.

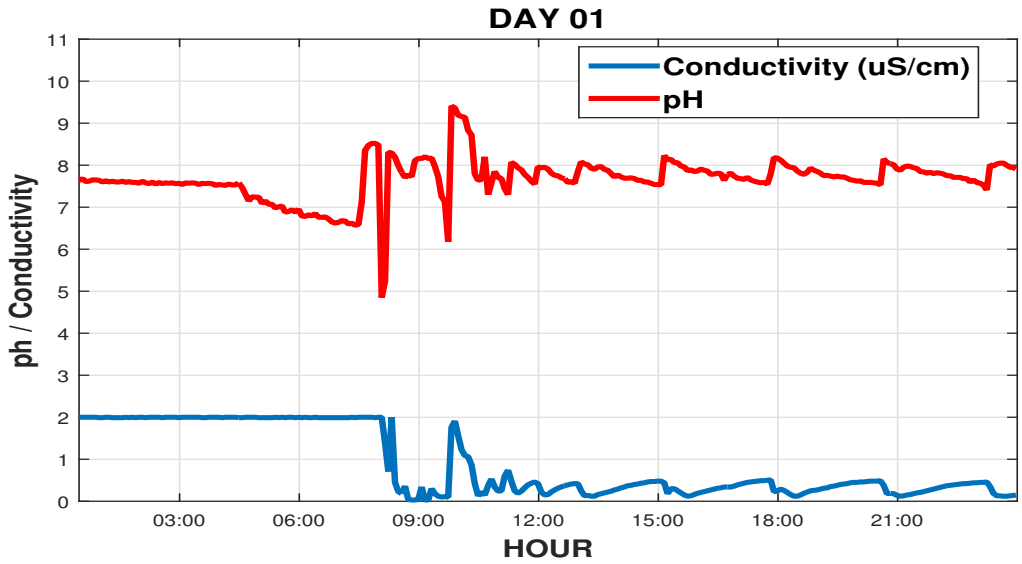

Figure 16. pH readings and RO conductivity during one day of intervention.

This second intervention takes a long time, about 6 hours long, so the loop system was interrupted for a long time outside its normal cycle, as can be seen in Figure 17, its noted that the PW tank level operates at normal cycle (ranging from 600 to 1200 L), until there was a shutdown of the system for maintenance and sanitization (cleaning) of the system (around 8:50 hs A.M.), we can observe that this maintenance continues until 5 hs P.M., the system restarts to lower the PW tank level, maintenance will continue the next day.

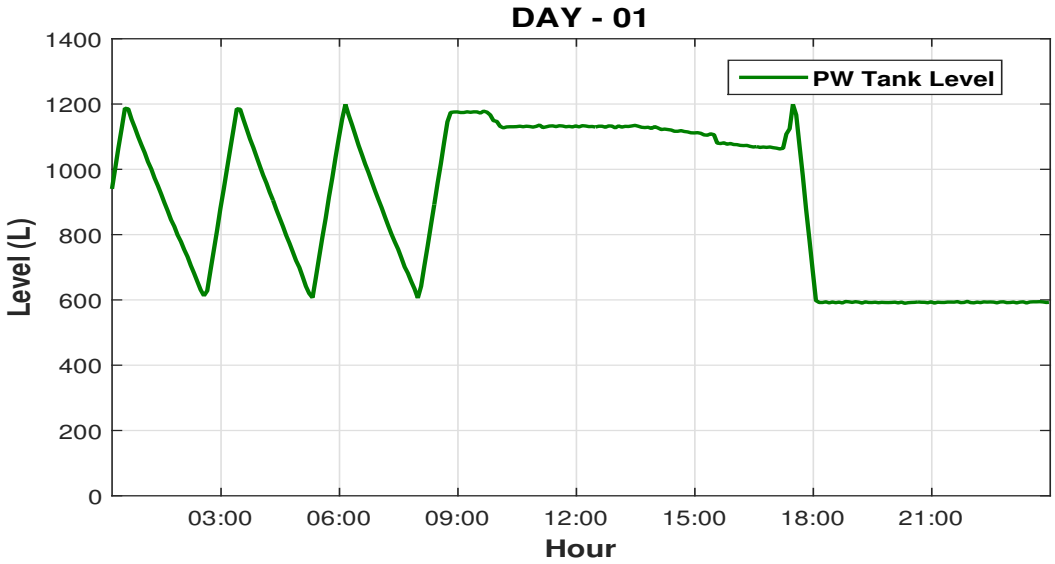

Figure 17. Sketch of graphical PW level reads during an intervention.

On the following day (second day) operators continued system maintenance, Figure 18 shows the graphic outline of tank level behavior on the second day of the intervention. Note that the system was out of operation, the operators dried the entire tank to produce whole new water. So, around 10 A.M. (after maintenance) the distribution and loop system, was reactivated and the PW tank level returned to work in its normal cycle, ranging from 600 to 1200 L.

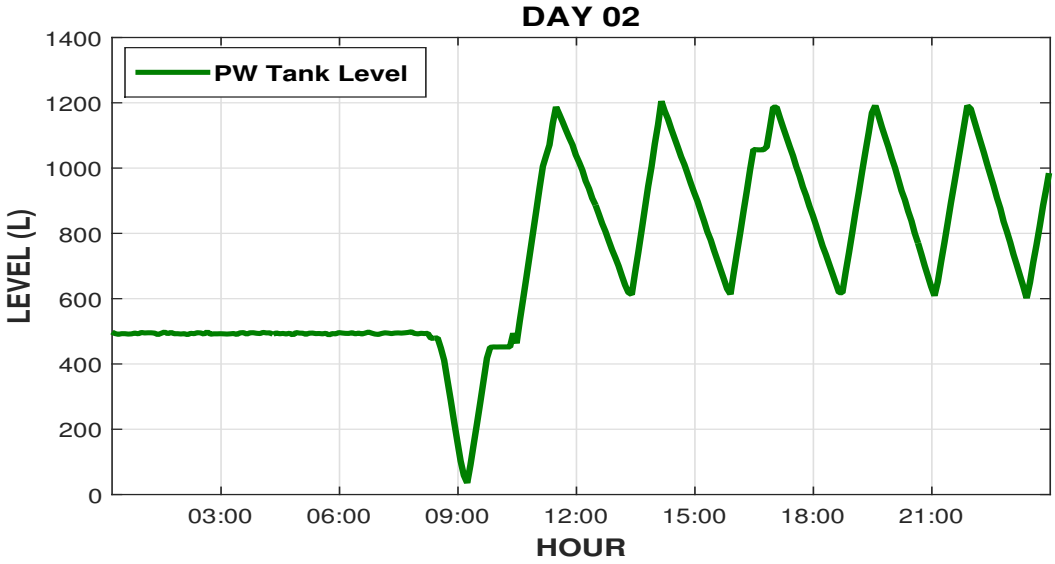

Figure 18. Readings of the PW tank level on the second intervention day.

We can see that the conductivity, which before the intervention was 2 µS/cm, is now below the setpoint (0.7 µS/cm), and the pH that was varying above 8, now varying within the desired range near 7.5, as shown in Figure 19.

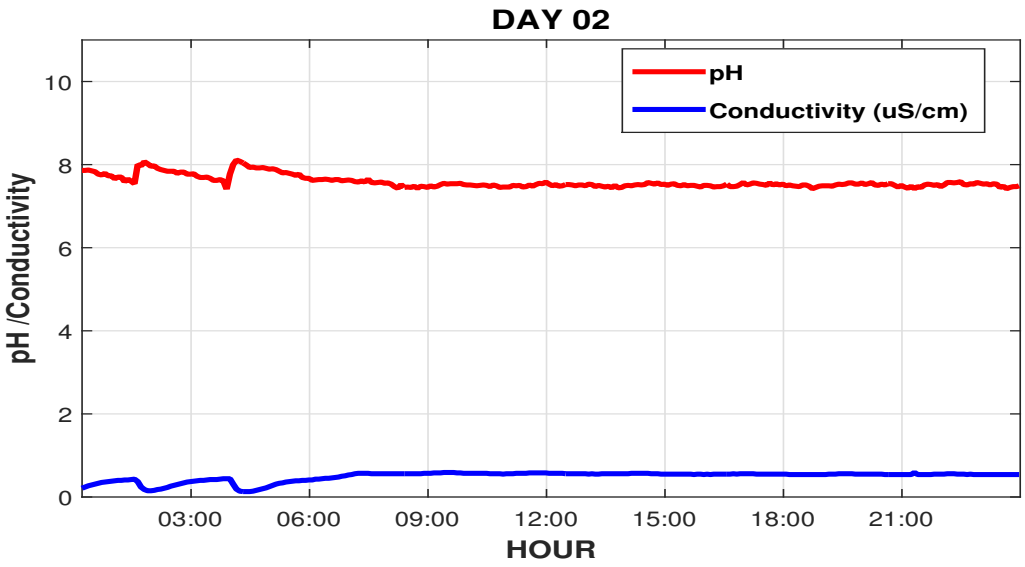

Figure 19. pH and RO conductivity readings on the second intervention day.

Figures 20 illustrates the system behavior on the day following the interventions (third day), showing the regular rise and fall cycle of the PW tank (600 to 1200 L). Figure 21 shows the graphs of pH reading and osmosis conductivity graphs, respectively, which are within their reading and control ranges (0.7 µS/cm).

Thus, collecting this data in real-time greatly facilitated the diagnosis for operator intervention in the plant, made the system more transparent so that the supervisor can see if the procedures and interventions of the operators in the system are correct, as well as prove that the data collected matches the truth of the water validation process and is within the required standards.

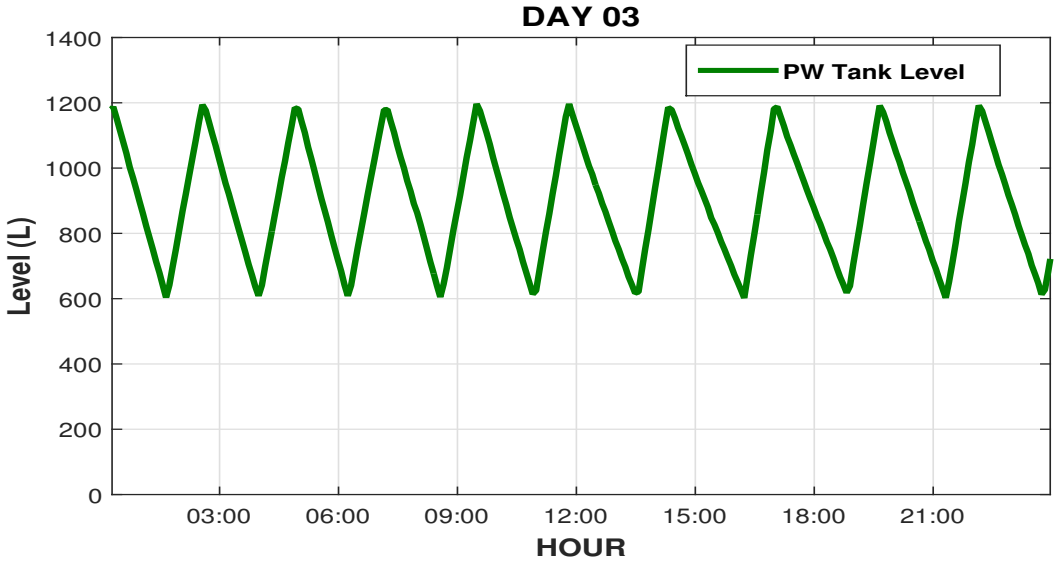

Figure 20. Readings of the PW tank level on the third day.

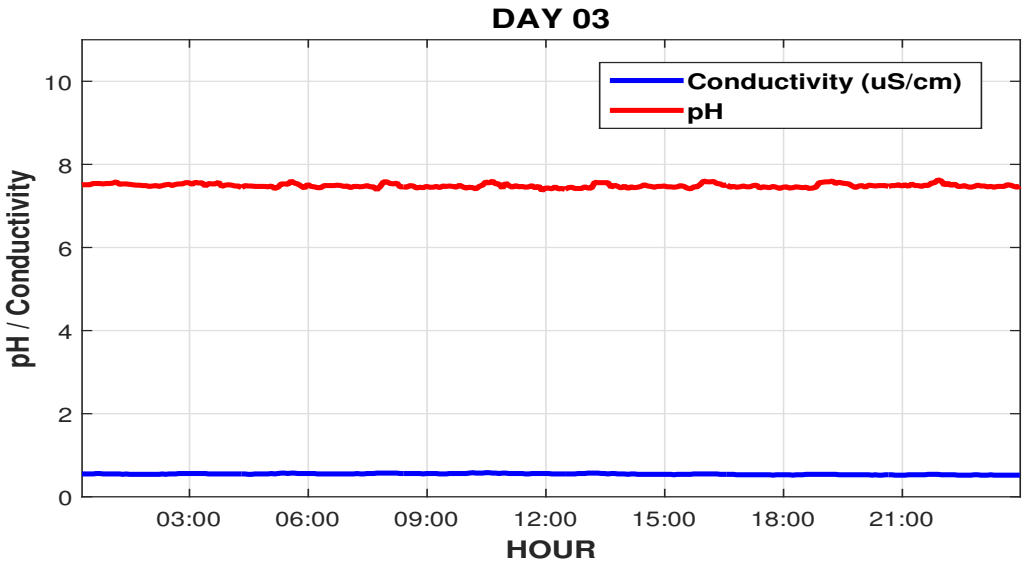

Figure 21. pH readings and RO conductivity on day 3.

5. Conclusions

This paper presented the implementation of a series of adjustments in the plant of the water treatment plant for pharmaceutical purposes concerning automation. The initial proposal consists of the implementation of a communication link between a controller, sensors and actuators network and a SCADA system as a solution to enhance the connectivity of the WTS. The most relevant contribution of the proposed solution is that all the operations of the WTS are performed automatically and autonomously. The developed SCADA system (SISETA) implements functionalities required by the Brazilian regulatory agency (ANVISA) such as audit trail, asset management, access control, electronic signature, etc. Besides, the presented system takes advantage of the already available components, regarding the implementation of the paradigms that govern the concept of industry 4.0.

The presented results prove the feasibility of the proposed solution for this first step of the project; that is, the information of the sensors, actuators, and controllers are effectively shared and managed through the Fieldbus, available for higher hierarchical level applications. This step will serve as the basis for the implementation of the Industry 4.0 concept. Future works include the addition of more industry 4.0 features like IoT and Cloud storage. Interoperability between instruments can be achieved

through a data acquisition interface compatible with the sensor of the application field. Protocols like MODBUS TCP, that is an open de facto standard, and is used for some automation and control systems, and can be implemented as an IoT protocol.

Author Contributions: Conceptualization, F.R.M.d.S. and D.A.d.M.F.; Data curation, F.R.M.d.S., D.A.d.M.F. and W.L.A.d.S.; Formal analysis, F.R.M.d.S., D.A.d.M.F., E.R.L.V. and A.O.S.; Funding acquisition, A.O.S.; Investigation, F.R.M.d.S., D.A.d.M.F. and E.R.L.V.; Methodology, F.R.M.d.S., W.L.A.d.S., D.A.d.M.F. and A.O.S.; Project administration, F.R.M.d.S., E.R.L.V., A.O.S. and G.A.E.E.; Resources, F.R.M.d.S., D.A.d.M.F. and A.O. S.; Software, F.R.M.d.S. and D.A.d.M.F.; Supervision, F.R.M.d.S., E.R.L.V., A.O.S. and G.A.E.E.; Validation, F.R.M.d.S. D.A.d.M.F. and W.L.A.d.S. ; Visualization, F.R.M.d.S., D.A.d.M.F. and A.O.S.; Writing—original draft, F.R.M.d.S., D.A.d.M.F. and E.R.L.V.; Writing—review & editing, F.R.M.d.S., D.A.d.M.F., W.L.A.d.S., E.R.L.V. and A.O.S.

Funding: This research was funded in part by the Coordenação de Aperfeiçoamento de Pessoal de Nível Superior—Brasil (CAPES)—Finance Code 001 and Conselho Nacional de Desenvolvimento Científico e Tecnológico (CNPq), and supported by Universidad Nacional de San Agustin de Arequipa (UNSA) Investiga under the grant number IAI-019-2018-UNSA.

Conflicts of Interest: The authors declare no conflict of interest.

Abbreviations

The following abbreviations are used in this manuscript:

WTS	Water treatment station
NUPLAM	Núcleo de Pesquisa em Alimentos e Medicamentos
PW	Purified water
HPW	Highly Purified Water
WFI	Water For Injection
GMP	Good Manufacturing Practices
SCADA	Supervisory Control and Data Acquisition
WFI	Water for injections
CFU	Chain forming unit
HMI	Human-Machine Interface
PLC	Programmable Logic Controller
TOC	Total organic carbon
RO	Reverse osmosis
ORP	Oxidation Reduction Potencial
PWT	Purified Water Tank
DB	Data block
ANVISA	Agência Nacional de Vigilancia Sanitaria
SISETA	Sistema Supervisorio da Estaçao de Tratamento de Água

References

1. Agency, E.M. Guideline on the Quality of Water for Pharmaceutical Use. Available online: https://www.ema.europa.eu/en/documents/scientific-guideline/draft-guideline-quality-water-pharmaceutical-use_en.pdf (accessed on 27 April 2019).
2. Kadajji, V.G.; Betageri, G.V. Water soluble polymers for pharmaceutical applications. *Polymers* **2011**, *3*, 1972–2009. [CrossRef]
3. World Health Organization. *Quality Assurance of Pharmaceuticals: A Compendium of Guidelines and Related Materials*; Good Manufacturing Practices and Inspection; World Health Organization: Geneva, Switzerland, 2007; Volume 2.
4. Simpson, D.R. Biofilm processes in biologically active carbon water purification. *Water Res.* **2008**, *42*, 2839–2848. [CrossRef]
5. Kawai, M.; Yamaguchi, N.; Nasu, M. Rapid enumeration of physiologically active bacteria in purified water used in the pharmaceutical manufacturing process. *J. Appl. Microbiol.* **1999**, *86*, 496–504. [CrossRef]
6. Haleem, R.M.; Salem, M.Y.; Fatahallah, F.A.; Abdelfattah, L.E. Quality in the pharmaceutical industry—A literature review. *Saudi Pharm. J.* **2015**, *23*, 463–469. [CrossRef]

7. Ministerio da Saúde. *Farmacopeia Brasileira*; Agencia Nacional de Vigilancia Sanitaria: Anvisa, Brazil, 2010. Available online: http://portal.anvisa.gov.br/documents/33832/260079/5%C2%AA+edi%C3%A7%C3%A3o+-+Volume+1/4c530f86-fe83-4c4a-b907-6a96b5c2d2fc (accessed on 15 April 2019).
8. Brasil. Ministerio da Saude. ANVISA-Agencia Nacional de Vigilancia Sanitaria. RDC n. 17, 16 April 2010. Available online: http://portal.anvisa.gov.br/documents/33880/2568070/res0017_16_04_2010.pdf/b9a8a293-f04c-45d1-ad4c-19e3e8bee9fa (accessed on 11 January 2019).
9. Gough, A.G.; Robottom, I. Towards a socially critical environmental education: Water quality studies in a coastal school. *J. Curric. Stud.* **1993**, *25*, 301–316. [CrossRef]
10. Calderón Godoy, A.; González Pérez, I. Integration of sensor and actuator networks and the scada system to promote the migration of the legacy flexible manufacturing system towards the industry 4.0 concept. *J. Sens. Actuator Netw.* **2018**, *7*, 23. [CrossRef]
11. Gilchrist, A. *Industry 4.0: The Industrial Internet of Things*; Apress: New York, NY, USA, 2016.
12. Nicolae, A.; Korodi, A.; Silea, I. Identifying Data Dependencies as First Step to Obtain a Proactive Historian: Test Scenario in the Water Industry 4.0. *Water* **2019**, *11*, 1144. [CrossRef]
13. Legat, C.; Vogel-Heuser, B. A configurable partial-order planning approach for field level operation strategies of PLC-based industry 4.0 automated manufacturing systems. *Eng. Appl. Artif. Intell.* **2017**, *66*, 128–144. [CrossRef]
14. Silva, F.R.M.d. Implantação e Desenvolvimento de uma Rede de Automação Industrial e Sistema SCADA para Estação de Tratamento de Água Purificada. Master's Thesis, Federal University of Rio Grande do Norte, Natal, Brazil, 2017.
15. Brasil, Ministerio da Saude. ANVISA-Agencia Nacional de Vigilancia Sanitaria. Consulta Pública n 312 Cofar, v.1. 2017. Available online: http://portal.anvisa.gov.br/documents/10181/2949405/CONSULTA+PUBLICA+N+312+COFAR.pdf/31ad3eb8-888c-434e-b7e6-119191479504 (accessed on 18 January 2019).
16. Santos, K.d.; Cruz, E. Sistemas de Geração e Distribuição de Água Purificada na Indústria Farmacêutica. *Farmacos Medicam.* **2008**, *50*, 34–41.
17. Valentini, S.A.; Vieira, L.d.J. Qualidade Físico-Química da Água Purificada das Farmácias de Manipulação da Cidade de Campo Mourão. *Revista Iniciare* **2017**, *2*, 49–52.
18. Brandão, I.A.P. Validação do Sistema de Agua Purificada na Industria Farmaceutica. Master's Thesis, Fundação Oswaldo Cruz, Rio de Janeiro, Brazil, 2015.
19. Agalloco, J.P.; Carleton, F.J. *Validation of Pharmaceutical Processes*; CRC Press: Boca Raton, FL, USA, 2007.
20. Park, H.G.; Kwon, Y.N. Long-Term Stability of Low-Pressure Reverse Osmosis (RO) Membrane Operation—A Pilot Scale Study. *Water* **2018**, *10*, 93. [CrossRef]
21. Kim, D.H.; Park, S.; Yoon, Y.; Park, C. Removal of Total Dissolved Solids from Reverse Osmosis Concentrates from a Municipal Wastewater Reclamation Plant by Aerobic Granular Sludge. *Water* **2018**, *10*, 882. [CrossRef]
22. Yokogawa, E.C. Reverse Osmosis: Application Note. Available online: https://web-material3.yokogawa.com/AN10B01B20-06E_020.pdf (accessed on 9 January 2019).
23. Martelli, C.; Pereira, E.; de Sousa, M.C.; Llehmann, E.L.; Guilherme, M.P.; Gonçalves, W.N. Uso Sustentável dos Recursos Hídrico e Energético do Instituto de Química: Uma Economia Anual de 1 Milhão de Litros de Água Potável e uma Experiência Disseminada. *Revista Eletronica do SIMTEC* **2016**, *1*, 96–97.
24. Scapini, L. Avaliação do Desempenho da Osmose Reversa e da Troca Iônica para Tratamento de Efluente de Curtume (Aimore Couros LTDA-Encantado) Visando a Reutilização da Água. Master's Thesis, University of Santa Cruz do Sul, Santa Cruz do Sul, Brazil, 2007.
25. Roy, S.; Ragunath, S. Emerging Membrane Technologies for Water and Energy Sustainability: Future Prospects, Constraints and Challenges. *Energies* **2018**, *11*, 2997. [CrossRef]
26. Brasil, Ministerio da Saude. ANVSA-Agencia Naciona de Vigilancia Sanitaria. Guia de Qualidade para Sistemas de Purificação de Água para Uso Farmacêutico. 2013. Available online: http://portal.anvisa.gov.br/resultado-de-busca?p_p_id=101&p_p_lifecycle=0&p_p_state=maximized&p_p_mode=view&p_p_col_id=column-1&p_p_col_count=1&_101_struts_action=%2Fasset_publisher%2Fview_content&_101_assetEntryId=350002&_101_type=document (accessed on 11 January 2019).
27. Fujioka, T.; Ishida, K.P.; Shintani, T.; Kodamatani, H. High Rejection Reverse Osmosis Membrane for Removal of N-Nitrosamines and Their Precursors. *Water Res.* **2018**, *131*, 45–51. [CrossRef]

28. Anand, A.; Unnikrishnan, B.; Mao, J.Y.; Lin, H.J.; Huang, C.C. Graphene-Based Nanofiltration Membranes for Improving Salt Rejection, Water Flux and Antifouling—A Review. *Desalination* **2018**, *429*, 119–133. [CrossRef]
29. Chee, K.P.; Wai, K.P.; Koo, C.H.; Chong, W.C. Performance Evaluation of Reverse Osmosis Desalination Pilot Plants using ROSA Simulation Software. In *E3S Web of Conferences*; EDP Sciences: Les Ulis, France, 2018; Volume 65, p. 05022.
30. Food and Drug Administration (FDA). Guide to Inspections of High Purity Water Systems. 1993. Available online: http://www.fda.gov/ICECI/Inspections/InspectionGuides/ucm074905.htm (accessed on 20 April 2019).
31. Health Sciences Authority. *Regulatory Guidance: Water Systems for Manufactures of Non-Sterile Products*; HSA: Singapore, 2008.
32. Dias, F.N. Avaliação de Eficácia da Sanitização de um Sistema de Purificação de Água. Esterilização de Artigos Médicos, Dissipação Residual do Óxido de Etileno e uso da Proteína Verde Fluorescente (GFP) como Indicador de Controle do Processo. Ph.D. Thesis, Universidade de São Paulo, São Paulo, Brazil, 2007.
33. Pereira, D.A.R. Projeto de um Sistema de Automação Industrial para uma Indústria de Produtos Saneantes. Undergraduate Thesis, University of Brasilia, Brasília, Brazil, 2015.
34. González, I.; Calderón, A.; Barragán, A.; Andújar, J. Integration of Sensors, Controllers and Instruments Using a Novel OPC Architecture. *Sensors* **2017**, *17*, 1512. [CrossRef]
35. Calderón, A.; González, I. Some Hardware and Instrumentation Aspects of the Development of an Automation System for Jar Tests in Drinking Water Treatment. *Sensors* **2017**, *17*, 2305. [CrossRef]
36. Jaloudi, S. Communication Protocols of an Industrial Internet of Things Environment: A Comparative Study. *Future Internet* **2019**, *11*, 66. [CrossRef]
37. Wollschlaeger, M.; Sauter, T.; Jasperneite, J. The future of industrial communication: Automation networks in the era of the internet of things and industry 4.0. *IEEE Ind. Electron. Mag.* **2017**, *11*, 17–27. [CrossRef]
38. Liu, Y.; Xu, X. Industry 4.0 and cloud manufacturing: A comparative analysis. *J. Manuf. Sci. Eng.* **2017**, *139*, 034701. [CrossRef]
39. Battaglia, F.; Iannizzotto, G.; Bello, L.L. JxActinium: A runtime manager for secure REST-ful CoAP applications working over JXTA. In Proceedings of the 31st Annual ACM Symposium on Applied Computing, Pisa, Italy, 4–8 April 2016; pp. 1611–1618.
40. Bruckner, D.; Stănică, M.P.; Blair, R.; Schriegel, S.; Kehrer, S.; Seewald, M.; Sauter, T. An introduction to OPC UA TSN for industrial communication systems. *Proc. IEEE* **2019**, *107*, 1121–1131. [CrossRef]
41. Neumann, P. Communication in industrial automation—What is going on? *Control Eng. Pract.* **2007**, *15*, 1332–1347. [CrossRef]
42. MODBUS Application Protocol. V1. 1b3, Modbus Organization. Inc. Retrieved. 2013. Available online: http://www.modbus.org/docs/Modbus_Application_Protocol_V1_1b.pdf (accessed on 15 February 2019).
43. ELIPSE. Elipse Scada, Driver M-PROT. 2015. Available online: https://www.elipse.com.br/downloads/?cat=48&key=mprot&language=ptbr#header-main (accessed on 11 April 2019).
44. Comer, D. *Interligação de Redes com TCP/IP: Princípios, Protocolos e Arquitetura*; Elsevier: Rio de Janeiro, Brazil, 2016; Volume 1.
45. Al-Dalky, R.; Abduljaleel, O.; Salah, K.; Otrok, H.; Al-Qutayri, M. A Modbus Traffic Generator for Evaluating the Security of SCADA Systems. In Proceedings of the IEEE 2014 9th International Symposium on Communication Systems, Networks & Digital Sign (CSNDSP), Manchester, UK, 23–25 July 2014; pp. 809–814.
46. Siemens AG. *SIMATIC S7-1200 Easy Book*; Siemens AG: Nürnberg, Germany, 2011. Available online: https://euroec.by/assets/files/siemens/s71200_easy_book_en-US_en-US.pdf (accessed on 22 April 2019).
47. Siemens AG. *SIMATIC S7-1200 Programmable Controller*; Siemens AG: Nürnberg, Germany, 2013. Available online: https://cache.industry.siemens.com/dl/files/593/109741593/att_895681/v1/s71200_system_manual_en-US_en-US.pdf (accessed on 23 April 2019).
48. Scada, E. HMI/SCADA SOFTWARE-Manual do Usuário. 2010. Available online: http://www.meccomeletronica.com/site/data/uploads/manual-scada.pdf (accessed on 20 April 2019).

© 2019 by the authors. Licensee MDPI, Basel, Switzerland. This article is an open access article distributed under the terms and conditions of the Creative Commons Attribution (CC BY) license (http://creativecommons.org/licenses/by/4.0/).

ResearchGate

See discussions, stats, and author profiles for this publication at: https://www.researchgate.net/publication/326688969

Development and Analysis of a Cryptographic Algorithm for Genetically Optimized Wireless Sensor

Article *in* Przeglad Elektrotechniczny · July 2018

DOI: 10.15199/48.2018.08.21

CITATIONS
0

READS
158

5 authors, including:

Xiankleber Cavalcante Benjamim
Universidade Federal do Rio Grande do Norte
10 PUBLICATIONS **12** CITATIONS
SEE PROFILE

Felipe Gama
Universidade Federal do Rio Grande do Norte
10 PUBLICATIONS **7** CITATIONS
SEE PROFILE

Rodrigo Soares Semente
Universidade Federal Rural do Semi-Árido - UFERSA
12 PUBLICATIONS **15** CITATIONS
SEE PROFILE

Elmer ROLANDO LLANOS Villarreal
Universidade Federal Rural do Semi-Árido - UFERSA
52 PUBLICATIONS **59** CITATIONS
SEE PROFILE

Some of the authors of this publication are also working on these related projects:

Detecção de Vazamentos em Dutos View project

Automação da Medição View project

All content following this page was uploaded by Andrés Ortiz Salazar on 30 July 2018.

The user has requested enhancement of the downloaded file.

Xiankleber C. BENJAMIM[1], Felipe O. S. GAMA[1], Rodrigo S. SEMENTE[2],Elmer R. L. VILLAREAL[2], Andrés O. SALAZAR[1]

Universidade Federal do Rio Grande do Norte (1), Universidade Federal Rural do Semi-Árido (2)

doi:10.15199/48.2018.08.21

Development and Analysis of a Cryptographic Algorithm for Genetically Optimized Wireless Sensor

Abstract. *This article proposes a methodology for obtaining a cryptographic algorithm, optimized for wireless sensor networks, through genetic algorithm. With the objective of increasing the level of security, computational efficiency and highlighting the energy consumption, considering that the autonomy of the wireless sensor devices is directly influenced by this factor. In aptitude function of genetic algorithm, were used metrics of algorithm runtime, maximum deviation and irregular, space occupied in memory and correlation coefficient (a new proposed metric), in order to find a safe and fast algorithm. The results obtained through computational simulations show the efficiency of the proposed methodology, in terms of processing time, coefficient of correlation and occupation of memory.*

Streszczenie. *W tym artykule zaproponowano metodologię uzyskiwania algorytmu kryptograficznego, zoptymalizowanego dla bezprzewodowych sieci czujników, za pomocą algorytmu genetycznego. W celu zwiększenia poziomu bezpieczeństwa, wydajności obliczeniowej i podkreślenia zużycia energii, biorąc pod uwagę fakt, że ten czynnik ma bezpośredni wpływ na autonomię bezprzewodowych czujników. W funkcji uzdatniania algorytmu genetycznego wykorzystano metryki czasu pracy algorytmu, maksymalnego odchylenia i nieregularności, miejsca zajmowanego w pamięci i współczynnika korelacji (nowa proponowana metryka), aby znaleźć bezpieczny i szybki algorytm. Wyniki uzyskane za pomocą symulacji obliczeniowych pokazują efektywność proponowanej metodologii, pod względem czasu przetwarzania, współczynnika korelacji i zajęcia pamięci.* ***(Opracowanie i analiza kryptograficznego algorytmu dla zoptymalizowanego genetycznie czujnika bezprzewodowego)***

Keywords: Cryptographic Algorithm, Genetic Programming, Wireless Sensor Networks
Słowa kluczowe: Algorytm kryptograficzny, Programowanie genetyczne, Sieci czujników bezprzewodowych

Introduction

The wireless sensor networks consist of nodes interconnected by wireless channels with sensing, control and actuation capacity. The data obtained and transmitted by the wireless sensor nodes in an industrial environment, especially when the sensor nodes are installed outdoors, must be confidential. For this purpose, are available in the literature various techniques that aim to maintain the confidentiality of the information transmitted. Among them, there is an approach that employs the increase of data security transmitted in wireless sensor networks, it is the use of cryptography techniques, according to [1].

Cryptographic security is responsible for keeping the information confidential, preventing the system from being invaded. By allowing the inclusion of false information in the system, an invasion can lead to even greater failures in the entire monitoring and control process, according to [1].

The most widely used standard in wireless sensor networks is the IEEE 802.15.4 [2], created in parallel with the Network Protocol ZigBee [3]. The standard IEEE 802.15.4 defines the physical layer and the Medium Acces Control (MAC) layer, as well as the recommended encryption technique for system security, the Advanced Encryption Standard (AES) [4].

The AES-128 is an efficient technique in terms of data processing and security. There are some reports of security breaches in partial versions of the algorithm, which does not mean that it is unsafe. However, there are studies indicating that it can be broken in a timely manner in the coming decades [5, 6].

It is important to emphasize that the energy efficiency of the nodes of the wireless sensor networks is more critical than in designed systems in which it does not need an autonomy of months and even years. In this context, electronic devices of low power and complexity are used, such as 8-bit and low memory microprocessors [7, 8].

There are papers in the literature that demonstrate that it is possible to create cryptographic algorithms with acceptable performance and security characteristics using genetic programming (GP) [9, 10, 11]. However, none of these papers presented results focusing on devices with only 8-bit processing capacity, taking into account both energy efficiency, occupied memory space and security, or a more robust comparative study, including cryptographic algorithms in effect.

Taking all these aspects into account and seeking to improve the security efficiency of wireless sensor networks, new algorithms can be developed for this purpose [12]. However, this work proposes the use of genetic algorithms with the objective of obtaining an optimized cryptographic algorithm for the wireless sensor networks, based on the Maximum and Irregular Deviation Ratio (MIDR), correlation coefficient, occupied memory and the execution time of the algorithm.

To demonstrate the feasibility of using the GP technique in the development of cryptographic algorithms, two classical encryption algorithms Advanced Encription Standart, XXTEA, and the CRYSEED algorithm presented in the paper [12]. The results presented in this work demonstrate that the use of GA can create efficient cryptographic algorithms, being a significant advance for the diffusion of artificial intelligence techniques.

Cryptographic Algorithms

This section presents two cryptographic algorithms which were used in this work to compare performance of the proposed algorithm.

The Advanced Encryption Standard (AES), is the chosen algorithm by the US government for the protection of data traffickedby digital means [13]. AES can use keys of 128, 192 and 256 bits.

The Algorithm considers groups of 16 bytes that form one state, which in other words is simply a 4×4 array with each element being a byte. This algorithm can be divided into four basic operations:

- AddRoundKey: Each byte of a state is combined with a byte of the key through the XOR (OR Exclusive) bit by bit.
- SubBytes: A nonlinear substitution where each byte is replaced by another according to a table lookup.
- ShiftRows: The bytes of each line undergo a shift cyclic by a certain amount of steps.
- MixColumns: Each column of state $a(x)$ is combined according to a known matrix $c(x)\ 4 \times 4$, which multiplied by state columns returns a new column for the resulting

state $b(x)$. The operation is reversible, simply by multiplying the columns of state $b(x)$ by a matrix $d(x)$, the result will be state $a(x)$.

Given these four operations, the algorithm can be divided into four stages, where the third step is usually repeated 20 times:

1. Key expansion based on key scheduling;
2. Start round: AddRoundKey;
3. Rounds:
   - SubBytes;
   - ShiftRows;
   - MixColumns;
   - AddRoundKey
4. Final round (without column mixing):
   - SubBytes;
   - ShiftRows;
   - MixColumns;

In the work [14] he developed the block encryption, Tiny Encryption Algorithm (TEA), which was notable for its simplicity and few lines of code, but that soon presented a security flaw that made the maximum size of its equal key 126 bits, making it so easy to break it such as a hash table or cryptographic scatter, tables substitutions created by spreading functions.

In 1997 the TEA was improved with an extension, thus generating Block TEA, or as it is better known the XTEA (eXtended TEA), which keys with a size of 128 bits [15]. Due to other security issues, the algorithm was restructured a second time, creating the XXTEA [16].

The XTEA is based on the classical Feistel network, varying only the Feistel function, as can be observed in Figure 1. XOR and modular sum operations are represented, respectively, by the square and the circle in Figure 1. The left and right shift operations are also used, but with a fixed number of offsets, 4 bits and 5 bits respectively.

XXTEA is an unbalanced Feistel network, whose input block is divided into N parts, each part being called X_R. So, the encryption of each die depends both his predecessor and successor neighbors , as observed in Figure 2, which presents the Feistel function that depends on both the X_{R-1} and X_{R+1}. Also used is K_R, which applies a left-hand cyclic shift of 2 bits each round.

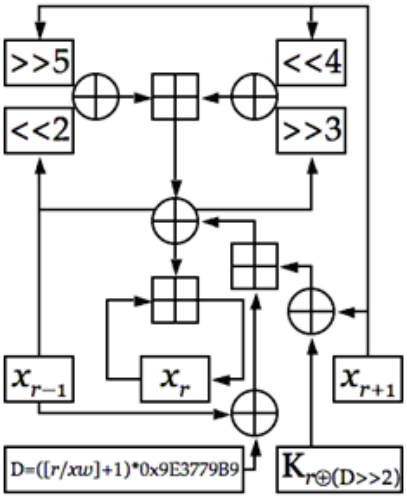

Fig. 1. XXTEA Flowchart. Source [18]

A fault in the XXTEA has already been found, with key breaking through differential cryptanalysis, performing a number of queries of only 2^{59} [19]. This method is a little difficult to apply in practice in an RSSF, since you have to choose the correct plain text for comparison. The data generated by a node of the RSSF are obtained with each measurement, they are not data that can be known by an attacker, being difficult to carry out this attack. Even so, this break can mean the existence of other faults, which may indicate the non-recommendation of its use, even in the Wireless sensor network.

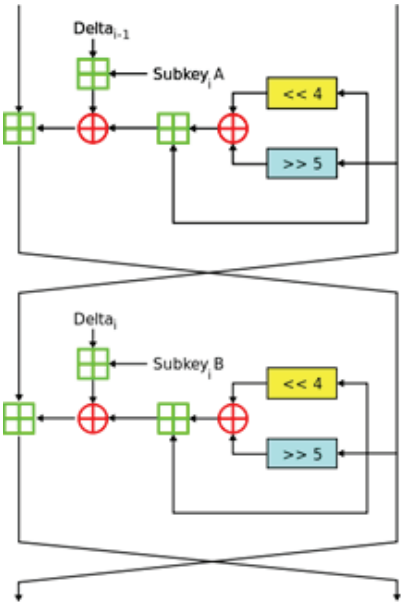

Fig. 2. XXTEA Feistel function. Source [17]

Genetic Programming

Based on natural evolution, several computational program solution methods have been developed, such as genetic algorithm, evolutionary programming, evolutionary strategies and genetic programming. The genetic algorithm allows the creation of programs to solve a problem, created automatically by the computer using a procedure inspired by evolution [20]. This program is usually represented by a tree structure, where each node and a function, where it receives an input from the son and returns an output to the parent, and the root node returns the final output of the program.

Genetic programming can be represented by a tree structure, where each node is a function, which receives an input from each child and returns an output to the parent, and where the root node returns the final output of the program. Thus PG follows the following steps:

- Initial population: it is the initial step of the genetic algorithm is the creation of an initial population of individuals. In this work the initial population is created in a random way.
- Fitness Function : it is the evaluation of the performance of each individual of the population, measuring the how much the result of that species is better compared to the others.
- Selection: it select the individuals with better aptitude from the previous population to generate the population. These individuals may pass through reproduction, crossover or mutation.
- Reproduction: choose the individuals with better aptitude from the previous population to generate the next population. These individuals may pass through reproduction, crossover or mutation.

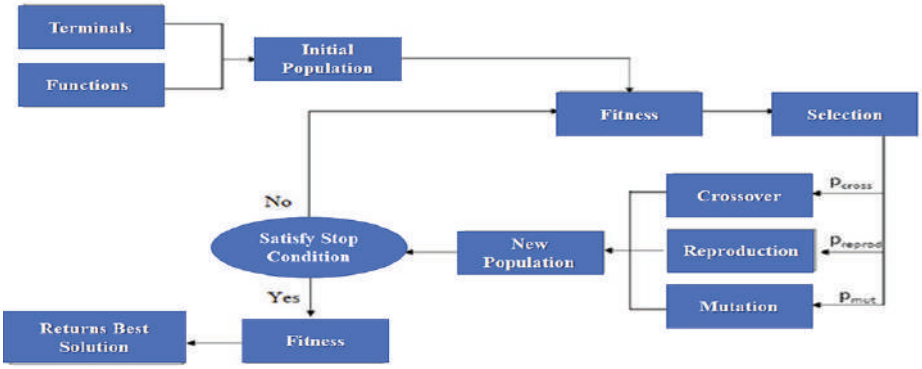

Fig. 3. Diagram of execution of a genetic programming.

- Crossover: each gene can be exchanged between two individuals, according to a uniform probability, generating two son.
- Mutation: is small probability of one or more random genes being exchanged for any other, generating a new individual slightly modified.
- New population: from the processes of reproduction, crossover and mutation a new population is generated.
- Satisfy Stop Condition: stop criteria are checked, which can contain: maximum number of iterations, so that the program can stop (mandatory condition); rate of population, stopping the program if it is not able to vary the population further.
  - If the stopping criterion is satisfied, the aptitude test must be performed, returning the best individual of the current population.
  - If it is not satisfied you should return to the second step.

The Figure 3 presents the order of execution of these steps, presented the probabilities of crossover P_{cross}, probability of reproduction P_{reprod} and probability of mutation P_{mut}. Some genetic programming do not use the reproduction step, since the crossover is similar in some respects to the first one, changing genes between two individuals [20].

Implementation

In this work, a C-library (Lil-GP) was used, making it possible to create algorithms that work in 8-bit microcontrollers, as proposed in this work. The use of the C language is also important, since it is used to program in the main microcontrollers. With the objective of embarking the genetic programming in the microcontroller, modifications were made. The following are the changes in the library:

- Adaptation so that all data operated by the cryptographic algorithms were 8-bits, through the type unsigned char. Although the DATATYPE variable type allows you to change most of the library, some parts, such as in preview and printing, needed to be adjusted in code.
- Parameter creation limiting the minimum number of nodes of the trees generated. This was created to prevent the generated programming from being trivial, such as simple assignments or denials, and to fit only performance parameters, not security parameters.
- Presentation of new fitness variables to better visualize the values of each plots of more complex fitness functions.
- Creations of variable weights to allow automatic execution of several genetic algorithms, each with different weight in the fitness functions.

In this work we used the coefficient of correlation in Fitness Function of genetic programming, where this metric is a measure of similarity between two variables [21, 22, 23]. If the two variables are an image and its encryption, then they are in perfect correlation (that is, coefficient of correlation equals one) if they are highly dependent (identical). In this situation, the encryption process failed to hide the details of the original image. If the correlation coefficient is zero, then the original image and the encrypted image are totally different, that is, the encrypted image has no recognizable feature and is highly uncorrelated from the original image. If the coefficient of correlation equals -1, this means that the encrypted image is the negative of the original image. The parameters used in the genetic programming were: a population of 200 individuals, 8192 test samples with 100 generations. Two weights were used for variable balancing of the fitness formula, varied ten times for each, thus creating the equivalent of 100 individual tests. A total of four test batteries were made, totaling 400 samples.

The evaluation function used in this phase follows as defined by:

$$(1) Fit = \left(\frac{T_N}{100} + \left(\Delta R \frac{MIDR}{MIDR_B} + \Delta C \frac{CC_S}{CC} \right) \right),$$

where ΔR and ΔC are the variation weights of the MIDR and coefficient of correlation parameters, CC_S is the lowest correlation coefficient between the algorithms studied for each image, and $MIDR_B$ is the Maximum and Irregular Deviation Ratio of best individual. This variation has as main objective to find the relation between the two metrics, a balance of difficult balance. It was noticed that small variations (with difference of 0.1 between the weights) did not present significant changes in the results, so variations were used in the order of 10^{-N}, with N being the execution index of each of the genetic programming individually.

Results Obtained

In this section presents algorithm obtained through computational simulation. In the development of the algorithm the Maximum and Irregular Deviation Ratio, and Correlation Coefficient were considered, the algorithm obtained through the proposed methodology of this work was named CRYSEED2. The execution time was used for the fitness function in genetic programming. The calculation of the occupied memory was calculated after the final results, because a reliable calculation of the occupied memory through the structures of trees created by genetic programming is not feasible. To compensate for this problem, we used a 50-node number limitation on the tree. Another factor that also helps to compen-

sate for this limitation is the use of runtime optimization due to the relationship of small algorithms to runtime. Also in this section a performance analysis is performed of the algorithm obtained.

The sets of functions used in this work were based on the functions used in the work [24]. Randomly generated constants were also added. The evaluation function used in this phase is given by:

$$Fit = \left(0,2T_N + \frac{0,4DM}{DM_M} + \frac{0,4DI_M}{DI}\right). \quad (2)$$

After 20 interactions, the PG converged to an algorithm with a tree function $(add(shift\ a_{10}\ a_{12})(xor\ a_5\ a_2))$. In Algorithms 1 and 2 they present the pseudocodes of the encryptor and decryptor CRYSEED2, respectively.

Algorithm 1 Encryption Pseudocode CRYSEED2

for $t = 0$ to number of rounds **do**
  for $j = 0$ to 16 **do**
    $v_1(j) = v_2(j) \wedge$ round key
  end for
  for $k = 0$ to 16 **do**
    for $j = 0$ to 16 **do**
      $v_2(j) = v_1((k+j)\%8)$
    end for
    $T_1 = v_2(10) \ll v_2(12)$
    $T_2 = (v_2(5) \wedge v_2(2))$
    $v_1(k) = (T_1 + T_2) \wedge v_2(0)$
  end for
  for $j = 0$ to 8 **do**
    $v_2(j) = v_1(j)$
  end for
end for

Algorithm 2 Pseudocode of decryptor CRYSEED2

for $t = 0$ to number of rounds **do**
  for $j = 0$ to 16 **do**
    $v_1(j) = v_2(j) \wedge$ round key
  end for
  for $i = 1$ to 16 **do**
    for $j = 0$ to 16 **do**
      $v_2(j) = v_1((k+j)\%8)$
    end for
    $T_1 = v_2(10) \gg v_2(12)$
    $T_2 = (v_2(5) \wedge v_2(2))$
    $v_1(k) = (T_1 - T_2) \wedge v_2(0)$
  end for
  for $j = 0$ to 8 **do**
    $v_2(j) = v_1(j)$
  end for
end for

Table 1 presents the execution time of the obtained algorithm and the reference algorithms. Comparing the results presented in Table 1, one can verify that the algorithm proposed in this work has a processing time reduction of 28%. In particular, it can be seen that CRYSSED2 has a processing time reduction of 84% over XXTEA. These times demonstrate the low computational cost of the proposed algorithm when compared with the reference algorithms, thus increasing the energy efficiency of the wireless sensor devices. It is important to note that the tests were performed on a computer with an Intel Core i5-2520M 2.5 GHz processor, with 8 GB of RAM DDR3-1333 SDRAM, Windows 7 Ultimate 64-bit operating system.

Table 1. Cryptographic Algorithm Execution Time.

Algorithm	Execution time (μs)		
	Encryption Time	Decryption time	Total time
AES	0.708	0.706	1.414
XXTEA	1.1097	1.097	2.294
Cryseed	0.2718	0.22	0.4918
Cryseed2	0.175	0.175	0.35

The level of quality of an encryption depends on how much greater the difference between the original data and the encrypted data, and even if it spreads the data in an irregular way, therefore a good cryptographic algorithm must be able to generate large values of D_M (maximum deviation) and small D_I values (irregular deviation). In this context, a performance analysis of the proposed algorithm through the MIDR, where the MIDR is given by:

$$MIDR = \left(\frac{D_M}{D_I} \times \frac{DI_M}{DM_M}\right), \quad (3)$$

where DM_M and DI_M are the maximum and irregular deviations of the best individual.

The images used for the comparative test among the algorithms were: lena, the most used image in scientific articles; cameraman, used for having shades of gray and light and dark areas; mandrill, an image with high contrast of high frequency colors; testpat, an image with squares of various sizes of various shades of gray and in the center the image lena. These images are shown in Figure 4. All images were obtained from The USC-SIPI Image Database [25]. Tests with other images were also performed to obtain more significant results from the proposed technique, these images are illustrated in Figure 5. The results of this encryption were used to feed the adjust the importance of each metric in the quality assessment cryptographic. In the figure below we can observe the images used in encryption.

Table 2 show the results obtained through simulations the performance of the proposed algorithm and the reference algorithms, in terms of MIDR, each value of the images refers to the Maximum and Irregular Deviation Deviation of each algorithm related to the figures. It is observed that CRYSSED 2 had a considerable gain over other reference algorithms such as AES and XXTEA. It is observed that this gain of CRYSEED2 in the MIDR occurs through its encryption of the proposed algorithm, showing that the encrypted algorithm is superior to its predecessors comparing the means MIDR obtained by the reference algorithms, thus becoming the best algorithm analyzed in this work demonstrating the metric Coefficient of Correlation applied was better in the cryptographic analysis of the images.

Coefficient of Correlation (CC) is a measure of similarity between two variables [22, 23, 21]. If the two variables are an image and its encryption, then they are in perfect correlation (that is, CC equals one) if they are highly dependent (iden-

tical). In this situation, the encryption process failed to hide the details of the original image. If the correlation coefficient is zero, then the original image and the encrypted image is totally different, that is, the encrypted image has no recognizable feature and is highly uncorrelated from the original image. If the CC equals -1, this means that the encrypted image is the negative of the original image. The CC is measured by:

$$cc = \frac{cov(x,y)}{\sigma_x \sigma_y} = \frac{\sum_{i=1}^{N}(x_i - E(x))(y_i - E(y))}{\sqrt{\sum_{i=1}^{N}(x_i - E(x))^2}\sqrt{\sum_{i=1}^{N}(y_i - E(y))^2}} \tag{4}$$

Where $E(x) = \frac{1}{N}\sum_{n}^{i=1} x_i$, and x and y are the gray values of the original and encrypted image pixel. The success of the encryption process means lower CC values

The standardized CC is given by:

$$CC_N = \frac{CC_M}{CC} \times 100 \tag{5}$$

Where CCN is the normalized value in percentage and CCM is the lowest correlation coefficient between the algorithms studied for each image.

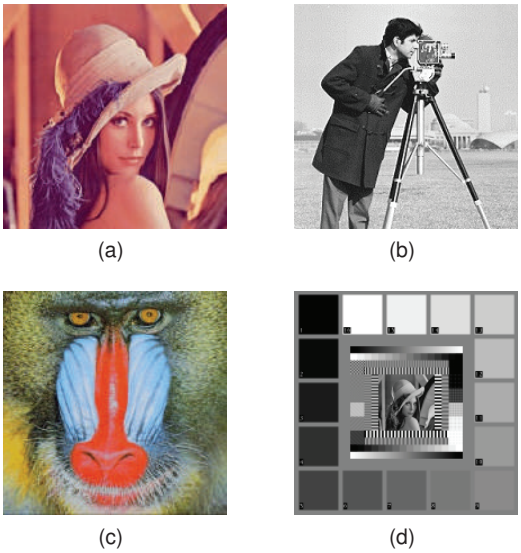

(a) (b) (c) (d)

Fig. 4. Standard images: (a) lena; (b) cameraman; (c) mandril (d) testpat.

Table 2. Maximum and Irregular Deviation Ratio.

Algorithm	Maximum and Irregular Deviation Ratio							
	lena	cman	mandrill	testpat	black	arial	random	earth
AES	1.24	1.93	1.86	1.67	0.58	0.80	0.58	1.50
XXTEA	0.89	2.19	2.67	1.04	0.25	0.79	0.34	2.46
CRYSEED	1.14	2.62	2.05	1.37	0.34	0.65	0.25	1.77
CRYSEED2	1.12	2.61	2.06	1.39	0.34	0.65	0.34	1.81

The results obtained in the computational simulations with the objective of measuring the correlation coefficient can be seen in 3. It should be noted that the results obtained with the images lena, black, arial and mandrill were the better results.The proposed technique obtained good gains in the correlation coefficient showing that the analyzed images are different from the originals,since CC is negative. So it shows the efficiency of the proposed technique.

Table 3. Coefficient of Correlation.

Algorithm	Coefficient of Correlation							
	lena	cman	mandrill	testpat	black	arial	random	earth
AES	0.14	−0.01	0.005	−0.05	−0.27	−0.10	−0.07	−0.02
XXTEA	0.014	−0.002	−0.003	−0.02	0.02	0.002	−0.001	0.01
CRYSEED	−0.1	−0.18	−0.07	−0.10	−0.19	−0.03	0.01	−0.05
CRYSEED2	−0.16	−0.17	−0.07	−0.08	−0.20	−0.03	0.01	−0.08

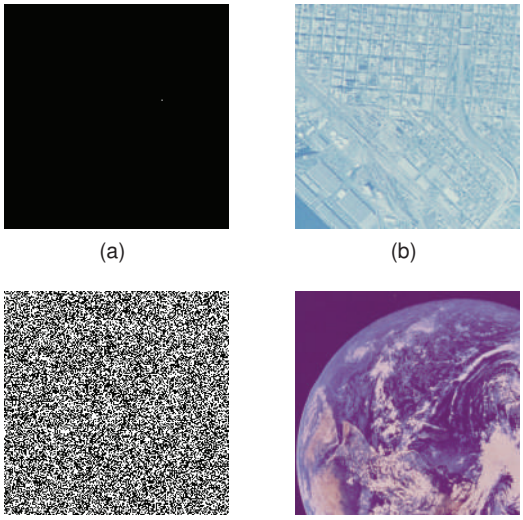

(a) (b) (c) (d)

Fig. 5. Standard images: (a) black; (b) arial; (c) random (d) earth.

The Table 4 presents the performance of the algorithms analyzed in terms of occupied memory, in which one can analyze the gain of the proposed algorithm, specifically if we compare CRYSEED2 in relation to AES.

Table 4. Cryptographic Occupied memory.

Algorithm	Occupied memory (Bytes)
AES	$9,437$
XXTEA	$1,570$
CRYSEED	$1,078$
CRYSEED2	$1,078$

Conclusions

The genetic programming methodology was applied and improved for the development of cryptographic algorithm for 8-bit devices, widely used in wireless sensor networks. The CRYSEED2 algorithm was automatically developed from the use of the lil-GP library, adapted to find an efficient cryptographic algorithm for 8-bit devices with high-quality encryption. Also shown performed comparative tests between the algorithm proposed in relation to widely used algorithms literature, in which the following comparison metrics were used: runtime and Maximum and Irregular Deviation Ratio, space occupied in memory and correlation coefficient. The obtained results demonstrate that CRYSEED2 is competitive in comparison to the other presented algorithms. Making possible the insertion of the proposed algorithm in wireless sensor networks, since CRYSEED 2 has low computational complexity and good cryptographic performance. Finally, these results help to prove that genetic programming can create efficient cryptographic algorithms and is a significant advance in the diffusion of artificial intelligence techniques.

***Authors**: Msc. Xiankleber C. Benjamim, Brazil, E-mail: xiankleber@dca.ufrn.br: Msc. Felipe O. S. Gama, Brazil, E-mail:felipe.gama@dca.ufrn.br: Dr. Rodrigo S. Semente, Brazil, E-mail: rodrigo.semente@ufesa.edu.br: Dr. Elmer R. L. Villarrea, Brazil, E-mail: Dr. Andrés O. Salazar, Brazil, andres@dca.ufrn.br*

REFERENCES

[1] Shim, K.A. A Survey of Public-Key Cryptographic Primitives Issues in Wireless Sensor Networks **2012**.

[2] IEEE Standards 802.15.4. Technical report, The Institute of Electrical and Electronics Engineers, Inc., New York, USA., 2003.

[3] ZigBee Specification Version 1.0. Technical report, ZigBee Aliance, 2004.
[4] IEEE 802.15.4e - IEEE Standard for Local and metropolitan area networks–Part 15.4: Low-Rate Wireless Personal Area Networks (LR-WPANs) Amendment 1: MAC sublayer. Technical report, The Institute of Electrical and Electronics Engineers, Inc., New York, USA., 2012.
[5] Biryukov A., Dunkelman O., Keller N., Khovratovich D., Shamir A.: Key recovery attacks of practical complexity on AES-256 variants with up to 10 rounds **2010**. pp. 299–319.
[6] Biryukov, A., Großschädl J.: Cryptanalysis of the full AES using GPU-like special-purpose hardware. *Fundamenta Informaticae* **2012**, *114*, 221–237.
[7] Rinne S., Eisenbarth T., Paar C.: Performance analysis of contemporary light-weight block ciphers on 8-bit microcontrollers. Ecrypt Workshop SPEED. Citeseer, 2007, pp. 33–43.
[8] Meiser G., Eisenbarth T., Lemke-Rust K., Paar C.: Efficient implementation of eSTREAM ciphers on 8-bit AVR microcontrollers. Industrial Embedded Systems, 2008. SIES 2008. International Symposium on. IEEE, 2008, pp. 58–66.
[9] Polimón J., Hernández-Castro J.C., Estévez-Tapiador J.M., Ribagorda A.: Automated design of a lightweight block cipher with Genetic Programming. *International Journal of Knowledge-based and Intelligent Engineering Systems* **2008**, *12*, 3–14.
[10] Estevez-Tapiador J.M., Hernandez-Castro J.C., Peris-Lopez P., Ribagorda A.: Automated Design of Cryptographic Hash Schemes by Evolving Highly-Nonlinear Functions. *Journal of Information Science & Engineering* **2008**, *24*.
[11] Picek S., Carlet C., Jakobovic D., Miller J.F., Batina L.: Correlation immunity of boolean functions: an evolutionary algorithms perspective **2015**. pp. 1095–1102.
[12] Semente R.S., Salazar A.O., Oliveira F.D.: CRYSEED: An automatic 8-bit cryptographic algorithm developed with genetic programming. Instrumentation and Measurement Technology Conference (I2MTC) Proceedings, 2014 IEEE International. IEEE, 2014, pp. 1065–1068.
[13] Daemen J., Rijmen V.: AES proposal: Rijndael **1999**.
[14] Wheeler D.J., Needham R.M.: TEA, a tiny encryption algorithm. International Workshop on Fast Software Encryption. Springer, 1994, pp. 363–366.
[15] Needham R.M., Wheeler D.J.: Tea extensions. *Report (Cambridge University, Cambridge, UK, 1997) Google Scholar* **1997**.
[16] Wheeler D.J., Needham R.M.: Correction to xtea. *Unpublished manuscript, Computer Laboratory, Cambridge University, England* **1998**.
[17] Gaba S., Aggarwal I., Pandey S.: Design of efficient XTEA using Verilog. *International Journal of Scientific and Research Publications* **2012**, *2*.
[18] Zafar F. *Tiny encryption algorithm for cryptographic gradient noise*; University of Maryland, Baltimore County, 2010.
[19] Yarrkov E. Cryptanalysis of XXTEA. *IACR Cryptology ePrint Archive* **2010**, *2010*, 254.
[20] Koza J.R. Hierarchical Genetic Algorithms Operating on Populations of Computer Programs. IJCAI, 1989, pp. 768–774.
[21] Ahmad J., Ahmed F.: Efficiency analysis and security evaluation of image encryption schemes. *International Journal of Video and Image Processing and Network Security* **2010**, *23*, 25.
[22] Ahmed H.E.d.H., Kalash H.M., Allah O.F.: Encryption efficiency analysis and security evaluation of RC6 block cipher for digital images. Electrical Engineering, 2007. ICEE'07. International Conference on. IEEE, 2007, pp. 1–7.
[23] El Fishawy N.F., Zaid O.M.A.: Quality of encryption measurement of bitmap images with RC6, MRC6, and Rijndael block cipher algorithms. *IJ Network Security* **2007**, *5*, 241–251.
[24] Hernandez-Castro J.C., Estevez-Tapiador J.M., Ribagorda-Garnacho A., Ramos-Alvarez B.: Wheedham: An automatically designed block cipher by means of genetic programming. Evolutionary Computation, 2006. CEC 2006. IEEE Congress on. IEEE, 2006, pp. 192–199.
[25] SIPI, U. The usc-sipi image database, 2016.

View publication stats

Benchmark of a PI Controller Implemented in Java and Native Code on the Android™ Platform Embedded on ARM

R. R. Melo, E. Caratti Filho, D. S. S. Casillo and E. R. L. Villarreal

***Abstract*— This paper presents a performance analysis of a PI controller implemented on the Android™ platform in embedded ARM. To perform the analysis are presented two execution strategies. The first strategy is the execution of PI controller from its implementation in Java. The second strategy is the execution of the PI controller from its implementation in native code. In the analysis of the experiment with two suggested strategies, it was found that the controller obtained better performance and stability while running in native code.**

***Keywords*— PI Controller, Android, ARM microcontroller, java code, native code.**

I. Introdução

RECENTEMENTE, a plataforma Android vem sendo utilizada em diversos dispositivos móveis. Seu surgimento se deu para o uso em celulares, mas seu uso vem ganhando espaço para uma gama cada vez maior de dispositivos, sendo estes não móveis também [1].

Na plataforma Android a maioria das aplicações são programadas na linguagem Java. Geralmente os programas escritos em Java são mais lentos do que os escritos em C/C+. Mas na plataforma Android é permitido também o desenvolvimento de aplicações escrito em C/C++ [2]. Alguns trabalhos mostram que a execução de algoritmos escritos em C/C++ é mais eficiente do que executados em Java na plataforma Android [3]-[6].

Muito dos dispositivos com Android são baseados na tecnologia ARM. Esta tecnologia é utilizada em Unidades Microcontroladas (MCUs, do inglês *Microcontroller Units*), componente este, presente em uma variedade de dispositivos, que vão desde uso doméstico a uso industrial. Estes dispositivos para uso em automação industrial e controle podem dispor de sistemas operacionais embarcados, oferecendo mais funcionalidades e melhor desempenho do que equipamentos de controle convencional [7]-[9]. Alguns trabalhos mostram o desempenho de algoritmos de controle embarcados em placas ARM, algumas dispostas por sistemas operacionais embarcados baseados em Linux [10]-[14].

Em MCUs ARM dois tipos de sistemas operacionais podem ser portados, os sistemas operacionais em tempo real e os sistemas operacionais de uso geral [15], como o Android discutido anteriormente. Em sistemas de controle embarcado, os sistemas operacionais em tempo real são importantes para atender requisitos críticos de tempo em uma aplicação. Em [16]-[19] é discutido a temática sobre o desempenho e uso da plataforma Android em aplicações de tempo real.

Este trabalho trata da utilização da plataforma Android embarcada em um microcontrolador ARM para resolver um dos processos mais encontrados na indústria, o controle de nível de líquido, onde frequentemente é usado um controlador Proporcional Integral Derivativo (PID).

As seções a seguir estão divididas da seguinte forma: na seção 2 serão abordados os conceitos da plataforma Android e do mecanismo JNI. Na seção 3 será apresentado o modelo de um controlador PI para nível de líquido e as estratégias de implementação deste controlador em uma plataforma Android embarcada em ARM. A seção 4 descreverá sobre os componentes e a montagem do experimento de controle. Na seção 5 são apresentados os resultados obtidos com o experimento realizado.

II. Sistema Operacional Android e Interface Nativa Java

Nas seções A e B será descrito uma visão geral da plataforma Android e do mecanismo JNI utilizado nesta plataforma.

A. Android

O sistema operacional android foi projetado principalmente para plataformas móveis, sendo de código aberto e baseado no Kernel do Linux (Versão 2.6). A plataforma permite ao desenvolvedor escrever aplicações principalmente em Java, mas com suporte para linguagens C/C++ [20].

A arquitetura do sistema operacional android é divida em camadas de software como pode ser visto na Fig. 1. A base do sistema é composta pelo kernel do Linux (versão 2.6), fornecendo as funcionalidades básicas do sistema, como gerenciamento de memória, segurança, drivers de hardware, interface de rede, gerenciamento de energia, entre outros.

Logo acima do kernel existe o conjunto de bibliotecas nativas em C/C++, que inclui a bionic (libc), suporte para vídeo, áudio, gráficos (OpenGL-ES), SQlite para banco de dados, SSL e Webkit para navegador web e segurança na internet.

R. R. Melo, Universidade Federal Rural do Semi-Árido (UFERSA), Rio Grande do Norte, Brasil, reuberegis@gmail.com.

E. Caratti Filho, Universidade Federal Rural do Semi-Árido (UFERSA), Rio Grande do Norte, Brasil, egm.filho@gmail.com.

D. S. S. Casillo, Universidade Federal Rural do Semi-Árido (UFERSA), Rio Grande do Norte, Brasil, danielle@ufersa.edu.br.

E. R. L. Villarreal, Universidade Federal Rural do Semi-Árido (UFERSA), Rio Grande do Norte, Brasil, elmerllanos@ufersa.edu.br.

Figura 1. Arquitetura da Plataforma Android.

Também na camada de software superior ao Kernel, possui a parte principal que representa o sistema Android, denominado de tempo de execução Android. Nesta parte estão incluídos dois componentes, o núcleo de bibliotecas Android e a Dalvik VM. O núcleo de bibliotecas Android fornece muito das funcionalidades disponíveis no núcleo de bibliotecas Java, como também biblioteca especifica para o sistema Android. A Dalvik VM é uma maquina virtual baseada em registradores, onde foi otimizada para trabalhar com múltiplas instâncias de forma eficiente executando *bytecode Dalvik*. Estes *bytecodes Dalvik* são gerados da compilação de aplicações Java para android, portanto vale ressaltar que o Android não executa *bytecode* java. A Dalvik VM se baseia no Kernel para gerenciamento de threads e de memória de baixo nível.

A camada de framework de aplicações fornece classes java necessárias para criar uma aplicação Android. Nesta camada também permite uma abstração genérica para acesso ao hardware, gerenciamento de interface do usuário e recursos das aplicações. Na camada de aplicação encontram-se todas as aplicações desenvolvidas para o sistema operacional android, nativas e de terceiros [1].

B. Interface Nativa Java

A Interface Nativa Java (JNI, do inglês *Java Native interface*) é um mecanismo que trabalha de forma bidirecional, ou seja, permite que aplicativos Java acessem códigos nativos, geralmente escrita em C/C++, e o código nativo acesse o aplicativo Java [21], [22]. É possível também utilizar este mecanismo na plataforma Android, utilizando o pacote de desenvolvimento nativo do Android, o NDK [2]. Com este pacote as bibliotecas nativas podem ser incorporadas em uma aplicação android, permitindo chamadas as funções nativas a partir do aplicativo em execução na maquina virtual Dalvik. Lembrando que este aplicativo é escrito em Java, por isso o mecanismo JNI pode ser usado.

A vantagem de utilizar código nativo em uma aplicação android esta relacionado ao tipo de solução que se quer buscar. Nem sempre usar código nativo representa um aumento de desempenho na aplicação. Aplicações que necessite de operações intensas, simulações físicas e processamentos de sinais, são as mais indicadas a usarem códigos nativos.

A Fig. 2 mostra um exemplo de um mecanimo JNI. Primeiro o método nativo em java é declarado, depois este método é implementado em código nativo. O código nativo é chamado a partir de uma biblioteca compartilhada, *IOPortsARM.so*, carregada pelo aplicativo Android através do *System.loadLibrary()*.

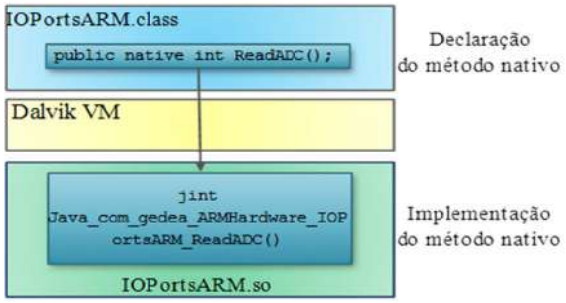

Figura 2. Exemplo de uma função nativa chamada pelo JNI.

III. Sistema de Controle de Nível de Líquido

O experimento realizado neste trabalho foi um sistema de controle de nível de água. Como planta a ser controlada, foi utilizado o sistema experimental de tanques acoplados de fabricação Quanser®, e para o controle foi utilizado o kit de desenvolvimento para ARM, o Tiny6410® [23], fabricado pela *Friendly* ARM. Foi desenvolvida uma aplicação Android para realização do algoritmo de controle e gravação da resposta do sistema a diferentes *setpoints*.

A. Modelo do controlador PI

O controle de malha fechada utilizado neste trabalho é mostrado na Fig. 3, onde V_{p1}é o valor de voltagem da bomba gerado pelo controlador PI, e o V_{p_ff} é o valor de ação *feedforward* para compensar a não linearidade do sistema. Os valores de K_{i_1}, K_{p_1} e K_{ff_1} são calculados de acordo com o modelo proposto em [24].

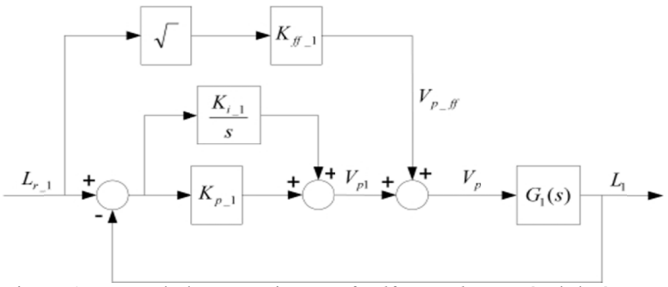

Figura 3. Controlador PI mais ação *feedforward* para nível de água.

A função de transferência para o sistema experimental de tanques acoplados da Quanser® é definido como:

$$G_1(s) = \frac{K_{dc_1}}{\tau_1 s + 1} \tag{1}$$

com:

$$K_{dc_1} = \frac{K_p \sqrt{gL_{10}}\sqrt{2}}{A_{ol} g} \quad e \quad \tau_1 = \frac{\sqrt{gL_{10}} A_{\tau 1}\sqrt{2}}{A_{ol} g} \tag{2}$$

Nas equações em (2) temos:
K_{dc_1}: *ganho DC(cm/V)*
τ_1: *constante de tempo em malha aberta (s).*
K_p: *constante de vazão por volt da bomba.*
g: *gravidade.*
L_{10}: *nível de operação no tanque 1.*
A_{ol}: *área do orifício inferior do tanque 1*
$A_{\tau 1}$: *área do tanque 1.*

Para a ação de *feedforward* no sistema de controle PI é definido K_{ff_1} como:

$$K_{ff_1} = \frac{A_{ol}\sqrt{2}\sqrt{g}}{K_p} \tag{3}$$

Para o cálculo dos ganhos proporcional e integral do controlador PI são determinadas as seguintes expressões:

$$K_{p_1} = \frac{2\zeta_1 \omega_{n1} \tau_1 - 1}{K_{dc_1}} \tag{4}$$

$$K_{i_1} = \frac{{\omega_{n1}}^2 \tau_1}{K_{dc_1}} \tag{5}$$

onde:

$$\zeta_1 = \frac{\left|\ln\left(\frac{1}{100}PO_1\right)\right|}{\sqrt{\ln\left(\frac{1}{100}PO_1\right)^2 + \pi^2}} \quad e \quad \omega_{n1} = \frac{4}{\zeta_1 t_{s_1}} \tag{6}$$

Em (6) temos:
PO_1: *máximo sobressinal* $\leq 11\%$.
t_{s_1}: *tempo de subida* $\leq 5s$.

O erro para o controlador PI é encontrado por:

$$(e) = L_{r_1} - L_1 \tag{7}$$

onde:
L_{r_1}: *nível de referência.*
L_1: *nível do tanque.*

B. Estratégias de implementação

Neste trabalho o modelo do controlador PI é disposto em duas estratégias de implementação na plataforma Android™ embarcada em ARM. A primeira estratégia é a implementação em java na aplicação Android, como mostrada na Fig. 4. Nesta estratégia o controlador PI é executado na máquina virtual Dalvik do sistema Android. As leituras do sensor de nível da planta e o envio de sinais de controle da bomba são realizados através das chamadas via JNI a biblioteca nativa da aplicação, que por sua vez acessam os drivers das portas *Analog-to-Digital Converter* (ADC) e *Pulse Width Modulation* (PWM).

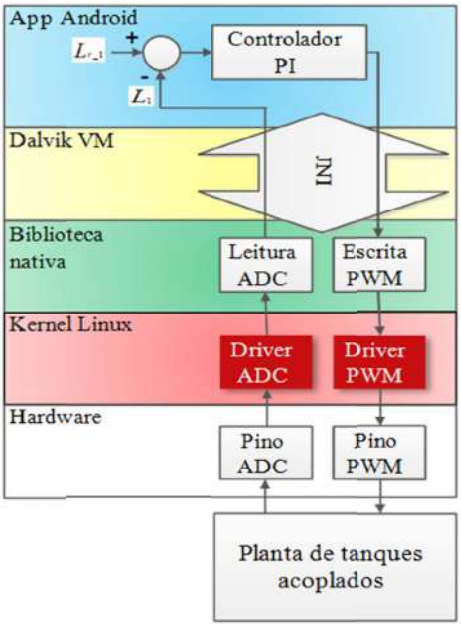

Figura 4. Estratégia de implementação em Java.

A segunda estratégia é a implementação do controlador PI em código nativo. Nesta estratégia a aplicação Android executa o controlador PI diretamente em código nativo, como pode ser visto na Fig. 5. As leituras do sensor e envio dos sinais de controle também são realizadas em código nativo. Nesta estratégia não ocorre chamadas via JNI durante a execução do controle.

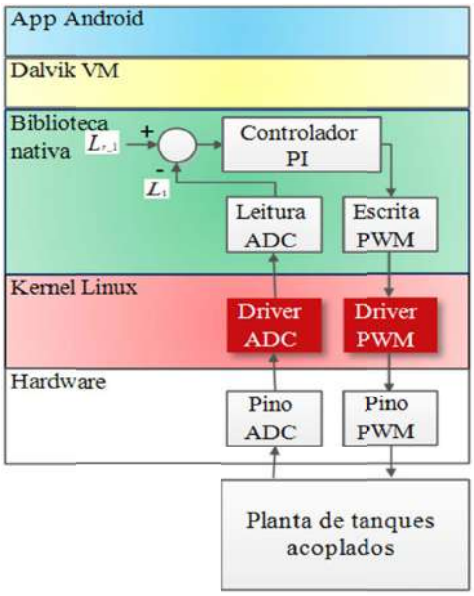

Figura 5. Estratégia de implementação em código nativo.

Uma vantagem de usar a primeira estratégia em relação a segunda é que o aplicação Android fica menos complexa, não perdendo a mobilidade do código nem sua segurança. Por sua vez ao se trabalhar em código nativo, que é o caso da segunda

estratégia, se ganha desempenho na realização dos cálculos do controlador PI.

IV. Montagem do Experimento

Os materiais utilizados na realização do experimento foram: planta didática, a placa Tiny6410®, resistores e transistor para montagem de um divisor de tensão e driver PWM, módulo de potencia VoltPaq-X1®, cabos para comunicação e fonte de tensão. A seguir são detalhados os componentes que foram utilizados no experimento.

- Planta didática Quanser de tanques acoplados – Nesse sistema, dois tanques e uma bomba podem ser dispostos em três configurações de forma a simular diferentes sistemas de controle de nível. Para esta aplicação foi utilizada a configuração 1, mostrada na Fig. 6, na qual a bomba alimenta o tanque 1, localizado na parte superior da planta, com o objetivo de controlar o nível daquele tanque. O tamanho do orifício de vazão do tanque utilizado foi 0,3175cm. Na base do tanque possui um sensor de pressão para emitir o sinal do nível em tensão 0-5V. A bomba da planta suporta uma tensão de até 23V por curtos períodos de tempo e de 12V de forma ininterrupta [25].

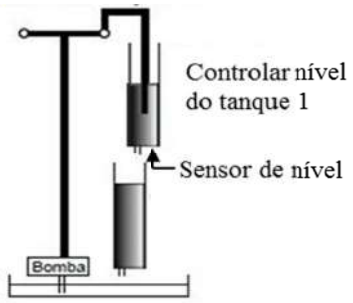

Figura 6. Estrutura da planta de tanques acoplados.

- Módulo de potência VoltPaq-X1® - Este módulo recebe o sinal do sensor de pressão presente no fundo do tanque 1 e emiti um ganho de tensão 3 vezes para a bomba da planta [26]. O módulo é mostrado na Fig. 7.

Figura 7. Módulo de potencia VoltPaq-X1®.

- Divisor de tensão - A porta analógica do microcontrolador ARM da placa Tiny6410® trabalha com sinais de tensão que variam entre 0-3.3V, sendo que o sinal do sensor do tanque 1 da planta didática possui valores entre 0-5V. De forma a compatibilizar esses sinais dos sensores com a entrada analógica do microcontrolador foi estabelecido o circuito divisor de tensão da Fig. 8.

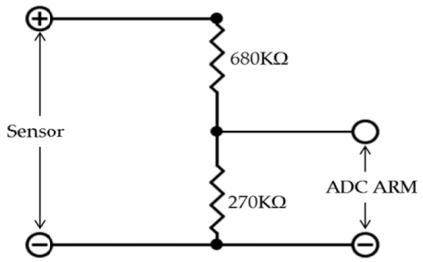

Figura 8. Divisor de tensão para porta analógica do ARM.

- Driver PWM - Para o sinal de controle da bomba foi utilizado uma porta PWM do microcontrolador ARM. A Fig. 9 mostra o driver utilizado para modularização do sinal de tensão de 0-7V ao módulo de potência. No módulo de potência esse sinal possui um ganho de 3 vezes para alimentar a bomba da planta.

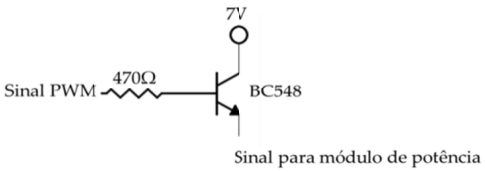

Figura 9. Driver PWM.

Este experimento foi realizado no laboratório do Grupo de Estudo e Desenvolvimento em Energia e Automação (GEDEA) localizado no prédio do Centro Integrado de Inovação Tecnológica do Semi-Árido (CITED) da Universidade Federal Rural do Sermi-Árido (UFERSA). A estrutura de montagem do experimento é mostrada na Fig. 10.

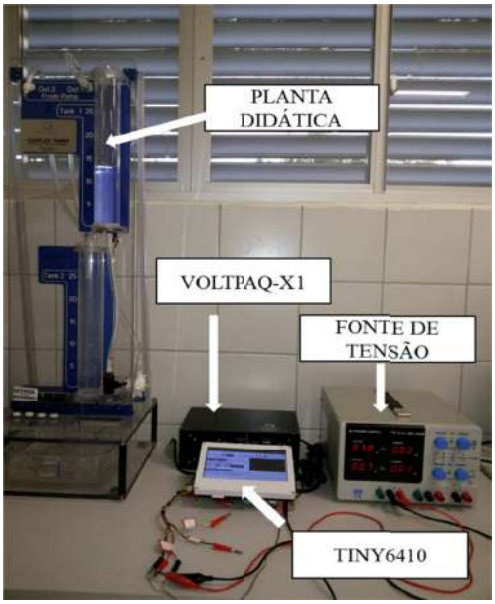

Figura 10. Montagem do experimento de controle de nível de tanque.

As ligações entre o módulo de potência e a placa Tiny6410 foram feitas através de cabos. A fonte de tensão fez a alimentação do driver PWM para envio de sinal para bomba. A planta didática, como já mencionado anteriormente foi configurada de modo a realizar o controle do tanque 1.

Antes da realização do experimento foram realizadas calibrações do sensor do tanque 1. Essa calibração foi realizada ajustando os potenciômetros de *offset* e ganho do sensor. Estes potenciômetros ficam localizados na base da planta. O primeiro ajuste foi do *offset* com o tanque vazio para zerar a leitura feita pela aplicação Android™ na placa Tiny6410®. Depois foi ajustado o ganho com o tanque no nível de 15cm.

V. Resultados

Para analisar o tempo de execução do controlador PI em cada estratégia sugerida, foi utilizado a função *clock_gettime()* em C/C++. Essa função foi chamada a cada loop realizado pelo controlador. Para uma melhor análise foi determinado uma média de 150 leituras do sensor de nível para cada loop.

Na Figura 11 é mostrada a resposta do controlador PI implementado em Java na aplicação android. O eixo x mostra o tempo em segundos e o eixo y mostra o nível do tanque em centímetros. Para a análise dos primeiros 20 segundos de execução do controlador PI na Fig. 11, o sistema não alcançou um desempenho satisfatório, o tempo de atraso para o *setpoint* de 15cm foi de 7,35 segundos e o tempo de subida foi de 12,69 segundos. Nesta análise o sistema conseguiu um máximo sobressinal de 2,3%. O tempo de acomodação para um critério de 5% foi de 12,18 segundos.

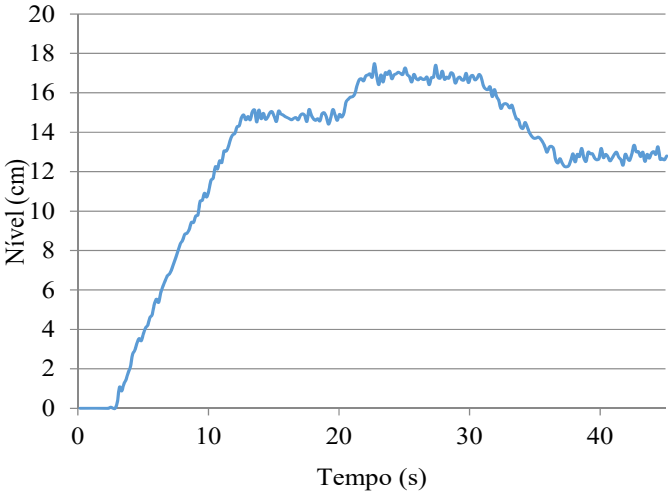

Figura 11. Resposta do controlador implementado em Java.

A segunda análise foi realizada com controlador implementado em código nativo. A resposta do sistema é mostrada na Fig. 12. Nesta análise, o tempo de atraso do sistema foi de 6,78 segundos, o tempo de subida foi de 12,3 segundos, o máximo sobressinal foi de 0,6% e o tempo de acomodação foi de 11,66 segundos a critério de 2%.

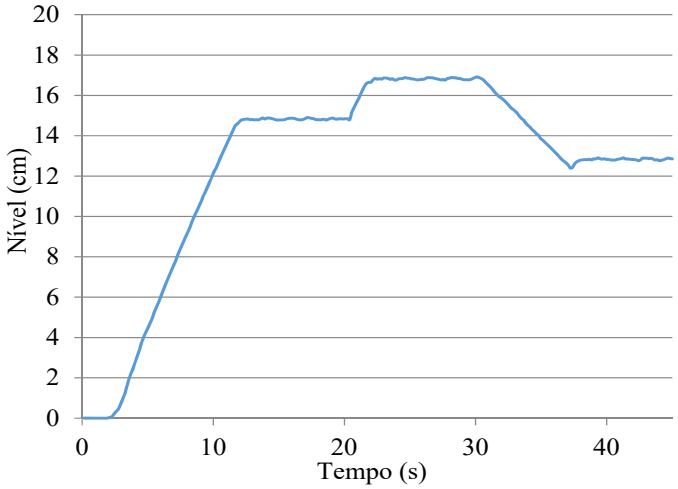

Figura 12. Resposta do sistema implementado em código nativo.

Fazendo uma análise comparativa das duas implementações pode-se notar que o controlador PI obteve um melhor desempenho ao ser executado em código nativo.

Outra análise realizada neste trabalho foi o tempo de execução de cada loop de controle no decorrer das simulações. As Fig. 13 e 14 mostram o tempo gasto entre cada *loop* de controle durante a execução na maquina virtual Dalvik e execução em código nativo, respectivamente. O eixo x mostra o número de *loops* realizados pelo controlador PI e o eixo y mostra o tempo gasto por cada *loop*.

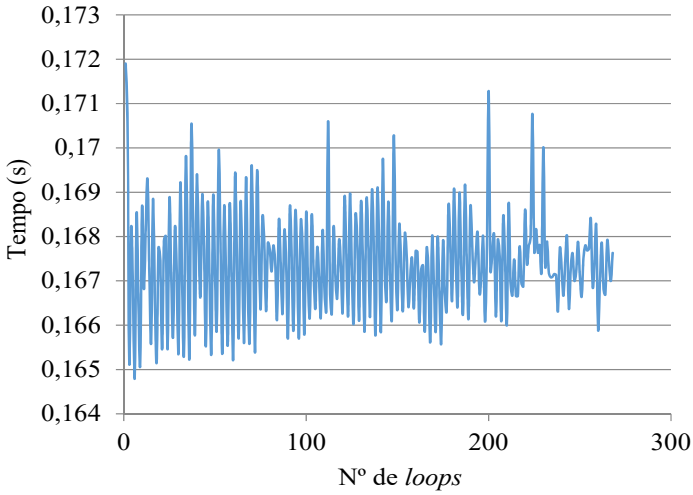

Figura 13. Tempo gasto pelos *loops* do controlador em Java.

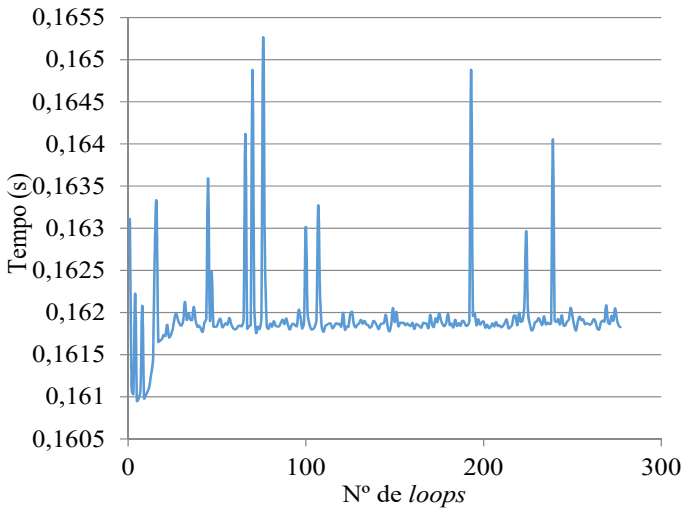

Figura 14. Tempos gasto pelos *loops* do controlador em código nativo.

Na análise das leituras podemos notar que o controlador PI executado na máquina virtual Dalvik gasta mais tempo para realizar as leituras e processar o controle do sistema. O que também é possível notar é que as leituras são mais irregulares do que as leituras quando realizadas a partir do código nativo.

VI. Conclusão e Trabalhos Futuros

Este trabalho mostrou os conceitos da plataforma Android e o mecanismo JNI para acesso ao código nativo em uma aplicação Android. Ao analisar a execução de um controlador PI em uma plataforma Android embarcada em um microcontrolador ARM, concluiu-se que quando este controlador é executado em código nativo, possui um melhor desempenho e melhor estabilidade em relação a sua execução na máquina virtual Dalvik. O mecanismo JNI foi necessário para realização da execução do controlador PI na Dalvik VM, mas influenciou negativamente no desempenho do controlador. Com o controlador executando em código nativo, não houve a necessidade da utilização do mecanismo JNI e nem da Dalvik VM, elevando assim seu desempenho.

Como trabalhos futuros é possível explorar modelos de controladores neurais para a planta de tanques de nível utilizada neste trabalho, e assim implementar esses controladores na plataforma Android embarcado em ARM. Seguindo a ideia apresentada em [27], as entradas e saídas obtidas pelo controlador PI deste trabalho podem ser utilizadas para o treinamento de um controlador neural. Dessa forma, comparações entre o controlador PI e os controladores neurais podem ser feitas para verificar o comportamento na plataforma embarcada. Assim como foi realizado neste trabalho, os controladores neurais podem também ser implementados em Java e código nativo, verificando os diferentes comportamentos.

VII. Agradecimentos

Os autores agradecem o apoio estrutural da UFERSA e apoio financeiro da CAPES.

Referências

[1] Meier, Reto. *Professional Android 4 application development*. John Wiley & Sons, 2012.

[2] Yaghmour, Karim. *Embedded Android: Porting, Extending, and Customizing*. O'Reilly, 2013.

[3] Lee, Sangchul, and Jae Wook Jeon. Evaluating performance of Android platform using native C for embedded systems. *Control Automation and Systems (ICCAS), 2010 International Conference on*. IEEE, 2010.

[4] Lin, Cheng-Min, et al. Benchmark dalvik and native code for android system. *Innovations in Bio-inspired Computing and Applications (IBICA), 2011 Second International Conference on*. IEEE, 2011.

[5] Kim, Yeong-Jun, et al. Benchmarking Java application using JNI and native C application on Android. *Control, Automation and Systems (ICCAS), 2012 12th International Conference on*. IEEE, 2012.

[6] Son, Ki-Cheol, and Jong-Yeol Lee. The method of android application speed up by using NDK. *Awareness Science and Technology (iCAST), 2011 3rd International Conference on*. IEEE, 2011.

[7] Ruimei, Zhao, and Wang Mei. Design of ARM-based embedded Ethernet interface. *Computer Engineering and Technology (ICCET), 2010 2nd International conference on*. Vol. 4. IEEE, 2010.

[8] Melo, Reuber R., et al. New Approach in Building Supervision Systems, Automation and Control Based on ARM. *Intelligent Manufacturing Systems*. Vol. 11. No. 1. 2013

[9] Li, Gan-ping. Design of an embedded control and acquisition system for industrial Local Area Networks based on ARM. *Computer Science and Education (ICCSE), 2010 5th International Conference on*. IEEE, 2010.

[10] SUDHEER, L. SHRIMANTH, JP BHASKAR IMMANUEL, and CS PARVATHI. Arm7 microcontroller based fuzzy logic controller for liquid level control system. *International Journal of Electronics* (2013).

[11] Krivic, Senka, et al. Design and implementation of fuzzy controller on embedded computer for water level control. *MIPRO, 2012 Proceedings of the 35th International Convention*. IEEE, 2012.

[12] Franc, Hanžič, and R. Šafarič. ARM-Cortex Microcontroller fuzzy position control on an automatic door test-bed. *Robotics in Alpe-Adria-Danube Region (RAAD), 2010 IEEE 19th International Workshop on*. IEEE, 2010.

[13] Anish, M. K. Internal Model Control of pressure process using ARM microcontroller. *Computing, Electronics and Electrical Technologies (ICCEET), 2012 International Conference on*. IEEE, 2012.

[14] Yang, He, Li Kejian, and Cai Qizhong. Design of ARM-based human-machine interface of plastic injection blow molding machine. *Computer Application and System Modeling (ICCASM), 2010 International Conference on*. Vol. 1. IEEE, 2010.

[15] Sloss, Andrew, Dominic Symes, and Chris Wright. *ARM System Developer's Guide: Designing and Optimizing System Software*. Morgan Kaufmann, 2004.

[16] Maia, Cláudio, Luís Nogueira, and Luis Miguel Pinho. Evaluating android os for embedded real-time systems. *Proceedings of the 6th International Workshop on Operating Systems Platforms for Embedded Real-Time Applications, Brussels, Belgium*. 2010.

[17] Perneel, Luc, Hasan Fayyad-Kazan, and Martin Timmerman. Can Android be used for real-time purposes?. *Computer Systems and Industrial Informatics (ICCSII), 2012 International Conference on*. IEEE, 2012.

[18] Mongia, Bhupinder S., and Vijay K. Madisetti. Reliable real-time applications on android os. *IEEE Electrical and Computer Engineering Electrical and Computer Engineering* (2010).

[19] Nagata, Kyosuke, and Saneyasu Yamaguchi. An Android application launch analyzing system. *Computing Technology and Information Management (ICCM), 2012 8th International Conference on*. Vol. 1. IEEE, 2012.

[20] Rogers, Rick, et al. *Android application development: Programming with the Google SDK*. O'Reilly Media, Inc., 2009.
[21] Liang, Sheng. *The Java™ Native Interface: Programmer's Guide and Specification*. Addison-Wesley Professional, pp. 3-19, 1999.
[22] Schildt, Herbert, and Danny Coward. *Java: The Complete Reference*. McGraw-Hill, pp. 302-306, 2011.
[23] FRIENDLYARM. *User's Guide to Tiny6410 System Installation*. 2012. Disponível em: <http://www.friendlyarm.net/products/tiny6410>. Acesso em: fev. 2012.
[24] QUANSER. *Coupled Tanks - Instructor Manual.* 2013. Disponível em: <www.quanser.com>. Acesso em: abr. 2013.
[25] QUANSER. *Coupled Tanks-User Manual*. 2013. Disponível em: <www.quanser.com>. Acesso em: abr. 2013.
[26] QUANSER. *VoltPAQX1-User Manual.* 2013. Disponível em: <http://www.quanser.com>. Acesso em: abr. 2013.
[27] OLIVEIRA., J. C. P. (2009). Avaliação de Controle Neural a um Processo de Quatro Tanques Acoplados. Tese de Doutorado em Engenharia Elétrica, Publicação PPGENE. TD-044/09, Departamento de Engenharia Elétrica, Universidade de Brasília, Brasília, DF, 115p.

Reuber Regis de Melo possui graduação em Ciência da Computação pela Universidade Federal Rural do Semi-Árido - UFERSA (2011), mestrado em Controle e Automação no Programa de Pós-Graduação em Sistemas de Comunicação e Automação-PPGSCA na UFERSA (2013), Mossoró-RN, Brasil.

Egmídio Caratti Filho possui graduação em engenharia mecânica na Universidade Federal do Ceará – UFC 1995, mestrado em Controle e Automação no Programa de Pós-Graduação em Sistemas de Comunicação e Automação-PPGSCA na UFERSA (2014), Mossoró, Brasil.

Danielle Simone S. Casillo possui graduação em Engenharia de Computação pela Universidade Potiguar (2001), mestrado (2004) e doutorado (2009) na área de Automação e Controle em Engenharia Elétrica e de Computação pela Universidade Federal do Rio Grande do Norte. Atualmente é professora Adjunto II do curso de Ciências da Computação do Departamento de Ciências Exatas e Naturais da Universidade Federal Rural do Semiárido. Tem experiência na área de Engenharia Elétrica, com ênfase em Controle e Automação de Processos.

Elmer Rolando Llanos Villarreal possui graduação em Matemática (Bacharel)- Universidad Nacional de Ingenieria Lima(Diploma Revalidado pela UFSC) (1993), mestrado em Engenharia Elétrica pela Universidade de São Paulo (1997) e doutorado em Engenharia Elétrica pela Universidade Federal de Santa Catarina (2002). Atualmente é professor adjunto III da Universidade Federal Rural do Semi-Árido. Possui artigos publicados em periódicos e em eventos científicos. Tem experiência na área de Engenharia Elétrica e Matemática Aplicada, com ênfase em Sistemas de Controle e Matemática Aplicada, atuando principalmente na área de Controle Multivariável, Controle Adaptativo, Otimização, Análise Numérica, Educação Matemática e Análise Matemática.

COMPUTATIONAL & APPLIED MATHEMATICS

Volume 31, N. 1, pp. 143–168, 2012
Copyright © 2012 SBMAC
ISSN 0101-8205 / ISSN 1807-0302 (Online)
www.scielo.br/cam

A new approach for data transmission system on topological surfaces

JOÃO D. LIMA[1]*, FRANCISCO M. SILVA[1] and ELMER R.L. VILLAREAL[2]

[1]Mestrado em Ciência da Computação, Universidade do Estado do Rio Grande do Norte
59633-010 Mossoró, RN, Brazil

[2]Departamento de Ciências Exatas, Universidade Federal do Semi-Árido
59610-090, Mossoró, RN, Brazil

E-mails: jddeus@uol.com.br / miguel.silva@ufersa.edu.br / evillareal@hotmail.com

Abstract. This work introduces a new data transmission system in which the main blocks, coding, modulation and channel are designed on a Riemannian manifolds. An intrinsic algebraic structure to the manifolds (surface), the homology group will be used to compose an error corrector code, a partition on the surface extracted from the embedding of a graph, which will compose the modulation design, and the channel design is the result of an association rule applied to the embedded graph.

Mathematical subject classification: Primary: 06B10; Secondary: 06D05.

Key words: modulation, coding, graph embedding, homology group.

1 Introduction

Modulation on Riemannian manifold introduced in the 1960s [13], called twister modulation, has been the subject of recent works [1, 9, 14], due to the good performance presented and of course because of these surfaces which will be the new spaces to be addressed. On a smaller scale, the first proposals for coding on Riemannian manifolds are emerging [2, 8]. The great source of mathematical results achieved in Riemannian geometry has aroused the interest of researchers in the search of new projects of modulations and codification.

#CAM-345/11. Received: 13/III/11. Accepted: 23/VIII/11.
*Corresponding author is supported by MCC-UERN-UFERSA.

In this work, the main components of a data transmission system, the coding, modulation and the channel, will be offered on a Riemannian manifold from an embedding of a graph. As these components are connected by an embedding of a graph, the relation is called compatibility. The data transmission system in which the coding, modulation and channel are compatible among themselves and called of integrated system.

There are many algebraic structures existing in the Riemannian manifolds theory that can be used to compose error corrector codes, however, the homology group is the more natural and is related to the embedded graph [8]. To meet the compatibility relation, we are presenting this structure as a component of a compatible code which attends to the pattern of an integrated system.

The logical principles in which the relations of compatibilities among coding, modulation and channel have been established and their respective geometric constructions that gave rise to the definitions of these components are showed in Section 2. The integrated system definition and a brief comment on the performance are discussed in Section 3. The identification process of compatible modulations is described in Section 4. An example of compatible code, which give information on the integrated system performance is the topic of Section 5. The complete process of the integrated system components' identification will be discussed in Section 6. The conclusions are in Section 7.

2 Compatibility concepts

Aiming to introduce the compatibility concepts, it is assumed that a data transmission system uses an *alphabet m-ary*, indicated by set $\mathbb{Z}_m$, where m is a positive integer, to transmit data through a discrete memoryless channel, DMC, with m-ary input and n-ary output, denoted by $C_{m,n}$. The labeling of the graph vertices, symbols and codewords of this system are represented through a trellis Φ, which section is a sub graph of the complete graph $K_{m,n}$. A particular case of this representation is shown in Figure 1. Note that the sequence $\gamma = (0, 2, 2, 1, 0)$ corresponds to a codeword $u = (02\ 22\ 21\ 10)$, it is defined on a channel $C_{4,4}$. Thus, γ is associated to a connected path of the trellis. The connectivity of the path, results from the fact that a bit information is sent by channel in each interval, condition represented by the trellis. As consequence,

every source coding sequence or every codeword are represented by a connected path on the trellis.

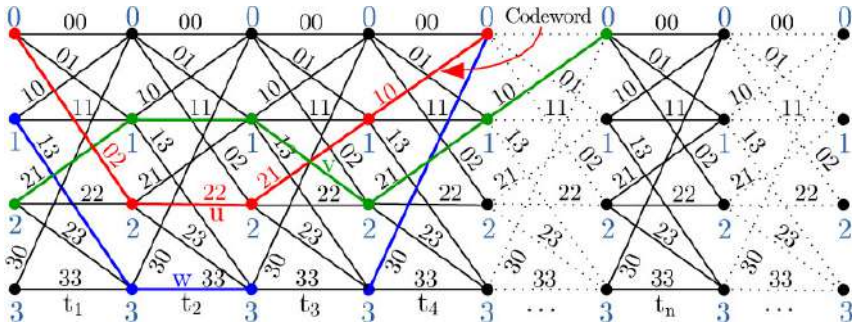

Figure 1 – Trellis corresponding a channel $C_{4,4}$.

Observe that $\gamma_1 = (2, 1, 1, 2, 1, 0)$ and $\gamma_2 = (1, 3, 3, 3, 0)$ sequences correspond, respectively, to codewords $v = (21\ 11\ 12\ 21\ 10)$ and $w = (13\ 33\ 30)$, but we can not consider those as codewords coming from trellis Φ. The transition 12 in v is not a trellis edge, and w is not defined on a connected path of the Φ.

2.1 Compatibility between coding and channel

In the trellis Φ are observed two properties: (I) every sequence on the channel $C_{4,4}$ it will be formed by elements of $\mathbb{Z}_4$; and (II), if the channel transition of the vertices i to vertices j is represented by ij, then $C_{4,4}$ does not have the transitions 03, 12, 20, 31. Thus, it makes sense to use these two conditions to introduce the concept of compatibility between coding system and channel. To do so, let $\mathbb{Z}_m$ be the input of the alphabet and output of the channel $C_{m,m}$.

Definition 2.1. *It is said that a* coding is compatible with the channel $C_{m,m}$ *if every codeword u contains only elements of $\mathbb{Z}_m$ and the whole subsequence ij of u is one transition of $C_{m,m}$. Otherwise, we said that coding and channel are* incompatible.

If a codeword u satisfies the Definition 2.1, it is easy to see that u is represented by a unique connected path on the $C_{m,m}$ trellis, important condition that establishes the uniqueness of the codewords. The compatibility between

source coding and channel depends on only the properties (I) and (II). It was observed that linear, blocs and convolutional codes, among others, are important code classes compatible with channels. As it is known that, codewords of linear codes are generated from operations on a generator matrix, then by Definition 2.1, every set of sequences of $\mathbb{Z}_m$ associated with connected paths of the trellis are considered a code compatible with a channel $C_{m,m}$. As there are sets that do not come from linear structures, the compatible code classes incorporate other classes of different codes from linear codes. It will be seen later that exists a natural structure of linear code related with this process.

2.2 Compatibility between modulation and channel

The natural representative of a discrete memoryless channel $C_{m,n}$ is a bipartite graph $K_{m,n}$ or a sub graph that one. In both cases, a modulation project is necessarily a metrical space partitioned in *n decision regions* (or *Voronoi regions*), where signal is present in the center each respective region. One way that such partitions can be obtained is through the dual embedding of 2-cells of bipartite graph $K_{m,n}$. While the embedding condition implies the uniqueness of the channel transitions, the 2-cell embedding implies the uniqueness of the partition. This condition was established by Dyck [4] and later proved by Youngs [12] through the following enunciate.

Theorem 2.2. *There is an one-to-one correspondence between rotation system of the graph G and its embeddings on orientable surfaces.*

Our purpose is to obtain a modulation project on the metric space that accurately represents the channel transitions and has well defined the Voronoi regions. This is possible if and only if the project is realizable on a surface coming from a graph embedding.

The idea to obtain a modulation project associated with a DMC coming from Lima-Palazzo's work [8]. Later Lima-Lima [7] has showed that is possible to obtain this project through an embedding of a complete graph. A recent analysis in the Lima-Lima's work by Lima-Matias [5], has showed that association process can be simplified and established through any connected graph. It is not a trivial process, it evolves concepts of orientable graph and its dual.

2.3 Association process

The process established by Lima-Lima-Matias consists in taking a connected graph $G_{p,q}$, embedding it on a surface Ω as 2-cells embedding, constructing the dual embedding, and to define two modulation projects called *quadrature amplitude modulations on surface* (QAMS). To be more specific, let's suppose that the embedding is of form

$$G_{p,q} \hookrightarrow \Omega \equiv \cup_{i=1}^{k} R_{\alpha_i}$$

where R_α represents a region of α edges defined by sequence $\gamma = (\gamma_1, \gamma_2, \cdots, \gamma_\alpha)$ called *orbital sequence*. In the orbital sequence γ, $\gamma_i \in \{0, 1, \cdots, p-1\}$, corresponds to the vertex v_{γ_i} of G, and γ defines the closed path on surface Ω corresponding the region frontier R_a. Furthermore, the dual embedding of G is given by $G'_{k,q} \hookrightarrow \Omega \equiv \cup_{j=1}^{p} R_{\alpha_j}$. As a modulation project for a constellation of m signals might divide the metric space (Ω, δ) in m Voronoi regions, in particular, we have two partitions on Ω: the embedding partition in k regions $\cup_{i=1}^{k} R_{\alpha_i}$, and the dual partition in p regions $\cup_{j=1}^{p} R_{\alpha_j}$. So, we have two projects of modulation, the modulation k-QAMS coming from embedding of $G_{p,q}$, and dual modulation p-QAMS. Of course there are modulations for k and p signals, respectively. Once that the signals of the constellation are associated to points of Ω, k signals of k-QAMS correspond to the k vertexes of dual G', and p signals of p-QAMS correspond to the p vertexes of G. Finally, we might associate the channels $C_{k,k}$ and $C_{p,p}$ to modulations k-QAMS and p-QAMS, process that will be described following.

2.4 Channel compatible with a modulation

In the Heawood's description process [11] of the graph embedding $G_{p,q} \hookrightarrow \Omega \equiv \cup_{i=1}^{k} R_{\alpha_i}$, the partition $\cup_{i=1}^{k} R_{\alpha_i}$ is obtained through the orientable graph (or digraph). In this process, an orientation on vertexes of G defines k regions of partition (Voronoi regions of k-QAMS). But on the digraph G, each edge $e = (v_i, v_j)$ contains its inverse $e^{-1} = (v_j, v_i)$, and so, each edge $e = (v_i, v_j)$ of G defines two transitions on the channel $C_{k,k}$, and each edge $e = (v_h, v_k)$ of dual G' defines two transitions on the channel $C_{p,p}$. Thus, we can define a channel $C_{k,k}$ compatible with a modulation k-QAMS, for this.

Let $G_{p,q} \hookrightarrow \Omega \equiv \cup_{i=1}^{k} R_{\alpha_i}$ be a 2-cells embedding of a graph G, and $G'_{k,q} \hookrightarrow \Omega \equiv \cup_{j=1}^{p} R_{\alpha_j}$, is a dual embedding. Suppose that $A = \{s_0, s_1, \ldots, s_{k-1}\}$ and $A' = \{s'_0, s'_1, \ldots, s'_{p-1}\}$ are the respectively alphabetic symbols used in the channels $C_{k,k}$ and $C_{p,p}$.

Definition 2.3. *It is said that the* modulation *k-QAMS* (*p-QAMS*) is compatible with the channel $C_{k,k}$ ($C_{p,p}$)*, if each edge* $e = (v_i, v_j)$ ($e' = (v_h, v_k)$) *of the graph* G (G') *defines two transitions* (s_i, s_j) *and* (s_j, s_i) ((s_h, s_k) *and* (s_k, s_h)) *of the channel* $C_{k,k}$ ($C_{p,p}$).

If a modulation m-QAMS and a channel $C_{k,k}$ satisfy the condition of Definition 2.3, it still will said that the channel $C_{k,k}$ is compatible with the modulation k-QAMS.

In this process it is has been considered a discrete memoryless channel. The 2-cell embedding can even be used in this kind of project, it is missed only the condition of uniqueness, because exist identical modulations coming from distinct embeddings. But it is impossible discard the embedding condition, therefore, there would not be uniformity of channel transitions. A modulation is the process to broadcast a signal, but here, we are going to consider the modulations as a space metric (Ω, d) with a region partition $\cup R_\alpha$ (where R_α is an α-gon) on Ω, denoted by $\Xi = (\Omega, d, \cup R_\alpha)$. By Theorem 2.2, the modulation Ξ compatible with channel $C_{m,n}$ is well defined by rotation system of complete graph, $\Theta(K_{m,n})$. If the objective is to describe a modulation relating to its all components, then we write

$$\Xi : K_{m,n}(\Theta) \hookrightarrow \Omega \equiv \cup R_\alpha.$$

A modulation m-QAMS is compatible with a channel $C_{m,m}$, when the rotation system Θ and the 2-cells embedding are fixed. From the algebraic point of view, it is always possible to identify the kind of regions, genus surface and the own partition, but, the topological embedding is highly complex. In this work, it will be seen some non trivial examples.

In Figure 2, trellis section consists in a graph $K_{4,4}(8, 9)$ associated to the channel $C_{4,4}$, which the rotation system is given by

$$\Theta(K_{4,4}) = \big\{0(135), 1(062), 2(137), 3(042), 4(357), 5(04), 6(17), 7(264)\big\}.$$

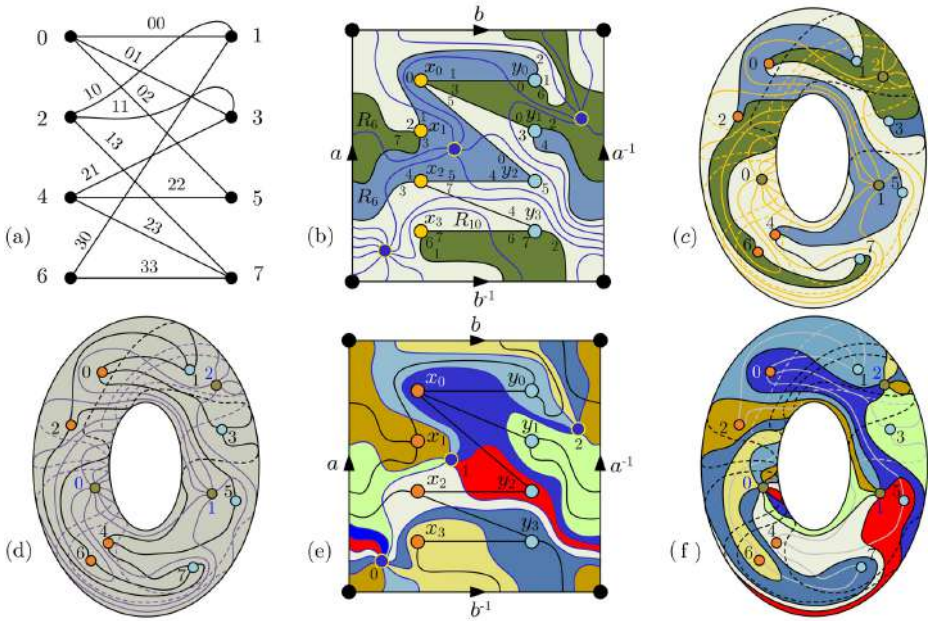

Figure 2 – Steps of a topological modulation projects.

This partition embedding is composed by a single region 22-gon defined by orbital sequence $\gamma = (1, 0, 3, 4, 5, 0, 1, 6, 7, 4, 3, 2, 7, 6, 1, 2, 3, 0, 5, 4, 7, 2)$. It is a maximal embedding on bi-torus of the kind $K_{4,4}(8, 9) \hookrightarrow 2T \equiv R_{22}$. As is not used modulation for one signal, only dual modulation is defined. As $K_{4,4}$ has 8 vertexes, the dual modulation is the form 8-QAMS, each decision region is composed by 1-gon. To better understand this process, we will see the next example. Choosing other rotation system for graph $K_{4,4}(8, 9)$, for example,

$$\Theta'(K_{4,4}) = \{0(135), 1(026), 2(137), 3(024), 4(357), 5(04), 6(17), 7(264)\}$$

(see Figure 2(a)), we obtain a different embedding $K_{4,4}(8, 9) \hookrightarrow T \equiv 2R_6 + R_{10}$ defined by sequences $\gamma_1(0, 3, 2, 7, 6, 1)$, $\gamma_2(0, 5, 4, 3, 2, 1)$ and $\gamma_3(3, 5, 4, 7, 2, 1, 6, 7, 4)$ (see Figure 2(b-c)). The dual embedding is given by $K'(3, 9) \hookrightarrow T \equiv 2R_2 + 6R_3$, and defined by dual $\gamma_{x_0}(1, 0, 2)$, $\gamma_{y_0}(1, 2, 0)$, $\gamma_{x_1}(1, 0, 2)$, $\gamma_{y_1}(1, 2, 0)$, $\gamma_{x_2}(1, 0, 0)$, $\gamma_{y_2}(1, 0)$, $\gamma_{x_3}(0, 2)$ e $\gamma_{y_3}(0, 2, 0)$ (see Figure 2(c-e)).

In Figure 2, embeddings (b) and (c) correspond to the planar and spacial topological projects of modulation 3-QAMS on the torus for a constellation

of three signals which decision regions are defined by orbital sequences γ_1, γ_2, γ_3. Its compatible channel $C_{3,3}$ is shown in Figure 3(a). Embeddings (d) and (e) of the Figure 2 correspond to the planar and spacial topological projects of dual modulation 8-QAMS on the torus for a constellation of eight signals which decision regions are defined by orbital sequences $\gamma_{x_0}, \gamma_{y_0}, \ldots, \gamma_{x_3}, \gamma_{y_3}$. Its compatible channel $C_{8,8}$ is shown in Figure 3(a). The embeddings of $K_{4,4}(8, 9)$ and their dual, shown in Figure 2, represent the complete steps of a topological modulation projects 3-QAMS and 8-QAMS compatible with the channels $C_{3,3}$ and $C_{8,8}$ which associated graph was fixed by rotation in (a). The plane model in (b) illustrates the partition on the torus caused by embedding of $K_{4,4}$ and its dual. The dual graph partition embedding together is shown in (e). The constructions (b) and (d) are very important because they are necessary to construct the modulation on torus, through its parametric equation, and to lead the problem to the Riemann Geometry environment. Finally, (c) and (e) show the spacial models corresponding to the embeddings (b) and (d). The goal of these constructions is to verify that topological modulation is compatible with channel which can be constructed on a topological riamannian manifolds.

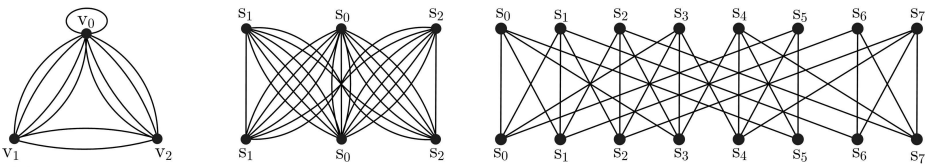

(a) Dual graph K' (b) Compatible channel $C_{3,3}$ (c) Channel $C_{8,8}$ compatible with 8-QAMS

Figure 3 – Dual graph and compatible channels.

It is observed that, the channel $C_{k,k}$ compatible with modulation k-QAMS is defined on the dual partition from an embedding of graph

$$G_{p,q} \hookrightarrow \Omega \equiv \cup_{i=1}^{k} R_{\alpha_i}.$$

But $K_{m,n}$ and its dual, are both embeddings in Ω and is a dual in another. On the other hand, if the dual defines the modulation p-QAMS compatible with the channel $C_{p,p}$, this is, defined on the graph $G_{p,q}$. Thus, embedding of $K_{m,n}$ defines a compatible modulation, called *directed compatible modulation with* $C_{n,n}$. Sometimes we will call *dual compatible modulation* to refer the compatible modulation coming from the dual embedding. Despite of the compatible

modulation on the embedding partition is not always uniform, the dual always will be, if the vertices degree of the associated channel is considered satisfying a determined condition.

Proposition 2.4. *Let $G(p,q) \hookrightarrow \Omega \equiv \cup_{i=1}^{k} R_{\alpha_i}^{i}$ be a 2-cells embedding of graph G. If $C_{k,k}$ and $C_{p,p}$ are DMC channels compatible with modulations k-QAMS and p-QAMS, then are true the followings affirmations:*

(i) *For all k, $\gamma(G_{p,q}) \leq m \leq \gamma_M(G_{p,q})$, there are directed and dual compatible modulation in $m\Omega$.*

(ii) *The directed and dual compatible modulations are modulations on Ω for a constellation of k and p signals, respectively.*

(iii) *The dual compatible modulation is uniform if, and only if, all vertices of $G_{p,q}$ have the same degree.*

Proof. The affirmation (i) follows by Theorem 2.2, (ii) is an embedding partition consequence and dual definition, and (iii) is due the number of edges of one dual region, the vertex degree in its inner, as the uniform modulation, all regions have the same number of the edges. □

By Proposition 2.4, it follows that dual modulations coming from complete graph K_n and bipartite complete graph of the form $K_{n,n}$, are uniform modulations.

3 Data transmission integrated system

In the Definitions 2.1 and 2.3, we have the necessary conditions that we have been looking for to define data transmission system to our interest.

Definition 3.1. *We said that a data transmission system is an* integrated system *(IS), if the coding and the modulation projects are compatible with the channel.*

It is still said that in the IS, the coding, modulation and channel are compatible among themselves. In the IS block model shown in Figure 4, the combination m-ary input in the modulator, the physical channel, and the n-ary output in

the demodulator are modeled as a discrete memoryless channel (DMC), denoted by C_n. The modulation design come from the partition of 2-cells embedding of the complete graph K_n in the surface Ω_3.

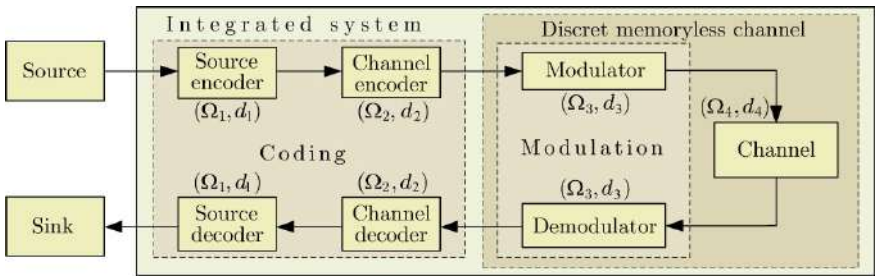

Figure 4 – Integrated system block model.

It's known [8] that the modulation efficiency depends on the genus and uniformity degree α (number of regions of the same kind), additionally, it is shown in [7] that they still depend on the number of edges of the regions. The identification of these parameters is very important in order to know the IS performance. In Figure 5 $P_e(\alpha)$ indicates the error probability in IS when is used an uniform modulation of degree α. In IS, the metric spaces can be considered the same or not [1]. About the compatibility conditions in Definitions 2.1 and 2.3, there are relations one-to-one among coding, modulation and channel, since these are directly related to the channel. This gave us the assurance that IS, in terms of implementation, is the one which has the lowest complexity, since there is no need to introduce additional devices of incompatibility control. Furthermore, someone should consider that the project is done on a Riemannian manifold, space that offers some options for projects with interest properties [1].

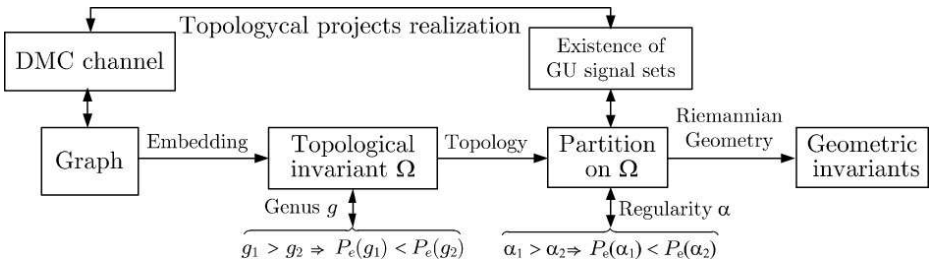

Figure 5 – Proposal overview (Adapted by [1]).

4 Identification process of compatible modulations

We notice the existence not only of a unique compatible modulation with a channel, but a whole compatible modulations set. Although this set was for a finite number of elements, which it grows quickly with increasing signs and channel transitions, it follows the more important topological invariants and results used in the identification process of the IS components.

If $V(G)$ is set of the vertices of G and $\deg(v)$ is the degree of the vertex $v \in V$, then it is easy to verify that graph G has

$$\prod_{v \in V(G)} (\deg(v) - 1)! \text{ rotations.} \tag{1}$$

If v, e and f are, respectively, the vertex, edges and regions number, then the Eüler's characteristic of the surface Ω is given by

$$\chi(\Omega) = v - e + f. \tag{2}$$

The genus g and $\widetilde{g}$ of the orientable Ω and non-orientable $\widetilde{\Omega}$ surfaces, in relation to the $\chi(\Omega)$, are given by

$$\chi(\Omega) = 2 - 2g \quad \text{and} \quad \chi\left(\widetilde{\Omega}\right) = 2 - \widetilde{g}. \tag{3}$$

Let $\{x\}$ be the smallest integer greater than or equal to the number x. The minimal genus of the orientable surface [11] is given by

$$g(m, n) = \{(m-2)(n-2)/4\}, \text{ for } m \text{ and } n \geq 2. \tag{4}$$

Let $[x]$ be the greatest integer less than or equal to number x. The maximal genus of the orientable surface [10] is given by

$$\gamma_M(K_{m,n}) = \left[\frac{1}{2}(m-1)(n-1)\right], \text{ for } m \text{ and } n \geq 2. \tag{5}$$

The following theorem [3] gave the orientable surfaces set where is present in the compatible modulation with a channel $C_{m,n}$.

Theorem 4.1. *If G has 2-cell embeddings on surfaces of genus m and n, then for every integer k, $m \leq k \leq n$, G has a 2-cell embedding on the surface of genus k.*

For example, if we take the bipartite complete graph $K_{4,4}$, what would be modulations coming from embedding of $K_{4,4}$ and their compatible channels? The first step of the identification process is to choose one of the four surfaces families: Non-orientable and orientable with and without component boards. It will be identified modulations for the two cases of surfaces without boards.

4.1 Compatible modulations on orientable surfaces

In relation to the orientable without board case, the equality (1) shown that $K_{4,4}$ has 1 679 616 rotations. Then there are 1 679 616 options to choose a rotation, but, not all the partitions are distinct, then it is possible to find them. By equalities (4)-(5), it is deducted that minimal and maximal embeddings of $K_{4,4}$ it has been found in surfaces of genus $\gamma = 1$ and $\gamma_M = 4$. So, by Theorem 4.1, orientable surfaces set to the $K_{4,4}$ embeddings is given by $\mathbb{S}(K_{m,n}) = \{T, 2T, 3T, 4T\}$. On the other hand, $K_{4,4}$ has 16 edges, the regions of the $K_{4,4} \hookrightarrow \Omega$ have 32 edges and embedding regions of $K_{4,4}$ only contain an even number of the edges larger than or equal to four. These affirmations conclude that 2-cell embeddings of $K_{4,4}$ must necessarily be listed in the Table 2, where partition of mT is the same of $2mP$. The notation $R_{a_1,a_2,\cdots,a_k}$ used in Table 2 indicates the embedding partition of $K_{m,n}$ in k regions with $a_1, a_2, \cdots, a_k$ edges.

An attribute of great interest in a modulation is its uniformity or, equivalently, the condition: Voronoi's regions are all congruent. Condition equivalent to the geometrically uniform signal space, here, correspondents to the embeddings with regions of the same kind, as examples, the partitions $8R_4$ of T and $4R_8$ of $3T$.

The Theorem 4.1 gave us the guarantee for the existence of, at least, an embedding with element of $\mathbb{S}$. Soon, we do not have doubt that the minimal embedding $K_{4,4} \hookrightarrow T \equiv 8R_4$ exists, an example of uniform compatible modulation. We still check the existence of the regular embedding $K_{4,4} \hookrightarrow 3T \equiv 4R_8$, other important example of regularity. These examples illustrated in Figure 6 shows that $K_{m,n}$ embeddings are a rich source of uniform compatible modulation. It is observe that directed and dual modulations coming from minimal embedding $K_{4,4}$ are equals. This one is an uniform modulation for a constellation of 8 signals, with Voronoi's regions of the kind 4-gon. Its dual graph and compatible

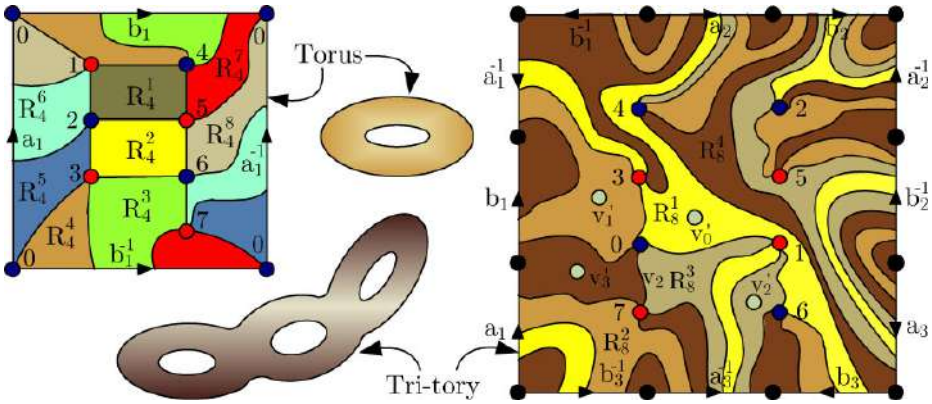

Figure 6 – Uniform modulations QAMS on the torus and 3-tory coming from $K_{4,4}$ embeddings.

channel is the same kind of channel in Figure 7(c). And 3-tory one, directed compatible modulation have 4 signals, with Voronoi's regions of the kind 8-gon. Dual graph (a) and compatible channel (b) is shown in Figure 7. Dual compatible modulations are uniform modulations for a constellation of 8 signals with decision regions of the kind 4-gon (see its channel in (c)). It is showing that geometrically uniform signal space is not privilege only of hyperbolic spaces.

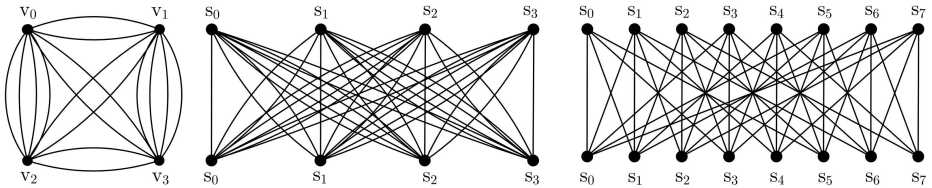

(a) Dual Graph K_4' (b) Channel $C_{4,4}$ compatible with 4-QAMS (c) Channel $C_{8,8}$ compatible with 8-QAMS

Figure 7 – Dual graph and compatible channels with the uniform modulations on $3T$ in the Figure 6.

An embedding of a graph G, and thus, its compatible modulations, are determined by a rotation system Θ of G, dual embedding, and sets of orbital sequences of embeddings of G and dual G'. This process can be realized only with algebraic resource, using a algorithm descriptor of embedding [6]. (See algebraic description process in Table 1).

Ω	Rotation	Orbital sequence γ_i	Ξ
T	$(1573)_0$,$(0426)_1$,$(1537)_2$,$(0264)_3$, $(1375)_4$,$(0624)_5$,$(1735)_6$,$(0462)_7$	$(1254)_1$,$(2365)_2$,$(3476)_3$,$(0143)_4$ $(0327)_5$,$(1672)_6$,$(0745)_7$,$(0561)_8$	$8R_4$
$3T$	$(1753)_0$,$(0642)_1$,$(1375)_2$,$(0642)_3$ $(1573)_4$,$(0642)_5$,$(1357)_6$,$(0642)_7$	1(30163412), 2(03654725) 3(10761452), 4(70567432)	$4R_8$

Table 1 – Uniform compatible modulations with $C_{4,4}$.

In Table 1, the notation $(1573)_0$ used in second column corresponds to the rotation of the vertex 0, $(1254)_1$ used in the 3^{rd} column indicated the orbital sequence γ_1 on the torus, and Ξ indicated the partition. It was verified even that the $R_{6,6,8,10}$ is the unique partition of the Table 2 non existent in one orientable embedding of $K_{4,4}$ [5]. It would be this partition in a non orientable embedding of $K_{4,4}$?

4.2 Irregular compatible modulation with $C_{4,4}$

In Table 2, most of the embeddings of $K_{4,4}$ are irregulars. Using the embedding method through homology curves incises [8], plane (b) and space (a) models of a compatible modulations with $K_{4,4}$ are illustrated in Figure 8. This is an embedding of the form $K_{4,4} \hookrightarrow 3T \equiv R_{4,6,6,16}$ (see plane model in (a)). It can be used as a non-uniform directed compatible modulation project for constellation of 4 signals, where decision regions R_4, R_6, R_6, R_{16} correspond orbital sequences $\gamma_1(4563)$, $\gamma_2(052743)$, $\gamma_3(012367)$, $\gamma_4(1032541650721476)$, respectively, and an uniform dual compatible modulation for constellation of 8 signals coming from dual partition $K_{4,4} \hookrightarrow 3T \equiv 8R_4$ (see embedding (e)), witch decision regions are defined by $\gamma_1(4243)$, $\gamma_2(4434)$, $\gamma_3(4432)$, $\gamma_4(1324)$, $\gamma_5(1244)$, $\gamma_6(1424)$, $\gamma_7(1443)$, $\gamma_8(2434)$.

It is concluded, therefore, that each embedding of $K_{4,4}$ defines two compatible modulations: that directly coming from the embedding partition and the dual partition. Despite of the compatible modulation on the embedding partition of the graph G is not always uniform, the dual always will be, if the vertices degree of G are equals. For example, when G is the complete graph or bipartite complete graph.

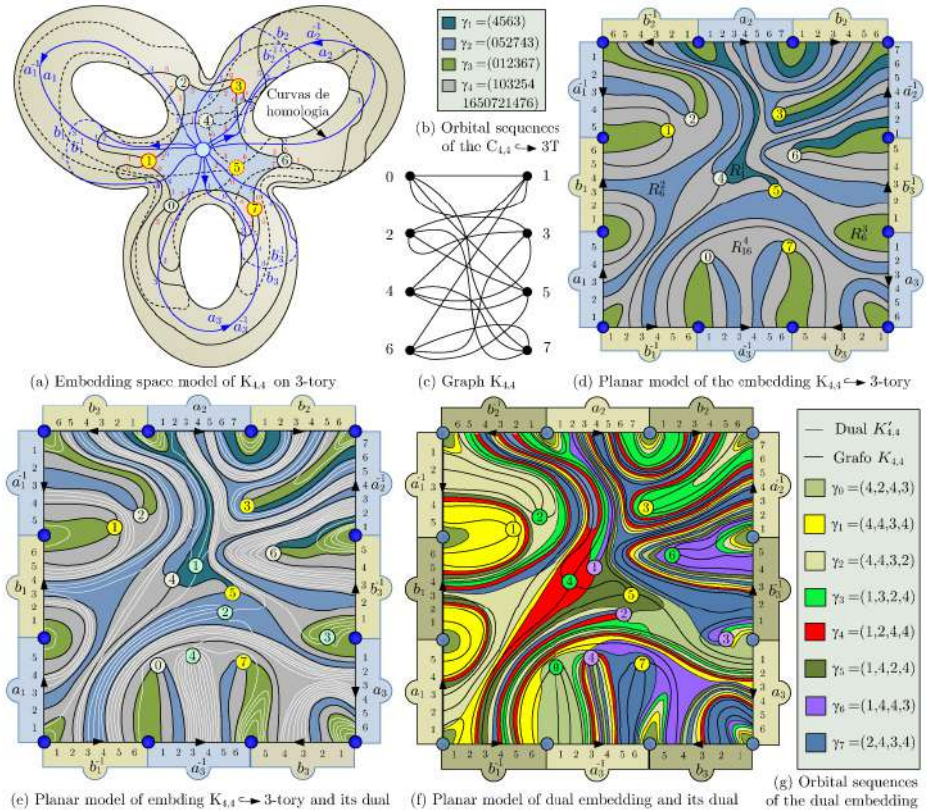

Figure 8 – Irregular modulations in 3-tory.

4.3 Compatible modulation on non-orientable surfaces

The identification process of modulation on non-orientable surfaces is similar to the orientable case. The difference is the variation of Eüler characteristic, it is of two in two unities in the orientable case and one to one it is the non-orientable case. As consequence, there are partitions in non-orientable surfaces that are not found in an orientable embeddings.

An orientable surface has been represented by a connected sum of g tory, denoted by gT. Similarly, a non-orientable surface it will be indicated by a connected sum of $\widetilde{g}$ projective planes P, denoted by $\widetilde{g}P$. Taking into account the fact that the embedding of $K_{4,4}$ only has regions of the kind $2k$-gon, $k \geq 2$, and sum of the region edges is 32, it is concluded that directed compatible

modulations with the channel $C_{4,4}$ in non-orientable surface are as the related models in Table 2.

$\widetilde{g}P$	Partitions	N^0
$2P$	$R_{4,4,4,4,4,4,4,4}$	1
$3P$	$R_{4,4,4,4,4,4,8}, R_{4,4,4,4,4,6,6}$	2
$4P$	$R_{4,4,4,4,4,12}, R_{4,4,4,4,6,10}, R_{4,4,4,4,8,8}, R_{4,4,4,6,6,8}, R_{4,4,6,6,6,6}$	5
$5P$	$R_{4,4,4,4,16}, R_{4,4,4,6,14}, R_{4,4,4,8,12}, R_{4,4,4,10,10}, R_{4,4,6,6,12}$ $R_{4,4,6,8,10}, R_{4,4,8,8,8}, R_{4,6,6,6,10}, R_{4,6,6,8,8}, R_{6,6,6,6,8}$	10
$3T$	$3R_4R_{20}, R_{4,4,6,18}, R_{4,4,8,16}, R_{4,4,10,14}, R_{4,4,12,12}, R_{6,6,6,14}, R_{6,6,8,12}, 4R_8$ $R_{4,6,6,16}, R_{4,6,8,14}, R_{4,6,10,12}, R_{4,8,8,12}, R_{4,8,10,10}, R_{6,6,10,10}, R_{6,8,8,10}$	15
$7P$	$R_{4,4,24}, R_{4,6,22}, R_{4,8,20}, R_{4,10,18}, R_{4,12,16}, R_{4,14,14}, R_{8,12,12}$ $R_{6,8,18}, R_{6,10,16}, R_{6,12,14}, R_{8,8,16}, R_{8,10,14}, R_{6,6,20}, R_{10,10,12}$	14
$8P$	$R_{4,28}, R_{6,26}, R_{8,24}, R_{10,22}, R_{12,20}, R_{14,18}\ R_{16,16}$	7
$9P$	R_{32}	1

Table 2 – Directed compatible modulations coming from $K_{4,4}$ embeddings on non-orientable surfaces.

Observe that partitions of non-orientable embeddings are always the same of the orientable embeddings always $\widetilde{g}$ is an even number, and in the cases where $\widetilde{g}$ is odd, the number of partitions is still quickly greater than the orientable partitions. So the non-orientable embeddings of $K_{4,4}$, when compared to orientable case, is a modulation source with more than double of elements of the orientable case, can have the same kind of partitions and present different options of embeddings and regularities. In relation to topological projects, these can be constructed with same difficulty degree of orientable embeddings, as shown the Figure 9. A compatible directed modulation with the channel $C_{12,12}[4, 4]$ is illustrated in (a). In the graph $K_{6,6}$, $\deg v = 4$ and rotation is given by

$$\begin{aligned}\Theta = \big\{&0(1,3,11,9), 1(0,10,2,4), 2(1,11,9,5), 3(0,4,6,8),\\ &4(1,5,7,3), 5(2,6,8,4), 6(3,7,9,5), 7(4,8,10,6), 8(5,3,11,7),\\ &9(6,10,0,2), 10(9,7,11,1), 11(10,8,0,2)\big\}.\end{aligned}$$

The plane model in (b) and spacial model in (c) represent homeomorphic embeddings corresponding to the partition $K_{6,6}(12, 24) \hookrightarrow 2P \equiv 12R_4$, is so

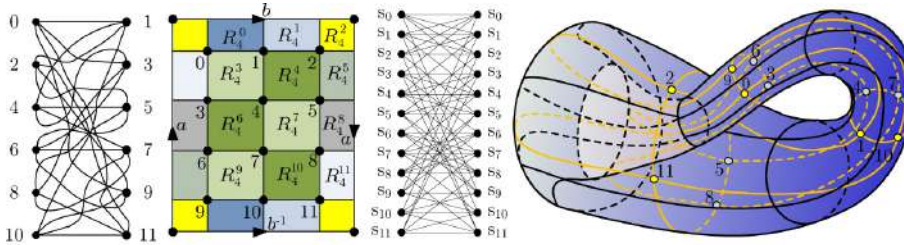

Figure 9 – Compatible modulation with channel C_{12} coming from $K_{6,6}[4]$ on the surface Klein's Bottle.

an example of a compatible uniform modulation on a non-orientable surface of genus 2, the Klein's bottle, of the same homeomorphis class of the surface $2P$. As the dual is equal to the own embedding, directed and dual compatible modulation are identical. This is a very important example because it is possible to be realized, a Differential Geometry level, through its parametric equations.

5 Homology group and compatible code

It has been seen that a compatible code with a DMC can be taken in different ways. The more natural way to do this choice [8] is that it should be through the homology group. The reason is because this group can be determined, when the Betti's method is applied from a triangulation obtained from a graph embedding. Thus, the proposal is to establish a compatible linear code extracted directly from the calculus process of homology group via Betti's method. In this sense, it is known that homology group of orientable and non-orientable surfaces is given by

$$H_1(\Omega) = \begin{cases} \mathbb{Z}^{2m}, \text{ if } \Omega \equiv mT \\ \mathbb{Z}_2 \oplus \mathbb{Z}^{m-1}, \text{ if } \Omega \equiv mP, \end{cases} \tag{6}$$

where $\mathbb{Z}$ is the additive group of the integers, $\mathbb{Z}_2$ is the binary group and $\mathbb{Z} \oplus \mathbb{Z}$ is a directed sum of $\mathbb{Z}$ with its own.

A strong reason for choice the homology group structure as an error-correcting code provider, beyond the uniqueness of this one, are the facts of the 2-cells embedding introduce a unique modulation and the rotation system provide a unique channel, conditions in which the own IS is determined by a unique way.

Moreover, the Betti's method determines the homology group through linear system which is associated to the matrix that can be used as an error-correcting code generator, similarly to linear codes. The idea is to identify and analyze the correct error capacity of these structures.

Suppose the graph $K_{m,n}$ is embedding on the surfaces $2T$ and $4P$, as a 2-cells embeddings. It is easy to construct the triangulation on these embeddings. Thus, let Υ be a triangulation or a simplicial complex on Ω. But Υ is a triangulation with many edges, which makes the homology group calculation more laborious. As the homology group is independent of the triangulations Υ, this calculus can be minimized using the *central triangular diagrams* (CTD) [8]. For surfaces $2T$ and $4P$ the CTD are shown in Figure 10.

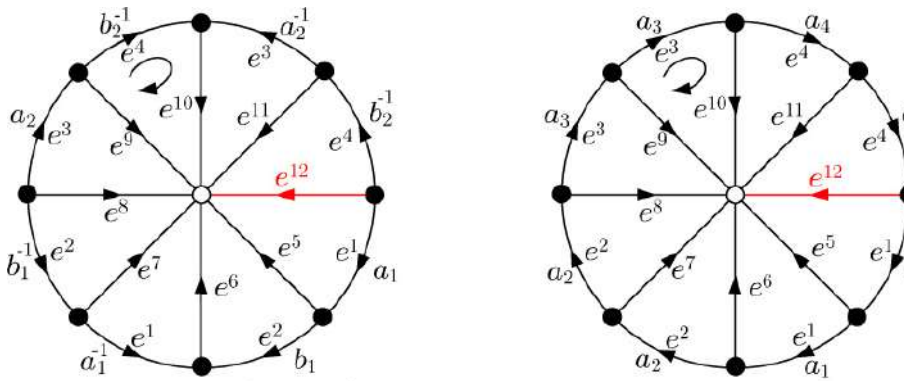

(a) $2T \equiv a_1 b_1 a_1^{-1} b_1^{-1} a_2 b_2 a_2^{-1} b_2^{-1}$ (b) $4P \equiv a_1 a_1 a_2 a_2 a_3 a_3 a_4 a_4$

Figure 10 – Central triangular diagrams on $2T$ and $4P$.

From Betti's method, the first homology group, indicated by $H_1(\Omega)$, of the surfaces $2T$ and $4P$ are given, respectively, by solutions of the linear systems

$$H\,(2T): \begin{cases} z_1 + z_2 + z_6 = 0 \\ z_1 + z_6 - z_7 = 0 \\ z_2 + z_7 - z_8 = 0 \\ z_3 - z_8 + z_9 = 0 \\ z_3 + z_4 + z_{10} = 0 \\ z_4 - z_9 + z_{10} = 0 \end{cases}, \quad H\,(4P): \begin{cases} 2z_1 + z_6 = 0 \\ z_2 + z_7 - z_6 = 0 \\ z_2 + z_8 - z_7 = 0 \\ z_3 + z_9 - z_8 = 0 \\ z_3 + z_{10} - z_9 = 0 \\ z_{10} - 2z_{11} = 0 \end{cases}$$

and using the fields $\mathbb{Z}_2$ and $\mathbb{Z}_3$ it follows the matrices

$$G = \begin{bmatrix} 1 & 1 & 0 & 0 & 1 & 0 & 0 & 0 & 0 \\ 0 & 1 & 0 & 0 & 0 & 1 & 0 & 0 & 0 \\ 0 & 0 & 1 & 0 & 0 & 0 & 1 & 1 & 0 \\ 0 & 0 & 0 & 1 & 0 & 0 & 1 & 1 & 1 \end{bmatrix},$$

$$\widetilde{G} = \begin{bmatrix} 1 & 0 & 0 & 2 & 0 & 0 & 0 & 0 & 0 \\ 0 & 1 & 0 & 0 & 2 & 1 & 0 & 0 & 0 \\ 0 & 0 & 1 & 0 & 0 & 0 & 2 & 1 & 0 \\ 0 & 0 & 0 & 1 & 0 & 0 & 0 & 0 & 1 \\ 0 & 0 & 0 & 0 & 1 & 1 & 1 & 0 & 0 \\ 0 & 0 & 0 & 0 & 0 & 0 & 1 & 1 & 1 \end{bmatrix}.$$

Therefore, $G(\Omega)$ is a binary matrix and $G(\widetilde{\Omega})$ is a 3-ary matrix. These properties will be used to obtain the linear codes in orientable and non-orientable surfaces, coming from homology group, with algebraic structures in the fields $\mathbb{Z}_2$ and $\mathbb{Z}_3$ and patterns of a IS. Then, considering $G(2T)$ as a generated matrix of an error-correcting code, it has a binary linear code $(C_1, 4, 9)$ with source sequences and codewords of lengths 4 and 9, respectively. Similarly, it is deduced that matrix $G(4P)$ generates a 3-ary linear code $(C_2, 6, 9)$. These structures of codes are formalized bellow.

Definition 5.1. *Let $K_{m,n} \hookrightarrow \Omega$ a 2-cells embedding of the graph $K_{m,n}$, and $\Xi(\Omega)$ the CDT on Ω. It is called* compatible generalized code*, the linear code (H, s, t) generated by matrix $G(\Omega)_{s\times t}$, obtained from linear system $H_1(\Omega)$.*

The demands imposed are: the linear independence of the $G(\Omega)$ lines and, to effect of correcting errors, the lines corresponding to the variables z_{2g+2} e z_{6g-4} are eliminated. Of course, these last conditions can be refused since they are not lost on condition of linear independence. The parameter s tells us the source code is a linear subspace of the space $\mathbb{Z}_2^s$ with 2^s elements and sequences of lengths s. The parameter t indicated the code is a linear subspace of the space $\mathbb{Z}_2^t$ with 2^t elements and codewords of lengths t.

Remark 5.2. If Ω is a compact surface of genus g, then $2g$-gon $\equiv \Omega$, and all vertices of the boundary of the orientable polygon $2g$-gon are transformed into

a single vertex, after the geometric realization of $2g$-gon in Ω. This property is essential to proof the follow affirmation.

Proposition 5.3. *The CDT $\Xi(\Omega)$ satisfies the following properties:*

a) *The maximal tree on $\Xi(\Omega)$ is composed by a unique 1-simplex* (*red edges in Figure* 10).

b) *$\Xi(\Omega)$ is composed by $6g$ 1-simplexes, if $\Omega \equiv gT$ or $\Omega \equiv \widetilde{g}P$ where $\widetilde{g} = 2g$.*

c) *The system of the homology group presentation $H_1(\Omega)$, from $\Xi(\Omega)$ is composed by $4g$ trivial relations, being two of two terms and the rest of three terms.*

d) *The system $H(\Omega)$ contains $4g-2$ trivial relations and $6g-2$ variables.*

e) *$H(gT)$ has two equivalent lines to the trivial relations $z_{2g+4} \equiv 0$ and $z_{6g-4} \equiv 0$.*

f) *The rank of the matrix $G(\Omega)$ is $2g$ if $\Omega \equiv gT$ and $\widetilde{g}-2$ if $\Omega \equiv \widetilde{g}P$, $\widetilde{g} = 2g$.*

Proof. Suppose that the maximal tree A has another 1-simplex e^j different of e^{12}. If e^j is an edge on the boundary of the $2n$-gon, then e^j is a loop of Ω. If e^j is a ray of the $2n$-gon, then, by Remark 5.2, e^j and e^{12} have two interceptions, in the center and on the boundary, and so A has a loop. Both on this case, A would not be a tree, which proofs the affirmation a). As $\widetilde{g} = 2g$, then, both the surfaces gT and $2gP$ present polygonal forms $2g$-gon. So its respective CDT $\Xi(\Omega)$ has g different 1-simplexes on the boundary and $2g$ 1-simplexes in the interior of $2g$-gon, a total of $6g$ 1-simplexes, which proves b). In the Betti's method, each trivial relation r_i comes from a 2-simplex or triangle t_i, and by one property known [8], the number of the r_i terms are equal to the number of 1-simplex in t_i that does not belong to maximal tree $\Xi(\Omega)$. As only there are two 2-simplexes of $\Xi(\Omega)$ has 1-simplex on A, it follows affirmation c). The number of system variables $H(\Omega)$ is equal to the number of 1-simplex, i.e., $6g$ and $H(\Omega)$ is obtained replacing the two trivial relations of two terms in two of three terms. As each replacement missed one variable, then $H(\Omega)$ is formed by $4g-2$ trivial relations and $6g-2$ variables, which proof d). The affirmation e)

was checked during the resolution of homology groups, including the solution on CDT of a generic surface. In particular case of $H(2T)$, he have

$$\begin{bmatrix} 1 & 1 & 0 & 0 & 0 & 1 & 0 & 0 & 0 & 0 \\ 1 & 0 & 0 & 0 & 0 & 1 & -1 & 0 & 0 & 0 \\ 0 & 1 & 0 & 0 & 0 & 0 & 1 & -1 & 0 & 0 \\ 0 & 1 & 0 & 0 & 0 & 0 & 0 & -1 & 1 & 0 \\ 0 & 0 & 1 & 1 & 0 & 0 & 0 & 0 & 0 & 1 \\ 0 & 0 & 0 & 1 & 0 & 0 & 0 & 0 & -1 & 1 \end{bmatrix} \Rightarrow \begin{bmatrix} 1 & 1 & 0 & 0 & 0 & 1 & 0 & 0 & 0 & 0 \\ 0 & 1 & 0 & 0 & 0 & 0 & 1 & 0 & 0 & 0 \\ 0 & 0 & 0 & 0 & 0 & 0 & 0 & -1 & 0 & 0 \\ 0 & 0 & 1 & 0 & 0 & 0 & 0 & -1 & 1 & 0 \\ 0 & 0 & 0 & 1 & 0 & 0 & 0 & -1 & 1 & 1 \\ 0 & 0 & 0 & 0 & 0 & 0 & 0 & -1 & 0 & 0 \end{bmatrix}$$

Notice that the 3^{th} and 4^{th} lines in the second matrix above are identical and both indicate that $z_8 = 0$. For the coding purpose, this type of line does not cause any effect, therefore their exclusion, amongst with variables which contain the null columns in the composition of the generator matrix of compatible code. Therefore, the generator matrix of compatible code on $2T$, instead of 6×10, it is a matrix of order 4×9 (in $\mathbb{Z}_2$, it is equal to the matrix G above). The affirmation f) result of the equality (6), a classic theorem of the homology groups of the algebraic topology. □

Constructing the DTC for generic surface Ω and its corresponding generate matrices $G(\Omega)$, it is possible to conclude that, for all embedding $K_{m,n} \hookrightarrow \Omega$, exists a unique generalized code compatible G on a Riemann manifold Ω which the graph associated to the channel $C_{m,n}$ has a 2-cells embedding.

Theorem 5.4. *If $K_{m,n} \hookrightarrow \Omega \equiv \cup_{i=1}^{k} R_{\alpha_i}^i$ is a 2-cells embedding, then exists a unique binary generalized code H, if $\Omega \equiv gT$, or a unique 3-ary generalized code $\widetilde{H}$, if $\Omega \equiv gT$, compatibles with C_k, defined by following parameters,*

$$H = \begin{cases} (H, 4g-4, 6g-3), \ \textit{if } \Omega \equiv gT \\ (\widetilde{H}, 2\widetilde{g}-2, 3\widetilde{g}-3), \ \textit{if } \Omega \equiv \widetilde{g}P. \end{cases} \tag{7}$$

Proof. By Definition 5.1, the generate matrix $G(\Omega)$ of code H coming from a matrix $H(\Omega)$ associated to the coefficients of a simplified system of trivial relations with three terms, obtained from the presentation of the homology group of Ω, through Betti's method. As $G(\Omega)$ is obtained through fundamental operations, then $G(\Omega)$ is equivalent to $H(\Omega)$ and so the code generated by $G(\Omega)$ is a unique binary code. If $\Omega \equiv gT$, by Proposition 5.3(d), $H(\Omega)$ has $2g-2$ trivial

relations and and $6g-2$ variables. As $G(\Omega)$ is the matrix of the coefficients of $H(\Omega)$ by eliminating two from the line of this one, it following that $G(\Omega)$ is a binary matrix of order $(4g-4)\times(6g-3)$. In an analogous way, it is conclude that $G(\widetilde{g}P)$ has a 3-ary matrix of order $(2g-2)\times(3g-3)$. As the order $s\times t$ of $G(\Omega)$ defines the parameters (H,s,t) of a linear code, which proves the equalities (8). □

Corollary 5.5. *Dual code of a generalized code compatible with a channel C_{m+n} is of the form:*

$$H' = \begin{cases} (H', 2g+1, 6g-3), \ \textit{if } \Omega \equiv gT \\ (\widetilde{H}', \widetilde{g}-1, 3\widetilde{g}-3), \ \textit{if } \Omega \equiv \widetilde{g}P. \end{cases} \tag{8}$$

Proof. Directed consequence of the dual code and Theorem 5.4. □

As examples, the generalized codes $(H_1, 4, 9)$ e $(H_2, 6, 9)$ above, relatives the generated matrices $G(2T)$ e $G(4P)$, have as dual codes $(H_1, 5, 9)$ e $(H_2, 3, 9)$, respectively.

6 Identification process of IS components

In the case of bipartite complete graph, the main components of IS, the modulations, coding and channel, are obtained through the followings steps.

6.0.1 Surface sets

Equalities (4) given the genus γ of the minimal orientable embedding of $K_{m,n}$. (The minimal non-orientable embedding $\widetilde{\gamma}$ satisfies the condition $\widetilde{\gamma}=\gamma$ or $\widetilde{\gamma}=\gamma+1$). Thus, by Theorem 4.1, the orientable and non-orientable surface sets for embeddings of $K_{m,m}$ are given by

$$\begin{aligned} \mathbb{S}(\Omega) &= \left\{\gamma T, (\gamma+2)T, (\gamma+4)T, \ldots, \gamma_M T\right\} \\ \mathbb{S}(\widetilde{\Omega}) &= \left\{\widetilde{\gamma} P, (\widetilde{\gamma}+1)P, (\widetilde{\gamma}+2)P, \ldots, \widetilde{\gamma}_M P\right\}, \end{aligned}$$

where γ_M and $\widetilde{\gamma}_M$ are the orientable and non orientable maximal genus of $K_{m,n}$.

6.0.2 *Modulation models*

It is determined the Eüler characteristic $\chi(\gamma T)$ by equalities (3) and the region number τ of the minimal embedding (equalities (2)). As the regions of a $K_{m,n}$ embedding partition have $2mn$ edges and one region is the form R_{2k}, $k \geq 2$, the modulation models are composed by all possible combinations of partitions $\cup_{i=1}^{t} R_{\alpha_i}^i$ such that

$$t = \begin{cases} \tau, \tau+2, \tau+4, \ldots, 5, 3, 1, & \text{if } t \text{ is odd} \\ \tau, \tau+2, \tau+4, \ldots, 6, 4, 2\ , & \text{if } t \text{ is even.} \end{cases}$$

In the non-orientable case, is determined the partitions $\cup_{i=1}^{\widetilde{t}} R_{\alpha_i}^i$ such that $\widetilde{t} = \widetilde{\tau}, \widetilde{\tau}+1, \widetilde{\tau}+2, \ldots, 3, 2, 1$, where $\widetilde{\tau}$ is the region number of the non-orientable minimal embedding.

6.0.3 *Compatible code*

Equalities (8) given an algebraic structures for composition of correcting-code error, Theorem 5.4 provides the generalized code compatible with channel $C_{m,n}$, and Corollary 5.5 provides the dual code.

As an application of the method we consider the IS components compatible with channel $C_{4,4}$ identified in the Table 3. The elements of the associated graph $K_{4,4}$ are: $v = 8$ and $e = 16$.

$g(\Omega)$	Ω	α	N^o	$H_1(\Omega)$	Code	Dual
gT	T	8	1	$\mathbb{Z}^2$	$(H, 1, 3)$	$(H', 2, 3)$
	$2T$	6	4	$\mathbb{Z}^4$	$(H, 4, 9)$	$(H', 6, 9)$
	$3T$	4	13	$\mathbb{Z}^6$	$(H, 8, 15)$	$(H', 7, 15)$
	$4T$	2	6	$\mathbb{Z}^8$	$(H, 12, 21)$	$(H', 9, 21)$
$\widetilde{g}P$	$2P$	8	1	$\mathbb{Z}_2 \oplus \mathbb{Z}$	$(H, 2, 3)$	$(H', 1, 3)$
	$3P$	7	2	$\mathbb{Z}_2 \oplus \mathbb{Z}^2$	$(H, 4, 6)$	$(H', 3, 6)$
	$4P$	6	4	$\mathbb{Z}_2 \oplus \mathbb{Z}^3$	$(H, 6, 9)$	$(H', 3, 9)$
	$5P$	5	10	$\mathbb{Z}_2 \oplus \mathbb{Z}^4$	$(H, 8, 12)$	$(H', 4, 12)$
	$6P$	4	13	$\mathbb{Z}_2 \oplus \mathbb{Z}^5$	$(H, 10, 15)$	$(H', 5, 15)$
	$7P$	3	14	$\mathbb{Z}_2 \oplus \mathbb{Z}^6$	$(H, 12, 18)$	$(H', 6, 18)$
	$8P$	2	6	$\mathbb{Z}_2 \oplus \mathbb{Z}^7$	$(H, 14, 21)$	$(H', 7, 21)$
	$9P$	1	1	$\mathbb{Z}_2 \oplus \mathbb{Z}^8$	$(H, 16, 24)$	$(H', 6, 24)$

Table 3 – IS components coming from $K_{4,4}$ embeddings.

By equalities (4) and (1), we have

$$\gamma(K_{4,4}) = \left\{ \frac{1}{4}(4-2)(4-2) = 1 \text{ and } \gamma_M(K_{4,4}) = \left[\frac{(4-1)(4-1)}{4} \right] \right\} = 4.$$

Then, the orientable embedding surface sets is $\mathbb{S}(K_{4,4}) = \{T, 2T, 3T\}$, non-orientable embedding surface sets is $\mathbb{S}(K_{4,4}) = \{2P, 3P, \cdots, 8P\}$ (2^{nd} column) and the these partitions are related in the 3^{rd} column. The 4^{th} column indicates the number α of the regions which it is constant in each surface. In the last three columns are the structures of compatible codes.

The generalized codes on the sphere and torus are degenerated cases. By Theorem 5.4, only dual code is defined on the torus. Indeed, generalized codes are more appropriated for surfaces of large genus. As $H_1(S) = 0$ the sphere is the unique case where the code coming from homology group is degenerated.

7 Conclusion

The integrated system is an ambitious idea, which intends to integrate the three main components of the data transmission system: codification, modulation and channel. In this first approach, the goal is to establish mathematic definitions considering the dependence relations of these components. In principle, the aim is to design a new data transmission system more efficient than the currently used. However, many other advantages are observed. The topological invariants such as orientability, genus, border component and partition, provide quick answers to questions about the modulation efficiency. It is not different with homology group. It is an important algebraic invariant which gives quick answers related to probably code class that could be projected in metrical spaces, such as Riemannian manifolds. The initial project, the topological constructing and identification of IS components, already has been solved in this work. The final project, has found in Algebraic Topology environments and Riemann's Geometry, recognized as promising areas for the communication problem. For further works, the proposal for the suggestions is to development embedding methods, constructing modulations that have been identified in this work (or new projects) using Riemann's Geometry tools and Algebraic Topology, and using the invariants as efficiency analysis instruments of the data transmission system.

Acknowledgements. Our warmest thanks go to Dr. Reginaldo Palazzo Jr., from State University of Campinas – Brazil, as well as to the anonymous reviewers for their important comments and suggestions.

REFERENCES

[1] R.G. Cavalcante, H. Lazary, J.D. Lima and R. Palazzo Jr., *A new approach to the design of digital communication systems*. Series in Discret Mathematics an Theorical Computer Science, (2005), 145–177.

[2] R.G. Cavalcante, H. Lazary, J.D. Lima and R. Palazzo Jr., *Coset space approach for the design of geometrically uniform codes in homogeneous spaces*. In: XVIII Escola de Álgebra, 2004, Campinas. Anais da XVIII Escola de Álgebra. Campinas, (2005), 1–26.

[3] R.A. Duck, *The genus, regional number, and Betti number of a graph*. Canad. J. Math., **18** (1966), 817–822.

[4] W. Dyck, *Reitrage zur Analysis Situs*. Math. Ann., **32** (1888), 457–512.

[5] J.D. Lima and E.V. Matias, *Modulation for signal constellations on Riemannian manifolds: associated channel and performance measure*. Master Dissertation, Computer Science Mester, University of the State of the Rio Grande do Norte, Brazil, (2011). (in Portuguese).

[6] J.D. Lima, L.P.R.C. Lima and W.C.D. de Melo, *Modulation for large signal constellations comming from embedding of complete graph*, in ITS 2010 – VII International Telecomunications Symposium, 2010, Manaus – AM. Proceedings of ITS 2010 – International Telecommunications Symposim. Rio de Janeiro – RJ: Sociedade Brasileira de Telecomunicações, **32** (2010), 1–5.

[7] L.P.R.C. Lima, *Modulation projects on topological surface associated to the discrete memoryless channels: a solution for the integrated system*. Master Dissertation, Computer Science Mester, University of the State of the Rio Grande do Norte, Brazil, (2009). (in Portuguese).

[8] J.D. Lima, *Identification and algebraic structure of compact surfaces with and without borders derived from embedding of discrete memoryless channels*. Doctoral Dissertation, School of Electrical and Computer Engineering, State University of Campinas, Brazil, (2002), (in Portuguese).

[9] H.M. Oliveira, D.R. Oliveira and R.M. Souza, *A unit quaternion-based spherical trigonometry and a new two-carrier phasequadrature quaternion modulation*

system. XXIX Simpósio Brasileiro de Telecomunicações – SBrT 2011, Curitiba, Paraná, (2011), 0–5.

[10] R.D. Reigensen, *Determining all compact orientable 2-manifolds upon which $K_{m,n}$ has 2-cell embeddings*. J. Combinatorial Theory, **12** (1972), 101–104.

[11] G. Ringuel, *Das Geschlecht des vollständigen paaren Graphen*. Math. Sem. Univ. Hamburg, **28** (1995), 139–150.

[12] J.W.T. Youngs and F. Ciryl, *Minimal imbeddings and the genus of a graph*. J. Math. Mech., **12** (1963), 303–316.

[13] J.M. Wozencraft and I.M. Jacobs, *Principles of Comunication Engineering*, 1st Edition, New York, (1966).

[14] Y. Wang, F. Alajaji and T. Linder, *Hybrid digital-analog coding with bandwidth compression for Gaussian source-channel pairs*. IEEE Transactions on Communications, **57** (2009), 997–1012.

STABILITY ANALYSIS OF A NEURO-IDENTIFICATION SCHEME WITH ASYMPTOTIC CONVERGENCE

José A. R. Vargas [1], Elder M. Hemerly[2] and Elmer R. L. Villarreal[3]

[1]Department of Electrical Engineering, Universidade de Brasília, Brasília, DF, Brazil
vargas@unb.br
[2]Department of System and Control, Instituto Tecnológico de Aeronáutica, SP, Brazil
hemerly@ita.br
[3]Department of Exact and Natural Sciences, Universidade Federal Rural do Semiárido, RN, Brazil
elmerllanos@ufersa.edu.br

ABSTRACT

This paper focuses on the stability and convergence analysis of a neuro-identification scheme for uncertain nonlinear systems. Based on linearly parameterized neural networks and the previous knowledge of upper bounds for the approximation error and disturbances, a robust modification of the descent gradient algorithm is proposed to make the overall identification process stable, and, in addition, the on-line residual prediction error asymptotically null, despite the presence of approximation error and disturbances. A simulation study to show the application and comparative performance of the proposed algorithm is presented.

KEYWORDS

On-line identification, nonlinear estimators, uncertain systems, neural networks.

1. INTRODUCTION

System neuro-identification is important not only to predict the behavior of the system, but also for providing an appealing system parameterization, which can later be used in the synthesis of control algorithms, since mathematical characterization is often a prerequisite to observer and controller design, see for instance [1-10] and the references therein.

Neural identification models usually employed are the dynamic ones, being their weights mainly adjusted using gradient and backpropagation algorithms or their robust modifications [3-10]. Most used robust modifications in neuro-identification are the σ, switching-σ, ε_1, parameter projection, and dead zone [3-10] which avoid the parameter drift. Nevertheless, these modifications, at present, can not ensure that the prediction error converges asymptotically to zero in the presence of approximation error and bounded disturbances.

For instance in [3], the identification of a general class of uncertain continuous-time dynamical systems was proposed, and a σ-modification adaptive law for the weights of recurrent high-order neural networks (RHONNs) was chosen to ensure that the state error converges to the

DOI : 10.5121/ijaia.2012.3403

neighborhood of the origin, which can be arbitrarily reduced by setting a sufficiently large number of high-order connections in the RHONN model.

In [4], dynamic NNs with a gradient descent algorithm for weights adjustment were used to identify a general class of uncertain nonlinear systems. Under the crucial assumption that the unknown system can be exactly modeled by a NN model, that is, the disturbance and approximation errors are identically null, it was shown that the state error converges asymptotically to zero, whereas the weight errors remain bounded or, in case that the hidden-layer activation function signal is persistently exciting, the weight errors converge to zero.

Similarly, also others relevant works, such as [5-10], showed that the dead zone, modified $\delta-$ rule, and ε_1-modification and others robust modifications can be used in weight adjustment laws to make the entire identification process stable in the presence of approximation error and disturbances.

Although the assumption of free disturbance may be interesting from a theoretical point of view, from a practical perspective it is a restrictive assumption since the presence of approximation errors are, in general, unavoidable, since the structure of the unknown system and the neural model are unrelated. It is well-known that adaptive laws designed for the disturbance or modeling error free case may suffer from parameter drift [11]. In fact, this lack of robustness in adaptive systems in the presence of unmodeled dynamics or bounded disturbances was reported in the early 1980s. Several robust modifications to counteract this [11] have been proposed since then.

Hence, in this paper we propose a robust modification for the weight adaptive law in neuro-identification problems which ensures, in contrast to previous works, that the residual prediction error converges to zero in the presence of approximation error and disturbances, provided that some conditions on the design parameters are satisfied. The adaptive law consists of a leakage modification of a standard gradient descent algorithm. However, in contrast to commonly leakage modifications [3-10] which aim at stability in the presence of approximation errors and disturbances, we introduce the leakage term here for, in addition to stability, ensuring that the residual prediction error converges to zero. More precisely, it is show by using usual Lyapunov arguments and an adaptive bounding technique [12] that the residual prediction error converges asymptotically to zero, whereas the others error signals remain bounded.

Throughout the paper $tr(\cdot)$ denotes the trace operator, $\lambda_{\min}(\cdot)$ denotes the minimum eigenvalue operator, $\|\cdot\|$ denotes the 2-norm and $\|\cdot\|_F$ denotes the Frobenius norm.

2. LINEARLY PARAMETERIZED NEURAL NETWORKS

Linearly parameterized neural networks (LPNNs) can be expressed mathematically as

$$\rho_{nn}(W,\zeta)=W\pi(\zeta) \tag{1}$$

where $W\in\Re^{n\times L_\rho}$, $\zeta\in\Re^{L_\zeta}$, $\pi:\Re^{L_\zeta}\mapsto\Re^{L_\rho}$ is the so-called basis function vector, which can be considered as a nonlinear vector function whose arguments are preprocessed by a scalar function $\pi(\cdot)$, and n,L_ρ,L_ζ are integers strictly positive. Commonly used scalar functions $\pi(\cdot)$ include sigmoid, tanh, gaussian, Hardy's, inverse Hardy's multiquadratic, etc [3,13]. However, here we are only interested in the class of LPNNs for which $\pi(\cdot)$ is bounded, since in this case we have,

$$\left\|\pi(\zeta)\right\| \le \pi_0 \tag{2}$$

being π_0 a strictly positive constant.

The class of LPNNs considered in this work includes HONN [3], RBF networks [13], wavelet networks [14], and also others linearly parameterized approximators as Takagi-Sugeno fuzzy systems [15]. Universal approximation results in [3,13,14,15] indicate that:

***Property 1*:** Given a constant $\varepsilon_0 > 0$ and a continuous function $f : \Omega \mapsto \Re^n$, where $\Omega \subset \Re^{L_\zeta}$ is a compact set, there exists a weight matrix $W = W^*$ such that the output of the neural network architecture (where L_ρ may depend on ε_0 and f) satisfies

$$\sup_{\zeta\in\Omega}\left| f(\zeta) - W^*\pi(\zeta)\right| \le \varepsilon_0 \tag{3}$$

where $|\cdot|$ denotes the absolute value if the argument is a scalar. If the argument is a vector function in $\Re^n$ then $|\cdot|$ denotes any norm in $\Re^n$.

3. PROBLEM FORMULATION

Consider the following nonlinear differential equation

$$\dot{x} = F(x,u,v,t), \qquad x(0) = x_0 \tag{4}$$

where $x \in X$ is the *n*-dimensional state vector, $u \in U$ is a *m*-dimensional admissible input vector, $v \in V \subset \Re^q$ is a vector of time varying uncertain variables and $F : X \times U \times V \times [0,\infty) \mapsto \Re^n$ is a continuous map. In order to have a well-posed problem, we assume that X, U, V are compact sets and F is locally Lipschitzian with respect to x in $X \times U \times V \times [0,\infty)$, such that (4) has a unique solution.

We assume that the following can be established

Assumption 1: On a region $X \times U \times V \times [0,\infty)$

$$\left\|h(x,u,v,t)\right\| \le h_0 \tag{5}$$

where

$$h(x,u,v,t) = F(x,u,v,t) - f(x,u) \tag{6}$$

f is an unknown map, h are internal or external disturbances, and $\bar{h}_0$, such that $\bar{h}_0 > h_0 \ge 0$, is a known constant.

Hence, except for the Assumption 1, we say that $F(x,u,v,t)$ is an unknown map and our aim is to design a NNs-based identifier for (4) to ensure the asymptotical state error convergence, that is,

the state error converges asymptotically to zero, which will be accomplished despite the presence of approximation error and disturbances.

4. IDENTIFICATION MODEL AND STATE ESTIMATE ERROR EQUATION

We start by presenting the identification model and the definition of the relevant errors associated with the problem.

Let $\bar{f}$ be the best known approximation of *f*, $B \in \Re^{n\times n}$ a scaling matrix defined as $B = diag(b_i)$, $b_i \neq 0$, $\bar{g} = B^{-1}g$, and $g(x,u) = f(x,u) - \bar{f}(x,u)$. Then, by adding and subtracting $\bar{f}(x,u)$, (4) can be rewritten as

$$\dot{x} = \bar{f}(x,u) + B\bar{g}(x,u) + h(x,u,v,t) \tag{7}$$

Remark 1: It should be noted that if the designer has no previous knowledge of *f*, then $\bar{f}$ is simply assumed as being the zero vector.

From (3), by using LPNNs, the nonlinear mapping $\bar{g}(x,u)$ can be replaced by $W^{*}\pi(x,u)$ plus an approximation error term $\varepsilon(x,u)$. More exactly, (7) becomes

$$\dot{x} = \bar{f}(x,u) + BW^{*}\pi(x,u) + B\varepsilon(x,u) + h(x,u,v,t) \tag{8}$$

where $W^{*} \in \Re^{nxL}$ is an "optimal" or ideal matrix, which can be defined as

$$W^{*} := \arg\min_{\hat{W}\in\Gamma} \left\{ \sup_{\substack{x\in X,\\ u\in U}} \left| \bar{g}(x,u) - \hat{W}\pi(x,u) \right| \right\} \tag{9}$$

with $\Gamma = \left\{ \hat{W} \mid \left\| \hat{W} \right\| \leq \alpha_{\hat{W}} \right\}$, $\alpha_{\hat{W}}$ is a strictly positive constant, $\hat{W}$ is an estimate of W^{*}, and $\varepsilon(x,u)$ is an approximation error term, corresponding to W^{*}, which can be defined as

$$\varepsilon(x,u) := \bar{g}(x,u) - W^{*}\pi(x,u) \tag{10}$$

The approximation, reconstruction, or modeling error ε is a quantity that arises due to the incapacity of LPNNs to match the unknown map $\bar{g}(x,u)$. Since *X*, *U* are compact sets and from (2), the following can be established

Assumption 2: On a region $X \times U$, the approximation error is upper bounded by

$$\left\| \varepsilon(x,u) \right\| \leq \bar{\varepsilon}_0 \tag{11}$$

where $\bar{\varepsilon}_0$, such that $\bar{\varepsilon}_0 > \varepsilon_0 \geq 0$, is an known constant.

Remark 2: Assumption 1 is usual in identification or robust control literature. Assumption 2 is quite natural since $\bar{g}$ is continuous and their arguments evolve on compact sets. The previous knowledge of upper bounds for approximation error and disturbances is common in the robust on-line parameter estimation literature. For instance, the dead zone algorithm uses a previous knowledge of bounds for the approximation errors, as can be seen in [5,6], or disturbances, as reported in [11].

Remark 3: Note that any $\bar{\pi}_0 > \pi_0$, $\bar{h}_0 > h_0$, and $\bar{\varepsilon}_0 > \varepsilon_0$ also satisfy (2), (5), and (11). Hence, to avoid confusion, we define π_0, h_0, and ε_0 to be the smallest constants such that (2), (5), and (11) are satisfied.

Remark 4: It should be noted that W^* and $\varepsilon(x,u)$ might be nonunique. However, $\|\varepsilon(x,u)\|$ is unique from (9).

Remark 5: It should be noted that W^* was defined as being the value of $\hat{W}$ that minimizes the L_∞- norm difference between $\bar{g}(x,u)$ and $\hat{W}\pi(x,u)$. Hence, the scaling matrix B in (7) is introduced to manipulate the magnitude of $\bar{g}(x,u)$, and therefore of $\|W^*\|_F$, since any increasing of $|b_i|$ implies that the corresponding $|\bar{g}_i(x,u)|$ decreases and, eventually, from (9), that $\|W^*\|_F$ decreases too. The matrix *B* provides an additional degree of freedom for shaping the transient performance.

Remark 6: Notice that the proposed neuro-identification scheme is a black-box methodology, hence the external disturbances and approximation error are related. Based on the system input and state measurements, the uncertain system (including the disturbances) is parameterized by a neural network model plus an approximation error term. However, the parameterization (8) is motivated by the fact that neural networks are not adequate for approximating external disturbances, since the basis function depends on the input and states, whereas the disturbances depend on the time and external variables. The aim for presenting the uncertain system in the form (8), where the disturbance *h* is explicitly considered, is also to highlight that the proposed scheme is in addition valid in the presence of unexpected changes in the systems dynamics that can emerge, for instance, due to environment change, aging of equipment or faults.
The structure (8) suggests an identification model of the form

$$\dot{\hat{x}} = \bar{f}(x,u) + B\hat{W}\pi(x,u) - L(\hat{x} - x) \tag{12}$$

where $\hat{x}$ is the estimated state, $L \in \Re^{n\times n}$ is a positive definite feedback gain matrix introduced to attenuate the effect of the nonzero uncertainties and the initial condition x_0. It will be demonstrated that the identification model (12) used in conjunction with a convenient adjustment law for $\hat{W}$, to be proposed in the next section, ensures the asymptotic convergence of the state error to zero, even in the presence of the approximation error and disturbances.

Remark 7: It should be noted that in our formulation, the LPNN is only required to approximate $B^{-1}[f(x,u) - \bar{f}(x,u)]$ (whose magnitude is often small) instead of the entire function $B^{-1}[f(x,u)]$. Hence, standard identification methods (to obtain some previous $\bar{f}$) can be used together with the proposed algorithm to improve performance.

By defining the state estimation error as $\tilde{x} := \hat{x} - x$, from (8) and (12), we obtain the state estimation error equation

$$\dot{\tilde{x}} = -L\tilde{x} + B\tilde{W}\pi(x,u) - B\varepsilon(x,u) - h(x,u,v,t) \tag{13}$$

where $\tilde{W} := \hat{W} - W^*$.

5. ADAPTIVE LAWS AND STABILITY ANALYSIS

Once the identification model and the relevant error equations associated with the problem of estimation were presented, the following step is the design of adaptive laws for the weights to achieve desired stability and convergence properties. Typically, in the literature [3-10], this is performed based on Lyapunov-like analysis via an enlargement process, where the error equation previously determined is used. Therefore, suitable weight adaptive laws are chosen to make $\dot{V}$, a time derivative of a Lyapunov function candidate V, negative semi-definite outside a ball whose radius is proportional to the worst-case of approximation error. However, this procedure ensures only practical stability. In this section we remove the aforementioned drawback by using dynamic leakage gain to make the Lyapunov derivative negative semi-definite in all error space. This choice is motivated by the fact that dynamic leakage gains can be considered as bounding functions and then can be used to dominate positive terms in $\dot{V}$ and hence improve the performance. Dynamic leakage gains have been used previously in [16].

Before presenting the main theorem, we state a fact, remark and lemma, which will be used in the stability analysis.

Fact 1: Let $W^*, W_0, \hat{W}, \tilde{W} \in \Re^{n \times L_\rho}$ and $\overline{C} \in \Re^{n \times n}$ be a diagonal matrix such that $\overline{C}^T \overline{C} = C$, where $C = diag(c_i)$, $c_i > 0$. Then, with the definition of $\tilde{W} = \hat{W} - W^*$, the following equalities are true:

$$\begin{aligned} 2tr\left[\tilde{W}^T C\left(\hat{W} - W_0\right)\right] &= \left\|\overline{C}\tilde{W}\right\|_F^2 + \left\|\overline{C}\left(\hat{W} - W_0\right)\right\|_F^2 - \left\|\overline{C}\left(W^* - W_0\right)\right\|_F^2 \\ 2tr\left[\hat{W}^T W_0\right] &= \left\|\hat{W}\right\|_F^2 + \left\|W_0\right\|_F^2 - \left\|\hat{W} - W_0\right\|_F^2 \end{aligned} \tag{14}$$

Remark 8: The first equality in (14) leads to the following inequality:

$$2tr\left[\tilde{W}^T C\left(\hat{W} - W_0\right)\right] \geq c_{i\min}\left\|\tilde{W}\right\|_F^2 + c_{i\min}\left\|\hat{W} - W_0\right\|_F^2 - c_{i\max}\left\|W^* - W_0\right\|_F^2 \tag{15}$$

where $c_{i\max} = \max(c_i)$ and $c_{i\min} = \min(c_i)$.

Lemma 5.1: Let a scalar bounding function be given by

$$\dot{\hat{\psi}} = -\gamma_\psi \left\|\tilde{x}\right\| \left[2\alpha_1 l\left(\hat{\psi}, \psi^*\right)\hat{\psi} - \alpha_2\left(\left\|\hat{W}\right\|_F^2 + \left\|W_0\right\|_F^2\right) - 2\alpha_1 l\left(\hat{\psi}, \psi^*\right)\psi^* \right] \tag{16}$$

where

$$l(\hat{\psi},\psi^*)=\frac{2l_0}{\hat{\psi}+\psi^*} \tag{17}$$

and $\gamma_\psi, l_0, \alpha_1, \alpha_2, \psi^* > 0$. Then, subject to the condition

$$\hat{\psi}(0)\geq \bar{\delta}\psi^* \tag{18}$$

where $\bar{\delta}=\frac{4\alpha_1 l_0+\alpha_2\|W_0\|_F^2}{4\alpha_1 l_0}$, the bounding function is lower bounded, for all $t\geq 0$, by

$$\hat{\psi}(t)\geq \bar{\delta}\psi^* \tag{19}$$

Proof: Consider the Lyapunov-like function

$$V_\psi = \hat{\psi}\,\gamma_\psi^{-1}\hat{\psi}\,/2 \tag{20}$$

By taking the derivative of (20) along (16) we obtain

$$\dot{V}_\psi=-\hat{\psi}\|\tilde{x}\|\left[2\alpha_1 l\hat{\psi}-\alpha_2\left(\|\hat{W}\|_F^2+\|W_0\|_F^2\right)-2\alpha_1 l\psi^*\right] \tag{21}$$

Furthermore, based on (16) and (18) it follows that $\hat{\psi}(t)>0$ for all $t\geq 0$. Then, with the definition (17), the Lyapunov derivative (21) can be lower bounded as

$$\dot{V}_\psi \geq -2\alpha_1 l\hat{\psi}\|\tilde{x}\|\left[\hat{\psi}-\bar{\delta}\psi^*\right] \tag{22}$$

Hence, if $\hat{\psi}\leq\bar{\delta}\psi^*$ we have $\dot{V}_\psi\geq 0$, which implies that the bounding function is directed towards the outside or boundary of the region $\left\{\hat{\psi}\;|\hat{\psi}\leq\bar{\delta}\psi^*\right\}$. Consequently, based on (18), it follows that $\hat{\psi}\geq\bar{\delta}\psi^*$ for all $t\geq 0$.

We now state and prove the main theorem of the paper.

Theorem 5.1: Consider the class of general nonlinear systems described by (4), which satisfies Assumptions 1-2. Let the weight law be given by

$$\dot{\hat{W}}=-\gamma_W\left\{2C\left(\hat{\psi}-\psi^*\right)\left[\hat{W}-\left(I-\alpha_2 C^{-1}\right)W_0\right]\|\tilde{x}\|+BK\tilde{x}\pi^T(x,u)\right\} \tag{23}$$

where $\hat{\psi}$ is given by (16), $\gamma_W>0$, I is an identity matrix, $K=P^T+P$, P is the unique positive definite solution of the Lyapunov equation

$$L^T P+PL=Q \tag{24}$$

where $L>0$ and $Q>0$. Then, subject to the condition (18), and if

$$\psi^* = \frac{2\alpha_4 \|KB\|_F}{\alpha_1 l_0} \tag{25}$$

$$\alpha_2 < c_{i\min} \tag{26}$$

$$W_0 \in \Omega_0 \tag{27}$$

$$l_0 \in [\beta_1, \beta_2] \tag{28}$$

Where

$$\Omega_0 = \{W_0 \mid tr(W^{*T} W_0) \le 0\},\ \beta_1 = \frac{2c_{i\max}}{\alpha_1}\|W^* - W_0\|_F^2,\ \beta_2 = \frac{\sqrt{c_{i\max}\alpha_2}\|W_0\|_F}{4\alpha_1}\|W^* - W_0\|_F,$$
$$\alpha_4 = \bar{\varepsilon}_0 + \|B^{-1}\|_F \bar{h}_0,\ \alpha_3 = \lambda_{\min}(Q) \tag{29}$$

the error signals $\tilde{x}, \tilde{W}, \tilde{\psi}$ are uniformly bounded and $\lim_{t\to\infty} \tilde{x}(t) = 0$.

Proof: Consider the Lyapunov function candidate

$$V = \tilde{x}^T P \tilde{x} + tr(\tilde{W}^T \gamma_W^{-1} \tilde{W})/2 + \tilde{\psi}\gamma_\psi^{-1}\tilde{\psi}/2 \tag{30}$$

where $\tilde{\psi} = \hat{\psi} - \psi^*$.

By evaluating (30) along the trajectories of (13), (16) and (23), and using the representation $tr(\tilde{W}^T BK\tilde{x}\pi^T) = \tilde{x}^T KB\tilde{W}\pi$, we obtain

$$\begin{aligned}\dot{V} = &-\tilde{x}^T(L^T P + PL)\tilde{x} - \tilde{x}^T K(B\varepsilon + h)\\ &- 2\tilde{\psi}\|\tilde{x}\| tr[\tilde{W}^T C(\hat{W} - W_0)] - 2\alpha_2\tilde{\psi}\|\tilde{x}\| tr(\tilde{W}^T W_0)\\ &- 2\alpha_1 l\tilde{\psi}\hat{\psi}\|\tilde{x}\| + \alpha_2\left(\|\hat{W}\|_F^2 + \|W_0\|_F^2\right)\tilde{\psi}\|\tilde{x}\| + 2\alpha_1 l\psi^*\tilde{\psi}\|\tilde{x}\|\end{aligned} \tag{31}$$

By using Fact 1, the representation $2\tilde{\psi}\hat{\psi} = \tilde{\psi}^2 + \hat{\psi}^2 - \psi^{*2}$, and (24), the Lyapunov derivative can be written as

$$\begin{aligned}\dot{V} = &-\tilde{x}^T Q\tilde{x} - \tilde{x}^T KB(\varepsilon + B^{-1}h)\\ &- \tilde{\psi}\|\tilde{x}\|\left[\|\bar{C}\tilde{W}\|_F^2 + \|\bar{C}(\hat{W} - W_0)\|_F^2 - \|\bar{C}(W^* - W_0)\|_F^2\right] + 2\alpha_2\tilde{\psi}\|\tilde{x}\| tr(W^{*T} W_0)\\ &- \alpha_1 l\left(\tilde{\psi}^2 + \hat{\psi}^2 - \psi^{*2}\right)\|\tilde{x}\| + \alpha_2\|\hat{W} - W_0\|_F^2\tilde{\psi}\|\tilde{x}\| + 2\alpha_1 l\psi^*\tilde{\psi}\|\tilde{x}\|\end{aligned} \tag{32}$$

Furthermore, by using Remark 8, condition (27), Lemma 5.1, and notation (29), the Lyapunov derivative (32) can be upper bounded as

$$\begin{aligned}\dot{V} \le & \left\|\tilde{x}\right\| \cdot \Big[-\alpha_3 \left\|\tilde{x}\right\| + \alpha_4 \left\|KB\right\|_F \\ & - \tilde{\psi} \left(c_{i\min} \left\|\tilde{W}\right\|_F^2 + c_{i\min} \left\|\hat{W} - W_0\right\|_F^2 - c_{i\max} \left\|W^* - W_0\right\|_F^2 \right) \\ & - \alpha_1 l \left(\tilde{\psi}^2 + \hat{\psi}^2 - \psi^{*2} \right) + \alpha_2 \left\|\hat{W} - W_0\right\|_F^2 \tilde{\psi} + 2\alpha_1 l \psi^* \tilde{\psi} \Big]\end{aligned} \tag{33}$$

Further using (26) and rearranging terms, we obtain

$$\begin{aligned}\dot{V} \le & \left\|\tilde{x}\right\| \cdot \Big[-\alpha_3 \left\|\tilde{x}\right\| - c_{i\min} \tilde{\psi} \left\|\tilde{W}\right\|_F^2 - \alpha_1 l \tilde{\psi}^2 \\ & + \alpha_4 \left\|KB\right\|_F + c_{i\max} \tilde{\psi} \left\|W^* - W_0\right\|_F^2 \\ & - \alpha_1 l \left(\hat{\psi}^2 - \psi^{*2} \right) + 2\alpha_1 l \psi^* \tilde{\psi} \Big]\end{aligned} \tag{34}$$

By employ the definition of ψ^*, see (25), recalling that $\tilde{\psi} = \hat{\psi} - \psi^*$, and using Lemma 5.1, (34) reduces to

$$\begin{aligned}\dot{V} \le & \left\|\tilde{x}\right\| \cdot \Big[-\alpha_3 \left\|\tilde{x}\right\| - c_{i\min} \tilde{\psi} \left\|\tilde{W}\right\|_F^2 - \alpha_1 l \tilde{\psi}^2 \\ & + \left(\alpha_1 l_0 / 2 + c_{i\max} \left\|W^* - W_0\right\|_F^2 \right) \hat{\psi} - c_{i\max} \psi^* \left\|W^* - W_0\right\|_F^2 \\ & - \alpha_1 l \hat{\psi}^2 + \alpha_1 l \psi^{*2} + 2\alpha_1 l \psi^* \tilde{\psi} \Big]\end{aligned} \tag{35}$$

which, by using (17), implies

$$\begin{aligned}\dot{V} \le & \left\|\tilde{x}\right\| \cdot \Big[-\alpha_3 \left\|\tilde{x}\right\| - c_{i\min} \tilde{\psi} \left\|\tilde{W}\right\|_F^2 \\ & + \left(\alpha_1 l_0 / 2 + c_{i\max} \left\|W^* - W_0\right\|_F^2 \right) \hat{\psi} - c_{i\max} \psi^* \left\|W^* - W_0\right\|_F^2 \\ & - \frac{2\alpha_1 l_0}{\hat{\psi} + \psi^*} \hat{\psi}^2 + 4\alpha_1 l_0 \psi^{*2} / \hat{\psi} \quad \Big]\end{aligned} \tag{36}$$

Thus by using Lemma 5.1 and rearranging terms in (36), we finally obtain

$$\begin{aligned}\dot{V} \le & \left\|\tilde{x}\right\| \cdot \Big\{ -\alpha_3 \left\|\tilde{x}\right\| - c_{i\min} \tilde{\psi} \left\|\tilde{W}\right\|_F^2 \\ & - \psi^* \left(c_{i\max} \left\|W^* - W_0\right\|_F^2 - \frac{(4\alpha_1 l_0)^2}{\alpha_2 \left\|W_0\right\|_F^2} \right) \\ & - \frac{\alpha_1 \hat{\psi}^2}{\hat{\psi} + \psi^*} \left[l_0 - \left(l_0 / 2 + c_{i\max} \left\|W^* - W_0\right\|_F^2 / \alpha_1 \right) \right] \\ & - \frac{\alpha_1 \hat{\psi}}{\hat{\psi} + \psi^*} \left[l_0 \hat{\psi} - \left(l_0 / 2 + c_{i\max} \left\|W^* - W_0\right\|_F^2 / \alpha_1 \right) \psi^* \right] \Big\}\end{aligned} \tag{37}$$

It addition, we note from (28) that

$$\left\|W^* - W_0\right\|_F^2 \geq \frac{(4\alpha_1 l_0)^2}{\alpha_2 c_{i\max}\left\|W_0\right\|_F^2}, \quad \frac{l_0}{2} \geq c_{i\max}\left\|W^* - W_0\right\|_F^2 \Big/ \alpha_1 \tag{38}$$

By substituting (38) into (37), and using Lemma 5.1, we arrive at

$$\dot{V} \leq -\alpha_3 \left\|\tilde{x}\right\|^2 \tag{39}$$

Hence, the error signals $\tilde{x}, \tilde{W}, \tilde{\psi}$ are uniformly bounded. Further, since V is bounded from below and non increasing with time, we have

$$\lim_{t\to\infty} \int_0^t \left\|\tilde{x}(\tau)\right\|^2 d\tau \leq \frac{V(0) - V_\infty}{\alpha_3} < \infty \tag{40}$$

where $\lim_{t\to\infty} V(t) = V_\infty < \infty$. Notice that with the bounds on $\tilde{x}, \tilde{W}, \tilde{\psi}, \varepsilon$ and h, $\left\|\tilde{x}\right\|^2$ is uniformly continuous. Thus from (13), it follows that $\dot{\tilde{x}}$ is bounded. Hence by Barbalat´s lemma [11], we conclude that $\lim_{t\to\infty} \tilde{x}(t) = 0$.

Remark 9: Conditions (18), (24), and (26) are trivial since them are defined by the user according to a desired performance. Condition (25) implies the previous knowledge of upper bounds for the approximation error and disturbances. Conditions (27) and (28) require at least that the sign of some entry of W^* and bounds for the ideal weights are known. The previous knowledge of bounds for the modeling error and ideal weights is not peculiar to the proposed scheme. Most robust modifications in the literature, as for example, switching-σ, parameter projection, and dead-zone require *a priori* information on the plant or modeling error for ensuring stability, as reported in [3,5,6,11]. Despite the aforementioned drawback, the relevance of the proposed algorithm consist in the introduction of a new robust modification and the establishment of conditions, on the design parameters, for which the residual prediction error converges to zero, even in the presence of approximation error and disturbances.

Remark 10: There is at least one way of selecting the design parameters to satisfy the interval condition (28): by selecting a conservative $\left\|W_0\right\|_F$ (large enough) and, in the sequence, by adjusting $\left\|W^* - W_0\right\|_F$ (small enough), what can be achieved by appropriate selection of the scaling matrix *B*.

6. SIMULATIONS

To illustrate the application of the proposed scheme, we consider an engine model operating under idle [17,18] described by

$$\dot{P} = k_p\left(\dot{m}_{ai} - \dot{m}_{ao}\right) \tag{41}$$

$$\dot{N} = k_n\left(T_i - T_l\right) \tag{42}$$

where

$$\dot{m}_{ai} = \left(1 + k_{m1}\theta + k_{m2}\theta^2\right) g(P),$$

$$\dot{m}_{ao} = -k_{m3}N - k_{m4}P + k_{m5}NP + k_{m6}NP^2,$$

$$g(P) = \begin{cases} 1 & P \le 50.6625 \\ 0.0197\sqrt{101.325P - P^2} & P > 50.6625 \end{cases},$$

$$T_i = -39.22 + 325024 m_{ao} - 0.0112\delta^2 + 0.635\delta$$
$$+ (2\pi/60)(0.0216 + 0.000675\delta)N - (2\pi/60)^2 0.000102N^2,$$

$T_l = (N/263.17)^2 + T_d$, $m_{ao} = \dot{m}_{ao}(t-\tau)/(120N)$, $k_p = 42.40$, $k_n = 54.26$, $k_{m1} = 0.907$, $k_{m2} = 0.0998$, $k_{m3} = 0.0005968$, $k_{m4} = 0.1336$, $k_{m5} = 0.0005341$, $k_{m6} = 0.000001757$,

P is the manifold pressure (kPa),

N is engine speed (rpm),

δ is the spark advance (degrees),

θ is the throttle angle (degrees),

$\dot{m}_{ai}$ is the mass flow rate into the manifold,

$\dot{m}_{ao}$ is the mass flow rate out of the manifold and into the cylinder,

T_d are disturbances which act on the engine as unmeasured accessory torque (N-m)

T_i is the internally developed torque (N.m),

T_l is the load torque made up of accessory torque T_d and shaft torque (N.m),

$g(P)$ is a manifold pressure influence function,

m_{ao} is the air mass in the cylinder, and

τ is a dynamic transport time delay,

The meaning of the main variables of the model is shown in Fig. 1 ([18]).

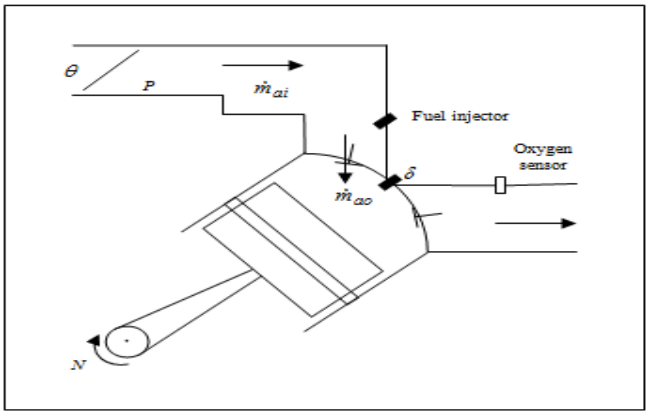

Figure 1- The main engine subsystem.

Since the engine operation is highly nonlinear system, because it presents time delays that vary inversely with engine speed and is time-varying due to aging of components and environment changes such as engine warm-up after a cold star [17], and their dynamical equations entail a great deal of uncertainty [18], the neural parameterization of the engine is relevant and useful. The neural model is valid for any operation points, in contrast to others models derived from steady-state map data and other empirical information.

We define $x=[P \quad N]^T$, $u=[\theta \quad \delta]^T$, and select, as in [19], θ as being a square wave with amplitude 20°, frequency 0.25 rad/s, δ as a sine wave with amplitude 30°, frequency 0.5 rad/s, T_d as a sawtooth wave with amplitude 10 N.m, frequency 0.5 rad/s, $\tau=0$, and $x(0)=[10 \quad 500]^T$. It should be noted that system (41)-(42) is only used for generation of state trajectory, which is used in the implementation of the algorithm.

To identify the uncertain system (41)-(42) the proposed identification model (12) and the adaptive laws (16) and (23) were implemented. The initial eigenvalues of the gain matrix *L* were freely chosen since the system dynamic is not accessible. The basis function vector was chosen to be very simple, to evaluate the performance of the proposed method in the presence of several approximation errors. Hence, a conservative bound α_4 was selected. In the sequence, by a trial and error procedure, the others design parameters were adjusted for providing an adequate transient and residual state error performance. The design parameter were chosen as

$$\alpha_4=3535.53,\ \hat{x}(0)=-[5 \quad 5]^T,\ \hat{W}(0)=0,\ \hat{\psi}(0)=\bar{\delta}\psi^*,\ \psi^*=20,\ l_0=0.5,\ \bar{f}=0,$$
$$L=20I,\ B=I,\ K=000.1I,\ W_0=\begin{bmatrix}1 & 0 & 0 & 0\\ 0 & 1 & 0 & 0\end{bmatrix},\ \pi=[s(x_1) \quad s(x_2) \quad s(u_1) \quad s(u_2)]^T,$$
$$s(\cdot)=10/[1+\exp-0.5(\cdot)],\ \gamma_W=\gamma_\psi=1,\ C=100I,\ \alpha_1=1, \text{ and } \alpha_2=75. \qquad (43)$$

Notice that the design parameters in (43) satisfy the conditions (18) and (26). It is supposed that condition (25) is satisfied when $\psi^*=20$. Another arbitrary large upper bound can be obtained by reducing the entries of *K* and, correspondingly, for shaping the transient performance, by increasing the entries of *L*. Hence, condition (25) is mild, since α_4 can be arbitrarily enlarged by reducing *K*, as already mentioned.

Based on (43), condition (28) becomes

$$0.02 \le \left\| W^* - W_0 \right\|_F \le 0.05 \qquad (44)$$

It should be noted that others large upper and small lower bounds for (44) can be obtained by adjusting the design parameters.

The performance in the estimation of the manifold pressure and engine speed are shown in Figures 2-3. We can see that the simulations confirm the theoretical results, that is, the algorithm is stable and the residual state error is small. Figure 4 shows the behavior of the weights, where a logarithmic scale is used for the time axis.

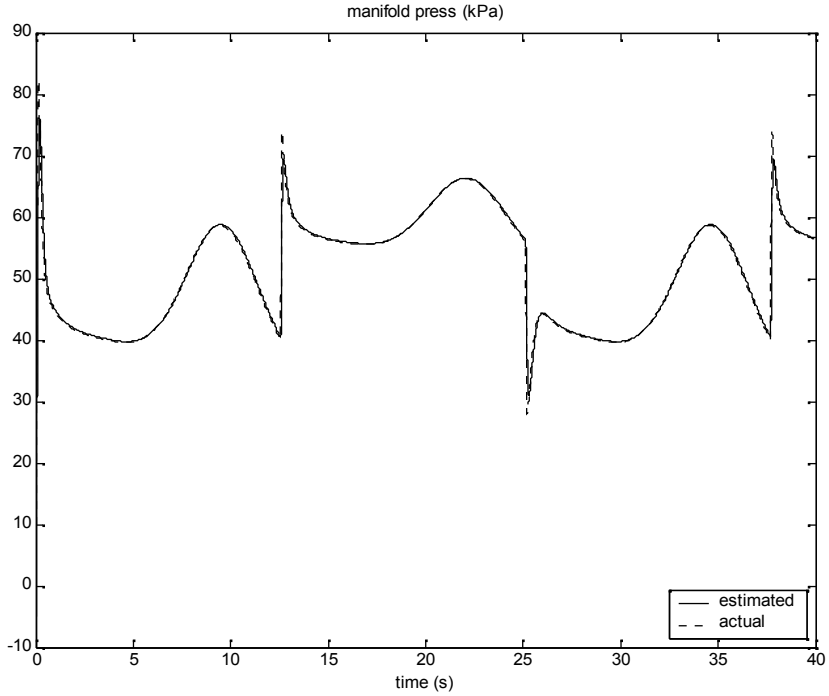

Figure 2- Performance in the estimation of *P*.

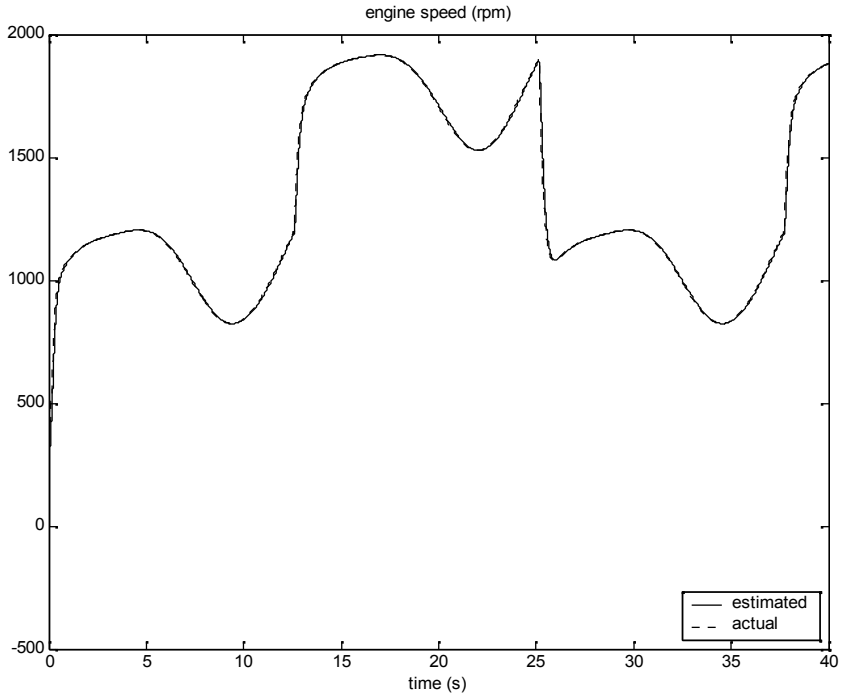

Figure 3- Performance in the estimation of *N*.

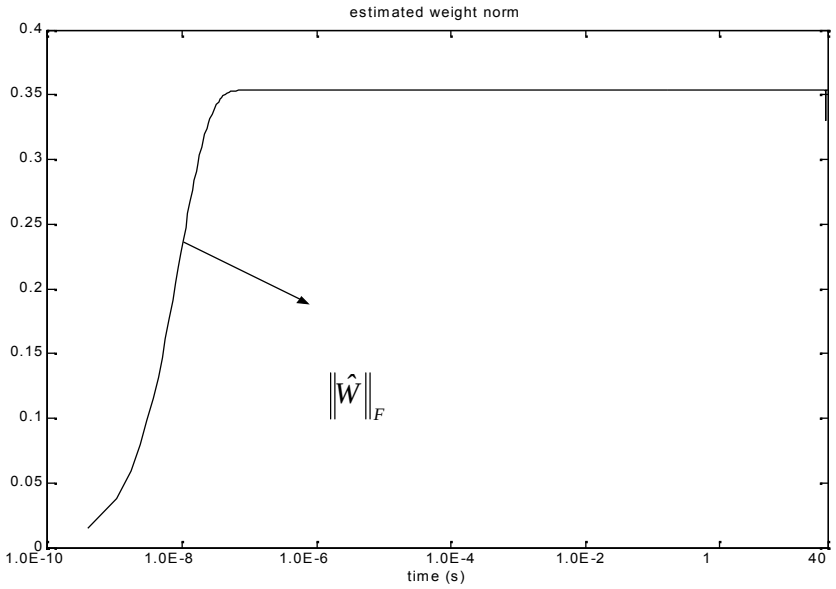

Figure 4- Frobenius norm of the estimated weights.

In Figures 5-6, we compare the performance and robustness, in the presence of uncertainties, of the proposed algorithm and that in [19]. These figures illustrate several points: 1) the proposed algorithm exhibit robustness in the presence of uncertainties, 2) concerning the residual estimation state error, the proposed algorithm presents good performance, and 3) it is not necessary to use arbitrary high gains to obtain arbitrary small residual estimation state errors, as can be seen from the design parameters (43).

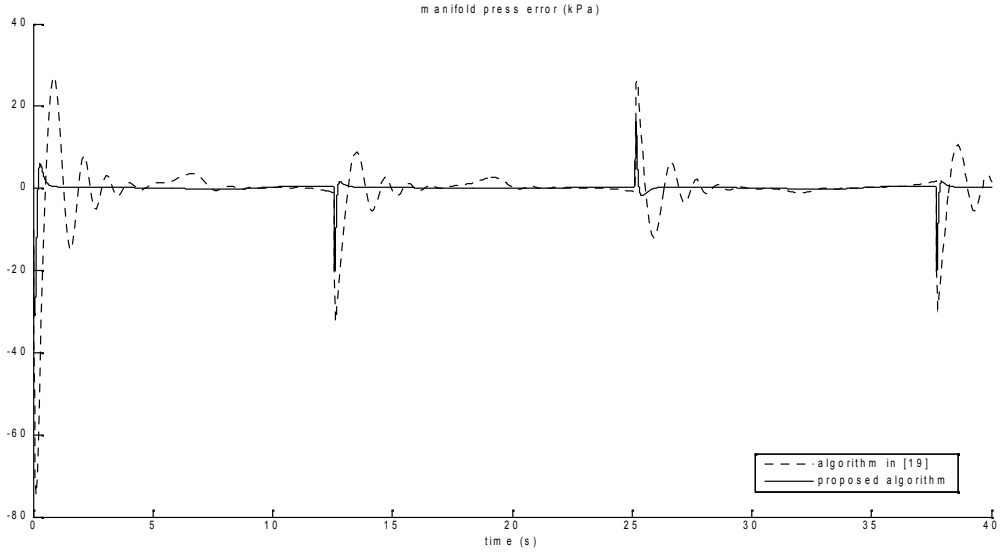

Figure 5- Performance comparison in the estimation of *P*.

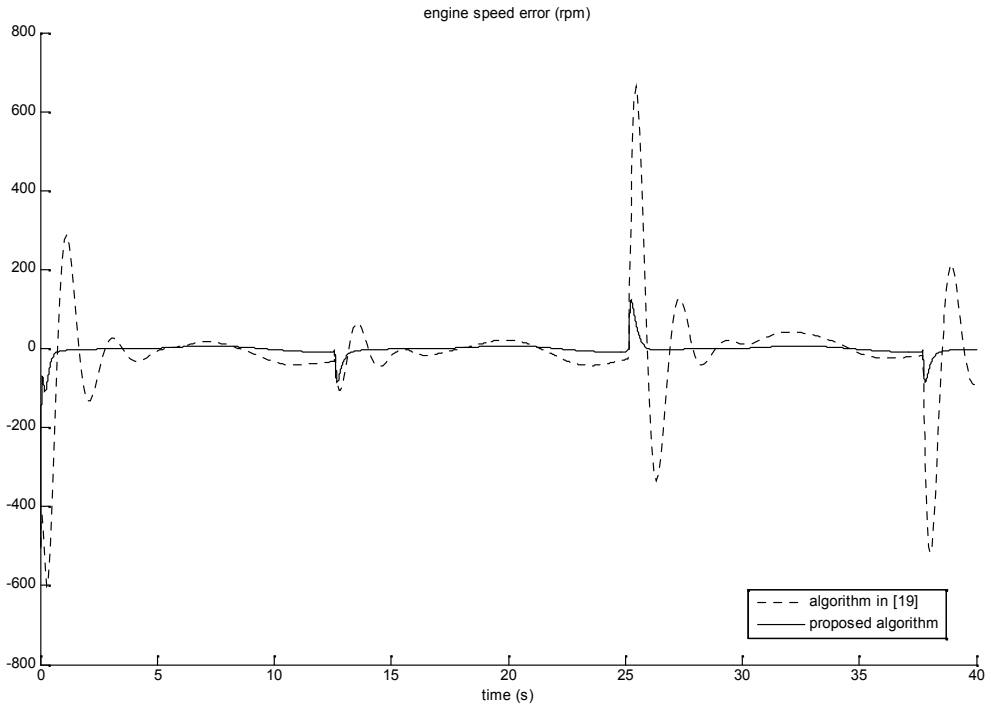

Figure 6- Performance comparison in the estimation of *N*.

7. CONCLUSIONS

In this work, by using Lyapunov-like analysis, we have proved that a robust modification based on a dynamic leakage gain can also ensure residual state error convergence to zero in neuro-identification algorithms, even in the presence of approximation error and disturbances. The proposed algorithm is based on a dynamic ε_1-modification and relies on the previous knowledge of upper bounds for the ideal weight, approximation error and disturbances to ensure asymptotic convergence. Although these bounds are usually unknown in practice, the proposed scheme has stability properties similar to others robust modification since it is based on a ε_1-modification. However, in contrast to previous works, the proposed algorithm has better convergence properties, since it can also guarantee asymptotic convergence even in the presence of approximation error and disturbances, if some conditions on the design parameters are verified.

REFERENCES

[1] K. S. Narendra, K. Parthasarathy, (1990) Identification and control of dynamical systems using neural networks, IEEE Trans. Neural Networks, Vol. 1 no. 1, pp. 4-27.

[2] F. O. Souza, R. M. Palhares, (2010) Interval time-varing delay stability for neural networks, Neurocomputing, Vol. 73, pp. 2789-2792.

[3] E. B. Kosmatopoulos, M. M. Polycarpou, M. A. Christodoulou, P. A. Ioannou, (1995) High-order neural network structures for identification of dynamical systems, IEEE Trans. Neural Networks, Vol. 6, no. 2, pp. 422-431.

[4] R. R. Selmic, F. L. Lewis, (2001) Multimodel neural networks identification and failure detection of nonlinear systems, Proc. 2001 CDC, Orlando, Florida USA, pp. 3128-3133.
[5] Q. Song, (1998) Robust training algorithms of multilayered neural networks for identification of nonlinear dynamical systems, IEE Proc.- Control Theory Appl., Vol. 145, no. 1, pp. 41-46.
[6] S. Jagannathan, F. L. Lewis, (1996) Identification on nonlinear dynamical systems using multilayered neural networks, Automatica, Vol. 32 no. 12, pp. 1707-1712.
[7] F. Abdollahi, H. A. Talebi, R. V. Patel, (2006) Stable identification of nonlinear systems using neural networks: Theory and experiments, IEEE/ASME Trans. on Mechatronics, Vol. 11, no. 4, pp. 488-495.
[8] A. Bazaei, M. Moallem, (2007) Online neural identification of multi-input multi-output systems, IET Control Theory Appl., Vol. 1, no. 1, pp. 44-50.
[9] I. Chairez, A. Poznyak, T. Poznyak, (2009) Stable weights dynamics for a class of differential neural network observer, IEE Proc.- Control Theory Appl., Vol. 3, no. 10, pp. 1437-1447.
[10] A. Y. Alanis, E. N. Sanchez, A. G. Loukianov, E. A. Hernandez, (2010) Discrete-time recurrent high order neural networks for nonlinear identification, Journal of the Franklin Institute, Vol. 347, pp. 1253-1265.
[11] P.A. Ioannou, J. Sun, (1996) Robust adaptive control, Prentice-Hall, Inc., Englewood Cliffs, New Jersey.
[12] M. Corless, (1993) Control of uncertain nonlinear systems, Trans. ASME J. Dyn. Sys., Meas., Control, Vol. 115, pp. 362-372.
[13] S. S. Ge, C. C. Hang, T. H. Lee, T. Zhang, (2002) Stable adaptive neural network control, Kluwer academic publishers.
[14] Q. Zhang and A. Benveniste, (1992) Wavelet networks, IEEE Trans. Neural Networks, Vol. 3, no. 6, pp. 889-898.
[15] L. X. Wang, (1994) Adaptive fuzzy system and control: design and stability analysis, Prentice-Hall, Inc., Englewood Cliffs, New Jersey.
[16] T.Y. Chai, Z. Tao, (1994) A new model reference robust adaptive controller in the presence of unmodeled dynamics and bounded disturbances, Automatica, Vol. 30, no. 5, pp. 865-869.
[17] G. V. Puskorius, L. A. Feldcamp, (1994) Neurocontrol of nonlinear dynamical systems with Kalman filter trained recurrent networks, IEEE Trans. Neural Networks, Vol. 5, no. 2, , pp. 279-297.
[18] G. Vachtsevanos, S. S. Farinwata, D. K. Pirovolou, D. K., (1993) Fuzzy logic control of an automotive engine, IEEE Control Systems Magazine, Vol. 13, no. 3, pp. 62-68.
[19] W. Yu, X. Li, (2001) Some new results on system identification with dynamic neural networks, IEEE Trans. Neural Networks, Vol. 12, no. 2, pp. 412-417.

Authors

José A. R. Vargas is Professor of Control Systems in the Electrical Engineering Department, University of Brasília, DF-Brazil. He received the Dr.Sc. degree in electronics and computer engineering from Instituto Tecnológico de Aeronáutica, in 2003. His current research interests include on-line identification, state estimation and adaptive control.

Elder M. Hemerly is Professor of Control Systems in the Electronics Division, Technological Institute of Aeronautics, SP-Brazil. He received the Ph.D. degree in electrical engineering from Imperial College, London, in 1989. His current research interests include robotics, system identification and adaptive control.

Elmer R. L. Villarreal is Professor of Control Systems in the Exact and Natural Sciences Department, Univesidade Federal Rural do Semi-árido, RN-Brazil. He received the Dr.Sc. degree in electrical engineering from University of Santa Catarina, in 2002. His current research interests include system identification and nonlinear control.

TEMA Tend. Mat. Apl. Comput., **10**, No. 1 (2009), 99-110.
© *Uma Publicação da Sociedade Brasileira de Matemática Aplicada e Computacional.*

Static Output Feedback Stabilization using Invariant Subspaces and Sylvester Equations

E.R.L. VILLAREAL[1], Departamento de Ciências Exatas e Naturais, Universidade Federal Rural do Semi-árido DCEN/UFERSA, BR 110, Km 47, Bairro Costa e Silva, 59625-900 Mossoró, RN, Brasil.

J.A. RUIZ VARGAS[2], E.M. HEMERLY[3], Instituto Tecnológico de Aeronáutica, Praça Mal. Eduardo Gomes, 50, ITA-IEE-IEES Vila das Acácias, 12228-900 São Jose dos Campos, SP, Brasil.

Abstract. This paper presents systematic computational algorithms for obtaining the output feedback gain matrix in linear systems stabilization problems. Based on the concept of (C, A, B)-invariant subspaces, introduced previously by the first author, that has related the existence of a gain matrix to the solution of coupled Sylvester equations, two algorithms are presented: 1) in the Syrmos-Lewis algorithm, a modification is proposed to provide a more adequate framework to numerical solution, and 2) by using orthogonal transformations, the Alexandridis-Paraskevopoulos algorithm is modified to overcome, in part, the Kimura condition. Numerical examples are provided to illustrate the application of the proposed algorithms.

Keywords. Stabilization, Output Feedback, Invariant Subspace, Sylvester equations.

1. Introduction

It is well known that the static output feedback stabilization problem is a relevant and challenging problem, due to its simple implementation, in contrast to more sophisticated dynamic methods, and because it is not easy to find a feedback matrix to make the closed-loop system asymptotically stable [5], [15], [10], [8], [2], unlike to the state feedback case.

The determination of procedures for obtaining the feedback matrix in output feedback control to asymptotically stabilize linear systems is actually an open problem. Several methods have been proposed in the literature based on Lyapunov, Ricatti, linear matrix inequalities, or eigenstructure assignement. See, for instance [1]-[5], [8], [10]-[14], [16], and the references therein.

[1]elmerllanos@ufersa.edu.br
[2]vargas@ieee.org
[3]hemerly@ita.br

In particular, recently in [5] it was introduced the concept of (C, A, B)-invariant subspaces to relate the existence of a feedback gain matrix to the solution of two coupled Sylvester equations. However, this solution was mainly obtained under the Kimura condition [11] (i.e., $m + p > n$, where n, m, and p are the dimensions of the state, input, and output, respectively). Pathological cases where $m + p \leq n$, were only tackled by a trial and error procedure [5].

Hence, motivated by the previous facts, the main concern in this paper is the design, under a less restrictive than Kimura condition, of more efficient computational algorithms to the selection of the output feedback matrix. Based on the Syrmos-Lewis algorithm, a modification is proposed to provide a more adequate framework to numerical solution. Basically, by considering that the system is observable, controllable and under the Kimura condition, the coupled Sylvester equations are solved by assuming that the dimension of $\mathcal{V} = Im\,(V)$ is equal to the number of outputs p and the matrix $CV \in \Re^{p\times p}$ is invertible. Then the feedback matrix can be found as $G = W(CV)^{-1}$, where V,T, and W are design matrices. In the sequel, to obtain the feedback matrix, the Alexandridis-Paraskevopoulos algorithm is modified. A simple algorithm is proposed under a less restrictive Kimura condition (it is now assumed that $n \leq mp$). It should be noted that in contrast to [5], the proposed algorithm uses a coordinate transformation and reduced order system to alleviate the computational burden. Both techniques are based on the subspace intersection condition, $Ker\,(T) \cap Ker\,(C) = \{0\}$, which was obtained in [5].

Considered the linear time-invariant system described by

$$\dot{x}(t) = Ax(t) + Bu(t) \tag{1.1}$$

$$y(t) = Cx(t) \tag{1.2}$$

where $x \in \mathcal{X} \sim \Re^n$, $u \in \mathcal{U} \sim \Re^m$, $y \in \mathcal{Y} \sim \Re^p$. It is assumed that B is full column-rank , C is full row-rank and that (C, A, B) is stabilizable and detectable.

The problem here is to find a static output feedback control law

$$u(t) = Gy(t) \quad , \quad G \in \Re^{m\times p} \tag{1.3}$$

such that $\sigma(A + BGC) \in \mathcal{C}^-$, or equivalently, the closed-loop system is asymptotically stable, where $\sigma(A + BGC) = \{\lambda_1, \lambda_2, \ldots, \lambda_n\}$ is the set of eigenvalues of $A + BGC$.

The reminder of the paper is organized in as follows. In Section 2, basic concepts on geometric control are introduced. Section 3 presents the main contributions of the paper: the proposed algorithms for obtaining the feedback gain matrix with examples. Finally, in Section 4, the conclusions of the paper are presented.

2. Invariant Subspaces and Coupled Sylvester Equations

In this Section some concepts and definitions on geometric control theory are introduced [17]. A subspace $\mathcal{V} \subset \mathcal{X}$ is (A, B)-invariant if there exists $K : \mathcal{X} \longrightarrow \mathcal{Y}$, such that $(A + BK)\mathcal{V} \subset \mathcal{V}$, or, equivalently , if $A\mathcal{V} \subset \mathcal{V} + Im\,B$. In a dual manner, a

subspace $\mathcal{T} \subset \mathcal{X}$ is (C, A)-invariant if exist $F : \mathcal{Y} \longrightarrow \mathcal{X}$, such that $(A+FC)\mathcal{T} \subset \mathcal{T}$, or, equivalently, if $\mathcal{T} \supset A(\mathcal{T} \cap Ker\,(C))$.

Definition 2.1. *[14], [16] A subspace $\mathcal{V} \subset \mathcal{X}$, of dimension v , is (C, A, B)-invariant if $\mathcal{V}$ is (A, B)-invariant and (C, A)-invariant.*

Consider $V \in \Re^{v\times v}$, such that $Im\,(V) = \mathcal{V}$, and let $T \in \Re^{(n-v)\times v}$ be a left annihilator of V, *i.e.*, $Ker\,(T) = Im\,(V)$. The definition 2.1 is equivalent to the existence of matrices ($H_V \in \Re^{v\times v}$, $W \in \Re^{m\times v}$) and ($H_T \in \Re^{n-v\times n-v}$, $U \in \Re^{(n-v)\times v}$), which are solutions of the following *coupled Sylvester Equations*

$$AV - VH_V = -BW \tag{2.1}$$
$$TA - H_T T = -UC \tag{2.2}$$
$$TV = 0. \tag{2.3}$$

The definition 2.1 and the equations (2.1) , (2.2), and (2.3) have a crucial importance in static output feedback via eigenstructure assignment [12] [14].

The properties of stabilizability and detectability are considered, respectively, by using two definitions
(i) a subspace (A, B)-invariant $\mathcal{V}$ is (A, B)-inner stabilizable subspace, or, equivalently, there exists K such that $(A + BK)|\mathcal{V}$ is asymptotically stable ; and
(ii) a subspace (C, A)-invariant $\mathcal{V}$ is (C, A)-outer detectable subspace if there exist F such that $(A + FC)|\mathcal{X}/\mathcal{V}$ is asymptotically stable.

Definition 2.2. *[14] A subspace $\mathcal{V}$, of dimension v, is (C, A, B)-invariant output stabilizable subspace , (or simply O.S. (C, A, B)-invariant [4]) if $\mathcal{V}$ is (A, B)-inner stabilizable and (C, A)-outer detectable.*

Thus, a necessary and sufficient condition for the existence of $\mathcal{V} = Im(V)$ or *O.S.* (C, A, B)-invariant subspace is that (2.1), (2.2) and (2.3) are verified with the additional condition of stability

$$\sigma(H_V) \in \mathcal{C}^- \tag{2.4}$$
$$\sigma(H_T) \in \mathcal{C}^- . \tag{2.5}$$

Theorem 2.1, in what follows, relates the concept of *O.S.* (C, A, B)-invariant subspace to the existence of a static output feedback control law (1.3), which stabilizes the closed loop system.

Theorem 2.1. *[5] There exists a static output feedback matrix $G : \mathcal{Y} \longrightarrow \mathcal{U}$ such that $\sigma(A + BGC) \in \mathcal{C}^-$, if and only if the following conditions hold true for some matrices ($V \in \Re^{n\times v}, H_V \in \Re^{v\times v}, W \in \Re^{m\times v}$), ($T \in \Re^{n-v\times n}, H_T \in \Re^{n-v\times n-v}, U \in \Re^{n-v\times v}$), and for some positive integer $v \leq n$*

$$AV - VH_V = -BW, \textit{ with } \sigma(H_V) \in \mathcal{C}^- \tag{2.6}$$
$$TA - H_T T = -UC, \textit{ with } \sigma(H_T) \in \mathcal{C}^- \tag{2.7}$$
$$TV = 0 \tag{2.8}$$
$$Ker\,(CV) \subseteq Ker\,(W) \tag{2.9}$$
$$Ker\,(B'T') \subseteq Ker\,(U') \tag{2.10}$$

[4] Output Stabilizable (C,A,B)-invariant [14] [4]

where $rank\,(V) = v$ *and* $rank\,(T) = n - v$.

It is interesting to notice that these results have been presented and explored under different forms in the literature related to eigenstructure assignment by output feedback (see [15]). The presented statement corresponds to Theorem 3.2 in [14]. The *coupled Sylvester Equations* (2.6), (2.7), and (2.8) describe some geometric properties of the subspace $\mathcal{V} = Im\,(V)$. Under stability of the matrix H_V, the equation (2.6) means that the subspace $\mathcal{V} = Im\,(V)$ must be (A, B)-inner stabilizable. In a dual manner, the subspace $Ker\,(T) = \mathcal{V}$ must be (C, A)-outer detectable, see (2.7). Thus, the coupling condition (2.8), the existence of $\mathcal{V} = Ker\,(T)$ $O.S.$ (C, A, B)-invariant subspace, and the conditions (2.9) and (2.10), are necessary and sufficient conditions for the existence of a matrix G.

Also, note that the conditions (2.9) and (2.10) correspond to the existence of a matrix $G \in \Re^{m\times p}$, which verifies the following two equalities

$$GCV = W \tag{2.11}$$

$$TBG = U, \tag{2.12}$$

where the closed loop system has eigenvalues given by

$$\sigma(A + BGC) = \sigma(H_V)\,\dot{\cup}\,\sigma(H_T).$$

3. Algorithmic Aspects

In this section, based on a subspace intersection condition, i.e., $Ker\,(T) \cap Ker\,(C) = \{0\}$ [5], two algorithms to eigenstructure assignment are presented. Motivated by the algorithm of Syrmos and Lewis [12], the first technique solves the coupled Sylvester equations in two steps, and can directly be applied to systems that verify the Kimura condition [11]. The second technique is based on the algorithm proposed by Alexandridis and Paraskevopoulos [1]. It uses a system representation in an adequate base of the state space to rewrite the Sylvester equations in a set of bilinear algebraic equations. The Proposed techniques assume that the dimension p of the output is the same as $\mathcal{V} = Im\,(V)$. Also, it is guaranteed that the matrix $CV \in \Re^{p\times p}$ is invertible, so that $G = W(CV)^{-1}$, see (2.11).

The set of the desired closed loop poles is denoted by $\Lambda = \{\lambda_1, \ldots, \lambda_{n-p}, \lambda_{n-p+1}, \ldots, \lambda_n\} = \{\Lambda_T, \Lambda_V\}$, where Λ_T and Λ_V are autoconjugated. $H_V \in \Re^{p\times p}$ and $H_T \in \Re^{(n-p)\times(n-p)}$ are defined as $\sigma(H_T) = \Lambda_T = \{\lambda_1, \ldots, \lambda_{n-p}\}$ and $\sigma(H_V) = \Lambda_V = \{\lambda_{n-p+1}, \ldots, \lambda_n\}$. For simplicity, it is considered that the elements of $\Lambda = \sigma(A + BGC)$ are all distinct.

3.1. Modified algorithm of Syrmos and Lewis

Based on Theorem 2.1, the following algorithm, considered in [12], can be used to obtain an output feedback matrix that stabilizes the closed loop system, when the Kimura condition, $n < m + p$, is verified.

Step 1: Select the matrix $H_T \in \Re^{n-p\times n-p}$, where $\sigma(H_T) = \Lambda_T \in \mathcal{C}^-$, and solve (2.7) to find the matrix $T \in \Re^{n-p\times n}$, such that

$$rank\left(\left[\begin{array}{c} T \\ C \end{array}\right]\right) = n \Longleftrightarrow Ker\ T \cap Ker\ C = \{0\}. \tag{3.1}$$

Step 2.1: Solve (2.6) for some matrix $H_V \in \Re^{p\times p}$, where $\sigma(H_V) = \Lambda_V \in \mathcal{C}^-$, whereas the matrix V satisfy the coupling condition (2.8) and $rank\,(V)$ is equal to p.
Step 2.2: By construction, the relation (3.1) guarantees that rank $(CV) = p$. Then G can be calculated as unique solution of (2.11).

Remark 3.1. *Steps* 1 *and* 2 *can be implemented by using standard techniques for eigenstructure assignment. By considering* H_T *e* H_V *in the Jordan form, the following procedure can be adopted:*

Step 1: *Find* $t_j \in \mathcal{C}^n$ *and* $u_j \in \mathcal{C}^p$*, such that*

$$\left[\begin{array}{cc} t_j' & u_j' \end{array}\right]\left[\begin{array}{c} A-\lambda_j I \\ C \end{array}\right] = 0\ \forall\ j = 1,\ldots,n-p \tag{3.2}$$

The row matrix $T \in \Re^{(n-p)\times n}$*, denoted for* T_j*, is constructed by using the vectors* t_j*, as follows*

- *if* $\lambda_j \in \Re$*, then* $T_j = t_j'$*;*
- *if* $\lambda_j \in \mathcal{C}$*, then* $\lambda_{j+1} = \lambda_j^*$ *and* $\left\{\begin{array}{c} T_j = Re\,(t_j') \\ T_{j+1} = Imag\,(t_j') \end{array}\right.$.

Step 2 : *To determine* $v_i \in \mathcal{C}^n$ *and* $w_i \in \mathcal{C}^n$ *we have*

$$\left[\begin{array}{cc} A-\lambda_i I & B \\ T & 0 \end{array}\right]\left[\begin{array}{c} v_i \\ w_i \end{array}\right] = 0\ \forall\ i = n-p+1,\ldots,n. \tag{3.3}$$

In similar form to the previous case, the used matrices V *and* W *can only be built with real elements. In particular, if* $\lambda_i \in \mathcal{C}$*, then* $\lambda_{i+1} = \lambda_i^*$ *and*
$\left\{\begin{array}{ll} V_i = Re\,(v_i), & V_{i+1} = Imag\,(v_i) \\ W_i = Re\,(w_i), & W_{i+1} = Imag\,(w_i) \end{array}\right.$ *, where* v_i *and* w_i *denote the columns of the matrices* V *and* W*, respectively.*

Remark 3.2. *[5] Step* 1*, in Remark 3.1, is concerned with the choice of a matrix* T*, which verifies (3.2). Step* 2 *is concerned with the solution of (2.6) and (2.8), to obtain the (A,B)-invariant of* $Ker\,(T)$*. This property is associated to the "zero equation" (3.3) [3]. To guarantee the freely placement of the eigenvalues* λ_i *in step* 2 *, the system matrix* $P(\lambda) = \left[\begin{array}{cc} A-\lambda I & B \\ T & 0 \end{array}\right]$ *of dimension* $(2n-p)\times(n+m)$*, must be row-full rank* $\forall\lambda$*. The algorithm is based in the fact that under Kimura condition,* $m+p > n$*,* $P(\lambda)$ *does not lose rank for almost all triples* (A,B,T) *[13]. Thus the zero equation (3.3) has solutions for all* λ_i*. In the presence of invariant zeros, it is possible to remake Step* 1 *to search other solutions for the Sylvester equation (2.6).*

Remark 3.3. *In the less restrictive case $m+p=n$, $P(\lambda)$ is square of dimension $(2n-p)\times(2n-p)$, and all triple (A,B,T) has p finite invariant zeros [12]. In this case, the basic procedure can produce stabilizing solutions only if T, found in step 1, generates p stable invariant zeros, which have to be used to solve (3.3) [3].*

Example 3.1. *Consider the linear system defined by [9]:*

$$A=\begin{bmatrix} 0 & 1 & 0 & 0 \\ 1 & 1 & 0 & 0 \\ -1 & 0 & 0 & 0 \\ 0 & 0 & 0 & 0 \end{bmatrix};\quad B=\begin{bmatrix} 0 & 0 \\ 1 & 0 \\ 0 & 0 \\ 0 & 1 \end{bmatrix};\quad C=\begin{bmatrix} 1 & 0 & 0 & 0 \\ 0 & 0 & 1 & 0 \\ 0 & 0 & 0 & 1 \end{bmatrix}.$$

The system is controllable and observable and $m+p=5>n$. The desired eigenvalues are $\Lambda_T=\{-4\}\cup\Lambda_V=\{-3,-2,-1\}$.
Step 1: *By considering that $\lambda_1=-4$, and using (3.2) we have* $T=\begin{bmatrix} -0.3148 & 0.0630 & -0.2406 & -0.2425 \end{bmatrix}$, *where (A,B,T) has not invariant zeros*
Step 2.1: *For $\lambda_2=-3$, $\lambda_3=-2$ and $\lambda_4=-1$, by using (3.3) we have*

$$V=\begin{bmatrix} 0.0727 & 0.1324 & 0.2425 \\ -0.2182 & -0.2649 & -0.2425 \\ 0.0242 & -0.0662 & 0.2225 \\ -0.1751 & -0.3064 & -0.6184 \end{bmatrix},\quad W=\begin{bmatrix} 0.7999 & 0.6622 & -0.2424 \\ 0.5254 & 0.6128 & -0.6184 \end{bmatrix}.$$

Step 2.2: *Based on $GCV=W$, we have* $G=\begin{bmatrix} -46.9778 & -20.7333 & -26.9444 \\ -16.1410 & -9.3519 & -10.9968 \end{bmatrix}$. *The closed loop matrix $A_G=A+BGC$ is then*

$$A_G=\begin{bmatrix} 0.0000 & 1.0000 & 0.0000 & 0.0000 \\ -45.97778 & 1 & -20.7333 & -26.9444 \\ -1.0000 & 0.0000 & 0.0000 & 0.0000 \\ -16.1410 & 0.0000 & -9.3519 & -10.9968 \end{bmatrix}.$$

3.2. Modified algorithm of Alexandridis and Paraskevopoulos

The presented technique is based on the use of coordinate transformations, obtained from the matrix C, that allows the solution of equation (3.2) by using a auxiliary system of reduced order $n-p$.

This type of decomposition is used in control theory, mainly for the construction of minimum order observers [1], [6]. From a geometric point of view, it aims at the construction of a subspace $\mathcal{V}=Ker\,(T)$ outer stabilizable, and to guarantee $Ker\,(T)\cap Ker\,(C)=\{0\}$.

Consider a base change given by

$$x=\begin{bmatrix} P_1 & P_2 \end{bmatrix}\begin{bmatrix} x_1 \\ x_2 \end{bmatrix}, \tag{3.4}$$
$$P_1\in\Re^{n\times p},\quad P_2\in\Re^{n\times n-p},$$

where $P=\begin{bmatrix} P_1 & P_2 \end{bmatrix}$ is nonsingular such that

$$C\begin{bmatrix} P_1 & P_2 \end{bmatrix}=\begin{bmatrix} C_1 & 0 \end{bmatrix}, \tag{3.5}$$
$$\text{with}\quad C_1\in\Re^{p\times p}\quad\text{and}\quad rank(C_1)=p.$$

The inverse of P is denoted for $\bar{P} = \begin{bmatrix} \bar{P}_1' \\ \bar{P}_2' \end{bmatrix}$, where $\bar{P}_1 \in \Re^{n\times p}$, $\bar{P}_2 \in \Re^{n\times n-p}$, and $\begin{bmatrix} P_1 & P_2 \end{bmatrix} \begin{bmatrix} \bar{P}_1' \\ \bar{P}_2' \end{bmatrix} = I_n$.

In this base, the open loop system can be rewritten as

$$\begin{aligned} \begin{bmatrix} \dot{x_1}(t) \\ \dot{x_2}(t) \end{bmatrix} &= \begin{bmatrix} A_{11} & A_{12} \\ A_{21} & A_{22} \end{bmatrix} \begin{bmatrix} x_1(t) \\ x_2(t) \end{bmatrix} + \begin{bmatrix} B_1 \\ B_2 \end{bmatrix} u(t) \\ y(t) &= \begin{bmatrix} C_1 & 0 \end{bmatrix} \begin{bmatrix} x_1(t) \\ x_2(t) \end{bmatrix} \end{aligned} \tag{3.6}$$

where, in particular, $A_{12} \in \Re^{p\times n-p}$ and $A_{22} \in \Re^{n-p\times n-p}$.

Lemma 3.1. *If (C, A) is observable, then there exists a $T \in \Re^{n-p\times p}$ such that (2.7) is verified and $Ker\,(T) \cap Ker\,(C) = \{0\}$.*

Proof. As shown in [6], the observability of the pair (C, A) is equivalent to the observability of the pair (A_{12}, A_{22}). $T_2 \in \Re^{(n-p)\times(n-p)}$, with $rank\,(T_2) = n - p$, and $T_1 \in \Re^{(n-p)\times p}$, are solutions of the Sylvester equations of *order-reduced*

$$T_2 A_{22} - H_T T_2 = -T_1 A_{12} \;\;,\;\; \sigma(H_T) \in \mathcal{C}^- \tag{3.7}$$

where $H_T \in \Re^{n-p\times n-p}$ is chosen such that $\sigma(H_T) \in \mathcal{C}^-$. Note that in general it is possible to find T_2 invertible when H_T does not contain the eigenvalues from matrix A_{22} [1]. Then, calculate $U \in \Re^{n-p\times p}$ as unique solution of

$$UC_1 = -\left(T_1 A_{11} + T_2 A_{21} - H_T T_1\right). \tag{3.8}$$

Jointly, (3.7) and (3.8) verify

$$\begin{bmatrix} T_1 & T_2 \end{bmatrix} \begin{bmatrix} A_{11} & A_{12} \\ A_{21} & A_{22} \end{bmatrix} - H_T \begin{bmatrix} T_1 & T_2 \end{bmatrix} = U \begin{bmatrix} C_1 & 0 \end{bmatrix}$$

which, in the original base, corresponds to Sylvester equation (2.7). Moreover, as T_2 is invertible, we have

$$rank\left(\begin{bmatrix} T \\ C \end{bmatrix} = \begin{bmatrix} T_1 & T_2 \\ C_1 & 0 \end{bmatrix} \begin{bmatrix} \bar{P}_1' \\ \bar{P}_2' \end{bmatrix}\right) = n \Longleftrightarrow Ker\,(T) \cap Ker\,(C) = \{0\}. \qquad \square$$

Equations (2.7) and (3.7) are related to the construction of minimum order observers [6] [1]. Consider the eigenvalues of $(A_{22} + L_2 A_{12})$, where $L_2 \in \Re^{n-p\times p}$ is such that

$$T_2 L_2 = T_1. \tag{3.9}$$

Then, substituting (3.9) into (3.7) it follows that

$$T_2(A_{22} + L_2 A_{12}) = H_T T_2 \tag{3.10}$$

or

$$\sigma(H_T) = \sigma(A_{22} + L_2 A_{12}) \in \mathcal{C},$$

Note that the decomposition of P is not unique. In particular, it can computationally be obtained through ortogonal transformations, $\bar{P} = P'$ [1] [4]. In what follows, in Theorem 3.1, a better alternative than the introduced by Alexandridis-Paraskevopoulos in [1] is proposed to alliviate the computational burden.

Theorem 3.1. *Given the system (1.1), (1.2). Consider a decomposition in the form (3.6). Then, the matrix G verifies* $\sigma(A + BGC) = \sigma(H_V) \dot{\cup} \sigma(H_T)$*, if and only if,*

$$\left[\begin{array}{cc} T_1 & T_2 \end{array} \right] \left[\begin{array}{c} \bar{P}_1' \\ \bar{P}_2' \end{array} \right] V \;\; = \;\; 0, \tag{3.11}$$

where $(W \in \Re^{m\times p}, V \in \Re^{n\times p})$ *and* $(T_1 \in \Re^{n-p\times p}, T_2 \in \Re^{n-p\times n-p})$ *satisfy the Sylvester equation (2.6) and (3.7),respectively, with* $det\,(CV) \neq 0$*.*

Proof. Necessity: It is considered that there exists an output feedback matrix $G \in \Re^{m\times v}$, so that the closed loop system is asymptotically stable, i.e., the Sylvester equations are verified for some positive $v \leq n$ and matrices T and V, such that $TV = 0$. More precisely,

$$\begin{array}{rcl} AV - VH_V & = & -BW \;, \;\; \text{with } \sigma(H_V) \in \mathcal{C}^- \\ TA - H_T T & = & -UC \;, \;\; \text{with } \sigma(H_T) \in \mathcal{C}^- \\ TV & = & 0 \\ Ker\,(CV) & \subseteq & Ker\,(W) \\ Ker\,(B'T') & \subseteq & Ker\,(U') \end{array}$$

where $rank\,(V) = v$ and $rank\,(T) = n - v$.

Under observability (detectability) condition, it is possible to find a matrix T. Once the matriz T is constructed, Step 2 allows the solution of (2.6) and (2.8), i.e., the (A,B)-invariant of $Ker\,(T)$.

Consider

$$x = \left[\begin{array}{cc} P_1 & P_2 \end{array} \right] \left[\begin{array}{c} x_1 \\ x_2 \end{array} \right] \qquad P_1 \in \Re^{n\times p}, \;\; P_2 \in \Re^{n\times n-p}, \tag{3.12}$$

where $P = \left[\begin{array}{cc} P_1 & P_2 \end{array} \right]$ is a nonsingular matrix so that

$$C \left[\begin{array}{cc} P_1 & P_2 \end{array} \right] = \left[\begin{array}{cc} C_1 & 0 \end{array} \right] \;, \;\; \text{with} \;\; C_1 \in \Re^{p\times p} \;\; \text{and} \;\; rank(C_1) = p. \tag{3.13}$$

The inverse of P is denoted by $\bar{P} = \left[\begin{array}{c} \bar{P}_1' \\ \bar{P}_2' \end{array} \right]$. Based on (3.6) and Lemma 3.1, it is possible to conclude that the observability of (C, A) is equivalent to the observability of (A_{12}, A_{22}). With change of base (3.4), we obtain T_1 e T_2 as

$$T_2 A_{22} - H_T T_2 \;\; = \;\; -T_1 A_{12} \;\; , \;\; \sigma(H_T) \in \mathcal{C}^- \;\; .$$

Hence, $\left(\left[\begin{array}{c} TV \end{array} \right] = \left[\begin{array}{cc} T_1 & T_2 \end{array} \right] \left[\begin{array}{c} \bar{P}_1' \\ \bar{P}_2' \end{array} \right] V \right) = 0$. Consequently,

$$\begin{array}{rcl} AV - VH_V & = & -BW \;, \;\; \text{with } \sigma(H_V) \in \mathcal{C}^- \\ T_2 A_{22} - H_T T_2 & = & -T_1 A_{12} \;\; , \;\; \sigma(H_T) \in \mathcal{C}^- \\ TV & = & 0. \end{array}$$

Sufficiency: Consider

$$\left[\begin{array}{cc} T_1 & T_2 \end{array}\right]\left[\begin{array}{c} \bar{P}_1' \\ \bar{P}_2' \end{array}\right] V \;=\; 0 \tag{3.14}$$

Then, the matrices $(W \in \Re^{m\times p}, V \in \Re^{n\times p})$ and $(T_1 \in \Re^{n-p\times p}, T_2 \in \Re^{n-p\times n-p})$ satisfy (2.6) and (3.7), respectively, where $det\,(CV) \neq 0$.

The matrix $H_T \in \Re^{n-p\times n-p}$ is choosed so that $\sigma(H_T) = \Lambda_T \in \mathcal{C}^-$ and (2.7) is resolved to find $T \in \Re^{n-p\times n}$ such that

$$rank\,\left(\left[\begin{array}{c} T \\ C \end{array}\right]\right) = n \Longleftrightarrow Ker\; T \cap Ker\; C = \{0\} \tag{3.15}$$

Equation (2.6) is solved, for some matrix $H_V \in \Re^{p\times p}$, so that $\sigma(H_V) = \Lambda_V \in \mathcal{C}^-$ and by considering that V verifies (2.8) and $rank\,(V)$ must be p. By construction, (3.1) ensures that $\text{rank}\,(CV) = p$ and G can be computed as the unique solution of (2.11). □

From the formulation presented in Theorem 3.1, the following procedure is proposed in [1] to poles assignment, when $mp \geq n$.

3.2.1. Procedure for the determination of output feedback matrix

Considering that H_V and H_T are in Jordan form, from (2.6) W and V can be written as

$$W = \left[\begin{array}{cccc} w_1, & w_2, & \ldots, & w_p \end{array}\right]; \tag{3.16}$$

$$V = \left[\begin{array}{cccc} X^1 w_1, & X^2 w_2, & \ldots, & X^p w_p \end{array}\right]. \tag{3.17}$$

where

$$X^i = (\lambda_i I - A)^{-1} B, \quad for \quad i = 1, \ldots, p. \tag{3.18}$$

Similarly, from (3.7) T_1 and T_2 can be written as

$$T_1 = \left[\begin{array}{c} \phi_{p+1}' \\ \phi_{p+2}' \\ \vdots \\ \phi_n' \end{array}\right] \quad and \quad T_2 = \left[\begin{array}{c} \psi_{p+1}' \\ \psi_{p+2}' \\ \vdots \\ \psi_n' \end{array}\right]$$

where ψ_j , $\forall j = p+1, \ldots, n$, can be obtain as

$$\psi_j' = \phi' A_{12} (\lambda_j I - A_{22})^{-1}. \tag{3.19}$$

From the notation above, the coupling equation (3.11) can be written in the form of a bilinear system of algebraic equations. Thus, substituting (3.18) and (3.19) in (3.11), we have

$$\begin{array}{l} \phi_j' \left[\begin{array}{cc} I_p & A_{12}[\lambda_j I - A_{22}]^{-1} \bar{P}_1' \\ \bar{P}_2' & \end{array}\right] X^i w_i = 0 \\ for \quad i = 1, , \ldots, p \quad and \quad j = p+1, \ldots, n. \end{array} \tag{3.20}$$

By solving (3.20), the parameters for w_i and ϕ'_j are determined. Then, the matrices W and V are defined based on (3.16), and the output feedback matrix G is directly calculated from (2.11). By using this formulation, the justification to the case $n \leq mp$ is given in [1]. "The equation (3.16) provides $p(m-1)$ free parameters (based on the arbitrary elements of $w_1, w_2, \ldots, w_p$). Additionally the equation (3.19) provides $(p-1)(n-p)$ free parameters (from the arbitrary elements of $\phi_{p+1}, \phi_{p+2}, \ldots, \phi_n$). On the other hand the equation (3.20) results in a system of $p(n-p)$ independent equations. Hence, for the solution existence, the number of equations must be equal or smaller than the addition of free parameters. After algebraic manipulations, the condition $mp \geq n$" is obtained .

Example 3.2. *Consider the previous example where* $C = \begin{bmatrix} 0 & 0 & 1 & 0 \\ 0 & 0 & 0 & 1 \end{bmatrix}$. *The corresponding system is controllable and observable* $mp = 4 = n$, $p = 2$ *and* $m = 2$. *The desired eigenvalues are* $\Lambda_V = \{-1, -2\}$ *and* $\Lambda_T = \{-3, -4\}$. *By using (3.6), a decomposition* P *is founded i.e.,* $P = \begin{bmatrix} 0 & 0 & 1 & 0 \\ 0 & 0 & 0 & 1 \\ 1 & 0 & 0 & 0 \\ 0 & 1 & 0 & 0 \end{bmatrix}$ *such that* $C \begin{bmatrix} P_1 & P_2 \end{bmatrix} = \begin{bmatrix} \bar{C}_1 & 0 \end{bmatrix} = \begin{bmatrix} 1 & 0 & 0 & 0 \\ 0 & 1 & 0 & 0 \end{bmatrix}$. *Then* $\begin{bmatrix} A_{12} \\ A_{22} \end{bmatrix} = \begin{bmatrix} \bar{P}'_1 \\ \bar{P}'_2 \end{bmatrix}$ $AP_2 = \begin{bmatrix} 0 & 0 \\ -1 & 0 \\ 0 & 1 \\ 0 & 0 \end{bmatrix}$.

For $\lambda_1 = -1, \lambda_2 = -2$, *two free parameters in* $\begin{bmatrix} w_1 & w_2 \end{bmatrix} = \begin{bmatrix} 1.0 & 1.0 \\ w_{12} & w_{22} \end{bmatrix}$ *are fixed,* $w_{12} = -2.2$ *and* $w_{22} = 2.8$. *On the other hand, for* $\lambda_3 = -3, \lambda_4 = -4$, *two free parameters in* $\begin{bmatrix} \phi'_3 \\ \phi'_4 \end{bmatrix} = \begin{bmatrix} 1.0000 & \phi_{32} \\ 1.0000 & \phi_{42} \end{bmatrix}$ *are fixed to obtain* $\phi_{32} = -1.6364$ *and* $\phi_{42} = -1.8824$. *By using the previous procedure, the matrices* (W, V) *and* (T_1, T_2, T), *which satisfy the Sylvester equations (2.6), (3.7) and (3.20), with* $det(CV) \neq 0$, *are determined as follows*

$$V = \begin{bmatrix} 0.6 & -0.8 \\ -1.6 & 0.6 \\ 1.6 & -1.2 \\ 0.6 & -0.4 \end{bmatrix}; \quad W = \begin{bmatrix} 1.0 & 1.0 \\ -2.2 & 2.8 \end{bmatrix};$$

$$T_1 = \begin{bmatrix} 1.0000 & -1.6364 \\ 1.0000 & -1.8824 \end{bmatrix}; \quad T_2 = \begin{bmatrix} -0.5455 & 0.1818 \\ -0.4706 & 0.1176 \end{bmatrix};$$

$$T = \begin{bmatrix} T_1 & T_2 \end{bmatrix} \begin{bmatrix} \bar{P}'_1 \\ \bar{P}'_2 \end{bmatrix} = \begin{bmatrix} -0.5455 & 0.1818 & 1.0000 & -1.6364 \\ -0.4706 & 0.1176 & 1.0000 & -1.8824 \end{bmatrix}.$$

The system (A, B, T) *has stable eigenvalues,* $\{-1, -2\}$, *as invariant zeros. The output feedback matrix* G *is determined by* $GCV = W$, *i.e.,* $G = \begin{bmatrix} -12.5 & 35.0 \\ -10.0 & 23.0 \end{bmatrix}$.

The closed loop matrix $A_G = A + BGC$*, whose eigenvalues are the desired ones, is given by* $A_G = \begin{bmatrix} 0.0 & 1.0 & -12.5 & 35.0 \\ 0.0 & 0.0 & 1.0 & 0.0 \\ 0.0 & 0.0 & -10.0 & 24.0 \\ -1.0 & 0.0 & 0.0 & 0.0 \end{bmatrix}$.

4. Conclusion

In this paper two computational algorithms were proposed to obtain the output feedback matrix gain in stabilization problems of linear systems. In the first, two coupled Sylvester equations, based on the concept of *O.S.* (C, A, B)-invariant subspace, were presented to compute the output feedback matrix. In the second, the Syrmos-Lewis and Alexandridis-Paraskevopoulos algorithms were modified by using the presented methodology to alleviate the computational burden and previous asumption on system structure.

Resumo. Este artigo apresenta em forma sistemática algoritmos computacionais para se obter a matriz de realimentação de saídas em problemas de estabilização de sistemas lineares. Baseado no conceito de (C, A, B)-subespaços invariantes, introduzido anteriormente pelo primeiro autor, e através do uso da solução de equações de Sylvester acopladas obtém-se a matriz de realimentação de saída. Dois algoritmos são apresentados: 1) modificação do algoritmo Syrmos-Lewis para fornecer um método mais adequado para solução numérica, e 2) utilizando transformações ortogonais modifica-se o algoritmo de Alexandridis-Paraskevopoulos com o objetivo de superar, em parte, a condição de Kimura. Exemplos numéricos são apresentados para ilustrar a aplicação dos algoritmos.

References

[1] A.T. Alexandridis, P.N. Paraskevopoulos, A new approach to eigenstructure assignment by output feedback, *IEEE Transactions on Automatic Control*, **41**, No. 7 (1996), 1046–1050.

[2] O. Bachelier, J. Bosche, D. Mehdi, On pole placement via eigenstructure assignment approach, *IEEE Transactions on Automatic Control*, **51**, No. 9 (2006), 1554–1558.

[3] E.B. Castelan, J.C. Hennet, Eigenstructure assignment for state constrained linear continuos time systems, *Automatica*, **28**, No. 3 (1993), 605–611.

[4] E.B. Castelan, J.C. Hennet, E.R.Ll. Villarreal, Quadratic characterization and use of output stabilizable subspaces, in "Proceedings (CD) of the 8th Mediterranean Conference on Control and Automation", Greece, 2000.

[5] E.B. Castelan, J.C. Hennet, E.R.Ll. Villarreal, Quadratic characterization and use of output stabilizable subspaces, *IEEE Transactions on Automatic Control*, **48**, No. 4 (2003), 654–660.

[6] C.T. Chen, "Linear System Theory ans Design", Holt, Rinehart and Winston, 1996.

[7] L. Dai, "Singular Control System", Springer-Verlag, 1989.

[8] J. Dong, G.-H. Yang,Static output feedback control synthesis for linear systems with time-invariant parametric uncertainties, *IEEE Transactions on Automatic Control*, **52**, No. 10 (2007), 1930–1936.

[9] L.R. Fletcher, J. Kautsky, G.K.G. Kolka, N.K. Nichols, Eigenstructure assingment by output feedback in descriptor systems, *IEEE Transactions on Automatic Control*, **42**, No. 4 (1985), 1457–1468.

[10] Y. He, Q.-G. Wang, An improved ILMI method for static output feedback control with application to multivariable PID control, *IEEE Transactions on Automatic Control*, **51**, No. 10 (2006), 1678–1683.

[11] H. Kimura, Pole assignment by gain ouptup feedback, *IEEE Transactions on Automatic Control*, **20**, No. 4 (1975) 509–516.

[12] V.L. Syrmos, F.L. Lewis, Output feedback eigenstructure assignment using two Sylvester equations, *IEEE Transactions on Automatic Control*, **38**, No. 3 (1993), 495–499.

[13] V.L. Syrmos, F.L. Lewis, Transmission zero assignment using descriptions, *IEEE Transactions on Automatic Control*, **38**, No. 7 (1993), 1115–1120.

[14] V.L. Syrmos, F.L. Lewis, Bilinear formulation for the output feedback problem in linear system, *IEEE Transactions on Automatic Control*, **39**, No. 2 (1994), 410–414.

[15] V.L. Syrmos, C.T. Abdallah, P. Dorato, K. Grigoriadis, Static output feedback - a survey, *Automatica*, **33**, No. 2 (1997), 125–137.

[16] E.R.Ll. Villarreal, J.D. Lima, Approach for stabilization by output feedback, invariant subspaces and Sylvester equations, in "Anais CNMAC 2008", Belém, PA, Brasil.

[17] W.M. Wonahm, "Linear Multivariable Control, a Geometric Approach", Springer-Verlag, 1979.

where $\xi = (1-d)\beta_0 + d\mu_0$. It follows that $M > 0$, if and only if

$$\frac{1}{\epsilon} > \nu_0 + \frac{\xi^2}{4\alpha_0 d(1-d)} = \nu_0 + \frac{1}{4\alpha_0}\left(\mu_0\sqrt{\frac{d}{1-d}} + \beta_0\sqrt{\frac{1-d}{d}}\right)^2$$

holds. Note that the function $f(s) = as + b/s$ $(a, b, s > 0)$ takes the minimum $2\sqrt{ab}$ at $s^* = \sqrt{b/a}$. Therefore, ϵ^* is the maximum value such that $M > 0$ for all $\epsilon \in (0, \epsilon^*)$, which in turn ensures asymptotic stability for the feedback system in Fig. 5. ■

It should be mentioned that if $\mathcal{B}_{x_0}$ in Assumptions (i) and (ii) is replaced by R^n with n the dimension of the state variable vector $x_0(t)$ as in (12), then global or semiglobal asymptotic stability can be claimed in both Theorem 3.5 and Corollary 3.6. In this case, there is a strong connection between our results and that of [2].

IV. Conclusion

Asymptotic stability is investigated for a class of nonlinear feedback systems which employ linear actuators. Two different approaches are employed to analyze and derive conditions for asymptotic stability of the closed-loop nonlinear system, of which one applies to linear actuator dynamics that are strictly minimum phase and have nonsingular high-frequency gain, and the other applies to band-limited linear actuator dynamics that are strictly causal and involve a high-gain integrator. Although precise quantification of the maximum gain parameter ϵ^* is not available, estimates of its positive lower bounds are given explicitly. Hence, the results of this note provide guidance to selection and design of linear actuators to be implemented in the nonlinear feedback system, which is initially designed in absence of the linear actuator.

Acknowledgment

The authors would like to thank one of the anonymous reviewers for bringing [2] to their attention.

References

[1] M. Arcak and P. Kokotović, "Robust nonlinear control of systems with input unmodeled dynamics," *Syst. Control Lett.*, vol. 41, pp. 115–122, 2000.
[2] P. D. Christofides and A. R. Teel, "Singular perturbations and input-to-state stability," *IEEE Trans. Automat. Contr.*, vol. 41, pp. 1645–1650, Nov. 1996.
[3] P. Kokotović, H. K. Khalil, and J. O'Reilly, *Singular Perturbation Methods in Control*. Philadelphia, PA: SIAM, 1999.
[4] Z.-P. Jiang and M. Arcak, "Robust global stabilization with ignored input dynamics: An ISS small-gain approach," *IEEE Trans. Automat. Contr.*, vol. 46, pp. 1411–1415, Sept. 2001.
[5] Z.-P. Jiang, A. R. Teel, and L. Praly, "Small gain theorem for ISS systems and applications," *Math. Control Signals, Syst.*, pp. 95–120, 1994.
[6] I. M. Y. Mareels and D. J. Hill, "Monotone stability of nonlinear feedback systems," *J. Math. Syst. Estimation Control*, pp. 275–291, 1992.
[7] Z. Qu, "Model reference robust control of systems with significant unmodeled dynamics," *Int. J. Robust Nonlinear Control*, vol. 7, pp. 951–974, 1997.
[8] I. W. Sandberg, "An observation concerning the application of the contraction mapping fixed-point theorem and a result concerning the norm-boundedness of solutions of nonlinear functional equations," *Bell Syst. Tech. J.*, pp. 1809–1812, 1965.
[9] E. D. Sontag, "Smooth stabilization and input-to-state stability," *IEEE Trans. Automat. Contr.* , vol. 34, pp. 435–443, Apr. 1989.
[10] ——, "Further facts about input-to-state stabilization," *IEEE Trans. Automat. Contr.*, vol. 35, pp. 376–473, Mar. 1990.
[11] M. Vidyasagar, *Nonlinear Systems Analysis*. Upper Saddle River, NJ: Prentice-Hall, 1993.
[12] J. C. Willems, *The Analysis of Feedback Systems*. Cambridge, MA: MIT Press, 1971.
[13] G. Zames, "On the input-output stability of time-varying nonlinear feedback systems, Part I," *IEEE Trans. Automat. Contr.*, vol. AC-11, pp. 228–238, Apr. 1966.

Quadratic Characterization and Use of Output Stabilizable Subspaces

Eugênio B. Castelan, Jean-Claude Hennet, and Elmer R. Llanos Villarreal

***Abstract*—This note treats the problem of stabilization of linear systems by static output feedback using the concept of (C, A, B)-invariant subspaces. The work provides a new characterization of output stabilizable (C, A, B)-invariant subspaces through two coupled quadratic stabilization conditions. An equivalence is shown between the existence of a solution to this set of conditions and the possibility to stabilize the system by static output feedback. An algorithm is provided and numerical examples are reported to illustrate the approach.**

***Index Terms*—Convex programming, geometric approach, Lyapunov equations, output feedback, quadratic stabilizability.**

I. Introduction

Stabilization of linear systems by static output feedback is recognized as an important and still open problem in control theory. A review of existing approaches and techniques to treat different versions of this problem can be found, for instance, in [14]. Other recent results not covered by this note are found in [1], [7], [9], and [10]

A common feature shared by different methods (Lyapunov, Riccati, linear matrix inequality, or eigenstructure assignment) is that the output feedback stabilization problem is equivalent to obtaining the solution of a coupled set of matrix equations. In particular, through the use of coupled Sylvester equations [11], [13], the output feedback control problem can be decomposed into two stages: 1) determination of a (C, A)-outer detectable subspace and 2) inner stabilization of this subspace.

This note proposes a quadratic counterpart of this result, under a similar decomposition into two stages. In particular, we show that solutions for the first stage can be obtained as solutions of a reduced-order Lyapunov equation. The method then defines a set of coupled Lyapunov- like equations that can be used for construction of an output stabilizable (C, A, B)-invariant subspace, as an intermediate mechanism in the process of designing a static output feedback controller. Furthermore, the quadratic characterization of both stages by Lyapunov

Manuscript received July 17, 2000; revised May 21, 2001, July 9, 2002, and October 10, 2002. Recommended by Associate Editor K. M. Grigoriadis. This work was supported in part by CNPq/Brazil. An earlier version of this note was presented at the 8th IEEE Mediterranean Conference on Control and Automation—MED 2000, Greece, July 2000.

E. B. Castelan and E. R. Llanos Villarreal are with Departamento de Automação e Sistemas 88040-900 Florianópolis (S.C), Brazil (e-mail: eugenio,llanos@das.ufsc.br).

J.-C. Hennet is with the Laboratoire d'Analyse et d'Architecture des Systèmes-LAAS du CNRS, 31077 Toulouse, Cedex 4, France (e-mail: hennet@laas.fr).

Digital Object Identifier 10.1109/TAC.2003.809774

0018-9286/03$17.00 © 2003 IEEE

equations provides a convenient framework for the numerical resolution of the problem through orthogonal transformations and convex programming techniques.

The second section recalls, with a geometric interpretation, a known result that relates the existence of a stabilizing static output feedback to the solution of coupled Sylvester equations. In the third section, the output stabilizing conditions are reformulated in the form of coupled Lyapunov equations. Some connections are established between this characterization and the quadratic stabilizability framework. An algorithmic procedure based on the use of orthogonal decomposition and convex programming techniques is proposed and discussed in Section IV. This approach is illustrated in Section V through numerical examples and some concluding remarks are finally presented.

Notation: For any given matrix $A \in \Re^{n\times n}$, $\mathrm{Im}\ A$ and $\mathrm{Ker}\ A$ represent its Image and Kernel, respectively. The set of eigenvalues of A is represented by $\sigma(A)$. $A \geq B (A > B)$ means that $A - B$ is positive semidefinite (positive definite). If $\mathcal{V} \subset \Re^n$ represents an A-invariant subspace, then $A|\mathcal{V}$ is the restriction of A to $\mathcal{V}$ and $A|(\Re^n)/\mathcal{V})$ is the map induced by A in the quotient space $\Re^n/\mathcal{V}$ [15].

II. Preliminaries

The considered linear time-invariant systems are described by

$$\dot{x}(t) = Ax(t) + Bu(t) \tag{1}$$

$$y(t) = Cx(t) \tag{2}$$

where: $x \in \Re^n$, $u \in \Re^m$, $y \in \Re^p$ and the involved matrices have appropriate dimensions. It is also assumed that B is full column-rank, C is full row-rank and that (C, A, B) is stabilizable and detectable. The studied problem is to find a static output feedback control law

$$u(t) = Ky(t) \tag{3}$$

such that $\sigma(A + BKC) \in \mathcal{C}^-$ or, equivalently, the closed-loop system is asymptotically stable.

Let $V \in \Re^{v\times v}$ be such that $\mathrm{span}(V) = \mathcal{V}$ and $T \in \Re^{(n-v)\times v}$ be a left annihilator of V, i.e, $\mathrm{Ker}\ T = \mathrm{Im}\ V$. The following theorem relates the existence of a stabilizing static output feedback control law (3) to the solution of two coupled Sylvester equations.

Theorem 2.1: There exists a static output feedback matrix $K \in \Re^{m\times p}$ such that $\sigma(A + BKC) \in \mathcal{C}^-$ if and only if the following conditions hold true for some matrices ($V \in \Re^{n\times v}$, $H_V \in \Re^{v\times v}$, $W \in \Re^{m\times v}$), ($T \in \Re^{(n-v)\times n}$, $H_T \in \Re^{(n-v)\times(n-v)}$, $U \in \Re^{(n-v)\times p}$), and for some positive integer $v \leq n$

$$AV - VH_V = -BW, \qquad \text{with } \sigma(H_V) \in \mathcal{C}^- \tag{4}$$

$$TA - H_T T = -UC, \qquad \text{with } \sigma(H_T) \in \mathcal{C}^- \tag{5}$$

$$TV = 0 \tag{6}$$

$$\mathrm{Ker}\, CV \subseteq \mathrm{Ker}\, W \tag{7}$$

$$\mathrm{Ker}\, B'T' \subseteq \mathrm{Ker}\, U' \tag{8}$$

where: $\mathrm{rank}(V) = v$ and $\mathrm{rank}(T) = n - v$. □

The aforementioned result has been presented and exploited under different forms mainly in the literature related to the eigenstructure assignment by output feedback (see [14]). Equations (4), (5), and (6) are recognized as coupled Sylvester equations and describe some geometric properties of subspace $\mathcal{V} = \mathrm{Im}\ V$, that can be summarized as follows (see [13]). Under the stability constraint imposed on matrix H_V, (4) means that $\mathcal{V} = \mathrm{Im}(V)$ must be an (A, B)-inner stabilizable subspace, that is there exists F such that $(A + BF)|\mathcal{V}$ is asymptotically stable. In a dual manner, (5) means that $\mathrm{Ker}\ T$ has to be a (C,A)-outer detectable subspace, that is there exists L such that $(A + LC)|(\Re^n/\mathrm{Ker}\, T)$ is asymptotically stable. Thus, under the coupling condition (6), relations (4) and (5) mean that $\mathcal{V} = \mathrm{Ker}\ T$ is an output stabilizable (OS) (C, A, B) invariant subspace, as defined in [13]. Notice also that inclusion conditions (7) and (8) can be equivalently replaced by

$$KCV = W \tag{9}$$

$$TBK = U. \tag{10}$$

From these comments, we see that the statement of Theorem 2.1 is essentially equivalent to the one of [13, Th. 3.2]. For algorithmic purposes, we shall assume in the sequel that $\mathcal{V}$ is a p-dimensional subspace. This assumption has been also adopted in many works that, explicitly or implicitly, use the coupled-Sylvester equations for eigenstructure assignment by output feedback [1], [8], [11]. Notice also the key role played by coupling condition (6). From a numerical point of view, it introduces a nonlinearity in terms of unknown matrices V and T, in general not easy to handle. However, when Kimura's condition $n < m + p$ is verified, this nonlinearity can be overcome and the coupled Sylvester equations can be solved sequentially. Thus, based on the conditions of Theorem 2.1, the following algorithm allows to compute a stabilizing output feedback when $n < m + p$ [11].

Step 1) Solve (5) to find a matrix $T \in \Re^{(n-p)\times n}$ such that

$$\mathrm{rank}\left(\begin{bmatrix} T \\ C \end{bmatrix}\right) = n \Longleftrightarrow \mathrm{Ker}\, T \cap \mathrm{Ker}\, C = \{0\}. \tag{11}$$

Step 2) Solve (4) and (6) to find $V \in \Re^{n\times p}$ and $W \in \Re^{m\times p}$.

Step 3) By construction, (11) guarantees that $\mathrm{rank}(CV) = p$ and K can be computed by

$$K = W(CV)^{-1}. \tag{12}$$

Steps 1) and 2) can be solved by standard eigenstructure assignment techniques. In particular, solutions for (5) such that (11) is verified can be obtained from an auxiliary reduced order system which is defined from an appropriate decomposition of output matrix C (see the Appendix). Once T has been determined, Step 2) can be solved by using the nonsquare "zero equation"

$$\begin{bmatrix} A - \lambda_i I & B \\ T & 0 \end{bmatrix} \begin{bmatrix} v_i \\ w_i \end{bmatrix} = \begin{bmatrix} 0 \\ 0 \end{bmatrix} \tag{13}$$

where v_i and w_i, $i = 1, \ldots, p$, form the columns of V and W, respectively.

Remark 2.1: To guarantee that the eigenvalues λ_i of Step 2) are freely assignable, the system matrix

$$P(\lambda) = \begin{bmatrix} A - \lambda I & B \\ T & 0 \end{bmatrix}$$

must verify the rank condition: $\mathrm{rank}(P(\lambda)) = 2n - p, \forall\ \lambda$. Otherwise, system ($A$, B, T) has invariant zeros, in which case they must be used to obtain the (A, B)-invariance of $\mathrm{Ker}\, T$ [3]. Notice however that, under Kimura's condition, $m + p > n$, $P(\lambda)$ does not lose rank for almost all triples (A, B, T) [12]. Furthermore, for particular *pathological* cases, where the corresponding $P(\lambda)$ does not verify the rank condition, other solutions T for Step 1) may be found such that $\mathcal{V} = \mathrm{Ker}\ T$ can be internally stabilized. This can be done, for instance, by slightly changing the eigenvalues chosen to be initially placed through Step 1) [11].

III. New Quadratic Stabilizability Characterization

A quadratic characterization of Theorem 2.1 can be obtained by replacing the $(A,\ B)$-inner stabilizability and the $(C,\ A)$-outer detectability requirements by the two equivalent quadratic Lyapunov stability conditions [6]

$$\sigma(H_V) \in \mathcal{C}^- \Longleftrightarrow \exists\, \Pi = \Pi' > 0 \text{ such that}$$
$$\Pi H_V' + H_V \Pi = -Q_V \qquad \forall\, Q_V = Q_V' > 0 \quad (14)$$
$$\sigma(H_T) \in \mathcal{C}^- \Longleftrightarrow \exists\, \Gamma = \Gamma' > 0 \text{ such that}$$
$$H_T'\Gamma + \Gamma H_T = -Q_T \qquad \forall\, Q_T = Q_T' > 0. \quad (15)$$

Theorem 3.1: There exists an output feedback $K \in \Re^{m\times p}$ such that $\sigma(A+BKC) \in \mathcal{C}^-$, if and only if the following conditions hold true for some full-rank matrices $V \in \Re^{n\times v}$ and $T \in \Re^{(n-v)\times n}$, with integer $v \leq n$, such that $TV = 0$

i) $\forall\, Q_V = Q_V' > 0$, $Q_V \in \Re^{v\times v}$, there exist $P = P' \geq 0$, $P \in \Re^{n\times n}$ and $Y \in \Re^{m\times n}$ such that

$$AP + PA' + BY + Y'B' = -VQ_VV' \quad (16)$$
$$V'PV > 0;\ TPT' = 0 \quad (17)$$
$$Y = W_\Pi V' \text{ for some } W_\Pi \in \Re^{m\times v}; \quad (18)$$

ii) $\forall\, Q_T = Q_T' > 0$, $Q_T \in \Re^{(n-v)\times(n-v)}$, there exist $S = S' \geq 0$, $S \in \Re^{n\times n}$ and $Z \in \Re^{n\times p}$ such that

$$A'S + SA + C'Z' + ZC = -T'Q_TT \quad (19)$$
$$TST' > 0;\ V'SV = 0 \quad (20)$$
$$Z = T'U_\Gamma \text{ for some } U_\Gamma \in \Re^{(n-v)\times p}; \quad (21)$$

iii)

$$\operatorname{Ker} CP \subseteq \operatorname{Ker} Y \quad (22)$$
$$\operatorname{Ker} B'S \subseteq \operatorname{Ker} Z'. \quad (23)$$

Proof: *Necessity*: Consider that $\mathcal{V} \subset \Re^n$ is an *OS*$(C,\ A,\ B)$-invariant subspace and, hence, that the coupled Sylvester equations (4), (5), and (6) are verified. Let us first show the necessity of part i). For any $Q_V = Q_V' > 0$, the quadratic stability condition given by (14) holds true, and we get

$$V\left(\Pi H_V' + H_V\Pi\right)V' = V\Pi H_V'V' + VH_V\Pi V' = -VQ_VV' \leq 0. \quad (24)$$

From (4), we also have $AV + BW = VH_V$, which can be used in(24) to obtain

$$V\Pi V'A' + V\Pi W'B' + AV\Pi V' + BW\Pi V' = -VQ_VV' \quad (25)$$

Thus, by setting $P = P' = V\Pi V'$ and $Y = W\Pi V'$, and by considering that $\operatorname{rank}(V) = v$ and that

$$\Pi > 0 \Longrightarrow \begin{cases} V'V\Pi V'V > 0 \\ T'V\Pi V'T = 0 \end{cases}$$

(25) can be equivalently replaced by (16), (17), and (18).

Using similar arguments, we can show the necessity of part ii). Thus, from (5) and (15), for any $Q_T = Q_T' > 0$ we obtain

$$T'\left(H_T'\Gamma + \Gamma H_T\right)T = A'T'\Gamma T + C'U'\Gamma T + T'\Gamma TA + T'\Gamma UC = -T'Q_TT \quad (26)$$

By setting $S = T'\Gamma T$ and $Z = T'\Gamma U$, (26) can replaced by (19) and (21). Furthermore, since $\operatorname{rank}(T) = n - v$ and $\Gamma > 0$, we also have

$$\begin{cases} TT'\Gamma TT' > 0 \\ V'T'\Gamma TV = 0 \end{cases}.$$

The necessity of part iii), (22), and (23) follows from (7) and (8), respectively, by taking into account the aforementioned definitions of P, Y, S and Z.

Sufficiency: Consider that parts i), ii), and iii) are verified. By definition, V and T have, respectively, full-column rank and full-row rank. Thus, from (17) and (20), we get

$$V'PV = \bar{P} = \bar{P}' > 0 \Longrightarrow P = V(V'V)^{-1}\bar{P}(V'V)^{-1}V' \quad (27)$$
$$TST' = \bar{S} = \bar{S}' > 0 \Longrightarrow S = T'(TT')^{-1}\bar{S}(TT')^{-1}T. \quad (28)$$

We shall now show that the verification of part i) implies that $\mathcal{V} = \operatorname{Im} V$ is a $(A,\ B)$-inner stabilizable invariant subspace. Similar arguments can be used to show that $\mathcal{V} = \operatorname{Ker} T$, which is implied by the coupling condition, is also a (C,A)-outer detectable subspace.

From (27) and (28), we have

$$P = \begin{bmatrix} V & T' \end{bmatrix}\begin{bmatrix} \Pi & 0 \\ 0 & 0 \end{bmatrix}\begin{bmatrix} V' \\ T \end{bmatrix} \geq 0 \quad \text{for}$$
$$\Pi = \Pi' = (V'V)^{-1}\bar{P}(V'V)^{-1} > 0. \quad (29)$$

From (22), there exists K such that

$$KCP = Y \quad (30)$$

Thus, by substituting (30) into (16), we get

$$P(A+BKC)' + (A+BKC)P = -VQ_VV' \quad (31)$$

Let us now take into account (29), the similarity equation

$$(A+BKC)\begin{bmatrix} V & T' \end{bmatrix} = \begin{bmatrix} V & T' \end{bmatrix}\begin{bmatrix} \bar{A}_{11} & \bar{A}_{12} \\ \bar{A}_{21} & \bar{A}_{22} \end{bmatrix} \quad (32)$$

and the fact that

$$VQ_VV' = \begin{bmatrix} V & T' \end{bmatrix}\begin{bmatrix} Q_V & 0 \\ 0 & 0 \end{bmatrix}\begin{bmatrix} V' \\ T \end{bmatrix} \geq 0. \quad (33)$$

From (31), we obtain

$$\begin{bmatrix} V & T' \end{bmatrix}\left(\begin{bmatrix} \Pi\bar{A}_{11}' & \Pi\bar{A}_{21}' \\ 0 & 0 \end{bmatrix} + \begin{bmatrix} \bar{A}_{11}\Pi & 0 \\ \bar{A}_{21}\Pi & 0 \end{bmatrix}\right)\begin{bmatrix} V' \\ T \end{bmatrix} = -\begin{bmatrix} V & T' \end{bmatrix}\begin{bmatrix} Q_V & 0 \\ 0 & 0 \end{bmatrix}\begin{bmatrix} V' \\ T \end{bmatrix} \geq 0. \quad (34)$$

Hence, (34) implies that

- $\mathcal{V} = \operatorname{Im} V$ is $(A+BKC)$-invariant, since $\bar{A}_{21}\Pi = 0$ iff $\bar{A}_{21} = 0$;
- $\mathcal{V}$ is inner-stabilizable, since $\Pi\bar{A}_{11}' + \bar{A}_{11}\Pi = -Q_V < 0$ implies the stability of $(A+BKC)|\mathcal{V}$.□

To complete this section, we present some remarks complementary to Theorem 3.1.

Remark 3.1: From the proof of Theorem 3.1, it can be seen that any pair of matrices (P, S) solution to parts i) and ii) verifies: $\operatorname{Ker} S = \operatorname{Im} \mathcal{V} = \operatorname{Im} P$, or equivalently

$$SP = 0. \quad (35)$$

Remark 3.2: Let us consider the following coupled quadratic equations that have been used to analyze the output stabilization problem:

$$A\mathcal{P} + \mathcal{P}A' + B\mathcal{W} + \mathcal{W}'B' < 0 \quad \mathcal{P} > 0 \quad (36)$$

$$\mathcal{S}A + A'\mathcal{S} + \mathcal{Y}C + C'\mathcal{Y}' < 0 \quad \mathcal{S} > 0 \tag{37}$$

$$\mathcal{S}\mathcal{P} = I_n. \tag{38}$$

The coupling condition (35) captures the major conceptual difference between the quadratic output stabilizing conditions obtained in Theorem 3.1 and the coupled quadratic conditions previously expressed. Indeed, the obtained stabilizing conditions are directly related to the geometric properties: $\mathrm{Ker}\ S = \mathrm{Im}\ \mathcal{V} = \mathrm{Im}\ P$, while the coupled conditions (36), (37), and (38) are mainly related to the invariance and contractivity of an ellipsoidal set defined from a Lyapunov function $l(x) = x'\mathcal{S}x$.

Thus, in our opinion, Theorem 3.1 bridges a gap between the geometric approach and the quadratic stabilizibility to treat the static output feedback stabilization problem. This is particularly clear in the algorithm of the next section.

Remark 3.3: The previous theoretical results allow to readily associate a quadratic Lyapunov function to the closed-loop system. Consider a solution (P, S, V, T) to the conditions in Theorem 3.1 and let K be the corresponding stabilizing output feedback matrix. Define matrices $\bar{T} \in \Re^{v\times n}$ and $\bar{V} \in \Re^{n\times(n-v)}$ as

$$\bar{T} = \overbrace{(V'V)^{-1}V'}^{V^\dagger} + D_l T;\ \bar{V} = \overbrace{T'(TT')^{-1}}^{T^\dagger} + V D_l \tag{39}$$

where $D_l \in \Re^{v\times(n-v)}$ is such that $D_l H_T - H_V D_l = -V^\dagger(A + BKC)T^\dagger$. Then

$$\begin{aligned} l(x) &= x'\mathcal{S}x, \text{ where} \\ \mathcal{S} &= \begin{bmatrix}\bar{T}' & T'\end{bmatrix}\begin{bmatrix}\Pi^{-1} & 0\\ 0 & \Gamma\end{bmatrix}\begin{bmatrix}\bar{T}\\ T\end{bmatrix} \\ &= \begin{bmatrix}V & \bar{V}\end{bmatrix}\begin{bmatrix}\bar{P}^{-1} & 0\\ 0 & \bar{S}\end{bmatrix}\begin{bmatrix}V'\\ \bar{V}'\end{bmatrix} \end{aligned} \tag{40}$$

is strictly decreasing along the trajectories of the closed-loop system $\dot{x}(t) = (A + BKC)x(t)$, since $\dot{l}(x) = x'((A + BKC)'\mathcal{S} + \mathcal{S}(A + BKC))x < 0\ \forall\, x \neq 0$.

IV. Algorithm for Output Feedback Stabilization

Theorem 3.1 gives a necessary and sufficient condition for the existence of a stabilizing output feedback. This result involves coupled-matrix equations that are nonlinear and nonconvex in the considered decision variables T, V, P and S. However, the quadratic characterization of Theorem 3.1 may be used to construct $OS(C, A, B)$-invariant subspaces that lead to stabilizing output feedback matrices K. Based on these results, and in light of the Syrmos and Lewis algorithm [11] outlined in Section II, the following basic procedure is proposed to compute a stabilizing static output feedback when $m + p > n$.

Step 1)

- Find a decomposition $C[M_1\ M_2] = [C_1\ 0]$ and set $\begin{bmatrix}A_{12}\\ A_{22}\end{bmatrix} = \begin{bmatrix}\bar{M}_1'\\ \bar{M}_2'\end{bmatrix} A M_2$, where $M_1 \in \Re^{n\times p}$, $M_2 \in \Re^{n\times(n-p)}$ and $[M_1\ M_2]\begin{bmatrix}\bar{M}_1'\\ \bar{M}_2'\end{bmatrix} = I_n$.
- Solve the *reduced-order* generalized Lyapunov equation (41) to find S_{21} and $S_{22} = S_{22}' > 0$

$$A_{22}'S_{22} + S_{22}A_{22} + A_{12}'S_{21}' + S_{21}A_{12} = -Q_T, \qquad \text{for } Q_T > 0. \tag{41}$$

- Set $T = [S_{21}\ S_{22}]\begin{bmatrix}\bar{M}_1'\\ \bar{M}_2'\end{bmatrix}$. If the triple ($A$, B, T) has nonminimum phase (infinite or unstable) invariant zeros then repeat Step 1) for a new decomposition of C (see Remark 4.4). Otherwise, go to Step 2).

Step 2)

- Compute $V \in \Re^{n\times p}$ as an orthogonal basis of $\mathrm{Ker}\ T$, i.e: $TV = 0$ with $V'V = I_p$.
- Solve (16), (17), and (18) to find $P = P' \geq 0$, Y and W_Π.

Step 3) Compute the stabilizing output feedback matrix K as the unique solution of

$$KCP = Y \Longleftrightarrow KCV\bar{P} = W_\Pi, \text{ since } V'V = I_p.$$

A. Some Remarks About the Proposed Basic Procedure

The steps of the previous basic algorithm can be justified as follows.

Remark 4.1: The key step of the algorithm is the construction of an adequate matrix $T \in \Re^{(n-p)\times n}$ in Step 1). This construction is based on the use of a reduced-order system, represented by matrices $A_{12} \in \Re^{p\times(n-p)}$ and $A_{22} \in \Re^{(n-p)\times(n-p)}$, obtained from the representation of the open-loop system in the basis formed by the columns of matrix $M = [M_1\ M_2]$. It is important to remark that the reduced-order Lyapunov equation (41) is always solvable since, by assumption, the pair (A_{12}, A_{22}) is detectable. Hence, any feasible solution for (41) produces a candidate matrix T such that $\mathrm{Ker}\ T \cap \mathrm{Ker}\ C = \{0\}$ and such that $\mathrm{Ker}\ T = \mathcal{V}$ is (C,A)-outer detectable (for details, see Lemma 7.1 in the Appendix).

Notice that the resolution of (41) is not sufficient for finding a stabilizing output feedback. This has been pointed out by Corollary 1 in [9], but it can be also interpreted under the terms of Remark 2.1, because the (A, B)-inner stabilizability of $\mathrm{Ker}\ T = \mathcal{V}$ is guaranteed if and only if the candidate T is such that $\mathrm{rank}(P(\lambda)) = 2n + p, \forall\, \lambda \notin \mathcal{C}^-$. Recall, however, that the system matrix $P(\lambda)$ verifies this rank condition for almost all triples (A, B, T), when $m + p > n$.

Remark 4.2: Step 2 is used to solve the set of conditions (16), (17), and (18) for $\mathcal{V} = \mathrm{Ker}\ T$. Thus, a feasibility test has been set at the end of Step 1) so that the computations involved in Step 2) are carried out only when a stabilizing solution is feasible. Numerical experiments, reported in the next section, show the effectiveness of the proposed approach.

Remark 4.3: Convex programming techniques can be used to find feasible solutions for the involved Lyapunov-like conditions [2]. Although in the present study, asymptotic stability is the only closed-loop requirement, the degrees-of-freedom existing in the quadratic approach given here could be exploited to achieve other requirements as, for instance, regional pole placement.

Remark 4.4: The decomposition used in Step 1) is not unique. In particular, it can be obtained computationally through orthogonal transformations. Then, the set of all decompositions (43) can be described from a chosen orthogonal matrix M as

$$CMD = C\begin{bmatrix}M_1 & M_2\end{bmatrix}\begin{bmatrix}D_1 & 0\\ D_{21} & D_2\end{bmatrix} = \begin{bmatrix}\bar{C}_1 & 0\end{bmatrix} \tag{42}$$

for all nonsingular matrices $D_1 \in \Re^{p\times p}$ and $D_2 \in \Re^{(n-p)\times(n-p)}$. Furthermore, for any particular choice of matrix D, the new (detectable) reduced-order pair can be easily computed

$$\begin{aligned} \begin{bmatrix}A_{12}^n\\ A_{22}^n\end{bmatrix} &= \begin{bmatrix}D_1^{-1} & 0\\ -\bar{D}_{21} & D_2^{-1}\end{bmatrix}\begin{bmatrix}A_{12}\\ A_{22}\end{bmatrix} D_2 \\ &= \begin{bmatrix}D_1^{-1}A_{12}D_2\\ \left(D_2^{-1}A_{22} - \bar{D}_{21}A_{12}\right)D_2\end{bmatrix}. \end{aligned}$$

It is important point out that it is not a simple task neither to determine an *a priori* good decomposition M nor to define an optimization cri-

TABLE I
SUMMARY OF RANDOMLY GENERATED EXAMPLES

Systems order	Compensator's order	Number of examples	Rate of success		
			Basic procedure	1 iteration	2 iterations
$n=5$ $m=p=3$	$\nu=0$	20 000	99.6%	0.4%	-
$n=5$ $m=2;p=3$	$\nu=1$	1 000	98.4%	1.6%	-
$n=5$ $m=2;p=2$	$\nu=2$	1 000	99.1%	0.9%	-
$n=4$ $m=p=2$	$\nu=0$	100	27%	21%	16%

terium guaranteeing that the numerical resolution of (41) will produce an adequate matrix T (see also [9]). For computational purposes, the above parameterization can be used in unfrequent pathological cases where a first particular choice of decomposition M does not produce an adequate matrix T in Step 1). Hence, matrix D can be used to define a new reduced-order pair and to produce a new solution to equation (41) so that Step 2) becomes feasible. This scheme has no guarantee of numerical convergence, but its use produces good results in practice, as shown in the next section.

Remark 4.5: The given algorithmic procedure is not directly adapted for more difficult cases where $m+p \leq n$, although a "trial-and-error" search may be carried out to find a "good" T, through the definition of decompositon M. In the case $m+p=n$, $P(\lambda)$ is square and almost all triple (A, B, T) has p finite invariant zeros [12]. In this particular case, the basic procedure can produce stabilizing solutions only if T found in Step 1) generate p minimum-phase (asymptotically stable) invariant zeros, which have to be used to solve (13) [3].

Finally, it is worth recalling that stabilizing solutions can be also computed from the dual system (A', C', B'). Also, for more difficult cases, $m+p \leq n$, the procedure can be systematically used to compute v-order stabilizing dynamic output compensators, by recovering the Kimura's condition, with $v > n-(m+p)$.

V. EXAMPLES

The examples reported in this section were solved with the aid of the software Scilab (developed at INRIA, France). In all the tests, the matrix decomposition in Step 1) has been firstly obtained from the QR decomposition of matrix C.

A. Randomly Generated Examples

First, 20 000 random triples (A, B, C) have been generated, verifying the Kimura's condition $m+p > n$, with $n=5$, $m=p=3$, and such that A is unstable. Feasible solutions for the coupled Lyapunov-like conditions have been found without considering additional requirements. The basic procedure computed stabilizing solutions in 99.6% of cases, without the need of iterations over Step 1). In the examples not solved by the basic algorithm, only one iteration was necessary to obtain a stabilizing solution. This iteration was carried out using Remark 4.4, with

$$D=\begin{bmatrix} I_p & 0 \\ D_{21} & I_{n-p} \end{bmatrix}$$

for a random matrix D_{21}. Thus, under the Kimura's condition, the algorithm was always successful.

Table I summarizes the computational experiments for randomly generated examples. In particular, it shows the effectiveness of the proposed algorithm to compute both static and dynamic stabilizing controllers when Kimura's condition is either verified or recovered. Thus, comparing theses results to the results reported by [10, Tables I and II], we can infer that, in terms of success in computing stabilizing solutions, the proposed approach has a performance comparable to the performance of the cone complementarity linearization algorithm. Furthermore, the data in the last row show that the approach may also be used to search for stabilizing solutions even when Kimura's condition is not verified.

B. Numerical Example

The objective of the next example is to describe the numerical results obtained at each step. Consider the following data [8]:

$$A=\begin{bmatrix} 0 & 1 & 0 & 0 \\ 1 & 1 & 0 & 0 \\ -1 & 0 & 0 & 0 \\ 0 & 0 & 0 & 0 \end{bmatrix}$$

$$B=\begin{bmatrix} 0 & 0 \\ 1 & 0 \\ 0 & 0 \\ 0 & 1 \end{bmatrix}$$

$$C=\begin{bmatrix} 1 & 0 & 0 & 1 \\ 0 & 0 & 1 & 0 \\ 0 & 0 & 0 & 1 \end{bmatrix}.$$

The triple (C, A, B) is controllable and observable and verify $m+p=5>n$. Also, to obtain closed-loop eigenvalues with real parts less than $-\alpha=-2$, computations are done using $(A+\alpha I)$ instead of A.

Using an orthogonal matrix M that performs Step 1), a matrix $T=[S_{21}\ S_{22}]\begin{bmatrix} M_1' \\ M_2' \end{bmatrix}$ is readily found in Step 2)

$$T=[0.0006 \quad 0 \quad -4.1142 \quad 1]\begin{bmatrix} -0.5257 & 0 & 0 & -0.8507 \\ 0 & 0 & -1 & 0 \\ 0.8507 & 0 & 0 & -0.5257 \\ 0 & 1 & 0 & 0 \end{bmatrix}$$
$$=[-3.5001 \quad 1 \quad 0 \quad 2.1625].$$

It implies, in Step 2), $V = \begin{bmatrix} 0.5107 & 0 & 0.2362 \\ -0.0660 & 0 & 0.9695 \\ 0 & 1 & 0 \\ 0.8572 & 0 & -0.0660 \end{bmatrix}$. A feasible solution for Step 2) is then found

$$P = \begin{bmatrix} 19\,753.561 & -41\,669.85 & 6418.2843 & 51\,240.969 \\ -41\,669.85 & 237\,613.71 & -6863.8855 & -177\,323.06 \\ 6418.2843 & -6863.8855 & 3104.1283 & 13\,562.213 \\ 51\,240.969 & -177\,323.06 & 13\,562.213 & 164\,934.04 \end{bmatrix}$$

$$Y = \begin{bmatrix} -51\,685.095 & -747\,434.01 & -14\,350.967 & 261\,981.08 \\ -33\,408.348 & 639\,608.61 & -4267.0209 & -349\,845.47 \end{bmatrix}$$

$$W_{\text{II}} = \begin{bmatrix} 247\,529.57 & -14\,350.967 & -754\,116.8 \\ -359\,186.68 & -4267.0209 & 635\,288.97 \end{bmatrix}.$$

The corresponding stabilizing output feedback

$$K = \begin{bmatrix} -67.1094 & 56.3478 & 84.9136 \\ 34.6173 & -26.0568 & -45.3505 \end{bmatrix}$$

gives

$$\sigma(A + BKC) = \{-2.5001;\ 2.1333;\ 2.5499 \pm 4.4622j\}$$

where the eigenvalue -2.5001 corresponds to Step 2), through (46).

VI. Concluding Remarks

The concept of (C, A, B)-invariance has been revisited to obtain a quadratic characterization of the so-called OS (C, A, B)-invariant subspaces, which play a fundamental role in output feedback stabilization of linear systems. This note has focused both on theoretical and algorithmic aspects. In particular, a necessary and sufficient condition for the existence of a stabilizing output feedback has been obtained in terms of two coupled Lyapunov-like equations. An algorithm has also been proposed to compute a stabilizing output feedback matrix under Kimura's condition $m + p > n$.

Some extensions of the proposed approach are possible. In particular, an interesting approach consists of replacing strict pole placement by regional pole placement, using, for example, the conditions given in[4] and [5]. Among the remaining open questions for future studies, one may consider the use of the existing degrees of freedom to include additional control requirements and the possibility to treat in a systematic way the more difficult case $mp \geq n$ [1].

Appendix

Lemma 7.1: Under the assumption that (C, A) is detectable, there always exist $S = S' \geq 0$ and Z verifying (19), (20), and (21) for some $T \in \Re^{(n-p)\times n}$, with rank $(T) = n - p$, such that $\operatorname{Ker} T = \mathcal{V}$ is (C, A)-outer detectable and $\operatorname{Ker} T \cap \operatorname{Ker} C = \{0\}$.

Proof: Consider the following change of basis: $x = [M_1 \quad M_2]\begin{bmatrix} x_1 \\ x_2 \end{bmatrix}$, $M_1 \in \Re^{n\times p}$, $M_2 \in \Re^{n\times(n-p)}$, where $M = [M_1 \quad M_2]$ is a nonsingular matrix such that

$$C[M_1 \quad M_2] = [C_1 \quad 0], \quad \text{with } C_1 \in \Re^{p\times p} \text{ and } \operatorname{rank}(C_1) = p. \tag{43}$$

The inverse of matrix M is denoted by $\bar{M} = \begin{bmatrix} \bar{M}_1' \\ \bar{M}_2' \end{bmatrix}$ with $\bar{M}_1 \in \Re^{n\times p}$, $\bar{M}_2 \in \Re^{n\times(n-p)}$.

In this basis, the open-loop system takes the form

$$\begin{bmatrix} \dot{x_1} \\ \dot{x_2} \end{bmatrix} = \begin{bmatrix} A_{11} & A_{12} \\ A_{21} & A_{22} \end{bmatrix}\begin{bmatrix} x_1 \\ x_2 \end{bmatrix} + \begin{bmatrix} B_1 \\ B_2 \end{bmatrix} u \tag{44}$$

$$y = [C_1 \quad 0]\begin{bmatrix} x_1 \\ x_2 \end{bmatrix} \tag{45}$$

where the matrices involved have the appropriate dimensions.

As shown in [6], detectability of the pair (C, A) implies detectability of the pair (A_{12}, A_{22}). Thus, for any given matrix $Q_T = Q_T' > 0$, let $S_{22} \in \Re^{(n-p)\times(n-p)}$, with $S_{22} = S_{22}' > 0$ and $S_{21} \in \Re^{(n-p)\times p}$ be solutions to the generalized reduced-order Lyapunov equation (41). Let $L_2 \in \Re^{(n-p)\times p}$ be such that

$$S_{22}L_2 = S_{21} \tag{46}$$

and consider also a Choleski decomposition of $S_{22} = S_{22}' > 0$ given by

$$S_{22} = T_2'T_2. \tag{47}$$

Thus, from (41), (46), and (47), we get $T_2'T_2(A_{22} + L_2A_{12}) + (A_{22}' + A_{12}'L_2')T_2'T_2 = -Q_T$, where, by construction, $\sigma(A_{22} + L_2A_{12}) \in \mathcal{C}^-$.

Since T_2 is, by definition, nonsingular, we can define the asymptotically stable matrix $H_T \in \Re^{(n-p)\times(n-p)}$ from the similarity relation

$$T_2(A_{22} + L_2A_{12}) = H_TT_2. \tag{48}$$

Furthermore, since C_1 is invertible, a matrix $U \in \Re^{(n-p)\times p}$ can always be computed from

$$UC_1 = -(T_2L_2A_{11} + T_2A_{21} - H_TT_1). \tag{49}$$

Thus, by defining $T_1 = T_2L_2$, (48) and (49) can be replaced by

$$[T_1 \quad T_2]\begin{bmatrix} A_{11} & A_{12} \\ A_{21} & A_{22} \end{bmatrix} - H_T[T_1 \quad T_2] = -U[C_1 \quad 0]. \tag{50}$$

Hence, $T = [T_1 \quad T_2]\begin{bmatrix} \bar{M}_1' \\ \bar{M}_2' \end{bmatrix}$ is such that

- $\operatorname{Ker} T$ is (C, A)-outer detectable, since $H_T = (A + LC)|\Re^n/\mathcal{V}$ is such that $\sigma(H_T) \in \mathcal{C}^-$ for $L = T'(TT')^{-1}U$;
- $\operatorname{Ker} T \cap \operatorname{Ker} C = \{0\}$ or, equivalently

$$\left(\operatorname{rank}\begin{bmatrix} T \\ C \end{bmatrix} = \begin{bmatrix} T_1 & T_2 \\ C_1 & 0 \end{bmatrix}\begin{bmatrix} \bar{M}_1' \\ \bar{M}_2' \end{bmatrix}\right) = n$$

since $\operatorname{rank}(T_2) = n - p$.

Furthermore, let $\Gamma = \Gamma' > 0$ be the unique solution of $H_T'\Gamma + \Gamma H_T = -Q_T$. Thus, the following matrices Z and $S = S' \geq 0$ verify (19), (20), and (21) for T defined as before: $Z = [M_1 \quad M_2]\begin{bmatrix} T_1' \\ T_2' \end{bmatrix}U\Gamma$ and

$$S = [M_1\ M_2]\begin{bmatrix} S_{11} & S_{21}' \\ S_{21} & S_{22} \end{bmatrix}\begin{bmatrix} \bar{M}_1' \\ \bar{M}_2' \end{bmatrix}$$

with

$$\begin{bmatrix} S_{11} & S_{21}' \\ S_{21} & S_{22} \end{bmatrix} = \begin{bmatrix} T_1' \\ T_2' \end{bmatrix}\Gamma[T_1\ T_2]. \qquad \square$$

ACKNOWLEDGMENT

The authors would like to thank the anonymous reviewers for their helpful comments and suggestions.

REFERENCES

[1] A. T. Alexandridis and P. N. Parakevopoulos, "A new approach to Eigenstructure assignment by output feedback," *IEEE Trans. Automat. Contr.*, vol. 41, pp. 1046–1050, July 1996.
[2] S. P. Boyd, L. El Ghaoui, E. Feron, and V. Balakrishhnan, *Linear Matrix Inequalities in System and Control Theory*. Philadelphia, PA: SIAM, 1994.
[3] E. B. Castelan and J. C. Hennet, "Eigenstructure assignment for state constrained linear continuous time systems," *Automatica*, vol. 28, no. 3, pp. 605–611, 1993.
[4] E. B. Castelan, E. R. Llanos Villareal, and J. C. Hennet, "Output feedback design by coupled Lyapunov-like equations," presented at the 15th IFAC World Congr., Barcelona, Spain, 2002.
[5] E. B. Castelan, E. R. Llanos Villareal, A. S. e Silva, and S. Tarbouriech, "Regional pole placement by output feedback for a class of descriptor systems," presented at the 15th IFAC World Congr., Barcelona, Spain, 2002.
[6] C. T. Chen, *Linear System Theory and Design*. New York: Holt, Rinehart, and Winston, 1984.
[7] C. A. R. Crusius and A. Trofino, "Sufficient LMI conditions for output feedback," *IEEE Trans. Automat. Contr.*, vol. 44, pp. 1053–1057, May 1999.
[8] L. R. Fletcher, J. Kautsky, G. K. G. Kolka, and N. K. Nichols, "Some necessary and sufficient conditions for eigenstructure assignment," *Int. J. Control*, vol. 42, no. 6, pp. 1457–1468, 1985.
[9] J. C. Geromel, P. L. D. Peres, and S. R. de Souza, "Convex analysis of output feedback control problems: stability and performance," *IEEE Trans. Automat. Control.*, vol. 41, pp. 997–1002, July 1996.
[10] L. El Ghaoui, F. Oustry, and M. AitRami, "A cone complementarity linearization algorithm for static output-feedback and related problems," *IEEE Trans. Automat. Contr.*, vol. 42, pp. 1171–1176, Aug. 1997.
[11] V. L. Syrmos and F. L. Lewis, "Output feedback Eigenstructure assignment using two Sylvester equations," *IEEE Trans. Automat. Contr.*, vol. 38, pp. 495–499, Mar. 1993.
[12] ——, "Transmission zero assignment using semistate descriptions," *IEEE Trans. Automat. Contr.*, vol. 38, pp. 1115–1120, July 1993.
[13] ——, "A bilinear formulation for the output feedback problem in linear systems," *IEEE Trans. Automat. Contr.*, vol. 39, pp. 410–414, Feb. 1994.
[14] V. L. Syrmos, C. T. Abdallah, P. Dorato, and K. Grigoriadis, "Static output feedback—a survey," *Automatica*, vol. 33, no. 3, pp. 125–137, 1997.
[15] W. M. Wonham, *Linear Multivariable Control, a Geometric Approach*. New York: Springer-Verlag, 1979.

On Hopf Bifurcations in Singularly Perturbed Systems

L. Yang, Y. Tang, and D. Du

***Abstract*—It has been shown recently that, under some generic assumptions, there exists a Hopf curve $\boldsymbol{\lambda = \lambda(\varepsilon)}$ for singularly perturbed systems of the form $\boldsymbol{\dot{x} = f(x, y, \lambda), \varepsilon\dot{y} = g(x, y, \lambda)}$ near the singular surface defined by $\det\, \boldsymbol{g_y = 0}$. In this note, we are concerned with the Hopf curve and obtain three results. 1) We prove that the eigenvalue crossing condition for the Hopf curve holds without additional assumption. 2) We provide an improved form of an existing derivative formula for the Hopf curve which is more suitable for practical computations. 3) We give a quite precise description of the spectrum structure of the linearization along the Hopf curve. All three results (stated in the main theorem) are useful for a better understanding of Hopf bifurcations in singularly perturbed systems. Our analysis is based on a factorization of parameter dependent polynomials (Lemma 2.3).**

***Index Terms*—Eigenvalue crossing condition, singularity induced bifurcation, singularity induced Hopf bifurcation, singularly perturbed system, spectrum structure.**

I. INTRODUCTION AND MAIN RESULTS

Let us consider singularly perturbed systems of the form

$$\begin{cases} \dot{x} = f(x, y, \lambda),\ f : \mathbb{R}^n \times \mathbb{R}^m \times \mathbb{R} \to \mathbb{R}^n \\ \varepsilon\dot{y} = g(x, y, \lambda),\ g : \mathbb{R}^n \times \mathbb{R}^m \times \mathbb{R} \to \mathbb{R}^m \end{cases} \tag{1.1}$$

where $\varepsilon \in \mathbb{R}$ is a small perturbation parameter and $\lambda \in \mathbb{R}$ a bifurcation parameter. A large class of physical systems (power systems, nonlinear networks, etc.) can be modeled by (1.1). Venkatasubramanian [15], [16] first explored the existence of a Hopf curve $\lambda = \lambda(\varepsilon)$ for the system (1.1) near the singular surface defined by $\det g_y = 0$, namely, the linearization of the system (1.1) at equilibriums $(x(\lambda), y(\lambda), \lambda)$ has a pair of purely imaginary eigenvalues for $\lambda = \lambda(\varepsilon)$. This implies that (1.1) could have a family of periodic solutions bifurcating from the equilibriums, in other words, a Hopf bifurcation could occur, which is often called singularity induced Hopf bifurcation (SIHB) in the literature. The SIHB closely relates to duck solutions and duck oscillations; see, for instance, [2], [8], [11], [13], and [14].

Using the method of matrix pencils Beardmore has given a detailed discussion on the existence of the Hopf curve and related issues; see [5] and [6]. In fact the existence of the Hopf curve is a consequence of a new bifurcation, called singularity induced bifurcation (SIB) [16]. The SIB often occurs in differential-algebraic equations of the form $\dot{x} = f(x, y, \lambda)$, $0 = g(x, y, \lambda)$ obtained from (1.1) with $\varepsilon = 0$, and also in quasi-linear ordinary differential equations [12] and infinite-dimensional systems. For a more precise description of the SIB, see [5] and [18].

There are three contributions concerning the Hopf curve in this note. 1) We prove that the eigenvalue crossing condition for the Hopf curve automatically holds. This condition is necessary for a Hopf bifurcation to occur. So far as we know, there has been no discussion on the validness of the condition in the literature. 2) We provide an improved form

Manuscript received March 26, 2001; revised August 4, 2001 and March 1, 2002. Recommended by Associate Editor H. Wang. This work was supported by the National Key Basic Research Special Fund under Grant G1 998 020 309 and by the National Natural Science Foundation of China under Grant 19 990 510.

The authors are with the Department of Mathematical Sciences, Tsinghua University, Beijing 100084, P.R. China (e-mail: lyang@math.tsinghua.edu.cn; tangyun@mail.tsinghua.edu.cn; dudongyun@263.net).

Digital Object Identifier 10.1109/TAC.2003.809772

0018-9286/03$17.00 © 2003 IEEE

Analysis and Modeling of an Electromagnetic Speed Regulator for Wind Energy Conversion Systems

Andrés O. Salazar, Daniel C. C. Crisóstomo, Glauco G. C. Maniçoba, Evandro A. D. F. Nunes, and Elmer R. L. Villarreal , *IEEE Senior Member*

***Abstract*—Nowadays, the growing increase in energy demand worldwide intensifies the search for clean and renewable energy sources used and, among the current technologies, wind energy has been highlighted like one of the most promising. This work presents a new proposal for a wind turbine conversion system using a Frequency Electromagnetic Regulator (FER) that replace gearbox functionalities and improve mechanical transmission system performance due to the high reliability and reduction of mechanical losses and maintenance costs. Besides, FER can be useful in several transmission systems wherein mechanical output speed control is the goal. The modeling is based on the wind power extraction rules, conventional three-phase symmetrical and balanced induction machine, kinematic coupling and motion equations and its performance are validated using simulation results that employ Finite Element Method (FEM) to deal with differential equations approximations.**

Keywords: Finite Element Method, Frequency Electromagnetic, Regulator.

I. Introduction

CURRENTLY, electricity generation from renewable energy sources is increasing continuously due to government incentives and environmental restrictions. Among the alternative sources, wind energy has received special attention from the energy sector and the scientific community. In Brazil, which in 2021 was at US 8^{th} in the world ranking of countries with the largest installed capacity in wind farms, the participation of this natural resource in the energy matrix shows an exponential growth reaching 42.373 GWh in 2021 that represents an amount of 6.8% of the whole generated energy in the country [1].

Andrés Ortiz Salazar and Glauco George Cipriano Maniçoba are Department of Computer Engineering and Automation, Federal University of Rio Grande do Norte DCA/UFRN, Natal, RN, Brazil, e-mail:(andres@dca.ufrn.br https://orcid.org/0000-0001-5650-3668 ; glaucogeorge@yahoo.com.br https://orcid.org/0000-0002-6906-2328).

Daniel Carlos de Carvalho Crisóstomo is Department of Science and Technology, Federal Rural University of Semi-arid DCT/UFERSA, Caraúbas, RN, Brazil, e-mail:(daniel.crisostomo@ufersa.edu.br https://orcid.org/0000-0002-9752-688X).

Evandro Ailson de Freitas Nunes is an the Federal Institute of Education, Science and Technology of Bahia IFBA, Salvador, Brazil, e-mail:(evandro.nunes@ifba.edu.br https://orcid.org/0000-0002-4237-0777).

Elmer Rolando Llanos Villarreal is Department of Natural Sciences, Mathematics, and Statistics, Federal Rural University of Semi-arid DCME/UFERSA, Mossoró, RN, Brazil. (Correspondence: elmerllanos@ufersa.edu.br https://orcid.org/0000-0002-3059-3340).

This study was financed in part by the Coordenação de Aperfeiçoamento de Pessoal de Nível Superior Brasil (CAPES) Finance Code 001

Copyright ISSN 0719-5567; IEEE eCF 551889.

IEEE ICA/ACCA2022: Talca, Chile, October 24-28, 2022.
978-1-6654-9408-3/22/$31.00 ©2022 IEEE

One of the most important steps in traditional wind power systems is speed reduction, which makes the angular velocity of the low-rotation axis compatible with that of the high-rotation axis that drives the electric generator. In [2] is presented speed control of sensorless induction generator by the artificial neural network in wind energy conversion system, where a new strategy for estimating the states (rotor flux and speed) and the load torque to implement a multivariable controller for a sensorless three-phase squirrel-cage induction machine in wind energy conversion systems. In [3] presents the implementation of a fuzzy control strategy for speed regulation of an electromagnetic frequency regulator (EFR) prototype, aiming to eliminate the dependence on knowledge of physical parameters in the most diverse operating conditions. Speed multiplication is one of the most important steps in wind power generation. To overcome these drawbacks, there are two lines of research that have been receiving special attention from the scientific community. The first one aims to eliminate the dependence gearboxes, giving rise to direct connection systems. The second one aims to replace gearboxes for less problematic networks. alternative transmission systems. Among the researches that fit the second trend line, the Frequency Electromagnetic Regulator (FER) is a device with promising performance. An example of a FER based wind power system is depicted in Fig. 1.

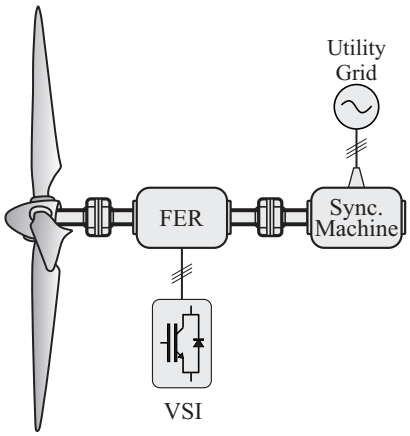

Fig. 1. FER based wind power system.

II. Preliminary concepts

In order to find solutions for finite discrete elements in the computational simulation, Maxwell's equations are adopted

according to (1) up to (3). The equations that will be described in the subsections are governed by Maxwell's equations indicated by the equations (1) for (3), which were implemented in the computational simulation to find solutions for finite discrete elements.

$$\nabla.E = \frac{-\partial B}{\partial t}. \quad (1)$$

$$\nabla.H = J. \quad (2)$$

$$\nabla.B = 0. \quad (3)$$

The combination of this equation set with the constitutive relations of material properties results in the following equations, which are computationally solvable.

$$\frac{\partial A}{\partial t} + \nabla.H + \sigma v.B = J_e. \quad (4)$$

$$\nabla.A = B. \quad (5)$$

A is the magnetic vector potential, s is the electrical conductivity of the material, v is the conductor velocity, and J_e is an externally generated current density. Thus, an equivalent equation is usually solved, which results from the three equations (1) for (3). To this end, an auxiliary vector quantity called of Vector Potential, which in principle has no physical meaning, serving only to make the numerical solution feasible.

A. Power Extracted from Winds

The wind turbine captures the kinetic energy realized through the movement of the wind turbine blades. This energy in the air with a mass m moving at a velocity v_v is given by the equation (6):

$$E_c = \frac{1}{2}mv_v^2. \quad (6)$$

Since the mass of volumetric air (m) is given by $\rho A v_v$ then the power is given by equation (7):

$$P_v = \frac{1}{2}\rho A v_v^3. \quad (7)$$

The rotor blades are designed to extract maximum power from the wind. Incoming wind with the power of P_v and rotor swept an area of radius R is reduced by the wind turbine with a fraction of C_p called power efficiency coefficient. Turbine power P_t is described as follows:

$$P_t = c_p P_v = \frac{1}{2}\rho A v_v^3 c_p. \quad (8)$$

Random wind velocity behavior must be taken into account, including the effect of turbulence. The mechanical output power provided by a wind turbine is obtained according to [4].

$$P_M = \frac{\rho}{2}\pi R^2 c_p(\lambda,\beta) v_w^3. \quad (9)$$

where:

ρ: is air density;

R: is the length of the propeller blades;

c_p: is the power coefficient of the wind turbine, as a function of the λ, β

$\lambda = \frac{\omega_r}{v_w} R$

ω_r: is angular velocity of the machine

β: is pitch angle of blades

v_w: is wind velocity

The energy extracted from the wind is transmitted, mechanically by the wind turbine, through the rotating axes of the turbine. When this power is transmitted through the axis, a torque T_v is obtained by solving the following equation

$$T_v = C_t \rho \pi R^2 v_v^2 D. \quad (10)$$

C_t : is the turbine torque coefficient; D: is the external diameter of the turbine; T_v: is the torque in the turbine.

B. Electromagnetic frequency regulator

In [5] it is described as a conventional three-phase balanced induction machine that can be mathematically represented by the following equations:

$$v_s = R_s I_s + L_{ss}\frac{di_s}{dt} + L_{sr}(\theta)\frac{di_r}{dt} + \frac{\delta}{\theta}[L_{sr}(\theta)][i_r]\frac{d\theta}{dt}. \quad (11)$$

$$v_r = R_r I_r + L_{rr}\frac{di_r}{dt} + L_{rs}(\theta)\frac{di_s}{dt} + \frac{\delta}{\theta}[L_{rs}(\theta)][i_s]\frac{d\theta}{dt}. \quad (12)$$

where v_s, v_r are stator and rotor terminals voltages, respectively. For squirrel cage rotor the short circuited rotor terminals leads to $V_r = 0$. R_s and R_r represent the stator and rotor resistance matrices, respectively.

$$[R_s] = \begin{bmatrix} R_s & 0 & 0 \\ 0 & R_s & 0 \\ 0 & 0 & R_s \end{bmatrix} \quad [R_r] = \begin{bmatrix} R_r & 0 & 0 \\ 0 & R_r & 0 \\ 0 & 0 & R_r \end{bmatrix}. \quad (13)$$

L_{ss} and L_{rr} represent the stator and the rotor proper inductance matrices, respectively, as follows;

$$[L_{ss}] = \begin{bmatrix} L_s & M_s & M_s \\ M_s & L_s & M_s \\ M_s & M_s & L_s \end{bmatrix} \quad [L_{rr}] = \begin{bmatrix} L_r & M_s & M_r \\ M_r & L_r & M_r \\ M_r & M_r & L_r \end{bmatrix}. \quad (14)$$

The phase coupling is eliminated using a Clark transformation that represents a three-phase system in a biphasic one ($\alpha\beta$ frame). As a result of applying this transformation at stator and rotor voltage and flows is the following new set of equations;

$$v_{s\alpha} = R_s i_{s\alpha} + \frac{d\lambda_{s\alpha}}{dt}. \quad (15)$$

$$v_{s\beta} = R_s i_{s\beta} + \frac{d\lambda_{s\beta}}{dt}. \quad (16)$$

$$\lambda_{s\alpha} = L_s i_{s\alpha} + L_m i_{r\alpha}. \quad (17)$$

$$\lambda_{s\beta} = L_s i_{s\beta} + L_m i_{r\beta}. \quad (18)$$

$$v_{r\alpha} = R_r i_{r\alpha} + \frac{d\lambda_{r\alpha}}{dt} + \omega_r \lambda_{r\alpha}. \quad (19)$$

$$v_{r\beta} = R_r i_{r\beta} + \frac{d\lambda_{r\beta}}{dt} + \omega_r \lambda_{r\beta}. \quad (20)$$

$$\lambda_{r\alpha} = L_r i_{r\alpha} + L_m i_{s\alpha} . \quad (21)$$

$$\lambda_{r\beta} = L_r i_{r\beta} + L_m i_{s\beta} . \quad (22)$$

where R_s, R_r, L_s, L_r, stator and rotor resistors and inductances, respectively, L_m is the mutual inductance. The electromagnetic torque is a function of the partial derivative of stored co-energy in the inductors concerning the displacement θ:

$$T_{mi} = \frac{\partial W(\theta, i)}{\partial \theta} \quad (23)$$

$$T_{mi} = p i^T_{s(dq)} \frac{\partial L_{sr}}{\partial \theta} i^T_{r(dq)} . \quad (24)$$

III. Kinematic coupling and motion equations

The rotor movement is a consequence of an internal effort in the working air gap. Due to the distribution of forces along the contour between the air gap and the rotor, torque is produced. Methods based on Maxwell mechanical tensor are generally used in force and torque calculations and for analysis using FEM electrical devices. The electromagnetic torque is obtained from a surface integral, expressed in equation (25).

$$T_e = \int_S r \left\{ \frac{1}{\mu_0}(B * n)B - \frac{1}{2\mu_0} B^2 n \right\} dS . \quad (25)$$

Where r is radial distance from the cylindrical coordinate system ($r = \sqrt{x^2 + y^2}$), μ_0 is magnetic vacuum permeability, B density of magnetic flux, n normal unit vector the surface.

In two-dimensional models, the surface integral can be reduced to an integral defined along the air gap. The torque is calculated by equation (26)

$$T_e = \frac{1}{\mu_0 (r_e - r_i)} \int_0^{2\pi} r^2 B_r B_\phi d\phi . \quad (26)$$

Where r_e and r_i are the outer and inner radius of the air gap, B_r and B_ϕ are the flux densities in the cylindrical coordinates r and ϕ respectively.

The rotational motion of the rotor is modeled using Ordinary Differential Equations (ODEs) and Algebraic Differential Equations (AEDs).

$$\frac{d\omega_m}{dt} = \frac{T_{FER} - T_e}{J_m} . \quad (27)$$

Where ω_m mechanical angular frequency in the rotor T_{FER} Mechanical torque on the FER and J_m Moment of Inertia in the rotor. Besides, we calculate the moment of inertia of the FER, which we will symbolize by I, expressed by the equation (28):

$$I = \int \rho.(x^2 + y^2).L . \quad (28)$$

Where ρ is the density of the rotor materials (kg/m^3), x and y are coordinates of the cylindrical axis and L length of the FER (meter).

The mechanical output torque of the FER (T_{FER}) is given by the sum of the electromagnetic torque (T_e) produced by the induction machine adapted with the mechanical torque produced by the turbine (T_v), is defined by:

$$T_{FER} = T_e + T_v . \quad (29)$$

IV. Losses in wind systems

The main operational problem that limits its global efficiency is the strong incidence of unplanned downtime and high maintenance costs over the life of the generators and the gearbox [6].

The authors in [7] have evaluated the losses in a wind power generation system. It was found that the maximum power that can be extracted from air masses varies between 40 and 60% of the available energy. The conversion of this energy into the electrical form also adds extra losses from the electromechanical systems and reaches values between 28% and 53%. In the latter, there is the involvement of electromechanical components that absorb the available energy and transforms into several losses by friction, thermal, inductive, etc., especially in the system that presents the gearbox. In Fig. 2 shows an example of a diagram of the global balance of the losses observed in the wind generators of Camelinho Park (Minas Gerais), considering each type of loss.

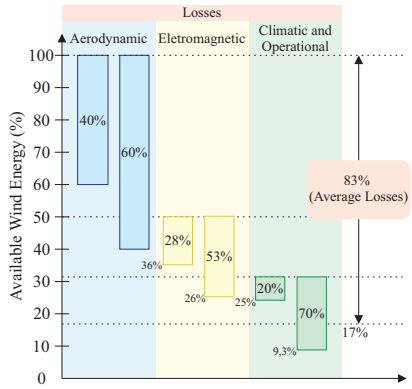

Fig. 2. Overall balance of the losses observed in the wind generators of the Camelinho Park (MG) Source: [7].

V. Frequency Electromagnetic regulator based topology

The rated speed of a wind turbine is relatively low varying from 20 up to 180 rpm and should be adapted to a higher rated velocity in the generator (1200 to 1800 rpm). These speeds levels depend, in the case of the turbine, on the area swept by the blades and the wind flow; in the case of the generator, the number of poles and the frequency of the network.

The efficiency of this control interferes with the frequency of the electric energy generated, the quality of the energy at the point of connection and the use of the kinetic energy of the wind by the turbine. From this point, a new machine was developed, in which the main control variable is the frequency in Fig. 1 [5].

As seen, depending on the number of generator poles, the presence of the gearbox is necessary to adapt the low speed

of rotation of the wind turbine to the high-speed axis of the electric generator. As has been seen, the gearbox has the objective of performing the coupling between the two systems operating at different velocities: the turbine and the generator. The gearbox seeks to ensure the synchronous speed demanded by the generator [8].

1) System structure: The FER is equipment that receives variable speed and offers a constant one. This equipment was developed from a machine that resembles an induction machine, and that allows the system to work with variable speed, coming from the winds, maintaining constant the output speed that, by moving a synchronous generator, does not use the box streaming. Unlike other topologies, this machine uses a VSI, which injects electrical currents into the armature, which is primarily responsible for speed control. The conventional stator of the machine (which is the asynchronous rotor), follows the axis of the wind turbine. An illustration of a wind turbine using the FER is depicted in Fig. 3. The wind turbine(1), the FER(2), the synchronous generator(3), and the VSI(4) present the topology of a wind turbine with the FER.

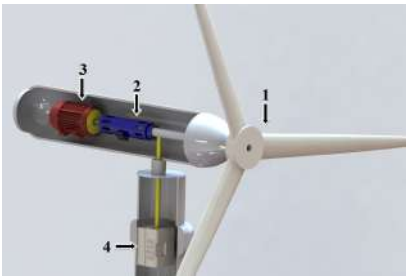

Fig. 3. Illustration of a wind turbine using the FER.

The FER based wind power system prototype is depicted in Fig. 4. The wind speed is emulated using a DC machine able to perform steady-state and transient behavior. The connection with FER asynchronous rotor is performed by mechanical coupling and supported by a mechanical bearing. These mechanical elements also perform the connection between FER rotor synchronous rotor and synchronous generator shaft.

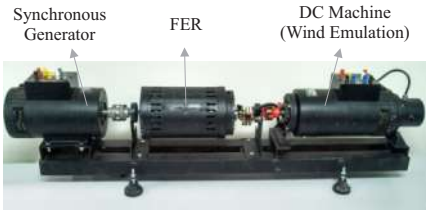

Fig. 4. FER based wind power system prototype.

The collector rings are placed on the axis of the asynchronous rotor to allow the electrical contact from VSI with the armature windings. The VSI feeds the armature to produce a rotating field ($W^{AR}_{CG_ASR}$). In Fig. 5 presents an illustrative image representing in section the physical structure of the prototype. In Fig. 6 it shows an exploded view of the FER.

The components illustrated in the Fig. 5 and Fig. 6 are listed in Table I .

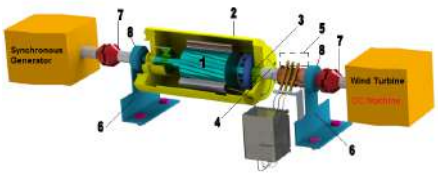

Fig. 5. Cut View of Physical Structure FER.

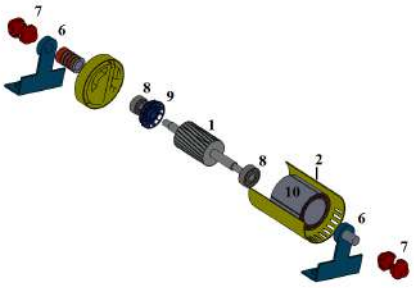

Fig. 6. Exploded View of the Physical Structure of the FER.

TABLE I
COMPONENTS OF THE FER PHYSICAL STRUCTURE.

Number	Component
1	Synchronous Rotor
2	Asynchronous Rotor
3	Asynchronous Rotor Bearing
4	Asynchronous Rotor Shaft
5	Collector ring
6	Bearings
7	Couplings
8	Bearing Bearings
9	Fans
10	Asynchronous Rotor windings

The reference system between the synchronous rotor and the asynchronous rotor remains equivalent to that of a conventional induction machine widely discussed in the literature. However, the relative speed between the synchronous rotor and the fixed reference axis (F) becomes different since the asynchronous rotor suffers a vector displacement (W_v) due to the turbine speed, resulting in a new reference axis (AR), as illustrated by the diagram in Fig. 7. Thus, the rotating fields of the two rotors remain stationary, an essential condition for maintaining the electromagnetic torque that moves the synchronous rotor.

It can be seen that for zero wind speed (W_v=0), we have the traditional reference system (F), with the asynchronous rotor field vector rotating with speed equal to the rotating field vector of the currents injected therein, we would have the speed of the asynchronous rotor field ($W^{F}_{C_ASR}$) equal to the speed of the synchronous rotor ($W^{F}_{C_SR}$) plus the slip:

$$W^{F}_{C_ASR}\rightarrow \;=\; W^{AR}_{C_ASR}\rightarrow + W_V\rightarrow . \qquad (30)$$

2) Scenarios of FER in current topologies: Employing FER, direct coupling of the generator with the power grid

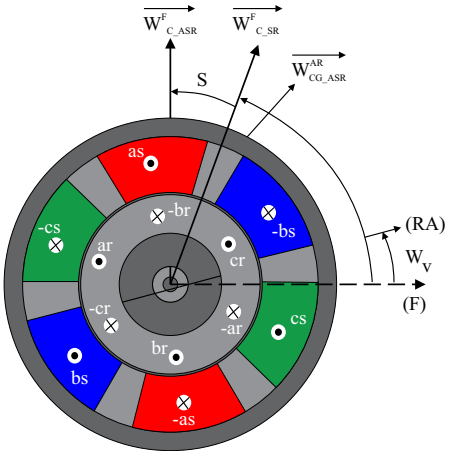

Fig. 7. Diagram with illustration of the reference system-FER.

can be done, avoiding the use of electronic power converters, widely used in traditional topologies, increasing efficiency, reliability and reducing costs.

The similarity of the FER with an induction motor with a cage rotor ensures the replacement of mechanical transmission by robust equipment with high reliability and efficiency.

In a generation of hybrid generation, FER will provide a system in which other sources of energy (batteries, solar panel, hydrogen cells) will be added to the amount of generated energy from the wind source, dispensing with the need of multiplicity of control of energy injection, since with it all energy sources will inject their contributions exclusively through the generator coupled to the FER [5].

VI. Finite Elements

In this type of study, the analytical resolutions are a non-trivial task, requiring a great mathematical effort. For this reason, in most cases, such equations are solved by methods of numerical approximation, among which the Finite Element Method stands out.

The use of FEM usually requires three basic steps: Pre-processing: In the pre-processor, the physical environment is created, that is, the model to be analyzed is inserted by its geometry, determining the properties of the materials, boundary conditions and the loop is generated. Processing: it is based on the application of a method to solve the equations that describe the problem. In the post-processing stage, the goal of this phase is to provide the user with a possible solution. The implementation is performed using COMSOL Multiphysics^o that enables 2D and 3D variables graphical evaluation. The main electrical and construction characteristics of FER are presented in Table II.

VII. Validation Results

The FEM is employed in the time domain solution, to analyze the performance of the machine under nominal conditions.

The electromagnetic processes in the active zone of the FER are described by a field equation that is solved by FEM. Taking into account the stator and the rotor end regions are modeled according to the equations of their domains. The discrete

TABLE II
FER SPECIFICATIONS.

Variables	Values
Rated voltage	380 V
Rated power	3 cv
Rated Speed	3400 rpm
Pair poles	1
Synchronous Rotor Resistance	2.3Ω
Asynchronous Rotor Resistance	2.8Ω
Synchronous Rotor Reactivity	3.7Ω
Reactivity of Asynchronous Rotor	3.9Ω
Mutual Inductance	220mH
Slots Number in Stator	24
Slots Number in Rotor	36
Gap Length	0.6mm
Rated voltage	380 V
Rated power	3 cv
Rated Speed	3400 rpm
Pair poles	1
Synchronous Rotor Resistance	2.3Ω
Asynchronous Rotor Resistance	2.8Ω
Synchronous Rotor Reactivity	3.7Ω
Reactivity of Asynchronous Rotor	3.9Ω
Mutual Inductance	220mH
Slots Number in Stator	24
Slots Number in Rotor	36
Gap Length	0.6mm

field, field equations and the time and discrete loop form a globally coupled system. The position of the rotor is taken into account while this coupled system is solved. The stator winding currents, torque, rotor speed, and other parameters were determined at each time step.

First, the distribution of induced magnetic flux inside the machine was analyzed with the open slots. The result is shown in Fig. 8. The contour lines represent the field lines and the surface is the magnetic flux density. The magnetic flux density has a higher intensity between the grooves.

The rotor bars are represented by closed grooves and investigated the behavior of the magnetic distribution induced in the rotor. The result is shown in Fig. 9. As can be seen with this groove type the field lines did not penetrate the rotor structure, causing insulation between the grooves of the rotor.

The time-domain performance analysis is depicted in Fig. 10. The experiment consists of evaluating the steady-state operation with no coupled load on the rotor called empty operation. The transient is evaluated when a 12 N.m load is coupled at the inception time equal to 1.5 seconds. Referring to the rotor speed shown in Fig. 10(a) it can be seen a good performance during the startup and a 2.16% of maximum slip that appears during the transient period and is almost mitigated after less than 0.25 seconds from the disturbance due to the load inception. According to Fig. 10(b) oscillations can be found at the output torque produced on the rotor. It occurs due to mechanical non-linearity that was not considered in the modeling. However, its mean values follow the desired behavior. Meanwhile, as can be seen in Fig. 10(c), when

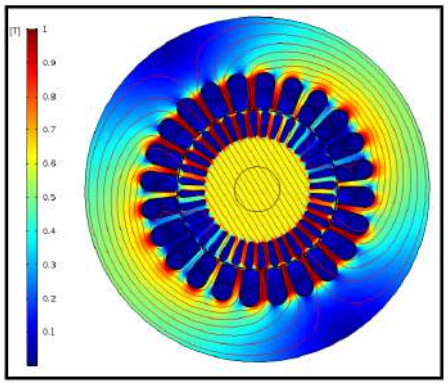

Fig. 8. Distribution of magnetic flux density and equipotential lines.

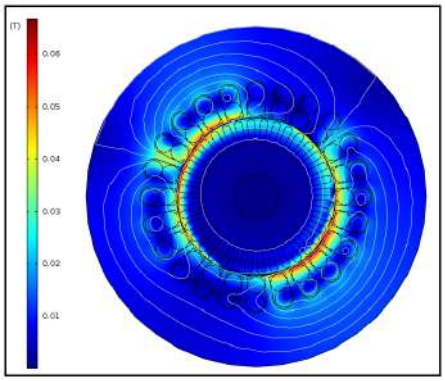

Fig. 9. Distribution of magnetic flux density and equipotential lines.

running on empty, it presents an average loss of approximately 0.95kW/m that equals to 123 W and at nominal load, the losses amount to 1.4 kW/m that is equivalent to 182 W. It results in an average rotor losses increase equals to 59 W with the load inception. The efficiency of the FER was also estimated, according to Fig. 11. When running on empty, FER performed a low efficiency of around 16%. It is similar to induction machines operating in the same conditions. Therefore, at the inception time, the efficiency experiments a marked increase and reaches an average value of 80%.

VIII. Conclusions

Among the new trends on the mechanical transmission of wind power systems, FER showed a promising performance and several advantages on replacing gearboxes. A new wind power topology was proposed to understand spacial devices distribution employing this configuration. To enable forward studies and system improvement this article focused on building a FER model. This model was elaborated using FEM applied to solve differential equations. The validation is performed with an analysis of the distribution of magnetic flux density and equipotential lines at two critical scenarios. Furthermore, a time-domain analysis improves the validation and shows good rotor speed, axle torque, rotor losses, and efficiency performance and ensures the obtained model applicability.A comparison between the power losses of a wind energy conversion system with a gearbox and a FER could be included in a future paper considering the VSC losses.

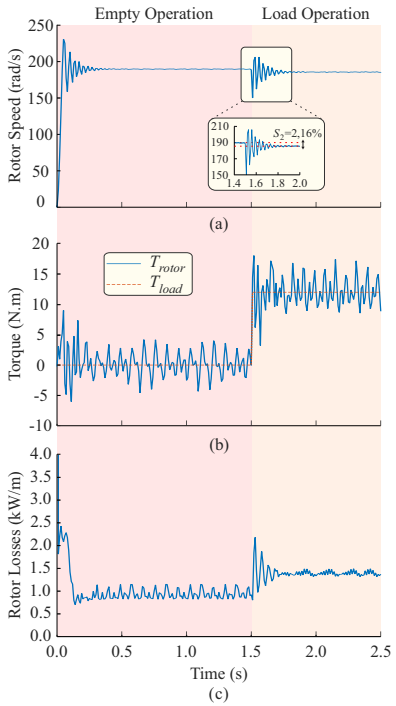

Fig. 10. Time-domain analysis of (a) speed rotor, (b) axle torque and (c) rotor losses.

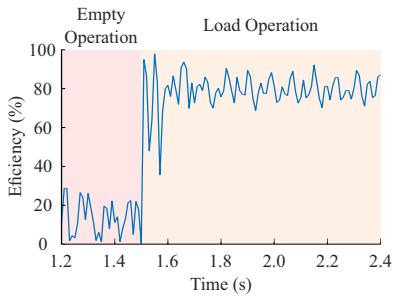

Fig. 11. Time-domain analysis of FER efficiency performance.

References

[1] B. Governo Federal, *Publicação dados abertos*. Empresa de Pesquisa Energética, Brasil, 2022.

[2] A. Merabet, A. A. Tanvir, and K. Beddek, "Speed control of sensorless induction generator by artificial neural network in wind energy conversion system," *IET Renewable Power Generation*, vol. 10(10), pp. 1597–1606, 2016.

[3] D. C. C. Crisóstomo, T. F. do Nascimento, E. A. D. F. Nunes, E. R. L. Villarreal, and A. O. Pinheiro, R. Salazar, "Fuzzy control strategy applied to an electromagnetic frequency regulator in wind generation systems," *Energies*, vol. 15(19), pp. 7011, 1–21, 2022.

[4] R. G. Hernandez and R. G. Ramirez, "Modeling and control of a wind turbine synchronous generator," in *2011 IEEE Electronics, Robotics and Automotive Mechanics Conference*, vol. 1, 2011, pp. 222–227.

[5] P. P. Vitor Silva, R. Ferreira Pinheiro, A. Ortiz Salazar, L. Pereira do Santos Junior, and C. Cesar de Azevedo, "A proposal for a new wind turbine topology using an electromagnetic frequency regulator," *IEEE Latin America Transactions*, vol. 13(4), pp. 989–997, 2015.

[6] R. Gasch and J. Twele, *Windkraftanlagen: Grundlagen, entwurf, planung und betrieb*. Empresa de Pesquisa Energética, Brasil, 2021.

[7] D. E. Castro, C. C. Pellegrini, A. H. Lisboa, and S. M. Pedreira, "Analysis of productive efficiency losses in wind energy conversion systems (wecs)," in *20th International Congress of Mechanical Enginering– COBEM, Proceedings of COBEM*, vol. 1, 2009, pp. 1–10.

[8] S. Y. Liu, *Direct power control on double-fed induction generator*. Master, Electrical engineering, UFMG, Brasil (in Portuguese), 2011.

Impulse elimination for singular second-order system : approach

Elmer R. L. Villarreal , *IEEE Senior Member*, Andrés O. Salazar, Werbert L. A. Da Silva, and Vitor M. D. S. Pereira

***Abstract*—This paper considers approaches to partial eigenvalue assignment in second-order descriptor systems via proportional plus derivative plus output feedback controller. The impulse elimination approach by output feedback control is addressed by combining the eigenstructure and the closed-loop system's finite eigenstructure. More precisely, based on the desired eigenstructure, the gains controller's parametric expressions making the closed-loop system impulse-free and assigning the finite eigenstructure are formulated. The simulation results are provided to verify the effectiveness of the proposed method. This study presents an approach to partial eigenvalue assignment for the descriptor system where an algorithm is presented for calculated the output feedback matrix by the Sylvester equation. Sylvester equations present the theorems. Two algorithms are implemented using the Sylvester equation, and examples were presented with finally their conclusions.**

Keywords: Impulse elimination, Second-order system, Sylvester equation.

I. Introduction

The second-order system model generated a lot interest and a wide variety of practical applications on the past decades [1], [2]. So there are several mathematical methods for solution model and controller design [3], [4], [5], [28], [9], [10], [11]. As is knowledge auto-structure assignment (ESA) and pole assignment are more effective approaches to improve the dynamic characteristics of the singular second-order system, including stabilization, impulse elimination and decoupling [5], [28], [9], [10], [11] [12], [13], [14]. The ESA based on state control and derivative feedback for second-order systems have several valuable results [5], [28], [9], [10], [11] [18], [15] [19] [20].

The existence of a solution in a generalized Sylvester equation was linked to a linear descriptor system and subject to some classification and regional pole placement restrictions. With the hypothesis of strong detectability of the descriptor system through a sequence of coordinate transformations, it was proposed in such a way that the considered problem is solved through a Sylvester equation linked to a detectable reduced-order normal system [37]. The output regulation process for the second-order system via feedback is presented in [16] [17]. Thus, the eigenvalue assignment with minimum sensitivity for second-order systems via proportional – derivative state feedback was proposed in [21]. The aforementioned parametric approach for The ESA in a second-order system via velocity plus-acceleration feedback is presented in [28], [9], [10], and the parametric news expressions of gain controllers assigning the eigenstructure via velocity-plus-acceleration feedback were formulated. Thus the partial pole assignment [22], [23] and partial eigenstructure assignment [24] [25] are focused with many approaches.

The Impulsive behavior was a relevant characteristic of descriptor systems. The Impulse terms destroy the system and thus are expected generate to be eliminated in singular systems. Therefore, there various impulse elimination approaches and results for singular systems [11] [26] [27] [28] . The impulsive modes was eliminated in singular systems via state feedback and output feedback [11] [28]. Thus, the impulse controllability and impulse observability was necessary conditions for impulse elimination in singular systems [28] [29], [31], [32].

The impulsive mode controllability was proposed for singular systems in [30], and the criteria referred to impulsive mode controllability was demonstrated. Thus, a structured output proportional and derivative feedback approach was presented for the problem of impulsive modes elimination in singular systems. Disturbance impulse controllability for the singular system was introduced in [32]. The controllability and observability important conditions of second-order linear systems were analyzed in [33]. The impulse elimination problems for second-order systems have not been explored in the literature. In this paper, the impulse elimination problem was explorer, respectively, via a class of feedback controllers by the ESA approach for a singular second-order system. The concept solvability of the proposed problem is given by analyzing the desired eigenstructure. Sob solvability conditions, news complete parametric expressions for controller gains of normalisation and impulse elimination were derived, respectively.

Elmer Rolando Llanos Villarreal is Department of Natural Sciences, Mathematics, and Statistics, Federal Rural University of Semi-arid (DCME-UFERSA), Mossoró 59625-900, Brazil. (Correspondence: elmerllanos@ufersa.edu.br).

Andrés Ortiz Salazar and Werbet Luiz Almeida da Silva are Department of Computer Engineering and Automation, Federal University of Rio Grande do Norte (DCA-UFRN), Natal 59072-970, Brazil.

Vitor Manoel De Souza Pereira is graduation Interdisciplinary in Science and Technology, Federal Rural University of Semi-arid (BC&T-UFERSA), Caraúbas, RN, 59780-000, Brazil.

email: (elmerllanos@ufersa.edu.br ; andres@dca.ufrn.br ; werbethluizz@hotmail.com ; vitodsouzap@gmail.com).

Correspondence: elmerllanos@ufersa.edu.br .

https://orcid.org/0000-0002-3059-3340; https://orcid.org/0000-0001-5650-3668; https://orcid.org/0000-0001-7197-6957; https://orcid.org/0000-0002-1140-2908.

This study was financed in part by the Coordenação de Aperfeiçoamento de Pessoal de Nível Superior Brazil (CAPES) Finance Code 001 and in part by the process 23091-014712/2019-87-UFERSA.

Copyright ISSN 0719-5567; IEEE eCF 551867. IEEE ICA/ACCA2021: 2021 IEEE International Conference on Automation /XXIV Congress of the Chilean Association of Automatic Control (ICA-ACCA), , Chile, March 22-26, 2021.
978-1-6654-0127-2/21/$31.00 ©2021 IEEE

Finally, showing examples are given.

It is considered the control of the following second-order singular dynamical linear system:

$$\begin{aligned} M\ddot{x} + D\dot{x} + Nx &= Bu \\ y_0 &= C_0 x \\ y_1 &= C_1 \dot{x} \\ y_2 &= C_2 \ddot{x} \end{aligned} \tag{1}$$

where $x \in R^n$ and $u \in R^m$ are the state vector and the control vector, respectively, and $M, D, N \in R^{n\times n}$, and $B \in R^{n\times m}$, $C_0, C_1, C_2 \in R^{p\times n}$ are the system coefficient matrices. In certain applications, the matrices M, D, and N being called the mass matrix, the structural damping matrix and the stiffness matrix, respectively [10] [6], [7], [8] . They know that descriptor system contains impulse terms in its state solution. Impulse elimination is to design a controller such that the state solution of the resulted closed-loop system has no impulsive terms. In [34] is formulated the condition for impulsive-mode controllability is derived and proved to be necessary and sufficient for the existence of admissible feedback controls eliminating related impulsive modes.

The article present in section II the problem formulation and preliminaries, in section III present the impulse elimination, in section IV present the problem eigenstructure assignment , and the section V the conclusions.

II. Problem formulation and preliminaries

These coefficient matrices satisfy the following assumptions.

Assumption 2.1: A_1: rank(M) = q, $0 < q \leq n$, rank(B) = m, and $rank(C_0) = rank(C_1) = rank(C_2) = p$.

For the second-order descriptor dynamical system (1), by choosing the following control law:

$$u(t) = -F_0 y_0(t) - F_1 y_1(t) - F_2 y_2(t) \tag{2}$$

with $F_0, F_1, F_2 \in R^{p\times n}$. For the feedback controller in the equation (2), the conditions are no longer be needed. Thus, the impulse elimination problem that we studied for the singular second-order system is not most considered in [5] [28] [9] [10] [6], [7] [8]. By feedback controller in the equation (2), the system (1) can be transformed into the closed-loop system as follows:

$$(M + BF_2C_2)\ddot{x} + (D + BF_1C_1)\dot{x} + (N + BF_0C_0)x = 0 \tag{3}$$

The respective quadratic polynomial matrix is given below:

$$P(\lambda) = \lambda^2(M + BF_2C_2) + \lambda(D + BF_1C_2) + N + BF_0C_0 \tag{4}$$

The system (3) can be written in the first-order state-space form

$$E_c\dot{z} = A_c z; \tag{5}$$

with

$$\begin{aligned} E_c &= \begin{bmatrix} I_n & 0 \\ 0 & (M + BF_2C_2) \end{bmatrix} \ and \\ A_c &= \begin{bmatrix} 0 & I \\ -(N + BF_0C_0) & -(D + BF_1C_1) \end{bmatrix} \end{aligned} \tag{6}$$

Simultaneously, rewrite the equation (2) as

$$u = -\begin{bmatrix} F_0 & F_{11} \end{bmatrix}\dot{z} - \begin{bmatrix} F_{12} & F_2 \end{bmatrix} z$$

where $F_{11} + F_{12} = F_1$. Substituting this into (2), we have

$$E_c\dot{z} = A_c z \tag{7}$$

with

$$\begin{aligned} E_e &= \begin{bmatrix} I_n & 0 \\ BF_{12}C_1 & M + BF_2C_2 \end{bmatrix}; \\ A_c &= \begin{bmatrix} 0 & I \\ -(N + BF_0C_0) & -(D + BF_{11}C_1) \end{bmatrix} \end{aligned} \tag{8}$$

$\dot{z} = \begin{bmatrix} \dot{x} \\ \ddot{x} \end{bmatrix}$ and $z = \begin{bmatrix} x \\ \dot{x} \end{bmatrix}$

Definition 2.1: The second-order dynamical system (1), is called S-controllable if and only if the corresponding extended first-order state-space representation (5), (6), is S-controllable. The main objective is to design the feedback controller (2) where the closed-loop system has $2n$ eigenvalues. This implies in the equation:

$$\begin{aligned} degdet[\lambda^2(M + BF_2C_2) + \lambda(D + BF_1C_1) + \\ N + BF_0C_0] = 2n \end{aligned} \tag{9}$$

III. Impulse elimination

In [34] prove the equivalence between impulsive-mode controllability and eliminating impulsive modes by feedback control. After impulsive modes being removed by feedback control, a nonsingular descriptor system has a unique smooth solution for each initial admissible condition and hence is free of impulse. Therefore, impulsive-mode elimination and impulse elimination are two different problems. The latter is equivalent to enabling the controlled system to have no impulsive modes and be nonsingular. In [30], impulsive behavior is an essential issue in the singular system, and therefore impulse terms are not expected to exist. A system is called impulse free, or equivalent, having no impulsive modes if there is no impulse term in the state solution. Likewise, the response of the second-order singular system (1) contains impulse terms. Consider the problem of impulse elimination for system (1) via feedback controller (2). By using the ESA method, we present the parametric expressions of gain controllers, ensuring the closed-loop system impulse-free. The following lemma, which is obtained directly by the results of [35], gives a simple rank criterion for a second-order system to be impulse-free.

Lemma 3.1: [30] The system (1) is impulse-free if and only if

$$rank\begin{bmatrix} M & D & N \\ 0 & M & D \\ 0 & 0 & M \end{bmatrix} = rank\begin{bmatrix} M & D \\ 0 & M \end{bmatrix} = n \tag{10}$$

This result gave an approach to detect a system's impulsive modes (1). In this section, the impulse elimination problem is research with based on the following lemma 3.2 instead of the considered Lemma 3.1.

Lemma 3.2: Considered if the system (5), (6) is impulse-free, then system (3) is impulse-free.

Lemma 3.2 previous was easy to prove the concept by matrix decomposition. Thus by Lemma 3.2, in this section, it is consider impulse elimination in the system (5), (6) by feedback controller (2) . The objective is to design the controller (2) such that system (5), (6) is impulse-free. For the system considered (7), (8) it is know that $rankE \geq degdet(sE - A)$ and closed-loop system is impulse-free if and only if $rankE = degdet(sE - A)$,

$$E = \begin{bmatrix} I & 0 \\ BF_{12}C_1 & M + BF_2C_2 \end{bmatrix} \tag{11}$$

$$A = \begin{bmatrix} 0 & I \\ -(N + BF_0C_0) & -(D + BF_{11}C_1) \end{bmatrix} \tag{12}$$

It is assumed that $n_1 = n + rank[M, B]$ is the number desired finite eigenvalues, with $n_2 = 2n - n_1$. Therefore, it is considered the equation (13) :

$$\begin{aligned} n_1 = degdet(sE - A) \leq rankE = n \\ + rank(M + BF_2C_2) \leq n + rank[M, B] \end{aligned} \tag{13}$$

Considered, $rankE = degdet(sE - A)$, where the closed-loop system is impulse-free. Then, based on the ESA approach and Lemma 3.2, news parametric expressions in gains controller make the closed-loop system impulse-free and assign the finite eigenstructure (i.e., Jordan structure of finite eigenvalues) in the closed-loop system is derived.

$$\begin{aligned} G &= diag(G_1, G_2, G_3, \cdots, G_p) \\ G_i &= diag(G_{i1}, G_{i2}, \cdots, G_{iq_i}) \\ G_{ij} &= \begin{bmatrix} \lambda_i & 1 & \cdots & \\ 0 & \lambda_i & 1 & \cdots \\ 0 & \cdots & \lambda_i & 1 \\ 0 & \cdots & \cdots & \lambda_i \end{bmatrix} \end{aligned} \tag{14}$$

where $G_{ij}, j = 1, 2, \cdots, q_i$, are the q_i Jordan blocks related with the eigenvalue λ_i. Thus, G is the Jordan matrix related with all the finite eigenvalues in closed-loop system.

The results significant are presented in the following theorem (3.1):

Theorem 3.1: It is assumed that the system (1) is $S-$controllable. Then, based on the prescribed finite eigenstructure with the form of (14), the controller gains for impulse elimination and arbitrary finite ESA by feedback controller (2) are given by:

$$\begin{aligned} \begin{bmatrix} F_{12} & F_2 \end{bmatrix} &= \begin{bmatrix} H_f G^{-1} & H_\infty \end{bmatrix} P^{-1} \\ \begin{bmatrix} F_0 & F_{11} \end{bmatrix} &= \begin{bmatrix} R_f & R_\infty \end{bmatrix} P^{-1} \end{aligned} \tag{15}$$

where $P \equiv \begin{bmatrix} P_f & P_\infty \end{bmatrix}$, $P_f \in C^{2n \times n_1}$, $H_f, R_f \in C^{r \times n_1}$

$$P_\infty = \begin{bmatrix} 0 \\ \tilde{P}_\infty \end{bmatrix} \in C^{2n \times n_2} \tag{16}$$

$H_\infty \in C^{r \times n_2}$ and

$$\begin{bmatrix} \tilde{P}_\infty \\ H_\infty \end{bmatrix} \in ker[M, B] \tag{17}$$

$R_\infty \in C^{r \times n_2}$ is any given matrix.

Proof:

It is assumed that system (1) is $S-$controllable. With based on the finite ESA results in Theorem 3 in [30], where is considered the equation (2) .

Write this as:

$$\begin{aligned} \begin{bmatrix} F_{12} & F_2 \end{bmatrix} P_f J &= H_f \\ \begin{bmatrix} F_0 & F_{11} \end{bmatrix} P_f &= R_f \end{aligned} \tag{18}$$

Let

$$\begin{bmatrix} F_{12} & F_2 \end{bmatrix} P_\infty = H_\infty \tag{19}$$

then $H_\infty \in C^{r \times n_2}$ and

For given R_∞, let

$$\begin{bmatrix} F_0 & F_{11} \end{bmatrix} P_\infty = R_\infty \tag{20}$$

Combining (18), with the equations (19), and (20), it is obtained

$$\begin{aligned} \begin{bmatrix} F_{12} & F_2 \end{bmatrix} &= \begin{bmatrix} H_f G^{-1} & H_\infty \end{bmatrix} P^{-1} \\ \begin{bmatrix} F_0 & F_{11} \end{bmatrix} &= \begin{bmatrix} R_f & R_\infty \end{bmatrix} P^{-1} \end{aligned} \tag{21}$$

where

$$P \equiv \begin{bmatrix} P_f & P_\infty \end{bmatrix} = \begin{bmatrix} \bar{P}_f & 0 \\ \tilde{P}_f & \tilde{P}_\infty \end{bmatrix}. \tag{22}$$

Thus, the proof is completed.

IV. Problem Eigenstructure Assignment

Considered the following linear time-invariant singular system

$$E\dot{x}(t) = Ax(t) + Bu(t); y(t) = Cx(t) \tag{23}$$

where $E, A \in R^{n \times n}$, $B \in R^{n \times m}$, $C \in R^{p \times n}$ and rank$E = q \leq n$. It is assumed that the matrix pencil$(\lambda E - A)$ is nonsingular matrix, i.e., rank$(\lambda E - A) = n$.

Proposition 4.1: [39] Considered the system (23) is controllable at infinity if and only if

$$rank[E, B] = rank[E, A, B] \tag{24}$$

Proposition 4.2: [39] Considered the system (23) is C-controllable if and only if condition (24) is satisfied together with

$$rank[\lambda E - A, B] = rank[E, A, B], \forall \lambda \in C. \tag{25}$$

Proposition 4.3: [39] Considered the system (23) is I-controllable if and only if

$$\begin{bmatrix} E & 0 & 0 \\ A & E & B \end{bmatrix} = rank[E, A, B] + rank[E]. \tag{26}$$

Proposition 4.4: [39] Considered the system (23) is S-controllable if and only if both the conditions (25) and (26) are satisfied.

A. Eigenstructure by equation Sylvester

Considered the system (3) is written formulated in the first-order state-space form (7) and (8). Thus for obtained the output feedback $K\ \sigma(E_d, A_d + B_d K C_d) \in C^-$, is used the Silvester equation in [38], [36].

Considered the following linear time-invariant singular system in [38], [36].

$$\begin{aligned} E_d\dot{x}(t) &= A_d x(t) + B_d u(t) \\ y(t) &= C_d x(t) \end{aligned} \tag{27}$$

The Sylvester equations in [38], [36].

$$A_d V_d - E_d V_d H_V = -B_d W_d, \qquad \sigma(H_V) \in \mathcal{C}^- \tag{28}$$

$$P_d A_d - H_P P_d E_d = -U_d C_d, \qquad \sigma(H_P) \in \mathcal{C}^- \tag{29}$$

the theorem (4.1) is based , [38].

Theorem 4.1: Let (1), be S-controllable, and $V_d \in R^{2n\times p}$ and $W_d \in R^{m\times p}$ satisfy the equation (28). Then, the following hold.

1) The matrices V_d and W_d given by (28),

$$\begin{bmatrix} A_d - \lambda_i E_d & B_d \\ P_d E_d & 0 \end{bmatrix} \begin{bmatrix} v_i \\ w_i \end{bmatrix} = \ i = 1, 2, \cdots, q. \tag{30}$$

satisfy Sylvester matrix equation (28) for, $i = 1, 2, \cdots, q$,

2) When

$$rank(\begin{bmatrix} V_i \\ W_i \end{bmatrix}) = m \ i = 1, 2, \cdots, q. \tag{31}$$

hold, (30) gives all the solutions.

Proof Based in [38], [36].

The following basic procedure is proposed in order to calculate the feedback controller matrix that stabilizes the closed-loop system when $m + p > q$. Closed-loop eigenvalues are positioned arbitrarily close to the set; they are symmetric sets of pre-specified eigenvalues. The (E_d, A_d, B_d, C_d) system is considered to be strongly controllable and strongly detectable.

Algorithm S_1

Step 1: Choose an array $H_P \in \Re^{q-p\times q-p}$ such that $\sigma(H_P) = \Lambda_P \in \mathcal{C}^-$ and Sylvester's equation (29) is solved to find a matrix

$P_d \in \Re^{n+q-p\times n+q}$ such that

$$rank\ \left(\begin{bmatrix} P_d E_d \\ C_d \end{bmatrix}\right) = q \tag{32}$$

Step 2: Sylvester's equation (28) is solved, for some $H_V \in \Re^{p\times p}$ matrix such that $\sigma(H_V) = \Lambda_V \in \mathcal{C}^-$ taking into account that the matrix V_d must taking into account that $rank\,(E_d V_d) = p$ (or $Ker\,(P_d E_d) = Ker\,(E_d) \oplus Im\,(V_d)$, where $\oplus$ represents the direct sum).

Step 3: By construction, the matrix V_d must verify that rank $(C_d V_d) = p$ and the matrix K can be calculated by:

$$K = W_d (C_d V_d)^{-1} \tag{33}$$

∘

Remark 4.1: steps 1 and 2 can be solved using standard techniques for positioning the self-structure. Similar to the previous case, the matrices V_d and W_d used for the calculation of K can be constructed only with real elements. In particular: if $\lambda_i \in \mathcal{C}$, it is considered $\lambda_{i+1} = \lambda_i^*$ e $\begin{cases} V_i = Re\,(v_i), & V_{i+1} = Imag\,(v_i) \\ W_i = Re\,(w_i), & W_{i+1} = Imag\,(w_i) \end{cases}$, where V_i and W_i denote the columns of the matrices V_d and W_d, respectively. In step 1, under the condition that the system is strongly observable (detectable). As will be seen later, degrees of freedom existing in the choice of V_d that satisfy the coupling condition $P_d E_d V_d = 0$, can also be used to guarantee obtaining K such that $K C_d V_d = W_d$ in [38].

B. Example

Consider a simple linear dynamical system (1) in [30]

$$M = \begin{bmatrix} 3 & 0 & 0 & 0 \\ 0 & 2 & 0 & 0 \\ 0 & 0 & 2 & 0 \\ 0 & 0 & 0 & 0 \end{bmatrix}$$

$$D = \begin{bmatrix} 25 & -15 & 0 & 0 \\ -15 & 35 & -20 & 0 \\ 0 & -20 & 60 & -40 \\ 0 & 0 & -40 & 40 \end{bmatrix}$$

$$N = \begin{bmatrix} 15 & -10 & 0 & 0 \\ -10 & 25 & -15 & 0 \\ 0 & -15 & 35 & -20 \\ 0 & 0 & -20 & 20 \end{bmatrix} \quad B = \begin{bmatrix} 1 & 0 \\ 0 & 0 \\ 0 & 0 \\ 0 & 1 \end{bmatrix}$$

$$C_0 = \begin{bmatrix} 1 & 0 & 0 & 1 \\ 0 & 0 & 0 & 1 \end{bmatrix}; \ C_1 = \begin{bmatrix} 1 & 0 & 0 & 0 \\ 0 & 1 & 0 & 0 \end{bmatrix}$$

$$C_2 = \begin{bmatrix} 1 & 0 & 0 & 1 \\ 0 & 1 & 0 & 1 \end{bmatrix}.$$

Considered the system in the equations (7), (8)

$$E_d = \begin{bmatrix} I_n & 0 \\ 0 & M \end{bmatrix}; \ A_d = \begin{bmatrix} 0 & I_n \\ -N & -D \end{bmatrix};$$

$$B_d = \begin{bmatrix} 0 \\ B \end{bmatrix} \ C_d = \begin{bmatrix} B' & 0 \end{bmatrix}$$

Algorithm $S1$

Resolved the equation (28) for calculate the matrices W_d, V_d, satisfies the equation (31) and the matrix K, such that $K C_d V_d = W_d$:

$$V_d = \begin{bmatrix} 0.0266594 & 0.012664 \\ 0.0532409 & 0.0292111 \\ 0.0526191 & 0.0275588 \\ 0.0428678 & 0.0204925 \\ -0.0799783 & -0.0506558 \\ -0.1597228 & -0.1168444 \\ -0.1578572 & -0.1102353 \\ -0.1286034 & -0.0819702 \end{bmatrix}$$

$$W_d = \begin{bmatrix} 0.9836714 & 0.9919888 \\ 0.9751273 & 0.9892803 \end{bmatrix}$$

$$K = \begin{bmatrix} -172.58241 & 135.085 \\ -173.19315 & 135.43792 \end{bmatrix}$$ where the eigenvalues are $\lambda_1 = -3$, $\lambda_2 = -4$, $\lambda_3 = -5.261107$, $\lambda_4 = -1.5034249$, $\lambda_5 = -0.509633$, $\lambda_6 = -0.7730653$, $\lambda_7 = -22.229984$, $\lambda_8 = -0.229984$.

C. Numerical algorithm

We first present an approach to the general solutions for $F_0, F_1 and F_2$. Let Q denote the matrix that its rows are comprised of orthonormal basis vectors of the null space, we have

$$[F_0, F_1, F_2] = VQ \tag{34}$$

where the parametric matrix V is to be determined based in the sylvester equation (28).

F_0, F_1 and F_2 must also implement some given eigenvalues assignment.

The theorem 4.2 is based in , [40] [38].

Theorem 4.2: Let (1), be S-controllable, and $V_d \in R^{2n\times p}$ and $W_d \in R^{m\times p}$ satisfy the equation (28). Then, the following hold.

1) The matrices V_d and W_d given by (35),

$$\begin{bmatrix} A_d - \lambda_i E_d & B_d \end{bmatrix} \begin{bmatrix} v_i \\ w_i \end{bmatrix} = \ i = 1, 2, \cdots, q. \tag{35}$$

satisfy Sylvester matrix equation (28) for, $i = 1, 2, \cdots, q$,

2) When

$$rank(\begin{bmatrix} V_i \\ W_i \end{bmatrix}) = m \ i = 1, 2, \cdots, q. \tag{36}$$

3) F_0, F_1, F_2 is such that it satisfies

$$(M + BF_2C_2)\ddot{q}(t) + (D + BF_1C_1)\dot{q}(t) + (N + BF_0C_0)q(t) = 0 \tag{37}$$

Proof Based in [37], [36], [38] and [40].

The following basic procedure is proposed in order to calculate the feedback controller matrix that stabilizes the closed loop system, when $m + p > q$. Closed loop eigenvalues are positioned arbitrarily close to the set ; they are symmetric sets of pre-specified eigenvalues. The (E_d, A_d, B_d, C_d) system is considered to be strongly controllable and strongly detectable.

Algorithm $Z1$ Input: M, D, N, B, C_0, C_1, C_2 Output: F_0, F_1, F_2

Step (1) Compute the left null space Q of the coefficient matrix in Equation (23).

Step (2) Compute v_i, w_i, $i =, 01, 2$ by Equations (28), (35), (36) to form V_0, V_1, V_2 and W_0, W_1, W_2.

Step(3) With the matrices W_0, W_1, W_2, V_0, V_1, V_2, satisfies the equation (35),(36) and the matrix F_0, F_1,F_2 such that $F_2C_2V_2 = W_2$, $F_1C_1V_1 = W_1$, and $F_0C_0V_0 = W_0$,

Step (4) Substitute V back into Equation (34) with (37) to give F_0, F_1, F_2.

◦

D. Example

Consider a simple linear dynamical system (1) in [30]

$$M = \begin{bmatrix} 3 & 0 & 0 & 0 \\ 0 & 2 & 0 & 0 \\ 0 & 0 & 2 & 0 \\ 0 & 0 & 0 & 0 \end{bmatrix}$$

$$D = \begin{bmatrix} 25 & -15 & 0 & 0 \\ -15 & 35 & -20 & 0 \\ 0 & -20 & 60 & -40 \\ 0 & 0 & -40 & 40 \end{bmatrix}$$

$$N = \begin{bmatrix} 15 & -10 & 0 & 0 \\ -10 & 25 & -15 & 0 \\ 0 & -15 & 35 & -20 \\ 0 & 0 & -20 & 20 \end{bmatrix}$$

$$B = \begin{bmatrix} 1 & 0 \\ 0 & 0 \\ 0 & 0 \\ 0 & 1 \end{bmatrix} \ C_0 = \begin{bmatrix} 1 & 0 & 0 & 1 \\ 0 & 0 & 0 & 1 \end{bmatrix};$$

$$C_1 = \begin{bmatrix} 1 & 0 & 0 & 0 \\ 0 & 1 & 0 & 0 \end{bmatrix}; C_2 = \begin{bmatrix} 1 & 0 & 0 & 1 \\ 0 & 1 & 0 & 1 \end{bmatrix}.$$

Considered the system in the equations (4), (5)

$$E_d = \begin{bmatrix} I_n & 0 \\ 0 & M \end{bmatrix}; A_d = \begin{bmatrix} 0 & I_n \\ -N & -D \end{bmatrix};$$

$$B_d = \begin{bmatrix} 0 \\ B \end{bmatrix} C_d = \begin{bmatrix} B' & 0 \end{bmatrix}$$

Algorithm Z1

Step (1) Compute the left null space Q of the coefficient matrix in Equation (23).

Step (2) Compute v_i, w_i, $i =, 01, 2$ by Equations (28), (35), (36) to form V_0, V_1, V_2 and W_0, W_1, W_2.

Step(3) With the matrices W_0, W_1, W_2, V_0, V_1, V_2, satisfies the equation (35),(36) and the matrix F_0, F_1,F_2 such that $F_2C_2V_2 = W_2$, $F_1C_1V_1 = W_1$, and $F_0C_0V_0 = W_0$,

Step (4) Substitute V back into Equation (34) with (37) to give F_0, F_1, F_2.

$$V_0 = V_1 = V_2 = \begin{bmatrix} 0.0266594 & 0.012664 \\ 0.0532409 & 0.0292111 \\ 0.0526191 & 0.0275588 \\ 0.0428678 & 0.0204925 \\ -0.0799783 & -0.0506558 \\ -0.1597228 & -0.1168444 \\ -0.1578572 & -0.1102353 \\ -0.1286034 & -0.0819702 \end{bmatrix}$$

$$W_0 = W_1 = W_2 = \begin{bmatrix} 0.98367140.9919888 \\ 0.97512730.9892803 \end{bmatrix}$$

$$F_0 = \begin{bmatrix} -6494.8334 & 10556.91 \\ -6511.9614 & 10584.49 \end{bmatrix}$$

where the eigenvalues are

$\lambda_1 = -3$, $\lambda_2 = -4$, $\lambda_3 = -26.609165$, $\lambda_4 = -0.4710995$, $\lambda_5 = -0.7617854$.

$$F_1 = \begin{bmatrix} -230.40991 & 133.84942 \\ -231.41824 & 134.19385 \end{bmatrix}$$

where the eigenvalues are $\lambda_1 = -3$, $\lambda_2 = -4$, $\lambda_3 = -22.523982$, $\lambda_4 = -0.5$, $\lambda_5 = -0.7672673$, $\lambda_6 = -2.7710422 + 0.7706989j$, $\lambda_7 = -2.7710422 - 0.7706989j$.

$$F_2 = \begin{bmatrix} -172.58241 & 135.085 \\ -173.19315 & 135.43792 \end{bmatrix}$$

where the eigenvalues are $\lambda_1 = -3$, $\lambda_2 = -4$, $\lambda_3 = -22.229984$, $\lambda_4 = -0.509633$, $\lambda_5 = -1.5034249$, $\lambda_6 = -5.2611072$, $\lambda_7 = -0.7730653$.

V. Conclusions

This paper has addressed the approach to partial eigenvalue assignment for the descriptor system with the condition of $S-$controllability. The impulse elimination problems were

considered via a class of feedback controllers for the second-order system using the ESA new approach, and Sylvester equations were addressed. Two theorems were presented using Sylvester's equations. Two algorithms were implemented based on the Sylvester equation, and examples were presented with their conclusions.

REFERENCES

[1] Y. Dumont, D. Goeleven and M. Rochdi, "Reduction of second order unilateral singular systems", Applications in mechanics, *J. Appl. Math. Mech.*, vol. 81, no. 4, pp. 219–245, 2001.

[2] W. Marszalek and H. Unbehauen, "Second order generalized linear systems arising in analysis of flexible beams", *Proceedings.* 31^{st} *Conference on Decision & Control*, Tucson, AZ, December, pp. 35143518, 1992.

[3] M. Hajarian, "Matrix form of the Bi-CGSTAB method for solving the coupled Sylvester matrix equations", *IET Control Theory Applications*, vol. 7, no. 14, pp. 1828–1833, 2013.

[4] M. Dehghan and M. Hajarian, "Efficient iterative method for solving the secondorder Sylvester matrix equation EVF2-AVF-CV=BW", *IET Control Theory Applications*, vol.3, no. 10, pp. 1401-1408, 2009.

[5] G. R. Duan, "Parametric eigenstructure assignment in second-order descriptor linear systems", *IEEE Trans. Automatic Control*, vol. 49, no. 10, pp. 1789–1795, 2004.

[6] T. H. S. Abdelaziz, "Eigenstructure assignment for second-order systems using velocity-plus-acceleration feedback", *Structure Control Health Monit.*, vol. 20, no. 4, pp. 465-482, 2013.

[7] T. H. S. Abdelaziz, "Robust pole placement for second-order linear systems using velocity-plus-acceleration feedback", *IET Control Theory Applications*, vol. 7, no. 14, pp. 1843-1856, 2013.

[8] T. H. S. Abdelaziz, "Parametric approach for eigenstructure assignment in descriptor second-order systems via velocity-plus-acceleration feedback", *Journal Dynamics Systems, Measurement, Control*, vol. 36, no.4, pp. 044505 (8 pages), 2014.

[9] G. R. Duan and G. P. Liu, "Complete parametric approach for eigenstructure assignment in a class of second order system", *Automatica*, vol. 38, no. 4, pp. 725–729, 2002.

[10] T. H. S. Abdelaziz and M. Valasek, "Eigenstructure assignment by proportional-plusderivative feedback for second-order linear control systems", *Kybernetika*, vol. 41, no. 5, pp. 661–676, 2005.

[11] G. R. Duan, "Analysis and design of descriptor linear systems", *Springer*, 2010.

[12] B. Zhang, "Parametric eigenstructure assignment by state feedback in descriptor systems", *IET Control Theory Applications*, vol. 2, no. 4, pp. 303–309, 2008.

[13] B. Zhou, Z. Y. Li and G. R. Duan, "Optimal pole assignment for discrete time systems via Stein equations", *IET Control Theory Application*, vol. 3, no.8, pp. 983-994, 2009.

[14] H. Ouyang, "A hybrid control approach for pole assignment to secondorder asymmetric systems", *Mech. Syst. Signal Process.*, vol.25, no. 1, pp. 123-132, 2011.

[15] J. M. Araújo, C. E.T. Dórea, L. M.G. Gonçalves and B. N. Datta, "State derivative feedback in second-order linear systems: A comparative analysis of perturbed eigenvalues under coefficient variation", *Mechanical Systems and Signal Processing*, vol. 76-77, pp. 33–46, 2016.

[16] Y. Teng and G. R. Duan, "Solvability and complete parametric approach for output regulation problems of matrix second-order systems via error feedback", *J. Harbin Inst. Technol.*, vol. 39, no. 5, pp. 691–695, 2007.

[17] X. Zhang and X. Liu, "Output regulation for matrix second order singular systems via measurement output feedback", *J. Franklin Inst.*, vol. 349, no.6, pp. 2124–2135, 2012.

[18] Y. Kim, H. S. Kim and J. L. Junkins, "Eigenstructure assignment algorithm for mechanical second-order systems", *AIAA J. Guidance Control Dyn.*, vol. 22, no. 5, pp. 729–731, 1999.

[19] D. J. Inman, "Vibration with control", *(John Wiley & Sons Ltd.)*, Chichester, England, 2006.

[20] N. K. Nichols and J. Kautsky, "Robust eigenstructure assignment in quadratic matrix polynomials: nonsingular case", *SIAM J. Matrix Anal. Application.*, vol. 23, no. 1, pp. 77–102, 2001.

[21] G. R. Duan and L. Huang, "Robust pole assignment in descriptor second-order dynamical systems", *Acta Autom. Sin*, vol.33, no. 8, pp. 888-892, 2007.

[22] S. Xu and J. Qian, "Orthogonal basis selection method for robust partial eigenvalue assignment problem in second-order control systems", *Journal Sound and Vibration*, vol.317, no. 12, pp. 1–19, 2008.

[23] M. G. Tehrani and H. Ouyang, "Receptance-based partial pole assignment for asymmetric systems using state-feedback", *Shock Vib.*, vol. 19, no. 5, pp. 1135–1142, 2012.

[24] J. Zhang, H. Ouyang and Y. Zhang, "Partial quadratic eigenvalue assignment in vibrating systems using acceleration and velocity feedback", *Inverse Probl Sci. Eng.* vol. 23, no.3, pp. 479–497, 2015.

[25] J. Zhang, H. Ouyang and J. Yang, "Partial eigenstructure assignment for undamped vibration systems using acceleration and displacement feedback", *Journal Sound Vibration*, vol. 333, no. 1, pp. 1–12, 2014.

[26] G. S. Zhang and W. Q. Liu, "Impulsive mode elimination for descriptor systems by a structured P-D feedback", *IEEE Trans. Automatic Control*, vol. 56, no. 12, pp. 2968–2973, 2011.

[27] M. Hou, "Controllability and elimination of impulsive modes in descriptor systems", *IEEE Trans. Automatic Control*, vol. 49, no. 10, pp. 1723–1727, 2004.

[28] G. R. Duan and A. G. Wu, "Impulse elimination via state feedback in descriptor systems", *Proc. Int. Conf. Impulsive Dyn. Sys. Appl.*, Wuxi, China, October, pp. 722–729, 2005.

[29] S. Shi, Q. Zhang and Z. Yuan, "Hybrid impulsive control for switched singular systems", *IET Control Theory Appl.*, vol 5, no. 1, pp. 103–111, 2011.

[30] P. Yu and G. Zhang, "Eigenstructure assignment and impulse elimination for singular second-order system via feedback control", *IET Control Theory & Applications*, vol. 10, no. 8, pp.869–876, 2016.

[31] A. G. Wu, G. R. Duan and S. M. Zhao, "Impulsive-mode controllablisability in descriptor linear systems", *IET Control Theory Appl.*, vol. 1, no. 3, pp. 558–563, 2007.

[32] Z. B. Yan, "Disturbance impulse controllability in descriptor system", *IEEE Trans. Autom. Control*, vol. 56, no. 4, pp. 946–951, 2011.

[33] P. Losse and V. Mehrmann, "Controllability and observability of second order descriptor systems", *SIAM J. Control Optim.*, vol. 47, no. 3, pp. 1351–1379, 2008.

[34] M. Hou, "Controllability and Elimination of Impulsive Modes in Descriptor Systems" *IEEE Transactions on Automatic Control*, vol. 49, no. 10, pp. 1723-1727, 2004.

[35] D. Henrion, J. C. Zúñiga, "Detecting infinite zeros in polynomial matrices", *IEEE Trans. Circuits Syst. II-Express Briefs*, vol. 52, no. 12, pp. 744–745, 2005.

[36] E. B. Castelan, "Estabilização de sistemas descritores por realimentação de saídas via subespaços invariantes", *Revista Controle & Automação*, vol.16 no.4, pp. 467–477,Outubro,2005.

[37] E. B. Castelan, and V. G. Da Silva, "On the solution of a sylvester equation appearing in descriptor systems control theory", *Systems and Control Letters*, vol. 54, no.2, pp 109-117. 2005.

[38] E. R. L. Villarreal, "Abordagem Geométrica para Estabilização por Realimentação de Saídas e sua Extensão aos Sistemas Descritores", *Doutorado em Engenharia Elétrica-UFSC*, Florianopolis, SC, Brasil, 2002.

[39] V. K. Mishra, N. K. Tomar and M. K. Gupta "On Controllability and Normalizability for Linear Descriptor Systems", *Journal of Control, Automation and Electrical Systems* vol. 27, pp.19–28, 2016.

[40] J. Zhang, Y. Yuan and H. Liu, "An Approach to Partial Quadratic Eigenvalue Assignment of Damped Vibration Systems Using Static Output Feedback", *International Journal of Structural Stability and Dynamics*, vol. 18, no. 1, 1850012, pp. 1–18, 2018.

Approach to partial eigenvalue assignment using Sylvester equation in system-second order

Elmer R. L. Villarreal , *IEEE Senior Member,* Andrés O. Salazar, and Paulo V. F. Vieira

***Abstract*—The article considers an approach for partial eigenvalue assignment in singular second order systems via proportional controller plus derived control plus output feedback controller. It is shown that the problem is closely related to a so-called second-order Sylvester matrix equation. This study presents an approach to partial the eigenstructure assignment for the descriptor system where an algorithm is presented for calculated the output feedback matrix by Sylvester equation. The paper is proposed two complete parametric methods for an approach to partial eigenstructure assignment problems. Both methods are respectively given simples complete parametric expressions for feedback gains and the closed-loop eigenvector matrices. The first one mainly depends on a series of singular value decompositions. The second one utilizes methodology for the system's factorization and enables the closed-loop eigenvalues to be set undetermined and search via specific optimization procedures. The theorems are presented using the Sylvester equations. Two algorithms are implemented using the Sylvester equation, and examples are presented with their conclusions.**

Keywords: Descriptor System, Second-order system, Sylvester equation.

I. Introduction

Second-order linear systems did capture the dynamic behavior of many natural phenomena. They were used for found applications in many fields, such as vibration and structural analysis, spacecraft control, and robotics control and, hence, have attracted much attention, [1], [2], [3], [4], [5].

A generalized Sylvester equation's solution is related to a linear singular system and subject to some rank and regional pole-placement constraints. Thus, under the hypothesis of strong-detectability of the descriptor system, a sequence of coordinate transformations is proposed such that the considered problem can be solved through a Sylvester equation related to a detectable reduced-order standard system [6].

Considered the following second-order singular dynamical linear system:

$$\begin{aligned} M\ddot{x} + D\dot{x} + Nx &= Bu \\ y_0 &= C_0 x \\ y_1 &= C_1 \dot{x} \\ y_2 &= C_2 \dot{x} \end{aligned} \tag{1}$$

where $x \in R^n$ and $u \in R^m$ are the state vector and the control vector, respectively, and $M, D, N \in R^{n\times n}$, and $B \in R^{n\times m}$, $C_0, C_1, C_2 \in R^{p\times n}$ are an system coefficient matrices. In diverse applications, the matrices M, D, and N being called the mass matrix, the structural damping matrix, and the stiffness matrix, respectively. These matrices of respective coefficients must satisfy the following assumptions.

Assumption 1.1: A_1: rank(M) = q, $0 < q \leq n$, rank(B) = m, and $rank(C_0) = rank(C_1) = rank(C_2) = p$.

With respect to concerning the control of the second-order linear system (1) most of the results are focused on stabilization (see, for example, pole assignment [1], [2], and partial pole assignment [3], [4]. Furthermore, various theoretical results for second-order systems were developed via the corresponding extended first-order singular state-space model.

Eigenstructure assignment is a very important problem in linear control systems design, the solution of a generalized Sylvester equation related with a linear singular system where the proposed results are motivated from its use for designing minimal-order observers and for computing output feedback control laws by a particular technique in [6], [7], [8]. In the design, the degree of freedom is supplied by eigenstructure assignment, and it is utilized to minimize the condition number of closed-loop system. The article present in section II the problem formulation, in section III present the solution to problem SSE, in section IV present the solution to problem ESA, in section V present the eigenstructure assignment and the section VI the conclusions.

II. Problem Formulation

Considered the second-order singular dynamical system (1), by choosing the following control law:

$$u(t) = -F_0 y_0(t) - F_1 y_1(t) - F_2 y_2(t) \tag{2}$$

with the matrices $F_0, F_1, F_2 \in R^{p\times n}$. It is obtained the closed-loop system as follows:

Elmer Rolando Llanos Villarreal is Department of Natural Sciences, Mathematics, and Statistics, Federal Rural University of Semi-arid (DCME-UFERSA), Mossoró, RN, 59625-900, Brazil. (Correspondence: elmerllanos@ufersa.edu.br).

Andrés Ortiz Salazar is Department of Computer Engineering and Automation, Federal University of Rio Grande do Norte (DCA-UFRN), Natal, RN, 59072-970, Brazil.

Paulo Victor Fernandes Vieira is graduation Interdisciplinary in Science and Technology, Federal Rural University of Semi-arid (BC&T-UFERSA), Mossoró, RN, 59625-900, Brazil.

e-mail:(elmerllanos@ufersa.edu.br ; andres@dca.ufrn.br ; fernandes_victor2001@hotmail.com).

Correspondence: elmerllanos@ufersa.edu.br .

https://orcid.org/0000-0002-3059-3340; https://orcid.org/0000-0001-5650-3668; https://orcid.org/0000-0003-2668-5362.

This study was financed in part by the Coordenação de Aperfeiçoamento de Pessoal de Nível Superior Brasil (CAPES) Finance Code 001 and in part by the process 23091-014712/2019-87-UFERSA.

Copyright ISSN 0719-5567; IEEE eCF 551868. IEEE ICA/ACCA2021: 2021 IEEE International Conference on Automation /XXIV Congress of the Chilean Association of Automatic Control (ICA-ACCA), Santiago, Chile, March 22-26, 2021.

978-1-6654-0127-2/21/$31.00 ©2021 IEEE

$$(M+BF_2C_2)\ddot{x}+(D+BF_1C_1)\dot{x}+(N+BF_0C_0)x \quad = \quad 0 \tag{3}$$

Thus, the system (3) is written in the first-order state-space form:

$$E_c\dot{z} \quad = \quad A_cz; \tag{4}$$

with

$$\begin{aligned} E_c &= \begin{bmatrix} I_n & 0 \\ 0 & (M+BF_2C_2) \end{bmatrix} \quad and \\ A_c &= \begin{bmatrix} 0 & I \\ -(N+BF_0C_0) & -(D+BF_1C_1) \end{bmatrix} \end{aligned} \tag{5}$$

It is here require the closed-loop matrix pair $(E_c; A_c)$ to be nondefective, that is, the Jordan form of matrix pair $(E_c; A_c)$ possesses a diagonal form. Further, following the pole assignment theory for first-order descriptor linear systems, under the controllability of system (1), $n+q$ finite eigenvalues can be assigned to the closed-loop system (4), (5). Therefore, the desired Jordan form of the matrix pair $(E_c; A_c)$ takes the form

$$\Lambda = diag(\lambda_1, \lambda_2, \ldots, \lambda_{n+q}) \tag{6}$$

where $\lambda_i, i = 1, 2, \ldots n+q$, are clearly the eigenvalues of matrix pair $(E_c; A_c)$. It is based on lemma in [14], thus is obtained the following lemma (2.1)

Lemma 2.1: Let E_c, A_c be given by (4), (5) , and by (6) Then, the following hold. 1) There exist matrices $V_1, V_2 \in R^{n\times n+q}$ satisfying

$$A_c\begin{bmatrix} V_1 \\ V_2 \end{bmatrix} = E_c\begin{bmatrix} V_1 \\ V_2 \end{bmatrix}\Lambda \tag{7}$$

if and only if

$$\begin{aligned} (M+BF_2C_2)V_1\Lambda^2+(D+BF_1C_1)V_1\Lambda+ \\ (N+BF_0C_0)V_1 = 0 \end{aligned} \tag{8}$$

and

$$V_2 = V_1\Lambda \tag{9}$$

2) There exist matrices V_∞, $V_\infty^{'} \in R^{n\times q}$ satisfying

$$E_c\begin{bmatrix} V_\infty^{'} \\ V_\infty \end{bmatrix} = 0, and, rank(\begin{bmatrix} V_\infty^{'} \\ V_\infty \end{bmatrix}) = n-q \tag{10}$$

if and only if $V_\infty^{'} = 0$ and consider the matrix $M_1 = (M + BF_2C_2)$

$$M_1V_\infty = 0 \; rank(V_\infty) = n-q \tag{11}$$

III. SOLUTION TO PROBLEM SSE

Consider the following linear time-invariant descriptor system

$$E_1\dot{x}(t) \quad = \quad A_1x(t)+B_1u(t); y(t) = CC_1x(t) \tag{12}$$

where $E_1, A_1 \in R^{n\times n}$, $B_1 \in R^{n\times m}$, $CC_1 \in R^{p\times n}$ and rank$E_1 = q \leq n$. Assume that the matrix pencil$(\lambda E_1 - A_1)$ is nonsingular, i.e., rank$(\lambda E_1 - A_1) = n$.

Proposition 3.1: [9] Considered the system (12) is controllable at infinity if and only if

$$rank[E_1, B_1] = rank[E_1, A_1, B_1] \tag{13}$$

Proposition 3.2: [9] Considered the system 12 is C-controllable if and only if condition (13) is satisfied together with

$$rank[\lambda E_1 - A_1, B_1] = rank[E_1, A_1, B_1], \forall\lambda \in C. \tag{14}$$

Proposition 3.3: [9] The system (12) is I-controllable if and only if

$$\begin{bmatrix} E_1 & 0 & 0 \\ A_1 & E_1 & B_1 \end{bmatrix} = rank[E_1, A_1, B_1] + rank(E_1). \tag{15}$$

Proposition 3.4: [9] Considered the system (12) is S-controllable if and only if both the conditions (14) and (15) respectively are satisfied.

Letting

$$\begin{aligned} W = F_1C_1V\lambda + F_0C_0V = \\ \begin{bmatrix} F_0C_0 & F_1C_1 \end{bmatrix}\begin{bmatrix} V \\ V\Lambda \end{bmatrix} \end{aligned} \tag{16}$$

then (8) becomes

$$\begin{aligned} (M+BF_2C_2)V\Lambda^2+DV\Lambda+NV = \\ BF_1C_1V\Lambda+(BF_0C_0)V \end{aligned} \tag{17}$$

$$(M+BF_2C_2)V\Lambda^2+DV\Lambda+NV \quad = \quad BW \tag{18}$$

Denote

$$V = \begin{bmatrix} v_1 & v_2 & \cdots & v_q \end{bmatrix} \tag{19}$$

$$W = \begin{bmatrix} w_1 & w_2 & \cdots & w_q \end{bmatrix} \tag{20}$$

It is converted the second-order Sylvester matrix equation (18) into the following column form:

$$(\lambda_i^2(M+BF_2C_2)+\lambda_iD+N)v_i \quad = \quad Bw_i \; i = 1, 2, \cdots, q. \tag{21}$$

The equations in (21), it is further written in the following form:

$$\Pi_i\begin{bmatrix} v_i \\ w_i \end{bmatrix} = 0 \; i = 1, 2, \cdots, q. \tag{22}$$

where

$$\Pi_i = \begin{bmatrix} \lambda_i^2M+\lambda_iD+N & -B \end{bmatrix}, \; i = 1, 2, \cdots, q. \tag{23}$$

This states that

$$\begin{bmatrix} v_i \\ w_i \end{bmatrix} \in Ker\,\Pi_i \; i = 1, 2, \cdots, q. \tag{24}$$

Thus, the following algorithm produces two sets of constant matrices T_i and U_i, $i = 1, 2, \cdots, q$, to be used in the representation of the solution found to the matrix equation (18), the following simple procedure is used and with based in [14].

Algorithm new P_1

Solving T_i and U_i, $i = 1, 2, \cdots, q$,

Step 1) Through applying SVD to the matrix Π_i, $i = 1, 2, \cdots, q$, is obtained two sets of matrices $P_i \in C^{n\times n}$ and $Q_i \in C^{n+m\times n+m}$, $i = 1, 2, \cdots, q$, satisfying

$$P_i\Pi_i Q_i = \begin{bmatrix} diag(\sigma_1, \sigma_2, \cdots, \sigma_q) & 0 \\ 0 & 0 \end{bmatrix}, \; i = 1, 2, \cdots, q. \tag{25}$$

where, $\sigma_i > 0$, $i = 1, 2, \cdots, q$, are the singular values of Π_i

$$q = rank \begin{bmatrix} \lambda^2(M + BF_2C_2) + \lambda D + N & B \end{bmatrix}, \tag{26}$$

Step 2) It is obtained the matrices $T_i \in R^{n\times n+m-q}$ and $U_i \in R^{m\times n+m-q}$, $i = 1, 2, \cdots, q$, by partitioning the matrix Q_i as follows

$$Q_i = \begin{bmatrix} * & T_i \\ * & U_i \end{bmatrix}, \; i = 1, 2, \cdots, q. \tag{27}$$

Thus, as a result of the equations (25) and (27), the matrices $T_i \in R^{n\times n+m-q}$ and $U_i \in R^{m\times n+m-q}$, $i = 1, 2, \cdots, q$, is obtained through Algorithm P_1 that satisfy

$$\Pi_i \begin{bmatrix} T_i \\ U_i \end{bmatrix} = 0,$$

$$rank \begin{bmatrix} T_i \\ U_i \end{bmatrix} = n + m - q \; i = 1, 2, \cdots, q. \tag{28}$$

Therefore, the columns of $\begin{bmatrix} T_i \\ U_i \end{bmatrix}$ form a set of basis for kerΠ_i. i. The previous deduction clearly yields the following result, where the theorem 3.1 is with based in [14].

Theorem 3.1: Let (1) S-controllable with the condition (26), and the conditions (14) and (15) respective are satisfied.

$T_i \in R^{n\times n+m-q}$ and $U_i \in R^{m\times n+m-q}$, $i = 1, 2, \cdots, q$, it is obtained via Algorithm new P_1. Then, all the matrices V and W satisfying the second-order Sylvester matrix equation (18) can be parameterized by columns as follows

$$\begin{bmatrix} v_i \\ w_i \end{bmatrix} = \begin{bmatrix} T_i \\ U_i \end{bmatrix} f_i \; i = 1, 2, \cdots, q. \tag{29}$$

$f_i \in R^{n+m-q}$, $i = 1, 2, \cdots, q$, are a set of arbitrary parameter vectors.

Thus, regarding the S-controllability of (1), it is obtained the following primary result, which is a general extension of the well-known PHB criterion [10].

Lemma 3.1: The second-order dynamical system (1), is S-controllable if and only if

$$rank \begin{bmatrix} \lambda_i^2(M + BF_2C_2) + \lambda_i D + N & B \end{bmatrix} = n, \; \forall\lambda \in C. \tag{30}$$

The solution for this case depends on a pair of polynomial matrices $T(\lambda) \in R^{n\times n+m-q}$ and $U(\lambda) \in R^{m\times n+m-q}$, satisfying

$$\begin{bmatrix} \lambda_i^2(M + BF_2C_2) + \lambda_i D + N \end{bmatrix} T(\lambda) = BU(\lambda). \tag{31}$$

In the case where (1), is regular, that is, det$(\lambda_i^2(M+BF_2C_2)+\lambda_i D+N)$ is not identically zero, the aforementioned equation can be written as

$$\begin{bmatrix} \lambda_i^2(M + BF_2C_2) + \lambda_i D + N \end{bmatrix}^{-1} B = T(\lambda)U^{-1}(\lambda). \tag{32}$$

which can be viewed as the right factorization of the following transfer function

$$G(\lambda) = \begin{bmatrix} \lambda_i^2(M + BF_2C_2) + \lambda_i D + N \end{bmatrix}^{-1} B.$$

For simplicity, we also call (31) the factorization of (1), where the theorem 3.2 is based in [14]

Theorem 3.2: Let (1), be S-controllable, and $T(\lambda) \in R^{n\times n+m-q}$ and $U(\lambda) \in R^{m\times n+m-q}$ satisfy the factorization (31). Then, the following hold.

1) The matrices V and W given by (19), (20)

$$\begin{bmatrix} v_i \\ w_i \end{bmatrix} = \begin{bmatrix} T(\lambda_i) \\ U(\lambda_i) \end{bmatrix} f_i \; i = 1, 2, \cdots, q. \tag{33}$$

satisfy the second-order Sylvester matrix equation (18) for $f_i \in C^{n+m-q}$, $i = 1, 2, \cdots, q$,

2) When

$$rank \begin{bmatrix} T(\lambda_i) \\ U(\lambda_i) \end{bmatrix} = n + m - q \; i = 1, 2, \cdots, q. \tag{34}$$

The factorization (31) performs a fundamental role in the solution (33). When (1), is regular and $\lambda_i, i = 1, 2, \cdots, q$, are chosen to be different from the zeros of det$(\lambda^2 M + \lambda D + N)$,$M_1 = (M + BF_2C_2)$ we can take

$$\begin{cases} T(\lambda_i) = Adj(\lambda^2 M_1 + \lambda D + N)B \\ U(\lambda_i) = det(\lambda^2 M_1 + \lambda D + N)I_m \end{cases}$$

For general numerical algorithms solving such factorizations, one can refer to [12], [13]. The following simple procedure can also be used and is based in [14].

Algorithm new P_2 (new coprime factorization)

Step 1) Under the S-controllability of system (1), find a pair of unimodular matrices $P(\lambda)$ and $Q(\lambda)$, of appropriate dimensions, satisfying

$$P(\lambda) \begin{bmatrix} \lambda^2 M_1 + \lambda D + N & B \end{bmatrix} Q(\lambda) = \begin{bmatrix} I_n & 0 \end{bmatrix}$$

Step 2) It is obtained the pair of polynomial matrices $T(\lambda) \in R^{n\times m}$ and $U(\lambda) \in R^{m\times m}$ by partitioning the unimodular matrix $Q(\lambda)$

$$Q(\lambda) = \begin{bmatrix} * & T(\lambda) \\ * & U(\lambda) \end{bmatrix}$$

It is worth pointingout that the pair of polynomial matrices $T(\lambda) \in R^{n\times m}$ and $U(\lambda) \in R^{m\times m}$ satisfying the right factorization (31), it is obtained from the Algorithm new P_2 are coprime

$$rank \begin{bmatrix} T(\lambda) \\ U(\lambda) \end{bmatrix} = m \ \forall \lambda \in C \tag{35}$$

IV. THE SOLUTION TO PROBLEM ESA

Following from the results in Section III, it is obtained the following two theorems regarding the solution to Problem ESA. Where the theorems 4.1 and 4.2 is based in [14].

Theorem 4.1: Let n_i $i = 1, 2, \cdots, n+q$ with condition expressed in (26), and $T_i \in R^{n\times n+m-q}$ and $U_i \in R^{m\times n+m-q}$, $i = 1, 2, \cdots, n+q$, be given by Algorithm P_1. Then, the following hold.

1) Problem ESA has solutions if and only if there exist a group of parameters $f_i \in C^{n+m-q}$ $i = 1, 2, \cdots, n+q$, satisfying the following constraints.

Constraint $Co_1 : f_i = \bar{f}_j$ if $\lambda_i = \bar{\lambda}_j$.

Constraint $C2_a$: det$V_c \neq 0$, with

$$V_c = \begin{bmatrix} T_1 f_1 & T_2 f_2 \cdots & T_{n+q} f_{n+q} & 0 \\ \lambda_1 T_1 f_1 & \lambda_2 T_2 f_2 \cdots & \lambda_{n+q} T_{n+q} f_{n+q} & V_\infty \end{bmatrix} \tag{36}$$

2) When this condition is met, all the solutions to problem ESA are given by

$$V = \begin{bmatrix} T_1 f_1 & T_2 f_2 & \cdots & T_{n+q} f_{n+q} \end{bmatrix} \tag{37}$$

and

$$\begin{bmatrix} F_0 C_0 & F_1 C_1 \end{bmatrix} = \begin{bmatrix} U_1 f_1 & U_2 f_2 & \cdots & U_{n+q} f_{n+q} & W_\infty \end{bmatrix} V_c^{-1} \tag{38}$$

where $f_i \in R^{n+m-q}$, $i = 1, 2, \cdots, n+q$, are arbitrary parameter vectors satisfying constraints Co_1 and C_{2a} and $W_\infty \in C^{m\times(n-q}$ is an arbitrary parameter matrix.

Theorem 4.2:

Let (1), be S-controllable, and $T(\lambda) \in R^{n\times m}$ and $U(\lambda) \in R^{m\times m}$ be a pair of polynomial matrices satisfying the right factorization (31) and condition (34). Then

1) Problem ESA has solutions if and only if there exist a group of parameters $f_i \in C^m$ $i = 1, 2, \cdots, n+q$, satisfying Co_1 and Constraint C_{2b}: det$V_{cb} \neq 0$ with

$$V_{cb} = \begin{bmatrix} T(\lambda_1) f_1 & T(\lambda_2) f_2 \cdots & T(\lambda_{n+q}) f_{n+q} & 0 \\ \lambda_1 T(\lambda_1) f_1 & \lambda_2 T(\lambda_2) f_2 \cdots & \lambda_{n+q} T(\lambda_{n+q}) f_{n+q} & V_\infty \end{bmatrix} \tag{39}$$

2) When this condition is met, all the solutions to problem ESA are given by

$$V = \begin{bmatrix} T(\lambda_1) f_1 & T(\lambda_2) f_2 \cdots & T(\lambda_{n+q}) f_{n+q} \end{bmatrix} \tag{40}$$

and

$$\begin{bmatrix} F_0 C_0 & F_1 C_1 \end{bmatrix} = \begin{bmatrix} U(\lambda_1) f_1 & U(\lambda_2) f_2 & \cdots & U(\lambda_{n+q}) f_{n+q} & W_\infty \end{bmatrix} V_{cb}^{-1} \tag{41}$$

where $f_i \in R^m$, $i = 1, 2, \cdots, n+q$, are arbitrary parameter vectors satisfying Constraints Co_1 and C_{2b} and $W_\infty \in C^{m\times(n-q)}$ is an arbitrary parameter matrix.

V. PROBLEM EIGENSTRUCTURE ASSIGNMENT: APPROACH

Strong stability can be interpreted in terms of the closed-loop system's self-structure: 1. Asymptotic stability is equivalent to that all finite poles are inside the left semi plane of the complex plane. 2.The absence of impulsive modes is equivalent to having q finite poles in a closed-loop. 3. Regularity is guaranteed if the system is free from impulsive modes. Based on this interpretation, necessary and sufficient conditions for the existence of S-stabilizable output feedback are established from a set of generalized coupled Sylvester equations, [6], [7], [8].

A. Eigenstructure by equation Sylvester

The system (3) is written in the first-order state-space form (4) and (5). Thus for obtained the output feedback matrix K $\sigma(E_d, A_d + B_d K C_d) \in C^-$, is used the Silvester equation in [8], [7].

Consider the following linear time-invariant descriptor system in [8], [7].

$$\begin{aligned} E_d \dot{x}(t) &= A_d x(t) + B_d u(t) \\ y(t) &= C_d x(t) \end{aligned} \tag{42}$$

The Sylvester equations in [8], [7].

$$A_d V_d - E_d V_d H_V = -B_d W_d, \qquad \sigma(H_V) \in \mathcal{C}^- \tag{43}$$

$$P_d A_d - H_P P_d E_d = -U_d C_d, \qquad \sigma(H_P) \in \mathcal{C}^- \tag{44}$$

The theorem 5.1 is based in [14], [8].

Theorem 5.1: Let (1), be S-controllable, and $V_d \in R^{2n\times p}$ and $W_d \in R^{m\times p}$ satisfy the equation (43). Then, the following hold.

1) The matrices V_d and W_d given by (45),

$$\begin{bmatrix} A_d - \lambda_i E_d & B_d \end{bmatrix} \begin{bmatrix} v_i \\ w_i \end{bmatrix} = \ i = 1, 2, \cdots, q. \tag{45}$$

satisfy Sylvester matrix equation (43) for, $i = 1, 2, \cdots, q$,

2) When

$$rank(\begin{bmatrix} V_i \\ W_i \end{bmatrix}) = m \ i = 1, 2, \cdots, q. \tag{46}$$

hold, (45) gives all the solutions.

Proof Based in [7], [8].

The following basic procedure is proposed to calculate the feedback controller that stabilizes the closed loop system, when $m+p > q$. Closed loop eigenvalues are positioned arbitrarily close to the set ; they are symmetric sets of pre-specified eigenvalues. The (E_d, A_d, B_d, C_d) system is considered to be strongly controllable and strongly detectable.

Algorithm $S1$

Step 1: Choose an array $H_P \in \Re^{q-p\times q-p}$ such that $\sigma(H_P) = \Lambda_P \in \mathcal{C}^-$ and Sylvester's equation (44) is solved to find a matrix

$P_d \in \Re^{n+q-p\times n+q}$ such that

$$rank\left(\left[\begin{array}{c} P_dE_d \\ C_d \end{array}\right]\right) = q \tag{47}$$

Step 2: Sylvester's equation (43) is solved, for some $H_V \in \Re^{p\times p}$ matrix such that $\sigma(H_V) = \Lambda_V \in \mathcal{C}^-$ taking into account that the matrix V_d taking into account that $rank\,(E_dV_d) = p$ (or $Ker\,(P_dE_d) = Ker\,(E_d) \oplus Im\,(V_d)$, where $\oplus$ represents the direct sum).

Step 3: By construction, the matrix V_d must verify that rank $(C_dV_d) = p$ and the matrix K can be calculated by:

$$K \quad = \quad W_d(C_dV_d)^{-1} \tag{48}$$

∘

In step 1, under the condition that the system is strongly observable (detectable). As will be seen later, degrees of freedom existing in the choice of V_d, can also be used to guarantee obtaining K such that $KC_dV_d = W_d$ in [8].

B. Example

Consider a simple linear dynamical system (1) in [14]

$M = \left[\begin{array}{ccc} 1 & 0 & 0 \\ 0 & 1 & 0 \\ 0 & 0 & 0 \end{array}\right]$

$D = \left[\begin{array}{ccc} 2.5 & -0.5 & 0 \\ -0.5 & 2.5 & -2 \\ 0 & -2 & 2 \end{array}\right]$

$N = \left[\begin{array}{ccc} 10 & -5 & 0 \\ -5 & 25 & -20 \\ 0 & -20 & 20 \end{array}\right]$ $B = \left[\begin{array}{cc} 1 & 0 \\ 0 & 0 \\ 0 & 1 \end{array}\right]$

Considered the system in (4), (5) $E_d = \left[\begin{array}{cc} I_n & 0 \\ 0 & M \end{array}\right]$;

$A_d = \left[\begin{array}{cc} 0 & I_n \\ -N & -D \end{array}\right]$;

$B_d = \left[\begin{array}{c} 0 \\ B \end{array}\right]$ $C_d = \left[\begin{array}{cccccc} 1 & 0 & 0 & 0 & 0 & 0 \\ 0 & 1 & 1 & 0 & 0 & 0 \end{array}\right]$

$C_0 = \left[\begin{array}{ccc} 1 & 0 & 1 \\ 0 & 1 & 1 \end{array}\right]$; $C_1 = \left[\begin{array}{ccc} 1 & 0 & 0 \\ 0 & 1 & 1 \end{array}\right]$

$C_2 = \left[\begin{array}{ccc} 1 & 0 & 0 \\ 0 & 1 & 0 \end{array}\right]$.

Considered the system in the equations (7), (8)

$E_d = \left[\begin{array}{cc} I_n & 0 \\ 0 & M \end{array}\right]$; $A_d = \left[\begin{array}{cc} 0 & I_n \\ -N & -D \end{array}\right]$;

$B_d = \left[\begin{array}{c} 0 \\ B \end{array}\right]$ $C_d = \left[\begin{array}{cccccc} 1 & 0 & 0 & 0 & 0 & 0 \\ 0 & 1 & 1 & 0 & 0 & 0 \end{array}\right]$

Algorithm S1

Resolved the equation (43) for calculate the matrices W_d, V_d, satisfies the equation (46) and the matrix K, such that $KC_dV_d = W_d$:

$V_d = \left[\begin{array}{cc} 0.1095906 & 0.0695801 \\ 0.0973067 & 0.0550873 \\ 0.1567901 & 0.1249138 \\ -0.3287717 & -0.2783205 \\ -0.2919201 & -0.2203492 \\ -0.4703702 & -0.4996553 \end{array}\right]$

$W_d = \left[\begin{array}{c} 0.91971790.9480201 \\ 0.8327670.8379183 \end{array}\right]$

$K = \left[\begin{array}{cc} -36.816339 & 19.498243 \\ -30.793252 & 16.558322 \end{array}\right]$

$\lambda_1 = -3$, $\lambda_2 = -4$, $\lambda_3 = -1.0795178 + 6.1019018j$, $\lambda_4 = -1.0795178 - 6.1019018j$, $\lambda_5 = -4.4381969$.

C. Numerical algorithm

It is first present an approach to the general solutions for F_0, F_1 and F_2. Let Q denote the matrix that its rows are comprised of orthonormal basis vectors of the null space, and it is has:

$$[F_0, F_1, F_2] = VQ \tag{49}$$

where the parametric matrix V is determined based on the Sylvester equation (43).

The matrices F_0, F_1 and F_2 must also implement some given eigenvalues assignment.

The theorem 5.2 is based in , [8] [11] .

Theorem 5.2: Let (1), be S-controllable, and $V_d \in R^{2n\times p}$ and $W_d \in R^{m\times p}$ satisfies the equation (43). Then, the following hold.

1) The matrices V_d and W_d given by (50),

$$\left[\begin{array}{cc} A_d - \lambda_i E_d & B_d \end{array}\right]\left[\begin{array}{c} v_i \\ w_i \end{array}\right] = \; i = 1, 2, \cdots, q. \tag{50}$$

satisfy Sylvester matrix equation (43) for, $i = 1, 2, \cdots, q$,

2) When

$$rank(\left[\begin{array}{c} V_i \\ W_i \end{array}\right]) = m \; i = 1, 2, \cdots, q. \tag{51}$$

3) F_0, F_1, F_2 is such that it satisfies

$$(M + BF_2C_2)\ddot{q}(t) + (D + BF_1C_1)\dot{q}(t) + (N + BF_0C_0)q(t) = 0 \tag{52}$$

Proof Based in [7], [8], and [11].

The following basic procedure is proposed to calculate the feedback controller that stabilizes the closed loop system, when $m+p > q$. Closed loop eigenvalues are positioned arbitrarily close to the set ; they are symmetric sets of pre-specified eigenvalues. The (E_d, A_d, B_d, C_d) system is considered to be strongly controllable and strongly detectable.

Algorithm Z1 Input: M, D, N, B, C_0, C_1, C_2 Output: F_0, F_1, F_2

Step (1) Compute the left null space Q of the coefficient matrix in Equation (49).

Step (2) Compute v_i, w_i, $i =, 01, 2$ by Equations (43), (50), (51) to form V_0, V_1, V_2 and W_0, W_1, W_2.

Step(3) With the matrices W_0, W_1, W_2, V_0, V_1, V_2, satisfies the equation (50),(51) and the matrix F_0, F_1,F_2 such that $F_2C_2V_2 = W_2$, $F_1C_1V_1 = W_1$, and $F_0C_0V_0 = W_0$,

Step (4) Substitute V back into Equation (49) with (52) to give F_0, F_1, F_2.

○

D. Example

Consider a simple linear dynamical system (1) in [14]

$$M = \begin{bmatrix} 1 & 0 & 0 \\ 0 & 1 & 0 \\ 0 & 0 & 0 \end{bmatrix} \quad D = \begin{bmatrix} 2.5 & -0.5 & 0 \\ -0.5 & 2.5 & -2 \\ 0 & -2 & 2 \end{bmatrix}$$

$$N = \begin{bmatrix} 10 & -5 & 0 \\ -5 & 25 & -20 \\ 0 & -20 & 20 \end{bmatrix} \quad B = \begin{bmatrix} 1 & 0 \\ 0 & 0 \\ 0 & 1 \end{bmatrix}.$$

Considered the system in (4), (5) $E_d = \begin{bmatrix} I_n & 0 \\ 0 & M \end{bmatrix}$; $A_d = \begin{bmatrix} 0 & I_n \\ -N & -D \end{bmatrix}$; $B_d = \begin{bmatrix} 0 \\ B \end{bmatrix}$

$$C_0 = \begin{bmatrix} 1 & 0 & 0 & 1 \\ 0 & 0 & 0 & 1 \end{bmatrix}; \; C_1 = \begin{bmatrix} 1 & 0 & 0 & 0 \\ 0 & 1 & 0 & 0 \end{bmatrix}$$

$$C_2 = \begin{bmatrix} 1 & 0 & 0 & 1 \\ 0 & 1 & 0 & 1 \end{bmatrix}.$$

Considered the system in the equations (4), (5)

$$E_d = \begin{bmatrix} I_n & 0 \\ 0 & M \end{bmatrix}; \; A_d = \begin{bmatrix} 0 & I_n \\ -N & -D \end{bmatrix};$$

$$B_d = \begin{bmatrix} 0 \\ B \end{bmatrix}$$

$$C_d = \begin{bmatrix} 1 & 0 & 0 & 0 & 0 & 0 \\ 0 & 1 & 1 & 0 & 0 & 0 \end{bmatrix} \; C_0 = \begin{bmatrix} 1 & 0 & 1 \\ 0 & 1 & 1 \end{bmatrix};$$

$$C_1 = \begin{bmatrix} 1 & 0 & 0 \\ 0 & 1 & 1 \end{bmatrix}; \; C_2 = \begin{bmatrix} 1 & 0 & 0 \\ 0 & 1 & 0 \end{bmatrix}.$$

Algorithm Z1

Step (1) Compute the left null space Q of the coefficient matrix in Equation (21).

Step (2) Compute v_i, w_i, $i =, 01, 2$ by Equations (43), (50), (51) to form V_0, V_1, V_2 and W_0, W_1, W_2.

Step(3) With the matrices W_0, W_1, W_2, V_0, V_1, V_2, satisfies the equation (50),(51) and the matrix F_0, F_1,F_2 such that $F_2C_2V_2 = W_2$, $F_1C_1V_1 = W_1$, and $F_0C_0V_0 = W_0$,

Step (4) Substitute V back into Equation (49) with (52) to give F_0, F_1, F_2.

$$V_0 = V_1 = V_2 = \begin{bmatrix} 0.1095906 & 0.0695801 \\ 0.0973067 & 0.0550873 \\ 0.1567901 & 0.1249138 \\ -0.3287717 & -0.2783205 \\ -0.2919201 & -0.2203492 \\ -0.4703702 & -0.4996553 \end{bmatrix}$$

$$W_0 = W_1 = W_2 = \begin{bmatrix} 0.9197179 & 0.9480201 \\ 0.832767 & 0.8379183 \end{bmatrix}$$

$$F_0 = \begin{bmatrix} 51.199353 & -50.054933 \\ 42.823231 & -41.616079 \end{bmatrix}$$

where the eigenvalues are

$\lambda_1 = -3$, $\lambda_2 = -4$, $\lambda_3 = -1.9669794 + 4.0571187j$, $\lambda_4 = -1.9669794 - 4.0571187j$, $\lambda_5 = -9.3303829$.

$$F_1 = \begin{bmatrix} -36.816339 & 19.498243 \\ -30.793252 & 16.558322 \end{bmatrix}$$

$\lambda_1 = -3$, $\lambda_2 = -4$, $\lambda_3 = -1.0795178 + 6.1019018j$, $\lambda_4 = -1.0795178 - 6.1019018j$, $\lambda_5 = -4.4381969$.

$$F_2 = \begin{bmatrix} 56.687413 & -54.391796 \\ 48.612123 & -46.190671 \end{bmatrix}$$

where the eigenvalues are $\lambda_1 = -3$, $\lambda_2 = -4$, $\lambda_3 = -10$, $\lambda_4 = -2 + 4.1836895j$, $\lambda_5 = -2 - 4.1836895j$.

VI. Conclusions

The paper has presented an approach to partial eigenvalue assignment in second-order descriptor linear systems via proportional plus derivative plus output feedback controller was presented. The approach to partial eigenstructure assignment is shown using a proportional plus-derivative plus output feedback in the second-order linear system. This study presented an approach to partial the eigenstructure assignment for the descriptor system where an algorithm is presented for calculating the output feedback matrix by equation de Sylvester. Two theorems were presented using Sylvester's equations. Two algorithms were implemented using the Sylvester equation as a basis, and examples are presented with their conclusions.

References

[1] J. N. Juang, K. B. Lim, and J. L. Junkins, "Robust eigensystem assignment for flexible structures", *J. Guindace, Control Dynamics*, vol. 12, no. 3, pp.381–387, 1989.

[2] E. K. Chu and B. N. Datta, "Numerically robust pole assignment for second-order systems", *International Journal of Control*, vol. 64, no. 4, pp. 1113–1127, 1996.

[3] B. N. Datta, S. Elhay, and Y. Ram, "Orthogonality and partial pole assignment for the symmetric definite quadratic pencil", *Linear Algebra and its Applications*, vol. 257, pp. 29–48, 1997.

[4] B. N. Datta, W. W. Lin, and J. N. Wang, "Robust and minimum gain partial pole assignment in vibrating structures with aerodynamics effects", *Proc. IEEE Conference Decision Control*, pp. 2358–2363, 2003.

[5] J. M. Araújo, and C. E.T. Dórea and L. M.G. Gonçalves and B. N. Datta, "State derivative feedback in second-order linear systems: A comparative analysis of perturbed eigenvalues under coefficient variation", *Mechanical Systems and Signal Processing*, vol. 76-77, pp. 33–46, 2016.

[6] E. B. Castelan, and V. G. Da Silva, "On the solution of a sylvester equation appearing in descriptor systems control theory", *Systems and Control Letters*, vol. 54, no.2, pp. 109–117. 2005.

[7] E. B. Castelan, "Estabilização de sistemas descritores por realimentação de saídas via subespaços invariantes", *Revista Controle & Automação*, vol.16 no.4, pp. 467–477, Outubro, 2005.

[8] Elmer R. L. Villarreal, "Abordagem Geométrica para Estabilização por Realimentação de Saídas e sua Extensão aos Sistemas Descritores", *Doutorado em Engenharia Elétrica-UFSC*, Florianopolis, SC, Brasil, 2002.

[9] V. K. Mishra, N. K. Tomar and M. K. Gupta, "On Controllability and Normalizability for Linear Descriptor Systems", *Journal of Control, Automation and Electrical Systems* vol. 27, pp.19–28, 2016.

[10] A. Laub and W. F. Arnold, "Controllability and observability criteria for multivariate linear second-order models", *IEEE Transactions on Automatic Control*, vol. AC-29, pp. 163–165, Feb. 1984.

[11] J. Zhang, Y. Yuan and H. Liu, "An Approach to Partial Quadratic Eigenvalue Assignment of Damped Vibration Systems Using Static Output Feedback", *International Journal of Structural Stability and Dynamics* vol. 18, no. 1, pp. 1–18, 2018.

[12] N. F. Almuthairi and S. Bingulac, "On coprime factorization and minimal-realization of transfer-function matrices using the pseudo-observability concept", *International Journal of Systems Science*, vol. 25, no. 27, pp. 1819–1844, 1994.

[13] T. G. J. Beelen and G. W. Veltkamp, "Numerical computation of a coprime factorization of a transfer-function matrix", *Systems & Control Letters*, vol. 9, no. 4, pp. 281–288, 1987.

[14] G. R. Duan, "Parametric Eigenstructure Assignment in Second-Order Descriptor Linear Systems", *IEEE Transactions on Automatic Control*, vol. 49, no. 10, pp.1789–1795, 2004.

Radial Position Control of a Bearingless Machine with Active Disturbance Rejection Control Fuzzy an approach

Werbet L. A. Da Silva, Andrés O. Salazar, Paulo V. F. Vieira, Maxwell C. Jácome, and Elmer R. L. Villarreal , *IEEE Senior Member*

***Abstract*—This paper is presented a new approach to fuzzy active-disturbance rejection position controller of the bearingless induction machine (BIM) servo system. The paper deals with applying the Fuzzy technique of Active Disruption Rejection Control (ADRC) in stabilizing and controlling the radial position of the rotor of an bearingless induction machine with split winding. A control model for the radial position problem is proposed, and the ADRC-Fuzzy control is used in order to improve the dynamics of the closed-loop system when a load change occurs at the output. The simulations show that the controller stabilizes the plant and rejects disturbances. These results served as the basis for future experimental validation in the problem.**

Keywords: **Control ADRC-Fuzzy, induction motor, magnetic levitation, robust controller**.

I. Introduction

Many Bearingless electric machines, they used structure based on induction motors that can meet industrial demand for less noisy motors, that can reach higher speeds and not contaminate the respective processes. So, the development of this technology process, has a diverse range of sectors that can take advantage of it [1] [2] [3]. For example, in the aerospace industry, where bearingless machines have been adopted, the number of maintenance events in space systems has been significantly reduced. In the biomedical area, the pumping systems where they replace the human heart are able to extend the period of operation to an interval of more than ten years thanks to the elimination of mechanical contacts [4].

The industrial systems with magnetically suspended rotors, as the bearingless machine with split winding proposed by [5], work without mechanical bearings, which are usually the first component to fail in electrical machines [6]. Linear controllers often does not achieve a stable and rapid response to suspension of the machine rotor. The emergence of microprocessors and power electronic devices supply conditions for applying advanced control theories, such as predictive controllers, by sliding modes, based on artificial neural networks, Fuzzy, and others [7].

With respect to this technique, the effects of internal and external disturbances, variations in parameters and other uncertainties are estimated through a state observer and compensated in real time by the control routine [8]. Thus, its architecture makes ADRC a control technique whose performance does not depend on the knowledge of the mathematical models of the process. In [9] was proposed a permanent magnet synchronous motor (PMSM) position, servo control system based on fuzzy active-disturbance rejection. Thus, presenting fuzzy logic control in the design of the ADRC controller, improving and tuning the self-tuning of the nonlinear state parameter nonlinear error feedback controller that maintains the original features controller and reduces the tunable parameter adjustable and improves the performance of the control system. Combined with the speed loop and the position loop, a new Fuzzy-ADRC position regulator is designed, which improves robustness and maintains the dynamic peculiarities of the system in same time. In [10] was proposed, a control model for the radial position problem, and the ADRC control is used to improve the closed-loop system dynamic when a changing load occurs on the output in the system. .

This paper studies the application of an ADRC controller in the position control of a bearingless machine with split winding. In addition to this introductory section, in the section (II), the modeling of the radial position system is performed. In section (III) explains the ADRC and shows its mathematical implementation. Section (IV) presents the Fuzzy Controller. section (V) presents the Fuzzy-ADRC Controller. In section (VI) presents the results of the simulated runs, followed by section (VII), in which the final considerations are made.

Werbet Luiz Almeida Da Silva and Andrés Ortiz Salazar are Department of Computer Engineering and Automation, Federal University of Rio Grande do Norte (DCA-UFRN), Natal, RN, 59072-970, Brazil.

Paulo Victor Fernandes Vieira is graduation Interdisciplinary in Science and Technology, Federal Rural University of Semi-arid (BC&T-UFERSA), Mossoró, RN, 59625-900, Brazil.

Maxwell Cavalcante Jácome is Program Postgraduate in Engineering Mechanical Federal University of Rio Grande do Norte (PPGEM/CT-UFRN), Natal, RN, 59072-970, Brazil.

Elmer Rolando Llanos Villarreal is Department of Natural Sciences, Mathematics, and Statistics, Federal Rural University of Semi-arid (DCME-UFERSA), Mossoró, RN, 59625-900, Brazil. (Correspondence: elmerllanos@ufersa.edu.br).

e-mail:(werbethluizz@hotmail.com ; andres@dca.ufrn.br ; fernandes_victor2001@hotmail.com ; maxwellc.jacome@hotmail.com ; elmerllanos@ufersa.edu.br .)

https://orcid.org/0000-0001-7197-6957; https://orcid.org/0000-0001-5650-3668; https://orcid.org/0000-0003-2668-5362; https://orcid.org/0000-0001-6635-3632; https://orcid.org/0000-0002-3059-3340.

This study was financed in part by the Coordenação de Aperfeiçoamento de Pessoal de Nível Superior Brasil (CAPES) Finance Code 001 and in part by the process 23091-014712/2019-87-UFERSA.

Copyright ISSN 0719-5567; IEEE eCF 551889.

IEEE ICA/ACCA2021: 2021 IEEE International Conference on Automation /XXIV Congress of the Chilean Association of Automatic Control (ICA-ACCA), Santiago, Chile, March 22-26, 2021.
978-1-6654-0127-2/21/$31.00 ©2021 IEEE

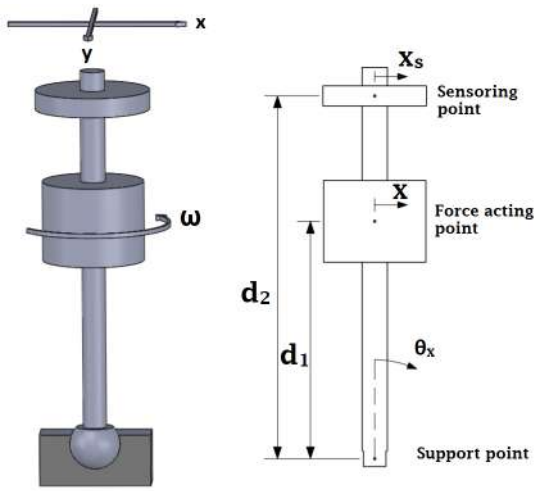

Fig. 1. Rotor free body diagram.

II. System Modeling

Nowadays several topologies topologies of bearingless machines are available in the literature. The topology to be used in this article was studied by [11], which develops a dynamic model of the rotor's radial position based on the basic characteristics of a real experimental prototype. This prototype operates vertically and is supported on the lower end of the shaft by a pivoted bearing that prevents radial and axial movements, but allows several important angular movements. Therefore, this type of system has two degrees of freedom for position control [12], and the rotor displacement occurs in the directions of the x and y axes.

Starting from the operation of the second motion law to Figure (1), [11] developed a new $G(s)$ function that relates the new control signal $U(s)$ to the new output position $Y(s)$ of the rotor. The dynamics part of the x-axis is equal to the y-axis, and both are described by:

$$G(s) = \frac{3.69 \times 10^6}{(s + 90.52)(s - 90.52)} \tag{1}$$

Therefore, the referred equation (1) shows that the radial position model has an unstable pole, so a controller is essential for the functioning of the operating system. Because they are mechatronic systems, which combine mechanical and electronic components, such as sensors and amplifiers, the dynamic models involve the combination of systems of different natures.

III. ADRC controller

The new version of the ADRC controller was presented by Jingqing Han, in an article entitled Automatic disturbance rejection controller and its applications [13]. In order to further advance the theory and practice of control engineering, Jingqing Han researched the characteristics of closed-loop nonlinear control problems and proved the efficiency of the controllers as mentioned above designed from them. As shown in [14], when compared to linear functions, nonlinear ones are potentially more effective in tolerating uncertainties and disturbances; is at improve the dynamics of the proposed systems.

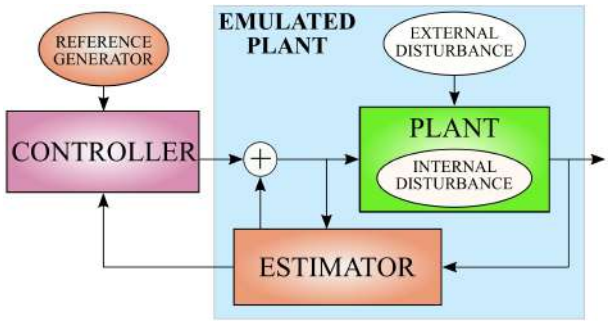

Fig. 2. ADRC - Overview.

In one article, Han introduced ADRC control as a closed-loop digital system control technique, developed based on a digital platform with a strong root in computer simulations, which is based on the proportional integral derivative controller (PID) the main feature most successful: a law control based mainly on error, and not just on the model of that plant; in addition, it also uses state observers, a technique from the theory of modern controllers; and also makes use of nonlinear control tools to perform of its fundamental structure [15].

Thus, the ADRC controller proposed in the engineering project uses a state observer to estimate any unknown information (dynamics, disturbances, nonlinearities, variations in parameters, etc.) about the system's actual reference to be controlled. Therefore, the algorithm subtracts the estimated information from the system dynamics to computationally emulate a model with simpler general behavior. In the ADRC controller structure, there is the observer, a reference generator, and a controller block (Figure 2). Thus, in order to achieve its objective, the ADRC controller groups all the uncertainties involved in the process into a single parameter called "generalized disturbance". The parameter is then defined as a state variable of the system to be estimated through the observer. Once estimated, this parameter is subtracted from the system's control loop, which the controller sees as a simpler system, formed only by cascade integrators (a canonical form of Han), whose control has already been widely studied in the literature. Thus, Han's mentioned canonical form is taken into account for the design of the control block, and the referred knowledge about the real parameters of the system is not fundamental.

A. ADRC mathematical description

The ADRC control structure is based mainly on non-linear functions, and its original full version consists of three blocks: an extended state observer (ESO), a tracking differentiator with tracking (TD), and a non-linear control law (Figure 3).

1) tracking differentiator: Considered the TD operates on the reference signal in order to filter it and smooth its transition. For a second-order system given by:

$$\begin{cases} \dot{p}_1 = p_2 \\ \dot{p}_2 = u \end{cases} \tag{2}$$

the optimal basic solution for this system is given by:

$$u = -rsign(p_1 - p + \frac{p_2|p_2|}{2r}) \tag{3}$$

Thus, the system is rewritten as:

$$\begin{cases} \dot{p}_1 = p_2 \\ \dot{p}_2 = -rsign(p_1 - p(t) + \frac{p_2|p_2|}{2r}) \end{cases} \tag{4}$$

with, $p_1(t)$ follows the input signal $p(t)$ with a speed adjusted by variable r. The new variable $p_2 = \dot{p}_1$ is an approximation of the derivative of $p(t)$.

2) ESO: As an observer-based method, ESO in the ADRC control introduces more phase lag when the observer's order becomes higher. The central impairment of the phase delay is the reduction of the loop stability. It consists of an estimator with nonlinear gains that detect information about the plant's states in real-time from observing the inputs and the output. It is an essential block of the controller, as it is responsible for detecting disturbances involved in the process. The observer design, for this paper, is given from the second-order system by:

$$\begin{cases} \dot{x}_1 = x_2 \\ \dot{x}_2 = h(x_1(t), x_2(t), w(t), t) + bu \\ y = x_1 \end{cases} \tag{5}$$

where y is variable the measured output that is controlled; $h(x_1(t), x_2(t), w(t), t) = H(t)$ is a multivariate function of states $(x_1(t), x_2(t))$, external disturbances $(w(t))$, and time (t); i.e., the total disturbance. Assuming in the paper that the variable $H(t)$ is a system state variable, $H(t) = x_3$ and $\dot{H}(t) = L(t)$ is its derivative respective. Thus, the extended representation of the system given by (5) is:

$$\begin{cases} \dot{x}_1 = x_2 \\ \dot{x}_2 = x_3 + bu \\ \dot{x}_3 = L(t) \\ y = x_1 \end{cases} \tag{6}$$

From this representation used, the observers' structure is proposed in [16]:

$$\begin{cases} \dot{z}_1 = z_2 - \beta_{01} fal(e, \alpha_1, d_1), \\ \dot{z}_2 = z_3 - \beta_{02} fal(e, \alpha_2, d_2) + b_0 u \\ \dot{z}_3 = -\beta_{03} fal(e, \alpha_3, d_3), \end{cases} \tag{7}$$

the fal function is defined by:

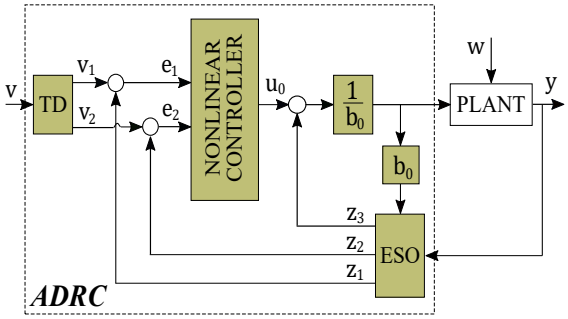

Fig. 3. ADRC - Control structure.

$$fal(e) = \begin{cases} |e|^{\alpha} sign(e), & |e| > d \\ \frac{e}{d^{1-\alpha}}, & |e| \leq d \end{cases} \tag{8}$$

The variables α_1, α_2, α_3, d_1, d_2 e d_3 are the obtained parameters of nonlinear functions. Thus, the observer output give the values of the states z_1, z_2 and z_3, i.e., it is estimated the numerical values of the states z_1, z_2 and of the function $H(t)$. From this, the effect of $H(t)$ is removed from the system dynamics through operation:

$$u = \frac{u_0 - H(t)}{b_0} \tag{9}$$

So, the computational emulated dynamics of the system becomes:

$$\begin{cases} \dot{x}_1 = x_2 \\ \dot{x}_2 = u_0 \\ y = x_1 \end{cases} \tag{10}$$

Which corresponds to a simple double integrating system, whose control is differently known in the current literature.

3) Control law: The paper [15] provided the following nonlinear strategy:

$$u_0 = \beta_1 fal(p_1 - z_1, \alpha_1, \delta) + \beta_2 fal(p_2 - z_2, \alpha_2, \delta) \tag{11}$$

Besides, it is emphasized that different strategies are used in the control law block.

IV. Fuzzy Controller

The basic structure of a rules-based fuzzy controller consists of three process: process fuzzification, process inference, and process defuzzification [17]. In the process fuzzification, input data are converted into fuzzy values, i.e., qualitative values comprehensible by the inference mechanism.

A. Rules Basis

Defining the rule sets is directly related to the aim of the control. Since the bearingless motor aims to keep the rotor centralized, the main task is to minimize the position tracking error. The higher the error, the higher the control input. However, a change in error also affects the value of the control input. Consequently, the error and change in error are used in the control rules as the linguistic variables. The variables $e[k]$ is the actual error and $e[k-1]$ the error calculated in the previous sample of k. These are defined as:

$$e_1 = \ error_1 = p_1 - z_1 \tag{12}$$

$$e_2 = \ error_2 = p_2 - z_2 \tag{13}$$

$$\begin{aligned} \Delta e_1 = \ & change\ in\ error_1 = e_x[k] - e_x[k-1] \\ \Delta e_2 = \ & change\ in\ error_2 = e_y[k] - e_y[k-1] \end{aligned} \tag{14}$$

wherein e is the error signal. The a, b, c and d mean Δ_{ex} , e_x , Δ_{ey} and e_y, respectively.

The rules of fuzzy controller are of the form:

$$If\ error_1 = A\ and\ change\ in\ error_1 = B \quad Then\ u = C \tag{15}$$

$$If\ error_2 = C\ and\ change\ in\ error_2 = D \quad Then\ u = G \tag{16}$$

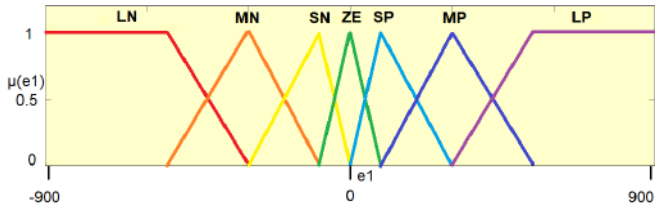

Fig. 4. Membership functions of input variables.

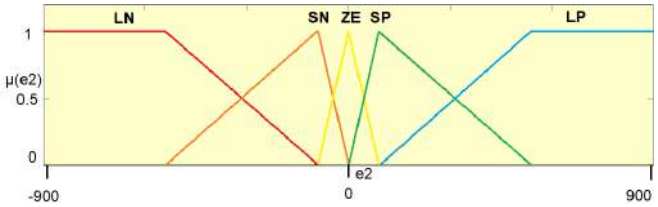

Fig. 5. Membership functions of input variables.

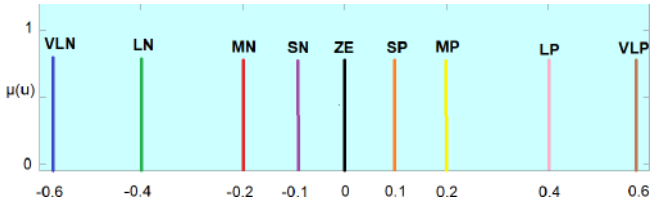

Fig. 6. Membership functions of input variables.

V. FUZZY ADRC CONTROLLER

Considering the synchronous rotation coordinate system, in which the vector control strategies, using the equation (5), it is obtained position loop two order dynamic equation of BIM:

$$\ddot{\theta} = -\frac{B\omega}{J} - \frac{T_L}{J} + \frac{1.5p\psi_f}{J}u(t) \tag{17}$$

$h(x_1(t), x_2(t), w(t)) = -\frac{B\omega}{J} - \frac{T_L}{J}$, $b = \frac{1.5p\psi_f}{J}$.

$u(t) = i_q$, where $h(x_1(t), x_2(t), w(t))$ is the known friction disturbance of system, $w(t)$ is the unknown load disturbances of system, through these two parts can estimate the total disturbance of system and compensate for it, making the system has great robustness to the load and friction disturbance. Under the condition of position sensor, ω is the known quantity, its the differential is also a known quantity and the state equation of position loop is available:

$$\begin{aligned} \dot{x}_1 &= x_2 = \frac{d\theta}{dt} \\ \dot{x}_2 &= \frac{d^2\theta}{dt^2} = h(x_1(t), x_2(t), w(t)) + bu(t) \\ y &= x_1 = \theta \end{aligned} \tag{18}$$

According to rotational transformation is obtaining parameters $\beta_0, \beta_1, \beta_2$. Finally, with the principles of Fuzzy ADRC parameters tuning, we can obtain Fuzzy-ADRC. Its structure is shown in Figure (7) and Its structure with rotational transformation is shown in Figure (8).

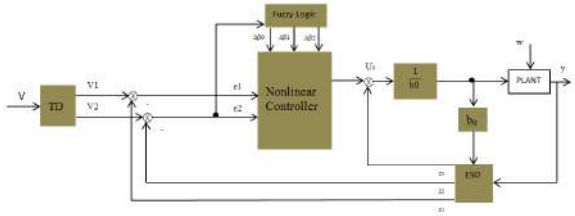

Fig. 7. Fuzzy-Self-adapted ADRC structure.

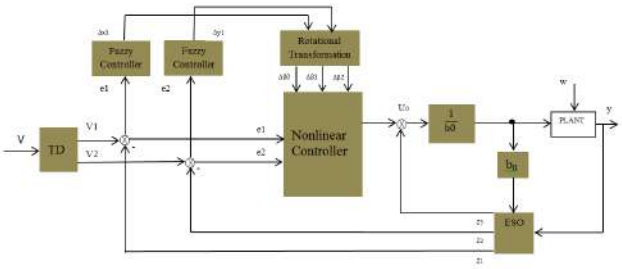

Fig. 8. Fuzzy-Self-adapted ADRC structure with rotational transformation.

It can be seen, every part of the position Fuzzy-ADRC controller can be designed, Its whole control structure is shown in Figure (8). In it, θ^* is the given rotor position, i_q^* is the given $q-$axis current, θ is the rotor position feedback signal, p_1 is the tracking signal of θ^* , p_2 is the differential signal of θ^* , z_1 is the tracking signal of θ , z_2 is differential signal for z_1, z_3 is system observation of the uncertain part of the disturbance that is $w(t)$ as the observation for the certain part, where the differential is different from the differential signal in a controller, its effect is not amplified, but disincentive to the noise signal.

A. Fuzzy controller model

Based in [18], this article introduces the fuzzy logic controller, according to the input of , e_1, Δe_1, e_2, Δe_2 and using fuzzy control rules to change the ADRC parameters $\{\Delta i_x, \Delta i_y\}$, with rotational transformation is obtained approaching the optimal parameters $\{\beta_0, \beta_1, \beta_2\}$. To meet the requirements of the $\{e_1,\ \Delta e_1,\ e_2,\ \Delta e_2\}$ parameters of the Fuzzy ADRC, in the controller, the fuzzy variables are e_1, e_2, $\{\Delta i_x, \Delta i_y,$, in your domain, five language sets defined such as {Large Negatives (NB), Small Negatives (NS), Zero (ZO), Small positives (PS), Large positives (PB) }. In the select the input variables e_1, e_2 for the Gaussian association function, output variables $\{\Delta i_x, \Delta i_y\}$ for triangular membership function. In this article, the basics e_1, domains are $[-900, +900]$, a range variation of $[-10, +10]$ and e_2 domains are $[-900, +900]$ for a range variation of $[-10, +10]$. Thus the variables $\{\Delta i_x, \Delta i_y\}$, with rotational transformation is obtaneid $\Delta\beta_0\}$ $\Delta\beta_1\}$,$\Delta\beta_2\}$ domains are $[-6, +6]$, $[-6, +6]$,

TABLE I
LINGUISTIC LABELS ADOPTED TO DESCRIBE FUZZY SETS.

Label	Signification
VLN	Very Large Negative
LN	Large Negatives
MN	Medium Negatives
SN	Small Negatives
ZE	Zero
SP	Small Positives
MP	Medium Positives
LP	Large Positives
VLP	Very Large Positives

$[-0.6, +0.6]$. Fuzzy reasoning using the Mamdani type and defuzification is the weight average method. According rules of the human mind, diffuse control rules are devised by

summarizing the technical knowledge of the engineering team and practical experience.

An initial rule base is developed using prior knowledge of the system. Then, respective adjustments were made based on the behavior of the system during the experiments. These rules were changed until they could no longer improve the response, so the association functions were adjusted. The adjustments to the rules are interspersed with the adjustments to the membership functions, never both at the same time. The adjustments gave rise to the error and the change in the error pertinence functions illustrated in Figures (4), (5) and the output pertinence functions represented in Figure (6) and the rules summarized in Table (II).

For $\{\Delta i_x, \Delta i_y\}$ parameter configuration, fuzzy control table are established, as shown in Tables (II) and (III) .

TABLE II
RULES FOR X-AXIS FUZZY CONTROLLER.

a \ b	LN	MN	SN	ZE	SP	MP	LP
LP	VLN	VLN	VLN	VLN	LN	SN	MN
SP	VLN	MN	MN	SN	SP	LP	LP
ZE	LN	SN	ZE	ZE	ML	LP	VLP
SN	VLN	MN	SN	ZE	SP	LP	LP
LN	MP	MP	LP	LP	SP	VLP	VLP

TABLE III
RULES FOR Y-AXIS FUZZY CONTROLLER.

c \ d	LN	MN	LN	ZE	SP	MP	LP
LP	VLN	VLN	VLN	LN	MN	MN	LN
MP	VLN	MN	MN	MN	ZE	SP	MP
ZE	LN	MN	ZE	ZE	SP	MP	MP
SN	SN	ZE	SP	SP	MP	LP	VLP
LN	LP	MP	LP	LP	SP	VLP	VLP

According to the table of allocation of members of fuzzy set Tables (II) and (III) . and the fuzzy control model of parameters, and with diffuse synthetic reasoning to project diffuse matrix, then defuzzification and correction parameters found $\{\Delta i_x, \Delta i_y\}$, with rotational transformation is obtaneid $\{\Delta\beta_0, \Delta\beta_1, \Delta\beta_2\}$ and replaced it in the equation:

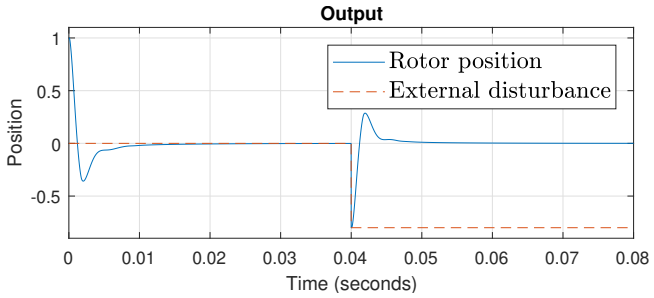

Fig. 9. System output.

$$\beta_0 = \beta_0^{'} + \Delta\beta_0 \tag{19}$$

$$\beta_1 = \beta_1^{'} + \Delta\beta_1 \tag{20}$$

$$\beta_2 = \beta_2^{'} + \Delta\beta_2 \tag{21}$$

Where variables $\beta_0, \beta_1, \beta_2$ is the nonlinear controller initial value.

VI. RESULTS

For the results described in this section, the following considerations were used:

- Given that the dynamic response is the same for x and y axes, the results for only one axis is showed.
- The control goal is to maintein the radial position of the machines rotor in $(x = 0, y = 0)$ position, so the reference signal p is kept in 0 and the TD block of the Figure (3) is not necessary
- The observer ESO was implemented according to (7) and the control law is given by (9).
- The controller tuning was carried out by trial and error.
- The system is simulated with initial conditions: $x_1(0) = 1$ and $x_2(0) = 0$. This situation initial is indicated that the machine rotor was stopped in an unwanted position before the controller start acting.
- A step-shaped disturbance is added at the output of the system at the instant $t = 0.05$ seconds. In a real situation, disturbances of this type are caused by loads added to the axis of the machine in operation.

In figure (9) shows the plant's output controlled with ADRC control. The controller corrected the plant output to the desired reference value and recovered this condition even under a load change condition.

In the study of the efficiency of the ADRC in controlling the output of the system depends directly on the ability of ESO to estimate the states of the plant, that is: $x_1 \to z_1$, $x_2 \to z_2$ and $H(t) \to z_3$. The figure (10) where it compares the real states' dynamic response with their respective values estimated by the observer used. Considering Figure (10), ESO's ability to provide adequate plant states estimates can be seen. Thus, the Fuzzy ADRC controller's efficiency in controlling the output of the system depends directly on the ability of the ESO observer to estimate the states of the plant.

The results of the simulations obtained are part of a project that seeks to carry out experiments with the ADRC controller

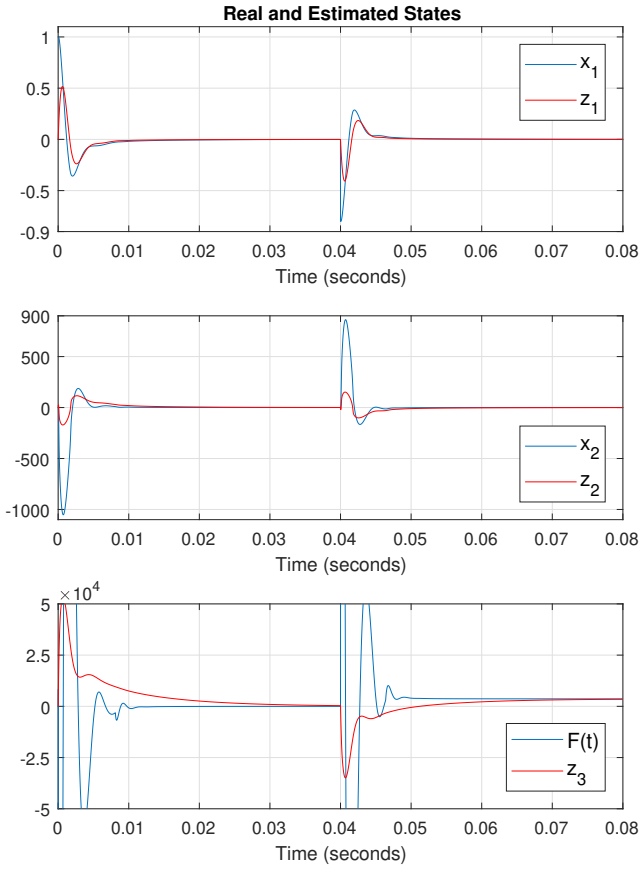

Fig. 10. Performance of the extended state observer.

and a bearingless machine prototype. A experimental setup (Figure 11) at Federal University of Rio Grande do Norte be used in experiments.

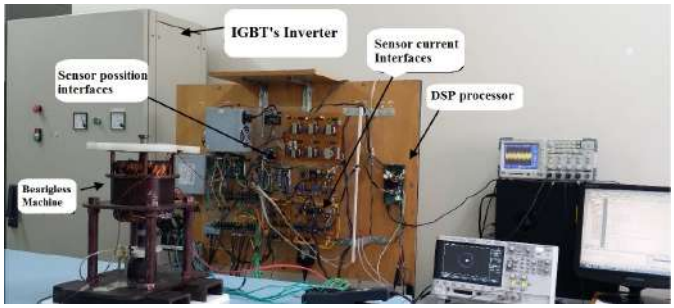

Fig. 11. Experimental setup.

VII. Conclusions

Following the practical requirements obtained, this article applies, Fuzzy -ADRC theory for high-performance permanent AC magnetic servo system and two-order Fuzzy-ADRC designs position regulator to increase the anti-interference ability of the the system, and using ESO to estimate the disturbance, which achieving high precision control of the servo motor with the position sensor. The results of the simulation and the experiment show that Fuzzy-ADRC has good dynamic and static performance for BIM. This paper studied the application of an ADRC fuzzy controller to a simulated radial position control system of an bearingless machine induction with split winding. The results proved the efficiency of the controller in keeping the rotor in the desired position. Future paper aims to apply this controller to an experimental system whose dynamics were subject to a higher number of disturbances and uncertainties.

References

[1] D. Gerada, , A. Brown, Neil L Mebarki, C. Gerada, A. Cavagnino, and A. Boglietti, "High-speed electrical machines: Technologies, trends, and developments," *IEEE Transactions on Industrial Electronics*, vol. 61, no. 6, pp. 2946–2959, 2013.

[2] T. Wellerdieck, T. Nussbaumer, P. Peralta, and J. W. Kolar, "Contributions to an ultra-high temperature (250 c/500 f) bearingless pump," in *2015 18th International Conference on Electrical Machines and Systems (ICEMS)*. IEEE(ICEMS), 2015, pp. 1158–1164.

[3] M. N. Recheis, , P. Fulmek, B. Schweighofer, and H. Wegleiter, "Selection of magnetic materials for bearingless high-speed mobile flywheel energy storage systems," *IEEE Transactions on Magnetics*, vol. 50, no. 4, pp. 1–4, 2014.

[4] N. Kurita, N. Saito, T. Ishikawa, T. Masuzawa, and D. L. Timms, "A double-sided stator type axial bearingless motor development for total artificial heart," *IEEE Transactions on Industry Applications*, vol. 55, no. 2, pp. 1516–1523, 2018.

[5] A. O. Salazar and R. Stephan, "A bearingless method for induction machines," *IEEE Transactions on Magnetics*, vol. 29, no. 6, pp. 2965–2967, 1993.

[6] K. Li, G. Cheng, D. Zhao, X. Sun, and Z. Yang, "Direct torque and suspension force control for bearingless induction motors based on active disturbance rejection control scheme," *IEEE Access*, vol. 7, pp. 86 989–87 001, 2019.

[7] Z. Yang, J. Ji, X. Sun, H. Zhu, and Q. Zhao, "Active disturbance rejection control for bearingless induction motor based on hyperbolic tangent tracking differentiator," *IEEE Journal of Emerging and Selected Topics in Power Electronics*, 2019.

[8] M. Ran, Q. Wang, C. Dong, and L. Xie, "Active disturbance rejection control for uncertain time-delay nonlinear systems," *Automatica*, vol. 112, p. 108692, 2020.

[9] Z. Gao, "A new fuzzy active-disturbance rejection controller applied in pmsm position servo system," in *Proceedings 17th International Conference on Electrical Machines and Systems (ICEMS), China*, vol. 1, 2014, pp. 2055–2059.

[10] "Radial position control of a bearingless machine with active disturbance rejection control, author=Da Silva, Werbet L. Almeida and Andrés O. Salazar and Ronaldo José N. Cabral Neto and Elmer R. L. Villarreal, booktitle=XXVII International Conference on Electronics, Electrical Engineering and computings (IEEE-INTERCON 2020), Peru, volume=1, pages=1–4, year=2020."

[11] F. E. C. Souza, "Otimização da estrutura de acionamento para o controle de posição radial de um motor de indução trifásico sem mancais com enrolamento dividido," 2018.

[12] A. Chiba, T. Fukao, O. Ichikawa, M. Oshima, M. Takemoto, and D. G. Dorrell, *Magnetic bearings and bearingless drives*, 2005.

[13] D. Huang, D. Min, Y. Jian, and Y. Li, "Current-cycle iterative learning control for high-precision position tracking of piezoelectric actuator system via active disturbance rejection control for hysteresis compensation," *IEEE Transactions on Industrial Electronics*, 2019.

[14] J. Li, Y. Xia, X. Qi, and Z. Gao, "On the necessity, scheme, and basis of the linear–nonlinear switching in active disturbance rejection control," *IEEE Transactions on Industrial Electronics*, vol. 64, no. 2, pp. 1425–1435, 2016.

[15] J. Han, "From pid to active disturbance rejection control," *IEEE transactions on Industrial Electronics*, vol. 56, no. 3, pp. 900–906, 2009.

[16] Z. Gao, "Scaling and bandwidth-parameterization based controller tuning," in *Proceedings of the American control conference*, vol. 6, 2006, pp. 4989–4996.

[17] M. G. Simoes and I. S. Shaw, *Fuzzy Control and Modelling*. Editora Blucher, Brazil (in Portuguese), 2007.

[18] E. A. D. F. Nunes, A. O. Salazar, E. R. L. Villarreal, F. E. C. Souza, L. P. D. J. S. B. Lopes, and J. C. C. Luque, "Proposal of a fuzzy controller for radial position in a bearingless induction motor," *IEEE ACCESS*, vol. 7, pp. 114 808–114 816, 2019.

Application of Active Disturbance Rejection Control (ADRC) in the Radial Position Control of a Bearingless Induction Machine With Split Winding

Werbet L. A. Silva[1]*, Elmer R. L. Villarreal[2]†, Jossana M. S. Ferreira[1]‡, José A. Paiva[3]§, Andrés O. Salazar[1]¶ and Andre L. Maitelli[1]‖

[1] Universidade Federal do Rio Grande do Norte, Natal-RN, Brazil
werbethluizz@hotmail.com
jossana@ect.ufrn.br
maitelli@dca.ufrn.br
andres@dca.ufrn.br
[2] Universidade Federal Rural do Semi-Árido, Mossoró-RN, Brazil.
elmerllanos@ufersa.edu.br
[3] Instituto Federal de Educação, Ciência e Tecnologia do Rio Grande do Norte, Natal-RN, Brazil.
jalvaro.paiva@gmail.com

Abstract

In this work, the Active Disturbance Rejection Control (ADRC) technique was applied to control a simulated plant that represents the radial displacement of a bearingless induction machine with split winding. Active Disturbance Rejection Controllers have a robust operation when applied to systems with uncertainties, nonlinearities, and in the presence of disturbances. The work employed the linear and nonlinear versions of the ADRC to control the radial displacement. The simulations were performed in the Scilab software. The system response under parameter variation and external load are presented to compare the performance and implementation of both techniques.

1 Introduction

The emergence of electrical machines with magnetic suspension of the rotor meets industry demand for motors that could generate less noise, reach higher speeds and avoid process contamination. In the past two decades, magnetic bearing technology has received significant attention due to its potential application to high-speed and harsh environments applications, where maintenance routines are more complicated. In this way, different machine types have been tested under the magnetic suspension scheme, and new structures appeared to overcome the natural problems of this technology.

Electrical machines that combine motor functions for torque generation and magnetic bearings in the same system, known as bearingless machines, are considered the greatest advance in this area of knowledge [10][13]. The bearingless technology has been applied in different electrical machine types; the induction motor, e.g., is often chosen due to its robustness, simplicity, and low cost [17][1][20]. [12] proposed a bearingless induction motor in which the group of

*Designed and implemented the control system
†Run simulations and tests and studied the model
‡Did numerous tests and provided a lot of suggestions
§Did the literature review and o wrote the main sections
¶Literature, text review and orientation
‖Literature, text review and orientation

coils that generate rotational torque also generates radial forces. This structure, known as split winding, aims to simplify the operation and improve the internal use of space of the motor. The same approach was used by [2] to propose the use of split windings in a traditional three-phase induction motor, obtaining a system capable of generating greater radial forces.

Since the magnetic shaft suspension is a naturally unstable system, the bearingless machine strongly depends on well-designed control routines. These systems are multivariable, non-linear, and coupled [20]. So linear position controllers, as the Proportional-Integral-Derivative (PID) [11], may not achieve a response fast and stable enough for proper shaft suspension. The use of microprocessors and power electronics devices enabled the application of advanced control theories, such as predictive control, sliding mode control, neural network control, Fuzzy control, and others [19]. In recent years, the Active Disturbance Rejection Control (ADRC) "is emerging as a promising alternative in many tough control scenarios, due to its structure simplicity and capability in dealing with the model uncertainties, nonlinearity and external disturbances within a unified framework" [16].

The ADRC has been widely studied in virtue of its anti-disturbance ability and its independence of a precise system model [6]. Its main idea is to group all the uncertainties of the plant – such as non-modeled dynamics, external disturbances, and variations in parameters – as an additional state variable to be estimated in real-time through the input and output variables. Thus, the additional state can be estimated and compensated in the control loop. This task is achieved thanks to the core element of the ADRC: the Extended State Observer (ESO). Employing the ESO, the output and its derivatives, as well as the lumped disturbance, the desired control performance can be achieved by a simple linear state feedback control algorithm with online disturbance rejection [18]. This works aims to apply the ADRC technique to control the rotor radial position of a four-pole bearingless induction machine with split winding.

The original concept of the ADRC controller proposed a completely non-linear structure. Despite being very efficient for non-linear systems, this structure is relatively complicated to be tuned because it has a large number of parameters. Gao's work sought to obtain a linear model of the ADRC controller that would maintain the good performance of the original controller.

This work is the first stage of a project that aims to apply the ADRC controller in the radial position control of an induction bearingless machine with split coil. Initially, we simulated the application of a linear and a non-linear ADRC structure to control a radial position system in order to understand the implementation, evaluate advantages and disadvantages, and assess the performance of the closed-loop control system. These results are the grounding foundation for the following stages of the project.

The results of these experiments are described in this text, which is organized as follows: in addition to this introductory section, section 2 provides a brief presentation of the radial displacement model used; section 3 describes the linear and non-linear structures of ADRC; section 4 shows the results of the simulations; finally, the conclusion section shows the most important points that were evaluated from this work.

2 Bearingless machine with split winding

2.1 Operation principle

In the stator of a three-phase bearing motor, there are three groups of windings divided to generate radial force and torque. The coils are split in the stator as shown in Figure 1. Considering a four-pole three-phase motor, Figure 2 can be used to explain the principle of generating radial magnetic forces in the rotor.

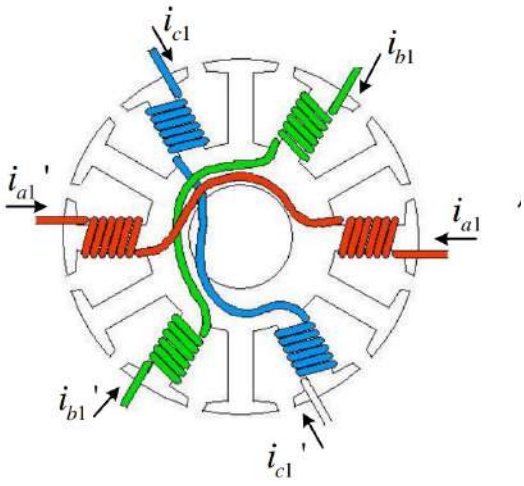

Figure 1: Winding's distribution.

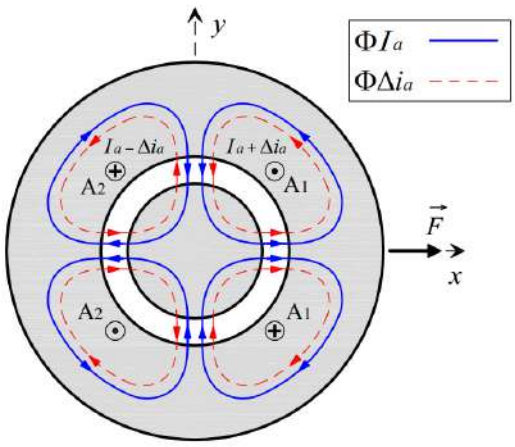

Figure 2: Radial forces generation.

Phase A is divided into two groups of coils: A1 and A2. When the same current (I_a) flows through coils A1 and A2, a magnetic flux is created, as represented in Figure 2 by solid blue lines. When the current increases by Δi_a in coil A1 and simultaneously decreases by Δi_a in coil A2, the flux density increases on one side of the rotor while it decreases on the opposite direction with the same magnitude. The unbalance in the original flux generated by Δi_a generates radial force in the positive direction of the axis X. Likewise, it occurs in the opposite direction when the additional current is added to coil A2 and subtracted from coil A1.

Extending this mode of operation to the three phases and decomposing the coordinate system of the position of the coils as shown in Figure 1 in the coordinate system xy, it is possible to control the radial position in the entire bounded plane for xy.

2.2 Radial displacement model

This prototype works vertically and is supported on the lower end of the shaft by a pivoted bearing that prevents radial and axial movements, but allows angular movements. This type of system has two degrees of freedom for position control and the rotor displacement occurs in the directions of x and y axes.

From the application of the second motion law to Figure 3, [15] developed a linear dynamical representation for the rotor radial displacement system:

$$\ddot{y} = 8374y + 3680000u + w \tag{1}$$

where y is the radial position, u is the input current signal that can vary from $-1A$ to $1A$ and w is an output disturbance. In the form of a transfer function that relates the control signal $U(s)$ to the output position $Y(s)$ of the rotor, the dynamics of the x-axis is equal to the y-axis and both are described by:

$$G(s) = \frac{3.68 \times 10^6}{(s + 91.51)(s - 91.51)} \tag{2}$$

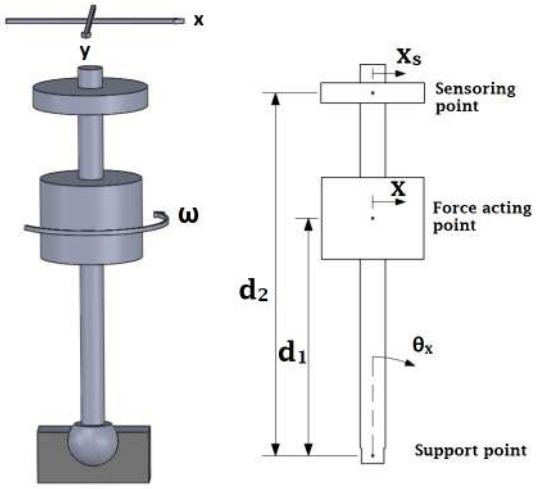

Figure 3: Rotor free body diagram.

Equation (2) shows that the radial position model has an unstable pole, thus a controller is fundamental to the system operation.

3 Active Disturbance Rejection Controller

The first version of the ADRC was presented in Chinese by its creator, Jingqing Han, in the work entitled "Auto disturbances rejection controller and its applications" in 1998 [7]. To promote advances in the theory and practice of control engineering, Jingqing Han researched the characteristics of nonlinear elements into closed-loop control problems and proved the efficiency of the controllers designed from them. According to [9], when compared to linear functions, nonlinear ones are potentially more effective in tolerating uncertainties and disturbances as well in improving systems dynamics.

In a more recent publication, Han described the ADRC as a digital closed-loop control technique, rooted in computer simulations, which inherits from the proportional-integral-derivative (PID) controller its characteristic of greatest success: a control law mainly based on error, and not just on the plant model; in addition, it uses state observers, a technique from the theory of modern controllers; and also makes use of nonlinear control tools for the realization of its structure [5].

Aiming to simplify the ADRC controller, [4] used only linear gains to propose a kind of linear ADRC that uses concepts of controller scaling and parameterization to make the controller parameters functions of the closed-loop bandwidth of the system. The version is called Linear ADRC (LADRC) and brought a new perspective to the industrial application of the technique once it maintained the controller abilities in rejecting disturbances and simplified the tuning process.

Both versions of ADRC (NADRC and LADRC) have exactly the same operation idea: using two control loops to emulate a simplified system, similar to a system composed only by cascaded integrators, in which the dynamic behavior can be controlled by a simple control law (feedback loop). To reach this task, an extended state observer estimates any unknown information (dynamics, disturbances, nonlinearities, parameter variations, time-delays, etc) by

the input-output data of the controlled system and removes this information in the control loop (feedforward loop). This structure makes the ADRC independent of the plant model, where the same structure can handle a large variety of dynamic systems. Furthermore, a Reference Generator can be used to provide a smooth version of the reference and its derivatives. This structure is shown in Figure 4.

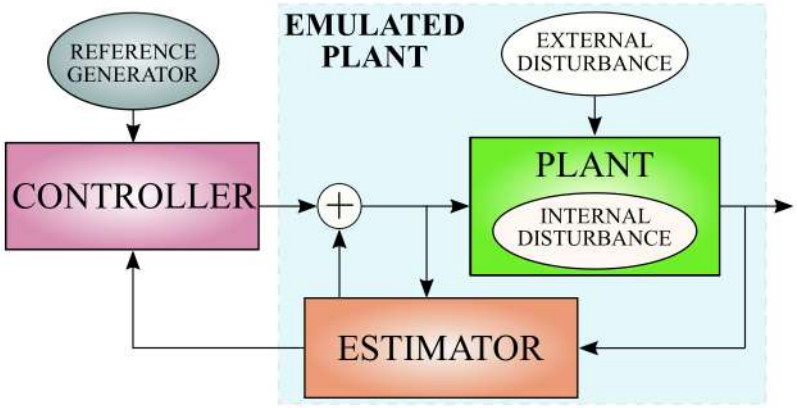

Figure 4: ADRC general idea.

The relative order of the plant is the only information necessary to build a controller based on ADRC. This information is needed because all the blocks described in Figure 4 are designed according to a specific dynamical order behavior. The following sections describe the design of the NADRC and the LADRC to a second-order system, once this is the relative order of our plant.

3.1 ADRC Structure

The mathematical description of the ADRC is based on [4]. A generic second-order system, to be controlled with ADRC, is represented by the following differential equation:

$$\ddot{y} = -a\dot{y} - by + w + bu \tag{3}$$

y is the output; u is the input; w represents an external disturbance; a and b are system parameters.

To apply the ADRC technique, there must be some information about the b parameter. Assuming an approximate value given by $b \approx b_0$, equation 3 can be rewritten as follows:

$$\ddot{y} = -a\dot{y} - by + w + (b - b_0)u + b_0u = f + b_0u \tag{4}$$

The term f in the above equation is denoted by generalized disturbance and is equal to $f = -a\dot{y} - by + w + (b - b_0)u$. The term $b - b_0$ represents the difference between the actual value of b and the approximation b_0, which must be specified to implement the algorithm. In state space form, assuming that $x_1 = y$ and $x_2 = \dot{x}_1$ the system given by 4 can be represented by:

$$\begin{cases} \dot{x}_1 = x_2 \\ \dot{x}_2 = b_0u + f \\ y = x_1 \end{cases} \tag{5}$$

Assuming that f can be estimated, the ADRC technique cancels its effect on the system output by applying the following relationship to the control loop:

$$u = \frac{u_0 - f(t)}{b_0} \tag{6}$$

Hence the total (emulated) dynamics of the system 5 becomes:

$$\begin{cases} \dot{x}_1 = x_2 \\ \dot{x}_2 = u_0 \\ y = x_1 \end{cases} \tag{7}$$

This is a simple double integrator system, whose control has been widely performed in the literature.

The concepts described above indicate that an estimation method that provides an accurate approximation of the value of f is fundamental for an adequate application of the ADRC technique. Furthermore, the control block must be able to meet performance expectations dynamic. The following sections describe two possible frameworks for fully implementing an ADRC-based controller.

3.2 NADRC Structure

The nonlinear structure of an ADRC controller is usually composed by three blocks: a Tracking Differentiator (TD), an Extended State Observer (ESO), and the nonlinear controller (Figure 5).

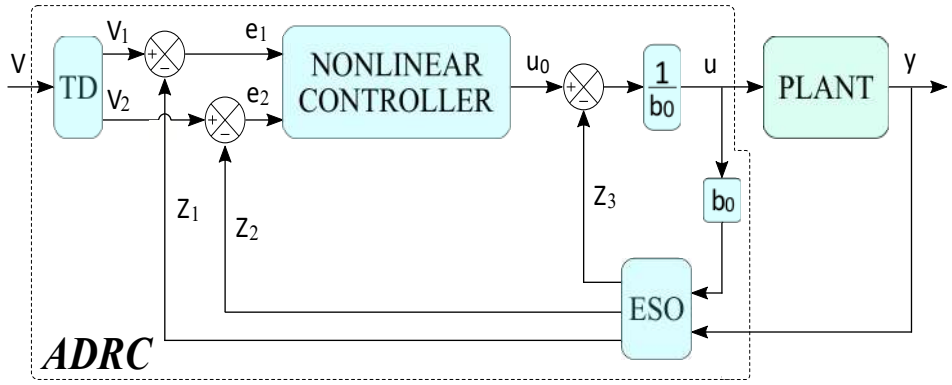

Figure 5: ADRC control loop structure.

3.2.1 Tracking Differentiator

The TD can be seen as a reference generator. It provides smooth versions of the reference signals that usually are put on the system input as a step function. Furthermore, it provides derivatives of the input without the noisy amplification of the traditional derivatives operations. For a second-order system given by:

$$\begin{cases} \dot{v}_1 = v_2 \\ \dot{v}_2 = u \end{cases} \tag{8}$$

an optimal solution is given by:

$$u = -rsign(v_1 - v + \frac{v_2|v_2|}{2r}) \tag{9}$$

This solution is named optimal because it can make the output of 8 reach the desired input fast and with low overshoot. The system can be rewritten as:

$$\begin{cases} \dot{v}_1 = v_2 \\ \dot{v}_2 = -rsign(v_1 - v(t) + \frac{v_2|v_2|}{2r}) \end{cases} \tag{10}$$

thus, $v_1(t)$ follows the input signal $v(t)$ with a speed adjusted by r. The variable $v_2 = \dot{v}_1$ is an approximation of the derivative of $v(t)$. The *sign* is given by:

$$sgn(e) = \begin{cases} 1, & e \geq 0 \\ -1, & e < 0 \end{cases} \tag{11}$$

3.2.2 Nonlinear Extended State Observer

The ESO is the most important block of the ADRC. In its structure the generalized disturbance f is considered as an additional state of the system 5:

$$\begin{cases} \dot{x}_1 = x_2 \\ \dot{x}_2 = x_3 + b_0 u \\ \dot{x}_3 = h \\ y = x_1 \end{cases} \tag{12}$$

where $x_3 = f$ is the augmented state and $h = \hat{f}$, its derivative. h is seen as an unknown disturbance. The above system can be rewritten by:

$$\begin{aligned} \dot{x} &= Ax + Bu + Eh \\ y &= Cz \end{aligned} \tag{13}$$

where:

$$\mathrm{A} = \begin{bmatrix} 0 & 1 & 0 \\ 0 & 0 & 1 \\ 0 & 0 & 0 \end{bmatrix}, \mathrm{B} = \begin{bmatrix} 0 \\ b_0 \\ 0 \end{bmatrix}, \mathrm{C} = \begin{bmatrix} 1 & 0 & 0 \end{bmatrix}, \mathrm{E} = \begin{bmatrix} 0 \\ 0 \\ 1 \end{bmatrix}$$

From the augmented system 12, it is possible to construct an observer to estimate numerical values to z_1, z_2 e z_3, which are the estimated values of the states x_1, x_2 e x_3. The work [3] proposed a nonlinear structure in which the ESO is such as:

$$\begin{aligned} \dot{z}_1 &= z_2 - \beta_1 fal(e, \alpha_1, d_1), \\ \dot{z}_2 &= z_3 - \beta_2 fal(e, \alpha_2, d_2) + b_0 u \\ \dot{z}_3 &= -\beta_3 fal(e, \alpha_3, d_3), \end{aligned} \tag{14}$$

where β_1, β_2 and β_3 are the observer gains of the nonlinear fal functions, whose definition is given by:

$$fal(e, \alpha, d) = \begin{cases} |e|^{\alpha} sgn(e), & |e| > d \\ \frac{e}{d^{1-\alpha}}, & |e| \leq d \end{cases} \tag{15}$$

the value of e is the error between the system output and its estimate $(\hat{y} - y)$ and α and d are tuning parameters.

3.2.3 Nonlinear Control Law

Among the control law alternatives proposed by [5], we can highlight the following:

$$u_0 = -K_P fal(e_1, \alpha_4, d_4) - K_D fal(\dot{e}_1 \alpha_5, d_5) \tag{16}$$

where e_1 is the error signal from the difference between the reference and the system output; K_P and K_D are gains; α_4, α_5, d_4, and d_5 are tuning parameters.

3.3 LADRC

Since there is no linear implementation of the Tracking Differentiator on the LADRC version proposed by [4], only the linear ESO and control law of the LADRC are described below.

3.3.1 LESO

The linear ESO proposed by [4] is built by removing the nonlinear terms of 14, such as:

$$\begin{cases} \dot{z}_1 = z_2 - \beta_1 e \\ \dot{z}_2 = z_3 - \beta_2 e + b_0 u \\ \dot{z}_3 = -\beta_3 e \end{cases} \tag{17}$$

where $e = (z_1 - y)$. This is equivalent to a tradicional Luenberger observer and can be rewritten as:

$$\begin{aligned} \dot{z} &= Az + Bu - L(\hat{y} - y) \\ \hat{y} &= Cz \end{aligned} \tag{18}$$

where the vector L if composed by the observer gains:

$$\mathrm{L} = \begin{bmatrix} \beta_1 & \beta_2 & \beta_3 \end{bmatrix}^T$$

These gains can be found by any method of pole allocation. In order to simplify the determination of the gains of the vector L, the tuning method proposed by [4] allocates all the poles in $-\omega_0$. ω_0 is assumed as the bandwidth of the observer. Solving $|s\mathbf{I} - (\mathbf{A} - \mathbf{LC})| = (s + \omega_0)^3$ gives:

$$\mathrm{L} = \begin{bmatrix} 3\omega_0 & 3\omega_0^2 & \omega_0^3 \end{bmatrix}^T$$

This procedure offers a systematic way to obtain the tuning parameters of the LESO. The ESO has advantages over nonlinear ESO considering the control complexities [8].

3.3.2 Linear Control Law

The state feedback method can be applied to control the emulated system of the LADRC. Considering the feedback law $u = -Kx$ gives:

$$u_0 = -K_1(r - z_1) - K_2(r - z_2) \tag{19}$$

K_1 and K_2 are the controller gains. The closed loop poles can be found by the allocation of all poles in $-\omega_c$. Solving $|s\mathbf{I} - (\mathbf{A} - \mathbf{BK})| = (s + \omega_c)^2$ and putting the gains grouped in a vector K:

$$\mathrm{K} = \begin{bmatrix} \omega_c^2 & 2\omega_c \end{bmatrix}$$

As for the ESO, the control law of the LADRC has a systematic way to tune the controller parameters.

4 Results

We simulated the control of the plant given by (2) using LADRC and NADRC to compare the performance of both techniques. For the results described in this section, the following considerations must be made:

- Since the dynamic response for the x and the y axis are equal, the results for only one axis are shown;
- The control goal is to maintain the radial position of the machine's rotor in $(x = 0, y = 0)$ position, so the reference signal v is kept in 0 and the Tracking Differentiator is not needed. Therefore the control loop implemented is showed on the Figure 6.

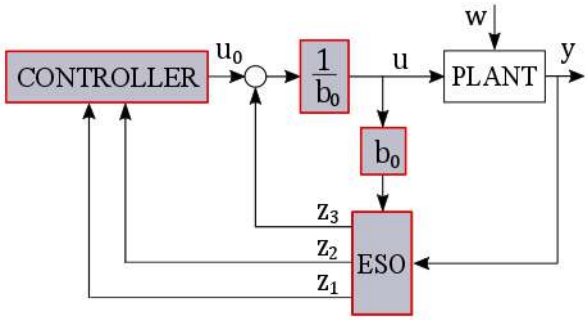

Figure 6: Control loop.

- The nonlinear ADRC was implemented using the equations (14) and the control law is given by (16);
- The linear ADRC was implemented using the equations (17) and the control law is given by (19);
- The controllers tuning was carried out by trial and error;
- The initial conditions are $x_1(0) = 1$ and $x_2(0) = 0$. This situation indicates that the machine rotor was stopped in an unwanted position before the controller starts acting;
- Two step-shaped disturbances were added at the output of the system at the instants $t = 0.1$ and $t = 0.3$ seconds. In a practical situation, disturbances of this type are caused by loads added to the axis of the machine in operation.
- Parameters variations in practice usually come from the natural heat by Joule effect of the circuits and power supplies. This condition is simulated in this work changing the plant dynamic according to:

$$\ddot{y} = (8374 + 8374 * 10 * t)y + 3680000u + w \tag{20}$$

Tables 1 and 2 show the controllers parameters used in the simulations for the LADRC and NADRC. The gains of the nonlinear ADRC blocks used the same of the LADRC.

Parameter	Value
step-size	0.0001 s
$x_1(0)$	1
$x_2(0)$	0
ω_c	147
ω_0	$5 * \omega_c$
b_0	2000000

Table 1: LADRC parameters.

Parameter	Value
step-size	0.0001 s
$x_1(0)$	1
$x_2(0)$	0
K_p	ω_c^2
Kd	$2\omega_c$
β_1	$3\omega_0$
β_2	$3\omega_0^2$
β_3	ω_0^3
b_0	2000000
$fal - ESO$	$d = 0,5;\ \alpha = 0,5$
$fal - Controller$	$d = 2;\ \alpha = 2$

Table 2: NADRC parameters.

Figure 7 shows the plant output for the two versions of the ADRC controller and the detailed views of relevant regions of the dynamical response.

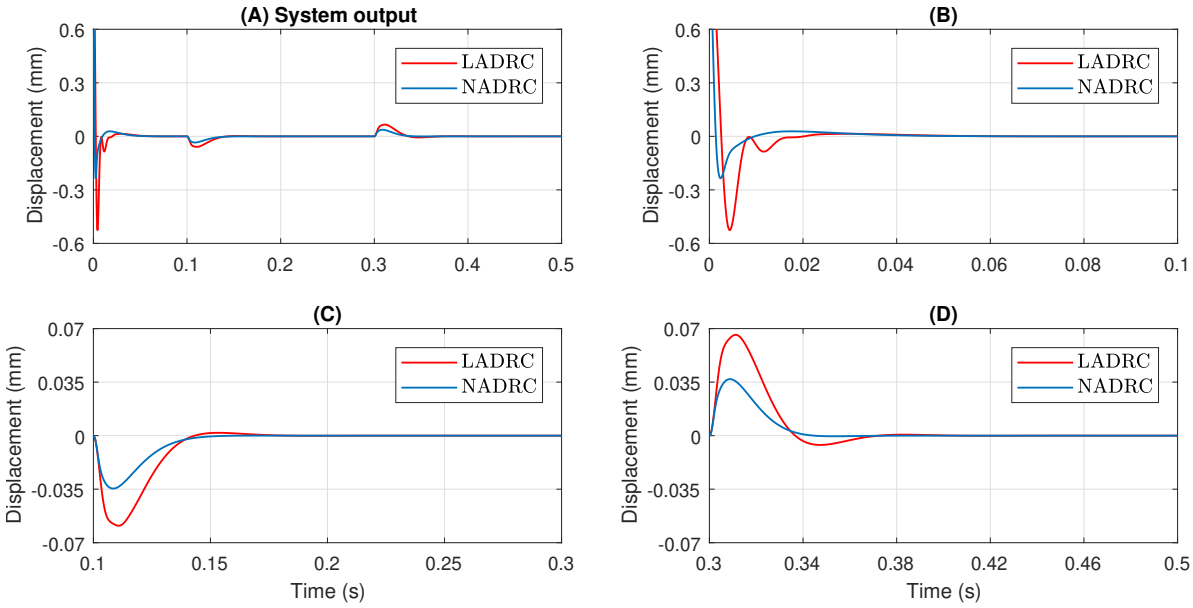

Figure 7: Plant response for LADRC and NADRC.

Figure 7(A) shows that both controllers corrected the plant output to the setpoint and were able to recover this condition even under a load change condition. Figures 7(B), 7(C) and 7(D) show a detailed view of the transitory regions. Figure 7 (B) indicates that the nonlinear model of ADRC can reach the reference faster and with less overshoot. Figures 7(C) and (D) are the response to the step external loads and indicates that the NADRC is more robust to disturbance.

The efficiency of the ADRC in controlling the output of the system depends directly on the ability of ESO to estimate the states of the plant, that is: $x_1 \rightarrow z_1$, $x_2 \rightarrow z_2$ e $F(t) \rightarrow z_3$. Figure 8 compares the dynamic response of the real states with their respective values estimated by the observer. It is clear the ability of the linear and nonlinear ESOs in providing proper estimations of the plant states.

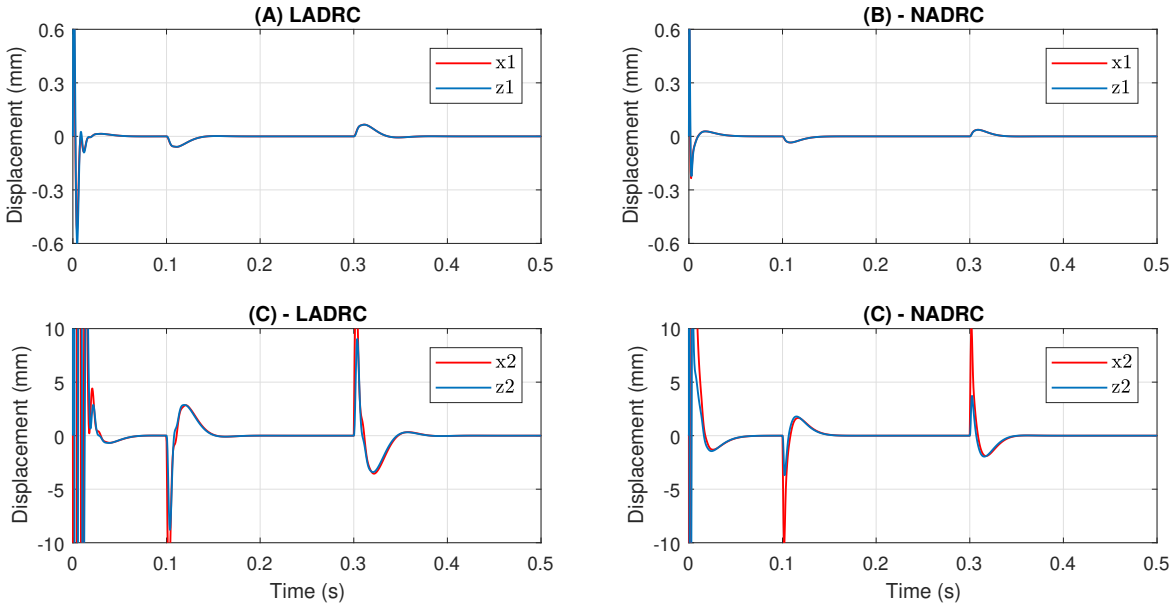

Figure 8: States estimation.

Figure 9 shows the generalized disturbance f and its estimation z_3. Despite some mismatch in the transitory period, the ESOs were successful in estimate the general behavior of the generalized disturbances.

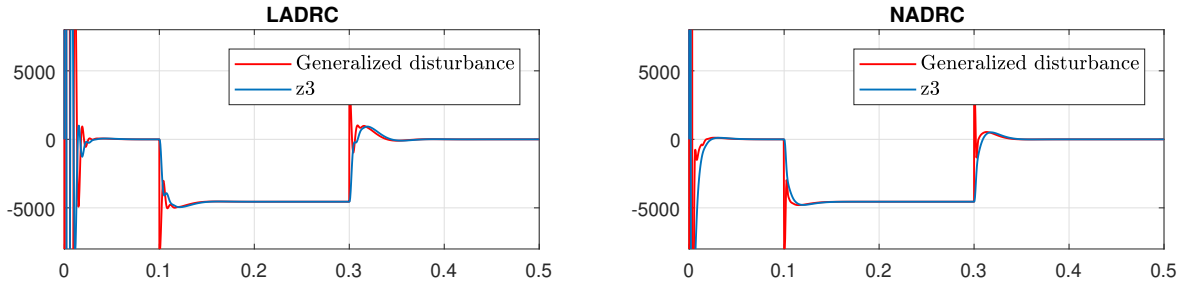

Figure 9: Generalized disturbance estimation.

5 Conclusions

This work studied the application of the ADRC technique to control a simulated plant that represent the rotor radial displacement of a bearingless machine with split winding.

From the simulated results, it was possible to notice that for both the linear and nonlinear controllers the ADRC was successful in providing a stable response to the system even in the presence of perturbations and parameters variations. Despite this, in a more precise point of view, the nonlinear ADRC structure presents a faster and more damped response when compared with the linear ADRC.

Since the performances for both controllers were similar, it is important to evaluate if it is necessary to use the NADRC, which is a more complex structure with more parameters to be tuned, instead of LADRC, which is easier to be built and tuned. Due the nonlinear nature of NADRC and the number of parameters of its implementation, in some cases researchers adopt optimization algorithms [14] instead of trial and error tuning. Again, it means an additional effort to use the NADRC technique that must be taken in account to make project decisions.

As the initial step of a project that aims to evaluate the ADRC to control a real prototype, this works provided the initial experience with this control paradigm and helped to test two different implementations of the ADRC. These results will be useful to future experimental implementations.

6 Acknowledgments

This work was supported by Comissão de Aperfeiçoamento de Pessoal do Nível Superior (CAPES), Programa de Pós-graduação em Engenharia Elétrica e de Computacão (PPgEEC/UFRN) and Conselho Nacional de Desenvolvimento Científico e Tecnológico (CNPq).

References

[1] Jiahao Chen and Eric L. Severson. Optimal design of the bearingless induction motor for industrial applications. In *2019 IEEE Energy Conversion Congress and Exposition (ECCE)*, pages 5265–5272, 2019.

[2] Jossana Maria de Souza Ferreira. Modelagem de máquina de indução trifásica sem mancais com bobinado dividido. 2006.

[3] Zhiqiang Gao. From linear to nonlinear control means: A practical progression. *ISA transactions*, 41(2):177–189, 2002.

[4] Zhiqiang Gao. Scaling and bandwidth-parameterization based controller tuning. In *Proceedings of the 2003 American Control Conference, 2003.*, volume 6, pages 4989–4996, 2003.

[5] Jingqing Han. From pid to active disturbance rejection control. *IEEE transactions on Industrial Electronics*, 56(3):900–906, 2009.

[6] Zhengjie Hao, Yang Yang, Yimin Gong, Zhengqiang Hao, Chenchen Zhang, Hongda Song, and Jiannan Zhang. Linear/nonlinear active disturbance rejection switching control for permanent magnet synchronous motors. *IEEE Transactions on Power Electronics*, 36(8):9334–9347, 2021.

[7] Deqing Huang, Da Min, Yupei Jian, and Yanan Li. Current-cycle iterative learning control for high-precision position tracking of piezoelectric actuator system via active disturbance rejection control for hysteresis compensation. *IEEE Transactions on Industrial Electronics*, 2019.

[8] Prashant Kumar, Abdul Rahiman Beig, Devara Vijaya Bhaskar, Khaled Ali Al Jaafari, Utkal Ranjan Muduli, and Ranjan kumar Behera. An enhanced linear active disturbance rejection controller for high performance pmbldcm drive considering iron loss. *IEEE Transactions on Power Electronics*, pages 1–1, 2021.

[9] Jie Li, Yuanqing Xia, Xiaohui Qi, and Zhiqiang Gao. On the necessity, scheme, and basis of the linear–nonlinear switching in active disturbance rejection control. *IEEE Transactions on Industrial Electronics*, 64(2):1425–1435, 2016.

[10] Ke Li, Guoyu Cheng, Xiaodong Sun, Dean Zhao, and Zebin Yang. Direct torque and suspension force control for bearingless induction motors based on active disturbance rejection control scheme. *IEEE Access*, 7:86989–87001, 2019.

[11] Yujun Liu, Hejin Xiong, and Heng Zhang. Research on active disturbance rejection control of active magnetic bearing-rotor system. In *2021 6th Asia Conference on Power and Electrical Engineering (ACPEE)*, pages 873–877, 2021.

[12] A.O. Salazar and R.M. Stephan. A bearingless method for induction machines. *IEEE Transactions on Magnetics*, 29(6):2965–2967, 1993.

[13] Eric Severson, Robert Nilssen, Tore Undeland, and Ned Mohan. Design of dual purpose no voltage combined windings for bearingless motors. In *2016 IEEE Energy Conversion Congress and Exposition (ECCE)*, pages 1–10, 2016.

[14] Suiyuan Shen and Jinfa Xu. Trajectory tracking active disturbance rejection control of the unmanned helicopter and its parameters tuning. *IEEE Access*, 9:56773–56785, 2021.

[15] Francisco Elvis Carvalho Souza. Otimização da estrutura de acionamento para o controle de posição radial de um motor de indução trifásico sem mancais com enrolamento dividido. 2018.

[16] Li Sun, Wenchao Xue, Donghai Li, Hongxia Zhu, and Zhi-gang Su. Quantitative tuning of active disturbance rejection controller for fopdt model with application to power plant control. *IEEE Transactions on Industrial Electronics*, pages 1–1, 2021.

[17] Xiaodong Sun, Long Chen, and Zebin Yang. Overview of bearingless induction motors. *Mathematical Problems in Engineering*, 2014, 2014.

[18] Thuy Vi Tran, Kyeong-Hwa Kim, and Jih-Sheng jason Lai. Optimized active disturbance rejection control with resonant extended state observer for grid voltage sensorless lcl-filtered inverter. *IEEE Transactions on Power Electronics*, pages 1–1, 2021.

[19] Zebin Yang, Jialei Ji, Xiaodong Sun, Huimin Zhu, and Qian Zhao. Active disturbance rejection control for bearingless induction motor based on hyperbolic tangent tracking differentiator. *IEEE Journal of Emerging and Selected Topics in Power Electronics*, 2019.

[20] Zebin Yang, Chengling Lu, Xiaodong Sun, Jialei Ji, and Qifeng Ding. Study on active disturbance rejection control of a bearingless induction motor based on an improved particle swarm optimization–genetic algorithm. *IEEE Transactions on Transportation Electrification*, 7(2):694–705, 2021.

REVIEW ABOUT CONTROL AND ESTIMATION STRATEGIES APPLIED TO BEARINGLESS MACHINES

José Á. De Paiva[1], Werbet L. A. Da Silva[2], Jossana M. D. S. Ferreira[2], André L. Maitelli[2], Andrés O. Salazar[2], and Elmer R. L. Villarreal[3]

[1] Federal Education, Science and Technology of Rio Grande do Norte (IFRN), Natal-RN, Brazil
alvaro.paiva@ifrn.edu.br
[2] Federal University of Rio Grande do Norte (UFRN), Natal-RN, Brazil
werbethluizz@hotmail.com
jossana@ect.ufrn.br
maitelli@dca.ufrn.br
andres@dca.ufrn.br
[3] Federal Rural of Semiarid (UFERSA), Mossoró-RN, Brazil
elmerllanos@ufersa.edu.br

Abstract

Motors with magnetic bearings and bearingless machines have as a basic principle magnetic levitation to reduce wear on mechanical parts to increase their useful life and reduce the need for preventive and corrective maintenance, especially in equipment that operates in difficult-to-access environments. However, in order for them to achieve the desired performance, their respective control systems must operate efficiently and synchronously on: the radial rotor position, the torque, speed, and supply currents of these machines. In this context, the first systems developed used in a broad and unrestricted way the classic controllers PI (Proportional-Integrative), PD (Proportional-Derivative), and PID (Proportional-Integrative-Derivative), allied to state estimators based on inverse models of these machines to avoid the use of costly sensors. During the research, however, it was found that the non-linearities and parametric variations inherent to these special machines could affect the performance of the control and estimation systems developed. In order to compensate for these limitations, from the 2000s onwards, new researches were developed using the main modern control and state estimation techniques successfully applied to conventional electrical machines. In this context, the development of microelectronics and new microcontrollers such as, for example, the DSP (Digital Signal Processor) was fundamental to enable the implementation of these new systems. To recover the history of these works and contribute to the development of future systems, this article presents an overview of the main control and estimation techniques applied to different types of machines without bearings and levitation systems developed so far, highlighting, critically, the advantages and limitations of each of the techniques discussed.

Bearingless, Induction motor, DSP, Estimation techniques, control techniques.

1 Introduction

Electric machines that operate with the radial magnetic suspension of the rotor shaft provide a significant reduction in mechanical wear and, consequently, in the number of predictive and corrective maintenance of this equipment [1]. This advantage over conventional electric machines has resulted in the study and development of new models with the most varied topologies over the past decades. In this context, several types of machines that use the magnetic suspension protocol in their operation have been developed over the years. Among them, we can list: Active Bearing Machines (AMB), Bearingless Induction Machine (BIM) with double winding and split winding bearingless motors, permanent magnet and bearingless motors of variable reluctance. Each of these engines has characteristics that fit specific applications. The projects and the performance improvement obtained with these special machines were only possible due to the advances of microelectronics together with the control and estimation techniques developed for conventional electrical machines. However, these machines have nonlinearities, which significantly limits the application only of classic controllers based on plants with constant and known parameters. In order to get around the nonlinearities of bearingless machines, many control systems use the combination of two or more control and/or estimation techniques with the classic methods (based on machine parameters) for tuning the controllers optimally. In the next sections, the basic characteristics and applications of the main estimation and control techniques applied to the various types of bearingless induction machines or Active Bearing Motors are presented, highlighting their respective advantages and disadvantages. Finally, a general analysis of these techniques is presented to contribute to the development and/or optimization of other control systems applied to these special machines.

2 General Model of Control System applied to bearingless machines

To start the discussions on the control and estimation strategies applied to machines without bearings and magnetic levitation systems, Figure (1) presents the universal block diagram, in which the main stages are present in most of the systems already implemented. The difference between them is evident from the techniques used to control variables and state estimation of the controlled machines. Among the most studied variables are forces and radial positioning, rotational speed, electrical torque, flux position, and machine parameters.

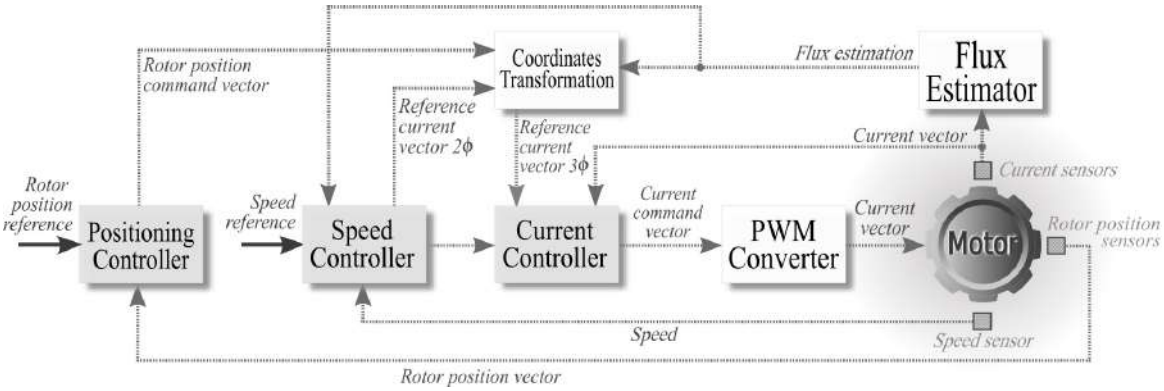

Figure 1: General diagram of a generic estimation and control system applied to bearingless machines and magnetic bearings.

This structure makes it possible to identify the following blocks: the radial positioning controller, the speed controller, the current controller, The PWM converter, the coordinate transformation block, and the flux estimator. The controllers most used in these stages are PI (Proportional-Integrative) or PD (Proportional-Derivative), or PID (Proportional-Integrative-Derivative). The estimator block is implemented by a flux-oriented vector model based on the inverse of the machine model. However, for plants with non-linear models with variable and unknown parameters, is necessary to replace or modify these control or estimation strategies with modern techniques based on artificial intelligence to improve the performance of these specialized machines. The PWM converter block is responsible for supplying the motor from the reference currents generated by the current controller; The coordinate transformation block converts two-phase control signals into three-phase reference signals, using the synchronous angle generated by the flux estimator. To this end, other strategies have been by using and implemented in recent years to assist the tuning of classic or modern controllers, making systems more robust to disturbances and parametric uncertainties. The estimation and control techniques covered in this article will be described in the following sections.

3 ESTIMATION TECHNIQUES APPLIED TO THE BEARINGLESS MACHINES

The states estimation and parameters of electrical machines aim to compensate for the difficulties of measuring these quantities in equipment with limited access or those which present significant variations under the influence of external phenomena, such as temperature and electrical and mechanical disturbances. The first estimation techniques developed were based on the internal model of the machine through which measurements of its inputs and outputs were made and, from the developed model, the values of the desired quantities were obtained. However, in most cases, the inverse models used for the estimation are linearized, operating at specific points. In addition, these models consider the machine parameters constant and immune to variations resulting from the influence of external agents. Several techniques have been studied and developed in the last decades to solve the limitations imposed by linearized models. One of those machines that have non-linearities is bearingless machines and machines with magnetic bearings. In order to understand the principle of operation and its respective applications, this article brought together the main estimation and control techniques applied to bearingless machines developed in the last decades. The description of the state of the art of these works as well as their applications will be presented in the following sections.

3.1 Estimation techniques based on the machine model

Each type of electric machine has a specific mathematical model, which depends essentially on its topology and construction technology. Thus, some machines have relatively simple and approximately linear models, such as DC machines. AC machines have more complex models with non-linear characteristics, as the machines are based on the principle of magnetic levitation. The following subsections describe the characteristics and applications of the main estimation techniques based on the bearingless machines inverse model.

3.1.1 Vector Model

The vector control techniques with flux guidance for induction machines, unlike scalar control of the V/F (voltage/frequency) type, present high performance both in the permanent regime and during the transients of these machines. The decoupling between the torque and flux controllers is achieved by transforming the model of the induction machine into a model similar to DC machines, whose control is much simpler and effective for both high and low speeds. The main requirement of vector controllers is to know the exact value of the magnitude and the position of the rotating flux. This factor generates the need for the use of flux sensors placed inside the machine, which is often not feasible for certain systems, either due to the difficulty of access or even the high cost of these sensors. For this reason, is very common to use flux estimators instead of sensors. In the vector control technique, a flux reference is chosen to obtain the model. The usual flux references are the stator flux vector the air gap flux vector, and the rotor flux vector. Each of these references has advantages and disadvantages in relation to the number of state equations and implementation difficulties. Initially, vector control was developed for the three-phase induction machine. However, features such as simplicity of equation and ease of implementation allowed the expansion of its applications to other types of machines. In [14], the vector model of an induction bearingless machine with split winding was developed. In this work, it was possible to prove that the model developed is similar to the vector model of a conventional three-phase induction machine when the rotor is centralized by the action of the radial position controller.

3.1.2 LSE based on zero-sequence voltage equations

The zero-sequence voltage equations to represent the models of three-phase electric induction machines are based on the representation in symmetric components widely used in multi-phase power systems. To make this representation possible, this model considers that all parameters of the induction machine are constant. From this model, it is possible to use the least-squares (LS) strategy to estimate the parameters through a regression equation composed by a prediction vector that depends on a regression vector and the parameter vector. To illustrate an application of this type of estimator, the work described in [30] presents an independent radial force control system on a double coiled induction bearing machine operating at high speed. In this work, the limitations of the control guided by the air gap flux are identified in relation to the delays inherent to the digital processing of the algorithm in a DSP for machines operating at high speeds. To compensate for these limitations, the developed estimator uses the least-squares technique (LSE) on the model of zero sequence equations of the machine. The proposed algorithm performs the estimation of stator parameters such as the mutual inductances between the windings and the resistance from the reading. With these estimated parameters, it is possible to independently control the electromagnetic torque and radial forces without direct dependence on the stator flux.

3.2 Artificial Neural Network (ANN)

Among the techniques for estimating nonlinear plants in evidence, estimators based on Artificial Neural Networks (ANNs) stand out [16]. This highlight is due to its wide range of applications and the ability to adapt and learn neural estimators concerning the behavior of the states to be estimated. One of the most promising research areas for implementing the artificial neural networks is in the control area and estimation of parameters and states of electrical machines. Induction machines have non-linearities in their models and suffer variations in the values of their parameters due to internal factors such as the rotor magnetic saturation and the temperature variation. In order to circumvent these problems, neural estimators can be trained under different load conditions and at various points of operation to contemplate and compensate for variations in machine parameters and maintain the desired performance for system controllers, whether they are classic or modern. Among the possible applications of RNAs in electrical machines is the induction bearingless machine with split winding. This machine type presents complex modeling in the function of the variation of

the values of its parameters in function of the radial position and the non-linearities present in its equations.

Flux-oriented vector control depends on the exact position of the chosen reference flux, be it the stator, the rotor, or the air gap. However, the flux estimation through the conventional model of the machines does not consider the parametric variations due to the action of external agents, such as temperature variations. In order to compensate and allow a self-adjustment of the estimator in relation to these variations, a radial position and speed control system for a bearingless motor with split winding was implemented in [15] using the ANNs to estimate the rotor flux through Backpropagation networks with offline training. The results obtained showed that the performance of the system operating under the guidance of estimated rotor flux through the neural estimator was superior to the conventional estimator based on the machine model in terms of stability of the control of the radial position and the speed of the response of the speed control. In [18], by using neural network configurations were tested for speed control of the same type of machine, and the simulations proved that other RNA topologies could be used for flux estimation.

3.3 Adaptive Neuro-Fuzzy Inference System (ANFIS)

Neuro-Fuzzy networks combine the characteristics of Fuzzy Inference (FIS) systems with the ability to learn artificial neural networks (ANNs), resulting in a system known as Adaptive Neuro-Fuzzy Inference System (ANFIS). With the combination of the characteristics of the Fuzzy controllers and the Neural Networks, it is possible to develop estimators that adapt to the parametric variations of the plant under control. An application of the ANFIS networks is presented in [17] to estimate the rotor flux necessary for the vector control of a three-phase induction machine with split winding. In this work, the control system's performance using a conventional rotor flux estimator is compared with an ANFIS estimator. In this comparison, it is possible to observe that the flux estimated by the ANFIS network accurately follows the flux estimated by the conventional estimator, and its responses of speed, torque, and machine currents offer better performance. Thus, ANFIS-type networks emerge as an important tool for treating non-linearities in bearingless machines split-coil or in other machines with similar characteristics.

Each of the estimation techniques described above has its advantages and limitations (see Table (2)). For this reason, choosing the ideal technique for each type of machine is an important step towards achieving the desired dynamic performance. This choice depends on the machine's constructive characteristics and the performance specifications foreseen for each application. However, the good dynamic performance of the machine is only possible if there is a perfect connection between the chosen estimation technique and the most suitable control strategy for each type of control variable of machines without bearings or levitation systems. In this context, several control techniques have been proposed to compensate for the limitations imposed by the classical controllers widely used in the first works, as discussed in the next section.

4 CONTROL STRATEGIES APPLIED TO THE BEARINGLESS MACHINES AND LEVITATION SYSTEMS

As shown in Figure (1), it is common for control systems to have state estimators operating together with the controllers so that the machine without bearings or levitation system achieves the desired performance within the conditions defined in the project. For this, several types of controllers have been developed, tested, and compared to each other to overcome the limitations imposed by the controlled machine to guarantee operating stability, rejection to external disturbances, and robustness to parametric variations. The following sections present and discuss the basic design and operation principles of the main control techniques applied to bearingless machines and magnetic levitation systems.

4.1 Classic Controllers (PI, PD e PID)

Conventional PI, PD, and PID controllers were the first to be used in the control loops of systems applied to bearingless machines or even in magnetic levitation systems [1], [11] [13]. Because they are easy to implement and have consolidated theory, they are still widely used in the control systems of electrical machines that operate under constant torque and speed conditions. They are controllers with designs based on linear models with fixed parameters. However, due to non-linearities and parametric uncertainties, the tuning of these controllers becomes ineffective for some types of applications. In these cases, it is common to use a hybrid system composed of meshes implemented with PI, PD, and PID controllers, but with the aid of some modern estimation and control techniques

for the online adjustment of its parameters [15], [26], [29], [30]. Thus, even with the emergence of modern control techniques, classical controllers should not be disregarded at first [5], [10], [12], [20], [21], [25], [27]. Initially, it is important to test them to identify possible limitations and define which estimation and/or control techniques should be added to compensate for them.

4.2 Convergent Control Algorithm

The convergent control algorithm (CC) is a control technique that operates in the frequency domain in which the Fourier coefficients of the controller input signal operating at excitation frequency are obtained by an adaptive control law [2]. If the excitation is composed of several frequencies, the convergent control algorithm must be applied to each excitation frequency separately through adaptive loops until the performance conditions are reached. Some works implement convergent control in machines without bearings to compensate for possible mechanical vibrations of the rotor at certain frequencies. The work presented in [3]. implements an active control of flexural vibration of the rotor using an adaptive harmonic controller LQR to attenuate the components of low-frequency vibrations, together with a convergent controller for radial positioning. The results obtained in the simulation show that the union of the techniques embedded in the system presents itself as a viable strategy for the control of vibrations at low frequencies in flexible rotors in an induction machine without cage bearings. In [2], the rotor's flexural vibrations with a two-pole cage rotor are studied. For this, the machine is equipped with a radial forces actuator and a supplementary winding located inside the stator slots. The model obtained from the machine uses the movement of the rotor coupled to the voltage and flux equations. The actuator built into the machine is a controller based on the Convergent Control Algorithm (CC) to attenuate periodic vibrations. The results showed that the controller used was able to attenuate the flexural vibrations of the rotor by up to 85%. In addition, the control technique implemented can also be used in the monitoring and diagnostics of machine failures.

4.3 Linear Quadratic Regulator (LQR)

The Optimal Control theory of a system considers that a good performance system depends on operating dynamics with minimal cost. Considering that a set of linear differential equations can represent the dynamics of the system and that the cost function is defined from a linear quadratic equation, the Quadratic Linear Regulator (LQR) is a control technique based on state feedback, stable and robust, whose main objective is to minimize the cost function. For this, the LQR control algorithm performs the adjustment of its coefficients through an iterative process. Some studies using LQR controllers have shown good results in the application of this control technique. In [28], the authors propose a decentralized LQR controller (LQRd) to control the radial position of a bearingless machine with double winding. In it, a direct comparison of the performance of the LQRd controller is made in relation to a conventional PD controller for radial positioning. The results obtained showed that the LQRd controller has a superior behavior to the PD controller and that the LQRd controller can be considered a PD controller with optimized parameters. Another work presented in [9] proposes an LQR controller combined with the theory of the Linear Inequality Matrix (LMI) for the optimization of the parameters of the Multiple Resonant controllers (MRC) to compensate the periodic oscillations generated by the disturbances on a multisector machine permanent magnet (MSPM). The results demonstrated that the control system combining the mentioned techniques presented a robust and efficient behavior in relation to oscillations in the radial position. Another application of the LQR controller is presented in [22]. In this work, a pole positioning controller is combined with the LQR controller to act in the radial position control of a permanent magnet dual machine with 4 degrees of freedom, double wound, and 10 kW. The article presents tests and simulations to check the stability of the radial position control at low speeds. When comparing the adopted controllers in relation to the PID controllers, it is shown that the LQR controller surpasses the performance in the radial positioning of the rotor. In addition, designing an LQR controller is simpler by using intuitive adjustments.

4.4 Decoupled torque and force control technique (FTD) and FTD with Harmonic Compensation (HFTD)

The articles that involve this technique use a machine structure without bearings with a permanent magnet rotor in which a single set of stator coils is responsible for generating the radial positioning forces and electromagnetic torque. In this machine model, the stator is divided into sectors, and a three-phase inverter controls each sector. The objective is to obtain an independent control of the x and y axes of radial position from the interaction of the magnetic fields resulting from each sector.

The FTD technique expresses the radial force F as a vector that can be decomposed into vectors on the x and y axes. These vectors, in turn, can be decomposed into three other axes (each axis corresponds to a spatial sector of the stator). The FTD technique uses the flux-oriented field control theory and shows that is possible to control radial and rotational forces in an uncoupled manner. In this technique, the "d" axis is responsible for controlling the radial positioning forces, and the "q" axis is responsible for the control of the electromagnetic torque. From this, as the intensity of the force F is controlled by the intensity of the component "d" of current of each sector, it has that the force F is maximum in the direction "d" of a determining sector when the resulting vector F is aligned with that "d" direction. The FTD technique controls the angle of force alignment F in relation to each sector's "d" components to carry out the radial position control. The control using the FTD technique does not include any compensation for synchronous disturbances. Therefore, the response of the position control system is highly interfered with by the action of an magnectic force F_m, resulting from the action of the centrifugal force caused by the unbalance of the rotor mass. To compensate for these synchronous disturbances, a modification in the FTD technique was proposed, resulting in the HFTD (Harmonic Force Torque Decoupled) technique. The HFTD technique alters the control law by including some parameters related to the synchronous frequency, which must be calculated using finite elements. Therefore, the HFTD control technique offers a harmonic compensation in a table form that must be updated according to the rotor position and the load torque to ensure the machine's stable operation. The work presented in [7] performs a direct comparison between the FTD, HFTD, and Pseudo Inverse Matrix (PIM) techniques, described in the following section. In this work, it was possible to prove that the FTD technique offers a good magnitude of radial forces and simplicity of computational implementation. However, the quality of these forces and the losses due to the Joule effect were significantly impaired by synchronous oscillations during the operation of the machine. When comparing the mentioned techniques, the HFTD technique provided an effective compensation for synchronous oscillations. However, its computational implementation is more complex than that required by the Pseudo Inverse Matrix technique (PIM).

4.5 Pseudo Inverse Matrix

The control technique through the Inverse Pseudo Matrix [7], [8], [10] was developed from the inverse model of a multi-sector permanent magnet bearingless motor (MSPM) with 18 slots and 6 poles with reconfigured winding. The mathematical modeling of the machine in question was based on the conventional permanent magnet machine in which the magnetic decoupling between sectors is considered, maintaining the geometric and symmetry characteristics. A matrix of K_E coefficients is found from the model obtained that characterizes the electro-magneto-mechanical outputs obtained by reading the currents responsible for the radial forces and torque. With these coefficients in place, the control action of the currents mentioned above is defined by obtaining the inverse K_E matrix. However, the matrix generates only three equations that differ from the number of state variables that depend on the number of sectors. In this way, the system of equations obtained presents infinite possibilities for solutions. Therefore, it is necessary to define a single solution that meets the minimum performance requirements. In order to minimize losses due to the joule effect, a solution using the Moore-Penrose pseudo matrix is proposed as a generalization of the inverse K_E matrix. In [7], the control technique is compared with the Decoupled Force and Torque (FTD) and Decoupled Force and Torque control techniques with Harmonic compensation (HFTD). The results obtained demonstrate that parameters such as: Magnitude and quality of radial forces minimize losses by Joule effect are equivalent between the HFTD and PIM techniques and better than FTD. However, the control technique based on the Pseudo Inverse Matrix (PIM) offers a simpler computational implementation than the HFTD technique. The only difficulty with the proposed technique is obtaining the Inverse Matrix K_E. For this, the computational technique SVD (Single Value Decomposition) is used with offline processing to minimize the computational effort during the Control System operation.

4.6 Support Vector Machine (SVM)

A support vector machine (SVM) is a concept in computer science for a set of supervised learning methods that analyze data and recognize patterns used for classification and regression analysis. The standard SVM takes a set of data as input and predicts each given input, which of two possible classes the input is part of, which makes SVM a non-probabilistic binary linear classifier. Given a set of training examples, each marked as belonging to one of two categories. An SVM training algorithm builds a model that assigns new examples to one category or another. An SVM model represents examples as points in space, mapped so that the examples in each category are divided into a clear space that is as wide as possible. The new examples are then mapped into the same space and predicted to belong to a category based on which side of the space they are placed on. The

SVM technique has been applied in some control systems of bearingless machines. In some cases, SVM is used in conjunction with other techniques. In [21], a decoupled control system based on the Least Squares Inverse Support Vector machine (LSSVMI) is proposed, applied on an induction machine of 5 degrees of freedom. This work presents the structure of the motor and its inverse mathematical model, which is obtained using the regression capacity of the nonlinear theory of the least squares support vector machine. In addition, the work proposes an optimization algorithm for the parameters, which improves the accuracy of the model's adjustment and prediction. The initial simulation results demonstrate the efficiency of the control strategy.

4.7 Active Disturbance Rejection Control (ADRC)

Active Disturbance Rejection Control (ADRC) is a robust controller based on non-linear functions that estimate and compensates for various disturbances and variations in plant parameters. For this, the equations of the ADRC controller consider the total disturbance (composed of unmodulated dynamics, nonlinearities, uncertainties, and load variations) as a new state of the system to be estimated in real-time through an extended state observer. These characteristics make the controller's performance independent to the plant model, which is ideal for controlling electrical machines. As a disadvantage for applying this technique, we can mention a large number of the controller parameters and the lack of a systematic method of tuning. As an application example of the ADRC controller, the work presented in [4] proposes an ADRC controller based on the inverse model of the rotor flux for the radial positioning and speed controls of a double winding induction machine, replacing the conventional PID controllers. The implemented ADRC controller considers the cross-couplings of torque and radial position, parametric variations, and loads as disturbances within the control law. An extended state observer (ESO) estimates the total disturbance and compensated by a non-linear state error controller. The simulation results showed that the proposed control system has the robustness and better performance in the responses of rotation speed and radial positioning in relation to the system implemented with conventional PI controllers. Another application of the ADRC controller is found in [19]. In this work, the performance of the proposed ADRC controller is compared to the performance of the PID controller. Among the control variables compared are: the response to the positioning step in the x and y directions, the radial displacement of the rotor, the speed response during the start and with the application of load variations. All the results obtained showed that the ADRC controller had a superior performance because they reduced the speed overshoot, quickness in the transient responses, and robustness to the parametric variations.

4.8 Sliding Mode Control (SMC)

Sliding mode control is a strategy with several applications in recent decades. It is indicated for plant control systems with strong nonlinear characteristics with great sensitivity to disturbances and parametric variations. The technique consists of direct control in two modes directing the system to a hyperplane, representing the plant's desired dynamic behavior. The trajectory of the outputs within this surface is known as operation in sliding modes. The technique has the advantages of quick response, negligible effects of unmodulated dynamics, and does not depend on plant parameters and external disturbances. The main problem with the SMC is that the control signal is applied at a high frequency to keep the output on a hyperplane to result in an unwanted phenomenon known as "Chattering". To decrease the Chattering effect, it is necessary to apply corrections to the control signal, replacing the discontinuous signal by a function with the saturation or the sigmoid function and limiting the signal level. Consequently, it is common for a finite error to appear permanently due to this correction of the control signal. In [23], a system for controlling the suspension of the rotor by sliding modes for an engine without variable reluctance bearings (BLSRM) is proposed. The results obtained in simulations with the proposed radial position control system demonstrated that the rotor remained stable both during acceleration and during the steady-state, with low vibrations. The rotor suspension and stabilization times were satisfactory.

4.9 Multi-Ressonant Controller (MRC)

Like the HFTD controllers applied to motors with magnetic bearings and machines without bearings, the Multiple Resonant Controllers (MRC) are used to mitigate the effects of periodic disturbances in the control of the radial position of the rotor. These disturbances arise mainly due to the misalignment of the geometric axis in relation to the center of mass of the rotor and the position sensing surface's constructive and magnetic imperfections. It is common to have cyclical disturbances of different frequencies in the same system, so the controller must be able to attenuate each one of them. In position control systems with MRC, there is usually a controller responsible for stabilizing

the radial position operating in conjunction with the MRC controller dedicated to promoting the rejection of cyclic disturbances. This controller produces an infinite gain whenever the error has a frequency ωr. The reference tracking problem can be addressed by using n resonant controllers that lead to multiple resonances or multiple resonant controllers. The main idea is to generate an oscillating dynamic (sinusoidal mode) corresponding to the fundamental frequency of the signal of interest and its respective most significant harmonics. To exemplify an application of this type of controller, the system described in [9] implements an LQR type controller for a machine without a permanent magnet multi-sector bearing (MSPM) in which a mathematical model was developed to generate optimally current references. To minimize losses by Joule effect. In it, an MRC controller is incorporated into the system to compensate for periodic disturbances. The experimental results demonstrated the effective rejection of oscillations on the radial position, which significantly improved the performance of the magnetic levitation system.

4.10 Fuzzy Controller

The Fuzzy controller seeks to embody the human way of thinking in a control system. It emerged as an alternative to the classic control method as it does not require the knowledge of its mathematical modelling, thus facilitating control in non-linear systems that are difficult to modelling. The controller design is based on deductive reasoning, on the experience of the system operators, or on a desired behavior for the system. Fuzzy controllers are an important application of the fuzzy set theory (Fuzzy sets) and can be used in conjunction with other types of controllers such as PID and Neuro-Controllers. A recent proposal for applying Fuzzy controllers for a three-phase induction machine without bearings with split winding is presented in [5]. This article presents a Fuzzy controller with PD controller characteristics for radial positioning. The design of the controller took into account the knowledge of the desired performance of the system when using a PD controller to keep the rotor axis centralized. From this condition, the input and output pertinence functions were defined together with the rules of the Fuzzy controller. The work results showed that the Fuzzy controller with PD characteristics applied to the x and y axes offers good performance and robustness in the control of the radial position, as long as the operating frequency of the motor is close to the nominal frequency of the machine. However, for operation at frequencies below 60 Hz, the Fuzzy control performance was impaired, indicating the need for modifications in the adjustment of the controller parameters. Even with significant oscillations, the rotor has not exceeded the stability limits, which demonstrates the viability of the technique for some simpler applications.

4.11 H_∞ Controller

The H_∞ controller is a feedback controller of the same order as the plant. The H_∞ controller synthesis must be understood as a system optimization technique in the frequency domain. Its main objective is to minimize the norm of the system's frequency response when it is desired to guarantee its stability and good performance. The norm of a system is related to the maximum gain existing between the inputs and outputs in the entire spectrum of possible operating frequencies. A thesis paper was presented in [6]. In it, an H_∞ controller is proposed for the radial positioning of a bearingless motor in order to maintain stability and robustness even with parametric variations. The thesis provides a detailed description of the concepts necessary to understand the H_∞ control. Soon after, the work describes the theory, the design, and the synthesis of the controller H_∞ , performs several simulations to verify stability in radial positioning and its behavior under the action of harmonic disturbances, and presents the implementation and operation of the prototype. After analyzing the results of the tests, it was found that the H_∞ control system meets the specified performance requirements. Thus, the work concludes that the H_∞ controller is a very promising technique for application in bearingless motors because it is a complex and non-linear modeling plant.

4.12 μ-Synthesis

The μ-Synthesis control technique is an extension of the H_∞ method and presents itself as a robust controller for plants with a high degree of uncertainty, whether parametric or dynamic. However, for the application of this method, it is necessary to know the uncertainties of the plant in detail and in a structured way. In addition, the μ-Synthesis method generates a higher-order controller, which requires a recursive process of interactions to obtain the optimal solution, which must meet the performance conditions required for the plant. The robust control technique μ-Synthesis has some recent applications in levitation systems as described in [24]. In this work, the μ-Synthesis control technique acts in the recovery of levitation of an active magnetic bearing (AMB). The proposed strategy uses the model in the theory-Synthesis controller theory to find the controller parameters to provide the necessary forces that prevent the saturation of the control signals that occur during large

deflections due to levitation problems. After the design and synthesis of the controller, experimental tests were carried out in which the levitation system was brought to instability simulating failures during operation. The work proposes that the μ-Synthesis controller is automatically activated in case of loss of support of the rotor. The results obtained demonstrated that the control system responded quickly to the recovery of levitation. However, the system was studied in a simplified model, which does not generate the need to expand research on machines with more complex models.

4.13 PWM modulation control techniques for inverters

To control the static switches of the inverters responsible for driving the electrical machines, is traditionally used the pulse width modulation (PWM) technique. Unfortunately, this high-frequency switching causes harmonic distortions that affect the quality of voltages and currents applied to electrical machines. In order to minimize these distortions and approximate these signals to perfect sine waves, several techniques were developed and implemented, significantly improving machine performance and control systems performance. The following subsections provide a brief description of these switching techniques.

4.13.1 Space Vector Modulation (SVM)

The technique known as Space Vector Modulation (SVM) is a strategy applied to the PWM (Pulse Width Modulation) signals that control the PWM inverters of an AC converter. Its operation can be defined by a specific sequence in the activation of the inverter switches so that the converter's output approaches the maximum of a sinusoidal signal. The main objective of this technique is to minimize the effect of harmonic components present in switched signals. Several works use the SVM technique combined with conventional control techniques to optimize the reference voltages and currents applied to the machines. An example of this combination of the SVM control technique applied to the PWM signals of the inverters is presented in [19]. Although this work is dedicated to the implementation of ADRC controllers for radial positioning, speed, and electromagnetic torque, the power stage uses SVM modulation in conjunction with a DTC (Direct Torque Controller) controller, resulting in a controller (SVM-DTC) for the supply of optimized voltage reference signals for the individual converters, for the supply of the two-pole windings (responsible for the radial positioning control) and four-pole windings (for the torque control) in order to guarantee the decoupling between the controllers and the reduction of high frequency harmonic components.

4.13.2 Direct Levitated Force Control

For the radial positioning control of bearingless machines, it is common to use flux-oriented vector control techniques synchronized with the torque and speed control. However, this type of control is strongly influenced by the machine parameters causing its radial levitation forces to be controlled indirectly. As a consequence of the indirect radial suspension force control, it is common the occurrence of lags on the flux angle that guides the radial positioning, resulting in the appearance of oscillations and sensitivity to disturbances. In order to ensure operating stability, minimize oscillations and make the positioning control more robust, the work presented in [12] proposes a new strategy for the direct control of levitation forces for an induction bearingless machine double-winding. This strategy executes an algorithm with predictive characteristics that calculates the future value of the angular position of the radial positioning flux from the difference between the current values of this angle and the angular position of the air gap flux, responsible for the torque and velocity control. For this, is necessary that in addition to the magnitude and phase values of the radial positioning flux predicted in the previous step, the magnitude and phase of the air gap flux are available, either through a sensor or calculated using a vector estimator flux. In this sense, to avoid using sensor flux, the cited work introduces an optimized model for the flux estimator responsible for the torque. For the optimized control of the inverter switching, the proposed system uses the SVPWM (Space Vectorial Pulse Width Modulation) technique.

The results obtained in the simulations and experimentally demonstrated that the technique of direct control of the levitation forces proposed improved the stability of the control of the radial position of the rotor, reduced the oscillations in the rotor levitation, and increased the disturbances rejection.

4.13.3 Direct Torque Control(DTC) and Direct Suspension Force Control (DSFC)

The Direct Torque Control (DTC) technique is a technique that allows direct control of stator flux and torque through optimal drive state selection using designer-defined switching tables. Due to

the simplicity of its structure, it is common for the appearance of high levels of ripple in the torque signals, which significantly affects the performance of the DTC controller. Therefore, works such as the one presented in [19] propose adding other switching techniques added to the DTC controller. In this work, the SVM-DTC technique was proposed to smooth the torque ripple effect, resulting in a significant improvement in the performance of the torque and flux control system. In addition to torque and flux controls, control systems for bearingless machines must ensure efficient control of the radial positioning of the rotor. In general, radial positioning control uses the torque vector controller itself to generate the command of lifting forces necessary for radial positioning. However, most of the time, this over-radial positioning action only occurs after modulation of the torque controller, which results in indirect control. This characteristic makes it considerably difficult to calculate the exact suspension forces required for radial positioning, impairing the overall behavior of the control system. To solve this limitation, the work presented in [19] proposes a direct control algorithm based on the strategy presented in [12], called Direct Levitation Force Control, resulting in the control technique DSFC (Direct Suspension Force Control). With these techniques, suspension forces are calculated using the flux link read and updated in real-time. In this way, the algorithm uses the difference between the suspension forces to calculate the ideal flux for the machine windings responsible for radial positioning. Also, in [19], ADRC controllers are implemented to modulate the signals from SVM-DTC controllers for torque and flux and DSFC for radial positioning to replace PID controllers. The results obtained in the simulation confirm the efficiency of the proposed system.

5 General analysis of the techniques presented

By analyzing the various works listed in this article, essential aspects of implementation could be extracted as a way to collaborate in the development of future systems. Are they:

- Originally, most estimation systems were based on the inverse models of the machines under study. However, uncertainties related to parametric variations and nonlinearities led to the search for more robust estimation techniques to these limitations.

- Since the first works, the classic PI, PD, and PID controllers have been used due to their ease of implementation and many industrial applications in electrical machines. Therefore, even in advanced control systems, it is common to use them together with the proposed controllers.

- For the implementation of each estimation or control technique, it is essential to know the system's behavior operating with estimators based on the inverse model and the classic controllers mentioned above. This knowledge makes it possible to identify the limitations of classical strategies and the correct choice of the advanced estimation and/or control technique to be used, according to the individual characteristics of each type of bearingless machine or levitation system. of the estimation and/or control strategies demand a significant computational processing capacity. For this reason, before implementing systems on an industrial scale, it is necessary to analyze the resources and specifications of the hardware devices available at the time of the control system's development to make it possible to choose the most suitable model for each application.

- Some estimation techniques are dedicated to parameter estimation, others to state estimation. Therefore, knowledge and identification of the difficulties and limitations of each machine or system are one of the first steps in choosing the appropriate technique for that problem (see table 3).

- In general, advanced control techniques seek to compensate for some limitations of classic controllers (PI, PD, and PID) related to aspects such as: speed of response, stabilization time, robustness to parametric uncertainties and disturbances. For this reason, carrying out intensive tests of the machine under study, under the command of these controllers under the most diverse operating conditions, is essential for choosing the most appropriate control and/or estimation technique(s). (see table 4).

It is important to emphasize that this article does not intend to exhaust and address all the contents related to the estimation and control techniques developed so far and applied to machines without bearings and magnetic levitation systems. However, by relating the strategies presented in this work, it was possible to verify the importance and influence of advanced and technical techniques for other types of electrical machines in order to expand the possibilities of new tools in the coming years in view that, until the moment, there is no single type of controller or estimator, operating individually

or together, that definitively compensates the performance limitations of all types of bearingless machines in their various applications.

Tables (1) and (2) with representation (Fig. (2) and Fig. (3)) show the chronological sequences of the works analyzed and their respective control and estimation techniques implemented. Next tables (3) and (4) with representation (Fig. (4) and Fig.(5)) present a general summary of the advantages and limitations of the control and estimation techniques analyzed in this article.

	2003	2004	2005	2006	2007	2008	2009	2010	2011	2012	2013	2014	2015	2016	2017	2018	2019	2020
Vector Model		[16]	[2]	[17]		[19]							[12]			[13]	[14]	
LSE based on zero sequence voltage equations													[3]					
Neuro-Fuzzy Networks (ANFIS)	[6]																[5]	[4]
Artificial Neural Network (ANN)										[7]								

Figure 2: Timeline: Main estimation techniques applied to machines bearingless.

	2003	2004	2005	2006	2007	2008	2009	2010	2011	2012	2013	2014	2015	2016	2017	2018	2019	2020
ClassicControllers (PI, PD and PID)		[3] [9]	[1] [2]	[10]		[5]		[11]	[12]		[7]	[13]		[14]	[16]		[15] [17] [27]	
Convergent Control Algoritm						[19]										[20]		
Linear Quadratic Regulator (LQR)						[21]							[6]				[22]	
Decoupled torque and force control technique (FTD)														[24]				
Decoupled torque and force control technique including Harmonic Compensation (HFTD)														[24]				
Pseudo Inverse Matrix														[24]	[25]			
Support Vector Machine (SVM)														[14]			[15]	
Active Disturbance Rejection Control (ADRC)															[26]		[27]	
Sliding Mode Control (SMC)																[28]		
Multi-Ressonant Controller (MRC)																	[22]	
Fuzzy Controllers																	[17]	
H∞ Controller											[29]							
μ-Synthesis															[30]			
Space Vector Modulation (SVM)																	[27]	
Direct Levitated Force Control																	[15]	
Direct Torque Control																	[27]	
Direct Suspension Force Control																	[27]	

Figure 3: Timeline : Main control techniques applied to the bearingless machines.

6 Conclusions

This article presented a general analysis of the main estimation and control techniques applied to machines that use the principle of magnetic levitation in their operation. Throughout the research, it was observed that most of the systems proposed in the analyzed works are based on control systems already developed and consolidated for conventional electrical machines. However, these special types of electrical machines have characteristics such has non-linearities and parametric uncertainties that

Estimation tecnique	Main advantages	Limitations
Vector Model	▸ The vector model approximates a direct-current machine, which facilitates its implementation. ▸ Provides good performance both in steady-state and during transient state.	▸ The model obtained depends heavily on knowledge of plant parameters. ▸ To ensure decoupling between flux and torque, it is necessary to have exact knowledge of the position and magnitude of the electromagnetic flux. ▸ The choice of the flow reference reflects the dimension and complexity of the model obtained.
LSE based on zero sequence voltage equations	▸ Its implementation only requires reading the voltages and currents applied to the machine windings. ▸ The accuracy of the estimation is not influenced by any other machine parameters.	▸ It demands high computational effort for real-time applications.
Neuro-Fuzzy Networks (ANFIS)	▸ Adapt to machine parametric variations and uncertainties. ▸ Allows learning and estimating non-linear plants.	▸ It demands high computational effort for real-time applications. ▸ The learning process can slow down plant dynamics.
Artificial Neural Network (ANN)	▸ It combines the learning characteristics of Neural Networks with the relationships and rules of the excellent performance of the Fuzzy controllers' system, allowing the representation of non-linear models with a high degree of uncertainty.	▸ It demands high computational effort for real-time applications. ▸ The process of learning and selfadjusting the rules can slow down the dynamics of the plant.

Figure 4: Main estimation techniques applied to machines bearingless.

make it difficult to implement estimators based on their models based on constant parameters and classical controllers (PI, PD, and PID). From this study, it was possible to gather and systematize the advantages and limitations of the strategies presented to collaborate with the development of new works.

7 Acknowledgments

This work was suported by Comissão de Aperfeiçoamento de Pessoal do Nível Superior (CAPES), Programa de Pós-graduação em Engenharia Elétrica e de Computação (PPgEEC/UFRN) and Conselho Nacional de Desenvolvimento Científico e Tecnológico (CNPq).

References

[1] O. Ichikawa M. Oshima M. Takemoto A. Chiba, T. Fukao and D. G. Dorrell. *Magnetic bearings and bearingless drives*. Elsevier, 2005.

[2] J. Orivuori Anssi Sinervo Kai Zenger A. Laiho, K. Tammi and Anter Arkkio. Electromechanical interaction in eccentric-rotor cage induction machine equipped with a self-bearing force actuator. In *11th International Symposium on Magnetic Bearings, ISMB 2008, Nara*, volume 1, 2008.

[3] K. Zenger A. Laiho, K. Tammi and A. Arkkio. A model-based flexural rotor vibration control in cage induction electrical machines by a built-in force actuator. *Electr Eng 90*, 34(4):407–421, 2008.

[4] W. S. Bu and Y. Q. Huang. Active disturbance rejection control of bearingless induction motor. *DEStech Transactions on Engineering and Technology Research*, 2017.

[5] E. R. L. Villarreal F. E. C. Souza L. P. D. S. Júnior J. S. B. Lopes E. A. D. F. Nunes, A. O. Salazar and J. C. C. Luque. Proposal of a fuzzy controller for radial position in a bearingless induction motor. *IEEE Access*, 7:114808–114816, 2019.

[6] A. R. Franco. *Posicionamento de eixo com motor mancal magnético, utilizando controle H_∞*. Programa de Pós-graduação em Engenharia Elétrica (COPPE), UFRJ, 2013.

[7] A. Formentini C. Gerada G. Valente, L. Papini and P. Zanchetta. Radial force control of multi-sector permanent magnet machines. In *2016 XXII International Conference on Electrical Machines (ICEM)*, volume 1, pages 2595–2601, 2016.

[8] A. Formentini C. Gerada G. Valente, L. Papini and P. Zanchetta. Radial force control of multisector permanent-magnet machines for vibration suppression. *IEEE Transactions on Industrial Electronics*, 65(7):5395–5405, 2018.

[9] L. Papini C. Gerada G. Valente, A. Formentini and P. Zanchetta. Performance improvement of bearingless multisector pmsm with optimal robust position control. *IEEE Transactions on Power Electronics*, 34(4):3575–3585, 2019.

[10] L. Papini P. Zanchetta G. Valente, A. Formentini and C. Gerada. Position control study of a bearingless multi-sector permanent magnet machine. In *IECON 2017-43rd Annual Conference of the IEEE Industrial Electronics Society*, volume 1, pages 8808–8813, 2017.

[11] F. E. F. Castro S. N. D. Lisboa A. O. Salazar J. A. De Paiva, J. M. D. S. Ferreira and A. L. Maitelli. New approach for a bearingless three-phase induction machine with divided winding. In *Ninth International Symposium on Magnetic Bearings, ISMB 2004, Lexongton-KY*, volume 1, 2004.

[12] X. Sun C. Bao J. Lu, Z. Yang and X. Chen. Direct levitation force control for a bearingless induction motor based on model prediction. *IEEE Access*, 7:65368–65378, 2019.

[13] A. 0. Salazar F. E. F. Castro J. M. S. Ferreira, J. A. De Paiva and S. N. D. Lisboas. Dsp utilization in radial positioning control of bearingless machine. In *2003 IEEE International Symposium on Industrial Electronics*, volume 1, 2003.

[14] A. O. Salazar J. M. S. Ferreira, M. Zucca and L. Donadio. Analysis of a bearingless machine with divided windings. *IEEE Transactions on Magnetics*, 41(10):3931–3933, 2005.

[15] A. L. Maitelli J. Á. De Paiva, A. O. Salazar and R. M. Stephan. Performance improvement of a split winding bearingless induction machine based on a neural network flux observer. In *11th International Symposium on Magnetic Bearings, ISMB 2008, Nara*, volume 1, 2008.

[16] A. O. Salazar J. Á. De Paiva and A. L. Maitelli. Review of control strategies and model estimation techniques applied to bearingless induction machine with divided winding. In *Proceedings 13th International Symposium on Magnetic Bearings, ISMB 2013, Rio de Janeiro*, volume 1, 2013.

[17] F.E. C. Souza L. P. D. Santos Junior J. A. De Paiva J.S. B. Lopes, J. D. Fernandes and A. O. Salazar. Adaptative neuro-fuzzy inference system for estimation of rotor flux of a bearingless induction motor applied to speed control. In *13th International Symposium on Magnetic Bearings, ISMB 2013, Rio de Janeiro*, volume 1, 2013.

[18] F.E. C. Souza L. P. D. Santos Junior J. A. De Paiva J.S. B. Lopes, J. D. Fernandes and A. O. Salazar. Using feed-forward back propagation for rotor flux estimation of a bearingless induction motor applied in the speed vector control. In *13th International Symposium on Magnetic Bearings, ISMB 2015, Kitayushu*, volume 1, pages 180–187, 2015.

[19] X. Sun D. Zhao K. Li, G. Cheng and Z. Yang. Direct torque and suspension force control for bearingless induction motors based on active disturbance rejection control scheme. *IEEE Access*, 7:86989–87001, 2019.

[20] J. T. D. Carvalho Neto V. F. Victor L. P. Junior, J. S. B. Lopes and A. O. Salazar. Robust speed control of a bearingless ac motor type divided winding, based on a conventional squirrel cage induction motor. In *22nd International Conference on Magnetically Levitated Systems and Linear Drives (MAGLEV)*, volume 1, pages 1–15, 2014.

[21] X. Sun Z. Chen L. Wan, Z. Yang and L. Chen. Decoupling control of a 5-degree-of- freedom bearingless induction motor based on least squares support vector machine inverse. *Advances in Mechanical Engineering*, 8(10):1–11, 2016.

[22] N. Nevaranta R. Jastrzebski P. Jaatinen, J. Vuojolainen and O. Pyrhonen. Control system commissioning of fully levitated bearingless machine. *Modeling, Identification and Control*, 40(1):27–39, 2019.

[23] G. V. N. Kumar P. V. S. Sobhan and P. V. R. Rao. Rotor suspension and stabilization of bearingless srm using sliding mode controller. *International Journal of Engineering & Technology, [S.l.]*, 7(1.8):214–218, 2018.

[24] A. H. Pesch and J. T. Sawicki. Active magnetic bearing online levitation recovery through μ-synthesis robust control. *Actuators*, 6(2):1–14, 2017.

[25] P. Jaatinen R. P. Jastrzebski and O. Pyrhonen. Modeling and control design simulations of a linear flux-switching permanent-magnet-levitated motor. In *Mechanical Engineering Journal*, volume 1, 2017.

[26] J. A. Santisteban R. R. Gomes and R. M. Stephan. Optimized performance of a motor -bearing. In *Symposium Series in Mechatronics*, volume 1, pages 417–424, 2006.

[27] E. F. Rodriguez and J. A. Santisteban. An improved control system for a split winding bearingless induction motor. *IEEE Transactions on Industrial Electronics*, 58(8):3401–3408, 2011.

[28] R. M. Stephan Domingos W. L. Kauss, A. C. D. N. Gomes and F. B. David. Lqr control of a bearingless macine implemented with a dsp. In *11th International Symposium on Magnetic Bearings, ISMB 2008, Nara*, volume 1, pages 2595–2601, 2008.

[29] Z. Wang and X. Liu. An improved rotor flux oriented control system of bearingless induction motors. In *2010 Chinese Control and Decision Conference*, volume 1, pages 2733–2737, 2010.

[30] X. Meng Z. Deng, X. Wang and Y. Yan. An independent controller of radial force subsystem for super-high-speed bearingless induction motors. In *Proceedings Ninth International Symposium on Magnetic Bearings, ISMB 2004, Lexongton-KY*, volume 1, 2004.

Control tecnique	Main advantages	Limitations
ClassicControllers (PI, PD and PID)	▸Consolidated theory in academia and industry. ▸Large number of applications in electrical machines. ▸It is easy to implement.	▸Difficulty of tuning in non-linear plants. ▸It has high sensitivity to parametric variations and disturbances.
Convergent Control Algoritm	▸Allows attenuation of vibrations generated by periodic power signals.	▸Needs accurate identification of frequencies responsible for vibrations.
Linear Quadratic Regulator (LQR)	▸High performance and simple implementation.	▸It is Sensitive to disturbances and parametric variations.
Decoupled torque and force control technique (FTD)	▸Provides decoupling of radial force and torque controllers ▸It is easy to implement computationally. ▸Provides high magnitude of radial forces.	▸Has low quality of radial force signals. ▸Generate high losses due to the joule effect. ▸It does not show good performance in the attenuation of total harmonic distortions (THD). ▸Generates considerable errors in the directions of radial forces compared to other techniques such as HFTD and PIM.
Decoupled torque and force control technique including Harmonic Compensation (HFTD)	▸Provides decoupling of radial force and torque controllers. ▸Provides high magnitude of radial forces. ▸Presents good quality of radial force signals. ▸Provides efficient attenuation of total harmonic distortions (THD). ▸Considerably reduces errors in radial force directions compared to FTD technique.	▸Needs accurate identification of frequencies responsible for vibrations. ▸The computational implementation is more complex.
Pseudo Inverse Matrix	▸Provides a reduction in computational effort for online operation compared to other techniques such as HFTD. ▸It is able to compensate for imbalances in radial forces. ▸Provides stable generation of radial forces without the need for additional control stages. ▸Allows the generalization of the technique to other plants of a higher order. ▸Allows the generation of optimized reference currents resulting in a reduction in copper joule losses.	▸Provides intermediate performance in reducing total harmonic distortion compared to other techniques such as HFTD. ▸It presents high computational effort for the online processing of the matrix.
Support VectorMachine (SVM)	▸It allows the supervised learning used to estimate a function that classifies the input data of the plants for the recognition of patterns with performance superior to the ANNs. ▸They are robust for large data sets.	▸It is sensitivity to the choice of parameter values and the difficulty of interpreting the model.
Active Disturbance Rejection Control (ADRC)	▸It does not require the exact model of the machine. ▸Estimates and cancels the disturbance effects. ▸High degree of adaptability and resistance to disturbance.	▸There is no a systematic tuning method. ▸The number of parameters makes difficult the controller tuning.
Sliding Mode Control (SMC)	▸Fast dynamic responses. ▸Disregards the effects of the plant nonmodeled dynamics. ▸Regardless of the parameters of the plant and the disturbances on it	▸It presents unwanted oscillations caused by the high-frequency switching (Chattering) of the inverters.
Multi-Ressonant Controller (MRC)	▸Provides the suppression of oscillations in the radial position caused by disturbances of a periodic nature.	▸Needs accurate identification of frequencies responsible for vibrations. ▸System dimension becomes large for a large amount of disturbance frequencies.
Fuzzy Controllers	▸It allows the representation of models with a high degree of uncertainty through rules of inputs and outputs.	▸They depend on the operator's knowledge for tuning the controllers.
H∞ Controller	▸It provides good dynamic response and robustness to parametric variations and rejection of disturbances.	▸Controller design is complex for multiple input and multiple output systems. ▸Tuning parameters (weights) and choosing controller functions tend to be difficult, especially in a high-order system. ▸The high computational effort for highorder controllers.
μ-Synthesis	▸Provides a reduced settling time. ▸It is suitable for plants with a high degree of uncertainty. ▸Allows the processing of multiple parametric uncertainties and their interactions. ▸It is robust to parametric variations and disturbances.	▸The large number of method iterations can result in long calculation times, which can degrade the overall performance of the system.
Space Vector Modulation (SVM)	▸Optimizes control of inverter switch states to make the output nearly sinusoidal. ▸Reduces harmonic distortions caused by switching. ▸Reduces heat losses and torque ripple. ▸Allows digital implementation of switch control, including for multilevel inverters.	▸Its implementation requires a little more processing than conventional PWM modulation. However, it can become easier when used in multilevel inverters.
Direct Levitated Force Control	▸It is a controller based on a predictive model that provides direct control of radial forces. ▸Minimizes the controller's dependence on machine parameters present in the traditional vector model.	▸There is still a strong dependence on the accuracy of flow observers (torque and levitation) used. ▸The computational effort for real-time operation of observers together with controllers tends to be high.
Direct Torque Control	▸The structure of the control algorithm is simple. ▸Allows direct control of stator torque and flux. ▸Allows the generation of approximately sinusoidal stator fluxes and currents. ▸Provides high dynamic performance. ▸No need for coordinate transformations. ▸No need for modulation blocks or the addition of other controllers for flux and torque. ▸Provides fast torque responses.	▸They can generate instability during machine startups. ▸They need flux and torque estimators, which creates the need for exact knowledge of the parameters. ▸Its torque and flux signals are ripple.
Direct Suspension Force Control	▸It is a controller based on a predictive model that provides direct control of radial forces. ▸It minimizes the controller's dependence on the machine parameters present in the vector model.	▸There is still a strong dependence on the accuracy of flow observers (torque and levitation) used. ▸The computational effort for real-time operation of observers together with controllers tends to be high.

Figure 5: Main control techniques applied to the bearingless machines.

Radial Position Control of a Bearingless Machine with Active Disturbance Rejection Control

1st Werbet L. A. Silva
Dept. of Computation Engineering
Federal University of
Rio Grande do Norte
Natal, Brazil
werbethluizz@hotmail.com

2nd Andres O. Salazar
Dept. of Computation Engineering
Federal University of
Rio Grande do Norte
Natal, Brazil
andres@dca.ufrn.br

3rd Ronaldo José N. Cabral Neto
Dept. of Computation Engineering
Federal University of
Rio Grande do Norte
Natal, Brazil
ronaldojncneto@gmail.com

4th Elmer R. L. Villarreal
Department of Natural Sciences, Mathematics, and Statistics (DCME)
Federal Rural University of Semi-Arid (UFERSA)
Mossoró, Brazil
elmerllanos@ufersa.edu.br

***Abstract*—This work investigates the application of the Active Disturbance Rejection Control (ADRC) technique on the stabilization and control of the rotor radial position of a bearingless induction machine with split winding. A control model for the radial position problem is proposed and the ADRC is used aiming to improve the closed-loop system dynamic when a change load occurs on the output. The simulations showed that the controller is able to stabilize the plant and reject disturbances. These results will guide to a future experimental validation of the problem.**

***Index Terms*—magnetic levitation, induction motor, robust controller**

I. Introduction

Bearingless electric machines based on induction motors appeared to meet an industrial demand for less noisy motors, which could reach higher speeds and would not contaminate processes. With the development of this technology, a wide range of sectors could take benefit of it [1] [2] [3]. As an example, the aerospace industry, which adopted bearingless machines because they are able to significantly reduce the number of maintenance events in systems operating in space. In the biomedical area, pumping systems that replace the human heart were able to extend its operational period to an interval of more than ten years thanks to the elimination of mechanical contacts [4].

The systems with magnetically suspended rotors, as the bearingless machine with split winding proposed by [5], work without mechanical bearings which are usually the first component to fail in electrical machines [6]. These special machine type have an operation that is strongly dependent on well-designed control routines since the magnetic shaft suspension is a naturally unstable system. Also, these systems are multivariable, nonlinear and have strong coupling between variables, especially when load changes occurs on the rotor during the machine operation. Linear controllers may not achieve a stable and fast response for the proper suspension of the machine rotor. The emergence of microprocessors and power electronic devices provided conditions for applying advanced control theories, such as predictive controllers, by sliding modes, based on artificial neural networks, Fuzzy, and others [7].

Among the control techniques available, the application of controllers that promote the active detection and rejection of disturbances has been investigated as an viable alternative for a suitable control of bearingless machines. ADRC has been successfully implemented due to its simplicity of implementation and performance [8] [9]. With this technique, the effects of internal and external disturbances, parameter variations, and other uncertainties are estimated through a state observer and compensated in real-time by the control routine [10]. Its architecture makes the ADRC a control technique whose performance is independent of the mathematical model's knowledge of the process.

This work studies the application of an ADRC controller in the position control of a bearingless machine with split winding. In addition to this introductory section, in the Section 2 the modeling of the radial position system is performed. Section 3 explains the ADRC and shows its mathematical implementation. Section 4 presents the results of the simulated runs, followed by section 5, in which the final considerations are made.

II. System modeling

Currently, several topologies of bearingless machines are available in the literature. The topology used in this work was studied by [11], which developed the dynamic model

This study was financed in part by the Coordenação de Aperfeiçoamento de Pessoal de Nível Superior – Brasil (CAPES) – Finance Code 001 and in part by the process 23091-014712/2019-87-UFERSA.

978-1-7281-9377-9/20/$31.00 ©2020 IEEE

Authorized licensed use limited to: Universidade Federal Rural do Semiarido. Downloaded on October 22,2020 at 19:36:41 UTC from IEEE Xplore. Restrictions apply.

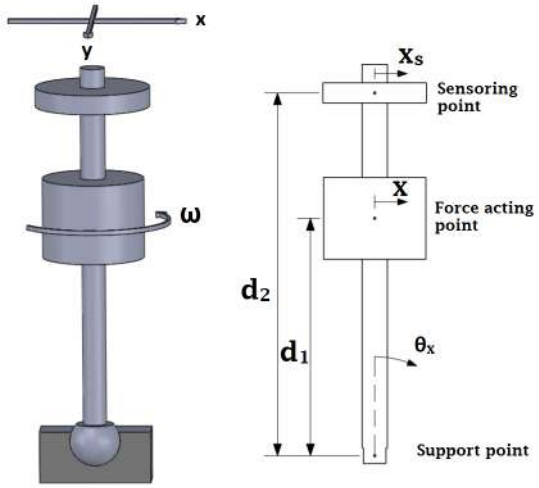

Fig. 1. Rotor free body diagram.

of the rotor radial position from the characteristics of a real experimental prototype. This prototype works vertically and is supported on the lower end of the shaft by a pivoted bearing that prevents radial and axial movements, but allows angular movements. This type of system has two degrees of freedom for position control [12] and the rotor displacement occurs in the directions of x and y axes.

Starting from the application of the second motion law to Figure 1, [11] developed a $G(s)$ function that relates the control signal $U(s)$ to the output position $Y(s)$ of the rotor. The dynamics of the x-axis is equal to the y-axis and both are described by:

$$G(s) = \frac{3.68 \times 10^6}{(s + 91.51)(s - 91.51)} \quad (1)$$

Equation (1) show that the radial position model has a unstable pole, thus a controller is fundamental to the system operation.

III. ADRC CONTROLLER

The first version of the ADRC controller was presented in chinese by its creator, Jingqing Han, in work entitled "Auto disturbances rejection controller and its applications" in 1998 [13]. In order to promote advances in the theory and practice of control engineering, Jingqing Han researched the characteristics of nonlinear into closed-loop control problems and proved the efficiency of the controllers designed from them. According to [14], when compared to linear functions, nonlinear ones are potentially more effective in tolerating uncertainties and disturbances; and in improving systems dynamics.

In a more recent publication, Han described the ADRC as a digital closed-loop system control technique, developed from a digital platform rooted in computer simulations, which inherits from the proportional-integral-derivative (PID) controller its characteristic of greatest success: a control law mainly based on error, and not just on the plant model; in addition, it

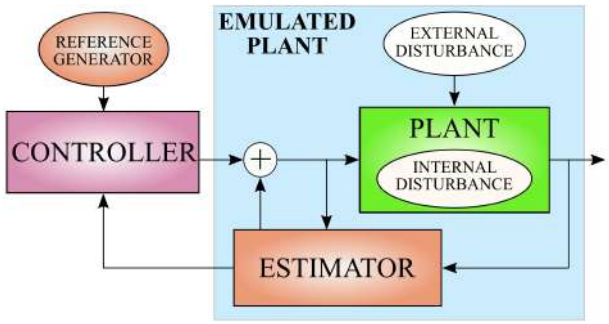

Fig. 2. ADRC - General idea.

uses state observers, a technique from theory of modern controllers; and also makes use of nonlinear control tools for the realization of its structure [15].

The ADRC controller uses a state observer to estimate any unknown information (dynamics, disturbances, nonlinearities, parameter variations, time-delays etc) about the real system to be controlled. Then, the algorithm subtracts the estimated information from the system dynamics in order to emulate a model with simpler general behavior. On the ADRC structure there is the observer, a references generator and a controller block (Figure 2). To achieve its goal, the ADRC groups all the uncertainties involved in the process into a single parameter named "generalized disturbance". This parameter is then defined as a state variable of the system to be estimated through the observer. Once estimated, this parameter is subtracted from the system's control loop, which is seen by the controller as a simpler system, formed only by cascated integrators (Han's canonical form), whose control has already been extensively studied in the literature. Therefore, for the design of the control block, the Han's canonical form is taken in account and the knowledge about the real system parameters is not important.

A. Mathematical Description of ADRC

The ADRC structure is based mainly on nonlinear functions and its original complete version is composed by three blocks: an extended state observer (ESO), a tracking differentiator (TD), and a nonlinear control law (Fig. 3).

1) tracking differentiator: The TD operates on the reference signal in order to filter it and smooth its transition. For a

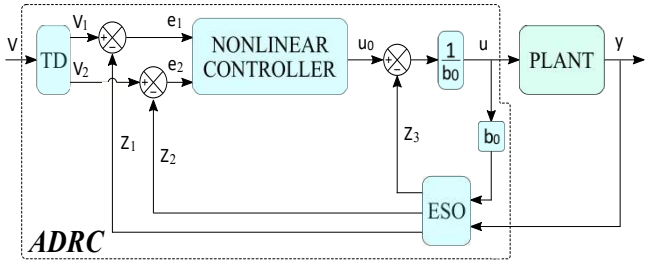

Fig. 3. ADRC - Control strucuture.

Authorized licensed use limited to: Universidade Federal Rural do Semiarido. Downloaded on October 22,2020 at 19:36:41 UTC from IEEE Xplore. Restrictions apply.

second-order system given by:

$$\begin{cases} \dot{v}_1 = v_2 \\ \dot{v}_2 = u \end{cases} \tag{2}$$

the optimal solution for this system is given by:

$$u = -rsign(v_1 - v + \frac{v_2|v_2|}{2r}) \tag{3}$$

Therefore, the system can be rewritten as:

$$\begin{cases} \dot{v}_1 = v_2 \\ \dot{v}_2 = -rsign(v_1 - v(t) + \frac{v_2|v_2|}{2r}) \end{cases} \tag{4}$$

thus, $v_1(t)$ follows the input signal $v(t)$ with a speed adjusted by r. The variable $v_2 = \dot{v}_1$ is an approximation of the derivative of $v(t)$.

2) ESO: it consists of an estimator with nonlinear gains that detects information about the states of the plant in real-time from the observation of the inputs and the output. It is the most important block of the controller, as it is responsible for detecting disturbances involved in the process. The observer design, for this work, is given from the second order system by:

$$\begin{cases} \dot{x}_1 = x_2 \\ \dot{x}_2 = f(x_1(t), x_2(t), w(t), t) + bu \\ y = x_1 \end{cases} \tag{5}$$

where y is the measured output that must be controlled;; $f(x_1(t), x_2(t), w(t), t) = F(t)$ is a multivariate function of states $(x_1(t), x_2(t))$, external disturbances $(w(t))$, and time (t); i.e., the total disturbance. Assuming that $F(t)$ is a system state variable, $F(t) = x_3$ and $\dot{F}(t) = G(t)$ is its derivative. Therefore, the extended representation of the system given by (5) is:

$$\begin{cases} \dot{x}_1 = x_2 \\ \dot{x}_2 = x_3 + bu \\ \dot{x}_3 = G(t) \\ y = x_1 \end{cases} \tag{6}$$

From this representation, the observer's structure is proposed [16]:

$$\begin{cases} \dot{z}_1 = z_2 - \beta_{01} fal(e, \alpha_1, d_1), \\ \dot{z}_2 = z_3 - \beta_{02} fal(e, \alpha_2, d_2) + b_0 u \\ \dot{z}_3 = -\beta_{03} fal(e, \alpha_3, d_3), \end{cases} \tag{7}$$

the fal function is defined by:

$$fal(e) = \begin{cases} |e|^{\alpha} sign(e), & |e| > d \\ \frac{e}{d^{1-\alpha}}, & |e| \leq d \end{cases} \tag{8}$$

The variables α_1, α_2, α_3, d_1, d_2 e d_3 are the parameters of the nonlinear functions. The observer output give the values of the states z_1, z_2 e z_3, i.e., it estimates the numerical values of the states z_1, z_2 and of the function $F(t)$. From this, the effect of $F(t)$ is removed from the system dynamic through the operation:

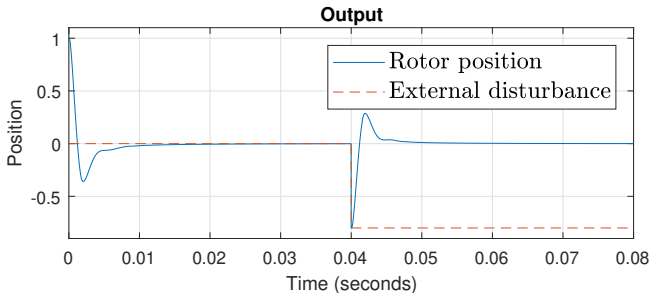

Fig. 4. System output.

$$u = \frac{u_0 - F(t)}{b_0} \tag{9}$$

So, the emulated dynamics of the system becomes:

$$\begin{cases} \dot{x}_1 = x_2 \\ \dot{x}_2 = u_0 \\ y = x_1 \end{cases} \tag{10}$$

which corresponds to a simple double integrator system, whose control is widely known in the literature.

3) Control law: the work [15] indicates the following nonlinear strategy:

$$u_0 = \beta_1 fal(v_1 - z_1, \alpha_1, \delta) + \beta_2 fal(v_2 - z_2, \alpha_2, \delta) \tag{11}$$

However, it emphasizes that different strategies can be used in the the control law block.

IV. Results

We simulated the control of the plant given by (1) using ADRC. For the results described in this section, the following considerations must be made:

- Given that the dynamic response is the same for x and y axes, the results for only one axis is showed.
- The control goal is to maintain the radial position of the machine's rotor in $(x = 0, y = 0)$ position, so the reference signal v is kept in 0 and the TD block of the Figure 3 is not necessary.
- ESO was implemented according to (7) and the control law is given by (9).
- The controller tuning was carried out by trial and error.
- The system was simulated with initial conditions: $x_1(0) = 1$ and $x_2(0) = 0$. This situation indicates that the machine rotor was stopped in an unwanted position before the controller start acting.
- A step-shaped disturbance was added at the output of the system at the instant $t = 0.04$ seconds. In a practical situation, disturbances of this type are caused by loads added to the axis of the machine in operation.

The Fig. 4 shows the output of the plant controlled with ADRC. The controller corrected the plant output to the desired reference value and was able to recover this condition even under a load change condition.

Authorized licensed use limited to: Universidade Federal Rural do Semiarido. Downloaded on October 22,2020 at 19:36:41 UTC from IEEE Xplore. Restrictions apply.

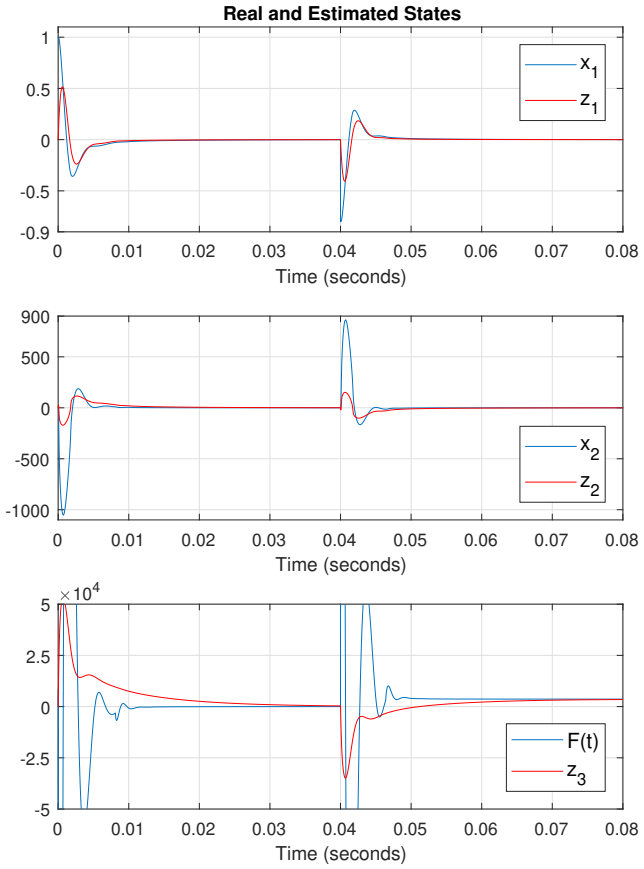

Fig. 5. Performance of the extended state observer.

The efficiency of the ADRC in controlling the output of the system depends directly on the ability of ESO to estimate the states of the plant, that is: $x_1 \rightarrow z_1$, $x_2 \rightarrow z_2$ e $F(t) \rightarrow z_3$. Fig. 5 compares the dynamic response of the real states with their respective values estimated by the observer. From the Figure, it is clear the ability of the ESO in provide proper estimates of the plant states.

The simulations results are part of a project that aim to carry on experiments with ADRC controller and a bearingless machine prototype. A experimental setup (Fig. 6) at Federal University of Rio Grande do Norte will be used in future experiments.

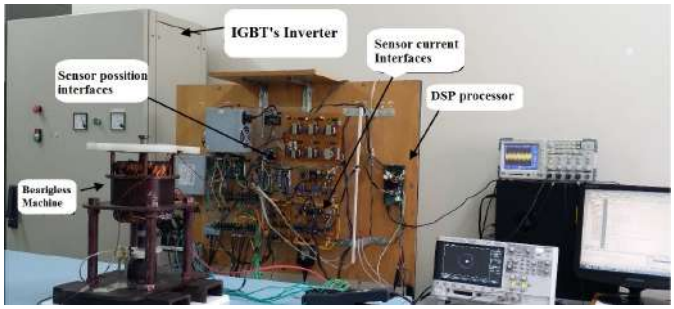

Fig. 6. Experimental setup.

V. Conclusions

This work studied the application of an ADRC controller to a simulated radial position control system of an induction machine without bearings with split winding. The results proved the efficiency of the controller in keeping the rotor in the desired position. Future work aims to apply this controller to an experimental system whose dynamics are subject to a higher number of disturbances and uncertainties.

References

[1] D. Gerada, A. Mebarki, N. L. Brown, C. Gerada, A. Cavagnino, and A. Boglietti, "High-speed electrical machines: Technologies, trends, and developments," *IEEE Transactions on Industrial Electronics*, vol. 61, no. 6, pp. 2946–2959, 2013.

[2] T. Wellerdieck, P. Peralta, T. Nussbaumer, and J. W. Kolar, "Contributions to an ultra-high temperature (250 c/500 f) bearingless pump," in *2015 18th International Conference on Electrical Machines and Systems (ICEMS)*. IEEE, 2015, pp. 1158–1164.

[3] M. N. Recheis, B. Schweighofer, P. Fulmek, and H. Wegleiter, "Selection of magnetic materials for bearingless high-speed mobile flywheel energy storage systems," *IEEE Transactions on Magnetics*, vol. 50, no. 4, pp. 1–4, 2014.

[4] N. Kurita, T. Ishikawa, N. Saito, T. Masuzawa, and D. L. Timms, "A double-sided stator type axial bearingless motor development for total artificial heart," *IEEE Transactions on Industry Applications*, vol. 55, no. 2, pp. 1516–1523, 2018.

[5] A. O. Salazar and R. Stephan, "A bearingless method for induction machines," *IEEE Transactions on Magnetics*, vol. 29, no. 6, pp. 2965–2967, 1993.

[6] K. Li, G. Cheng, X. Sun, D. Zhao, and Z. Yang, "Direct torque and suspension force control for bearingless induction motors based on active disturbance rejection control scheme," *IEEE Access*, vol. 7, pp. 86 989–87 001, 2019.

[7] Z. Yang, J. Ji, X. Sun, H. Zhu, and Q. Zhao, "Active disturbance rejection control for bearingless induction motor based on hyperbolic tangent tracking differentiator," *IEEE Journal of Emerging and Selected Topics in Power Electronics*, 2019.

[8] S. Chen, W. Xue, and Y. Huang, "On active disturbance rejection control for nonlinear systems with multiple uncertainties and nonlinear measurement," *International Journal of Robust and Nonlinear Control*, vol. 30, no. 8, pp. 3411–3435, 2020.

[9] V. Nguyen, C. Lin, S. Su, W. Sun, and M. J. Er, "Global finite time active disturbance rejection control for parallel manipulators with unknown bounded uncertainties," *IEEE Transactions on Systems, Man, and Cybernetics: Systems*, pp. 1–12, 2020.

[10] M. Ran, Q. Wang, C. Dong, and L. Xie, "Active disturbance rejection control for uncertain time-delay nonlinear systems," *Automatica*, vol. 112, p. 108692, 2020.

[11] F. E. C. Souza, "Otimização da estrutura de acionamento para o controle de posição radial de um motor de indução trifásico sem mancais com enrolamento dividido," 2018.

[12] A. Chiba, T. Fukao, O. Ichikawa, M. Oshima, M. Takemoto, and D. G. Dorrell, *Magnetic bearings and bearingless drives*. Elsevier, 2005.

[13] D. Huang, D. Min, Y. Jian, and Y. Li, "Current-cycle iterative learning control for high-precision position tracking of piezoelectric actuator system via active disturbance rejection control for hysteresis compensation," *IEEE Transactions on Industrial Electronics*, 2019.

[14] J. Li, Y. Xia, X. Qi, and Z. Gao, "On the necessity, scheme, and basis of the linear–nonlinear switching in active disturbance rejection control," *IEEE Transactions on Industrial Electronics*, vol. 64, no. 2, pp. 1425–1435, 2016.

[15] J. Han, "From pid to active disturbance rejection control," *IEEE transactions on Industrial Electronics*, vol. 56, no. 3, pp. 900–906, 2009.

[16] Z. Gao, "Scaling and bandwidth-parameterization based controller tuning," in *Proceedings of the American control conference*, vol. 6, 2006, pp. 4989–4996.

Authorized licensed use limited to: Universidade Federal Rural do Semiarido. Downloaded on October 22,2020 at 19:36:41 UTC from IEEE Xplore. Restrictions apply.

Proposed of active suspension with fuzzy control

Maxwell C. Jácome, B.S.,[1] and
Elmer R. L. Villarreal, Dr.[2]

[1]Bachelor of Science and Technology, Engineering Center, UFERSA, Av. Francisco Mota, 572, Bairro Costa e Silva, CEP 59625900, Mossoró, RN.; e-mail: maxwellc.jacome@htmail.com

[2]Postgraduate Program in Communications and Automation Systems-UFERSA, Center of Exact and Natural Sciences, CCEN-UFERSA, Av. Francisco Mota, 572, Bairro Costa e Silva, CEP 59625900, Mossoró-RN.; email: elmerllanos@ufersa.edu.br

ABSTRACT

Automotive suspensions are part of the system that controls the vibration generated in the locomotion of the vehicle, which are generally composed by simple components such as springs and dampers, whose parameters are fixed, which limit its activities to prioritize comfort or safety. Other more efficient methods such as active and semi-active suspensions demand the application of an external actuator, what requires the development of a control strategy for its operation. In this work, we developed a mathematical method to determine the transfer function from the differential equations that describe a quarter car model. The transfer function will act on a Simulink® blocks circuit. From the structural formulation of an active suspension, which considers a simplified template corresponding to a quarter car, the use of a controller based on fuzzy language is proposed. Twenty-five fuzzy rules were established to determine the output variable value that corresponds to the force applied by an actuator based on absolute and relative speed, between a sprung mass and a mass of the tire-wheel assembly for the relative one. The results show a stabilization of the built system, evaluating the strength, displacement and acceleration responses. The stabilization time reduced by 50% and the overshot reduced by 30%, showing the fuzzy control pertinency.

1. INTRODUCTION

The operation of mechanisms in general present unwanted vibrations. In the case of automotive vehicles, the system aimed at controlling these vibrations arising from the vehicle dynamics is the suspension system. This system guarantees the comfort and stability necessary to drive the car.

As to the way of acting, the literature presents three modalities regarding its autonomy: passive, semi-active and active system. Despite the wide usability of the passive system, due to its simplicity of operation caused by the fixed parameters of rigidity and damping, the development of new control techniques and more efficient actuators allows the proposal of active and semi-active approaches, which improve the time and response quality of the system addressed. Thus, as implied, increased efficiency is associated with an efficient control theory.

The modeling of the dynamic system will be described in terms of its differential equations and, from these, we can represent the systems in terms of their transfer functions, in a relation between input and output. The transfer functions are present in several control modalities, as well as being applied in signal processing, communication theory, and circuit analysis.

After describing the mathematical foundation behind the transfer functions, mainly the Laplace transform, the theory will be applied in a mechanical system representing the active suspension of a wheel of a car, which makes use of an external actuator capable of applying a force to control vibrations.

In order for the actuator to apply the appropriate force to each perturbation submitted to the suspension system, a safe control strategy is required, which correlates the data obtained by sensing from the variations of the lane to generate an exit action, culminating in the force applied by the actuator. The type of controller used for this purpose is based on fuzzy logic, which is inserted in a control circuit together with the transfer function.

In this work, the transfer function, which will be inserted in a control system in a Simulink® environment, will be calculated from the differential equations describing a quarter car suspension model, with the aim of stabilizing the system.

It is proposed in this work the application of fuzzy language, similar to human decision making, allowing half truths and half lies. The fuzzy language presents itself as an alternative to several industry sectors, especially when there are problems of difficult mathematical formulation, and also when the accuracy of the answer is expensive to the control system. From the absolute velocity and relative velocity data, the controller will be able to result in a response to the force.

2. VEHICULAR SUSPENSION

According to Rao (2008), a vibratory system (where bodies have oscillatory movements and associated forces) includes a medium for storing potential energy (spring and/or elasticity), a medium for storing kinetic energy (mass or inertia), and a medium of gradual energy loss (damper), as illustrated in Figure 1.

In automotive vehicles, the suspension establishes the connection between the vehicle body and the wheels with the tires and, in essence, enables vertical wheel movement to compensate runway irregularities.

It can be said that the suspension system is also responsible for isolating the vehicle body from internal disturbances (disturbances created by curves, acceleration or deceleration), giving comfort to drive. In addition, it is useful for lifting the vehicle body weight, reacting to load variations, and maintaining a firm contact between the road and the tires in order to perform well in handling, which means safety in the direction (Xue Et al., 2011).

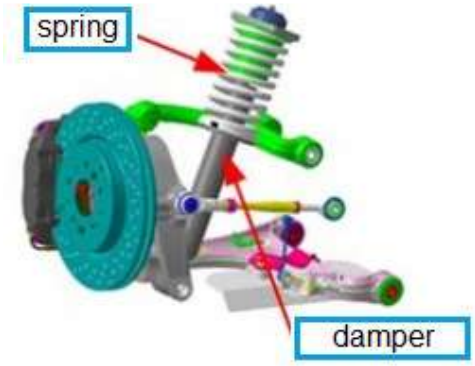

Figure 1. Illustration of a vehicular suspension. Adapted from Xue et al. (2011).

In the interest of improving the overall performance of automotive vehicles in recent years, suspensions that incorporate active components have been developed (Gillespie, 1992).

2.1 Passive suspension

It consists of conventional components with spring and damper properties that are invariant over time. It is the most common system due to its long service life, simple and firm structure, small volume, low weight, low cost and high reliability. In contrast, it hardly meets good levels of comfort and performance mutually (Xue et al., 2011).

2.2 Semi-active suspension

The semi-active term refers to systems that do not require additional external energy, besides that necessary to trigger devices such as valves, coils, actuators, among others (Montini, 2006).

The presence of a control is able to change the damping coefficient, altering, this way, the reaction force of the damper. Such force is supplied to this system for the purpose of dissipating the energy of the vibrations. It has the advantage of improving the damping characteristics by applying a simple control, and low cost.

2.3 Active suspension

This type of suspension has an actuator that, through the application of a force, can both dissipate energy and store, as well as apply external energy to stabilize the vehicle using data from sensors connected to the vehicle (Xue et al., 2011).

Despite being the most efficient in performance, it has the disadvantage of extra energy demand (reducing engine or battery power), as well as the need for an efficient control system that guarantees good suspension functionality.

2.4 Lógica fuzzy

The fuzzy language is able to model and manipulate mathematically vague and imprecise information, similar to human decision making.

Given a subset A of a universe set U, a set is considered fuzzy subset of U if it is described as a set of ordered pairs as follows (Montini, 2006):

$$A = \{(x, \mu_A(x));\ x \in U \text{ e } \mu_A(x) \in [0,1]\} \quad (1)$$

Considering a membership interval of [0,1] where 0 indicates that an element does not belong to the set, 1 points to a complete membership of the set, and values between 0 and 1 represent intermediate degrees of pertinence. Thus, in fuzzy logic, an element belongs to a set with a certain degree of pertinence, so that a given sentence may be partially true and partially false (Marro, 2016).

In order to define the response of the fuzzy control, rules based on the "if and then" model are used. After this step, fuzzy inference is performed, which formulates a mapping of a given input to a certain output, by which control decisions are made.

For control action to be performed, basically three steps are required. In fuzzification, the input variables are organized into different membership functions. In defuzzification, the value of the linguistic variable of the inference process of the fuzzy rules is converted into a discrete signal, which also represents a degree of relevance of the output variable (Tusset, 2008).

3. TRANSFER FUNCTION

Although many physical relationships are usually represented by linear equations, in most cases real relationships are not exactly so, because they only behave in this way in limited ranges of operation. Non-linearities of the quadratic law type may occur in some components, such as shock absorbers, used in physical systems, which have linearity in low speed operations, but can become nonlinear at high speeds, with a damping force proportional to the square of the operation speed (Ogata, 2010).

In case the system operates around a break-even point, when the signals involved are small, it is possible to approach the non-linear system by a linear system in a limited operating range.

The transfer function of a system represented by time-invariant linear differential equations is defined as the ratio between the Laplace transform of the output signal (response

function) and the Laplace transform of the input signal (excitation function), starting from the premise that the initial value problem presents all zero initial conditions (Ogata, 2010).

3.1 Laplace transform

The Laplace Transform is a mathematical resource to determine the particular solution of a differential equation.

In the context of control theories, this tool can be used to study the characteristics of the complete response of feedback systems, as well as the transient response (Franklin, Powell and Emami-Naeini, 2013).

Be the function f defined in [0,+∞[. The function F of complex variable "s" given by

$$F(s) = \int_0^{+\infty} e^{-st} f(t)dt \tag{1}$$

a Laplace transform of f is determined. The domain of F(s) is the set of all s values for which the improper integral is convergent.

3.2 Theorem 1

The following theorem shows how the Laplace transform destroys derivatives. Considering that the function f, as well as its derivative are continuous in the domain [0,+∞[.

$$\int_0^{+\infty} e^{-st} f'(t)dt = s\int_0^{+\infty} e^{-st} f(t)dt - f(0)$$

$$\int_0^{+\infty} e^{-st} f''(t)dt = s^2\int_0^{+\infty} e^{-st} f(t)dt - sf(0) - f'(0)$$

As a consequence:

$$\int_0^{+\infty} e^{-st} f'(t)dt = sF(s) - f(0)$$

$$\int_0^{+\infty} e^{-st} f''(t)dt = s^2F(s) - sf(0) - f'(0) \tag{2}$$

In an expression with the presence of a function, its first and second derivative, applying this theorem, it is possible to highlight the function in the domain of the F(s) complexes, which will be useful to obtain the Laplace transform of the problem.

3.3 Theorem 2

The Lerch's theorem ensure that if the Laplace transform of two functions (defined in [0, + ∞ [, continuous and exponential orders) are equal, then these two functions are equal. If

$$\int_0^{+\infty} e^{-st} f_1(t)dt = \int_0^{+\infty} e^{-st} f_2(t)dt$$

then

$$f_1(t) = f_2(t) \text{ in } [0,+\infty[\qquad (3)$$

This theorem ensures the applicability of the Laplace transform in the two members of an equation.

4. MODELING AND SIMULATION

The quarter car model simplifies the analysis of the suspension of an automobile, considering that the mass of the vehicle distributes evenly on the four wheels, and adopting the independent action of each damper. It has two degrees of freedom, and considers that the vehicle tire does not lose touch with the ground.

The model consists of two masses, the suspension (one-fourth the mass of the chassis plus passengers) and the non-suspended mass (wheel and suspension elements).

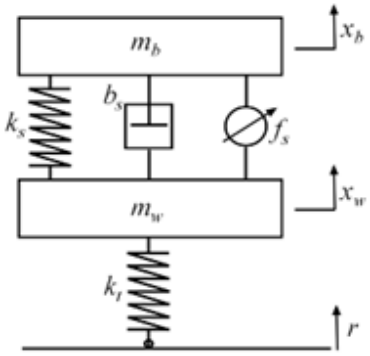

Figure 2. Quarter car model.

The Figure 2 exemplifies the active suspension, with the application of a variable force (f_s), and a static shock absorber (b_s). In addition to spring k_s, the elastic deflection presented by the tire equals the behavior of a spring, represented in the model by k_l.

The displacements r, x_w, and x_b represent the movements of the tire, wheel and body, respectively. Spring elements are present between the masses and in the ground contact, as well as energy storage elements.

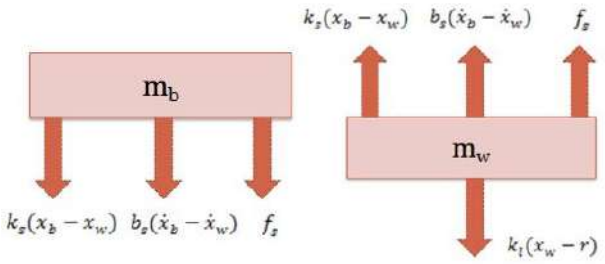

Figure 3. Force diagrams in the blocks of mass.

After the sum of forces in both blocks of mass in Figure 3, it is possible to get the second order differential equations that describes the movement.

$$m_b\ddot{x}_b + b_s(\dot{x}_b - \dot{x}_w) + k_s(x_b - x_w) + f_s = 0 \quad (4)$$

$$m_w\ddot{x}_w + b_s(\dot{x}_b - \dot{x}_w) + k_s(x_w - x_b) - k_l(r - x_w) - f_s = 0 \quad (5)$$

The physical systems have their dynamics modeled mathematically in terms of their differential equations and, from these, we can represent the systems in terms of their transfer functions, in a relation between input and output. Assuming the denominator as Δ:

$$\Delta = s^4 + s^3\left(\frac{b_s}{m_w} + \frac{b_s}{m_b}\right) + s^2\left(\frac{k_s}{m_w} + \frac{k_l}{m_w} + \frac{k_s}{m_b}\right) + s\frac{b_s k_l}{m_b m_w} + \frac{k_s k_l}{m_b m_w} \quad (6)$$

$$X_b(s) = \frac{R(s)\left(s\frac{b_s k_l}{m_b m_w} + \frac{k_s k_l}{m_b m_w}\right) - F(s)\left(\frac{s^2}{m_b} - \frac{k_l}{m_b m_w}\right)}{\Delta} \quad (7)$$

The expression can be compiled in the form of a block diagram as in Figure 4, which is actually performed in Simulink® simulation.

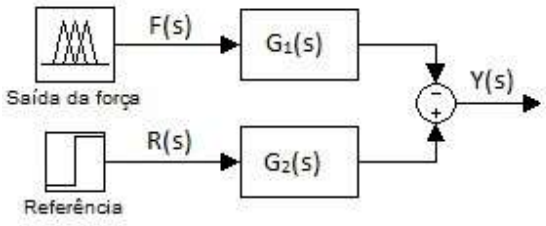

Figure 4. Transfer function in block diagram.

In which,

$$G_1(s) = \frac{\left(\frac{s^2}{m_b} - \frac{k_w}{m_b m_w}\right)}{\Delta}, \quad (8)$$

$$G_2(s) = \frac{\left(s\frac{bk_w}{m_b m_w} + \frac{k_s k_w}{m_b m_w} \right)}{\Delta} \qquad (9)$$

and Y(s) is the response to the displacement of the suspended mass.

From an initial step perturbation, concerning the signal R (s), the displacement response was initially obtained for a passive suspension, i.e., without the application of force.

Note that for this transfer function, two input signals (referring to the force and displacement of the reference), and one output (related to the displacement of the suspended mass) are required.

The values of the parameters were based on the problem retranslated in the work of Montini (2006), as shown in Table 1.

Variable	Module	Units	Description
k_s	20000	N/m	Spring stiffness (suspension)
b_s	1000	Ns/m	Damping static
m_b	400	Kg	Suspense mass
m_w	50	Kg	Mass of tire-wheel assembly
k_l	250000	N/m	Stiffness constant (tire)
f_s	-	N	Variable force

Table 1: Parameter values.

Based on the rules referenced by Montini (2006), a set of 25 fuzzy rules were elaborated, whose input parameters were absolute velocity (Figure 5) and relative velocity (Figure 6), represented in the equation by $\dot{x}_b$ - $\dot{x}_w$, and the output parameter as the force of the actuator (Figure 7). All parameters were distributed in 5 degrees of pertinence: large negative; negative mean; zero; positive mean; and large positive (Table 2).

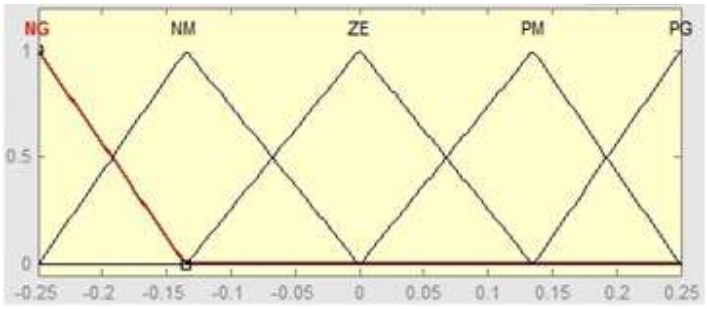

Figure 5: Pertinence functions of absolute velocity.

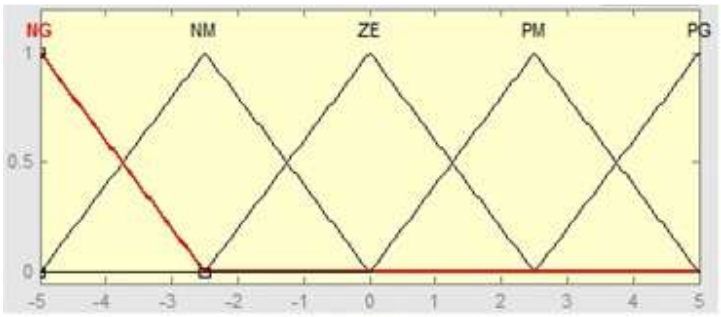

Figure 6: Pertinence functions of relative velocity.

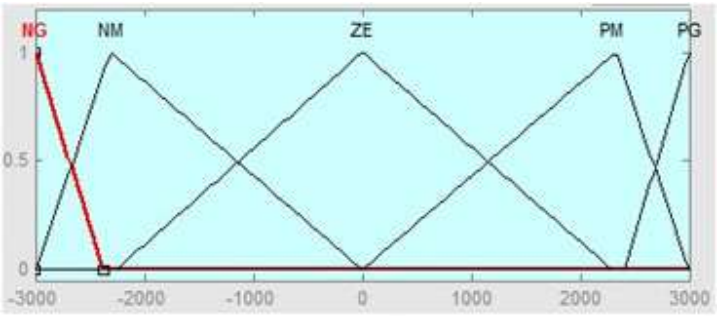

Figure 7: Pertinence functions of actuating force.

Actuating force		Absolute speed				
		NG	NM	ZE	PM	PG
Relative speed	NG	NG	NG	NM	NM	NM
	NM	NG	NM	NM	NM	NM
	ZE	NM	NM	ZE	PM	PM
	PM	PM	PM	PM	PM	PG
	PG	PM	PM	PM	PG	PG

Table 2: Fuzzy rules.

The efficiency of the result is evaluated based on the degree of acceleration of the upper mass, since it is the variable sensitive to human comfort. Data were also obtained from the force required by the actuator to stabilize the system after a step disturbance.

The system was assembled in the Simulink® (Figure 8), adding the elaborated fuzzy controller to the transfer function, obtained through equations 2 and 3, having two input signals (force and displacement of reference frame "r"), and an output signal (mass displacement).

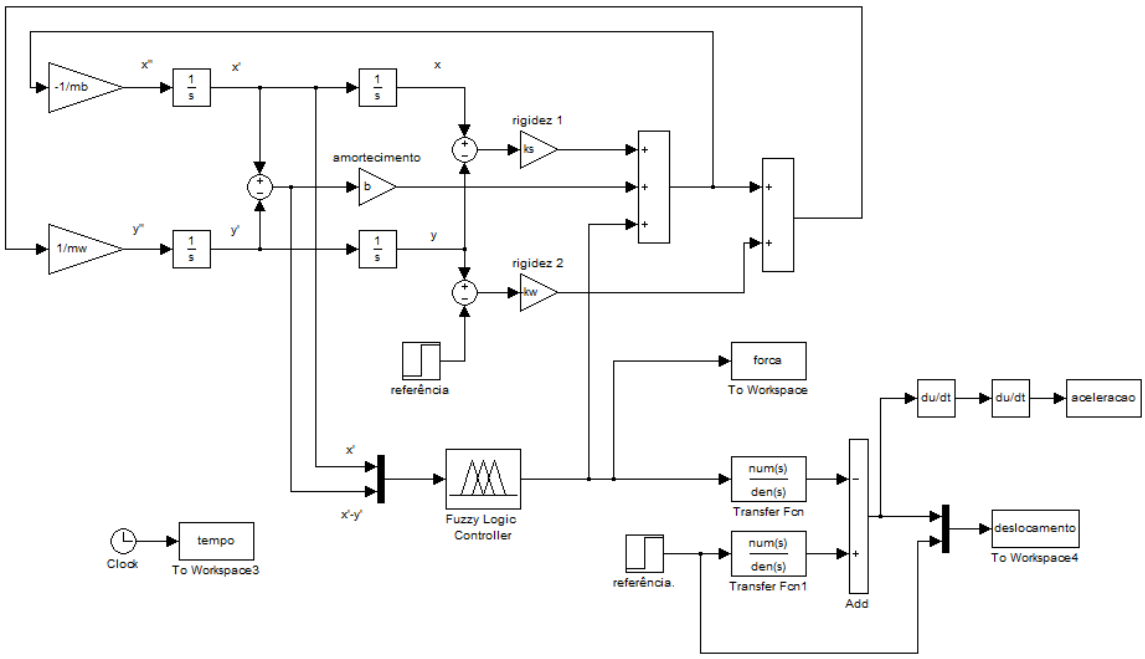

Figure 8: Bloke circuit in Simulink®.

From an initial step disturbance corresponding to a variation in the lane, referring to the signal R(s), the displacement response was initially obtained for a passive suspension, i.e., without the application of force.

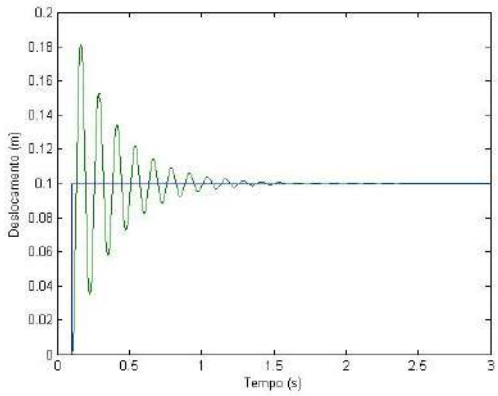

Graphic 1. Response of the displacement in y for a passive suspension.

Comparing the Graphic 1 with the following response in Graphic 2, now for an active suspension, it is noted that the established control was efficient to optimize the stabilization of the system.

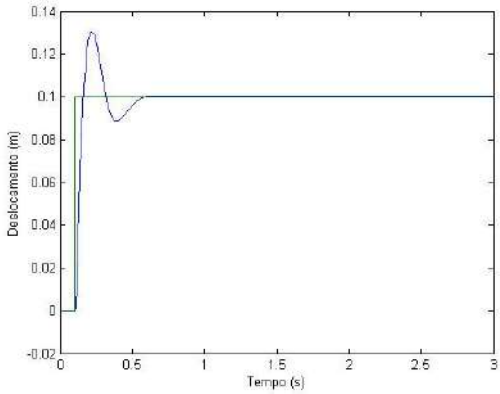

Graphic 2. Displacement of the suspended mass.

Stabilization was achieved in little more than 0.5 seconds, which presents a satisfactory result, mainly because the peak of the graph did not exceed 30% of the initial disturbance.

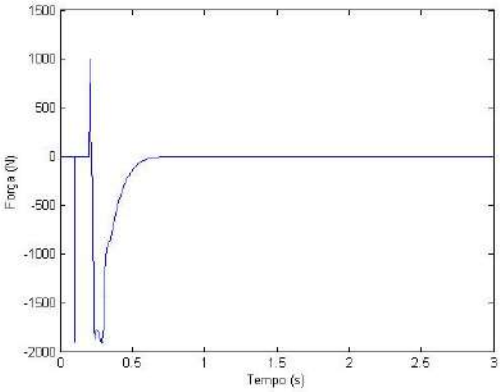

Graphic 3. Force required by the actuator.

The performance of the force in Graphic 3 indicated the force is that one applied by the actuator in the control of the vibratory system. The need arises to develop actuators able to provide the magnitudes of force in agile time.

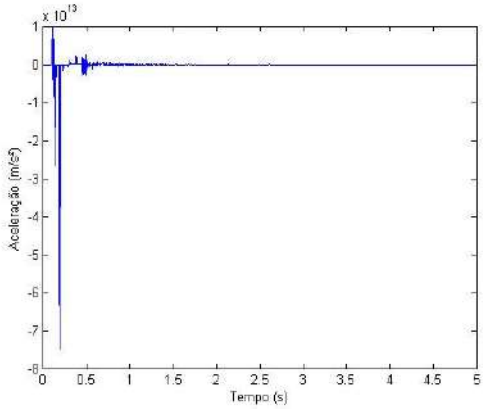

Graphic 4. Acceleration of the suspended mass.

Finally, it was tried to discover the value of the acceleration by which the suspended mass is submitted (Graphic 4), reflecting in the sensation of the passengers and the driver, since the human body is a good accelerometer. Large peaks were observed, corresponding to the intense application of force by the actuator. It is interesting that softer values are achieved, so that stability does not imply in a sudden acceleration. This result can be obtained by changing the fuzzy controller's membership functions.

5. CONCLUSION

With the simulation and achievement of quite strong results in the stabilization of the vibration system, the control based on the fuzzy logic proved to be a good alternative for the control of active suspensions, being more efficient than the conventional passive models. However, one should seek better parameters for acceleration, since it is felt by the human body, which can cause discomfort. This can be achieved by varying the parameters of the fuzzy controller, which is responsible for the signal output of the force. In addition, it is possible to manipulate values in the controller's elaboration to obtain more adequate results.

Parallel to the study of control theory, it is necessary to look for elements that provide an applicability of it, as in the development of intelligent buffers, capable of executing the actions of control instantaneously.

REFERENCES

Franklin, G. F., Powell, J. D., Emami-Naeini, A. (2013). "Sistemas de Controle para Engenharia". 6. ed. Porto Alegre: Bookman.

Gillespie, T. (1992). "Fundamentals of Vehicle Dynamics". Warrendale, Usa: Society Of Automotive Engineers.

Marro, A. A. et al. (2016). "Lógica Fuzzy: conceitos e aplicações." <http://aquilesburlamaqui.wdfiles.com/local--files/logica-aplicada-a-computacao/texto_fuzzy.pdf> (Dec. 5, 2016).

Ogata, Katsuhiko. (2010). "Engenharia de Controle Moderno." 5. ed. São Paulo: Pearson.

Rao, Singiresu. (2008). "Vibrações Mecânicas." 4. ed. São Paulo: Pearson.

Tusset, A. M. (2008). "Controle ótimo aplicado em modelo de suspensão veicular não-linear controlada através de amortecedor magneto-reológico." 174 f. Tese (Doutorado), Programa de Pós-graduação em Engenharia Mecânica, Universidade Federal do Rio Grande do Sul, Porto Alegre.

Xue, X. D. et al. (2011). "Study of art of automotive active suspensions." 4th International Conference On Power Electronics Systems And Applications, [s.l.], p.1-7, jun. 2011. Institute of Electrical & Electronics Engineers (IEEE). http://dx.doi.org/10.1109/pesa.2011.5982958.

2015 Workshop on Research, Education and Development of
Unmanned Aerial Systems (RED-UAS)
November 23-25, 2015. Cancun, Mexico

A Comparative Study of Altitude and Yaw Controllers for Rotorcraft UAV

Alexandre da S. Fernandes†, Alexandre S. Brandão† and Elmer R. Llanos Villarreal⋆

Abstract— **The paper presents a brief study of quadrotor vehicle, its principle of operation and its high-level dynamic model. The proposal of altitude and yaw controllers is also presented. PID, LQR (LQRI) and Lyapunov based control techniques are here compared according to Integral Absolute Error (IAE) and Control Signal Energy criteria. The performance is analyzed in terms of the response time and energy spent to accomplish the task. The optimum controller gains are defined by simulation, after establishing the maximum value of the criteria. In the sequence, some experiments are run to validate the controllers and to compared them in real scenarios of regulation and trajectory tracking tasks.**

I. Introduction

The study and development of Unmanned Aerial Vehicles (UAVs) have grown considerably in recent years, both in academic and scientific circles. Such growth is mainly generated by technological advances in sensors, control techniques and data processing, which make these vehicles more economically feasible [1], [2], [3]. Additionally, UAVs have a wide range of applications, covering various areas from civil applications to those intended for military use [3], [4], [5]. Among the numerous applications, mapping areas for cartography, inspection in hazardous areas, aerial photographs and movie videos can be mentioned.

In this paper a specific type of rotating wing vehicles is used: the quadrotor. This vehicle is in the class of Vertical Takeoff and Landing (VTOL) machines because it has the ability to take off and land vertically, perform hovering tasks hovered, changing its heading, move along and laterally while maintaining the same vertical cote. It also can change its flight direction completely or even stop suddenly. These skills enable the quadrotor to be an aircraft useful in tasks that require a high degree of mobility [2]. The study presented in [6] shows the behavior of each type of VTOL vehicle according to skills, cost and complexity of the structure. Table I shows the score of each vehicle for each feature.

The quadrotor has some strengths, such as mechanical simplicity and aerodynamic with excellent stability in flights at low and high speeds. On the other hand, they have certain deficiencies related to the high power cost (low flight range). Among all the features listed in the Table I, the quadrotor has the highest score. In addition, the quadrotor is perfect for indoor applications, since it does not need much space to takeoff, execute maneuvers and landing. In short, the advantages presented have motivated the use of this type of vehicle, for

TABLE I

Features of VTOL vehicles (1=Bad, 4=Very Good)[6]

Features	A	B	C	D	E	F	G	H
Power cost	2	2	2	2	1	4	3	3
Control cost	1	1	4	2	3	3	2	1
Payload/volume	2	2	4	3	3	1	2	1
Maneuverability	4	3	2	2	3	1	3	3
Mechanics simplicity	1	2	3	1	4	4	1	1
Aerodynamics complexity	1	1	1	1	4	3	1	1
Low speed flight	4	3	4	3	4	4	2	2
High speed flight	2	4	1	2	3	1	3	3
Miniaturization	2	3	4	2	3	1	2	4
Survivability	1	3	3	1	1	3	2	3
Stationary flight	4	4	4	4	4	3	1	2
Total	**24**	**28**	**32**	**23**	**33**	**28**	**22**	**24**

A=Single rotor, B=Axial rotor,
C=Coaxial rotors, D=Tandem rotors, E=Quadrotor,
F=Blimp, G=Bird-like, H=Insect-like

*This work was supported by two brazilian organizations: CNPq and FUNARBE.

†Núcleo de Especialização em Robótica, Department of Electrical Engineering, Federal University of Viçosa, 36570-000 Viçosa MG, Brazil
alexandrefernandes2112@hotmail.com
alexandre.brandao@ufv.br

⋆Department of Exact and Natural Sciences, Federal Rural University of Semi-Árido, 59625-620 Mossoró RN, Brazil
elmerllanos@ufersa.edu.br

controller and task validation. Thus, the present paper shows the study of a AR.Drone quadrotor by Parrot Inc. during an observation tasks (altitude and yaw manuever).

In recent years the number of users of UAVs has greatly increased, especially the quadrotor. Due to its applicability, it has been much explored in academia, especially in modeling and control studies.

White box modeling considers the physical and mathematical equations governing the system, while the black box modeling considers only the inputs and outputs of the system without needing the knowledge of the system in detail. Gray box modeling comes from the combination of these two modeling. In this paper the white box modeling is applied, once the equations have great importance for a dynamic evaluation of quadrotor. Newton-Euler and Euler-Lagrange equations are examples of techniques based on white box modeling, whose quadrotor model description can be found in [7], [8], [9], [10] and [11].

Once having the system model, it is possible to control a UAV in distinct tasks. There are several control techniques found in the literature. A PD controller is a widely used. In [12], it is applied to guide a quadrotor in the vertical (z-axis) movement. PID controllers are used in [13] and [11] for control of a quadrotor, analyzing performance in computer simulations. In [1] and [14] Fuzzy-Based LQR Controller are used to control the movements of a quadrotor. Moreover, a junction among two or more control methods can be used simultaneously, as shown in [15], where a hybrid fuzzy PID controller is used for autonomous navigation of a quadrotor.

Another technique also very explored is the LQR (Linear Quadratic Regulator) and LQRI (LQR with Integrative term) controllers. A Learning-Based Fuzzy LQR Controller, Linearized LQR and Classical LQR are used respectively in [9], [16] and [17] in altitude control of a quadrotor. The data presented in the first two works are obtained by simulation, while the third one presents experimental results.

In [18], the author compares the PID and LQR controllers for all possible movements of quadrotor in three-dimensional plane by computer simulation. Thus, in an attempt to develop a more consistent work, the focus of this study is to compare the altitude and yaw controls of AR.Drone Parrot quadrotor through the LQR (LQRI), PID and Lyapunov controllers in order to establish the advantages and disadvantages of each through computer simulation and practice validation.

In this work, the gains of the three controllers in this paper are tuned by an artificial intelligence strategy (genetic algorithm), in contrast with [19] where the author presents a comparison of the performance of PID controller using manual tuning and optimization gradient.

In this work, PID, LQR (LQRI) and Lyapunov based control techniques are here compared according to Integral Absolute Error (IAE) and Control Signal Energy criteria. The performance is analyzed in terms of the response time and energy spent to accomplish the task. The optimum controller gains are defined by simulation, after establishing the maximum value of the criteria. In the sequence, some experiments are run to validate the controllers and to compared them in real scenarios of regulation and trajectory tracking tasks. To accomplish it this work is split as following: Section II presents the quadrotor model, designed by a white box modeling. Section IV introduces the methods adopted to compare the controllers and also presents the comparison criteria. In the sequel, Section III introduces the controller design for guiding the altitude and yaw movement. Next, Section V presents the simulation and experimental results obtained for each controller according to regulation and trajectory tracking missions. Finally, some concluding remarks and suggestions for future works are presented in Section VI.

II. The Quadrotor Model

This section presents the quadrotor model adopted in this work. First, the posture of quadrotor shown in Figure 1 in 3-D space in relation to the reference system $\langle g \rangle$ defines the vector $\mathbf{q} = \begin{bmatrix} \xi & \eta \end{bmatrix}^T$, where $\xi = \begin{bmatrix} x & y & z \end{bmatrix}^T$ is the vector with the position parameters of quadrotor and $\eta = \begin{bmatrix} \phi & \theta & \psi \end{bmatrix}^T$ is the vector with the angle parameters, where ϕ, θ and ψ are roll, pitch and yaw angles, respectively.

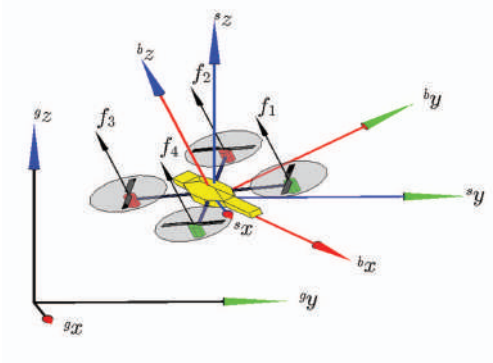

Fig. 1. Reference systems used in the modeling of quadrotor.

The dynamic modeling of the high level used in this paper can be seen in [7], [20], and the compact representation which can be described by

$$\begin{cases} m\ddot{x} = (\cos\phi\sin\theta\cos\psi + \sin\phi\sin\psi)\,U_1 \\ m\ddot{y} = (\cos\phi\sin\theta\sin\psi - \sin\phi\cos\psi)\,U_1 \\ m\ddot{z} = (\cos\phi\cos\theta)\,U_1 - mg \\ I_{xx}\ddot{\phi} = (I_{yy} - I_{zz})\,\dot{\theta}\dot{\psi} + U_2 \\ I_{yy}\ddot{\theta} = (I_{zz} - I_{xx})\,\dot{\phi}\dot{\psi} + U_3 \\ I_{zz}\ddot{\psi} = U_4 \end{cases} \tag{1}$$

where m is the mass of quadrotor, g is the gravity acceleration, I_{xx},I_{yy}, I_{zz} are the moments of inertia of the quadrotor and the parameters U_1, U_2, U_3 and U_4 are the control signals given by

$$\begin{cases} U_1 = f_1 + f_2 + f_3 + f_4 \\ U_2 = \dfrac{\tau_\phi + \tau_\theta}{2} = k_1\,(f_2 - f_4) \\ U_3 = \dfrac{\tau_\phi - \tau_\theta}{2} = k_1\,(f_1 - f_3) \\ U_4 = \tau_\psi = k_2\,(f_1 - f_2 + f_3 - f_4) \end{cases} \tag{2}$$

where f_i are the the propulsive force of the engines, τ_ϕ, τ_θ, τ_ψ are the torques of quadrotor due to control inputs, k_1 is the distance between the origin of quadrotor reference system $\langle b\rangle$ to the point of application of propulsive force, and k_2 is the relationship between the torque generated by the engine and its corresponding propulsion.

III. The Control Strategy

A. LQR (LQRI) Controller

Two versions LQR controller are here used. For altitude control, integrative factor error is added to compensate to gravitational force, resulting in a LQRI controller, as shown in [21].

Considering $\bar{u} = \ddot{z}$ in (1) and applying Laplace Transform, one has

$$U_1(s) = m\bar{U}(s) + \frac{mg}{s}. \tag{3}$$

Moreover, with the equation $\bar{u} = \ddot{z}$ and insertion of integrative term, the state space equation is given by

$$\dot{X} = AX + B\bar{U}$$
$$\begin{bmatrix} \dot{x_1} \\ \dot{x_2} \\ \dot{x_3} \end{bmatrix} = \begin{bmatrix} 0 & 1 & 0 \\ 0 & 0 & 0 \\ 1 & 0 & 0 \end{bmatrix} \begin{bmatrix} x_1 \\ x_2 \\ x_3 \end{bmatrix} + \begin{bmatrix} 0 \\ 1 \\ 0 \end{bmatrix} \bar{U}, \tag{4}$$

where $x_1 = z - z_d$, $x_2 = \dot{z}$, $x_3 = \int_0^t (z - z_d)dt$, $\bar{U} = KX = \begin{bmatrix} k_{1z} & k_{2z} & k_{3z} \end{bmatrix} \begin{bmatrix} x_1 \\ x_2 \\ x_3 \end{bmatrix}$ and $K = R^{-1}B^*P$, where P is the solution of Riccati Equation given by

$$A^TP + PA - PBR^{-1}B^TP + Q = 0 \tag{5}$$

In the case of altitude-yaw control, the classic version of LQR controller is used. Thus, Equation (8) in state space results is

$$\dot{Y} = AY + BU_4$$
$$\begin{bmatrix} \dot{y_1} \\ \dot{y_2} \end{bmatrix} = \begin{bmatrix} 0 & 1 \\ 0 & 0 \end{bmatrix} \begin{bmatrix} y_1 \\ y_2 \end{bmatrix} + \begin{bmatrix} 0 \\ \dfrac{1}{I_{zz}} \end{bmatrix} U_4, \tag{6}$$

where $y_1 = \psi - \psi_d$, $y_2 = \dot{\psi}$ and $U_4 = KY = \begin{bmatrix} k_{1\psi} & k_{2\psi} \end{bmatrix} \begin{bmatrix} y_1 \\ y_2 \end{bmatrix}$, where $K = R^{-1}B^*P$ and P is the solution of (5).

So it needs to determine the matrices Q and R to implement the LQR (LQRI) controller.

Figure 2 illustrates the system representation, containing the LQR (LQRI) controller and the altitude and yaw systems.

B. PID Controller

The frequency domain of PID controller is

$$U(s) = \left(K_p + \frac{K_i}{s} + K_d\,s\right) E(s). \tag{7}$$

Its representation for altitude and yaw control system can be seen in Figure 3. In our case, the same structure is used for both controllers.

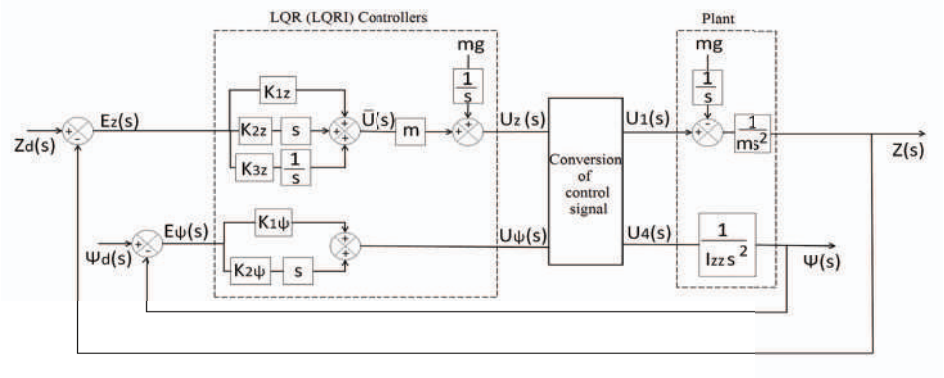

Fig. 2. Block diagram of the LQR (LQRI) controllers.

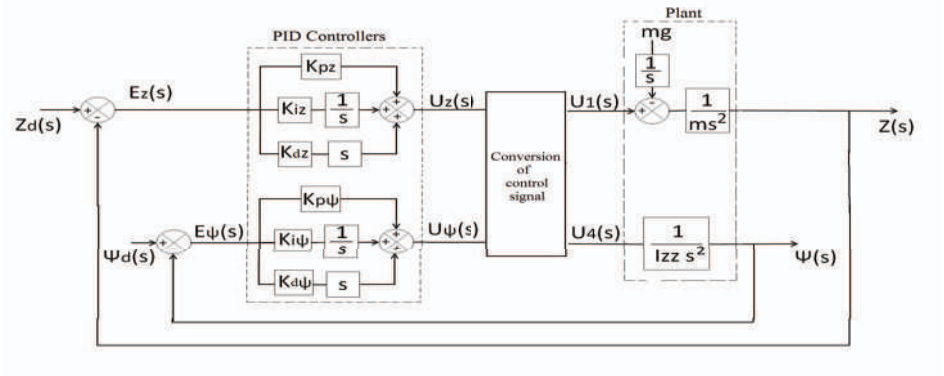

Fig. 3. Block diagram of the PID controllers.

C. Lyapunov-based Controller

The controller proposed based on Lyapunov theory apply the inverse dynamic concept on (8), at the time domain. Thus, the control signals are given by

$$U_1 = m[\ddot{z}_d + k_{dz1}\tanh(k_{dz2}\dot{\tilde{z}}) + k_{pz1}\tanh(k_{pz2}\tilde{z}) + g]$$
$$U_4 = I_{zz}[\ddot{\psi}_d + k_{d\psi 1}\tanh(k_{d\psi 2}\dot{\tilde{\psi}}) + k_{p\psi 1}\tanh(k_{p\psi 2}\tilde{\psi})],$$

where $\tilde{z} = z_d - z$ and $\tilde{\psi} = \psi_d - \psi$ (subscript d represents the desire value). Moreover k_{dz1}, k_{dz2}, k_{pz1}, k_{pz2}, $k_{d\psi 1}$, $k_{d\psi 2}$, $k_{p\psi 1}$ and $k_{p\psi 2} \in \mathbb{R}_+$ are the controller gains. Finally the nonlinear function $\tanh(\cdot)$ is here used to avoid physical saturation of the propellers by saturating mathematically the control signals sent to them. This control technique was based on the paper developed by [22].

IV. Materials and Methods

This study is split into two distinct steps. First, a computer simulation of the PID, LQR (LQRI)and Lyapunov controller performance for altitude and yaw movements of a quadrotor is done. Then, experimental tests are run using Ar.Drone Parrot quadrotor considering the controller gains tuned by simulation.

Both in simulation and in experiment tests, Aurora platform developed software in $Matlab^{®}$ is used to validate the controllers. AuRoRA platform structure is designed to operate in quasi-real time (it works in Windows Operational System). The actions require a permission for execution flag, whose permission is given only when the time interval related to the sampling period of each simulated UAV is reached. In the case of AR.Drone Parrot quadrotor, the sampling period is $T_s = \frac{1}{30}$s. Thus, the computational effort is minimized by preventing the execution of a series of instructions each iteration, and by avoiding the sending of multiple control signals to vehicles in one sampling period. Another item of extreme importance in the platform is the overlapping of the control signals for joystick commands sent by a human operator. Details about AuRoRA platform can be found in

[23].

The criteria adopted for tuning the controller gains are the Integral Absolute Error (IAE) and the Control Signal Energy (S), given respectively by

$$IAE = \int_0^T |e(t)|\, dt \quad \text{and} \quad S = \int_0^T u^2(t)\, dt$$

where $e(t)$ is the error between the output value and the desired value and $u(t)$ is the control signal.

Moreover, the maximum value of the control signal has been analyzed, since quadrotor engines have physical limitations (for instance, the voltage to be applied to them). Therefore, the rotating speed of the propellers saturates. In practice, the value of altitude control signal must be less than $25\,[N]$ and the yaw control signal should not exceed $0,3\,[N \cdot s]$. These maximum values are found experimentally by applying control signals and observing the perfect functioning of the AR.Drone Parrot quadrotor. Another item observed during the controller gain tuning is the quadrotor behavior in steady-state conditions.

Adopting the considerations aforementioned, the best set of controller gain is obtained for each situation by using an artificial intelligence strategy (genetic algorithm). The performance of the controllers in a Ar.Drone Parrot quadrotor is carried out by its connection to the computer through the wireless network link between it and AuRoRA platform.

In this work we are interested only in altitude and yaw control of quadrotor. Therefore, the behavior of other variables are disregarded, i.e., ϕ and θ are equal to $0\,[rad]$, resulting in simplification of the system given in 1. Thus, a reduced system in frequency domain is given by

$$\begin{cases} ms^2 Z(s) = U_1(s) - \dfrac{mg}{s} \\ I_{zz} s^2 \Psi(s) = U_4(s) \end{cases} \tag{8}$$

The control signals expressed in (8) are converted inside the AuRoRA platform in voltage signals to be applied in quadrotor engines, and then in normalized joystick commands to be sent to AR.Drone quadrotor.

Table II presents the high-level dynamic model parameters of Ar.Drone Parrot quadrotor, that are used in the computer simulation and experiments.

TABLE II

PARAMETERS OF THE HIGH-LEVEL DYNAMIC MODEL OF AR.DRONE PARROT QUADROTOR [20]

$m = 0,380\,[Kg]$	$I_{xx} = 9,57 \cdot 10^{-3}\,[Kgm^2]$
$k_1 = 0,1782\,[m]$	$I_{yy} = 18,57 \cdot 10^{-3}\,[Kgm^2]$
$k_2 = 0,0290\,[Nms^2]$	$I_{zz} = 25,52 \cdot 10^{-3}\,[Kgm^2]$

V. RESULTS AND DISCUSSION

After the depth-first search of the controller parameters, graphs highlighting the Integral Absolute Error (IAE) and Signal Control Energy (S) values were obtained for each iteration done. Thus, the optimal set of controller gains is linked to the lower value of these criteria. However, it is also necessary to verify the stabilization of the system and whether it is critically damped, since real systems respond better for such case. Thus, in the simulation, we obtained the graphics for altitude and yaw control of quadrotor. Experimentally, the results obtained in the simulation were validated by carrying out indoor tests.

A. Computer Simulation

Figure 4 shows the computer simulation for altitude and yaw control for the three controllers and their control signals. Figure 4(a) can be visualized the altitude control and the respective control signal. In Figure 4(b) is given the yaw value and the corresponding control signal. In the simulation, the three controllers behaved in a very similar way, with emphasis on the Lyapunov control which had a less energy consumption.

B. Real Experiment

Figure 5 shows the real experiment for altitude-yaw control for the three controllers and their control signals. Figure 5(a) illustrates the altitude control and the respective control signal. In Figure 5(b) it is given the yaw profile and the corresponding control signal.

In the real experiment, the system response for the PID and Lyapunov controllers were very similar and had better results, whereas the LQR (LQRI) controller consumed less energy. This can be seen in both cases: altitude and yaw control.

Table III shows the values of gains to the controllers used in this work and Table IV shows the values of Integral Absolute Error (IAE) and

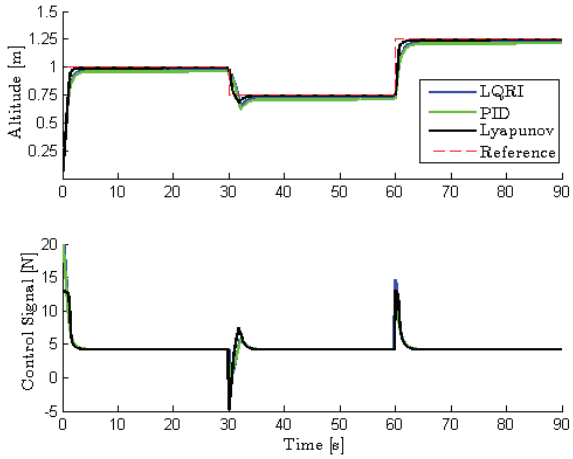

(a) Altitude

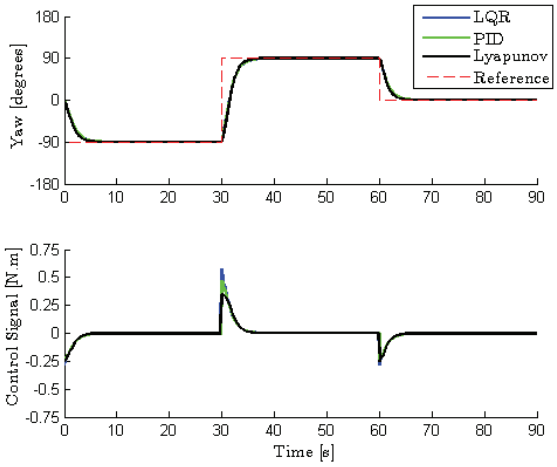

(b) Yaw

Fig. 4. Simulation data for altitude and yaw control.

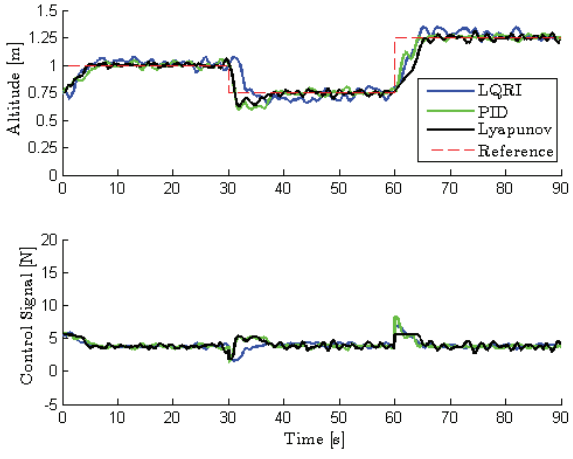

(a) Altitude

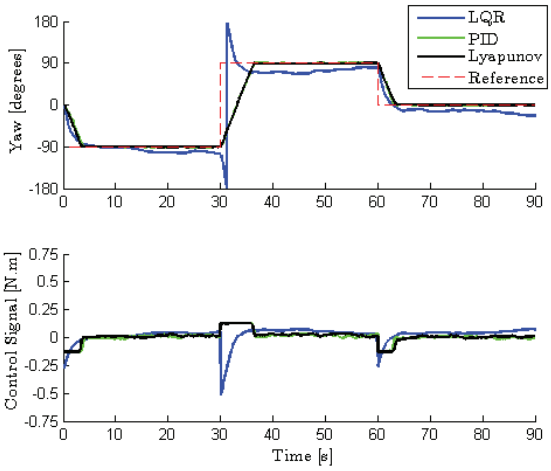

(b) Yaw

Fig. 5. Experimental data for altitude and yaw control.

Control Signal Energy (S) to each controller during regulation experiment.

C. Case Study: Sinusoidal Trajectory

Figure 6 shows the system response to a sinusoidal trajectory. LQR (LQRI) controller does not respond appropriately for a trajectory tracking mission (such controller is a regulator one). Lyapunov controller was more satisfactory in the case of altitude. The PID and Lyapunov controllers responded similarly in yaw maneuver. However, the Lyapunov controller required less energy to execute the flight mission. Moreover some tracking delays are observed in the PID controller.

After comparing the controllers we can conclude Lyapunov controller responds more efficiently in

TABLE III

CONTROLLER GAINS.

LQR(LQRI)	$Q_z = \begin{pmatrix} 15 & 0 & 0 \\ 0 & 0.001 & 0 \\ 0 & 0 & 0.002 \end{pmatrix}$ $Q_\psi = \begin{pmatrix} 5 & 0 \\ 0 & 0.001 \end{pmatrix}$	$R_z = 0.005$ $R_\psi = 15$
PID	$K_{pz} = 17$ $K_{iz} = 3.5$ $K_{dz} = 0.001$	$K_{p\psi} = 0.15$ $K_{i\psi} = 0.0003$ $K_{d\psi} = 0.00002$
Lyapunov	$K_{dz1} = 25$ $K_{dz2} = 6$ $K_{pz1} = 1$ $K_{pz2} = 5$	$K_{d\psi1} = 15$ $K_{d\psi2} = 0.5$ $K_{p\psi1} = 1$ $K_{p\psi2} = 0.5$

regulation and trajectory tracking mission. Despite consuming more energy than LQR (LRQI) and PID controllers, it spending less time to reach and remain at the goal.

TABLE IV

PERFORMANCE DATA FOR ALTITUDE AND YAW CONTROL.

	Controllers	IAE	S
Simulation	LQR (LQRI)	11.5314	2,018.8510
	PID	12.1384	1,953.7688
	Lyapunov	10.4613	1,945.4334
Experiment	LQR (LQRI)	5.5386	1,437.1908
	PID	3.7577	1,470.5558
	Lyapunov	3.8432	1,473.0290

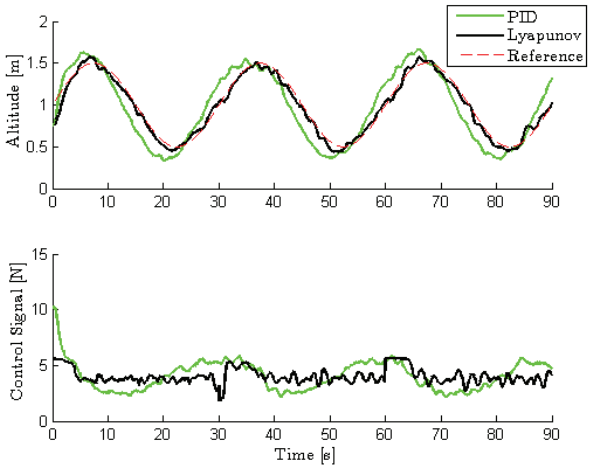

(a) Altitude

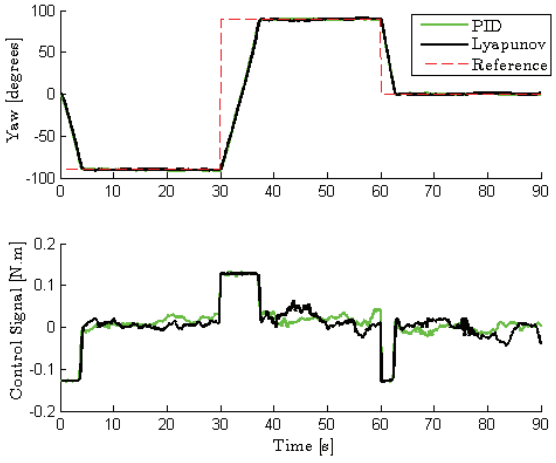

(b) Yaw

Fig. 6. Experimental data for sinusoidal trajectory.

VI. CONCLUDING REMARKS AND FUTURE WORKS

In this paper three control techniques (PID, LQR (LQRI) and Lyapunov-based) are used for guiding a quadrotor during altitude and yaw movement, in real scenarios of regulation and trajectory tracking tasks. Integral Absolute Error (IAE) and Control Signal Energy criteria are used to define the best set of controller gains by simulation. These gains are also used in the experimental test and the performance is analyzed in terms of the response time and energy spent to accomplish the task. This work highlights the simulated data are effectively verified in practice, achieving the expected results.

It is observed that the time response required to achieve the yaw reference is greater than that one required for achieving the altitude regulation. It occurs due to the overlapping of control signals. Equation (2) describes that the altitude and yaw controllers act together for the quadrotor, interfering in the individual performance.

This work deals only with the altitude and yaw variables. For future work, the authors propose to execute the control of all movements of quadrotor in three-dimensional space, and analyzing the application of other control techniques and gains optimization algorithms.

ACKNOWLEDGMENT

The authors thank CNPq and FUNARBE for financial support for this research. They also thank UFV for making possible this work.

REFERENCES

[1] Younes AI-Younes and M. A. Jarrah. Attitude stabilisation of quadrtor uav using backstepping fuzzy logic & backstepping least-mean-square controllers. In *International Symposium on Mechatronics and its Applications*, Amman, Jordan, May 2008. IEEE.

[2] João Paulo Ferreira Guimarães, Armando Sanca Sanca, Michel Santana de Deus, Tania Luna Laura, Alessandro Nakoneczny Schildt, Adelardo Adelino Dantas de Medeiros, and Pablo Javier Alsina. Estratégia de estabilização para um helicóptero quadri-rotor autônomo. In *Anais do XIX Congresso Brasileiro de Automática*, Campina Grande, Paraíba, Setembro 2012. CBA.

[3] Erick Pfeifer. Projeto e controle de um uav quadrirotor. Master's thesis, Universidade de São Paulo, São Paulo, SP, 2013.

[4] Anil Güçlü. *Attitude and altitude control of an outdoor quadrotor*. PhD thesis, School of Natural and Applied Sciences of Atilim University, Ankara, Turkey, July 2012.

[5] Pedro Castillo, Rogelio Lozano, and Alejandro Dzul. Stabilization of a mini rotorcraft with four rotors. *IEEE Control Systems Magazine*, December 2005.

[6] Samir Bouabdallah, Marcelo Becker, and Roland Siegwart. Autonomous miniature flying robots: coming soon! *IEEE Robotics & Automation Magazine*, September 2007.

[7] Alexandre S. Brandão, Igor H. B. Pizetta, Mario Sarcinelli Filho, and Ricardo Carelli. Modelagem e controle não linear subatuado de um quad-rotor: Parte 1. In *Anais do XIX Congresso Brasileiro de Automática*, pages 449–454, Campina Grande - PB, Brasil, Setembro 2012. CBA.

[8] Samir Bouabdallah. *Design and Control of Quadrotors with Application to Autonomous Flying*. PhD thesis, École Polytechnique Fédérale de Lausanne, Tlemcen, Algérie, Février 2007.

[9] Z. X. Liu, C. Yuan, Y. M. Zhang, and J. Luo. A learning-based fuzzy lqr control scheme for height control of an unmanned quadrotor helicopter. pages 936–941, Orlando, FL, USA, May 27-30 2014. International Conference on Unmanned Aircraft Systems (ICUAS), IEEE.

[10] Aydin Yesildirek and Bara Imran. Nonlinear control of quadrotor using multi lyapunov functions. pages 3844–3849, Portland, Oregon, USA, June 4-6 2014. American Control Conference (ACC), IEEE.

[11] Minh Nguyen Duc, Thang Nguyen Trong, and Yang Sheng Xuan. The quadrotor mav system using pid control. pages 506–510, Beijing, China, August 2-5 2015. International Conference on Mechatronics ant Automation, IEEE.

[12] Miguel Enrique Parra Muñoz. Modelagem matemática e controle de um quadrimotor. Master's thesis, Universidade de Brasília, Brasília - DF, Brasil, Outubro 2012.

[13] Bin Yua, Youmin Zhang, and Yaohong Qu. Fault tolerant control using pid structured optimal technique against actuator faults in a quadrotor UAV. pages 167–174, Orlando, FL, USA, May 27-30 2014. International Conference on Unmanned Aircraft Systems (ICUAS), IEEE.

[14] Soroush Sheikhpour and Saeed Bagheri Shouraki. A model-based fuzzy controller using the parallel distributed compensation method for quadrotor attitude stabilization. *IEEE*, 2013.

[15] M. Zareb, R. Ayad, and W. Nouibat. Fuzzy-pid hybrid control system to navigate an autonomous mini-quadrotor. 3^{rd} *International Conference on Systems and Control*, October 2013.

[16] Zhao Shulong, An Honglei, Zhang Daibinga, and Shen Lincheng. A new feedback linearization lqr control for attitude of quadrotor. pages 1593–1597, Marina Bay Sands, Singapore, December 10-12 2014. 13th International Conference on Control, Automation, Robotics & Vision, IEEE.

[17] Dong Yiqun, Fu Jun, Yu Bin, Zhang Youmin, and Ai Jianliang. Position and heading angle control of an unmanned quadrotor helicopter using lqr method. pages 5566–5571, Hangzhou, China, July 28-30 2015. Proceedings of the 34th Chinese Control Conference, IEEE.

[18] Shahida Khatoon, Dhiraj Gupta, and L .K. Das. PID & LQR control for a quadrotor: Modeling and simulation. pages 796–802. International Conference on Advances in Computing,Communications and Informatics (ICACCI), IEEE, 2014.

[19] Jiangcheng Zhu, Endong Liu, Shan Guo, and Chao Xu. A gradient optimization based pid tuning approach on quadrotor. pages 1588–1593. 27th Chinese Control and Decision Conference (CCDC), IEEE, 2015.

[20] Alexandre S Brandão, Igor H B Pizetta, Mario Sarcinelli-Filho, and Ricardo Carelli. Modelagem e controle nao linear subatuado de um quadrotor: Parte 2. In *Anais do XIX Congresso Brasileiro de Automática*, Campina Grande, PB, 2012.

[21] Victor G. Adîr and Adrian M. Stoica. Integral LQR control of a star-shaped octorotor. *Incas Bulletin*, 4:3–18, February 2012.

[22] Alexandre Santos Brandão, Mário Sarcinelli Filho, and Ricardo Carelli. High-level underactuated nonlinear control for rotorcraft machines. In *International Conference on Mechatronics*, Vicenza, 2013. IEEE.

[23] Igor Henrique Beloti Pizetta, Alexandre Santos Brandao, and Mario Sarcinelli Filho. A hardware-in-loop platform for rotary-wing unmanned aerial vehicles. In *Unmanned Aircraft Systems (ICUAS), 2014 International Conference on*, pages 1146–1157. IEEE, 2014.

FUZZY PITCH CONTROLLER APPLIED TO VARIABLE-SPEED WIND TURBINE

Francisco das Chagas Barbosa De Sena, **José Patrocinio da Silva** , **Adriano Aron Freitas de Moura**
E-mail: fcbsena@hotmail.com; patroc@ct.ufrn.br; adrianoaron@ufersa.edu.br
Elmer Rolando Llanos Villarreal, Emmanuel Ramon Marques Dantas,
Curso de Pósgraduação em Sistemas de Comunicação e Automação -UFERSA
59625-900, Mossoró, RN Brazil.
E-mail: elmerllanos@ufersa.edu.br ; manel.mrq@hotmail.com

Abstract

The development of a mathematical model for a system of wind power generation is complex, can be strongly affected by the wind variation and its a nonlinear problem. Due to these characteristics the analysis can be performed using a control system based on fuzzy logic, which improves a better adjust of the system to be controlled. In this paper, the performance of a variable-speed wind turbine controlled by a classic proportional controller (CPC), and a fuzzy logic controller (FLC) to adjust the angle of inclination of the blades is analyzed. In this case, its possible to verify the effectiveness of the application of fuzzy logic, the ability to avoid fluctuations and improvement of the quality of electric power output, regardless of the original features of the proportional control applied. The CPC and the FLC were implemented using the Fuzzy Logic Toolbox^{TM} and SIMULINK software packages available in MATLAB. The results show that the application of fuzzy logic to adjust the parameters of a controller can improve the dynamic performance of the wind turbine with respect to reducing the onset of fatigue loads, weather fluctuations and stabilization of electric power output.

1. INTRODUCTION

In recent years, is possible to realize the steadily growing in generation of electricity by using green energy, particularly, energy from sun and wind. However, due to this kind of production to be really dependent of the weather, the control system has an important function in the process of generation and on the final price of the generated *KW*.

The energy from wind is captured by using wind turbine, that technology has over the years suffered great evolution in its construction. As a result, the productions capacity passed from KW to MW. Horizontal axes turbines can be classified into two models: fixed speed, and variable speed. The second one is most used than the first, because its able to improve power generations quality over a wide range of wind speed.

According to Baygildina, [1] the main challenges for the conventional wind turbine control is achieving maximum power conversion from the wind within an acceptable wind speed range and damp harmful mechanical oscillations, caused by the wind stochastic behavior.

Among several advantages from using a pitch angle control we can emphasize the optimizing the power output of the wind turbine for wind speed bellow turbines rated speeds, preventing input mechanical power exceeds the designed limits, for winds above turbines rated speeds and Minimizing fatigue loads of the turbines mechanical components, avoiding aerodynamic overload on turbines structure [2].

In [3], has that the proportional-integral controller (PI), which is part of the modern control theory, are widely used as a basic control technology in industry nowadays. However, this technic carries some inconvenient, for example, to get a good performance of wind turbines is necessary to know the correct aims of the controller, but due to domain behavior, it may be a difficult task. Furthermore, *PI* controller is not appropriate for system that involves high nonlinearities or the reference changes with high frequency [5]. In case of high nonlinearity technique such as gain scheduling and neural network can get better results [6].

Control via fuzzy logic, has over the last years increased in popularity among engineers. This increase can be attributed to the fact of this technic allows to the control incorporates human reasoning, differently from the traditional control. In other words, the controller designed using fuzzy logic implements cognitive human reasoning thats programmed by membership functions, rules and interpretation rules (fuzzy logic language). Some of the bigger fuzzy controllers advantage is that it doesnt need completed mathematic knowledge of the analyzed system. Its also suitable for systems containing strong non-linearity. Therefore, on this paper is modeled and analyzed the performance of a FLC applied specifically to the pitch angle controller of a variable-speed wind turbine. In the next section, the wind turbine modeling is presented. The fuzzy logic theory is briefly explained in section 3. The proposed method is presented in the section 4. The simulations and comparisons of the different pitch angle control strategies are showed in section 5 and finally the main

conclusions are given at the end.

2. WIND TURBINE MODELING

A. Description

Pitch control is responsible to move wind turbines blades continually, the one hand this action occurs in order to get a better performance for the generated power, on the other hand it also reduces mechanical efforts. This moving occurs through sophisticated hydraulics and electronics devices that drive the blades around their longitudinal axes. Its important to highlight that the attack angle of the blades varies according to wind speed [4].

This paper discusses the pitch control, which has the characteristic of moving blades continually in other, on the one hand this action occurs in order to get a better performance for the power generated, on the other hand, it also reduces mechanical efforts. This moving occurs through sophisticated hydraulics and electronics devices that drive the blades around their longitudinal axes. Where the attack angle varies according with wind speed variation [4]. The Figure (1) shows a general scheme of a Wind Energy Conversion System (WECS) where three types of energy states are presented: wind, mechanical, and electrical.

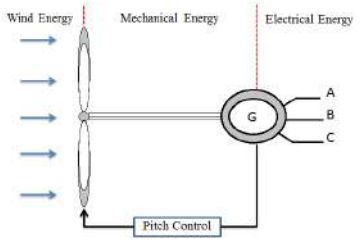

Figure 1. General scheme of a WECS specifying the three models of energy conversion

Considering a packet of air with mass, m, moving at a speed vwind on the x direction. Its kinetic energy, U, is given by the following mathematical relation:

$$\frac{1}{2}\rho A\frac{dx}{dt}v_{wind}^2 \tag{1}$$

The aerodynamic model equations allows to calculate the mechanical power value applied to the shaft of the electric generator, considering different wind speeds and different positions of the blade pitch angle. This model depends on the type of turbine to be represented. How in this paper is considering a longitudinal turbine of has that the power in the wind, P_w, is the time derivative of the kinetic energy:

$$P_w = \frac{dU}{dt} = \frac{1}{2}\rho A\frac{dx}{dt}v_{wind}^2 = \frac{1}{2}\rho A v_{wind}^3 \tag{2}$$

The aerodynamic model equations allows to calculate the mechanical power value applied to the shaft of the electric generator, considering different wind speeds and different positions of the blades. This model depends of the type of wind turbine is being represented, in this will be considered a longitudinal turbine where the wind power Pw is the time derivative of the kinetic energy, represented in the equation (2):

The the equation (2) is used to determinate the full power from wind, however just a part of this energy can be converted into electric energy. The fraction of power extracted from the wind power is normally called performance coefficient or power coefficient, given by the symbol C_p. So the actual mechanical power output can be written as follow:

$$P_{mec} = \frac{1}{2}\rho A v_{wind}^3 C_p(\lambda,\beta) \tag{3}$$

As can be appreciated in Equation (3), C_p is a function of tip speed ratio and blade pitch angle. Where the tip speed ratio is defined as:

$$\lambda = \frac{w_{rotor}R}{V_{wind}} \tag{4}$$

Where: P_{mec} =mechanical power (W) ρ =air density (Kg/m^3) A=area swept by blades β=blade pitch angle $(^o)$ λ= tip speed ration R= turbine rations radiou (m) w_{rotor}= turbine rotor speed (rad/s)

The power coefficient, referent to the aerodynamic model, its not dependent of the type of electric generator or the type of control used in the power converters. The structure of C_p is represented at the equation (5) according to [7]:

$$C_p(\lambda,\beta) = k_1[\frac{k_2}{\lambda_i} - k_3\beta - k_4\beta^{k_5} - k_6]e^{\frac{-k_7}{\lambda_i}} \tag{5}$$

Where:

$$\lambda_i = \frac{1}{\frac{1}{\lambda+k_8} - \frac{k_9}{\beta^3+1}} \tag{6}$$

The constants used in equation (5) and (6) are showed at the Table (1).

Coefficient	Value
K_1	0.73
K_2	151
K_3	0.58
K_4	0.58
K_5	0.58
K_6	0.58
K_7	0.58
K_8	0.002
K_9	0.03

Table 1. Power curve coefficients

Characteristics of C_p for different values of pitch angle are shown in Figure (2). It's possible to realize that for each value of pitch angle theres a maximum

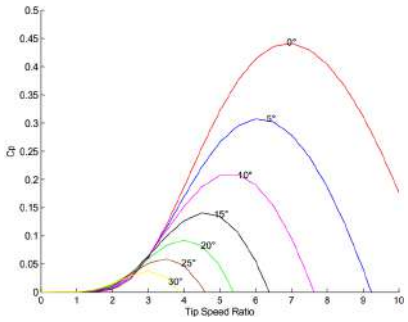

Figure 2. Power coefficient versus tip speed ratio

value for C_p and the increasing of the tip speed ratio leads to a quick decreasing of C_p.

B. Conversational Pitch Control

Passive stall technology is the simpler way to achieve power limitation however pitch control is able to get faster answer and better controllability. This kind of control is normally preferred from medium to large wind turbines [8].

Variable-pitch has been used to provide a chancing in the attack angle of the blades, because of that is possible to modify the aerodynamic characteristic of the blades and avoid, for example, fatigue damage and overload. This action carries to improvement of mechanical loads, and output power, at higher wind speed. Block diagram of the first-order of a variable-pitch control system is highlighted at Figure (3) .

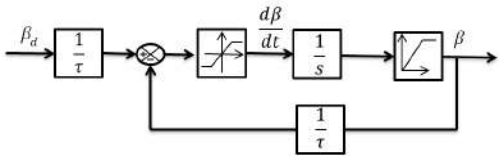

Figure 3. Model of a pitch angle actuator

Pitch angle actuator is a nonlinear servo that generally rotates all the blades or parts of them together and unison, depend of the type of system used on the wind farm. In closed loop the pitch actuator can be modeled as a first-order dynamic system with saturation in the amplitude and derivate of the output signal as is possible to check at Figure (3). The Equation (7) specifies the dynamic behavior for this particular model, operating in its linear region [8].

$$\frac{d\beta}{dt} = -\frac{1}{\tau}\beta + \frac{1}{\tau}\beta_d \tag{7}$$

where

β =actual blade pitch angle $(^o)$

β_d =desired blade pitch angle $(^o)$

The behavior of the pitch angle control can be summarized as the follow: when the wind speed is below than the rated speed, the attack angle is kept at its rated value; when the wind speed is higher than the rated speed, the attack angle is reduced, consequently the lift forces decrease as well; when the blades are completely pitched, the attack angle is aligned with the wind and no forces lift will act on the blades, so the wind turbine will stop its rotation.

3. FUZZY LOGIC

A. Description

Fuzzy systems are based on the fuzzy sets and fuzzy logic theory proposed by Loft A. Zadeh in the 1960s [9]. According to Dumitrescu [10] fuzzy logic has been applied to several areas with satisfactory results, such as optimization, control of processes and system design.

With the versatility of this technic is possible to shape and manipulate mathematically imprecise information, natural of the human language and thus provided by experts (not mathematical) to characterize the problem analyzed. This manipulation occurs though the composition of chosen variables to model mathematically the process, when the involvement of independents variables on the dependent is established by a set of linguistic rules based on experts knowledge [11]. Regarding the definition of the set of rules, as well as setting the attributes in terms of fuzzy sets both tasks can be performed by an expert or automatic methods, when the data representatives of the problem are available [12], [13].

3.1. Process identification for analysis

Thus, the essential concepts that must be observed for identification, by the expert user, of important set of variables of the process in study belong to the class of fuzzy variables. The first concept according to [15] is associated to the definition of fuzzy sets, for example, be a subset from a set is considered fuzzy subset if it is described as a set of ordered pairs as following [15]:

$$A = \{(x, \mu_A(x));\ x \in U\ \mu_A(x) \in [0,1]\} \tag{8}$$

Where $\mu A(x)$ is a membership function that deter-mines to what degree x is in A:

$\mu A(x) = 1$, x belongs totally to the set A; $0 < \mu A(x) < 1$, x belongs partly to the set A; $\mu A(x) = 0$, x not belong to the set A.

Notice that the algebra fuzzy sets doesnt follow the usual classical theory, especially due to the fact that the operations of union and intersection of a set and its complements are different from 1 and empty respectively and therefore specific operations between fuzzy sets must be established.

C. Structure of Fuzzy Controller

In general, a fuzzy system does correspond to each fuzzy input a fuzzy output. However, it is expected that each input (either a real number or pair of real numbers, or n-tuple of real numbers) to make a corresponding output. In this case a fuzzy system is a function of R^n in R, built in any specific way. At Figure (4) is represented the methodology for the construction of this function [16]:

1. Fuzzification Module: performs the mathematical modeling of the information of input variables

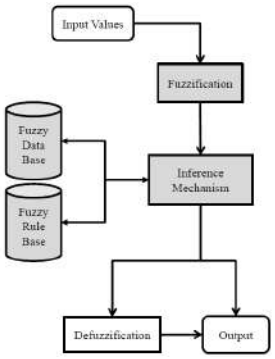

Figure 4. Fuzzy System

through of fuzzy sets. Its responsible for showing the great importance of specialist process is being analyzed, since each input variable should be assigned linguistic terms which represent the states of this variable, and each linguistic term, should be assigned a fuzzy set by a relevance function;

2. Base Rules Module: Its what constitutes the core of the system. This module recognize and store the linguistic variables and their classifications;

3. Inference Module: where is define what are the logical connectives used to establish the fuzzy relation which models the rule base. It is in this module that depends on the success of the fuzzy system as it will provide the fuzzy output (control) to be adopted by the controller from each fuzzy input;

4. Defuzzification Module: it translates the state of each fuzzy output variable to a numeric value.

4. THE PROPOSED METHOD

In this work, the FLC was developed using the Fuzzy Logic $Toolbox^{TM}$ available in $MATLAB^{R}$. The control was incorporated into $SIMULINK^{R}$, a dynamic simulation program where is possible to model, supervise, and provide appropriate adjustments to the system, in this case, a pitch angle controller of a wind turbine. The fuzzy inference system (FIS) was defined using two inputs, they are: signal error, that is the difference between the reference point (set point) and the actual rotors speed, and the change in the error signal. Triangular and trapezoid membership functions were used to represent the systems inputs and output, in order to provide more sensitivity to the system modeled. The development of the present article has been used the follow terms to describe each rule: negative large (NL), negative medium (NM), zero (ZE), positive small (PS), positive medium (PM), and positive large (PL). The first rule set is named Error, where has been used a range varying from -1 to 1 and a total of 5 membership functions, as is possible to see in Figure (5).

The second rule set is named Change Error, where has been used a range varying from -0.1 to 0.1. It was used 7 membership functions, shown in Figure (6).

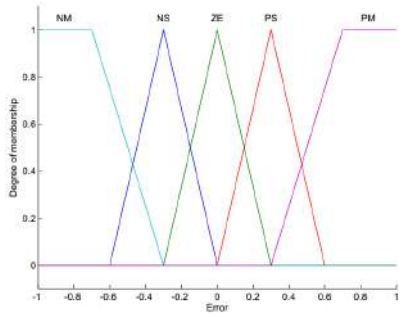

Figure 5. Error defined in terms of fuzzy sets

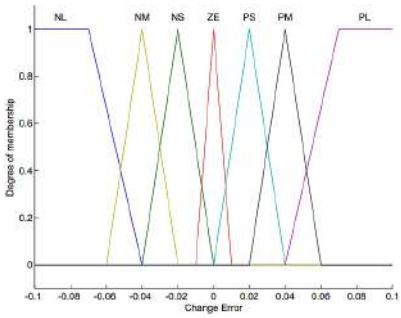

Figure 6. Change in the Error defined in terms of fuzzy sets

The output of the system is named Pitch Angle, where has been used a range varies from -10^{o} to 10^{o}, seen in Figure (7). Its responsible to send the value of pitch angle to the blades.

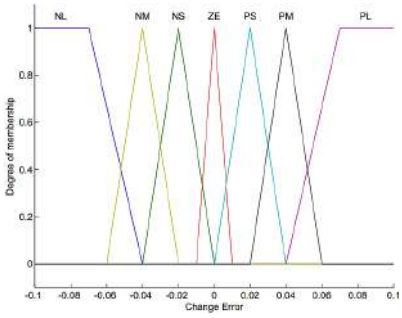

Figure 7. Output variable defined in terms of fuzzy sets

The Table (2) shows the rules of FLC responsible to direct the acting of the controller according to values of inputs.

Figure (8) shows the surface diagram as result of all 35 fuzzy rules for the designed FLC. For the defuzzification, was employed the center of gravity method.

Next, will be present the experiments and results from this FLC comparing it with a classical proportional controller as a way to identify how it reacts to different regime of wind speed, and if its able to improve the characteristics of the CPC and what are its additional main advantages due to utilize this intelligent technic to

Erro ‖*ChangeError*	NM	NS	ZE	PS	PM
NL	NL	NL	NM	NM	NS
NM	NL	NL	NM	NS	ZE
NS	NL	NM	NS	ZE	PS
ZE	NM	NS	ZE	PS	PM
PS	NS	ZE	PS	PM	PL
PM	ZE	PS	PM	PL	PL
PL	PS	PM	PL	PM	PL

Table 2. Set of rules defined for the fuzzy control system

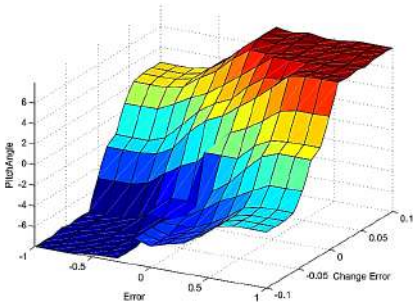

Figure 8. Visualization of the control surface

complement traditional controller technic.

5. EXPERIMENTS AND RESULTS

In Figure (9) shows the behavior of the wind used to verify the ability of each controller keeps the systems quality and efficiency. Also, its used to check the speed tracking performance of the proposed control strategy. Notice that the first 2 seconds has a tough region with different levels of wind speed, being above and under rated speed of the wind turbine. Remembering that $12m/s$ $(1pu)$ represent the rated wind speed for the wind generator, in this condition its able to produce a maximum electric power of 6 kW $(1pu)$.

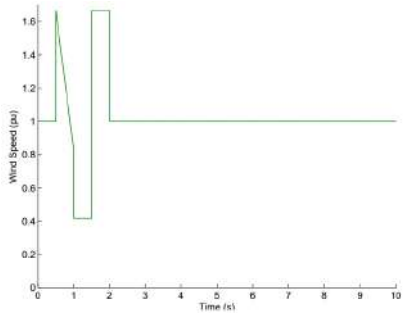

Figure 9. Wind Speed per unit (pu)

It was utilized a sinusoidal three-phase machine as generator, more specifically, a permanent magneto synchronous machine (PMSM), with salient-pole rotor, connected to a resistive three-phase load of 25 Ohms. In Figure (10) is seen the classical model of blade angle control, using CPC block (pitch gain of 500). This diagram has the actual

Figure 10. Model of classical proportional pitch controller

In Figure (11) can be seen the new block diagram, where the inputs and output were kept, but the classical model of blade angle control was replaced for a fuzzy logic controller block, furthermore, as possible to see a new block called integer delay that is responsible to delay the error signal in 4 sample periods creating the change in error signal.

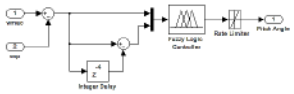

Figure 11. Proposed Fuzzy Controller

The results obtained by comparing the classical proportional pitch controller with the fuzzy pitch controller are showed at Figure (12) and (13). Analyzing Figure (12), that represents generators rotor speed has that the CPC had an overshoot of 29.0046% and a settling time of 2.8886 seconds while the FLC had an overshoot of 29.0053% and a settling time of 3.9701. However, the *FLC* had a softer settling than the classical control, that shown less effective to avoid oscillations.

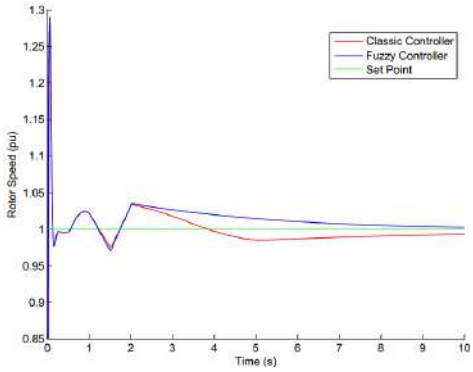

Figure 12. Comparison between rotor speed for each controller

About the electric power, shown in Figure (13), has that the CPC had an overshoot of 59.0278% and a settling time of 7.6591 seconds while the FLC had an overshoot of 59.0295% and a settling time of 5.7801 seconds. The numbers show a modest difference between both overshoot but, the *FLC* had settling time much better than the *CPC*, approximately 2 seconds of difference, shown more effective to avoid oscillations ensuring the final quality of the electric power. The classical technic was not able to track totally the set point, differently from the *FLC*.

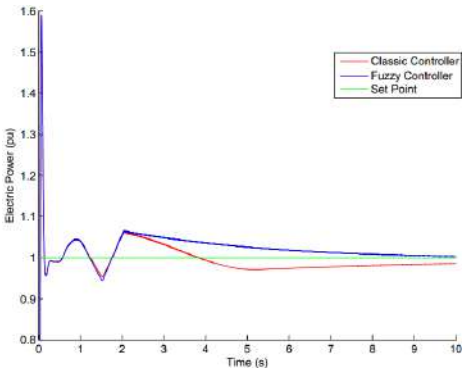

Figure 13. Comparison between electric power for each controller

The initial high value of overshoot is justified due to the fact of the systems startup, and generally, the proportional mode is added when wish to obtain a specific rising time not being able to eliminate this disadvantage. To achieve this objective, an integral mode is more indicate. But, after the startup, the overshoot is very small although the difficult regimes of wind speed.

6. CONCLUSIONS

In this paper, was analyzed the additional advantages to apply fuzzy logic to the control of pitch angle of variable-speed wind turbine instead of a classical proportional controller. The parameters observed were wind speed, generators rotor speed and electric power output. In conclusion, simulation results demonstrated that the FLC showed more appropriate to the problem of power control than the CPC. It was able to keep the system within acceptable operation limits, without large power fluctuation, even with a difficult wind regime. Also it showed an important ability to attenuate oscillations and capability of returning totally to the set point in a shorter settling time.

7. ACKNOWLEDGMENTS

The authors acknowledge the structural support of UFERSA, UFRN and financial support of FAPERN and ANP - PRH -56.

References

[1] Baygildina, E.; Hynynen, K. M.; Pyrhonen, O., Wind turbine adaptive controller modeling, *Conference Power Electronics and Machines in Wind Applications (PEMWA)*, v. 1, n. 1, pp.1-6, 2012.

[2] Jianzhong Zhang; Ming Cheng; Zhe Chen; Xiaofan Fu, Pitch angle control for variable speed wind turbines,*Electric Utility Deregulation and Restructuring and Power Technologies, Third International Conference on*, v. 1, n. 1, pp.2691-2696, 2008.

[3] Jin, H.P., Su, W.S. and Lee, I.B., An Enhanced PID Control Strategy for Unstable Processes. *Automatica*, v 4, n. 6 pp. 751-756, 1998.

[4] W. W. Tan, A.L. Dexter, A self-learning fuzzy controller for embedded applications, *Automatica*, v. 36, n.1, pp. 1189-1198, 2000.

[5] M. Kawato, Y. Uno, M. Isobe, and R. Suzuki, "Hierarchical neural network model for voluntary movement with application to robotics," *IEEE Control Systems Magazine*, v. 8(2), pp. 8-15, 1988.

[6] Macedo, A.V.A.; Mota, W.S., Wind turbine pitch angle control using Fuzzy Logic, *Transmission and Distribution: Latin America Conference and Exposition (TD-LA), Sixth IEEE/PES*, v. 1, n. 1, pp.1-6, 2012.

[7] S.N. Muyeen, T. Tamura, and T. Murata, "Stability Argumentation of a Grid-connected Wind farm", 1st Ed. London, Green Energy and Technology, 248p. XIV, Springer, 2009.

[8] Fernando D. Bianchi, Hernan de Battista, and Ricardo J Mantz, "Wind Turbine Control Systems, Principles, Modelling, and Gain Scheduing Design", 1st ed.,., Ed. London, Inglaterra: Springer, 2007.

[9] L. Zadeh, Fuzzy Sets, *Information and Control*, v. 8(3), pp. 338-353, 1965.

[10] D. Dumitrescu, B. Lazzerini, and L. Jair, "Fuzzy Sets and Their Application to Clustering and Training", Int. Series on Computational Intelligence. CBC Press., 2000.

[11] Simões, M.G. and Shaw, I. S., "Fuzzy Control and Modelling", Ed. Blucher, 2007.

[12] Dan Su; Kaichun Ren; Jianyuan Luo; Chunhan He; Liyong Wang; Xingqi Zhang, Programme and simulation of the fuzzy control list in fuzzy control, *Intelligent Control and Automation (WCICA), 8th World Congress on*, v. 1, n. 1, pp.1935-1940, 2010.

[13] M.E. Cintra and M.C., and Camargo Monard, Fuzzy and Classic Rule Learning Methods: A Comparative Analysis, in *World Conference on Soft Computing*, pp. 182-190, 2011.

[14] Cintra, M.E.; Monard, M.C.; Camargo, H.A., Using fuzzy formal concepts in the genetic generation of fuzzy systems, *Fuzzy Systems (FUZZY-IEEE), IEEE International Conference on* , v. 1, n. 1, pp.1-8, 2012.

[15] Amendola, M.; Souza, A.L; Barros, L.C. Manu-al do Uso da Teoria dos Conjuntos Fuzzy no MATLAB 6.5. FEAGRI IMECC/ UNICAMP, 2004. Disponivel 14/08/2014 em http://www.ime.unicamp.br/ laeciocb/.

[16] Q. Li, Y. Fang, and J. and Wang, J. Song, The Application of Fuzzy Control in Liquid Level System, in *International Conference on Measuring Technology and Mechatronics Automation*, 2010.

11th IFAC Workshop on Intelligent Manufacturing Systems
The International Federation of Automatic Control
May 22-24, 2013. São Paulo, Brazil

Proposal of a Fuzzy Control System for the Management of Traffic lights

C. A. Teixeira Jr., E. R. L. Villarreal, M. E. Cintra, N. W. B. Lima

Federal Territorial University of the Semi-Arid (UFERSA)
Dept. of Exact and Natural Sciences – Mossoro, RN, Brazil
(c5rlos@yahoo.com.br, {elmerllanos,cintra}@ufersa.edu.br,
nwontoon@gmail.com)

Abstract:
In this work, we describe the proposal of a fuzzy control system to manage the traffic in a critical point, in Mossoro - RN, composed by a traffic light that controls a pedestrian crossing point in a busy road, which is connect to a roundabout. The system includes access to two important universities, UFERSA - Federal Territorial University of the Semi-Arid, and UERN - State University of Rio Grande do Norte. The problem in this traffic system is related to traffic jams in rush hours, which block the access to both universities, blocking all entrances and exits of the roundabout. Several techniques have been used for traffic control, including local policies, as well as computational systems, such as fuzzy systems. The adopted methodology, a fuzzy control system, is justified by the interpretability and accuracy of the final model. The problem was tackled by measuring and analysing the traffic system in order to control the main element in case of traffic jams, the traffic lights. The control is performed by adjusting the green time for vehicles of the traffic lights in order to allow a suitable flow of vehicles while keeping the waiting time of pedestrians at reasonable levels. The rules to control the traffic lights were empirically defined by adjusting the fuzzy sets modelling the variables of the systems. Simulation results show that the proposed fuzzy control system is suitable to tackle the problem by providing an economic and feasible alternative, with promising results.

Keywords: Fuzzy Logic and Fuzzy Computing; Knowledge-Based Systems.

1. INTRODUCTION

Technological development has provided improvements to many aspects of our lives. It has also created new problems. Transportation is one of the aspects of our lives that has been greatly improved with new technologies. Nevertheless, the growing fleet of cars has caused serious traffic problems which have been studied by many research areas. Some proposals have already tackled relevant problems related to traffic systems in modern life, such as the adoption of traffic lights to control the flow of cars in busy roads. Traffic lights usually have a predefined time for green and for red lights. This strategy, however, is not suitable for all places. In the city of Mossor, the problem of congestion in traffic flow at the roundabout located at Francisco Mota street, also known as federal highway BR 110, occurs due to a traffic light located in front of UFERSA. The roundabout connects several sites, including the city of Areia Branca, UERN, the city centre, and the access to Natal and Fortaleza. A model of the traffic in the area is shown in Figure 1.

The distance from the traffic lights to the roundabout is approximately 300 meters and on busy days, during rush hours, the queue of vehicles from the roundabout to the traffic lights causes a massive jam in the roundabout, blocking access to most roads.

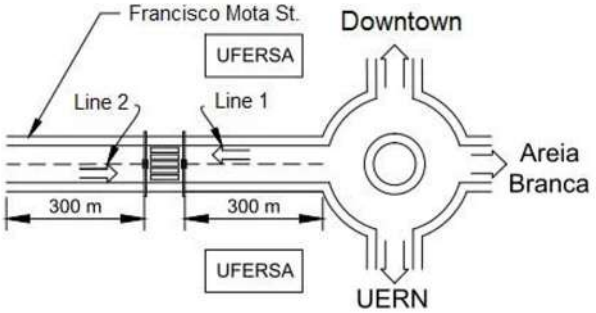

Fig. 1. Representation of the traffic system between UFERSA and UERN.

This type of problem, however, is not linear. This way, we selected the fuzzy logic to tackle it, since fuzzy logic handles non-linearity well, usually presenting good results. The proposed strategy consists of applying a fuzzy controller at the traffic lights system in order to adjust its green and red times, in order to properly handle different levels of traffic flow through the day.

The efficiency of the proposed method is shown in experimental results, as well as the positive analysis of experts.

This paper is organized as follows. Section 2 presents the basic concepts of fuzzy logic. Section 2 describes the problem and includes a review on methods to tackle traffic

978-3-902823-33-5/13/$20.00 © 2013 IFAC

jams. Section 3 presents the proposed method. Section 4 details the proposal. Section 5 presents the experiments and results, followed by the final conclusions and future work in Section 6.

2. FUZZY SYSTEMS

Fuzzy systems are based on the fuzzy sets and fuzzy logic theory proposed by Loft A. Zadeh in the 1960s (Zadeh, 1965). Fuzzy logic has been applied to several areas with satisfactory results, such as optimization, control of processes and system design (Dumitrescu et al., 2000; Pedrycz, 1996, 1998). Fuzzy logic is able to handle imprecise and uncertain data by means of fuzzy sets, which model variables of the real world in terms of how much a specific input value belongs to different sets.

For instance, let us consider a variable *Temperature*, ranging from 0 to 45 °Celsius. When discretizing this variable into four sets, *Low*, *Medium*, *High*, and *Very High*, in the classic set theory, 20 °can only belong to one set: *Medium* or *High*. When defining the fuzzy linguistic variable *Temperature*, using the same linguistic values, as shown in Figure 2, 20 °belongs to the *Medium* and *High* fuzzy sets, each one with a different membership degree: 0.66 for *High* and 0.33 for *Medium*.

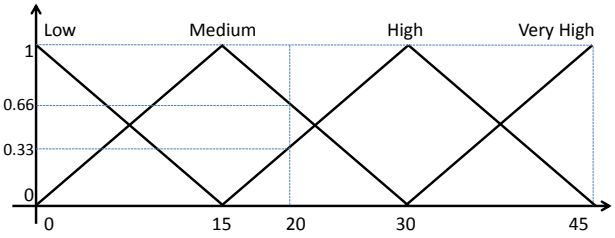

Fig. 2. Variable *Temperature*.

A fuzzy system is usually composed of a set of rules (fuzzy rule base), a fuzzy data base, which contains the definition of the attributes of the system in terms of fuzzy sets, and an inference mechanism, which processes the input values in order to generate the output, as shown in Figure 3.

The fuzzy rule base is composed of a set of *If Then* rules.

Notice that for classification problems, the output of the system is a (discreet) class, while for control systems, the output is usually a continuous value. This way, a defuzzification of the class might be necessary. This fact is shown in Figure 3, which depicts the defuzzification step as optional. In fact, the Mamdani model (Klir and Yuan, 1995) is usually used for classification (discreet outputs), while the Takagi-Sugeno-Kang (Klir and Yuan, 1995) model is used for continuous outputs. The Mamdani model can also be used in conjunction with a defuzzification step, providing a continuous output value.

Regarding the definition of the set of rules, as well as the definition of the attributes in terms of fuzzy sets, both tasks can be performed by a domain expert or by automatic methods (Cintra et al., 2011, 2012), when representative data of the problem is available.

Fuzzy systems allow the analysis of a problem from a human-like point of view, due to the use of linguist

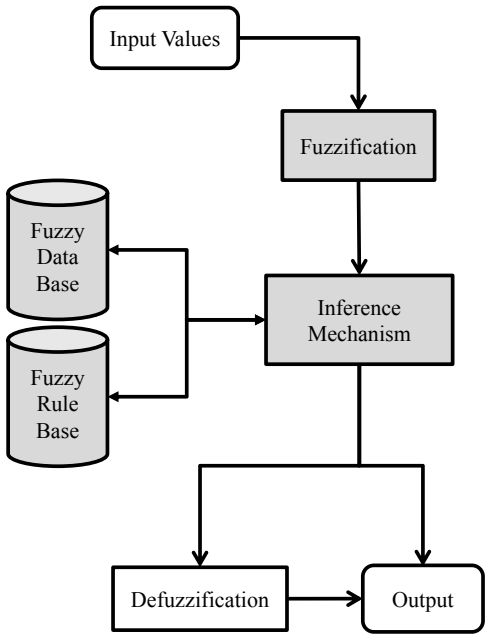

Fig. 3. Fuzzy System.

variables. It also allows a gradual transition between sets. Thus, fuzzy control systems can be modelled to emulate the same strategy humans use to solve problems. Therefore it is considered an intelligent system. This way, fuzzy systems provides a formal method to translate verbal, vague, imprecise and qualitative expressions, common in human communication, into numerical values (Simoes and Shaw, 2007).

Fuzzy logic is used in embarked systems in microcontrollers for several applications, from washing machines to digital cameras (Haruki, 1992; Banks and Hayward, 1993). Fuzzy controllers have also been used for traffic lights with promising results (Mehta, 2008).

Historical data reports the first application of fuzzy logic in urban traffic control in 1997 by Pappis and Mamdani (Pappis and Mamdani, 1977) and in the following decades its use in traffic control has been thoroughly tested (Rentera, 2002), including in Brazil (Koga et al., 2012).

3. CONTEXTUALIZATION

In countries considered "in development", such as Brazil, traffic problems are serious and part of the reality in many cities. Vehicle fleets are growing at an accelerated rate in many states. Nevertheless, solutions to the problems it brings often fail to accompany such growth.

According to the State Traffic Department - DETRAN-RN, the number of vehicles in the state of Rio Grande do Norte increased about 34% from 2008 to 2011 (DETRAN-RN, 2012). As expected, this phenomenon causes negative impacts in many cities. The city of Mossoro, located in the state of Rio Grande do Norte, for example has approximately 109,400 vehicles. The fleet in Mossoro has presented a rapid growth without a prior efficient planning of the public transport infrastructure, thus, facing several situations in its roads.

978-3-902823-33-5/13/$20.00 © 2013 IFAC

With the increasing number of vehicles in the cities, the control over how long the green time of traffic lights has posed a relevant problem to traffic engineers. The problem is aggravated when considering traffic lights for pedestrians,since the flow of vehicles and people presents large variations through the day and a reduction in the waiting time of pedestrians causes a reduction in the green time for vehicles.

Measures taken to minimize this problem include reducing the waiting time of pedestrians to cross a road. In Sao Paulo city, for instance, a reduction of 16%, on average, in the waiting time for pedestrian to cross roads was implemented in 18% of the total of 5847 crossing points of the city (CET, 2012). The measure was taken aiming at reducing the incidence of accidents since pedestrians tend to try to cross the street avoiding vehicles if the waiting time is long.

As previously explained, a serious complication is faced by drivers who go through the Leste-Oeste and BR-101 (aka, Francisco Mota) roads, near UFERSA and UERN, during rush hours. The traffic lights in front of the entrance to UFERSA, which allows pedestrians to cross BR-101, located 300 meters from a roundabout which gives access to UERN, the city centre, and the city of Areia Branca is a key element for the whole traffic in the area. In fact, when the queue of vehicles waiting at the traffic lights reach the roundabout, it creates a traffic jam that blocks all the exits of the roundabout (to UERN, city centre, and Areia Branca). A zoomed version of Figure 1 is shown in Figure 4. The yellow path represents the most problematic area for traffic jams.

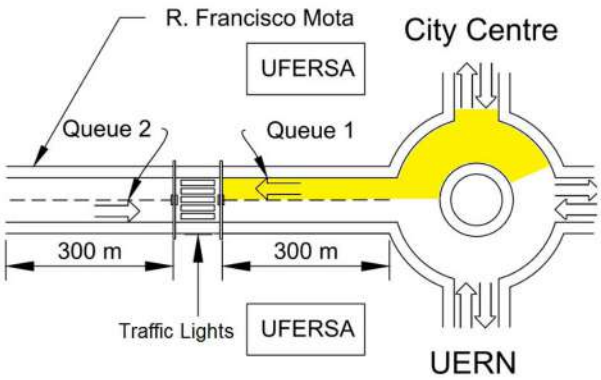

Fig. 4. Representation of the traffic system between UFERSA and UERN.

Based on this situation, we performed a case study in order to propose a solution to the risk generated when queue 1 reaches the roundabout blocking access to other directions.

The traffic lights located in front of UFERSA were implemented for the safety of pedestrians, specially people from the UFERSA community, since the university is divided into two campuses by BR 110 and students need to cross the road frequently to access different areas of the university.

Our proposal is based on the idea to automatically adjust the times of green and red at the traffic lights in order to avoid traffic jams in the area while allowing reasonable time for the crossing of pedestrians.

Another alternatives for this problem include the building of an elevated crossing platform or even a tunnel under the road. These alternatives, however, pose high costs and a considerable amount of time to be implemented.

The automatic adjust of the traffic light times is simple, economic, and can be efficient to tackle the problem. Moreover, the same situation is faced in several other crossing points and can also be tackled by our proposal with little adaptation.

Next, we detail the proposal.

4. PROPOSED METHOD

According to an on site evaluation, we defined two input variables to the fuzzy controller, both related to the size of the queues at the traffic lights. The output to the system is an increase or decrease value for the time of green of the traffic lights. Figure 5 shows the basic system, presenting the input variables, *Queue 1* and *Queue 2*, the output variable, *Variation*, as well as the adopted Mamdani Model.

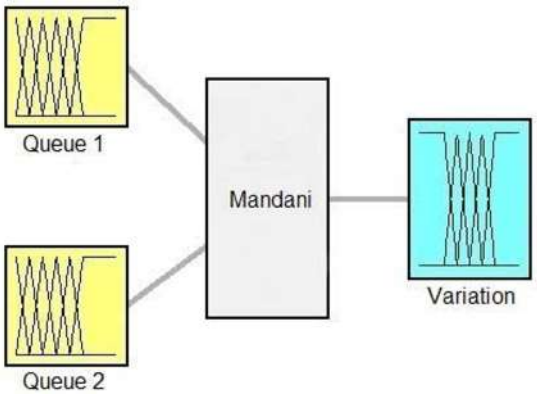

Fig. 5. Visualization of the inputs and output of the proposed fuzzy control system.

The domain of the input variables are related to the actual distance between the traffic lights and the roundabout, which is approximately 300 meters. For the construction of the rule set, we used the range of 0 to 75 meters, since there is a direct increase between the size of the queue and the time taken for the last car to move: the larger the queue size, the longer it takes to move, the larger it tends to become. This way, we considered that a queue larger than= 75 meters is the limit to set the variation of time to its maximum (20 seconds).

We empirically defined four triangular and one trapezoidal shaped fuzzy sets for this variable. The fuzzy sets are labelled as:

(1) Null: *F1-LLL*;
(2) Very Small: *F1-LL*,;
(3) Small: *F1-L*;
(4) Average: *F1-H*;
(5) Long: *F1-HH*;
(6) Very Long: *F1-HHH*.

The fuzzy labels are related to the size of the queue. Figure 6 presents variable *Line 1* defined in terms of 6 triangular-shaped fuzzy sets

978-3-902823-33-5/13/$20.00 © 2013 IFAC

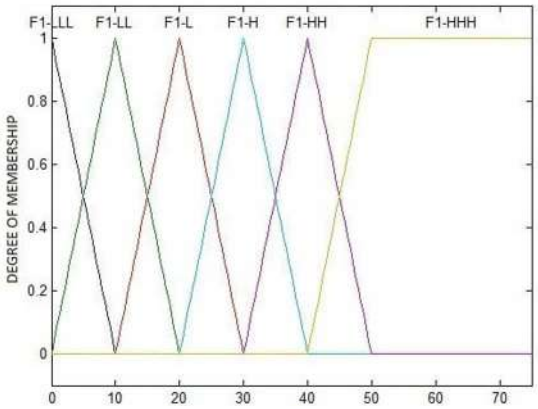

Fig. 6. Variable *Queue 1* defined in terms of fuzzy sets.

The second variable, *Queue 2*, represents the queue of vehicles formed on the opposite side of the traffic lights, roundabout-bound. The maximum size that it can reach is also approximately 300 meters. Nevertheless, the variable is limited to 75 meters. From that size, the queue is considered very long. The fuzzy labels of the variable are listed next.

(1) Null: *F1-LLL*;
(2) Very Small: *F1-LL,*;
(3) Small: *F1-L*;
(4) Average: *F1-H*;
(5) Long: *F1-HH*;
(6) Very Long: *F1-HHH*.

The second input variable of the systems is shown in Figure 7.

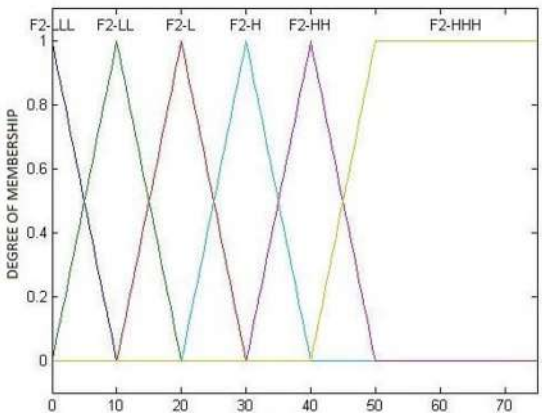

Fig. 7. Variable *Queue 2* defined in terms of fuzzy sets.

Table 1 presents the parameter values, in meters, for the input functions.

Table 1. Parameter values, in meters, for the input functions.

Fuzzy set	Queue 1	Queue 2
LLL	[-10, 0, 10]	[-10, 0, 10]
LL	[0, 10, 20]	[0, 10, 20]
L	[10, 20, 30]	[10, 20, 30]
H	[20, 30, 40]	[20, 30, 40]
HH	[30, 40, 50]	[30, 40, 50]
HHH	[40, 50, 75, 75]	[40, 50, 75, 75]

We set the variation of the time of green, *i.e.e*, the output variable, to plus or minus 20 seconds. This way, the time of green can be reduced in 20 seconds for short or null queues, as well as increased in 20 seconds for very long queues. Since the standard time of green is 60 seconds, the traffic lights will be opened for cars from the minimum of 40 seconds to the maximum of 80 seconds.

The output variable, *Variation*, was empirically defined with three triangular and two trapezoidal fuzzy sets:

(1) Big Reduction: *AJ-LL*;
(2) Small Reduction: *AJ-L*;
(3) No change: *AJ-M*;
(4) Small Increase: *AJ-H;*
(5) Big Increase: *AJ HH*.

The output variable is shown in Figure 8

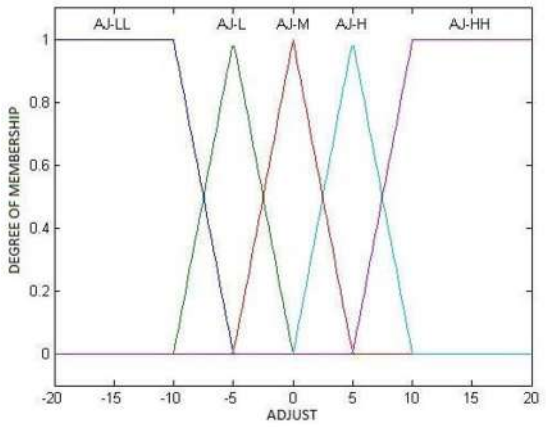

Fig. 8. Output variable representing the time variation for the traffic lights defined in terms of fuzzy sets.

Table 2 shows the parameters of the fuzzy sets the output variable.

Table 2. Parameter values, in meters, for the output variable.

Fuzzy Set	Variation
LL	[-20, -20, -10, -5]
L	[-10, -5, 0]
M	[-5, 0, 5]
H	[0, 5, 10]
HH	[5, 10, 20, 20]

Notice that variable *Queue 1* has a greater influence on the systems than *Queue 2*, since it is directly responsible for traffic jams at the roundabout. Thus, variable *Queue 1* is prioritized in the system by means of the fuzzy rule base, empirically defined.

The fuzzy rule base is shown in Table 3.

Notice that, according to the fuzzy logic, one or more rules might be triggered depending on the input values. The inference mechanism, however, is able to combine the triggered rules in order to provide a continuous output. This is done according to the centroid defuzzification method (Klir and Yuan, 1995), also known as mass centre or gravity centre. The defuzzification provides an exact amount of seconds to adjust the green time.

978-3-902823-33-5/13/$20.00 © 2013 IFAC

Table 3. Set of rules defined for the fuzzy control system.

Rule	Queue 1	Queue 2	Variation
1	-	H	H
2	-	HH	HH
3	-	HHH	HH
4	H	-	H
5	HH	-	HH
6	HHH	-	HHH
7	LLL	LLL	LL
8	LLL	LL	LL
9	LLL	L	LL
10	LL	LLL	LL
11	LL	LL	L
12	LL	L	L
13	L	LLL	LL
14	L	LL	L
15	L	L	M

To exemplify the inference process, let us consider there is a 15 meter queue in both directions of the traffic lights. According to the set of rules, 4 rules (11, 12, 14, and 15) are triggered. In this toy example, all rules present a 0.5 membership degree.

These rules can be read as follows.

(1) If ***Queue 1*** is *Very small* and ***Queue 2*** is *Very small*, then ***Variation*** is *Small*
(2) If ***Queue 1*** is *Small* and ***Queue 2*** is *Very small*, then ***Variation*** is *Small*
(3) If ***Queue 1*** is *Small* and ***Queue 2*** is *Very small*, then ***Variation*** is *Small*
(4) If ***Queue 1*** is *Small* and ***Queue 2*** is *Small*, then ***Variation*** is *Medium*

Using the output fuzzy sets of the triggered rules (Small and Medium), the inference mechanism calculates the number of seconds to adjust the green time of the traffic lights. In this case, the green time is reduced in 2.495 seconds.

Figure 9 shows the control surface obtained from the set of rules. As an example, a specific point is selected in the control surface, presenting a variation of 6.413 seconds for an input of 26.79 meters for *Queue 1* and 32.14 meters for *Queue 2*.

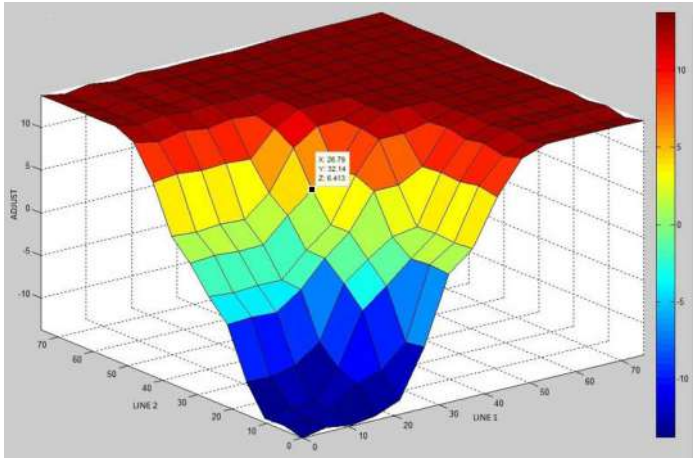

Fig. 9. Visualization of the control surface.

From the decision surface it is possible to notice that the greem time is reduced or kept the same for queues smaller than 25 meters, allowing a larger flow of vehicles, while for larger than 25 meters, the green time is augmented, allowing pedestrians to cross the road with a smaller waiting time.

Next, we present the experiments and results.

5. EXPERIMENTS AND RESULTS

Following the design of the system, *i.e.*, the definition of the variables, fuzzy data base, and fuzzy rule base, the system was simulated using a commercial software package, MATLAB (MATLAB, 2010).

For the simulations, we used an extensive set of values for *Queue 1* and *Queue 2* , in order to determine the variation of the green light. Notice that the system is proposed to update the green time at previously defined intervals in order to keep the queues at reasonable sizes, as well as the waiting time for pedestrians to cross the road.

Table 4 presents 38 of the simulation results. For space reasons, notice that the name of the variables are abbreviated. The columns representing the simulation number are light-gray shaded.

Table 4. Results of the simulations for different queue sizes.

#	Q 1	Q 2	Var	#	Q 1	Q 2	Var
1	1	1	-13.214	20	39	39	13.214
2	3	3	-12.04	21	41	41	13.658
3	5	5	-10.714	22	43	43	13.436
4	7	7	-9.077	23	45	45	13.205
5	9	9	-6.742	24	47	47	13.436
6	11	11	-4.33	25	49	49	13.658
7	13	13	-3.322	26	51	51	13.766
8	15	15	-2.495	27	53	53	13.766
9	17	17	-1.668	28	55	55	13.766
10	19	19	-0.659	29	57	57	13.766
11	21	21	0.659	30	59	59	13.766
12	23	23	1.668	31	61	61	13.766
13	25	25	2.495	32	63	63	13.766
14	27	27	3.322	33	65	65	13.766
15	29	29	4.33	34	67	67	13.766
16	31	31	6.742	35	69	69	13.766
17	33	33	9.077	36	71	71	13.766
18	35	35	10.714	37	73	73	13.766
19	37	37	12.04	38	75	75	13.766

The tests shown in Table 4 start from a queue representing one vehicle (1 meter), to the maximum size of queue the system considers, which is the limit of the domains of the input variable (75 meters). In this work we consider that the limit of 75 meters of queue is enough for about 20 cars.

Notice that, although the output variable, *Variation*, ranges from -20 to 20 seconds, the results of the system, see Table 4, range from -13.214 to 13.766 seconds. This is due to the defuzzification step which is calculated using the mass centre of the triggered fuzzy sets, considering the membership degrees achieved for the fuzzy sets of the triggered rules.

Although the maximum and minimum variations are not achieved, this does not pose a problem for the efficiency

978-3-902823-33-5/13/$20.00 © 2013 IFAC

of the system, since, as previously explained, the variation of green time is calculated constantly in order to adjust the queues before they reach an inadequate size. In other words,

The results obtained can be considered satisfactory as an alternative to more costly solutions. The gradual variation in the increase or decrease of the green time allows the system to avoid the formation of long queues.

Nevertheless, it is important to observe the fact that it is impossible to always avoid the formation of long queues, since the variables in question are not independent. In other words, it is not possible to open the traffic lights for cars until the queue is considered suitable while blocking the crossing of pedestrians indeterminately.

6. CONCLUSION AND FUTURE WORK

Traffic problems have presented a fast growth in the last years due to the increasing number of vehicles in the cities. Pedestrians are also affected by the number of vehicles.

In this work, we present a proposal to tackle the problem faced in Mossoro, more specifically, in the UFERSA and UERN area. The problem consists of a crossing point for pedestrians controlled by traffic lights, which is the bottleneck of the traffic system in the region. The traffic lights are located 300 meters from a roundabout which is blocked when the queue of vehicles that go towards the traffic lights reaches it.

The proposal consists of a fuzzy control system to adjust the green time of the traffic lights during rush hours, according to the queue of vehicles. The system was modelled using two input variables, related to the size of the queues in both sides of the traffic lights, and an output variable representing the adjustment of time for green. The output variable is responsible for the increase or decrease of the green time of the traffic lights.

The proposed fuzzy controller was simulated using MATLAB and presented promising results. The fuzzy controller allows a gradual transition between the largest decrease and the largest increase, which contributes to avoid the formation of long queues in the traffic lights.

As future work, we intend to further investigate the system in order to collect statistical data on the flow of vehicles in the area to be able to perform more accurate simulations. We also intend to present the proposal to the local traffic engineering secretary and investigate the possibility of its real implementation.

REFERENCES

Banks, W. and Hayward, G. (1993). Fuzzy logic in embedded microcomputers and control systems. URL `http://goo.gl/gBl3a`. Byte Craft Limited.

CET (2012). Pedestrians wait less time to cross in 1.047 traffic lights of sao paulo. CET - Traffic Engineering Centre. URL `http://goo.gl/OlpW7`.

Cintra, M.E., Monard, M.C., and Camargo, H.A. (2011). Fuzzy and classic rule learning methods: a comparative analysis. In *World Conference on Soft Computing, 2011*, volume 1, 182–190.

Cintra, M.E., Monard, M.C., Camargo, H.A., and Martin, T.P. (2012). A hybrid approach for the automatic generation of fuzzy systems using fuzzy formal concepts. In *2012 IEEE International Conference on Fuzzy Systems (FUZZ-IEEE 2012)*, volume 1, 1784–1791.

DETRAN-RN (2012). Distribution of the vehicle fleet of rio grande do norte according to car type. (in Portuguese).

Dumitrescu, D., Lazzerini, B., and Jair, L. (2000). *Fuzzy Sets and Their Application to Clustering and Training*. Int. Series on Computational Intelligence. CBC Press.

Haruki, T. (1992). Video camera system using fuzzy logic. *Consumer Electronics, IEEE Transactions on*, 38, 624–634.

Klir, G.J. and Yuan, B. (1995). *Fuzzy Sets and Fuzzy Logic - Theory and Applications*. Prentice-Hall.

Koga, C.A., Massette, G.V., and Travensolli, W.P. (2012). Controlador fuzzy de semforos. Universidade Tecnolgica Federal do Paran. 63p (in Portuguese).

MATLAB (2010). *version 7.10.0 (R2010a)*. The MathWorks Inc., Natick, Massachusetts.

Mehta, S. (2008). Fuzzy control system for controlling traffic lights. In *Proceedings of the International MultiConference of Engineers and Computer Scientists*, volume 1, 19–21.

Pappis, C.P. and Mamdani, E.H. (1977). A fuzzy logic controller for a traffic junction. *IEEE Transactions on Systems, Man, and Cybernetics*, 7-10, 707–717.

Pedrycz, W. (1996). *Fuzzy Modelling: Paradigms and Practice*. Kluwer Academic Press.

Pedrycz, W. (1998). *Computational Intelligence: An Introduction*. CRC Press.

Rentera, A.R. (2002). *Controle de semforos por lgica fuzzy e redes neurais*. Master's thesis, Electric Engeneering Department - Universidade Catlica do Rio de Janeiro.

Simoes, M.G. and Shaw, I.S. (2007). *Fuzzy Control and Modelling*. Blucher. (in Portuguese).

Zadeh, L. (1965). Fuzzy sets. *Information and Control*, 8, 338–353.

978-3-902823-33-5/13/$20.00 © 2013 IFAC

Solution of Equations of State and Output Feedback for a Line Transmission Via Invariant Subspaces

Clayton A. M. Oliveira*, Elmer R. L. Villarreal, Reuber R. Melo*****

**Graduate in Communication and Automation Systems, Universidade Federal do Semi-Árido, UFERSA, Av. Francisco Mota, 522, Mossoró/RN, CEP: 59625-900.*
Instituto Federal de Educação, Ciência e Tecnologia do Rio Grande do Norte, IFRN, Câmpus Mossoró/RN, Rua Raimundo Firmino de Oliveira, 400, Costa e Silva, Mossoró/RN, CEP: 59628-330 (e-mail: clayton.miranda@ifrn.edu.br).
***Department of Exact and Natural Sciences, Universidade Federal do Semi-Árido, UFERSA, Av. Francisco Mota, 522, Mossoró/RN, CEP: 59625-900 (e-mail: elmerllanos@ufersa.edu.br).*
****Graduate in Communication and Automation Systems, Universidade Federal do Semi-Árido, UFERSA, Av. Francisco Mota, 522, Mossoró/RN, CEP: 59625-900 (e-mail: reuberegis@gmail.com).*

Abstract: The objective of this paper is to find a solution by output feedback static for state matrices representing a transmission line whose parameters longitudinal do not take into account the effects of frequency. The transmission line is represented by a cascade of π circuits, and the results presented are based on the concept of (C, A, B)-invariance and on the coupled Sylvester equations. We present algorithms for computation of the output feedback matrix based on eigenvalues assignment techniques. The simulations are performed in MATLAB.

Keywords: Transmission line models, Output feedback, Linear systems.

1. INTRODUCION

The models of transmission lines of electric energy can be developed in the time domain or in the frequency domain. However, the electrical system in which the transmission lines are inserted, has several elements whose characteristics do not allow them to be represented as linear elements, making the representation of the electrical system in the frequency domain (Marti, 1988). Another advantage of models that represent the line directly in the time domain is that they are easily implemented in computational programs which perform simulations of electromagnetic transients in power systems.

In situations where it is desired to simulate the propagation of electromagnetic waves resulting from switching and operations maneuvers performed on transmission lines, we can represent them as being a cascade of circuit π. This model considers the line as being a large number of small line segments, and that each of these small segments is represented by a π circuit consisting of resistors, inductors and capacitors (Tavares, 1999). This model, which is developed directly in the time domain, is then implemented in software type EMTP.

Due to the fact that the EMTP type programs are not easy to use, many authors (Mamis, 2003; Mácias, 2005) suggest describe the currents and voltages in the cascade π circuit through state variables. The state equations are then transformed into difference equations and can be solved using any computational language.

Therefore, the state space model for the transmission lines is introduced into the electric system model for studies of transient with depicted in Fig. 1, where tensions are inputs to the model, and after interact with the states, result in the currents injected into the bar (Lemos, 2008).

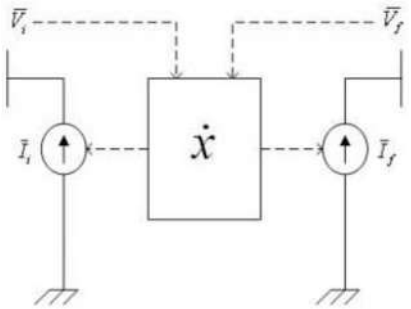

Fig. 1. Representation of the line per the state space.

It is known that a transmission line, whose parameters can be considered independent of frequency, can be represented, in an approximate way and obeying a series of restrictions, as being a cascade of circuits π (Charantola, 2007).

The Fig. 2 shows a single-phase transmission line of length *d* represented by *n* circuits type π connected in cascade.

978-3-902823-33-5/13/$20.00 © 2013 IFAC

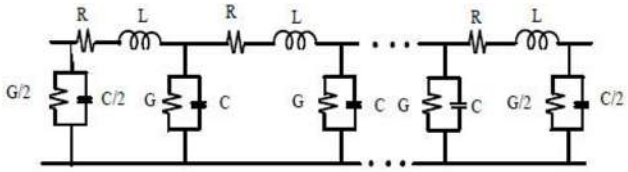

Fig. 2. Line represented by a cascade of *n* circuits type π.

In Fig. 2 the parameters *R* and *L* are, respectively, the resistance and inductance longitudinal of the line and the *G* and *C* parameters are respectively the conductance and capacitance transverse. These parameters are written as:

$$R = R'\frac{d}{n}; \qquad L = L'\frac{d}{n} \tag{1}$$

$$G = G'\frac{d}{n}; \qquad C = C'\frac{d}{n} \tag{2}$$

In equations (1) and (2) the terms R', L', G' and C' are the parameters of the line per unit length.

The representation of the line per means of state variables can be utilized in teaching basic concepts of wave propagation in transmission lines, in the analysis of the distribution of currents and voltages along the line and in the simulation of electromagnetic transients in transmission lines that have elements non-linears (Mamis, 2003; Kurokawa, 2007).

This type of representation presents advantages compared to representation by differential equations, since they, generally, are difficult to obtain, when taking into account the line losses.

Thus, the longitudinal current and the transverse voltage of the line represented by a cascade of π circuits, shown in Fig. 2, can be written in the form of equations of state, ie:

$$[\dot{X}] = [A][X] + [B]u(t) \tag{3}$$

In equation (3), [X] is the vector with state variables, while [A] and [B] are matrices of state of the circuit shown in Fig. 2.

For solution of equation (3), there are several numerical methods that can an approximation of exact solution of a differential equation. Examples of numerical methods of resolution, we can cite: Method of Euler, Heun formula (Trapezoid Rule) and the Method of Runge-Kutta (Charantola, 2007).

In this paper, we propose a solution to the equation of state of a transmission line by using control techniques, which allow the transmission line parameters may be controlled by altering its closed loop poles.

The method used is commonly called pole assignment technique, where it is assumed that all state variables are measurable and available for feedback. If the system is completely controllable, then the closed-loop poles can be located in any desired positions by means of state feedback through a feedback gain matrix of state appropriately (Ogata, 2010).

2. POLES PLACEMENT FOR THE CONTROL IN STATE SPACE.

As from the representation by equations of state, we have that the representation of transmission lines can be represented by a linear time-invariant system described by Ogata, 2010:

$$\dot{x}(t) = Ax(t) + Bu(t) \tag{4}$$

$$y(t) = Cx(t) \tag{5}$$

where: *x* = state vector (vector *n*); *y* = output signal (scalar); *u* = control signal (scalar); A = constant matrix *n* x *n*; B = constant matrix *n* x 1; C = constant matrix 1 x *n*.

We want to choose a control signal type:

$$u(t) = -Ky(t) \tag{6}$$

that representing a static output feedback with the feedback gain matrix of states K 1 x n. This matrix K is found from the desired closed loop poles from transient response requirements and / or the frequency response, such as response speed, damping coefficient, maximum overshoot, or bandwidth, as well as the requirements for system stationary (Ogata, 2010). Substituting (6) in (4) have:

$$\dot{x}(t) = (A - BK)x(t) \tag{7}$$

The matrix of gain K of state feedback forces the eigenvalues of A – BK to be λ_1, λ_2,..., λ_n (desired values). The stability and characteristic of time response are determined by these eigenvalues. If the matrix K is chosen correctly, the matrix A – BK can be asymptotically stable and, for all x(0) ≠ 0, you can do *x(t)* to tend to *0*, as *t* to tend to infinity (Ogata, 2010).

It is worth mentioning that there a necessary and sufficient condition for arbitrary allocation of poles: the system must be completely controllable.

There are many methods for determination the matrix K, as the use of direct substitution method, more indicated for low-order systems ($n \leq 3$), or even with the use of the matrix of transformation T. The MATLAB program can also be used to solve problems of pole placement using simple commands.

Another way to solve this type of problem, addressed in this paper, is with the use of Sylvester equations. Considering the equations (4) and (5), where we have: $x \in \Re^n, u \in \Re^m, y \in \Re^p$, and A, B and C are constant matrices where B is of full rank by columns (rank of B = m) and C is of full rank by lines (rank of C = p) (Villarreal, 2010). Thus, we can find a law control of the type of static output feedback:

$$u(t) = Ky(t), \qquad K \in \Re^{m \times p} \tag{8}$$

such that the closed-loop system has the following form:

$$\dot{x}(t) = (A + BKC)x(t), \;\; y(t) = Cx(t) \tag{9}$$

978-3-902823-33-5/13/$20.00 © 2013 IFAC

and be asymptotically stable, ie $\sigma(A + BKC) \in C^-$, where $\sigma(A + BKC) = \{\lambda_1, \lambda_2, \ldots, \lambda_n\}$ is the set of eigenvalues of $A + BKC$.

3. INVARIANT SUBSPACES AND COUPLED SYLVESTER EQUATIONS

As in Syrmos and Lewis, 1994, are used some concepts and definitions on geometric control theory (Wonahm, 1979). It is known that a subspace $V \subset X$ é (A,B)-invariant if there exists $F : X \rightarrow Y$ such that $(A + BF)V \subset V$, or equivalently, $AV \subset V + ImB$. By duality, a subspace $T \subset X$ is (C,A)-invariant if exists $L : Y \rightarrow X$ such that $(A + LC)T \subset T$, or equivalently, if $T \supset A(T \cap Ker\,(C))$.

Definition 3.1 *(Syrmos and Lewis, 1994) A subspace $V \subset X$ of dimension v, is (C, A, B)-invariant if V is (A, B)-invariant and (C, A)-invariant.*

Consider $V \in \Re^{v \times v}$ such that $Im(V) = V$ and let $T \in \Re^{(n-v)\times v}$ be a left annihilator of V *i.e., Ker (T) = Im (V).*

$$AV - VH_V = -BW \tag{10}$$

$$TA - H_T T = -UC \tag{11}$$

$$TV = 0 \tag{12}$$

The definition 3.1 and equations (10), (11) and (12) have a crucial importance in the static output feedback by eigenvalues assignment (Syrmos and Lewis, 1993, 1994). This study takes into account the properties of stabilizability and detectability through the two following definitions:

(i) a subspace *(A, B)*-invariant V is *(A, B)*-inner stabilizable subspace, if there exists F such that $(A + BF) \mid V$ is asymptotically stable, and

(ii) a subspace *(C, A)*-invariant V is *(C, A)*-outer detectable subspace if there exist L such that $(A + LC)|X/V$ is asymptotically stable.

Definition 3.2 *(Syrmos and Lewis, 1994) A subspace V of dimension v, is (C, A, B)-invariant stabilizable by output (or simply O.S. (C, A, B)-invariant) if V is (A, B)-inner stabilizable and (C, A)-outer detectable.*

Thus, a necessary and sufficient condition for the existence of a subspace $V = Im(V)$ or *O.S. (C, A, B)*-invariant that (10), (11) and (12) are verified with the additional conditions of stability:

$$\sigma(H_V) \in C^- \tag{13}$$

$$\sigma(H_T) \in C^- \tag{14}$$

The following theorem relates the concept of subspaces O.S. (C, A, B)-invariant to the existence by a control law as a static output feedback (3), which stabilizes the closed-loop system.

Theorem 3.1 *There exists a matrix of feedback static output $K : Y \rightarrow U$ such that $\sigma(A + BKC) \in C^-$, if and only if the following conditions hold true for some matrices $V \in \Re^{n\times v}, H_V \in \Re^{v\times v}, W \in \Re^{m\times v}$), $(T \in \Re^{n-v\times n}, H_T \in \Re^{n-v\times n-v}, U \in \Re^{n-v\times v})$ and for some positive integer $v \leq n$:*

$$AV - VH_V = -BW, with\ \sigma(H_V) \in C^- \tag{15}$$

$$TA - H_T T = -UC, with\ \sigma(H_T) \in C^- \tag{16}$$

$$TV = 0 \tag{17}$$

$$Ker(CV) \subseteq Ker(W) \tag{18}$$

$$Ker(B'T') \subseteq Ker(U') \tag{19}$$

where: rank $(V) = v$ e rank $(T) = n - v$.

It is interesting to notice that these results have been presented and explored under different forms in the literature related to eigenvalues assignment by output feedback. The presented statement corresponds to Theorem 3.2 in Syrmos and Lewis, 1994. As seen, the coupled Sylvester Equations (15), (16) and (17) describe some geometric properties of this subspace $V = Im(V)$. Under the restriction imposed on the stability of the matrix H_V, the equation (15) means that the subspace $V = Im(V)$ must be (A,B)-inner stabilizable. In a dual manner, the subspace $Ker\,(T) = V$ must be (C,A)-outer detectable. Thus, under the coupling condition (17), the existence of a subspace $V = Ker\,(T)$ *O.S.* (C,A,B)-invariant, and the conditions (18) and (19), are necessary and sufficient conditions for existence of solution of the problem considered. Also note that the conditions (18) and (19) correspond to the existence of a matrix $K \in \Re^{m\times p}$ which verifies the following two equalities:

$$KCV = W \tag{20}$$

$$TBK = U \tag{21}$$

It is important to note that assured the existence of a solution to Sylvester Equations and that K has been obtained such that (20) (or 21) be verified, the closed-loop eigenvalues are given by:

$$\sigma(A + BKC) = \sigma(H_V) \dot{U} \sigma(H_V) \tag{22}$$

4. ALGORITHMIC ASPECTS

The conditions established in matrix in the Theorem 3.1 are nonlinear with respect to matrix variables (V, H_V, W, T, H_T, U). In particular, the nonlinear terms VH_V and $H_T T$ present in (15) and (16), respectively, can be linearized by setting the matrices H_V e H_T, or equivalently by setting the desired eigenvalues for the closed loop system.

In this section are presented a technique algorithmic that are based in the eigenvalues assignment to the output feedback motivated by the algorithm of Syrmos and Lewis, 1993, that solves the coupled Sylvester equations in two steps, and can directly be applied to systems that verify the condition Kimura (Kimura, 1975) $m + p > n$. In this proposed technique assume that the dimension $V = Im(V)$ is the same than p of the output, because, it is guaranteed that the matrix $CV \in \Re^{p\times p}$ is invertible, so that to ensure the existence of $K = W(CV)^{-1}$, see (20).

978-3-902823-33-5/13/$20.00 © 2013 IFAC

Further, it is considered that the system represented by (*C,A,B*) is controllable and observable, condition necessary for the arbitrary choice of the poles to be placed in close loop. However, this condition can be relaxed to stabilizability and detectability of (*C,A,B*), which implies the use of eigenvalues uncontrollable and unobservable in the desired spectrum for the closed-loop system.

The set of the desired poles is denoted by $\Lambda = \{\lambda_1, \ldots, \lambda_{n-p}, \lambda_{n-p+1}, \ldots, \lambda_n\} = \{\Lambda_T, \Lambda_V\}$ where Λ_T and Λ_V are auto-conjugated. $H_V \in \Re^{p\times p}$ and $H_T \in \Re^{(n-p)\times(n-p)}$ are defined as: $\sigma(H_T) = \Lambda_T = \{\lambda_1, \ldots, \lambda_{n-p}\}$ and $\sigma(H_V) = \Lambda_V = \{\lambda_{n-p+1}, \ldots, \lambda_n\}$. For simplicity, it is considered that the elements of $\Lambda = \sigma(A + BKC)$ are all distinct.

4.1 Syrmos and Lewis algorithm

Based on the Theorem 3.1, the following algorithm, considered in Syrmos and Lewis, 1993, is used to obtain an output feedback matrix that stabilizes the closed loop system, when the Kimura condition, $n < m + p$, is verified:

Step 1: Select the matrix $H_T \in \Re^{n-p\times n-p}$ such that $\sigma(H_T) = \Lambda_T \in C^-$, and solve the Sylvester equation (16) to find a matrix $T \in \Re^{n-p\times n}$, such that

$$rank\left(\begin{bmatrix}T\\C\end{bmatrix}\right) = n \Leftrightarrow Ker\ T \cap Ker\ C = \{0\} \qquad (23)$$

Step 2: Solve the Sylvester equation (15) for some matrix $H_V \in \Re^{p\times p}$ where $\sigma(H_V) = \Lambda_V \in C^-$ whereas the matrix V must satisfy the coupling condition (17) and $rank\ (V)$ must be equal to p.

Step 3: By construction, the relation (23) guarantees that rank $(CV) = p$ and the matrix K can be calculated as only solution of (20).

To follow, are a few observations with the double purpose of showing aspects of the numerical solution of the steps of the algorithm and justify them theoretically.

Remark 4.1: Steps 1 and 2 can be implemented by using standard techniques for eigenvalues assignment. By considering H_T and H_V in the diagonal form of Jordan, the following procedure can be adopted:

Step 1: Find $t_j \in C^n$ and $u_j \in C^p$, such that:

$$[t_j' \quad u_j']\begin{bmatrix}A-\lambda_j I\\C\end{bmatrix} = 0 \ \ \forall\, j = 1, \ldots, n-p \qquad (24)$$

The row matrix $T \in \Re^{(n-p)\times n}$, denoted for T_j, is constructed by using the vectors t_j, as follows:

- if $\lambda_j \in \Re$, then $T_j = t_j'$;
- if $\lambda_j \in C$, then $\lambda_{j+1} = \lambda_j^*$ and $\begin{cases} T_j = Re(t_j') \\ T_{j+1} = Imag(t_j') \end{cases}$

Step 2 : To determine $v_i \in C^n$ and $w_i \in C^n$ we have:

$$\begin{bmatrix}A-\lambda_i I & B\\ C & 0\end{bmatrix}\begin{bmatrix}v_i\\w_i\end{bmatrix} = 0 \quad \forall \ \ i = n-p+1, \ldots, n \qquad (25)$$

In similar form to the previous case, the matrices V and W used to calculate K can only be built with real elements. In particular, if $\lambda_i \in C$, it is considered $\lambda_{i+1} = \lambda_j^*$ and $\begin{cases} V_i = Re(v_i), V_{i+1} = Imag(v_i) \\ W_i = Re(w_i), W_{i+1} = Imag(w_i) \end{cases}$, where v_i and w_i denote the columns of the matrices V and W, respectively.

Remark 4.2: In the step 1, under the condition of observability (detectability) is always possible to choice of a matrix T, which verifies (24) and, therefore, guarantee obtain of K via (20). Once determined the matrix T, step 2 is associated with the combined solution of equations (15) and (17), to obtain the (A,B)-invariant of *Ker* (*T*). This property is associated to the "zero equation" (25). To guarantee that the eigenvalues λ_i be freely allocable in step 2, the system matrix $P(\lambda) = \begin{bmatrix}A-\lambda_i I & B\\ C & 0\end{bmatrix}$ of dimension $(2n - p) \times (n + m)$, must be row-full rank $\forall\lambda$. The algorithm is based in the fact that under Kimura condition $m+p > n$, $P(\lambda)$ does not lose rank for almost all triples (A,B,T) (Castelan and Hennet, 1993). Thus the zero equation (25) has solutions for all λ_i. In the presence of invariant zeros, it is possible to remake Step 1 to search other solutions for the Sylvester equation (15).

Remark 4.3: In the less restrictive case $m + p = n$, $P(\lambda)$ is a matrix square of dimension $(2n - p) \times (2n-p)$, and almost all triple (A,B,T) has p finite invariant zeros (Syrmos and Lewis, 1993). In this case, the basic procedure can produce a matrix of output feedback which stabilizes the close loop systems only if T matrix, found in step 1, generate p stable invariant zeros, which have to be used to solve (25) (Castelan and Hennet, 1993).

5. MODEL TEST TRANSMISSION LINE

Consider a single-phase transmission line with length d, energized by voltage source u(t) and with open terminal, as shown in Fig. 3, as in Kurokawa, 2007.

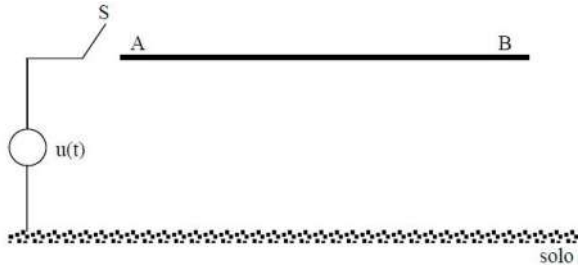

Fig. 3. Single-phase transmission line with open extremity B.

Disregarding the effect of frequency on the longitudinal parameters of the line and representing by two π circuits, there is circuit shown in Fig. 4 (Charantola, 2007).

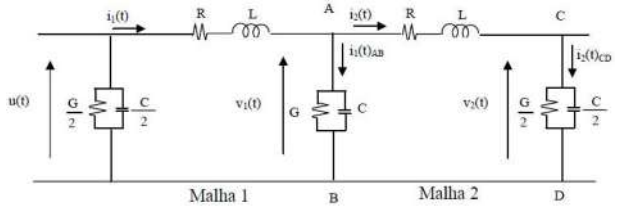

978-3-902823-33-5/13/$20.00 © 2013 IFAC

Fig. 4. Line representing by two π circuits

The Fig. 3 describe a single-phase line with length 10 Km. In the terminal A this line, is applied a constant voltage 20 KV, u(t) = 20 KV at instant t = 0.

The elements values R and L are obtained from the longitudinal parameters per unit. This parameters are shown in the Table 1 which also shows that the transverse parameters per unit of the line to determine the element G and C [3].

Table 1. Parameters of LT per unit

Parameters
R′ = 1,470 Ω/Km
L′ = 2,209 mH/Km
G′ = 0, 55 μS/Km
C′ = 11,11 μF/Km

Using this data is possible to build an equation of state as in (3) with the following matrices:

$$\mathbf{A} = \begin{bmatrix} -0.6700 & -0.0900 & 0 & 0 \\ 18.0000 & 0 & -18.0000 & 0 \\ 0 & -0.0900 & -0.6700 & -0.0900 \\ 0 & 0 & 36.0000 & 0 \end{bmatrix}$$

$$\mathbf{B} = \begin{bmatrix} 0.0900 \\ 0 \\ 0 \\ 0 \end{bmatrix}$$

5.1 Resolution by pole placement

The corresponding system, formulated earlier is controllable. The eigenvalues are arbitrarily chosen to position by: $\Lambda_T = \{-4,-3,-2,-1\}$.

In the MATLAB program can find the matrix of state feedback gain K (6) that resolves (7), through command ACKER. Hence the matrix K:

$$\mathbf{K} = \begin{bmatrix} 96.2222 & 15.7462 & -114.6024 & 12.1738 \end{bmatrix}$$

The matrix fed back assumes the following values:

$$\mathbf{A - BK} = \begin{bmatrix} -9.3300 & -1.5072 & 10.3142 & -1.0956 \\ 18.0000 & 0 & -18.0000 & 0 \\ 0 & -0.0900 & -0.6700 & -0.0900 \\ 0 & 0 & 36.0000 & 0 \end{bmatrix}$$

5.2 Resolution by Sylvester equations and by Syrmos e Lewis algorithm

For solving our model tests we inserts na entry in the matrix B and choose a matrix C, one of the following:

$$\mathbf{B} = \begin{bmatrix} 0.0900 & 0 \\ 0 & 0 \\ 0 & 0 \\ 0 & 1.0000 \end{bmatrix} \quad \mathbf{C} = \begin{bmatrix} -1 & 0 & 0 & -1 \\ 0 & 0 & 1 & 1 \\ 0 & 0 & 0 & 1 \end{bmatrix}$$

The corresponding system is controllable and observable and m+p = 5 > n, establishing the condition Kimura [9]. The eigenvalues are given by position: $\Lambda_T = \{-4\} \cup \Lambda_V = \{-3,-2,-1\}$.

Step 1: For $\lambda_1 = -4$, T is determined that verifies (24) and such that (A,B,T) has zeros invariant:

$$\mathbf{T} = \begin{bmatrix} 0.2504 & -0.0069 & -0.5555 & 0.0417 \end{bmatrix}$$

Step 2 : For $\lambda_2 = -3$, $\lambda_3 = -2$ and $\lambda_4 = -1$, V and W are determined using (25):

$$\mathbf{V} = \begin{bmatrix} -0.0263 & -0.0093 & 0.0046 \\ 0.0565 & -0.0693 & -0.0930 \\ -0.0232 & -0.0170 & -0.0108 \\ -0.1415 & -0.1824 & -0.1879 \end{bmatrix}$$

$$\mathbf{W} = \begin{bmatrix} 0.1530 & 0.0686 & -0.2133 \\ 0.9758 & 0.9782 & 0.9542 \end{bmatrix}$$

Step 3: K is determined such that KCV = W:

$$\mathbf{K} = \begin{bmatrix} 150.6101 & 278.4075 & -146.4646 \\ -64.4030 & -145.1280 & 85.6199 \end{bmatrix}$$

The closed loop matrix AK = A + BKC correspondent, whose eigenvalues are desired, it is

$$\mathbf{AK} = \begin{bmatrix} -14.2249 & -0.0900 & 25.0567 & -1.6800 \\ 18.0000 & 0 & -18.0000 & 0 \\ 0 & -0.0900 & -0.6700 & -0.0900 \\ 64.4030 & 0 & -109.1280 & 4.8949 \end{bmatrix}$$

6. CONCLUSION

Were presented in this paper a model of representation of transmission lines based on pi model, without taking into account the effects of frequency on the longitudinal parameters of the line. We represent the transmission line through equations of state, and simulated stability and behavior through feedback outputs.

It has also the concept of subspace *O.S.* (*C, A,B*)-invariant and its relation to solving the problem of stabilization using feedback outputs, via two Sylvester coupled equations.

It was found that the Syrmos and Lewis algorithm to pole placement via solution of the Sylvester coupled equations provided a satisfactory solution to the problem. Note was the fact that Syrmos and Lewis algorithm allow the solution to systems that verify the condition Kimura ($m + p > n$), which does not always happen in the representation of systems transmission lines.

A next article will explore the use of other forms of representation of transmission lines, which can be applied in its resolution algorithms for systems with invariant subspace with feedback output via pole placements and that verify the condition Kimura ($m + p > n$). And how this algorithm is applied to the case of projects of state observers be they of full order or of reduced order.

978-3-902823-33-5/13/$20.00 © 2013 IFAC

Another issue not discussed in this paper, is the definition of the types of actuators that should be used to change the parameters of the transmission line, so that the same operates within the requirements of the electric power system. We still have to research how to determine and define the types and configurations of electric power systems for which the equations of Sylvester and Kimura condition ($m + p > n$) together with the algorithm Syrmos and Lewis for pole assignment can be applied as a control solution suitable for power systems.

REFERENCES

Castelan, E. B. and Hennet, J. C. (1993). Eigenstructure Assignment for State Constrained Linear Continuos Time Systems. Automatica, vol. 28, number 3, pp. 605-611.

Castelan, E. B.; Hennet, J. C. and Villarreal, E. R. L. (2003). Quadratic Characterizacion and Use of Output Stablizable Subspace. IEEE Control System, vol. 48, number 4, pp. 654-660.

Charantola, D. J. (2007). Representação de Linhas de Transmissão Monofásicas por Meio de Variáveis de Estado: Comparação das Soluções Numérica e Analítica. UNESP – Campus de Ilha Solteira, Dissertação, São Paulo – SP.

Lemos, J. R. F. (2008). Modelagem de Linhas de Transmissão para Estudos de Transitórios Eletromecânicos. Politécnica UFRJ, Monografias, Rio de Janeiro – RJ.

Kimura, H. (1975). Pole Assignment by Gain Output Feedback. IEEE Trans. Automatic. Control, vol. 20, number 4, pp. 509-516.

Kurokawa, S.; Yamanaka, F. N. R.; Prado, A. J.; Bovolato, L. F. and Pissolato, J. (2007). "Representação de Linhas de Transmissão por Meio de Variáveis de Estado Levando em Consideração o Efeito da Frequência sobre os Parâmetros Longitudinais" – Revista Controle & Automação, vol. 18, nº 3.

Macías, J. A. R.; Expósito, A. G. and Soler, A. B. (2005). A Comparison of Techniques for State-space. Transient Analysis of Transmission Lines. IEEE Trans. On Power Delivery, vol. 20, nº 2, pp. 894-903.

Mamis, M. S. (2003). Computation of Electromagnetic Transients on Transmission Lines with Nonlinear Components. IEEE Proc. General Transmission and Distribution, vol. 150, n º 2, pp. 200-203.

Marti, J. R. (1988). Simulation of Transientes in Underground Cables with Frequency-dependent Modal Transformation Matrices. IEEE Trans. On Power Delivery, vol. 3(3), pp. 1099-1110.

Ogata, K. (2010). Engenharia de controle moderno. 5ª Edição, Pearson Prentice Hall, São Paulo – SP.

Syrmos, V. L. and Lewis, F. L. (1994). Bilinear Formulation for the Output Feedback Problem in Linear System. IEEE Trans. Automatic. Control, vol. 39, number 2, pp. 410-414.

Syrmos, V. L. and Lewis, F. L. (1993). Output Feedback Eigenstructure Assignment Using Two Sylvester Equations. IEEE Trans. Automatic. Control, vol. 38, number 3, pp. 495-499.

Tavares, M. C.; Pissolato, J. and Portela, M. C. (1999). Quasi-modes Multiphase Transmission Line Model. Electric Power Systems Research, nº 49, pp. 159-167.

Villarreal, E. R. L.; Vargas, J. A. R. and Hermerly, E. M. (2009). Static Output Feedback Stabilization using Invariant Subspace and Sylvester Equations. TEMA – Tendências em Matemática Aplicada e Computacional, vol. 10, nº 1, pp. 99-110.

Wonahm, W. M. (1979). Linear Multivariable Control, a Geometric Approach. 2nd edition, Springer-Verlag, New York.

978-3-902823-33-5/13/$20.00 © 2013 IFAC

11th IFAC Workshop on Intelligent Manufacturing Systems
The International Federation of Automatic Control
May 22-24, 2013. São Paulo, Brazil

New Approach in Building Supervision Systems, Automation and Control Based on ARM

Melo, R. R. * **Caratti Filho, E.** * **Casillo, D. S. S.** **
Villarreal, E. R. L. **

* *Mestrado em Sistema de Comunicação e Automação, Universidade Federal Rural do Semi-árido, UFERSA, 59625-900, Mossoró, RN,Brasil (e-mail: reuberegis@gmail.com, edmigiofilho@gmail.com).*
** *Depto de Ciências de Exatas e Naturais, DCEN,Universidade Federal Rural do Semi-árido, UFERSA, 59625-900, Mossoró, RN,Brasil(e-mail: elmerllanos@ufersa.edu.br, danielle@ufersa.edu.br)*

Abstract: A new approach to developing solutions and tools for the automation of general use is presented in this paper using as a basis a device formatted with ARM 11 processor encapsulated in a motherboard of low cost. A comparison with conventional solutions for control and data acquisition, microcontrollers based on this processor offers greater possibility of features and flexibility, with an overall design for reliability, durability and ease of installation. Thus this paper aims to present a new approach that consists in dividing into modules the ARM microcontroller functionality, leaving application level to end user. So, this proposal allow facilitate the building of a system for automation, supervision and control. The modules are independent Android applications, each one with specific functions.

Keywords: Embedded Systems, Scheduling and Control, Industrial Applications

1. INTRODUCTION

In the past years before the personal computer (PC) was widely incorporated into industrial automation systems, all the faults that occurred in industrial processes were checked and dealt with by trained or experienced operators. In recent decades, this picture has been dramatically changed due to the wide adoption of industrial PC in a wide range of industrial applications.

The combination of emerging information technologies with traditional condition monitoring systems allows for the continuous running status monitoring for essential equipment as well as comprehensive data processing and centralized resource management. It will significantly enhance the working efficiency of system operators and decision-makers. As a result, developing such systems with the aforementioned characteristics for achieving full industrial automation has a positive practical significance in both economy and technology perspectives Wang and Tan (2006).

Advances in the development of programs related to automation were also important, including the FORTRAN programming language (1955), the APT programming language for numerical control (NC) machine tool (1961), operation system (UNIX) (1969), the VAL language for programming robots (1979), Microsoft Windows (1985) and the Java programming language (1995). The advances and improvements of these technologies remain Groover (2007).

Currently there are a lot of equipment solutions for industrial automation, residential and vehicular. All these solutions follow industry standards and technical standards. The Micro Control Unit (MCU) was originally developed to equipment controls for various applications such as industries, household equipment such as TV, video games and elevator control Wan et al. (2010).

Earlier the language assembly was the usual by being native of this compact devices. With the emergence of compilers for languages like C and other high-level languages, there was an improvement in hardware devices, software and programming environments to reach the goal of this work. Many academic papers propose the use of 32bit MCUs in the automation systems design, such as ping Li (2010), Ruimei and mei (2010), Xu et al. (2006), Anish (2012).

Following this line of research and technological trend, the purpose of this work is to develop objective solutions and tools for automation of general use, using as a basis a device formatted with ARM 11 processor encapsulated in a motherboard at low cost. This equipment allows to be used with Linux, Windows CE and Android.

The aim of the proposal is to develop modules of independent programs, each block has a very specific function to handle an appeal board ARM 11, making this feature to be handled by the developer in high-level programming. This new approach behind the interaction of computing, breaking the paradigm of conventional solutions in automation.

978-3-902823-33-5/13/$20.00 © 2013 IFAC

2. NEW APPROACH OVERVIEW

The new approach uses a RISC microprocessor S3C6410, designed by Samsung to provide a low cost, low power consumption and high performance capabilities of the processor solutions and mobile phones and general applications Gao and Zhao (2012). A striking feature of the S3C6410 is your CPU core , an ARM 11 processor RISC 32-bit (533MHz) designed by Advanced RISC Machine, Ltd. The processor has low power consumption and small size and high yield and a response in real-time interrupt ping Li (2010). A controller based on ARM processor can handle much more control tasks than conventional controllers versions. The board development kit with the ARM processor is shown in Fig. 1.

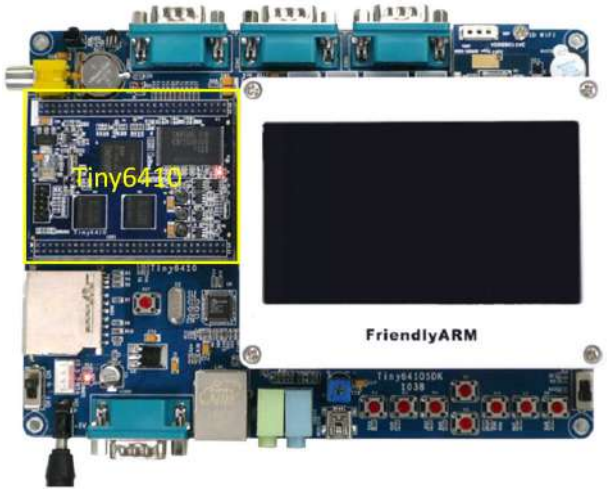

Fig. 1. FriendlyARM board for development on ARM

The Tiny6410 CPU board uses 2GB Nand flash memory for storage and 256MB of SDRAM CoreWind (2013). It features the Android operating system to implement the programs.

There are several types of board that can be attached to the motherboard and applied for numerous tiny6410 need, so for this paper we used a kit attached to the motherboard that already consists of features such as: four RS232 ports, two USB ports, touch LCD, SD Driver card, Ethernet buttons among others. In the case of applications that require ruggedness industrial developer can have multiple configurations market already ready.

The development of this work also includes the functionality in industrial applications considering both the physical robustness and all patterns of electric signals pertaining to the sensors and elements general for this kind of automation. To be compatible with these signal patterns industrial technology was developed by EGM (2013) one board being coupled ARM board. So this EGM board works as a board driver so that any element that make up the industrial automation as sensors, transducers and actuators, connect to it due to its ability to work with standard industrial signals. Communication between boards can be easily used to construct automation system via a proposed new approach to work. This physical construction is illustrated in Fig. 2.

Fig. 2. Physical structure the coupled boards

For communication between boards was made a network using I2C protocol, which is high performance and easy development and is a standard microcontroller and technologies in small electronic devices.

All this building will serve as a physical basis for the development of a group of programs developed for the Android platform, which will be installed on board ARM 11 Tiny 6410. So, are presented in high-level access and control to all elements actuators and industrial sensors. Is also presented modules (programs) with resources for developing logic and algorithm, access to databases and communications with other devices using RS232 and Ethernet physical means. These modules will be detailed in section 5.

3. DATA ACQUISITION AND TRANSDUCER

The board illustrated in Fig. 3 is used to perform the conversion of signals industrial standards concerning sensors, digital inputs and outputs, and proportional. This board uses a PIC18F452 microcontroller and communication with the ARM11 motherboard (Tiny 6410) is made with I2C protocol.

Fig. 3. Converter board industry standard

The firmware developed for the PIC18F452 interacts controlling the states of the following channels of plate technology EGM: 5 relay outputs that are ready, two PWM outputs proportional, 4 digital input simple optocouplers with 3 inputs, 4 analog inputs 10bits of 4 to 20mA or 0 to 10V, output transistor 1 and 8 digital outputs 0-5 V.

978-3-902823-33-5/13/$20.00 © 2013 IFAC

Using this board was deliberate, because she have 7 years in the oil and gas (onshore Brazil) and acting exactly directed to industrial automation and production surveys. An example of using this board in tackling this reading weight nonlinear described in Caratti Filho et al. (2012).

4. NEW APPROACH DESIGN

The structure of this new approach is to divide into modules the ARM microcontroller functionality . The main objective is to facilitate the development of building automation systems, supervisory control and bringing these features to application level. The modules are in fact Android applications independent , each with specific functions. The important point of this concept is that the tools modulated can reach any level of development so much for working on developing native language C or JAVA for example, or simply using the tool group proposed in this work. The modules are illustrated in Fig. 4.

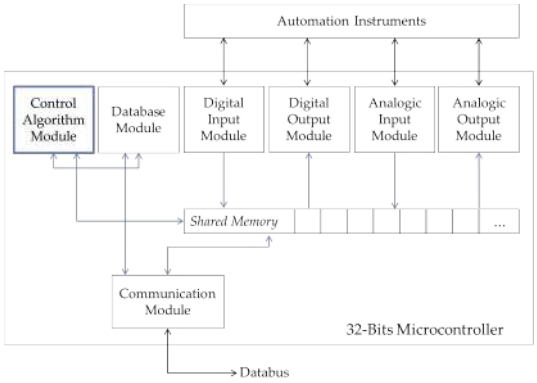

Fig. 4. Modular structure of the new approach

4.1 Inputs and Outputs Modules

The inputs and outputs module are elementary applications in automation. They make direct communication with the Android operating system the physical addresses of the ports for the ARM 11 microcontroller. These applications are the input and output module, analog and digital, leading the developer to have quick and easy to understand, demystifying and opening access through manipulation of variables (positions) shared memory, using a techniques known as "Shared Memory". Fig. 5 shows the schematic operation of inputs and outputs modules.

The modules are divided into four: AIM (analog input module), DIM (digital input module) AOM (analog outputs module) and DOM (digital output module) . These modules have the task to only communicate with automation tools, ie, act or acquire data on these instruments are the ports that can be physically with sensors, switches, solenoids, valves, proportional PWM among others, constantly accessing These four modules positions shared memory (Shared Memory). Thus one input module, for example, performs a read on a tool automation and writes that value into a shared memory location. Since the output module performs readings from a position of shared memory and sends this value to the actuator instrument automation. This strategy of using a shared memory allows another module access the information of inputs and

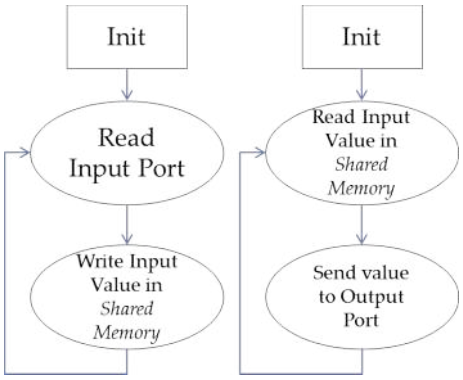

Fig. 5. Inputs and Outputs Modules Operations

outputs. The Fig. 6 show interface android for inputs and outputs modules.

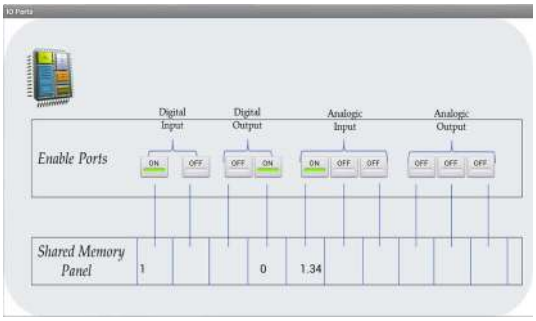

Fig. 6. Android Interface for Inputs and Outputs Modules

4.2 Database Module

The database module has the function of creating SQLite databases. The SQLite database is supported by a Android system and database created by this module can also be used by the module control algorithm, in order to back up information from automation.

In the database developer will store data according to the logic of its design and automation. When working with database developer gets all the benefits of performance, security, intrinsic operations, SQL statements, queries, filters, queries and other advantages.

4.3 Control Algorithm Module

In this module the user can observe values of shared variables that represent the physical inputs, and also develop a sequence of rules that schedules in the states of shared variables that represent the outputs can be changed through a set of rules, timers, logic, arithmetic among others. The developer will then dispose of module creation and will be the heart of manipulating variables and logic outputs, then the developer will have the input variables and outputs, teams of them, counters, variables, mathematical instructions, handlers database variables data, in order, this automation module will be developed from the data flow in previously planned project.

However the proposal to create applications with diverse functions makes this idea to have comprehensive solutions and conceptually simple since it has the android application level, the physical manipulation of the data from the

978-3-902823-33-5/13/$20.00 © 2013 IFAC

microcontroller. The Fig. 7 shows a small applying reading voltage of a solar panel using the proposed approach.

Fig. 7. ARM board and EGM board for read of solar panel

In this application the voltage readings of the solar panel are held by the board EGM. The board EGM send those values through I2C for ARM board which has the android applications. The Fig. 8 shows a simple Android application to keep the voltage read.

Fig. 8. Android Interface for voltage read in solar panel

4.4 Communication Module

The evolution of communication systems propose the use of industrial Ethernet in automation level of the shop floor level (usually referred to as "device level"), which is performed to transfer data between controllers and sensors / actuators Ruimei and mei (2010).

For this work proposes a new approach to the control system, automation and supervision is on a dedicated LAN as shown in Fig. 9. This system structure causes the layers of management and monitoring of automation of data access layers basic control and acquisition directly, differentiating the conventional structure of automation.

This module lets you choose the mode by which the physical system data can travel. The means may be by RS-232/485 serial port interface or Ethernet, and this last is considered the ARM device on a LAN. From this module you can access the variables of Shared Memory or data in the database.

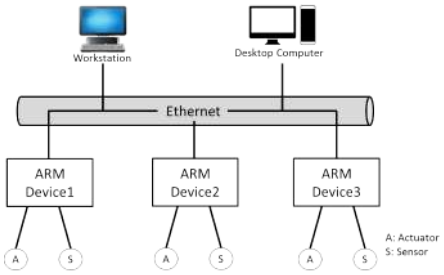

Fig. 9. Automation System with Ethernet

5. CONCLUSION

The use of ARM processor in automation and control has already been released in some academic work as seen on ping Li (2010). The use of the ARM presents as a new method for distributed control and data acquisition. It provides important and necessary functions to develop a rapid and efficient. Another benefit is the low cost and compact, making it useful for industrial applications.

To make more efficient building automation systems, control and supervision based on ARM, the new approach proposed in this work leave application level the main features of this device. This will allow any user or developer to use these features to build their systems. The new approach divides the features of ARM on brick structure.

The inputs and outputs modules are basic modules that allow you to access the physical ports on ARM. The database module SQLite allow banks to create backup of information. The control algorithm module allows to create control structures using the variables of inputs and outputs. The communication module enables interfaces ethernet and serial port for remote communication. Thus, this brick structure behind a new concept under development in automation, control and supervision based on ARM. He brings to high-level features of ARM developers making automation, supervisory control and build their systems quickly and easily, without deepening the concepts of low-level machine.

It is important to mention that these modules will not be the only or as few modules definitive. Work is not a turnkey solution to software level but a development concept, then nothing will stop in the short term, an increased amount of tools and solutions driven automation. One can cite for future work in ladder language modules, software builders supervisory board in android. Another important point is the fact that all development solutions in the application layer, then there is no reason to take any other existing solutions, and incorporates it into the development of a solution, for example an application that makes image processing, Biometric readers, speech synthesizers, and other media players Yuksekkaya et al. (2006).

REFERENCES

Anish, M. (2012). Internal model control of pressure process using arm microcontroller. In *Computing, Electronics and Electrical Technologies (ICCEET), 2012 International Conference on*, 351 –353. doi: 10.1109/ICCEET.2012.6203812.

Caratti Filho, E., Villarreal, E.R.L., Casillo, D.S.S., Pavão, A.C., and Melo, R.R. (2012). Linear systems applied in suspended weight of oil rigs. In *XV Congreso Latinoamericano de Control Automático.*, 134 –138.

CoreWind (2013). Tiny6410. `http://www.armdevs.com`.

EGM (2013). `http://www.egmtecnologia.com`.

Gao, Y. and Zhao, X. (2012). The implementation of buttons driver using the linux input subsystem based on s3c6410 platform. In *Industrial Informatics (INDIN), 2012 10th IEEE International Conference on*, 281 –286. doi:10.1109/INDIN.2012.6301361.

Groover, M.P. (2007). *Automation, Production Systems, and Computer-Integrated Manufacturing*. Prentice Hall Press, Upper Saddle River, NJ, USA, 3rd edition.

ping Li, G. (2010). Design of an embedded control and acquisition system for industrial local area networks based on arm. In *Computer Science and Education (ICCSE), 2010 5th International Conference on*, 35 – 39. doi:10.1109/ICCSE.2010.5593644.

Ruimei, Z. and mei, W. (2010). Design of arm-based embedded ethernet interface. In *Computer Engineering and Technology (ICCET), 2010 2nd International Conference on*, volume 4, V4–268 –V4–270. doi: 10.1109/ICCET.2010.5485599.

Wan, F., Duval, F., Savatier, X., Louis, A., and Belahcene, M. (2010). Study of susceptibility of an mcu control system in the automotive field. In *Electromagnetic Compatibility (APEMC), 2010 Asia-Pacific Symposium on*, 610 –613. doi:10.1109/APEMC.2010.5475715.

Wang, L. and Tan, K.C. (2006). *Modern Industrial Automation Software Design*. IEEE Press, 1rd edition.

Xu, R., Guo, W., and Li, C. (2006). A new type of embedded autolevelling control system based on arm microcontroller for carding machine. In *Industrial Electronics and Applications, 2006 1ST IEEE Conference on*, 1 –6. doi:10.1109/ICIEA.2006.257151.

Yuksekkaya, B., Kayalar, A., Tosun, M., Ozcan, M., and Alkar, A. (2006). A gsm, internet and speech controlled wireless interactive home automation system. *Consumer Electronics, IEEE Transactions on*, 52(3), 837 –843. doi: 10.1109/TCE.2006.1706478.

978-3-902823-33-5/13/$20.00 © 2013 IFAC

APPROACH ON SOLUTION TO SYLVESTER EQUATION STABILIZATION IN SINGULAR SYSTEM

Llanos Villarreal E. R. [*] **Martins Rodrigues W.** [*]
Deus Lima J. [**] **Ruiz Vargas J. A.** [***]

[*] *Depto de Cincias de Exatas e Naturais, DCEN,Universidade Federal Rural do Semi-árido, UFERSA, 59625-900, Mossoró, RN,Brasil (e-mail: elmerllanos@ufersa.edu.br, walterm@ufersa.edu.br).*
[**] *Departamento de Matemtica,Universidade do Estado do Rio Grande do Norte, UERN, Campus Mossoró, 59625000,Mossoró, RN, Brasil (e-mail: jddeus@uol.com.br).*
[***] *Universidade de Brasilia UNB, Departamento de Engenharia Elétrica, Laboratório de Automação e Controle - LARA,C. U. Darcy Ribeiro, 70.910-900, Brasília DF, Brasil e-mail: vargas@unb.br).*

Abstract: This paper presents new approach for the solution of the constrained Sylvester equation associated to linear singular systems. This problem has been recently studied in [32005Castelan,] and [62006Darouach,]. In the present paper, the new method is developed to solve this problem. The necessary and sufficient conditions are presented in the theorem. The algorithm is provided to illustrate the approach.

Keywords: Sylvester equation, Regional Pole placement, Singular Systems.

1. INTRODUCTION

It is known that the static output feedback stabilization problem is a relevant and challenging problem, due to its simple implementation, in contrast to more dynamic methods, and because it is not easy to find a feedback matrix to make the closed-loop system asymptotically stable [42003Castelan,], [81994Syrmos,]. The determination of procedures for obtaining the feedback matrix in output feedback control to asymptotically stabilize linear singular systems is actually an open problem. Several methods have been proposed in the literature based on Lyapunov and Ricatti linear matrix inequalities, or eigenstructure assignment [71988Fletcher,], [11996Alexandridis,],[42003Castelan,] [91993Syrmos,]. There are sufficient conditions for the solution to these equations under a rank constraint [32005Castelan,], [42003Castelan,],[62006Darouach,].

The problem of static output feedback by regional pole placement in a linear time-invariant singular system using output feedback is considered in this paper. There are approaches and techniques to treat different versions of this problem [42003Castelan,], [81994Syrmos,]. Many problems in systems control theory are solved when calculated the solution of Sylvester equations. The present paper considers the problem studied in [32005Castelan,], [62006Darouach,]. A new approach to solve these equations is developed, necessary and sufficient conditions are presented.

2. PRELIMINARES

Consider the linear time-invariant multivariable system described by

$$E\dot{x} = Ax + Bu \tag{1}$$

$$y = Cx \tag{2}$$

where $x \in \Re^n$ is the state vector $y \in \Re^p$ the output vector, and $u \in \Re^m$ the input vector. The matrices E, $A \in \Re^{n\times n}$, $B \in \Re^{n\times m}$, and $C \in \Re^{p\times n}$ are known constan matrices, with $\text{rank}(E) = q < n$, $\text{rank}(B) = m$ and $\text{rank}(C) = p < q$.

2.1 PROBLEM 1

Let $\mathcal{D}$ be a region in the open left half complex plane $\mathcal{D} \subset \mathcal{C}^-$, symmetric with respect to the real axis. The problem is to find matrices $V \in \Re^{p\times n}$, $W \in \Re^{m\times p}$ and $H_V \in \Re^{p\times p}$ such that

$$AV - EVH_V = -BW \tag{3}$$

with $\sigma(H_V) \subset \mathcal{D}$, under the rank constant

$$rank\,[\,EV\ \ AL\ \ B\,] = n \tag{4}$$

where $\sigma(H_V)$ is the spectrum of H_V and $L \in \Re^{n\times n-q}$ is any full row rank matrix obtained $EL = 0$.

The studied problem is to find a static output feedback control law $u(t) = Gy(t)$ such that the closed-loop system

$$E\dot{x}(t) = (A + BGC)x(t) \tag{5}$$

is S-stable: regular, assymptotically stable and free impulses.

2.2 SYLVESTER EQUATION

Let generalized Sylvester Equations where there exist matrices ($H_V \in \Re^{v\times v}$, $W \in \Re^{m\times v}$) and ($H_T \in \Re^{(q-v)\times(q-v)}$, $U \in \Re^{(q-v)\times v}$) solutions to the following *coupled-generalized Sylvester equations* :

$$AV - EVH_V = -BW, \qquad \sigma(H_V) \in \mathcal{C}^- \tag{6}$$

$$TA - H_T TE = -UC, \qquad \sigma(H_T) \in \mathcal{C}^- \tag{7}$$

$$TEV = 0 \tag{8}$$

The generalized Sylvester equation (6) -(8) has a close relation with many problems in linear control theory of singular systems, such as the eigenstructure assignment [71988Fletcher,], and the state observer design. The observer design problem can be formulated as follows [32005Castelan,], [62006Darouach,]:

For the descriptor system (1), (2), consider a reduced-order observer of the form

$$\dot{z}(t) = H_V z(t) + CVu(t) - Wy(t), \tag{9}$$

$$\tilde{x}(t) = Sz(t) + \bar{N}\bar{y} + \bar{M}y(t), \tag{10}$$

where $z \in \Re^{q-m}$ is the state of the observer and $\bar{y} \in \Re^{n-q}$ is a fictitious ouput. Based in shown in [32005Castelan,], [62006Darouach,], if Problem 1 is solved for some matrices V, W and H_V and if we compute the matrices S, $\bar{N}$ and $\bar{M}$ such that $[\,EV\ AL\ B\,]\begin{bmatrix} S \\ \bar{N} \\ \bar{M} \end{bmatrix} = I$, then, for observer (9), (10) we have:

i) $lim_{t\to\infty}(z(t) - EVx(t)) = 0$,

ii) for $\bar{y}(t) = -CLu(t)$, the estimated state $\tilde{x}(t)$ satisfies $lim_{t\to\infty}(x(t) - \tilde{x}(t)) = 0$

Remark 2.1. For $L = 0$, the Problem 1 is reduced to finding matrices $V \in \Re^{n\times n-m}$, $W \in \Re^{m\times n-m}$ and $H_V \in \Re^{n-m\times n-m}$, such that

$$AV - EVH_V = -BW$$

with $\sigma(H_V) \subset \mathcal{D}$, under the rank constraint

$$rank\,[\,EV\ B\,] = n \tag{11}$$

These conditions are those required for the observer design with order (m).

3. MAIN RESULTS

In this section we will present a new solution to problem 1. Consider the matrix $E \in \Re^{n\times n}$ is singular and rank$(E) = q < n$, there exist two nonsingular matrices M and N of appropriate dimensions such that

$$\tilde{E} = MEN = \begin{bmatrix} I_q & 0 \\ 0 & 0 \end{bmatrix}$$

$$\tilde{A} = MAN = \begin{bmatrix} A_{11} & A_{12} \\ A_{21} & A_{22} \end{bmatrix}$$

$$MB = \begin{bmatrix} B_1 \\ B_2 \end{bmatrix}$$

$$N^{-1}V = \begin{bmatrix} V_1 \\ V_2 \end{bmatrix}$$

$$N^{-1}L = \begin{bmatrix} L_1 \\ L_2 \end{bmatrix}$$

where $L \in \Re^{n\times n-q}$ is any matrix satisfying $EL = 0$.

Therefore, equation (4) can be write as

$$rank\begin{bmatrix} EV & AL & B \end{bmatrix} = \begin{bmatrix} V_1 & A_{12}L_2 & B_1 \\ 0 & A_{22}L_2 & B_2 \end{bmatrix} =$$

$$rank\begin{bmatrix} E_c M^{-1}V & A_c M^{-1}L & MB \end{bmatrix} = n \tag{12}$$

Now the equation 3 can be written as

$$A_c N^{-1}V - E_c N^{-1}VH_V = -MBW \tag{13}$$

using the above results we obtain

$$A_{11}V_1 - V_1H_V = \mathcal{B}_1\mathcal{J} \tag{14}$$

$$A_{21}V_1 = \mathcal{B}_2\mathcal{J} \tag{15}$$

with $\sigma(H_V) \subset \mathcal{D}$, and where $\mathcal{J} = \begin{bmatrix} V_2 \\ W \end{bmatrix}$, $\mathcal{B}_1 = [\,A_{12}\ B_1\,]$ and $\mathcal{B}_2 = [\,A_{22}\ B_2\,]$.

Define the following matrices $\mathcal{B} = \begin{bmatrix} \mathcal{B}_1 \\ \mathcal{B}_2 \end{bmatrix}$ and $\mathcal{V} = MEV$, the equation (14), (15) becomes

$$A_c\mathcal{V} - \mathcal{V}H_V = \mathcal{J} \tag{16}$$

and equation (12) can be written as

$$rank\,[\,\mathcal{V}\ \mathcal{B}\,] = n \tag{17}$$

where $\mathcal{V} = MEV = \begin{bmatrix} V_1 \\ 0 \end{bmatrix}$, which can also be written as

$$X\mathcal{V} = 0 \tag{18}$$

with $X = [\,0\ I_{n-q}\,]$.

Then the Problem 1 reduces to finding matrices $\mathcal{V}$, $\mathcal{J}$, and H_V with $\sigma(H_V) \in \mathcal{D}$, such that (16) -(18) are satisfied.

Before proceeding, let us give the following definition which is useful for the sequel.

Definition 3.1. System 1 is $\mathcal{D}$-strongly controllable if and only if the following conditions are satisfied

$$rank\,[\,A - \lambda E\ B\,] = n \forall \in \mathcal{C}, \lambda \notin \mathcal{D},$$

$$rank\,[\,E\ AL\ B\,] = n.$$

For the standard systems, where $E = I$, definition (3.1) becomes

Definition 3.2. Let $A \in \Re^{n\times n}$ and $B \in \Re^{n\times m}$ be constant matrices, then the pair (A, B) is said $\mathcal{D}$-controllable if and only if

$$rank\,[\,\lambda I - A\ B\,] = n \forall \in \mathcal{C}, \lambda \notin \mathcal{D}.$$

We establish the following lemma

Lemma 3.1. The following statements are equivalent

1. System (1) is $\mathcal{D}$-strongly controllable,

2. rank $\begin{bmatrix} \lambda I - A_c & B \\ X & 0 \end{bmatrix} = 2n - q \forall \in \mathcal{C}, \lambda \notin \mathcal{D}$ and $[\, A_{22} \;\; B_2 \,] = n - q$.

Proof 3.1. By using the above transformations we obtained:

$$rank \begin{bmatrix} A - \lambda E & B \end{bmatrix} = rank \begin{bmatrix} M(A - \lambda E)N & MB \end{bmatrix} = rank \begin{bmatrix} \lambda I - A_{11} & -A_{12} & B_1 \\ -A_{21} & -A_{22} & B0_2 \end{bmatrix}$$

and

$$rank \begin{bmatrix} E & AL & B \end{bmatrix} = rank \begin{bmatrix} MEN & MANN^{-1}L & MB \end{bmatrix} = rank \begin{bmatrix} I_q & A_{12}L_2 & B_1 \\ 0 & A_{22}L_2 & B_2 \end{bmatrix} = q + rank \begin{bmatrix} A_{22} & B_2 \end{bmatrix}$$

which prove the lemma.

The necessary and sufficient conditions for the existence of the solution to Problem 1 are then given by the following theorem.

Theorem 3.1. Under the assumption that matrix $\mathcal{B}$ is of full column rank, or rank$\mathcal{B} = n - q + m$, the necessary and sufficient condition for the existence of the solution to Problem 1 is that system (1) must be $\mathcal{D}$-strongly controllable.

Proof 3.2. Under condition (17), there exists a matrix $\mathcal{R}$, such that $\mathcal{V} = \mathcal{R} - \mathcal{B}K$ and rank$[\, \mathcal{V} \;\; \mathcal{B} \,] = rank \, [\, \mathcal{R} \;\; \mathcal{B} \,] \begin{bmatrix} I & 0 \\ -K & I \end{bmatrix}$ if and only if the pair (Λ, Ω) is $\mathcal{D}$-controllable, and using lemma (3.1), we obtained the result of the theorem.

n, or rank$[\, \mathcal{R} \;\; \mathcal{B} \,] = n$. In this case (16) becomes equivalent to

$$A_c(\mathcal{R} - \mathcal{B}K) - (\mathcal{R} - \mathcal{B}K)H_V = \mathcal{B}\mathcal{J}, \tag{19}$$

or

$$\mathcal{R}H_V + \mathcal{B}K_1 + A_c\mathcal{B}K = A_c\mathcal{R} \tag{20}$$

where $K_1 = \mathcal{J} - KH_V$. From the equation (20) it is easy to see that the knowledge of matrices $\mathcal{R}$, H_V, K_1 and K is necessary and sufficient to determine the matrices V and W of the initial problem.

Now let $[\, \mathcal{R} \;\; \mathcal{B} \,]^{-1} = \begin{bmatrix} P_1 \\ Q_1 \end{bmatrix}$, then post multiplying the two sides of equation (20) by the nonsingular matrix $\begin{bmatrix} P_1 \\ Q_1 \end{bmatrix}$ leads to

$$H_V = P_1A_c\mathcal{R} - P_1A_c\mathcal{B}K \tag{21}$$

and

$$K_1 = Q_1A_c\mathcal{R} - Q_1A_c\mathcal{B}K \tag{22}$$

On the other hand, equation (18) can be written as $X(\mathcal{R} - \mathcal{B}K) = 0$ or

$$X\mathcal{B}K = X\mathcal{R} \tag{23}$$

The necessary and sufficient condition for the existence of a solution to (23) is that rank$X\mathcal{B} = rank \, [\, X\mathcal{R} \;\; X\mathcal{B} \,] = rankX = n - q$, which is equivalent to $[\, A_{22} \;\; B_2 \,]$ being of full row rank. Under this condition, the solution to (23) is given by

$$K = (XB)^{\dagger}X\mathcal{R} + (I - (XB)^{\dagger}(XB))Y \tag{24}$$

where $A^{\dagger}$ is any generalized inverse of matrix A, satisfying $AA^{\dagger}A = A$, and Y is an arbitrary matrix of appropriate dimension. The substituting this expression in (21) yields

$$H_V = \Lambda - \Omega Z \tag{25}$$

where $\Lambda = P_1A_c\mathcal{R} - P_1A_cB(XB^{\dagger})(X\mathcal{R})$ and $\Omega = P_1A_cB(I - (XB)^{\dagger}(XB))$.

From (25) $\sigma(H_V) \subset \mathcal{D}$ if and only if the pair (Λ, Ω) is $\mathcal{D}$-controllable, or equivalently rank$[\, \lambda I - A \;\; \Omega \,] = n \forall \in \mathcal{C}, \lambda \notin \mathcal{D}$.

Now, define the following full row matrices $S_1 = \begin{bmatrix} \mathcal{R} & \mathcal{B} & 0 \\ 0 & 0 & I \end{bmatrix}$, $S_2 = \begin{bmatrix} I & 0 & 0 \\ (X\mathcal{B})^{\dagger}X\mathcal{R} & (I - (X\mathcal{B})^{\dagger}(X\mathcal{B})) & (X\mathcal{B})^{\dagger} \end{bmatrix}$ and the nonsingular matrix $S_3 = \begin{bmatrix} 0 & P_1 \\ 0 & Q_1 \\ I & 0 \end{bmatrix}$, then we have

$$rank \begin{bmatrix} \lambda I - A_c & \mathcal{B} \\ X & 0 \end{bmatrix} = rankS_3 \begin{bmatrix} \lambda I - A_c & \mathcal{B} \\ X & 0 \end{bmatrix} S_1 = n - q + m + rank \begin{bmatrix} \lambda I - P_1A_c\mathcal{R} & -P_1A_c\mathcal{B} \\ X\mathcal{R} & X\mathcal{B} \end{bmatrix} S_2 = 2n - 2q + m + rank \begin{bmatrix} \lambda I - & \Omega \end{bmatrix} = 2n - q$$

From the above results we can give the algorithm to solve Problem 1.

4. ALGORITHM

Let the conditions of theorem (3.1) be satisfied, then following method computes the solution of Problem 1.

Step 1: Compute matrices M and N such that $MEN = \begin{bmatrix} I & 0 \\ 0 & 0 \end{bmatrix}$, then compute $A_c = MAN = \begin{bmatrix} A_{11} & A_{12} \\ A_{21} & A_{22} \end{bmatrix}$ and $MB = \begin{bmatrix} B_1 \\ B_2 \end{bmatrix}$.

Step 2: Find a matrix $\mathcal{R}$ that $[\, \mathcal{R} \;\; \mathcal{B} \,]$, is nonsingular and let $\begin{bmatrix} P_1 \\ Q_1 \end{bmatrix} = [\, \mathcal{R} \;\; \mathcal{B} \,]$. Define $\mathcal{D}$, and compute the gain matrix Y, using the pole placement method (see [21989Byers,] and [101996Tits,]), such that $H_V = \Lambda - \omega Y$, and $\sigma(H_V) \subset \mathcal{D}$, then K_1 and K from (21) and (24).

Step 3: Compute $\mathcal{J} = K_1 + KH_V$, $\mathcal{V} = \mathcal{R} - \mathcal{B}K =$, $V_1 = [\, I_q \;\; 0 \,]\mathcal{V}$, $V_2 = -[\, I_{n-q} \;\; 0 \,]\mathcal{J}$, then deduce $W = -[\, 0 \;\; I_p \,]\mathcal{J}$ and $V = M \begin{bmatrix} V_1 \\ V_2 \end{bmatrix}$.

Remark 4.1. Many transformations are used in addition to the resolution of a Sylvester equation, in our paper the problem is reduced to a pole placement one which can be solved by the existing robust methods.

Remark 4.2. In the above result, we have introduced a full column rank matrix $\mathcal{R}$ such that $[\mathcal{R}\ \mathcal{B}]$ is nonsingular, then there exists a regular matrix θ such that $\mathcal{R}\theta = \mathcal{R}$. By pre-multiplying (19) by θ we obtain $A_c(\mathcal{R} - \mathcal{B}\bar{K}) - (\bar{R} - \mathcal{B}\bar{K})H_V = \mathcal{B}\bar{J}$, where $\bar{J} = \mathcal{J}\theta$, $\bar{H}_V = \theta^{-1}H_V\theta$, and $\sigma(\bar{H}_V) = \sigma(H_V)$, which shows that the solution given above is independent of the choice of matrix $\mathcal{R}$.

5. REGIONAL POLE PLACEMENT

The LMI regions describe a convex regions in the complex plane which each point is symmetric in relation to the real axis.

Definition 5.1. A subset $\mathcal{D} = \{\lambda \in \mathcal{C}^- : f_{\mathcal{D}}(\lambda) < 0\}$ complex plane is called a *linear matrix inequalities* (LMI) *region* if there exist a symmetric matrix $\Delta = (\delta)_{kl} \in \Re^{n\times n}$ and $\Theta = (\theta)_{kl} \in \Re^{n\times n}$ such that $f_{\mathcal{D}}(\lambda) = \Delta + \lambda\Theta + \bar{\lambda}\Theta'$ with $\lambda, \bar{\lambda} \in \mathcal{C}^-$, where $\mathcal{C}^-$ denotes the complex half-plane, and $(\delta)_{kl}$, $(\theta)_{kl}$ represent the elements of the matrices Δ and Θ, for all $1 \leq k, l \leq n$.

The characteristic function $f_{\mathcal{D}}(\lambda)$ takes values in the space of Hermitian matrices of dimensions $n \times n$. The LMI region can be defined from $f_{\mathcal{D}}(\lambda)$ to characterize the properties of the eigenvalues of a real matrix in $\mathcal{D}$ [51996Chilali,].

This section is presented the solution of Problem 1 by regional pole placement in LMI regions of the complex plane. We shall use the same notations as [62006Darouach,] and [32005Castelan,] define the LMI region $\mathcal{D} \subset \mathcal{C}^-$ by the existence of two matrices $\Delta = \Delta' \in \Re^{m\times m}$ and $\Gamma \in \Re^{m\times m}$ such that $\mathcal{D} = (\lambda \in \mathcal{C} : f_{\mathcal{D}}(\lambda) = \Delta + \lambda\Gamma + \bar{\lambda}\Gamma' < 0)$, then we propose the following result.

Theorem 5.1. Let $\mathcal{D} \subset \mathcal{C}^-$ be an LMI region, and assume that system (1) is $\mathcal{D}$-strongly controllable, then there exists a solution to Problem 1, with $\sigma(H_V) \subset \mathcal{D}$ if and only if there exist a symmetric positive definite matrix $Y \in \Re^{m\times m}$ and a matrix $\phi \in \Re^{m\times m}$ such that

$$Y \otimes \Delta + (\Lambda Y) \otimes \Gamma - (\omega\phi) \otimes \Gamma + (\Lambda Y)' \otimes (\Gamma)' - (\omega\phi)' \otimes (\Gamma)' < 0 \qquad (26)$$

where $\Lambda = P_1A_c\mathcal{R} - P_1A_c\mathcal{B}(X\mathcal{B})^{\dagger}X\mathcal{R}$, $\omega = (P_1A_c\mathcal{B})(I - (X\mathcal{B})^{\dagger}(X\mathcal{B}))$, and $\otimes$ is the Kronecker's product. In this case $H_V = \Lambda - \omega Z$ with $Z = \phi Y^{-1}$.

Proof 5.1. The proof is direct, in fact from [62006Darouach,], $\sigma(H_V) \subset \mathcal{D}$ if and only if there exists a symmetric positive definite matrix $Y \in \Re^{m\ timesm}$ such that

$$Y \otimes \Delta + (H_VY) \otimes \Gamma + (H_VY)' \otimes (\Gamma)' < 0 \qquad (27)$$

From the above result we have $H_V = \Lambda - \omega Z$, and by substituting this value in (27) and by substitution $\phi = ZY$ we obtain the desired result.

6. CONCLUSIONS

In this paper, we have presented a new approach to solve the generalized Sylvester equation associated to Linear Singular System. This problem was considered in [32005Castelan,] where only sufficients conditions were given, and in [62006Darouach,], where necessary and sufficients conditions were given. We have also given the necessary and sufficients conditions for the existence of the solution. Solution by LMI regional pole placement was also presented.

REFERENCES

[Alexandridis, (1996)] Alexandridis A. T. and Paraskevopoulos P. N.(1996), "A New Approach to Eigenstruture Assignment by Output Feedback," *IEEE Trans. Automatic. Control*, 41 (7), July, 1046–1050.

[Byers, (1989)] R. Byers, S. G. Nash, Approaches to robust pole assignment, Int. J. Control. 49 (1) (1989) 97-117.

[Castelan, (2005)] Castelan E. B., Gomes da Silva V. (2005), "On the solution of a Sylvester equation appering in descriptor Systems control theory," *Systems e Control Letters*, 54, 109–117.

[Castelan, (2003)] Castelan E. B., Hennet J. C.J. C., Villarreal E. R. Ll.(2003), "Quadratic characterization and use of output stabilizable subspaces," *IEEE Trans. Automat. Control*, 48 (4), 654–660.

[Chilali, (1996)] Chilali M. , Gahinet P. (1996), " H_∞ Design with Pole Placement Constraints: An LMI Approach," *IEEE Trans. Automatic. Control*, 41 (3), 358–367.

[Darouach, (2006)] Darouach M. (2006), "Solution to Sylvester equation associated to linear descriptor systems," *Systems and Control Letters*, 55(10), October, 835–838.

[Fletcher, (1988)] Fletcher L. R.(1988), "Eigenstructure Assingment by Output Feedback in Descriptor Systems," *IEEE Proc.*, 135 (4), 302–308.

[Syrmos, (1994)] Syrmos V. L.,Lewis F. L. (1994), "Bilinear Formulation for the Output Feedback Problem in Linear System," *IEEE Trans. Automat. Control*, 39 (2) 410–414.

[Syrmos, (1993)] Syrmos V. L., Lewis F. L.(1993), "Output Feedback Eigenstructure Assignment Using Two Sylvester Equations," *IEEE Trans. Automat. Control*, 38 (3), 495–499.

[Tits,(1996)] Tits A. L., Yang Y. (1996), "Globally convergent algorithms for robust pole assignment by state feedback," *IEEE Trans. Automat. Control*, 41 (1) 1432–1452.

[Villarreal,(2009)] Villarreal E. R. Ll., Vargas J. A. R., Hemerly E. M.(2009), "Static Ouput Feedback stabilization using Invariant Subspaces and Sylvester Equations," *TEMA - Tend. Matema. Aplic. Computac.*, 10 (1), 99–110.

Modeling of mechanical system: output feedback and derivative feedback

Azevedo C.M.M. * **Villarreal E. R. LL.** ** **Garcia A. R. G.** **

* *Universidade Federal Rural do Semi Árido (UFERSA), Pós-Graduação em Sistemas de Comunicação e Automação Mossoró – RN – Brasil (e-mail:claudio.medeiros05@gmail.com).*

** *Universidade Federal Rural do Semi Árido (UFERSA), Departamento de Ciências Exatas e Naturais (DCEN), Mossoró – RN – Brasil (e-mail: elmerllanos@ufersa.edu.br);(gomesgarcia@gmail.com)*

Abstract: In this paper is study the stabilization problem of linear system find output feedback matrix and state feedback matrix, will be used the concept of $(C; A; B)$ invariant subspaces for the problem of mechanical suspension of a car. Based on this concept introduced, reported the existence of a output feedback matrix and state feedback matrix by solution of coupled Sylvester equations, with it will be necessary to present an algorithm that refers to Syrmos-Lewis, a modification is proposed to provide a more appropriate for numerical solution, in part, the condition of Kimura.

Keywords: Algorithms, Mechanical system, Output feedback, Control engineering.

1. INTRODUCTION

An important problem in the theory and practice of control system design is the design of feedback controllers, which place the closed-loop poles of a linear system at desired locations, Making a brief account of this engineering, it is clear that the Control engineering is focused on the study of the dynamics of physical systems. Among the main activities carried out by this engineering, they are modeling, analysis, simulation, design, implementation, and others. The model- ing stage is especially important for the study of a control system. At this stage, a mathematical model for a mechanical system is proposed, where the mechanical system refers to a suspension system of an automobile. It is based on it that the other activities are performed, and therefore essential to define a model that accurately represents its dynamics. In general, it should obtain a mathematical model, which is adequate to solve the specific problem in this analysis. However, it is important to emphasize that the results of this analysis are valid only for cases in which the model is valid. When we go to obtain a simplified model of a system, generally we ignore some physical properties of this system. If the effects that these properties have on the response of the system are small, then a good similarity between the results of mathematical analysis and practical results of the system is obtained. In general, the dynamic systems are nonlinear. However, the mathematical procedures for obtaining the solution of linear models are very complicated. For this reason, usually is substituted a nonlinear model by a linear model, with valid only in a limited region of operation, or to a point operating. A system is called linear if it applies the principle of superposition. Where the superposition principle establishes that the response produced by the simultaneous application of two different excitations is equal to the sum of two individual responses to each of the excitations. As a result, linear systems, the response to various inputs can be calculated by considering a single entry at a time and adding the results. So for a better understanding, the work outlined here will be subdivided into four main sections, where we will start talking about the invariant subspaces and coupled Sylvester equations, soon after will be presented the problem to be modeled, where will be presented the function transfer, In which is used to characterize the input-output relation of components or systems that can be written by differential equations linear time-invariant. Apresented the modified algorithm of Syrmos and Lewis based on Theorem 2.1 in Villarreal, Vargas (2009), that such shown the existence the output feedback matrix for the suspension system of an automobile. Then immediately will discuss the modeling of the problem and algorithmic aspects, to this, power make the formulation in space of states and ending with the matrix determination K with the use of transformation T, where the matrix K, is the output feedback matrix, and ending with the conclusion that it will present the results we have at work.

⋆ This work was supported in part by the CAPES.

2. COUPLED SYLVESTER EQUATIONS

As in Syrmos, Lewis (1994), makes use of some concepts and definitions of geometric control theory Wonahm (1979). It is known that a subspace $\mathcal{V} \subset \mathcal{X}$ (A, B)invariant if there $F : \mathcal{X} \longrightarrow \mathcal{Y}$ such that $(A + BF)V \subset \mathcal{V}$, or equivalently, $A\mathcal{V} \subset \mathcal{V}+ImB$. By subspace a duality $\mathcal{T} \subset \mathcal{X}$ is (C, A) considered to be invariant if there $L : \mathcal{Y} \longrightarrow X$, such that $(A + LC)\mathcal{T} \subset \mathcal{T}$, or equivalently, $\mathcal{T} \supset A(\mathcal{T} \cap Ker(C))$.

It is $V \in \Re^{v\times v}$ such that $Im(V) = V$ and is $T \in \Re^{n-v\times v}$ and a left anhilator of V, *i.e.*: $Ker(T) = Im(V)$.

$$AV - VH_V = -BW \tag{1}$$

$$TA - H_T T = -UC \tag{2}$$

$$TV = 0 \tag{3}$$

The equations play a fundamental role in the treatment of the control problem using static output feedback, especially for auto-structure placement Syrmos, Lewis (1994) Syrmos, Lewis (1993). And leading into account the properties of stabilizability and detectability by the two following definitions::

- A subspace (A, B) invariant $\mathcal{V}$ is (A, B) internally stabilizable if there F such that $(A + BF)|\mathcal{V}$ is asymptotically stable;
- A subspace (C, A) invariant $\mathcal{V}$ (C, A) externally detectable L such that $(A + B)|\mathcal{X}/V$ is asymptotically stable;

The necessary and sufficient condition for a subspace $\mathcal{V} = Im(\mathcal{V})$ $O.S$ (C, A, B) invariant that equation (3) be verified with the additional conditions stability by Villarreal, Vargas (2009):

$$\sigma(H_V) \in \mathcal{C}^- \tag{4}$$

$$\sigma(H_T) \in \mathcal{C}^- \tag{5}$$

The following theorem makes the relation concept of subspaces $O.S.(A, B, C)$ invariant to the existence of a control law of type static output feedback which stabilizes the closed system.

$$AV - VH_V = -BW, with\ \sigma(H_V) \in \mathcal{C}^- \tag{6}$$

$$TA - H_T T = -UC, with\ \sigma(H_T) \in \mathcal{C}^- \tag{7}$$

$$TV = 0 \tag{8}$$

$$Ker(CV) \subseteq Ker(W) \tag{9}$$

$$Ker(B'T') \subseteq Ker(U') \tag{10}$$

$$where: rank(V) = v\ and\ rank(T) = n - v$$

Note that the results have been presented and explored in different ways in the literature concerning the auto-structure placement using output feedback Syrmos, Lewis (1997). As seen, the coupled equations Sylvester (6), (7), (8) describe geometric properties of the subspace $\mathcal{V} = Im(\mathcal{V})$ should be (A, B) asymptotically stable; ally means that the subspaces $Ker(T) = \mathcal{V}$ should be (C, A) externally stabilizable. Thus, under the coupling condition, is that the existence of a subspace $\mathcal{V} = Ker(T)$ $O.S.$ (C, A, B) invariant, with the additional conditions (9), (10) is a necessary and sufficient condition for the existence of solution of the problem considered. Note also that the terms (9), (10) correspond to the existence of a matrix $K \in \Re^{m \times p}$ which verifies the two following equalities:

$$KCV = W \tag{11}$$

$$TBK = U \tag{12}$$

It is important to note that is guaranteed the existence of a solution to the equation of Sylvester, is K has been obtained and such (12) is verified, the eigenvalues in closed-loop are given by:

$$\sigma(A + BKC) = \sigma(HV) \dot{\cup} \sigma(H_T)$$

3. FORMULATION OF THE PROBLEM

In the translational mechanical systems, there are three mechanical elements that are involved: element of inertia, damping element, element of elasticity. Where the element of inertia (mass) is assumed that the mass is rigid. Thus the connection higher, should not move in relation to less connection, that is, both connections moving the second $x(t)$. already the damping element (damper) there is a relative displacement between the upper connection point and connection point lower. Therefore, there is a need to shift two variables to describe this element. The physical realization of this element is the viscous friction associated with the oil or air. The element of elasticity (spring) can be deformed by an external force, such that the deformation is directly proportional to this force.

There fore, the problem to be modeled consists of obtaining a transfer function of a moving automobile, where it passes through different obstacles (elevations) on the track which will be observed the mechanical system simplified of a system suspension of wheels a car. Then it will be assigned at a certain instant in that car passes by a certain elevation in $25cm$, which is applied to the force F. A schematic representation of a model for the car with a buffer (f) and a spring (k):The System of car suspension is illustrated in Figure 1:

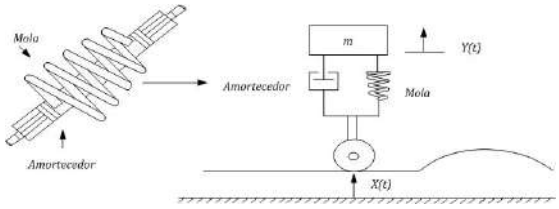

Fig. 1. Suspension System

This is a model corresponding to one of the four wheels of a car. The cylinder of damper contains air that passes from one side to another, when occurs a relative motion. He always applies a reaction force, that is contrary to the movement of his extremities. The viscous damper provides viscous friction, ie, it opposes any relative motion of the two ends, dissipating energy in form of heat. Will be illustrated now the mathematical model that provides the problem. see Figure 2

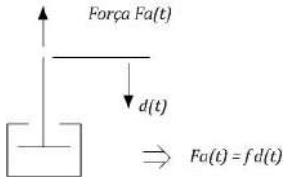

Fig. 2. Mathematical model

Where the forces on the mass m are expressed in Figure 3

With:

$$\begin{cases} \text{force of moll}: F_m = K(y - x) \\ \text{force of buffer}: F_a = f(\dot{y} - \dot{x}) \end{cases} \tag{13}$$

we know that:

$$\Sigma F_y = m.a \tag{14}$$

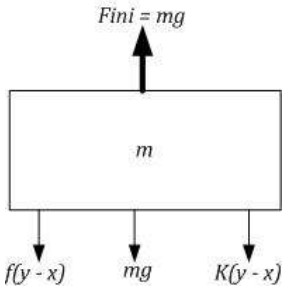

Fig. 3. Force on Mass

here fore, we obtain:

$$m.g - f(\dot{y} - \dot{x}) - m.g - K(y - x) = m\ddot{y} \tag{15}$$

Defined above, we know that the continuous transfer function is the relation between the Laplace transform of the output, $Y(s)$, by Laplace transform of the input, $X(s)$. The relation $G(s)$ is a ratio of two polynomials in s:Thus, applying to laplace C.I. zero we obtain

$$\begin{cases} -f(sY(s) - sX(s)) - K[Y(s) - X(s)] = ms^2Y(s) \\ Y(s)[ms^2 + fs + k] = [sf + k]X(s) \\ \dfrac{Y(s)}{X(s)} = \dfrac{sf + k}{ms^2 + fs + k} = G(s) \end{cases} \tag{16}$$

where f is the reaction force, K is a spring constant and mis the mass of the car.

4. MODELING THE PROBLEM

To illustrate the usefulness of MATLAB in this analysis, assume that an automobile in Motion passes through different obstacles (elevations) on the track. In Figure 4 we have presented an outline of a representative model for the car with a buffer (f) and a spring (k):

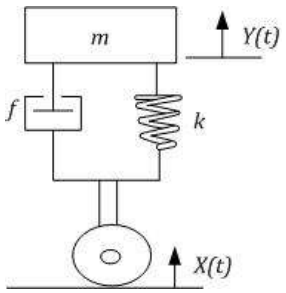

Fig. 4. Model of buffer

Suppose now that this same car passes through a elevation of $d = 25cm$, as shown in Figure 5.

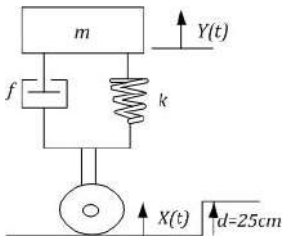

Fig. 5. Representation of elevation

This elevation corresponds to the entry system and is called the step input. To observe the response of the system (movement of the mass-spring system, shock absorber, the alleged car), based on the transfer function of the damper seen previously, we apply the values the instant the car passes this elevation, where invariants are: $m = 1000, f = 500$ e $K = 200$.

Thus, the function acquired in 16 will:

$$\frac{Y(s)}{X(s)} = \frac{500s + 200}{1000s^2 + 500s + 200} = G(s) \tag{17}$$

Writing the transfer function obtained in 17 we have:

$$\frac{Y(s)}{U(s)} = \frac{numerator\ polynomial\ in\ s}{denominator\ polynomial\ in\ s} = \frac{num}{den} \tag{18}$$

Once we have this expression of type transfer function, the command in MATLAB:

$$[A, B, C, D] = tf2ss(num, den) \tag{19}$$

described in Ogata (2010) provides a state-space representation. It is important to note that the representation in the state space of any system is not unique. There are many (actually infinite) representations for the same system. The command in MATLAB provides a possible representations in space data. From the transfer function obtained in 17, and changing some values, we can visualize so with the values of matrices A, B, C e D we get the following function:

$$\frac{Y(s)}{U(s)} = \frac{0.5s + 0.2}{s^2 + 0.5s + 0.2} \tag{20}$$

As from the transfer function 20, the values matrices A, B e C will be:

$$A = \begin{bmatrix} -0.5 & -0.2 \\ 1 & 0 \end{bmatrix}_{2\times2} \quad B = \begin{bmatrix} 1 & 0 \\ 0 & 1 \end{bmatrix}_{2\times1} \quad C = [\,0.5\ \ 0.2\,]_{1\times2}$$

Will be presented following two methods, in which shall be responsible for submitting of arrays of state feedback and output feedback.

4.1 Feedback States

In this section will reported the method 1 in Ogata (2010), in which it gets the matrix G state feedback, where:

$$\dot{x} = Ax + Bu \tag{21}$$

$$y(t) = Cx + Du \tag{22}$$

Choose the control signal as:

$$u = Gx \tag{23}$$

To calculate the state feedback matrix of G we will use MATLAB, where we have two commands *acker* and *place*. the commands *acker* is based on the Ackerman formula that applies only to systems of one input and one output. the commands *place* can be used for both systems as an entry for multiple inputs, it requires that the multiplicity

of the desired closed loop poles does not exceed the rank of B. To use the commands *acker* ou *place* we will use the matrices A, B and J. The matrices A and B, have been previously defined and the matrix J is the one that consists of closed-loop poles, so that:

$$J = [\,\mu_1 \;\; \mu_2 \;\; \cdots \;\; \mu_n\,] \tag{24}$$

Applying the mechanical system, the matrix J is:

$$J = [\,-1 \;\; -2\,]$$

As from the matrix J, we introduce:

$$G = place(A, B, J)$$

Therefore, the matrix G is:

$$G = \begin{bmatrix} 0.5000 & 0.2000 \\ 1.0000 & 2.0000 \end{bmatrix}$$

To determine the matrix we use $A_G = A - B * K$, then the matrix AG will:

$$A_G = \begin{bmatrix} -1 & 0 \\ 0 & -2 \end{bmatrix}$$

Now, we will use the command $eig(AG)$, to verify that the matrix provides the desired eigenvalues:

$$[\,-1 \;\; -2\,]$$

Thus will be shown following graph the resultant curve from the rung response of unitary based on the matrices. A, B, C, D and the matrix of the state feedback G, adquired from the transfer function (20), in Figure 6.

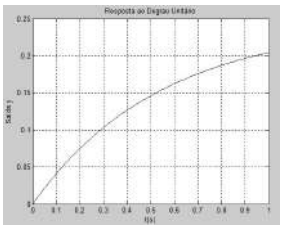

Fig. 6. Unitary rung response

The graph shown in Figure 6, shows the stability of values appropriate for the desired which was obtained from the state feedback matrix.

4.2 Modified algorithm of Syrmos and Lewis

Based on Theorem 2.1 in Villarreal, Vargas (2009), the following algorithm, considered in Syrmos, Lewis (1993), can be used to obtain an output feedback matrix that stabilizes the closed loop system, when the Kimura condition, $n < m + p$, is verified.

Step 1: Select the matrix $H_T \in \Re^{n-p\times n-p}$, where $\sigma(H_T) = \Lambda_T \in \mathcal{C}^-$, and solve (6) to find the matrix $T \in \Re^{n-p\times n}$, such that

$$rank\left(\begin{bmatrix} T \\ C \end{bmatrix}\right) = n \Longleftrightarrow Ker\; T \cap Ker\; C = \{0\} \tag{25}$$

Step 2.1: Solve (6) for some matrix $H_V \in \Re^{p\times p}$, where $\sigma(H_V) = \Lambda_V \in \mathcal{C}^-$, whereas the matrix V satisfy the coupling condition (8) and $rank\,(V)$ is equal to p.

Step 2.2: By construction, the relation (25) guarantees that rank $(CV) = p$. Then G can be calculated as unique solution of (11).
∘

Steps 1 and 2 can be implemented by using standard techniques for eigenstructure assignment. By considering H_T e H_V in the Jordan form, the following procedure can be adopted:

Step 1: Find $t_j \in \mathcal{C}^n$ and $u_j \in \mathcal{C}^p$, such that :

$$\begin{bmatrix} t_j' & u_j' \end{bmatrix} \begin{bmatrix} A - \lambda_j I \\ C \end{bmatrix} = 0 \;\forall\; j = 1, \ldots, n-p \tag{26}$$

The row matrix $T \in \Re^{(n-p)\times n}$, denoted for T_j, is constructed by using the vectors t_j, as follows :

- if $\lambda_j \in \Re$, then $T_j = t_j'$;
- if $\lambda_j \in \mathcal{C}$, then $\lambda_{j+1} = \lambda_j^*$ and $\begin{cases} T_j = Re\,(t_j') \\ T_{j+1} = Imag\,(t_j') \end{cases}$.

Step 2 : To determine $v_i \in \mathcal{C}^n$ and $w_i \in \mathcal{C}^n$ we have :

$$\begin{bmatrix} A - \lambda_i I & B \\ T & 0 \end{bmatrix} \begin{bmatrix} v_i \\ w_i \end{bmatrix} = 0 \;\forall\; i = n - p + 1, \ldots, n \tag{27}$$

In similar form to the previous case, the used matrices V and W can only be built with real elements. In particular, if $\lambda_i \in \mathcal{C}$, then $\lambda_{i+1} = \lambda_i^*$ and $\begin{cases} V_i = Re\,(v_i), & V_{i+1} = Imag\,(v_i) \\ W_i = Re\,(w_i), & W_{i+1} = Imag\,(w_i) \end{cases}$, where v_i and w_i denote the columns of the matrices V and W, respectively. Castelan, Hennet, Villarreal (2003) Step 1, in Remark 3.1, is concerned with the choice of a matrix T, which verifies (26). Step 2 is concerned with the solution of (6) and (8), to obtain the (A,B)-invariant of $Ker\,(T)$. This property is associated to the "zero equation" (27) Castelan, Hennet, Villarreal (2003). To guarantee the freely placement of the eigenvalues λ_i in step 2 , the system matrix $P(\lambda) = \begin{bmatrix} A - \lambda I & B \\ T & 0 \end{bmatrix}$ of dimension $(2n-p)\times(n+m)$, must be row-full rank $\forall\lambda$. The algorithm is based in the fact that under Kimura condition, $m + p > n$, $P(\lambda)$ does not lose rank for almost all triples (A, B, T) Syrmos, Lewis (1994). Thus the zero equation (27) has solutions for all λ_i. In the presence of invariant zeros, it is possible to remake Step 1 to search other solutions for the Sylvester equation (6). In the less restrictive case $m + p = n$, $P(\lambda)$ is square of dimension $(2n - p) \times (2n - p)$, and all triple (A, B, T) has p finite invariant zeros Syrmos, Lewis (1997). In this case, the basic procedure can produce stabilizing solutions only if T, found in step 1, generates p stable invariant zeros, which have to be used to solve (27) Castelan, Hennet, Villarreal (2003).

: Consider the linear system defined by Fletcher, Kautsky, Kolka et. al. (1985) :

$$A = \begin{bmatrix} 0 & 1 & 0 & 0 \\ 1 & 1 & 0 & 0 \\ -1 & 0 & 0 & 0 \\ 0 & 0 & 0 & 0 \end{bmatrix} \;;\; B = \begin{bmatrix} 0 & 0 \\ 1 & 0 \\ 0 & 0 \\ 0 & 1 \end{bmatrix} \;;\; C = \begin{bmatrix} 1 & 0 & 0 & 0 \\ 0 & 0 & 1 & 0 \\ 0 & 0 & 0 & 1 \end{bmatrix}$$

The system is controllable and observable and $m + p = 5 > n$. The desired eigenvalues are : $\Lambda_T = \{-4\} \cup \Lambda_V = \{-3, -2, -1\}$.

Step 1 : By considering that $\lambda_1 = -4$, and using (26) we have

$T = [\,-0.3148 \;\; 0.0630 \;\; -0.2406 \;\; -0.2425\,]$, where (A, B, T) has not invariant zeros

Step 2.1 : For $\lambda_2 = -3$, $\lambda_3 = -2$ and $\lambda_4 = -1$, by using (27) we have:

$$V = \begin{bmatrix} 0.0727 & 0.1324 & 0.2425 \\ -0.2182 & -0.2649 & -0.2425 \\ 0.0242 & -0.0662 & 0.2225 \\ -0.1751 & -0.3064 & -0.6184 \end{bmatrix} \;,\; W = \begin{bmatrix} 0.7999 & 0.6622 & -0.2424 \\ 0.5254 & 0.6128 & -0.6184 \end{bmatrix}$$

Step 2.2 : Based on $GCV = W$, we have $G = \begin{bmatrix} -46.9778 & -20.7333 & -26.9444 \\ -16.1410 & -9.3519 & -10.9968 \end{bmatrix}$. The closed loop matrix $A_G = A + BGC$ is then

$$A_G = \begin{bmatrix} 0.0000 & 1.0000 & 0.0000 & 0.0000 \\ -45.97778 & 1 & -20.7333 & -26.9444 \\ -1.0000 & 0.0000 & 0.0000 & 0.0000 \\ -16.1410 & 0.0000 & -9.3519 & -10.9968 \end{bmatrix}.$$

△

4.3 Output Feedback

In this section we will present a technique based on algorithmic procedures for auto-structure placement to obtain a output feedback Villarreal, Vargas (2009)Castelan, Hennet, Villarreal (2003). Where the technique proposed by Lewis and Syrmos[6] solves the coupled Sylvester equations in two steps and can be directly applied to systems that verify the condition $m + p > n$, condition known as Kimura [4]. It is clear that the dimension of $V = Im(V)$ equals the number of outputs p, seeking to ensure that the matrix $CV \in \Re^{p \times p}$ is invertible and, so that the matrix of feedback gains can be found, from equation (11), the form $K = W(CV)^{-1}$.

It will be also shown that if, the considered system is completely state controllable, then the poles of closed-loop system can be placed in any desired position by means of a state feedback, using an appropriate gain matrix,with that, limit our discussion to systems an input and an Output. The requirement is that the system is completely controllable.

Consider the following system defined on [3].

$$\dot{x} = Ax + Bu \tag{28}$$

$$y = Cx + Du \tag{29}$$

Choose the control signal as:

$$u = -Kx \tag{30}$$

This means that the control signal u is determined by an instantaneous state. This scheme is called state feedback. The matrix $K_{1\times n}$ is called state feedback matrix . Thus, the mechanical system represented in state space is represented as follows:

The electrical system represented in state space is:

$$\begin{bmatrix} \dot{x_1} \\ \dot{x_2} \end{bmatrix} = \begin{bmatrix} -0.5 & -0.2 \\ 1 & 0 \end{bmatrix} \begin{bmatrix} x_1 \\ x_2 \end{bmatrix} + \begin{bmatrix} 1 & 0 \\ 0 & 0 \end{bmatrix} u$$

$$y = [\,0.5 \;\; 0.2\,] \begin{bmatrix} x_1 \\ x_2 \end{bmatrix}$$

Further, it is considered that the system represented by (C, A, B) is controllable and observable, this necessary condition for the arbitrary choice of the poles to be placed in closed loop. This condition can however be relaxed for the stabilization and detectability of (C, A, B), which implies the use of non-controllable eigenvalues non-observable in the spectrum for the desired closed-loop system. Assume that T can be found from the matrices $[A, B, C]$ As determined in Villarreal, Vargas (2009)Castelan, Hennet, Villarreal (2003):

$$A = \begin{bmatrix} -0.5 & -0.2 \\ 1 & 0 \end{bmatrix}_{2\times 2}$$

$$B = \begin{bmatrix} 1 & 0 \\ 0 & 1 \end{bmatrix}_{2\times 1}$$

$$C = [\,0.5 \;\; 0.2\,]_{1\times 2}$$

The corresponding system is controllable and observable and $m + p = 3 > n$. Then determine the matrix T verified the equation (17) in Villarreal, Vargas (2009) Castelan, Hennet, Villarreal (2003). Thus the matrix T Thus the matrix:

$$T = [\,-0.7071 \;\; -0.0000\,]_{1\times 2}$$

The matrices V and W are determined using the equation (18) in Villarreal, Vargas (2009) Castelan, Hennet, Villarreal (2003):

$$V = [\,0.0000 \;\; -0.4454\,]_{1\times 2}$$

$$W = [\,0.0891 \;\; 0.8909\,]_{1\times 2}$$

be determined K such that $KCV = W$:

$$K = \begin{bmatrix} -1.0000 \\ -10.0000 \end{bmatrix}_{2\times 1}$$

The closed-loop matrix $A_k = A + BCK$ *correspondent, whose eigenvalues are the desired, is:*

$$A_k = \begin{bmatrix} -1.0000 & 0.0000 \\ -4.0000 & -2.0000 \end{bmatrix}_{2\times 2}$$

$$A_{k1} = \begin{bmatrix} -1 \\ -2 \end{bmatrix}_{2\times 1}$$

5. CONCLUSION

The present paper was considered the stabilization problem by output feedback and state feedback to stabilize a mechanical system. Introduced the concept of subspaces O.S.(C, A, B) invariants and their relation to the solution of the stabilization problem of using output feedback by Sylverter coupled equations, showing that they play a

key role in the response of stabilization problem of linear systems. The paper has focused on theoretical and algorithmic aspects. In particular, a necessary and sufficient condition for the existence of a output feedback. An algorithm has been proposed to calculate a feedback matrix using condition to Kimura $m + p > n$. Aim is to develop future studies aimed at deepening the applications, and so, can be presented other techniques mentioned in Ogata (2010). in order to further facilitate the analysis proposed in the paper.

REFERENCES

Abdelaziz T.H.S. and Valask, M.. Pole-placement for siso linear systems by state-derivative feedback. IEEE Proceedings-Controle Theory and Application, 151(4):377-385, 2004.

Assunção E., Teixeira M.C.M., Faria F.A., Silva N.A.P. da , and Cardim R.. Robust state-derivative feedback LMI-based designs for multivariable systems. International and Infrastructure Engeneering, 20(6):431-499, 2005.

Castelan E.B. , Hennet J. C. , Villarreal E. R. L.. Quadratic characterization and use of output stabilizable subspace. pages 654 660. IEEE Control Systems V48, 2003.

Chen C.T.. Linear system theory and design. The Oxford series in electrial and computer enginnering. Oxford, New York, 3rd edition, 1999.

Dorf R.C. and Bishop R.H.. Sistemas de controle modernos. LTC(Livros Tcnicos e Cientficos Editora S.S.) Rio de Janeiro, 8 edition, 2001.

Duan G.R., Irwin G.W., Liu G.P.. Robust stabilization of descriptor linear systems via proportional-plus-derivative state feedback. In: AMERICAN CONTROL CONFERENCE, 1999, San Diego. *Proceedings of the 1999 American Control conference*. San Diego: American Automatic Control Council, 1999 pages 1304-1308

Villarreal E. R. L. , Vargas J. A. R., Hemerly E. M.. Static output fedback stabilization using invariant sub space and sylvester equations, Revista TEMA - Tendências em Matemática Aplicada e Computacional. Vol. (1), pages 99 110. 2009.

Fletcher R., Kautsky J., Kolka G. K. G., and Nichols N. K.. Eigenstructure ass- ingment by output feedback in descriptor systems. In IEEE Trans. Automatic. Control, vol. 42, pages 1457 1468. Systems and Control Letters 24(2). 1985.

Garcia M. P. Regularizing generalized linear systems by means a derivative feedback. In: PHYSICS AND CONTROL, 2003. In: *Physcon 2003 Proceedings*. St. Petersburg: IEEE. Proceedings, 2003. Pages 1134-1140.

Kimura H.. Pole assignment by gain output feedback. In IEEE Transactions on Automatic Control vl. 20, page 509 516. Systems and Control Letters 24(2). 1975.

OGATA, K. Engenharia de Controle Moderno. Estabilização por realimentação de saídas. In Prentice-Hall, editor,pages 594 657. 2010.

Syrmos L. and Lewis F. L. . Bilinear formulation for the output feedback problem in linear system. In IEEE Trans. Automatic. Control, vol. 39, number 2, pages 410 414. 1994.

Syrmos V. L., Abdallah C. T., Dorato P., and Grigoriadis K. . Static output feedback. In A Survey Automatica, vol. 33, number 2, pages 125 137. 1997.

Syrmos V. L. and Lewis F. L. . Output feedback eigenstructure assignment using two sylvester equations. In IEEE Trans. Automatic. Control, vol. 38, number 3, pages 495 499. Springer-Verlag. 1993.

Rossi F. Q., Assunção E. , and Teixeira M. C.M. , Controlador Robusto com Realimentação derivativa e alocação de polos usando LMI para supressao de vibração em sistema mecânico. 7 Brazilian Conference on Dynamics, Control and Applications. DINCON 2008, Unesp at Presidente Prudente, SP, Brazil.

Wonahm W. M. (1979). Linear multivariable control, a geometric approach. Springer- Verlag.

Linear Systems Applied in Suspended Weight of Oil Rigs

Caratti E. F. * **Villarreal E. R. Ll.** * **Casillo D. S. S.** ** **Pavão A. C.** *** **Melo R. R.** *

* *Mestrado de Sistema de Comunicação e Automação, Universidade Federal Rural do Semi-árido, UFERSA, 59625-900, Mossoró, RN,Brasil (e-mail: edmigiofilho@gmail.com).*
** *Depto de Cincias de Exatas e Naturais, DCEN,Universidade Federal Rural do Semi-árido, UFERSA, 59625-900, Mossoró, RN,Brasil (e-mail: elmerllanos@ufersa.edu.br, danielle@ufersa.edu.br).*
*** *Depto de Cincias Ambientais e Tecnologia, DCAT,Universidade Federal Rural do Semi-árido, UFERSA, 59625-900, Mossoró, RN,Brasil(e-mail: augusto.pavao@ufersa.edu.br).*

Abstract: In this paper we present an analysis in linear systems, based on a practical situation of control and automation in oil rigs. It is presented in weight suspended in probe, practical problems encountered and the solutions to supervisory level to determine the actual weight. Then we present a mathematical model to prove the controllability and observability of the system, using algorithmic resources to obtain an output feedback matrix, and an algorithm to obtain a state feedback matrix.

Keywords: Stabilization, Output feedback, oil rigs, suspended weight.

1. INTRODUCTION

Increasingly, the automation and process control in oil drilling, are being applied in the field. The requirements are based on the concept make operations more safe and accurate accident operational, physical and environmental. This paper proposes a study to support a control theory usually practiced in the probe, for reading suspended of weight systems, systems using mathematical theories, which prove the controllability and observability of the solutions currently used in supervisory control.

Fig. 1.

2. CONCEPTS OF PRACTICE

The current automation systems, done in oil rigs, readers have sprung weight on the winch from the probe, which is now linked with automation through a supervision system in the probes. This winch, commonly called "Catarina", is responsible for most of the drilling operations and can working with great efforts , so have the highest degree of importance in service survey. It is a winch for "maneuver", introduction and removal of tubes and tools into the well, responsible for maneuvering heavy equipment and is located right above the well.

There is then a constant concern with the actual reading of weight, everyday process instrumentation, and that became important from the new contracts signed between Petrobras and company service providers, in addition to the instrument players weight should having a history stored in the database via automation of all operations, including the main reading that the weight is suspended from the main hook, called the "weight of Catarina" .

Fig. 2.

3. PROBLEMS ENCOUNTERED

By 2007, it was customary, the weight readings through automation, with serious mistakes were made, which had a nonlinear response of the sensor with respect to the actual weight suspended from the hook.

Peso no leitor (libras) Weight in Reader	Peso na Automação (libras) Reading weight in automation	Erro
10000	10000	0%
15000	14560	3%
20000	19120	4%
25000	23680	5%
30000	28240	6%
35000	32800	6%
40000	37360	7%
45000	41920	7%
50000	46480	7%
55000	51040	7%

Fig. 3. Table 1

These errors shown in Table 1, physically happen because of mechanical losses from reductions in pulleys. The system dynamic tension of the cable, presents a reduction of effort in the distribution of pulleys.

When the system uses low weights, friction and bending losses of the cable means, represent much error in reading instrument.
The measurement of weight measurement automation system , was done with low weights. When there's weight gain, the distortion occurred in reading, because as the weight increases will bow down to getting as close to a straight, which means that losses, no longer has significant importance for high loads. Below the schematic figure of the drive train weight

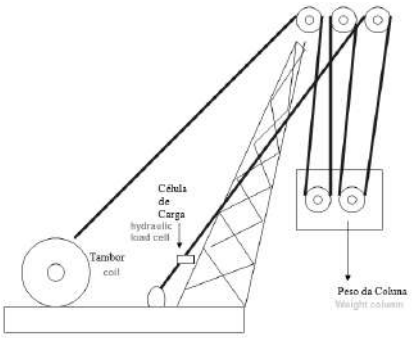

Fig. 4.

There was an increase of error in the reading of the automation for equipment calibrated probe. Were introduced then weigth correction techniques described in this text.

4. TEST WEIGHT MEASUREMENT USING THE MARTIN DECKER EQUIPMENT (LAB)

The reader Mark Martin Decker weight, *lum* is an instrument to measure weight using a hydraulic load cell attached to the anchor wire rope of main winch system of the probe. The hydraulic system that let you read a weight by a change in fluid pressure caused by tension in steel cable.

Fig. 5.

The experiment consists of placing a pressure sensor from ifm brand PA 3024, with the response from 4 to 20 mA, in parallel to the hydraulic system to read exactly the same pressure of the reader in weight. With an auxiliary pump and using a gauge of pressure, positioned at intervals of 5000 pounds in weight and reader, mark the pressure via electrical signal in mA and the transformation of automation for voltage in volts (0 to 5V). First and second columns of Table 2. Using resources of supervisory software (Auto control), we use a set of factors represented by the expression

$$Y = aX + bX + c.$$

The weight stored by automation, with adjustments for factors, $a = 26,000$, $b = 35000$, $c = -4000$, presented a satisfactory average error of order 0.1, for all grinding equipment Martin Decker. Where X represents the the voltage value in volts of the automation system. This values are listed in Table 2.

5. MATHEMATICAL MODELING OF THE CONTROL SYSTEM.

The initial problem is to set up the equations that represent entry and exit control system. Given the equation,

$$Y = aX^2 + bX + c$$

With a supervisory control of the error for satisfying instrumentation and substituting the value found for a, b and c, the actual practical to have:

$$Y = 26000X^2 + 35000X - 4000 \quad (1)$$

With this equation, was assembled in the laboratory the spreadsheet and graph of Figure 5 and Figure 6.

Where X is the real value of the voltage in volts and the output of the system, responding to the weight in pounds given by Y this is obtained from the transfer function and then for find the state space.

Then calling the output function, where X is the sensor voltage and the input function would be $Y = 1$, because the system is only observation and not generates return control measures.

Applying Laplace Transform to generate the transfer function, have the equation:

$$G(s) = \frac{L(Y)}{L(1)} \quad (2)$$

For Laplace Transform table we have:

sensor ifm mA (ifm)	Tensão (V)	Peso certificado Peso Mart.Dck	Peso Automação
4,00	0,000000	0	0
4,59	0,184375	5.000	4.516
4,92	0,287500	10.000	10.097
5,22	0,381250	15.000	15.522
5,47	0,459375	20.000	20.265
5,71	0,534375	25.000	24.990
5,96	0,612500	30.000	30.078
6,20	0,687500	35.000	35.112
6,47	0,771875	40.000	40.940
6,67	0,834375	45.000	45.364
6,91	0,909375	50.000	50.787
7,11	0,971875	55.000	55.398
7,32	1,037500	60.000	60.327
7,50	1,093750	65.000	64.621
7,70	1,156250	70.000	69.464
7,90	1,218750	75.000	74.382
8,07	1,271875	80.000	78.618
8,28	1,337500	85.000	83.923
8,49	1,403125	90.000	89.303
8,70	1,468750	95.000	94.758
8,85	1,515625	100.000	98.699
9,06	1,581250	105.000	104.278
9,25	1,640625	110.000	109.386
9,44	1,700000	115.000	114.551
9,63	1,759375	120.000	119.770
9,82	1,818750	125.000	125.045
10,00	1,875000	130.000	130.091
10,20	1,937500	135.000	135.754
10,38	1,993750	140.000	140.900
10,57	2,053125	145.000	146.382
10,73	2,103125	150.000	151.037
10,91	2,159375	155.000	156.317
11,09	2,215625	160.000	161.641
11,26	2,268750	165.000	166.709
11,42	2,318750	170.000	171.514
11,56	2,362500	175.000	175.747
11,75	2,421875	180.000	181.532
11,91	2,471875	185.000	186.440
12,07	2,521875	190.000	191.380
12,21	2,565625	195.000	195.730
12,37	2,615625	200.000	200.731
12,52	2,662500	205.000	205.448

Fig. 6. Table 2

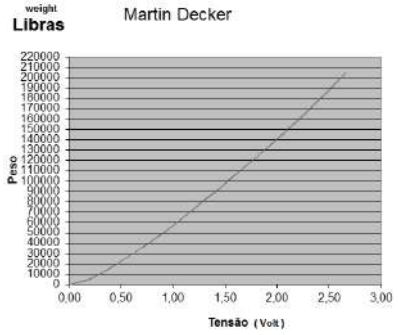

Fig. 7. Grafico 1 -with the standard used by MartinDeck Sotep. In the graph shows the curve (function) if pressure sensor with respect to the weight shown in martinDeck. The polynomial function $y = f(x)$ shown in blue on the side, is the result of (pounds) of the signal coming from sensor X (volts), ie, the signal from 4 to 20 mA sensor that comes through the geolograf equipment (barrier and plate), this signal is converted to a scale of 0 to 5 volts, in turn, the software plays in this value function, applying the factors a, b, CEZ giving the result of the suspended weight in pounds. To ensure better accuracy divided into two curves, one for lower value of X and equal to 1volt and one for values greater than 1volt. The blue curve represents the x MartinDeck Tension Rosy Reading and the curve x Voltage Software.

$$L(T^n) = \frac{n!}{s^{(n+1)}} \tag{3}$$

and

$$L(1) = \frac{1}{s} \tag{4}$$

Where $L(Y)$ is the Laplace Transform function $Y(X)$ and $L(1)$ is the Laplace Transform to 1, which represents the system input.

Substituting in the equation we have:

$$G(s) = \frac{\frac{as^3}{3} + \frac{bs^2}{3} + c + K}{\frac{1}{s1}} \tag{5}$$

Replacing the practical results of the laboratory in variables a, b and c , then we have:

$$G(s) = \frac{\frac{26000s^3}{3} + \frac{35000s^2}{3} - 4000}{\frac{1}{s1}} \tag{6}$$

We consider $c+K$ a constant zero correction of the weight curve of the reader need only be represented by c. In practice this is necessary because the equipment mechanical readers need a manual adjustment. The constant C reresenta well this adjustment.

6. FINDING THE MATRICES THAT REPRESENT THE STATE SPACE FOR THE CONTROL

The concept of controllability and observability were defined by Kalman. They play an important role in the control system of the state space. These concepts can help us in identifying the existence of a complete solution for project control and automation.

A time-invariant linear system , is completely controllable if, given any set of initial data $X(to)$ at instant of initial time$t = 0$, this state can be transferred to a set of final states$t > 0$, through a control signal $u(t)$, defined within the same interval $[t = 0, t > 0]$.

A time-invariant linear system , is said to completely observable if, given the input variables and output of the system at any instant of time, belonging to interval $[t = 0, t > 0]$, one can determine all state vectors $x(to) = x(0)$, and therefore the values of $x(t)$, for any time t.

Using Matlab, we find from the equation $G(s)$, and the $[A, B, C, D] = tf2ss(num, den)$, we have:

$$A = \begin{bmatrix} 0 & 0 & 0 \\ 1 & 0 & 0 \\ 0 & 1 & 0 \end{bmatrix},$$

$$B = \begin{bmatrix} 1 \\ 0 \\ 0 \end{bmatrix}$$

and

$$C = [\,333333\ \ 17500\ \ -4000\,]$$

Proving the existence of output feedback matrices, using the algorithm in (1). To use the algorithm in (2), (3), (4) it was necessary to use artifice that was an increase in input and output monitoring system weight, This was done so that the system satisfied the Kimura conditions :

Given a matrix $A_{n\times n}, B_{m\times n}, C_{p\times n}$, Then, $m + p > n$:

Thus, with the input matrices in MATLAB we obtain:

$$A = \begin{bmatrix} 0 & 0 & 0 \\ 1 & 0 & 0 \\ 0 & 1 & 0 \end{bmatrix}$$

,

$$B = \begin{bmatrix} 1 & 0 \\ 0 & 0 \\ 0 & 1 \end{bmatrix}$$

and

$$C = \begin{bmatrix} 333333 & 17500 & -4000 \\ 0 & 0 & 1 \end{bmatrix}$$

Using the algorithm in (2), (3) (4), we have an array of feedback:

$$AK = 1.0e+004 \begin{bmatrix} 0.0390 & 0.00200 & -0.0004 \\ 0.0001 & 0 & 0 \\ 3.5541 & 0.1867 & -0.0396 \end{bmatrix}$$

With their eigenvalues,

$$ak12 = \begin{bmatrix} -3 \\ -2 \\ -1 \end{bmatrix}$$

The observability and controllability properties of the control system are taken from the rank of **ab** and **ca**, represent below. These eigenvalues were taken from the information of the algorithm:

$$ab = [B, AB, A^2B], \tag{7}$$

$$rank(ab) = 3 \tag{8}$$

(controllable system)

$$ca = [C; CA; CA^2], \tag{9}$$

$$rank(ca) = 3 \tag{10}$$

(observable System)

Using the algorithm in (1) solved the problem of pole placement with commands "acker" to calculate the gain matrix K feedback. We use the algorithm because it is a system with only one input and one output. Using the matrix A:

$$A = \begin{bmatrix} 0 & 0 & 0 \\ 1 & 0 & 0 \\ 0 & 1 & 0 \end{bmatrix}$$

Using the matrix B in the original format, we have:

$$B = \begin{bmatrix} 1 \\ 0 \\ 0 \end{bmatrix}$$

For a matrix A of order 3, we have:

$$J = [\,-1\ \ -2\ \ -3\,]$$

Using then the algorithm in (1) Allocation of poles, then we have:

$$K = [\,6\ \ 11\ \ 6\,]$$

and the eigenvalues :

$$eig(A - B * K) = \begin{bmatrix} -3 \\ -2 \\ -1 \end{bmatrix}$$

The pole placement method is to allocate the poles of the closed-loop system in pre-specified positions. The poles thus chosen determine the closed-loop characteristic polynomial.
For this study, it was important to the theory of control system in state space with emphasis to the case of control with pole placement. The model was in some state space, we find the matrix :

$$K = [\,6\ \ 11\ \ 6\,]$$

Then applied the pole placement theory by state feedback to the observation of known outputs. We used MATLAB software tool for simulation of closed-loop system, then the software in question was made to verify the behavior of output variables and further understanding of the results obtained in simulation, where we got the curves of each of the states system which can later be compared with the actual behavior of the weight reading on the probes automation .

In practice we can use a control system where the feedback occurs through the processed information to meet a need. In the specific case of a probe, we can shoot hydraulic valves and relieve the weight hanging on the "Catherine" or even to perform a tensile strength with the operation.

7. CONCLUSION

Our work in mathematical modeling of the system supervisory for weight suspended in rigs probe, was a priority, find matrices for computational work problems involving control system. This was done based on real numeros of control for a particular type of automation, describing the behavior of specific equipment called Martin Decker, and widely used in oil rigs. However, two methods were used and an analysis of a comparative nature. As expected, for both cases, the feedback matrix are distinct, but that the eigenvalues of the algorithm in (2), (1) and (5) arrays are identical.
Eigenvalues of the matrix in both cases was given by,

$$eig = \begin{bmatrix} -3 \\ -2 \\ -1 \end{bmatrix}$$

In addition, we found the observability and controllability of the system, using [2] algorithm for a system that in practice it was a system completely observable and controllable. Could not be different, because the system is used in probes for many years, and to periodically the system is measured for certification and calibration, by teams of instrumentation.

Another fact to be mentioned is that we develop a linearization of a polynomial system that is currently used in the supervisory system of oil rigs.

REFERENCES

[1] Castelan E. B., Hennet J. C.J. C., Villarreal E. R. Ll.(2003), "Quadratic characterization and use of output stabilizable subspaces," *IEEE Trans. Automat. Control*, 48 (4), 654–660.

[2] Villarreal E. R. Ll., Vargas J. A. R., Hemerly E. M.(2009), "Static Ouput Feedback stabilization using Invariant Subspaces and Sylvester Equations," *TEMA - Tend. Matema. Aplic. Computac.*, 10 (1), 99–110.

[3] Fletcher L. R.(1988), "Eigenstructure Assingment by Output Feedback in Descriptor Systems," *IEEE Proc.*, 135 (4), 302–308.

[4] Kimura, H. (1975), "Pole assignment by gain output feedback," *IEEE Transactions on Automatic Control.*, 24(2). 509-516.

[5] OGATA, K. Engenharia de Controle Moderno. Prentice-Hall, editor,pp. 594657. 2010.

[6] Syrmos, L. and Lewis, F. L. (1994) "Bilinear formulation for the output feedback problem in linear system," *IEEE Trans. Automatic. Control*, 39,(2), 410 414.

[7] Syrmos, V. L., Abdallah, C. T., Dorato, P., and Grigoriadis, K. (1997), "Static output feedback A Survey," *Automatica*, 33, (2), 125137.

[8] Syrmos, V. L. and Lewis, F. L. (1993), "Output feedback eigenstructure assignment using two sylvester equations" *IEEE Trans. Automatic. Control,* 38, (3), 495 499.

[9] Wonahm, W. M. Linear multivariable control, a geometric approach. Springer- Verlag, 1979.

2012 12th International Conference on Computational Science and Its Applications

Stabilization: Algorithms for Mechanical System using Output Feedback and State Feedback

Cláudio Márcio Medeiros de Azevedo
Universidade Federal Rural do Semi Árido (UFERSA)
Pós-Graduação em Sistemas de Comunicação e Automação
Mossoró – RN – Brazil
Email: claudio.matematic@gmail.com

Elmer Rolando Llanos Villarreal
Universidade Federal Rural do Semi Árido (UFERSA)
Departamento de Ciências Exatas e Naturais (DCEN)
Mossoró – RN – Brazil
Email: elmerllanos@ufersa.edu.br

***Abstract*—The present article aims to show systematically computational algorithms to obtaining the transfer function, and find the matrices (A, B, C) state space representation. In the stabilization problem of linear system find output feedback matrix and state feedback matrix, will be used the concept of $(C; A; B)$ invariant subspaces for the problem of mechanical suspension of a car. Based on this concept introduced, reported the existence of a output feedback matrix and state feedback matrix by solution of coupled Sylvester equations, with it will be necessary to present an algorithm that refers to Syrmos- Lewis, a modification is proposed to provide a more appropriate for numerical solution, in part, the condition of Kimura. With this will be presented with numerical examples, where are provided to illustrate the application of the proposed algorithms.**

***Keywords*: Computational algorithm, Mechanical system, Output feedback, Control engineering.**

I. Introduction

The Control Engineering is focused on the study of the dynamics of physical systems. Among the main activities carried out by this engineering, they are modeling, analysis, simulation, design, implementation, and others. The modeling stage is especially important for the study of a control system. At this stage, a mathematical model for a mechanical system is proposed, where the mechanical system refers to a suspension system of an automobile. It is based on it that the other activities are performed, and therefore essential to define a model that accurately represents its dynamics. In general, it should obtain a mathematical model, which is adequate to solve the specific problem in this analysis. However, it is important to emphasize that the results of this analysis are valid only for cases in which the model is valid. When we go to obtain a simplified model of a system, generally we ignore some physical properties of this system. If the effects that these properties have on the response of the system are small, then a good similarity between the results of mathematical analysis and practical results of the system is obtained. In general, the dynamic systems are nonlinear. However, the mathematical procedures for obtaining the solution of linear models are very complicated. For this reason, usually is substituted a nonlinear model by a linear model, with valid only in a limited region of operation, or to a point operating. A system is called linear if it applies the principle of superposition. Where the superposition principle establishes that the response produced by the simultaneous application of two different excitations is equal to the sum of two individual responses to each of the excitations. As a result, linear systems, the response to various inputs can be calculated by considering a single entry at a time and adding the results. So for a better understanding, the work outlined here will be subdivided into four main sections, where we will start talking about the invariant subspaces and coupled Sylvester equations, soon after will be presented the problem to be modeled, where will be presented the function transfer, In which is used to characterize the input-output relation of components or systems that can be written by differential equations linear time-invariant. Apresented the modified algorithm of Syrmos and Lewis based on Theorem 2.1 in [4], that such shown the existence the output feedback matrix for the suspension system of an automobile. Then immediately will discuss the modeling of the problem and algorithmic aspects, to this, power make the formulation in space of states and ending with the matrix determination K with the use of transformation T, where the matrix K, is the output feedback matrix, and ending with the conclusion that it will present the results we have at work.

II. Coupled Sylvester Equations

As in [9], makes use of some concepts and definitions of geometric control theory [14]. It is known that a subspace $\mathcal{V} \subset \mathcal{X}$ (A, B)invariant if there $F : \mathcal{X} \longrightarrow \mathcal{Y}$ such that $(A + BF)V \subset \mathcal{V}$, or equivalently, $A\mathcal{V} \subset \mathcal{V} + ImB$. By subspace a duality $\mathcal{T} \subset \mathcal{X}$ is (C, A) considered to be invariant if there $L : \mathcal{Y} \longrightarrow X$, such that $(A + LC)\mathcal{T} \subset \mathcal{T}$, or equivalently, $\mathcal{T} \supset A(\mathcal{T} \cap Ker(C))$.

It is $V \in \Re^{v \times v}$ such that $Im(V) = V$ and is $T \in \Re^{n-v \times v}$ and a left anhilator of V, $i.e.$: $Ker(T) = Im(V)$.

$$AV - VH_V = -BW \quad (1)$$

$$TA - H_T T = -UC \quad (2)$$

$$TV = 0 \quad (3)$$

The equations play a fundamental role in the treatment of the control problem using static output feedback, especially for auto-structure placement [9] [13]. And leading into account the properties of stabilizability and detectability by the two following definitions::

978-0-7695-4710-7/12 $26.00 © 2012 IEEE
DOI 10.1109/ICCSA.2012.25

Authorized licensed use limited to: Universidade Federal Rural do Semiárido - Campus Mossoró. Downloaded on October 01,2024 at 18:16:27 UTC from IEEE Xplore. Restrictions apply.

- A subspace (A, B) invariant $\mathcal{V}$ is (A, B) internally stabilizable if there F such that $(A+BF)|\mathcal{V}$ is asymptotically stable;
- A subspace (C, A) invariant $\mathcal{V}$ (C, A) externally detectable L such that $(A + B)|\mathcal{X}/\mathcal{V}$ is asymptotically stable;

The necessary and sufficient condition for a subspace $\mathcal{V} = Im(\mathcal{V})$ $O.S$ (C, A, B) invariant that equation (3) be verified with the additional conditions stability by [4]:

$$\sigma(H_V) \in \mathcal{C}^- \tag{4}$$

$$\sigma(H_T) \in \mathcal{C}^- \tag{5}$$

The following theorem makes the relation concept of subspaces $O.S.(A, B, C)$ invariant to the existence of a control law of type static output feedback which stabilizes the closed system.

$$AV - VH_V = -BW, with\ \sigma(H_V) \in \mathcal{C}^- \tag{6}$$

$$TA - H_T T = -UC, with\ \sigma(H_T) \in \mathcal{C}^- \tag{7}$$

$$TV = 0 \tag{8}$$

$$Ker(CV) \subseteq Ker(W) \tag{9}$$

$$Ker(B'T') \subseteq Ker(U') \tag{10}$$

$$where : rank(V) = v\ and\ rank(T) = n - v$$

Note that the results have been presented and explored in different ways in the literature concerning the auto-structure placement using output feedback [12]. As seen, the coupled equations Sylvester (6), (7), (8) describe geometric properties of the subspace $\mathcal{V} = Im(\mathcal{V})$ should be (A, B) asymptotically stable; ally means that the subspaces $Ker(T) = \mathcal{V}$ should be (C, A) externally stabilizable. Thus, under the coupling condition, is that the existence of a subspace $\mathcal{V} = Ker(T)$ $O.S.$ (C, A, B) invariant, with the additional conditions (9), (10) is a necessary and sufficient condition for the existence of solution of the problem considered. Note also that the terms (9), (10) correspond to the existence of a matrix $K \in \Re^{m\times p}$ which verifies the two following equalities:

$$KCV = W \tag{11}$$

$$TBK = U \tag{12}$$

It is important to note that is guaranteed the existence of a solution to the equation of Sylvester, is K has been obtained and such (12) is verified, the eigenvalues in closed-loop are given by:

$$\sigma(A + BKC) = \sigma(HV)\dot{\cup}\sigma(H_T)$$

III. Formulation of the problem

In the translational mechanical systems, there are three mechanical elements that are involved: element of inertia, damping element, element of elasticity. Where the element of inertia (mass) is assumed that the mass is rigid. Thus the connection higher, should not move in relation to less connection, that is, both connections moving the second $x(t)$. already the damping element (damper) there is a relative displacement between the upper connection point and connection point lower. Therefore, there is a need to shift two variables to describe this element. The physical realization of this element is the viscous friction associated with the oil or air. The element of elasticity (spring) can be deformed by an external force, such that the deformation is directly proportional to this force.

There fore, the problem to be modeled consists of obtaining a transfer function of a moving automobile, where it passes through different obstacles (elevations) on the track which will be observed the mechanical system simplified of a system suspension of wheels a car. Then it will be assigned at a certain instant in that car passes by a certain elevation in $25cm$, which is applied to the force F. A schematic representation of a model for the car with a buffer (f) and a spring (k):The System of car suspension is illustrated in Figure 1:

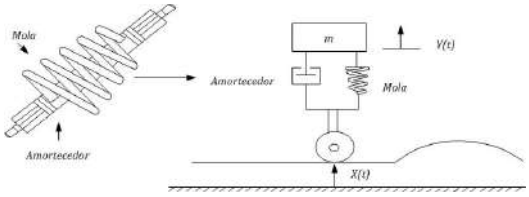

Fig. 1. Suspension System

This is a model corresponding to one of the four wheels of a car. The cylinder of damper contains air that passes from one side to another, when occurs a relative motion. He always applies a reaction force, that is contrary to the movement of his extremities. The viscous damper provides viscous friction, ie, it opposes any relative motion of the two ends, dissipating energy in form of heat. Will be illustrated now the mathematical model that provides the problem. see Figure 2

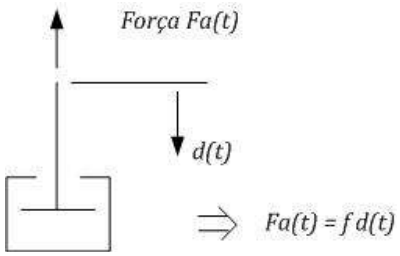

Fig. 2. Mathematical model

Where the forces on the mass m are expressed in Figure 3 With:

$$\begin{cases} \text{force of moll} : F_m = K(y - x) \\ \text{force of buffer} : F_a = f(\dot{y} - \dot{x}) \end{cases} \tag{13}$$

we know that:

$$\Sigma F_y = m.a \tag{14}$$

here fore, we obtain:

$$m.g - f(\dot{y} - \dot{x}) - m.g - K(y - x) = m\ddot{y} \tag{15}$$

Authorized licensed use limited to: Universidade Federal Rural do Semiárido - Campus Mossoró. Downloaded on October 01,2024 at 18:16:27 UTC from IEEE Xplore. Restrictions apply.

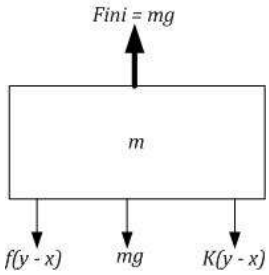

Fig. 3. Force on Mass

Defined above, we know that the continuous transfer function is the relation between the Laplace transform of the output, $Y(s)$, by Laplace transform of the input, $X(s)$. The relation $G(s)$ is a ratio of two polynomials in s:Thus, applying to laplace C.I. zero we obtain

$$\begin{cases} -f(sY(s) - sX(s)) - K[Y(s) - X(s)] = ms^2Y(s) \\ Y(s)[ms^2 + fs + k] = [sf + k]X(s) \\ \frac{Y(s)}{X(s)} = \frac{sf+k}{ms^2+fs+k} = G(s) \end{cases} \tag{16}$$

where f is the reaction force, K is a spring constant and mis the mass of the car.

IV. Modeling the Problem

To illustrate the usefulness of MATLAB in this analysis, assume that an automobile in Motion passes through different obstacles (elevations) on the track. In Figure 4 we have presented an outline of a representative model for the car with a buffer (f) and a spring (k):

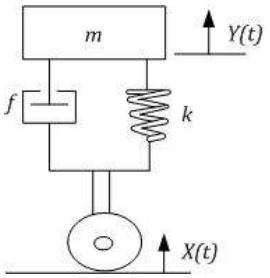

Fig. 4. Model of buffer

Suppose now that this same car passes through a elevation of $d = 25cm$, as shown in Figure 5.

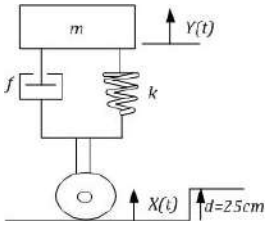

Fig. 5. Representation of elevation

This elevation corresponds to the entry system and is called the step input. To observe the response of the system (movement of the mass-spring system, shock absorber, the alleged car), based on the transfer function of the damper seen previously, we apply the values the instant the car passes this elevation, where invariants are: $m = 1000, f = 500$ e $K = 200$.

Thus, the function acquired in 16 will:

$$\frac{Y(s)}{X(s)} = \frac{500s + 200}{1000s^2 + 500s + 200} = G(s) \tag{17}$$

Writing the transfer function obtained in 17 we have:

$$\frac{Y(s)}{U(s)} = \frac{numerator\ polynomial\ in\ s}{denominator\ polynomial\ in\ s} = \frac{num}{den} \tag{18}$$

Once we have this expression of type transfer function, the command in MATLAB:

$$[A, B, C, D] = tf2ss(num, den) \tag{19}$$

described in [8] provides a state-space representation. It is important to note that the representation in the state space of any system is not unique. There are many (actually infinite) representations for the same system. The command in MATLAB provides a possible representations in space data. From the transfer function obtained in 17, and changing some values, we can visualize so with the values of matrices A, B, C e D we get the following function:

$$\frac{Y(s)}{U(s)} = \frac{0.5s + 0.2}{s^2 + 0.5s + 0.2} \tag{20}$$

As from the transfer function 20, the values matrices A, B e C will be:

$A = \begin{bmatrix} -0.5 & -0.2 \\ 1 & 0 \end{bmatrix}_{2\times2}$ $B = \begin{bmatrix} 1 & 0 \\ 0 & 1 \end{bmatrix}_{2\times1}$ $C = \begin{bmatrix} 0.5 & 0.2 \end{bmatrix}_{1\times2}$

Will be presented following two methods, in which shall be responsible for submitting of arrays of state feedback and output feedback.

A. Feedback States

In this section will reported the method 1 in [8], in which it gets the matrix G state feedback, where:

$$\dot{x} = Ax + Bu \tag{21}$$

$$y(t) = Cx + Du \tag{22}$$

Choose the control signal as:

$$u = Gx \tag{23}$$

To calculate the state feedback matrix of G we will use MATLAB, where we have two commands $acker$ and $place$. the commands $acker$ is based on the Ackerman formula that applies only to systems of one input and one output. the

Authorized licensed use limited to: Universidade Federal Rural do Semiárido - Campus Mossoró. Downloaded on October 01,2024 at 18:16:27 UTC from IEEE Xplore. Restrictions apply.

commands $place$ can be used for both systems as an entry for multiple inputs, it requires that the multiplicity of the desired closed loop poles does not exceed the rank of B. To use the commands $acker$ ou $place$ we will use the matrices A, B and J. The matrices A and B, have been previously defined and the matrix J is the one that consists of closed-loop poles, so that:

$$J = \begin{bmatrix} \mu_1 & \mu_2 & \cdots & \mu_n \end{bmatrix} \tag{24}$$

Applying the mechanical system, the matrix J is:

$$J = \begin{bmatrix} -1 & -2 \end{bmatrix}$$

As from the matrix J, we introduce:

$$G = place(A, B, J)$$

Therefore, the matrix G is:

$$G = \begin{bmatrix} 0.5000 & 0.2000 \\ 1.0000 & 2.0000 \end{bmatrix}$$

To determine the matrix we use $A_G = A - B * K$, then the matrix AG will:

$$A_G = \begin{bmatrix} -1 & 0 \\ 0 & -2 \end{bmatrix}$$

Now, we will use the command $eig(AG)$, to verify that the matrix provides the desired eigenvalues:

$$\begin{bmatrix} -1 & -2 \end{bmatrix}$$

Thus will be shown following graph the resultant curve from the rung response of unitary based on the matrices. A, B, C, D and the matrix of the state feedback G, acquired from the transfer function (20), in Figure 6.

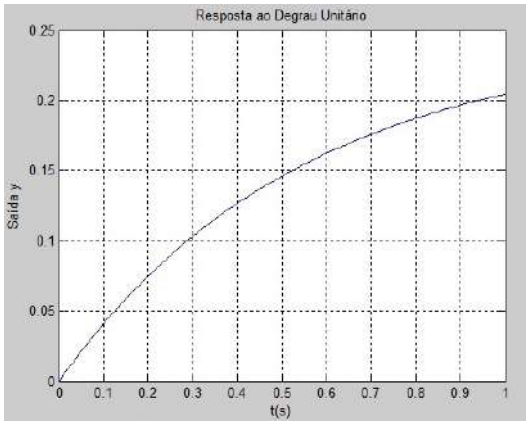

Fig. 6. Unitary rung response

The graph shown in Figure 6, shows the stability of values appropriate for the desired which was obtained from the state feedback matrix.

B. Modified algorithm of Syrmos and Lewis

Based on Theorem 2.1 in [4], the following algorithm, considered in [10], can be used to obtain an output feedback matrix that stabilizes the closed loop system, when the Kimura condition, $n < m + p$, is verified.

Step 1: Select the matrix $H_T \in \Re^{n-p \times n-p}$, where $\sigma(H_T) = \Lambda_T \in \mathcal{C}^-$, and solve (6) to find the matrix $T \in \Re^{n-p \times n}$, such that

$$rank \left(\begin{bmatrix} T \\ C \end{bmatrix} \right) = n \Longleftrightarrow Ker\ T \cap Ker\ C = \{0\} \tag{25}$$

Step 2.1: Solve (6) for some matrix $H_V \in \Re^{p \times p}$, where $\sigma(H_V) = \Lambda_V \in \mathcal{C}^-$, whereas the matrix V satisfy the coupling condition (8) and $rank\,(V)$ is equal to p.

Step 2.2: By construction, the relation (25) guarantees that rank $(CV) = p$. Then G can be calculated as unique solution of (11).
∘

Remark 4.1: Steps 1 and 2 can be implemented by using standard techniques for eigenstructure assignment. By considering H_T e H_V in the Jordan form, the following procedure can be adopted:

Step 1: Find $t_j \in \mathcal{C}^n$ and $u_j \in \mathcal{C}^p$, such that :

$$\begin{bmatrix} t'_j & u'_j \end{bmatrix} \begin{bmatrix} A - \lambda_j I \\ C \end{bmatrix} = 0 \ \forall\ j = 1, \ldots, n-p \tag{26}$$

The row matrix $T \in \Re^{(n-p) \times n}$, denoted for T_j, is constructed by using the vectors t_j, as follows :

- if $\lambda_j \in \Re$, then $T_j = t'_j$;
- if $\lambda_j \in \mathcal{C}$, then $\lambda_{j+1} = \lambda_j^*$ and $\begin{cases} T_j = Re\,(t'_j) \\ T_{j+1} = Imag\,(t'_j) \end{cases}$.

Step 2 : To determine $v_i \in \mathcal{C}^n$ and $w_i \in \mathcal{C}^n$ we have :

$$\begin{bmatrix} A - \lambda_i I & B \\ T & 0 \end{bmatrix} \begin{bmatrix} v_i \\ w_i \end{bmatrix} = 0 \ \forall\ i = n - p + 1, \ldots, n \tag{27}$$

In similar form to the previous case, the used matrices V and W can only be built with real elements. In particular, if $\lambda_i \in \mathcal{C}$, then $\lambda_{i+1} = \lambda_i^*$ and
$\begin{cases} V_i = Re\,(v_i), & V_{i+1} = Imag\,(v_i) \\ W_i = Re\,(w_i), & W_{i+1} = Imag\,(w_i) \end{cases}$, where v_i and w_i denote the columns of the matrices V and W, respectively.

Remark 4.2: [3] Step 1, in Remark 3.1, is concerned with the choice of a matrix T, which verifies (26). Step 2 is concerned with the solution of (6) and (8), to obtain the (A,B)-invariant of $Ker\,(T)$. This property is associated to the "zero equation" (27) [1]. To guarantee the freely placement of the eigenvalues λ_i in step 2 , the system matrix $P(\lambda) = \begin{bmatrix} A - \lambda I & B \\ T & 0 \end{bmatrix}$ of dimension $(2n - p) \times (n + m)$, must be row-full rank $\forall \lambda$. The algorithm is based in the fact that under Kimura condition, $m + p > n$, $P(\lambda)$ does not lose rank for almost all triples (A, B, T) [11]. Thus the zero equation (27)

Authorized licensed use limited to: Universidade Federal Rural do Semiárido - Campus Mossoró. Downloaded on October 01,2024 at 18:16:27 UTC from IEEE Xplore. Restrictions apply.

has solutions for all λ_i. In the presence of invariant zeros, it is possible to remake Step 1 to search other solutions for the Sylvester equation (6).

Remark 4.3: In the less restrictive case $m + p = n$, $P(\lambda\ )$ is square of dimension $(2n - p) \times (2n - p)$, and all triple (A, B, T) has p finite invariant zeros [10]. In this case, the basic procedure can produce stabilizing solutions only if T , found in step 1, generates p stable invariant zeros, which have to be used to solve (27) [1].

Example 4.1: : Consider the linear system defined by [6] :

$$A = \begin{bmatrix} 0 & 1 & 0 & 0 \\ 1 & 1 & 0 & 0 \\ -1 & 0 & 0 & 0 \\ 0 & 0 & 0 & 0 \end{bmatrix} \ ; \ B = \begin{bmatrix} 0 & 0 \\ 1 & 0 \\ 0 & 0 \\ 0 & 1 \end{bmatrix} \ ; \ C = \begin{bmatrix} 1 & 0 & 0 & 0 \\ 0 & 0 & 1 & 0 \\ 0 & 0 & 0 & 1 \end{bmatrix}$$

The system is controllable and observable and $m + p = 5 > n$. The desired eigenvalues are : $\Lambda_T = \{-4\} \cup \Lambda_V = \{-3, -2, -1\}$.

Step 1 : By considering that $\lambda_1 = -4$, and using (26) we have

$T = \begin{bmatrix} -0.3148 & 0.0630 & -0.2406 & -0.2425 \end{bmatrix}$, where (A, B, T) has not invariant zeros

Step 2.1 : For $\lambda_2 = -3$, $\lambda_3 = -2$ and $\lambda_4 = -1$, by using (27) we have:

$$V = \begin{bmatrix} 0.0727 & 0.1324 & 0.2425 \\ -0.2182 & -0.2649 & -0.2425 \\ 0.0242 & -0.0662 & 0.2225 \\ -0.1751 & -0.3064 & -0.6184 \end{bmatrix} \ , \ W = \begin{bmatrix} 0.7999 & 0.6622 & -0.2424 \\ 0.5254 & 0.6128 & \end{bmatrix}$$

[4][2]:

Step 2.2 : Based on $GCV = W$, we have $G = \begin{bmatrix} -46.9778 & -20.7333 & -26.9444 \\ -16.1410 & -9.3519 & -10.9968 \end{bmatrix}$. The closed loop matrix $A_G = A + BGC$ is then

$$A_G = \begin{bmatrix} 0.0000 & 1.0000 & 0.0000 & 0.0000 \\ -45.97778 & 1 & -20.7333 & -26.9444 \\ -1.0000 & 0.0000 & 0.0000 & 0.0000 \\ -16.1410 & 0.0000 & -9.3519 & -10.9968 \end{bmatrix}.$$

△

C. Output Feedback

In this section we will present a technique based on algorithmic procedures for auto-structure placement to obtain a output feedback [4][2]. Where the technique proposed by Lewis and Syrmos[6] solves the coupled Sylvester equations in two steps and can be directly applied to systems that verify the condition $m + p > n$, condition known as Kimura [4]. It is clear that the dimension of $V = Im(V)$ equals the number of outputs p, seeking to ensure that the matrix $CV \in \Re^{p \times p}$ is invertible and, so that the matrix of feedback gains can be found, from equation (11), the form $K = W(CV)^{-1}$.

It will be also shown that if, the considered system is completely state controllable, then the poles of closed-loop system can be placed in any desired position by means of a state feedback, using an appropriate gain matrix,with that, limit our discussion to systems an input and an Output. The requirement is that the system is completely controllable.

Consider the following system defined on [3].

$$\dot{x} = Ax + Bu \quad (28)$$
$$y = Cx + Du \quad (29)$$

Choose the control signal as:

$$u = -Kx \quad (30)$$

This means that the control signal u is determined by an instantaneous state. This scheme is called state feedback. The matrix $K_{1\times n}$ is called state feedback matrix . Thus, the mechanical system represented in state space is represented as follows:

The electrical system represented in state space is:

$$\begin{bmatrix} \dot{x_1} \\ \dot{x_2} \end{bmatrix} = \begin{bmatrix} -0.5 & -0.2 \\ 1 & 0 \end{bmatrix} \begin{bmatrix} x_1 \\ x_2 \end{bmatrix} + \begin{bmatrix} 1 & 0 \\ 0 & 0 \end{bmatrix} u$$

$$y = \begin{bmatrix} 0.5 & 0.2 \end{bmatrix} \begin{bmatrix} x_1 \\ x_2 \end{bmatrix}$$

Further, it is considered that the system represented by (C, A, B) is controllable and observable, this necessary condition for the arbitrary choice of the poles to be placed in closed loop. This condition can however be relaxed for the stabilization and detectability of (C, A, B), which implies the use of non-controllable eigenvalues non-observable in the spectrum for the desired closed-loop system. Assume that T can be found from the matrices $[A, B, C]$ As determined in 0 6184

$$A = \begin{bmatrix} -0.5 & -0.2 \\ 1 & 0 \end{bmatrix}_{2\times 2}$$

$$B = \begin{bmatrix} 1 & 0 \\ 0 & 1 \end{bmatrix}_{2\times 1}$$

$$C = \begin{bmatrix} 0.5 & 0.2 \end{bmatrix}_{1\times 2}$$

The corresponding system is controllable and observable and $m+p = 3 > n$. Then determine the matrix T verified the equation (17) in [4] [2]. Thus the matrix T Thus the matrix:

$$T = \begin{bmatrix} -0.7071 & -0.0000 \end{bmatrix}_{1\times 2}$$

The matrices V and W are determined using the equation (18) in [4] [2]:

$$V = \begin{bmatrix} 0.0000 & -0.4454 \end{bmatrix}_{1\times 2}$$

$$W = \begin{bmatrix} 0.0891 & 0.8909 \end{bmatrix}_{1\times 2}$$

be determined K such that $KCV = W$:

$$K = \begin{bmatrix} -1.0000 \\ -10.0000 \end{bmatrix}_{2\times 1}$$

The closed-loop matrix $A_k = A+BCK$ *correspondent, whose eigenvalues are the desired, is:*

$$A_k = \begin{bmatrix} -1.0000 & 0.0000 \\ -4.0000 & -2.0000 \end{bmatrix}_{2\times 2}$$

$$A_{k1} = \begin{bmatrix} -1 \\ -2 \end{bmatrix}_{2\times 1}$$

Authorized licensed use limited to: Universidade Federal Rural do Semiárido - Campus Mossoró. Downloaded on October 01,2024 at 18:16:27 UTC from IEEE Xplore. Restrictions apply.

V. Conclusion

The present paper was considered the stabilization problem by output feedback and state feedback to stabilize a mechanical system. Introduced the concept of subspaces O.S.(C, A, B) invariants and their relation to the solution of the stabilization problem of using output feedback by Sylverter coupled equations, showing that they play a key role in the response of stabilization problem of linear systems. The paper has focused on theoretical and algorithmic aspects. In particular, a necessary and sufficient condition for the existence of a output feedback. An algorithm has been proposed to calculate a feedback matrix using condition to Kimura $m+p > n$. Aim is to develop future studies aimed at deepening the applications, and so, can be presented other techniques mentioned in [8]. in order to further facilitate the analysis proposed in the paper.

References

[1] E. B. Castelan and J. C. Hennet, "Eigenstructure Assignment for State Constrained Linear Continuos Time Systems", *Automatica*, vol.28.

[2] E.B. Castelan, J. C. Hennet, E. R. L. V.. Quadratic characterization and use of output stabilizable subspace. pages 654 660. IEEE Control Systems V48, 2003.

[3] E. B. Castelan and J. C. Hennet and E. R. Ll. Villarreal, "Quadratic Characterization and Use of Output Stabilizable Subspaces",*Automatic Control IEEE Transactions on*, vol.48, no.4.

[4] Elmer R. L. Villarreal, J. A. R. Vargas, E. M. Hemerly.. Static output fedback stabilization using invariant sub space and sylvester equations, Revista TEMA - Tendências em Matemática Aplicada e Computacional. Vol. (1), pages 99 110. 2009.

[5] Fletcher, R., Kautsky, J., Kolka, G. K. G., and Nichols, N. K.. Eigenstructure ass- ingment by output feedback in descriptor systems. In IEEE Trans. Automatic. Control, vol. 42, pages 1457 1468. Systems and Control Letters 24(2). 1985.

[6] L. R. Fletcher and J. Kautsky and G. K. G. Kolka and N. K. Nichols, "Eigenstructure Assingment by Output Feedback in Descriptor Systems", *Automatic Control IEEE Transactions on*, vol.42, no.4, pp.1457-1468, 1985.

[7] Kimura, H.. Pole assignment by gain output feedback. In IEEE Transactions on Automatic Control vl. 20, page 509 516. Systems and Control Letters 24(2). 1975.

[8] OGATA, K. Engenharia de Controle Moderno. Estabilização por realimentação de saídas. In Prentice-Hall, editor,pages 594 657. 2010.

[9] Syrmos, L. and Lewis, F. L. . Bilinear formulation for the output feedback problem in linear system. In IEEE Trans. Automatic. Control, vol. 39, number 2, pages 410 414. 1994.

[10] V. L. Syrmos and F. L. Lewis, "Output Feedback Eigenstructure Assignment Using Two Sylvester Equations", *Automatic Control IEEE Transactions on*, vol.38, no.3, pp.495-499, 1993.

[11] V. L. Syrmos and F. L. Lewis, "Transmission Zero Assignment using Descriptions", *Automatic Control IEEE Transactions on*, vol.38, no.7, pp.1115-1120, 1993.

[12] Syrmos, V. L., Abdallah, C. T., Dorato, P., and Grigoriadis, K. . Static output feedback. In A Survey Automatica, vol. 33, number 2, pages 125 137. 1997.

[13] Syrmos, V. L. and Lewis, F. L. . Output feedback eigenstructure assignment using two sylvester equations. In IEEE Trans. Automatic. Control, vol. 38, number 3, pages 495 499. Springer-Verlag. 1993.

[14] Wonahm, W. M. (1979). Linear multivariable control, a geometric approach. Springer- Verlag.

Authorized licensed use limited to: Universidade Federal Rural do Semiárido - Campus Mossoró. Downloaded on October 01,2024 at 18:16:27 UTC from IEEE Xplore. Restrictions apply.

Applied in Fuzzy Logic Controller in Smart Structures

Villarreal E. R. Ll.* Lima N. W. B*., Silva. R. D.*, Rodrigues W. M.*

**Universidade Federal Rural do Semiárido*
Departamento de Ciências Exatas e Naturais
5962-5900, Mossoró, RN, Brasil
e-mail: elmerllanos@ufersa.edu.br; wontoon_@hotmail.com;
reginaldodantasfla@hotmail.com;walterm@ufersa.edu.br

Abstract: This paper presents studies related to active control of vibration of piezoelectric smart structures that show that these materials generally exhibit nonlinear characteristics or behaviors and noted the optimal location of piezoelectric patch by the D-optimal design principle. This makes the use of conventional methods disadvantageous. Due to this fact the present article aims to show the application of fuzzy logic controllers, a process that increases efficiency and reduces the complexity of calculations. In it are discussed methods of Mamdani and Takagi-Sugeno-Kang. The fuzzy rules were established based on the analysis of the movements of a cantilever.

Key words: Smart Structures, Fuzzy logic controllers, Piezoelectric Materials.

1. INTRODUCTION

We are witnessing a world that has as one of the main goals to make discoveries that enable innovation. In this context, one of the techniques that has gained prominence in industries related to aeronautics and civil structures is the use of intelligent control systems that are structural in which sensors are connected, control laws, associated electronics, actuators, signal processing, etc. In other words, structures are able to react and modify certain actions by the environment. This paper presents an optimization method using the D-optimal design principle simplified to determine an optimal principle for the best location of piezoelectric elements, and then designs a fuzzy logic controller to control the beam's vibratiom.

An example of application of these structures is the use of such composite materials are intelligent microfibers forming a web piezoelectric interconnected. Through this, researchers were able to assemble materials with active and passive layers where part of this work as a sensor, actuator, etc. as another. So the fact problematic ultralight composites have reduced capacity of adaptability, as lighter materials are subject to more intense vibrations, can be solved and these can help produce more efficient vehicles with lower fuel consumption and higher performance .

Another area of emphasis related to smart structures is the use of unconventional methods in process control of them which has enabled the use of more complex systems, with the largest number of variables and parameters inaccurate. This advantage coupled with piezoelectric materials that are equipped with features such as low weight, great strength of performance, response to stimuli from the external environment in a short period of time, ability to direct conversion of electrical energy into mechanical, has called the attention of major centers research as NASA Langley and several industry sectors. So, piezoelectric is a kind of Smart material, due to the following two characteristics: the first is direct and inverse piezoelectic effects and the second is the ability to be used as the sensor or the actuator in active vibration control systems. Among the unconventional methods we can mention the fuzzy logic and neural networks.

There are conventional techniques of classical control that give good results for systems with a linear or slightly non-linear and exhibiting only one inlet and one outlet, but it can not be applied to systems that run from this pattern. The feedback

control with proportional gain constant is a classic example of a technique for controlling vibrations in structures with piezoelectric.

How many current problems involving complex systems are more unconventional methods studied. Two models using fuzzy logic for control structures are the model of Mamdani and Takagi-Sugeno-Kang. This first one is considered a linguistic fuzzy model which makes it the most intuitive, since it is more like our ways of manipulating information. The second is based on a set of rules and provides as output a real number or result exact - so it is not as intuitive - which increases their processing efficiency, since the accounts involved in the computational process becomes simpler and this makes it more accurate.

Another disadvantage of the method of Mamdani is that it can reduce the vibration with the passage of time, but there comes a point when the vibration is relatively low, the controller itself induces a residual vibration in the beam. The controller based on the method of Takagi-Sugeno-Kang and suppresses vibrations more efficiently perform this process in a shorter time period.

2. MODELING

In order to reduce the vibration of smart structures, this article shows the piezoelectric correction method based on Takagi-Sugeno-Kang, and uses fuzzy logic to control the vibration of smart structures. The fuzzy logic controller (FLC) was developed based on projects that use the displacement and velocity of the balance beams as inputs, and control power balance on the beams as the output. This new method improves efficiency and reduces the complexity of the calculations. The simulation results with Matlab illustrate that the proposed method has better control and performance than conventional methods.

The placement of piezoelectric patches plays an important role in the design procedure of the active structures. The researchers have focused on development of the optimal piezoelectric patch location. (Guo, et al., 2004) presented a global optimization of sensor locations based on the damage detection method for structural health monitoring systems. (Martin Kögl, et al., 2004) presented a novel approach to the design os piezoelectric plates and Shell actuators using topology optimization.

However, in order to make use of the above-mentioned measures, a flexible structure state space equation should be modeled by the given location of piezoelectric patches. The D-optimal design principle is an optimization method presented by (Bayard, et al., 1988) which suggests that the máximum determinant of Fisher Information Matrix Criteria is chosen as the optimization function and then simplified to determine an optimal principle for the best location for piezoelectric elements.
Now to understand the model should be considered as beam or plate structures connected to sensors and piezoelectric actuators in a rectangular shape. The sensors and actuators are placed symmetrically on both sides of the same frame position, as shown in Figure 1.

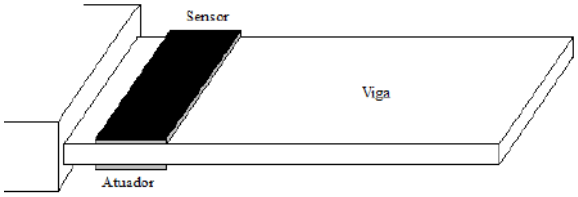

Fig. 1. Sensors and actuators on the beam

The finite element method may be used to analyze the model arbitrary geometry and the anisotropic properties of the piezoelectric materials.

Indeed, the sensors are used to estimate the state parameter. Well we play the imput and output data and based on the theory of mathematical statistics, the determinant of Fisher Information Matrix det(F) has inverse ratio to low bound of variance of parameter unbiased estimation. Due to the symmetrical collocation of the piezoelectric patches, if the locations of sensors have been confirmed, the actuators will be at the same locations as the sensors. For a slightly damped structure, the principle used can be simplified to decouple the problems of placement of actuators, sensors and control input. The principle can be written as:

$$Max(\det F) \tag{1}$$

Subject to $$\beta \in B_m, B_m = \left\{ \sum_{k=1}^{M} \beta_k = m \right\}$$

where $\boldsymbol{\beta}$ β is the location selection matrix and B_m is the set of possible locations. The function can also be written as:

$$S(m) = \max_{\beta} \sum_{i=1}^{N} \log\left(\sum_{k=1}^{M} \beta_k \frac{\left(\gamma_k^T \phi_i\right)^2}{\varphi_k^2} \right) \tag{2}$$

where N and M are the number of models and the possible locations of, m is the number of the sensors, β_k is composed of 0 and 1 – if $\beta_k = 1$, there is a sensor located on the location, in contrast, if $\beta_k = 0$, then on site has no sensor –, γ_k is a vector coefficient related to kth location of sensor, φ_i is a normalized mode shape vector, φ_k is the noise covariance of the sensor signal and can be defined as 1.

The physical meaning of (2) can be considered to find the location of peak loads. Therefore, $\gamma_k^T \phi_i$ is equivalent to the output of load sensors. If we assume that the area of the sensor is sufficiently small compared with the beam (plate), the load sensor can be written as:

$$q = D \times A = A \times \left(D_x + D_y\right) \tag{3}$$

$$D_x = d_{31} E_{pe} \varepsilon_x = d_{31} E_{pe} \frac{\partial^2 \omega}{\partial x^2} \frac{t_p}{2} \tag{4}$$

$$D_y = d_{31} E_{pe} \varepsilon_y = d_{31} E_{pe} \frac{\partial^2 \omega}{\partial y^2} \frac{t_p}{2} \tag{5}$$

where D_x is the offset voltage generated by an electrical axis X, D_y is the electric displacement generated by an effort on the shaft Y and A is the area of the sensor. For the beam structure, the electric displacement is generated by a unidirectional voltage. d_{31} is the piezoelectric voltage constant. E_p and t_p are the Young's modulus and the thickness of the piezoelectric section. ω is the deflection of the structure.

Based on the differential equation of second order scheme, $\frac{\partial^2 \omega}{\partial x^2}\Big|_k$ and $\frac{\partial^2 \omega}{\partial y^2}\Big|_k$ can be expressed as:

$$\frac{\partial^2 \omega}{\partial x^2}\Big|_k \approx d_x^2 \omega = \frac{\omega(i) + \omega(j) - 2\omega(k)}{(dx)^2} \tag{6}$$

$$\frac{\partial^2 \omega}{\partial y^2}\Big|_k \approx d_y^2 \omega = \frac{\omega(m) + \omega(n) - 2\omega(k)}{(dy)^2} \tag{7}$$

Substituting (4), (5), (6) e (7) into (3) we obtain

$$q = d_{31} E_{pe} A \lambda_y \tag{8}$$

where

$$\lambda_y = \frac{t_p}{2}\left(\frac{\omega(i) + \omega(j) - 2\omega(j)}{(dx)^2} + \frac{\omega(m) + \omega(n) - 2\omega(j)}{(dy)^2} \right);$$

The deflection of the structure ω can be expressed in terms of ϕ_i

$$\omega = \sum_{i=1}^{N} \eta_i \phi_i \tag{9}$$

in which η_i is a generalized form of coordinate. Substituting (9) into (8), arrive at $\sum_{i=1}^{N} \gamma_k^T \phi_i = q$, γ_k^T can be written as:

$$\gamma_k^T = \frac{1}{2} \eta_i A d_{31} E_{pe} \lambda_k^i \tag{10}$$

where

$$\lambda_k^i = \phi_i \frac{t_p}{2}\left(\begin{array}{l}\frac{1}{(dx)^2}\begin{bmatrix}0 & 1_i & -2_k & 1_j & 0\end{bmatrix}+\\ \frac{1}{(dy)^2}\begin{bmatrix}0 & 1_m & -2_k & 1_n & 0\end{bmatrix}\end{array}\right)$$

and ϕ_i is a normalized mode shape vector. Substituting (10) into (2), we can make a simplification:

$$S(m) = \max_{\beta} \sum_{i=1}^{N}\left(\sum_{k=1}^{M}\eta_i \beta_k \lambda_k^i\right)$$

(11)

With the power generation of vibration, the equation of motion in the form of coordinates can be written as:

$$\ddot{\eta}_i(t) + 2\xi_i\omega_i\dot{\eta}_i(t) + \omega^2\eta_i(t) = \frac{1}{M_i}f(t)$$

(12)

where $\ddot{\eta}_i$, $\dot{\eta}_i$ and η_i represent the acceleration mode, velocity and displacement, respectively, ω_i and ξ_i are the natural frequency and damping mode. Due to the flexible structure and the absence of damping inside, $\xi_i = 0$.

For a different strength, each form has a different proportion in the way of vibration of a structure. Assuming that vibration generating force is taken as a unit impulse, the structure vibrates in accordance with the bottom shape and other shapes can be ignored. Thus, the piezoelectric sections should be placed at most all stains (piezoelectric). The spot mode unit can be written as:

$$\overline{\lambda_k^i} = \lambda_k^i / \max(\phi_i)$$

(13)

Integrating the equation (13) and (11), we can write a new function:

$$S^*(m) = \max \sum_{i=1}^{N}\left(\sum_{k=1}^{M}\beta_k \overline{\lambda_k^i}\right)$$

(14)

Thus, the performance criteria of local sensors can be obtained using the shapes of the structures.

3. FUZZY LOGIC CONTROLLER APPLIED TO SMART STRUCTURES

The fuzzy logic controller uses a form of quantification of inaccurate data (input fuzzy sets) to generate an inference relating to a knowledge base of the control force to be applied in the system. The advantage of this quantification is the set of inaccurate data can be represented by a unique linguistic expression such as small, medium and large.

In this article the inputs are the displacement and swing speed of the output beam and the control force is about the same. Basing on the control rules, the signal is translated to the driver. The function of fuzzy logic controller is making the imput fuzz up. In other words, it is the fuzzy control that executes the process of fuzzed. The fuzzy contol's basic was the rule database which was composed of several rules. The method of control vibration is minimized the response of displacement of cantilever beam.

In fuzzification, the offset is set in the range of -5 to 5 (-5,-4,-3,-2,-1,0,1,2,3,4,5), the speed is set to -2 to 2 (-2,-1,0,1,2) and force control is set from -7 to 7 (-7,-6,-5,-4,-3,-2,-1,0,1,2,3,4,5,6,7). Two membership functions commonly adopted in the fuzzy logic controller are the triangular and trapezoidal.

The ultimate goal of the controller based on fuzzy logic is to make inaccurate data closer to reality and its function is to provide a force to minimize the vibration of the beam.

The rules were implemented according to fuzzy rule base shown in Fig. 2. From it we extract the following:

(1) If the PS and the speed offset is PB, the tip of the beam (beam end) is away from the equilibrium position. It is therefore a need to add strength NB down, causing the tip of the beam is close to the reference value.

(2) If CP is displacement speed and PS is the tip of the beam is up, ie the displacement is maximum. Therefore, you must add an NS force down and this will cause the vibrating motion of the beam passes close to the reference value (stability).

(3) If the CP and is displacement speed NS, the tip of vibration of the beam is below the equilibrium position. Thus, it is necessary to add a force NS to the tip of the beam is near the equilibrium value.

(4) If the PS and the speed offset is NB, the tip of the vibrating beam is below the equilibrium position. It is necessary to add a force NB so that the tip of the beam is close to the reference value.
(5) If the offset is NS and speed is NB , the tip of the vibrating beam is far from equilibrium position. Thus, a force must be added to CP that the vibration in the beam becomes close to the reference value.
(6) If the displacement is NB and the speed is NS, the tip of the beam will have the maximum displacement to down. Thus, an upward force PS should be added so that the end of the beam is near the reference values.
(7) If the displacement is NB and the speed PS, to leave the beam close to the reference value is priciso add a force PS.
(8) If the offset is NS and PB is the speed, the tip of the vibrating beam has a maximum displacement upwards. Therefore, for this shift is near the equilibrium position, it is necessary under the addition of a CP.
(9) If the offset is PM and the speed NS, presents the instability of the beam vibration. So that the beam must be balanced by addition of an NM force.
(10) If the displacement is NM and the speed NS, the tip of the vibrating beam is not in equilibrium. This is a force required for the motion PM beam is close to the reference value (balance).

F / D / V	NB	NM	NS	ZO	PS	PM	PB
NB	PS	PM	PB	ZO	NB	NM	NS
NS	PS	PM	PB	ZO	NB	NM	NS
ZO	ZO	ZO	ZO	ZO	ZO	ZO	ZO
PS	PS	PM	PB	ZO	NB	NM	NS
PB	PS	PM	PB	ZO	NB	NM	NS

Fig 2. Fuzzy rule base

The simulation system is carried out by software Matlab / Simulink, as shown in Fig. 3. Fig. 4 shows the control surface. The simulation results digital graphs showing the time required for equilibration of the beam (x axis) and the same displacement (y axis) is displayed in Fig. 5. The fuzzy rules are explained in Fig. 6.

Fuzzy Logic Controllers is designed to control nonlinear vibration of a Smart structure and the effects of the controllers over the system are examined. Fuzzy logic controller using in such system which has nonlinear vibrations gives a good result as tip position control of a Smart structure. Observing Fig 5, we see settling time of system is approximately 7s, and the displacemente of the tip of the bean decrease over time, so this method has practical value in preventing vibration of displacement. Accordi ng to these results, suitable performance of fuzzy logic controller is determined for tip position control of a Smart structure system. The fuzzy logic controller designed is established properly and this new controller can be used for such kind of system.

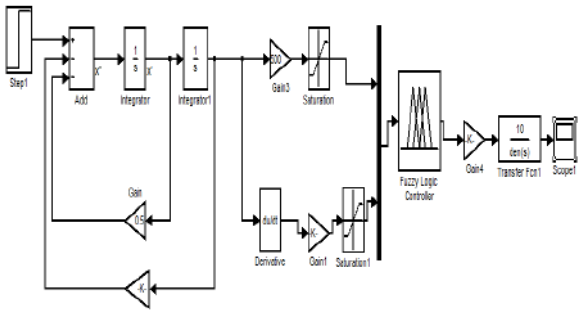

Fig. 3. Fuzzy Logic in Control system

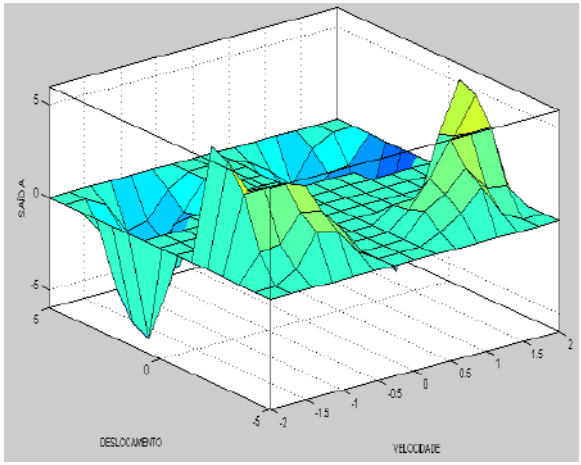

Fig. 4. Control surface

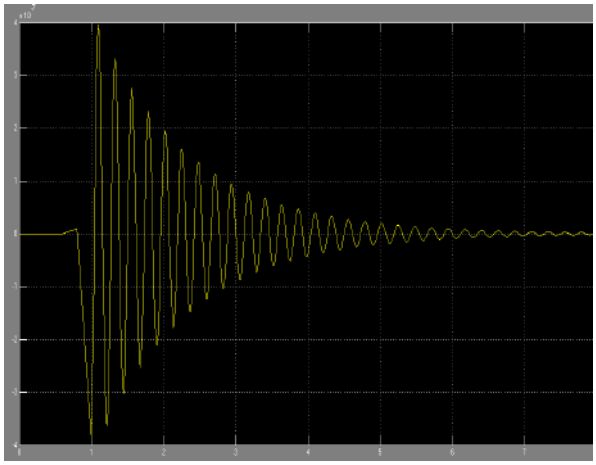

Fig. 5. In response to the position of the tip of the cantilever over time

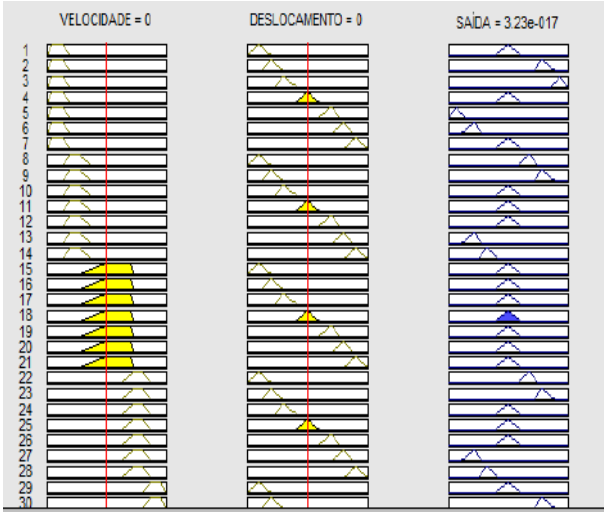

Fig. 6. Viewer of the rules

4. CONCLUSION

Given the current development and the search for new technologies, methods that can improve the performance of structures and machines, we conclude that the smart structures play a key role with regard to the fact that open ways to achieve greater efficiency in many areas of industry, such as aeronautics and civil. We also found that among the various methods the controller that uses fuzzy logic is what gives the best results, as well as provide more accurate results allows the use of more complex systems with more variables.

REFERENCES

Abreu, G.L.; Ribeiro, J.F. (1999). Controle ativo de vibração usando controladores baseados em lógica fuzzy. In: *Anais Congresso Brasileiro de Engenharia Mecânica*, 15. Águas de Lindóia, 1999.

Agrawal; B.N.; Treanor, K. E. (1999). Shape control of a beam using piezoelectric actuators. *Smart Material and Structures*, v. 8, p. 729-740.

Babuska, R.; Verbruggen, H.B. (1996). An overview of fuzzy modeling for control. *Control Engineering Practice*, v. 4, n. 11, p. 1593-1606.

Bayard D. S., Hadaegh, F. Y. and Meldrum, D. R., (1988), Optimal experiment design for edentification of large space structures, *Automatica*, 24(3): 357-364.

Blanguernon, A.; Léné, F.; Bernadou, M. (1999). Active control of a beam using a piezoceramic element, *Smart Material and Structure*, v. 8, p. 116-124.

Crawley, E. F.; de Luis, J. (1987). Use of piezoelectric actuators as elements of inteligente structures, *AIAA Journal*, v. 25, n. 8, p. 1373-1385.

Guo, H. Y. Zhang, L. L. and Zhou, J. X., 2004, Optimal placement of sensors for structural health monitoring using improved genetic algorithms, *Smart Materials and Structure*, 13:528-534.

Hwang, W.S.; Park, H.C. (1993). Finite element modeling of piezoelectric sensors and actuators. *AIAA Journal*, v. 31, n. 5, p. 930-937.

Ikeda, T. (1990). *Fundamentals of Piezoelectricity*. Oxford, Oxford Science Publications.

Martin Kögl and Emílio, C. N., Silva, 2004, Topology optimization of smart structures: design of piezoelectric plate and shell actuators, *Smart Materials and Structure*, 14:387-399.

New Approach in pH Neutralization Process Using Fuzzy Controller

Morais F.A*, Villarreal E. R. L.*, Gurgel D. P. * Rodrigues M. W. *

* UFERSA-Universidad Federal Rural do Semi-Arid - DCEN - Department of Exact and Natural Sciences, BCT-Bachelor of Science and Technology, Av Francisco Mota 572, 59625-900 Mossoró RN.

(e-mail: aldo_apodi@hotmail.com), (e-mail: elmerllanos@ufersa.edu.br) , (diego_dji@hotmail.com), (walterm@ufersa.edu.br)

ABSTRACT - This paper studies the control of a pH neutralization process using a fuzzy controller. Because of high non-linearity of the process, the fuzzy controller may not operate properly. The hydrogen potential, providing an indication of the degree of acidity, neutrality or alkalinity. To ensure a complete efficiency of the controller, is used to detect an auxiliary variable region of process operation. Thus the controller has three inputs; auxiliary variable, and error control and error variation and a control output, change in control action. The fuzzy logic controller designed using this auxiliary variable, can provide satisfactory performance in all regions.

Keywords: Fuzzy Control, nonlinearity, process techniques, error control.

1. INTRODUCTION

In an very competitive world, industries are increasingly seeking to profit and it is important to master all the parties involved in a process. Thus, companies are required to continuously improve the productivity of its plants. The process of pH control is very important in chemical, petrochemical and biological fields, with various applications, for example, in the manufacture of detergents and soft.

The idea of control is to specify a pH value to achieve certain goals, such as speed up and improve process, obtaining a product with higher quality and, thus, generating more profit for corporations. The great difficulty in controlling pH is its high nonlinearity. Because of this, conventional controllers, such as PID, have presented disadvantages to this type of process. These problems can be best treated by the use of adaptive intelligent, predictive controllers, or combination of these techniques. In this work, we presented a model using fuzzy logic to control a pH neutralization plant.

So this paper is structured as follows. In section 2, we discussed the basis of pH neutralization. Section 3 presents and took out the application of fuzzy logic controller of the pH neutralization process. In section 4 shows the results obtained in this study. In the end, some conclusions are presented in section 5.

2. BASIC CONCEPTS OF THE NEUTRALIZATION PROCESS PH

The hydrogen potential (pH), is a quantity that represents the concentration of hydrogen íons H^+, providing an indication of the degree of acidity, neutral or alkaline aqueous solutions (Berni, 2004). The pH ranges from 0 to 14. For values above 7, the solution is considered to be basic, and as the pH is equal to 7, the solution is neutral.

In an acid base reaction is the release of, and OH^-In an acid-base reaction, it is the release of H^+ and OH^-. Thus, we have in a solution the hydrogen ion concentration [H^+] OH-ions concentration [OH^-] are inversely correlated, i.e. the increase results in a drop of the other and vice versa. Thus, in an acidic solution for more than ions H^+ than ion OH^-, whereas in alkaline solutions. There are ions OH than H + ions, and as their concentration are equal, there is a neutral solution. The "equation 1" below shows the mathematical expression of the hydrogen potential.

$$pH = -\log_{10}[H^+] \quad (1)$$

Since [H^+] is the concentration of hydrogen ions in moles / liter.

You can calculate the OH-ions concentration potential through the mathematical expression shown in "Equation 2" below:

$$pOH = -\log[OH^-] \quad (2)$$

The "equation 3" below shows the relationship between the hydrogen potential and OH-ion concentration.

$$14 = pH + pOH \quad (3)$$

So just knowing the concentration of H^+ or OH^- ions can calculate pH and pOH of the solution.

A neutralization reaction is a reaction between an acid and a base to form salt and water. The reaction can take two forms, partial and total. In the partial form only part of H^+ ions of the acid and OH^- ions react base; while the total form, all of the acid H^+ and OH^- ions react all base.

3. FUZZY LOGIC

Fuzzy logic is considered inaccurate because it works with vague approximations of data (Sturm, 2005). Through a given rule, which varies according to what purpose fuzzy logic is used, the data collected characterized as uncertain are analyzed according to the rule implemented and approximate numbers to allow the interpretation of the machines and computers. The "Figure 1" shows that the fuzzy logic system between the input and output data has a fuzzificator, a rule base, an inference module and a defuzzificator, as described below: 1) Fuzzification module: it is mathematically modeling the information of the input variables by means of fuzzy sets. It is the module that shows the great importance of the expert process to be analyzed, for each input variable, it must be assigned linguistic terms representing the states of this variable, and each linguistic term should be combined with a fuzzy set by a function relevance; 2) Module of basic rules: this is what constitutes the core of the system. This is the module where keep the linguistic variables and their classifications; 3) Inference module: it is where you define the logical connectives used to establish the relationship that form the fuzzy rule base. It is this module that depends on the success of the fuzzy system as it will provide the output (control) to be adopted by the fuzzy controller from each input fuzzy, and 4) Defuzzification module: it reflects the state of the fuzzy output variable to a numeric value.

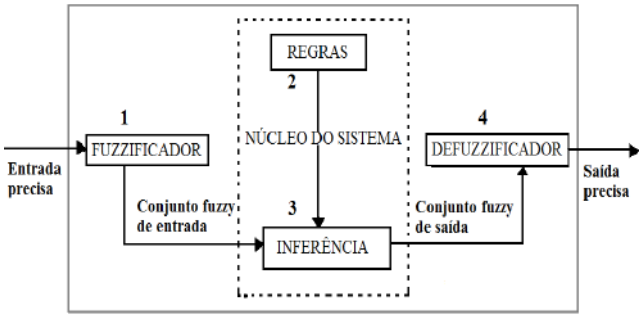

Figure 1 - Parts that make up a fuzzy system.

3.1 Fuzzy controller neutralization process pH.

Most industrial processes have considerable non-linearity with respect to different regions of operation, as with the process of pH. Depending on the process characteristics such as gain (Gp) and the regions of the process may be classified as high gain, medium gain and low gain, as shown in "Figure 2". If an auxiliary variable (AV) is used to indicate the different regions of the non-linear process, thus the process of non-linearity can be represented by the following relations fuzzy (Qin, Borders, 1994):

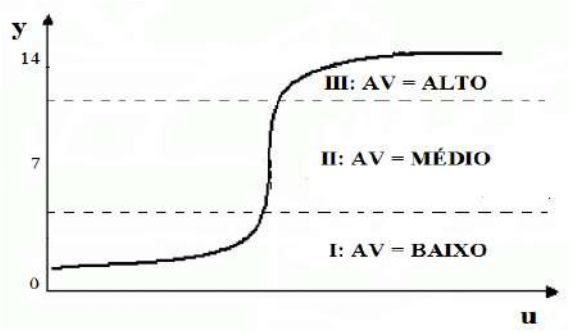

Figure 2 - Example of a gain on a non-linear process.

AV is the SE Region I THEN gain is low

AV is the SE Region II THEN gain is high

AV is the SE Region III THEN gain is low

To design a fuzzy controller that provides satisfactory performance for different regions of nonlinear gain, we use a fuzzy controller with three inputs "Figure 3". In addition, using the error control and error variation of control as inputs, an auxiliary variable is used as gain input to determine in which region the process is operating. This variable may be an auxiliary control variable (Uk) and leaving the process (yk), depending where the operating regions are defined.

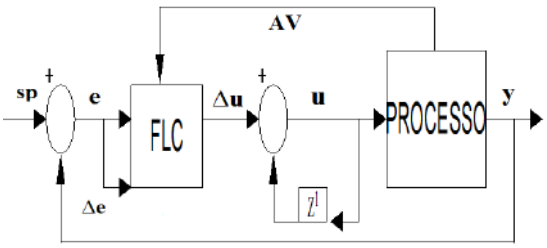

Figure 3 - Structure of fuzzy controller that uses an auxiliary variable to detect where the process is working and to compensate non-linearity to win.

In Nie et al. (1996) it is propose a modeling and identification of pH neutralization process using neuro-fuzzy approach of providing a new model that is not just for control purposes, but also to a better understanding of the processes of analyzing pH and, thus, its applicability ability of the neuro-fuzzy modeling when applied to complex systems.

3.2 *Definitions of rules*

The rule of fuzzy inference to generate this controller has three inputs and one output is: If AV is Ai, and is Bi, Ci is ΔE, then DU is Di. Where Ai, Bi, Ci and Di are the adjectives for the auxiliary variable (AV), error (E), change in control error (ΔE) and a change of control action (ΔU), respectively. These adjectives could be described as Negative, Positive, Zero and so on. A key requirement for these rules is that they have to run a negative feedback control because of stability. An example set of rules is listed in "Table 1", which in a real process has to be adjusted via the control experience of human operators.

As you can see there is a set of rules for each region of the process. In general, when the process is operating in a region of low gain, an aggressive control action is required, which is obtained by activating a large control action. To make more aggressive actions, positive or negative, large control movements are activated. Moreover, when the process is in the region of high gain, it requires a control action low.

Table 1 - A set of rules for a driver fuzzy three regions

Region AV = Low

	ΔE					
E	Neg	Neg Méd	Zero Neg	Zero Pos	Pos Méd	Pos
Neg	Pos	Pos	Pos	Pos-M	Z-Pos	Zero
Neg Méd	Pos	Pos	Pos	Pos-M	Zero	Z-Neg
Zero Neg	Pos	Pos-M	Z-Pos	Zero	Z-Neg	Neg-M
Zero Pos	Pos-M	Z-Pos	Zero	Neg-M	Neg	Neg
Pos Méd	Z-Pos	Zero	Z-Neg	Neg-M	Neg	Neg
Pos	Zero	Z-Neg	Neg-M	Neg	Neg	Neg

Region AV = average

	ΔE					
E	Neg	Neg Méd	Zero Neg	Zero Pos	Pos Méd	Pos
Neg	Pos-M	Pos-M	Pos-M	Z-Pos	Z-Pos	Zero
Neg Méd	Pos-M	Pos-M	Pos-M	Z-Pos	Zero	Z-Neg
Zero Neg	Pos-M	Pos-M	Z-Pos	Zero	Z-Neg	Neg-M
Zero Pos	Pos-M	Z-Pos	Zero	Z-Neg	Neg-M	Neg-M
Pos Méd	Z-Pos	Zero	Z-Neg	Neg-M	Neg-M	Neg-M
Pos	Zero	Z-Neg	Z-Neg	Neg-M	Neg-M	Neg-M

Region AV = high

	ΔE					
E	Neg	Neg Méd	Zero Neg	Zero Pos	Pos Méd	Pos
Neg	Pos	Pos	Pos	Pos-M	Z-Pos	Zero
Neg Méd	Pos	Pos	Pos	Pos-M	Zero	Z-Neg
Zero Neg	Pos	Pos-M	Z-pos	Zero	Z-Neg	Neg-M
Zero Pos	Pos-M	Z-Pos	Zero	Neg-M	Neg	Neg
Pos Méd	Z-Pos	Zero	Z-Neg	Neg-M	Neg	Neg
Pos	Zero	Z-Neg	Neg-M	Neg	Neg	Neg

Thus, looking at the table above it can be seen 108 rules that are necessary for a complete comprehension system.

3.3 *Implementation of the controller in a process pH neutralization.*

In order to implement the fuzzy controller to the process explained in the section above, you must first set the number of regions to divide the performance system. For this process, three regions of nonlinear gains can be identified: high pH medium pH and low pH. In the regions of high pH and low pH the gain of the process is extremely small, ie considerably large changes that have to be made in the rate of flow of acid to make significant changes in the pH. While in the average pH of the process the gain is extremely high, ie a small change in flow rate of acid results in a major change in the pH value.

The second step is to decide the auxiliary variable of the process to be used as an additional input for the fuzzy controller. In this case, after some experimentation, it is chosen as the reference the auxiliary variable pH (Casado; Robles, 2001). This variable is divided into three regions, ie three membership functions can usually be defined using the human knowledge on the process. The "Figure 4" shows the partition of the AV. It is possible to see in this particular case that the region of high gain is to high pH.

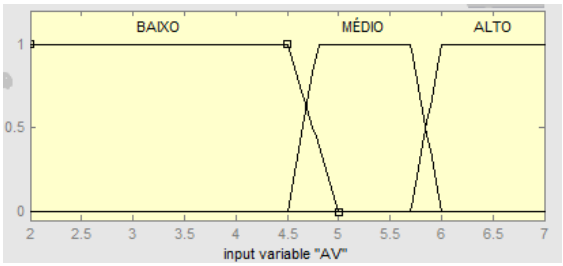

Figure 4 - Definition for the variable auxiliary input for a fuzzy controller: Low, Medium and High.

Now, it is necessary to define the fuzzy membership functions associated with the inputs of the controller, the control error and the change in control error and the controller output (ΔU), based on prior knowledge about the process. The number of membership functions for each variable may vary depending on the resolution required for this variable. Generally, the membership functions offer more degrees of freedom for the functional relationship of the controller

However, it is required more effort to implement it. Therefore, the effect of using more than two membership functions only the addition of non-linearity. It should be noted that the change in control action (ΔU) generally requires higher resolution than other variables, because the controller must be able to perform actions to control aggressive and less aggressive depending on the nonlinearity of the process.

The "Figures 5, 6 and 7" show the membership functions selected for this problem (Casado; Robles, 2001). As you can see, the membership functions for the controller output is greater than the input (six for each entry E and ΔE), and in this configuration the control law is less aggressive on the high yields. In these figures the meaning of adjectives are: Negative, Negative-Medium, Zero Negative, Zero, Zero Positive, Positive-Medium, and Positive.

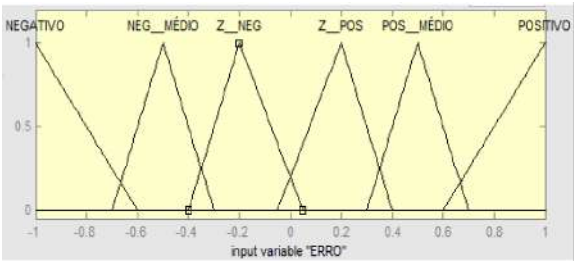

Figure 5 - Composition of functions for input variable, control error for the fuzzy controller.

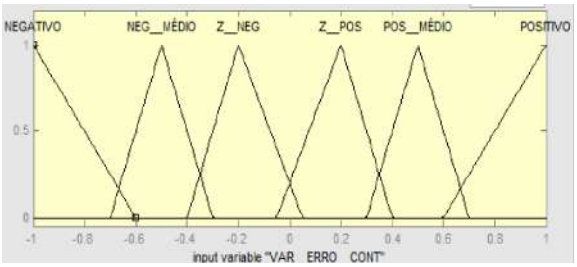

Figure 6 - Composition of functions for the input variable, change in control error for the fuzzy controller.

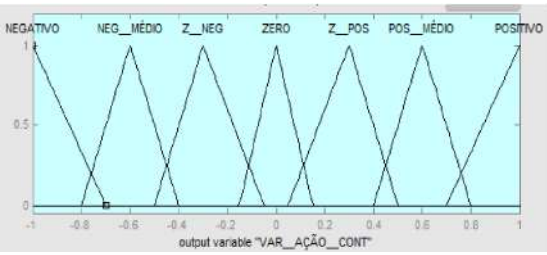

Figure 7 - Composition of functions for variable output, range of control action for the fuzzy controller.

These values show that the universe of discourse for all variables are in [-1,1], and the membership functions are symmetrical in this range.

4 RESULTS

After the implementation of the fuzzy controller, it can be seen that when the auxiliary variable AV is lower, it shows the same set of rules than when it is high in the region, as it can be seen in "Figure 8". . Therefore, it is possible to override 36 rules. In the middle region, the rules are different and can not be eliminated, then the total set of rules for the fuzzy controller rules is 72, not 108. It is very important because a large number of rules requires more computation time and more memory, then by reducing the number of rules, this means less work, less spending and, therefore more profit.

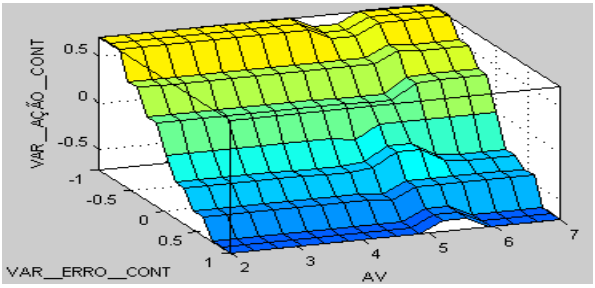

Figure 8 - The gain in the process in the regions, low, medium and high in pH neutralization process.

When analyzing the chart above, one can see that the gain in the process for the low and high region is the same, and, now, to the middle region, the gain is different. What does this according to the model proposed by (Fuentes et al., 2002). Thus, the final set of fuzzy rules to the process of neutralization of the pH is shown in "Table 2". This fuzzy controller was implemented by using the Fuzzy Logic Toolbox of MATLAB. The data are acquired and sent to the real plant through the toolbox of MATLAB in real time.

Table 2 - final set of fuzzy rules to a process for neutralization of pH

	ΔE					
E	Neg	Neg Méd	Zero Neg	Zero Pos	Pos Méd	Pos
Neg	Pos	Pos	Pos	Pos-M	Z-Pos	Zero
Neg Méd	Pos	Pos	Pos	Pos-M	Zero	Z-Neg
Zero Neg	Pos	Pos-M	Z-Pos	Zero	Z-Neg	Neg-M
Zero Pos	Pos-M	Z-Pos	Zero	Neg-M	Neg	Neg
Pos Méd	Z-Pos	Zero	Z-Neg	Neg-M	Neg	Neg
Pos	Zero	Z-Neg	Neg-M	Neg	Neg	Neg

Region AV = AV = High or Low

Region AV = average

	ΔE					
E	Neg	Neg Méd	Zero Neg	Zero Pos	Pos Méd	Pos
Neg	Pos-M	Pos-M	Pos-M	Z-Pos	Z-Pos	Zero
Neg Méd	Pos-M	Pos-M	Pos-M	Z-Pos	Zero	Z-Neg
Zero Neg	Pos-M	Pos-M	Z-Pos	Zero	Z-Neg	Neg-M
Zero Pos	Pos-M	Z-Pos	Zero	Z-Neg	Neg-M	Neg-M
Pos Méd	Z-Pos	Zero	Z-Neg	Neg-M	Neg-M	Neg-M
Pos	Zero	Z-Neg	Z-Neg	Neg-M	Neg-M	Neg-M

Thus, these results show that the actual plant controlled by this control diffuse operates properly in the desired range of pHs, with acceptable control actions.

5 CONCLUSIONS

This paper presents the control of a real process, a pH neutralization process using a fuzzy controller composed of three inputs and one output. The inputs are the control error, the change in control error and an auxiliary variable that indicates the various regions of the non-linear process. The output is the change in control action in order to implement a nonlinear fuzzy controller. The results show that the performance of the Multiregional fuzzy controller is very suitable for controlling non-linear processes, without the need for a complex mathematical model of the system.

REFERENCES

Berni, C. C. *Implementação em Hardware/Firmware de um sensor virtual utilizando algoritmo de identificação nebulosa.* São Paulo. 2004.

Casado, O. and Robles, C. *Desarrollo e implementación de um controlador borroso en una planta de pH.* Technical report, University of Valladolid, 2001**.**

Fuentes, M. J., Robles, C., Casado, O., Tadeo, F. *Fuzzy control of a neutralization process, Proceedings of IEEE International Conference Applications, September 18-20, 2002, Glasgow, Scontland, U.K.*

Nie, J., Loh, A. P., Hang, C. C. *"Modeling pH neutralization Processs using Fuzzy-neural approaches"*. Fuzzy sets systems, 1996. Vol. 78, no. 1, pp 5-22.

Qin, S. J. and Borders, G. *A multiregion fuzzy logic controller for nonlinear process control.* IEEE Trans. *on Fuzzy* Systems, 274-81, 1994.

Sturm, W. *Avaliação do potencial de uso da lógica fuzzy para a identificação de indicadres de competência no currículo lattes*. Curitiba, 2005.

ResearchGate

See discussions, stats, and author profiles for this publication at: https://www.researchgate.net/publication/280298398

MECHANICAL SYSTEM MODELING AND FEEDBACK-STATE OUTPUTS

Conference Paper · October 2012

CITATIONS
0

READS
1,151

3 authors:

Claudio MARCIO MEDEIROS DE Azevedo
Universidade Federal Rural do Semi-Árido - UFERSA
2 PUBLICATIONS **0** CITATIONS
SEE PROFILE

Elmer ROLANDO LLANOS Villarreal
Universidade Federal Rural do Semi-Árido - UFERSA
77 PUBLICATIONS **138** CITATIONS
SEE PROFILE

Antonio Ronaldo G. Garcia
Universidade Federal Rural do Semi-Árido - UFERSA
44 PUBLICATIONS **502** CITATIONS
SEE PROFILE

All content following this page was uploaded by Elmer ROLANDO LLANOS Villarreal on 29 May 2019.

The user has requested enhancement of the downloaded file.

Mechanical System Modeling, Feedback and Feedback-state Outputs

Cláudio Medeiros
Universidade Federal Rural do Semiárido (UFERSA)
Department of Exact and Natural Sciences
Mossoró – RN – Brazil
Email: claudio.matematic@gmail.com

Elmer Villarreal
Universidade Federal Rural do Semiárido (UFERSA)
Department of Exact and Natural Sciences
Mossoró – RN – Brazil
Email: evillarea@hotmail.com

***Abstract*—The present article aims show systematically computational algorithms for obtaining the transfer function, and find the matrices (A, B, C) – state space representation and output of gain feedback in linear problems and stabilization systems. will be used the concept of $(C; A; B)$– invariant subspaces of a problem of mechanical suspension of a car. Based on this concept introduced, reported the existence of a gain matrix for the solution of coupled Sylvester equations, with it will be necessary to present an algorithm that refers to Syrmos-Lewis, where a modification is proposed to provide a more appropriate for numerical solution, in part, the condition of Kimura.With this will be presented with numerical examples, where are provided to illustrate the application of the proposed algorithms.**

***Keywords*-Computational algorithm, Mechanical system, Output feedback, Control engineering.**

I. Introduction

The Control Engineering is focused on the study of the dynamics of physical systems. Among The main activities carried out by this engineering, they are modeling, analysis, simulation, design, implementation, and others. The modeling stage is especially important for the study of a control system. At this stage, a mathematical model for a mechanical system is proposed, where the mechanical system refers to a system suspension of an automobile. It is based on it that the other activities are performed, and therefore essential to define a model that accurately represents its dynamics.

In general should obtain a mathematical model, which is adequate to solve the specific problem in this analysis. However, it is important to emphasize that the results of this analysis are valid only for cases in which the model is valid. When we go obtain a simplified model of a system, generally ignore some physical properties of this system. If the effects that these properties have on the response of the system are small, then a good similarity between the results of mathematical analysis and practical results of the system is obtained. In general, dynamic systems are nonlinear. However, the mathematical procedures for obtaining the solution of linear models are very complicated. For this reason, usually is substituted a nonlinear model linear by a model, with valid only in a limited region of operation, or to a point operating.

A system is called linear if it applies the principle of superposition. Where the principle of superposition establishes that the response produced by the simultaneous application of two different excitations is equal to the sum of two individual responses to each of the excitations. As a result, linear systems, the response to various inputs can be calculated by considering a single entry at a time and adding the results.

So for a better understanding, the work outlined here will be subdivided into four main sections, where we will start talking about the invariant subspaces and coupled equations of silvester, soon after will be presented the problem to be modeled, where will be presented the function transfer , In which is used to characterize the input-output relationships of components or systems that can be written by differential equations linear time-invariant, then immediately will discuss the modeling of the problem and algorithmic aspects, to this, power make the formulation in space of states and ending with the matrix determination K with the use of transformation T, where the matrix K, is the feedback gain matrix, and ending with the conclusion that it will present the results we have at work.

A. invariant subspaces and coupled Sylvester equations

As in [6], makes use of some concepts and definitions of geometric control theory [9]. It is known that a subspace $\mathcal{V} \subset \mathcal{X}$ (A, B)invariant if there $F : \mathcal{X} \longrightarrow \mathcal{Y}$ such that $(A+BF)V \subset \mathcal{V}$, or equivalently, $A\mathcal{V} \subset \mathcal{V} + ImB$. By subspace a duality $\mathcal{T} \subset \mathcal{X}$ is (C, A) considered to be invariant if there $L : \mathcal{Y} \longrightarrow X$, such that $(A + LC)\mathcal{T} \subset \mathcal{T}$, or equivalently, $\mathcal{T} \supset A(\mathcal{T} \cap Ker(C))$.

Is $V \in \Re^{v\times v}$ such that $Im(V) = V$ and is $T \in \Re^{n-v\times v}$ and a left diriment of V, $i.e.$: $Ker(T) = Im(V)$.

$$AV - VH_V = -BW \tag{1}$$

$$TA - H_T T = -UC \tag{2}$$

$$TV = 0 \tag{3}$$

The equations play a fundamental role in the treatment of the control problem using static output feedback, especially for self-positioning and structure [6] [8]. And leading into account the properties of stabilizability and detectability by the two following definitions::

- A subspace (A, B) invariant $\mathcal{V}$ is (A, B) internally stabilizable if there F such that $(A+BF)|\mathcal{V}$ is asymptotically stable;
- A subespace (C, A) invariant $\mathcal{V}$ (C, A) externally detectable L such that $(A+B)|\mathcal{X}/\mathcal{V}$ is asymptotically stable;

The necessary and sufficient condition for a subspace $\mathcal{V} = Im(\mathcal{V})$ seja $O.S$ (C, A, B) invariant that 3 be verified with the additional conditions stability by [2] [1]:

$$\sigma(H_V) \in \mathcal{C}^- \tag{4}$$
$$\sigma(H_T) \in \mathcal{C}^- \tag{5}$$

The following theorem makes the relationship concept of subspaces $O.S.(A, B, C)$ be invariant to the existence of a control law of type static output feedback which stabilizes the closed system.

$$AV - VH_V = -BW, com\sigma(H_V) \in \mathcal{C}^- \tag{6}$$
$$TA - H_T T = -UC, com\sigma(H_T) \in \mathcal{C}^- \tag{7}$$
$$TV = 0 \tag{8}$$
$$Ker(CV) \subseteq Ker(W) \tag{9}$$
$$Ker(CV) \subseteq Ker(U') \tag{10}$$

$onde : posto(V) = veposto(T) = n - v$

Note that the results have been presented and explored in different ways in the literature concerning the positioning of self-structure using output feedback [7]. As seen, the coupled equations Sylvester (6),(7),(8) describe geometric properties of the subspace $\mathcal{V} = Im(\mathcal{V})$ should be (A, B) asymptotically stable; ally,means that the subspaces $Ker(T) = \mathcal{V}$ should be (C, A) externally stabilizable. Thus, under the condition of coupling , is that the existence of a subspace $\mathcal{V} = Ker(T)O.S.(C, A, B)$ invariant, with the additional conditions (9),(10) is a necessary and sufficient condition for the existence of solution of the problem considered. Note also that the terms (9),(10) correspond to the existence of a matrix $K \in \Re^{m \times p}$ which verifies the two following equalities:

$$KCV = W \tag{11}$$
$$\tag{12}$$
$$TKK = U \tag{13}$$

It is important to note that is guaranteed the existence of a solution to the equation of Sysvester, is K has been obtained and such (13) is checked, the eigenvalues ??in mesh closed are given by:

$$\sigma(A + BKC) = \sigma(HV)\dot{\cup}\sigma(H_T)$$

1) Formulation of the problem: Us systems translational mechanical , there are three mechanical elements that are involved: element of inertia, damping element, element of elasticity. Where the element of inertia (mass) is assumed that the mass is rigid. Thus the connection higher, should not move in relation to less connection, that is, both connections moving the second $x(t)$. already the damping element (damper) there is a relative displacement between the upper connection point and connection point lower. Therefore, there is a need to shift two variables to describe this element. The physical realization of this element is the viscous friction associated with the oil or air. The element of elasticity (spring) can be deformed by an external force, such that the deformation is directly proportional to this force.

There fore, the problem to be modeled consists of obtaining a transfer function of a moving automobile, where it passes through different obstacles (elevations) on the track which will be observed the mechanical system simplified of a system suspension of wheels a car. Then it will be assigned at a certain instant in that car passes by a certain elevation of 25 cm, which is applied to the force F. Um representante esquemtica de um modelo para o carro com um amortecedor(f) and a spring (k):The System of suspension of car this illustrated in Figure 1:

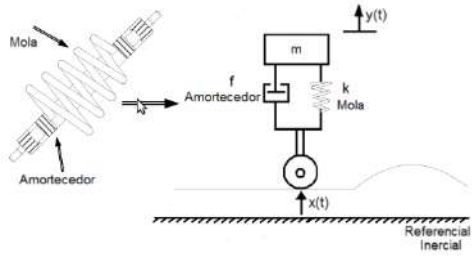

Figure 1. Suspension system

This is a model corresponding to one of the four wheels of a car. The cylinder of damper contains air that passes from one side to another, when occurs a relative motion. He always applies a reaction force, that is contrary to the movement of his extremities. The viscous damper provides viscous friction, ie, it opposes any relative motion of the two ends, dissipating energy in form of heat. Will be illustrated now the mathematical model that provides the problem. see Figure 2:

Where the forces on the mass m are expressed in Figure 3:
With:

$$force\ of\ moll : F_m = K(y - x) \tag{14}$$
$$force\ of\ buffer : F_a = f(\dot{y} - \dot{x}) \tag{15}$$

we know that:

$$\Sigma F_y = m.a \tag{16}$$

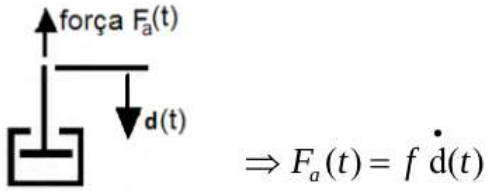

Figure 2. Mathematical model

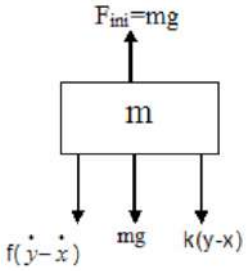

Figure 3. Force on mass

there fore, we obtain::

$$m.g - f(\dot{y} - \dot{x}) - m.g - K(y - x) = m\ddot{y} \tag{17}$$

Defined above, we know that the continuous transfer function is the relationship between the Laplace transform of the output, $Y(s)$, by Laplace transform of the input, $X(s)$.the relationship G(s) is a ratio of two polynomials in s:Thus, applying to laplace C.I. zero we obtain

$$-f(sY(s) - sX(s)) - K[Y(s) - X(s)] = msY(s) \tag{18}$$

$$Y(s)[ms + fs + k] = [sf + k]X(s) \tag{19}$$

$$\frac{Y(s)}{X(s)} = \frac{sf + k}{ms + fs + k} = G(s) \tag{20}$$

This mathematical model of the transfer function is shown in Figure 4

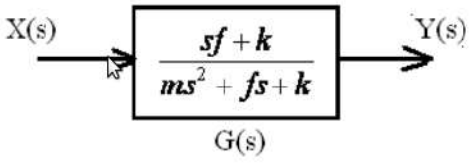

Figure 4. Transfer function

where f is the reaction force, K is a spring constant and $m$is the mass of the car.

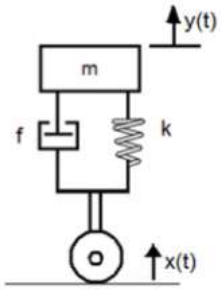

Figure 5. Model of buffer

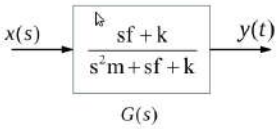

Figure 6. Transfer function

B. Modeling the Problem

To illustrate the usefulness of MATLAB in this analysis, assume that an automobile in Motion passes through different obstacles (elevations) on the track. In Figure 6 we have presented an outline of a representative model for the car with a buffer (f) and a spring (k):

Suppose now that this same car passes through a elevation of $d = 25cm$, as shown in Figure 7.

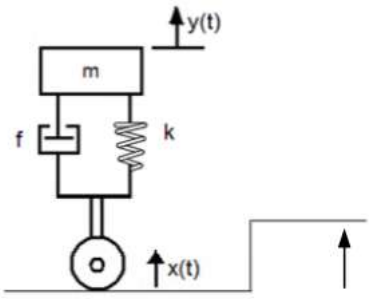

Figure 7. Representation of elevation

This elevation corresponds to the entry system and is called the step input. To observe the response of the system (movement of the mass-spring system, shock absorber, the alleged car), based on the transfer function of the damper seen previously, we apply the values the instant the car passes this elevation, where invariants are: $m = 1000$, $f = 500$ e $K = 200$.
Thus, the function acquired in 19 will:

$$\frac{Y(s)}{X(s)} = \frac{500s + 200}{1000s + 500s + 200} = G(s) \tag{21}$$

Writing the transfer function obtained in 20 we have:

$$\frac{Y(s)}{U(s)} = \frac{numerator\ polynomial\ in\ s}{denominator\ polynomial\ in\ s} = \frac{num}{den}$$

Once we have this expression of type transfer function, the command in MATLAB:

$$[A, B, C, D] = tf2ss(num, den)$$

described in [5] provides a state-space representation. It is important to note that the representation in the state space of any system is not unique. There are many (actually infinite) representations for the same system. The command in MATLAB provides a possible representations in space data.

From the transfer function obtained in 19, and changing some values, we can visualize so with the values of matrices A, B, C e D we get the following function:

$$\frac{Y(s)}{U(s)} = \frac{0.5s + 0.2}{s + 0.5s + 0.2} \tag{22}$$

As from the transfer function 21, the values matrices A, B, C e D will be:

$A = \left[\begin{array}{cc} -0.5 & -0.2 \\ 1 & 0 \end{array} \right]_{2\times2}$ $B = \left[\begin{array}{cc} 1 & 0 \\ 0 & 1 \end{array} \right]_{2\times1}$ $C = \left[\begin{array}{cc} 0.5 & 0.2 \end{array} \right]_{1\times2}$ $D = \left[\begin{array}{c} 0 \end{array} \right]_{1\times1}$

Will be presented following two methods, in which shall be responsible for submitting of arrays of state feedback and output feedback.

C. Feedback States

In this section will reported the method 1 in [5], in which it gets the matrix G state feedback,

where:

$$\dot{x} = Ax + Bu \tag{23}$$

$$y = Cx + Du \tag{24}$$

Choose the control signal as:

$$u = -GX \tag{25}$$

To calculate the state feedback matrix of G we will use MATLAB, where we have two commands $acker$ and $place$. the commands $acker$ is based on the Ackerman formula that applies only to systems of one input and one output. the commands $place$ can be used for both systems as an entry for multiple inputs, it requires that the multiplicity of the desired closed loop poles does not exceed the rank of **B**.To use the commands $acker$ ou $place$ we will use the matrices **A**, **B** and **J**. the matrices **A** and **B**, have been previously defined and the matrix J is the one that consists of poles of mesh closed, so that:

$$J = \left[\begin{array}{cccc} \mu_1 & \mu_2 & \cdots & \mu_n \end{array} \right]$$

Applying the mechanical system, the matrix J is:

$$J = \left[\begin{array}{cc} -1 & -2 \end{array} \right]$$

As from the matrix J, we introduce:

$$G = place(A, B, J)$$

Therefore, the matrix G is:

$$G = \left[\begin{array}{cc} 0.5000 & 0.2000 \\ 1.0000 & 2.0000 \end{array} \right]$$

To determine the matrix we use $AG = A - B * K$, then the matrix AG will:

$$AG = \left[\begin{array}{cc} -1 & 0 \\ 0 & -2 \end{array} \right]$$

Now, we will use the command $eig(AG)$, to verify that the matrix provides the desired eigenvalues:

$$eig(AG) = \left[\begin{array}{c} -2 \\ -1 \end{array} \right]$$

D. Output Feedback

In this section we will present a technique based on algorithmic procedures for placement of self-structure to obtain a output feedback [2] [1]. Where the technique proposed by Lewis and Syrmos[6] solves the coupled Sylvester equations in two steps and can be directly applied to systems that verify the condition $m+p > n$, condition known as Kimura [4]. It is clear that the dimension of $V = Im(V)$ equals the number of outputs p, seeking to ensure that the matrix $CV \in \Re^{pxp}$ is invertible and, so that the matrix of feedback gains can be found, from 11, the form $K = W(CV)^{-1}$.

It will be shown also that if, the considered system is completely state controllable, then the poles of closed-loop system can be placed in any desired position by means of a state feedback, using an appropriate gain matrix,with that, limit our discussion to systems an input and an Output. The requirement is that the system is completely controllable.Consider the following system defined on [3].

$$\dot{x} = Ax + Bu \tag{26}$$

$$y = Cx + Du \tag{27}$$

Choose the control signal as:

$$u = -KX \tag{28}$$

This means that the control signal u is determined by an instantaneous state. This scheme is called state feedback. The matrix $K1 \times n$ is called feedback gain matrix of state. Thus, the mechanical system represented in state space is represented as follows:

$$\left[\begin{array}{c} \dot{x_1} \\ \dot{x_2} \end{array} \right] = \left[\begin{array}{cc} -0.5 & -0.2 \\ 1 & 0 \end{array} \right] \left[\begin{array}{c} x_1 \\ x_2 \end{array} \right] + \left[\begin{array}{cc} 1 & 0 \\ 0 & 0 \end{array} \right] u$$

$$y = \left[\begin{array}{cc} 0.5 & 0.2 \end{array} \right] \left[\begin{array}{c} x_1 \\ x_2 \end{array} \right]$$

Further, it is considered that the system represented by (C, A, B) is controllable and observable, this necessary condition for the arbitrary choice of the poles to be placed in closed loop. This condition can however be relaxed for the stabilization and detectability of (C, A, B), which implies the use of non-controllable eigenvalues non-observable in the spectrum for the desired closed-loop system. Assume

that T can be found from the matrices $[A, B, C]$ As determined in [2] [1]:

$$A = \begin{bmatrix} -0.5 & -0.2 \\ 1 & 0 \end{bmatrix}_{2\times 2}$$

$$B = \begin{bmatrix} 1 & 0 \\ 0 & 1 \end{bmatrix}_{2\times 1}$$

$$C = \begin{bmatrix} 0.5 & 0.2 \end{bmatrix}_{1\times 2}$$

The corresponding system is controllable and observable and $m+p = 3 > n$. Then determine the matrix T checking (17) in Elmer [2] [1]. Thus the matrix T Thus the matrix:

$$T = \begin{bmatrix} -0.7071 & -0.0000 \end{bmatrix}_{1\times 2}$$

The matrices V and W are determined using (18) in [2] [1]:

$$V = \begin{bmatrix} 0.0000 & -0.4454 \end{bmatrix}_{1\times 2}$$

$$W = \begin{bmatrix} 0.0891 & 0.8909 \end{bmatrix}_{1\times 2}$$

be determined K such that $KCV = W$:

$$K = \begin{bmatrix} -1.0000 \\ -10.0000 \end{bmatrix}_{2\times 1}$$

The closed-loop matrix $A_k = A + BCK$ *correspondent, whose eigenvalues are the desired, is:*

$$A_k = \begin{bmatrix} -1.0000 & 0.0000 \\ -4.0000 & -2.0000 \end{bmatrix}_{2\times 2}$$

$$A_{k1} = \begin{bmatrix} -1 \\ -2 \end{bmatrix}_{2\times 1}$$

II. Conclusion

We considered the problem of output feedback to stabilize a mechanical system.Introduced the concept of subspaces $O.S.(C, A, B)$ – invariants and their relation to the solution of the problem of stabilization using output feedback via Sylverter coupled equations, showing that play a key role in the response of output stabilization of linear systems.The paper has focused on theoretical and algorithmic aspects. In particular, a necessary and sufficient condition for the existence of a output feedback. An algorithm has been proposed to calculate a feedback array of stabilization of the product about condition to Kimura $m+p > n$.Aim is to develop future studies aimed at deepening the applications, and so, can be presented other techniques mentioned in [5]. in order to further facilitate the analysis proposed in the article.

References

[1] E.B. Castelan, J. C. Hennet, E. R. L. V. (2003). Quadratic characterization and use of output stabilizable subspace. In IEEE Control Systems V48 NAo a, pages 654660. Universidade Federal Rural do Semi-Arido.

[2] E.R.LL Villareal, J. A. R. Vargas, E. H. (2009). Static output fedback stabilization using invariant sub space and sylvester equations. In Advances in Computer Science, pages 99110. Universidade Federal Rural do Semi-Arido.

[3] Fletcher, R., Kautsky, J., Kolka, G. K. G., and Nichols, N. K. (1985). Eigenstructure ass- ingment by output feedback in descriptor systems. In IEEE Trans. Automatic. Control, vol. 42, pages 14571468. Systems and Control Letters 24(2).

[4] Kimura, H. (1975). Pole assignment by gain output feedback. In IEEE Transactions on Automatic Control vl. 20, page 509 516. Systems and Control Letters 24(2).

[5] OGATA, K. (2010). EstabilizaAAo de sistemas descritores por realimentaAAo de saAdas via subespaAos invariantes. In Prentice-Hall, editor, Advances in Computer Science, pages 594657. Universidade Federal Rural do Semi-Arido.

[6] Syrmos, L. and Lewis, F. L. (1994). Bilinear formulation for the output feedback problem in linear system. In IEEE Trans. Automatic. Control, vol. 39, number 2, pages 410 414.

[7] Syrmos, V. L., Abdallah, C. T., Dorato, P., and Grigoriadis, K. (1997). Static output feedback. In A Survey Automatica, vol. 33, number 2, pages 125137.

[8] Syrmos, V. L. and Lewis, F. L. (1993). Output feedback eigenstructure assignment using two sylvester equations. In IEEE Trans. Automatic. Control, vol. 38, number 3, pages 495499. Springer-Verlag.

[9] Wonahm, W. M. (1979). Linear multivariable control, a geometric approach. Springer- Verlag.

View publication stats

Copyright © 2002 IFAC
15th Triennial World Congress, Barcelona, Spain

ELSEVIER
IFAC
PUBLICATIONS
www.elsevier.com/locate/ifac

REGIONAL POLE PLACEMENT BY OUTPUT FEEDBACK FOR A CLASS OF DESCRIPTOR SYSTEMS

Eugênio B. Castelan[†] , Aguinaldo S. Silva[‡]
Elmer R. Llanos Villarreal[†] and Sophie Tarbouriech[§]

[†] *LCMI / DAS / UFSC ;* [‡] *GSP / EEL / UFSC*
88040-900 - Florianópolis (S.C) - Brazil
E-mail: {*eugenio , llanos*}*@lcmi.ufsc.br , aguinald@labspot.ufsc.br*

[§] *LAAS du CNRS*
31077 - Toulouse Cédex 4 - France ; E-mail: *tarbour@laas.fr*

Abstract: The problem of regional pole placement by static output feedback is studied for a class of linear descriptor systems that presents two caracteristics found in some physical models: regularity and absence of direct action of control inputs on the algebraic variables. Thus the structure of the mathematical model of this class of systems is exploited. We show, in particular, how some results from the classical theory of normal (differential) linear systems can be used to solve the considered problem. The paper provides a set of necessary and sufficient conditions to characterize the existence of an output feedback that places the finite closed-loop poles in particular regions of the complex plane. A technique based on the use of an orthogonal decomposition and on the solution of two-coupled Lyapunov equations is also proposed. A numerical example illustrates the approach. *Copyright © 2002 IFAC*

Keywords: Output feedback, Stabilization, Pole placement, Descriptor systems, Lyapunov equations, Convex programming.

1. INTRODUCTION

Linear descriptor systems arise naturally in the modelling of several systems such as circuits, power systems and other interconnected systems (Dai, 1989), (Verghese et al., 1981). Although a purely differential representation for these systems can usually be obtained, there are advantages in keeping the original descriptor system model. In the case of power systems, not only the descriptor systems arises naturally from the system modeling but also the reduction to a purely differential form can pose computational restrictions owing to the large dimension that power systems can present. The high sparsity found in the descriptor system matrices is lost when the differential system is obtained. Analysis techniques have been developed to deal with power system models in the descriptor form, preserving sparsity. On the other hand few design techniques for power system controllers can be found that use the descriptor system formulation. These techniques use output feedback, which is the usual approach for the design of power system controllers (Freitas et al., 1997) (Freitas et al., 1995).

This paper tackles the problem of the regional pole placement, called $\mathcal{D}$-stabilization problem, of a particular algebraic-differential descriptor model by output feedback. This model is assumed to present several characteristics: regularity and absence of impulsive behaviour and no direct action of control inputs on the algebraic variables. Although these assumptions may seem to be restrictive, some physical models of interconnected systems models, comply with them. It is shown that the output feedback $\mathcal{D}$-stabilization of the considered linear descriptor system can be viewed as the classical problem of output feedback stabilization of a reduced-order normal system, to which $\mathcal{D}$-stabilization techniques by output feedback can be applied (Syrmos et al., 1997), (Chilali

* This work has been partially supported by CNPq/Brazil.

and Gahinet, 1996). Furthermore, it is shown how these techniques can be directly applied to the full-order descriptor system. To illustrate this point, an approach based on the solution of two coupled-Lyapunov equations is utilized (Castelan et al., 2000).

This paper is organized as follows. Section 2 poses the problem of output feedback stabilization. Section 3 presents some basic concepts of the descriptor system theory and introduces the general reduced-order $\mathcal{D}$-stabilization methodology. In section 3, the coupled-Lyapunov equations approach is presented and adapted to the considered descriptor system. Finally, convex programming techniques are used to solve a numerical example. The last section presents some conclusions.

2. PROBLEM PRESENTATION

Let us consider a linear descriptor system described by a set of algebraic and differential equations of the form:

$$\begin{bmatrix} I_q & 0 \\ 0 & 0 \end{bmatrix} \begin{bmatrix} \dot{x}_1(t) \\ \dot{x}_2(t) \end{bmatrix} = \begin{bmatrix} J_1 & J_2 \\ J_3 & J_4 \end{bmatrix} \begin{bmatrix} x_1(t) \\ x_2(t) \end{bmatrix} + \begin{bmatrix} B_1 \\ 0 \end{bmatrix} u(t) \quad (1)$$

$$y(t) = \begin{bmatrix} C_1 & C_2 \end{bmatrix} \begin{bmatrix} x_1(t) \\ x_2(t) \end{bmatrix} \quad (2)$$

where: $x_1 \in \Re^q$, $x_2 \in \Re^{(n-q)}$, $u \in \Re^m$, and $y \in \Re^p$. I_q is the q-dimensional identity matrix and $J_4 \in \Re^{(n-q)\times(n-q)}$ is assumed to be full-rank. The other involved matrices are of appropriate dimensions and it is also assumed that $rank(B_1) = m$.

Some structural particularities of system (1) , (2) are the following: *i*) matrix J_4 is invertible, which characterizes the absence of impulsive behavior in the dynamic response of this system and its regularity as well (Bender and Laub, 1997);
ii) there is no direct action of control inputs on algebraic variables, as emphasized by the structure of input matrix $\begin{bmatrix} B_1' & 0 \end{bmatrix}'$.

The particular structure of this descriptor system may lead to some useful results concerning its stabilization by static output feedback $u(t) = Ky(t)$. Thus, we are interested in solving the following *Output Feedback $\mathcal{D}$-stabilization problem:*

Given the Descriptor System model (1) and (2), find a static output feedback control law

$$u(t) = Ky(t) = K[C_1 \; C_2] \begin{bmatrix} x_1(t) \\ x_2(t) \end{bmatrix} \quad (3)$$

where $K \in \Re^{m\times p}$, such that the closed-loop system given by

$$\begin{bmatrix} I_q & 0 \\ 0 & 0 \end{bmatrix} \begin{bmatrix} \dot{x}_1 \\ \dot{x}_2 \end{bmatrix} = \begin{bmatrix} J_1 + B_1KC_1 & J_2 + B_1K_2C_2 \\ J_3 & J_4 \end{bmatrix} \begin{bmatrix} x_1 \\ x_2 \end{bmatrix} \quad (4)$$

has its finite closed-loops poles belonging to a given region of the complex-plane, denoted $\mathcal{D}$.

The regions $\mathcal{D}$ considered in this work are defined from LMI regions, which can describe a wide class of pole clustering regions (Chilali and Gahinet, 1996):

Definition 2.1. A subset $\bar{\mathcal{D}}$ of the complex plane is called an LMI region if there exist a symmetric matrix $\alpha = [\alpha_{kl}] \in \Re^{n\times n}$ and a matrix $\beta = [\beta_{kl}] \in \Re^{n\times n}$ such that $\bar{\mathcal{D}} = \{\lambda \in \mathcal{C} : f_{\bar{\mathcal{D}}}(\lambda) = \alpha + \lambda\beta + \bar{\lambda}\beta' < 0\}$.

From definition 2.1, LMI regions describe convex regions in the complex plane that are symmetric with respect to the real axis. The characteristic function $f_{\bar{\mathcal{D}}}(\lambda)$ takes values in the space of $m \times m$ Hermitian matrices, and Linear Matrix Inequalities can be set from $f_{\bar{\mathcal{D}}}(\lambda)$ to characterize the property that the eigenvalues of a real matrix belong to $\bar{\mathcal{D}}$ (Chilali and Gahinet, 1996).

3. BACKGROUND

In order to better understand and solve the stated output feedback $\mathcal{D}$-stabilization problem, some known concepts of descriptor systems theory are first recalled (Bender and Laub, 1997), (Dai, 1989). A general descriptor systems takes the form :

$$\bar{E}\dot{x}(t) = \bar{A}x(t) + \bar{B}u(t) \quad (5)$$

$$y(t) = \bar{C}x(t) \quad (6)$$

where: $x \in \Re^n$, $u \in \Re^m$, $y \in \Re^p$ and $\bar{E} \in \Re^{n\times n}$ verifies $rank(\bar{E}) = q$; the other matrices have adequate dimensions.

Descriptor system (5), (6) is called *regular* if $det(\lambda\bar{E} - \bar{A}) \neq 0$. If we assume that it is regular, the set of poles of this system (finite and infinite) represents the set of generalized eigenvalues of the pair $(\bar{E}, \bar{A})$. The *finite poles* of $(\bar{E}, \bar{A})$ are the roots of the characteristic equation $\Delta(\bar{E}, \bar{A}) = det(\lambda\bar{E} - \bar{A}) = 0$. If the number of finite poles is less than $rank(\bar{E}) = q$, then the descriptor system has impulsive modes. It is *impulse-free* if it has exactly q finite poles. We say that this system is *$\mathcal{D}$-stable* if all its finite poles are in $\mathcal{D} \subseteq \mathcal{C}^-$, where $\mathcal{C}^-$ denotes the open left-hand complex semiplane. Concerning structural properties of triples $(\bar{E}, \bar{A}, \bar{B})$ and $(\bar{C}, \bar{A}, \bar{E})$ that are to be used in the sequel, we say that descriptor system (5), (6) is *$\mathcal{D}$-stabilizable* if and only if

$$rank\left(\begin{bmatrix} \lambda\bar{E} - \bar{A} & \bar{B} \end{bmatrix}\right) = n \;\; , \;\; \forall\, \lambda \notin \mathcal{D} \quad (7)$$

and it is *$\mathcal{D}$-detectable* if and only if

$$rank\left(\begin{bmatrix} \lambda\bar{E} - \bar{A} \\ C \end{bmatrix}\right) = n \;\; , \;\; \forall\, \lambda \notin \mathcal{D} \quad (8)$$

Let us also consider the output feedback control law $u(t) = K\,y(t)$, with $K \in \Re^{m\times p}$ and assume

that (7) is not verified for some finite $\lambda \notin \mathcal{D}$. This is equivalent to the existence of a non-null vector $\xi \in \Re^n$ such that $\xi'\left(\lambda\bar{E} - \bar{A}\right) = 0$ and $\xi'\bar{B} = 0$. Thus, if we premultiply the closed-loop state matrix by ξ', we get $\xi'(\bar{A} + \bar{B}K\bar{C}) = \xi'\bar{A} = \xi'\lambda\bar{E}$, which means that λ is necessarily a finite closed-loop pole. Hence, controllability of the finite open-loop poles that do not belong to $\mathcal{D}$ is a necessary condition for $\mathcal{D}$-stabilization of descriptor systems by output feedback. By duality, observability of the finite open-loop poles that do not belong to $\mathcal{D}$ is also a necessary condition for $\mathcal{D}$-stabilization of descriptor systems by output feedback.

Let $\tilde{Q} \in \Re^{n\times n}$ and $\tilde{P} \in \Re^{n\times n}$ be two nonsingular matrices and consider the change of coordinates $x = \tilde{P}\tilde{x}$. Then, the following system is an equivalent representation of system (5), (6):

$$\tilde{E}\dot{\tilde{x}}(t) = \tilde{A}\tilde{x}(t) + \tilde{B}u(t) \tag{9}$$

$$y(t) = \tilde{C}\tilde{x}(t) \tag{10}$$

where: $\tilde{E} = \tilde{Q}\bar{E}\tilde{P}$, $\tilde{A} = \tilde{Q}\bar{A}\tilde{P}$, $\tilde{B} = \tilde{Q}\bar{B}$ and $\tilde{C} = \bar{C}\tilde{P}$. It can be shown that $\mathcal{D}$-stabilizability and $\mathcal{D}$-detectability are preserved under change of coordinates. Furthermore, the finite poles of $(\bar{E}, \bar{A})$ and $(\tilde{E}, \tilde{A})$ are the same (Bunse et al., 1992).

Descriptor systems considered in this work are special cases of system (5), (6) where, in particular, matrices $\bar{E}$ and $\bar{B}$ are given in equation (1). Notice also that the case $\bar{E} = I_n$ corresponds to the classical case of differential systems which will be referred as *normal* systems. By considering the algebraic-differential model (1), (2), conditions (7) and (8) can be equivalently replaced by

$$rank\left(\begin{bmatrix} \lambda I - J_1 & -J_2 & B_1 \\ -J_3 & -J_4 & 0 \end{bmatrix}\right) = n \quad ,\forall\, \lambda \notin \mathcal{D} \tag{11}$$

and

$$rank\left(\begin{bmatrix} \lambda I_q - J_1 & -J_2 \\ -J_2 & -J_4 \\ C_1 & C_2 \end{bmatrix}\right) = n \quad ,\forall\, \lambda \notin \mathcal{D} \tag{12}$$

Furthermore, since J_4 is invertible, the considered descriptor systems are impulse-free and the q open-loop finite poles are the eigenvalues of matrix $(J_1 - J_2J_4^{-1}J_3)$. In the sequel, the dependence of the variables on t is ommited.

3.1 *Output feedback stabilization*

We shall now show that under the assumptions of finite $\mathcal{D}$-stabilizability and $\mathcal{D}$-detectability of system (1), (2), the stated output feedback $\mathcal{D}$-stabilization problem may be viewed as a classical problem of output feedback $\mathcal{D}$-stabilization for a reduced-order normal system. To do this, we shall consider matrices $\tilde{Q} = I_n$ and $\tilde{P} = \begin{bmatrix} I_q & 0 \\ -J_4^{-1}J_3 & I_{n-q} \end{bmatrix}$ and the change of coordinates $x = \tilde{P}z$:

$$\begin{bmatrix} x_1 \\ x_2 \end{bmatrix} = \begin{bmatrix} I_q & 0 \\ -J_4^{-1}J_3 & I_{n-q} \end{bmatrix}\begin{bmatrix} z_1 \\ z_2 \end{bmatrix} \tag{13}$$

Thus, the closed-loop system (4) is equivalent to

$$\begin{bmatrix} I_q & 0 \\ 0 & 0 \end{bmatrix}\begin{bmatrix} \dot{z}_1 \\ \dot{z}_2 \end{bmatrix} = \begin{bmatrix} J_1(K) & J_2(K) \\ 0 & J_4 \end{bmatrix}\begin{bmatrix} z_1 \\ z_2 \end{bmatrix} \tag{14}$$

where : $J_1(K) = (J_1 - J_2J_4^{-1}J_3) + B_1K(C_1 - C_2J_4^{-1}J_3)$ and $J_2(K) = J_2 + B_1KC_2$.

From the structure of matrices involved in representation (14), the closed-loop finite poles correspond exactly to the set of eigenvalues of matrix $J_1(K)$, and are given by the roots of the characteristic equation $det\ (\lambda I_q - J_1(K)) = 0$.

From the development above, we conclude that matrix K must be such that the spectrum of $J_1(K)$, which gives the finite closed-loop poles, lies in the region $\mathcal{D} \subset \mathcal{C}^-$. In fact, the problem to be solved in this step may be viewed as the output feedback $\mathcal{D}$-stabilization, by considering $u = Ky$, of the *reduced-order* normal system:

$$\dot{\zeta}_1 = A\,\zeta_1 + Bu \tag{15}$$

$$y = C\,\zeta_1 \tag{16}$$

where: $A = (J_1 - J_2J_4^{-1}J_3)$, $B = B_1$ and $C = (C_1 - C_2J_4^{-1}J_3)$.

Necessary conditions for $\mathcal{D}$-stabilizing a reduced-order normal system (A, B, C) by output feedback are related to the $\mathcal{D}$-stabilizability and $\mathcal{D}$-detectability of pairs (A, B) and (C, A) (see, for instance, (Syrmos et al., 1997)).

Lemma 3.1. The reduced-order system (15), (16) is $\mathcal{D}$-stabilizable and $\mathcal{D}$-detectable if and only if descriptor system (1), (2) is $\mathcal{D}$-stabilizable and $\mathcal{D}$-detectable.

Proof: Based on the invariance of controllability and observability under the change of coordinates. □

We can summarize the previous development by the following algorithm for $\mathcal{D}$-stabilizing descriptor systems (1), (2) by output feedback:

Step A: Compute (the unique) $X \in \Re^{(n-q)\times q}$ such that $J_4X = J_3$ and set: $A = J_1 - J_2X$; $B = B_1$; $C = C_1 - C_2X$.
Step B: Compute $K \in \Re^{m\times p}$ such that $\sigma(A + BKC) \in \mathcal{D}$.

The Step B of the algorithm is now commented. Since it is assumed that the descriptor system (1), (2) is $\mathcal{D}$-stabilizable and $\mathcal{D}$-detectable, pairs (A, B) and (C, A) involved in Step B are $\mathcal{D}$-stabilizable and $\mathcal{D}$-detectable. Thus, the necessary conditions for solving the output feedback stabilization problem in Step B are fullfilled. However, there is no closed solution for the problem of stabilization of normal linear systems by output feedback, but different techniques exist in the literature to treat this problem and may be

candidates to be used in Step B. The choice of an appropriate one depends, in many cases, of the structure of the involved matrices and on the knowledge and experience of the designer as well (Syrmos et al., 1997).

Although different output feedback stabilization techniques can be considered to be applied to the reduced-order system, the chosen technique can also be directly applied to the full order descriptor model (1),(2). To show that, a particular technique that brings together elements from the geometric and the quadratic approaches (Castelan et al., 2000) will be considered. In particular the use of the full-order model can be attractive from numerical and computational storage point of views mainly for high dimensional systems where the involved matrices have some (sparse) structure that are lost in the reduced-order triple (A, B, C) (Freitas et al., 1997), (Freitas et al., 1995).

4. A $\mathcal{D}$-STABILIZATION APPROACH VIA LMI REGIONS

Let us first recall a result that relates the existence of a stabilizing output feedback, for the reduced-order system, to the solution of two coupled-Sylvester equations (Syrmos and Lewis, 1994):

Theorem 4.1. There exists an output feedback matrix $K \in \Re^{m\times p}$ such that $\sigma(A+BKC) \in \mathcal{C}^-$ if and only if the following conditions hold true for some matrices $(V_1 \in \Re^{q\times(q-v)}, H_V \in \Re^{(q-v)\times(q-v)}, W \in \Re^{m\times(q-v)}, T_1 \in \Re^{v\times q}, H_T \in \Re^{v\times v}, U \in \Re^{m\times p})$ and some positive scalar $v \leq q$:

$$AV_1 - V_1H_V = -BW\ ,\quad \sigma(H_V) \in \mathcal{C}^- \tag{17}$$

$$T_1A - H_TT_1 = -UC\ ,\quad \sigma(H_T) \in \mathcal{C}^- \tag{18}$$

$$T_1V_1 = 0 \tag{19}$$

$$Ker\, CV_1 \subseteq Ker\, W \tag{20}$$

$$Ker\, B'T_1' \subseteq Ker\, U' \tag{21}$$

where: $rank(V_1) = (q-v)$ and $rank(T_1) = v$.

The above result has been exploited mainly in the literature related to the eigenstructure assignment by output feedback (see (Syrmos et al., 1997)). The coupled-Sylvester equations (17),(18) and (19) can be interpreted in terms of geometric properties of the subspace $\mathcal{V} = Ker\ T_1$ (for details, see (Syrmos and Lewis, 1994) and (Castelan et al., 2000)). Once the coupled Sylvester equations have been solved, the associated stabilizing output feedback can be computed by solving

$$KCV_1 = W \quad \text{or} \quad T_1BK = U \tag{22}$$

The closed-loop spectrum is given by:

$$\sigma(A+BKC) = \sigma(H_V) \dot{\cup} \sigma(H_T) \tag{23}$$

In this work, two new coupled-Lyapunov like equations, that can be obtained from Theorem 4.1, will be presented. The proposed coupled-Lyapunov equations are such that convex programming techniques can be used to solve the output feedback $\mathcal{D}$-stabilization problem. Thus, in the sequel, it is considered that the desired pole placement region $\mathcal{D}$ is defined from two LMI regions associated to H_V and H_T:

$$\begin{matrix}\sigma(H_V) \in \mathcal{D}_V \\ \sigma(H_T) \in \mathcal{D}_T\end{matrix} \implies \mathcal{D} = \mathcal{D}_V \cup \mathcal{D}_T \tag{24}$$

Thus, the LMI regions $\mathcal{D}_V$ and $\mathcal{D}_T$ are defined by the following two quadratic Lyapunov $\mathcal{D}$-stability conditions (Chilali and Gahinet, 1996):

$$\begin{matrix}\sigma(H_V) \in \mathcal{D}_V \Longleftrightarrow \exists\ \Pi = \Pi' > 0 \text{ such that} \\ \alpha_V \otimes \Pi + \beta_V' \otimes (\Pi H_V') + \beta_V \otimes (H_V\Pi) < 0\end{matrix} \tag{25}$$

$$\begin{matrix}\sigma(H_T) \in \mathcal{D}_T \Longleftrightarrow \exists\ \Gamma = \Gamma' > 0 \text{ such that} \\ \alpha_T \otimes \Gamma + \beta_T' \otimes (H_T'\Gamma) + \beta_T \otimes (\Gamma H_T) < 0\end{matrix} \tag{26}$$

where $\otimes$ stands for the Kronecker Product.

The following result can be obtained in a similar way as in (Castelan et al., 2000), by considering the coupled-Sylvester equations under the regional pole placement constraint on the spectra of H_V and H_T. For algorithmic purposes, it is considered that $v = m$. The set of closed-loop poles, denoted Λ, will verify $\Lambda = \Lambda_V \cup \Lambda_T$, with $\Lambda_V = \{\lambda_1, \ldots, \lambda_{q-m}\} \in \mathcal{D}_V$ e $\Lambda_T = \{\lambda_{q-m+1}, \ldots, \lambda_q\} \in \mathcal{D}_T$.

Theorem 4.2. There exists $K \in \Re^{m\times p}$ such that $\sigma(A+BKC) = \Lambda \in \mathcal{D}$, for $\mathcal{D} = \mathcal{D}_V \cup \mathcal{D}_T$, if and only if there exist $(P_1 = P_1' \geq 0,\ P_1 \in \Re^{q\times q}$, $Y \in \Re^{m\times q}$, $S_1 = S_1' \geq 0,\ S_1 \in \Re^{q\times q}$ and $Z \in \Re^{q\times p})$ such that the following conditions hold true for some matrices $V_1 \in \Re^{q\times(q-m)}$ and $T_1 \in \Re^{m\times q}$ verifying $T_1V_1 = 0$:

$$\alpha_V \otimes P_1 + \beta_V \otimes (AP_1 + BY) + \beta_V' \otimes (P_1A' + Y'B') \leq 0 \tag{27}$$

$$V_1'P_1V_1 = \bar{P}_1 > 0\ ;\ T_1P_1T_1' = 0 \tag{28}$$

$$Y = W_\Pi V_1' \text{ for some } W_\Pi \in \Re^{m\times(q-m)} \tag{29}$$

$$\alpha_T \otimes S_1 + \beta_T \otimes (S_1A + ZC) + \beta_T' \otimes (A'S_1 + C'Z') \leq 0 \tag{30}$$

$$T_1S_1T_1' = \bar{S}_1 > 0;\ V_1'SV_1 = 0 \tag{31}$$

$$Z = T_1'U_\Gamma \text{ for some } U_\Gamma \in \Re^{m\times p} \tag{32}$$

$$Ker\, CP_1 \subseteq Ker\, Y \tag{33}$$

$$Ker\, B'S \subseteq Ker\, Z' \tag{34}$$

Proof: ommited. □

4.1 *Algorithm*

Theorem 4.2 gives a necessary and sufficient condition for the existence of a $\mathcal{D}$-stabilizing output feedback. Unfortunately, this result involves equations that are non-linear in the considered unknows. However the quadratic characterization of Theorem 4.2 may be used to compute $\mathcal{D}$-stabilizing output feedback matrices K. This can be done, for instance, by taking into account the

coupling requirement and solving subsequently equations (27) and (30). Notice that, for guaranteeing that the inclusion (34) is verified and, hence, that a solution for $S_1BK = Z$ exists, it was considered that $v = m$. In the light of the algorithms proposed in (Syrmos and Lewis, 1993) and (Castelan et al., 2000), the following basic procedure can be used to compute a $\mathcal{D}$-stabilizing output feedback when $m + p > q$ is verified:

Step 1: Determine $V_1 \in \Re^{q\times(q-m)}$, such that (27), (28) and (29) can be verified and such that (A, V_1, C) has no invariant zeros;
Step 2: Compute T_1 from $T_1V_1 = 0$ and solve (30), (31) and (32) to find S, Z and U_Γ.
Step 3: Compute the $\mathcal{D}$-stabilizing output feedback matrix from $S_1B_1K = Z$.

The above procedure is a dual formulation of the basic procedure presented in (Castelan et al., 2000) for output feedback stabilization of normal systems. In the more difficult case $m + p \leq q$, the procedure can be systematically used to compute ν-order $\mathcal{D}$-stabilizing dynamic output compensators, with $\nu > q - (m + p)$. In the sequel, it is shown that the computations involved in Steps 1 and 2 can be done by using directly the descriptor model (1), (2), instead of using the reduced order matrices. Some comments are given to show how the proposed computations lead to a desired solution.

Step 1: *Computations*
1.1) Find an orthogonal decomposition:

$$\begin{bmatrix} M_1' \\ M_2' \end{bmatrix} B_1 = \begin{bmatrix} \bar{B}_1 \\ 0 \end{bmatrix} \tag{35}$$

where: $\bar{B}_1 \in \Re^{m\times m}$, $rank(\bar{B}_1) = m$, $\begin{bmatrix} M_1 & M_2 \end{bmatrix} \in \Re^{q\times q}$. Compute the matrix $\begin{bmatrix} M_3 & M_4 \end{bmatrix}$ that verifies:

$$J_3 \begin{bmatrix} M_1 & M_2 \end{bmatrix} + J_4 \begin{bmatrix} M_3 & M_4 \end{bmatrix} = \begin{bmatrix} 0 & 0 \end{bmatrix} \tag{36}$$

$$\text{and set: } \begin{bmatrix} A_{21} & A_{22} \end{bmatrix} = M_2' \begin{bmatrix} J_1 & J_2 \end{bmatrix} \begin{bmatrix} M_1 & M_2 \\ M_3 & M_4 \end{bmatrix} \tag{37}$$

1.2) Find P_{12} and $P_{22} = P_{22}' > 0$ verifying the *reduced-order* generalized Lyapunov equation

$$\begin{aligned} \alpha_V \otimes (P_{22}) + \beta_V \otimes (A_{22}P_{22} + A_{21}P_{12}) + \\ \beta_V' \otimes (P_{22}A_{22}' + P_{12}'A_{21}') < 0. \end{aligned} \tag{38}$$

1.3) Set $V_1 = \begin{bmatrix} M_1 & M_2 \end{bmatrix} \begin{bmatrix} P_{12} \\ P_{22} \end{bmatrix}$ and define:
$\mathcal{A} = J_1$, $\mathcal{B} = [-J_2 \; V_1]$, $\mathcal{C} = \begin{bmatrix} -J_3 \\ C_1 \end{bmatrix}$ and $\mathcal{E} = \begin{bmatrix} -J_4 & 0 \\ C_2 & 0 \end{bmatrix}$.
If $(\mathcal{A}, \mathcal{B}, \mathcal{C}, \mathcal{E})$ has no invariant zeros, then go to Step 2; else, repeat Step 1 using a new decomposition for B_1.

Comments: In the first part of Step 1, an auxiliary pair of matrices ($A_{22} \in \Re^{(q-m)\times(q-m)}$, $A_{21} \in \Re^{(q-m)\times m}$) is computed. It appears from decomposition (35) through

$$\begin{bmatrix} A_{11} & A_{12} \\ A_{21} & A_{22} \end{bmatrix} = \begin{bmatrix} M_1' \\ M_2' \end{bmatrix} \left(J_1 - J_2J_4^{-1}J_3\right) \begin{bmatrix} M_1 & M_2 \end{bmatrix}.$$

Thus, by defining $\begin{bmatrix} M_3 & M_4 \end{bmatrix} = -J_4^{-1}J_3 \begin{bmatrix} M_1 & M_2 \end{bmatrix}$, which corresponds to (36), one obtains (37).

Since the the open-loop system is assumed to be $\mathcal{D}$-stabilizable, it follows that the pair (A_{22}, A_{21}) is $\mathcal{D}$-stabilizable. Thus a solution (P_{22}, P_{12}) to (38) exists and is such that: $\sigma(A_{22} + A_{21}P_{12}(P_{22})^{-1}) = \sigma(H_V) \in \mathcal{D}_V$ (for details, see (Castelan et al., 2000). Notice also that (38) is an LMI in decision variables P_{12} and P_{22}. Then, standard convex programming techniques can be used to find feasible solutions to this matrix inequality (Boyd et al., 1994).

The last part of Step 1 is set to verify whether the computed matrix V_1 will produce or not feasible solutions in Step 2. This can be done by verifying the existence of invariant zeros for the triple (A, V_1, C). From the theory presented in section 2, it can be shown that the invariant zeros of this reduced-order triple correpond to the invariant zeros of $(\mathcal{A}, \mathcal{B}, \mathcal{C}, \mathcal{E})$. Thus, if $(\mathcal{A}, \mathcal{B}, \mathcal{C}, \mathcal{E})$ has no invariant zeros, then the system matrix $P_\lambda = \begin{bmatrix} \lambda I_q - J_1 & -J_2 & V_1 \\ -J_3 & -J_4 & 0 \\ C_1 & C_2 & 0 \end{bmatrix}$ has full normal column rank, equal to $n + m - q$, and Step 2 will produce feasible solutions. In general, the existence of invariant zeros do not allow to solve Step 2. However, in the unfrequent cases where invariant zeros may appear, other solutions to Step 1 can be generated from a new, not necessarily orthogonal, decomposition (35) so that Step 2 becomes feasible (Castelan et al., 2000).

Step 2: *Computations*

2.1) Compute T_1 such that

$$T_1V_1 = 0 \text{ with } T_1T_1' = I_m \tag{39}$$

2.2) Solve the following two equations, under constraints (31) and (32), to find S_1, Z:

$$\begin{aligned} \alpha_T \otimes S_1 + \beta_T \otimes (S_1J_1 + S_2J_3 + ZC_1) + \\ \beta_T' \otimes (J_1'S_1 + J_3'S_2' + C_1'Z') \leq 0 \end{aligned} \tag{40}$$

$$S_1J_2 + S_2J_4 + ZC_2 = 0 \tag{41}$$

Comments: Notice first that inequality (40) is obtained from (30), by defining $S_2 = -(S_1J_2 + ZC_2)J_4^{-1}$, which is equivalent to (41). From (39), T_1 has orthogonal rows and, from any feasible solution obtained in Step 2, the corresponding $\mathcal{D}$-stabilizing output feedback matrix verifies $S_1B_1K = Z \iff \bar{S}T_1B_1K = U_\Gamma$.

The computations in the second part of Step 2 can also be done by using standard convex programming techniques. For computational purposes, (40) can be treated as an equality, where the left hand side takes the form $-(T_1' \otimes I_m)Q_T(I_m \otimes$

T_1). Thus, $Q_T \in \Re^{m^2 \times m^2}$ can be considered as a free variable matrix. Additional requirements in the form of linear matrix inequalities can then be added to obtain other closed-loop requirements.

5. EXAMPLE

Consider the following data (Duan et al., 1999):

$$\bar{A} = \begin{bmatrix} 0 & 0 & 1 & 0 \\ 1 & 0 & 0 & 0 \\ 0 & 1 & 0 & 1 \\ 0 & 0 & 1 & 1 \end{bmatrix} \quad , \quad \bar{B} = \begin{bmatrix} 1 & 0 \\ 1 & -1 \\ 0 & 1 \\ 0 & 0 \end{bmatrix}$$

$$\bar{E} = \begin{bmatrix} 1 & 0 & 0 & 0 \\ 0 & 1 & 0 & 0 \\ 0 & 0 & 1 & 0 \\ 0 & 0 & 0 & 0 \end{bmatrix} \quad , \quad \bar{C} = \begin{bmatrix} 1 & 0 & 0 & 1 \\ 0 & 1 & 0 & -1 \end{bmatrix}$$

The corresponding system $(\bar{C}, \bar{A}, \bar{E}, \bar{B})$ is controllable and observable and $m + p = 4 > q$. The open-loop poles are: 0.7549, $-0.8774 \pm 0.7449j$.

The LMI region $\mathcal{D}_V$ is a vertical strip defined by: $\mathcal{D}_V = \{x + jy \in \mathcal{C} \; ; \; -3.5 < x < -2.5\}$. The LMI region $\mathcal{D}_T$ is defined from the intersection of a conic sector and a disk, defined by: $\{x + jy \in \mathcal{C} \; ; \; x < -2.5, |x + jy| < 5 \text{ and } tan\, 45° x < |y|\}$. Thus, standard convex programming techniques are applied to find feasible solutions for the pole placement equations, without considering additional requirements.

The matrix $\begin{bmatrix} M_1 & M_2 \\ M_3 & M_4 \end{bmatrix} = \begin{bmatrix} -0.7071 & 0.4082 & -0.5774 \\ -0.7071 & -0.4082 & 0.5774 \\ 0 & 0.8165 & 0.5774 \\ 0 & -0.8165 & -0.5774 \end{bmatrix}$ found in the step 1.1 leads to: $A_{22} = -0.6667$ $A_{21} = \begin{bmatrix} -0.8165 & -0.9428 \end{bmatrix}$. A solution for step 1.2 is: $P_{22} = 1$, $P_{12} = \begin{bmatrix} 2.6616 & 0.0011 \end{bmatrix}'$, that gives in step 1.3: $V_1 = \begin{bmatrix} -0.986 & -0.239 & 0.986 \end{bmatrix}'$. This solution has no invariant zeros and it implies, in the step 2.1: $T_1 = \begin{bmatrix} 0.2034 & 0.0501 & 0.9778 \\ -0.4590 & 0.8870 & 0.0501 \end{bmatrix}$. A feasible solution for the step 2.2 is then found: $Z = \begin{bmatrix} 546.5093 & 26024.205 \\ -25080.366 & -156113.26 \\ -54283.375 & -241688.35 \end{bmatrix}$ and $\begin{bmatrix} S_1 & S_2 \end{bmatrix} = \begin{bmatrix} 1092.1903 & -4276.1339 & -5006.97 & 30484.665 \\ -4276.1339 & 33000.084 & 56298.632 & -187331.53 \\ 5006.97 & 56298.632 & 105776.54 & -293181.51 \end{bmatrix}$.

The corresponding stabilizing output feedback, $K = \begin{bmatrix} 0.1052 & -9.2545 \\ -1.2062 & 4.7089 \end{bmatrix}$, gives: $\sigma(A + BKC) = \{-2.8409, -3.0511 \pm 1.5106j\} \subset \mathcal{D} = \mathcal{D}_V \cup \mathcal{D}_T$. The eigenvalue $-2.8409 \subset \mathcal{D}_V$ corresponds to step 1.

6. CONCLUSION

The problem of output feedback for regional pole placement of a class of descriptor systems has been studied. The particular structure of the model has been exploited to propose an approach based on the solution of a set of coupled-Lyapunov equations. The proposed design technique can be thought as an alternative to eigenstructure assignment to treat both pole placement and other performance requirements. The application of the proposed technique for power systems control design is at present being studied.

7. REFERENCES

L. Dai, *Singular Control System.* Springer Verlag, 1989.

V. L. Syrmos and F. L. Lewis, "Output Feedback Eigenstructure Assignment Using Two Sylvester Equations." *IEEE Tr. Autom. Cont.*; Vol 28, No 3, pp. 495-499, 1993.

V. L. Syrmos and F. L. Lewis, "A Bilinear Formulation for the Output Feedback Problem in Linear Systems." *IEEE Tr. Autom. Cont.*; Vol 39, No 2, pp. 410-414 1994.

S.P. Boyd, L. El Ghaoui, E. Feron and V. Balakrishhnan, *Linear Matrix Inequalities in System and Control Theory.* SIAM, 1994.

G. C. Verghese, B. C. Lèvy and T. Kailath, "A General State Space for Singular Systems." *IEEE Tr. Autom. Cont.*; Vol 26, pp. 811-831, 1981.

F. D. Freitas, A. S. e Silva and A. J. A. Simoes Costa, "Coordinate Setting of Stabilizers for Synchronous Generators." *CIGRÉ Symp. Power Electr. Power Syst.*; pp. 320-323, 1995.

A. J. A. Simoes Costa, F. D. Freitas and A. S. e Silva, "Design of Descentralized Controllers for Large Power Systems." *IEEE Tr. Power Syst.*; Vol 12, No 1, pp. 144-152, 1997.

V.L. Syrmos, C.T. Abdallah, P. Dorato and K. Grigoriadis, "Static Output Feedback - A Survey." *Automatica*; 33,3, pp. 125-137, 1997.

D. J. Bender and A. J. Laub, "The Linear Quadratic Optimal Regulator for Descriptor Systems." *IEEE Tr. Autom. Cont.*; vol AC-32, No 8, pp. 672-688, 1997.

A. Bunse- Gerstner, V. Mehrmann and N. K. Nichols, "Regularization of Descriptor Systems by Derivative and Proportional." *Siam J. Matrix Anal. Appl.*; Vol 13, No 1, pp. 46-67, 1992.

E. B. Castelan, J. C. Hennet and E. R. Llanos V, *"Quadratic characterization and use of output stabilization subspaces".* 8^{th} IEEE-MED Conf. Contr. and Automation, Patras, 2000. Also submitted to IEEE Tr. Autom. Cont.

G. R. Duan, G. W. Irwin and G. P. Liu, "Robust Stabilization of Descriptor Linear Systems via Proportional-plus-derivative State Feedback." *Proc. American Cont. Conf.*; San Diego, California, 1999.

M. Chilali and P. Gahinet, "H_∞ Design with Pole Placement Constraints: An LMI Approach." *IEEE Tr. Autom. Cont.*; Vol 41, No 3, pp. 358-367, 1996.

Copyright © 2002 IFAC
15th Triennial World Congress, Barcelona, Spain

ELSEVIER
IFAC
PUBLICATIONS
www.elsevier.com/locate/ifac

OUTPUT FEEDBACK DESIGN BY COUPLED LYAPUNOV-LIKE EQUATIONS

Eugênio B. Castelan , Elmer R. Llanos Villarreal
LCMI / DAS / UFSC
88040-900 - Florianópolis (S.C) - Brazil
E-mail: {*eugenio , llanos*}*@lcmi.ufsc.br ; Fax: +55 48 331 99 34*

Jean-Claude Hennet
LAAS du CNRS
31077 - Toulouse Cedex 4 - France
E-mail: *hennet@laas.fr ; Fax: +33 5 61 33 69 36*

Abstract: This note presents two coupled Lyapunov-like conditions under which a linear discrete-time system can be stabilized by static output feedback. The originality of these conditions is their relation to the well-known coupled Sylvester equations that describe both the (A, B) and (C, A)-invariance of a subspace. For systems verifying Kimura's condition, we show that output feedback stabilizing gain matrices can be computed through the successive resolution of two standard convex programming problems. Numerical results are provided to show the effectiveness of the proposed approach. *Copyright © 2002 IFAC*

Keywords: Output Feedback, Stabilization, Invariant Subspaces, Lyapunov Equations, Convex Programming.

1. INTRODUCTION

[1] A common feature shared by different methods to treat the static output feedback stabilization problem of linear systems is that it is equivalent to obtaining solutions of coupled sets of matrix equations (Castelan et al., 2000). In particular, through the use of coupled Sylvester equations (Syrmos and Lewis, 1993) (Syrmos and Lewis, 1994), the output feedback stabilization problem can be decomposed into two stages: (*i*) determination of a (C, A)-outer detectable subspace, an (*ii*) inner stabilization of this subspace. Thus, when the number of inputs, m, plus the number of outputs, p, is greater than the number of states, n, known as Kimura's condition $(m + p > n)$ (Kimura, 1975), the Sylvester equations involved in the two stages can be solved by standard eigenstructure assignment techniques.

This paper extends to the case of discrete-time systems the results presented in (Castelan et al., 2000) for continuous-time systems. It is shown that the above mentioned geometric approach based on the solution of coupled Syslvester equations has a quadratic counterpart, so that coupled linear matrix inequalities and equalities can also be used for construction of an output stabilizable (C, A, B)-invariant subspace as an intermediate mechanism in the process of designing a static output feedback. The quadratic characterization of both stages by Lyapunov equations provides a convenient framework for the numerical resolution of the problem through standard convex programming. In particular, we show that the first stage can be accomplished through the solution of a reduced-order strict LMI. The proposed problem decomposition as two subsequent convex programming problems may be also convenient for the integration of some additional performance and robustness requirements represented in the form of **Ms** .

The second section of the paper presents the key result that links the solution of the static output feedback stabilization problem to the coupled Sylvester equations and decomposes the basic solution into two steps. In the third section, the

[1] This work has been partially supported by CNPq/Brazil.

equivalent quadratic characterization is obtained. Then, section 4 is devoted to the presentation of the proposed algorithm, based on the use of orthogonal transformations and convex programming solutions of $LMIs$. In section 5, numerical examples are reported to illustrate the effectiveness of the proposed approach. We finally present some concluding remarks.

2. PRELIMINARIES

The considered linear discrete time-invariant systems are described by

$$x_{k+1} = Ax_k + Bu_k \quad (1)$$

$$y_k = Cx_k \quad (2)$$

where: $x \in \Re^n$, $u \in \Re^m$, $y \in \Re^p$. It is also assumed that B is full column-rank, C is full row-rank and that (C, A, B) is stabilizable and detectable. The studied problem is to find a static output feedback control law $u_k = Ky_k$, such that the closed-loop system

$$x_{k+1} = (A + BKC)x_k \quad (3)$$

is asymptotically stable, i.e. its spectrum satisfies:

$$\sigma(A + BKC) = \{\lambda_1, \lambda_2, \ldots, \lambda_n\} \text{ with,}$$

$$\text{for } i = 1, ..., n, \quad \lambda_i \in \mathcal{C}^s = \{\lambda \in \mathcal{C}; |\lambda| < 1\}.$$

The following basic result relates the existence of a stabilizing output feedback to the solution of two coupled Sylvester equations.

Theorem 2.1. There exists a static output feedback $K : \Re^p \longrightarrow \Re^m$ such that $\sigma(A+BKC) \in \mathcal{C}^s$ if and only if the following conditions hold true for some matrices ($H_V \in \Re^{v \times v}$, $V \in \Re^{n \times v}$, $Z_v \in \Re^{m \times v}$, $H_T \in \Re^{n-v \times n-v}$, $T \in \Re^{n \times (n-v)}$, $Z_T \in \Re^{p \times n-v}$) and for some positive scalar $v \leq n$:

$$AV - VH_V = -BZ_V \ , \quad \text{with} \quad \sigma(H_V) \in \mathcal{C}^s \quad (4)$$

$$T'A - H_T T' = -Z_T'C \ , \quad \text{with} \quad \sigma(H_T) \in \mathcal{C}^s \quad (5)$$

$$T'V = 0 \quad (6)$$

$$Ker(CV) \subseteq Ker(Z_V) \quad (7)$$

$$Ker(B'T) \subseteq Ker(Z_T') \quad (8)$$

where: $\text{rank}\,(T) = n - v$ and $\text{rank}\,(V) = v$. □

The above result has been presented and exploited under different forms in the literature related to the eigenstructure assigment by output feedback (see (Syrmos et al., 1997)). The equations (4) to (5) are recognized as coupled Sylvester equations. Under the stability constraint imposed on matrix H_V, (4) means that $\mathcal{V} = Im(V)$ must be a (A, B)-inner stabilizable subspace, that is there exists F such that $(A+BF)|\mathcal{V}$ is stable. Dually, (5) means that $Ker\ T'$ has to be a (C, A)-outer detectable subspace, that is there exists L such that $(A + LC)|(\Re^n / Ker\ T')$ is stable.

Under the coupling condition (6), (4) and (5) mean that $\mathcal{V} = Ker\ T'$ is an Output Stabilizable (C, A, B) invariant subspace, as defined in (Syrmos and Lewis, 1994). Notice also that inclusions (7) and (8) can be equivalently replaced by:

$$KCV = Z_V \quad (9)$$

$$T'BK = Z_T' \quad (10)$$

From the above remarks we see that the statement of theorem 2.1 is essentially equivalent to the one of theorem 3.2 stated in (Syrmos and Lewis, 1994). For algorithmic purposes, we specialize the design to the case where $\mathcal{V} = Im\ V$ is a p-dimensional subspace. This assumption has also been adopted in many other works that, explicitly or implicitly, use the coupled-Sylvester equations for eigenstructure assignment by output feedback (Alexandridis and Parakevopoulos, 1996) (Syrmos and Lewis, 1993) (Fletcher et al., 1985). Its main advantage is to provide a straightforward solution to equation (9). Thus, based on the conditions of theorem 2.1, the following procedure generically leads to a stabilizing output feedback when the Kimura's condition $n < m + p$ is verified (Syrmos and Lewis, 1993) :

Step 1: Find a matrix $T \in \Re^{n \times n-p}$ verifying (5), and such that

$$rank \begin{bmatrix} T' \\ C \end{bmatrix} = n \Leftrightarrow Ker\ T' \cap Ker\ C = \{0\} \quad (11)$$

Step 2: Solve (4), taking into account that V must verify (6) and rank(V) must be equal to p.
Step 3: By construction (11) guarantees that $\text{rank}(CV) = p$ and K can be computed by:

$$K = Z_V (CV)^{-1} \quad (12)$$

Steps 1 and 2 can be solved by using standard eigenstructure assignment techniques. In particular, once T has been found, step 2 can be solved by using the "zero equation":

$$\begin{bmatrix} A - \lambda_i I & B \\ T' & 0 \end{bmatrix} \begin{bmatrix} v_i \\ z_{vi} \end{bmatrix} = \begin{bmatrix} 0 \\ 0 \end{bmatrix} \quad (13)$$

where v_i and z_{vi}, $i = 1, \ldots, p$, form the columns of V and Z_V, respectively.

Remark 2.1. To guarantee that the eigenvalues λ_i of step 2 are freely assignable, the system matrix $P(\lambda) = \begin{bmatrix} A - \lambda I & B \\ T' & 0 \end{bmatrix}$ must have full normal row

rank: $rank(P(\lambda)) = 2n - p$, $\forall \lambda$. Otherwise the system (A, B, T') has invariant zeros, in which case they must be used to obtain the (A, B)-invariance of $Ker\, T'$. The genericity of the above procedure relies on the fact that, for $m + p > n$, $P(\lambda)$ does not lose rank for almost all triples (A, B, T') (Syrmos and Lewis, 1993).

Remark 2.2. In the case $m+p = n$, $P(\lambda)$ is square and almost all triple (A, B, T') has p finite invariant zeros (Syrmos and Lewis, 1993). Thus, the basic procedure can produce stabilizing solutions in this more difficulty case only if T found in step 1 generates p minimum-phase invariant zeros, which have to be used to solve (13) (Castelan and Hennet, 1993). However, to our knowledge, no systematic procedure exists for the search of a good T, although a "try-and-error" search may be carried-out.

3. COUPLED MATRIX INEQUALITY CONDITIONS

A quadratic characterization of Theorem 2.1 can also be obtained by replacing the stability constraints on matrices H_V and H_T by the following equivalent conditions that are obtained from Schur complement applied to the classical discrete-time Lyapunov stability conditions (Crusius and Trofino, 1999):

$$\begin{cases} H_V' \bar{\Pi} H_V - \bar{\Pi} < 0 \\ \bar{\Pi} > 0 \end{cases} \Longleftrightarrow \begin{cases} \begin{bmatrix} -\Pi & \Pi H_V' \\ H_V \Pi & -\Pi \end{bmatrix} = -Q_V \\ Q_V = Q_V' > 0 \\ \Pi = \bar{\Pi}^{-1} > 0 \end{cases} \quad (14)$$

$$\begin{cases} H_T \bar{\Gamma} H_T' - \bar{\Gamma} < 0 \\ \bar{\Gamma} > 0 \end{cases} \Longleftrightarrow \begin{cases} \begin{bmatrix} -\Gamma & \Gamma H_T \\ H_T' \Gamma & -\Gamma \end{bmatrix} = -Q_T \\ Q_T = Q_T' > 0 \\ \Gamma = \bar{\Gamma}^{-1} > 0 \end{cases} \quad (15)$$

Theorem 3.1. There exists an output feedback $K : \Re^p \longrightarrow \Re^m$ such that $\sigma(A + BKC) \in C^g$, if and only if the following conditions hold true for some full rank matrices $T \in \Re^{n \times n-v}$, $V \in \Re^{n \times v}$, with $v > 0$, such that $T'V = 0$:

(i) $\exists P = P' \geq 0, P \in \Re^{n \times n}$, $W \in \Re^{m \times n}$;

$$\begin{bmatrix} -P & PA' + W'B' \\ AP + BW & -P \end{bmatrix} = \begin{bmatrix} V & 0 \\ 0 & V \end{bmatrix} Q_V \begin{bmatrix} V' & 0 \\ 0 & V' \end{bmatrix} \quad (16)$$

$$V'PV > 0 \; ; \; T'PT = 0 \quad (17)$$

$$W = Z_\Pi V' \; for \; some \; Z_\Pi \in \Re^{m \times v} \quad (18)$$

(ii) $\exists S = S' \geq 0, S \in \Re^{n \times n}$, $Y \in \Re^{n \times p}$;

$$\begin{bmatrix} -S & SA + YC \\ A'S + C'Y' & -S \end{bmatrix} = \begin{bmatrix} T & 0 \\ 0 & T \end{bmatrix} Q_T \begin{bmatrix} T' & 0 \\ 0 & T' \end{bmatrix} \quad (19)$$

$$T'ST > 0 \; ; \; V'SV = 0 \quad (20)$$

$$Y = TZ_\Gamma' \; for \; some \; Z_\Gamma \in \Re^{p \times n-v} \quad (21)$$

(iii) $Ker\, CP \subseteq Ker\, W$ (22)

$Ker\, B'S \subseteq Ker\, Y'$ (23)

Proof (outline):

Necessity: Consider that K is a stabilizing output feedback and, hence, that the conditions (4) to (5) of theorem 2.1 are all verified.

By recalling that the quadratic stability condition (14) holds true, we obtain:

$$\begin{bmatrix} V & 0 \\ 0 & V \end{bmatrix} \begin{bmatrix} -\Pi & \Pi H_V' \\ H_V \Pi & -\Pi \end{bmatrix} \begin{bmatrix} V' & 0 \\ 0 & V' \end{bmatrix} = \begin{bmatrix} -V\Pi V' & V\Pi H_V' V' \\ V H_V \Pi V' & -V\Pi V' \end{bmatrix} \leq 0.$$

Then, condition (16) is obtained using $AV + BZ_V = VH_V$, setting $Z_\Pi = Z_V \Pi$, $P = P' = V\Pi V'$ and $W = Z_\Pi V'$.

Now, condition (17) is obtained considering that $rank(V) = p$ and that $\Pi > 0 \Longrightarrow \begin{cases} V'V\Pi V'V > 0 \\ T'V\Pi V'T = 0 \end{cases}$.

Using similar arguments, we can show the necessity of part (ii):

$$\begin{bmatrix} T & 0 \\ 0 & T \end{bmatrix} \begin{bmatrix} -\Gamma & \Gamma H_T \\ H_T' \Gamma & -\Gamma \end{bmatrix} \begin{bmatrix} T' & 0 \\ 0 & T' \end{bmatrix} = \begin{bmatrix} -T\Gamma T' & T\Gamma H_T T' \\ T H_T' \Gamma T' & -T\Gamma T' \end{bmatrix} \leq 0.$$

Thus, by using $T'A + Z_T' C = H_T T'$, and setting $S = T\Gamma T'$ and $Y = T\Gamma Z_T'$, we obtain (19) and (21). Furthermore, since $rank(T) = n - v$ and $\Gamma > 0$, we also have $\begin{cases} T'T\Gamma T'T > 0 \\ V'T\Gamma T'V = 0 \end{cases}$, corresponding to condition (20).

Necessity of (22), (23) is derived from (7), (8), respectively, and from the definition of the matrices involved in these conditions.

Sufficiency: For simplicity of the presentation we show only that the verification of part(i) is equivalent to the (A, B)-inner stabilizability of the subspace $\mathcal{V} = Ker\, T'$. We first have:

$$\begin{bmatrix} V' \\ T' \end{bmatrix} P \begin{bmatrix} V & T \end{bmatrix} = \begin{bmatrix} \bar{P} & 0 \\ 0 & 0 \end{bmatrix} \geq 0; \; \bar{P} = \bar{P}' > 0 \quad (24)$$

Thus, we can decompose P as:

$$P = \begin{bmatrix} V & T \end{bmatrix} \begin{bmatrix} \Pi & 0 \\ 0 & 0 \end{bmatrix} \begin{bmatrix} V' \\ T' \end{bmatrix} \geq 0 \quad \text{for} \quad (25)$$

$$\Pi = \Pi' = V'(V'V)^{-1} \bar{P} (V'V)^{-1} V > 0 \quad (26)$$

From (22), there exists a matrix K such that:

$$KCP = W \tag{27}$$

Thus, by substituting (27) into (16), we get

$$\begin{bmatrix} -P & P(A+BKC)' \\ (A+BKC)P & -P \end{bmatrix} = -\tilde{Q}_V \tag{28}$$

where $\tilde{Q}_V \in \Re^{2n\times 2n}$ is defined from $Q_V = \begin{bmatrix} Q_{V11} & Q'_{V21} \\ Q_{V21} & Q_{V22} \end{bmatrix}$ by $\tilde{Q}_V =$

$$\begin{bmatrix} V & T & \\ & & V & T \end{bmatrix} \begin{bmatrix} \begin{bmatrix} Q_{V11} & 0 \\ 0 & 0 \end{bmatrix} & \begin{bmatrix} Q'_{V21} & 0 \\ 0 & 0 \end{bmatrix} \\ \begin{bmatrix} Q_{V21} & 0 \\ 0 & 0 \end{bmatrix} & \begin{bmatrix} Q_{V22} & 0 \\ 0 & 0 \end{bmatrix} \end{bmatrix} \begin{bmatrix} V' & \\ T' & \\ & V' \\ & T' \end{bmatrix}.$$

Taking into account (26) and the similarity equation:

$$(A+BKC)\begin{bmatrix} V & T \end{bmatrix} = \begin{bmatrix} V & T \end{bmatrix} \begin{bmatrix} \bar{A}_{11} & \bar{A}_{12} \\ \bar{A}_{21} & \bar{A}_{22} \end{bmatrix} \tag{29}$$

we obtain from (28):

$$\begin{bmatrix} -\begin{bmatrix} \Pi & 0 \\ 0 & 0 \end{bmatrix} & \begin{bmatrix} \Pi\bar{A}'_{11} & \Pi\bar{A}'_{21} \\ 0 & 0 \end{bmatrix} \\ \begin{bmatrix} \bar{A}_{11}\Pi & 0 \\ \bar{A}_{21}\Pi & 0 \end{bmatrix} & -\begin{bmatrix} \Pi & 0 \\ 0 & 0 \end{bmatrix} \end{bmatrix} = -\begin{bmatrix} \begin{bmatrix} Q_{V11} & 0 \\ 0 & 0 \end{bmatrix} & \begin{bmatrix} Q'_{V21} & 0 \\ 0 & 0 \end{bmatrix} \\ \begin{bmatrix} Q_{V21} & 0 \\ 0 & 0 \end{bmatrix} & \begin{bmatrix} Q_{V22} & 0 \\ 0 & 0 \end{bmatrix} \end{bmatrix} \tag{30}$$

By construction, $\Pi > 0$, thus from (30), $\bar{A}'_{21} = 0$, which implies that $\mathcal{V} = Im\,V$ is a $(A+BKC)$-invariant subspace. And also from (30),

$$\begin{bmatrix} -\Pi & \Pi\bar{A}'_{21} \\ \bar{A}_{21}\Pi & -\Pi \end{bmatrix} = -Q_V < 0$$

which means that the restriction of $(A+BKC)$ to $\mathcal{V} = Im\,V$ is stable. □

Remark 3.1. For any pair of matrices (P, S) solution to parts (i) and part (ii), the coupling condition between the given matrix inequality conditions (16) and (19) can be restate as $Ker\ S = Im\ \mathcal{V} = Im\ P$, or, equivalently: $SP = 0$. The coupled matrix inequality conditions (i) and (ii), together with this condition show how the geometric approach and Lyapunov conditions have been combined in our approach.

4. AN ALGORITHM FOR OUTPUT FEEDBACK STABILIZATION

Theorem 3.1 gives a necessary and sufficient condition for the existence of a stabilizing output feedback. Unfortunately, this result involves coupled matrix inequality conditions that are non-convex in the considered decision variables T, V, P and S. However these conditions may be used to adequately construct Output Stabilizable (C, A, B)-invariant subspaces that lead to stabilizing output feedback matrices K. As in the eigenstructure assignment approach presented in section 2 (Syrmos and Lewis, 1993), this can be done by taking into account the coupling requirement and solving subsequently part (ii) and part (i) of theorem 3.1. The following procedure is proposed to compute a stabilizing output feedback when $m+p > n$ [2].

Step 1:

- Find an orthogonal decomposition $C\begin{bmatrix} M_1 & M_2 \end{bmatrix} = \begin{bmatrix} C_1 & 0 \end{bmatrix}$, where $C_1 \in \Re^{p\times p}$ is non-singular, and set $\begin{bmatrix} A_{12} \\ A_{22} \end{bmatrix} = \begin{bmatrix} M'_1 \\ M'_2 \end{bmatrix} AM_2$;
- Solve the reduced-order (strict) LMI condition below to find $S_{21} \in \Re^{n-p\times p}$ and $S_{22} \in \Re^{n-p\times n-p}$: $S_{22} > 0$ and

$$\begin{bmatrix} -S_{22} & S_{22}A_{22} + S_{21}A_{12} \\ A'_{22}S_{22} + A'_{12}S'_{21} & -S_{22} \end{bmatrix} < 0 \tag{31}$$

- Define $T' = \begin{bmatrix} S_{21} & S_{22} \end{bmatrix} \begin{bmatrix} M'_1 \\ M'_2 \end{bmatrix}$.

Step 2:

- Compute V from (6) as an orthogonal basis of $Ker\ T'$, *i.e.* $V'V = I_p$;
- Solve conditions (16), (17) and (18) to find P, W and Z_Π.

Step 3: Compute the stabilizing output feedback matrix as the unique solution of:
$KCP = W \iff KCV\bar{P} = Z_\Pi$, since $V'V = I_p$.

Remark 4.1. In step 1, a candidate matrix T is constructed such that $Ker T' \cap Ker C = \{0\}$. In the basis formed by the columns of matriz $M = \begin{bmatrix} M_1 & M_2 \end{bmatrix}$, the open-loop system takes the form

$$\begin{bmatrix} \dot{x}_1 \\ \dot{x}_2 \end{bmatrix} = \begin{bmatrix} A_{11} & A_{12} \\ A_{21} & A_{22} \end{bmatrix} \begin{bmatrix} x_1 \\ x_2 \end{bmatrix} + \begin{bmatrix} B_1 \\ B_2 \end{bmatrix} u \tag{32}$$

$$y = \begin{bmatrix} C_1 & 0 \end{bmatrix} \begin{bmatrix} x_1 \\ x_2 \end{bmatrix} \tag{33}$$

where the matrices involved have the appropriate dimensions. As shown in (Chen, 84), the detectability of the pair (C, A) implies the detectability of the pair (A_{12}, A_{22}). Thus, a feasible solution to LMI (31) can always be find. Let $L_2 \in \Re^{n-p\times p}$ be such that $S_{22}L_2 = S_{21}$ and consider a Choleski decomposition of S_{22} given by: $S_{22} = T'_2T_2$. Since, by construction L_2 stabilizes

[2] If $m+p = \bar{\nu} \leq n$, a dynamic compensator of order $\nu > n - \bar{\nu}$ can be considered to recover this condition.

$(A_{22} + L_2 A_{12})$, we can define $H_T \in \mathcal{C}^s$ from the similarity relation

$$T_2 (A_{22} + L_2 A_{12}) = H_T T_2 \qquad (34)$$

Furthermore, since C_1 is invertible, a matrix $Z_T \in \Re^{p \times (n-p)}$ can always be computed from:

$$Z_T' C_1 = -(T_2 L_2 A_{11} + T_2 A_{21} - H_T T_1) \quad (35)$$

where: $T_1 = T_2 L_2$. Hence, (34) and (35) can be equivalently replaced by

$$\begin{bmatrix} T_1 & T_2 \end{bmatrix} \begin{bmatrix} A_{11} & A_{12} \\ A_{21} & A_{22} \end{bmatrix} - H_T \begin{bmatrix} T_1 & T_2 \end{bmatrix} = -Z_T' \begin{bmatrix} C_1 & 0 \end{bmatrix}, \quad with\ \sigma(H_T) \in \mathcal{C}^s. \quad (36)$$

By construction, $\begin{bmatrix} T' \\ C \end{bmatrix} = \begin{bmatrix} T_1 & T_2 \\ C_1 & 0 \end{bmatrix} \begin{bmatrix} M_1' \\ M_2' \end{bmatrix}$. Thus, $rank \begin{bmatrix} T' \\ C \end{bmatrix} = n \iff Ker\, T' \cap Ker\, C = \{0\}$.

Furthermore , let $\Gamma = \Gamma' > 0$ be a solution to (15). Thus, the following matrices Y and $S \geq 0$ verify (16) ,(17) and (18) for $Y = T Z_T' \Gamma$;

$$S = \begin{bmatrix} M_1 & M_2 \end{bmatrix} \begin{bmatrix} S_{11} & S_{21}' \\ S_{21} & S_{22} \end{bmatrix} \begin{bmatrix} M_1' \\ M_2' \end{bmatrix}, \quad \text{with}$$

$$\begin{bmatrix} S_{11} & S_{21}' \\ S_{21} & S_{22} \end{bmatrix} = \begin{bmatrix} T_1' \\ T_2' \end{bmatrix} \Gamma \begin{bmatrix} T_1 & T_2 \end{bmatrix}.$$

Remark 4.2. Step 2 is used to solve the set of conditions for $\mathcal{V} = Ker T'$. Recall that these conditions are generically solvable in the sense that when $m + p > n$, $P(\lambda)$ has full row rank for almost all triples (A, B, T') (remark 2.1).

Remark 4.3. The decomposition for step 1 is not unique. The set of all decompositions can be obtained from a chosen orthogonal matrix M by

$$CMD = C \begin{bmatrix} M_1 & M_2 \end{bmatrix} \begin{bmatrix} D_1 & 0 \\ D_{21} & D_2 \end{bmatrix} = \begin{bmatrix} \bar{C}_1 & 0 \end{bmatrix} \quad (37)$$

for all non-singular matrices $D_1 \in \Re^{p \times p}$, $D_2 \in \Re^{n-p \times n-p}$. For instance, in the unfrequent cases where step 2 fails, a new basis (not necessarily orthogonal) can be constructed by $M^n = MD$; the new detectable pair (A_{12}^n, A_{22}^n) satisfies:

$$\begin{bmatrix} A_{12}^n \\ A_{22}^n \end{bmatrix} = \begin{bmatrix} D_1^{-1} & 0 \\ -\bar{D}_{21} & D_2^{-1} \end{bmatrix} \begin{bmatrix} A_{21} \\ A_{22} \end{bmatrix} D_2 = \begin{bmatrix} D_1^{-1} A_{21} D_2 \\ (D_2^{-1} A_{22} - \bar{D}_{21} A_{21}) D_2 \end{bmatrix}$$

with $\bar{D}_{21} = D_2^{-1} D_{21} D_1^{-1}$. In this way, other solutions to step 1 can be found so that step 2 becomes feasible.

Finally, it is worth recalling that stabilizing solutions can also be computed from the use of the dual system (A', C', B'). In addition, standard convex programming techniques can be used to find feasible solutions for the considered Lyapunov-like conditions and also to include some additional.

5. NUMERICAL EXAMPLE

The numerical examples reported in this section were solved with Scilab (INRIA, France). Standard convex programming techniques have been applied to find feasible solutions for the coupled Lyapunov-like conditions.

The first 1 000 random triples (A, B, C) generated with unstable A verify the Kimura's condition $m + p > n$, with; $n = 5$, $m = p = 3$. The basic procedure computed stabilizing solutions in 99.6% of cases. In the other 4 examples, only one iteration was necessary to obtain a stabilizing solution; this iteration was carried out using Remark 4.3, with $D = \begin{bmatrix} I_p & 0 \\ D_{21} & I_{n-p} \end{bmatrix}$, with a random matrix D_{21}. Thus, under the Kimura's condition, the algorithm was always successful and had a performance comparable to the performance reported in (El Ghaoui et al., 1997) for the cone complementarity linearization algorithm.

Some computational experiments have also been carried out for the less restrictive case $m + p = n$, with; $n = 4$, $m = p = 2$ (see Remark 2.2). For 20 random triples (A, B, C) the basic procedure computed stabilizing solutions in 50 % of cases. Once more, only one iteration was necessary to produce a stabilizing solution, for each one of the remaining 10 examples. These results also show that the approach may be effective when Kimura's condition is not verified.

The objective of the next example is to show the numerical results obtained at each step. The following model has been obtained from a discretization of the system studied in (Fletcher et al., 1985): $A = \begin{bmatrix} 1.0502 & 0.3551 & 0 & 0 \\ 0.3551 & 1.4054 & 0 & 0 \\ -0.3049 & -0.0502 & 1 & 0 \\ 0 & 0 & 0 & 1 \end{bmatrix}$, $B = \begin{bmatrix} 0.0502 & 0 \\ 0.3551 & 0 \\ -0.0049 & 0 \\ 0 & 0.3 \end{bmatrix}$, $C = \begin{bmatrix} 1 & 0 & 0 & 1 \\ 0 & 0 & 1 & 0 \\ 0 & 0 & 0 & 1 \end{bmatrix}$, with open-loop spectrum $\sigma(A) = \{1;\ 1.6248;\ 0.8308;\ 1\}$. The corresponding triple (C, A, B) is controllable and observable and $m + p = 5 > n$. Using an orthogonal matrix M that performs step 1, a matrix $T' = \begin{bmatrix} S_{21} & S_{22} \end{bmatrix} \begin{bmatrix} M_1' \\ M_2' \end{bmatrix}$ is readily found:

$$T' = \begin{bmatrix} 1 & 0.1868 & 0.1611 & 0.1585 \end{bmatrix} \begin{bmatrix} -0.7071 & 0 & 0 & -0.7071 \\ 0 & 0 & -1 & 0 \\ 0.7071 & 0 & 0 & -0.7071 \\ 0 & 1 & 0 & 0 \end{bmatrix}$$

$= \begin{bmatrix} -0.5932 & 0.1585 & -0.1868 & -0.8210 \end{bmatrix}$.

It implies, in step 2: $V = \begin{bmatrix} -0.7879 & -0.1793 & 0.1521 \\ 0.0764 & 0.0174 & 0.9853 \\ -0.0900 & 0.9795 & 0.0174 \\ 0.6044 & -0.0900 & 0.0764 \end{bmatrix}$.

A feasible solution for the second part of step 2 is then found by minimizing the trace of matrix P:

$$P = 10^{-3} \begin{bmatrix} 0.5630 & -0.3142 & 0.3740 & -0.5525 \\ -0.3142 & 1.4728 & 0.7512 & 0.3403 \\ 0.3740 & 0.7512 & 1.8026 & -0.5354 \\ -0.5525 & 0.3403 & -0.5354 & 0.5867 \end{bmatrix},$$

$$W = 10^{-3} \begin{bmatrix} -0.5647 & -3.8352 & -1.9805 & 0.1183 \\ 0.3027 & -1.3523 & -0.5114 & -0.3634 \end{bmatrix};$$

$$Z_\Pi = 10^{-3} \begin{bmatrix} 0.4018 & -1.9160 & -3.8899 \\ -0.5153 & -0.5460 & -1.3230 \end{bmatrix}.$$

The corresponding stabilizing output feedback, $K = \begin{bmatrix} -21.4364 & -3.5490 & -1.7870 \\ -4.1273 & -1.0505 & -1.3373 \end{bmatrix}$, gives:

$$\sigma(A + BKC) = \{0.1355;\ 0.0098;\ 0.8056 \pm 0.1336i\}.$$

where the eigenvalue 0.1355 corresponds to step 1.

6. CONCLUDING REMARKS

Stabilization of linear systems by static output feedback is recognized a basic and still open problem in control theory. A review of existing approaches and techniques to treat different versions of this problem can be found in (Syrmos et al., 1997); other recent results not covered by this survey paper are, for instance, (Alexandridis and Parakevopoulos, 1996), (Crusius and Trofino, 1999), (Geromel et al., 1998), (El Ghaoui et al., 1997) and (Castelan et al., 2000).

The present paper has extended the results reported in (Castelan et al., 2000) to the case of discrete-time systems. The basis of the study has been the coupled Sylvester equations approach, often used in the eigenstructure assignment literature. From these equations, a quadratic approach based on the solution of two-coupled Lyapunov-like conditions has been obtained.

The effectiveness of the proposed algorithm has been shown through numerical examples for cases where the Kimura's condition are verified. Thus, stabilizing solutions can also be used in the cases where this condition is not verified by using dynamical compensators that recovers Kimura's condition for the associated augmented system.

The use of the proposed approach to integrate additional closed-loop performance requirements and also to solve less restrictive cases are the subject of underlying researches.

7. REFERENCES

A.T. Alexandridis and P.N. Parakevopoulos, "A new approach to Eigenstructure Assignment by Output Feedback." *IEEE Trans. Automatic Control*; Vol. 41, No 7, pp. 1046-1050, 1996.

S.P. Boyd, L. El Ghaoui, E. Feron and V. Balakrishhnan, *Linear Matrix Inequalities in System and Control Theory*. SIAM, 1994.

E.B. Castelan and J. C. Hennet, "Eigenstructure Assignment for State Constrained Linear Continuous Time Systems." *Automatica*; Vol. 28, No 3, pp. 605-611, 1993

C.T. Chen, *Linear system theory and design* : New York, Holt, Rinehart and Winston, INC, 1984.

C.A.R. Crusius and A. Trofino, "Sufficient LMI Conditions for Output Feedback." *IEEE Trans. Automatic Control*; Vol. 44, No 5, pp. 1053-1057, 1999.

L.R. Fletcher, J. Kautsky, G.K.G Kolka and N.K Nichols, "Some necessary and sufficient conditions for eigenstructure assignment." *Int. J. Control*; Vol. 42, No 6, pp. 1457-1468, 1985.

J.C. Geromel, C.C. de Souza and R.E. Skelton, "Static Output Feedback Controllers: Stability and Convexity." *IEEE Trans. Automatic Control*; Vol. 43, No 1, pp. 120-125, 1998.

L. El Ghaoui, F. Oustry and M. AitRami, "A Cone Complementarity Linearization Algorithm for Static Output-Feedback and Related Problems." *IEEE Trans. Automatic Control*; Vol. 42, No 8, pp. 1171-1176, 1997.

H. Kimura, "Pole Assignment by Gain Output Feedback." *IEEE Trans. Automatic Control*; Vol. 20, pp. 509-516, 1975.

V.L. Syrmos and F.L. Lewis, "Output Feedback Eigenstructure Assignment Using Two Sylvester Equations." *IEEE Trans. Automatic Control*; Vol. 38, No 3, pp. 495-499, 1993.

V.L. Syrmos and F.L. Lewis, "A Bilinear Formulation for the Output Feedback Problem in Linear Systems." *IEEE Trans. Automatic Control*; Vol. 39, No 2, pp. 410-414, 1994.

V.L. Syrmos and F.L. Lewis, "Transmission Zero Assignment Using Semistate Description." *IEEE Trans. Automatic Control*; Vol. 38, No 7, 1993.

V.L. Syrmos, C.T. Abdallah, P. Dorato and K. Grigoriadis, "Static Output Feedback - A Survey." *Automatica*; 33,3, pp. 125-137, 1997.

W.M. Wonham, *Linear Multivariable Control, a Geometric Approach*. Springer Verlag, 1979.

E. B. Castelan, J. C. Hennet and E. R. Llanos V, *"Quadratic characterization and use of output stabilization subspaces"*. 8^{th} IEEE-MED Conf. on Contr. and Automation, Patras, 2000.

Copyright © IFAC System Structure and Control,
Prague, Czech Republic, 2001

IFAC
Publications
www.elsevier.com/locate/ifac

QUADRATIC CHARACTERIZATION AND USE OF OUTPUT STABILIZABLE SUBSPACES FOR DESCRIPTOR SYSTEMS

Eugênio B. Castelan * Elmer R. Llanos V.*
Sophie Tarbouriech **

* *UFSC - Departamento de Automação e Sistemas*
P.O. Box 476, 88040-900 Florianópolis, SC, BRAZIL
** *LAAS du CNRS - 7, Avenue du Colonel Roche*
31077 Toulouse Cedex 4 - France

Abstract: The study is based on the characterization of Output Stabilizable (C,A,E,B)-invariant subspaces through two coupled quadratic stabilization conditions as an extension of the results developed in (Castelan *et al.* 2000). The paper shows the equivalence between the existence of a solution to this set of conditions and the possibility to stabilize the system by static output feedback. A numerical example is provided to illustrate the approach. *Copyright* © 2001 *IFAC.*

Keywords: Output feedback, geometric approach, quadratic stabilizability, descriptor systems.

1. INTRODUCTION

Due both to its practical and theoretical interests, the problem of output feedback stabilization of dynamical systems has attracted the attention of many researchers in the control community. In the case of normal systems (classical dynamical systems described by a set of first order linear differential equations), a review of existing approaches and techniques to treat different versions of this problem can be found in (Syrmos *et al.* 1997). Other recent results not covered by this survey paper are found, for instance, in (Crusius and Trofino 1999), (Castelan *et al.* 2000), (Geromel *et al.* 1998) and (El Ghaoui *et al.* 1997) .

This paper tackles the problem of stabilization by static output feedback for linear descriptor systems. Remind that an n-dimensional descriptor system consists of a mixture of $n-q$ algebraic equations and q first order differential equations. Descriptor systems arise naturally in the modelling of several dynamical systems commonly used in engineering applications such as circuits, power systems and other interconnected systems (Dai 1989), (Lewis 1986).

Due to their nature, the stabilization for descriptor systems is a much more involving problem than the one of stabilizing normal systems. Besides guaranteeing the closed-loop asymptotical stability, two other properties are also desired in practice: closed-loop regularity and absence of impulsive behavior. The problem of computing a suitable static output feedback, from which these closed-loop properties are verified, is called output feedback strong-stabilization problem or, simply, S-stabilization problem. These three desired properties can be described in terms of the closed-loop eigenstructure: (i) the asymptotic stability is equivalent to have all the finite poles in the left half complex plane; (ii) the absence of impulsive modes is equivalent to have q finite closed-loop poles; and (iii) the regularity is guaranteed if the system is impulse-free.

From the interpretation given above, necessary and sufficient conditions for the existence of a S-stabilizing output feedback can be found as a set of *coupled* (generalized) *Sylvester equations* (see (Duan 1999), (Fletcher 1988)). As in the case of normal systems, it turns out that the *coupled Sylvester equations* can be interpreted in geometric terms and may also be used to solve the considered problem.

Thus, the main objective of this paper is to show that the *coupled Sylvester equations* have a counterpart in the quadratic stabilizability framework, so that coupled Lyapunov like equations can also be used to obtain a set of necessary and sufficient conditions for the existence of a S-stabilizing output feedback. In this way, we extend to the descriptor systems case, the framework used in (Castelan *et al.* 2000) for treating the output feedback stabilization of normal systems. In particular we introduce the key notion of (strongly) Output Stabilizable (C,E,A,B)-invariant subspaces, and in the light of the algorithms presented in (Castelan *et al.* 2000) and (Syrmos and Lewis 1993), we show how this concept can be used as an intermediate mechanism for designing the output feedback controller.

The paper is organized as follows. The second section presents the problem, introduces the basic geometric concepts and recalls the necessary and sufficient conditions for the existence of a solution. Section 3 is devoted to present the main results in the form of coupled Lyapunov equations. A numerical example that outlines the basic steps that may be used to solve the problem is presented in the fourth section. Finally, some concluding remarks end the paper.

2. PRELIMINARIES

The considered linear time-invariant descriptor systems are described by

$$E\dot{x}(t) = Ax(t) + Bu(t) \tag{1}$$

$$y(t) = Cx(t) \tag{2}$$

where: $x \in \mathcal{X} \subset \Re^n$, $u \in \mathcal{U} \subset \Re^m$, $y \in \mathcal{Y} \subset \Re^p$. It is assumed that $E \in \Re^{n\times n}$ is singular, with $\text{rank}(E) = q < n$, B is full column-rank, C is full row-rank. Furthermore, the system represented by (C,A,E,B) is supposed to be strongly stabilizable and strongly detectable. The studied problem is to find a static output feedback control law

$$u(t) = Ky(t), \qquad K \in \Re^{m\times p} \tag{3}$$

such that the closed-loop system

$$E\dot{x}(t) = (A + BKC)x(t) \tag{4}$$

is regular, asymptotically stable and impulse free. In the sequel, the above problem will be referred to as *S-stabilization problem.*

Aiming to treat the considered problem in a similar framework to the one used in (Castelan *et al.* 2000), the mathematical analysis uses some concepts and definitions from the geometric control theory (Lewis and Ozcaldiran 1989), (Lewis and Ozcaldiran 1990), (Wonham 1979). Noticing that Im and Ker stand, respectively, for the image and null space of linear maps, it is first recalled that a subspace $\mathcal{V} \subset \mathcal{X}$ is (A,E,B)-invariant if there exists $F : \mathcal{X} \longrightarrow \mathcal{Y}$ such that $(A+BF)\mathcal{V} \subset E\mathcal{V}$, or equivalently $A\mathcal{V} \subset E\mathcal{V} + Im\,B$. In addition, an (A,E,B)-invariant subspace $\mathcal{V}$ is regularizable, that is there exists F such that the pencil $(E, A+BF)$ is regular, if and only if $Ker\,E \cap \mathcal{V} = \{\emptyset\}$. In a dual way, a subspace $\mathcal{V} \subset \mathcal{X}$ is (C,A,E)-invariant, if there exists $L : \mathcal{Y} \longrightarrow \mathcal{X}$ such that $(A+LC)\mathcal{V} \subset E\mathcal{V}$, or equivalently $A(\mathcal{V} \cap Ker\,C) \subset E\mathcal{V}$.

Definition 2.1. A v-dimensional subspace $\mathcal{V} \subset \mathcal{X}$ is (C,A,E,B)-invariant if it is both (A,E,B)-invariant and (C,A,E)-invariant. If, in addition, $\mathcal{V}$ is such that $Ker\,E \cap \mathcal{V} = \{\emptyset\}$, then it is called strongly (C,A,E,B)-invariant.

Let $V \in \Re^{n\times v}$ be such that $span(V) = \mathcal{V}$. Then the condition $Ker\,E \cap \mathcal{V} = \{\emptyset\}$ can be equivalently replaced by (Lewis and Ozcaldiran 1989):

$$rank(EV) = v \tag{5}$$

Assuming that (5) is verified, a matrix $T \in \Re^{(q-v)\times n}$ is a generalized left annihilator of EV, if $TEV = 0$ and $Ker\,T \cap Im\,E = \{\emptyset\}$. Thus, the subspace $\mathcal{V} = span(V)$ is strongly (C,A,E,B)-invariant if and only if there exist matrices $(H_V \in \Re^{v\times v}, \quad W \in \Re^{m\times v})$ and $(H_T \in \Re^{(q-v)\times(q-v)}, U \in \Re^{(q-v)\times v})$ solutions to the following *coupled-generalized Sylvester equations*:

$$AV - EVH_V = -BW \tag{6}$$

$$TA - H_TTE = -UC \tag{7}$$

$$TEV = 0 \tag{8}$$

Definition 2.1 and equations (6), (7) and (8) play a fundamental role in treating the problem of control by static output feedback, mainly by eigenstructure assignment (Fletcher 1988). This

study rather focuses on the properties of stabilizability and detectability by considering that:
(i) an (A,E,B)-invariant subspace $\mathcal{V}=Im\,V$ is (A,E,B)-inner stabilizable if there exists F such that $(E,A+BF)|\mathcal{V}$, is (asymptotically) stable, that is $(A+BF)V=EVH_V$, with $\sigma(H_V)\in\mathcal{C}^-$;
(ii) a (C,A,E)-invariant subspace $\mathcal{V}=Im\,V$ is (C,A,E)-outer detectable if there exists L such $(E,A+LC)|\mathcal{X}/\mathcal{V}$ is (asymptotically) stable, that is $T(A+LC)=H_TTE$, with $\sigma(H_T)\in\mathcal{C}^-$.

Definition 2.2. A v-dimensional subspace $\mathcal{V}$ is an Output Stabilizable (C,A,E,B)-invariant if $\mathcal{V}$ is (A,E,B)-inner stabilizable and (C,A,E)-outer detectable. If, in addition, $\mathcal{V}$ is such that $Ker\,E\cap\mathcal{V}=\{\emptyset\}$, then $\mathcal{V}$ is a strongly Output Stabilizable (C,A,E,B)-invariant subspace.

Thus, a necessary and sufficient condition for $\mathcal{V}=ImV$ to be *strongly Output Stabilizable* (or simply, strongly OS) (C,A,E,B)-invariant subspace is that (6), (7), and (8) hold true for some H_V,H_T,W and U, with the additional stability conditions:

$$\sigma(H_V)\in\mathcal{C}^- \tag{9}$$
$$\sigma(H_T)\in\mathcal{C}^- \tag{10}$$

The following theorem relates the concept of strongly $OS(C,A,E,B)$-invariant subspaces to the existence of an output feedback that solves the *S-stabilization problem:*

Theorem 2.1. There exists an output feedback matrix $K:\mathcal{Y}\longrightarrow\mathcal{U}$ such that the closed-loop system (4) is regular, asymptotically stable and impulse free if and only if there exists a v-dimensional strongly $OS(C,A,E,B)$-invariant subspace $\mathcal{V}=Im\,V$, with $V\in\Re^{n\times v}$ and such that

$$Ker\,CV\subseteq Ker\,W \tag{11}$$
$$Ker\,B'T'\subseteq Ker\,U' \tag{12}$$

where: W, T and V verify (6) to (8).

Proof: We first notice that relations (11) and (12) can be equivalently replaced by the existence of $K:\mathcal{Y}\longrightarrow\mathcal{U}$ such that

$$KCV=W \tag{13}$$
$$TBK=U \tag{14}$$

Necessity: Assuming that the closed-loop system is asymptotically stable and impulse free, and hence regular, the following equations hold true for some scalar $v\geq 0$ (see (Duan 1999)):

$$(A+BKC)\begin{bmatrix}V & \bar{V}\end{bmatrix}=E\begin{bmatrix}V & \bar{V}\end{bmatrix}\begin{bmatrix}H_V & 0\\ 0 & H_T\end{bmatrix} \tag{15}$$
$$\begin{bmatrix}\bar{T}\\ T\end{bmatrix}(A+BKC)=\begin{bmatrix}H_V & 0\\ 0 & H_T\end{bmatrix}\begin{bmatrix}\bar{T}\\ T\end{bmatrix}E \tag{16}$$
$$\begin{bmatrix}\bar{T}\\ T\end{bmatrix}E\begin{bmatrix}V & \bar{V}\end{bmatrix}=\begin{bmatrix}I_v & 0\\ 0 & I_{q-v}\end{bmatrix} \tag{17}$$

where: $H_V\in\Re^{v\times v}$ *and* $H_T\in\Re^{(q-v)\times(q-v)}$ are such that $\sigma(E,A+BKC)=\sigma(H_V)\dot{\cup}\sigma(H_T)\in\mathcal{C}^-$, and $\begin{bmatrix}V & \bar{V}\end{bmatrix}\in\Re^{n\times q}$ and $\begin{bmatrix}\bar{T}\\ T\end{bmatrix}\in\Re^{q\times n}$ are two full rank matrices, accordingly partitioned.

The equations (15), (16) and (17) are related to the finite closed-loop eigenstructure (Fletcher 1988). From the closed-loop regularity it follows that $rank\,(EV)=v$. Thus, by setting $KCV=W$ in (15) and $TBK=U$ in (16), we can deduce that $\mathcal{V}=ImV$ is a strongly $OS(C,A,E,B)$-invariant v-dimensional subspace.
Sufficiency: Assume the existence of a v-dimensional strongly $OS(C,A,E,B)$-invariant subspace $\mathcal{V}=Im\,V$ and that conditions (11) and (12) hold true. Since $rank\,(EV)=v$ and $rank\,(TE)=q-v$, we can define two (full rank matrices) $\bar{T}'\in\Re^{n\times v}$ and $\bar{V}\in\Re^{n\times(q-v)}$ such that, for some $D_l\in\Re^{v\times(q-v)}$ and $D_r\in\Re^{v\times(q-v)}$, they verify (17):

$$\bar{T}=(V'E'EV)^{-1}V'E'+D_lT; \tag{18}$$
$$\bar{V}=E'T'(TEE'T')^{-1}+VD_r \tag{19}$$

Thus, by using the coupled-generalized Sylvester equations (6), (7) and (8), and replacing conditions (11) and (12) respectively by (13) and (14), we get:

$$(A+BKC)\begin{bmatrix}V & \bar{V}\end{bmatrix}=E\begin{bmatrix}V & \bar{V}\end{bmatrix}\begin{bmatrix}H_V & H_{V2}\\ 0 & H_{V3}\end{bmatrix} \tag{20}$$
$$\begin{bmatrix}\bar{T}\\ T\end{bmatrix}(A+BKC)=\begin{bmatrix}H_{T1} & 0\\ H_{T3} & H_T\end{bmatrix}\begin{bmatrix}\bar{T}\\ T\end{bmatrix}E \tag{21}$$

where the bloc-triangular forms of $\begin{bmatrix}H_V & H_{V2}\\ 0 & H_{V3}\end{bmatrix}$ and $\begin{bmatrix}H_{T1} & 0\\ H_{T3} & H_T\end{bmatrix}$ arise from the (A,E,B)-invariance and (C,A,E)-invariance of the $Im\,V$. But, pre-multiplication of (20) by $\begin{bmatrix}\bar{T}\\ T\end{bmatrix}$ and post-multiplication of (21) by $\begin{bmatrix}V & \bar{V}\end{bmatrix}$ show that : $H_{T3}=0$; $H_{V2}=0$; $H_{V3}=H_T$; $H_{T1}=H_V$. Thus, the closed-loop system has q finite closed-loop poles, given by

$$\sigma(E,A+BKC)=\sigma(H_V)\dot{\cup}\sigma(H_T) \tag{22}$$

Hence, the closed-loop system is impulse free and, consequently, regular. The asymptotical stability is also guaranteed since it is assumed that $\sigma(H_V) \cup \sigma(H_T) \in \mathcal{C}^-$. □

The following basic procedure may be used to find a S-stabilizing controller, particularly when $q < m + p$. It can be considered as a generalization of the Syrmos and Lewis algorithm proposed in (Syrmos and Lewis 1993) for normal systems. Eigenstructure assignment techniques may be used to solve the coupled-generalized Sylvester equations when $q < m + p$:

1) Find a matrix $T \in \Re^{(q-p)\times n}$ verifying (6), with $\sigma(H_T) \in \mathcal{C}^-$ and such that

$$rank\left(\begin{bmatrix} TE \\ C \end{bmatrix}\right) = q \tag{23}$$

2) Solve equation (7) under constraint (8), taking into account that $rank\,(EV) = p$ (or $Ker\,TE = Ker\,E \oplus Im\,V$, where $\oplus$ represents the direct sum) and $\sigma(H_V) \in \mathcal{C}^-$;

3) By construction, V verifies $rank\,(CV) = p$ and K can be computed by

$$K = W(CV)^{-1} \tag{24}$$

Notice that relation (23) is equivalent to $Ker\,C \cap Ker\,TE = \{\emptyset\}$ and also guarantees that $rank\,(TE) = q - p$ (or equivalently $Ker\,T \cap Im\,E = \{\emptyset\}$).

3. A QUADRATIC STABILIZABILITY CHARACTERIZATION

A quadratic characterization of $OS(C, A, E, B)$-invariant subspaces can be obtained from Definition 2.2 by replacing the (A, E, B)-inner stabilizability condition (9) and the (C, A, E)-outer detectability condition (10) by the two equivalent quadratic Lyapunov stability conditions (Chen 1984):

$$\sigma(H_V) \in \mathcal{C}^- \Longleftrightarrow \exists\, \Pi = \Pi' > 0 \text{ such that}$$
$$\Pi H_V' + H_V \Pi = -Q_V, \forall\, Q_V = Q_V' > 0 \tag{25}$$
$$\sigma(H_T) \in \mathcal{C}^- \Longleftrightarrow \exists\, \Gamma = \Gamma' > 0 \text{ such that}$$
$$H_T'\Gamma + \Gamma H_T = -Q_T, \forall\, Q_T = Q_T' > 0 \tag{26}$$

Lemma 3.1. Let $V \in \Re^{n\times p}$ be a basis of a p-dimensional subspace $\mathcal{V} \subset \mathcal{X}$ such that $Ker\,E \cap \mathcal{V} = \{\emptyset\}$. Let $T \in \Re^{(q-p)\times n}$ be a generalized left annihilator of EV. Then, $\mathcal{V}$ is a strongly $OS(C, A, E, B)$-invariant subspace if and only if:

(i) $\forall\, Q_V = Q_V' > 0$, $Q_V \in \Re^{p\times p}$, there exist $P = P' \geq 0$, $P \in \Re^{n\times n}$ and $Y \in \Re^{m\times n}$ such that

$$APE' + EPA' + BYE' + EY'B' = -EVQ_VV'E' \tag{27}$$

$$V'PV > 0 \;;\; TEPE'T' = 0 \tag{28}$$
$$Y = W_\Pi V' \text{ for some } W_\Pi \in \Re^{m\times p} \tag{29}$$

(ii) $\forall\, Q_T = Q_T' > 0$, $Q_T \in \Re^{(q-p)\times(q-p)}$, there exist $S = S' \geq 0$, $S \in \Re^{n\times n}$ and $Z \in \Re^{n\times p}$ such that

$$A'SE + E'SA + C'Z'E + E'ZC = -E'T'Q_TTE \tag{30}$$
$$TST' > 0 \;;\; V'E'SEV = 0 \tag{31}$$
$$Z = T'U_\Gamma \text{ for some } U_\Gamma \in \Re^{(q-p)\times p} \tag{32}$$

Proof:

Necessity: Consider that $\mathcal{V} \subset \mathcal{X}$ is a strongly $OS(C, A, E, B)$-invariant subspace and, hence, that the coupled generalized Sylvester equations (6), (7) and (8) are verified.

Let us first show the necessity of part *(i)*. For any $Q_V = Q_V' > 0$, the quadratic stability condition given by (25) holds true, and we get :

$$EV\left(\Pi H_V' + H_V\Pi\right)V'E' = EV\Pi H_V'V'E' + EVH_V\Pi V'E' = -EVQ_VV'E' \tag{33}$$

From (6) we also have $AV + BW = EVH_V$, which can be used in (33) to obtain

$$EV\Pi V'A' + EV\Pi W'B' + AV\Pi V'E' + BW\Pi V'E' = -EVQ_VV'E' \tag{34}$$

Thus, by setting $P = P' = V\Pi V'$ and $Y = W\Pi V'$, and by considering that $rank(V) = p$ and the fact that $\Pi > 0 \Longrightarrow \begin{cases} V'V\Pi V'V > 0 \\ TEV\Pi V'E'T' = 0 \end{cases}$, (34) can be equivalently replaced by (27), (28) and (29).

Using similar arguments, we can show the necessity of part *(ii)*. Thus, from (7) and (26), for any $Q_T = Q_T' > 0$ we obtain:

$$E'T'(H_T'\Gamma + \Gamma H_T)TE = (A'T'\Gamma + C'U'\Gamma)TE + E'T'(\Gamma TA + \Gamma UC) = -E'T'Q_TTE \tag{35}$$

By setting $S = T'\Gamma T$ and $Z = T'\Gamma U$, (35) can replaced by (30) and (32). Furthermore, since $rank(T) = q - p$ and $\Gamma > 0$, we have $\begin{cases} TT'TTT' > 0 \\ V'E'T'\Gamma TEV = 0. \end{cases}$

Sufficiency: Consider that parts *(i)* and *(ii)* are verified. By definition, V and T have, respectively, full column and row ranks. Thus, from (28) and (31), we get:

$$V'PV = \bar{P} = \bar{P}' > 0 \Longrightarrow P = V(V'V)^{-1}\bar{P}(V'V)^{-1}V' \tag{36}$$
$$TST' = \bar{S} = \bar{S}' > 0 \Longrightarrow S = T'(TT')^{-1}\bar{S}(TT')^{-1}T \tag{37}$$

We shall now show that the verification of part (i) implies that $\mathcal{V} = Im\,V$ is an (A, E, B)-inner stabilizable invariant subspace. Thus, similar arguments can be used to demonstrate that $\mathcal{V}$, is also a (C, A, E)-outer detectable subspace.

From (36) and (37) we have:

$$P = \begin{bmatrix} V & T' \end{bmatrix} \begin{bmatrix} \Pi & 0 \\ 0 & 0 \end{bmatrix} \begin{bmatrix} V' \\ T \end{bmatrix} \geq 0$$

$$\text{for } \Pi = \Pi' = (V'V)^{-1}\bar{P}(V'V)^{-1} > 0 \qquad (38)$$

Consider also a matrix F such that $F = W_\Pi V'V\bar{P}^{-1}V'$. By construction, such a matrix F verifies $FP = W_\Pi V' = Y$. Thus, from (27) we get

$$EP(A+BF)' + (A+BF)PE' = -EVQ_V V'E' \quad (39)$$

Let us now take into account (38), relation

$$(A+BF)\begin{bmatrix} V & T' \end{bmatrix} = E\begin{bmatrix} V & T' \end{bmatrix}\begin{bmatrix} \bar{A}_{11} & \bar{A}_{12} \\ \bar{A}_{21} & \bar{A}_{22} \end{bmatrix} \quad (40)$$

and the fact that

$$EVQ_V V'E' = E\begin{bmatrix} V & T' \end{bmatrix}\begin{bmatrix} Q_V & 0 \\ 0 & 0 \end{bmatrix}\begin{bmatrix} V' \\ T \end{bmatrix}E' \geq 0 \quad (41)$$

From the quadratic equation (39), we obtain:

$$E\begin{bmatrix} V & T' \end{bmatrix}\begin{bmatrix} \Pi\bar{A}'_{11} + \bar{A}_{11}\Pi & \Pi\bar{A}'_{21} \\ \bar{A}_{21}\Pi & 0 \end{bmatrix}\begin{bmatrix} V' \\ T \end{bmatrix}E' = -E\begin{bmatrix} V & T' \end{bmatrix}\begin{bmatrix} Q_V & 0 \\ 0 & 0 \end{bmatrix}\begin{bmatrix} V' \\ T \end{bmatrix}E' \leq 0 \quad (42)$$

Since $E\begin{bmatrix} V & T' \end{bmatrix}$ is a full column rank matrix, (42) implies that:

- $\mathcal{V} = Im\,V$ is $(E, A+BF)$-invariant, since $\bar{A}_{21}\Pi = 0$ if and only if $\bar{A}_{21} = 0$; and
- $\mathcal{V}$ is inner-stabilizable, since $\Pi\bar{A}'_{11} + \bar{A}_{11}\Pi = -Q_V < 0$ implies the stability of $(E, A+BF)|\mathcal{V}$. □

From the proof given above, we can restate the coupling condition between parts (i) and (ii) of Lemma 3.1 as follows.

Corollary 3.1. If $\mathcal{V} \subset \mathcal{X}$ is a strongly $OS(C, A, E, B)$-invariant subspace, then any pair of matrices (P, S) solution to parts (i) and (ii) of Lemma 3.1 verifies : $SEP = 0$.

The quadratic stabilizability conditions of Lemma 3.1 can now be used to reformulate the necessary and sufficient condition, given in Theorem 2.1, for the existence of a stabilizing static output feedback.

Theorem 3.1. There exists an output feedback $K : \mathcal{Y} \longrightarrow \mathcal{U}$ such that the closed-loop system (4) is regular, asymptotically stable and impulse free if and only if there exist matrices $P = P' \geq 0$, Y, $S = S' \geq 0$ and Z such that the coupled quadratic stabilization conditions of Lemma 3.1 hold true for some matrices V and T verifying $TEV = 0$, and such that:

$$KCP = Y \ , \ SBK = Z$$

As in (Castelan *et al.* 2000), the previous theoretical results allow to associate a quadratic Lyapunov function $V(x)$ that is strictly decreasing along the trajectories of the closed-loop system (4). Thus, for: $V(x) = x'E'\mathcal{S}Ex$ where

$$\mathcal{S} = \begin{bmatrix} \bar{T}' & T' \end{bmatrix}\begin{bmatrix} \Pi^{-1} & 0 \\ 0 & \Gamma \end{bmatrix}\begin{bmatrix} \bar{T} \\ T \end{bmatrix} = \begin{bmatrix} V & \bar{V} \end{bmatrix}\begin{bmatrix} \bar{P}^{-1} & 0 \\ 0 & \bar{S} \end{bmatrix}\begin{bmatrix} V' \\ \bar{V}' \end{bmatrix} \geq$$

we get, for $x \neq 0$ and $x \notin Ker\,E$:

$$\dot{V}(x) = x'\left((A+BKC)'\mathcal{S}E + E'\mathcal{S}(A+BKC)\right)x < 0\,.$$

Theorem 3.1 gives a necessary and sufficient condition for the existence of a stabilizing output feedback. Unfortunately, this result involves equations that are nonlinear in the considered unknowns. However the quadratic characterization of Lemma 3.1 may be used to adequately construct strongly $OS(C, A, E, B)$-invariant subspaces that lead to S-stabilizing output feedback matrices K. As for normal systems case (Castelan *et al.* 2000), (Syrmos and Lewis 1993) this can be done, for instance, by taking into account the coupling requirement and solving subsequently part (ii) and part (i) of Lemma 3.1, as outlined in section 2.

4. NUMERICAL EXAMPLE

The example in this section is devoted both to verify numerically the previous results and to show, how the quadratic characterization may also be used to find a S-stabilizing controller.

Consider the following data (Chu *et al.* 1997):

$$E = \begin{bmatrix} 0 & 0 & -0.82 & 0 & 0 \\ 0 & 0 & 0 & 0 & 0 \\ 0 & 0 & 0 & 0 & 0 \\ 1.72 & 0 & 0 & 0 & 0 \\ 0 & 0 & 0 & 0 & 1 \end{bmatrix} \ ; \ B = \begin{bmatrix} 0.41 & -2.34 \\ 0 & 0.45 \\ 0 & 0 \\ 1.72 & 0 \\ 7 & -1 \end{bmatrix}$$

$$A = \begin{bmatrix} 0 & 0 & 1.23 & 0 & 0 \\ 1.1 & 0 & 0 & 0 & 0 \\ 0 & 1.56 & 0 & 0 & 1.01 \\ 0 & 0 & 1.98 & 0 & 0 \\ 0 & 0 & 0 & 0 & 0 \end{bmatrix} \ ; \ C = \begin{bmatrix} -1 & 0 & 0 & -1 & 0 \\ 0 & 0 & 0 & 1 & 1 \end{bmatrix}$$

The corresponding descriptor system is non-regular and its finite poles are given by: $\sigma(E, A) = \{0, 0, -1.5\}$. The system (C, E, A, B)

is both strongly controllable and strongly observable and $m+p=4>q$.

In a *first step*, eigenstructure assignment is used to compute a matrix T that imposes $\lambda=-1$ as a closed-loop finite pole and such that (23) is also verified. Using the classical relation

$$\begin{bmatrix} t' & u' \end{bmatrix} \begin{bmatrix} \lambda E - A \\ -C \end{bmatrix} = 0,$$

we choose: $T = t' = \begin{bmatrix} -0.314 & -0.355 & -0.723 & 0.037 & 0 \end{bmatrix}$ We also notice that, from $H_T=-1$, $Q_T=2$ and $\Gamma=1$, the part (i) of Lemma 3.1 is verified for

$$S = T'\Gamma T = \begin{bmatrix} 0.099 & 0.112 & 0.227 & -0.011 & 0 \\ 0.112 & 0.126 & 0.256 & -0.013 & 0 \\ 0.227 & 0.256 & 0.522 & -0.027 & 0 \\ -0.011 & -0.013 & -0.027 & 0.001 & 0 \\ 0 & 0 & 0 & 0 & 0 \end{bmatrix};$$

$$\bar{S} = TST' = 0.560 \;\; ; \;\; U_\Gamma = \begin{bmatrix} 0.355 & 0.355 \end{bmatrix}$$

$Z = T'U_\Gamma = \begin{bmatrix} -0.112 & -0.126 & -0.256 & 0.013 & 0 \\ -0.112 & -0.126 & -0.256 & 0.013 & 0 \end{bmatrix}'$. From T defined above, we set V as an orthogonal matrix such that $TEV=0$ and $Ker\,TE = Ker\,E \oplus Im\,V$:

$$V = \begin{bmatrix} -0.836 & -0.252 & 0.487 & 0 & 0 \\ -0.410 & 0.877 & -0.252 & 0 & 0 \end{bmatrix}'$$

In a *second step*, standard convex programming techniques are applied to find a feasible solution for the equations of part (ii) of Lemma 3.1, without additional requirements that could improve the numerical solution or closed-loop performance:

$$P = \begin{bmatrix} 388.013 & -327.648 & -7.887 & 231.034 & -22.811 \\ -327.648 & 2821.159 & -1242.212 & -1989.279 & -304.718 \\ -7.887 & -1242.212 & 613.126 & 875.919 & 159.478 \\ 231.034 & -1989.279 & 875.919 & 19286.532 & 299.026 \\ -22.811 & -304.718 & 159.478 & 299.026 & 12950.852 \end{bmatrix}$$

$$\bar{P} = \begin{bmatrix} 768.735 & -967.271 \\ -967.271 & 3053.564 \end{bmatrix} \;\; ; \;\; W_\Pi = \begin{bmatrix} -397.589 & -1392.012 \\ -600.959 & -1086.416 \end{bmatrix}$$

$$Y = \begin{bmatrix} 903.839 & -1119.951 & 156.716 & 0 & 0 \\ 948.477 & 800.918 & -19.276 & 0 & 0 \end{bmatrix}.$$

Finally, the corresponding S-stabilizing output feedback, is $K = \begin{bmatrix} 2.211 & -0.140 \\ 2.444 & 0 \end{bmatrix}$. The closed-loop finite poles are given by: $\{ -1.846 \pm 2.187i \, , -1 \}$.

5. CONCLUDING REMARKS

We have considered the problem of existence and computation of a static output feedback that strongly stabilizes a descriptor system. It was shown that the known *coupled-Sylvester equation* approach, used mainly in eigenstructure assignment techniques, has a counterpart in the quadratic stabilizability framework. Thus, coupled Lyapunov like equations can also be used for the construction of a strongly output stabilizable (C,E,A,B)-invariant subspace as an intermediate mechanism in the process of designing output feedback controllers.

The quadratic characterization by Lyapunov equations provides a convenient framework for the numerical resolution of the problem (through LMIs and LMEs, for instance) and possibly for the integration of additional requirements. A study is now being carried out to solve the first step of the algorithm through the use of a *reduced-order Lyapunov equation*. Among some open questions for future studies one may consider the possible extension of the outlined technique to treat less restrictive cases than the $m+p>q$ case.

6. REFERENCES

Castelan, E. B., J. C. Hennet and E. R. Llanos V. (2000). Quadratic characterization and use of output stabilizable subspaces. In: *8th Mediterranean Conference on Control and Automation*.

Chen, C.T. (1984). *Linear system theory and design*. Holt, Rinehart and Winston. New York.

Chu, D. L., H. C. Chan and D. W. C. Ho (1997). A general framework for state feedback pole assignment of singular systems. *Int. J. Control* **67**(2), pp. 135–152.

Crusius, C. A. R. and A. Trofino (1999). Sufficient lmi conditions for output feedback. *IEEE Trans. Automatic Control* **44**(5), pp. 1053–1057.

Dai, L. (1989). *Singular Control System*. Springer-Verlag. New York.

Duan, G. R. (1999). Eigenstruture assignment in descriptor systems via output feedback : a new complete parametric approach. *Int. J. Control* **72**(4), pp. 345–364.

Fletcher, L.R. (1988). Eigenstructure assignment by output feedback in descriptor systems. *IEEE Proceedings* **135**(4), pp. 302–308.

Geromel, J. C., C.C. de Souza and R.E. Skelton (1998). Static output feedback controllers: Stability and convexity. *IEEE Trans. Automatic Control* **43**(1), pp. 120–125.

El Ghaoui, L., F. Oustry and M. AitRami (1997). A cone complementarity linearization algorithm for static output-feedback and related problems. *IEEE Trans. Automatic Control* **42**(8), pp. 1171–1176.

Lewis, F. L. (1986). A survey of linear singular systems. *Circuits Syst. Signal Process* **5**(1), pp. 3–36.

Lewis, F. L. and K. Ozcaldiran (1989). Geometric structure and feedback in singular systems. *IEEE Trans. Automatic Control* **AC-34**, pp. 450–455.

Lewis, F. L. and K. Ozcaldiran (1990). On the regularizability of singular systems. *IEEE Trans. Automatic Control* **35**(10), pp. 1156–1160.

Syrmos, V.L. and F.L. Lewis (1993). Output feedback eigenstructure assignment using two sylvester equations. *IEEE Trans. Automatic Control* **38**(3), pp. 495–499.

Syrmos, V.L., C.T. Abdallah and K. Grigoriadis (1997). Static output feedback - a survey. *Automatica* **33**(3), pp. 125–137.

Wonham, W.M. (1979). *Linear Multivariable Control, a Geometric Approach*. Springer Verlag. New York, Heidelberg, Berlin.

Proceedings of the 8th IEEE Mediterranean Conference
on Control and Automation (MED 2000)
Rio, Patras, GREECE 17-19 July, 2000

QUADRATIC CHARACTERIZATION AND USE OF OUTPUT STABILIZABLE SUBSPACES

EUGENIO B. CASTELAN[1] , JEAN-CLAUDE HENNET[2] and ELMER R. LLANOS VILLAREAL[1]

[1] LCMI/DAS/UFSC, 88040-900 - Florianópolis (S.C) - Brazil Fax +55 (48) 331 99 34, eugenio@lcmi.ufsc.br, llanos@lcmi.ufsc.br
[2] LAAS-CNRS, 31077 - Toulouse Cedex 4 - France Fax +33 5 61 33 69 36, hennet@laas.fr

Abstract. The study is based on the characterization of Output Stabilizable (C,A,B)-invariant subspaces through two coupled quadratic stabilization conditions. The paper shows the equivalence between the existence of a solution to this set of conditions and the possibility to stabilize the system by output feedback. An algorithm and a numerical example are provided to illustrate the approach.

Key Words. Output feedback, geometric approach, quadratic stabilizability, LMIs.

1 INTRODUCTION

The stabilization of linear systems by output feedback is recognized as an important and still open problem in control theory. A review of existing approaches and techniques to treat different versions of this problem can be found in [10]. Other recent results not covered by this survey paper are found, for instance, in [1], [7], [4] and [6].

A commom feature shared by different methods (Lyapunov, Riccati, LMI or Eigenstructure Assignment) is that the output feedback stabilization problem is equivalent to obtaining the solution of a coupled set of matrix equations. In particular, through the use of coupled Sylvester equations [8] [9], the output feedback control problem can be decomposed into two stages :

- determination of a (C,A)-outer detectable subspace
- inner stabilization of this subspace.

This paper shows that this geometric approach based on the solution of coupled Sylvester equations has a quadratic counterpart, so that coupled Lyapunov like equations can also be used for construction of an output stabilizable (C, A, B)-invariant subspace as an intermediate mechanism in the process of designing a static output feedback controller. In particular, we show that solutions for the first stage can be obtained as solutions of a reduced-order Lyapunov equation.

Furthermore, the quadratic characterization of both stages by Lyapunov equations provides a convenient framework for the numerical resolution of the problem (through LMIs for instance) and for the integration of additional performance requirements, such as regional pole placement, robustness to structured parametric uncertainties and disturbance attenuation.

The second section of the paper introduces the key notion of *Output Stabilizable* (C, A, B)-invariant subspace and the basic equivalence between existence of such a subspace and static output stabilizability of the system. The third and fourth sections provide a generic formulation of the output stabilization problem in the form of coupled Lyapunov equations. An orthogonal decomposition technique and an algorithm to solve the problem are also proposed in section 4. This approach is illustrated in section 5 through a numerical example and some concluding remarks are finally presented.

2 PRELIMINARIES

Linear time-invariant systems are considered :

$$\dot{x}(t) = Ax(t) + Bu(t) \quad (1)$$

$$y(t) = Cx(t) \quad (2)$$

where : $x \in \mathcal{X} \subset \Re^n$, $u \in \mathcal{U} \subset \Re^m$, $y \in \mathcal{Y} \subset \Re^p$. B is assumed full column-rank, C full row-rank and (C, A, B) stabilizable and detectable. The studied problem is to find a static output feedback control law

$$u(t) = Ky(t) \quad (3)$$

such that $\sigma(A+BKC) \in \mathcal{C}^-$, or equivalently, the closed-loop system is asymptotically stable.

As in [9], the mathematical analysis is based on some known concepts and definitions from the geometric control theory [11]. It is first recalled that a subspace $\mathcal{V} \subset \mathcal{X}$ is (A, B)-invariant if there exists $F : \mathcal{X} \longrightarrow \mathcal{Y}$ such that $(A + BF)\mathcal{V} \subset \mathcal{V}$, or equivalently , $A\mathcal{V} \subset \mathcal{V} + Im\, B$. In a dual way, a subspace $\mathcal{T} \subset \mathcal{X}$ is (C, A)-invariant if there exists $L : \mathcal{Y} \longrightarrow \mathcal{X}$ such that $(A + LC)\mathcal{T} \subset \mathcal{T}$, or equivalently, $\mathcal{T} \supset A(\mathcal{T} \cap Ker\, C)$.

Definition 2.1 *[9] : A v-dimensional subspace $\mathcal{V} \subset \mathcal{X}$ is (C, A, B)-invariant if $\mathcal{V}$ is both (A, B)-invariant and (C, A)-invariant.*

Let $V \in \Re^{v \times v}$ be such that $span(V) = \mathcal{V}$ and $T \in \Re^{(n-v)\times v}$ be a left annihilator of V, *i.e* : $Ker\, T = Im\, V$. Thus, definition 2.1 is equivalent to the existence of matrices ($H_V \in \Re^{v\times v}$, $W \in \Re^{m\times v}$) and ($H_T \in \Re^{(n-v)\times(n-v)}$, $U \in \Re^{(n-v)\times p}$) solutions to the following *coupled-Sylvester equations*:

$$AV - VH_V = -BW \quad (4)$$
$$TA - H_T T = -UC \quad (5)$$
$$TV = 0 \quad (6)$$

Definition 2.1 and equations (4),(5) and (6) play a fundamental role in treating the problem of control by static output feedback, mainly by eigenstructure assignment [8] [9]. This study rather focuses on the properties of stabilizability and detectability. It is recalled that :
(i) a (A, B)-invariant subspace $\mathcal{V}$ is (A, B)-inner stabilizable if there exists F such that $(A+BF)|\mathcal{V}$ is (asymptotically) stable; and
(ii) a (C, A)-invariant subspace $\mathcal{V}$ is (C, A)-outer detectable if there exists L such $(A+LC)|\mathcal{X}/\mathcal{V}$ is (asymptotically) stable.

Definition 2.2 *[9] : A v-dimensional subspace $\mathcal{V}$ is an Output Stabilizable (C, A, B)-invariant subspace if $\mathcal{V}$ is (A, B)-inner stabilizable and (C, A)-outer detectable.*

Thus, a necessary and sufficient condition for $\mathcal{V} = Im(V)$ to be an *Output Stabilizable* (or simply, OS)(C, A, B)-invariant subspace is that (4), (5), and (6) hold true for some H_V, H_T, W and U, with the additional stability conditions :

$$\sigma(H_V) \in \mathcal{C}^- \quad (7)$$
$$\sigma(H_T) \in \mathcal{C}^- \quad (8)$$

The following theorem relates the concept of $OS(C, A, B)$-invariant subspaces to the existence of a stabilizing output feedback control law (3).

Theorem 2.1 *: There exists a static output feeback matrix $K : \mathcal{Y} \longrightarrow \mathcal{U}$ such that $\sigma(A + BKC) \in \mathcal{C}^-$ if and only if there exists a matrix $V \in \Re^{n\times v}$ spanning a v-dimensional subspace $\mathcal{V} = Im\, V$ that is $OS(C, A, B)$-invariant and such that*

$$Ker\, CV \subseteq Ker\, W \quad (9)$$
$$Ker\, B'T' \subseteq Ker\, U' \quad (10)$$

It is important to note that the above result has been presented and exploited under different forms in the literature related to the eigenstructure assignment by output feedback. The above statement is essentially equivalent to the one of theorem 3.2 stated in [9]. In the sequel, we shall assume that v, the dimension of $\mathcal{V}$, is p. This assumption has been also adopted in many works that, explicitly or implicitly, use the coupled-Sylvester equations for eigenstructure assignment by output feedback [1] [8] [5]. Furthermore, (9) and (10) can then be equivalently replaced by

$$KCV = W \quad (11)$$
$$TBK = U \quad (12)$$

In particular, if $CV \in \Re^{p\times p}$ is full rank, $Ker\, CV = \{0\}$ is always included in $Ker\, W$ and K verifies:

$$K = W(CV)^{-1} \quad (13)$$

It is also easy to verify that $Ker\, CV = \{0\}$ if and only if $Ker\, T \cap Ker\, C = \{0\}$, or, equivalently, that $rank(CV) = p$ if and only if $rank\left(\begin{bmatrix} T \\ C \end{bmatrix}\right) = n$. For algorithmic purposes, this condition on T may be considered, for instance, in the solution of the second Sylvester equation and shall lead, subsequently, to the solutions of (4) such that (13) holds true [8].

3 A QUADRATIC STABILIZABILITY CHARACTERIZATION

A quadratic characterization of $OS(C, A, B)$-invariant subspaces can be obtained from definition 2.2 by replacing the (A, B)-inner stabilizability condition (7) and the (C, A)-outer detectability condition (8) by the two equivalent quadratic Lyapunov stability conditions [3] :

$$\sigma(H_V) \in \mathcal{C}^- \Longleftrightarrow \exists\, \Pi = \Pi' > 0 \text{ such that}$$
$$\Pi H_V' + H_V \Pi = -Q_V, \forall\, Q_V = Q_V' > 0 \quad (14)$$
$$\sigma(H_T) \in \mathcal{C}^- \Longleftrightarrow \exists\, \Gamma = \Gamma' > 0 \text{ such that}$$
$$H_T'\Gamma + \Gamma H_T = -Q_T, \forall\, Q_T = Q_T' > 0 \quad (15)$$

Theorem 3.2 *: Let $V \in \Re^{n\times p}$ be a basis of a p-dimensional subspace $\mathcal{V} \subset \mathcal{X}$ and $T \in \Re^{(n-p)\times n}$ be such that $TV = 0$. Then, $\mathcal{V}$ is an $OS(C, A, B)$-invariant subspace if and only if :*

(i) $\forall\ Q_V = Q_V' > 0$, $Q_V \in \Re^{p\times p}$, *there exist* $P = P' \geq 0$, $P \in \Re^{n\times n}$ *and* $Y \in \Re^{m\times n}$ *such that*

$$AP + PA' + BY + Y'B' = -VQ_VV' \quad (16)$$
$$V'PV > 0 \quad ; \quad TPT' = 0 \quad (17)$$
$$Y = W_\Pi V' \text{ for some } W_\Pi \in \Re^{m\times p} \quad (18)$$

(ii) $\forall\ Q_T = Q_T' > 0$, $Q_T \in \Re^{n-p\times n-p}$, *there exist* $S = S' \geq 0$, $S \in \Re^{n\times n}$ *and* $Z \in \Re^{n\times p}$ *such that*

$$A'S + SA + C'Z' + ZC = -T'Q_TT \quad (19)$$
$$TST' > 0 \quad ; \quad V'SV = 0 \quad (20)$$
$$Z = T'U_\Gamma \text{ for some } U_\Gamma \in \Re^{n-p\times p} \quad (21)$$

Proof (outline):
Necessity: Consider that $\mathcal{V} \subset \mathcal{X}$ is an $OS(C,A,B)$-invariant subspace and, hence, that the coupled Sylvester equations (4), (5) and (6) are verified.

Let us first show the necessity of part (i). For any $Q_V = Q_V' > 0$, the quadratic stability condition given by (14) holds true, and we obtain :

$$V(\Pi H_V' + H_V\Pi)V' = V\Pi H_V'V' + VH_V\Pi V' = -VQ_VV' \leq 0 \quad (22)$$

From (4) we also have $AV + BW = VH_V$, which can be used in (22) to obtain

$$V\Pi V'A' + V\Pi W'B' + AV\Pi V' + BW\Pi V' = \quad (23)$$
$$-VQ_VV' \quad (24)$$

Thus, by setting $P = P' = V\Pi V'$ and $Y = W\Pi V'$, and by considering that $rank(V) = p$ and that $\Pi > 0 \Longrightarrow \begin{cases} V'V\Pi V'V > 0 \\ T'V\Pi V'T = 0 \end{cases}$, (24) can be equivalently replaced by (16), (17) and (18).

Using similar arguments, we can show the necessity of part (ii). Thus, from (5) and (15), for any $Q_T = Q_T' > 0$ we obtain :

$$T'(H_T'\Gamma + \Gamma H_T)T = A'T'\Gamma T + C'U'\Gamma T \quad (25)$$
$$+T'\Gamma TA + T'\Gamma UC = -T'Q_TT \quad (26)$$

By setting $S = T'\Gamma T$ and $Z = T'\Gamma U$, (26) can replaced by (19) and (21). Furthermore, since $rank(T) = n - p$ and $\Gamma > 0$, we also have $\begin{cases} TT'\Gamma TT' > 0 \\ V'T'\Gamma TV = 0 \end{cases}$.

Sufficiency: By using arguments from the geometric theory, it can be shown that the verification of condition (i) implies that $\mathcal{V} = Im\,V$ is a (A,B)-inner stabilizable invariant subspace. Similar arguments can be used to show that $\mathcal{V} = Ker\,T$, which is implied by the coupling condition, is also a (C,A)-outer detectable subspace.
□

The coupling condition between parts (i) and (ii) of theorem 3.2 can be restated as follows:

Corollary 3.1 *If* $\mathcal{V} \subset \mathcal{X}$ *is an* $OS(C,A,B)$*-invariant subspace, then any pair of matrices* (P,S) *solutions to parts* (i) *and* (ii) *of theorem 3.2 verifies* $Ker\ S = Im\ \mathcal{V} = Im\ P$, *or, equivalently:*

$$SP = 0 \quad (27)$$

4 OUTPUT FEEDBACK STABILIZATION

The quadratic conditions of theorem 3.2, which could be applied to verify whether an arbitrary subspace $\mathcal{V} \subset \mathcal{X}$ is an $OS(C,A,B)$-invariant subspace or not, will now be used to reformulate the necessary and sufficient condition, given in theorem 2.1, for the existence of a stabilizing static output feedback.

Theorem 4.3 : *There exists an output feedback* $K : \mathcal{Y} \longrightarrow \mathcal{U}$ *such that* $\sigma(A + BKC) \in \mathcal{C}^-$ *if and only if there exist positive semi-definite matrices* $P = P' \geq 0$, Y, $S = S' \geq 0$ *and* Z *such that the coupled quadratic stabilization conditions of theorem 3.2 hold true for some matrices* V *and* T *verifying* $TV = 0$, *and such that :*

$$Ker\,CP \subseteq Ker\,Y \quad (28)$$
$$Ker\,B'S \subseteq Ker\,Z' \quad (29)$$

Proof: It remains to show that (28) and (29) are, respectively, equivalent to conditions (9) and (10) of theorem 2.1. Thus, from theorem 3.2, (28) can be equivalently replaced by

$$\exists\ K \text{ such that } KCV\Pi V' = W\Pi V' \quad (30)$$

where $\Pi = \Pi' > 0$ and V' has full row rank. Hence, relation (30) (or, equivalently, (28)), is verified if and only (9) holds. Similar arguments show the equivalence between (29) and (10) . □

The previous theoretical results allow to readily associate a quadratic Lyapunov function to the closed-loop system.

Corollary 4.2 *Consider that* P, S, V *and* T *have been found such that theorem 4.3 holds true and let* K *be the corresponding stabilizing output feedback matrix. Define matrices* $\bar{T} \in \Re^{p\times n}$ *and* $\bar{V} \in \Re^{n\times(n-p)}$ *as:*

$$\bar{T} = \overbrace{(V'V)^{-1}V'}^{V^\dagger} + D_lT \quad ; \quad \bar{V} = \overbrace{T'(TT')^{-1}}^{T^\dagger} + VD_l \quad (31)$$

where $D_l \in \Re^{p\times(n-p)}$ *is such that:*

$$D_lH_T - H_VD_l = -V^\dagger(A + BKC)T^\dagger \quad (32)$$

Then, $v(x) = x'\mathcal{S}x$, *where* (33)

$$\mathcal{S} = \begin{bmatrix} \bar{T}' & T' \end{bmatrix}\begin{bmatrix} \Pi^{-1} & 0 \\ 0 & \Gamma \end{bmatrix}\begin{bmatrix} \bar{T} \\ T \end{bmatrix} = \begin{bmatrix} V & \bar{V} \end{bmatrix}\begin{bmatrix} \bar{P}^{-1} & 0 \\ 0 & \bar{S} \end{bmatrix}\begin{bmatrix} V' \\ \bar{V}' \end{bmatrix}$$

is strictly decreasing along the trajectories of the closed-loop system $\dot{x}(t) = (A + BKC)x(t)$.

Proof: From the definition of matrices $\bar{T}$ and $\bar{V}$, it can be verified that

$$\begin{bmatrix} \bar{T} \\ T \end{bmatrix} \begin{bmatrix} V & \bar{V} \end{bmatrix} = \begin{bmatrix} I_p & 0 \\ 0 & I_{n-p} \end{bmatrix}. \quad (34)$$

Furthermore, by considering the equivalence between theorems 4.3 and 2.1, we also get

$$\begin{bmatrix} \bar{T} \\ T \end{bmatrix} (A+BKC) \begin{bmatrix} V & \bar{V} \end{bmatrix} = \begin{bmatrix} H_V & H_{12} \\ 0 & H_T \end{bmatrix} \quad (35)$$

where, from (32), $H_{12} = D_l H_T - H_V D_l + V^\dagger (A + BKC) T^\dagger = 0$. Thus, relation (35) can be rewritten:

$$\begin{bmatrix} \bar{T} \\ T \end{bmatrix} (A+BKC) = \begin{bmatrix} H_V & 0 \\ 0 & H_T \end{bmatrix} \begin{bmatrix} \bar{T} \\ T \end{bmatrix} \quad (36)$$

From (14) and (15), we also have:
$\begin{bmatrix} H_V' & 0 \\ 0 & H_T' \end{bmatrix} \begin{bmatrix} \Pi^{-1} & 0 \\ 0 & \Gamma \end{bmatrix} + \begin{bmatrix} \Pi^{-1} & 0 \\ 0 & \Gamma \end{bmatrix} \begin{bmatrix} H_V & 0 \\ 0 & H_T \end{bmatrix} =$

$\begin{bmatrix} -Q_{\bar{V}} & 0 \\ 0 & -Q_T \end{bmatrix}$ where: $Q_{\bar{V}} = Q_{\bar{V}}' = \Pi^{-1} Q_V \Pi^{-1} > 0$. (37)

Thus, by taking into account (36), left and right multiplications of (37) by respectively $\begin{bmatrix} \bar{T}' & T' \end{bmatrix}$ and $\begin{bmatrix} \bar{T} \\ T \end{bmatrix}$, give: $(A+BKC)' \begin{bmatrix} \bar{T}' & T \end{bmatrix} \begin{bmatrix} \Pi^{-1} & 0 \\ 0 & \Gamma \end{bmatrix} \begin{bmatrix} \bar{T} \\ T \end{bmatrix} +$

$\begin{bmatrix} \bar{T}' & T \end{bmatrix} \begin{bmatrix} \Pi^{-1} & 0 \\ 0 & \Gamma \end{bmatrix} \begin{bmatrix} \bar{T} \\ T \end{bmatrix} (A+BKC) < 0$. Hence, $\dot{v}(x) = x'((A+BKC)'\mathcal{S} + \mathcal{S}(A+BKC))x < 0 \ \forall \ x \neq 0$. Furthermore, $\mathcal{S}$ can also be written as:

$$\begin{aligned} \mathcal{S} &= \begin{bmatrix} V & T' \end{bmatrix} \begin{bmatrix} \bar{P}^{-1} & 0 \\ 0 & \Gamma \end{bmatrix} \begin{bmatrix} V' \\ T \end{bmatrix} \\ &= \begin{bmatrix} V & \bar{V} \end{bmatrix} \begin{bmatrix} \bar{P}^{-1} & 0 \\ 0 & \bar{S} \end{bmatrix} \begin{bmatrix} V' \\ \bar{V}' \end{bmatrix}. \end{aligned}$$ □

4.1 Algorithm

Theorem 4.3 gives a necessary and sufficient condition for the existence of a stabilizing output feedback. Unfortunately, this result involves equations that are nonlinear in the considered unknows. However the quadratic characterization of theorem 3.2 may be used to adequately construct $OS(C,A,B)$-invariant subspaces that lead to stabilizing output feedback matrices K. This can be done, for instance, by taking into account the coupling requirement and solving subsequently part (ii) and part (i) of theorem 3.2.

Before presenting a procedure based on this last comment, a result will be formulated allowing the use of a reduced-order generalized Lyapunov equation both to solve part (ii) and to consider the inclusion (9). The proof given for the next lemma sets into evidence some connections between the adopted quadratic approach and the Sylvester equations approach. The choice of using orthogonal transformations is due both to their known numerical interests and simplicity for deriving the theoretical results.

Lemma 4.1 *Under the assumption that (C,A) is detectable, there always exist $S = S' \geq 0$ and Z verifying (19), (20) and (21) for some $T \in \Re^{n-p \times n}$, with rank $(T) = n-p$, such that $Ker\, T = \mathcal{V}$ is (C,A)-outer detectable and*

$$Ker\, T \cap Ker\, C = \{0\}$$

Proof: Consider the following change of basis :

$$x = \begin{bmatrix} M_1 & M_2 \end{bmatrix} \begin{bmatrix} x_1 \\ x_2 \end{bmatrix} \quad (38)$$

where $[M_1 \ \ M_2]$ is an orthogonal matrix such that :

$$C \begin{bmatrix} M_1 & M_2 \end{bmatrix} = \begin{bmatrix} C_1 & 0 \end{bmatrix} \quad (39)$$

with $C_1 \in \Re^{p \times p}$ and $rank(C_1) = p$.

In this basis, the open-loop system takes the form

$$\begin{bmatrix} \dot{x_1} \\ \dot{x_2} \end{bmatrix} = \begin{bmatrix} A_{11} & A_{12} \\ A_{21} & A_{22} \end{bmatrix} \begin{bmatrix} x_1 \\ x_2 \end{bmatrix} + \begin{bmatrix} B_1 \\ B_2 \end{bmatrix} u \quad (40)$$

$$y = \begin{bmatrix} C_1 & 0 \end{bmatrix} \begin{bmatrix} x_1 \\ x_2 \end{bmatrix} \quad (41)$$

where the involved matrices have appropriate dimensions.

As shown in [3], the detectability of the pair (C,A) implies the detectability of the pair (A_{12}, A_{22}). Thus, for any given matrix $Q_T = Q_T' > 0$, let $S_{22} \in \Re^{n-p \times n-p}$, with $S_{22} = S_{22}' > 0$ and $S_{21} \in \Re^{n-p \times p}$ be solutions to the following generalized reduced-order Lyapunov equation :

$$A_{22}' S_{22} + S_{22} A_{22} + A_{12}' S_{21}' + S_{21} A_{12} = -Q_T \quad (42)$$

Let $L_2 = \Re^{n-p \times p}$ be such that

$$S_{22} L_2 = S_{21} \quad (43)$$

and consider also a Choleski decomposition of $S_{22} = S_{22}' > 0$ given by:

$$S_{22} = T_2' T_2 \quad (44)$$

Thus, from (42), (43) and (44), we get

$$T_2' T_2 (A_{22} + L_2 A_{12}) + (A_{22}' + A_{12}' L_2') T_2' T_2 = -Q_T$$

where, by construction, $\sigma(A_{22} + L_2 A_{12}) \in \mathcal{C}^-$.

Since T_2 is, by definition, non-singular, we can define the asymptotically stable matrix $H_T \in \Re^{n-p \times n-p}$ from the similarity relation

$$T_2 (A_{22} + L_2 A_{12}) = H_T T_2 \quad (45)$$

Furthermore, since C_1 is invertible, a matrix $U \in \Re^{n-p \times p}$ can always be computed from:

$$U C_1 = -(T_2 L_2 A_{11} + T_2 A_{21} - H_T T_1) \quad (46)$$

Thus, by defining $T_1 = T_2 L_2$, (45) and (46) can be replaced by $\begin{bmatrix} T_1 & T_2 \end{bmatrix} \begin{bmatrix} A_{11} & A_{12} \\ A_{21} & A_{22} \end{bmatrix} - H_T \begin{bmatrix} T_1 & T_2 \end{bmatrix} = -U \begin{bmatrix} C_1 & 0 \end{bmatrix}$.

Hence, $T = \begin{bmatrix} T_1 & T_2 \end{bmatrix} \begin{bmatrix} M_1' \\ M_2' \end{bmatrix}$ is such that;

- $Ker\, T$ is (C, A)-outer detectable, since $H_T = (A + LC)|\mathcal{X}/\mathcal{V}$ is such that $\sigma(H_T) \in \mathcal{C}^-$ for $L = T'(TT')^{-1}U$;
- $Ker\, T \cap Ker\, C = \{0\}$, since the invertibility of T_2 implies $rank \left(\begin{bmatrix} T \\ C \end{bmatrix} = \begin{bmatrix} T_1 & T_2 \\ C_1 & 0 \end{bmatrix} \begin{bmatrix} M_1' \\ M_2' \end{bmatrix} \right) = n$.

Furthermore, let $\Gamma = \Gamma' > 0$ be the unique solution of $H_T'\Gamma + \Gamma H_T = -Q_T$. Thus, the following matrices $S = S' \geq 0$ and Z verify (19), (20) and (21) for T defined above:

$$S = \begin{bmatrix} M_1 & M_2 \end{bmatrix} \begin{bmatrix} S_{11} & S_{21}' \\ S_{21} & S_{22} \end{bmatrix} \begin{bmatrix} M_1' \\ M_2' \end{bmatrix}, \qquad (47)$$

$$\text{with } \begin{bmatrix} S_{11} & S_{21}' \\ S_{21} & S_{22} \end{bmatrix} = \begin{bmatrix} T_1' \\ T_2' \end{bmatrix} \Gamma \begin{bmatrix} T_1 & T_2 \end{bmatrix}$$

$$\text{and } Z = \begin{bmatrix} M_1 & M_2 \end{bmatrix} \begin{bmatrix} T_1' \\ T_2' \end{bmatrix} U\Gamma \qquad (48)$$

□

From the proof given above, it can also be verified that $V = \begin{bmatrix} M_1 & M_2 \end{bmatrix} \begin{bmatrix} V_1 \\ V_2 \end{bmatrix}$ such that $Im\, V = Ker\, T$ can be obtained as a basis of the null-space of $\mathcal{T} = \begin{bmatrix} S_{21} & S_{22} \end{bmatrix} \begin{bmatrix} M_1' \\ M_2' \end{bmatrix}$:

$$\mathcal{T}V = 0 \qquad (49)$$

Based on these results, and in the light of the algorithm proposed in [9], the following basic procedure is proposed to compute a stabilizing output feedback when $m + p > n$ [1]:

Step 1: Find the orthogonal decomposition $C = \begin{bmatrix} C_1 & 0 \end{bmatrix} \begin{bmatrix} M_1' \\ M_2' \end{bmatrix}$ and set $\begin{bmatrix} A_{12} \\ A_{22} \end{bmatrix} = \begin{bmatrix} M_1' \\ M_2' \end{bmatrix} AM_2$;

Step 2: Solve the *reduced-order* generalized Lyapunov equation (42) to find S_{21} and S_{22};

Step 3: Compute V from (49) as an orthogonal basis of $Ker\, \mathcal{T}$, *i.e.* $V'V = I_p$;

Step 4: Solve equations (16), (17) and (18) to find P, Y and W_Π;

Step 5: Compute the stabilizing output feedback matrix as the unique solution of

$$KCP = Y \iff KCV\bar{P} = W_\Pi, \text{ since } V'V = I_p.$$

[1] If $m + p = \bar{\nu} \leq n$, a dynamic compensator of order $\nu > n - \bar{\nu}$ can be considered to recover this condition.

The steps of this procedure have a correspondence with those of the algorithm proposed in [8] to compute an output feedback matrix K that assigns stable closed-loop eigenvalues. An example in the next section shows that even in the case $m+p > n$ the basic procedure may fail and some iterations can be necessary to adequately define $\mathcal{V}$.

Although in this study, stability is the only closed-loop requirement, the degrees-of-freedom existing in the quadratic approach given here could be exploited to consider other numerical and closed-loop performance requirements. In particular, additional requirements may be associated to the Lyapunov function defined in corollary 4.2. Also, Q_V and Q_T may be let as free variables in steps 2 and 4, respectively, and convex optimization techniques may be used to solve the corresponding equations [2].

5 EXAMPLES

Consider the following data [5]:

$$A = \begin{bmatrix} 0 & 1 & 0 & 0 \\ 1 & 1 & 0 & 0 \\ -1 & 0 & 0 & 0 \\ 0 & 0 & 0 & 0 \end{bmatrix} \quad ; \quad B = \begin{bmatrix} 0 & 0 \\ 1 & 0 \\ 0 & 0 \\ 0 & 1 \end{bmatrix}$$

Two different output matrices C are considered. In both cases, the corresponding triples (C, A, B) are controllable and observable and $m + p = 5 > n$. Also, to obtain closed-loop eigenvalues with real parts less than $-\alpha = -2$, computations are done using $(A+\alpha I)$ instead of A. Standard convex programming techniques are applied to find feasible solutions for the coupled quadratic equations, without additional requirements that could improve the numerical solution or the closed-loop performance.

1^{st} *Case*: Consider first the following output matrix: $C = \begin{bmatrix} 1 & 0 & 0 & 1 \\ 0 & 0 & 1 & 0 \\ 0 & 0 & 0 & 1 \end{bmatrix}$.

Using an orthogonal matrix M to perform step 1, a matrix $\mathcal{T} = \begin{bmatrix} S_{21} & S_{22} \end{bmatrix} \begin{bmatrix} M_1' \\ M_2' \end{bmatrix}$ is readily found in step 2:

$$\mathcal{T} = \begin{bmatrix} 0.0006 & 0 & -4.1142 & 1 \end{bmatrix} \begin{bmatrix} -0.5257 & 0 & 0 & -0.8507 \\ 0 & 0 & 1 & 0 \\ 0.8507 & 0 & 0 & -0.5257 \\ 0 & 1 & 0 & 0 \end{bmatrix}$$

$$= \begin{bmatrix} -3.5001 & 1 & 0 & 2.1625 \end{bmatrix}.$$

It implies, in step 3: $V = \begin{bmatrix} 0.5107 & 0 & 0.2362 \\ -0.0660 & 0 & 0.9695 \\ 0 & 1 & 0 \\ 0.8572 & 0 & -0.0660 \end{bmatrix}$.

A feasible solution for step 4 is then found:

$$P = \begin{bmatrix} 19753.561 & -41669.85 & 6418.2843 & 51240.969 \\ -41669.85 & 237613.71 & -6863.8855 & -177323.06 \\ 6418.2843 & -6863.8855 & 3104.1283 & 13562.213 \\ 51240.969 & -177323.06 & 13562.213 & 164934.04 \end{bmatrix},$$

$Y = \begin{bmatrix} -51685.095 & -747434.01 & -14350.967 & 261981.08 \\ -33408.348 & 639608.61 & -4267.0209 & -349845.47 \end{bmatrix}$

$W_{\Pi} = \begin{bmatrix} 247529.57 & -14350.967 & -754116.8 \\ -359186.68 & -4267.0209 & 635288.97 \end{bmatrix}$.

The corresponding stabilizing output feedback $K = \begin{bmatrix} -67.1094 & 56.3478 & 84.9136 \\ 34.6173 & -26.0568 & -45.3505 \end{bmatrix}$ gives:

$\sigma(A + BKC) = \{ -2.5001 ; -2.1333 ; -2.5499 \pm 4.4622j ; \}$ where the eigenvalue -2.5001 corresponds to step 2, through (43).

2^{nd} *Case*: Consider now the output matrix used in [5]:

$C = \begin{bmatrix} 1 & 0 & 0 & 0 \\ 0 & 0 & 1 & 0 \\ 0 & 0 & 0 & 1 \end{bmatrix}$.

In this example, convex programming techniques do not produce a feasible solution in step 4, due to the particular matrices $\mathcal{T}$ selected in step 2. However, a stabilizing solution exists. It has been found in [5] by eigenstructure assignment. Thus, the left eigenvector of this solution is selected as a candidate T:

$T = [\ 35 \quad -7 \quad -28 \quad -10\ ]$ so that $\lambda = -4$ must be assigned as a closed-loop eigenvalue, and:

$$V = \begin{bmatrix} 0.2153 & 0.6027 & 0.1507 \\ -0.0185 & -0.0518 & 0.9871 \\ -0.0740 & 0.7928 & -0.0518 \\ 0.9736 & -0.0740 & -0.0185 \end{bmatrix}.$$

Hence, a feasible solution for step 4 can now be obtained:

$$P = \begin{bmatrix} 40952.514 & -88879.744 & 14627.136 & 164593.46 \\ -88879.744 & 601592.13 & -19920.323 & -676416.69 \\ 14627.136 & -19920.323 & 6758.6188 & 46215.07 \\ 164593.64 & -676416.69 & 46215.07 & 920167.23 \end{bmatrix}$$

$W_{\Pi} = \begin{bmatrix} 603289.9 & -79801.264 & -1989176.3 \\ -1990617.4 & -25183.375 & 2876237.8 \end{bmatrix}$;

$Y = \begin{bmatrix} -217972.83 & -1970444.2 & -4872.8597 & 630050.05 \\ -10282.026 & 2877121.4 & -21648.917 & -1989355.1 \end{bmatrix}$

The corresponding stabilizing output feedback $K = \begin{bmatrix} -116.2499 & 158.3979 & 13.5233 \\ 97.4749 & -122.0786 & -13.4663 \end{bmatrix}$ gives: $\sigma(A + BKC) = \{ -4.0 ; -2.2319 ; -3.1172 \pm 6.6548j \}$.

6 CONCLUDING REMARKS

The concept of (C, A, B)-invariance has been revisited to obtain a quadratic characterization of the so-called *Output Stabilizable* (C, A, B)-invariant subspaces, which have a fundamental role for output feedback stabilization in linear systems. The paper has focused on both theoretical and algorithmic aspects, and some links with the coupled Sylvester equations approach have been stressed. In particular, a necessary and sufficient condition for the existence of a stabilizing output feedback has been obtained in terms of two coupled-quadratic equations. An algorithm has also been proposed to compute a stabilizing output feedback matrix when $m + p > n$.

Among the remaining open questions for future studies, one may consider the use of the existing degrees of freedom to include additional control requirements, the possible extension to the less restricitive case $mp \geq n$ [1], and numerical and theoretical comparisons with other quadratic approaches.

REFERENCES

[1] A.T. Alexandridis and P.N. Parakevopoulos : *A new approach to Eigenstructure Assignment by Output Feedback*. IEEE Trans. Automatic Control, Vol. 41, No 7, pp. 1046-1050, July 1996.

[2] S.P. Boyd, L. El Ghaoui, E. Feron and V. Balakrishhnan : *Linear Matrix Inequalities in System and Control Theory*. Philadelphia, PA: SIAM, 1994.

[3] C.T. Chen : Linear system theory and design, Holt, Rinehart and Winston, INC, New York, 1984.

[4] C.A.R. Crusius and A. Trofino : *Sufficient LMI Conditions for Output Feedback*. IEEE Trans. Automatic Control, Vol. 44, No 5, pp. 1053-1057, May 1999.

[5] L.R. Fletcher, J. Kautsky, G.K.G Kolka and N.K Nichols : *Some necessary and sufficient conditions for eigenstructure assignment*. Int. J. Control, Vol. 42, No 6, pp. 1457-1468, 1985.

[6] J.C. Geromel, C.C. de Souza and R.E. Skelton : *Static Output Feedback Controllers: Stability and Convexity*. IEEE Trans. Automatic Control, Vol. 43, No 1, pp. 120-125, January 1998.

[7] L. El Ghaoui, F. Oustry and M. AitRami : *A Cone Complementarity Linearization Algorithm for Static Output-Feedback and Related Problems*. IEEE Trans. Automatic Control, Vol. 42, No 8, pp. 1171-1176, August 1997.

[8] V.L. Syrmos and F.L. Lewis : *Output Feedback Eigenstructure Assignment Using Two Sylvester Equations*. IEEE Trans. Automatic Control, Vol. 38, No 3, pp. 495-499, March 1993.

[9] V.L. Syrmos and F.L. Lewis : *A Bilinear Formulation for the Output Feedback Problem in Linear Systems*. IEEE Trans. Automatic Control, Vol. 39, No 2, pp. 410-414, February 1994.

[10] V.L. Syrmos, C.T. Abdallah and K. Grigoriadis : *Static Output Feedback - A Survey*. Automatica, Vol. 33, No 3, pp. 125-137, 1997.

[11] W.M. Wonham: *Linear Multivariable Control, a Geometric Approach*, Springer Verlag, New York, Heidelberg, Berlin, 1979.

Proceeding Series of the Brazilian Society of Computational and Applied Mathematics, v. 10, n. 1, 2023.

Trabalho apresentado no XLII CNMAC, Universidade Federal de Mato Grosso do Sul - Bonito - MS, 2023

Proceeding Series of the Brazilian Society of Computational and Applied Mathematics

Tuning Method in the Implementation Fuzzy ADRC Controllers for a Mass-Spring-Damper System: An approach

Lucas D. da Silva [1]
Engenharia Mecânica Centro de Engenharias ,
Universidade Federal Rural do Semi-árido EM/UFERSA, Mossoró, RN.
Walter M. Rodrigues [2]
Departamento de Ciências Naturais, Matemática e Estatística,
Universidade Federal Rural do Semi-árido, DCME/UFERSA, Mossoró, RN.
Nathan R. da Silva [3]
Engenharia Elétrica Centro de Engenharias ,
Universidade Federal Rural do Semi-árido EM/UFERSA, Mossoró, RN.
Maxwell C. Jácome [4]
Instituto Federal Institute de Rio Grande do Norte,
IFRN, Campus João Câmara, RN.
Andres O. Salazar [5]
Departamento de Engenharia de Computação e Automação,
Universidade Federal do Rio Grande do Norte DCA/UFRN, Natal, RN.
Elmer R. L. Villarreal [6]
Departamento de Ciências Naturais, Matemática e Estatística,
Universidade Federal Rural do Semi-árido DCME/UFERSA, Mossoró, RN.

Abstract. This article presents a new approach that describes a mass-spring-damper system as a second-order system. Thus, the first part implements the Active Disturbance Rejection Control (ADRC) controller, and then the implementation of the fuzzy ADRC controller will be simplified by the tuning technique. The article also presents a simulation of the mass-spring-damper system using the output plant transfer function. The paper implements a controller to control the closed-loop system. Finally, a graphical comparison of the respective controllers is shown in the mass-spring-damper system.

Keywords. Control ADRC, Control Fuzzy ADRC, Mass-Spring-Damper System, Second Order Differential Equation

[1]lucasdantas742@gmail.com
[2]walterm@ufersa.edu.br
[3]nathanrgsilva@gmail.com
[4]maxwellc.jacome@gmail.com
[5]andres@dca.ufrn.br
[6]elmerllanos@ufersa.edu.br

 © 2023 SBMAC

1 Introduction

The study of the movement experienced by a mass suspended from the free end of a spring is discussed in most introductory physics courses from theoretical and experimental outlooks. Springs, dampers, and masses are typical components of a mechanical system. In [1], propose a vibration suppression control method for a mass-spring-damper system with one or two dynamic damper(s). The feedback is designed by the interconnection and damping assignment passivity-based control, where the system is transformed into a system having a skyhook damper with an artificial modification of the structure matrix.

Semi-Active Suspension Control Design for Vehicles is described in [4]. In a Semi-active suspension system, the damping coefficient of the shock absorber or spring constant is electronically controlled, without adding external energy to the system, except the device control that changes the damping coefficient or the elastic constant characterizes a semi-active suspension; mostly of the cases, is the damping coefficient of the dissipative element that varies in semi-active suspensions in [4]. The motion equations and state-space model are the same for passive suspension systems, so none of the parameters are changed. In contrast, for semi-active suspension systems, these parameters may vary. The paper [6] presents a new approach to the fuzzy active-disturbance rejection position controller of the bearingless induction machine. In the paper, [5] proposed a control variable for the radial position problem, and the ADRC control is used to improve the closed-loop system dynamic when a changing load occurs on the output system.

The mechanism and Lagrange methods model the mass-spring-damping resonance system and analyze the system stability. The mechanism and Lagrange methods model the mass-spring-damping resonance system, and the system stability is analyzed. The extended state observer (ESO) algorithm analyzes and controls the mass-spring-damping system based on active disturbance rejection control ADRC theory. The ADRC solution, as a generic controller, does not require detailed model information beyond the integral dynamics. Therefore, it is interesting to explore what benefits, if any, can be obtained by incorporating such knowledge into the ADRC solution, perhaps in reducing the load on the estimation of the total disturbance [7]. The ADRC uses the tracking characteristics of the extracted differential signal to formulate the signal transition arrangement between the input and differential signals. When the signal response changes abruptly, the tracking differentiator (TD) can promptly provide the smooth signal as the input signal to the controlled system, thereby ensuring that a large overshoot due to the mutations is not incurred and the system stability is enhanced in [2].

This paper studies implementing a Fuzzy ADRC control in the mass-spring-damper system. The article presents a guide to the introduction section. The section 2 presents the mathematical model and the ADRC controller. The section 3 presents results using Fuzzy ADRC Controller and discussions. In section 4, the conclusions are made.

2 Mathematical model and ADRC Controller

In [3], it is formulated that as a two-degree-of-freedom active disturbance-rejection method, the equivalent-input-disturbance (EID) approach shows its validity for structural control. It uses a state observer to estimate the effect of disturbances on a control input channel. A stability condition of the system with prescribed control performance is derived in the form of a linear matrix inequality (LMI) that is used to design the gain of the state feedback. To simulate the mass-spring-damper system and apply the Proportional-Integral-Derivative (PID) controller and ADRC controllers, it is first necessary to mathematically model the entire system to obtain the plant transfer function. Applying the sum of the forces concerning the mass of the system block, it is possible to obtain equation (1) , where $u(t)$ is the applied external force, m is the block mass

DOI: 10.5540/03.2023.010.01.0107 © 2023 SBMAC

, k is the spring constant, and f_v is the viscous force of the damper. The motion is in a line which we can take to be the y-axis.

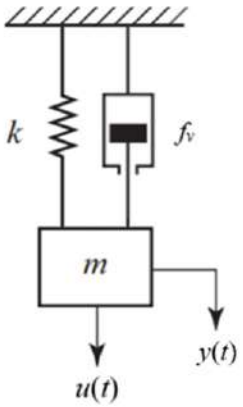

Figure 1: Mass-spring-damper system.

$$u(t) = m\frac{d^2y}{dt^2} + f_v\frac{dy}{dt} + ky \tag{1}$$

Since equation (1) is an ordinary differential equation it is possible to apply the Laplace transform, thus obtaining an external force in the Laplace domain U(s) and also the position Y (equation (2)).

$$U(s) = ms^2 + f_v s + kY \tag{2}$$

The plant transfer function is classified as the ratio of output and input, thus rewriting equation (2) the plant transfer function was obtained the equation (3).

$$P(s) = \frac{Y(s)}{U(s)} = \frac{1}{ms^2 + f_v s + kY} \tag{3}$$

$$P(s) = \frac{1/m}{s^2 + \frac{f_v}{m}s + \frac{k}{m}Y}$$

For the transfer function in terms of natural frequency (ω_n) and damping coefficient (ϵ) we have:

$$H(s) = \frac{\omega_n^2}{s^2 + 2\epsilon\omega_n s + \omega_n^2} \tag{4}$$

where $\omega_n = \sqrt{\frac{k}{m}}$ and $\epsilon = \frac{f_v}{2m\omega_n}$

The mass-spring-damper system is characterized as a second-order system, thus the ADRC controller for a second-order system is given as:

$$\ddot{y} = f(y, \dot{y}, d, t) + bu \tag{5}$$

Where y is the position, u is the input parameter, b is a constant, d is an unknown parameter (external perturbation) and $f(y, \dot{y}, d, t)$ is known as the generalized perturbation of the system and

 © 2023 SBMAC

its knowledge not required for controller design and implementation. The only information needed is its real-time estimated value. Let $\tilde{f}$ be the estimate $f(y, \dot{y}, d, t)$ at a time t, then the control law proposed by the ADRC method is as follows:

$$u = \frac{-\tilde{f} + u_0}{b} \tag{6}$$

3 Results using Fuzzy ADRC Controller and discussions

ADRC adopts a nonlinear state error feedback strategy, which can significantly improve the efficiency of feedback control. Non-linear state error feedback is based on the principle of "small error, large gain, large error, small gain", appropriate selection of parameters and linear interval for segmentation, and the use of different gain control in different intervals can obtain the effect of rapid adjustment. Fuzzy-Self-adapted ADRC structure, its structure is shown in Figure (2) and Fuzzy-Self-adapted ADRC structure with rotational transformation, its structure with rotational transformation is shown in Figure (3).

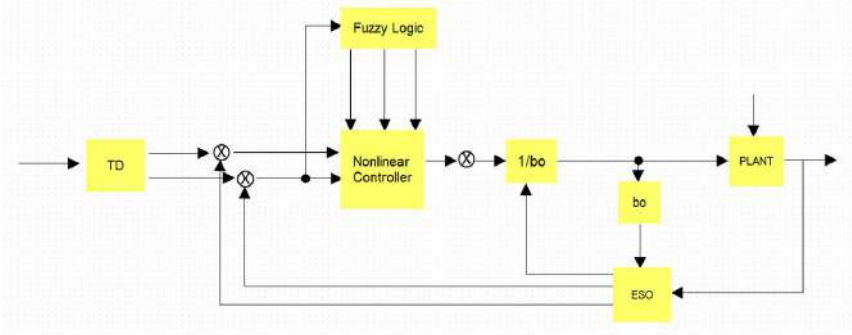

Figure 2: Fuzzy-Self-adapted ADRC structure.

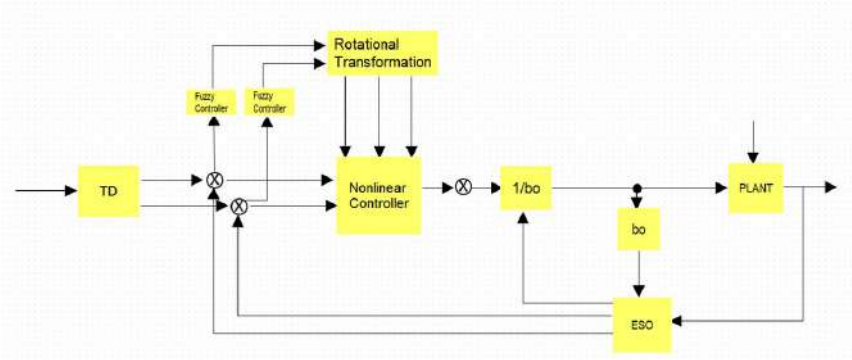

Figure 3: Fuzzy-Self-adapted ADRC structure with rotational transformation.

The following results were based on the articles [5], [6]. So the notations, inputs, outputs, error and other parameters can be seen in detail in [5], [6]. This article introduces the fuzzy logic controller, according to the input of , e_1, Δe_1, e_2, Δe_2 and using fuzzy control rules to change the ADRC parameters $\{\Delta i_x, \Delta i_y\}$, with rotational transformation is obtained approaching the optimal

 © 2023 SBMAC

parameters $\{\beta_0, \beta_1, \beta_2\}$. To meet the requirements of the $\{e_1,\ \Delta e_1,\ e_2,\ \Delta e_2\}$ parameters of the Fuzzy ADRC, in the controller, the fuzzy variables are e_1, e_2, $\{\Delta i_x, \Delta i_y,$, in your domain, seven language sets defined such as { (NB), (NM), (NS), (QZ), (PS), (PM), (PB) }. For $\{\Delta i_x, \Delta i_y\}$ parameter configuration, fuzzy control table is formed, as demonstrated in Tables (2) and (3). The adjustments gave rise to the error and the change in the error pertinence functions illustrated in Figures (4), (5) and the output pertinence functions represented in Figure (6) and the rules summarized in Table (2).

Table 1: Linguistic labels adopted to describe fuzzy sets.

Label	Signification
NB	Negative Big
NH	Negative Huge
NM	Negative Medium
NS	Negative Small
QZ	Quasi- Zero
PH	Positive Huge
PS	Positive Small
PM	Positive Medium
PB	Positive Big

Table 2: Rules for x-axis fuzzy controller.

d \ f	NB	NM	NS	QZ	PS	PM	PB
NB	NH	NH	NH	NB	NM	NS	QZ
NM	NH	NH	NB	NM	NS	QZ	PS
NS	NH	NB	NM	NS	QZ	PS	PM
QZ	NB	NM	NS	QZ	PS	PM	PB
PS	NM	NS	QZ	PS	PM	PB	PH
PM	NS	QZ	PS	PM	PB	PH	PH
PB	QZ	PS	PM	PB	PH	PH	PH

Table 3: Rules for y-axis fuzzy controller.

g \ h	NB	NM	NS	QZ	PS	PM	PB
NB	NH	NH	NB	NB	NM	NS	QZ
NM	NH	NB	NB	NM	NS	QZ	PS
NS	NB	NB	NM	NS	QZ	PS	PS
QZ	NB	NM	NS	QZ	PS	PS	PM
PS	NM	NS	QZ	PS	PS	PM	PB
PM	NS	QZ	PS	PS	PM	PB	PH
PB	QZ	PS	PS	PM	PB	PH	PH

It is said to see that, each piece of the position Fuzzy-ADRC controller is construed, Its entire control frame is demonstrate in Figure (2). The x_1 is the monitoring signal of θ^* , x_2 is the differential signal of θ^* , z_1 is the monitoring signal of θ , z_2 is differential signal for z_1, z_3 is system observation of the incertitude piece of the perturbance that is $w(t)$ as the observation for

 © 2023 SBMAC

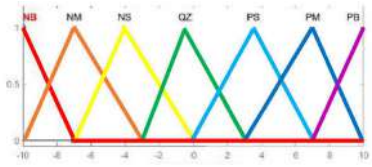

Figure 4: Membership functions of input variables.

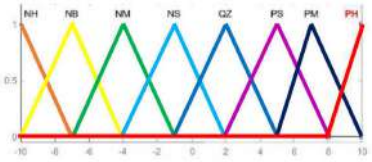

Figure 5: Membership functions of input variables.

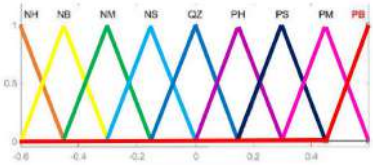

Figure 6: Membership functions of output variables.

the certain part, where the differential is different from the differential signal in a controller, its effect is not amplified, but disincentive to the noise signal. According to the table of allocation of members of fuzzy set Tables (2) and (3) and the fuzzy control model of parameters, and with diffuse synthetic reasoning to project diffuse matrix, then defuzzification and correction parameters found $\{\Delta i_x, \Delta i_y\}$, with rotational transformation is obtaneid $\{\Delta\beta_0, \Delta\beta_1, \Delta\beta_2\}$ and replaced it in the equation:

$$\beta_0 = \beta_0^{'} + \Delta\beta_0 \tag{7}$$

$$\beta_1 = \beta_1^{'} + \Delta\beta_1 \tag{8}$$

$$\beta_2 = \beta_2^{'} + \Delta\beta_2 \tag{9}$$

Where variables $\beta_0, \beta_1, \beta_2$ is the nonlinear controller initial value. According to rotational transformation is obtaining parameters $\beta_0, \beta_1, \beta_2$. Finally, with the principles of Fuzzy ADRC parameters tuning, we can obtain Fuzzy-ADRC. In the Figure (7) presents a comparison between the simulations. With $\beta_0^{'} = 0$, $\beta_1^{'} = 0$, $\beta_2^{'} = 0$, $\{\Delta\beta_0\}$ $\{\Delta\beta_1\}$,$\{\Delta\beta_2\}$ domains are $[-6, +6]$, $[-6, +6]$, $[-0.6, +0.6]$. Thus $\beta_0 = \Delta\beta_0$, $\beta_1 = \Delta\beta_1$ and $\beta_2 = \Delta\beta_2$. The fuzzy adrc controller is well optimized because there is a good tuning of the fuzzy adrc controller.

4 Conclusions

The article presents a new approach that describes a mass-spring-damper system as a second-order system. Thus, when implementing the Fuzzy ADRC controller in the mass-spring-damper system. The implementation of the Fuzzy ADRC controller was simplified by the technique used.

 © 2023 SBMAC

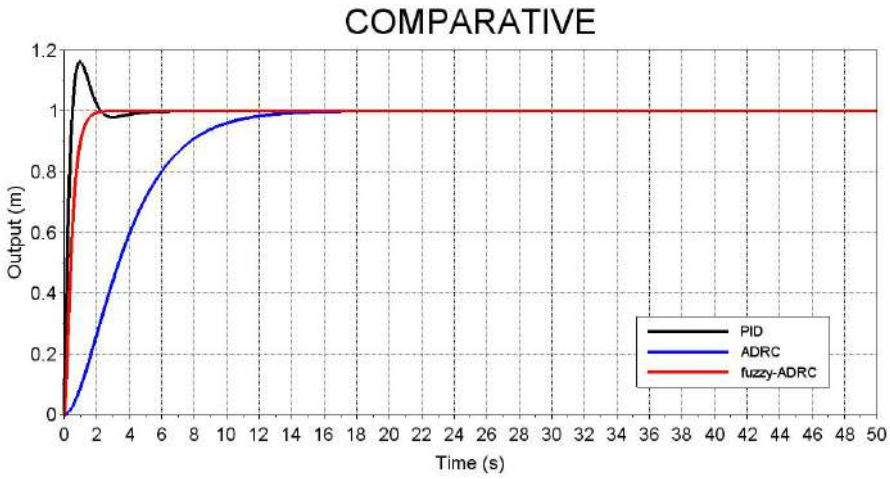

Figure 7: Comparison between simulations.

Acknowledgment

This work was suported by Comissão de Aperfeiçoamento de Pessoal do Nível Superior (CAPES) and Conselho Nacional de Desenvolvimento Científico e Tecnológico (CNPq).

References

[1] T. Aoki, Y. Yamashita, and D. Tsubakino. "Vibration Suppression of Mass-Spring-Damper System with Dynamic Dampers using IDA-PBC". In: **IFAC Proceedings Volumes** 45(1) (2012), pp. 42–47. DOI: /10.3182/20120829-3-IT-4022.00021.

[2] Y. Fan et al. "Active Disturbance Rejection Control Design Using the Optimization Algorithm for a Hydraulic Quadruped Robot". In: **Computational Intelligence and Neuroscience** ID 6683584 (2021), pp. 1–22. DOI: 10.1155/2021/6683584.

[3] K. Miyamoto et al. "Active Structural Control of Base-Isolated Building Using Equivalent-Input-Disturbance Approach With Reduced-Order State Observer". In: **J. Dyn. Syst. Meas. Control** 144 (9) (2022), pp. 1–14. DOI: 10.1115/1.4054819.

[4] S. M. Savaresi et al. **Semi-Active Suspension Control Design for Vehicles**. Elsevier Science, 2010. ISBN: 9780080966793.

[5] W. L. D. Silva et al. "Radial Position Control of a Bearingless Machine with Active Disturbance Rejection Control Fuzzy an approach". In: **XXVII International Conference on Electronics, Electrical Engineering and computings (IEEE-INTERCON 2020), Peru** 1 (2020), pp. 1–4. DOI: 10.1109/INTERCON50315.2020.9220221.

[6] W. L. D. Silva et al. "Radial Position Control of a Bearingless Machine with Active Disturbance Rejection Control Fuzzy an approach". In: **2021 IEEE International Conference on Automation/XXIV Congress of the Chilean Association of Automatic Control (ICA-ACCA)** 1 (2021), pp. 1–4. DOI: 10.1109/ICAACCA51523.2021.9465177.

[7] H. Zhang, S. Zhao, and Z. Gao. "An active disturbance rejection control solution for the two-mass-spring benchmark problem". In: **2016 American Control Conference (ACC)** 1 (2016), pp. 1566–1571. DOI: 10.1109/ACC.2016.7525139.

 © 2023 SBMAC

Trabalho apresentado no XLI CNMAC, Unicamp - Campinas - SP, 2022.

Proceeding Series of the Brazilian Society of Computational and Applied Mathematics
Preprint

Eigenvalue Assignment in Second order systems Using Sylvester equations: Approach

Elmer R. L. Villarreal [1]
Departamento de Ciências Naturais, Matemática e Estatística,
Universidade Federal Rural do Semi-árido DCME/UFERSA, Mossoró, RN.
Andres O. Salazar [2]
Departamento de Engenharia de Computação e Automação,
Universidade Federal do Rio Grande do Norte DCA/UFRN, Natal, RN.
Thiago F. do Nascimento [3]
Departamento de Engenharia de Computação e Automação,
Universidade Federal do Rio Grande do Norte DCA/UFRN, Natal, RN.
Lucas D. da Silva [4]
Engenharia Mecânica Centro de Engenharias ,
Universidade Federal Rural do Semi-árido EM/UFERSA, Mossoró, RN.
Walter M. Rodrigues [5]
Departamento de Ciências Naturais, Matemática e Estatística,
Universidade Federal Rural do Semi-árido, DCME/UFERSA, Mossoró, RN.

Abstract. Second-order systems are those whose models can be written by a second-order differential equation. That is, they are those that have two poles. The present article proposes an approach to solve the output feedback control with eigenvalues for second-order systems using Sylvester equations. The matrices are prescribed in advance and depend greatly on the controllability conditions, being assigned the system's observability eigenvalues. Furthermore, the real-value spectral decomposition $T(\lambda)$ is explored to establish conditions so that the feedback gain matrices do not overflow over the eigenvalue assignment. However, it should be noted that the proposed algorithms may present complex computational problems. Two theorems were presented using Sylvester equations. The algorithms were implemented based on Sylvester equations, and examples were presented with their conclusions.

Keywords. Sylvester equations, Eigenvalue assignment, Output feedback control, Second order system.

1 Introduction

Second-order linear systems capture the dynamic behavior of many natural phenomena, and have found applications in many fields, such as vibration and structural analysis, spacecraft control and robotics control and, hence, have attracted much attention [3]. In [6] presented impulse elimination approach to partial eigenvalue assignment for the descriptor system with the condition of

[1]elmerllanos@ufersa.edu.br
[2]andres@dca.ufrn.br
[3]thiago.figueiredo@ufrn.br
[4]lucasdantas742@gmail.com
[5]walterm@ufersa.edu.br

 © 2022 SBMAC

$S-$controllability. In [5] presented an approach for partial eigenvalue assignment in singular second order systems via proportional controller plus derived control plus output feedback controller.

The problem of partially eigenvalue allocation for amortization vibrancy in the second-order system by static output feedback in [8]. In this note, it is considered that the controller follows a second-order singular linear system:

$$\begin{aligned} P_0\ddot{x} + Q_0\dot{x} + R_0x &= Bu \\ y_0 &= C_0x \\ y_1 &= C_1\dot{x} \\ y_2 &= C_2\ddot{x} \end{aligned} \tag{1}$$

where $x \in \mathbb{R}^n$ and $u \in \mathbb{R}^m$ are the state vector and the control vector, respectively, and $P_0, Q_0, R_0 \in \mathbb{R}^{n\times n}$, and $B \in \mathbb{R}^{n\times m}$, $C_0, C_1, C_2 \in \mathbb{R}^{p\times n}$ are the system coefficient matrices. In particular demand, the matrices P_0, Q_0, and R_0 being denominated the mass matrix, the structural damping matrix and the stiffness matrix, respectively. As for the control of the second-order linear system (1), more of the results are focus on stabilization), pole assignment [1], [2], and partial pole assignment, [3]. The system (1), is expressed in the form:

$$E_f\dot{z} = A_fz + B_fu \tag{2}$$

with

$$E_f = \begin{bmatrix} I_n & 0 \\ 0 & P_0 \end{bmatrix} \;;\; A_f = \begin{bmatrix} 0 & I \\ -R_0 & -Q_0 \end{bmatrix} \; B_f = \begin{bmatrix} 0 \\ B \end{bmatrix} \tag{3}$$

$\dot{z} = \begin{bmatrix} \dot{x} \\ \ddot{x} \end{bmatrix}$ and $z = \begin{bmatrix} x \\ \dot{x} \end{bmatrix}$

Therefore, these results eventually involve manipulations on $2n$ dimensional matrices E_f, A_f and B_f.

The remaining of the paper is organized in the following Sections: Section 2 in presented problem formulation. Section 3 is presented Eigenstructure by Sylvester equation. Section 4 is presented Numerical Algorithm of Eigenvalue Assignment by SOF (Static Output Feedback) and numerical Examples. Finally, Section 5 concludes the paper.

2 Problem formulation

For the second-order descriptor dynamical system (1), by choosing the following control law:

$$u(t) = -L_0y_0(t) - L_1y_1(t) - L_2y_2(t) \tag{4}$$

with $L_0, L_1, L_2 \in \mathbb{R}^{p\times n}$. It obtains the closed-loop system as follows:

$$(P_0 + BL_2C_2)\ddot{x} + (Q_0 + BL_1C_1)\dot{x} + (R_0 + BL_0C_0)x = 0 \tag{5}$$

System (5) can be written in the first-order state-space form

$$E_b\dot{z} = A_bz; \tag{6}$$

 © 2022 SBMAC

with

$$E_b = \begin{bmatrix} I_n & 0 \\ 0 & (P_0 + BL_2C_2) \end{bmatrix} \text{ and}$$
$$A_b = \begin{bmatrix} 0 & I \\ -(R_0 + BL_0C_0) & -(Q_0 + BL_1C_1) \end{bmatrix}$$

System (1) gives rise to the quadratic eigenvalue problem of the open-loop vibration system with solving the eigenvalues λ_k and the associated eigenvectors $x_k \neq 0$, which satisfy

$$T(\lambda_k)x_k = 0 \; k = 1, 2, \cdots 2n \tag{7}$$

where

$$T(\lambda) = \lambda^2 P_0 + \lambda Q_0 + R_0 \tag{8}$$

By definition in [8],

$$\mu_i^2(P_0 + BL_2C_2)y_i + \mu_i(Q_0 + BL_1C_1)y_i + (R_0 + BL_0C_0)y_i = 0, \; i = 1, 2, \cdots, p. \tag{9}$$

In general, the open-loop 2n eigenvalues are also called the open-loop poles of system (1). Correspondingly, the system (5) leads to the closed-loop quadratic eigenvalue problem.

$$T(\lambda)y = (\lambda^2(P_0 + BL_2C_2) + (Q_0 + BL_1C_1)\lambda + (R_0 + BL_0C_0))y = 0 \tag{10}$$

3 Eigenstructure by Sylvester equation

The system (5) can be written in the first-order state-space form (6) and (7). Thus, for obtaining the output feedback matrix K $\sigma(E_s, A_s + B_sKC_s) \in \mathcal{C}^-$, is used the Sylvester equation in [4].

Consider the following linear time-invariant descriptor system in [4].

$$\begin{aligned} E_s\dot{x}(t) &= A_sx(t) + B_su(t) \\ y(t) &= C_sx(t) \end{aligned} \tag{11}$$

The Sylvester equations in [4].

$$A_sV_s - E_sV_sH_V = -B_sW_s, \qquad \sigma(H_V) \in \mathcal{C}^- \tag{12}$$
$$T_sA_s - H_TT_sE_s = -U_sC_s, \qquad \sigma(H_T) \in \mathcal{C}^- \tag{13}$$
$$T_sE_sV_s = 0 \tag{14}$$

The theorem 3.1 is based in [4], [8].

Theorem 3.1. *Let (1), be S-controllable, and $V_s \in \mathbb{R}^{n\times p}$ and $W_s \in \mathbb{R}^{m\times p}$ satisfy the equation (12). Then, the following hold.*

1) The matrices V_s and W_s given by (12),

$$\begin{bmatrix} A_s - \lambda_i E_s & B_s \\ T_sE_s & 0 \end{bmatrix} \begin{bmatrix} v_i \\ w_i \end{bmatrix} = 0 \; i = 1, 2, \cdots, q. \tag{15}$$

 © 2022 SBMAC

satisfy Sylvester matrix equation (12) for, $i = 1, 2, \cdots, q$,

2) When

$$rank(\begin{bmatrix} V_i \\ W_i \end{bmatrix}) = m \; i = 1, 2, \cdots, q. \tag{16}$$

hold, (14) gives all the solutions.

Proof. Based in [4]. □

Theorem 3.2. *Let* $E_s, A_s \in \mathbb{R}^{n\times n}$, $B_s \in \mathbb{R}^{n\times m}$, $H_V \in \mathbb{R}^{p\times p}$ *satisfy*

$$rank[A_s - \lambda E_s \; B_s] = n, \quad for \; any \; \lambda \in \sigma(H_V). \tag{17}$$

Further, let $H \in \mathbb{R}^{(n+m)\times m}[\lambda]$ *be a polynomial matrix satisfying* $[A_s - \lambda E_s \; B_s]H(\lambda) = 0_{n\times m}$.

Then:

(1) The matrices $V_s \in \mathbb{R}^{n\times p}$ *and* $W_s \in \mathbb{R}^{m\times p}$ *given by*

$$\begin{bmatrix} V_s \\ W_s \end{bmatrix} = Syl(H(\lambda), H_V, Z) \tag{18}$$

satisfy the matrix equation (12) for any matrix $Z \in \mathbb{R}^{m\times p}$. *(2) When* $rankH(\lambda) = r$ *for any* $\lambda \in \sigma(H_V)$, *all the matrices* V_s *and* W_s *satisfying the matrix equation (12) can be explicitly expressed by (18).*

Proof. Based in [4] and [7]. □

4 Numerical Algorithm

Let $G(\lambda)$ and X be defined as

$G(\lambda) = [A_s - \lambda E_s \; B_s]$; $X = \begin{bmatrix} V_s \\ W_s \end{bmatrix}$

The following basic procedure is proposed to calculate the feedback controller that stabilizes the closed loop system, when $m + p > q$. Closed loop eigenvalues are positioned arbitrarily close to the set ; they are symmetric sets of pre-specified eigenvalues. The (E_s, A_s, B_s, C_s) system is considered to be strongly controllable and strongly detectable.

Algorithm

Step 1: Choose an array $H_T \in \mathbb{R}^{q-p\times q-p}$ such that $\sigma(H_T) = \Lambda_T \in \mathcal{C}^-$ and Sylvester equation (13) is solved to find a matrix $T_s \in \mathbb{R}^{q-p\times n}$ such that

$$rank \left(\begin{bmatrix} T_s E_s \\ C_s \end{bmatrix} \right) = q \tag{19}$$

Step 2: Sylvester equation (12) is solved, for some $H_V \in \mathbb{R}^{p\times p}$ matrix such that $\sigma(H_V) = \Lambda_V \in \mathcal{C}^-$ taking into account that the matrix V_s must check the condition of the coupling (14) and taking into account that $rank\,(E_s V_s) = p$ .The condition (19) guarantees, in particular, that $rank(T_s E_s) = q$.

Step 3: By construction, the matrix V_s must verify that rank $(C_s V_s) = p$ and the matrix K can be calculated by:

$$K \quad = \quad W_s (C_s V_s)^{-1} \tag{20}$$

◇

 © 2022 SBMAC

Remark 4.1. *steps* 1 *and* 2 *can be solved using standard techniques for positioning the self-structure. Similar to the previous case, the matrices* V_s *and* W_s *used for the calculation of* K *can be constructed only with real elements. In particular: if* $\lambda_i \in \mathcal{C}^-$*, it is considered* $\lambda_{i+1} = \lambda_i^*$ *e* $\begin{cases} V_i = Re\,(v_i), & V_{i+1} = Imag\,(v_i) \\ W_i = Re\,(w_i), & W_{i+1} = Imag\,(w_i) \end{cases}$*, where* V_i *and* W_i *denote the columns of the matrices* V_s *and* W_s*, respectively.*

In step 1, under the condition that the system is strongly observable (detectable). As will be seen later, degrees of freedom existing in the choice of V_s that satisfy the coupling condition $T_s E_s V_s = 0$, can also be used to guarantee obtaining K such that $KC_sV_s = W_s$ in [4].

4.1 Example

Consider a simple linear dynamical system (1) in [8]

$$P_0 = \begin{bmatrix} 1.56 & 0.66 & 0.54 & -0.39 & 0 & 0 \\ 0.66 & 0.36 & 0.39 & -0.27 & 0 & 0 \\ 0.54 & 0.39 & 3.12 & 0 & 0.54 & -0.39 \\ -0.39 & -0.27 & 0 & 0.72 & 0.39 & -0.27 \\ 0 & 0 & 0.54 & 0.39 & 3.12 & 0 \\ 0 & 0 & -0.39 & -0.27 & 0 & 0.72 \end{bmatrix}$$

$$Q_0 = \begin{bmatrix} 0.72 & 1.08 & -0.72 & 1.08 & 0 & 0 \\ 1.08 & 2.16 & -1.08 & 1.08 & 0 & 0 \\ -0.72 & -1.08 & 1.44 & 0 & -0.72 & 1.08 \\ 1.08 & 1.08 & 0 & 4.32 & -1.08 & 1.08 \\ 0 & 0 & -0.72 & -1.08 & 1.44 & 0 \\ 0 & 0 & 1.08 & 1.08 & 0 & 4.32 \end{bmatrix}$$

$$R_0 = \begin{bmatrix} 12 & 18 & -12 & 18 & 0 & 0 \\ 18 & 36 & -18 & 18 & 0 & 0 \\ -12 & -18 & 24 & 0 & -12 & 18 \\ 18 & 18 & 0 & 72 & -18 & 18 \\ 0 & 0 & -12 & -18 & 24 & 0 \\ 0 & 0 & 18 & 18 & 0 & 72 \end{bmatrix}$$

$$B = \begin{bmatrix} 1 & 0 & 0 & 0 \\ 1 & 1 & 0 & 0 \\ 0 & 0 & 1 & 1 \\ 0 & 0 & 0 & 0 \\ 0 & 0 & 0 & 0 \\ 0 & 0 & 0 & 1 \end{bmatrix}; C_0 = \begin{bmatrix} 1 & 0 & 0 & 0 & 0 & 1 \\ 0 & 1 & 0 & 0 & 0 & 1 \\ 0 & 0 & 1 & 0 & 0 & 1 \\ 0 & 0 & 0 & 1 & 0 & 1 \end{bmatrix};$$

$$C_1 = \begin{bmatrix} 1 & 0 & 0 & 0 & 0 & 0 \\ 0 & 1 & 0 & 0 & 0 & 0 \\ 0 & 0 & 1 & 0 & 0 & 0 \\ 0 & 0 & 0 & 1 & 0 & 0 \end{bmatrix}; C_2 = \begin{bmatrix} 1 & 0 & 0 & 0 & 0 & 1. \\ 0 & 1 & 0 & 0 & 0 & 1 \\ 0 & 0 & 1 & 0 & 0 & 0 \\ 0 & 0 & 0 & 1 & 0 & 0 \end{bmatrix}.$$

Considered the system in the equations (8), (9)

$$E_f = \begin{bmatrix} I_n & 0 \\ 0 & M \end{bmatrix}; A_s = \begin{bmatrix} 0 & I_n \\ -R & -Q \end{bmatrix};$$

 © 2022 SBMAC

$$B_f = \begin{bmatrix} 0 \\ B \end{bmatrix} \; C_f = \begin{bmatrix} 1 & 0 & 0 & 0 \\ 0 & 1 & 0 & 0 \\ 0 & 0 & 1 & 0 \\ 0 & 0 & 0 & 1 \\ 0 & 0 & 0 & 0 \\ 1 & 1 & 1 & 1 \\ 0 & 0 & 0 & 0 \\ 0 & 0 & 0 & 0 \\ 0 & 0 & 0 & 0 \\ 0 & 0 & 0 & 0 \\ 0 & 0 & 0 & 0 \\ 0 & 0 & 0 & 0 \end{bmatrix}^T$$

Algorithm basic S1

Resolved the equation (11) for calculate the matrices W_s, V_s, satisfies the equation (14) and the matrix K, such that $KC_sV_s = W_s$:

$$T_s = \begin{bmatrix} 0.0191586 & 0.0067923 \\ 0.002596 & -0.0048225 \\ -0.1142892 & -0.0984266 \\ 0.0291704 & 0.0464583 \\ -0.1560708 & -0.1242605 \\ 0.1411607 & 0.1285409 \\ -0.041492 & -0.0123643 \\ 0.0355007 & 0.0117136 \\ 0.050413 & 0.0245556 \\ 0.0223914 & 0.0129728 \\ 0.0354971 & 0.0116523 \\ 0.0102292 & 0.0214763 \end{bmatrix}^T$$

$$V_s = \begin{bmatrix} 0.0521304 & 0.0439039 & 0.0383248 & 0.0348497 \\ -0.076474 & -0.0719608 & -0.0708508 & -0.0726528 \\ 0.0070045 & 0.0070247 & 0.0066577 & 0.0061644 \\ 0.0043382 & 0.0040844 & 0.0037361 & 0.0028785 \\ 0.0017522 & 0.0004953 & -0.0002459 & -0.0006246 \\ 0.0074559 & 0.008552 & 0.0083765 & 0.0071757 \\ -0.1563912 & -0.1756154 & -0.1916239 & -0.2090984 \\ 0.229422 & 0.2878434 & 0.3542541 & 0.435917 \\ -0.0210135 & -0.0280988 & -0.0332887 & -0.0369862 \\ -0.0130146 & -0.0163374 & -0.0186804 & -0.0172712 \\ -0.0052567 & -0.0019812 & 0.0012293 & 0.0037475 \\ -0.0223678 & -0.0342079 & -0.0418824 & -0.043054 \end{bmatrix}$$

$$W_s = \begin{bmatrix} -0.3242153 & -0.2210717 & -0.2005616 & -0.273146 \\ -1.1272841 & -1.1120762 & -1.1044034 & -1.092142 \\ 0.3896079 & 0.3995321 & 0.4373715 & 0.4820908 \\ 0.6208033 & 0.6569759 & 0.6137823 & 0.5062952 \end{bmatrix}$$

$$K = \begin{bmatrix} -6.1606949 & 5.4435459 & -14.456099 & 53.214836 \\ 4.1704143 & 13.62053 & -4.0775774 & -31.944519 \\ -9.9164149 & -12.267784 & -18.247316 & 33.716473 \\ 3.875054 & 3.1614239 & 31.649585 & 12.754786 \end{bmatrix}$$ where the eigenvalues are

$\lambda_1 = -1$, $\lambda_2 = -2$, $\lambda_3 = -3$, $\lambda_4 = -4$, $\lambda_5 = -5$, $\lambda_6 = -6$, $\lambda_7 = -4.649849$, $\lambda_8 = -37.149593$, $\lambda_9 = -0.9921309 + 3.8887332i$, $\lambda_{10} = -0.9921309 - 3.8887332i$, $\lambda_{11} = -0.4872684 + 0.2499814i$,

 © 2022 SBMAC

$\lambda_{12} = -0.4872684 - 0.2499814i$.

5 Conclusions

This article proposes an approach to resolve the eigenvalue assignment output feedback control problem for second-order systems using the Sylvester equations. So the matrices are simply prescribed in advance and highly dependent on the conditions of controllability and observability of the system where the eigenvalues are assigned. The numerical method presented applies to the active vibration control design of multiple inputs and outputs of practical engineering structures.

Acknowledgment

This work was suported by Comissão de Aperfeiçoamento de Pessoal do Nível Superior (CAPES) and Conselho Nacional de Desenvolvimento Científico e Tecnológico (CNPq).

References

[1] A. Bhaya and C. Desoer. "On the design of large flexible space structures (LFSS)". In: **IEEE Transactions on Automatic Control** AC30 (1985), pp. 1118–1120. DOI: 10.1016/0024-3795(93)90467-3.

[2] E. K. Chu and B. N. Datta. "Numerically robust pole assignment for second-order systems". In: **International Journal of Control** 64(4) (1996), pp. 1113–1127. DOI: 10.1080/00207179608921677.

[3] B. N. Datta, W. W. Lin, and J. N. Wang. "Robust and minimum gain partial pole assignment in vibrating structures with aerodynamics effects". In: **Proceedings IEEE Conf. Decision Control** 1 (2003), pp. 2358–2363. DOI: 10.1109/CDC.2003.1272971.

[4] E. R. L. Villarreal, J. A. V. Ruiz, and E. M. Hemerly. "Static Output Feedback Stabilization using Invariant Subspaces and Sylvester Equations". In: **TEMA Tend. Mat. Apl. Comput** 10 (1) (2009), pp. 99–110. DOI: 10.5540/tema.2009.010.01.0099.

[5] E. R. L. Villarreal, A. O. Salazar, and P. V. F. Vieira. "Approach to partial eigenvalue assignment using Sylvester equation in system-second order". In: **2021 IEEE International Conference on Automation/XXIV Congress of the Chilean Association of Automatic Control (ICA-ACCA)** 1 (2021), pp. 1–6. DOI: 10.1109/ICAACCA51523.2021.9465267.

[6] E. R. L. Villarreal et al. "Impulse elimination for singular second-order system: approach". In: **2021 IEEE International Conference on Automation/XXIV Congress of the Chilean Association of Automatic Control (ICA-ACCA)** 1 (2021), pp. 1–6. DOI: 10.1109/ICAACCA51523.2021.9465327.

[7] A. G. Wu et al. "Solving the generalized Sylvester matrix equation AV+BW=EVF via a Kronecker map". In: **Applied Mathematics Letters** 21 (10) (2008), pp. 1069–1073. DOI: 10.1016/j.aml.2007.12.004.

[8] J. Zhang, Y. Yuan, and H. Liu. "An Approach to Partial Quadratic Eigenvalue Assignment of Damped Vibration Systems Using Static Output Feedback". In: **International Journal of Structural Stability and Dynamics** 18(1) (2018), pp. 1–18. DOI: 10.1142/S0219455418500128.

 © 2022 SBMAC

Trabalho apresentado no XLI CNMAC, Unicamp - Campinas - SP, 2022.

Proceeding Series of the Brazilian Society of Computational and Applied Mathematics
Preprint

An Approach to Partial Quadratic Eigenvalue Assignment of Vibration Systems Using Sylvester equations

Elmer R. L. Villarreal [1]
Departamento de Ciências Naturais, Matemática e Estatística,
Universidade Federal Rural do Semi-árido DCME/UFERSA, Mossoró, RN.
Andres O. Salazar [2]
Departamento de Engenharia de Computação e Automação,
Universidade Federal do Rio Grande do Norte DCA/UFRN, Natal, RN.
Thiago F. do Nascimento [3]
Departamento de Engenharia de Computação e Automação,
Universidade Federal do Rio Grande do Norte DCA/UFRN, Natal, RN.
Lucas D. da Silva [4]
Engenharia Mecânica Centro de Engenharias ,
Universidade Federal Rural do Semi-árido EM/UFERSA, Mossoró, RN.
Walter M. Rodrigues [5]
Departamento de Ciências Naturais, Matemática e Estatística,
Universidade Federal Rural do Semi-árido DCME/UFERSA, Mossoró, RN.

Abstract. This article proposes an approach to resolve the partial eigenvalue assignment output feedback control problem for second-order damped vibration systems. The matrices are prescribed in advance and highly depend on controllability conditions, and the system's observability eigenvalues are assigned. In addition, the real value spectral decomposition $P(\lambda)$ is exploited to establish conditions so that the feedback gain matrices do not spill over eigenvalue assignment. Thus, the numerical method presented applies to the active vibration control design of multiple inputs and outputs of functional engineering structures. However, it should be noted that the proposed algorithm can present complex computational problems if the mass matrix of the system is almost singular, as it involves the inverse calculation of the mass matrix. Two theorems were presented using Sylvester equations. Three algorithms were implemented based on the Sylvester equation, and examples were presented with their conclusions.

Keywords. Sylvester equations, Partial eigenvalue assignment, Output feedback control.

1 Introduction

Second-order linear systems capture the dynamic behavior of many natural phenomena have therefore found applications in vibration and structural analysis. Second-order linear systems have found applications in fields such as spacecraft control and robotic control. Therefore, they have

[1]elmerllanos@ufersa.edu.br
[2]andres@dca.ufrn.br
[3]thiago.figueiredo@ufrn.br@dca.ufrn.br
[4]lucasdantas742@gmail.com
[5]walterm@ufersa.edu.br

 © 2022 SBMAC

attracted a lot of attention, in [1], [2], [3], [4], [5]. In [8] he presented an impulse elimination approach for partial assignment of eigenvalues to the descriptor system with the condition of $S-$controllability. In [7] presented an approach for assigning partial eigenvalues in second-order singular systems via proportional controller, derived control, and output feedback controller.

A solution of the generalized Sylvester equation is linked to a linear singular system subjected to any restriction on poles classification and regional placement. The problem of partially eigenvalue allocation for amortization vibrancy in the second-order system by static output feedback in [9]. In this note, it is considered that the controller follows a second-order singular linear system:

$$\begin{aligned} M_0\ddot{x} + D_0\dot{x} + N_0x &= Bu \\ y_0 &= C_0x \\ y_1 &= C_1\dot{x} \\ y_2 &= C_2\ddot{x} \end{aligned} \tag{1}$$

where $x \in \mathbb{R}^n$ and $u \in \mathrm{R}^m$ are the state vector and the control vector, respectively, and $M_0, D_0, N_0 \in \mathbb{R}^{n\times n}$, and $B \in \mathbb{R}^{n\times m}$, $C_0, C_1, C_2 \in \mathbb{R}^{p\times n}$ are the system coefficient matrices. In particular demand, the matrices M_0, D_0, and N_0 being denominated the mass matrix, the structural damping matrix and the stiffness matrix, respectively. The coefficient matrix satisfies the follow assumption. A_1: rank(M) $= q$, $0 < q \leq n$, $rank(B) = m$, and $rank(C_0) = rank(C_1) = rank(C_2) = p$.

As for the control of the second-order linear system (1), more of the results are focus on stabilization), pole assignment [3], [4], and partial pole assignment, [5]. In addition, several theoretical results for second-order systems are progressed over the convenient enlarged first-order singular state-space model. The system (1), is expressed in the form:

$$E_d\dot{z} = A_dz + B_du \tag{2}$$

with

$$E_d = \begin{bmatrix} I_n & 0 \\ 0 & M_0 \end{bmatrix} \; ; \; A_d = \begin{bmatrix} 0 & I \\ -N_0 & -D_0 \end{bmatrix} \; B_d = \begin{bmatrix} 0 \\ B \end{bmatrix} \tag{3}$$

$\dot{z} = \begin{bmatrix} \dot{x} \\ \ddot{x} \end{bmatrix}$ and $z = \begin{bmatrix} x \\ \dot{x} \end{bmatrix}$

Therefore, these results eventually involve manipulations on $2n$ dimensional matrices E_d, A_d and B_d.

The remaining of the paper is organized in the following Sections: Section 2 in presented problem formulation. Section 3 is presented Eigenstructure by Sylvester equation . Section 4 is presented Numerical Algorithm of Partial Eigenvalue Assignment by SOF (Static Output Feedback). Section 5 is presented Numerical Examples. Finally, Section 6 concludes the paper.

2 Problem formulation

For the second-order descriptor dynamical system (1), by choosing the following control law:

$$u(t) = -K_0y_0(t) - K_1y_1(t) - K_2y_2(t) \tag{4}$$

with $K_0, K_1, K_2 \in \mathbb{R}^{p\times n}$. It obtains the closed-loop system as follows:

 © 2022 SBMAC

$$(M_0 + BK_2C_2)\ddot{x} + (D_0 + BK_1C_1)\dot{x} + (N_0 + BK_0C_0)x = 0 \quad (5)$$

System (5) can be written in the first-order state-space form

$$E_c\dot{z} = A_c z; \quad (6)$$

with

$$E_c = \begin{bmatrix} I_n & 0 \\ 0 & (M_0 + BK_2C_2) \end{bmatrix} \quad and$$
$$A_c = \begin{bmatrix} 0 & I \\ -(N_0 + BK_0C_0) & -(D_0 + BK_1C_1) \end{bmatrix}$$

System (1) gives rise to the quadratic eigenvalue problem of the open-loop vibration system with solving the eigenvalues λ_f and the associated eigenvectors $x_f \neq 0$, which satisfy

$$P(\lambda_f)x_f = 0 \; f = 1, 2, \cdots 2n \quad (7)$$

where

$$P(\lambda) = \lambda^2 M_0 + \lambda D_0 + N_0 \quad (8)$$

By definition in [9],

$$\mu_i^2(M_0 + BK_2C_2)y_i + \mu_i(D_0 + BK_1C_1)y_i + (N_0 + BK_0C_0)y_i = 0, \; i = 1, 2, \cdots, p. \quad (9)$$

In general, the open-loop $2n$ eigenvalues are also called the open-loop poles of system (1). Correspondingly, the system (5) leads to the closed-loop quadratic eigenvalue problem.

$$P(\lambda)y = (\lambda^2(M_0 + BK_2C_2) + (D_0 + BK_1C_1)\lambda + (N_0 + BK_0C_0))y = 0 \quad (10)$$

3 Eigenstructure by Sylvester equation

The system (5) can be written in the first-order state-space form (6) and (7). Thus, for obtaining the output feedback matrix F $\sigma(E_p, A_p + B_pFC_p) \in \mathcal{C}^-$, is used the Sylvester equation in [6].

Consider the following linear time-invariant descriptor system in [6].

$$E_p\dot{x}(t) = A_p x(t) + B_p u(t) \quad (11)$$
$$y(t) = C_p x(t)$$

The Sylvester equations in [6].

$$A_pV_p - E_pV_pH_V = -B_pW_p, \qquad \sigma(H_V) \in \mathcal{C}^-. \quad (12)$$
$$P_pA_p - H_PP_pE_p = -U_pC_d, \qquad \sigma(H_P) \in \mathcal{C}^-. \quad (13)$$
$$P_pE_pV_p = 0 \quad (14)$$

The theorem 3.1 is based in [6], [9].

 © 2022 SBMAC

Theorem 3.1. *Let (1), be S-controllable, and $V_p \in \mathbb{R}^{n\times p}$ and $W_p \in \mathbb{R}^{m\times p}$ satisfy the equation (12). Then, the following hold.*

1) The matrices V_p and W_p given by (12),

$$\begin{bmatrix} A_p - \lambda_i E_p & B_p \\ P_p E_p & 0 \end{bmatrix} \begin{bmatrix} v_i \\ w_i \end{bmatrix} = 0 \; i = 1, 2, \cdots, q. \tag{15}$$

satisfy Sylvester matrix equation (12) for, $i = 1, 2, \cdots, q$,

2) When

$$rank(\begin{bmatrix} V_i \\ W_i \end{bmatrix}) = m \; i = 1, 2, \cdots, q. \tag{16}$$

hold, (14) gives all the solutions.

Proof. Based in [6]. □

4 Numerical Algorithm of Partial Eigenvalue Assignment by SOF

4.1 A sufficient condition and the associated matrix equation

For the acceleration, velocity and displacement output feedback, substituting $\Delta N = BK_0C_0$; $\Delta D = BK_1C_1$, $\Delta M = BK_2C_2$ in [9] is obtained

$$\begin{bmatrix} K_0 & K_1 & K_2 \end{bmatrix} \begin{bmatrix} \overline{C}_0 \\ \overline{C}_1 \\ \overline{C}_2 \end{bmatrix} = 0 \tag{17}$$

The matrices K_0, K_1, K_2 are obtain from the homogeneous matrix equation (17) in [9]. The coefficient matrix of (17) in [9] involves only those few eigenvalues and the corresponding eigenvectors to be assigned and the analytical matrices of the system (1), and is a real matrix. Let $rank(A) = q$, then the matrix equation 17 in [9] has non-trivial solutions.

4.2 Numerical algorithm

We first present an approach to the general solutions of (17) in [9] for K_0, K_1, K_2. It is to determine the left null space of the coefficient matrix A using the singular value decomposition. Let Q denote the matrix that its rows are comprised of orthonormal basis vectors of the null space, and it is has

$$[K_0, K_1, K_2] = VQ \tag{18}$$

where the parametric matrix V is to be determined below. Secondly, K_0, K_1, K_2 must also implement some given eigenvalues assignment. The projection is characterized by the parametric vector μ_i where

$$\mu_i = (\Gamma^T(\lambda_i)(\lambda_i))^{-1}\Gamma^T(\lambda_i)x_i \tag{19}$$
$$y_i = \Gamma(\lambda_i)\mu_i \tag{20}$$
$$w_i = \Phi(\lambda_i)\mu_i \tag{21}$$

 © 2022 SBMAC

$$V(N[\overline{CY}]) \quad = \quad \overline{W} \tag{22}$$

Equation (22) is of the form $ZE = S$, where S and E are given matrices of appropriate dimensions, and the matrix Z needs to be determined. The necessary and sufficient condition for the existence of solutions on this type of matrix equation is $SE^{+}E = S$ where the superscript $^{+}$ denotes the Moore-Penrose inverse of a matrix, and it is obtained the minimal S-norm solution

$$V \quad = \quad \overline{W}(N[\overline{CY}])^{+} \tag{23}$$

Substituting the obtained V back into (18), then output feedback gain matrices K_0, K_1, K_2 are eventually determined, in the closed-loop quadratic pencil $P(\lambda)$ of (8). When M_0 is nonsingular, this requirement guarantees that no impulses occur in the closed-loop system owing to infinite eigenvalues. It naturally involves with the problem of finding the distance of M_0 to the nearest singular matrix. The matrices K_0, K_1 and K_2 must also implement some given eigenvalues assignment. The theorem 4.1 is based in [6], [9].

Theorem 4.1. *Let (1), be S-controllable, and $V_p \in \mathbb{R}^{2n\times p}$ and $W_p \in \mathbb{R}^{m\times p}$ satisfy the equation (12). Then, the following hold.*

1) The matrices V_p and W_p given by (12),

$$\left[\begin{array}{cc} A_p - \lambda_i E_p & B_p \end{array}\right] \left[\begin{array}{c} v_i \\ w_i \end{array}\right] = 0 \; i = 1, 2, \cdots, q. \tag{24}$$

satisfy Sylvester matrix equation (12) for, $i = 1, 2, \cdots, q$,

2) When

$$rank(\left[\begin{array}{c} V_i \\ W_i \end{array}\right]) = m \; i = 1, 2, \cdots, q. \tag{25}$$

3) K_2, K_1, K_0 is such that it satisfies

$$\begin{aligned}(M_0 + B_p K_2 C_2)\ddot{q}(t) + (D_0 + B_p K_1 C_1)\dot{q}(t) + \\ (N_0 + B_p K_0 C_0)q(t) = 0\end{aligned} \tag{26}$$

Proof. Based in [6], [7], [8], [9]. □

Algorithm basic $Z1$ Input: M_0, D_0, N_0, B_p, C_0, C_1, C_2 Output: K_0, K_1, K_2

Step (1) Compute S_1 and the left null space Q of the coefficient matrix in Equation (18).

Step (2) Compute y_i, w_i, $i = 1, 2, \cdots, p$ by Equations (24), (25), (20) to form Y and W.

Step(3) Solve Equation (22) for V with Equation (23) after checking the existence of the solution.

Step (4) Substitute V back into Equation (18) to give K_0, K_1, K_2.

5 Numerical Examples

To demonstrate the performance of the present approach, two numerical examples are analyzed in this section. All codes are run in MATLAB with machine precision 10^{-16} on a personal computer.

Consider a simple linear dynamical system (1) with $M_0, D_0, N_0, B, C_0, C_1, C_2$ in [9].

 © 2022 SBMAC

Algorithm basic $Z1$ Input: M_0, D_0, N_0, B, C_0, C_1, C_2 Output: K_0, K_1, K_2

Step (1) Compute S_1 and the left null space Q of the coefficient matrix in Equation (18).

Step (2) Compute y_i, w_i, $i = 1, 2, \cdots, p$ by Equations (24), (25), (20) to form Y and W.

Step(3) Solve Equation (22) for V with Equation (23) after checking the existence of the solution.

Step (4) Substitute V back into Equation (18) with (21) to give K_0, K_1, K_2 and the matrix K_0, K_1,K_2 such that $K_2C_2V_2 = W_2$, $K_1C_1V_1 = W_1$, and $K_0C_0V_0 = W_0$,

$$V_0 = \begin{bmatrix} 0.0521304 & 0.0439039 & 0.0383248 & 0.0348497 \\ -0.076474 & -0.0719608 & -0.0708508 & -0.0726528 \\ 0.0070045 & 0.0070247 & 0.0066577 & 0.0061644 \\ 0.0043382 & 0.0040844 & 0.0037361 & 0.0028785 \\ 0.0017522 & 0.0004953 & -0.0002459 & -0.0006246 \\ 0.0074559 & 0.008552 & 0.0083765 & 0.0071757 \end{bmatrix}$$

$$W_0 = \begin{bmatrix} -0.3242153 & -0.2210717 & -0.2005616 & -0.273146 \\ -1.1272841 & -1.1120762 & -1.1044034 & -1.092142 \\ 0.3896079 & 0.3995321 & 0.4373715 & 0.4820908 \\ 0.6208033 & 0.6569759 & 0.6137823 & 0.5062952 \end{bmatrix}$$

$$K_0 = \begin{bmatrix} -6.1606949 & 5.4435459 & -14.456099 & 53.214836 \\ 4.1704143 & 13.62053 & -4.0775774 & -31.944519 \\ -9.9164149 & -12.267784 & -18.247316 & 33.716473 \\ 3.875054 & 3.1614239 & 31.649585 & 12.754786 \end{bmatrix}$$

where the eigenvalues are $\lambda_1 = -1$, $\lambda_2 = -2$, $\lambda_3 = -3$, $\lambda_4 = -4$, $\lambda_5 = -5$, $\lambda_6 = -6$, $\lambda_7 = -37.149593$, $\lambda_8 = -4.649849$, $\lambda_9 = -0.9921309 + 3.8887332j$ $\lambda_{10} = -0.9921309 - 3.8887332j$ $\lambda_{11} = -0.4872684 + 0.2499814j$, $\lambda_{12} = -0.4872684 - 0.2499814j$.

$$V_1 = \begin{bmatrix} 0.0446926 & 0.0374525 & -0.0291067 & -0.0236673 \\ -0.0783949 & -0.0746852 & 0.0726337 & 0.0678909 \\ 0.0038137 & 0.0046988 & -0.0012483 & -0.0011304 \\ 0.0060943 & 0.0051477 & -0.00533 & -0.0026561 \\ 0.0018332 & 0.000595 & -0.0000931 & 0.0001565 \\ 0.0069051 & 0.0089582 & 0.0038211 & 0.0050015 \end{bmatrix}$$

$$W_1 = \begin{bmatrix} 0.5059455 & -0.4979435 & 0.7124262 & 0.8776696 \\ -1.1048955 & -1.0545573 & 0.8970177 & 0.7237905 \\ 0.3395982 & 0.2477809 & -0.6899967 & -0.6205126 \\ 0.5704727 & 0.6765353 & 0.2266264 & 0.3581733 \end{bmatrix}$$

$$K_1 = \begin{bmatrix} 5.914908319.21919963.56123381.056327 \\ -1.85692637.5686617 - 39.087756 - 45.860668 \\ -11.322169 - 13.724264 - 107.3790129.407447 \\ 17.77522416.570007230.3076732.279694 \end{bmatrix}$$ where the eigenvalues are $\lambda_1 = -1$, $\lambda_2 = -2$, $\lambda_3 = -3$, $\lambda_4 = -4$, $\lambda_5 = -5$, $\lambda_6 = -6$, $\lambda_7 = -38.653889$, $\lambda_8 = -3.695664$, $\lambda_9 = -2.8420891 + .6086082j$ $\lambda_{10} = -2.8420891 - .6086082j$.

$$V_2 = \begin{bmatrix} 0.0488385 & 0.0403992 & -0.025387 & -0.0181925 \\ -0.0797826 & -0.0784526 & 0.0687017 & 0.0611566 \\ 0.0038728 & 0.0040052 & -0.0006003 & -0.0004777 \\ 0.0056806 & 0.005733 & -0.0052843 & -0.0023258 \\ 0.0017419 & 0.000654 & -0.0001266 & 0.0000899 \\ 0.0066251 & 0.0062879 & 0.0053903 & 0.0062784 \end{bmatrix};$$

$$W_2 = \begin{bmatrix} -0.440617 & -0.4841541 & 0.777753 & 0.9964393 \\ -1.1356319 & -1.1110555 & 0.8038804 & 0.5579771 \\ 0.3574743 & 0.3837874 & -0.7035365 & -0.5846476 \\ 0.5476882 & 0.4999696 & 0.3360751 & 0.449065 \end{bmatrix}$$

$$K_2 = \begin{bmatrix} 7.7654659 & 19.487249 & 1.609387 & 96.48342 \\ -3.4471017 & 5.1972494 & -58.282258 & -59.589812 \\ -4.6306656 & -8.6625354 & -57.413782 & 35.723326 \\ 9.2594212 & 10.475041 & 163.1129 & 29.705745 \end{bmatrix}$$ where the eigenvalues are

$\lambda_1 = -1$, $\lambda_2 = -2$, $\lambda_3 = -3$, $\lambda_4 = -4$, $\lambda_5 = -5$, $\lambda_6 = -6$,

$\lambda_1 = -3$, $\lambda_2 = -4$, $\lambda_3 = -22.229984$, $\lambda_4 = -0.509633$, $\lambda_5 = -1.5034249$, $\lambda_6 = -5.2611072$, $\lambda_7 = -4.1601947$, $\lambda_8 = -40.283544$, $\lambda_9 = -1.2514216 + 5.4279253j$. $\lambda_{10} = -1.2514216 - 5.4279253j$.

 © 2022 SBMAC

6 Conclusions

This article proposes an approach to resolve the partial eigenvalue assignment output feedback control problem for second-order damped vibration systems. So the matrices are simply prescribed in advance and highly dependent on the conditions of controllability and observability of the system where the eigenvalues are assigned. In addition, the real value spectral decomposition $P(\lambda)$ is exploited to establish conditions so that the feedback gain matrices do not spill over eigenvalue assignment. The numerical method presented applies to the active vibration control design of multiple inputs and outputs of practical engineering structures.

Acknowledgment

This work was suported by Comissão de Aperfeiçoamento de Pessoal do Nível Superior (CAPES) and Conselho Nacional de Desenvolvimento Científico e Tecnológico (CNPq).

References

[1] J. M. Araujo et al. "State derivative feedback in second-order linear systems: A comparative analysis of perturbed eigenvalues under coefficient variation". In: **Mechanical Systems and Signal Processing** 76-77 (2016), pp. 33–46. DOI: 10.1016/j.ymssp.2016.02.014.

[2] M. J. Balas. "Trends in large space structure control theory: Fondest hopes, wildest dreams". In: **IEEE Transactions on Automatic Control** 27 (3) (1982), pp. 522–535. DOI: 10.1109/TAC.1982.1102953.

[3] A. Bhaya and C. Desoer. "On the design of large flexible space structures (LFSS)". In: **IEEE Transactions on Automatic Control** AC30 (1985), pp. 1118–1120. DOI: 10.1016/0024-3795(93)90467-3.

[4] E. K. Chu and B. N. Datta. "Numerically robust pole assignment for second-order systems". In: **International Journal of Control** 64(4) (1996), pp. 1113–1127. DOI: 10.1080/00207179608921677.

[5] B. N. Datta, W. W. Lin, and J. N. Wang. "Robust and minimum gain partial pole assignment in vibrating structures with aerodynamics effects". In: **Proceedings IEEE Conf. Decision Control** 1 (2003), pp. 2358–2363. DOI: 10.1109/CDC.2003.1272971.

[6] E. R. L. Villarreal, J. A. V. Ruiz, and E. M. Hemerly. "Static Output Feedback Stabilization using Invariant Subspaces and Sylvester Equations". In: **TEMA Tend. Mat. Apl. Comput** 10 (1) (2009), pp. 99–110. DOI: 10.5540/tema.2009.010.01.0099.

[7] E. R. L. Villarreal, A. O. Salazar, and P. V. F. Vieira. "Approach to partial eigenvalue assignment using Sylvester equation in system-second order". In: **2021 IEEE International Conference on Automation/XXIV Congress of the Chilean Association of Automatic Control (ICA-ACCA)** 1 (2021), pp. 1–6. DOI: 10.1109/ICAACCA51523.2021.9465267.

[8] E. R. L. Villarreal et al. "Impulse elimination for singular second-order system: approach". In: **2021 IEEE International Conference on Automation/XXIV Congress of the Chilean Association of Automatic Control (ICA-ACCA)** 1 (2021), pp. 1–6. DOI: 10.1109/ICAACCA51523.2021.9465327.

[9] J. Zhang, Y. Yuan, and H. Liu. "An Approach to Partial Quadratic Eigenvalue Assignment of Damped Vibration Systems Using Static Output Feedback". In: **International Journal of Structural Stability and Dynamics** 18(1) (2018), pp. 1–18. DOI: 10.1142/S0219455418500128.

 © 2022 SBMAC

Trabalho apresentado no XLI CNMAC, Unicamp - Campinas - SP, 2022.

Proceeding Series of the Brazilian Society of Computational and Applied Mathematics
Preprint

Stabilization in semiactive systems using Sylvester equations: Approach

Maxwell C. Jácome [1]
Instituto Federal do Rio Grande do Norte
Campus João Câmara IFRN,
BR-406 KM 73 3500 Perímetro Rural, João Câmara - RN.
Lucas D. da Silva [2]
Engenharia Mecânica Centro de Engenharias ,
Universidade Federal Rural do Semi-árido EM/UFERSA, Mossoró, RN.
Andrés O. Salazar [3]
Departamento de Engenharia de Computação e Automação,
Universidade Federal do Rio Grande do Norte DCA/UFRN, Natal, RN.
Walter M. Rodrigues
[4]Departamento de Ciências Naturais, Matemática e Estatística,
Universidade Federal Rural do Semi-árido DCME/UFERSA, Mossoró, RN.
Elmer R. L. Villarreal [5]
Departamento de Ciências Naturais, Matemática e Estatística,
Universidade Federal Rural do Semi-árido DCME/UFERSA, Mossoró, RN.

Abstract. Active suspension systems for the vehicle control problem are formulated using output feedback. The present article proposes solving the output feedback control with eigenvalues for active suspension systems using Sylvester equations. The matrices are prescribed in advance and depend greatly on the controllability conditions, being assigned the system's observability eigenvalues. The theorems were presented using Sylvester equations. The algorithm was implemented based on Sylvester equation, and an example was presented with their conclusions.

Keywords. Sylvester equations, Eigenvalue assignment, Output feedback control, semi-active suspension systems.

1 Introduction

In moving mechanical systems, efforts are always made to reduce the influence of unwanted vibrations. In the case of automotive vehicles, the system responsible for such action is that of suspension. Not only in terms of comfort, but this system is necessary also for the safety and stability of the vehicle in maneuvers and when driving on terrains uneven. From the restrictions of projects with passive suspensions, whose parameters are fixed, and with the progress in technological and microelectronics development, as well as in the field of new actuators, active damper systems have

[1]maxwellc.jacome@gmail.com
[2]lucasdantas742@gmail.com
[3]andres@dca.ufrn.br
[4]walterm@ufersa.edu.br
[5]elmerllanos@ufersa.edu.br

 © 2022 SBMAC

evolved more and more, increasing the efficiency of these equipments and demanding, therefore, strategies of control of in order to provide an adequate action from the motion sensors. Allied to that, the development of control systems and its importance in the stability of systems mechanics (such as active suspension and control of flexible structures) motivate the study of efficient control techniques [4]. The semi-active system tries to vary the damping coefficient instead of a constant damping of the passive system. This is the main system that combines simplicity of control and quality in stabilization. The objective of this work is to develop the modeling of a control system of a semi-active damping system based on Sylvester's equations.

The remaining of the paper is organized in the following Sections: Section 2 in presented problem formulation. Section 4 Semi-active suspension systems is presented. Section 5 is presented Eigenstructure by Sylvester equation Sylvester. Section 6 is presented Numerical Algorithm of Eigenvalue Assignment by SOF (Static Output Feedback) and numerical example. Finally, Section 6 concludes the paper.

2 Problem formulation and control

Vehicle suspension plays a fundamental role concerning the level of passenger comfort. The mathematical model of a suspension system vehicle representing a quarter of a vehicle is used by most bibliographies available on the subject. The motion equation for the suspended mass is described by equation (1), where M_2 is the mass of a quarter car, k_f is the spring coefficient, d_s is the displacement of M_2 and d_r is the displacement of the wheel, spring and damper system.

$$M_2\ddot{d}_s = -k_f(d_s - d_r) - B_a(\dot{d}_s - \dot{d}_r) \tag{1}$$

The motion equation for the unsprung mass is described by equation (2), where M_1 is the mass of the system composed of the wheel, spring and damper.

$$M_1\ddot{d}_r = k_f(d_s - d_r) + B_a(\dot{d}_s - \dot{d}_r) - k_p(d_r - d_p) \tag{2}$$

Applying the state space model to Equation (1) and Equation (2), we arrive at the following state equation:

$$\begin{aligned} \dot{z}(t) &= A_p z(t) + B_p u(t) \\ y(t) &= Cz(t) \end{aligned} \tag{3}$$

with

$$A_p = \begin{bmatrix} 0 & 1 & 0 & 0 \\ -\frac{k_f}{M_1} & \frac{-B_a}{M_1} & \frac{k_f}{M_1} & \frac{B_a}{M_1} \\ 0 & 0 & 0 & 1 \\ -\frac{k_f}{M_2} & \frac{B_a}{M_2} & \frac{-(k_p+k_f)}{M_1} & \frac{-B_a}{M_2} \end{bmatrix}$$

$$B_p = \begin{bmatrix} 0 \\ 0 \\ 0 \\ \frac{k_p}{M_2} \end{bmatrix}.$$

Let the the normal dynamical system (4)

$$\begin{aligned} \dot{x}(t) &= Ax(t) + Bu(t) \\ y(t) &= Cx(t) \end{aligned} \tag{4}$$

Therefore, n dimensional matrices $A \in \mathbb{R}^{n\times n}$, state space $B \in \mathbb{R}^{n\times m}$ input matrix and $C \in \mathbb{R}^{p\times n}$ output matrix .

DOI: 10.5540/03.2022.009.01.0310 © 2022 SBMAC

For the normal dynamical system (4), by choosing the following control law:

$$u(t) = -Ly(t) \tag{5}$$

with $L \in \mathbb{R}^{p\times n}$. It obtains the closed-loop system as follows:

$$\begin{aligned} \dot{x}(t) &= (A + BLC)x \\ y(t) &= Cx(t) \end{aligned} \tag{6}$$

Modern control is based on differential equations in the form of state space, and introduced to the control area from the 1960s onwards [1], [3]. Designing a controller for a dynamic system requires a model that represents the system's dynamic response. Most systems physics are complex and non-linear. Generally, the design needs to be based on a simplified but robust version of the model so that the control meets the performance requirements when applied to the actual device. In closed-loop control, the system includes a sensor to measure the output signal. The data acquired by the sensor is feedback to the controller that makes a comparison with the reference; the result of this comparison is the plant error. The controller sends a control effort signal to act on the process control variable from the error. A feature of both types of systems is the presence of the actuator. The actuator is a device that somehow influences the process control variable and receives the control effort signal directly from the controller in [3].

3 Semi-active suspension system

Active suspension systems the vehicle is described in [2]. Semi-Active Suspension Control Design for Vehicles is described in [4]. In a Semi-active suspension system, varying the damping coefficient of the shock absorber or spring constant through electronic control without inputting external energy to the system, except the device control that changes the damping coefficient or the elastic constant characterizes a semi-active suspension; mostly of the cases, the damping coefficient of the dissipative element in the system varies semi-active in [4]. In Figure (1), it is observed the semi-active suspension model. Where d_p, d_r and d_s represent the vertical displacements of the tire, wheel, and body, respectively. The spring is represented by its spring constant k_f and the damper by its coefficient B_a, while the constant k_p represents the tire elasticity. The masses of the body and wheel are respectively represented by M_1 and M_2.

Note that the semi-active suspension system is quite similar to the passive suspension system. The difference is that in the passive system the parameter B_a is constant, while in the semi-active system the B_a is variable, allowing the implementation of a control system to determine its value. Regarding the motion equations and state-space model of this example, both are the same as the passive suspension system. The only difference is that none of the parameters are changed in practice in the latter. In the semi-active suspension system, these parameters can be changed. Regarding the simulation, both the systems adjust the parameters in advance. Therefore, the simulation of both does not have considerable differences. There are several devices to implement a semi-active suspension system. In order to exemplify, here are three devices that are already used commercially: by the automotive industry: electro-hydraulic (EH), magnetorheological dampers (MR) and electrorheological (ER). EH dampers can be distinguished from traditional dampers due to the presence of electronic solenoid valves in your model, unlike of the conventional model that features only passive valves. These solenoid valves can vary the damping coefficient by changing the size of its orifices which, in turn, allow a greater or lesser flow of the fluid between the device's compression and traction chambers in [4].

 © 2022 SBMAC

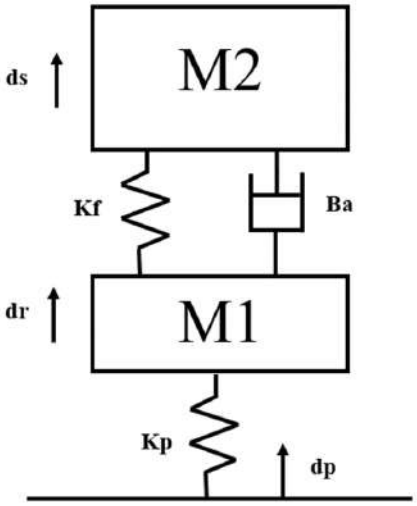

Figure 1: Model of semi-active suspension system of a car room.

The state equations, to obtain the state matrix A, the matrix input B , output matrix C , and forward transition matrix D.

$$\begin{aligned} \dot{x}(t) &= Ax(t) + Bu(t) \\ y(t) &= Cx(t) + Du(t) \end{aligned} \tag{7}$$

4 Eigenstructure by Sylvester equation

Consider the following linear time-invariant descriptor system in [5].

$$\begin{aligned} E_s\dot{x}(t) &= A_s x(t) + B_s u(t) \\ y(t) &= C_s x(t) \end{aligned} \tag{8}$$

The Sylvester equations in [5].

$$A_s V_s - E_s V_s H_V = -B_s W_s, \qquad \sigma(H_V) \in \mathcal{C}^- \tag{9}$$

$$T_s A_s - H_T T_s E_s = -U_s C_s, \qquad \sigma(H_T) \in \mathcal{C}^- \tag{10}$$

$$T_s E_s V_s = 0 \tag{11}$$

Consider the $E_s = I_n$.

The system (4) can be written in the first-order state-space form (9), (10) (11). Thus, for obtaining the output feedback matrix K $\sigma(E_s, A_s + B_s K C_s) \in \mathcal{C}^-$, is used the Sylvester equation in [5].

The theorem 4.1 is based in [5], [7].

Theorem 4.1. *Let the system (8), be S-controllable, and $V_s \in \mathbb{R}^{n\times p}$ and $W_s \in \mathbb{R}^{m\times p}$ satisfy the equation (9). Then, the following hold.*

1) The matrices V_s and W_s given by (12),

 © 2022 SBMAC

$$\begin{bmatrix} A_s - \lambda_i E_s & B_s \\ T_s E_s & 0 \end{bmatrix} \begin{bmatrix} v_i \\ w_i \end{bmatrix} = 0 \; i = 1, 2, \cdots, q. \tag{12}$$

satisfy Sylvester matrix equation (9) for, $i = 1, 2, \cdots, q$,

2) When

$$rank(\begin{bmatrix} V_i \\ W_i \end{bmatrix}) = m \; i = 1, 2, \cdots, q. \tag{13}$$

hold, (11) gives all the solutions.

Proof. Based in [5]. □

Theorem 4.2. *Let* $E_s, A_s \in \mathbb{R}^{n\times n}$, $B_s \in \mathbb{R}^{n\times m}$, $H_V \in \mathbb{R}^{p\times p}$ *satisfy*

$$rank[A_s - \lambda E_s \; B_s] = n, \quad for \; any \; \lambda \in \sigma(H_V). \tag{14}$$

Further, let $H \in \mathbb{R}^{(n+m)\times m}[\lambda]$ *be a polynomial matrix satisfying* $[A_s - \lambda E_s \; B_s]H(\lambda) = 0_{n\times m}$.

Then:

(1) The matrices $V_s \in \mathbb{R}^{n\times p}$ *and* $W_s \in \mathbb{R}^{m\times p}$ *given by*

$$\begin{bmatrix} V_s \\ W_s \end{bmatrix} = Syl(H(\lambda), H_V, Z) \tag{15}$$

satisfy the matrix equation (9) for any matrix $Z \in \mathbb{R}^{m\times p}$. *(2) When* $rank H(\lambda) = r$ *for any* $\lambda \in \sigma(H_V)$, *all the matrices* V_s *and* W_s *satisfying the matrix equation (9) can be explicitly expressed by (15).*

Proof. Based in [5] and [6]. □

5 Numerical Algorithm

Let $G(\lambda)$ and X be defined as

$G(\lambda) = [A_s - \lambda E_s \; B_s]$; $X = \begin{bmatrix} V_s \\ W_s \end{bmatrix}$

The following basic procedure is proposed to calculate the feedback controller that stabilizes the closed loop system, when $m + p > n$. Closed loop eigenvalues are positioned arbitrarily close to the set ; they are symmetric sets of pre-specified eigenvalues. The (E_s, A_s, B_s, C_s) system is considered to be strongly controllable and strongly detectable.

Algorithm

Step 1: Choose an array $H_T \in \mathbb{R}^{q-p\times q-p}$ such that $\sigma(H_T) = \Lambda_T \in \mathcal{C}^-$ and Sylvester equation (10) is solved to find a matrix $T_s \in \mathbb{R}^{q-p\times n}$ such that

$$rank \left(\begin{bmatrix} T_s E_s \\ C_s \end{bmatrix} \right) = q \tag{16}$$

Step 2: Sylvester equation (9) is solved, for some $H_V \in \mathbb{R}^{p\times p}$ matrix such that $\sigma(H_V) = \Lambda_V \in \mathcal{C}^-$ taking into account that the matrix V_s must check the condition of the coupling (11) and taking into account that $rank\,(E_s V_s) = p$ .The condition (16) guarantees, in particular, that $rank(T_s E_s) = q$.

 © 2022 SBMAC

Step 3: By construction, the matrix V_s must verify that rank $(C_sV_s) = p$ and the matrix K can be calculated by:

$$K \quad = \quad W_s(C_sV_s)^{-1} \tag{17}$$

$\diamond$

Remark 5.1. *steps* 1 *and* 2 *can be solved using standard techniques for positioning the self-structure. Similar to the previous case, the matrices* V_s *and* W_s *used for the calculation of* K *can be constructed only with real elements. In particular: if* $\lambda_i\mathcal{C}^-$*, it is considered* $\lambda_{i+1} = \lambda_i^*$ *e* $\begin{cases} V_i = Re\,(v_i), & V_{i+1} = Imag\,(v_i) \\ W_i = Re\,(w_i), & W_{i+1} = Imag\,(w_i) \end{cases}$*, where* V_i *and* W_i *denote the columns of the matrices* V_s *and* W_s*, respectively.*

In step 1, under the condition that the system is strongly observable (detectable). As will be seen later, degrees of freedom existing in the choice of V_s that satisfy the coupling condition $T_sE_sV_s = 0$, can also be used to guarantee obtaining K such that $KC_sV_s = W_s$ in [5].

5.1 Example

Consider a simple linear dynamical system (4) with $M_1 = 40$; $M_2 = 450$; $B_a = 1.2$; $k_f = 30$; $k_p = 160$; in the matrizes A, B, C :

$$A = \begin{bmatrix} 0 & 1 & 0 & 0 \\ -\frac{k_f}{M_1} & \frac{-B_a}{M_1} & \frac{k_f}{M_1} & \frac{B_a}{M_1} \\ 0 & 0 & 0 & 1 \\ -\frac{k_f}{M_2} & \frac{B_a}{M_2} & \frac{-(k_p+k_f)}{M_1} & \frac{-B_a}{M_2} \end{bmatrix}$$

$$B = \begin{bmatrix} 0 & 0 \\ 0 & \frac{-1}{M_1} \\ 0 & 0 \\ \frac{k_p}{M_2} & \frac{1}{M_2} \end{bmatrix};$$

$$C = \begin{bmatrix} 1 & 0 & 0 & 0 \\ 0 & 0 & 1 & 0 \\ 0 & 0 & 0 & 1 \end{bmatrix};$$

Thus the matrizes A, B, C are following:

$$A = \begin{bmatrix} 0 & 1 & 0 & 0 \\ -0.75 & -0.03 & 0.75 & 0.03 \\ 0 & 0 & 0 & 1 \\ 0.0667 & 0.0027 & -0.4222 & -0.0027 \end{bmatrix}$$

$$B = \begin{bmatrix} 0 & 0 \\ 0 & -0.0250 \\ 0 & 0 \\ 0.3556 & 0.0022 \end{bmatrix};$$

$$C = \begin{bmatrix} 1 & 0 & 0 & 0 \\ 0 & 0 & 1 & 0 \\ 0 & 0 & 0 & 1 \end{bmatrix};$$

Algorithm basic

Resolved the equation (9) for calculate the matrices W_s, V_s, satisfies the equation (17) and the matrix K, such that $KC_sV_s = W_s$:

$T_s = \begin{bmatrix} -0.3851 & 0.3970 & -0.9512 & -0.0095 \end{bmatrix}$

 © 2022 SBMAC

$$V_s = \begin{bmatrix} -0.0045 & -0.0023 & -0.0014 & -0.0014 \\ 0.0090 & 0.0069 & 0.0055 & 0.0055 \\ 0.0057 & 0.0039 & 0.0030 & 0.0030 \\ -0.0113 & -0.0118 & -0.0119 & -0.0119 \end{bmatrix}$$

$$W_s = \begin{bmatrix} 0.0650 & 0.0985 & 0.1314 & 0.1641 \\ 0.9978 & 0.9950 & 0.9912 & 0.9864 \end{bmatrix}$$

$$K = \begin{bmatrix} -134.4978 & -177.1450 & -41.1356 \\ -35.5740 & -20.1672 & -83.9791 \end{bmatrix}$$ where the eigenvalues are $\lambda_1 = -1$, $\lambda_2 = -2$, $\lambda_3 = -3$, $\lambda_4 = -8.8859$.

6 Conclusions

This paper proposes solving the output feedback control problem with eigenvalues for a semi-active suspension system using Sylvester equations. Thus, the matrices formulated are simply prescribed in advance and highly dependent on the controllability and observability conditions of the system where the eigenvalues are assigned. The numerical method presented applies to the control design of the semi-active suspension system with multiple inputs and outputs.

Acknowledgment

This work was suported by Comissão de Aperfeiçoamento de Pessoal do Nível Superior (CAPES) and Conselho Nacional de Desenvolvimento Científico e Tecnológico (CNPq).

References

[1] R. C. Dorf and Bishop R. H. **Sistemas de controle modernos**. LTC, 2009. ISBN: 9788521617143.

[2] S. P. Dutra. **Controle H-infinito de sistemas de suspensão ativa veicular**. UFSC Joinville, 2016.

[3] K. Ogata. **Engenharia de controle moderno**. Pearson Prentice Hall, 2011. ISBN: 9788576058106.

[4] S. M. Savaresi et al. **Semi-Active Suspension Control Design for Vehicles**. Elsevier Science, 2010. ISBN: 9780080966793.

[5] E. R. L. Villarreal, J. A. V. Ruiz, and E. M. Hemerly. "Static Output Feedback Stabilization using Invariant Subspaces and Sylvester Equations". In: **TEMA Tend. Mat. Apl. Comput** 10 (1) (2009), pp. 99–110. DOI: 10.5540/tema.2009.010.01.0099.

[6] A. G. Wu et al. "Solving the generalized Sylvester matrix equation AV+BW=EVF via a Kronecker map". In: **Applied Mathematics Letters** 21 (10) (2008), pp. 1069–1073. DOI: 10.1016/j.aml.2007.12.004.

[7] J. Zhang, Y. Yuan, and H. Liu. "An Approach to Partial Quadratic Eigenvalue Assignment of Damped Vibration Systems Using Static Output Feedback". In: **International Journal of Structural Stability and Dynamics** 18(1) (2018), pp. 1–18. DOI: 10.1142/S0219455418500128.

 © 2022 SBMAC

One Cycle Control Applied to a Three-Phase PWM Rectifier

1st Rodrigo de Andrade Teixeira
Department of Computer Engineering and Automation,
Federal University of Rio Grande do Norte (DCA-UFRN)
Natal, Brazil
email : rodrigoandradeteixeira@gmail.com

2nd Andres Ortiz Salazar
Department of Computer Engineering and Automation
Federal University of Rio Grande do Norte (DCA-UFRN)
Natal, Brazil
email : andres@dca.ufrn.br

3rd Elmer Rolando Llanos Villarrreal
Department of Natural Sciences, Mathematics, and Statistics
Federal Rural University of Semi-arid (DCME-UFERSA), Mossoró, RN, 59625-900, Brazil
Mossoró, Brazil
email: elmerllanos@ufersa.edu.br

4th Werbet Luiz Almeida Da Silva
Department of Computer Engineering and Automation
Federal University of Rio Grande do Norte (DCA-UFRN)
Natal, Brazil
email: werbethluizz@hotmail.com

5th João Teixeira de Carvalho Neto
The Federal Institute of Education, Science and Technology
of Rio Grande do Norte (IFRN)
Natal, Brazil
email: joao.teixeira@ifrn.edu.br

***Abstract*—This work has as proposal the use of the one-cycle control technique to control a three-phase rectifier based on the boost topology, without the use of voltage sensors at the coupling point of the system. In addition, unlike most of the work developed with the OCC technique the digital implementation using *DSP TMS320F28335* from Texas Instruments was used. The objective of the proposed implementation is to obtain a sinusoidal current at the rectifier input with a power factor as close as possible to unity, while the rectifier output is controlled at a fixed voltage value. To evaluate the proposed system, simulations were performed and the practical results were verified using a laboratory prototype.**

***Index Terms*—component, formatting, style, styling, insert**

I. Introdução

In power quality two of the main concerns are excessive harmonic content and low PF power factor. A high harmonic content can cause undue actuation of protection devices, on the other hand, a low power factor decreases the active power made available by the network. In the last decades several studies have been done in the area of power quality, especially to meet the IEC61000-3-4 and IEEE-519-1992 standards.

Several control loop-based methods have been proposed to achieve unity power factor in PWM rectifiers, in these cases, for input current to follow the reference voltage it is necessary to detect the three-phase grid voltages, the DC-side voltage, the three-phase currents and eventually it is necessary to use a PLL-type synchronization circuit. Control techniques based on this concept usually use SVM vector modulation, Park/Clark transforms and control with coupled terms such as VOC, DPC [1], MPC [2], fuzzy control [3] and neural networks [4].

The one-cycle control (OCC) technique is a resistor emulation method originally based on [5] hardware, implemented by some commercial ICs. Originally the technique uses variable amplitude carrier and addition and subtraction operations, which results in a control technique with great arithmetic simplicity and fast dynamic response.

Although OCC has been applied several times in APF active power filters [6] and [7], FACT transmission systems [8], grid-connected PV inverters GCI [9] [10] and [11], the OCC presented problems [5], [12], [13], which to solve them required adding extra circuitry to the system, complicating control and reducing the simplicity of the hardware. To solve OCC-related problems and preserve its fast dynamic response, DSP-emulated OCC control was proposed in [14]. This version increases the calculability of OCC and makes it possible to use the technique in more complex control problems than hardware-OCC [15], [16].

II. Control Strategy

One-loop control can be used in resistance emulation in three-phase converters. The following shows how the technique can be applied to control the waveforms of the currents at the input of a three-phase rectifier circuit with boost topology. Given the three-phase rectifier shown in Figure 1, it is considered that:

- The three-phase system to which the rectifier is connected is balanced and symmetrical; semiconductor switches in each arm operate in a complementary way; average value

of the input voltage $v_g(t)$ and of the phase current $i_g(t)$ are zero;

- The switching frequency is fixed and much higher than the line frequency.

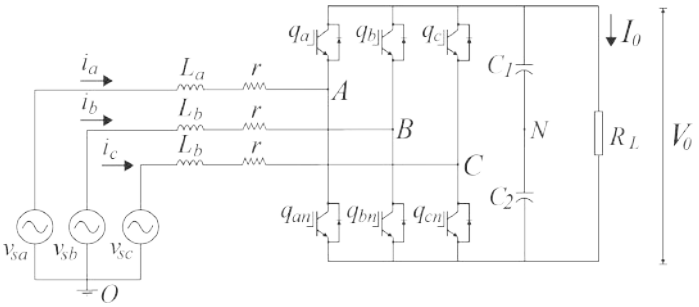

Fig. 1. PWM Three-Phase Rectifier

In one-cycle control it is assumed that the converter operates in continuous conduction mode with a small current variation, as a consequence the average current is proportional to the phase current [3] Equation 1. In this expression i_{gs} is the average phase current and K_1 is an introduced constant given in Ohm.

$$\frac{L}{T}\int i_g dt = K_1 i_{gs} = V_0(1 - d_{gn}) \tag{1}$$

In a controlled rectifier the equivalent input impedance must behave as a resistance R_e, furthermore, the link-DC voltage must also be regulated at a fixed value v_{ref}. In this sense, to solve both problems the constant K_1 can be seen as an emulated resistance R_e Equation 2.

$$R_e i_{gs} = V_0(1 - d_{gn}) \tag{2}$$

Although Equation 2 relates the duty cycle to the average of the phase currents this expression does not fully represent the OCC proposal. In this sense, the best way to represent the OCC PWM modulator is through the key drive expression.

$$q_{gn} = \begin{cases} 1 & \text{se} \quad i_{gs} \geq \frac{V_0}{R_e} A_{tri}(t) \\ 0 & \text{se} \quad i_{gs} < \frac{V_0}{R_e} A_{tri}(t) \end{cases}$$

The previous expression is based on the essence of the OCC method since the switches are activated when i_{gs} is greater than or equal to the variable amplitude carrier $v_0 A_{tri}(t)/R_e$. The average control current can be obtained using an integrator circuit or a low-pass filter as commented earlier. However, unlike conventional methods in this approach an advance-delay compensator LLC is used as the method of calculating the average controlled current [16]. The function of the LLC Equation 3 is to average the phase current without phase angle delays.

$$\frac{I_{gs}(s)}{I_g(s)} = G_0 \frac{(1 + s\tau_1)}{(1 + s\tau_2)} \tag{3}$$

The block diagram of the control system is shown in Figure 2. The average phase currents are obtained through the LLC controllers, the emulated resistance R_e is obtained at the output of the PI controller used for voltage regulation of the link-DC, and the maximum and minimum limiters are used at the controller output to limit the average values of the phase currents. The minimum resistor R_{emin} controls the maximum average current and the maximum resistor R_{emax} controls the minimum average current. The control signal is divided by the link-DC voltage, and then it is multiplied by the average of the phase currents obtained at the outputs of the *LLC* controllers. The resulting multiplication signals are compared with the triangular carrier $A_{tri}(t)$ to obtain the command pulses of the semiconductor switches.

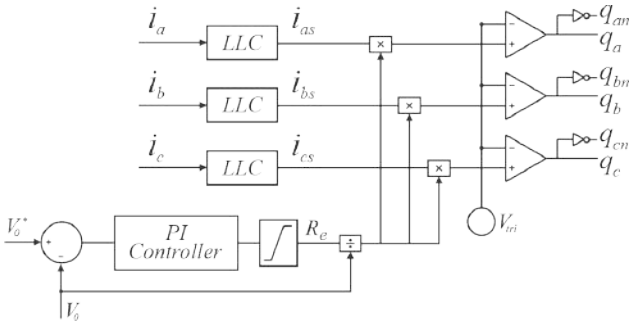

Fig. 2. OCC Block Diagram

III. System Parameters

The objective of the control system is to make the output voltage follow the reference independently of disturbances in the grid voltage and variations in the load current. In this sense, the studied converter was analyzed by simulation in permanent regime and when subjected to disturbances in the input voltage and variations in the load current. The converter was also analyzed operating at high load and no load. In these conditions stability was achieved by varying the parameters of the LLC controller and the maximum emulated resistor limiter R_{emax}.

The stability of the system was analyzed by simulation and the practical performance was observed on an experimental platform (Figure 3) that uses a TMS320F28335 type digital signal controller and a supervisory system implemented in Labview. The model of the rectifier circuit used in the tests is shown in Figure 1 and the parameter values of the simulated and experimentally verified rectifiers are arranged in Tables I and II. The time constants of the LLC controllers, the switching frequency f_s and the maximum and minimum values of the emulated resistors at the rectifier input for the simulation tests are arranged in Tables III and IV.

TABLE I
Simulation and Experimental Parameters - Network and Circuit.

Parameter	$R(\Omega)$	$\omega(rad/s)$	$L(mH)$	$C_1(uF)$
Simulation	1	377	1	470
Experimental	1	377	1	2200

Fig. 3. Experimental Platform

TABLE II
SIMULATION AND EXPERIMENTAL PARAMETERS - NETWORK AND CIRCUIT.

Parameter	$C_2(uF)$	$v_{sg}(V)$
Simulation	470	110
Experimental	2200	21

TABLE III
SIMULATION PARAMETERS - CONTROL.

Parameter	τ_1	τ_2	$f_s(kHz)$
Parameters 1	$1,1e^{-3}$	$2,5e^{-3}$	10
Parameters 2	$0,5e^{-3}$	$1,8e^{-3}$	10

TABLE IV
SIMULATION PARAMETERS - CONTROL.

Parâmetro	R_{emin}	R_{emax}
Parameters 1	$0,8376$	$1,9942$
Parameters 2	$0,1$	1000

A. Simulation and Experimental Results

B. Simulation Results

In Figures 4 and 5 the simulation results of the link-DC voltage for the startup conditions and for load variations on the rectifier are shown. In Figure 4 the system startup transient is shown, while in Figures 5, 6 and 7 are shown respectively the voltage variation of the link-DC for a load increase of 50%, the voltage variation in the link-DC for a load reduction of 50%, and the fine adjustment of the voltage controller during the stabilization of the link-DC voltage at the reference value.

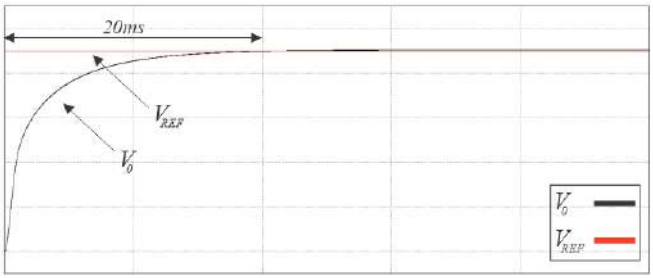

Fig. 4. Entry into Operation

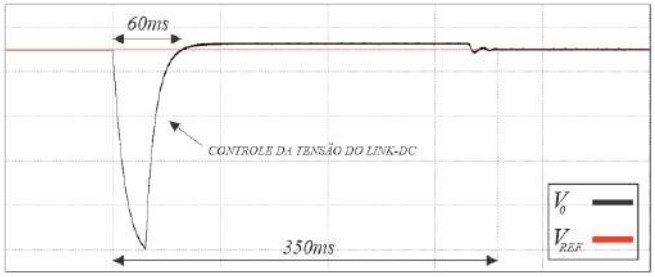

Fig. 5. Load increase 50%

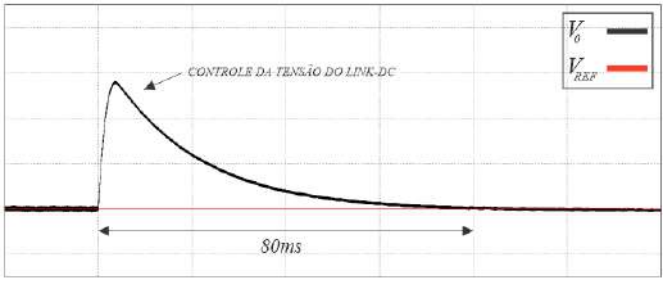

Fig. 6. Load reduction 50%

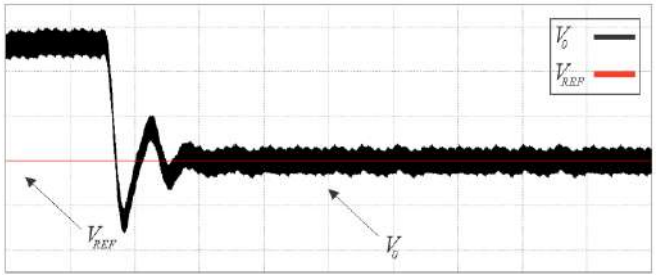

Fig. 7. Fine tuning V_0

Figures 8 and 9 show the simulation results for the emulated resistance R_e and the input and output currents of the rectifier circuit during load increase and decrease transients.

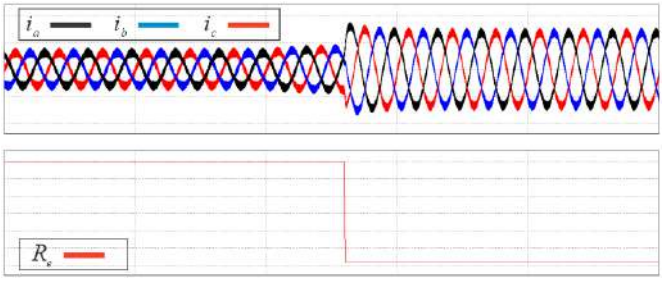

Fig. 8. i_{abc} e R_e.

Figures 8 and 9 show the simulation results for the emulated resistance R_e and the input and output currents of the rectifier circuit during transients of increase and reduction of load.

In Figure 9 the phase currents and emulated resistance at the input of the circuit during load reduction are shown, while in

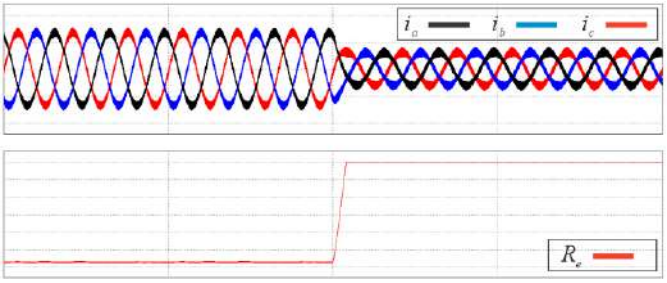

Fig. 9. i_{abc} e R_e.

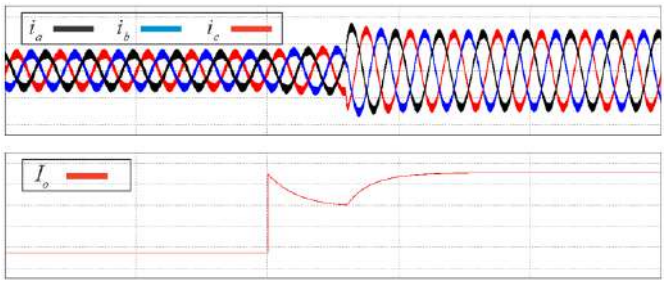

Fig. 10. i_{abc} e I_0.

Figure 11 the direct relationship between the input and output currents of the rectifier circuit.

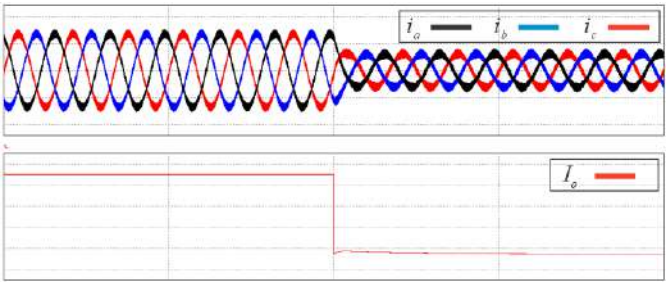

Fig. 11. i_{abc} e I_0.

C. Experimental Results

The experimental result shown in Figure 12 shows voltage and current in phase at the connection point of the rectifier circuit with phase A. The high distortion in the input voltage was not observed in the simulation results Figures 13 and 14 due to ideal simulation characteristics.

Figure 15 shows the three currents at the input of the rectifier and the sum of these currents. In this figure it is possible to see the distortion present in the input currents of the circuit, this distortion can also be observed in Figures 13 and 14 obtained by simulation.

Figure 16 shows one of the experimental results obtained during the startup of the rectifier circuit. This figure shows the load current I_0, the resistance R_e, the voltage and current at the point of connection of the rectifier with phase A. Observing the figure, it is possible to see the proportional relationship between the load current and phase currents observed in

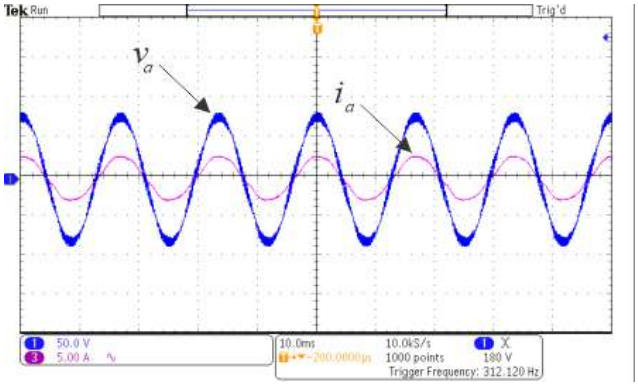

Fig. 12. Phase A voltage and current. $V_{Sg} = 50V/div$. $I_g = 5A/div$

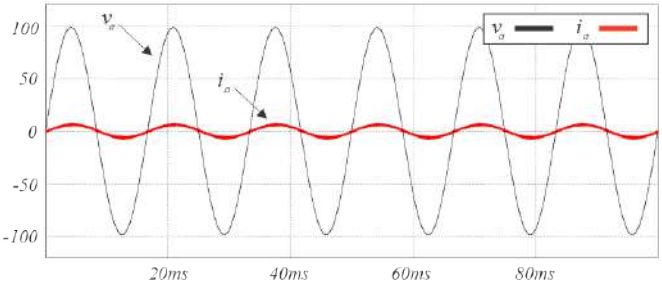

Fig. 13. Voltage and current (Phase A) operation at high load. $V_{Sg} = 110V$. $V_o = 450V$. $Vert.: 50V/div$. $Hor.: 20ms/div$

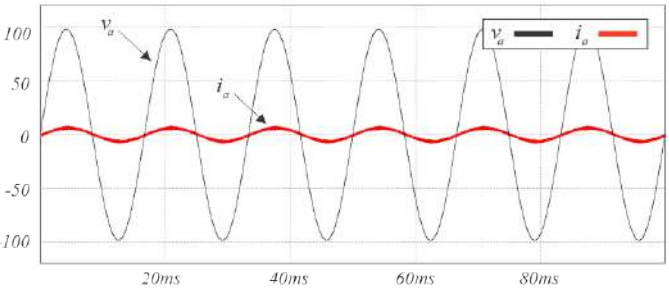

Fig. 14. Voltage and current (Phase A) low load operation. $V_{Sg} = 110V$. $V_o = 450V$. $Vert.: 50V/div$. $Hor.: 20ms/div$

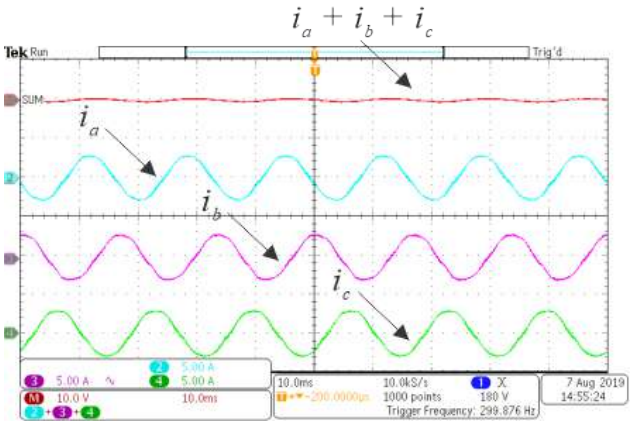

Fig. 15. Sum of phase currents and ABC phase currents. $SUM = 5A/div$. $I_g = 5A/div$

Figures 10 and 11. It is also possible to notice the reduction of R_e during the load increase transient, this characteristic was also observed in the simulation result of Figure 8. Observing the phase current and voltage waveforms it is possible to see the rapid adjustment of the current in phase A after the system goes into operation, this fast adjustment is in accordance with the control of a cycle, also observed during the transients of load of Figures 8 and 9. The start-up transient shown in Figure 16 and commented earlier can be seen in more detail in Figure 17.

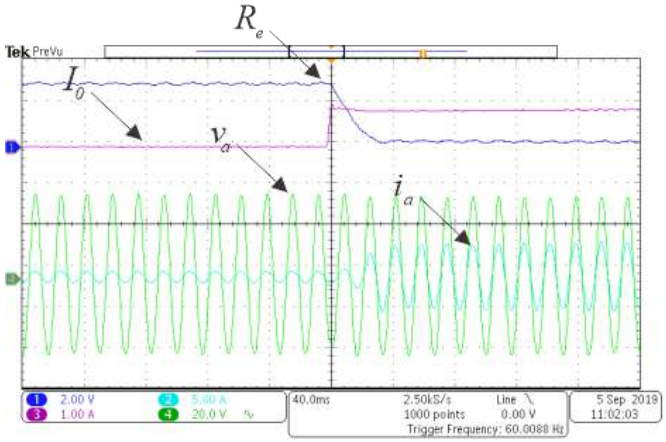

Fig. 16. Transition from no load to high load. $I_L = 1A/div$. $I_o = 5A/div$. $R_e = 2V/div$. $V_{Sg} = 20V/div$

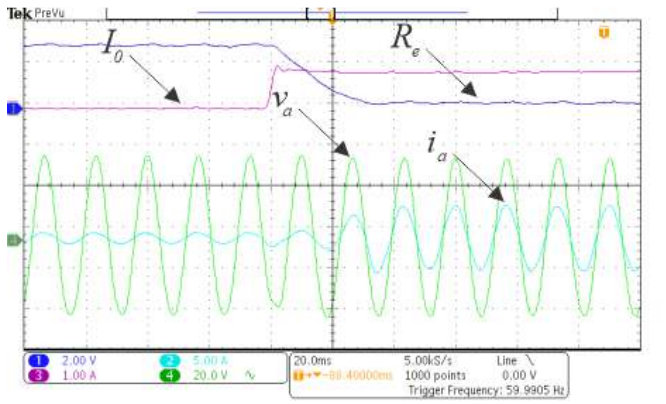

Fig. 17. Transition from no load to high load. $I_L = 1A/div$. $I_o = 5A/div$. $R_e = 2V/div$. $V_{Sg} = 20V/div$

Figure 18 shows one of the experimental results obtained during the circuit's load-drop transient. This figure also shows the load current I_0, the resistance R_e, the phase A voltage and current during the transient. Observing this figure it is also possible to see the proportional relationship between the load current and the phase currents observed in Figures 10 and 11.

Still in relation to Figure 18 it is possible to notice the increase of R_e during this transient, this characteristic was also observed in the simulation result of Figure 9. Regarding the phase voltage and current for this operating condition, as

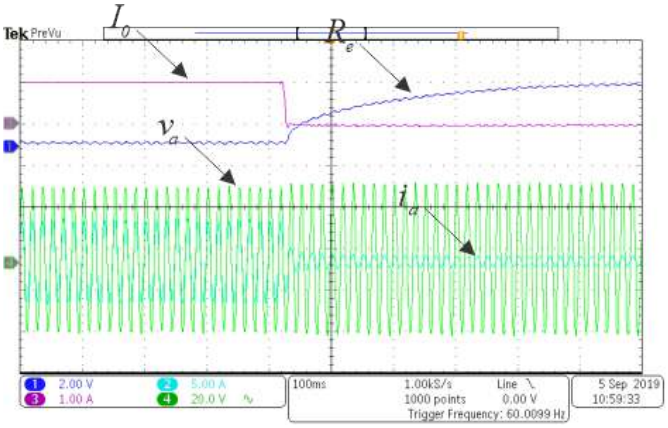

Fig. 18. Transient high load to no load. $I_L = 1A/div$. $I_o = 5A/div$. $R_e = 2V/div$. $V_{Sg} = 20V/div$

well as the results obtained for the circuit input into operation Figures 16 and 17, the system quickly adjusted the phase current, this adjustment is also in accordance with the control of a cycle. The load shedding transient shown in Figure 18 can be seen in more detail in Figure 19.

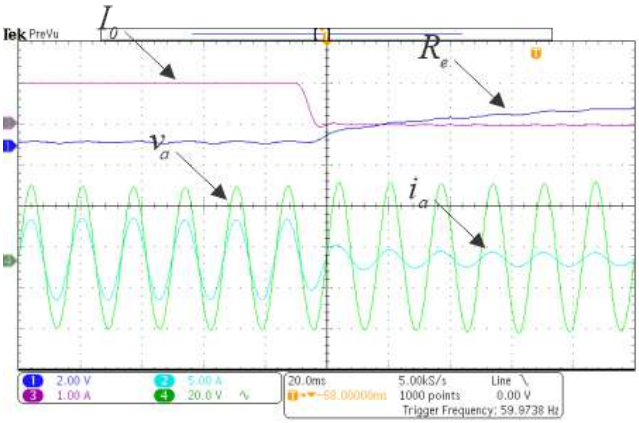

Fig. 19. Transient high load to no load. $I_L = 1A/div$. $I_o = 5A/div$. $R_e = 2V/div$. $V_{Sg} = 20V/div$

IV. Conclusion

The simulation results showed that the implemented control behaves stably during the start-up transients and load variation. The start-up transients showed stabilization time around $20ms$ (1 cycle) with a maximum of $1s$ (60 cycles) for setting the output voltage to the reference value. The load swing transients had settling times of at most $80ms$ (5 cycles) with a maximum time of $350ms$ (20 cycles) for the DC-link voltage to reach the reference. During the analysis of the results, the fast dynamics of the phase currents of the circuit in accordance with the *OCC* technique became clear.

The experimental results initially showed the emulation of the resistance R_e of the converter circuit. It was also possible to see the proportional relationship between phase and load currents during the system load transients. In addition to

these characteristics, it was also possible to note the direct relationship between the resistance effectively emulated at the input of the rectifier circuit and the phase and load currents during transients.

ACKNOWLEDGMENT

This work was suported by Comissão de Aperfeiçoamento de Pessoal do Nível Superior (CAPES) and Conselho Nacional de Desenvolvimento Científico e Tecnológico (CNPq).

REFERENCES

[1] Mohammad Monfared, Hassan Rastegar, and Hossein Madadi Kojabadi. High performance direct instantaneous power control of pwm rectifiers. *Energy Conversion and Management*, 51(5):947–954, 2010.

[2] Abdelouahab Bouafia, Jean-Paul Gaubert, and Fateh Krim. Design and implementation of predictive current control of three-phase pwm rectifier using space-vector modulation (svm). *Energy Conversion and Management*, 51(12):2473–2481, 2010.

[3] Juan W Dixon, Jose M Contardo, and Luis A Moran. A fuzzy-controlled active front-end rectifier with current harmonic filtering characteristics and minimum sensing variables. *IEEE Transactions on Power Electronics*, 14(4):724–729, 1999.

[4] Resul Coteli, Hakan Acikgoz, Ferhat Ucar, and Besir Dandil. Design and implementation of type-2 fuzzy neural system controller for pwm rectifiers. *international journal of hydrogen energy*, 42(32):20759–20771, 2017.

[5] Chongming Qiao and Keyue Ma Smedley. Unified constant-frequency integration control of three-phase standard bridge boost rectifiers with power-factor correction. *IEEE Transactions on Industrial Electronics*, 50(1):100–107, 2003.

[6] Chongming Qiao and Keyue Ma Smedley. Three-phase bipolar mode active power filters. *IEEE Transactions on Industry Applications*, 38(1):149–158, 2002.

[7] Chongming Qiao, Taotao Jin, and Keyue Ma Smedley. One-cycle control of three-phase active power filter with vector operation. *IEEE Transactions on Industrial Electronics*, 51(2):455–463, 2004.

[8] Taotao Jin, Lihua Li, and Keyue Ma Smedley. A universal vector controller for four-quadrant three-phase power converters. *IEEE Transactions on Circuits and Systems I: Regular Papers*, 54(2):377–390, 2007.

[9] Yang Chen and Keyue Ma Smedley. A cost-effective single-stage inverter with maximum power point tracking. *IEEE transactions on power electronics*, 19(5):1289–1294, 2004.

[10] Mario Fortunato, Alessandro Giustiniani, Giovanni Petrone, Giovanni Spagnuolo, and Massimo Vitelli. Maximum power point tracking in a one-cycle-controlled single-stage photovoltaic inverter. *IEEE Transactions on Industrial Electronics*, 55(7):2684–2693, 2008.

[11] Yang Chen and Keyue Smedley. Three-phase boost-type grid-connected inverter. *IEEE Transactions on Power Electronics*, 23(5):2301–2309, 2008.

[12] Dharmraj V Ghodke, ES Sreeraj, Kishore Chatterjee, and BG Fernandes. One-cycle-controlled bidirectional ac-to-dc converter with constant power factor. *IEEE Transactions on Industrial Electronics*, 56(5):1499–1510, 2009.

[13] Keyue M Smedley, Luowei Zhou, and Chongming Qiao. Unified constant-frequency integration control of active power filters-steady-state and dynamics. *IEEE Transactions on Power Electronics*, 16(3):428–436, 2001.

[14] Alberto Soto Lock, Edison R da Silva, Malik E Elbuluk, and Darlan A Fernandes. A hybrid current control for a controlled rectifier. In *2010 IEEE Energy Conversion Congress and Exposition*, pages 920–926. IEEE, 2010.

[15] Alberto Soto Lock, Malik E Elbuluk, Edison R da Silva, and Darlan A Fernandes. Torque control of induction motor drives based on one-cycle control method. In *2012 IEEE Industry Applications Society Annual Meeting*, pages 1–8. IEEE, 2012.

[16] Alberto Soto Lock, Edison Roberto Cabral da Silva, Malik E Elbuluk, and Darlan A Fernandes. An apf-occ strategy for common-mode current rejection. *IEEE Transactions on Industry Applications*, 52(6):4935–4945, 2016.

Proceeding Series of the Brazilian Society of Computational and Applied Mathematics

Controle MPC com Atrasos e Perdas de Pacotes

Elmer Rolando Llanos Villarreal[1]
Departamento de Ciências Naturais, Matemática e Estatística,
Universidade Federal Rural do Semi-árido, 59625900, Mossoró, RN, Brasil.
Rosana Cibely Batista Rego[2]
Centro Multidisciplinar de Pau dos Ferros
Universidade Federal Rural do Semi-árido,
59625900, Mossoró, RN, Brasil.
Xiankleber Cavalcante Benjamin[3]
Departamento de Engenharia de Computação e Automação
Universidade Federal de Rio Grande do Norte,
59078-970, Natal, RN, Brasil.
Andrés Ortiz Salazar[4]
Departamento de Engenharia de Computação e Automação
Universidade Federal de Rio Grande do Norte,
59078-970, Natal, RN, Brasil.
Alberto Soto Lock[5]
Departamento de Engenharia Elétrica
Universidade Federal Paraiba, 58051-900, João Pessoa, PB, Brasil.
Carlos Ramon Pantaleon Dionisio[6]
Faculdade de Computação
Universidade Federal Uberlandia, 38400-902, Uberlandia, MG, Brasil.

Resumo. Este artigo estuda o modelo de controle preditivo dos sistemas de controle em rede sem fio, onde podem ocorrer atrasos e perdas indesejáveis induzidas arbitrariamente pelo sistema wifi , em ambos os controles do controlador e controlador para o atuador. É proposto um modelo aumentado, que é especialmente adequado à lei de controle por realimentação de saída , com base em qual proposta de MPC em sistema de controle em rede sem fio é proposta estendendo o anterior para WCS com apenas perdas de pacotes. Mostra-se que a estabilidade proposta é garantida pela estabilidade fechada, satisfazendo as restrições de entrada, de estado e saída. **Palavras-chave**. Sistema de controle em rede sem fio, Realimentação de saídas, Controle Peditivo.

Este artigo tem como objetivo contribuir para a melhoria da solução do controle de processos com atraso. Dá-se ênfase aos problemas associados ao controle de processos com atrasos e restrições, quando se utilizam controladores preditivos baseados em modelo. A escolha do modelo de predição é o ponto chave no MPC: um bom projeto deve buscar obter o melhor modelo possível, que deve ser completo o suficiente para capturar adequadamente a dinâmica do processo e permitir o cálculo das predições da saída do processo, ser intuitivo e ao mesmo tempo permitir uma análise teórica do sistema. As diferentes

[1]elmerllanos@ufersa.edu.br
[2]cibely@gmail.com
[3]xiankleber@dca.ufrn.br
[4]andres@dca.ufrn.br
[5]aslock@cear.ufpb.br
[6]carlos.dionisio@ufu.br

estratégias de MPC utilizam diferentes formas para representar as relações entre entradas manipuladas, perturbações e saídas do processo. Estimar, a cada instante de tempo discreto , uma predição da saída do processo por exemplo é o horizonte de predição. Esta predição se realiza com base em um modelo do processo, e depende dos valores conhecidos (das entrada e saídas passadas) até o instante tempo t e dos valores da sequência de incrementos dos sinais de controle futuro. Estabelecer uma trajetória de referência para a saída, sobre o horizonte de predição. Calcular a seqüencia de ações de controle futuro. Aplicar ao processo apenas o primeiro elemento da sequência de incrementos de ações futuras de controle, desprezando o restante dos valores. As técnicas do controlador MPC são particularmente interessantes para tratar o problema de controle sob restrições. O propósito principal do controlador MPC é aplicar a melhor ação de controle possível minimizando uma determinada função de custo, em [4]. Os sistemas de controle em rede sem fio (WNCS) são sistemas de controle em que a malha de controle é fechado nos sistemas em rede sem fio . A inserção do sistema de rede sem fio não traz apenas as vantagens para a implementação física, mas também alguns problemas desafiadores, como atrasos induzidos pelo sistema de rede sem fio, distúrbios de pacotes, perdas de pacotes e quantizações de dados. Assim, as teorias de controle convencionais para sistemas de controle ponto-a-ponto devem ser reavaliadas antes de aplicá-las aos (WNCS). Nos últimos anos, várias metodologias foram propostas para modelagem, análise de estabilidade e projeto de controladores para (WNCS). O Controle Preditivo Baseado em Modelo (Model Predictive Control, MPC) refere-se a uma classe de estratégias de controle onde, em cada instante de amostragem, um problema de otimização deve ser resolvido para obter as políticas de controle para a corrente e um período de tempo futuro. A solução ideal é usada para gerar o movimento de controle atual. Em [3], um modelo aumentado de ciclo fechado e a abordagem de síntese correspondente ao controlador MPC são dadas para o sistema WNCS com perdas de pacotes limitadas no sensor para controlador (SC) e o controlador para atuador (CA). Este trabalho tem como objetivo generalizar os principais resultados para incorporar atrasos limitados. Para a lei de controle invariante no tempo, [5] e [9] combinaram os atrasos SC e CA. No entanto, para a lei de controle MPC atualizada on-line , a abordagem de combinar os atrasos em ambos os sistemas não é favorável. No controlador MPC, uma vez que o controlador deve estimar quando os dados recebidos foram enviados e prever quando o comando de controle que chegará ao atuador, é necessário analisar os atrasos nos dois sistemas, respectivamente. Em [6], um modelo de sistema linear de salto é fornecido com base em cadeias de Markov, onde os atrasos em ambos os sistemas em rede sem fio são considerados respectivamente, mas o controle MPC é arbitrário. Para obter a matriz de realimentação de saídas K foi usado os artigos de [1] e [7]. O artigo está dividido da seguinte maneira. A Seção 2 estabelece o modelo de $WNCS$ e o resultado básico de estabilidade, apresenta-se os teoremas para obter a matriz de realimentação de saídas K. A Seção 3 aborda a abordagem de síntese do MPC em sistemas em rede sem fio. Finalmente, a seção 4 apresenta algumas observações finais. Notação: I é a matriz de identidade com dimensão apropriada. Para qualquer vetor x e a matriz W, $x_W^2 := x^T W x$. $x(k+i|k)$ é o valor do vetor x num tempo futuro $k+i$ previsto no tempo k. O símbolo $*$ é usado para induzir matrizes simétricas. Um valor com o sobrescrito $*$ corresponde à solução ideal do problema de otimização.

1 Modelagem de WNCS com atrasos e perdas de pacote

Conforme ilustrado na Figura 1 abaixo, a planta é

$$x(k+1) = Ax(k) + Bu(k), k \geq 0 \quad (1)$$

$$y(k) = Cx(k) \quad (2)$$

onde A, B e C são matrizes constantes de dimensões apropriadas; $u(k) \in R^m$, $x(k) \in R^n$ e $y(k) \in R^p$ são o controlador o estado da planta e a saída, respectivamente. $\tilde{u}(k) \in R^m$ e $\tilde{x} \in R^n$ são o controlador e o estado da planta, respectivamente. Os seguintes pressupostos são válidos neste artigo.

- (i) Os dados x e $\tilde{u}$ são marcados com o tempo.
- (ii) O sensor deve ser accionado , isto é, envia $x(k)$ para a rede em cada instante de amostragem k.
- (iii) O controlador é conduzido por eventos, ou seja, na amostra instantânea k, se e somente se buffer 1 recebe novos dados, então o controlador escolhe os dados com o último período e, se o controlador recebe dados com um aumento de tempo, então ele calcula o movimento de controle.
- (iv) O atuador é conduzido por eventos, ou seja, no momento de amostragem k, se o buffer 2 receber novos dados, o atuador escolhe os dados com o último período e, se o atuador receber dados com um aumento de hora, então atualiza a entrada da planta.

Para o sistema SC, são considerados os atrasos induzidos pelo sistema em rede sem fio, distúrbios de pacotes e perdas de pacotes. Assim, os seguintes quatro casos podem acontecer.

- (i) Não há nenhum pacote chegando no buffer 1. O movimento de controle não é calculado.
- (ii) Existe um pacote de dados que chega ao buffer 1. Se o tempo-limite desses dados for posterior ao dos dados utilizados anteriormente, esses dados são utilizados pelo controlador para calcular o movimento de controle.
- (iii) Mais de um pacote de dados chegar ao buffer 1. O controlador escolhe os dados com o último período e executa como no caso (ii).
- Existe um pacote de dados que chega ao buffer 1. Se o tempo desses dados for normal ao dos dados utilizados anteriormente, esses dados não são utilizados pelo controlador para calcular o movimento de controle.

Para o sistema CA, os atrasos induzidos pelo sistema em rede sem fio, As distúrbios de pacotes e as perdas de pacotes são consideradas. Assim, de forma semelhante, deve ser obtida a sequência de tempo $I_0 := \{i_1, i_2, i_3, ...\}$, onde $i_l (l \geq 1)$ é o ponto de tempo quando o atuador atualiza o controle para a planta. Defina (como o índice tal que $u(\eta)$ é $\tilde{u}(\eta)$. é claro que $(\eta_{i_l} \in \Gamma_0$. Seja $\tau_1 := max_{j_l \in \Gamma_0}(j_l - k_{j_l})$ e $\tau_2 := max_{i_l \in I_0}(i_l - \eta_{i_l})$ são os limites máximos de atraso máximo em sistemas SC e CA, respectivamente. Se $\tau_1 = \tau_2 = 0$, o controlador e o atuador nunca utilizam os dados com tempo atrasado. Sejam d_1 e d_2 os limites máximos de perda de pacotes máximos nos sistemas SC e CA, respectivamente em [3]. Correspondientemente, $d_1 + \tau_1 := max_{j_l, j_{l+1} \in J_0}(j_{l+1} - j_l)$ e $d_2 + \tau_2 := max_{i_l, i_{l+1} \in I_0}(i_{l+1} - i_l)$ são limites de intervalo intermitente máximo em sistemas SC e CA, respectivamente.

Definição 1.1. *[2] O processo de atraso limitado é definido como* $\{\rho_{sc}(j_l) := j_l - k_{j_l} | j_l \in \Gamma_0\}$, $\{\rho_{ca}(i_l) := i_l \in \Gamma_0\}$ *onde* $P_{sc}(j_l)$ *e* $P_{ca}(i_l)$ *tomam valores nos conjuntos finitos* $\Im_1 := \{0, 1, ..., \tau_1\}$ *e* $\Im_2 := \{0, 1, ..., \tau_2\}$, *respectivamente.*

Definição 1.2. *[2] O processo de intervalo intermitente limitado é definido como* $\{\eta_{s-c}(j_l) := j_{l+1} - j_l | j_l, j_{l+1} \in \Gamma_0\}$, $\eta_{sc}(j_l) := i_{l+1} - i_l | i_l, i_{l+1} \in \Gamma_0\}$ *onde* $\eta_{sc}(j_l)$ *e* $\eta_{c-a}(i_l)$ *tomam valores nos conjuntos finitos* $M_1 := \{1, 2, ..., d_1 + \tau_1\}$ *e* $M_2 := \{1, 2, ..., d_2 + \tau_2\}$, *respectivamente.*

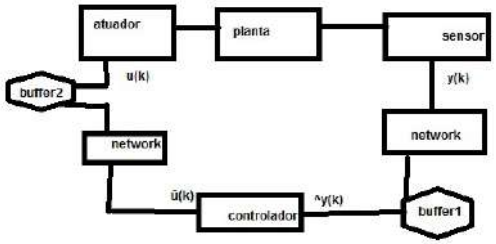

Figura 1: Sistemas de controle em rede sem fio com atrasos

1.1 Sequências de tempo em sistema em malha fechada

Com base nas análises acima, são encontradas as sequências de dados que são utilizadas pelo controlador e a planta, respectivamente. No entanto, alguns dados correspondentes às duas sequências podem não afetar o sistema em malha fechada. Há duas razões para isso. Primeiro, se $\{u(i_l), u(i_{l+1}), \ldots, u(i_{l+c})\}$ são os mesmos que $\tilde{u}$ calculou-se (então $\tilde{u}(\zeta_{i_l}), \tilde{u}(\zeta_{i_{l+1}}), ..., \tilde{u}(\zeta_{i_{l+c}})$ não afetam o sistema em malha fechada. Em segundo lugar, se $\tilde{u}(j_s)$ é descartado ou perdido, então $\tilde{x}(j_s)$ não afeta o sistema em malha fechada. Vamos definir $I := \{i_1, i_2, i_3, ...\}$ e $J := \{j_1, j_2, j_3, ...\}$ para que $\tilde{u}(\eta_{i_n})$ e $\tilde{x}(j_n)(n \geq 1)$ representem completamente os dados que afetam o sistema em malha fechada . Sejam I e J que satisfazem

a) $I \subseteq \{i_1, i_2, i_3\}$, $J \subseteq \{j_1, j_2, j_3\}$;

b) para qualquer número inteiro $c > 0$, se e somente se $\zeta_{i_{c+l}} \neq \zeta_{i_c}$ então $i_{c+l} \in I$. Especialmente, $i_{c+l} \in I$;

c) $j_s \in I_0$ se somente existe $l \geq 1$ tal que $\zeta_{i_l} = j_s$ então $i_{c+l} \in I$. Especialmente, $i_{c+l} \in I$;

É mostrado que $\{j_r, i_r\}$ é um par que satisfaz $j_r = \zeta_{i_r}$ e $j_r \leq i_r$ para todo $r \geq 1$.

Proposição 1.1. *Considerando o tempo t onde I_t é a sequência de tempo $I_0 := \{i_1, i_2, i_3, ...\}$, onde $i_l (l \geq 1)$ é o ponto de tempo quando o atuador atualiza o controle para a planta. Para os atrasos limitados e as perdas de pacotes conforme definido nas definições (1.1)–(1.2) ,*

$$j_r - k_{j_r} \in \Im_1 \tag{3}$$
$$i_r - j_r + 1 \in M_2 \tag{4}$$
$$i_r - k_{j_r} + 1 \in \tau_3 \tag{5}$$
$$i_{r+1} - i_r, i_{r+1} - j_r, i_r - k_{j_r} \in M_3 \tag{6}$$

onde $\tau_3 := \{1, 2, ..., \tau_1 + \tau_2 + d_2\}$ e $M_3 := \{1, 2, ..., \tau_1 + \tau_2 + d_2 - 1\}$.

O Teorema a seguir estabelece à existência de uma lei de controle do tipo realimentação estática de saídas $u = Fy$ que estabiliza o sistema em malha fechada. O referido teorema foi adaptado em tempo discreto. A aplicação do Teorema abaixo é aplicado em uma região circular de raio unitário, denotada por $\mathcal{C}^s = \{\lambda \in \mathcal{C}; |\lambda| < 1\}$, que corresponde à estabilidade no caso de sistemas discretos no tempo.

Teorema 1.1. *[1] Existe uma matriz de realimentação de saídas $K : \mathcal{Y} \longrightarrow \mathcal{U}$ tal que $\sigma(A + BKC) \in \mathcal{C}^s$, se e somente se as seguintes condições são verificadas para algumas matrizes $(V \in \Re^{n \times v}, H_V \in \Re^{v \times v}, W \in \Re^{m \times v})$, $(T \in \Re^{n-v \times n}, H_T \in \Re^{n-v \times n-v}, U \in$*

$\Re^{n-v\times v}$) *e para algum escalar positivo* $v \leq n$*:*

$$\begin{aligned} AV - VH_V &= -BW \ , \quad com\ \sigma(H_V) \in \mathcal{C}^s && (7)\\ TA - H_T T &= -UC \ , \quad com\ \sigma(H_T) \in \mathcal{C}^s && (8)\\ TV &= 0 && (9)\\ Ker\,(CV) &\subseteq Ker\,(W) && (10)\\ Ker\,(B'T') &\subseteq Ker\,(U') && (11) \end{aligned}$$

onde: $posto\,(V) = v$ *e* $posto\,(T) = n - v$ *.* □

Observação 1.1. *Então existe uma matriz por realimentação de saídas* K *que satisfaz as equações de Sylvester expressas nas equações (7), (8), (9), (10) e (11).*

1.2 Modelo em malha fechada no WCS e resultados

Seja o sistema (1), (2) com a lei de controle por realimentação de saídas dado no Teorema (1.1)

$$u = Ky = FCx \tag{12}$$

Suponha a lei de controle $\tilde{u} = K\tilde{y}$ onde K é projetado. Em cada j_l, o controlador calcula $\tilde{u}(j_l)$. Para $j_l \leq K_{j_{l+1}}$, $\tilde{u}(k) = \tilde{u}(j_l)$ é enviado para a rede. Assim o controlador $\tilde{u}(j_l)$ pode ser ou não ser aplicado na planta, da qual o controlador não conhece a priori. Considerando a entrada de controle $u(i_r) = K\tilde{y}(j_r) = Ky(k_{j_r}) = FCx(k_{j_r})$ e as definições de I e J o sistema em malha fechada para todos os $k \geq i_1$ torna-se

$$\begin{aligned} x(k+1) = A^{k-i_r+l}x(i_r) + B_{k-i_r+l}KCx(k_{j_r}),\\ i_r \leq k \leq i_{r+l} \end{aligned} \tag{13}$$

onde $B_j = \sum_{s=0}^{j-1} A^S B$ para qualquer número inteiro $j > O$.

De acordo com a Proposição (1.1), um número de modelos determinísticos diferentes $d_1(\tau_1+\tau_2+d_2)+\frac{1}{2}(\tau_1+\tau_2+d_2)(\tau_1+\tau_2+d_2-1)$ podem ser desenhados de (13). Semelhante a [3], [2], defini-se $z(k) = [x(k)^T x(k_l)^T x(k-2)^T \dots x(k-\tau_1-\tau_2-d_2+l)^T]^T$ e levando em consideração todos os modelos determinísticos, (13) pode ser re-escrito como o seguinte modelo com o estado aumentado $z(i_r)$.

$$\begin{aligned} z(i_r) = \Phi(i_r)z(i_r),\ \Phi(i_r) = \sum_{p\in\tau}\sum_{t\in\tau_3} \omega_p(i_r)\lambda_t(i_r)\Phi_{pt},\\ \omega_p(i_r) = \begin{cases} 1, & i_{r+1} - i_r = p \\ 0, & de\ outra\ forma \end{cases}\\ \lambda_t(i_r) = \begin{cases} 1, & i_r - kj_r + 1 = t \\ 0, & de\ outra\ forma \end{cases} \end{aligned} \tag{14}$$

onde $\tau(t) = \{1, 2, ..., \tau_1+d_1+\tau_2+d_2-t\}$, $\Phi_{pt} \in R^{(\tau_1+\tau_2+d_2)n\times(\tau_1+\tau_2+d_2)n}$, $\Phi_{pt} = \begin{bmatrix} \phi_{pt} \\ I \quad 0 \end{bmatrix}$, $\phi_{pt} \in R^{(min\{\tau_1+\tau_2+d_2,p\}n)\times(\tau_1+\tau_2+d_2)n}$, $\phi_{pt} = [\phi_{pt}^1\, \phi_{pt}^2 ..., \phi_{pt}^{\tau_1+\tau_2+d_2}]$, $\phi_{pt}^s \in R^{(min\{\tau_1+\tau_2+d_2,p\}n)\times n}$, $s \in \tau$; $\phi_{pl}^s = 0, s \neq 1$ e

$$\Phi_{pl}^1 = \begin{bmatrix} A^p + B_pKC \\ A^{p-1} + B_{p-1}KC \\ \vdots \\ A^{max\{1,p-\tau_1-\tau_2-d_2+1\}} + B_{max\{1,p-\tau_1-\tau_2-d_2+1\}}KC \end{bmatrix}^T$$

para $t \neq 1$, $\phi_{pt}^{s} = 0$, $s \neq \{1, t\}$ e

$$[\phi_{pt}^{1} \ \phi_{pt}^{t}] = \begin{bmatrix} A^{p} & B_{p}KC \\ A^{p-1} & B_{p-1}KC \\ \vdots & \vdots \\ A^{max\{1,p-\tau_1-\tau_2-d_2+1\}} & B_{max\{1,p-\tau_1-\tau_2-d_2+1\}}KC \end{bmatrix}$$

Mostra-se que a análise da estabilidade de (14) é equivalente à equação (13) em [**?**]. Uma vez que este artigo e [2] introduzem a técnica de espaço aumentado para estudar WCS, No modelo WCS (14) será usado o controle por realimentação de saídas F obtido no Teorema (1.1) . Ao generalizar "Observação 8"em [3], é fácil mostrar que, o sistema de malha fechada (14) é assintoticamente estável se existirem matrizes positivas definidas P_{pt}, de modo que

$$\Phi_{pt}^{T} P_{hl} \Phi_{pt} - P_{pt} < 0, t, l \in \tau_3, p \in \tau(t), h \in \tau_l. \tag{15}$$

Para reduzir a carga computacional, seja $P_{pt} = P$ para todos $t \in \tau_3$ e todos $p \in \tau(t)$. Denota-se $Q = P^{-1}$

$$G_{pt} = \begin{bmatrix} G_{pt}^{11} & G_{pt}^{12} & ... & G_{pt}^{1,\tau_1+\tau_2+d_2} \\ G_{pt}^{21} & G_{pt}^{22} & ... & G_{pt}^{2,\tau_1+\tau_2+d_2} \\ \vdots & \vdots & \vdots & \vdots \\ G_{pt}^{\tau_1+\tau_2+d_2,1} & G_{pt}^{\tau_1+\tau_2+d_2,2} & ... & G_{pt}^{\tau_1+\tau_2+d_2,\tau_1+\tau_2+d_2} \end{bmatrix}$$

$G_{pt}^{t,s} = G$, $s \in \tau_3$ onde cada bloco em G_{pt} é da mesma dimensão. Então, a realimentação de saídas foi projetado em termos de um conjunto de LMIs.

Teorema 1.2. *Considere o sistema (1), (2) onde os atrasos delimitados e as perdas de pacotes que ocorrem como nas definições (1.1)–(1.2). Então existe um controlador de realimentação de saídas $u = Ky = FCx$, onde K é obtido baseado no teorema (1.1) de modo que o sistema de malha fechada (13) seja assintoticamente estável, se houver matrizes Y, G_{pt} e Q tais que*

$$A_{pt} = \begin{bmatrix} G_{pt}^{T} + G_{pt} - Q & * \\ \phi_{pt} G_{pt} & Q \end{bmatrix} > 0, t \in \tau_3, p \in \tau(t) \tag{16}$$

onde $KG = FCG$ em $\Phi_{pt} G_{pt}$ satisfaz Y. Neste caso o ganho por realimentação de saídas é dado por $K = FC = YG^{-1}$.

2 Aplicação de sintesis do controle preditivo

Uma das maiores vantagens do controle MPC é considerar explicitamente as restrições físicas. As restrições de entrada e estado considerados neste artigo são:

$$\begin{aligned} -\bar{u} \leq u(i_1 + h) \leq \bar{u} \\ -\bar{\Phi} \leq \Phi x(i_1 + h + l) \leq \bar{\Phi}, \forall h \geq 0 \end{aligned} \tag{17}$$

onde $\bar{u} := [\bar{u}_1, \bar{u}_2, \ldots, \bar{u}_m]^T$, $\bar{u}_j > 0$, $j \in m := \{1, 2, ..., m\}$; $\bar{\Phi} := [\bar{\phi}_1, \bar{\phi}_2, ..., \bar{\phi}_q]^T$, $\bar{\phi}_s > 0$, $j \in q := \{1, 2, ..., q\}$; $\Phi \in R^{q \times n}$. Portanto, o objetivo é projetar um controlador MPC em sistema em rede sem fio que estabilize o sistema (14), ao mesmo tempo que satisfaça (17).

2.1 Problema de otimização para MPC

A abordagem de síntese do controle MPC permite que $K = FC$ seja variável no tempo e seja otimizado. Assim, a lei de controle determinada é

$$\tilde{u}(k) = \tilde{u}(j_l) = K(j_l)\tilde{y}(j_l) = F(j_l)C(j_l)\tilde{x}(j_l)\, para \\ j_l \leq k \leq j_{l+1}\ e\ l \geq 1 \tag{18}$$

Um sensor envia $S_{act} = [s_{act}(k-1), s_{act}(k-2), ..., s_{act}(k-\tau_1-\tau_2-d_2+1)$ juntamente com $x(k)$ para o controlador, em cada tempo k.

3 Conclusões

No presente artigo foi considera uma abordagem típica do controlador MPC.Este artigo generalizou principais resultados para incorporar atrasos limitados. O atraso induzido pela rede é conhecido como uma fonte potencial de degradação do desempenho e até mesmo causando instabilidade. Ao analisar os efeitos dos atrasos e das perdas de pacotes, nos sistemas SC e CA, respectivamente, no sistema de circuito fechado, é estabelecido um modelo inovador que pode ser usado para lidar com o problema da lei de controle atualizado em WNCS. É apresentado como obter uma matriz de realimentação de saídas K.

Referências

[1] E. B. Castelan, J. C. Hennet, E. R. Ll. Villarreal, Quadratic Characterization and Use of Output Stabilizable Subspaces, *IEEE Trans. Automatic Control*, 48(4):654–660, 2003.

[2] B. Ding and X. Tang and H. Pan and T. Zou, "On MPC of Linear System Over Networks with Bounded Delays and Packet Losses, *Proceeding of the* 11^{th} *World Congress on Intelligent Control and Automation Shenyang*, vol1, China, 2014.

[3] B. Ding, Stabilization of linear systems over networks with bounded packet loss and its use in model predictive control,*Automatica*, 47:2526–2533, 2011.

[4] C. B. S. Dutra, Controle Preditivo Multiobjetivo para processos em atraso, Tese doutorado, Universidade Federal de Santa Catarina, Brasil, 2003.

[5] H. Gao, T. Chen, and J. Lam, A new delay system approach to network-based control, *Automatica*, 44:39–52, 2008.

[6] Y. Shi and B. Yu, "Robust mixed H_2/H_∞ control of networked control systems with random time delays in both forward and backward communication links,*Automatica*, 47:754–760, 2011.

[7] E. R. Ll. Villarreal, J. A. R. Vargas, E. M. Hemerly, Static Ouput Feedback stabilization using Invariant Subspaces and Sylvester Equations, *TEMA - Tend. Mat. Apl. Comput.*, 10(1):99–110, 2009.

[8] D. Yue, Q. L. Han, and Lam, Network-based robust H_{infty} control of systems with uncertainty, *Automatica*, 41:999–107, 2005.

[9] W. Zhang and L. Yu, A robust control approach to stabilization of networked control systems with time-varing delays, *Automatica*, 45:2440–2445, 2009.

Trabalho apresentado no XXXVIII CNMAC, Campinas - SP, 2018.

Proceeding Series of the Brazilian Society of Computational and Applied Mathematics

Output Feedback Control in Descriptor System Admissible

Elmer Rolando Llanos Villarreal[1]
Departamento de Ciências Naturais, Matemática e Estatística,
Universidade Federal Rural do Semi-árido, 59625900, Mossoró, RN, Brasil.
Andrés Ortiz Salazar[2]
Departamento de Engenharia de Computação e Automação
Universidade Federal de Rio Grande do Norte,
59078-970, Natal, RN, Brasil.
Alberto Soto Lock[3]
Departamento de Engenharia Elétrica
Universidade Federal Paraiba, 58051-900, João Pessoa, PB, Brasil.
Walter Martins Rodrigues[4]
Departamento de Ciências Naturais, Matemática e Estatística,
Universidade Federal Rural do Semi-árido, 59625900, Mossoró, RN, Brasil.

Resumo. In this paper, are propose new techniques for synthesis of output feedback controllers of descriptor system to attain the closed loop admissibility. A necessary and sufficient condition are shown for the existence of such a controller in terms of linearized LMIs whose solution yields a controller that satisfy the specification. Considered the existence problem and the compute of output feedback that stabilizable in descriptor systems. This paper show that based the coupled Sylvester equations and the coupled Lyapunov like equations can also be used to obtain a set of necessary and sufficient conditions for the existence of a output feedback controller, such that closed-loop system is admissible.

Palavras-chave. Output Feedback Control, Descriptor System,

1 Introduction

This paper deals the problem of stabilization by static output feedback for descriptor systems. Remind that an n-dimensional descriptor system consists of a mixture de n-q algebraic equations and q firts order diferential equations. Descriptor systems arise naturally in modelling of several dynamical systems commonly used engineering applications such as biological system, power systems and other interconnected systems [7], [10].

In the available literature on descriptor systems, there are two kinds of stabilization problems for singular continuous-time systems. One consists in designing a output-feedback controller in such a way that the closed-loop system is regular, impulse-free, and stable or equivalently admissible. The other is to design a output feedback controller in order to make the closed-loop system regular and stable.

The problem of computing a suitable static output feedback, from which these closed-loop propierties are verified. These three desired properties can be described in terms of the closed-loop eigenstructure: (i) the asymptotic stability is equivalent to have all the finite

[1]elmerllanos@ufersa.edu.br
[2]andres@dca.ufrn.br
[3]aslock@cear.ufpb.br
[4]walterm@ufersa.edu.br

DOI: 10.5540/03.2018.006.02.0309 © 2018 SBMAC

poles in the left half complex plane; (ii) the absence of impulsive modes is equivalent to have q finite closed-loop; and (iii) the regularity is guaranteed if the system is impulse-free. Thus the necessary and sufficient conditions for the existence of a stabilizing output feedback are obtained as a set of coupled (generalized) Sylvester equations in [8], [9], [4], [5] [14] .

This paper is organized as follows. The second section, presents the problem, based in the basic concepts, the necessary and sufficient conditions for existence of a solution. In section 3 presents some results main with formulation the theorems . In section 4 presents the aspects algorithmic and presents The numerical example illustrate the application of the algorithm that outlines the basic steps are used to solve the problem is presented in the fourth section. In the section 5 presents the regulator problem. Finally, concluding remarks are apresented.

2 Preliminaries

The considered linear descriptor systems are described by :

$$\begin{aligned} E\dot{x}(t) &= Ax(t) + Bu(t) \quad (1)\\ y(t) &= Cx(t) + Du(t) \quad (2) \end{aligned}$$

where: $x \in \mathcal{X} \sim \Re^n$, $u \in \mathcal{U} \sim \Re^m$, $y \in \mathcal{Y} \sim \Re^p$ and $E \in \Re^{n\times n}$, $rank\,(E) = q < n$; as the other matrices is an appropriate size with $rank\,(B) = m$, $rank\,(C) = p$ and $rank\,(D) = m$. The pair (E, A) is called regular if there exists $s \in \mathcal{C}$ such that $det(sE - A) \neq 0$ Thus a regular descriptor system is in [13] and [7].

i) stable if all finite roots of $det(sE - A) = 0$ are in the open left half complex plane;

ii) impulse free if it exhibits no impulse behavior;

iii) finite dynamics detectable if there exists L such that $(E, A + LC)$ is regular and stable;

iv) impulse observable if there exists L such that $(E, A + LC)$ is regular and impulse-free;

Considered the descriptor system

$$E\dot{x}(t) = Ax(t) \quad (3)$$

Consider as follow definitions

Definition 2.1. *[15] The system (1), (2) is said to be regular if* $det(sE - A) \neq 0$.

Definition 2.2. *[15] The system (1), (2) is said to be impulse-free is* $deg(det(sE - A)) = rank(E)$.

Definition 2.3. *[15] The system (1), (2) is said to be stable if all the roots of deg(det(sE-A))=0 have negative real part.*

Definition 2.4. *[15] The system (1), (2) is said to be admissible if it is regular, impulse-free and stable.*

The objective the paper is to find a static output feedback controller

$$u(t) = Gy(t), \quad (4)$$

such that the closed-loop system is admissible.

$$\begin{aligned} E\dot{x}(t) &= (A + BGC)x(t),\\ y(t) &= Cx(t) \quad (5) \end{aligned}$$

DOI: 10.5540/03.2018.006.02.0309 © 2018 SBMAC

Theorem 2.1. *The system (1), (2) is admissible if and only if there exist a scalar $\epsilon > 0$ and matrices $\tilde{P} > 0$, $\tilde{U} > 0$, $\tilde{W} > 0$ and $\tilde{Q} > 0$ such that*

$$\begin{pmatrix} -E'\tilde{P}E - \tilde{W} & \epsilon A' + E' & \epsilon A' & \tilde{Q}'S' \\ \epsilon A + E & -\tilde{U} & 0 & 0 \\ \epsilon A & 0 & -I & 0 \\ S\tilde{Q} & 0 & 0 & -I \end{pmatrix} < 0 \tag{6}$$

$$\tilde{W} < (\epsilon A' - \tilde{Q}'S')(\epsilon A - S\tilde{Q}), \tag{7}$$

$$\tilde{P}\tilde{U} = I \tag{8}$$

where $S \in \Re^{n\times(n-r)}$ is any matrix with full column rank and satisfies $E'S = 0$.

The presented a version of the generalized Lyapunov theorem in [11].

Theorem 2.2. *[11] Let (E, A) be regular and (E, A, C) be impulse observable and finite dynamics detectable. Then (E, A) is stable and impulse-free if and only if there exists a solution (P, Q) to the equation:*

$$A'P + Q'A + C'C = 0; \quad Q'E = E'P \geq 0 \tag{9}$$

3 Main results

This paper show that based the coupled Sylvester equations and the coupled Lyapunov like equations can also be used to obtain a set of necessary and sufficient conditions for the existence of a output feedback controller $u = \epsilon^{-1}\tilde{K}y(t)$ $u = Gy$ with $G = \epsilon^{-1}\tilde{K}$, such that closed-loop system (5) is admissible.

Theorem 3.1. *Given the continuous descriptor systems (1), (2). There exists a static output feedback controller (4) such that closed-loop system (5) is admissible if there exist a scalar $\epsilon > 0$, matrices $\tilde{P} > 0$, $\tilde{U} > 0$, $\tilde{W} > 0$ and $\tilde{Q} > 0$ such that*

$$\begin{pmatrix} -E'\tilde{P}E - \tilde{W} & \epsilon A' + E' & \epsilon A' & \tilde{Q}'S' \\ \epsilon A + E & -\tilde{U} & 0 & 0 \\ \epsilon A & 0 & -I & 0 \\ S\tilde{Q} & 0 & 0 & -I \end{pmatrix} < 0 \tag{10}$$

$$\tilde{W} < (\epsilon A' - \tilde{Q}'S')(\epsilon A - S\tilde{Q}), \tag{11}$$

$$\tilde{P}\tilde{U} = I \tag{12}$$

where $S \in \Re^{n\times(n-r)}$ is any matrix with full column rank and satisfies $E'S = 0$. in this case, a desired static output feedback control law can be chosen as

$$u(t) = \epsilon^{-1}\tilde{K}Cx(t) \tag{13}$$

$$u(t) = Gy(t) \tag{14}$$

Remark 3.1. *The Theorem (3.1) presents necessary and sufficient conditions for the admissibility of continuous descriptor systems (1), (2). The Theorem (3.1) provides a sufficient condition for existence of the output feedback controller for continuous descriptor systems.*

DOI: 10.5540/03.2018.006.02.0309 © 2018 SBMAC

The Theorem is presented as follows:

Theorem 3.2. *If there exist a scalar $\epsilon > 0$, matrices $\tilde{P} > 0$, $\tilde{U} > 0$, $\tilde{W} > 0$ and $\tilde{Q} > 0$ such that the equations (10) , (11) and (12) are satisfied.Then there exists an output feedback matrix $G : \mathcal{Y} \longrightarrow \mathcal{U}$ such that closed-loop system (5) is admissible. if the sufficient following conditions are verified for some positive scalar $v \leq n$ and for some pair of matrices $V \in \Re^{n\times v}$ and $T \in \Re^{q-v\times n}$, that such $TEV = 0$, where $rank\,(EV) = rank\,(TE) = q$:*
(i) Let $Q = C'C$, $Q \in \Re^{n\times n}$, there exist matrices $P = P' \geq 0$, $P \in \Re^{n\times n}$ and $Y = WV' \in \Re^{m\times n}$, such that:

$$APE' + EPA' = -EC'CE' \tag{15}$$

$$Pd = V'PV > 0 \quad ; \quad TEPE'T' = 0 \tag{16}$$

$$Y = GCP \tag{17}$$

The theorem (3.2) is propose numerically solution algorithm to determine the output feedback matrix in descriptor systems, where the equations (10) , (11) and (12) are satisfied and such that closed-loop system (5) is admissible. The theorem (3.2) it is similarly at [2], [5].

4 Aspects algorithmic

Is shown below that based coupled Sylvester equations and the coupled Lyapunov like equations can also be used to obtain the sufficient conditions for the existence of a output feedback, such that closed-loop system (5) is admissible.

4.1 The Syrmos-Lewis algorithm

Considered the Theorem (3.1) where a scalar $\epsilon > 0$, matrices $\tilde{P} > 0$, $\tilde{U} > 0$, $\tilde{W} > 0$ and $\tilde{Q} > 0$ such that the equations (10), (11), (12) are satisfied. Then for the calculation of the output feedback that stabilizes the closed-loop system, when $m + p > q$.

Therefore determined The Syrmos-Lewis algorithm the existence of a output feedback, such that closed-loop system (5) is admissible.

4.2 Example

Considered the following data [6] :

$$E = \begin{bmatrix} 1.00 & 0.00 & 0.00 & 0.00 \\ 0.00 & 0.00 & 1.00 & 0.00 \\ 0.00 & 0.00 & 0.00 & 0.00 \\ 0.00 & 0.00 & 0.00 & 0.00 \end{bmatrix};$$

$$A = \begin{bmatrix} 0.00 & 1.00 & 0.00 & 0.00 \\ 0.00 & 0.00 & 0.00 & 1.00 \\ 1.00 & 1.00 & 0.00 & 0.00 \\ 0.00 & -1.00 & 1.00 & 1.00 \end{bmatrix}$$

DOI: 10.5540/03.2018.006.02.0309 © 2018 SBMAC

$$B = \begin{bmatrix} 0.00 & 0.00 \\ 0.00 & 0.00 \\ 1.00 & 0.00 \\ 0.00 & 1.00 \end{bmatrix}; \; C = \begin{bmatrix} 1 & 0 & 0 & 0 \end{bmatrix}$$

The corresponding descriptor system with finite poles are given by: $\sigma(E, A) = \{0.0,\, 0.0,\, -1.0\}$. The system (C, E, A, B) is both stronlgy controllable and observable.

In a first step, considered a scalar $\epsilon > 0$, matrices $\tilde{P} > 0$, $\tilde{U} > 0$, $\tilde{W} > 0$ and $\tilde{Q} > 0$ such that the equations (10), (11) and (12) in theorem (3.1) are satisfied.

In a second step, eigenstructure assignment is used thus the eigenvalues to positioned are given for : $\Lambda_T = \{-1\} \cup \Lambda_V = \{-3.5\}$.

Step 1 : For $\lambda_1 = -1$, $t_j \in \mathcal{C}^n$ and $u_j \in \mathcal{C}^p$, such that :

$$\begin{bmatrix} t_j' & u_j' \end{bmatrix} \begin{bmatrix} A - \lambda_j E \\ C \end{bmatrix} = 0 \;\; \forall \;\; j = 1, \ldots, q - p \tag{18}$$

determined T that verified (18) and such that $TEP = 0$ is also verified and (A, B, T, E) have not invariant zeros :

$$T = \begin{bmatrix} 0.00 & 0.00 & 0.7071 & -0.7071 \end{bmatrix}$$

Step 3 : For $\lambda_2 = -3.5$,

$$\begin{bmatrix} A - \lambda_i E & B \\ TE & 0 \end{bmatrix} \begin{bmatrix} P_i \\ Y_i \end{bmatrix} = 0 \, \forall \; i = q - p + 1, \ldots, q \tag{19}$$

determined P and Y using (19) :

$$P = \begin{bmatrix} 0.1762 \\ -0.6167 \\ 0.1626 \\ -0.5693 \end{bmatrix} \;\; ; \;\; Y = \begin{bmatrix} 0.4405 \\ -0.2101 \end{bmatrix};$$

Step 4 : Determined G that such $GCP = Y$:

$$G = \begin{bmatrix} 2.5000 \\ -1.1923 \end{bmatrix};$$

$$A + BGC = \begin{bmatrix} 0.0 & 1.0 & 0.0 & 0.0 \\ 0.0 & 0.0 & 0.0 & 1.0 \\ 3.5000 & 1.0 & 0.0 & 0.0 \\ -1.1923 & -1.0 & 1.0 & 1.0 \end{bmatrix}.$$

The corresponding closed-loop system $(E, A + BGC)$ has the desired generalized eigenvalues.

5 Regulator Problem

Consider the optimal regulator problem that minimizes

$$J = \frac{1}{2} \int_0^\infty ||y(t)||^2 dt \tag{20}$$

DOI: 10.5540/03.2018.006.02.0309 © 2018 SBMAC

subject to (1), (2) and with

$$lim_{t\longrightarrow\infty}x(t) = 0 \tag{21}$$

We assume that (E, A, B) be impulse controllable and finite dynamics stabilizable and that (E, A, C) be impulse observable and dynamics detectable. Let G be a output feedback matrix such that $(E, A + BGC)$ is stable and impulse-free, such that closed-loop system (5) is admissible. Thefore if there exist a scalar $\epsilon > 0$, matrices $\tilde{P} > 0$, $\tilde{U} > 0$, $\tilde{W} > 0$ and $\tilde{Q} > 0$ such that the equations (10), (11) and (12) in theorem (3.1) are satisfied.

Then from the symmetric version of Theorem (2.2), there exists a solution P to

$$\begin{aligned}(A + BGC)'P + P'(A + BGC) + QQ + (GC)'SS' + \\ SSGC + (CG)'R(CG) = 0; \quad E'P = PE \geq 0\end{aligned} \tag{22}$$

where $QQ = C'C$, $SS = C'D$, $R = D'D > 0$. It can be shown that the the performance index is expressed as

$$J = \frac{1}{2}x_o'P'E'Px_0 \geq 0 \tag{23}$$

6 Concluding remarks

In this paper, we proposed new techniques for synthesis of output feedback controllers of descriptor system to attain the closed loop admissibility. A necessary and sufficient condition is shown for the existence of such a controller in terms of linearized LMIs whose solution yields a controller that satisfy the specification. Considered the existence problem and the compute of output feedback that strongly stabilizable in descriptor systems.

Referências

[1] P. Bernhard, On singular implicit linear dynamical systems, *SIAM Journal on Control and Optimization*, 20(5):612–633, 1982.

[2] E. B. Castelan and Elmer R. Llanos Villarreal and Sophie Tarbouriech, Quadratic Characterization and Use of Output Stabilizable Subspaces in Descriptor Systems, *Proceedings (CD) 1st IFAC Symposium on System Structure, Prague,2001*, vol. 1, 207–212, 2001.

[3] E. B. Castelan and J. C. Hennet and E. R. Ll. Villarreal, Quadratic Characterization and Use of Output Stabilizable Subspaces,*IEEE Trans. Automatic. Control*, 48(4):654–660, 2003.

[4] E. B. Castelan and J. C. Hennet and E. R. Llanos Villarreal, Output Feeedback Design by Coupled Lyapunov-Like Equations, *Proceedings of the* 15^{th} *Ifac Congress on the International Federation of Automatic Control*, vol. 35. p. 207–212,2002.

[5] E. B. Castelan, Estabilização de Sistemas Descritores por Realimentação de Saídas via Subespaços Invariantes, *Revista de Controle e Automação*, 16(4):467–477, 2005.

[6] D. L. Chu and H. C. Chan and D. W. C. Ho, Necessary and Suficient Conditions for the Output Feedback Regularization of Descriptor Systems *IEEE Trans. Automatic. Control*, 44(2):1457–1468, 1999.

 © 2018 SBMAC

[7] L. Dai, Singular Control System, Springer-Verlag, 1989.

[8] , G. R. Duan, Eigenstructure assignment in descriptor systems via output feedback: a new complete parametric approach, *Int J. Control*, 72(4):345–364, 1999.

[9] L. R. Fletcher, Eigenstructure Assingment by Output Feedback in Descriptor Systems, *IEE Proceedings*, vo135(4):302–308, 1998.

[10] F. L. Lewis, A Survey of Linear Singular Systems, *Circuits Systems Signal Process*, 5(1):3–36, 1986.

[11] K. Tabaka, N. Morihira and T. Katayama, A generalized Lyapunov theorem for descriptor system, *Systems & Control Letters*, 24:49–51, 1995.

[12] A. Varga, On stabilization methods of descriptor systems, *Systems & Control Letters*, 24(2):133–138, 1995.

[13] G. C. Verghese, B C. Levy, and T. Kailath, A Generalized State-Space for Singular Systems, *IEEE Trans. Automatic. Control* AC-26(4):811–831, 1981.

[14] E. R. Ll. Villarreal, J. A. R. Vargas, E. M. Hemerly, Static Ouput Feedback stabilization using Invariant Subspaces and Sylvester Equations, *TEMA - Tend. Mat. Apl. Comput.*, 10(1):99–110, 2009.

[15] S. Xu and J. Lam, Robust Control and Filtering of Singular Systems, *Lecture Notes in Control and Information Sciences, Springer* 1:11–29, 2006.

DOI: 10.5540/03.2018.006.02.0309 © 2018 SBMAC

Proceeding Series of the Brazilian Society of Applied and Computational Mathematics, v. 6, n. 1, 2018.

Trabalho apresentado no XXXVII CNMAC, S.J. dos Campos - SP, 2017.

Proceeding Series of the Brazilian Society of Computational and Applied Mathematics

Aplicação da equação diferencial de Sylvester

Elmer Rolando Llanos Villarreal[1]
Centro de Ciências Exatas e Naturais, UFERSA, Mossoró, RN.
Maxwell Cavalcante Jácome, [2]
Engenharia Mecânica, UFERSA, Mossoró, RN.
Edpo Rodrigues de Morais[3]
Programa de Pós-Graduação em Sistemas de Comunicação e Automação, UFERSA, Mossoró, RN.
João Victor de Queiroz [4]
Programa de Pós-Graduação em Sistemas de Comunicação e Automação, UFERSA, Mossoró, RN.
Walter Martins Rodrigues[5]
Centro de Ciências Exatas e Naturais, UFERSA, Mossoró, RN.

Resumo: *O presente artigo te por objetivo encontrar algoritmo de controle para rastreamento de sistemas dinâmicos não-lineares aplicados em VANT via realimentação de saídas. O algoritmo de controle tem um quadro interno para testar controlabilidade do sistema variando no tempo via transformada de Lyapunov. Calcular a matriz de realimentação de saídas, e apresenta-se uma aplicação de controle em VANT.*

Palavras chave. Realimentação de saídas, Equação de Sylvester, VANT.

1 Introdução

Este artigo apresenta um algoritmo de controle para rastreamento de sistemas dinâmicos não-lineares aplicados em VANT via realimentação de saídas . O problema de rastreamento leva a equações linearizadas de erro variando no tempo. Daí novas noções de autovalores são introduzidas para sistemas de variação linear do tempo, um esquema de posicionamento de autoestrutura é proposto para uma estrutura linear variando no tempo via uma equação diferencial Sylvester. Também é mostrado que sistemas de malha fechada podem ser estabilizada pelo posicionamento de autovalores apropriadas. O desempenho desejado poderia ser obtido atribuindo-se valores aos autovetores. O presente algoritmo de controle tem um quadro interno para testar controlabilidade do sistema variando no tempo via transformada de Lyapunov.

Controle por posicionamento de polos para uma planta variando no tempo foi proposta em [7]. Em [4] foi proposta um projeto de posicionamento de autoestrutura para sistemas lineares variando no tempo via a equação diferencial de Sylvester, que foi baseado numa proposta de posicionamento de autoestrutura em [9]. Em [5] desenvolveu um controle LTI para $VANTS$

O artigo é organizado a seguir. Na seção 2 formula-se o problema seguindo algumas pre-liminares em sistemas descritores. Na seção 3 temos os sistemas lineares invariantes

[1]elmerllanos@ufersa.edu.br
[2]maxwellc.jacome@hotmail.com
[3]edpo_morais@hotmail.com
[4]joao.queiroz@ufersa.edu.br
[5]walterm@ufersa.edu.br

 © 2018 SBMAC

no tempo. Na seção 4 temos os sistemas lineares variantes no tempo. Na seção 5 temos aplicação de controle em $VANT$. Na seção 6 temos os resultados e discussões. Finalmente, às conclusões finais na seção 7.

2 Sistema descritor

Seja um sistema descritor com variáveis de estado, x, controle u dado por um conjunto de N equações

$$E\dot{x}(t) = f(x,u). \tag{1}$$

Considere o sistema descritor invariante no tempo descrito por:

$$E\dot{x}(t) = Ax(t) + Bu(t) \tag{2}$$
$$y(t) = Cx(t), \tag{3}$$

onde: $x \in \mathcal{X} \sim \Re^n$ é variável de estado, $u \in \mathcal{U} \sim \Re^m$ é variável de controle (entrada variável), $y \in \mathcal{Y} \sim \Re^p$ é a variável de saída e $E \in \Re^{n\times n}$, $posto\,(E) = q < n$; como as outras matrizes com dimensões apropriadas, onde $posto\,(B) = m$ e $posto\,(C) = p$.

Assim, o problema de controle é encontrar uma lei controle por realimentação de saídas $u(t) = Ky(t)$, tal que o sistema em malha fechada

$$E\dot{x}(t) = (A + BKC)x(t), \tag{4}$$

é S-estável: regular, assintoticamente estável e livre de impulsos em [1], [8].

3 Sistemas lineares invariantes no tempo

Considere a seguir o sistema quando a matriz E é uma matriz identidade $E = I_{n\times n}$ em [3], [2]. Assim seja um sistema dinâmico com variaveis de estado, x, controle u dado por um conjunto de N equações

$$\dot{x}(t) = f(x,u). \tag{5}$$

Considerando um sistema linearizado. Seja as equações a seguir:

$$\dot{x}(t) = Ax(t) + Bu(t) \tag{6}$$
$$y(t) = Cx(t). \tag{7}$$

Procura-se uma matriz de controle saída $K(t)$.

$$u(t) = K(t)y(t), \tag{8}$$

com o sistema em malha fechada

$$\dot{x}(t) = (A + BK(t)C)x(t). \tag{9}$$

DOI: 10.5540/03.2018.006.01.0326 © 2018 SBMAC

O problema fundamental é escolher os elementos de $K(t)$ de tal forma que o desempenho é satisfatório. Isto é muitas vezes realizado colocando os polos (autovalores) do sistema de malha fechada em locais específicos. Para isso colocamos o problema do autovalor:

$$(A + BK(t)C)\phi_i \quad = \quad \lambda_i \phi_i, \tag{10}$$

onde, ϕ_i é um autovalor à direita. Introduzimos um vetor parâmetro auxiliar

$$h_i \quad = \quad K(t)C\phi_i, \tag{11}$$

o que leva a

$$(A - \lambda_i I)\phi_i \quad = \quad -Bh_i. \tag{12}$$

A montagem de todas estas equações leva às equações de Sylvester em [2].

$$AV - VH_V \quad = \quad -BW. \tag{13}$$

4 Sistemas lineares variáveis no tempo

Contudo, no caso dos sistemas com variação temporal, tem havido uma investigação muito limitada, em parte devido à complexidade do problema.

$$\dot{x}(t) \quad = \quad A(t)x(t) + B(t)u(t). \tag{14}$$

Procura-se uma matriz de controle variando no tempo $K(t)$.

$$u(t) \quad = \quad K(t)y(t), \tag{15}$$

com o sistema em malha fechada:

$$\dot{x}(t) \quad = \quad (A(t) + B(t)K(t)C(t))x(t). \tag{16}$$

Agora, realizamos uma transformação de Lyapunov para converter as equações em forma canônica. O problema de transformar um sistema linear variando no tempo para uma forma canônica complementar como é considerado em [6]. Depois de converter $A(t)$ em forma canônica, obtemos uma matriz complementar. Agora definimos o problema correspondente ao autovalor para os sistemas da seguinte maneira:

$$(A_c(t) + \tilde{B}(t)\tilde{K}\tilde{C}(t))p_i(t) - \rho_i(t)p_i(t) \quad = \quad \dot{p}_i(t) \tag{17}$$

$$(A_c(t) + \tilde{B}(t)\tilde{K}\tilde{C}(t))q_i(t) - \rho_i(t)q_i^T(t) \quad = \quad -\dot{q}_i^T(t), \tag{18}$$

onde, $p_i(t)$ e $q_i(t)$ são os autovetores a esquerda e a direita respectivamente, correspondente ao autovalor $\rho_i(t)$.

O objetivo do presente artigo é encontrar a matriz de controle variando no tempo $K(t)$ de tal forma que os autovalores da malha fechada sejam posicionados de forma correta exatamente com seus os autovetores próprios desejados.

Se definimos um vetor parâmetro,

DOI: 10.5540/03.2018.006.01.0326 © 2018 SBMAC

$$h_i(t) = \tilde{K}(t)\tilde{C}(t)p_i(t). \tag{19}$$

Então a forma de matriz da equação de Sylvester diferencial pode ser escrita como:

$$A_c(t)P(t) - P(t)U(t) + \tilde{B}(t)W(t) = \dot{P}(t), \tag{20}$$

onde,

$$\begin{aligned} P(t) &= [p_1(t), p_2(t), ..., p_N(t)] && (21)\\ U(t) &= diag[\rho_1(t), \rho_2(t), ..., \rho_N(t)] && (22)\\ W(t) &= [w_1(t), w_2(t), ..., w_N(t)]. && (23) \end{aligned}$$

Para uma matriz autovalores $U(t)$ que não gera um conjunto atrativo de autovalores em malha fechada, um conjunto de autovetores próprios desejados em malha fechada pode ser seleccionado como

$$P_d(t) = [p_{d1}, p_{d2}, ..., p_{dN}]. \tag{24}$$

Depois de escolhidos, calcula-se uma matriz auxiliar, $\tilde{H}(t)$.

$$\tilde{H}(t) = -B^{+}(t)[A_c(t)P_d(t) - P_d(t)U_d(t) - \dot{P}_d], \tag{25}$$

onde, B^{+} denota a matriz seudo-inversa. Ao substituir esta solução pela matriz $\tilde{H}(t)$ e resolvendo com ajuda da matriz de autovetor direita admissível, encontra-se $P_a(t) \neq P_d(t)$. A matriz resultante é o mais próximo possível e satisfaz exatamente a seguinte equação:

$$A_c(t)P_a(t) - P_a(t)U_d(t) + \tilde{B}\tilde{H} = -\dot{P}_a(t)]. \tag{26}$$

Na forma vectorial temos que:

$$\dot{\bar{P}}_a = (I \otimes A_c\bar{P}_a(t)) + (U_d(t) \otimes (-I))\bar{P}_a + \bar{D}(t), \tag{27}$$

onde, $\otimes$ representa o produto Kronecker. Finalmente, a matriz de ganho variável no tempo é dada por:

$$\tilde{K}(t) = \tilde{W}(t)P_a^{-1}. \tag{28}$$

Assim temos a lei de controle (para as equações transformadas)

$$\tilde{u}(t) = \tilde{K}(t)\tilde{y}(t). \tag{29}$$

Assim, calcula-se $\tilde{K}(t)$ para o sistema em malha fechada com uma resposta satisfatória.

DOI: 10.5540/03.2018.006.01.0326 © 2018 SBMAC

5 Aplicação de controle em VANT

Esta seção apresenta uma aplicação do autovetor e um controle linear tempo-variando para as equações de erro do modelo rastreamento $VANT$. Um veículo aéreo tem seis graus de liberdade de corpo rígido comumente chamados de surge(u), sway(v), heave(w), roll(p), pitch (q) e yaw (r). O quadrotor $VANT$ move-se com seis graus de liberdade, mas apenas quatro deles são controlados por quatro variáveis de controle elevador total e três torques) diretamente para obter um sistema estável. As quatro variáveis de controle correspondem a quatro movimentos básicos: heave(w), roll(p), pitch(q) e yaw(r). O movimento pode ser definido em coordenadas corpo-fixas ou coordenadas terra-fixas, e as orientações angulares são definidas usando uma sequência de ângulos de Euler. Toda a questão dos modelos de aeronaves pode ser bastante complexa; assim para, determinar o modelo para usar o controle pode ser bastante complicado. Neste trabalho será realizado um estudo sobre um modelo dinâmico não-linear de 3 DOF para o veículo aéreo não tripulado $VANT$ seja considerado a seguir :

$$\dot{u} = rv + \frac{F_x}{m} \tag{30}$$

$$\dot{v} = -rv + \frac{F_y}{m} \tag{31}$$

$$\dot{r} = R_4 l + R_7 n \tag{32}$$

$$F_x = -\frac{1}{2\rho V^2 S C_{DO}} \tag{33}$$

$$F_y = \frac{1}{2\rho V^2 S (C_{Y\beta} tan^{-1}(\frac{v}{u}))} \tag{34}$$

$$l = \frac{1}{2\rho V^2 S (C_{l\beta} tan^{-1}(\frac{v}{u}) + \frac{C_{lr} br}{2V^2} + C_{l\delta_a}\delta_a)} \tag{35}$$

$$n = \frac{1}{2\rho V^2 S (C_{n\beta} tan^{-1}(\frac{v}{u}) + \frac{C_{nr} br}{2V^2} + C_{n\delta_a}\delta_a)} \tag{36}$$

onde,

$$R_4 = \frac{J_{xy}}{R} \tag{37}$$

$$R_7 = \frac{((J_x - J_y)J_x + J_{xz}^2)}{R} \tag{38}$$

$$R = J_x J_z - J_{xz}^2, \tag{39}$$

o modelo do quadrotor $VANT$ tem apenas $\delta_a(t)$ como o controle de entrada.

Definimos um vetor de estado

$$\dot{x} = [\dot{u}\ \dot{v}\ \dot{r}]^T \tag{40}$$

$$x = [u\ v\ r]^T. \tag{41}$$

 © 2018 SBMAC

Em seguida, especifica-se funções de tempo desejadas: $x_d(t)$ $\dot{x}_d(t)$ e uma função $\delta_{ad}(t)$ normalmente fixada.

$$\dot{x}_d = [\dot{u}_d \ \dot{v}_d \ \dot{r}_d]^T \quad (42)$$
$$x_d = [u_d \ v_d \ r_d]^T. \quad (43)$$

As equações de erro são:

$$\bar{x}(t) = \dot{x}_d - x(t). \quad (44)$$

Linearizando as equações acima, as equações de erro podem ser escritas como equações lineares variáveis no tempo como mostrado abaixo

$$\bar{x}(t) = A\bar{x} + B\bar{u}, \quad (45)$$

onde $x_d(t)$ é uma função da trajetória desejada, e $u(t)$ é o ângulo de airelon (entrada de controle). No algoritmo de controle descrito na seção anterior será aplicado às equações lineares de erro variando no tempo. Aplica-se o seguinte procedimento nas equações de erro acima.

- Tomar a transformação de Lyapunov para transformar um sistema linear variável no tempo na forma canônica complementar.Escolha do espectro $\lambda(t)$ em malha fechada desejada e a matriz modal desejada direita para o sistema transformado.
- Calcular a matriz de parâmetros $\tilde{W}(t)$. Resolver a equação diferencial de Sylvester com a matriz de parâmetros do passo acima para obter a matriz modal direita viável.
- Calcular a matriz de realimentação de saídas $\bar{K}(t)$. Como $\bar{K}(t)$ é obtido para o sistema transformado, tomamos a transformação de Lyapunov inversa para calcular a matriz de ganho de realimentação $K(t)$ para o sistema original.

6 Resultados e discussões

Primeiro, escolhe-se a trajetória de entrada desejada usando $\delta_a d(t) = Csen(t)$, onde C é um parâmetro constante. Escolhe-se para os autovalores e a matriz modal.

$$\delta_a d(t) = \begin{bmatrix} -e^{\alpha t} - s_1 & -e^{\alpha t} - s_2 & -e^{\alpha t} - s_3 \end{bmatrix} \quad (46)$$

$$P_d(t) = \begin{bmatrix} -\beta & 0 & 0 \\ 0 & -\beta & 0 \\ 0 & 0 & -\beta \end{bmatrix}. \quad (47)$$

Onde α, s_i e β_i são todos positivos e são parâmetros de entrada no projeto do controlador. O conjunto de equações para foram resolvidos em conjunto com as equações de erro linear em malha fechada numericamente. Isso considerando uma matriz realimentação de saída estável. Observe novamente que a própria matriz de ganho é uma função do tempo. É provável que diferentes escolhas dos autovalores e dos autovetores respectivamente resultem em diferentes graus de resposta. Os caminhos desejados são assumidos para a $VANT$ com base na aplicação que está realizando em uma situação particular.

 © 2018 SBMAC

7 Conclusões

Neste artigo, apresenta-se novas noções de autovalores para sistemas lineares, e desenvolveu uma estrutura de projeto de controle linear através de uma equação diferencial de Sylvester. Mostra-se que os sistemas em malha fechada poderiam ser estabilizados Através do posicionamento de autovetor apropriado, e um desempenho poderia ser obtido através da determinação do autovetores à direita. Com as especificações do projeto o exemplo de controle de vôo $VANT$ confirmou a utilidade e precisão do algoritmo de controle de rastreamento proposto. O algoritmo proposto é muito aplicável a sistemas de qualquer ordem de complexidade com qualquer grau ou tipo de não-linearidade.

Referências

[1] E. B. Castelan, E. R. Ll. Villarreal, and S. Tarbouriech, Quadratic Characterization and Use of Output Stabilizable Subspaces in Descriptor Systems, *Proceedings (CD) 1st IFAC Symposium on System Structure*, Prague, volume 1, pages 255-260, 2001.

[2] E. B. Castelan, J. C. Hennet, and E. R. Ll. Villarreal, Quadratic Characterization and Use of Output Stabilizable Subspaces, *IEEE Trans. Automatic. Control*, 48(4): 654–660, 2003.

[3] C. T. Chen, *Linear System Theory and Design*, Holt, Rinehart and Winston, 1996.

[4] H. Lee, and J. Choi,Linear time-varying eigenstructure assigment with flight control application. *IEEE Transactions on Aerospace and Electronic Systems*, 40(1):145–157, 2004.

[5] C. Nataraj, and P. Kasliwal, Linear time varying control of unmanned surface vehicles. In *Intelligent Ships Symposium VI*, American Society of Naval Engineers, 2005.

[6] L. Silverman, Transformation of time-variable systems to canonical (phase-variable) form, *IEEE Transactions on Automatic Control* 11(2):300–303, 1966.

[7] K. Tsakalis, and P. Ioannou, *Linear Time-Varying Systems*, Engelwood Cliffs, NJ: Prentice -Hall, 1993.

[8] E. R. Ll. Villarreal, J. A. R. Vargas, and E. M. Hemerly, Static Ouput Feedback stabilization using Invariant Subspaces and Sylvester Equations, *TEMA - Tend. Mat. Apl. Comput.*, 10(1):99–110, 2009.

[9] J. Zhu, A unified spectral theory for linear time-varying systems-progress and challenges. In *Proceedings of the 34th IEEE conference on Decision and Control*, volume 1, pages 2540-2546, 1995.

DOI: 10.5540/03.2018.006.01.0326 © 2018 SBMAC

Proceeding Series of the Brazilian Society of Applied and Computational Mathematics, v. 6, n. 1, 2018.

Trabalho apresentado no XXXVII CNMAC, S.J. dos Campos - SP, 2017.

Proceeding Series of the Brazilian Society of Computational and Applied Mathematics

Optimization Based Output Feedback Control Design in Descriptor Systems

Elmer Rolando Llanos Villarreal[1]
Centro de Engenharia, Modelagem e Ciências Exatas e Naturais, UFERSA, Mossoró, RN.
Maxwell Cavalcante Jácome, [2]
Engenharia Mecânica, UFERSA, Mossoró, RN.
Edpo Rodrigues de Morais[3]
Programa de Pós-Graduação em Sistemas de Comunicação e Automação, UFERSA, Mossoró, RN.
João Victor de Queiroz [4]
Programa de Pós-Graduação em Sistemas de Comunicação e Automação, UFERSA, Mossoró, RN.
Walter Martins Rodrigues[5]
Centro de Ciências Exatas e Naturais, UFERSA, Mossoró, RN.

This article proposes an algorithm to minimize the Frobenius norm of output feedback matrix of a regular, linear time invariant, continuous time descriptor system. The resulting gain matrix ensures that the closed loop system is impulse-free and the associated non singular matrix is well-conditioned. By characterizing a subset of the set of non singular matrices through a linear matrix inequality, the related optimization is formulated as a semi-definite program.

Keywords. Output Feedback, Descritor Systems, Stabilization.

1 Introduction

This paper deals with the problem of stabilization by static output feedback for linear descriptor systems. Remind that an $n-$dimensional descriptor system consists of a mixture of $n-q$ algebraic equations and q first order diferential equations. Descriptor systems arise naturally in the modelling of several dynamical systems commonly used in engineering applications, such as biological system, power systems and other interconnected systems [12]. Besides guaranteeing the closed-loop asymptotical stability, two other properties are desired in practice: closed-loop regularity and absence of impulsive behavior. The problem of computing a suitable static output feedback, from which these closed-loop propierties are verified, is called simply stabilization problem. These three desired properties can be

[1]elmerllanos@ufersa.edu.br
[2]maxwellc.jacome@hotmail.com
[3]edpo_morais@hotmail.com
[4]joao.queiroz@ufersa.edu.br
[5]walterm@ufersa.edu.br

 © 2018 SBMAC

described in terms of the closed-loop eigenstructure: (i) the asymptotic stability is equivalent to have all the finite poles in the left half complex plane; (ii) the absence of impulsive modes is equivalent to have q finite closed-loop; and (iii) the regularity is guaranteed if the system is impulse-free. Thus, the necessary and sufficient conditions for the existence of a S-stabilizing output feedback are obtained as a set of coupled (generalized) Sylvester equations in [9], [7] . In case of normal systems, it is shown that output stabilizable (C, A, B)-invariant subspaces are obtained through a pair of coupled Sylvester equations for systems verifying Kimura's condition, thus two algorithm are proposed to solve the coupled Sylvester equations in [6], [14].

Since the impulsive response is undesirable in practical applications. One of the effective ways to eliminate impulses from a linear time invariant (LTI) descriptor system is by designing a suitable output feedback matrix that reduces the nilpotent index to one or strangeness index to zero (see [12], [9], [10] and the references therein). In the process, one has to select a output feedback gain matrix such that an appropriate sub-matrix, in the closed loop, would be non singular. It has been shown in [12], [9] that the inverse of resulting non singular matrix plays important role while designing a output feedback control for assigning the closed loop finite poles at appropriate locations in the complex plane. Hence, the non singular matrix should be well-conditioned to avoid numerical errors in the finite pole placement. The choice of feedback output matrix that eliminates impulses from the response of a descriptor system is not unique [12], [10], [9]. On the other hand, a limited magnitude of control signal can be provided to the actuators and the cost of the actuator grows quickly with increasing the amplitude of control signal. Since the control signal amplitude is directly proportional to the norm of the output feedback matrix, the minimum norm output feedback matrix satisfying the desired objectives would be preferable [13].

In this article we propose a convex algorithm to minimize the norm of output feedback matrix for an LTI regular descriptor system, ensuring that i) the response of the closed loop system is impulse free and ii) the associated non singular matrix is well-conditioned. To obtain a well-conditioned non singular matrix, we formulate a linear matrix inequality (LMI) optimization that minimizes the largest singular value and maximizes the smallest singular value of non singular matrix, simultaneously. Although there are several existing algorithms for impulse elimination, to the best of our knowledge, no results in the literature available that combines the above objectives and formulated it as a convex optimization in [8]. Rest of the paper is organized as follows. In Section II we formulate the problem following to some preliminaries on descriptor systems. In Section III we formulate the optimization to minimize the norm of output matrix, while at the same time improve the condition number of associated non singular matrix. Finally, we conclude in Section IV.

Notations: The set of all $m \times n$ constant real matrices is denoted as $R^{m\times n}$. I_n stands for an identity matrix of size $n \times n$. The Frobenius norm of $A \in R^{m\times n}$ is denoted as $||A||_K$, and defined as $||A||_K := \sqrt{\sum_{i=1}^{m}\sum_{j=1}^{n}|a_{ij}|^2}$. $A > 0$ ($A \geq 0$) denotes that A is a symmetric positive definite (symmetric positive semi-definite) matrix.

DOI: 10.5540/03.2018.006.01.0410 © 2018 SBMAC

2 Problem formulation

Let us consider an LTI continuous time descriptor system represented by the following equation:

$$E\dot{x} = Ax + Bu \tag{1}$$
$$y = Cx \tag{2}$$
$$x(t_0) = x_0,$$

where, if algebraic constraints are present, $E \in R^{n\times n}$ is singular, $A \in R^{n\times n}$, and $B \in R^{n\times m}$, $x : R \longrightarrow R^n$ is the state vector with initial condition $x(t_0) = x_0$ and $u : R \longrightarrow R^m$ is an input to the system. We assume that system (1) is regular, i.e., there exists a complex number $s \in C$ such that $det(sE - A) \neq 0$ (where $det()$ stands for determinant of a matrix). We refer to the roots of polynomial $det(sE - A)$ as finite poles of system (1). Furthermore, we assume that system (1) is impulse controllable and the involved matrices have appropriate dimensions. It is also assumed that B is full column-rank, C is full row-rank and that (C, A, B) is stabilizable and detectable.

The studied problem is to find a static output feedback control law

$$u(t) = Ky(t), \tag{3}$$

such that $\sigma(E, A + BKC) \in C^-$ or, equivalently, the closed-loop system is asymptotically stable. Considered the system

$$E_1\dot{x}(t) = A_1x(t) + B_1u(t) \tag{4}$$
$$0 = A_2x(t) + B_2u(t). \tag{5}$$

Let $V \in R^{v\times v}$ be such that $span(V) = V$ and $T \in R^{n-v\times v}$ be a left annihilator of V , i.e, $KerTE = ImV$. The following theorem relates the existence of a stabilizing static output feedback control law (3), to the solution of two coupled Sylvester equations. The system (4) is impulse controllable, *i.e.* $rank[E\, AS_\infty\, B]$, where the coluns of the matrix S_∞ span the kernel of E. Then there exists a output feedback K such that $u = Ky$ where $K \in R^{m\times p}$, such that the closed loop system:

$$E\dot{x} = (A + BKC)x, \tag{6}$$

would be impulse free, equivalently,

$$E_1\dot{x}(t) = A_1x(t) + B_1K_1C_1u(t) \tag{7}$$
$$0 = A_2x(t) + B_2K_2C_2u(t), \tag{8}$$

is impulse-free and the matrix $H_K = \begin{bmatrix} E_1 \\ A_2 + B_2K_2C_2 \end{bmatrix} \in R^{n\times n}$ is non singular. Since E_1 is full row rank: $rank(E_1) = q$, there exists an orthogonal matrix $W \in R^{n\times n}$ such that $H_W := HW$ would be in the following form (obtained by QR decomposition):

 © 2018 SBMAC

$H_W = \begin{bmatrix} E_1 \\ A_2 \end{bmatrix} W = \begin{bmatrix} E_1 & 0 \\ A_{21} & A_{22} \end{bmatrix}$, where $E \in R^{q\times q}$ is non singular and $A_{22} \in R^{n-q\times n-q}$. Now, by defining the output feedback matrix K as follows: $K = \begin{bmatrix} 0 & K_2C_2 \end{bmatrix} W^T$, where $K_2 \in R^{n-q\times n-q}$, we obtain the following relation: $H_KW = \begin{bmatrix} E_1 \\ A_2 \end{bmatrix} W + \begin{bmatrix} 0 \\ B_2K_2C_2 \end{bmatrix} W = \begin{bmatrix} E_{11} & 0 \\ A_{21} & A_{22}+B_2K_2C_2 \end{bmatrix}$, where $A_{22} + B_2K_2C_2 \in R^{n-q\times n-q}$. Note that the matrix E_{11} is non singular, and hence to make the closed loop system impulse-free we have to ensure that $\det(A_{22} + B_2K_2C_2) \neq 0$. Furthermore, it is demonstrated in [12], [9] that the inverse of matrix $A_{22} + B_2K_2C_2$ is needed while computing output feedback matrix for assigning the closed loop finite poles at appropriate locations in the complex plane. Hence, to avoid numerical errors in the finite pole placement, special care must be taken while computing K_2C_2, so as to ensure that $A_{22}+B_2K_2C_2$ is well-conditioned. In this context, the problem of interest can be precisely posed as follows.

Problem 1: Find $inf||K||_K$ such that i) response of the closed loop system (6) is impulse-free that is, $\det(A_{22}+B_2K_2C_2) \neq 0$ and ii) the condition number of $A_{22}+B_2K_2C_2$ is small.

3 Controller Design

In this section we formulate a semi-definite program to compute a desired output feedback matrix K which will ensure that the closed loop system (6) is impulse free and such that the matrix $A_{22} + B_2K_2C_2$ is well-conditioned. For this purpose, let us define a set N as follows:

$$N = \{K_2 \in R^{m\times n-q}/det(A_{22} + B_2K_2C_2) \neq 0\}. \quad (9)$$

Problem 2: Find $min_{K_2\in N}||K||_K$ such that the matrix $A_{22}+B_2K_2C_2$ is well-conditioned. Note that Problem 2 is a non-convex optimization since the set N is non-convex. To convexity the problem we establish a sufficient condition on K_2 in the following result based in [8] .

Theorem 3.1. *Let us denote $A_{K2} = A_{22} + B_2K_2C_2$. If K_2 satisfies following condition:*

$$\begin{bmatrix} \frac{1}{2}(A_{K2} + A_{K2}^T) & \beta I_{n-q} \\ \beta I_{n-q} & I_{n-q} \end{bmatrix} \succ 0, \quad (10)$$

for some positive β then $A_{K2} \in R^{(n-q)\times(n-q)}$ is non singular.

Proof: According to the Schur complement relation, (9) can be written as follows:
$\frac{1}{2}(A_{K2} + A_{K2}^T) - \beta^2 I_{n-q} \succ 0 \Longrightarrow \lambda_{min}(\frac{1}{2}(A_{K2} + A_{K2}^T)) > \beta^2$
$\Longrightarrow sn(A_{K2}) \geq \lambda_{min}(\frac{1}{2}(A_{K2} + A_{K2}^T)) > \beta^2$ where $sn(A_{K2})$ is the smallest singular value of A_{K2} and $\lambda_{min}(\frac{1}{2}(A_{K2}+A_{K2}^T))$ is the minimum eigenvalue of $\frac{1}{2}(A_{K2}+A_{K2}^T)$. Since the smallest singular value of A_{K2} is greater than zero, the matrix A_{K2} is non singular. This completes the proof.

 © 2018 SBMAC

Note that Theorem (3.1) defines a sufficient condition on K_2 such that the matrix A_{K2} is non singular. Additionally, inequality (9) is an LMI in β and K_2. Let us define a set M as follows:

$$M = \{K_2 \in R^{m\times n-q}/LMI\ (10)\ holds\ for\ \beta > 0)\}. \tag{11}$$

Then, M is a convex set; furthermore, $M \subseteq N$. Hence, instead of using a non convex set in Problem 2, we perform optimization over a convex set M. Next, we discuss on formulating a semi-definite program to minimize $||K||_K$.

Let us denote k_i^T for $i = 1, 2, \ldots, m$ as the i^{th} row of K_2. Then, $||K||_K$ can be minimized resulted in a positive scalar λ which satisfies an LMI:

$$\begin{bmatrix} I & k \\ k^T & \lambda \end{bmatrix} \succ 0,$$

where $k = [k_1^T, k_2^T, \ldots, k_m^T]^T$. This can be seen as follows: applying the Schur complement formula, we have

$$k^T k < \lambda \Longrightarrow ||K_2||_K < \lambda.$$

Since W is orthogonal, we can write

$$||K||_K = ||\begin{bmatrix} 0 & K_2 \end{bmatrix} W^T||_K = ||K_2||_K < \lambda.$$

Hence, to compute minimum norm K that eliminate impulses from the response of the closed loop system (4), we formulate the following convex optimization:

Problem 3: Find $min_{k,\beta,\lambda}\lambda$ subject to i) $\begin{bmatrix} \frac{1}{2}(A_{K2} + A_{K2}^T) & \beta I_{n-q} \\ \beta I_{n-q} & I_{n-q} \end{bmatrix} \succ 0$; ii) $\begin{bmatrix} I & k \\ k^T & \lambda \end{bmatrix} \succ 0$ for $\beta > 0$.

The solution of Problem 3 will produce a non singular matrix $A_{22} + B_2K_2C_2$, and hence the closed loop system (4) would be impulse-free. However, with this setting, since we are allowing β to take any arbitrary small positive number, the smallest singular value of A_{K2} (sn(A_{K2})) will also be very small. Then, the condition number of A_{K2},

$$k(A_{K2}) = \frac{s_1(A_{K2})}{sn(A_{K2})}, \tag{12}$$

where $s1(A_{K2})$ is the largest singular value of A_{K2}, would be very large, and hence the resulting non singular matrix A_{K2} might be ill-conditioned. We formulate an optimization where $sn(A_{K2})$ is maximized and $s1(A_{K2})$ is minimized simultaneously. This strategy will help us in improving the condition number of A_{K2}. We have already shown in Theorem 1 that $sn(A_{K2}) \geq \beta^2$, and hence maximization of β will maximize A_{K2}. Now, we will show that minimization of λ essentially reduces the maximum singular value of A_{K2} ($s1(A_{K2})$). Note that $s1(A_{K2})$ can be written as follows:

$$s_1(A_{K2}) = s_1(A_{22} + B_2K_2C_2) \tag{13}$$
$$\leq s_1(A_{22}) + (s_1(B_2)s_1(K)s_1(C_2)) \tag{14}$$
$$\leq s_1(A_{22}) + s_1(B_2)\lambda s_1(C_2), \tag{15}$$

 © 2018 SBMAC

and hence $s1(A_{K2})$ can be reduced by minimizing λ. The above inequalities follows from [11, Theorem 3.3.16]. Hence, a relaxed optimization associated with Problem 2 can be formulated as follows:

Problem 4: Find $max_{k,\beta,\lambda}\beta - \lambda$ subject to i) $\begin{bmatrix} \frac{1}{2}(A_{K2} + A_{K2}^T) & \beta I_{n-q} \\ \beta I_{n-q} & I_{n-q} \end{bmatrix} \succ 0$; ii) $\begin{bmatrix} I_{mn} & k \\ k^T & \lambda \end{bmatrix} \succ 0$ for $\beta > 0$.

Since the constraints (i) and (ii) in Problem 4 are $LMIs$ and the objective function is linear, it is an LMI optimization problem, and hence can be solved by existing standard LMI solvers see [8]. Once K_2 is computed by solving Problem 4, the desired matrix K, which makes the closed loop system (4) impulse free, can be obtained from the relation (7). The optimization Problem 4 is always feasible since we have assumed that the system (1) is impulse controllable.

Remark 3.1. *Recall that the set N , defined in (9), is a non convex set. Hence, to convexity the related optimization we compute a set M, in (9), which is a convex subset of N , and perform optimization over M. As a result the optimal (sub-optimal) solution of Problem* 4 *is an upper bound for the minimum value of $||K||_K$. In the following section we consider a numerical example to verify the effectiveness of the proposed approach.*

4 CONCLUSION

In this work we develop a novel algorithm to compute a output feedback matrix for an LTI regular descriptor system to eliminate impulses from the response. We represent a subset of the set of non singular matrices by an LMI, which enables to formulate the associated problem as a semi-definite program. We demonstrated through numerical example that the objective of only minimizing the norm of gain matrix might produce numerical errors while assigning the closed loop finite poles. This difficulty is then overcome by defining a cost function which simultaneously minimizes the norm of gain matrix and improve the condition number of the associated non singular matrix. The proposed method can be extended in the direction of developing a convex algorithm to minimize the norm of output feedback matrix for assigning the finite poles at i) some fixed locations ii) within a stability region in the complex plane. These objectives are under current investigation.

References

[1] W. Blajer and K. Kodziejczyk, Control of underactuated mechanical systems with servo-constraints, *Nonlinear Dynamics*, 50(4):781–791, 2007.

[2] K. E. Brenan, S. L. Campbell, and L. R. Petzold, *Numerical Solution of Initial-Value Problems in Differential Algebraic Equations*. Philadelphia, PA: SIAM Publications, 2nd ed., 1996.

[3] K. E. Brenan, S. L. Campbell, and L. R. Petzold, *Numerical Solution of Initial-value Problem in Differential Algebraic Equations*. New York: SIAM, 1989.

 © 2018 SBMAC

[4] S. L. Campbell, P. Kunkel, and V. Mehrmann, *Control and Optimization with Differential-Algebraic Constraints, ch. Regularization of Linear and Nonlinear Descriptor Systems*. SIAM, 2012.

[5] E. B. Castelan and E. R. Llanos Villarreal and S. Tarbouriech, Quadratic Characterization and Use of Output Stabilizable Subspaces in Descriptor Systems, *Proceedings (CD) 1st IFAC Symposium on System Structure*, Prague, volume 1, pages 255-260, 2001.

[6] E. B. Castelan and J. C. Hennet and E. R. Ll. Villarreal, Quadratic Characterization and Use of Output Stabilizable Subspaces,*IEEE Trans. Automatic. Control*,48(4): 654–660, 2003.

[7] E. B. Castelan, J. C. Hennet, and Elmer R. Ll. Villarreal , Output Feedback Design by Coupled Lyapunov-Like Equations*15 th IFAC World Congress on Automatic Control*, Spain, volume 1 pages 207-212, 2002.

[8] S. Datta, Optimization Based State Feedback Control Design for Impulse Elimination in Descriptor Systems, *Indian Control Conference (ICC) Indian Institute of Technology Hyderabad*, India, 2016.

[9] G. R. Duan, *Analysis and design of descriptor linear systems*. New York, NY: Springer-Verlag, 2010.

[10] P. Kunkel and V. Mehrmann, Differential-Algebraic Equations. *Analysis and Numerical Solution*. Zürich, Switzerland: EMS Publishing House, 2006.

[11] B. Pal and B. Chaudhuri, *Robust control in power systems*. Springer : New York, Power electronics and power systems, 2005.

[12] L. Dai, *Singular Control Systems*. Berlin, Germany: Springer-Verlag, 1989.

[13] A. Varga, A numerically reliable approach to robust pole assignment for descriptor systems,*Future Generation Computer Systems*,19 (1):1221–1230, 2003.

[14] E. R. Ll. Villarreal, J. A. R. Vargas, and E. M. Hemerly, Static Output Feedback stabilization using Invariant Subspaces and Sylvester Equations, *TEMA - Tend. Mat. Apl. Comput.*, 10(1):99–110, 2009.

DOI: 10.5540/03.2018.006.01.0410 © 2018 SBMAC

DINCON 2017
CONFERÊNCIA BRASILEIRA DE DINÂMICA, CONTROLE E APLICAÇÕES
30 de outubro a 01 de novembro de 2017 – São José do Rio Preto/SP

Suspensão Semi-ativa com Controlador Fuzzy

Maxwell Cavalcante Jácome[1]
Italo Oliveira Rebouças[2]
Engenharia Mecânica, UFERSA, Mossoró, RN
Natanael Expedito de Carvalho Mendes[3]
Bacharelando em Ciência e Tecnologia, UFERSA, Mossoró, RN
Elmer Rolando Llanos Villarreal[4]
Walter Martins Rodrigues[5]
Centro de Ciências Exatas e Naturais, UFERSA, Mossoró, RN

Resumo. A suspensão automotiva é o sistema responsável pelo controle das vibrações oriundas das variações do nível do solo. A modelagem utilizada para análise de uma suspensão se baseia no modelo de um quarto do veículo, o qual será representado dinamicamente em ambiente Simulink®. Para propor um sistema mais eficiente do que a convencional suspensão passiva, cujos parâmetros de rigidez e amortecimento são fixos, propõe-se um sistema de suspensão semi-ativa, em que o parâmetro de amortecimento é variável através de um controlador baseado na linguagem fuzzy. Foram comparadas as respostas de deslocamento e aceleração a fim de verificar a aplicabilidade do controle fuzzy numa suspensão semi-ativa.

Palavras-chave. Suspensão semi-ativa, Controlador Fuzzy, Simulink.

1 Introdução

O funcionamento de mecanismos em geral apresentam naturalmente vibrações indesejadas. No caso de veículos automotivos, o sistema voltado para lidar com tais vibrações é o de suspensão, garantindo o conforto e a estabilidade necessários à condução do automóvel.

[1] maxwellc.jacome@hotmail.com
[2] italo_reboucas@hotmail.com
[3] necmendes07@gmail.com
[4] elmerllanos@ufersa.edu.br
[5] walterm@ufersa.edu.br

Os componentes desse sistema são, essencialmente, uma mola (com o objetivo de armazenar a energia das vibrações) e um amortecedor (com o fim de dissipá-la em forma de calor) [4].

Quanto à forma de atuação, a literatura apresenta três modalidades quanto a sua autonomia: sistema passivo, semi-ativo e ativo. Apesar do vasto uso do sistema passivo por sua simplicidade de atuação por conta dos parâmetros fixos de rigidez e amortecimento, o desenvolvimento de novas técnicas de controle e de atuadores mais eficientes permitem a proposta de abordagens ativas e semi-ativas, as quais aperfeiçoam o tempo e qualidade de resposta do sistema abordado. Assim, o aumento da eficiência está associado a uma teoria de controle eficiente.

Com o desenvolvimento de amortecedores em que se utiliza fluido eletroreológico ou magnetoreológico [2], é possível obter equipamentos cujo valor de amortecimento é variável de acordo com a perturbação submetida ao sistema de suspensão. É necessária, então, a elaboração de uma estratégia de controle que, a partir dos dados obtidos por sensoriamento proveniente das variações da pista, gere uma ação de saída, equivalente a um valor de amortecimento.

Propõe-se neste trabalho a aplicação da linguagem difusa (fuzzy), semelhante à tomada de decisões humanas, permitindo meias verdades e meias mentiras. A linguagem fuzzy se apresenta como uma alternativa a vários setores da indústria, principalmente quando a precisão da resposta custa caro ao sistema de controle. A partir dos dados da velocidade absoluta e velocidade relativa, o controlador será capaz de resultar numa resposta para o amortecimento.

Após uma explanação sobre as classificações dos sistemas de suspensão e do método de controle pela linguagem fuzzy, será realizada uma simulação de um sistema convencional (suspensão passiva), o qual será comparado com a resposta de um sistema de suspensão ativa.

2 Métodos

2.1 Suspensão veicular

Uma suspensão passiva consiste de componentes convencionais com propriedades de mola e amortecedor invariantes com o tempo. Os amortecedores são, usualmente, cilindros preenchidos com óleo hidráulico ou gás comprimido, dentro do qual um pistão conectado por uma haste se move. O fluido gera uma força de reação ao movimento do pistão proporcional à velocidade relativa entre as massas por ele interligadas [6].

Se tratando de suspensão semi-ativa, a mesma refere-se a sistemas que não necessitam de energia externa adicional, além daquela necessária para acionar dispositivos como válvulas, bobinas, atuadores, entre outros [3]. Contém elementos de mola e amortecedor, semelhante à suspensão passiva. No entanto, a presença de um controle é capaz de alterar o coeficiente de amortecimento, alterando assim a força de reação do amortecedor.

Por outro lado, a suspensão ativa possui um atuador que, através da aplicação de uma força, pode tanto dissipar energia como armazenar e aplicar uma energia externa para a estabilização do automóvel utilizando dados de sensores ligados ao veículo.

A composição de sua estrutura contém uma mola mecânica, um atuador e a presença ou não de um amortecedor estático. Geralmente os atuadores são hidráulicos ou pneumáticos e eletromagnéticos [6].

O modelo “um quarto de veículo” (do inglês quarter car) simplifica a análise da suspensão de um automóvel, adotando que a massa do veículo se distribui uniformemente

nas quatro rodas e que a atuação de cada amortecedor é independente. O modelo pode variar de acordo com o tipo de suspensão, caracterizado pela presença de um atuador de força no tipo ativo e por um amortecedor variável no caso semi-ativo, como ilustrado na Figura 1.

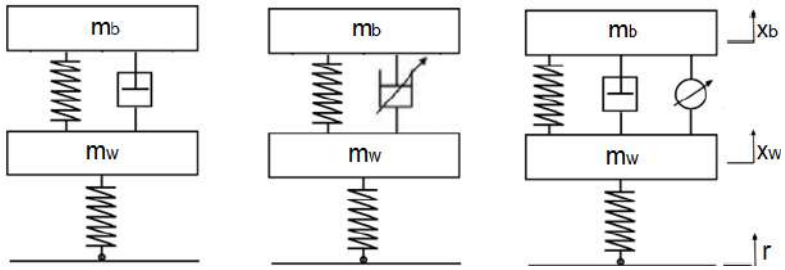

Figura 1: Modelos de suspensão passiva (esquerda), semi-ativa (centro) e ativa (direita)

A massa suspensa (m_b) representa a massa total do corpo (body) dividida por quatro, sendo sustentada imediatamente pela força elástica de uma mola de rigidez "k_s", um amortecedor com coeficiente de amortecimento "b". A massa (m_w) representando a massa fixa do pneu, roda (wheel) e demais componentes a ela associada.

A representação da mola inferior (entre m_w e o solo) se trata da compressibilidade do pneu (k_w). Os eixos x_b, x_w e r indicam, respectivamente, os deslocamentos da massa suspensa, da massa do conjunto pneu-roda, e da superfície de referência, representando esta as variações da pista, sendo assim a fonte das perturbações.

Ao ser feito o somatório de forças em ambos os blocos de massa, é possível chegar a equações diferenciais de segunda ordem que descrevem o movimento.

$$m_b\ddot{x}_b + b_s(\dot{x}_b - \dot{x}_w) + k_s(x_b - x_w) = 0 \quad (1)$$

$$m_w\ddot{x}_w + b_s(\dot{x}_b - \dot{x}_w) + k_s(x_w - x_b) - k_l(r - x_w) = 0 \quad (2)$$

2.2 Controle Fuzzy

A linguagem fuzzy surgiu desde os trabalhos de Lofti A. Zadeh em 1965, quando o mesmo estudava problemas de conjuntos que não apresentavam fronteira definida [5]. As características desta linguagem diferem da usual linguagem boleana de padrões restritos: 0 ou 1, sim ou não, verdadeiro ou falso. O método de controle por linguagem fuzzy se processa em três etapas: fuzzyficação, inferência e defuzzyficação.

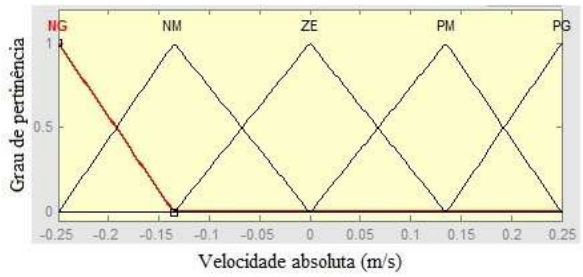

Figura 2: Funções de pertinência da velocidade absoluta.

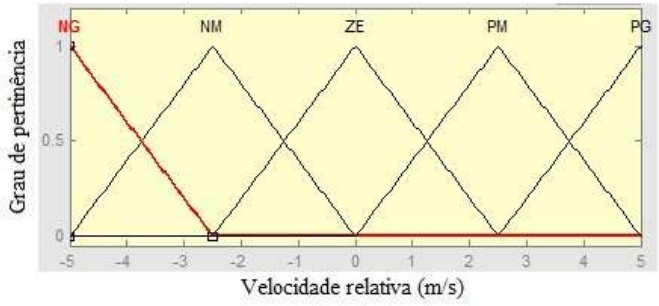

Figura 3: Funções de pertinência da velocidade relativa.

Na etapa de fuzzyficação são estabelecidas as funções de pertinência concernentes às variáveis de entrada, a velocidade absoluta da massa suspensa (Figura 2) e a velocidade relativa entre as massas (Figura 3), sendo necessário estabelecer o domínio de cada.

A resposta do controlador diz respeito à variável de amortecimento, a qual também é composta por cinco graus de pertinência, como na Figura 4.

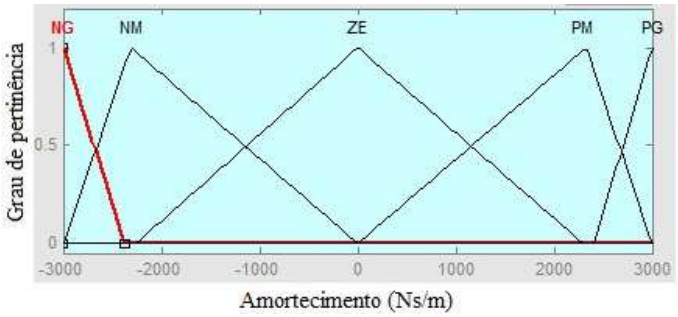

Figura 4: Funções de pertinência do amortecimento.

Através da Tabela 1 é possível notar que com 5 graus de pertinência em cada variável de entrada são necessárias 25 regras de inferência baseadas numa relação if then (se então).

Tabela 1: Regras de inferência.

Amortecimento		**Velocidade Absoluta**				
		NG	**NM**	**ZE**	**PM**	**PG**
Velocidade relativa	NG	NG	NG	NM	NM	NM
	NM	NG	NM	NM	NM	NM
	ZE	NM	NM	ZE	PM	PM
	PM	PM	PM	PM	PM	PG
	PG	PM	PM	PM	PG	PG

3 Resultados

Com base nas equações que descrevem o sistema, foi construído um circuito de blocos no ambiente Simulink® representando o fluxo de sinais do sistema (Figura 5). Inicialmente o bloco associado ao amortecimento apresenta valor constante, gerando os gráficos do deslocamento (Figura 6) e da aceleração (Figura 7) da massa suspensa, sendo as respostas que os passageiros estão sujeitos a sentir.

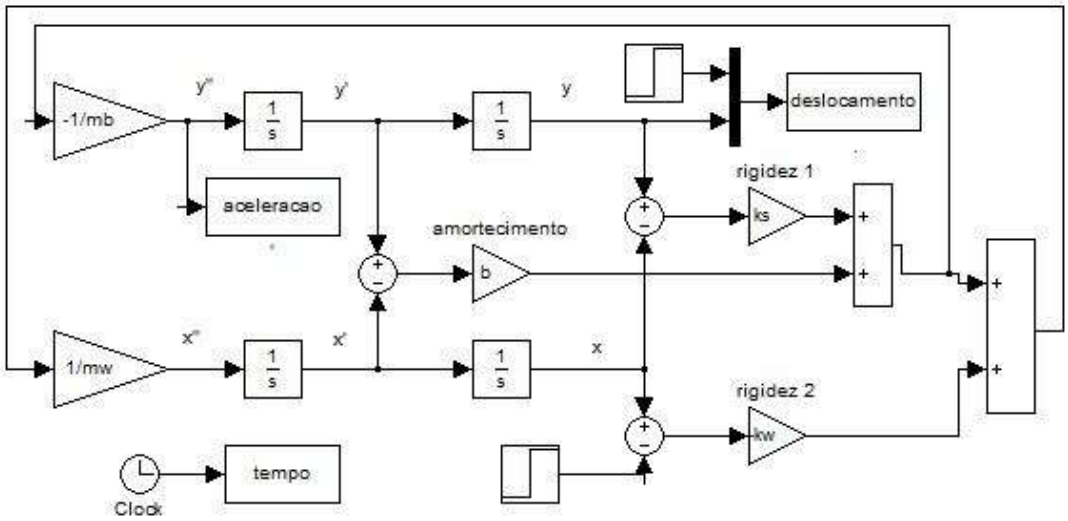

Figura 5: Circuito de blocos no Simulink® para o sistema passivo.

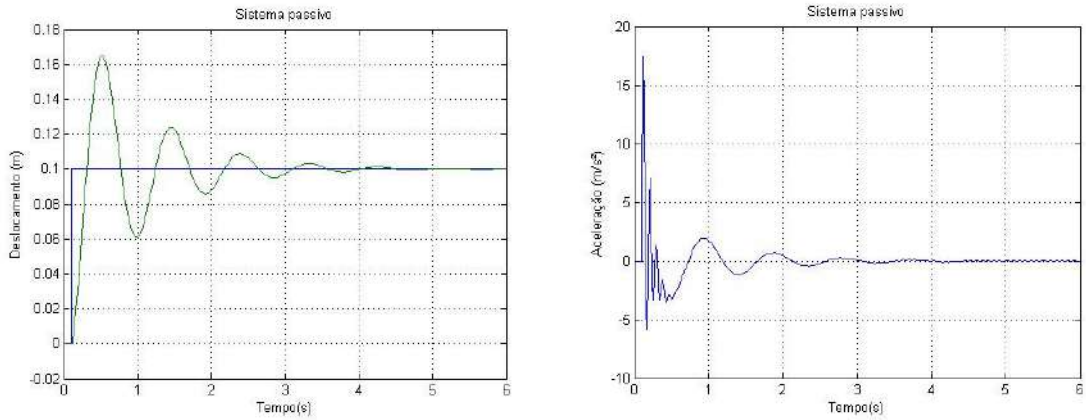

Figura 6: Gráfico do deslocamento (à esquerda) e da aceleração (à direita) da massa suspensa.

Em seguida, o bloco de amortecimento foi substituído pelo controlador fuzzy (Figura 7), o qual recebe como entradas os sinais de velocidade absoluta e relativa. Os gráficos são exibidos na Figura 8.

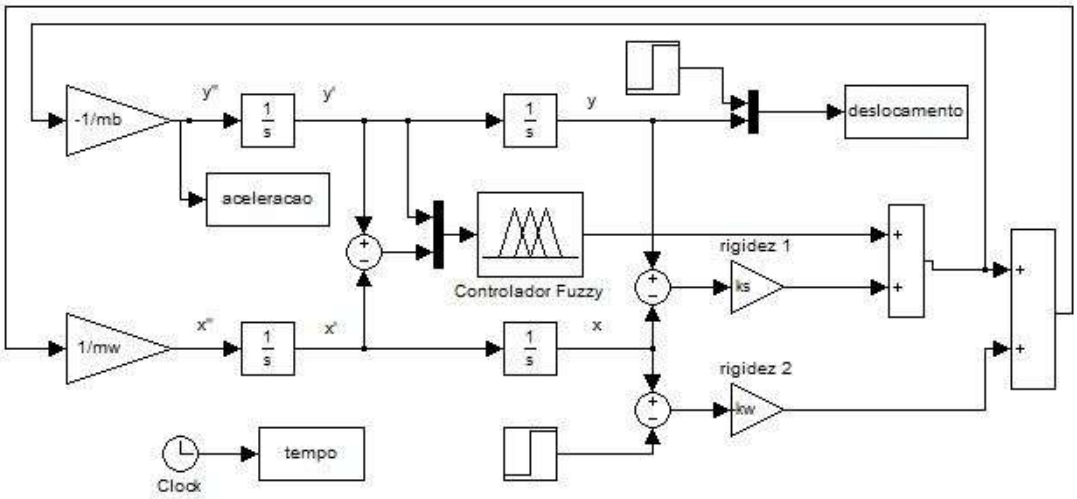

Figura 7: Circuito de blocos no Simulink® para o sistema semi-ativo.

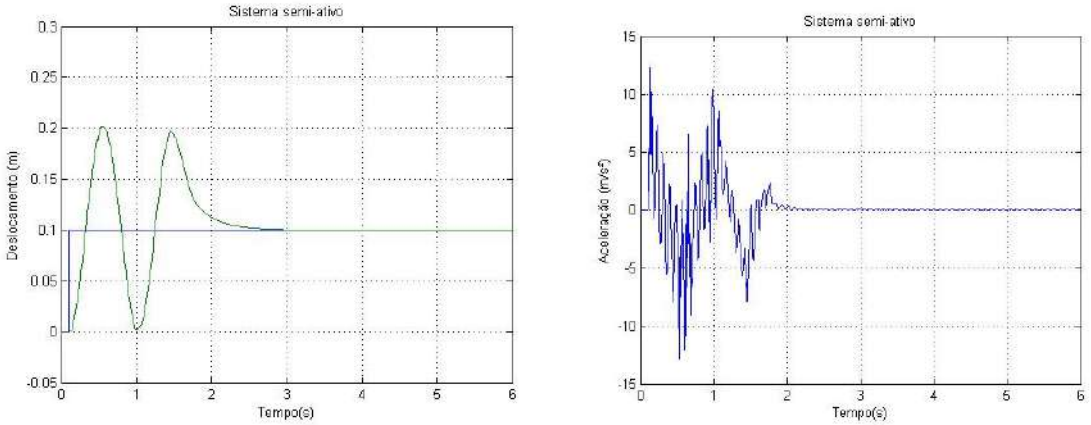

Figura 8: Gráfico do deslocamento (à esquerda) e da aceleração (à direita) da massa suspensa.

4 Discussões

Alterações na faixa de variação do amortecimento aumentaram o tempo de estabilização ou mesmo impediram que tal condição ocorrece. O controlador proposto se baseia em 25 regras de inferência, simplificando a atuação do controle se comparado às 49 regras utilizadas por Abu-Khudhair [1].

Comparando os resultados obtidos, o sistema semi-ativo reduziu o tempo de estabilização do deslocamento, embora tenha elevado os picos, o que é indesejável. Quanto à aceleração, o sistema proposto reduziu o tempo de estabilização e reduziu os picos, apesar de apresentar uma resposta mais irregular.

5 Conclusão

O estudo de novos métodos de controle de suspensões deve acompanhar a evolução dos equipamentos amortecedores. Foi possível demonstrar um modelo de suspensão semi-ativa, o qual se mostrou vantajoso em relação à redução do tempo de estabilização; em contrapartida, exige implementações que tornem a resposta mais regular e com menores picos de atuação. Apesar de adequações no controlador fuzzy se darem por mudanças de parâmetros baseada na tentativa e erro, tal característica permite várias implementações e fornece uma vertente de novos trabalhos que possam buscar uma melhor condição de funcionamento.

Agradecimentos

Agradecemos à Universidade Federal Rural do Semiárido (UFERSA) e ao Cento de Ciências Exatas e Naturais (CCEN) por possibilitarem a realização deste trabalho.

Referências

[1] A. Abu-Khudhair, R. Muresan and S. X. Yang, Fuzzy control of semi-active automotive suspensions, International Conference On Mechatronics And Automation, pp. 2118-2122, (2009), DOI: 10.1109/ICMA.2009.5246409.

[2] L. A. Gagg Filho, Controle semi-ativo de vibrações com fluido magnetoreológico utilizando LMis e lógica nebulosa otimizada por algoritmo genético, Dissertação de Mestrado em Engenharia Mecânica, Universidade Estadual Paulista Júlio de Mesquita Filho, (2013).

[3] A. W. Montini, Estratégia de controle fuzzy para suspensão ativa automotiva, Monografia de Engenharia Elétrica, Universidade São Francisco, (2006).

[4] S. Rao, Vibrações Mecânicas, 4. ed., Pearson, (2008).

[5] F. G. B. Sena, Controle fuzzy aplicado à otimização de um sistema eólico de velocidade variável, Dissertação de Mestrado em Sistemas de Comunicação e Automação, Universidade Federal Rural do Semiárido, (2015).

[6] X. D. Xue et al, Study of art of automotive active suspensions, 4th International Conference On Power Electronics Systems And Applications, vol. l, 1-7, (2011), DOI: 10.1109/PESA.2011.5982958.

COBENGE 2016
XLIV CONGRESSO BRASILEIRO DE EDUCAÇÃO EM ENGENHARIA
27 a 30 de setembro de 2016
UFRN / ABENGE

USO DO SIMULINK PARA SIMULAÇÃO DE UM SISTEMA DINÂMICO DESCRITO POR EQUAÇÕES DIFERENCIAIS

Maxwell Cavalcante Jácome – maxwellc.jacome@hotmail.com
Natanael Expedito de Carvalho Mendes – necmendes07@gmail.com
Elmer Rolando LLanos Villarreal – elmerllanos@ufersa.edu.br
Universidade Federal Rural do Semiárido, Departamento de Ciências Exatas e Naturais
R. Francisco Mota, 572 - Costa e Silva
59600-971 – Mossoró – RN

Resumo: *Diversos problemas da engenharia são descritos através de equações diferenciais, as quais necessitam de uma vasta compreensão matemática a fim de se chegar a uma função que, dada as suas derivadas, compõem uma determinada equação. No entanto, problemas complexos dificultam a obtenção de soluções exatas, enquanto o interessante é tão somente observar o comportamento gráfico do sistema. Por isso, ferramentas computacionais facilitam o estudo de determinados problemas, em que se dará ênfase à ferramenta Simulink do Matlab, a qual é capaz de simular sistemas dinâmicos modelados por um circuito de blocos. Pretende-se tornar esta ferramenta acessível a quem está conhecendo-a, em que será aplicada em um exemplo vibratório de uma suspensão veicular. Após a descrição matemática do problema, serão obtidas equações diferenciais a partir das quais será construído o circuito no Simulink, buscando-se uma resposta gráfica de estabilização do sistema massa mola amortecido.*
Palavras-chave: *Equações Diferenciais, Suspensão, Simulink, Vibrações Mecânicas*

1. INTRODUÇÃO

Muitos problemas da engenharia são modelados matematicamente através de equações diferenciais. Devido a sua complexidade de solução em diversos casos, surge então a opção de desenvolver algo que facilite as resoluções dessas equações. Para isso, é proposta nesse trabalho uma maneira de resolver equações diferenciais através da ferramenta Simulink (Matlab), que proporciona um ambiente de simulação em blocos para sistemas dinâmicos, fazendo com que seja mais conveniente trabalhar com um assunto de vasta aplicação.

Nos sistemas mecânicos em movimento, busca-se sempre a redução da influência de vibrações indesejadas. Se tratando de veículos automotivos, o sistema responsável por tal atuação é o de suspensão. Através da modelagem de um modelo simples de suspensão, referente a um quarto de veículo, pretende-se demonstrar a aplicabilidade da ferramenta computacional para a construção e simulação do sistema vibratório, explicando a utilização de alguns modos de operação do Simulink e demonstrando a eficácia da proposta por meio da resposta gráfica do sistema.

2. REFERENCIAL TEÓRICO

2.1. Equações diferenciais

Equações diferenciais é um conteúdo matemático que pode ser aplicado em diversas áreas de conhecimento, como na física, química, biologia, economia, estatística, geografia e em vários outros ramos diversificados (ALITOLEF, 2011). Como objeto de estudo deste trabalho, tem-se também as equações diferenciáveis aplicadas na solução de problemas práticos na engenharia. Não há em específico apenas uma ramificação de engenharia que vá utilizar os conhecimentos de equações diferenciais para efetuar melhorias, é um assunto que tem espaço em todas.

Por definição, sabe-se que uma equação diferencial é uma equação que contém as derivadas ou diferenciais de uma ou mais variáveis dependentes, em relação a uma ou mais variáveis independentes onde ela possui determinadas características que a classifica quanto à ordem, por exemplo, que é a ordem da derivada mais alta da equação. (ZILL, 2001).

Uma equação diferencial de segunda ordem possui a seguinte forma:

$$m\ddot{x} = -kx - \beta\dot{x} \tag{1}$$

A representação algébrica acima é de um esquema de sistema harmônico amortecido onde m é a massa de um corpo, k é a constante elástica da mola e β é uma constante de amortecimento, positiva. Temos que a equação (1) é um exemplo de equação diferencial de segunda ordem, sabendo que a ordem de uma equação é definida a partir da derivada mais alta, nesse caso $\ddot{x}$. Com as devidas manipulações matemáticas, obtém-se a seguinte expressão como solução geral:

$$x(t) = e^{-\lambda t}\left(c_1 cos\sqrt{\omega^2 - \lambda^2}t + c_2 sen\sqrt{\omega^2 - \lambda^2}t\right) \tag{2}$$

Pode ser observado que a solução de uma equação diferencial é bastante complexa para as pessoas que não estão habituadas a esse tipo de expressão algébrica e de difícil agilidade ao utilizá-la em algoritmos de programação. Dessa forma, é ressaltada a importância de avaliar o comportamento do gráfico dessa equação.

2.2. Suspensão veicular

Segundo Rao (2008), um sistema vibratório (onde corpos possuem movimentos oscilatórios e forças associadas) inclui um meio para armazenar energia potencial (mola e ou elasticidade), um meio para armazenar energia cinética (massa ou inércia) e um meio de perda gradual de energia (amortecedor).

Nos veículos automotivos, a suspensão estabelece a conexão entre a carroceria do veículo e as rodas com os pneus e, por essência, possibilita o movimento vertical da roda para compensar as irregularidades da pista de rolamento (BOSH, 2005).

Proceeding Series of the Brazilian Society of Computational and Applied Mathematics

Aplicação do Controle Servo Visual em um Quadrirrotor

Flavio de Abreu Bezerra Filho[1]

Bacharelando em Ciência e Tecnologia, Departamento de Ciências Exatas e Naturais, UFERSA, Av. Francisco Mota, 572, Bairro Costa e Silva, CEP 59625900 Mossoró, RN.

Maxwell Cavalcante Jácome[2]

Bacharelando em Ciência e Tecnologia, Departamento de Ciências Exatas e Naturais, UFERSA, Av. Francisco Mota, 572, Bairro Costa e Silva, CEP 59625900, Mossoró, RN.

Elmer Rolando Llanos Villareal[3]

Programa de Pós-graduação em Sistemas de Comunicações e Automação -UFERSA, Departamento de Ciências Exatas e Naturais DCEN-UFERSA, Av. Francisco Mota, 572, Bairro Costa e Silva, CEP 59625900, Mossoró-RN

Resumo. Uma das formas de controlar a dinâmica de um robô é a partir da visão computacional. Dentre as técnicas estabelecidas na literatura, pretende-se desenvolver um estudo sistemático a fim de classificar os conceitos referentes ao controle servo visual aplicado em um quadrirrotor.

Palavras-chave. Visão Computacional, Servo Visão, Quadrirrotor, IBVS, PBVS.

1 Introdução

Normalmente, os robôs são utilizados na indústria para a execução de atividades com maior rapidez e agilidade que o ser humano, porém, estes dependiam bastante do homem para ter a possibilidade de exercer algumas de suas funções devido à baixa eficiência de seus sensores.

Devido ao aumento da necessidade do homem, este cenário vem mudando gradativamente e as máquinas estão cada vez mais aptas a servirem ao seu usuário, atendendo a praticamente todas as suas exigências.

Essa mudança se deve, em partes, a um tipo de sensor com maior capacidade de desempenhar a obtenção de informações de um determinado local – o sensor visual – onde, a câmera, juntamente com os sistemas de informação que compõem o robô,

[1] flavioabreubf@gmail.com
[2] maxwellc.jacome@hotmail.com
[3] elmerllanos@ufersa.edu.br

 © 2016 SBMAC

fornecem localização e forma dos elementos em um espaço definido. Em função dessa alta eficiência na busca de informação, os sensores servo visuais têm sido bastante utilizados pelos pesquisadores e cientistas atuais para auxiliar no controle de robôs.

De início, pretende-se aplicar as técnicas, já utilizadas em robôs terrestres, em robôs aéreos, no caso, os VANT's – veículos aéreos não tripulados – mais especificamente nos quadrirrotores. Para isso, é necessária a implementação dessas técnicas, primeiramente, em locais fechados e de ambiente conhecido para que se possa passar por uma série de testes, para que, por fim, seja possível manipular os robôs em áreas sujeitas a alterações impostas pela natureza, onde as matérias existentes no meio possam alterar a sua posição.

O aperfeiçoamento dos veículos aéreos não tripulados, com o auxílio do controle servo visual, permitirá que ele monitore, por exemplo, grandes áreas, podendo assistir desde o tráfego urbano até o setor de plantações rurais, sendo adaptável a diferentes ambientes.

2 Objetivos

A interação dos quadrotores com os interesses humanos gera uma relação promissora na inspeção de grandes áreas. Seja na infraestrutura, na agricultura, na pecuária, no monitoramento da poluição ambiental e em todas as áreas que sejam compstas por ambientes hostis que se caracterizam pelo difícil acesso tanto do homem quanto de robores terrestres.

Desse modo, o foco principal desse estudo é a aplicação do controle servo visual nos VANT's, visando o aperfeiçoamento das técnicas de monitoramento e controle de diversos ambientes.

3 Materiais e Métodos

O principal objeto de estudo foi um quadrirrotor do tipo Ar.Drone Parrot (versão 1.0), com o qual inicialmente foram realizados os testes de voo e coleta de imagens com controle manual. O VANT pesa 420g e é equipado com quatro motores presos a hastes de fibra de carbono e um corpo de plástico. A principal característica do veículo para esse estudo são suas duas câmeras, uma voltada para a frente e outra apontada verticalmente para baixo. Ambas as câmeras são do tipo VGA (640x480). É alimentado por uma bateria capaz de fornecer uma autonomia de voo de aproximadamente doze minutos [4].

Figura 1: AR. Drone Parrot (versão 1.0).

DOI: 10.5540/03.2016.004.01.0004 © 2016 SBMAC

Sobre o ponto de vista de controle, foram analisados os circuitos de alguns toolboxes (traduzido livremente por caixas de ferramentas) os quais fornecem circuitos de simulação em ambiente Matlab (Simulink). Os arquivos disponíveis são livres, permitindo a modificação e adaptação, e foram bastante úteis na compreensão das etapas nas quais a imagem deve passar desde sua captura até a ação tomada pelo sistema de controle:

- Robotics Toolbox: é composto por um conjunto de ferramentas para simulação de robôs móveis.
- Machine Vision Toolbox: disponibiliza funções de controle visual em máquinas.
- Visual Servoing Toolbox: os recursos visuais dos robôs são aplicados no sistema de controle servo visual.

4 Resultados

A visão computacional é a ciência que busca desenvolver algoritmos e tecnologias, através dos quais sistemas computacionais são capazes de interpretar imagens ou quaisquer outros dados de várias dimensões e extrair informações em um determinado contexto [3].

A aplicação da visão computacional em robôs móveis tem se desenvolvido graças a crescente disponibilidade de recursos computacionais de alto desempenho, somada aos resultados de muitos projetos de pesquisa nessa vertente e na de processamento de imagens, permite-nos considerar a inclusão destes sistemas em malhas fechadas de controle [2].

A abordagem de controle servo visual envolve os problemas e aplicações da visão robótica no controle de sistemas, abrangendo aspectos de realimentação, dinâmica e estimação de parâmetros [2]. Assim, o sistema servo visual se trata do controle da informação visual com sua realimentação em malha fechada, o que diminui os erros associados às imagens já que a cada ciclo o manipulador tem sua posição corrigida, até atingir a posição desejada.

Uma particularidade notada no estudo da aplicação do controle servo visual em robôs aéreos como nos quadrirrotores é sobre o comportamento da imagem adquirida para fazer parte do controle frente aos movimentos de voo. Graças à dinâmica de voo de um quadrirrotor, os movimentos de rolagem e arfagem são responsáveis pela translação horizontal e provocam uma inclinação na câmera embarcada, isso gera uma rotação relativa na imagem captada no sentido inverso do movimento do veículo. Nota-se que é indispensável a análise do erro intrínseco ao modo de captura das imagens que serão utilizadas no controle servo visual.

A análise da literatura sobre servo visão permitiu resultados conceituais, sobre como a abordagem de controle visual terá sua melhor aplicação num quadrirrotor.

4.1 Classificação da câmera

Um critério de classificação do controle servo visual é quanto ao numero de câmeras pertencentes ao sistema, podendo ser Monocular (apenas uma câmera), Estéreo ou

DOI: 10.5540/03.2016.004.01.0004 © 2016 SBMAC

Binocular, que utiliza duas câmeras, e Redundante, quando se têm mais de duas câmeras. Outro critério é a posição entre a câmera e o robô, podendo ser câmera fixa ("eye-to-hand"), onde a câmera se encontra imóvel durante o processo, e câmera embarcada ("eye-in-hand"), quando esta se move junta ao robô [6].

Nesse sentido é fácil classificar o veículo em estudo, visto que possui duas câmeras (binocular) as quais estão contidas em sua estrutura, enquadrando-se como "eye-in-hand".

4.2 Definição do erro

Outra classificação comumente trabalhada na literatura é quanto à definição do erro inerente ao sistema de controle, como segue:

- Image-Based Visual Servoing (IBVS)

No controle servo visual baseado em imagem o erro é definido no espaço da imagem (bidimensional), usando parâmetros das características visuais diretamente no seu cálculo [4].

Os parâmetros da imagem podem ser representadas matematicamente pelo vetor $s = [s_1 \dots s_k]^T$, e s_d é o vetor de valores desejados. Assim, o erro é dado por:

$$E(s) = s - s_d = 0$$

Para relacionar a taxa de variação nos parâmetros da imagem, $\dot{s}$, à velocidade da câmera v_c, tem-se a relação

$$\dot{s} = L_s(r)v_c$$

onde L_s é a matriz de iteração (também chamada de Jacobiano da imagem) relacionada ao vetor de características visuais s, representada da forma:

$$\boldsymbol{L_s} = \frac{\partial \boldsymbol{s}}{\partial \boldsymbol{r}} = \begin{bmatrix} \frac{\partial s_1}{\partial r_1} & \cdots & \frac{\partial s_1}{\partial r_m} \\ \vdots & \ddots & \vdots \\ \frac{\partial s_k}{\partial r_1} & \cdots & \frac{\partial s_k}{\partial r_m} \end{bmatrix}$$

Pode-se observar que no circuito do Simulink existe um bloco com a função de calcular a matriz Jacobiana, referente à matriz de interação.

DOI: 10.5540/03.2016.004.01.0004

© 2016 SBMAC

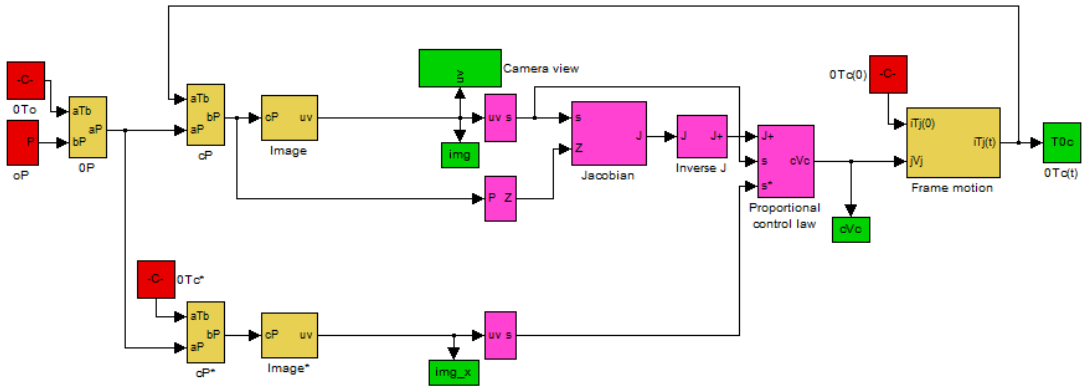

Figura 02: simulação do controle IBVS.

Além disso, nota-se que se trata de um sistema de malha fechada, com aquisição de imagens e realimentação do sistema de controle, conforme a definição de servo visual.

O modelo Simulink é um exemplo muito complexo que simula não só o robô, mas também a câmera e o algoritmo IBVS. A saída da câmera é a imagem em 2D, sendo o plano de coordenadas dos pontos de destino. Esses são usados para calcular a matriz Jacobiana da imagem que é invertida e multiplica o movimento desejado dos pontos de destino no plano da imagem. O movimento desejado é simplesmente a diferença entre os pontos do alvo observado e as posições dos pontos desejados [1].

- Position-Based Visual Servoing (PBVS)

O controle servo visual baseado em posição usa informações visuais para estimar a posição e orientação da câmera, e o erro se define no espaço da tarefa (tridimensional) [4].

Sendo a postura da câmera representada por $r = [X\ Y\ Z\ \phi\ \theta\ \psi]^T$ (onde X, Y e Z representam as coordenadas espaciais da câmera em relação a um sistema de coordenadas fixo no ambiente e ϕ, θ e ψ são os ângulos de rotação passíveis do veículo – rolagem, arfagem e guinada) e r_d a postura desejada, o erro é dado por:

$$E(r,t) = r(t) - r_d(t)$$

O posicionamento espacial definido em termos de três variáveis justifica a classificação do IBVS como 3D. De maneira análoga, o circuito pode ser representado por:

 © 2016 SBMAC

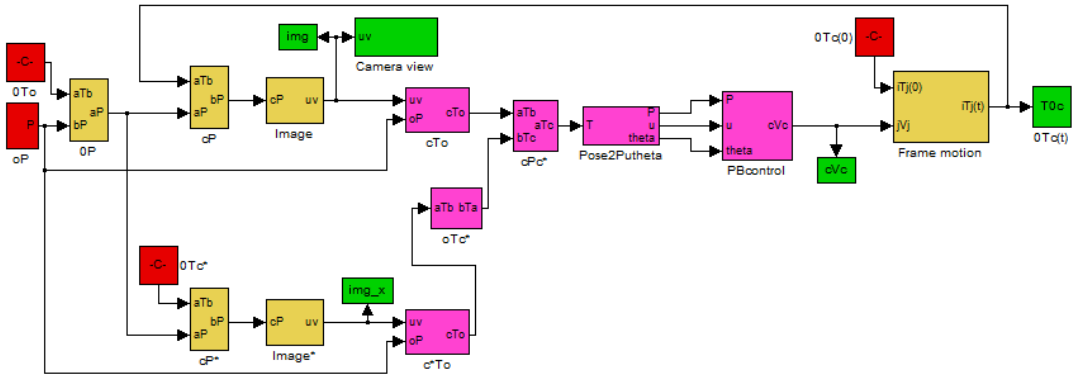

Figura 03: simulação do controle PBVS.

4.2 Comparação entre IBVS e PBVS

O fato de no PBVS se controlar a trajetória no espaço cartesiano facilita no projeto das leis de controle, ais quais serão mais simples, característica não pertinente à abordagem IBVS.

Tabela 1: Análise comparativa dos métodos de erro.

Método	Vantagens	Desvantagens
IBVS	Construção 2D (mais simples)	Estimação da profundidade
	Dispensa a calibração da câmera	
PBVS	Controla a trajetória no espaço cartesiano	Construção 3D (mais complexo)
		Estima a posição a cada iteração

A dificuldade da construção 3D diz respeito à necessidade de se ter a representação ideal das características do veículo ao qual a câmera estará a observar.

5 Discussões

Para solucionar os problemas contidos nas duas definições de erros, Menezes [4] e Gans [5] propõem a utilização de sistemas híbridos, em que tanto há a atuação de uma câmera embarcada como de uma fixa. Essa proposta atende a limitação do IBVS em se estimar a profundidade não dependendo apenas do método PBVS.

6 Conclusão

 © 2016 SBMAC

Essa exigência de aplicação do controle servo visual nos veículos aéreos se dá pela necessidade que o ser humano vem desenvolvendo ao longo dos anos. Isso permite que haja cada vez mais investimentos em pesquisas e testes acerca dessa tecnologia.

Tendo em vista esse estímulo, resultados positivos estão sendo obtidos, a partir de análises e manuseio de softwares, os quais trouxeram à tona características do VANT estudado como: a captura da imagem invertida pelo sistema binocular de câmeras embarcadas e a definição dos erros nos dois sitemas de controle, em duas dimensões (IBVS) ou em três dimensões (PBVS).

Diante do bom andamento dos estudos, a pesquisa continua sendo implementada em busca de novos resultados, a fim de contribuir para o aperfeiçoamento dessa tecnologia altamente promissora para a humanidade.

Agradecimentos

Agradecemos à CITED-UFERSA e ao CNPQ por subsidiarem os fatores ligados ao desenvolvimento do projeto.

Referências

[1] P. I. Corke, Robotics toolbox for Matlab, CSIRO, vol. 1, (2002).

[2] G. F. da Silveira Filho, Controle servo visual de veículos robóticos aéreos, Dissertação de Mestrado em Engenharia Elétrica, Unicamp, (2002).

[3] L. C. de Lima, Estudo sobre uma estratégia de controle adaptativo servo visual e sua aplicação em um robô industrial, Monografia para graduação em Engenharia de Controle e Automação, UFRJ, (2013).

[4] R. P. B. de Menezes, Controle servo visual de veículos aéreos multirrotores, Dissertação de Mestrado em Mecatrônica, UFBA, (2013).

[5] N. R. Gans and S. A. Hutchinson, Stable visual servoing through hybrid switched-system control, IEEE Transactions on Robotics, vol. 23, (2007).

[6] G. L. L. Muñoz, Análise comparativa das técnicas de controle servo-visual de manipuladores robóticos baseadas em posição e em imagem, Dissertação de Mestrado em Sistemas Mecatrônicos, UnB, (2011).

 © 2016 SBMAC

APLICAÇÃO DOS QUADRIRROTORES COMO OBJETO DE ESTUDO DE DIVERSAS ÁREAS DA ENGENHARIA

Elmer Rolando Llanos Villareal – elmerllanos@ufersa.edu.br
Universidade Federal Rural do Semiárido, Departamento de Ciências Exatas e Naturais
Av. Francisco Mota, 572, Bairro Costa e Silva
CEP 59625900 – Mossoró – RN

Flavio de Abreu Bezerra Filho – flavioabreubf@gmail.com
Universidade Federal Rural do Semiárido, Departamento de Ciências Exatas e Naturais
Av. Francisco Mota, 572, Bairro Costa e Silva
CEP 59625900 – Mossoró – RN

Luana Carla de Andrade – luana.cda@hotmail.com
Universidade Federal Rural do Semiárido, Departamento de Ciências Exatas e Naturais
Av. Francisco Mota, 572, Bairro Costa e Silva
CEP 59625900 – Mossoró – RN

Maxwell Cavalcante Jácome – maxwellc.jacome@hotmail.com
Universidade Federal Rural do Semiárido, Departamento de Ciências Exatas e Naturais
Av. Francisco Mota, 572, Bairro Costa e Silva
CEP 59625900 – Mossoró – RN

Resumo: *Os quadrirrotores têm se destacado por serem veículos com várias aplicações, graças às suas características que incluem o voo não tripulado, capacidade de permanecer imóvel no ar, de se deslocar em todas as direções, além da possibilidade de carregar objetos, em muitos casos câmeras, úteis tanto na captura de imagens do ambiente como para fins de automação. Tais funcionalidades vêm sendo cada vez mais adotados em aplicações nas diversas áreas da engenharia, o que torna o quadrirrotor um objeto promissor de estudo. Pretende-se utilizar tal veículo como estratégia de ensino de disciplinas relacionadas à engenharia, nas áreas de física, programação e controle, proporcionando a alunos recém-egressos um contato inicial com aplicações dos conteúdos a serem estudados bem como permitindo uma abordagem mais complexa para os estudantes com mais tempo de curso.*

Palavras-chave: *Quadrirrotor, Dinâmica, Controle, Programação.*

1. INTRODUÇÃO

A popularização dos quadrirrotores com fins de capturar imagens de lugares de difícil acesso não limita a aplicação desse Veículo Aéreo Não Tripulado (VANT) em sistemas de monitoramento de segurança e de lavouras, transporte de materiais a lugares de difícil acesso, graças às características desse veículo de levantar voos e pousar verticalmente e poder realizar

um voo pairado (sem se deslocar no ar) bem como rotacionando e transladando em todas as direções.

Esse conjunto de características permite uma abordagem em várias áreas das ciências exatas, podendo ser vista como uma estratégia de ensino de disciplinas que envolvem conceitos de dinâmica, controle, programação e mecânica dos fluidos, atraindo a atenção tanto de alunos ingressantes como daqueles que buscam uma aplicação mais complexa de seus conhecimentos.

2. DINÂMICA DE UM CORPO RÍGIDO

De maneira geral, os quadrirrotores são constituídos de quatro rotores fixos dispostos nos quatro cantos de uma estrutura cruzada, carregando em seu centro o conjunto de equipamentos necessários para sua automatização (COSTA, 2008).

Figura 1 – AR. Drone Parrot (versão 1.0).

Para a realização do voo é necessário que as pás que constituem cada rotor rotacionem em sentidos diferentes, alternadamente. Assim, dois rotores (opostos pelo centro) giram no sentido horário enquanto os outros dois no anti-horário. Tal restrição é um exemplo bastante didático da conservação do momento angular em um sistema físico. Geralmente essa situação é exemplificada nos helicópteros convencionais, onde é necessário que um haja um rotor na cauda dos helicópteros afim de evitar uma rotação indesejada oriunda do movimento rotacional das hélices, o que modifica o momento angular do sistema. Tal problema pode ser corrigido, no caso dos helicópteros, ao se utilizar dois sistemas de hélices, cada um girando num sentido para que o momento angular seja nulo. Já nos quadrirrotores, essa compensação é feita pelo sentido de giro de cada rotor.

O momento angular (L) de um corpo rígido que gira em torno de um eixo fixo é definido matematicamente por

$$L = I\omega \tag{1}$$

Como o momento de inércia (I) das hélices é o mesmo, o que pode variar o momento angular é a velocidade angular (ω), por se tratar de uma grandeza conservativa pela ausência de torque resultante externo. O sentido de cada momento é dado pela regra da mão direita, dependendo do sentido da rotação do corpo (HALLIDAY *et* al., 2008).

Assim, os movimentos de translação longitudinal nas situações (a) e (b) da "Figura 2" são realizados pela variação na velocidade com que as hélices 1 e 3, causando uma inclinação do veículo que o fará avançar, mantendo sempre o empuxo suficiente para ele não perder

DESENVOLVER UM CONTROLADOR FUZZY-PID PARA UM VEÍCULO AÉREO NÃO TRIPULÁVEL - VANT

Cauê Coelho Alves – caue20_@hotmail.com
Tiago Mateus Pereira Gonçalves – tiagomateuspg@gmail.com
Elmer Rolando Llanos Villareal – evillareal@hotmail.com
Universidade Federal Rural do Semi-Árido - UFERSA
Av. Francisco Mota, 572 - Costa e Silva.
59625-900 – Mossoró – Rio Grande do Norte.

Resumo: *Este presente artigo visa mostrar o estudo a respeito de um veiculo aéreo não tripulado – VANT, mais conhecido também como quadrotor, e um controlador para o mesmo. Esses quadrotores são pequenas aeronaves de tamanho e peso reduzido que podem ter diversas aplicações tanto no mundo da aviação como no ambiente militar. Com o estudo de um VANT torna-se possível aplicarem-se inúmeros assuntos estudados durante um curso de engenharia, como por exemplo, dinâmica, automação e controle, matemática aplicada, softwares simuladores, mecânica dos fluidos e etc.*

Palavras-chave: *Quadrotor, Controlador, Veículo aéreo, Engenharia, Aplicação.*

1. INTRODUÇÃO

Os quadrotores são equipamentos de voo sem tripulantes de tamanho pequeno que atraíram a atenção de uma grande quantidade de cientistas e pesquisadores devido a sua grande área de aplicação tanto na área militar como comercial. Os estudos envolvendo esse tipo de protótipo começaram no século vinte e se estendem até hoje, claro que antes não havia as tecnologias que existem hoje, tanto na parte de controle como na de sensores, o que dificultava a construção de um VANT, o que foi resolvido com o avanço da tecnologia e que permitiu hoje existir vários protótipos de variados tamanhos nas universidades. Os estudos a respeito desse assunto estão avançando cada vez mais, como por exemplo, protótipos desenvolvidos pelo método do Euler-Newton que trabalhou na visão de estabilização e controle de saída, também foi criada uma rede neural para controle servo visual para imagem do quadrotor. Vem utilizando-se também o filtro de Kalman para estimular a atitude do quadrotor e utilizar um controlador de lógica fuzzy combinado com um PID convencional. Desde o ultimo século que se faz uso também da lógica fuzzy nos sistemas dinâmicos, que foi implementada no controle de helicópteros e mais recentemente nos VANTs. Apesar de todas as vantagens do quadrotor, que serão apresentadas melhor mais a frente, ele ainda tem alguns problemas no que diz respeito à sua estabilização, justamente por causa do seu comportamento não linear, por isso utiliza-se o sistema fuzzy. Neste trabalho será apresentado

o sistema fuzzy para o controle do quadrotor, comparando com o clássico PID, mostrando o modelo matemático utilizado, os controladores, simulações e conclusões finais do trabalho.

2. QUADROTOR

O principal propósito do trabalho é desenvolver um controlador para controle do quadrotor, porém é importante explicar primeiramente os conceitos fundamentais a respeito do seu funcionamento. O quadrotor possui quatro rotores de mesma dimensão que estão conectados em forma de x, dois de extremidades opostas em relação ao centro da estrutura giram no sentido anti-horário enquanto os outros dois giram no sentido horário para anular o torque gerado. O movimento na vertical é chamado de throttle (aceleração), já o na horizontal pode ser realizado pelos comandos pitch (arfagem) e roll (rolagem). Com o comando pitch, a aeronave é inclinada para frente ou para trás e o roll para um lado ou para o outro. Já o do eixo vertical é feito pelo comando yaw (guinada). Grande simplicidade de construção, baixa manutenção e barulho, são umas das vantagens dessa máquina comparada com outras máquinas de voo.

Figura 1: Movimentos angulares.

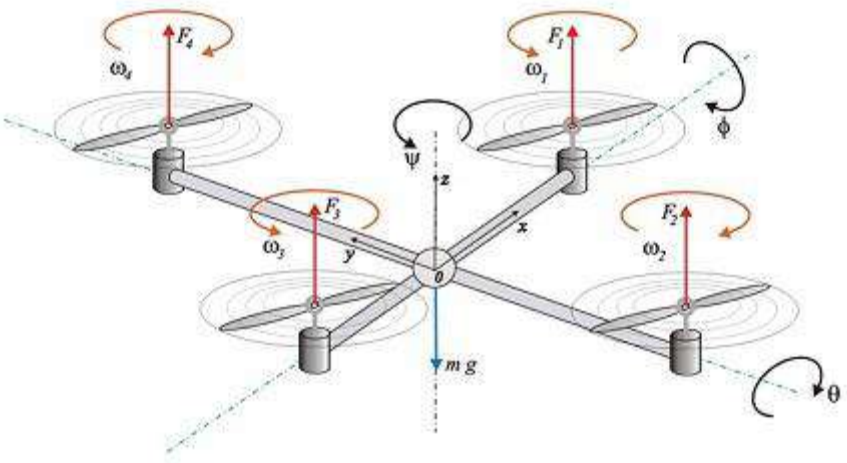

Quando se deseja que o equipamento movimente-se na vertical, basta variar igualmente a velocidade dos quatro rotores, ou seja, simultaneamente, já para se movimentar na horizontal (eixo x ou y), basta aumentar a velocidade de um rotor e diminuir na mesma intensidade a velocidade do rotor oposto, prevenindo um desequilíbrio.

3. CONTROLE FUZZY-PID

Será utilizada nesse trabalho a junção de dois controladores, como já foi dito anteriormente, o classico PID e o sistema lógico fuzzy, que terá a função de sintonizar os ganhos do PID. O controle PID consiste em calcular, a partir das informações do valor desejado e do valor atual da variável do processo, um valor de atuação sobre o processo, que será transformado em um sinal adequado ao atuador utilizado (válvula, relé), e deve garantir um controle estável e preciso. O controlador PID é composto de 3 partes:

Controlador proporcional (P): Possui a função de reduzir o tempo de crescimento. Se só o controlador proporcional for utilizado no sistema de controle, faltas permanentes ocorrem no sistema.
Controlador proporcional integral (PI): Aqui os faltos permanentes já não existem mais, o que pode levar a flutuações no sistema que podem ser imortais ou mortais. Para corrigir o controle, a parte derivativa é adicionada.
Controlador proporcional integral derivativo (PID): Permite ao controlador prevê o tipo de comportamento do sistema, e antes que o erro cresça, ele corrige a entrada do mesmo.

Figura 2: Esquema de um controlador PID.

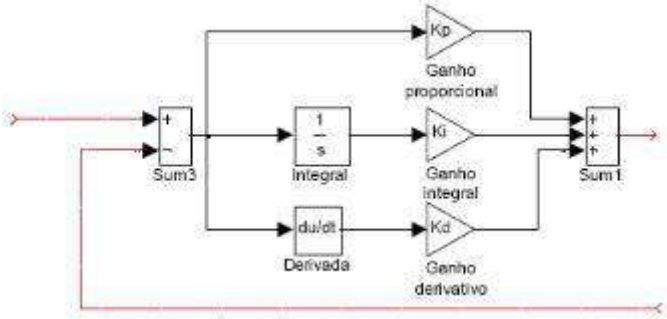

Com o desenvolvimento da lógica fuzzy, ficou mais fácil trabalhar e solucionar os problemas do dia a dia, pois existe, várias imperfeições difíceis de serem resolvidas, justamente pelo fato dessa lógica possuir um método de trabalhar com a não linearidade. A lógica fuzzy trabalha com uma grande variedade de informações vagas e incertas, as quais podem ser traduzidas por expressões do tipo: a maioria, mais ou menos, talvez, etc, que antes não tinham como ser processadas.

4. RESULTADOS E DISCUSSÃO

As figuras abaixo mostram o diagrama de bloco do controlador fuzzy pid auto-sintonizado. Como pode ser visto no diagrama, o sistema fuzzy possui duas entradas (e e ed) e nos dá três saídas (Kp, Ki, Kd). Este diagrama de bloco apenas mostra o controle de um grau liberdade do quadrotor e nós usamos dois outros controladores como esse para o controle da atitude do quadrotor. As funções de pertinência de todas as entradas e saídas foram escolhidas iguais. A figura Fig. 3 mostra as funções de pertinência.

As funções de pertinência são combinadas de triangular e gaussiana. A largura dos conjuntos fuzzy usados nos controladores não são as mesmas e foram determinadas por erro. A largura dos conjuntos fuzzy usados para saída, Kp, foram escolhidas [0.2 0.7], Ki, foi escolhida [0.001 0.01] e para Kd, [0.1 0.15]. E para as entradas, a gama para o erro foi escolhida [-1 1] e para a taxa do erro também [-10 10] e se essas entradas saírem dessa gama nós usamos saturação para colocar na gama de novo. O conjunto de regras linguísticas é parte essencial do controlador fuzzy. Em vários casos é fácil traduzir a experiência de um expert para essas regras, e qualquer número que essas regras possam ser criadas para definir as ações do controlador. Em outros casos essas regras podem vim de algum julgamento e abordagem de erro.

Figura 3: Funções de pertinências.

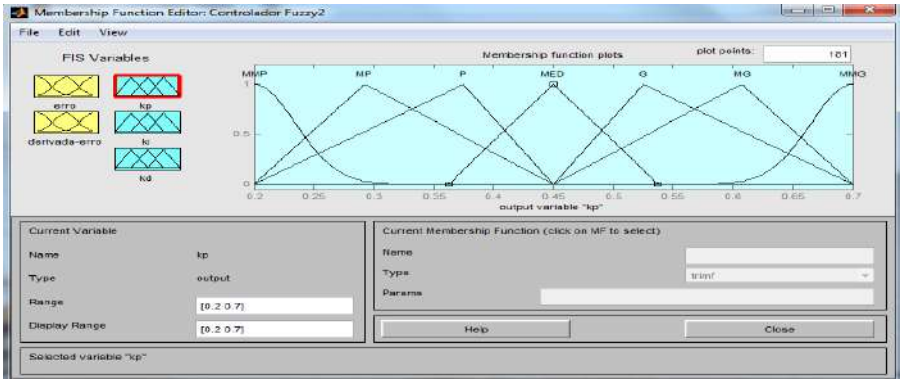

Figura 4: Estrutura básica do controlador fuzzy.

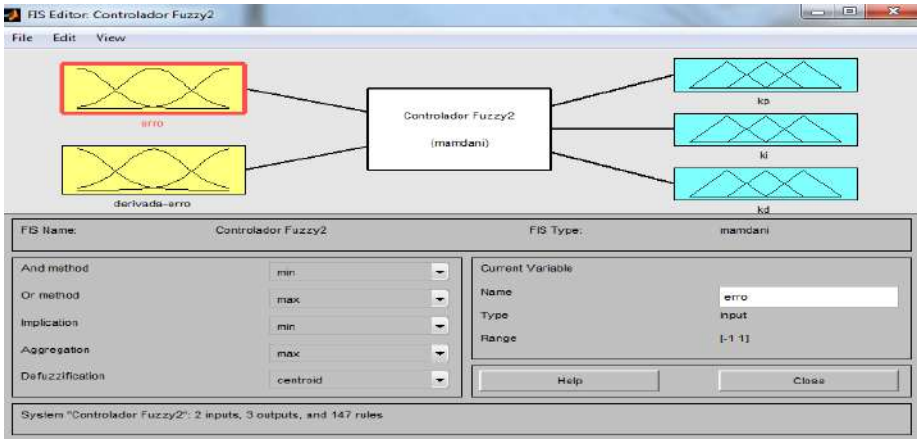

O modelo matemático dinâmico do quadrotor assim como os controladores, foi desenvolvido pelo simulink no Matlab para simulação. O objetivo dessa análise é testar o quanto os controladores conseguem estabilizar o quadrotor. O quadrotor é designado para mudar o ângulo para zero e se estabilizar, usando o sistema fuzzy para sintonizar os ganhos pid, os mesmos mudam ao longo da simulação.
Das figuras claramente conseguimos entender que usando o sistema fuzzy para sintonizar os ganhos do pid aumenta-se a performance.

Figura 5: Gráficos

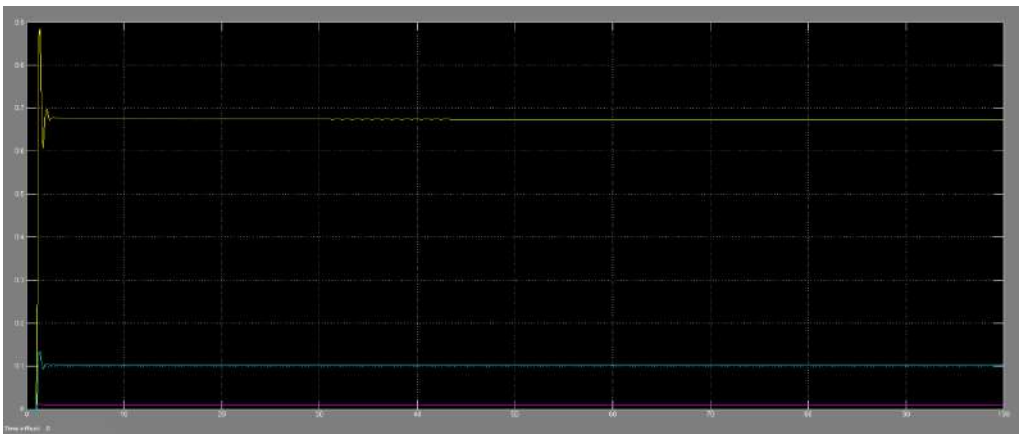

O desenvolvimento dessa pesquisa tornou-se muito interessante e importante pelo fato de que o estudo tem diversas aplicações práticas no dia a dia, podendo ser verificado desde utilização na aviação, no exército, pelo seu pequeno tamanho, o que facilita o voo em locais de difícil acesso, e até mesmo no reconhecimento de imagens. Isso permite que haja cada vez mais investimentos em pesquisas e testes acerca dessa tecnologia.
Uma sugestão para um trabalho futuro é desenvolver ainda mais método de controle utilizado, talvez complementando com uma rede neural de modo a adicionar uma inteligência adicional ao sistema.

5. CONSIDERAÇÕES FINAIS

Com o presente trabalho podemos concluir que o quadrotor é controlado bem com o controlador PID quando se trabalha numa rota fixa sem variações, mas quando o sistema final é exposto a muita turbulência como ventos e obstáculos, o sistema PID não responde muito bem, o que vem a ser necessário um sistema fuzzy em conjunto com o PID. A base teórica forneceu um grande suporte para o desenvolvimento de simulador utilizado para validar a técnica de controle escolhida, além de ficarem evidentes que os trabalhos voltados para desenvolvimento de quadrotores utilizavam vários sensores para avaliar sua posição e atitude em relação a um sistema de coordenadas. Diante do bom andamento dos estudos, a pesquisa continua sendo implementada em busca de novos resultados, a fim de contribuir para o aperfeiçoamento dessa tecnologia altamente promissora para a humanidade.

Agradecimentos

Agradecemos à CITED-UFERSA e ao CNPQ por subsidiarem os fatores ligados ao desenvolvimento do projeto.

REFERÊNCIAS BIBLIOGRÁFICAS

[1] KOHAGURA, T. Lógica fuzzy e suas aplicações. Trabalho de graduação em Ciência da computação-UEL, Londrina, 2007.

[2] COSTA, A. d.; RODRIGUEZ, A. G.; SIMAS, E. P.; ARAUJO, R. d. S. Lógica fuzzy: conceitos e aplicações. Relatório. São Leopoldo: Universidade do Vale do Rio dos Sinos, 2008.

[3] BRESCIANI, T. Modelling, identification and controlof a quadrotor helicopter.[S.1]: Department of Automatic Control, Lund University, 2008.

[4] ERENOGLU, I.; EKSIN, I.; YESIL, E.; GUZELKAYA, M. Na inteligente hybrid fuzzy pid controller. In: European Conference on Modelling and Simulation. [S.1.: s.n.], 2006.

[5] BOUABDALLAH, S. Design and control of quadrotors with application to autonomous flying. Ecole Polytechnique Federale de Lausanne, 2007.

DEVELOP A FUZZY - PID CONTROLLER FOR AIR VEHICLE NOT MANNED - UAV

Abstract: *This present article aims to show the study on an unmanned aerial vehicle - UAV , known also as quadrotor , and a controller for it. These are small quadrotores reduced size and weight of aircraft that can have several applications both in the aviation world as the military environment. With the study of a UAV becomes possible to apply up numerous subjects studied for an engineering degree , such as dynamic , automation and control , applied mathematics , software simulators , fluid mechanics , etc.*

Key-words: *Quadrotor , Controller , Air Vehicle , Engineering, Application*

Modeling and Control Output Feedback of a VANT

Elmer Rolando Llanos Villarreal
Programa de Pós-graduação em Sistemas de Comunicação e Automação da UFERSA Mossoró, RN, Brasil
Departamento de Ciências Exatas e Naturais (DCEN)-UFERSA Av. Francisco Mota 572 Mossoró, RN, Brasil
Email: elmerllanos@ufersa.edu.br

Alexandre Santos Brandão
Departamento de Engenharia Elétrica, UFV, Viçosa, MG.
Email: alexandre.brandao@ufv.br

Alex Sandro de Araújo Silva
Departamento de Ciências Ambientais e Tecnológicas (DCAT)-UFERSA,
Av. Francisco Mota 572 Mossoró, RN, Brasil.
Email: alex.araujo@ufersa.edu.br

***Abstract*—Attitude control is always considered as a nonlinear control problem. The statedependent Riccati quation (SDRE) method of nonlinear suboptimal regulation is applied here to the attitude control of VANT. This paper presents a study of mathematical modeling of a vehicle the quadrotor type. The dynamic model of the vehicle takes into account the dynamics of rotating wings and results in a non-linear system. For simplify the model nonlinear is realized the linearization. The stabilization problem by state feedback is studied for the new linear system.Them is projected to control LQR (Linear Quadratic Regulator) to find the state matrix F. The stabilization problem by output feedback is studied for the linear system. The implementation the algorithm using Sylvester equations to find the output feedback matrix K. It then makes a comparison between the two algorithms with numerical examples is apresented.**

Keywords: *Stabilization, Riccati Equation, Sylvester Equation, Quadrotor.*

I. Introduction

Currently , the quadrotor is emerging as a standard platform for the detection of motion and three-dimensional perception , because this kind of vehicle is one of the most flexible aerial platforms in the field of aerial robotics . It is known that the static output feedback stabilization problem is a relevant and challenging problem, due to its simple implementation, in contrast to more dynamic methods, and because it is not easy to find a feedback matrix to make the closed-loop system asymptotically [4], [14], [17],[3], [2], [18].

The modeling and attitude stabilization control problems of a four-rotor vertical takeoff and landing unmanned air vehicle (UAV) known as the quadrotor are investigated. The quadrotor's attitude is represented by the unit quaternion rather than Euler angles to avoid singularity problem. Taking dynamical behavior of motors into consideration and ignoring aerodynamic effect, a nonlinear controller is developed to stabilize the attitude.

The determination of procedures for obtaining the feedback matrix in output feedback control to asymptotically stabilize linear systems is actually an open problem. Several methods have been proposed in the literature based on Lyapunov and Riccati linear matrix inequalities, or eigenstructure assignment [7], [1],[4] [13]. There are sufficient conditions for the solution to these equations under a rank constraint [4]. This paper presents a study modeling mathematical e stabilization problem of the dynamics of a quadrotor.

In this paper is studied the stabilization problem by output feedback thus is obtained the output feedback matrix using the Sylvester equations, where the algorithm Syrmos and Lewis is implemented to find the output feedback matrix K, and so compare between them.

The paper is apresented in section two the quadrotor and its features can be seen. The third section describes the mathematical modeling of a quadrotor, then this is simplified and linearized resulting in the linear system. In section four the stabilization problem is obtained the state matrix F by LQR method . The next section presents the stabilization problem by output feedback and is obtained the output feedback matrix by the method of Sylvester equations, here are some examples to illustrate their methodology and conclusions of this study are mentioned in the final section.

II. The Quadrotor

A quadrotor is an aerial robot that has four engines , where adjacent motors rotate in the opposite direction . Performed by the propeller forces are perpendicular to the plane of the engines , the center of mass is located in the center of the vehicle . Compared to a classic helicopter quad provides great advantages for being a symmetrical vehicle, since its simplicity of construction and the robustness and maintainability [11]. The four-engine helicopter has the advantage of being controlled from the variation of the four angular velocities of the four engines , each force produced by the motor is equal to the square of the angular velocities [5].The motor rotates in a fixed direction , whereby the forces are always positive.

III. Mathematical Modeling

The first step before the control stage is the adequate modeling of the system dynamics. With mathematical modeling is a better understanding of the system and its limitations. This section presents the mathematical modeling of the quadrotor and its sensors, providing the mathematical basis for the application of the system dynamics in a simulation environment. Leonhard Euler defined the orientation of a rigid body can be expressed by three angles. This convention can be used in the rotation of a vector quantity between different references, as shown in [12]. This transformation should follow a non-commutative sequence of three rotations, presented below:

$$R_x = \begin{bmatrix} 1 & 0 & 0 \\ 0 & \cos\phi & sen\phi \\ 0 & \phi & \cos\phi \end{bmatrix} \tag{1}$$

$$R_y = \begin{bmatrix} \cos\theta & 0 & \theta \\ 0 & 1 & 0 \\ sen\theta & 0 & \cos\theta \end{bmatrix} \tag{2}$$

$$R_z = \begin{bmatrix} \cos\psi & sen\psi & 0 \\ \psi & \cos\psi & 0 \\ 0 & 0 & 1 \end{bmatrix} \tag{3}$$

Particularly for the xyz referential: R_x causes a rotation around the x-axis, R_y about the y-axis and R_z around the z-axis. Thus, for a given vector $N \in \Re^{3\times 1}$, the transformation of the standard NED for reference xyz ($NED \rightarrow xyz$) is given by:

$$N^q = RN^I \tag{4}$$

where R is the rotation matrix shown in Equation (6)

$$R = R_z R_y R_x \tag{5}$$

$$S = \begin{bmatrix} aa & bb & cc \\ dd & ee & jj \\ ff & gg & hh \end{bmatrix} \tag{6}$$

with
$aa = cos\psi cos\theta$
$bb = cos\psi sen\theta sen\phi - cos\phi sen\psi$
$cc = cos\psi sen\theta cos\phi + sen\psi sen\phi$
$dd = sen\psi sen\theta sen\phi + cos\psi cos\phi$
$ee = sen\psi sen\theta cos\phi + sen\phi cos\psi$
$jj = sen\psi sen\theta cos\phi + sen\phi cos\psi$
$ff = -sen\theta$
$gg = sen\phi cos\theta$
$hh = cos\theta cos\phi$

Notice that R is orthogonal matrix ($R^{-1} = R'$) and has determinant ($det(R) = 1$), A sequence of rotations $R\psi R\theta R\phi$ must be fulfilled. The transformation ($xyz \rightarrow NED$) is obtained by inverting the equation (7):

$$N^I = R' N^q \tag{7}$$

The state vector that defines the dynamics of attitude

$$x = \begin{bmatrix} p & q & r & \phi & \theta & \psi \end{bmatrix}' \tag{8}$$

Conversely, the Euler angles can be calculated by a rotation matrix:

$$\xi = \begin{bmatrix} \phi \\ \theta \\ \psi \end{bmatrix} = \begin{bmatrix} atan2(R_{2,3}, R_{3,3}) \\ arcsin(R_{1,3}) \\ atan2(R_{1,2}, R_{1,1}) \end{bmatrix} \tag{9}$$

The linear along the axis of the body speeds can be transformed by using the resulting inertia matrix

$$\dot{x} = \frac{d}{dt}\begin{bmatrix} x_E \\ y_E \\ z_E \end{bmatrix} = R \begin{bmatrix} uu \\ vv \\ ww \end{bmatrix} \tag{10}$$

$$\begin{bmatrix} \dot{x} \\ \dot{y} \\ \dot{z} \end{bmatrix} = R \begin{bmatrix} uu \\ vv \\ ww \end{bmatrix} \tag{11}$$

$$\dot{x} = a + b + c \tag{12}$$

where,

$$\begin{aligned} a &= (cos\psi cos\theta)uu \\ b &= (cos\psi sen\theta sen\phi - cos\phi sen\psi)vv \\ c &= (cos\psi sen\theta cos\phi + sen\psi sen\phi)ww \end{aligned}$$

$$\dot{y} = d + e + f \tag{13}$$

then,

$$\begin{aligned} d &= (sen\psi cos\theta)uu \\ e &= (sen\psi sen\theta sen\phi + cos\psi cos\phi)vv \\ f &= (sen\psi sen\theta cos\phi - sen\phi cos\psi)ww \end{aligned}$$

$$\dot{z} = -sen\theta uu + sen\phi cos\theta vv + cos\theta cos\phi ww \tag{14}$$

Angle along the body axis rates can be transformed into Euler rates, using the transformation matrix M as follows

$$\frac{d}{dt}\begin{bmatrix} \phi \\ \theta \\ \psi \end{bmatrix} = R \begin{bmatrix} p \\ q \\ r \end{bmatrix} \tag{15}$$

$$M = \begin{bmatrix} 1 & tan\theta sen\phi & tan\theta cos\phi \\ 0 & cos\phi & -sen\phi \\ 0 & sec\theta sen\phi & sec\theta cos\phi \end{bmatrix} \tag{16}$$

$$\begin{bmatrix} \dot{\phi} \\ \dot{\theta} \\ \dot{\psi} \end{bmatrix} = M \begin{bmatrix} p \\ q \\ r \end{bmatrix} \tag{17}$$

$$\dot{\phi} = p + qtan\phi + rtan\phi \tag{18}$$
$$\dot{\theta} = qcos\phi - rsen\phi \tag{19}$$
$$\dot{\psi} = qsec\theta sen\phi + rsec\theta cos\phi \tag{20}$$

For this system to "Newton's Second Law" can be written as

$$F_m = ma \tag{21}$$

$$(F_m + G)\frac{1}{m} = \frac{d}{dt}V_e = \begin{bmatrix} \dot{u}u & \dot{v}v & \dot{w}w \end{bmatrix}' + \begin{bmatrix} p & q & r \end{bmatrix}' \times \begin{bmatrix} uu & vv & ww \end{bmatrix} \tag{22}$$

IV. Linearization of the nonlinear equations of state

The state equations are nonlinear. These equations have to be linearized about the hovering stable condition. The process of Linearization in the nonlinear state equations are made using Jacobians of the nonlinear state equations with respect to the states and the inputs conditions hovering around $[\ 0 \quad 0 \quad 0 \quad 0 \quad 0 \quad 0.1\ ]$. Given a set of state equations $y = f(x)$ n state equations in n variables $x_1, ..., x_n$ a Jacobian matrix for a set of state equations can be calculated as shown in equation (23).

$$\frac{df}{dx} = \begin{bmatrix} \frac{df_1}{dx_1} & \frac{df_1}{dx_2} & \cdots \\ \frac{df_2}{dx_1} & \frac{df_2}{dx_2} & \cdots \\ \vdots & \vdots & \ddots \end{bmatrix} \tag{23}$$

The Jacobian matrix of the nonlinear states equations in relation to the initial conditions, starting from the point x_0.

V. Stabilization by LQR method

The quadrotor's attitude is represented by the unit quaternion rather than Euler angles to avoid singularity problem. Taking dynamical behavior of motors into consideration and ignoring aerodynamic effect, a nonlinear controller is developed to stabilize the attitude. The traditional method used to control is LQR to use such a nonlinear system must first linearize around a certain operating point. For this purpose , the Jacobians of the nonlinear states equations are derived for the states and the inputs. Thus, the state matrices A, B, C and D are obtained after replacing the amounts of states in the operating point. The attitude of the movement system is completely observable with the set of sensors used. The attitude of the moving system is completely observable with the set of sensors used. The observability analysis is also carried out by checking the rank of the observability matrix. Thus, these states that rule the attitude of the system can be controlled with the set of sensor chosen.

In the control problem of attitude stabilization technique using Riccati equations and will be used this technique being implemented from the paper [9].

Consider the state space representation of a time-invariant linear system:

$$\dot{x} = Ax + Bu \tag{24}$$
$$y = Cx \tag{25}$$

where $x \in \Re^n$ is the vector of state variables, $u \in \Re^m$ is the control input and $y \in \Re^p$ corresponds the output. For stabilization this system is necessary the find a state feedback matrix in the form

$$u = Fx \tag{26}$$

with $F \in \Re^{m \times n}$, a constant coefficient matrix control to be determined.

The LQR (Linear Quadratic Regulator) is a control technique in the form of equation (26), and matrix F_{LQR} that allows optimal control of the system (27) by minimizing the cost function:

$$J_{LQR} = \int_0^\infty (x^*Qx + u^*Su)dt \tag{27}$$

The symbol $*$ represent a matrix operation conjugate transposed. For example x^* is the conjugate transpose of x, i.e. the elements of the matrix x are transposed and complex elements, if any, are combined so composing the new matrix. Already Q and R are Hermitian matrices, that is the matrix is equal to its conjugate transpose.

In Equation (28) and (29) Q and S are matrices positive semidefinite weighting and set, respectively. These symbolize, respectively, the importance given by the user to the state variables and the control action. The rule Bryson proposes an initial estimate of Q and S based on maximum variation for the desired states and the system input. where $\max(x_i)$ is the highest value that the state variable x can assume and $\max(u_i)$ is the highest value that the control signal u can assume.

$$Q = \begin{bmatrix} \frac{1}{max(x_1)^2} & 0 & 0 \\ 0 & ... & 0 \\ 0 & 0 & \frac{1}{max(x_n)^2} \end{bmatrix}, \tag{28}$$

$$S = \begin{bmatrix} \frac{1}{max(u_1)^2} & 0 & 0 \\ 0 & ... & 0 \\ 0 & 0 & \frac{1}{max(u_m)^2} \end{bmatrix} \tag{29}$$

Using the method LQR the optimal matrix F_{LQR} is calculated by solving the algebraic Riccati equation in order to P_1

$$A'P_1 + P_1A - P_1BS^{-1}B'P_1 + Q = 0 \quad (30)$$

where a matrix F_{LQR} is obtained

$$F_{LQR} = S^{-1}B'P_1 \quad (31)$$

The steps of the LQR controller design is summarized in the following steps:

1) Transform the system equations in the state space equation format, as in the relationship, obtaining matrices A and B

2) Determine the matrices Q and S, where the elements are given in (28) and (29).

3) Find the matrix P_1 shown in equation (30).

4) Determine the matrix F_{LQR} using the equation (31).

Example 1: This example will use the method of LQR.

One linearized system (25) is considered , defined by [5]:

$$A = \begin{bmatrix} 0 & 0 & 0 & 0 & 0 & 0 \\ 0 & 0 & 0 & 0 & 0 & 0 \\ 0 & 0 & 0 & 0 & 0 & 0 \\ 1.000 & 0 & 0 & 0 & 0 & 0 \\ 0 & 0.9950 & -0.0998 & 0 & 0 & 0 \\ 0 & 0.0998 & 0.9950 & 0 & 0 & 0 \end{bmatrix}$$

;

$$B = \begin{bmatrix} 0 & 14.1622 & 0 & -14.1622 \\ 14.1622 & 0 & -14.1622 & 0 \\ -18.6049 & 18.6049 & -18.6049 & 18.6049 \\ 0 & 0 & 0 & 0 \\ 0 & 0 & 0 & 0 \\ 0 & 0 & 0 & 0 \end{bmatrix}$$

$$C = \begin{bmatrix} 1 & 0 & 0 & 0 & 0 & 0 \\ 0 & 1 & 0 & 0 & 0 & 0 \\ 0 & 0 & 1 & 0 & 0 & 0 \\ 0 & 0 & 0 & 1 & 0 & 0 \\ 0 & 0 & 0 & 0 & 1 & 0 \\ 0 & 0 & 0 & 0 & 0 & 1 \end{bmatrix}$$

The corresponding system is controllable and observable.

Since the matrix Q and S

$$Q = \begin{bmatrix} 1.000 & 0 & 0 & 0 & 0 & 0 \\ 0 & 0.001 & 0 & 0 & 0 & 0 \\ 0 & 0 & 1.000 & 0 & 0 & 0 \\ 0 & 0 & 0 & 0.001 & 0 & 0 \\ 0 & 0 & 0 & 0 & 1.000 & 0 \\ 0 & 0 & 0 & 0 & 0 & 0.001 \end{bmatrix}$$

$$S = \begin{bmatrix} 0.010 & 0 & 0 & 0 \\ 0 & 0.010 & 0 & 0 \\ 0 & 0 & 0.010 & 0 \\ 0 & 0 & 0 & 0.010 \end{bmatrix}$$

we obtain the matrices P_1 and F_{LQR}

$$P_1 = \begin{bmatrix} 0.005 & 0.000 & -0.000 & 0.000 & 0.000 & -0.000 \\ 0.000 & 0.001 & -0.000 & 0.000 & 0.005 & 0.000 \\ -0.000 & -0.000 & 0.002 & 0.000 & -0.000 & 0.000 \\ 0.000 & 0.000 & 0.000 & 0.031 & 0.000 & -0.000 \\ 0.000 & 0.005 & -0.000 & 0.000 & 0.015 & -0.003 \\ -0.000 & 0.000 & 0.000 & -0.000 & -0.003 & 0.031 \end{bmatrix};$$

$$F_{LQR} = -\begin{bmatrix} 0.000 & 0.741 & -5.002 & 0.000 & 7.137 & -0.155 \\ 7.072 & -0.002 & 5.000 & 0.223 & -0.066 & 0.158 \\ 0.000 & 0.737 & -4.998 & -0.000 & -7.003 & -0.161 \\ -7.072 & -0.002 & 5.000 & -0.223 & 0.066 & 0.158 \end{bmatrix}$$

with $A_F = A + BF_{LQR}$ and $\sigma(A_F \in C^-)$. Thus the matrix F stabilizes the given system.

A. Output Feedback Matrix Using Coupled Sylvester Equations

In this part a technique of stabilization by output feedback is presented.

Is considered to be time-invariant linear system:

$$\dot{x} = Ax + Bu \quad (32)$$

$$y = Cx \quad (33)$$

, where A, B, C are matrices of appropriate dimensions.

As in [14], use certain concepts and definitions of geometric control theory reported by [19]. It is known that a subspace is $V \subset X$ (A, B) if there is invariant $F : X \longrightarrow Y$ such that $(A + BF)V \subset V$, or equivalently, $AV \subset V + ImB$. By duality a subspace $\tau \subset X$ is (C, A) if there is invariant $L : Y \longrightarrow X$, such that $(A + LC)\tau \subset \tau$, or equivalently, $\tau \supset A(\tau \cap ker(C))$.

Definition 5.1: As in [14], a subspace $V \subset X$,of dimension v, is (C, A, B) invariant if V is $(A, B)-$ invariant and $(C, A)-$ invariant.

Let $V \in \Re v \times v$ such that $Im(V) = V$ and let $T \in \Re^{(n-v)\times v}$ a left annihilator of V, i.e.: Ker $(T) = Im(V)$. The definition is equivalent to the existence of matrices $(H_V \in \Re^{v\times v}, W \in \Re^{m\times v})$ and $(H_T \in \Re^{(n-v)\times(n-v)}, U \in \Re^{(n-v)\times v})$ solutions to the following equations coupled Sylvester:

$$AV - VH_V = -BW, \quad (34)$$

$$TA - H_TT = -UC, \quad (35)$$

$$TV = 0 \quad (36)$$

Considered the Sylvester equation (34), (35) and (36) the problem of control using static output feedback, mainly self-positioning structure [14] and [13]. The study takes into account the properties of detectability and stability, using the two following definitions:

(i) A subspace V $(A, B)-$ invariant is $(A, B)-$ internally stabilizable if there is F such that $(A + BF)\backslash V$ is asymptotically stable, and

(ii) A subspace $(C, A)-$invariant $V$is$(C, A)-$ externally detectable if there is L such that $(A + CL)\backslash X/V$ is asymptotically stable.

Definition 5.2: [4] A subspace V ,of dimension v, is $(C, A, B)-$ invariant stabilizable output (or simply O.S.)(C, A, B)-invariant if V is (A, B)-intern stabilizable and $(C, A)-$ external detectably.

Thus a necessary and sufficient condition for a subspace $V = Im(v)$ is *O.S.*$(C, A, B)-$invariant is that (34), (35) and (36) are verified with additional stability conditions:

$$\sigma(H_V) \in C^- \tag{37}$$

$$\sigma(H_T) \in C^- \tag{38}$$

In [4] and [16] the Theorem 5.1 relates the concept of subspaces O.S.$(C, A, B)-$ invariant to the existence of a output feedback matrix K that stabilizes the closed-loop system.

Theorem 5.1: [4] [16] There is a matrix of output feedback $K : Y \to U$ such that $\sigma(A + BKC) \in C^-$ if and only if the following conditions are verified for some matrices $(V \in \Re^{n\times v}, H_V \in \Re^{v\times v}, W \in \Re^{m\times v})$,$(T \in \Re^{(n-v)\times n}, H_T \in \Re^{(n-v)\times(n-v)}, U \in \Re^{(n-v)\times v})$ and for some positive scalar $v \leq n$:

$$AV - VH_V = -BW, \text{with } \sigma(H_V) \in C^- \tag{39}$$

$$TA - H_T T = -UC, \text{with } \sigma(H_T) \in C^- \tag{40}$$

$$TV = 0 \tag{41}$$

$$Ker(CV) \subseteq Ker(W) \tag{42}$$

$$Ker(B'T') \subseteq Ker(U') \tag{43}$$

where: rank$(V) = v$ and rank$(T) = n - v$

Subject to restriction of stability the matrix H_V, to Equation (39) means either que subspace $V = Im(V)$ should be $(A, B)-$ invariant stabilizable; dually, (40) means either que subspace $Ker\,(T) = V$ should be $(C, A)-$ stabilizable externally. Thus, to under coupling condition of (41), Which is a subspace existence has $V = Ker(T)$ O.S$(C, A, B)-$ invariant with the conditions (42) and (43) is a necessary and sufficient condition for the existence of solution of the problem considered. Que also note the conditions (42) and (43) correspond to an existence output feedback matrix $K \in \Re^{m\times p}$ verifying two the following equalities:

$$KCV = W \tag{44}$$

$$TBK = U \tag{45}$$

Important to note that guaranteed the existence of solution to the equations of Sylvester and the output feedback matrix K is obtained such that (44) and either (45) is verified, the eigenvalues loop closed are given by:

$$\sigma(A + BKC) = \sigma(H_V)\dot{\cup}\sigma(H_T)$$

B. Algorithms Aspects

In the Theorem (5.1) the matrix conditions of are not linear (V, H_V, W, T, H_T, U). In particular, the non-linear terms V; H_V and H_T; T present in (39) and (40), respectively, can be linearized when setting up the matrices H_T and H_V, or equivalently when setting up the desired results for the closed-loop system eigenvalues.

An algorithmic technique based on the procedures for self-positioning structure for obtaining an output feedback matrix will be displayed in this section. The technique to be worked on is the proposed [13] solves the coupled Sylvester equations in two steps and can be directly applied to systems which verify the condition $m + p > n$, known as Kimura condition [8]. For the development of the technique, it is assumed that the dimension $V = Im(V)$ is equal p, while ensuring that the matrix $CV \in \Re^{p\times p}$ is invertible and hence the output feedback matrix can be found from Equation (44) in the form $K = W(CV)^{-1}$.

Further, it is considered that the system represented by (C, A, B) is controllable and observable, this necessary condition for arbitrary choice of the poles to be placed in closed loop. This condition can however be relaxed to stabilizability and detectability of (C, A, B), which implies the use of non-controllable and unobservable eigenvalues to the desired closed-loop system spectrum.

The set of desired poles is denoted by $\Lambda = \{\lambda_1, \cdots, \{\lambda_{n-p}, \lambda_{n-p+1}, \cdots, \lambda_n\} = \{\lambda_T, \Lambda_V\}$ where λ_T and λ_V are self conjugates. These sets are associated matrices $H_V \in \Re^{p\times p}$ and $H_T \in \Re^{(n-p)\times(n-p)}$ in the following way:$\sigma(H_T) = \lambda_T = \{\lambda_1, \cdots, \lambda_{n-p}\}$ and $\sigma(H_V) = \lambda_V = \{\lambda_{n-p+1}, \cdots, \lambda_n\}$. For simplicity of presentation, it is considered that the elements of Λ=$\sigma(A+BKC)$ are distinct.

C. Algorithm Syrmos and Lewis

Based on the conditions expressed by Theorem (5.1), The following algorithm, proposed in [13], usually leads to an array of output feedback which stabilizes the closed-loop system when the condition Kimura $n < m + p$ is verified:

Step 1: Choose $H_T \in \Re^{(n-p)\times(n-p)}$ matrix such that $\sigma(H_T) = \Lambda_T \in C^-$ and solves the Sylvester equation (40) to find a matrix $T \in \Re^{p\times(n-p)}$ such that

$$rank \begin{bmatrix} T \\ C \end{bmatrix} = n \Leftrightarrow Ker\ T \cap Ker\ C = \{0\} \tag{46}$$

Step 2: Resolves to Sylvester equation (39), for any matrix $H_V \in \Re^{p\times p}$ such that $\sigma(H_V) = \Lambda_V \in C^-$ assuming the matrix V with the coupling condition (39) and rank the matrix (V) be equal to p.

Step 3: The equation (46) ensures that rank the matrix $(CV) = p$ and the output feedback matrix K and can be calculated using the equation (44).

The following presents some observations with dual aim of showing aspects of the numerical solution of the steps of the algorithm and justify it theoretically.

Note: The steps 1 and 2 can be solved using standard techniques for self-positioning structure. Whereas matrizes H_T and H_V in Jordan canonical form, we can adopt the following procedure:

Step 1: Find $t_j \in C^n$ and $u_j \in C^p$, such that:

$$\left[\begin{array}{cc} t'_j & u'_j \end{array} \right] \left[\begin{array}{c} A - \lambda_j I \\ C \end{array} \right] = 0 \ \forall j = 1, \cdots, \ n - p \qquad (47)$$

Step 2:

Determine $v_i \in C^n$ and $w_i \in C^n$ such that:

$$\left[\begin{array}{cc} A - \lambda_j I & B \\ C & 0 \end{array} \right] \left[\begin{array}{c} v_i \\ w_i \end{array} \right] = 0 \quad \forall \ i = \ n - p, \ \cdots, \ n \quad (48)$$

In a similar way to the previous case, the matrices V and W for the calculation of output feedback matrix K can be constructed with real elements. In particular, if $\lambda_i \in C$, we consider $\lambda_{i+1} = \lambda_i^*$ and

$$\left\{ \begin{array}{l} V_i = Re\,(v_i)\,, \quad V_{i+1} = Im(v_i) \\ W_i = Re\,(w_i)\,, \quad W_{i+1} = Im(w_i) \end{array} \right.$$

where v_i and w_i denote the columns of the matrices V and W, respectively.

$$TV \ = \ 0 \qquad (49)$$

Example 2:

A linear system (32), is considered defined by [15]:

$$A = \left[\begin{array}{cccccc} 0 & 0 & 0 & 0 & 0 & 0 \\ 0 & 0 & 0 & 0 & 0 & 0 \\ 0 & 0 & 0 & 0 & 0 & 0 \\ 1.000 & 0 & 0 & 0 & 0 & 0 \\ 0 & 0.9950 & -0.0998 & 0 & 0 & 0 \\ 0 & 0.0998 & 0.9950 & 0 & 0 & 0 \end{array} \right] ;$$

$$B = \left[\begin{array}{cccc} 0 & 14.1622 & 0 & -14.1622 \\ 14.1622 & 0 & -14.1622 & 0 \\ -18.6049 & 18.6049 & -18.6049 & 18.6049 \\ 0 & 0 & 0 & 0 \\ 0 & 0 & 0 & 0 \\ 0 & 0 & 0 & 0 \end{array} \right]$$

$$C = \left[\begin{array}{cccccc} 1 & 0 & 0 & 0 & 1 & 0 \\ 0 & 1 & 0 & 0 & 0 & 1 \\ 0 & 0 & 1 & 0 & 0 & 0 \\ 0 & 0 & 0 & 1 & 0 & 0 \end{array} \right]$$

The corresponding system is controllable and observable and $m + p = 8 > n$. The eigenvalues are given by : $\Lambda_T = \{-5; -6\} \cup \Lambda_V = \{-4; -3, -2, -1\}$.

Step 1 :

For $\lambda_1 = -5$, and $\lambda_2 = -6$, determines that the matrix T and such that (A, B, T) not has invariants zeros:

$$T = \left[\begin{array}{cccccc} -0.152 & -0.161 & -0.163 & -0.186 & -0.190 & -0.203 \\ -0.134 & -0.139 & -0.141 & -0.158 & -0.160 & -0.168 \end{array} \right];$$

Step 2 :

For $\lambda_3 = -4$, $\lambda_4 = -3$ $\lambda_5 = -2$ and $\lambda_6 = -1$, are determined V e W:

$$V = \left[\begin{array}{cccc} 0.2956 & 0.1264 & 0.0857 & -0.0102 \\ -.1592 & 0.1239 & 0.1150 & -0.0187 \\ -0.1208 & -0.2016 & -0.1781 & 0.0265 \\ -0.2956 & -0.0632 & -0.0286 & 0.0026 \\ 0.1361 & -0.0717 & -0.0441 & 0.0053 \\ 0.1361 & 0.0941 & 0.0552 & -0.0061 \end{array} \right]$$

,

$$W = \left[\begin{array}{cccc} 0.6645 & 0.6768 & 0.6773 & 0.7169 \\ 0.6517 & 0.6874 & 0.6948 & 0.7069 \\ 0.6533 & 0.6943 & 0.7016 & 0.7057 \\ 0.6726 & 0.7053 & 0.7129 & 0.7040 \end{array} \right]$$

Step 3 :

Determines K such that $KCV = W$:

$$K = \left[\begin{array}{cccc} 1.1432 & 1.0830 & 1.1147 & 1.1690 \\ 1.1417 & 1.0815 & 1.1133 & 1.1675 \\ 1.1415 & 1.0813 & 1.1130 & 1.1672 \\ 1.1416 & 1.0814 & 1.1131 & 1.1673 \end{array} \right]$$

The closed-loop matrix $A_K = A + BKC$ correspondent, whose eigenvalues are desired, is: $A_K = \left[\begin{array}{cccccc} 0.254 & 0.242 & 0.251 & 0.260 & 0.254 & 0.242 \\ 2.485 & 2.357 & 2.428 & 2.539 & 2.485 & 2.357 \\ -2.692 & -2.633 & -2.750 & -2.692 & -2.554 & \\ 0.001 & 0 & 0 & 0 & 0 & 0 \\ 0 & 0.001 & -0.0001 & 0 & 0 & \\ 0 & 0.0001 & 0.001 & 0 & 0 & 0 \end{array} \right]$.

VI. Conclusions

In this paper the modeling of a quadrotor attitude stabilization controller using quaternion feedback. The modeling of any quadrotor can approach a model of Newton-Euler based on an inertial reference frame. Assumptions that can reduce the complexity of the model and help increase the understanding of the behavior of the object in flight. For the stabilization problem by state feedback, the LQR control technical was used to find the state matrix F_{LQR} and for the stabilization problem by output feedback using the Sylvester equations in order to find the feedback output matrix K using the Sylvester equations. Implementation through the two algorithms for find the matrices. Aming some opens questions for future studies among may consider the possible extension of the outlined technique to treat less restrictive cases than the $m + p > q$ case.

References

[1] ALEXANDRIDIS A. T. and Paraskevopoulos P. N.(1996), *A New Approach to Eigenstruture Assignment by Output Feedback*, IEEE Trans. Automatic. Control, 41 (7), July, 1046–1050.

[2] ALVES, C. C.; GONÇALVES, T. M. P.; VILLARREAL, E. R. L. *Desenvolver um controlador Fuzzy PID para um veículo aéreo não tripulável-VANT*, Anais Congresso Brasileiro de Educação em Engenharia, COBENGE 2015, São Bernardo-SP. Setembro de 2015.

[3] BEZERRA FILHO, F. A., JÁCOME, M. C.; VILLARREAL, E. R. L. *Aplicação do Controle Servo Visual em um Quadrirrotor*Proceeding Series of the Brazilian Society of Computational and Applied Mathematics, DINCON-2015, Natal, RN, Vol 1 n.1, p.8-14, Outubro-2015.

[4] CASTELAN, E. B.; HENNET, J.-C.; VILLARREAL, E. L. *Quadratic characterization and use of output stabilizable subspaces.* Automatic Control, IEEE Transactions on, IEEE, v. 48, n. 4, p. 654-660, 2003.

[5] CASTILLO, P.; GARCIA, P.; LOZANO, R.; ALBERTOS, P. *Modelado y estabilizacion de un helicoptero con cuatro rotores.* Revista Iberoamericana de Automatica e Informatica Industrial RIAI, Elsevier, v. 4, n. 1, p. 41-57, 2007.

[6] DOMINGUES, J. M. B. *Quadrotor prototype.* Instituto Superior Tecnico, 2009.

[7] FLETCHER L. R.(1988), *Eigenstructure Assingment by Output Feedback in Descriptor Systems,* IEEE Proc., 135 (4), 302–308.

[8] KIMURA, H. *Pole assignment by gain output feedback.* Automatic Control, IEEE Transactions on, IEEE, v. 20, n. 4, p. 509-516, 1975.

[9] LUO, W.; CHU, Y.-C. *Attitude control using the sdre technique.* In: IEEE. Control, Automation, Robotics and Vision, 2002. ICARCV 2002. 7th International Conference on. [S.l.], 2002. v. 3, p. 1281-1286.

[10] PAULA, J. C. d. *Desenvolvimento de um vant do tipo quadrirotor para obtenção de imagens aereas em alta definição.* 2013.

[11] SHTESSEL, Y. B.; TOURNES, C. H.; FRIDMAN, L. *Advances in guidance and control of aerospace vehicles using sliding mode control and observation techniques.* Journal of the Franklin Institute, Pergamon, v. 349, n. 2, p. 685-699, 2012.

[12] STEVENS, B. L.; LEWIS, F. L. *Aircraft control and simulation.* Wiley-Interscience, 2003.

[13] SYRMOS, V.; LEWIS, F. *Output feedback eigenstructure assignment using two sylvester equations.* Automatic Control, IEEE Transactions on, IEEE, v. 38, n. 3, p. 495-499, 1993.

[14] SYRMOS, V.; LEWIS, F. *A bilinear formulation for the output feedback problem in linear systems.* Automatic Control, IEEE Transactions on, IEEE, v. 39, n. 2, p. 410-414, 1994.

[15] SYRMOS, V. L.; ABDALLAH, C. T.; DORATO, P.; GRIGORIADIS, K. *Static output feedback a survey.* Automatica, Elsevier, v. 33, n. 2, p. 125-137, 1997.

[16] VILLARREAL, E. R. L.; VARGAS, J. A. R.; HEMERLY, E. M. *Static output feedback stabilization using invariant subspaces and sylvester equations.* TEMA Tend. Mat. Apl. Comput, v. 10, n. 1, p. 99-110, 2009.

[17] VILLARREAL, E. R. L,;BRANDÃO, A. S. ; DE MORAIS, E. R., COLAÇA, C. F. *Modeling and Stabilization of a Quadrotor using Output Feedback*, Proceeding Series of the Brazilian Society of Computational and Applied Mathematics, DINCON-2015, Natal, RN, Vol 1 n.1, p.1-7,Outubro-2015.

[18] VILLARREAL, E. R. L.; JÁCOME, M. C.;BEZERRA FILHO, F. A. ;DE ANDRADE L. C. *Aplicao dos quadrirrotores como objeto de estudo de diversas áreas de engenharia*, Anais Congresso Brasileiro de Educação em Engenharia, COBENGE 2015, So Bernardo-SP. Setembro de 2015.

[19] WONHAM, W. M. *Linear multivariable control: a geometric approach.* [S.l.]: Springer-Verlag New York, 1979.

Proceeding Series of the Brazilian Society of Computational and Applied Mathematics

Modeling and Stabilization of a Quadrotor using Output Feedback

Elmer Rolando Llanos Villarreal[1]

Programa de Pós-graduação em Sistemas de Comunicação e Automação da UFERSA Mossoró, RN.

Departamento de Ciências Exatas e Naturais (DCEN)

Av. Francisco Mota 572 Mossoró, RN.

Alexandre Santos Brandão[2]

Departamento de Engenharia Elétrica, UFV, Viçosa, MG.

Edpo Rodrigues de Morais [3] Cássio Falcão Colaça,[4]

Programa Pós-graduação Sistemas de Comunicação e Automação da UFERSA Mossoró, RN.

Maxwell Cavalcante Jácome[5]

Departamento Ciências Exatas e Naturais (DCEN), UFERSA, Mossoró, RN.

Abstract: *This paper presents a study of mathematical modeling of a vehicle the quadrotor type. The dynamic model of the vehicle takes into account the dynamics of rotating wings and results in a non-linear system. For Simplifity the model nonlinear is linearization carried. Thus the new linear system is projected to control LQR (Linear Quadratic Regulator) to find the state matrix F. As well as is applied the algorithm using Sylvester equations to find the feedback output matrix K. It then makes a comparison between the two algorithms with numerical examples is presented.*

Keywords:. Stabilization, Riccati Equation, Sylvester Equation, Quadrotor, Output Feedback.

1 Introduction

Currently , the quadrotor is emerging as a standard platform for the detection of motion and three-dimensional perception , because this kind of vehicle is one of the most flexible aerial platforms in the field of aerial robotics . It is known that the static output feedback stabilization problem is a relevant and challenging problem, due to its simple implementation, in contrast to more dynamic methods, and because it is not easy to find a feedback matrix to make the closed-loop system asymptotically [2]. The determination of procedures for obtaining the feedback matrix in output feedback control to asymptotically stabilize linear systems is actually an open problem. Several methods have been proposed in the literature based on Lyapunov and Ricatti linear matrix inequalities, or

[1]elmerllanos@ufersa.edu.br
[2]alexandre.brandao@ufv.br
[3]edpo_morais@hotmail.com
[4]cassiofc@hotmail.com
[5]maxwellc.jacome@hotmail.com

eigenstructure assignment [4], [2] [7]. There are sufficient conditions for the solution to these equations under a rank constraint [2]. This paper presents a study modelling mathematical e stabilization problem of the dynamics of a quadrotor.

In this paper is studied the stabilization problem by output feedback thus is obtained the output feedback matrix using the Sylvester equations, where the algorithm Syrmos and Lewis is implemented to find the gain matrix K, and so compare between them. The paper is apresented in section two the quadrotor and its features can be seen. In section third the stabilization problem is obtained the state matrix F by LQR method . The next section presents the stabilization problem by output feedback and is obtained the output feedback matrix by the method of Sylvester equations, here are some examples to illustrate their methodology and conclusions of this study are mentioned in the final section.

2 The Quadrotor

A quadrotor is an aerial robot that has four engines , where adjacent motors rotate in the opposite direction . Performed by the propeller forces are perpendicular to the plane of the engines , the center of mass is located in the center of the vehicle . Compared to a classic helicopter quad provides great advantages for being a symmetrical vehicle, since its simplicity of construction and the robustness and maintainability [6]. These advantages are due to the fact that the quad has constant helix angle at all , thus avoiding the use of variation of the angles of the propellers systems that are complex and not robust systems that require much maintenance. The four-engine helicopter has the advantage of being controlled from the variation of the four angular velocities of the four engines , each force produced by the motor is equal to the square of the angular velocities $f_i = k_{w^2}$ [3].The motor rotates in a fixed direction , whereby the forces are always positive.

3 Stabilization by LQR method

The traditional method used to control the attitude stabilization system is LQR to use such a nonlinear system must first linearize around a certain operating point . For this purpose , the Jacobians of the nonlinear states equations are derived for the states and the inputs. Thus, the state matrices A, B, C and D are obtained after replacing the amounts of states in the operating point. The controllability of physical state is analyzed by checking out controllability matrix is considered and controlled by all twelve states. The attitude of the movement system is completely observable with the set of sensors used. The attitude of the moving system is completely observable with the set of sensors used . The observability analysis is also carried out by checking the rank of the observability matrix. Thus, these states that rule the attitude of the system can be controlled with the set of sensor chosen.

In the control problem of attitude stabilization technique using Riccati equations and will be used this technique being implemented from the article [5].

Consider the state space representation of a time-invariant linear system

$$\dot{x} = Ax + Bu \tag{1}$$
$$y = Cx \tag{2}$$

where $x \in \mathbf{R}^n$ is the vector of state variables of the system, $u \in \mathbf{R}^m$ is the control input and $y \in \mathbf{R^p}$ corresponds to the system output. For stabilization this system is necessary the find a feedback state matrix in the form

$$u = -Fx \tag{3}$$

with $F \in \mathbf{R}^{m\times n}$, a constant coefficient matrix control to be determined.

The LQR (Linear Quadratic Regulator) is a control technique in the form of equation (3), and matrix F_{LQR} that allows optimal control of the system (4) by minimizing the cost function:

$$J_{LQR} = \int_0^\infty (x^*Qx + u^*Ru)dt \tag{4}$$

The symbol $*$ represent a matrix operation conjugate transposed. For example x^* is the conjugate transpose of x, i.e. the elements of the matrix x are transposed and complex elements, if any, are combined so composing the new matrix. Already Q and R are Hermitian matrices, that is the matrix is equal to its conjugate transpose.

In Equation (5) Q and R are matrices positive semidefinite weighting and set, respectively.

$$Q = \begin{bmatrix} \frac{1}{max(x_1)^2} & 0 & 0 \\ 0 & ... & 0 \\ 0 & 0 & \frac{1}{max(x_n)^2} \end{bmatrix}; R = \begin{bmatrix} \frac{1}{max(u_1)^2} & 0 & 0 \\ 0 & ... & 0 \\ 0 & 0 & \frac{1}{max(u_m)^2} \end{bmatrix} \tag{5}$$

Using the method LQR the optimal matrix F_{LQR} is calculated by solving the algebraic Riccati equation in order to P_1

$$A'P_1 + P_1.A - P_1BR^{-1}B'P_1 + Q = 0 \tag{6}$$

where a matrix F_{LQR} is obtained

$$F_{LQR} = R^{-1}B'P_1 \tag{7}$$

The steps of the LQR controller design is summarized in the following steps:

1) Transform the system equations in the state space equation format, as in the relationship, obtaining matrices A and B

2) Determine the square matrices Q and R, where the elements are given by the equations (5).

3) Find the matrix P_1 by resolution of the Riccati equation shown in equation (6).

4) Determine the value of the F_{LQR} matrix equation (7).

Example 1: This example will use the method of LQR.

One linearized system (2) is considered , defined by [3] :

$$A = \begin{bmatrix} 0 & 0 & 0 & 0 & 0 & 0 \\ 0 & 0 & 0 & 0 & 0 & 0 \\ 0 & 0 & 0 & 0 & 0 & 0 \\ 1.000 & 0 & 0 & 0 & 0 & 0 \\ 0 & 0.9950 & -0.0998 & 0 & 0 & 0 \\ 0 & 0.0998 & 0.9950 & 0 & 0 & 0 \end{bmatrix}$$

$$B = \begin{bmatrix} 0 & 14.1622 & 0 & -14.1622 \\ 14.1622 & 0 & -14.1622 & 0 \\ -18.6049 & 18.6049 & -18.6049 & 18.6049 \\ 0 & 0 & 0 & 0 \\ 0 & 0 & 0 & 0 \\ 0 & 0 & 0 & 0 \end{bmatrix}; C = \begin{bmatrix} 1 & 0 & 0 & 0 & 0 & 0 \\ 0 & 1 & 0 & 0 & 0 & 0 \\ 0 & 0 & 1 & 0 & 0 & 0 \\ 0 & 0 & 0 & 1 & 0 & 0 \\ 0 & 0 & 0 & 0 & 1 & 0 \\ 0 & 0 & 0 & 0 & 0 & 1 \end{bmatrix}$$

The corresponding system is controllable and observable.
Since the matrix Q and R

$$\mathrm{Q} = \begin{bmatrix} 1.000 & 0 & 0 & 0 & 0 & 0 \\ 0 & 0.001 & 0 & 0 & 0 & 0 \\ 0 & 0 & 1.000 & 0 & 0 & 0 \\ 0 & 0 & 0 & 0.001 & 0 & 0 \\ 0 & 0 & 0 & 0 & 1.000 & 0 \\ 0 & 0 & 0 & 0 & 0 & 0.001 \end{bmatrix}; R = \begin{bmatrix} 0.010 & 0 & 0 & 0 \\ 0 & 0.010 & 0 & 0 \\ 0 & 0 & 0.010 & 0 \\ 0 & 0 & 0 & 0.010 \end{bmatrix}$$

we obtain the matrices P_1 and F_{LQR}

$$\mathrm{P}_1 = \begin{bmatrix} 0.005 & 0.000 & -0.000 & 0.000 & 0.000 & -0.000 \\ 0.000 & 0.001 & -0.000 & 0.000 & 0.005 & 0.000 \\ -0.000 & -0.000 & 0.002 & 0.000 & -0.000 & 0.000 \\ 0.000 & 0.000 & 0.000 & 0.031 & 0.000 & -0.000 \\ 0.000 & 0.005 & -0.000 & 0.000 & 0.015 & -0.003 \\ -0.000 & 0.000 & 0.000 & -0.000 & -0.003 & 0.031 \end{bmatrix};$$

$$\mathrm{F}_{LQR} = \begin{bmatrix} 0.000 & 0.741 & -5.002 & 0.000 & 7.137 & -0.155 \\ 7.072 & -0.002 & 5.000 & 0.223 & -0.066 & 0.158 \\ 0.000 & 0.737 & -4.998 & -0.000 & -7.003 & -0.161 \\ -7.072 & -0.002 & 5.000 & -0.223 & 0.066 & 0.158 \end{bmatrix}$$

with $A_F = A - BF_{LQR}$ and $\sigma(A_F \in C^-)$. Thus the matrix F stabilizes the given system.

3.1 Feedback Outputs Using Coupled Sylvester Equations

In this part a technique of stabilization by output feedback is presented.
Is considered to be time-invariant linear system:

$$\dot{x} = Ax + Bu \tag{8}$$
$$y = Cx \tag{9}$$

, where A, B, C are matrices of appropriate dimensions.

As in [2], use certain concepts and definitions of geometric control theory. It is known that a subspace is $V \subset X$ (A, B) if there is invariant $F : X \longrightarrow Y$ such that $(A+BF)V \subset V$, or equivalently, $AV \subset V + ImB$. By duality a subspace $\tau \subset X$ is (C, A) if there is invariant $L : Y \longrightarrow X$, such that $(A + LC)\tau \subset \tau$, or equivalently, $\tau \supset A(\tau \cap ker(C))$.

Definition 3.1. *As in [2], a subspace $V \subset X$,of dimension v, is (C, A, B) invariant if V is $(A, B)-$ invariant and $(C, A)-$ invariant .*

Definition 3.2. *A subspace V ,of dimension v, is $(C, A, B)-$ invariant stabilizable by output (or simply O.S.)(C, A, B)-invariant if V is (A, B)-intern stabilizable and $(C, A)-$ external detectably.*

In [2] and [8] Theorem 3.1 relates the concept of subspaces O.S.$(C, A, B)-$ invariant to the existence of a control law of the static type of feedback outputs $(u = Ky)$ that stabilizes the closed-loop system.

Theorem 3.1. *There is a matrix of output feedback $K : Y \to U$ such that $\sigma(A + BKC) \in C^-$ if and only if the following conditions are checked for some matrices $(V \in \mathbf{R}^{nxv}, H_V \in \mathbf{R}^{vxv}, W \in \mathbf{R}^{mxv})$,$(T \in \mathbf{R}^{n-vxn}, H_T \in \mathbf{R}^{n-vxn-v}, U \in \mathbf{R}^{n-vxv})$ and for some positive scalar $v \leq n$:*

$$AV - VH_V = -BW, \text{with } \sigma(H_V) \in C^- \tag{10}$$

$$TA - H_T T = -UC, \text{with } \sigma(H_T) \in C^- \tag{11}$$

$$TV = 0 \tag{12}$$

$$KCV = W \tag{13}$$

$$TBK = U \tag{14}$$

where: $\text{rank}(V) = v$ and $\text{rank}(T) = n - v$

Important to note that guaranteed the existence of solution to the equations of Sylvester and K is obtained such that (13) and either (14) is verified, the eigenvalues loop closed are given by:

$$\sigma(A + BKC) = \sigma(H_V) \dot{\cup} \sigma(H_T)$$

3.2 Algorithms Aspects

In the Theorem (3.1) the conditions not linear with respect to matrix variables (V, H_V, W) and (T, H_T, U). In particular, the non-linear terms V; H_V and H_T; T present in (10) and (11), respectively, can be linearized when setting up the matrices H_T and H_V, or equivalently when setting up the desired results for the closed-loop system eigenvalues.

An algorithmic technique based on the procedures for self-positioning structure for obtaining an output feedback will be displayed in this section. The technique to be worked on is the proposed [7] solves the coupled Sylvester equations in two steps and can be directly applied to systems which verify the condition $m+p > n$, known as Kimura condition . For the development of the technique, it is assumed that the dimension $V = Im(V)$ is equal to the number of outputs p, while ensuring that the matrix $CV \in \mathbf{R}^{pxp}$ is invertible and hence the feedback gain matrix can be found from Equation (13) in the form $K = W(CV)^{-1}$.

Further, it is considered that the system represented by (C, A, B) is controllable and observable, this necessary condition for arbitrary choice of the poles to be placed in closed loop. The set of desired poles is denoted by $\Lambda = \{\lambda_1, \cdots, \lambda_{n-p}, \lambda_{n-p+1}, \cdots, \lambda_n\} = \{\lambda_T, \Lambda_V\}$ where λ_T and λ_V are self conjugates. These sets are associated matrices $H_V \in R^{p\times p}$ and $H_T \in R^{(n-p)\times(n-p)}$ in the following way:$\sigma(H_T) = \lambda_T = \{\lambda_1, \cdots, \lambda_{n-p}\}$ and $\sigma(H_V) = \lambda_V = \{\lambda_{n-p+1}, \cdots, \lambda_n\}$. For simplicity of presentation, it is considered that the elements of $\Lambda = \sigma(A + BKC)$ are distinct.

3.3 Algorithm Syrmos and Lewis

Based on the conditions expressed by Theorem (3.1), The following algorithm, proposed in [7], usually leads to an array of output feedback which stabilizes the closed-loop system when the condition Kimura $n < m + p$ is verified:

Step 1: Choose $H_T \in \mathbf{R}^{(n-p)x(n-p)}$ matrix such that $\sigma(H_T) = \Lambda_T \in C^-$ and solves the Sylvester equation (11) to find a matrix $T \in \mathbf{R}^{pxn-p}$ such that

$$rank \begin{bmatrix} T \\ C \end{bmatrix} = n \Leftrightarrow KerT \cap KerC = 0 \tag{15}$$

Step 2: Resolves to Sylvester equation (10), for any matrix $H_V \in \mathbf{R}^{pxp}$ such that $\sigma(H_V) = \Lambda_V \in C^-$ assuming the matrix V should check the coupling condition (10) and put that (V) be equal to p.

Step 3: By condition, the equation (15) ensures that placed $(CV) = p$ and the matrix K can be calculated as a single solution (13).

The following presents some observations with dual aim of showing aspects of the numerical solution of the steps of the algorithm and justify it theoretically.

Note: The steps 1 and 2 can be solved using standard techniques for self-positioning structure. Whereas mothers H_T and H_V in Jordan canonical form, we can adopt the following procedure:

Step 1: Find $t_j \in C^n$ and $u_j \in C^p$, such that:

$$\begin{bmatrix} t'_j & u'_j \end{bmatrix} \begin{bmatrix} A - \lambda_j I \\ C \end{bmatrix} = 0 \ \forall j = 1, \cdots, \ n - p \tag{16}$$

Step 2: Determine $v_i \in C^n$ and $w_i \in C^n$ such that:

$$\begin{bmatrix} A - \lambda_j I & B \\ C & 0 \end{bmatrix} \begin{bmatrix} v_i \\ w_i \end{bmatrix} = 0 \quad \forall \ i = \ n - p, \ \cdots, \ n \tag{17}$$

In a similar way to the previous case, the matrices V and W for the calculation of K can be constructed with real elements. Where v_i and w_i denote the columns of the matrices V and W respectively. With $TV = 0$.

Example 2: A linear system (8) is considered defined by :

$$A = \begin{bmatrix} 0 & 0 & 0 & 0 & 0 & 0 \\ 0 & 0 & 0 & 0 & 0 & 0 \\ 0 & 0 & 0 & 0 & 0 & 0 \\ 1.000 & 0 & 0 & 0 & 0 & 0 \\ 0 & 0.9950 & -0.0998 & 0 & 0 & 0 \\ 0 & 0.0998 & 0.9950 & 0 & 0 & 0 \end{bmatrix};$$

$$B = \begin{bmatrix} 0 & 14.1622 & 0 & -14.1622 \\ 14.1622 & 0 & -14.1622 & 0 \\ -18.6049 & 18.6049 & -18.6049 & 18.6049 \\ 0 & 0 & 0 & 0 \\ 0 & 0 & 0 & 0 \\ 0 & 0 & 0 & 0 \end{bmatrix}; C = \begin{bmatrix} 1 & 0 & 0 & 0 & 1 & 0 \\ 0 & 1 & 0 & 0 & 0 & 1 \\ 0 & 0 & 1 & 0 & 0 & 0 \\ 0 & 0 & 0 & 1 & 0 & 0 \end{bmatrix}$$

The corresponding system is controllable and observable and $m + p = 8 > n$. The eigenvalues are given by : $\Lambda_T = \{-5; -6\} \cup \Lambda_V = \{-4; -3, -2, -1\}$.

Step 1 : For $\lambda_1 = -5$, and $\lambda_2 = -6$, determines that the matrix T and such that (A, B, T) not has invariants zeros: $T = \begin{bmatrix} -0.152 & -0.161 & -0.163 & -0.186 & -0.190 & -0.203 \\ -0.134 & -0.139 & -0.141 & -0.158 & -0.160 & -0.168 \end{bmatrix}$.

Step 2 : For $\lambda_3 = -4$, $\lambda_4 = -3$ $\lambda_5 = -2$ and $\lambda_6 = -1$, are determined V and W:

$$V = \begin{bmatrix} 0.2956 & 0.1264 & 0.0857 & -0.0102 \\ -.1592 & 0.1239 & 0.1150 & -0.0187 \\ -0.1208 & -0.2016 & -0.1781 & 0.0265 \\ -0.2956 & -0.0632 & -0.0286 & 0.0026 \\ 0.1361 & -0.0717 & -0.0441 & 0.0053 \\ 0.1361 & 0.0941 & 0.0552 & -0.0061 \end{bmatrix}; W = \begin{bmatrix} 0.6645 & 0.6768 & 0.6773 & 0.7169 \\ 0.6517 & 0.6874 & 0.6948 & 0.7069 \\ 0.6533 & 0.6943 & 0.7016 & 0.7057 \\ 0.6726 & 0.7053 & 0.7129 & 0.7040 \end{bmatrix}$$

Step 3 : Determines K such that $KCV = W : K = \begin{bmatrix} 1.1432 & 1.0830 & 1.1147 & 1.1690 \\ 1.1417 & 1.0815 & 1.1133 & 1.1675 \\ 1.1415 & 1.0813 & 1.1130 & 1.1672 \\ 1.1416 & 1.0814 & 1.1131 & 1.1673 \end{bmatrix}$.

The closed-loop matrix $A_K = A + BKC$ correspondent, whose eigenvalues are desired.

4 Conclusions

The LQR control was used to find the F_{LQR} state matrix and used Sylvester equations in order to find the matrix K feedback output using the Sylvester equations thus is obtained the state matrix and matrix feedback output through the two algorithms. Aming some opens questions for future studies among may consider the possible extension of the outlined technique to treat less restrictive cases than the $m + p > q$ case.

References

[1] A. T. Alexandridis and P.N. Paraskevopoulos, A New Approach to Eigenstruture Assignment by Output Feedback, IEEE Trans. Automatic. Control, vol. 41(7), July, 1046–1050, (1996).

[2] E. B. Castelan, J. C. Hennet and E. R. L. Villarreal, Quadratic characterization and use of output stabilizable subspaces, IEEE Trans. Automatic. Control, vol. 48(4), 654–660, (2003).

[3] P. Castillo, P. Garcia, R. Lozano and P. Albertos, Modelado y estabilizacion de un helicoptero con cuatro rotores, Revista Iberoamericana de Automatica e Informatica Industrial RIAI, ELSEVIER, vol. 4(1), 41–57, 2007.

[4] L. R. Fletcher, Eigenstructure Assingment by Output Feedback in Descriptor Systems, IEEE Proc., vol. 135(4), 302–308, (1988).

[5] W. Luo and Y. C. Chu, Attitude control using the sdre technique, IEEE Control, Automation, Robotics and Vision, 2002. ICARCV 2002. 7th International Conference on, vol. 3, 1281–1286, (2002).

[6] Y. B. Shtessel, C. H. Tournes and L. Fridman, Advances in guidance and control of aerospace vehicles using sliding mode control and observation techniques, Journal of the Franklin Institute, PERGAMON, vol. 349(2), 685–699, (2012).

[7] V. Syrmos and F. Lewis, Output feedback eigenstructure assignment using two sylvester equations, IEEE Trans. Automatic. Control, vol. 38(3), 495–499, (1993).

[8] E. R. L. Villarreal, J. A. R. Vargas and E. M. Hemerly, Static output feedback stabilization using invariant subspaces and sylvester equations TEMA, vol. 10(1), 99–110, (2009).

APPLICATION THE CONTROL IN TANKS USING FUZZY THEORY

ADELSON MENEZES LIMA*, SAMEQUE FARIAS CUNHA DE OLIVEIRA*, MISSILENE DA SILVA FARIAS*, TARCISIO DA SILVA BARRETO*, ELMER ROLANDO LLANOS VILLARREAL†

* *Simulation and Computacional Insfrastructure Laboratory Post-graduation Program in Communication Systems and Automation Federal University of the Semi-Arid Region(UFERSA) CEP-59.625-900, Mossoro, RN, BRASIL*

† *Department of Exact and Natural Sciences (DCEN), Federal University of the Semi-Arid region (UFERSA) CEP- 59.625-900, Mossoró, RN, BRASIL*
Simulation and Computacional Insfrastructure Laboratory Post-graduation Program in Communication Systems and Automation Federal University of the Semi-Arid Region(UFERSA)

Emails: adelsonmlima@gmail.com, samequefarias@hotmail.com, missilenefarias@hotmail.com, tarcisiofip2@gmail.com, elmerllanos@ufersa.edu.br

Abstract— The control of liquid level in tanks and flow between tanks is a basic problem in the process industries. The process industries require liquids to be pumped, store in tanks, then pumped to another tank. Through the use of Fuzzy Logic can control any process, in order to overcome the limitation imposed by the difficulty in obtaining accurate parameters of a conventional PI controller. In this paper, control is performed liquid level present in two water tanks QUANSER attached, and used the theory of fuzzy sets applied to the environment of high-level programming in MATLAB a for the design of Fuzzy Controller . In order to prove the effectiveness of the proposed control model, a comparison is made between the response of the controlled system exclusively by proportional integral (PI) to that obtained with the application of Fuzzy Controller, where you can observe the superiority of the latter in relation to conventional control.

Keywords— Fuzzy, Proportional Integral; Matlab, Level Control.

1 Introduction

The control of liquid level in tanks and flow between tanks is a basic problem in the process industries. The process industries require liquids to be pumped, store in tanks, then pumped to another tank. Many times the liquids will be processed by chemical or mixing treatment in the tanks, but always the level of fluid in the tanks must be controlled, and the flow between tanks must be regulated. Often the tanks are so coupled together that the levels interact and this must also be controlled. Level and flow control in tanks are at the heart of all chemical engineering systems. The Proportional-Integral (PI) has relatively simple structure and efficiency in control of a variety of industrial processes, as shown in Figure 1.

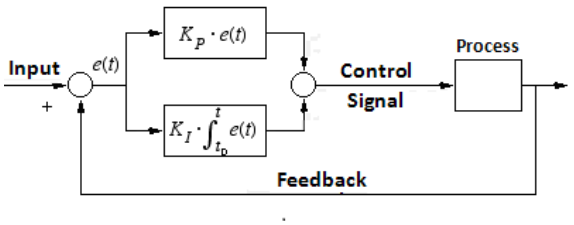

Figure 1: PI Controller

The integral action corresponds to a rate of change of the output signal relative to the input signal. So with a full action, improves the performance of the system response in steady state, tending to eliminate the steady state error due to the fact of increasing the order of the system, however, detract from the transitional regime, as it adds poles to the system tends to destabilize it, and thereby increase the settling time of the signal. The performance of a PI controller is the sum of the proportional action and integral action. This way you can improve both the transient, response with input from the proportional action, as the steady-state error corrected by the integral action. Despite the wide use in a range of processes, it is not hard to find PIs presenting unsatisfactory behavior, ie not passing correct the error or stationary presenting high values of overshoot due to the increased complexity, non-linearity, coupling between the variables, etc., making it difficult to define the parameters of control system. Thus, with the development of Modern Control Theory, made possible the development of more advanced control strategies such as the Fuzzy Controller, aiming to stabilize the plant effectively, thus increasing the accuracy of the system. In the case of having a narrow operating limit by fuzzy control can be achieved great effect in terms of control. The Fuzzy term have meanings that vary according to the context in which the basic concept revolves around the always vague, nebulous or uncertain. As its name suggests, has as main objective the computational modeling of human reasoning, sometimes inaccurate, ambiguous and vague, using fuzzy conditional statements, by quantifying the linguistic variables as (Amendola et al., 2005) and (Marro et al., 2006) . The paper is organized

as follows: The fuzzy controller is explained in section II. The principle of operation of the level control tank is coupled discussed in section III. The simulation system applied to a fuzzy controller, for controlling the level of liquid in tanks is provided in section IV. The results and findings are reported in Sections V and VI, respectively.

2 The Fuzzy Controller

2.1 Structure

According with (Shaw and Simoes, 2007) , intelligent systems are part of a new paradigm as logic "Fuzzy", Neural Networks, Expert Systems and genetic algorithms. These systems seek to provide answers that solve problems, as appropriate to the specific situations of these problems, even if new or unexpected. The fuzzy logic can be applied to a control system for solving problems in systems from simple, small, embedded microcontrollers, even in data acquisition systems based workstation and control. Can be implemented in hardware, software or a combination of both, thus providing a simple way to arrive at a definite conclusion based on information input vague or ambiguous, or even incomplete as (Qi et al., 2010). The algorithms fuzzy contain the functions necessary to solve problems in a process controlled by a fuzzy controller, in which it can emphasize its basic components: the knowledge base, the inference procedure, the interface fuzzyfication, and interface defuzzification as follows figure 2.

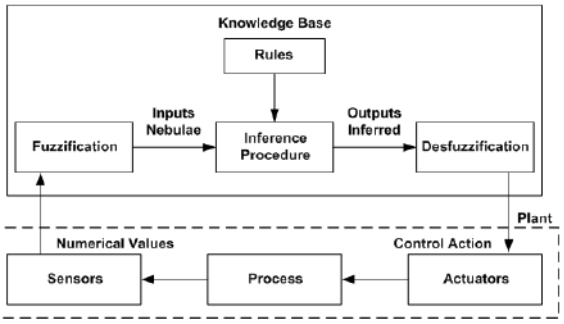

Figure 2: Fuzzy Controller

1. Knowledge Base: Contains settings that characterize the control strategy and goals.

2. Procedure of inference: Responsible for making decisions based on the information obtained in the system and act according to the rule base of the fuzzy logic decision making.

3. Fuzzification interface: Transforms the variables of the problem in real values for fuzzy sets.

4. Defuzzification interface: Convert the output fuzzy sets for real output value, ie, clear results.

2.2 Design of Fuzzy Controller

The design of a fuzzy controller mainly involves the following four steps:

1. Fuzzification

   In the fuzzy control, the actual values must be processed in fuzzy sets to be calculated on the fuzzy rules. It is called fuzzification using these sets that express real signals. The first step in the representation of fuzzy sets is the choice of the membership function. The choice of this function depends on the problem to be modeled and also computational capacity available to process what you want. For example, if the relevant interval is $[0, 1]$, where 0 means an element not belonging to a particular group and 1 means complete relevance to the set, it is requested to say that values between 0 and 1 representing degrees of partial pertinence. In other words, the fuzzy logic element belongs to a group with a certain degree of membership, causing a given sentence can be partially true and, at the same time, partially be considered false. Furthermore, the same element may have different degrees of pertinence from 0 to more than one fuzzy set as (Qi et al., 2010). There are different ways to define the fuzzy sets, but the method proposed by Singleton is the most commonly used, where the calculations can be simplified if we consider fuzzy subsets of the entries consist of true values and fuzzy transforms real input ϵ for one or two values of a single fuzzy set a, in which:

$$\mu(A) = \begin{cases} 1 & \epsilon = \epsilon^2 \\ 0 & other \end{cases} \quad (1)$$

   If the entry receives a disturbance, fuzzy sets reflect this uncertainty in the measurement process.

2. Establishment of Fuzzy Inference Rules

   Would be associated with a linguistic variable x, each of these terms associated with a fuzzy set in order to establish its meaning. Are the keys of the fuzzy controller as a device for correcting or compensating the traditional control systems. Usually expressed through conditional statements like "if ... else ..."

3. Selecting the synthesis algorithm for reasoning

   The optimal algorithm is one that can better adapt to frequent variations in load change

and regime changes in operating conditions of a given process. From an operational standpoint, simplicity is also desirable. The algorithm for implementation of fuzzy rules must be directly related to the vague reasoning, present in these rules, using functions of relevance established. Gaussian membership functions, membership trapezoidal membership functions of triangular function and are most commonly used.

4. Defuzzification Is to transform the fuzzy sets result in a sharp, or to return results in actual numeric values for the machine within the range stipulated by the fuzzy logic. There are several known methods, however, the two most commonly used methods are the method based on center of mass and the method based on the average of the maximum of the membership functions, also known as Mamdani, created by Professor Ebrahim Mamdani of the University of London (UK) in 1975. Through these methods is the most appropriate numerical value in "x" axis and turning the membership functions elaborated by the rules, you discover how numerically this value means in terms of linguistic variables.

3 Princíple of Control System of Liquid Level in Pond Coupled

The structure of the tank coupled system to control liquid level consists of two tanks in series of the same capacity, an outlet valve whose inflow is adjusted by an adjustable-speed pump, and a water level sensor to real-time changes in the reservoirs according to figure 3 as (Qi et al., 2010). According to the configuration of valves, the problem is to maintain the liquid level desired for the tanks, which decided on this system in controlling

Where as the system of Figure 3, the expression of its transfer function can be represented by equation 2 as (Qi et al., 2010):

$$G(s) = \frac{1}{[(A^2/K)s^2 + 2As + K]} \quad (2)$$

where:

A = area of the tank $0.15dm^2$;

K = constant flow of water $3.3cm^3/s/V$

Therefore, from the values of "A" and "K" can have equation (3):

$$G(s) = \frac{1}{[0.04s^2 + 0.3s + 3.3]} \quad (3)$$

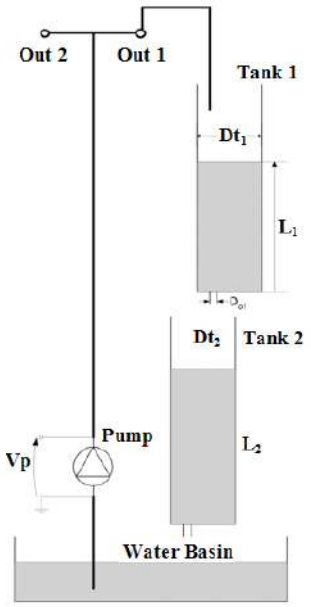

Figure 3: Scheme Plant Tank Coupled

4 Simulation System Apllied Fuzzy Control of Liquid Level

Generally to control the liquid level in tanks, traditionally used to control structure Proportional-Integral-Derivative (PID) to act on the valve installed in the liquid outlet. However, the main problem in this type of system is the transfer of oscillations that can occur to the load output flow. Only systems with small load fluctuations using the PID is satisfactory. For systems with large swings in load this driver, tuned to keep the level constant, the oscillations in the flow tank inlet propagate to the output, causing instability in the equipment installed downstream of the tanks. And in this case, a PI controller present in poor performance as (Amendola et al., 2005) and (Filho et al., 2002). So it is necessary to use a control algorithm that enables the damping of oscillations in the tanks, in other words, the ideal level controller must allow the level varied within an operating range (bandwidth) for the flow at the exit are less oscillatory and allow the oscillation of this controlled variable (level) within the limits (band), it is advisable to apply a control based on fuzzy logic as (Giovani, 2004). The PI control system, the input variable is the error measured by the liquid level e(t) in the tank, while the fuzzy control object has two inputs, one is the error e(t), the other is rate of change of error $\Delta e(t)$. The output voltage is proportional to the pump. Thus, the control system with fuzzy logic has dual input and single output.

4.1 Step Fuzzification

The range of error e(t) was defined in [-1,0,1]. Fuzzy corresponding values are (High, Ideal and

Low). The range rate error $\Delta e(t)$ is $[-0.1, 0, 0.1]$ the corresponding fuzzy sets are considered (negative, zero, positive). The model of the membership functions are Gaussian in figures 4 and 5.

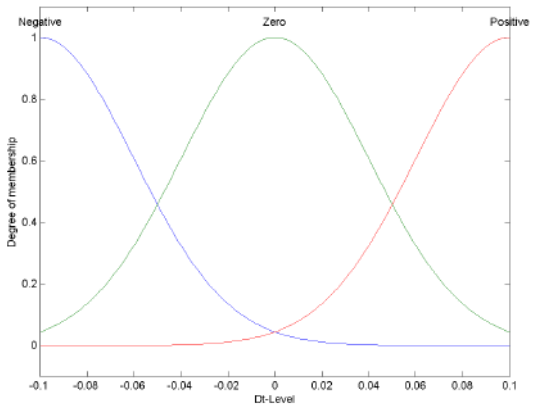

Figure 4: Input Membership Function for Error

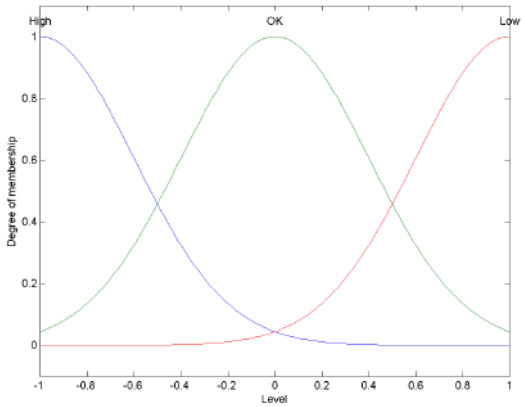

Figure 5: Membership function for the variation of the error

4.2 Establishment of Fuzzy Rules

We used the algorithm Mandani type Fuzzy Inference System, as shown in figure 6. To establish the process of fuzzy reasoning, fuzzy rules were chosen as follows and shown in Figure 7:

1. If the level is optimal, then the output voltage remains constant;
2. If the level is low, then the output voltage rises rapidly
3. If the level is high, then the voltage decreases rapidly;
4. If the level is ideal and its variation is positive, then the output voltage decreases slowly;
5. If the level is ideal and its variation is negative, then the output voltage increases slowly.

4.3 Defuzzification

In the problem shown here, the output variable was chosen as the voltage applied to the pump, whose domain is defined as [-1,0,1], and fuzzy sets were chosen (very low, low, stable, and high very high). The membership function has a triangular shape as shown in Figure 8.

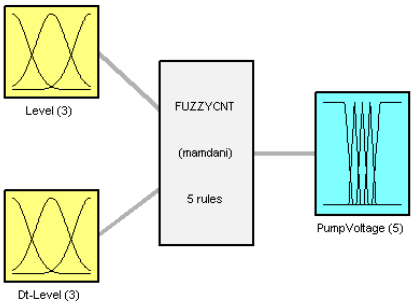

Figure 6: Mandani type Fuzzy Inference System

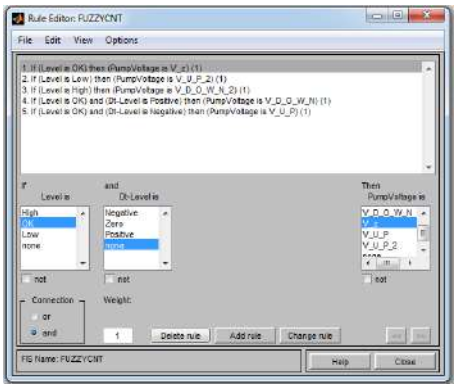

Figure 7: Rule bases

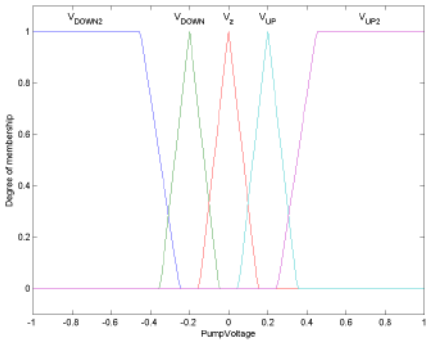

Figure 8: Member Function of the Output Variables

5 The Main Results

The simulated controllers are implemented in MATLAB® version 7.7 R2011 model for the PI

controller and the fuzzy logic and the results obtained in Figure 9.

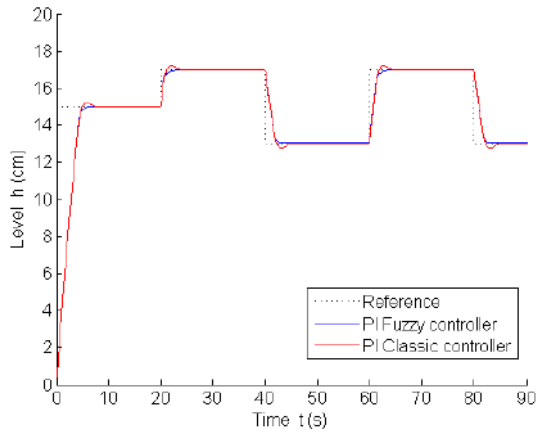

Figure 9: Comparison of Fuzzy and PI control

The responses to the controllers initially represent the average level in the tank 15cm. The test signal selected was applied with a setpoint change 2cm during a time interval varying the level up to 17cm and 13cm low level. The results obtained from the graphs in the system validates the modeling technique employed. The comparison between controllers shows the improvement in system performance using a fuzzy controller. The PI controller features an overshoot generating oscillations that occurs in the output flow of the pump.

6 Conclusion

This paper presents the result of simulations allowed the preliminary assessment of the behavior of the system when operated with the fuzzy controller. The Matlab/Simulink was very useful for the evaluation which showed that the fuzzy control system, the dynamic performance is better, no oscillation eliminated the maximum overshoot. The technique also appears to be quite useful for problems with non- linear systems. The system presented can be applied to more complex plants making up their adaptations.

References

Amendola, M., de Souza, A. L. and C.Barros, L. (2005). *Manual do Uso da Teorias dos Conjuntos Fuzzy no MATLAB 6.5*, FEAGRI-IMECC-UNICAMP.

Filho, F. M. L., Gosmann, H. L. and Bauchspiess, A. (2002). *Controle Fuzzy para Sistema de Nivel de Liquidos*, XIV Congresso Brasileiro de Automática.

Giovani, C. N. (2004). *Controle por Bandas: Conceitos básicos e aplicação no amortecimento de oscilações de carga em unidades de produção de petróleo*, Bol. Tec. Petrobras.

Marro, A. A., Souza, A. M. C., Cavalcante, E. R. S., Nunes, G. S. and Bezerra, R. O. (2006). *Lógica Fuzzy: Conceitos e Aplicações*, DIMAp-UFRN.

Qi, L., Yanjun, F., Jizhong, S. and Ji, W. (2010). *The Application of Fuzzy Control in Liquid Level System*, International Conference on Measuring Technology and mechatronic Automation.

Shaw, I. S. and Simoes, M. G. (2007). *Controle e Modelagem Fuzzy*, Edgard Blucher.

APPROACH IN NONLINEAR DESCRIPTOR SYSTEM USING OUTPUT FEEDBACK

ELMER ROLANDO LLANOS VILLARREAL*, ALEX SANDRO DE ARAUJO SILVA†, SAMEQUE FARIAS CUNHA DE OLIVEIRA ‡

* *Universidade Federal Rural do Semi-Árido (UFERSA)*

Departamento de Ciências Exatas e Naturais (DCEN)
Programa de Pós-graduação em Sistemas de Comunicação e Automação
Av. Francisco Mota 572 Mossoró, RN, Brasil.

† *Universidade Federal Rural do Semi-Árido (UFERSA)*

Departamento de Ciências Exatas,Tecnológicas- Humanas (DCETH)

Rua Gamaliel Martins Bezerra,s/n Angicos, RN, Brasil.

‡ *Programa de Pós-graduação em Sistemas de Comunicação e Automação/ UFERSA*
Mossoró, RN, Brasil.

Emails: elmerllanos@ufersa.edu.br, alex.araujo@ufersa.edu.br, samequefarias@hotmail.com

Abstract— The present paper study the Lipschitz nonlinear descriptor system. Considering the nonlinear fault-tolerant control system can be made solvable, causal, asymptotically stable. The main result provided condition for the design the output feedback controller, is presented using an LMI approach, where the theorem for existence the output feedback matrix is presented .

Keywords— Nonlinear Descriptor System; Output Feedback; LMI.

1 INTRODUCTION

The determination of procedures for obtaining the feedback matrix in output feedback control to asymptotically stabilize linear systems is actually an open problem. Several methods have been proposed in the literature based on Lyapunov and Ricatti linear matrix inequalities, or eigenstructure assignment (Fletcher, 1988), (Alexandridis and Paraskevopoulos, 1996),(Castelan et al., 2003).

Research into fault detection and diagnosis for dynamic system has long been recognized as one of the important aspects in practical control systems Several works on the fault detection and diagnosis for nonlinear descriptor systems can be found in (Vemuri et al., 2001), (Chen et al., 2003). In the work in (Gao and Ho, 2006) is presented $LMIs$ technique for a class of Lipschitz nonlinear descriptor systems.

In this paper is presented the approach is developed for nonlinear Lipschitz descriptor systems, thus the show the existence the output feedback matrix, based the paper in (Gao and Ding, 2007). The consider faults here may be unbounded, thus the plant may fail in the presence of faults. This motivates us to investigate fault-tolerant control topic, which is very important in many practical systems. However, to the best of our knowledge, very few effort has been made to investigate fault-tolerant control for non linear descriptor systems. In this study, based on the LMI technique and by using the estimated output and faults. The solvability, causality, asymptotic stability and performance are guaranteed. Moreover, the present fault- tolerant controller is output-space dynamic controller with original coefficient matrices, and it is thus realiable in computations.

2 SYSTEM DESCRIPTION

The original mathematical description of a system often consists of a set of differential and algebraic equations. However, in most literature on control theory it is assumed that the algebraic equations can be used to eliminate some variables. The result is a system description consisting only of differential equations that can be written in state-space form as

$$\dot{x} = F(t, x, u) \tag{1}$$

3 PRELIMINARIES AND PROBLEM STATEMENT

In the present paper, the notations are rather standard. R denotes the set of real numbers; C denotes the complex plane; $R_e(a)$ denotes the real part of the complex number a; $A^\dagger$ denotes the generalized inverse of A; $\lambda_i(A)$ denotes the ith eigenvalue de A; I_m denotes an identity matrix with the dimension $m \times m$; $O_{n\times p}$ denotes a $n \times p$ matrix with zero entries; $P > 0$ (or $P < 0$) indicates the symmetric matrix P is positive (or negative) definite; $\forall$ means "for all" ; $|.|$denotes the standard norm symbol ; $L_2[0T_f]$ represents the set of all signals which are square integrable and satisfy $\int_0^{T_f} d'(\tau)d(\tau)d\tau < \infty$; and $||d||_{T_f} := (\int_0^{T_f} d'(\tau)d(\tau)d\tau)^2$. The considered nonlinear descriptor systems are described by :

$$\begin{aligned} E\dot{x}(t) &= Ax(t) + Bu(t) + \phi(t, x, u) + B_d d + B_f f \\ y(t) &= Cx(t) \end{aligned} \tag{2}$$

where: $x \in \Re^n$, is the descriptor state vector; $u \in \Re^m$, $y \in \Re^p$ are, respectively, the control input and measurement output vectors and $E \in \Re^{n\times n}$,

$rank\,(E) = q < n$; as the other matrices is an appropriate size with $rank\,(B) = m$, $rank\,(C) = p$; $\phi(t,x,u) \in \Re^n$ is the real nonlinear vector function satisfying the following

$$||\phi(t,\tilde{x},u) - \phi(t,x,u)|| \leq ||U(\tilde{x}-x)||\,\forall(t,\tilde{x},u), \quad (t,x,u) \in \Re \times \Re^n \times \Re^m \qquad (3)$$

and $U \in \Re^{n\times n}$ is known constant matrix. Provided that

$$rank[U'C']' = rank(C), \qquad (4)$$

there exists a matrix $K = UC^{\dagger}$ such that

$$U = KC. \qquad (5)$$

Substitution of (5) into (3) yields

$$||\phi(t,\tilde{x},u) - \phi(t,x,u)|| \leq ||KC(\tilde{x}-x)|| \leq \theta_0||C(\tilde{x}-x)|| \leq \theta||\tilde{x}-x|| \qquad (6)$$

$\forall(t,\tilde{x},u),(t,x,u) \in \Re \times \Re^n \times \Re^m$

where θ_0 and θ are both positive scalars. In this paper, plant (2) satisfies Lipschitz constraint (6).

4 BASIC CONCEPTS

The pair (E,A) is called regular if there exists $s \in \mathcal{C}$ such that $det(sE-A) \neq 0$ Thus a regular descriptor system is in (Verghese et al., 1981) and (Dai, 1989).

i) stable if all finite roots of $det(sE-A) = 0$ are in the open left half complex plane;

ii) impulse free if it exhibits no impulse behavior;

iii) finite dynamics detectable if there exists L such that $(E, A+LC)$ is regular ans stable;

iv) impulse observable if there exists L such that $(E, A+LC)$ is regular and impulse-free;

v) finite dynamics stabilizable if there exists F such that $(E, A+BF)$ is regular and stable; (E,A,B) is finite dynamics stabilizable if $rank[sE-AB] = n$, $Re[s] \geq 0$.

vi) impulse controllable if there exists F such that $(E, A+BF)$ is regular and impulse-free. If there exists a F such that $(E, A+BF)$ has no impulsive then (E,A,B) is called impulse controllable.

5 MAIN RESULT FOR NONLINEAR SYSTEM

Consider the nonlinear system

$$\begin{aligned} E\dot{x} &= Ax + Bu + \phi(t,x,u) + B_d d + B_f f \qquad (7)\\ y(t) &= Cx(t) \end{aligned}$$

In form basic it is find an static output feedback control law $u(t) = Gy(t)$ such that the closed-loop system

$$E\dot{x}(t) = (A+BGC)x(t) \qquad (8)$$

is S-stable: regular, assymptotically stable and free impulses.

Consider

$$\begin{aligned} E\dot{x} &= (A+BGC)u + \phi(t,x,u) + B_d d + B\tilde{G}C\bar{e} \qquad (9)\\ y &= Cx \end{aligned}$$

Now we begin to discuss how to choose $G \in \Re^{p\times m}$ to make the plant (9) satisfy the following:

1) The plant (9) is solvable, causal and asymptotically stable.

2) $\forall\, T_f \geq 0$, the L_2-gain from the disturbance input d to the system output y is less than or equal to a prescribed H_∞ performance $\lambda > 0$, i.e.,

$$||y||_{T_f} \leq \lambda||d||_{T_f} \qquad (10)$$

We make a further assumption on $\phi(t,x,u) \in \Re^n$, i.e. $\phi(t,0,0) = 0$. Thus, from the Lipschitz constraint (6) one further has

$$||\phi(t,x,u)|| \leq \theta||x||, \forall(t,x,u) \in \Re \times \Re^n \times \Re^m \qquad (11)$$

Now we have the following statement

Theorem 1 *The closed-loop system (9) is solvable, causal and asymptotically stable, and* $||y||_{T_f} \leq \lambda||d||_{T_f}$ *if there exists a matrix* $P \in \Re^{n\times n}$ *and* $G \in \Re^{m\times p}$ *such that*

$$E'P = P'E \geq 0 \qquad (12)$$

$$(A+BGC)P + P(A+BGC)' + I + C'C + \frac{1}{\lambda^2}P'B_dB_d'P < 0 \qquad (13)$$

Proof:

The proof is composed of three parts such as (i) the proof of solvability, (ii) the proof of the asymptotic stability, and (iii) the proof of the guaranteed performance index.

(i) The proof of solvability: It is clear that (13) implies

$$\Lambda = (A+BGC)'P + P'(A+BGC) + I + \theta^2P'P < 0 \qquad (14)$$

and further indicates

$$(A+BGC)'P + P'(A+BGC) < 0 \qquad (15)$$

Moreover, (12) and (15) indicate that the pair $(E, A+BGC)$ is casual (or impulse free), asymptotically stable, and P is nonsingular.

Similar can find non-singular matrices $M = \begin{bmatrix} M_s' & M_f' \end{bmatrix}'$ and $N = \begin{bmatrix} N_s & N_f \end{bmatrix}$ such that

$$MEN = \begin{bmatrix} I_q & 0 \\ 0 & 0 \end{bmatrix}, \text{ q=rank(E)} \qquad (16)$$

$$M(A+BGC)N = \begin{bmatrix} A_s & 0 \\ 0 & -I_{n-q} \end{bmatrix} \qquad (17)$$

$$M'^{-1}PN = \begin{bmatrix} P_{11} & 0 \\ P_{21} & P_{22} \end{bmatrix},\ P_{11} = P_{11}' > 0 \qquad (18)$$

$$||M_f|| \leq 1,\ ||N_f|| < \frac{1}{\theta\sqrt{1+\epsilon}} \qquad (19)$$

where ϵ is a sufficient small positive number. Let $N^{-1}x = \begin{bmatrix} x_s' & x_f' \end{bmatrix}'$, the descriptor state equation of the plant (9) can be transformed into

$$\begin{cases} \dot{x}_s = A_s x_s + M_s[\phi(t,x,u) + B_d d + B\bar{G}C\bar{e}] \\ x_f = M_f[\phi(t,x,u) + B_d d + B\bar{G}C\bar{e}] \end{cases} \qquad (20)$$

With the error dynamic equation can be characterized as

$$\bar{e} = \bar{x} - x \tag{21}$$

By using (21) and (20), the closed-loop plant can be described as follows

$$\begin{cases} \begin{bmatrix} \dot{x}_s \\ \dot{\bar{e}} \end{bmatrix} = \begin{bmatrix} A_s & M_s B\tilde{G}C \\ 0 & \bar{S}^{-1}(\bar{A} - (1+\alpha_0)\bar{L}_p\bar{C}) \end{bmatrix} \begin{bmatrix} x_s \\ \bar{e} \end{bmatrix} \\ + \begin{bmatrix} M_s & 0 \\ 0 & \bar{S}^{-1} \end{bmatrix} \begin{bmatrix} M_s & 0 \\ 0 & \bar{S}^{-1} \end{bmatrix} \\ + \begin{bmatrix} \phi(t,x,u) \\ \tilde{\phi} \end{bmatrix} + \begin{bmatrix} B_d \\ -\tilde{B}_d \end{bmatrix} d + \begin{bmatrix} 0 \\ -\tilde{W} \end{bmatrix} f^{(q)} \\ x_f = M_f[\phi(t,x,u) + B_d d + B\tilde{G}C\bar{e}] \end{cases} \tag{22}$$

From the well-known contraction mapping theory, the closed-loop system (22) is causal and there exists a unique solution for x_f in the static equation in terms of x_s, u, d and $\bar{e}$. To show the existence and uniqueness of x_s in the dynamic equation of (22) we only need to show $J(t,u,x_s,x_f)$ is Lipschitz with respect to x_s.

Consider

$$||J(t,u,x_{s1},x_{f1}) - J(t,u,x_{s2},x_{f2})|| \leq \tag{23}$$
$$\sqrt{2}||\phi(t,N_s x_{s1} + N_f x_{f1},u) - \phi(t,N_s x_{s2} + N_f x_{f2},u)||$$

and

$$||J(t,u,x_{s1},x_{f1}) - J(t,u,x_{s2},x_{f2})|| \leq \tag{24}$$
$$\sqrt{2}\frac{\theta\sqrt{1+\epsilon}}{\sqrt{1+\epsilon}-1}||N_s||x_{s1} - x_{s2}||$$

which implies $J(t,u,x_s,x_f)$ is Lipschitz with respect to x_s. Thus, the existence and uniqueness of x_s in the dynamic equation of (22) has been verified. As a result, the equivalent plant (9) is causal and solvable.

(ii) The proof of the asymptotic stability: Letting

$$V_c(x) = x'E'Px = x'P'Ex \tag{25}$$

and taking the derivative and using (9) and (11), one has

$$\dot{V}_c(x) \leq x'\Lambda x + 2x'P'B\bar{G}C\bar{e} + x'P'B_d d. \tag{26}$$

Let

$$V_h(x,\bar{e}) = V_c(x) + \epsilon_h V_0(\bar{e}) \tag{27}$$

with

$$\dot{V}_0(\bar{e}) \leq -\nu||\bar{e}||^2 \tag{28}$$

and

$$V_h(x,\bar{e}) \leq e^{-\beta_h t/\alpha_h} V_h(x(0),\bar{e}(0)) \tag{29}$$

Noticing that

$$V_h(x,\bar{e}) = \begin{bmatrix} x_s' & \bar{e}' \end{bmatrix} \begin{bmatrix} P_{11} & 0 \\ 0 & \epsilon_h\bar{P} \end{bmatrix} \begin{bmatrix} x_s \\ \bar{e} \end{bmatrix} \tag{30}$$

and choosing

$$\psi = \lambda_{min} \begin{bmatrix} P_{11} & 0 \\ 0 & \epsilon_h\bar{P} \end{bmatrix} \tag{31}$$

equations (29), (30) and (31) imply that

$$\left|\left| \begin{matrix} x_s \\ \bar{e} \end{matrix} \right|\right| \leq \sqrt{\frac{V_h(x(0),\bar{e}(0))}{\psi}} e^{-\beta_h t/2\alpha_h} \tag{32}$$

Hence $x_s \to 0$ and $\bar{e} \to 0$ as $t \to \infty$. According to the output equation of (20) or (22) and under zero disturbances, one has

$$||x_f|| \leq \frac{\sqrt{1+\epsilon}}{\sqrt{1+\epsilon}-1}(||\theta||||N_s||||x_s|| + ||B\bar{G}C||||\bar{e}||). \tag{33}$$

Since $x_s \to 0$ and $\bar{e} \to 0$ as $t \to \infty$, the equation (33) implies $x_f \to 0$ when $t \to \infty$. Therefore, the plant (20) or (22) is asymptotically stable, and equivalently the plant (9) is asymptotically stable.

(iii) The proof of the guaranteed performance index: Define

$$H = \dot{V}_h(x,\bar{e}) + y'y - \lambda^2 d'd \tag{34}$$

Using (9)and (26), one can derive that

$$H \leq x_d'\bar{\Omega}x_d + \epsilon||x||||\bar{e}|| + \epsilon_h\dot{V}_0(\bar{e}), \tag{35}$$

where $x_d = [x'd']'$, $\bar{\Omega} = \begin{bmatrix} \Omega & P'B_d \\ B_d' & -\lambda^2 I \end{bmatrix}$

$$\Omega = \Lambda + C'C \tag{36}$$

Λ and ϵ_0 are defined as before. Applying the Schur complement to (13), we have equivalently $\bar{\Omega} < 0$. We denote

$$\nu_d = \lambda_{min}(-\bar{\Omega}) \tag{37}$$

Substituting (28) and (37) into (35), one has

$$H \leq -\nu_d||x_d||^2 + \epsilon_0||x||||\bar{e}|| - \nu_0\epsilon_h||\bar{e}||^2 \tag{38}$$

and choosing $\epsilon_h > \epsilon_0^2/\nu_{dc}\nu_o$ with $\nu_{dc} = min(\nu_c,\nu_d)$, we have

$$H \leq -\frac{\nu_d}{2}||x_d||^2 - \frac{\nu_0\epsilon_h}{2}||\bar{e}||^2 \tag{39}$$

Under zero initial conditions and from (34) and (39), we have

$$\int_0^{Tf}(y'y - \lambda^2 d'd)\tau \leq \int_0^{Tf} H d\tau \leq 0 \tag{40}$$

which means that (10) holds. This completes the proof.

Remark 1 *It is noticed that (13) is nonlinear matrix inequality, we thus have a continuous interest to transform (13) into the LMI form.*

Theorem 2 *The closed-loop system (9) is solvable, causal and asymptotically stable, and* $||y||_{T_f} \leq \lambda||d||_{T_f}$ *if there exists an non singular* $Q \in \Re^{n\times n}$ *and a matrix* $Y \in \Re^{m\times n}$ *such that*

$$Q'E' = EQ \geq 0 \tag{41}$$

$$\begin{bmatrix} (AQ+BY)' + AQ + BY & Q' & Q'C' & B_d \\ Q & -I & 0 & 0 \\ CQ & 0 & -I & 0 \\ B_d' & 0 & 0 & \lambda^2 I \end{bmatrix} < 0 \tag{42}$$

Furthermore, if a feasible solution (Q,Y) exists in the above LMIs,the output feedback gain can be $GC = YQ^{-1}$.

Proof:

Pre-multipliying P'^{-1} and post-multiplying P^{-1} on the inequalities (12) and (13), and letting

$P^{-1} = Q$, $GCP^{-1} = GCQ = Y$, then using the Schur complement, the inequalities (41) and (42) can be obtained immediately. This completes the proof.

Clearly , the equation (41) is a LMI, but not a strictly LMI. Thus, we will make a further development to give modified conditions in strictly LMI forms convenience of calculation.

Lemma 3 *(Ibrir, 2004) For any given vectors α, β and a positive definite matrix P with compatible dimension, one has*

$$\alpha'\beta + \beta'\alpha \leq \alpha' P\alpha + 2\beta' P^{-1}\beta. \tag{43}$$

Lemma 4 *(Gao and Ding, 2007) All $Z \in R^{n\times}$ satisfying*

$$Z'E' = EZ \geq 0 \tag{44}$$

can be parameterized as

$$Z = WE' + E_q^{\dagger}Q \tag{45}$$

where $W \geq 0 \in \Re^{n\times n}$ $Q \in \Re^{(n-q)\times n}$ are parameter matrices; $E_q^{\top} \in \Re^{n\times(n-q)}$ is a matrix such that $EE_q^{\top} = 0$ and rank($E_q^{\top}$)=n-rank(E)=n-q. Furthermore, when Z is nonsingular, $W > 0$.

Theorem 5 *The closed-loop system (9) is solvable, causal and asymptotically stable, and $||y||_{T_f} \leq \lambda||d||_{T_f}$ if there exists an positive definite matrix $W \in \Re^{n\times n}$, and matrices $S \in \Re^{(n-q)\times n}$ $Y \in \Re^{m\times n}$ such that*

$$\begin{bmatrix} \Lambda_{a_{11}} & (\Lambda_{a_{12}})' & (\Lambda_{a_{13}})' & B_d \\ \Lambda_{a_{12}} & -I & 0 & 0 \\ \Lambda_{a_{13}} & 0 & -I & 0 \\ B_d' & 0 & 0 & -\lambda^2 I \end{bmatrix} < 0 \tag{46}$$

where $\Lambda_{a_{11}} = (AWE' + AE_q^{\top}S + BY)' + AWE' + AE_q^{\top}S + BY$, $\Lambda_{a_{12}} = WE' + E_q^{\top}S$, $\Lambda_{a_{13}} = CWE' + CE_q^{\top}S$, $E_q^{\top} \in \Re^{n\times n-q}$ is a matrix such that $EE_q^{\top} = 0$ and rank($E_q^{\top}$)=$n - rank(E) = n-q$. Furthermore, if a feasible solution (W, S, Y) exists in the LMI (46), the output feedback gain can be computed as $GC = Y(WE' + E_q^{\top}S)^{-1}$.

Proof:

Based in Theorem (2) and Lemma (4) the result holds immediately.

6 CONCLUDING REMARKS

For Lipschitz nonlinear descriptor systems with bounded input disturbances, by solving a Lyapunov equation, a robust state-space observer was proposed in (Gao and Ding, 2007). In this paper were presented the approach is developed for nonlinear Lipschitz descriptor systems, where the solvability, causality, asymptotic stability and performance are guaranteed. The main result provided condition for the design the output feedback controller, was presented using an LMI approach, where the theorem for existence the output feedback matrix was presented.

References

Alexandridis, A. T. and Paraskevopoulos, P. N. (1996). A new approach to eigenstruture assignment by output feedback, *IEEE Trans. Automatic. Control* **41**(1): 1046–1050.

Castelan, E. B., Hennet, J.-C. and Llanos Villarreal, E. R. (2003). Quadratic characterization and use of output stabilizable subspaces, *IEEE Trans. Automatic. Control* **48**(4): 654–600.

Chen, Y., Weng, Z. and Shi, S. (2003). Robust fault diagnosis for nonlinear difference-algebraic system, *International Journal of Control* **76**(1): 1560–1569.

Dai, L. (1989). *Singular Control System*, Springer-Verlag.

Fletcher, L. R. (1988). Eigenstructure assingment by output feedback in descriptor systems, *IEE Proceedings* **135**(4): 302–308.

Gao, Z. and Ding, S. X. (2007). Actuator fault robust estimation and fault-tolerant control for a class of nonlinear descriptor system, *Automatica* **43**(1): 912–920.

Gao, Z. and Ho, D. W. C. (2006). State /noise estimator for descriptor systems with application to sensor fault diagnosis, *IEEE Transactions on Signal Processing* **54**(1): 1316–1326.

Ibrir, S. (2004). Robust state estimation with q-integral observers, *Proceedings of the American Control conference*, Salvador/Brasil, pp. 3466–3471.

Vemuri, A. T., Polycarpou, M. M. and Circ, A. R. (2001). Fault diagnosis of differential-algebraic systems, *IEEE Transactions on Systems Man Cybernatics :Part A* **31**(1): 143–151.

Verghese, G. C., Lèvy, B. C. and Kailath, T. (1981). A general state space for singular systems, *IEEE Trans. Automatic. Control* **26**: 811–831.

CNMAC2012
XXXIV CONGRESSO NACIONAL DE
MATEMÁTICA APLICADA E COMPUTACIONAL
17 a 21 de setembro de 2012 – Águas de Lindóia/SP
ISSN 1984-8218

Algorithmic for stabilization by regional pole placement

E. R. L. Villareal, **J. D. Lima**, **W. M. Rodrigues**, **S. D. M. Borjas**
Universidade Federal Rural do Semi-Árido - UFERSA, 59607-360, Mossoró, RN
Universidade do Estado do Rio Grande do Norte - UERN, 59607-360, Mossoró, RN
E-mail: elmerllanos@ufersa.edu.br, joaodeus@uern.br, walter@ufersa.edu.br, santos.borjas@ufersa.edu.br.

Abstract: *It is being proposed in this paper a computational algorithm for acquiring the output feedback gain matrix in linear systems stabilization problems by regional pole placement in LMI regions. The output feedback controller is obtained through the solution of the coupled Sylvester equations. It is shown the existence of output feedback matrix providing conditions in which this problem has a solution using Kimura and condition $m + p > n$. An algorithm is proposed to provide a more suitable framework for numerical solutions. The convex programming techniques are applied to find the regional pole placement equations.*

Palavras-chave: *Stabilization; Output Feedback; Regional Pole Placement.*

1 Introduction

It is known that the static output feedback stabilization problem is a relevant and challenging problem, due to its simple implementation in contrast to more dynamic methods, and also because it is not easy to find a feedback matrix to make the closed-loop system asymptotically [4, 11]. The determination of procedures for obtaining the feedback matrix in output feedback control to asymptotically stabilize linear systems is actually an open problem. Many methods have been proposed in the literature based on Lyapunov and Ricatti linear matrix inequalities, or eigenstructure assignment [1, 4, 12]. Recently, there are sufficient conditions for the solution to these equations under a rank constraint [3, 4, 8].

The problem of static output feedback by regional pole placement in a linear time-invariant multivariable system, using output feedback, are considered in this paper. There are approaches and techniques to treat different versions of this problem [4, 11]. Many problems in systems' control theory are solved when it is calculated the solution of Sylvester equations.

Recently [4, 13] it was introduced the concept of (C, A, B)-invariant subspaces to relate the existence of a feedback gain matrix to the solution of two coupled Sylvester equations. However, this solution was mainly obtained under the Kimura condition [18]. Pathological cases where $m + p \leq n$, were only tackled by a trial and error procedure [5].

If the system is observable, controllable and under the Kimura condition, the coupled Sylvester equations are solved by assuming that the dimension of $\mathcal{V} = Im(V)$ is equal to the number of outputs p and the matrix $CV \in \mathbb{R}^{p\times p}$ is invertible. Then, the feedback matrix can be found as $G = W(CV)^{-1}$, where C, V, W are matrices. The technique are based on the subspace intersection condition, $\ker T \cap \ker C = \{0\}$ [5].

Considering the linear time-invariant system described by

$$\dot{x} = Ax + Bu \tag{1}$$
$$y = Cx \tag{2}$$

where $x \in \mathcal{X} \subset \mathbb{R}^n$, $u \in \mathcal{U} \subset \mathbb{R}^m$ and $y \in \mathcal{Y} \subset \mathbb{R}^p$. It is assumed that B is full column-rank, C is full row-rank and that (C, A, B) is stabilizable and detectable. Let $\mathcal{D}$ be a region in the open left half complex plane $\mathcal{D} \subseteq \mathcal{C}^-$, symmetric in relation to the real axis. The problem here is to find a static output feedback control law

$$u(t) = Gy(t),\ G \in \mathbb{R}^{m\times p} \tag{3}$$

ISSN 1984-8218

such that $\sigma(A+BGC) \in \mathcal{D}^-$, that is, the closed-loop system is asymptotically stable, where $\sigma(A+BGC) = \{\lambda_1, \lambda_2, \ldots, \lambda_n\}$ is the set of eigenvalues of $A+BGC$.

This paper is organized as it follows. In Section 2, basic concepts on geometric control are introduced. Section 3 presents the main contributions of the paper, the algorithm for obtaining the feedback gain matrix. In Section 4, the conclusions of the paper are presented.

2 Preliminaries

In this Section some concepts and definitions on geometric control theory are introduced [17].

Definição 1 *[13] A subspace $\mathcal{V} \subset \mathcal{X}$ of dimension v is* (C,A,B)-invariant*, if $\mathcal{V}$ is (A,B)-invariant and (C,A)-invariant.*

Definição 2 *[13] A subspace (A,B)-invariant $\mathcal{V}$ is a* (A,B)-inner stabilizable subspace*, if there exists K such that $(A+BK)|\mathcal{V}$ is asymptotically stable. A subspace (C,A)-invariant $\mathcal{V}$ is a* (C,A)-outer detectable subspace*, if there exists F such that $(A+FC)|\mathcal{X}/\mathcal{V}$ is asymptotically stable.*

Definição 3 *[13] A subspace $\mathcal{V}$ of dimension v is a* (C,A,B)-invariant output stabilizable subspace*, if $\mathcal{V}$ is (A,B)-inner stabilizable and (C,A)-outer detectable.*

The condition for the existence of $\mathcal{V} = Im(V)$ or (C,A,B)-invariant output stabilizable subspace is that the coupled Sylvester equations are verified with the additional condition of stability given by

$$\sigma(H_V) \in \mathcal{C}^- \text{ and } \sigma(H_T) \in \mathcal{C}^-. \tag{4}$$

The solutions to the problem of stabilization is associated with the existence of $\mathcal{V} = \ker T$, a (C,A,B)-invariant output stabilizable subspace, due to the possibility by solving the coupled Sylvester equations, rewritten by

$$AV + VH_V = -BW \text{ with } \sigma(H_V) \in C^- \tag{5}$$

$$TA + HT_T = -UC \text{ with } \sigma(H_T) \in C^- \tag{6}$$

$$TV = 0 \tag{7}$$

$$\ker CV \subseteq \ker W \text{ and } \ker B'T' \subseteq \ker U'. \tag{8}$$

The conditions (5)-(8) to describe geometrical properties required for solving the stabilization problem.

The convex programming techniques can be used to find feasible solutions [5]. The quadratic characterization (C,A,B)-invariant output stabilizable subspace is obtained to replace stabilizability conditions expressed in Sylvester equations (5), (7) and additional conditions $\sigma(H_V) \in \mathcal{C}^-$ and $\sigma(H_T) \in \mathcal{C}^-$. Thus, the two Lyapunov stability conditions [7] are obtained

$$\sigma(H_V) \in C^- \Leftrightarrow \exists\ \Pi = \Pi' > 0;\ \Pi H_V' + H_V \Pi = -Q_V, \forall Q_V = Q_V' > 0 \tag{9}$$

$$\sigma(H_T) \in C^- \Leftrightarrow \exists\ \Gamma = \Gamma' > 0;\ H_T'\Gamma + \Gamma H_T = -Q_T, \forall Q_T = Q_T' > 0. \tag{10}$$

3 Regional pole placement

A solution to the stabilization problem is to obtain an output feedback matrix based on the arbitrary pole placement. There are solutions to the stabilization problem considering the displacement of α using $A+\alpha I$ instead of A. In the stabilization process, the poles are allocated in a determined LMI region $\mathcal{D}$ [8]. In this paper, the stabilization technique formulated [2] is improved to treat the regional pole placement problem in the LMI region [8].

Let $\mathcal{D}$ be a region in the open left half complex plane $\mathcal{D} \subseteq \mathcal{C}^-$, symmetric in relation to the real axis. The stabilization problem to be studied is to find an output feedback matrix $u = Gy$ such that $\sigma(A+BGC) \in \mathcal{D}$, or equivalently, the closed loop system is $\mathcal{D}$-stable.

It is said that a pair (A,B) is *D-stabilizable* if $\text{rank}\left[\ \lambda I - A\ B\ \right] = n$, for all $\lambda \notin D$, and (C,A) is *D-detectable*, if $\text{rank}\begin{bmatrix} \lambda I - A \\ C \end{bmatrix} = n$, for all $\lambda \notin D$.

ISSN 1984-8218

3.1 Basic Concepts of LMI regions

The LMI regions describe a convex regions in the complex plane which each point is symmetric in relation to the real axis.

Definição 4 *A subset $\mathcal{D} = \{\lambda \in \mathcal{C}^- : f_{\mathcal{D}}(\lambda) < 0\}$ complex plane is called a* linear matrix inequalities *(*LMI*) region if there is a symmetric matrix $\Delta = (\delta)_{kl} \in \Re^{n\times n}$ and $\Theta = (\theta)_{kl} \in \Re^{n\times n}$ such that $f_{\mathcal{D}}(\lambda) = \Delta + \lambda\Theta + \bar{\lambda}\Theta'$ with $\lambda, \bar{\lambda} \in \mathcal{C}^-$, where $\mathcal{C}^-$ denotes the complex half-plane, and $(\delta)_{kl}$, $(\theta)_{kl}$ represent the elements of the matrices Δ and Θ, for all $1 \leq k, l \leq n$.*

The characteristic function $f_{\mathcal{D}}(\lambda)$ takes values in the space of Hermitian matrices of dimensions $n \times n$. The LMI region can be defined from $f_{\mathcal{D}}(\lambda)$ to describe the properties of the eigenvalues of a real matrix in $\mathcal{D}$ [8]. Considering the linear system represented by

$$\dot{z}(t) = Hz(t), \quad \text{with} \quad H \in \Re^{n\times n} \tag{11}$$

The system (11) is $\mathcal{D}$-stable, where $\mathcal{D}$ is a LMI region if and only if there are matrices Δ and $\Theta \in \Re^{n\times n}$ satisfying the condition

$$f_{\mathcal{D}}(\Theta) = \Delta + \Theta\otimes H + \Theta'\otimes H', \tag{12}$$

where $\otimes$ represents the Kronecker product [11]. Note that the equation (12) can be rewritten as

$$f_{\mathcal{D}}(\theta) = (\delta)_{kl} + (\theta)_{kl}H + (\theta)'_{lk}H', \quad \forall\ 1 \leq k, l \leq n. \tag{13}$$

For two LMI regions $\mathcal{D}_1$ and $\mathcal{D}_2$ whose characteristics' functions are associated $f_{\mathcal{D}_1}$ and $f_{\mathcal{D}_2}$, respectively, the intersection $\mathcal{D} = \mathcal{D}_1 \cap \mathcal{D}_2$ is a LMI region with characteristic function $f_{\mathcal{D}_1\cap\mathcal{D}_2} = \text{diag}(f_{\mathcal{D}_1}, f_{\mathcal{D}_2})$.

3.2 $\mathcal{D}$-Stabilization by output feedback

The existence of an output feedback matrix that stabilizes the closed loop system can be associated with the solution of coupled Sylvester equations (5)-(7). By one existence theorem [5], these equations can be interpreted in terms of geometric properties of the subspace $\mathcal{V} = \ker T$. Once found the output feedback matrix which stabilizes the system, the spectrum of the closed loop is given by

$$\sigma(A + BGC) = \sigma(H_V)\ \dot{\cup}\ \sigma(H_T). \tag{14}$$

It is considered that the regional pole placement is defined from LMI regions associated to the matrices H_V and H_T. If $\sigma(H_V) \in \mathcal{D}_V$ and $\sigma(H_T) \in \mathcal{D}_T$ then $\mathcal{D} = \mathcal{D}_V \cup \mathcal{D}_T$. Assuming that $H_V \in \Re^{p\times p}$ and $H_T \in \Re^{n-p\times n-p}$, conditions of $\mathcal{D}$-stabilizability in LMI regions are equivalently replaced by the following two conditions

$$\sigma(H_V) \in \mathcal{D}_V \Leftrightarrow \exists\ \Pi = \Pi' > 0; \triangle_V \otimes \Pi + \Theta'_V \otimes \Pi H'_V + \Theta_V \otimes H_V\Pi = -Q_V < 0, \text{ and } \Pi \in \mathbb{R}^{p\times p} \tag{15}$$

$$\sigma(H_T) \in \mathcal{D}_T \Leftrightarrow \exists\ \Gamma = \Gamma' > 0; \triangle_T \otimes \Gamma + \Theta'_T \otimes H'_T\Gamma + \Theta_T \otimes \Gamma H_T = -Q_T < 0,\ \Gamma \in \mathbb{R}^{n-p\times n-p}. \tag{16}$$

The following result can be obtained considering the coupled Sylvester equations under the regional pole placement restricted to the spectrum of matrices H_V and H_T respectively. For algorithmic purposes, it is considered that $v = p$.

Teorema 1 *There is a static output feedback matrix $G \in \Re^{m\times p}$ with $\sigma(A+BGC) = \{\lambda_1, \lambda_2, \ldots, \lambda_n\} \in \mathcal{D}, \mathcal{D} = \mathcal{D}_V \cup \mathcal{D}_T$, where $\{\lambda_1, \cdots, \lambda_{n-p}\} \in \mathcal{D}_T$ and $\{\lambda_{n-p+1}, \cdots, \lambda_n\} \in \mathcal{D}_V$ if and only if there are matrices $P = P' \geq 0$, $P \in \Re^{n\times n}$, $Y \in \Re^{m\times n}$, $S = S' \geq 0$, $S \in \Re^{n\times n}$, $Z \in \Re^{n\times p}$, $V \in \Re^{n\times p}$ and $T \in \Re^{n-p\times n}$ with $TV = 0$, such that the following conditions are verified.*

$$\triangle_V \otimes P + \Theta_V \otimes (AP + BY) + \Theta'_V \otimes (PA' + Y'B') = -(V \otimes I_P)\, Q_{V_1}\, (V \otimes I_P)',\ Q_{V_1} > 0 \tag{17}$$

$$V'PV = \overline{P} > 0, TPT' = 0 \tag{18}$$

$$Y = W_\Pi V', \text{ for some } W_\Pi \in \mathbb{R}^{m\times p} \tag{19}$$

$$\triangle_T \otimes S + \Theta_T \otimes (SA + ZC) + \Theta'_T \otimes (A'S + C'Z') = -(T' \otimes I_{n-p})\, Q_{T_1}\, (I_{n-p} \otimes T),\ Q_{T_1} > 0 \tag{20}$$

$$TST' = \overline{S} > 0;\ V'SV = 0 \tag{21}$$

$$Z = T'U_\Gamma,\ \text{for some } U_\Gamma \in \mathbb{R}^{n-p\times n} \tag{22}$$

$$\ker CP \subseteq \ker Y \text{ and } \ker B'S \subseteq \ker Z'. \tag{23}$$

ISSN 1984-8218

Proof: By quadratic condition (15) and Kronecker product, the equality (15) can be replaced by

$$(\delta_V)_{kl}\, V\Pi V' + (\theta_V)_{lk}\, V\Pi H_V' V' + (\theta_V)_{kl}\, V H_V \Pi V' = -V\,(Q_V)_{kl}\, V', \tag{24}$$

for all $1 \leq k, l \leq n$, where $(Q_V)_{kl} = (Q_V)_{kl}' \in \Re^{p\times p}$. From (5) is obtained $AV + BW = VH_V$. Replacing this in (24) gave us

$$(\delta_V)_{kl}\,(V\Pi V') + (\theta_V)_{lk}\,(V\Pi V'A' + V\Pi W'V') + (\theta_V)_{kl}\,(AV\Pi V' + BW\Pi V') = -V\,(Q_V)_{kl}\,V'. \tag{25}$$

It is placing P by $P' = V\Pi V'$, Y by $W\Pi V'$ and considering that the $\operatorname{rank} V = p$, $\Pi > 0$, results in $V'V\Pi V'V > 0$ and $T'V\Pi V'T = 0$. Then, (25) results in conditions (17)-(19). Using similar arguments, the conditions (20) and (22) are showed. Furthemore, for all $1 \leq k, l \leq n$ with $(Q_T)_{kl} = (Q_T)_{kl}' \in \Re^{n-p\times n-p}$, we have

$$(\delta_T)_{kl}(T'\Gamma T) + (\theta_T)_{lk}(T'H_T'\Gamma T) + (\theta_T)_{kl}(T'\Gamma H_T T) = -T'(Q_T)_{kl}T, \tag{26}$$

By replacing of (20) and (22) in (26), the matrices $S = T'\Gamma T$ and $Z = T'\Gamma U$ are obtained. Moreover, $\operatorname{rank} T = q - p$, $\Gamma > 0$, $TT'\Gamma TT' > 0$ and $V'T'\Gamma TV = 0$. So the conditions in (16) follows the conditions $\ker CV \subseteq \ker W$ and $\ker B'T' \subseteq \ker U'$ respectively, taking into account the previous definitions P, Y, S and Z.

Reciprocally, it is considered that the equalities (17)-(23) are verified. By definition, V and T, are matrices with full column and full row respectively. Thus, from (18) and (21) are obtained

$$V'PV = \bar{P} = \bar{P}' > 0 \Rightarrow P = V(V'V)^{-1}\bar{P}(V'V)^{-1}V' \tag{27}$$

$$TST' = \bar{S} = \bar{S}' > 0 \Rightarrow S = T'(TT')^{-1}\bar{S}(TT')^{-1}T. \tag{28}$$

By conditions (17)-(18), it follows that $\mathcal{V} = \ker T$ is a (A, B)-invariant subspace and the spectrum of $(A, B)|\mathcal{V}$ is in $\mathcal{D}_V$. However, the conditions (27) and (28) result in

$$P = \begin{bmatrix} V & T' \end{bmatrix} \begin{bmatrix} \Pi & 0 \\ 0 & 0 \end{bmatrix} \begin{bmatrix} V' \\ T \end{bmatrix} \geq 0 \tag{29}$$

for $\Pi = \Pi' = (V'V)^{-1}\bar{P}(V'V)^{-1} > 0, \Pi \in \Re^{p\times p}$. From (23), it is stated that there is a matrix G such that $GCP = Y$. Thus, the replacing (8) in (17) result in

$$(\delta_V)_{kl}P + (\theta_V)_{lk}P(A + BGC)' + (\theta_V)_{kl}(A + BGC)P = -V(Q_V)_{kl}V', \tag{30}$$

for all $1 \leq k, l \leq n$. Now, taking into account (29), the similarity equation $(A+BGC)\begin{bmatrix} V & T' \end{bmatrix} = \begin{bmatrix} V & T' \end{bmatrix}\begin{bmatrix} \bar{A}_{11} & \bar{A}_{12} \\ \bar{A}_{21} & \bar{A}_{22} \end{bmatrix}$ and is indeed that $\begin{bmatrix} V & T' \end{bmatrix}\begin{bmatrix} (Q_V)_{kl} & 0 \\ 0 & 0 \end{bmatrix}\begin{bmatrix} V' \\ T \end{bmatrix} \leq 0$. Thus, from these two conditions, (29) and (30), it is obtained that

$$-\begin{bmatrix} V & T' \end{bmatrix}\begin{bmatrix} (Q_V)_{kl} & 0 \\ 0 & 0 \end{bmatrix}\begin{bmatrix} V' \\ T \end{bmatrix} = (\delta_V)_{kl}\begin{bmatrix} V & T' \end{bmatrix}\begin{bmatrix} \Pi & 0 \\ 0 & 0 \end{bmatrix}\begin{bmatrix} V' \\ T \end{bmatrix} +$$

$$(\theta_V)_{lk}\begin{bmatrix} V & T' \end{bmatrix}\begin{bmatrix} \Pi\overline{A}_{11}' & \Pi\overline{A}_{21}' \\ 0 & 0 \end{bmatrix}\begin{bmatrix} V' \\ T \end{bmatrix} + (\theta_V)_{lk}\begin{bmatrix} V & T' \end{bmatrix}\begin{bmatrix} \overline{A}_{11}\Pi & 0 \\ \overline{A}_{21}\Pi & 0 \end{bmatrix}\begin{bmatrix} V' \\ T \end{bmatrix}$$

$$= \begin{bmatrix} V & T' \end{bmatrix}\begin{bmatrix} (\delta_V)_{kl}\,\Pi + (\theta_V)_{lk}\,\Pi\overline{A}_{11}' + (\theta_V)_{kl}\,\overline{A}_{11}\Pi & (\theta_V)_{lk}\,\Pi\overline{A}_{21}' \\ (\theta_V)_{kl}\,\overline{A}_{21}\Pi & 0 \end{bmatrix}\begin{bmatrix} V' \\ T \end{bmatrix}.$$

Considering that $\Pi > 0$ and that $(\theta_V)_{kl} \neq 0$, follow from equalities above that: a)$\mathcal{V} = \ker T$ is a $(A + BGC)$-invariant subspace, since $(\theta_V)_{kl}\bar{A}_{21}\Pi = 0$ if and only if $\bar{A}_{21} = 0$ and; b) $\mathcal{V} = \ker T$ is $\mathcal{D}$-stabilizable, since $(\delta_V)_{kl}\Pi + (\theta_V)_{lk}\Pi\bar{A}_{11}' + (\theta_V)_{kl}\bar{A}_{11}\Pi < 0$, $\forall\ 1 \leq k, l \leq n$ implies $\mathcal{D}$-stability from $(A + BGC)|\mathcal{V}$. ■

If P, S, V and T have been found, then Theorem 1 is verified with G feedback output matrix corresponding. The coupling condition between the equalities (17)-(22) can be described by $SP = 0$.

ISSN 1984-8218

The Theorem 1, application of a circular region of the unit radius denoted by $\mathcal{C}^s = \{\lambda \in \mathcal{C}; |\lambda| < 1\}$, corresponds to the stability in the case of discrete-time systems [6]. There is an output feedback matrix $G \in \mathbb{R}^{m\times p}$ such that $\sigma(A+BGC) \in \mathcal{C}^s$ if and only if there are matrices ($P = P' \geq 0$, $P \in \mathbb{R}^{n\times n}$, $Y \in \mathbb{R}^{m\times n}$, $S = S' \geq 0$, $S \in \mathbb{R}^{n\times n}$ and $Z \in \Re^{n\times p}$) such that the following conditions are verified for any pair of matrices $V \in \Re^{n\times p}$ and $T \in \mathbb{R}^{n-p\times n}$ with $TV = 0$.

$$\begin{bmatrix} -P & PA'+Y'B' \\ AP+BY & -P \end{bmatrix} = \begin{bmatrix} V & 0 \\ 0 & V \end{bmatrix} Q_V \begin{bmatrix} V' & 0 \\ 0 & V' \end{bmatrix} \tag{31}$$

$$V'PV = \overline{P} > 0,\ TPT' = 0 \tag{32}$$

$$Y = W_\Pi V' \text{ for } W_\Pi \in \mathbb{R}^{m\times p}, \forall\, Q_T = Q_T' > 0,\ Q_T \in \mathbb{R}^{2n\times 2n} \tag{33}$$

$$\begin{bmatrix} -S & SA+ZC \\ A'S+C'Z' & -S \end{bmatrix} = \begin{bmatrix} T' & 0 \\ 0 & T' \end{bmatrix} Q_T \begin{bmatrix} T & 0 \\ 0 & T \end{bmatrix} \tag{34}$$

$$TST' = \overline{S} > 0,\ V'SV = 0 \tag{35}$$

$$Z = T'U_\Gamma \text{ for some } U_\Gamma \in \mathbb{R}^{m\times p} \tag{36}$$

$$\ker CP \subseteq \ker Y \text{ and } \ker B'S \subseteq \ker Z'. \tag{37}$$

4 Algorithm for Output Feedback Stabilization

The following basic procedure is proposed to compute a $\mathcal{D}$-stabilizing static output feedback matrix in the closed loop system when the condition $m+p > n$ is verified.

Algorihm 1 (Primal Algorithm) The output feedback stabilization is obtained through the following steps:

Step 1 Decomposition of matrix C:
1.1 For $C_1 \in \mathbb{R}^{p\times p}$ and $\operatorname{rank} C_1 = p$ find the matrix $\begin{bmatrix} M_1 & M_2 \end{bmatrix}$ satisfying the conditions

$$C \begin{bmatrix} M_1 & M_2 \end{bmatrix} = \begin{bmatrix} C_1 & C_2 \end{bmatrix}, \quad \begin{bmatrix} A_{21} \\ A_{22} \end{bmatrix} = \begin{bmatrix} \overline{M}_1' \\ \overline{M}_2' \end{bmatrix} \text{ and } \begin{bmatrix} M_1 & M_2 \end{bmatrix} \begin{bmatrix} \overline{M}_1' \\ \overline{M}_2' \end{bmatrix} = I_n;$$

1.2 Find S_{21} and $S_{22} = S_{22}' > 0$ in the follows LMI $\Delta_T \otimes (S_{22}) + \Theta_T \otimes (S_{22}A_{22} + S_{21}A_{12}) + \Theta_T' \otimes (A_{22}'S_{22} + A_{21}'S_{21}') < 0$.

Step 2 To determinate the matrix P and Y:
2.1 Find V as an orthogonal basis of $\ker T$, $TV = 0$, $V'V = I_p$;

2.2 Using (18) and (19) to find P and Y through the equation

$$\Delta_V \otimes P + \Theta_V \otimes (AP+BY) + \Theta_V' \otimes (PA'+Y'B') = -(V \otimes I_p) Q_{V1} (V \otimes I_p)' \leq 0.$$

Step 3 The $\mathcal{D}$-stabilizing output feedback matrix in the closed loop system is verified in $GCP = Y \Leftrightarrow GCV\bar{P} = W_\Pi$, $V'V = I_p$.

In the Step 1.2, a pair of matrices $A_{22} \in \mathbb{R}^{(n-p)\times(n-p)}$, $A_{12} \in \mathbb{R}^{p\times n-p}$ are calculated from the decomposition in Step 1.1. It is assumed that the open-loop system is $\mathcal{D}$-stabilizable. Then the pair (A_{12}, A_{22}) is $\mathcal{D}$-detectable. Therefore there are (S_{22}, S_{21}), solutions for Step 1.2., such that $\sigma(A_{22} + (S_{22})^{-1}S_{21}A_{12}) = \sigma(H_T) \in \mathcal{D}_T$. Note also that the equation in Step 1.2. is a LMI in variables S_{21} and S_{22}. Then, convex programming techniques can be used to find feasible solutions [3]. As a test of the feasibility Step 2, you should verify if the system (A, B, T) has no invariant zeros which belong to $\mathcal{D}_V$. Then go to the next step. The conditions are usually solved in the sense that the matrix system $P_\lambda = \begin{bmatrix} A-\lambda I_n & B \\ T & 0 \end{bmatrix}$ of dimension $(n+m)\times(2n-p)$ must have full row rank, for all λ. Thus, the Step 2 is only made feasible with stable solutions.

ISSN 1984-8218

For instance, consider the system (A, B, C) with data in [10]

$$A = \begin{bmatrix} 0 & 1 & 0 & 0 \\ 1 & 1 & 0 & 0 \\ -1 & 0 & 0 & 0 \\ 0 & 0 & 0 & 0 \end{bmatrix}, \quad B = \begin{bmatrix} 0 & 0 \\ 1 & 0 \\ 0 & 0 \\ 0 & 1 \end{bmatrix}, \quad C = \begin{bmatrix} 1 & 0 & 0 & 1 \\ 0 & 0 & 1 & 0 \\ 0 & 0 & 0 & 1 \end{bmatrix}.$$

The system (C, A, B) corresponding is controllable and observable, and $m + p = 5 > n$. The open-loop poles are $0.0, 0.0, 1.618, -0.6180$.

From Primal Algorithm, the LMI region $\mathcal{D}_T$ is a vertical band defined by $\mathcal{D}_T = \{\, x + jy \in \mathcal{C} \;;\; -5 < x < -1 \,\}$. The LMI region $\mathcal{D}_V$ is defined from the intersection of sectors and a conical disk defined by: $\{\, x + jy \in \mathcal{C} \;;\; x < -5,\, |x + jy| < 10 \text{ and } \tan 45x < |y| \}$. Thus, convex programming techniques are applied to find feasible solutions for the equations of regional pole placement without additional requirements. The matrix

$$\begin{bmatrix} M_1 & M_2 \end{bmatrix} = \begin{bmatrix} -0.7071 & 0.0000 & 0.7071 & 0.0000 \\ 0.0000 & 0.0000 & 0.0000 & 1.0000 \\ 0.0000 & -1.0000 & 0.0000 & 0.0000 \\ -0.7071 & 0.0000 & -0.7071 & 0.0000 \end{bmatrix}.$$

Found in step 1.1 result in $A_{12} = [-0.7071, 0.0000, 0.7071]'$ and $A_{22} = [1.0]$. A solution for Step 1.2 is given by $S_{22} = 333.3318$, and $S_{21} = [0.0000\ 0.0000\ -2080.8778]$, which results in Step 1.3 are $T = [-1471.4028\ 333.3318\ 0.0000\ 1471.4028]$. This solution has no zeros invariant and imply, in Step 2.1

$$V = \begin{bmatrix} 0.6982 & 0.0000 & 0.1582 \\ -0.0650 & 0.0000 & 0.9853 \\ 0.0000 & 1.0000 & 0.0000 \\ 0.7129 & 0.0000 & -0.0650 \end{bmatrix}.$$

A solution for Step 2.2 is then found

$$Y = \begin{bmatrix} 10887.2550 & 150744.2000 & 304.1292 & 45036.8680 \\ -4945.7042 & 52669.6190 & -336.9173 & -16877.4870 \end{bmatrix}$$

$$W_{\Pi} = \begin{bmatrix} 49513.0880 & 304.1292 & -149730.1600 \\ -18910.8790 & -336.9173 & 52208.9740 \end{bmatrix}$$

$$P = \begin{bmatrix} 585.8797 & -3033.8726 & 88.1286 & 1273.1736 \\ -3033.8726 & 23055.7690 & -320.7086 & -8256.9297 \\ 88.1286 & -320.7086 & 16.9370 & 160.7819 \\ 1273.1736 & -8256.9297 & 160.7819 & 3143.6997 \end{bmatrix}.$$

The output feedback matrix corresponding that stabilizes the closed loop system is $G = \begin{bmatrix} -218.6662 & 348.0591 & 303.7491 \\ 52.7244 & -78.8494 & -75.4133 \end{bmatrix}$, resulting $\sigma(A + BGC) = \{-3.4142, -5.7409, -6.2669 \pm 4.6210j\} \subset \mathcal{D}_V$. Where the eigenvalue $-3.4142 \subset \mathcal{D}_T$ corresponds to step 1.

5 Conclusion

We have proposed a computational algorithm for obtaining the output feedback gain matrix in linear systems stabilization problems by regional pole placement (LMI) regions. The design of output feedback controller is obtained through the solution of the coupled Sylvester equation. The proposed theorem for the existence output feedback matrix providing necessary and sufficient conditions in which this problem has a solution using Kimura condition of $m + p > n$. The computational algorithm is presented, a modification is proposed to provide a more suitable framework to numerical solution. The convex programming techniques were applied to find the regional pole placement equations without additional requirements.

ISSN 1984-8218

References

[1] N.J. Higham, "Handbook of Writing for the Mathematical Sciences", SIAM, Philadelphia, 1993.

[2] A.T. Alexandridis and P.N. Paraskevopoulos, A new approach to eigenstruture assignment by output feedback, *IEEE Trans. Automatic. Control*, 41 (1996) 1046-1050.

[3] S.P. Boyd, L.E. Ghaoui, E. Feron and V. Balakrishhnan "Linear Matrix Inequalities in System and Control Theory," SIAM, Philadelphia, 2005.

[4] E.B. Castelan and V.G. Silva, On the solution of a Sylvester equation appering in descriptor systems control theory, *Systems e Control Letters*, 54 (2005) 109-117.

[5] E.B. Castelan, J.C. Hennet and E.R.L. Villarreal Quadratic characterization and use of output stabilizable subspaces, *IEEE Trans. Automatic Control*, 48 (2003) 654-660.

[6] E.B. Castelan, J.C. Hennet E.R.L. Villarreal Output feeedback design by coupled Lyapunov-Like equations, *15 th IFAC World Congress on Automatic Control*, Spain, (2002) 1-6.

[7] C.T. Chen, "Linear System Theory and Design" Holt, Rinehart and Winston, 1996.

[8] M. Chilali, P. Gahinet, H_∞ Design with pole placement constraints: an LMI approach, *IEEE Trans. Automatic. Control*, 41 (1996) 358-367.

[9] M. Darouach, Solution to Sylvester equation associated to linear descriptor systems, *Systems and Control Letters*, 55 (2006) 835-838.

[10] L.R. Fletcher, J. Kautsky, G.K.G. Kolka and N.K. Nichols, Eigenstructure assingment by output feedback in descriptor systems, *IEEE Trans. Automatic. Control*, 42 (1985) 1457-1468.

[11] R.A. Horn and C.R. Jhonsons, "Topics in Matrix Analysis", Cambridge University Press, 1991.

[12] V.L. Syrmos, C.T. Abdallah, P. Dorato and K. Grigoriadis, A Survey of static output feedback, em "Automatica", pp 125–137, 1997.

[13] V.L. Syrmos and F.L. Lewis, Bilinear formulation for the output feedback problem in linear system *IEEE Trans. Automatic Control*, 39 (1994) 410-414.

[14] V.L. Syrmos and F.L. Lewis, Output feedback eigenstructure assignment using two Sylvester equations, *IEEE Trans. Automatic Control*, 38 (1993) 495-499.

[15] E.R.L. Villarreal, J.A.R. Vargas and E.M. Hemerly, Static ouput feedback stabilization using invariant subspaces and Sylvester equations, *TEMA - Tend. Mat. Apl. Comput.*, 10 (2009) 99-110.

[16] L. Zhoua and G. Lub, Detection and stabilization for discrete-time descriptor systems via a limited capacity, *Automatica*, 45 (2009) 2272-2277.

[17] W. M. Wonahm, "Linear Multivariable Control, a Geometric Approach", Springer Verlag, 1979.

[18] H. Kimura, Pole assignment by gain output feedback, *Automatic Contol IEEE Transactions*, 20 (1975) 509-516.

Equação Diferencial, Lógica Fuzzy em Estruturas Inteligentes

Nataniel Wontoon Barbosa Lima, **Reginaldo Dantas da Silva**,
Bacharelado em Ciência e Tecnologia, DCEN, UFERSA,
59625-900, Mossoró, RN
E-mail: nwontoon@gmail.com, reginaldodantasfla@hotmail.com

Elmer Rolando Llanos Villarreal , **Walter Martins Rodrigues**
DCEN, UFERSA
59625-900, Mossoró, RN
E-mail: elmerllanos@ufersa.edu.br, walterm@ufersa.edu.br

Reuber Regis de Melo
Mestrado em Sistemas de Comunicação e Automação, UFERSA
59625-900, Mossoró, RN
E-mail: reuberegis@gmail.com

Palavras-chave: *Equação diferencial, Lógica fuzzy, Materiais piezoelétricos*

Resumo: *Neste trabalho são apresentados estudos relacionados com controle ativo de vibração de estruturas inteligentes piezoelétricas que mostram que esses materiais geralmente apresentam características ou comportamentos não lineares. Isso torna a utilização de métodos convencionais, na resolução problemas que envolvam essas estruturas, desvantajosa, até por causa da pouca precisão dos resultados. Em virtude desse fato o presente artigo objetiva mostrar a aplicação da lógica fuzzy em controladores, um processo que aumenta a eficiência e reduz a complexidade de cálculos. Nele são abordados os métodos de Mamdani e o de Takagi-Sugeno-Kang e retratadas algumas de suas vantagens e desvantagens. As regras difusa foram estabelecidas com base na análise dos movimentos de viga em balanço. Como dados de entrada do controlador de lógica fuzzy (FLC) são utilizados a velocidade e o deslocamento da viga e como saída a força de controle, cuja finalidade é equilibrar a mesma atuando em direção oposta ao seu deslocamento.*

1 Introdução

Presenciamos um mundo que tem como uma das principais metas descobertas que possibilitem inovações. Nesse contexto de descobertas uma das técnicas que tem ganhado destaque dentro de indústrias como a aeronáutica e a civil é a utilização de estruturas inteligentes que são sistemas de controle estrutural nos quais são interligados sensores, leis de controle, eletrônica associada, atuadores, processamento de sinais etc. Em outras palavras, são estruturas capazes de reagir e se modificar mediante certas ações do ambiente. Um exemplo de aplicação dessas estruturas é o uso de tais materiais em compósitos inteligentes que são microfibras interligadas formando uma teia piezoelétrica [4,5]. Essa vantagem aliada aos materiais piezoelétricos que são dotados de características como baixo peso, grande força de atuação, resposta a estímulos do meio externo em curto prazo de tempo, capacidade de conversão direta de energia elétrica em mecânica, tem chamado a atenção de grandes centros de pesquisas como a NASA Langley e vários setores da indústria. Dentre os métodos não convencionais podemos citar a lógica difusa e as redes neurais [1,2,3]. O controle por realimentação com ganho constante proporcional é um exemplo de uma técnica clássica no controle de vibrações em estruturas com piezoelétricos [2,3]. Como vários problemas atuais envolvem sistemas complexos métodos não convencionais são mais estudados. Dois modelos que utilizam a lógica difusa para o controle das estruturas são o modelo de Mamdani e o de Takagi-Sugeno-Kang. Este primeiro é considerado um modelo difuso linguístico o que faz dele o método mais intuitivo, visto que é mais parecido com nossos hábitos de manipular informações. O segundo se baseia em um conjunto de regras e apresenta como saída ou resultado um número real exato - por isso não é tão intuitivo - o que aumenta a sua eficiência de processamento, visto que as contas envolvidas no processo computacional se tornam mais simples, e isso o torna mais preciso [3,6].

2 Modelagem Matemática

A lógica fuzzy do controlador (PLC) foi desenvolvida com base em projetos que utilizam o deslocamento e a velocidade do balanço de vigas como entradas, e a força de controle sobre as vigas de balanço como a saída. Este novo método melhora a eficiência e reduz a complexidade dos cálculos. Os resultados das simulações com o Matlab ilustram que o método proposto tem um melhor controle e desempenho do que os métodos convencionais. Agora para entendermos o modelo devemos considerar como viga ou placa as estruturas ligadas a sensores e atuadores piezoelétricos de forma retangular. Os sensores e atuadores são simetricamente colocados em ambos os lados da mesma posição da estrutura, conforme mostra a Figura 1.

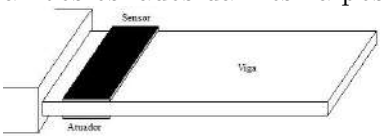

Figura 1: Posição dos sensores e atuadores na viga.

Na verdade, os sensores são utilizados para estimar o estado do parâmetro. Para uma estrutura ligeiramente amortecida, o princípio utilizado pode ser simplificado para dissociar os problemas de colocação de atuadores/sensores e controle de entrada. Ele pode ser escrito como:

$$Max(Det(F)) \tag{1}$$

Seja $\beta \in B_m$, $B_m = \beta \sum_{k=1}^{M} \beta_k = m$ onde β é a localização da matriz seleção e B_m é o conjunto de localizações possíveis. A função (1) pode também ser escrita na forma:

$$S(m) = max_\beta \sum_{k=1}^{N} log(\sum_{1}^{M} \beta_k \frac{(\lambda' \phi_i)^2}{{\phi_k}^2}) \tag{2}$$

onde N e M são o número de modelos e as possíveis localizações dos sensores, m é o número de sensores, β_k é composto por 0 e 1 - se $\beta_k = 1$, este denota que há um sensor na localização, em contraste, se $\beta_k = 0$, este indica que no local não tem nenhum sensor -, λ_k é um vetor coeficiente relacionado com kht localização no sensor, ϕ_i é um modo ith normalizado em forma de vetor, ϕ_k é a covariância de ruído do sinal do sensor e pode ser definido como 1 . O sentido físico de (2) pode ser considerado para encontrar a localização de cargas máximas. Portanto, $(\lambda_k)' \phi_i$ é equivalente às cargas de saída dos sensores. Se supusermos que a área do sensor é suficientemente pequena em comparação com a viga (placa), a carga do sensor pode ser escrito como:

$$q = DA = A(D_x + D_y) \tag{3}$$

$$D_x = d_{31} E_{pe} \epsilon_x = d_{31} E_{pe} \frac{\partial^2 w}{\partial x^2} \frac{t_p}{2} \tag{4}$$

$$D_y = d_{31} E_{pe} \epsilon_y = d_{31} E_{pe} \frac{\partial^2 w}{\partial y^2} \frac{t_p}{2} \tag{5}$$

onde D_x é o deslocamento elétrico gerado pelo X que é o eixo de tensão, D_y é o deslocamento elétrico gerado por um esforço no eixo Y e A é a área do sensor. Para a estrutura da viga, o deslocamento elétrico é gerado por uma tensão unidirecional. d_{31} é a tensão piezoelétrica constante. E_p e t_p são o módulo de Young e as espessuras do trecho piezoeléctrico. w é a deflexão da estrutura.

Baseado na equação diferencial de segunda ordem do esquema trabalhado, $\frac{\partial^2 w}{\partial x^2}|_K$ e $\frac{\partial^2 w}{\partial y^2}|_K$ podem ser expressas como

$$\frac{\partial^2 w}{\partial x^2}|_K \approx \partial_x^2 w = \frac{w(i) + w(j) - 2w(k)}{(dx)^2} \tag{6}$$

$$\frac{\partial^2 w}{\partial y^2}|_K \approx \partial_y^2 w = \frac{w(m) + w(n) - 2w(k)}{(dy)^2} \tag{7}$$

Substituindo (4), (5), (6) e (7) em (3) obtemos

$$q = d_{31} E_{pe} A \lambda_y \tag{8}$$

onde

$$\lambda_k = \frac{t_p}{2}\left(\frac{w(i) + w(j) - 2w(j)}{(dx)^2} + \frac{w(m) + w(n) - 2w(j)}{(dy)^2}\right)$$

A deflexão da estrutura w pode ser expressa em função de ϕ_i

$$w = \sum_{i=1}^{N} \mu_i \phi_i \tag{9}$$

na qual μ_i é uma forma ith de coordenada generalizada, substituindo (9) em (8) chegaremos a $\sum_{i=1}^{N} (\gamma_k)' \phi_i = q$, $(\gamma_k)'$ pode ser escrito como

$$(\gamma_k)' = \frac{1}{2} \mu_i A d_{31} E_{pe} \lambda_k^i \tag{10}$$

onde

$$\lambda_k^i = \phi_i \frac{t_p}{2}\left(\frac{1}{(dx)^2}[0...1_i - 2_k 1_j ...0] + \frac{1}{(dy)^2}[0...1_m - 2_k 1_n ...0]\right)$$

e ϕ_i é um vetor ith de modo normalizado. Substituindo (10) em (2), a função objetivo pode ser simplificada como:

$$S(m) = max_\beta \sum_{i=1}^{N} \left(\sum_{k=1} \mu_i \beta_k \lambda_k^i\right) \tag{11}$$

De (11), cocluímos que o objetivo da função de todos os passos e modos de vibração com o coeficiente μ_i. Com a geração da força de vibração, a equação do movimento em forma de coordenadas pode ser escrita como:

$$\dot{\mu_i}(t) + 2\epsilon_i w_i \dot{\mu_i}(t) + w^2 \mu_i(t) = \frac{1}{M_i} f(t) \tag{12}$$

onde $\ddot{\mu_i}, \dot{\mu_i}$, e μ_i representam o modo de aceleração, velocidade e deslocamento, respectivamente, w_i e ϵ_i são a frequência natural e o modo de amortecimento ith, vevido a estrutura flexível e a ausência de amortecimento em seu interior, $\epsilon_i = 0$. A fim de desenvolver o desempenho da vibração, cada modo de vibração deve ser considerada. Assim, os trechos piezoelétricos devem ser colocados no máximo em todas as manchas (piezoelétricas). A mancha no modo unitário pode ser escrito como:

$$\bar{\lambda_k^i} = \frac{\lambda_k^i}{max(\phi_i)} \tag{13}$$

Integrando a equação (13) e (11) , podemos escrever uma nova função objetivo:

Assim, o critério de desempenho dos sensores locais pode ser obtido usando as formas das estruturas.

3 Lógica fuzzy aplicada no controlador em estruturas inteligentes

O controlador de lógica fuzzy usa uma forma de quantificação dos dados imprecisos (conjuntos de entrada fuzzy) para gerar uma inferência relacionada a uma base de conhecimento do controle da força a ser aplicada no sistema. Nesse artigo as entradas são o deslocamento e a velocidade do balanço da viga e a saída é a força de controle sobre o balanço da viga. Na fuzificação, o deslocamento é definido no intervalo de -5 até 5 $(-5, -4, -3, -2, -1, 0, 1, 2, 3, 4, 5)$, a velocidade é definida de -2 até 2 $(-2, -1, 0, 1, 2)$ e a força de controle é definida de -7 até 7 $(-7, -6, -5, -4, -3, -2, -1, 0, 1, 2, 3, 4, 5, 6, 7)$. Duas funções de pertinência comumente adotados no controle da lógica fuzzy são as triangular e trapezoidal. O objetivo final do controlador baseado na lógica fuzzy é tornar os dados imprecisos mais próximos da realidade e sua função é fornecer uma força para reduzir ao máximo a vibração da viga. Na análise de uma viga em balanço, as regras foram implementadas do seguinte modo.

A base das regras fuzzy não é invariável, poderia ser modificado na prática. A base das regras fuzzy é mostrada na Figura 2.

F \ D / V	NB	NM	NS	ZO	PS	PM	PB
NB	PS	PM	PB	ZO	NB	NM	NS
NS	PS	PM	PB	ZO	NB	NM	NS
ZO	ZO	ZO	ZO	ZO	ZO	ZO	ZO
PS	PS	PM	PB	ZO	NB	NM	NS
PB	PS	PM	PB	ZO	NB	NM	NS

Figura 2: Base de regras fuzzy IF-THEN.

O sistema de simulação foi realizado pelo software MATLAB/Simulink, conforme mostra a Figura 2. De acordo com este resultado o controlador de lógica fuzzy é propício para o controle da posição de um sistema de estrutura inteligente. Logo, o controlador de lógica fuzzy projetado é adequado e pode ser usado para esse tipo de sistema.

4 Conclusões

Diante do atual desenvolvimento e da busca de novas tecnologias que possam melhorar o desempenho de estruturas e máquinas, concluímos que as estruturas inteligentes desempenham um papel fundamental no que diz respeito ao fato de abrir caminhos para se conseguir maior eficiência em diversas áreas da indústria, como a aeronáutica e a civil. Verificamos também que dentre os diversos métodos o controlador que utiliza a lógica difusa é o que apresenta os melhores resultados, visto que além de fornecer resultados mais precisos permite a utilização de sistemas mais complexos, com mais variáveis.

Referências

[1] Abreu, G.L.; Ribeiro, J.F. Controle ativo de vibração usando controladores baseados em lógica fuzzy. *Anais Congresso Brasileiro de Engenharia Mecânica,*. Águas de Lindóia, 1999.

[2] B.N. Agrawal; K. E. Treanor, Shape control of a beam using piezoelectric actuators. *Smart Material and Structures,* 8, (1999), 729-740.

[3] R. Babuska; H.B. Verbruggen, An overview of fuzzy modeling for control. *Control Engineering Practice,* 4, (11), (1996), 1593-1606.

[4] A. Blanguernon; F. Lene; M. Bernadou, Active control of a beam using a piezoceramic element, *Smart Material and Structure,* 8, (1999) 116-124.

[5] E. F. Crawley; J. Luis, Use of piezoelectric actuators as elements of inteligente structures, *AIAA Journal,* v. 25, n. 8, (1987), 1373-1385.

[6] W. S. Hwang; H. C. Park, Finite element modeling of piezoelectric sensors and actuators.AIAA Journal, 31, (5), (1993), 930-937.

CONTROLE PID PARA VÁZÃO, UMA AULA DIDÁTICA USANDO SIMULAÇÃO NA UFERSA

Elmer Rolando Llanos Villarreal – elmerllanos@ufersa.edu.br
Bacharelado em Ciência e Tecnologia (BCT),
Departamento de Ciências Exatas e Naturais (DCEN).
Mestrado em Sistemas de Comunicação e Automação.
Universidade Federal Rural do Semi-arido (UFERSA)
Rua Francisco Mota 572
59625900 – Mossoró – RN.
Alexandre Henrique Soares de Oliveira – ahso_eu@hotmail.com
Universidade Federal Rural do Semi-arido (UFERSA), Bacharelado em Ciência e Tecnologia (BCT)
Rua Francisco Mota 572
59625900 – Mossoró – RN.
Isau Macedo Balbino – isaumacedo@hotmail.com
Universidade Federal Rural do Semi-arido (UFERSA), Bacharelado em Ciência e Tecnologia (BCT)
Rua Francisco Mota 572
59625900 – Mossoró – RN.

Resumo: *O presente trabalho apresenta um* software *para auxílio no ensino de disciplinas de modelagem e controle de sistemas. Geralmente, os alunos sentem dificuldade em entender o funcionamento de controladores apenas a partir de seus modelos matemáticos. O programa apresentado permite ao professor, na própria sala de aula, de uma forma visual e interativa, demonstrar o funcionamento de um sistema de controle sem a necessidade de um sistema físico. Assim, é possível mostrar ao aluno, de maneira intuitiva, os conceitos envolvidos com as ações de controle proporcional, integral e derivativa (PID) antes da apresentação de suas funções matemática. Assim o trabalho implementa algoritmos de controle do tipo PID com sintonia de seus parâmetros para o controle de nível. O projeto consiste na sintonia de um controle convencional PID para controlar o nível de um sistema de tanques acoplados. O referido trabalho ajudara muito sala de aula na disciplina de modelagem e controle de sistemas na UFERSA.*
.

Palavras-chave: *Ensino, Didática, Controle de nível, Controle PID.*

1 INTRODUÇÃO

A necessidade de se controlar sistemas e processos físicos existe desde tempos remotos. Antigamente o controle manual, primeira forma de controle foi utilizada , e esta presente em muitos processos, tem-se a necessidade de um operador humano que deve conhecer o sistema e ter razoável experiência e habilidade. Contudo, com o avanço da tecnologia, os sistemas e processos ficaram ainda mais complexos, tornando ineficaz, ou até mesmo impossíveis, a

utilização dos controladores convencionais obtidos a partir da teoria clássica. Existe uma busca por novos métodos e estratégias de controle tais como: controle multivariável, controle adaptativo, controle preditivo, e sistemas de controle inteligente.

No presente trabalho é apresentada uma ferramenta computacional de fácil utilização que permite ao professor, na própria sala de aula, demonstrar o funcionamento de sistemas dinâmicos e controladores automáticos de uma forma visual e agradável para o aluno. A ferramenta permite também ao aluno a experimentação virtual das ações de controle proporcional, integral e derivativa de forma manual de modo a facilitar o entendimento de seu funcionamento automático.

2 CONCEITOS BÁSICOS DE CONTROLE

2.1 Controle realimentado ou controle em malha fechada é uma operação que reduz a diferença entre a saída (resposta) de um sistema ou planta a uma referência externa préestabelecida. Com o sistema de controle em malha fechada surge a figura do "controlador", que compara o valor desejado com o valor medido, e se houver um desvio entre estes valores, manipula a sua saída de forma a eliminar este desvio ou erro. Desta maneira, o controle em malha fechada mantém a variável do processo no seu valor desejado, compensando as perturbações externas e as possíveis não-linearidades do sistema (Massa, 2006).

2.2 Controle PID O controlador Proporcional –Integral- Derivativo (PID) é o algoritmo de controle mais tradicional na indústria. Um controlador PID calcula inicialmente o "erro" entre a sua variável controlada e seu valor desejado, e em função deste "erro" gera um sinal de controle, de forma eliminar este desvio. O algoritmo PID usa o erro em três módulos distintos para produzir a sua saída ou variável manipulada. O controlador Proporcional Integral e Derivativo (PID) gera a sua saída proporcionalmente ao erro, proporcionalmente à integral do erro e proporcionalmente à derivada do erro (Dazzo,2002), (Ogata, 2003). A seguir tem-se a formula do PID

$$u(t) = K_p e(t) + K_p \frac{1}{T_1} + \int e(t)dt + K_P T_D \frac{de(t)}{dt} + u_0 \qquad (1)$$

O fator multiplicativo (T_D) é conhecido como o tempo derivativo do controlador .
Para se obter a sintonia do controlador PID, para um processo com dinâmica conhecida, deve-se definir o critério de desempenho desejado para a malha. O principal critério para ajuste de uma malha de controle, e que deve ser satisfeito, é a estabilidade. Desta forma a sintonia deve ser tal que todos os pólos da função de transferência em malha fechada tenham a parte negativa. Ver figura 1

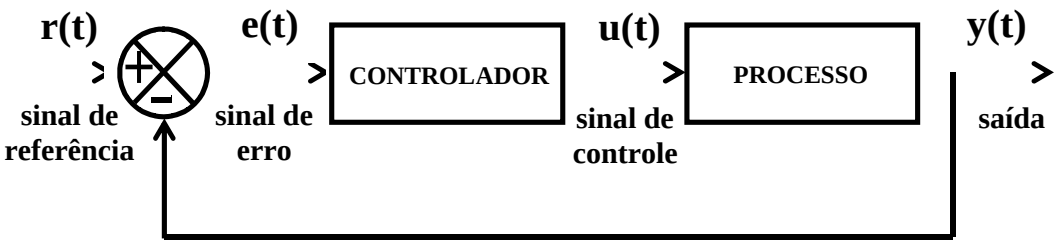

Figura 1 sistema malha fechada (sistema de malha fechada genérica).

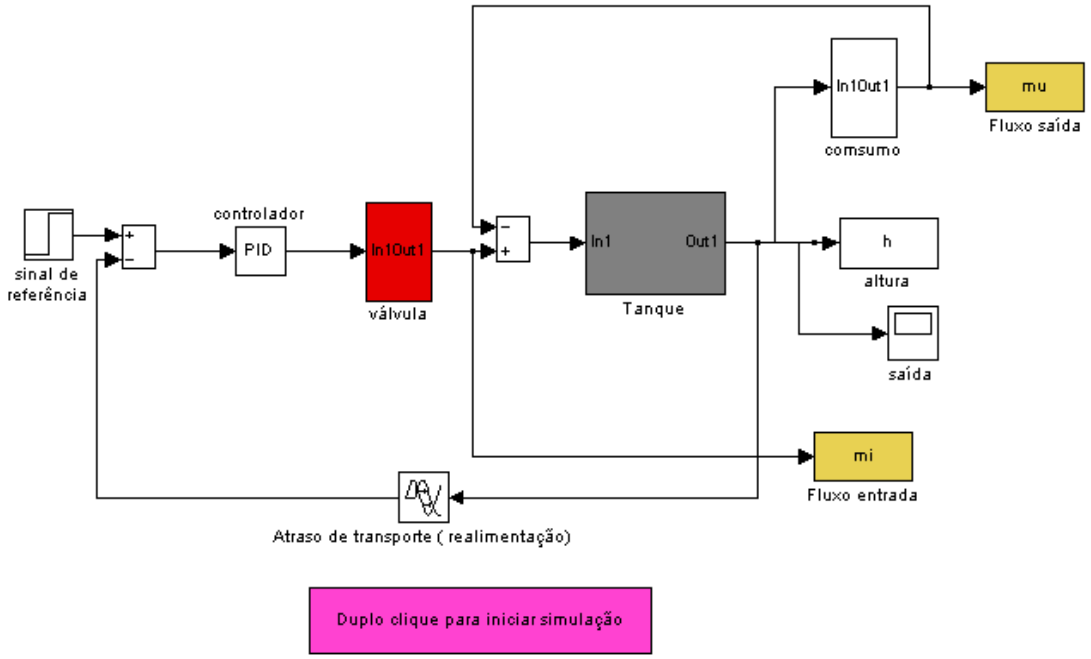

Figura 2 Simulink onde esta PID. (mostra a disposição do diagrama montado no *Simulink*, para a projeção da simulação).

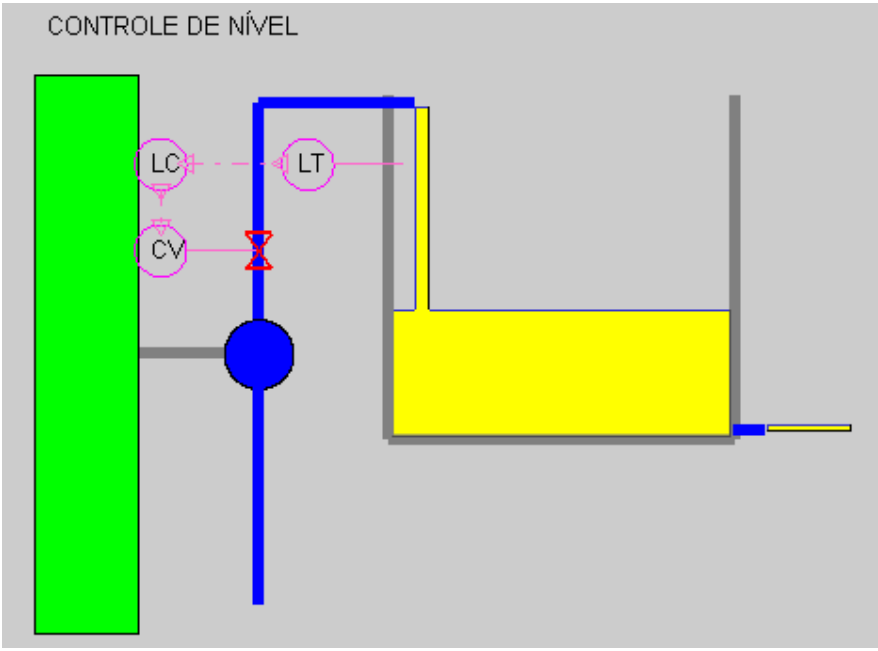

Figura 3 sistema de controle de vazão.(interface gráfica do sistema de controle de vazão).

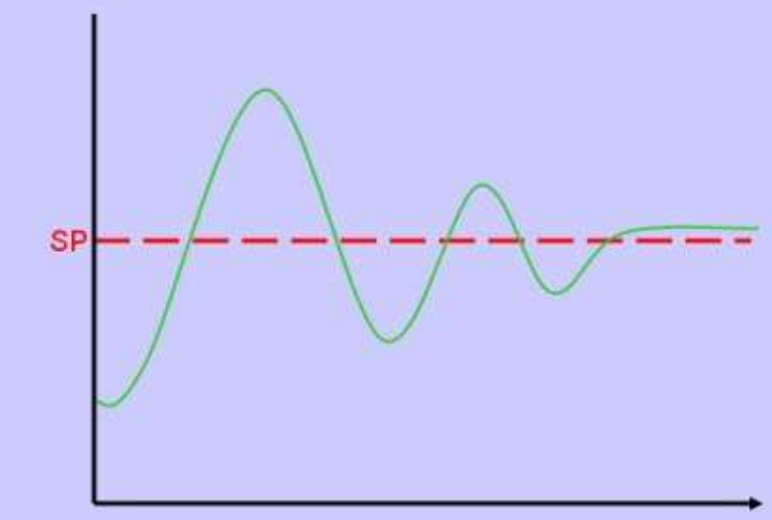

Figura 4 gráfico de comportamento do controlador PID.

3 CONTROLE DE NÍVEL

Um dos controles mais importantes nas unidades industriais é o dos níveis. Estes controles são responsáveis pelos "balanços de massa" das plantas. Isto é, para manter um nível de um tanque ou vaso constante é necessário que a vazão mássica de entrada (Me) seja igual à de saída (Ms), conforme a figura 5. Desta forma, quando ocorre um aumento na vazão de entrada de 10 kg/h para manter a estabilidade do sistema. Entretanto, este aumento não precisa ser no mesmo instante. Ao contrário, deve-se procurar sintonizar a malha de nível de forma a usar o volume do tanque para amortecer as variações de saída (Ms). Isto é, ao haver um aumento da vazão de entrada (Me), o controle pode, e deve em alguns casos, permitir um aumento temporário do nível, para que o aumento da vazão saída ocorra mais lentamente. Isto permite "isolar" duas áreas de planta, ou melhor, o vaso é utilizado como uma capacitância ou pulmão, de maneira a atenuar a interferência de uma parte da planta em outra que lhe seja subsequente (Massa, 2006). Desta maneira, uma perturbação em seção da planta não é transmitida rapidamente às transmitida rapidamente às outras seções.

Muitos problemas de controle e operação de unidades industriais decorrem de variações ou falhas na estratégias de ajuste de malha de nível. Em muitos casos, estes controles não são capazes de amortecer as perturbações por diversas razões:

- vasos ou tanques pequenos (baixa capacitância) que dão origem a um baixo tempo de residência, por erro de projeto, ou porque a unidade foi sendo ampliada ("revamp") e sua carga processada aumentou ao longo do tempo;
- má sintonia dos controles de nível;
- uma interação muito grande com as malhas de controle da unidade.

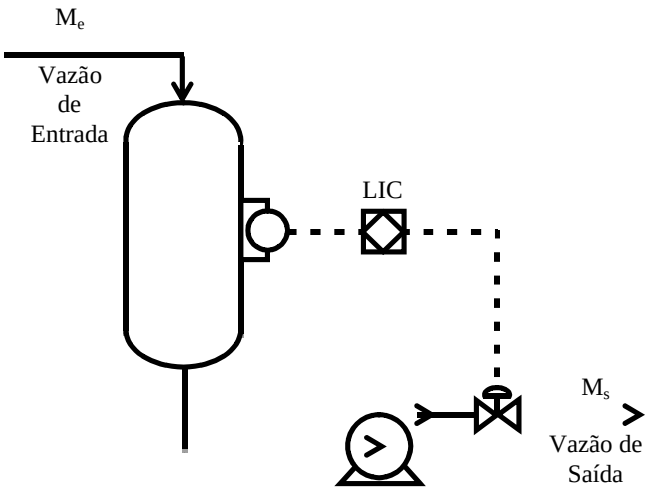

Figura 5 malha fechada com controle de vazão e cilindro vertical.

Considerando-se que o inventário de um tanque é a massa de produto armazenada no mesmo. Por isso, os controles de nível também são conhecidos como os controles de inventario dos sistemas.

O tempo de residência é calculado dividindo-se o volume disponível ou capacidade do tanque pela vazão volumétrica que escoa pelo mesmo. Por exemplo, se existe um volume de 20 m³ para fase líquida deum tanque, e a vazão é de 100 m³/h, o tempo de residência é de 0,2 hora (12 minutos).

Quanto maior for o tempo de residência, melhor para o controle, pois pode-se amortecer as perturbações mais facilmente e trabalhar isoladamente as diversas áreas da unidade. Entretanto, será necessário investir mais na construção de um vaso de dimensões maiores, e em caso de produto inflamável as consequências durante um incêndio seriam mais sérias, pois teríamos um estoque maior.

A geometria do vaso é importante para o controle. Na prática, pode-se encontrar esferas, cilindros horizontais e verticais. Controle em vasos cilíndricos verticais (figura 5) são mais simples de operar, pois independente de onde esteja o ponto de controle (“setpoint”), a resposta dinâmica do processo ou o aumento de nível será o mesmo para uma mesma variação de entrada. Todavia, no caso de uma esfera, ao se controlar o nível no meio da mesma teremos um resposta muito mais lenta do que no caso de se controlar o nível próximo às extremidades da esfera. Esta não-linearidade de acarreta uma dificuldade para o ajuste dos parâmetros de sintonia do controlador PID.

4 CONTROLE DE NIVEL COM PID

Para demonstração do controlador PID e de suas ações de controle, o programa conta com um modo de simulação automático em que o usuário pode definir os valores das contantes *Kp*, *Ki* e *Kd* e da referência de nível desejada.

O controlador PID realiza as funções de controle a partir do desvio entre variável de processo (PV) e o seu setpoint (SP). Quanto maior o desvio, maior a ação de controle, o

controlador deve atuar de forma a trazer o processo rapidamente para o equilíbrio. A relação não-linear entre desvio e a mudança na variável manipulada é produzida pela função “ganho não linear”.

A ação proporcional do controlador PID dentro da faixa ou banda (“gap”) deve ser mais suave do que fora, e podem existir várias faixas em função do problema a ser resolvido.

A transição da ação da banda proporcional do PID de dentro para fora da faixa e vice-versa deve ser feita sem variações abruptas;

A largura da faixa e a relação entre os ganhos são parâmetros ajustáveis que dependem do problema em questão.

Esta estratégia não-linear também pode ser utilizada para variar o tempo do controlador PID em função do erro atual do controlador (Massa,2006), (Shunta 1976).

Explicar os passos a serem seguidos para o controle de nível.

5 CONSIDERAÇÕES FINAIS

O presente trabalho mostrou a utilização de um *software* didático para o ensino de modelagem e controle de sistemas dinâmicos. O programa permite a atuação manual na vazão de entrada de um tanque, além da visualização da dinâmica do controle automático. É possível verificar independentemente a influência de cada ação de controle no sistema, bem como analisar e entender o processo de sintonia do controlador.

Com a utilização do programa, o professor tem a possibilidade de mostrar visualmente aos alunos o funcionamento de um controlador, permitindo o entendimento das equações matemáticas e sua associação com o sistema físico. O sistema permite, ainda, a conexão com um controlador real, possibilitando ao aluno o contato com um sistema de controle industrial sem colocar em risco uma planta real, dessa forma, a aprendizagem do aluno fica mais dinâmica e completa, pois possibilita uma agregação interativa de conhecimento, desenvolvendo no mesmo um raciocínio lógico e de programação.

Práticas de simulação tem grande vantagem no aprendizado, pois além de fornecer um contato direto com meios utilizados em processos industriais, barateia e acessibiliza o estudo de aspectos específicos e gerais das mais variadas áreas da engenharia, diretamente aplicada a processos de produção e controle industrial, mostrando a aplicabilidade de conceitos interdisciplinares na aplicação de equações matemáticas na execução de tarefas reais.

REFERÊNCIAS BIBLIOGRÁFICAS

Dazzo, J. J.; Houpis, C. H. Análise e projeto de sistemas de controle lineares. Guanabara Dois, Rio de Janeiro, 2002.

Massa de Campos M. C., Herbert Texeira C.G. Controles Típicos de equipamentos e processos industriais, Ed. Blucher, 2da Edição, 2006.

Ogata, K. Engenharia de controle moderna. 5ª edição, Pearson,Prentice Hall, São Paulo, 2011.

Shunta “Nonlinear Control of Liquid Level”, Instrumentation Technology, pp.43-48,1976.

Abstract:*This paper presents a software to aid in teaching subjects of modeling and control systems. Generally, students have difficulty in understanding the functioning of controllers only from their mathematical models. The program presented allows the teacher's own classroom, a visual and interactive way to demonstrate the operation of a control system without the need for a physical system. Thus it is possible to show the student, intuitively, the concepts involved with efforts to control proportional, integral and derivative (PID) before submission of mathematical functions. So the work implements control algorithms like PID-tuned its parameters to the control level. The project consists of a line of conventional PID control to control the level of a system of coupled tanks. That work helped a lot in the classroom discipline of modeling and control systems in UFERSA.*

Key-words: Learning, Didactic, Level control, PID control.

http://dx.doi.org/10.5540/DINCON.2011.001.1.0200

DINCON 2011
10ª Conferência Brasileira de Dinâmica, Controle e Aplicações
28 de agosto a 1º de setembro de 2011

STABILIZATION BY OUTPUT FEEDBACK IN REGIONAL POLE PLACEMENT

Elmer R. Ll. Villarreal[1], *Walter M. Rodrigues*[2], *Samara J. M. Bezerra*[3], *José A. R. Vargas*[4]

[1]Mestrado em Sistemas de Comunicação e Automação, Posgraduação/UFERSA, , Departamento de Ciências Exatas e Naturais, DCEN/UFERSA 59625900, Mossoró, Brasil, elmerllanos@ufersa.edu.br

[2]Departamento de Ciências Exatas e Naturais, DCEN/UFERSA, 59625900, Mossoró, Brasil, walterm@ufersa.edu.br

[3]Bacharelado em Ciência e Tecnologia-BCT-UFERSA, Mossoró, Brasil, samarajessicabm18@hotmail.com

[4]Universidade de Brasília UnB Laboratório de Automação e Controle - LARA Campus Universitário Darcy Ribeiro, 70.910-900, Brasília DF, Brasil.

Resumo: The present paper considers the stabilization problem for static output feedback by regional pole placement in Linear matrices inequalities, ($LMIs$) regions. A new approach for the design of output feedback controller is proposed and the respective output feedback gains are obtained through the solution of the coupled Sylvester equation which is related to the solution of Lyapunov equations that allow to obtain pole placement in LMI regions of the complex plane. It presented necessary and sufficient conditions for the existence of the static output feedback matrix. This paper also proposes a new numerically efficient solution algorithm for the coupled design equations to determine the output feedback matrix where the solution can be obtained using the condition $(m + p > n)$.

Palavras-chave: Stabilization; Output Feedback; Regional pole placement.

1. INTRODUCTION

The problem of static output feedback by regional pole placement in a linear, time-invariant, multivariable system using output feedback is considered in this paper. The stabilization of linear systems by output feedback is recognized as an important and still open problem in control theory. For normal systems, approaches and techniques to treat different versions of this problem, it can be found in [5], [13]. Approaches and techniques to treat descriptor systems by output feedback can be found in [17], [18]. Many problems in control theory systems are solved when calculated the solution of Sylvester equations. These equations have important applications in stability analysis and in the eigenvalue assignment (see [15]; [1]; [5]). There are necessary and sufficient conditions for the solution to these equations in [5]. The Solution of Sylvester equation associated to a linear descriptor system in [4], [10]. In this paper an output feedback approach and an algorithm are presented to compute solutions by LMI techniques. The solution of Sylvester equations is related to the solution of Lyapunov equations which allows to obtain pole placement in LMI regions. Thus, necessary and sufficient conditions are presented for the existence of the static output feedback matrix in pole placement. This paper also proposes a numerically efficient solution algorithm for the coupled Lyapunov equations to determine the output feedback matrix. Finally, many theoretical conditions have been offered for the existence of output feedback matrix.

This paper is organized as follows. The second section presents the problem based on the basic concepts and LMI regions basic concepts . In section 3, we present some results in the form of Sylvester equations, the Theorem for the existence of the output feedback matrix. Numerical examples illustrate the application of the algorithms which outline the basic steps used to solve the problem. They are presented in the fourth section. Finally, the concluding remarks are presented.

2. PRELIMINARIES

The solutions to the problem stabilization is associated to the existence of a subspace $\mathcal{V} = Ker\,(T)$ $O.S.$ $(C, A, B)-$invariant, due to the possibility of solving the coupled Sylvester equations, rewritten below:

$$AV + VH_V = -BW \;\; with \;\; \sigma(H_V) \in \mathcal{C}^- \quad (1)$$

$$TA + H_T T = -UC \;\; with \;\; \sigma(H_T) \in \mathcal{C}^- \quad (2)$$

$$TV = 0 \quad (3)$$

$$Ker\,(CV) \subseteq Ker\,(W) \quad (4)$$

$$Ker\,(B'T') \subseteq Ker\,(U') \quad (5)$$

In [5], the coupled equations Lyapunov can also be used to describe geometrical properties required for solving the stabilization problem .

Theorem 2.1 *: [5] There exists an output feedback matrix $G \in \Re^{m\times p}$ such that $\sigma(A + BGC) \in \mathcal{C}^-$, if and only if the conditions verified for some full-rank matrices $V \in \Re^{n\times v}$ and $T \in \Re^{n-v\times n}$, with integer $0 < v \leq n$, such that $TV = 0$:*
(i) $\forall\ Q_V = Q_V' > 0$, $Q_V \in \Re^{v\times v}$, there exist the matrices $P = P' \geq 0$, $P \in \Re^{n\times n}$ and $Y \in \Re^{m\times n}$ such that :

$$AP + PA' + BY + Y'B' = -VQ_VV' \quad (6)$$

$$V'PV > 0 \;\; ; \;\; TPT' = 0 \quad (7)$$

$$Y = W_\Pi V' \; for \; some \;\; W_\Pi \in \Re^{m\times v} \quad (8)$$

(ii) $\forall\ Q_T = Q_T' > 0$, $Q_T \in \Re^{n-v\times n-v}$, *there exist the matrices* $S = S' \geq 0$, $S \in \Re^{n\times n}$ *and* $Z \in \Re^{n\times v}$ *such that :*

$$A'S + SA + C'Z' + ZC = -T'Q_T T \tag{9}$$

$$TST' > 0\ ;\ V'SV = 0 \tag{10}$$

$$Z = T'U_\Gamma \text{ for some } U_\Gamma \in \Re^{n-v\times v} \tag{11}$$

(iii)

$$Ker\, CP \subseteq Ker\, Y \tag{12}$$

$$Ker\, B'S \subseteq Ker\, Z' \tag{13}$$

3. REGIONAL POLE PLACEMENT

A solution for the stabilization problem to obtain output feedback matrix was based on the arbitrary pole placement. There are solutions for the stabilization problem considering the displacement of α using $(A + \alpha I)$ instead of A. The possibility to stabilize and situate the poles in a determined LMI region $\mathcal{D}$ as in [9].

Let $\mathcal{D} \subseteq \mathcal{C}^-$ some region of the complex plane. The stabilization problem is to find an output feedback matrix $u = Gy$ that such $\sigma(A+BGC) \in \mathcal{D}$, or equivalently, the closed loop system is $\mathcal{D}$*-stable*.

A pair (A, B) is $\mathcal{D}$-stabilizable if and only if

$$rank\,([\ \lambda I - A \quad B\ ]) \ = \ n\ ,\ \forall\,\lambda\ \notin \mathcal{D} \tag{14}$$

and a pair (C, A) is $\mathcal{D}$-detectable if and only if

$$rank\left(\left[\begin{array}{c} \lambda I - A \\ C \end{array}\right]\right) \ = \ n\ ,\ \forall\,\lambda\ \notin \mathcal{D} \tag{15}$$

3.1. LMI regions basic concepts

The LMI regions describe convex regions in complex plane that are symmetric in relation to the real axis.

Definition 3.1 *A subset* $\mathcal{D}$

$$\mathcal{D} = \{\lambda \in \mathcal{C} : f_\mathcal{D}(\lambda) < 0\} \tag{16}$$

complex plane is called a LMI *region if there is a symmetric matrix* $\Delta = (\delta)_{kl} \in \Re^{n\times n}$ *and a matrix* $\Theta = (\theta)_{kl} \in \Re^{n\times n}$ *such that*

$$f_\mathcal{D}(\lambda) \ = \ \Delta + \lambda\Theta + \bar{\lambda}\Theta' \tag{17}$$

with $\lambda, \bar{\lambda} \in \mathcal{C}$, *where* $\mathcal{C}$ *denotes the complex half-plane* [1].

The characteristic function $f_\mathcal{D}(\lambda)$ takes values in the space of Hermitian matrices of dimensions $n \times n$. Linear matrices inequalities, $(LMIs)$ can be defined from $f_\mathcal{D}(\lambda)$ to characterize the properties of the eigenvalues of a real matrix belonging to $\mathcal{D}$ [9].

The LMI regions with their characteristic functions are given in [9].:

- A disk-centric $(-q, 0)$ with radius r, whose characteristic function is :

$$f_\mathcal{D}(\lambda) = \left(\begin{array}{cc} -r & q \\ q & -r \end{array}\right) + \left(\begin{array}{cc} 0 & 0 \\ 1 & 0 \end{array}\right)\lambda + \left(\begin{array}{cc} 0 & 0 \\ 1 & 0 \end{array}\right)'\bar{\lambda} \tag{18}$$

Consider the linear system represented by

$$\dot{z}(t) \ = \ Hz(t),\ \ with\ \ H \in \Re^{n\times n} \tag{19}$$

[1] $(\delta)_{kl}$ $((\theta)_{kl})$ represent the matrix elements Δ (Θ) $\forall\ 1 \leq k, l \leq n$

The system (19) is $\mathcal{D}$-stable, where $\mathcal{D}$ is a LMI region, if and only if there exist matrices Δ and $\Theta \in \Re^{n\times n}$

$$f_\mathcal{D}(\Theta) \ = \ \Delta + \Theta\otimes H + \Theta'\otimes H' < 0 \tag{20}$$

where $\otimes$ represents the Kronecker product in [12].
Is interesting to note that:

- the equation (20) can be rewritten as

$$f_\mathcal{D}(\theta) = (\delta)_{kl} + (\theta)_{kl}H + (\theta)_{lk}'H',\ \ \forall\ 1 \leq k, l \leq n \tag{21}$$

- for two LMI regions, $\mathcal{D}_1$ and $\mathcal{D}_2$, and whose characteristics functions are associated to $f_{\mathcal{D}_1}$ and $f_{\mathcal{D}_2}$, respectively, the intersection $\mathcal{D} = \mathcal{D}_1 \cap \mathcal{D}_2$ is an LMI region with characteristic function $f_{\mathcal{D}_1\cap\mathcal{D}_2} = Diag(f_{\mathcal{D}_1}, f_{\mathcal{D}_2})$.

3.2. $\mathcal{D}$-Stabilization by output feedback

Remember first that the existence of an output feedback matrix that stabilizes the closed loop system can be associated with to solution of coupled Sylvester equations (1) , (2) and (3). By Theorem in [5], these equations can be interpreted in terms of geometric properties of the subspace $\mathcal{V} = Ker\,(T)$. Once found the output feedback matrix which stabilizes the system, the spectrum of the closed loop is given by :

$$\sigma(A + BGC) = \sigma(H_V)\,\dot{\cup}\,\sigma(H_T) \tag{22}$$

Thus, in sequence it is considered that the desired regional pole placement is defined from LMI regions associated to the matrices H_V and H_T, as follows:

$$\begin{array}{l}\sigma(H_V) \in \mathcal{D}_V \\ \sigma(H_T) \in \mathcal{D}_T\end{array} \quad \Longrightarrow \ \mathcal{D} = \mathcal{D}_V\ \cup\ \mathcal{D}_T \tag{23}$$

Then, assuming that $H_V \in \Re^{p\times p}$ and $H_T \in \Re^{n-p\times n-p}$, $\mathcal{D}$-stabilizability conditions in LMI regions are equivalently replaced by the following two conditions :

$$\begin{array}{r}\sigma(H_V) \in \mathcal{D}_V \Longleftrightarrow \exists\ \Pi = \Pi' > 0 \text{ such that} \\ \Delta_V \otimes \Pi + \Theta_V' \otimes (\Pi H_V') + \Theta_V \otimes (H_V\Pi) = -Q_V < 0\end{array} \tag{24}$$

where $\Pi \in \Re^{p\times p}$

$$\begin{array}{r}\sigma(H_T) \in \mathcal{D}_T \Longleftrightarrow \exists\ \Gamma = \Gamma' > 0 \text{ such that} \\ \Delta_T \otimes \Gamma + \Theta_T' \otimes (H_T'\Gamma) + \Theta_T \otimes (\Gamma H_T) = -Q_T < 0\end{array} \tag{25}$$

where $\Gamma \in \Re^{n-p\times n-p}$.

The following result can be obtained similarly to the result in the previous section, considering as starting point the coupled Sylvester equations under the regional pole placement restricted to the spectrum of matrices H_V and H_T, respectively. For algorithmic purposes, it is considered that $v = p$. The necessary and sufficient conditions are presented for the existence output feedback matrix given by the following theorem.

Theorem 3.1 *There exists a static output feedback matrix* $G \in \Re^{m\times p}$ *such that* $\sigma(A + BGC) = \{\lambda_1, \lambda_2, \ldots, \lambda_n\} \in \mathcal{D}$, *for* $\mathcal{D} = \mathcal{D}_V \cup \mathcal{D}_T$, *where* $\{\lambda_1, \ldots, \lambda_{n-p}\} \in \mathcal{D}_T$ *and* $\{\lambda_{n-p+1}, \ldots, \lambda_n\} \in \mathcal{D}_V$, *if and only if there exist matrices* $(P = P' \geq 0,\ P \in \Re^{n\times n},\ Y \in \Re^{m\times n},\ S = S' \geq 0,$ $S \in \Re^{n\times n}$ *and* $Z \in \Re^{n\times p})$ *such that the following conditions are verified for any pair of matrices* $V \in \Re^{n\times p}$ *and* $T \in \Re^{n-p\times n}$ *such that* $TV = 0$*:*
i)

$$\begin{array}{r}\Delta_V\otimes P + \Theta_V \otimes (AP + BY) + \Theta_V' \otimes (PA' + Y'B') = \\ -(V\otimes I_p)Q_{V1}(V \otimes I_p)' \text{ for } Q_{V1} > 0\end{array} \tag{26}$$

$$V'PV = \bar{P} > 0\,;\; TPT' = 0 \tag{27}$$

$$Y = W_\Pi V' \textit{ for some } W_\Pi \in \Re^{m\times p} \tag{28}$$

ii)

$$\begin{array}{c}\Delta_T\otimes S + \Theta_T \otimes (SA + ZC) + \Theta'_T \otimes (A'S + C'Z') = \\ -(T'\otimes I_{n-p})Q_{T1}(I_{n-p}\otimes T) \textit{ for } Q_{T1} > 0\end{array} \tag{29}$$

$$TST' = \bar{S} > 0\,;\; V'SV = 0 \tag{30}$$

$$Z = T'U_\Gamma \textit{ for some } U_\Gamma \in \Re^{m\times p} \tag{31}$$

iii)

$$Ker\, CP \;\subseteq\; Ker\, Y \tag{32}$$

$$Ker\, B'S \;\subseteq\; Ker\, Z' \tag{33}$$

Proof:
Necessity: Consider that the coupled Sylvester equations (1),(2) and (3) are verified with the conditions (4) and (5). It first shows the necessity part (i). Since the quadratic condition given by (24) must be true, and using the definition of Kronecker product [2] :

$$\begin{array}{c}(\delta_V)_{kl}(V\Pi V') + (\theta_V)_{lk}(V\Pi H'_V V') + (\theta_V)_{kl}(VH_V\Pi V') = \\ -V(Q_V)_{kl}V' \;\; \forall\; 1\le k,l\le n\end{array} \tag{34}$$

where : $(Q_V)_{kl} = (Q_V)'_{kl} \in \Re^{p\times p}$.

From (1), it is also obtained $AV + BW = VH_V$, that can be used in (35) to obtain

$$\begin{array}{c}(\delta_V)_{kl}(V\Pi V') + (\theta_V)_{lk}(V\Pi V'A' + V\Pi W'B') + \\ (\theta_V)_{kl}(AV\Pi V' + BW\Pi V') = -V(Q_V)_{kl}V'\end{array} \tag{35}$$

Thus, by placing the matrices $P = P' = V\Pi V'$ and $Y = W\Pi V'$, and considering that the $rank\,(V) = p$ and that $\Pi > 0 \Longrightarrow \left\{ \begin{array}{l} V'V\Pi V'V > 0 \\ T'V\Pi V'T = 0 \end{array} \right.$, then (36) can be equivalently replaced by (26), (27) and (28).

Using similar arguments, it shows the necessity part (ii). Thus, from (2) and (25), it is obtained :

$$\begin{array}{c}(\delta_T)_{kl}(T'\Gamma T) + (\theta_T)_{lk}(T'H'_T\Gamma T) + (\theta_T)_{kl}(T'\Gamma H_T T) = \\ -T'(Q_T)_{kl}T \;\; \forall\; 1\le k,l\le n\end{array} \tag{36}$$

where: $(Q_T)_{kl} = (Q_T)'_{kl} \in \Re^{n-p\times n-p}$.

For the matrices $S = T'\Gamma T$ and $Z = T'\Gamma U$, (37) may be replaced by (29) and (31). Moreover, since $rank\,(T) = q-p$ and $\Gamma > 0$, it is obtained $\left\{ \begin{array}{l} TT'\Gamma TT' > 0 \\ V'T'\Gamma TV = 0 \end{array} \right.$.

The necessity of part *(iii)*, (32) and (33) follow the conditions $Ker\, CV \subseteq Ker\, W$ and $Ker\, B'T' \subseteq Ker\, U'$, respectively, taking into account the definitions above P, Y, S and Z.
Sufficiency :
It is considered that the part (i), (ii) and (iii) are verified.

4. OUTPUT FEEDBACK STABILIZATION ALGORITHM

4.1. Primal Algorithm

Based on the primal algorithm proposed in the previous section, the following basic procedure is proposed to compute a $\mathcal{D}$-stabilizing static output feedback matrix in the closed loop system when the condition $m+p > n$ is verified:
Step 1:
1.1) Find a decomposition

$$C\,[\;M_1 \quad M_2\;] = [\;C_1 \quad 0\;] \tag{37}$$

where: $C_1 \in \Re^{p\times p}$, $rank(C_1) = p$.

To compute matrices A_{12}, A_{22}:

$$\left[\begin{array}{c}A_{21}\\A_{22}\end{array}\right] = \left[\begin{array}{c}\bar{M}'_1\\ \bar{M}'_2\end{array}\right] AM_2 \;\text{ where }\; [\;M_1 \quad M_2\;]\left[\begin{array}{c}\bar{M}'_1\\ \bar{M}'_2\end{array}\right] = I_n \tag{38}$$

1.2) Solve the LMI to find S_{21} and $S_{22} = S'_{22} > 0$:

$$\begin{array}{c}\Delta_T \otimes (S_{22}) + \Theta_T \otimes (S_{22}A_{22} + S_{21}A_{12}) + \\ \Theta'_T \otimes (A'_{22}S_{22} + A'_{21}S'_{21}) < 0.\end{array} \tag{39}$$

1.3) Compute $T = [\;S_{21} \quad S_{22}\;]\left[\begin{array}{c}\bar{M}'_1\\ \bar{M}'_2\end{array}\right]$. If (A,B,T) has no invariant zeros, go to Step 2; or else, repeat the Step 1 using a new decomposition for C.
Step 2:
2.1) Compute V as an orthogonal basis of $Ker\,(T)$:

$$TV = 0 \;\; \text{with} \;\; V'V = I_p \tag{40}$$

2.2) Solve the following equation, under the constraints (27) and (28), to find P and Y:

$$\begin{array}{c}\Delta_V\otimes P + \Theta_V\otimes(AP + BY) + \Theta'_V\otimes(PA' + Y'B') = \\ -(V\otimes I_p)Q_{V1}(V\otimes I_p)' \le 0\end{array} \tag{41}$$

Step 3: The $\mathcal{D}$-stabilizing output feedback matrix in the corresponding closed loop system verifies

$$GCP = Y \iff GCV\bar{P} = W_\Pi, \;\text{ since }\; V'V = I_p.$$

Remark 4.1 *Note also that equation (40) is an LMI in the variables S_{21} and S_{22}. Then, convex programming techniques can be used to find feasible solutions in [2]. As a feasibility test for step 2, you should verify if the system (A,B,T) has no invariant zeros which belong to $\mathcal{D}_V$. Then go to the next step. The conditions are usually solved in the sense that the matrix system $P_\lambda = \left[\begin{array}{cc} A-\lambda I_n & B \\ T & 0\end{array}\right]$ of dimension $(n+m)\times(2n-p)$ must have full row rank $\forall\lambda$. Thus, the Step 2 is only feasible with stable solutions.*

4.2. Examples

Consider the system (A,B,C) with data in [11] ;

$$A = \left[\begin{array}{cccc} 0 & 1 & 0 & 0\\ 1 & 1 & 0 & 0\\ -1 & 0 & 0 & 0\\ 0 & 0 & 0 & 0\end{array}\right]\;;\; B = \left[\begin{array}{cc} 0 & 0\\ 1 & 0\\ 0 & 0\\ 0 & 1\end{array}\right];\; C = \left[\begin{array}{cccc} 1 & 0 & 0 & 1\\ 0 & 0 & 1 & 0\\ 0 & 0 & 0 & 1\end{array}\right]$$

The corresponding system (C,A,B) is stabilizable and detectable, and $m+p = 5 > n$. The open loop poles are: $0.0000\,,\; 0.0000\,, 1.6180\,, -0.6180$.
A)Primal Algorithm:

The LMI region $\mathcal{D}_\mathcal{T}$ is a vertical band defined by: $\mathcal{D}_T = \{\,x + jy \in \mathcal{C}\;;\; -5 < x < -1\,\}$. The LMI region $\mathcal{D}_V$ is defined from the intersection of sectors and a conical disk defined by: $\{\,x + jy \in \mathcal{C}\;;\; x < -5\,,\, |x+jy| < 10$ and $tan\,45^o x < |y|\}$. Thus, convex programming techniques are applied to find feasible solutions for the equations of regional pole placement without additional requirements.
The matrix $[\;M_1 \quad M_2\;] = \left[\begin{array}{cccc} -0.7071 & 0.0000 & 0.7071 & 0.0000\\ 0.0000 & 0.0000 & 0.0000 & 1.0000\\ 0.0000 & -1.0000 & 0.0000 & 0.0000\\ -0.7071 & 0.0000 & -0.7071 & 0.0000\end{array}\right]$ found in step 1.1 leads to: $A_{22} = 1.0000 \quad A_{12} = \left[\begin{array}{c} -0.7071\\ 0.0000\\ 0.7071\end{array}\right]$.

A solution for step 1.2 is:

$S_{22} = 333.3318\,,\; S_{21} = [\;0.0000 \quad 0.0000 \quad -2080.8778\;]\,,$

[2]Note that (24) can be equivalently replaced by: $(\delta_V)_{kl}\Pi + (\theta_V)_{lk}(\Pi H'_V) + (\theta_V)_{kl}(H_V\Pi) = -(Q_V)_{kl}\;\forall\; 1\le k,l\le n$

which results in step 1.3:

$$T = \begin{bmatrix} -1471.4028 & 333.3318 & 0.0000 & 1471.4028 \end{bmatrix}.$$

This solution has no invariant zeros and imply in step 2.1:

$$V = \begin{bmatrix} 0.6982 & 0.0000 & 0.1582 \\ -0.0650 & 0.0000 & 0.9853 \\ 0.0000 & 1.0000 & 0.0000 \\ 0.7129 & 0.0000 & -0.0650 \end{bmatrix}.$$

A solution for the step 2.2 is, then, found:

$$Y = \begin{bmatrix} 10887.2550 & 150744.2000 & 304.1292 & 45036.8680 \\ -4945.7042 & 52669.6190 & -336.9173 & -16877.4870 \end{bmatrix}$$

$$W_{\Pi} = \begin{bmatrix} 49513.0880 & 304.1292 & -149730.1600 \\ -18910.8790 & -336.9173 & 52208.9740 \end{bmatrix}$$

The corresponding output feedback matrix that stabilizes the closed loop system is:

$$G = \begin{bmatrix} -218.6662 & 348.0591 & 303.7491 \\ 52.7244 & -78.8494 & -75.4133 \end{bmatrix}$$

resulting: $\sigma(A + BGC) = \{-3.4142\,,\, -5.7409\,,\, -6.2669 \pm 4.6210j\,\} \subset \mathcal{D}_V$. Where the eigenvalue $-3.4142 \subset \mathcal{D}_T$ corresponds to step 1.

△

5. CONCLUDING REMARKS

In this paper, an output feedback approach and an algorithm were presented to compute solutions by LMI techniques. The solution of Sylvester equations was related to the solution of Lyapunov equations that allowed to obtain pole placement in LMI regions. Thus, necessary and sufficient conditions were presented for the existence of the static output feedback matrix. This paper also was proposed a numerically efficient solution algorithm for the coupled Lyapunov equations to determine the output feedback matrix.

REFERENCES

[1]DOI Alexandridis A. T. Paraskevopoulos P. N.(1996), "A New Approach to Eigenstruture Assignment by Output Feedbackt't', *IEEE Trans. Automatic. Control*,41, number 7,July, pp. 1046-1050.

[2] Boyd S. P., El Ghaoui L., Feron E. and Balakrishhnan V.(1994), "Linear Matrix Inequalities in System and Control Theoryt't' ,Philadelphia SIAM.

[3]DOI Byers R, Nash S G (1989) "Approaches to robust pole assignment,t't' *Int. J. Control*, 49 (1), pp.97-117.

[4]DOI Castelan E. B., Gomes Silva V. (2005) "On the solution of a Sylvester equation appering in descriptor Systems control theoryt't', *Systems e Control Letters* 54, pp. 109-117.

[5]DOI Castelan E. B., Hennet J. C., Villarreal E. R. Ll.(2003), "Quadratic Characterization and Use of Output Stabilizable Subspaces,t't' *IEEE Trans. Automatic Control*, 48, No. 4, pp. 654-660.

[6] Castelan E. B., Villarreal E. R. Ll., Tarbouriech S. (2002), "Quadratic characterization and use of output stabilizable subspaces for descriptor systems," in *Proceddings of the 15th Triennial World Congress of IFAC (IFAC'02)*, Barcelona, pp. 7-12.

[7]PUB Castelan E. B., Hennet J. C. Villarreal E. R. Ll. (2002), "Output Feeedback Design by Coupled Lyapunov-Like Equationst't', in *15 th IFAC(IFAC'02)*, Barcelona, pp. 7-12.

[8] Chen C. T.(1999), "Linear System Theory and Designt't', Holt, Rinehart and Winston.

[9]DOI Chilali M. , Gahinet P. (1996), " H_∞ Design with Pole Placement Constraints: An LMI Approacht't', *IEEE Trans. Automatic. Control*, 41,03, pp.358-367.

[10]DOI Darouach M (2006) "Solution to Sylvester equation associated to linear descriptor systemst't', *Systems and Control Letters* Vol. 55, Issue 10, October, pp. 835-838.

[11] Fletcher L. R., Kautsky J., Kolka G. K. G and Nichols N. K.(1988), "Eigenstructure Assingment by Output Feedback in Descriptor Systemst't', *IEEE Trans. Automatic. Control*, vol. 42, pp.1457-1468.

[12] Horn R. A. and Jhonsons C. R.(1991), "Topics in Matrix Analysist't',Cambridge University Press.

[13]DOI Syrmos V. L. Abdallah C. T. and Dorato P. and Grigoriadis K.(1997), "Static Output Feedback- A Surveyt't', *Automatica*, Vol. 33, No 2, pp. 125-137.

[14] Syrmos V. L.,Lewis F. L. (1994), "Bilinear Formulation for the Output Feedback Problem in Linear System t't', *IEEE Trans. Automatic Control*, 39, No. 2, pp. 410-414.

[15]DOI Syrmos V. L., Lewis F. L.(1993), "Output Feedback Eigenstructure Assignment Using Two Sylvester Equations, *IEEE Trans. Automatic Control*, **38**, No. 3, pp.495-499.

[16]DOI Tits A. L., Yang Y. (1996), "Globally convergent algorithms for robust pole assignment by state feedback *IEEE Trans. Automat. Control*, 41 (1) pp.1432-1452.

[17]PUB Villareal E. R. L., Vargas J.A.R., Hemerly E. M.(2009), "Static Ouput Feedback stabilization using Invariant Subspaces and Sylvester Equationst't', *TEMA - Tend. Mat. Apl. Comput.*, 10, No. 1, pp. 99-110.

[18]DOI Yagoubi M. (2010), "Static output feedback control design for descriptor system' *Journal of Control Science and Engineering*, 1, pp.1-8.

[19]DOI Zhoua L., Lub G. (2009), "Detection and stabilization for discrete-time descriptor systems via a limited capacity', *Automatica*, 45, No. 10, pp. 2272-2277.

DINCON'10
9th Brazilian Conference on Dynamics, Control and their Applications
June 07-11, 2010

SUFFICIENT CONDITIONS FOR STABILIZATION BY OUTPUT FEEDBACK IN DESCRIPTOR SYSTEMS

Elmer Rolando Llanos Villarreal[1], *Santos Demetrio Miranda Borjas*[2], *Walter Rodrigues Martins*[3], *José Alfredo Ruiz Vargas*[4]

[1,2,3]Departamento de Ciências Exatas e Naturais, Universidade Federal Rural do Semi-árido, UFERSA, Av. Francisco Mota 572, CEP: 59625-900 Costa e Silva Mossoró/RN, Brasil.
[1]elmerllanos@ufersa.edu.br
[2]santos.borjas@ufersa.edu.br
[3]walterm@ufersa.edu.br
[4]Faculdade de Tecnologia, Universidade de Brasilia (UNB), 70.910-900 Brasília DF, Brasil, vargas@ieee.org

Abstract

The principal aim of this paper is study the stabilization problem by static output feedback for linear descriptor system. Presented sufficient conditions for the existence of a S-stabilizing output feedback control in terms of two coupled matrix, where the solutions to these equations can be obtained using condition $(m + p > q)$.
Keywords: Stabilization, Output Feedback, Descriptor Systems.

1. INTRODUCTION

This paper deals with the stabilization for control problem by static output feedback for linear descriptor systems. Consider that an n-dimensional descriptor system consists of a mixture of $n - q$ algebraic equations and q first order diferential equations. Descriptor systems arise naturally in the modelling of several dynamic systems commonly used in engineering applications, such as biologic, power and other interconnected systems [7], [11], [16]. Besides guaranteeing the closed-loop asymptotic stability, two other properties are desired in practice: closed-loop regularity and absence of impulsive behavior. The problem of computing a suitable static output feedback, from which these closed-loop propierties are verified, is called S-stabilization problem. These three desired properties can be described in terms of the closed-loop eigenstructure: (i) the asymptotic stability is equivalent to have all the finite poles in the left half complex plane; (ii) the absence of impulsive modes is equivalent to have q finite closed-loop; and (iii) the regularity is guaranteed if the system is impulse-free. Thus, the necessary and sufficient conditions for the existence of a S-stabilizing output feedback are obtained as a set of coupled (generalized) Sylvester equations in [8], [9], [3], [1] . In case of normal systems, it is shown that output stabilizable (C, A, B)-invariant subspaces are obtained through a pair of coupled Sylvester equations by systems verifying Kimura's condition, thus, two algorithms are proposed to solve the coupled Sylvester equations in [2], [15].

This paper deals with the stabilization for control problem by output feedback in descriptor systems. Thus, a new approach for the design of output feedback controller is proposed and the respective output feedback gains are obtained through the solution of the Sylvester equation. Thus, it is presented sufficient conditions under which this problem has a solution. This paper also proposes a new numerically efficient solution algorithm for the coupled design equations to determine the output feedback matrix. Another consequence of this result is that the conditions also provide sufficient conditions to control the problem by output feedback. Of course, in case of these conditions are not met, this does not mean that the system is not stabilizable by output feedback.

This paper is organized as follows. The second section presents the problem based on the basic concepts, the necessary and sufficient conditions for the existence of a solution. In section 3, we present some results in the form of Lyapunov equations. The numerical examples illustrate the application of the algorithms which outline the basic steps used to solve the problem. They are presented in the fourth section. Finally, the concluding remarks are presented.

2. PRELIMINARIES

The considered descriptor time-invariant systems are described by :

$$E\dot{x}(t) = Ax(t) + Bu(t) \quad (1)$$
$$y(t) = Cx(t) \quad (2)$$

~

where: $x \in \mathcal{X} \sim \Re^n$ is the state variable, $u \in \mathcal{U} \sim \Re^m$ is the control variable(input variable), $y \in \mathcal{Y} \sim \Re^p$ is the output variable and $E \in \Re^{n\times n}$, $rank\,(E) = q < n$; as the other matrices have an appropriate size with $rank\,(B) = m$ and $rank\,(C) = p$.

Thus, the control problem is to find a static output feedback control law $u(t) = Ky(t)$, such that the closed-loop system

$$E\dot{x}(t) = (A + BKC)x(t) \quad (3)$$

is S-stable: regular, assymptotically stable and impulse free.

It presents to follow some concepts and definitions from the geometric control theory for the descriptor system.

Definition 2.1 *[13] A subspace $\mathcal{V}$, of dimension v, is (C, E, A, B)-invariant output stabilizable subspace , (or simply $O.S.$ (C, E, A, B)-invariant [1]) if $\mathcal{V}$ is (A, E, B)-inner stabilizable and (C, E, A)-outer detectable.*

For the closed loop system a subspace $\mathcal{V}$ $O.S.$ (C, A, E, B)-invariant to be associated does not regulate or have impulsive ways. Consider $V \in \Re^{v\times v}$ such that $Im\,(V) = \mathcal{V}$ and consider $T \in \Re^{(n-v)\times v}$ a left annihilator of V, $i.e.$: $Ker\,(T) = Im\,(V)$. A stronger definition that allows, particularly, regularizable property is considered in [12], as follows :

Definition 2.2 *[4] [1] A v-dimensional subspace $\mathcal{V} \subset \mathcal{X}$ is strongly $O.S.$ (C, A, E, B)-invariant if it is $O.S.$ (C, A, E, B)-invariant and $Ker\,E \cap \mathcal{V} = \{0\}$.*

As in [1], the definition 2.2 is equivalent an existence of matrices ($H_V \in \Re^{v\times v}$, $W \in \Re^{m\times v}$) and ($H_T \in \Re^{n-v\times n-v}$, $U \in \Re^{(n-v)\times v}$), solutions for the coupled Sylvester Equations :

$$AV - EVH_V = -BW \quad (4)$$
$$TA - H_TTE = -UC \quad (5)$$
$$TEV = 0 \quad (6)$$

The definition 2.2 and the equations (4) , (5) and (6) play a fundamental role in treating the control problem by output feedback, mainly for Eigenstructure Assignment [14], [13].

[1] Output Stabilizable (C,E,A,B)-invariant [13] [4]

The present study takes the properties of stabilizability and detectability into account through the two following definitions :
(i) a subspace (A, E, B)-invariant $\mathcal{V}$ is (A, E, B)-inner stabilizable subspace, that is there exist F such that $(A + BF)|\mathcal{V}$ is asymptotically stable ; and
(ii) a subspace (C, E, A)-invariant $\mathcal{V}$ is (C, E, A)-outer detectable subspace if there exists, L such that $(A + LC)|\mathcal{X}/\mathcal{V}$ is asymtotically stable.

Let $V \in \Re^{n\times v}$, such that $Span(V) = \mathcal{V}$. Then, the condition $Ker\,E \cap \mathcal{V} = \{0\}$ can be equivalently replaced by [12]:

$$rank(EV) = v \quad (7)$$

It is assumed that (7) is verified, a matrix $T \in \Re^{(q-v)\times n}$ is a generalized left annihilator of EV, if $TEV = 0$ and $Ker\,(T) \cap Im\,(E) = \{0\}$ [1]. Thus, a subspace $Span(V) = \mathcal{V}$ is strongly $O.S.$ (C, A, E, B)-invariant if and only if there exist matrices ($H_V \in \Re^{v\times v}$, $W \in \Re^{m\times v}$) and ($H_T \in \Re^{(q-v)\times(q-v)}$, $U \in \Re^{(q-v)\times v}$) solutions for the coupled-generalized Sylvester equations :

$$AV - EVH_V = -BW, \quad \sigma(H_V) \in \mathcal{C}^- \quad (8)$$
$$TA - H_TTE = -UC, \quad \sigma(H_T) \in \mathcal{C}^- \quad (9)$$
$$TEV = 0 \quad (10)$$

As [1] and [9] the definition 2.2 and equations (8) , (9) and (10) play a fundamental role in treating the control problem by static output feedback, mainly by eigenstructure assignment.

3. LYAPUNOV EQUATIONS AND OUTPUT FEEDBACK MATRIX

Two following theorems are used in the study of the S-stabilization problem. Thus, the Theorem 3.1 relates the concept of strongly $O.S.$ (C, A, E, B)-invariant subspaces to the existence of an output feedback $u(t) = Ky(t)$, such that solves the S-stabilization problem in the closed-loop system .

Theorem 3.1 *[4] [1] There exists an output feedback matrix $K : \mathcal{Y} \longrightarrow \mathcal{U}$ such that $\sigma(E, A + BKC) \in \mathcal{C}^-$ and the closed-loop system is regular, asymptotically stable and impulse free if and only if the following conditions are verified for some of the matrices ($V \in \Re^{n\times v}, H_V \in \Re^{v\times v}, W \in \Re^{m\times v}$), ($T \in \Re^{q-v\times n}, H_T \in \Re^{q-v\times q-v}, U \in \Re^{n-v\times n-v}$) and for some scalar positive $v \leq n$:*

$$AV - EVH_V = -BW, \quad \sigma(H_V) \in \mathcal{C}^- \quad (11)$$
$$TA - H_TTE = -UC, \quad \sigma(H_T) \in \mathcal{C}^- \quad (12)$$
$$TEV = 0 \quad (13)$$
$$Ker\,(CV) \subseteq Ker\,(W) \quad (14)$$
$$Ker\,(B'T') \subseteq Ker\,(U') \quad (15)$$

where: $rank\,(EV) = rank\,(TE) = q$.

A quadratic characterization of strongly subspaces $O.S.$ (C, A, E, B)-invariant is obtained by replacing conditions $\sigma(H_V) \in \mathcal{C}^-$ and $\sigma(H_T) \in \mathcal{C}^-$ by the two equivalent quadratic Lyapunov stability conditions [5] :

$$\sigma(H_T) \in \mathcal{C}^- \Longleftrightarrow \exists\ \Gamma = \Gamma' > 0$$
$$\text{such that } H_T'\Gamma + \Gamma H_T = -Q_T, \forall\ Q_T = Q_T' > 0 \quad (16)$$

Theorem 3.2 *[4], [1] : There exist an output feedback matrix $K : \mathcal{Y} \longrightarrow \mathcal{U}$, such that $\sigma(E, A+BKC) \in \mathcal{C}^-$, if and only if the following conditions are verified for some positive scalar $v \leq n$ and for some pair of matrices $V \in \Re^{n\times v}$ and $T \in \Re^{q-v\times n}$, such that $TEV = 0$, where $rank\,(EV) = rank\,(TE) = q$:*
(i) $\forall\ Q_V = Q_V' > 0$, $Q_V \in \Re^{v\times v}$, there exists matrices $P = P' \geq 0$, $P \in \Re^{n\times n}$ and $Y \in \Re^{m\times n}$, such that :

$$APE' + EPA' + BYE' + EY'B' = -EVQ_VV'E' \quad (17)$$
$$V'PV > 0\ ;\ TEPE'T' = 0 \quad (18)$$
$$Y = W_\Pi V' \text{ for some } W_\Pi \in \Re^{m\times v} \quad (19)$$

(ii) $\forall\ Q_T = Q_T' > 0$, $Q_T \in \Re^{q-v\times q-v}$, there exist matrices $S = S' \geq 0$, $S \in \Re^{n\times n}$ and $Z \in \Re^{n\times v}$, such that :

$$A'SE + E'SA + C'Z'E + E'ZC = -E'T'Q_TTE \quad (20)$$
$$TST' > 0\ ;\ V'E'SEV = 0 \quad (21)$$
$$Z = T'U_\Gamma \text{ for some } U_\Gamma \in \Re^{q-v\times v} \quad (22)$$

(iii)

$$Ker\,CP \subseteq Ker\,Y \quad (23)$$
$$Ker\,B'S' \subseteq Ker\,Z' \quad (24)$$

Remark 3.1 *Moreover, another approach based on the Lyapunov equation in [10] can be used for obtained the existence of a stabilizing output feedback in the descriptor system. For guarantee the stabilization, the same equations are used with the following conditions $Q = C'C$, and V, W obtained from the theorem 3.1 with Y=WV' and T obtained from the theorem 3.1 such that satisfied the equations 12 and 13.*

This paper shows that based coupled Sylvester equations and the coupled Lyapunov like equations can also be used to obtain the sufficient conditions for the existence of a S-stabilizing output feedback. The Theorem is presented as follows:

Theorem 3.3 *: There exists an output feedback matrix $K : \mathcal{Y} \longrightarrow \mathcal{U}$ such that $\sigma(E, A + BKC) \in \mathcal{C}^-$, if the sufficient following conditions are verified for some positive scalar $v \leq n$ and for some pair of matrices $V \in \Re^{n\times v}$ and $T \in \Re^{q-v\times n}$, that such $TEV = 0$, where $rank\,(EV) = rank\,(TE) = q$:*
(i) Let $Q = C'C$, $Q \in \Re^{n\times n}$, there exist matrices $Pc = Pc' \geq 0$, $Pc \in \Re^{n\times n}$ and $Y = WV' \in \Re^{m\times n}$, such that :

$$APcE' + EPcA' = -EC'CE' \quad (25)$$
$$Pd = V'PcV > 0 \quad ; \quad TEPcE'T' = 0 \quad (26)$$

$$Ker\,CPc \subseteq Ker\,Y \quad (27)$$

Proof:
Sufficiency:
Consider that $(E, A + BKC)$ is S-stable. It is known that there exists an unique symmetric nonnegative definite matrix P, such that

$$(A + BKC)PE' + EP(A + BKC)' - PBR^{-1}B'P + ECQC'E' = 0 \quad (28)$$

for real symmetric nonnegative definite matrix R. For F defined for

$$F = -KC \quad (29)$$

we obtain

$$K'(B'PB + R)K = SS \quad (30)$$

After the substitution from (29) to (26), the equation (28) is obtained. From detectability of (E, A, C) the existence of L such that $(E, A + LC)$ is guaranteed. Thus, also $[\ A+BKC\ [C'\ (KC)']']$ is detectable since

$$A + LC = (A + BKC) + [L\ -B][C'\ (KC)']']$$

Therefore, from (28), considering the previous arguments, the stability $(E, A + BKC)$ is obtained. $\diamond$

4. ALGORITHMIC ASPECTS

The theorem (3.2) is propose in a new numerically efficient solution algorithm to determine the output feedback matrix in descriptor systems.
The resulted algebraic of theorems (3.1) and (3.2) are used for the construction of the subspaces strongly $O.S.$ (C, A, E, B)-invariant leading to the calculation of output feedback matrix K.

4.1. The Syrmos-Lewis algorithm

For the calculation of the output feedback that stabilizes the closed-loop system, when $m + p > q$. The eigenvalues in closed-loop arbitrary assignment near the set $\Lambda = \Lambda_T \dot\cup \Lambda_V$, where $\Lambda_T = \{\lambda_1, \ldots, \lambda_{q-p}\}$ and $\Lambda_V = \{\lambda_{q-p+1}, \ldots, \lambda_q\}$ are symmetrical sets of pre-specified eigenvalues. The system (E, A, B, C) is considered stronlgy controllable and stronlgy detectable [1] .

Step 1:
Choose a matrix $H_T \in \Re^{q-p\times q-p}$ such that $\sigma(H_T) = \Lambda_T \in \mathcal{C}^-$ and solve the Sylvester equation (12) to find the matrix $T \in \Re^{q-p\times n}$, such that

$$rank\left(\left[\begin{array}{c} TE \\ C \end{array}\right]\right) = q \quad (31)$$

Step 2:
Solve the Sylvester equation (11), for some matrix $H_V \in \Re^{p\times p}$ such that $\sigma(H_V) = \Lambda_V \in \mathcal{C}^-$ carrying in consideration which the matrix V has verified the coupling condition (13) and to take it in account which $rank\,(EV) = v$ (or $Ker\,(TE) = Ker\,(E) \oplus Im\,(V)$, where $\oplus$ represents the direct sum) [2].
Step 3:
For the construction, the matrix V has verified that rank $(CV) = p$ and a matrix K is computed by:

$$K \quad = \quad W(CV)^{-1} \tag{32}$$

$\circ$

Remark 4.1 *The steps* 1 *and* 2 *are solving using standart technical for eigenstructure assignment. Consider the matrices* $H_T \in \Re^{q-p\times q-p}$ *and* $H_V \in \Re^{p\times p}$*:˜*

Step 1: *Find* $t_j \in \mathcal{C}^n$ *and* $u_j \in \mathcal{C}^p$*, such that :*

$$\left[\begin{array}{cc} t_j' & u_j' \end{array}\right] \left[\begin{array}{c} A-\lambda_j E \\ C \end{array}\right] = 0 \;\forall\; j = 1,\ldots,q-p \tag{33}$$

As matrix lines $T \in \Re^{(q-p)\times n}$*, denoted by* T_j*, are formed from the vector* t_j*, as follows:*

- *if* $\lambda_j \in \Re$*, then* $T_j = t_j'$*;*
- *if* $\lambda_j \in \mathcal{C}$*, considered* $\lambda_{j+1} = \lambda_j^*$ *and*

$$\left\{\begin{array}{c} T_j = Re\,(t_j') \\ T_{j+1} = Imag\,(t_j') \end{array}\right. .$$

Step 2 :
Determine $v_i \in \mathcal{C}^n$ *and* $w_i \in \mathcal{C}^n$*, such that :*

$$\left[\begin{array}{cc} A-\lambda_i E & B \\ TE & 0 \end{array}\right] \left[\begin{array}{c} v_i \\ w_i \end{array}\right] = 0 \,\forall\, i = q-p+1,\ldots,q \tag{34}$$

The matrices V *and* W *are constructed only with real elements, and it is used to calculate* K*. In particular: if* $\lambda_i \in \mathcal{C}$*, consider* $\lambda_{i+1} = \lambda_i^*$ *and*

$$\left\{\begin{array}{ll} V_i = Re\,(v_i), & V_{i+1} = Imag\,(v_i) \\ W_i = Re\,(w_i), & W_{i+1} = Imag\,(w_i) \end{array}\right. ,$$

where V_i *and* W_i *denoted the columns the matrices* V *and* W*, respectively.*

The degrees of freedom in the choice of V satisfying the coupling condition $TEV = 0$, also can be used to ensure the obtain of K such that $KCV = W$.

[2] The condition (31) guaranteed, in particular, that $rank\,(TE) = q$

4.2. Approach using the Lyapunov Algorithm

From the previous techniques in section 4.1, the step 1 under the condition which the system is strongly detectable is always possible to construct a matrix T that verified the condition (31), using standard technical for eigenstructure assignment. Thus, the $q-p$ finite poles is obtained. The step 2 is solving the equations of Lemma 3.3, where $Pd = V'PcV > 0$ and $TEPcE'T' = 0$. Thus, in the step 3 the other finite poles are obtained with $KCPc = Y$.

Example 4.1 *: Consider the following data [6] :*

$$E = \left[\begin{array}{cccc} 1.00 & 0.00 & 0.00 & 0.00 \\ 0.00 & 0.00 & 1.00 & 0.00 \\ 0.00 & 0.00 & 0.00 & 0.00 \\ 0.00 & 0.00 & 0.00 & 0.00 \\ 0.00 & 0.00 & 0.00 & 0.00 \end{array}\right];$$

$$A = \left[\begin{array}{cccc} 0.00 & 1.00 & 0.00 & 0.00 \\ 0.00 & 0.00 & 0.00 & 1.00 \\ 1.00 & 1.00 & 0.00 & 0.00 \\ 0.00 & -1.00 & 1.00 & 1.00 \end{array}\right]$$

$$B = \left[\begin{array}{cc} 0.00 & 0.00 \\ 0.00 & 0.00 \\ 1.00 & 0.00 \\ 0.00 & 1.00 \end{array}\right];$$

$$C = \left[\begin{array}{cccc} 1 & 0 & 0 & 0 \end{array}\right]$$

The corresponding descriptor system with finite poles is given by:

$$\sigma(E,A) = \{0.0,\, 0.0,\, -1.0\}.$$

The system (C,E,A,B) *is both stronlgy controllable and observable.*

In a first step, the eigenstructure assignment is used to find the eigenvalues that are given for : $\Lambda_T = \{-1\} \cup \Lambda_V = \{-3.5\}$.

Step 1 :
For $\lambda_1 = -1$*, determined* T *that verified (33) and such that (31) is also verified and* (A,B,T,E) *have not invariant zeros :*

$$T = \left[\begin{array}{cccc} 0.00 & 0.00 & 0.7071 & -0.7071 \end{array}\right]$$

Step 2 :
For $\lambda_2 = -3.5$*, determined* V *and* W *using (34) :*

$$V = \left[\begin{array}{c} 0.1762 \\ -0.6167 \\ 0.1626 \\ -0.5693 \end{array}\right];$$

$$W = \left[\begin{array}{c} 0.4405 \\ -0.2101 \end{array}\right];$$

Step 3 :

Determined K such that $KCV = W$:

$$K = \begin{bmatrix} 2.5000 \\ -1.1923 \end{bmatrix};$$

$$A + BKC = \begin{bmatrix} 0.0 & 1.0 & 0.0 & 0.0 \\ 0.0 & 0.0 & 0.0 & 1.0 \\ 3.5000 & 1.0 & 0.0 & 0.0 \\ -1.1923 & -1.0 & 1.0 & 1.0 \end{bmatrix}.$$

The corresponding closed-loop system

$$(E, A + BKC)$$

has the desired generalized eigenvalues.

Example 4.2 *: Consider the result obtained in the previous example. For the construction of the subspace $\mathcal{V} = Im\, V$ is strongly $O.S.$ (C, A, E, B)-invariant in relation the system (1), (2) used in example 4.1.*
In this case, are used $H_V = -3.5$, and $\Pi = 1$, that implies in

$$Q_V = \begin{bmatrix} 1 & 0 \\ 0 & 1 \end{bmatrix}.$$

From the corresponding matrices V and W, it is obtained :

$$P = VV' = \begin{bmatrix} 0.0310 & -0.1087 & 0.0287 & -0.10030 \\ -0.1087 & 0.3803 & -0.1003 & 0.3510 \\ 0.0287 & -0.1003 & 0.0265 & -0.0926 \\ -0.1003 & 0.3510 & -0.0926 & 0.3241 \end{bmatrix};$$

$$Y = WV' = \begin{bmatrix} 0.0776 & -0.2716 & 0.0716 & -0.2507 \\ -0.0370 & 0.1295 & -0.0342 & 0.1196 \end{bmatrix}$$

that verified a part (i) of Theorem 3.2. The corresponding S-stabilizing output feedback,

$$K = \begin{bmatrix} 4.3073 \\ -2.0542 \end{bmatrix}$$

The finite poles in closed-loop system are given by :

$$\sigma(E, A + BKC) = \begin{bmatrix} -5.3073 \\ -1.00 \end{bmatrix}$$

where the eigenvalue -1 corresponds to step 1.
$\triangle$

Example 4.3 *: Consider the result obtained in the previous example (4.1). In the step 1, for $\lambda_1 = -1$, determined T that verified (33) and such that (31). In the step 2, the equations are solving of Theorem (3.3), such that:*

$$Pc = \begin{bmatrix} 0.50 & -0.50 & -0.25 & -0.25 \\ -0.50 & 0.50 & 0.25 & 0.25 \\ -0.25 & 0.25 & 0.25 & -0.00 \\ -0.25 & 0.25 & -0.00 & 0.25 \end{bmatrix};$$

$$Pd = V'PcV = 0.5631$$

The corresponding S-stabilizing output feedback,

$$K = W(CVPd)^{-1}$$

$$K = \begin{bmatrix} 4.4393 \\ -2.1171 \end{bmatrix}$$

The finite poles in closed-loop system are given by :

$$\sigma(E, A + BKC) = \{ -5.4393 , -1.0000 \}$$

where the eigenvalue -1 corresponds to step 1.

5. CONCLUDING REMARKS

Consider the stabilization of control problem by output feedback in descriptor systems. Thus, a new approach for construction the output feedback controller was proposed, and the respective output feedback matrix was obtained through the solution of Sylvester equation. This paper show that based coupled Sylvester equations and the coupled Lyapunov like equations can also be used to obtain sufficient conditions for the existence of a S-stabilizing output feedback. Thus, a theorem was presented for the construction of the output feedback matrix. Some base results had been presented in this paper that basis the algorithms and theoretical results. The characterization of solution Lyapunov Equations in two steps still will be explored in the searche future to obtain poles regional assignment. Aiming some opens questions for future studies among may consider the possible extension of the outlined technique to treat less restrictive cases than the $m + p > q$ case.

References

[1] E. B. Castelan, "Estabilização de Sistemas Descritores por Realimentação de Saídas via Subespaços Invariantes," SBA, Sociedade Brasileira de Automática, Vol. 16 No. 4, pp. 467-477, 2005.

[2] E. B. Castelan, J. C. Hennet and E. R. Ll. Villarreal, "Quadratic Characterization and Use of Output Stabilizable Subspaces," IEEE Trans. Automatic. Control, Vol. 48, No. 4, pp. 654-660, 2003.

[3] E. B. Castelan and J. C. Hennet and E. R. Ll. Villarreal, "Output Feeedback Design by Coupled Lyapunov-Like Equations" (Paper No. 575) 15 th IFAC World Congress on Automatic Control, pp. 1-6, Barcelona, Pr., 2002.

[4] E. B. Castelan and E. R. Ll. Villarreal and Sophie Tarbouriech, "Quadratic Characterization and Use of Output Stabilizable Subspaces in Descriptor Systems," Proceedings 1st IFAC Symposium on System Structure, Prague, pp. 255-260, Praga, 2001.

[5] C. T. Chen, "Linear System Theory and Design," Holt, Rinehart and Winston, 1996.

[6] D. L. Chu and H. C. Chan and D. W. C. Ho, Necessary and Suficient Conditions for the Output Feedback Regularization of Descriptor Systems, *IEEE Trans. Automat. Contr.*, Vol. 44, No. 2, pp. 1457-1468, 1999.

[7] L. Dai, "Singular Control System", Springer-Verlag, 1989.

[8] , G. R. Duan, Eigenstructure assignment in descriptor systems via output feedback: a new complete parametric approach, *Int. J. Control*, Vol.72, No. 4, pp. 345-364, 1999.

[9] L. R. Fletcher, Eigenstructure Assingment by Output Feedback in Descriptor Systems, *IEE Proceedings*, Vol. 135, No. 4, pp. 302-308, 1988.

[10] J. Y. Ishihara and M. H. Terra, "A New Lyapunov equation for Discrete-time Descriptor Systems," American Control Conference, Denver Colorado, USA, Vol. 6 pp. 5078-5082, June 2003.

[11] F. L. Lewis, A Survey of Linear Singular Systems, *Circuits Systems Signal Process*, Vol. 5, No. 1, pp.3-36, 1986.

[12] K. S. Ozcaldiran and F. L. Lewis, On the Regularizability of Singular Systems, *IEEE Trans. Automat. Contr.* Vol. 35 No. 10, pp. 1156-1160, 1990.

[13] V. L. Syrmos and F. L. Lewis, Bilinear Formulation for the Output Feedback Problem in Linear System, *IEEE Trans. Automat. Contr.*, Vol. 39, No. 2, pp. 410-414,1994.

[14] V. L. Syrmos and F. L. Lewis, Output Feedback Eigenstructure Assignment Using Two Sylvester Equations, *IEEE Trans. Automat. Contr.*, Vol. 38, No 3, pp. 495-499, 1993.

[15] E. R. Ll. Villarreal and J. A. R. Vargas and E. M. Hemerly, Static Ouput Feedback stabilization using Invariant Subspaces and Sylvester Equations, *TEMA, Sociedade Brasileira de Matemática Aplicada*, Vol. 10, No. 1, pp. 99-110, 2009.

[16] L. Zhoua and G. Lub, Detection and stabilization for discrete-time descriptor systems via a limited capacity, *Atomática*, Vol. 45, No. 10, pp. 2272-2277, Outober 2009.

ResearchGate

See discussions, stats, and author profiles for this publication at: https://www.researchgate.net/publication/238733803

Approach for stabilization by output feedback, invariant subspace , Lyapunov Equations, and Ricatti Equations

Conference Paper · September 2009

CITATIONS
0

READS
97

2 authors, including:

Elmer ROLANDO LLANOS Villarreal
Universidade Federal Rural do Semi-Árido - UFERSA
77 PUBLICATIONS **138** CITATIONS

SEE PROFILE

All content following this page was uploaded by Elmer ROLANDO LLANOS Villarreal on 23 July 2015.

The user has requested enhancement of the downloaded file.

Approach for stabilization by output feedback, invariant subspace, Lyapunov Equations, and Ricatti Equations

Elmer Rolando Llanos Villarreal
Departamento de Ciências Exatas e Naturais,
Universidade Federal Rural do Semi-Árido, UFERSA,
BR 110, KM 47, 59625-900 Mossoró, RN
E-mail: elmerllanos@ufersa.edu.br

ABSTRACT

The algebraic Riccati equation is either of the following matrix equations:
the continuous time algebraic Riccati equation (CARE):

$$A'P + PA - PBB'P + Q = 0 \tag{1}$$

The use notion invariant subspaces (C, A, B) can be used as an intermediary for the construction of the feedback output. Thus, the paper presented anew approach to the design of output feedback controller is proposed, and the respective output feedback gains are obtained through the solution of a Riccati equation and Lyapunov equation using invariant subspaces.

The considered linear time-invariant system are described by :

$$\dot{x}(t) = Ax(t) + Bu(t) \tag{2}$$
$$y(t) = Cx(t) \tag{3}$$

where : $x \in \mathcal{X} \sim \Re^n$, $u \in \mathcal{U} \sim \Re^m$, $y \in \mathcal{Y} \sim \Re^p$. It is also assumed that B is full column-rank , C is full row-rank and that (C, A, B) is stabilizable and detectable. The studied problem is to find a static output feedback control law

$$u(t) = Gy(t) \quad , \quad G \in \Re^{m \times p} \tag{4}$$

such that $\sigma(A + BGC) \in \mathcal{C}^-$, or equivalently, the closed-loop system is asymptotically stable.

As in [4], some concepts and definitions are used geometric control theory [5]. It is know that an subspace $\mathcal{V} \subset \mathcal{X}$ is (A, B)-invariant if there exists $F : \mathcal{X} \longrightarrow \mathcal{Y}$ such that $(A + BF)\mathcal{V} \subset \mathcal{V}$, or equivalently , $A\mathcal{V} \subset \mathcal{V} + Im\, B$. For dually an subspace $\mathcal{T} \subset \mathcal{X}$ is (C, A)-invariant if exist $L : \mathcal{Y} \longrightarrow \mathcal{X}$ such that $(A + LC)\mathcal{T} \subset \mathcal{T}$, or equivalently, $\mathcal{T} \supset A(\mathcal{T} \cap Ker\,(C))$.

Given the system in the following state-space representation form:

$$\dot{x}(t) = Ax(t) + Bu(t);\ x(0) = x_0 \tag{5}$$
$$y(t) = Cx(t) \tag{6}$$

The next algebraic Riccati equation will play an important role in the analysis below:

$$A'P + PA - PBR^{-1}B'P + C'QC = 0 \tag{7}$$

Then the solution the Riccati equation use the following result in [6]:

Theorem 0.1 *[6] Assume that there exist P and G such that $X = P$ solves (7) with and $R^{-1}B'P = -GC = F$. Then exists for all y_0 and is attained by G. Moreover, conversely, if exists for all x_0, then there exist matrices X and G such that P, X satisfies (7), $\sigma(A - BR^{-1}B'X) \in \mathcal{C}^{-1}$ and $R^{-1}B'P = -GC = F$.*

From Theorem ([6]) that in case the optimization problem has a solution the optimal feedback is unique and given by $G = -R^{-1}B'XC'(CC')^{-1}$.

In The next step is then to verify whether the set linear equations

$$R^{-1}B'P = -GC = F \tag{8}$$

has a solution G.

The theorem (0.2) below relates the concept of (C, A, B)-invariant subspaces for the existence a output feedback control law $u(t) = Gy(t)$ that S-stabilizes the closed loop system.

Theorem 0.2 *Considered the system (2) , (3) with (A, B), stabilizable (C, A) detectable, with C full row rank. There exists an output feedback matrix $G : \mathcal{Y} \longrightarrow \mathcal{U}$, with $F = -GC$ such that $\sigma(A + BGC) \in \mathcal{C}^-$, if and only if the following conditions are verified for some exist $P = P'$ and G such that $X = P$ solves (7) with $Q = Q'$.* $\diamond$

Proof:
Similarly the proof of Theorem in [2], [1].

The following basic procedure is proposed to compute a stabilizing static output feedback when $m + p > n$.

Step 1 :
1.1) Find the decomposition $C \begin{bmatrix} M_1 & M_2 \end{bmatrix} = \begin{bmatrix} \bar{C}_1 & 0 \end{bmatrix}$ and calculate the matrices A_{12}, A_{22}.
1.2) Solve the Lyapunov equation where P_1 is the stabilizing solution of the Riccati equation

$$A'_{11}P_1 + P_1A_{11} - P_1B_1R^{-1}B'_1P_1 + C'_1QC_1 = 0 \tag{9}$$

Step 2 : Then $minJ(G)$ exists for all y_0 and is attained by $G^* = G$. Moreover, $J(G^*) = y'_0Py_0$. and P solves (7).
Step 3 : Calculate the output feedback matrix that stabilizes the closed loop system, as the only solution of $\sigma(A - BR^{-1}B'PC) \in \mathcal{C}^{-1}$ and $R^{-1}B'PC = -BGC$.

Conclusion

Some base results had been presented based in concept of (C, A, B) invariant subspace e its relation with the solution of stabilization problem using output feedback , by Lyapunov equations. Thus in this paper, the output feedback stabilization problem in linear systems was a new approach to the design of output feedback controller, by using the equations Riccati.

Key-words: *Stabilization, Equations Lyapunov and Riccati, Invariant Subspace.*

References

[1] E. B. Castelan and J. C. Hennet and E. R. Ll. Villarreal, Quadratic Characterization and Use of Output Stabilizable Subspaces, *IEEE Trans. Automatic. Control*, vol. 48, number 4, (2003) 654-660.

[2] Elmer R. Llanos Villarreal, *Abordagem Geométrica para Estabilização por Realimentação de Saídas e sua Extensão aos Sistemas Descritores*, Tese de doutorado em Engenharia Elétrica, Universidade Federal de Santa Catarina, 2002.

[3] V. L. Syrmos and F. L. Lewis, Transmission Zero Assignment using Descriptions, *IEEE Trans. Automatic. Control*, vol. 38, number 7, (1993) 1115-1120.

[4] V. L. Syrmos and F. L. Lewis, Bilinear Formulation for the Output Feedback Problem in Linear System, *IEEE Trans. Automatic. Control*, vol. 39, number 2, (1994) 410-414.

[5] W. M. Wonahm, "Linear Multivariable Control, a Geometric Approach", *Springer-Verlag*, 1979.

[6] Jacob Engwerdaa and Arie Weerenb, "A result on output feedback linear quadratic control´´ *Automatica* 44 (2008) 265-271.

View publication stats

ResearchGate

See discussions, stats, and author profiles for this publication at: https://www.researchgate.net/publication/238733803

Approach for stabilization by output feedback, invariant subspace , Lyapunov Equations, and Ricatti Equations

Conference Paper · September 2009

CITATIONS
0

READS
97

2 authors, including:

Elmer ROLANDO LLANOS Villarreal
Universidade Federal Rural do Semi-Árido - UFERSA
77 PUBLICATIONS **138** CITATIONS

SEE PROFILE

All content following this page was uploaded by Elmer ROLANDO LLANOS Villarreal on 23 July 2015.

The user has requested enhancement of the downloaded file.

Approach for stabilization by output feedback, invariant subspace, Lyapunov Equations, and Ricatti Equations

Elmer Rolando Llanos Villarreal
Departamento de Ciências Exatas e Naturais,
Universidade Federal Rural do Semi-Árido, UFERSA,
BR 110, KM 47, 59625-900 Mossoró, RN
E-mail: elmerllanos@ufersa.edu.br

ABSTRACT

The algebraic Riccati equation is either of the following matrix equations:
the continuous time algebraic Riccati equation (CARE):

$$A'P + PA - PBB'P + Q = 0 \tag{1}$$

The use notion invariant subspaces (C, A, B) can be used as an intermediary for the construction of the feedback output. Thus, the paper presented anew approach to the design of output feedback controller is proposed, and the respective output feedback gains are obtained through the solution of a Riccati equation and Lyapunov equation using invariant subspaces.

The considered linear time-invariant system are described by :

$$\dot{x}(t) = Ax(t) + Bu(t) \tag{2}$$
$$y(t) = Cx(t) \tag{3}$$

where : $x \in \mathcal{X} \sim \Re^n$, $u \in \mathcal{U} \sim \Re^m$, $y \in \mathcal{Y} \sim \Re^p$. It is also assumed that B is full column-rank , C is full row-rank and that (C, A, B) is stabilizable and detectable. The studied problem is to find a static output feedback control law

$$u(t) = Gy(t) \quad , \quad G \in \Re^{m \times p} \tag{4}$$

such that $\sigma(A + BGC) \in \mathcal{C}^-$, or equivalently, the closed-loop system is asymptotically stable.

As in [4], some concepts and definitions are used geometric control theory [5]. It is know that an subspace $\mathcal{V} \subset \mathcal{X}$ is (A, B)-invariant if there exists $F : \mathcal{X} \longrightarrow \mathcal{Y}$ such that $(A + BF)\mathcal{V} \subset \mathcal{V}$, or equivalently , $A\mathcal{V} \subset \mathcal{V} + Im\, B$. For dually an subspace $\mathcal{T} \subset \mathcal{X}$ is (C, A)-invariant if exist $L : \mathcal{Y} \longrightarrow \mathcal{X}$ such that $(A + LC)\mathcal{T} \subset \mathcal{T}$, or equivalently, $\mathcal{T} \supset A(\mathcal{T} \cap Ker\,(C))$.

Given the system in the following state-space representation form:

$$\dot{x}(t) = Ax(t) + Bu(t);\ x(0) = x_0 \tag{5}$$
$$y(t) = Cx(t) \tag{6}$$

The next algebraic Riccati equation will play an important role in the analysis below:

$$A'P + PA - PBR^{-1}B'P + C'QC = 0 \tag{7}$$

Then the solution the Riccati equation use the following result in [6]:

Theorem 0.1 *[6] Assume that there exist P and G such that $X = P$ solves (7) with and $R^{-1}B'P = -GC = F$. Then exists for all y_0 and is attained by G. Moreover, conversely, if exists for all x_0, then there exist matrices X and G such that P, X satisfies (7), $\sigma(A - BR^{-1}B'X) \in \mathcal{C}^{-1}$ and $R^{-1}B'P = -GC = F$.*

From Theorem ([6]) that in case the optimization problem has a solution the optimal feedback is unique and given by $G = -R^{-1}B'XC'(CC')^{-1}$.

In The next step is then to verify whether the set linear equations

$$R^{-1}B'P = -GC = F \tag{8}$$

has a solution G.

The theorem (0.2) below relates the concept of (C, A, B)-invariant subspaces for the existence a output feedback control law $u(t) = Gy(t)$ that S-stabilizes the closed loop system.

Theorem 0.2 *Considered the system (2) , (3) with (A, B), stabilizable (C, A) detectable, with C full row rank. There exists an output feedback matrix $G : \mathcal{Y} \longrightarrow \mathcal{U}$, with $F = -GC$ such that $\sigma(A + BGC) \in \mathcal{C}^-$, if and only if the following conditions are verified for some exist $P = P'$ and G such that $X = P$ solves (7) with $Q = Q'$.* $\diamond$

Proof:
Similarly the proof of Theorem in [2], [1].

The following basic procedure is proposed to compute a stabilizing static output feedback when $m + p > n$.

Step 1 :
1.1) Find the decomposition $C \begin{bmatrix} M_1 & M_2 \end{bmatrix} = \begin{bmatrix} \bar{C}_1 & 0 \end{bmatrix}$ and calculate the matrices A_{12}, A_{22}.
1.2) Solve the Lyapunov equation where P_1 is the stabilizing solution of the Riccati equation

$$A'_{11}P_1 + P_1A_{11} - P_1B_1R^{-1}B'_1P_1 + C'_1QC_1 = 0 \tag{9}$$

Step 2 : Then $minJ(G)$ exists for all y_0 and is attained by $G^* = G$. Moreover, $J(G^*) = y'_0Py_0$. and P solves (7).
Step 3 : Calculate the output feedback matrix that stabilizes the closed loop system, as the only solution of $\sigma(A - BR^{-1}B'PC) \in \mathcal{C}^{-1}$ and $R^{-1}B'PC = -BGC$.

Conclusion

Some base results had been presented based in concept of (C, A, B) invariant subspace e its relation with the solution of stabilization problem using output feedback , by Lyapunov equations. Thus in this paper, the output feedback stabilization problem in linear systems was a new approach to the design of output feedback controller, by using the equations Riccati.

Key-words: *Stabilization, Equations Lyapunov and Riccati, Invariant Subspace.*

References

[1] E. B. Castelan and J. C. Hennet and E. R. Ll. Villarreal, Quadratic Characterization and Use of Output Stabilizable Subspaces, *IEEE Trans. Automatic. Control*, vol. 48, number 4, (2003) 654-660.

[2] Elmer R. Llanos Villarreal, *Abordagem Geométrica para Estabilização por Realimentação de Saídas e sua Extensão aos Sistemas Descritores*, Tese de doutorado em Engenharia Elétrica, Universidade Federal de Santa Catarina, 2002.

[3] V. L. Syrmos and F. L. Lewis, Transmission Zero Assignment using Descriptions, *IEEE Trans. Automatic. Control*, vol. 38, number 7, (1993) 1115-1120.

[4] V. L. Syrmos and F. L. Lewis, Bilinear Formulation for the Output Feedback Problem in Linear System, *IEEE Trans. Automatic. Control*, vol. 39, number 2, (1994) 410-414.

[5] W. M. Wonahm, "Linear Multivariable Control, a Geometric Approach", *Springer-Verlag*, 1979.

[6] Jacob Engwerdaa and Arie Weerenb, "A result on output feedback linear quadratic control´´ *Automatica* 44 (2008) 265-271.

View publication stats

Aspect algorithm for stabilization by output feedback, Lyapunov Equations, and Ricatti Equations for class descriptor system

Elmer Rolando Llanos Villarreal
Departamento de Ciências Exatas e Naturais,
Universidade Federal Rural do Semi-Árido, UFERSA,
BR 110, KM 47, CEP:59625-900 Mossoró RN, Brasil
E-mail: elmerllanos@ufersa.edu.br

Abstract

A new approach to the design of output feedback controller is proposed, and the respective output feedback gains are obtained through the solution Riccati equation and Lyapunov equation using invariant subspaces. The objective is to reduce class descriptor system to a normal system, and gain from that change resolved the stabilization problem output feedback in the new system reduced using the Riccati Equation and Lyapunov Equations.
Keywords: Class Descriptor System, Stabilization, Riccati Equation, Lyapunov Equation.

1 Introduction

This paper deals the stabilization problem by static output feedback for class descriptor systems by using Riccati equations and Lyapunov Equations.

The class descriptor systems described by a set differential-algebraic equations in the form :

$$\begin{bmatrix} I_q & 0 \\ 0 & 0 \end{bmatrix}\begin{bmatrix} \dot{x}_1(t) \\ \dot{x}_2(t) \end{bmatrix} = \begin{bmatrix} J_1 & J_2 \\ J_3 & J_4 \end{bmatrix}\begin{bmatrix} x_1(t) \\ x_2(t) \end{bmatrix} + \begin{bmatrix} B_1 \\ 0 \end{bmatrix} u(t) \quad (1)$$

$$y(t) = \begin{bmatrix} C_1 & C_2 \end{bmatrix}\begin{bmatrix} x_1(t) \\ x_2(t) \end{bmatrix} \quad (2)$$

where : $x_1 \in \Re^q$, $x_2 \in \Re^{n-q}$, $u \in \Re^m$ and $y \in \Re^p$; I_q is the identity matrix the finite size q and $J_4 \in \Re^{n-q \times n-q}$ is the invertible matrix. A new approach to the design of output feedback controller is proposed, and the respective output feedback gains are obtained through the solution Riccati equation and Lyapunov equation using invariant subspaces. The objective is to reduce class descriptor system to a normal system, and gain from that change resolved the stabilization problem output feedback in the new system reduced using the Riccati Equation and Lyapunov Equations.

The paper is organized as follows. The second section 2, presents the problem, introduces the basic concepts, the presented in [1], in section 3 is presented the problem output feedback using the Riccati and Lyapunov equations , is formulated an existence theorem for the output feedback matrix. Some conclusive commentaries finally are presented.

2 Preliminaries

The considered descriptor time-invariant systems are described by :

$$\tilde{E}\dot{x}(t) = \tilde{A}x(t) + \tilde{B}u(t) \quad (3)$$

$$y(t) = \tilde{C}x(t) \quad (4)$$

where: $x \in \mathcal{X} \sim \Re^n$, $u \in \mathcal{U} \sim \Re^m$, $y \in \mathcal{Y} \sim \Re^p$ and $\tilde{E} \in \Re^{n \times n}$, $rank\,(\tilde{E}) = q < n$; as the other matrices is an appropriate size with $rank\,(\tilde{B}) = m$ and $rank\,(\tilde{C}) = p$.

The basic problem to be solved is finding a control law for static output feedback for descriptor systems.

Thus considered the system

$$\begin{bmatrix} I_q & 0 \\ 0 & 0 \end{bmatrix}\begin{bmatrix} \dot{z}_1(t) \\ \dot{z}_2(t) \end{bmatrix} = \begin{bmatrix} J_1 - J_2J_4^{-1}J_3 & J_2 \\ 0 & J_4 \end{bmatrix}\begin{bmatrix} z_1(t) \\ z_2(t) \end{bmatrix} + \begin{bmatrix} B_1 \\ 0 \end{bmatrix} u(t) \quad (5)$$

$$y(t) = \begin{bmatrix} C_1 - C_2J_4^{-1}J_3 & C_2 \end{bmatrix}\begin{bmatrix} z_1(t) \\ z_2(t) \end{bmatrix} \quad (6)$$

Thus, using $u(t) = Gy(t)$ for the system (5) , (6), obtained the equivalent representation the loop closed system for new coordinates change:

$$\begin{bmatrix} I_q & 0 \\ 0 & 0 \end{bmatrix}\begin{bmatrix} \dot{z}_1(t) \\ \dot{z}_2(t) \end{bmatrix} = \begin{bmatrix} J_1(G) & J_2(G) \\ 0 & J_4 \end{bmatrix}\begin{bmatrix} z_1(t) \\ z_2(t) \end{bmatrix} \quad (7)$$

where :

$$J_1(G) = (J_1 - J_2J_4^{-1}J_3) + B_1G(C_1 - C_2J_4^{-1}J_3)$$
$$J_2(G) = J_2 + B_1GC_2$$

3 Problem output feedback, Riccati Equations

In this section is considered the normal system, for resolved the class descriptor system. Given a system in the following state-space representation form:

$$\begin{aligned} \dot{x}(t) &= Ax(t) + Bu(t);\ x(0) = x_0 \quad (8) \\ y(t) &= Cx(t) \quad (9) \end{aligned}$$

where the matrices $A = J_1 - J_2 J_4^{-1} J_3$, $B = B_1$ and $C = C_1 - C_2 J_4^{-1} J_3$.

Define the functional $J(G)$ as follows:

$$J(G) = \frac{1}{2}\int_0^T [y'(t)Qy(t) + u'(t)Ru(t)]dt \quad (10)$$

where $u(t) = Gy(t)$ and $\sigma(A+BGC) \in C^-$; Assuming that the matrices Q and R are symmetric and R is positive definite with the positive semi-definite state weighting matrix Q and the positive definite control weighting matrix R.

Furthermore, the next algebraic Riccati equation will play an important role in the analysis below:

$$A'P + PA - PBR^{-1}B'P + C'QC = 0 \quad (11)$$

The next step is then to verify whether the set of linear equations

$$R^{-1}B'P = -GC = F \quad (12)$$

has a solution G in [4], [3].

3.1 Aspect algorithm the Output Feedback matrix

The theorem (3.1) below relates the concept of (C, A, B)-invariant subspaces for the existence of a output feedback control law $u(t) = Gy(t)$ that S-stabilizes the closed loop system.

Theorem 3.1 *Considered the normal system (8) , (9) with (A, B), stabilizable (C, A) detectable, with C full row rank. There exists an output feedback matrix $G : \mathcal{Y} \longrightarrow \mathcal{U}$, with $F = -GC$ such that $\sigma(A + BGC) \in \mathcal{C}^-$, if and only if the following conditions are verified for exist the matrices P and G such that P solves (11) with $Q = Q'$ and $R^{-1}B'P = -GC = F$.* $\diamond$

Proof:
The proof is similar to the proof of Theorem in [1], [2].
The following basic procedure is proposed to compute a stabilizing static output feedback when $m + p > q$.

Step 1 :
Considered the matrices $A = J_1 - J_2 J_4^{-1} J_3$, $B = B_1$ and $C = C_1 - C_2 J_4^{-1} J_3$ in the new normal system.

1.1) Find the decomposition $C\begin{bmatrix} M_1 & M_2 \end{bmatrix} = \begin{bmatrix} \bar{C}_1 & 0 \end{bmatrix}$ and calculate the matrices A_{12}, A_{22}:

$$\begin{bmatrix} A_{12} \\ A_{22} \end{bmatrix} = \begin{bmatrix} \bar{M}_1' \\ \bar{M}_2' \end{bmatrix} AM_2$$

where

$$\begin{bmatrix} M_1 & M_2 \end{bmatrix} \begin{bmatrix} \bar{M}_1' \\ \bar{M}_2' \end{bmatrix} = I_n;$$

1.2) Solve the Lyapunov equation where P_1 is the stabilizing solution of the Riccati equation

$$A_{11}'P_1 + P_1A_{11} - P_1B_1R^{-1}B_1'P_1 + C_1'QC_1 = 0 \quad (13)$$

Step 2 : Then $minJ(G)$ exists for all y_0 and is attained by $G^* = G$. Moreover, $J(G^*) = y_0'Py_0$. and P solves (11).
Step 3 : Calculate the output feedback matrix that stabilizes the closed loop system, as the only solution of $\sigma(A - BR^{-1}B'PC) \in \mathcal{C}^{-1}$ and $R^{-1}B'PC = -BGC$.

4 Conclusion

The main contribution was to present an adaptation of the characterization of the quadratic Lyapunov equations to solve the problem of stabilization for a class of descriptor systems with the aid of Riccati equations. Thus in this paper, the problem of output feedback stabilization of linear systems was a new approach to the design of output feedback controller by using Riccati equation.

References

[1] Elmer R. Llanos Villarreal, *Abordagem Geométrica para Estabilização por Realimentação de Saídas e sua Extensão aos Sistemas Descritores*, Tese de doutorado em Engenharia Elétrica, Universidade Federal de Santa Catarina, 2002.

[2] E. B. Castelan and J. C. Hennet and E. R. Ll. Villarreal, Quadratic Characterization and Use of Output Stabilizable Subspaces, *IEEE Trans. Automatic. Control*, vol. 48, number 4, (2003) 654-660.

[3] Jacob Engwerdaa and Arie Weerenb, "A result on output feedback linear quadratic control?? *Automatica* 44 (2008) 265-271.

[4] Adam Czornik*, Aleksander Nawrat, Andrzej Swierniak, "Bounds and sensitivity analysis for the solution of coupled algebraic Riccati equation?? , *conference/iccam2004*, Poland, 2004.

ResearchGate

See discussions, stats, and author profiles for this publication at: https://www.researchgate.net/publication/327468088

Approach For Stabilization by Output Feedback, Invariant Subspaces and Sylvester Equations

Conference Paper · September 2008

CITATIONS
0

READS
26

2 authors, including:

Elmer ROLANDO LLANOS Villarreal
Universidade Federal Rural do Semi-Árido - UFERSA
77 PUBLICATIONS **138** CITATIONS

SEE PROFILE

All content following this page was uploaded by Elmer ROLANDO LLANOS Villarreal on 29 May 2019.

The user has requested enhancement of the downloaded file.

Approach for stabilization by output feedback, invariant subspaces and Sylvester equations

Elmer Rolando Llanos Villarreal *
Departamento de Informática, FANAT,
Universidade do Estado do Rio Grande do Norte,
CEP:59610-090 , Campus Universitário Central, Setor II
BR 110, KM 48, Rua Prof. Antônio Campos, Costa e Silva, Mossoró, RN
E-mail: evillarrea@hotmail.com,

João de Deus Lima
Departamento de Matemática, FANAT,
Universidade do Estado do Rio Grande do Norte,
CEP:59610-090,Campus Universitário Central, Setor II
BR 110, KM 48, Rua Prof. Antônio Campos, Costa e Silva, Mossoró, RN
E-mail: jddeus@uol.com.br

1 Introduction

A system is continuous time when all the variables of the system are known in every moment of time. A control system is called invariant time when its parameters are stationary with respect to time. The representation will be through systems of state equations.

The Sylvester equations play an important role in numerical linear algebra. For example, they arise in the computation of invariant subspaces, in control problems, as linearizations of algebraic Riccati equations, and in the discretization of partial differential equations. For small systems, direct methods are feasible.

This article deals with the problems of stabilization and of regional pole placement by static output feedback in linear continuous-time systems. The results are based on the key notion of (C,A,B)-invariant subspaces which can be characterized through a pair of coupled Sylvester equations. Then, solutions to these equations can be obtained, for systems verifying Kimura's condition ($m + p > n$), into two steps using Syrmos and Lewis's algorithm.

The considered linear time-invariant system are described by :

$$\dot{x}(t) = Ax(t) + Bu(t) \quad (1)$$
$$y(t) = Cx(t) \quad (2)$$

where : $x \in \mathcal{X} \sim \Re^n$, $u \in \mathcal{U} \sim \Re^m$, $y \in \mathcal{Y} \sim \Re^p$.It is also assumed that B is full column-rank , C is full row-rank and that (C, A, B) is stabilizable and detectable. The studied problem is to find a static output feedback control law

$$u(t) = Gy(t) \quad , \quad G \in \Re^{m \times p} \quad (3)$$

such that $\sigma(A + BGC) \in \mathcal{C}^-$, or equivalently, the closed-loop system is asymptotically stable. That is: , where $\sigma(A + BGC) = \{\lambda_1, \lambda_2, \ldots, \lambda_n\}$ is the set of eigenvalues of $A + BGC$.

This presents the basic concepts of theory of geometric control theory that base the approach adopted for the solution of the problem [11], [13]. The coupled Sylvester equation are interpreted on the basis of geometric control theory. Thus, through these equations, the stabilization problem using output feedback can be decomposed in two stages [9]: (i) determination of a (C, A)-outer detectable subspace, and (ii) inner stabilization of this subspace.

In the search of solutions for the stabilization problem they are argued and they presented procedures for the solution of these coupled equations, with emphasis in techniques of eigenstruture assignment [1] [9]. Thus, it is introduced notion of $O.S.$ (C, A, B)-invariant subspace and presented the coupled Sylvester equation. Thus too presented the algorithmic aspects, illustrating them with numerical examples. Some conclusive commentaries finally are presented.

2 Invariant Subspaces and coupled Sylvester Equations

As in [11], some concepts and definitions are used of geometric control theory [13]. It is know that an subespace $\mathcal{V} \subset \mathcal{X}$ is (A, B)-invariant if there exists $F : \mathcal{X} \longrightarrow \mathcal{Y}$ such that $(A + BF)\mathcal{V} \subset \mathcal{V}$, or equivalently , $A\mathcal{V} \subset \mathcal{V} + Im\, B$. For dually an subspace $\mathcal{T} \subset \mathcal{X}$ is (C, A)-invariant if exist $L : \mathcal{Y} \longrightarrow \mathcal{X}$ such that $(A + LC)\mathcal{T} \subset \mathcal{T}$, or equivalently, $\mathcal{T} \supset A(\mathcal{T} \cap Ker\,(C))$.

*Researcher DCR, this work has been supported by FAPERN/CNPq

Definition 2.1 *[11] An subspace $\mathcal{V} \subset \mathcal{X}$, of dimension v , is (C, A, B)-invariant if $\mathcal{V}$ is (A, B)-invariant and (C, A)-invariant.*

Consider $V \in \Re^{v \times v}$ such that $Im(V) = \mathcal{V}$ and consider $T \in \Re^{(n-v)\times v}$ an left annihilator of V, *i.e.* : $Ker(T) = Im(V)$. The definition 2.1 is equivalent an existence of matrices ($H_V \in \Re^{v\times v}$, $W \in \Re^{m\times v}$) and ($H_T \in \Re^{n-v\times n-v}$, $U \in \Re^{(n-v)\times v}$), solutions for the following *coupled Sylvester Equations*:

$$AV - VH_V = -BW \quad (4)$$
$$TA - H_T T = -UC \quad (5)$$
$$TV = 0 \quad (6)$$

An definition 2.1 and the equations (4) , (5) and (6) they have a basic importance in the treatment of the control problem using static output feedback, mainly for Eigenstructure Assignment [9] [11]. The present study it takes in account the properties of stabilizability and detectability, through the two definition to follow:
(i) an subspace (A, B)-invariant $\mathcal{V}$ is (A, B)-inner stabilizable subspace, that is there exist F such that $(A + BF)|\mathcal{V}$ is asymptotically stable; and
(ii) an subspace (C, A)-invariant $\mathcal{V}$ is (C, A)-outer detectable subspace if there exist L such that $(A + LC)|\mathcal{X}/\mathcal{V}$ is asymtotically stable.

Definition 2.2 *[11] An subspace $\mathcal{V}$, of dimension v, is (C, A, B)-invariant output stabilizable subspace , (or simply O.S. (C, A, B)-invariant [1]) if $\mathcal{V}$ is (A, B)-inner stabilizable and (C, A)-outer detectable.*

Thus, a necessary and sufficient condition for the existence $\mathcal{V} = Im(V)$ subspace either *O.S.* (C, A, B)-invariant subspace is that (4), (5) and (6) they are verified with the conditions additional of stability :

$$\sigma(H_V) \in \mathcal{C}^- \quad (7)$$
$$\sigma(H_T) \in \mathcal{C}^- \quad (8)$$

A Theorem to follow it relates the concept of *O.S.* (C, A, B)-invariant subspace to the existence of a law of control of the type static output feedback (3) that it stabilizes the system in closed loop.

Theorem 2.1 *There exists an output feedback matrix $G : \mathcal{Y} \longrightarrow \mathcal{U}$ such that $\sigma(A + BGC) \in \mathcal{C}^-$, if and only if the following conditions are verified for some matrices ($V \in \Re^{n\times v}, H_V \in \Re^{v\times v}, W \in \Re^{m\times v}$), ($T \in \Re^{n-v\times n}, H_T \in \Re^{n-v\times n-v}, U \in \Re^{n-v\times v}$) to some scale positive $v \leq n$:*

$$AV - VH_V = -BW, \text{ with } \sigma(H_V) \in \mathcal{C}^- \quad (9)$$
$$TA - H_T T = -UC, \text{ with } \sigma(H_T) \in \mathcal{C}^- \quad (10)$$
$$TV = 0 \quad (11)$$
$$Ker(CV) \subseteq Ker(W) \quad (12)$$
$$Ker(B'T') \subseteq Ker(U') \quad (13)$$

where: $rank(V) = v$ e $rank(T) = n - v$. $\diamond$

It is important to notice that these results have been presented and explored under different forms in the literature related to the eigenstruture assignment by output feebaback (see [12]). The presented statement corresponds to the statement of the Theorem 3.2 de [11]. As it was seen, the *coupled Sylvester Equations* (9), (10) e (11) describe some geometric properties of subspace $\mathcal{V} = Im(V)$. Under the restriction of imposed stability a matrix H_V, the equation (9) means that the subspace $\mathcal{V} = Im(V)$ must be (A, B)-inner stabilizable subspace; In a dual manner, (10) means that the subspace $Ker(T) = \mathcal{V}$ must be (C, A)-outer detectable subspace. Thus, under the coupling condition (11), is had that the existence of $\mathcal{V} = Ker(T)$ *O.S.* (C, A, B)-invariant subspace,with the conditions you add (12) and (13) is a necessary and suficient condition for the existence solution of the considered problem. Also notices that the conditions (12) and (13) correspond to the existence of a matrix $G \in \Re^{m\times p}$ that it verifies the two following equalities:

$$GCV = W \quad (14)$$
$$TBG = U \quad (15)$$

Is important to observe that guaranteed the existence of solution for the Sylvester equations and that G has been gotten such that (14) (or 15) either verified, the eigenvalues in closed loop are given by:

$$\sigma(A + BGC) = \sigma(H_V) \dot{\cup} \sigma(H_T)$$

3 Algorithmic aspects

The established matrices conditions in the Theorem 2.1 are nonlinear in relation to the matrices variable (V, H_V, W, T, H_T, U). In particular, the terms nonlinear VH_V and $H_T T$ presented in (9) and (10), respectively, can be linear when fixing the matrices H_V and H_T, or equivalent when defining itself the eigenvalues desired for the system in closed loop.

In this section the basic procedure based in two algorithmic techniques of eigenstructure assignment for the attainment a output feedback are presented. The first technique, the algoritm proposed for Syrmos and Lewis in [9]

[1] Output Stabilizable (C,A,B)-invariant [11] [3]

solves the coupled Sylvester equations in two steps and it can directly be applied the systems that verify the condition $m + p > n$, known as condition of Kimura [8]. The second technique, the algorithm proposed for Paraskevopoulos in [1], uses a representation of the system in an adequate base of the state space, to rewrite the coupled Sylvester equations in the form of a set bilinear algebraic equations. In the two techniques, it is assumed that the dimension of $\mathcal{V} = Im\,(V)$ is equal to the number of output p, looking guaranteeing that a matrix $CV \in \Re^{p\times p}$ either invertible and, therefore, that the gain feedback matrix can be found, from (14), under the form $G = W(CV)^{-1}$.

In the sequence, it is considered system represented (C, A, B) is controlable and observable, is this necessary condition for the arbitrary choice of poles to be located in closed loop. This condition can be however to be relaxed for stabilizable and detectabilizable of (C, A, B), what it implies in the use of the non-controlable eigenvalues and non-observable in the spectrum desired for the system in closed loop.

In both the techniques to be presented, are considered that the set of poles desired is denoted by $\Lambda = \{\lambda_1, \ldots, \lambda_{n-p}, \lambda_{n-p+1}, \ldots, \lambda_n\} = \{\Lambda_T, \Lambda_V\}$ where Λ_T and Λ_V are auto-conjugated. These sets are associated the matrices $H_V \in \Re^{p\times p}$ and $H_T \in \Re^{(n-p)\times(n-p)}$ in the following form: $\sigma(H_T) = \Lambda_T = \{\lambda_1, \ldots, \lambda_{n-p}\}$ e $\sigma(H_V) = \Lambda_V = \{\lambda_{n-p+1}, \ldots, \lambda_n\}$. For simplicity, it is considered that the elements of $\Lambda = \sigma(A + BGC)$ are distinct.

3.1 Modified algorithm of Syrmos and Lewis

Based in the express conditions through Theorem 2.1, the following algorithm, considered in [9], generally it leads to a output feedback matrix that stabilizes the system in closed loop when the Kimura's condition $n < m + p$ is verified:

Step 1: It chooses the matrix $H_T \in \Re^{n-p\times n-p}$ such that $\sigma(H_T) = \Lambda_T \in \mathcal{C}^-$ and solve the Sylvester equation (10) for find an matrix $T \in \Re^{n-p\times n}$ such that

$$rank\left(\begin{bmatrix} T \\ C \end{bmatrix}\right) = n \Longleftrightarrow Ker\,T \cap Ker\,C = \{0\} \quad (16)$$

Step 2: Solve the Sylvester equation (9), for some matrix $H_V \in \Re^{p\times p}$ such that $\sigma(H_V) = \Lambda_V \in \mathcal{C}^-$ leading in consideration that the matrix V must verify the coupling condition (11) and that $rank\,(V)$ must be equal p.

Step 3: For construction, the relation (16) guarantees that the rank $(CV) = p$ and the matrix G can be calculated as only solution of (14).

∘

Is presented to follow it some comments with the double objective to show relative aspects to the numerical solution of steps algorithm and to justify them theoretically.

Remark 1.1 : The steps 1 and 2 can be resolved using techniques standards for eigenstructure assignment. Considering the matrices H_T e H_V in the diagonal form of Jordan, the following procedure can be adopted:

Step 1: Find $t_j \in \mathcal{C}^n$ and $u_j \in \mathcal{C}^p$, such that :

$$\begin{bmatrix} t_j' & u_j' \end{bmatrix}\begin{bmatrix} A-\lambda_j I \\ C \end{bmatrix} = 0 \;\forall\; j = 1, \ldots, n-p \quad (17)$$

The row matrix $T \in \Re^{(n-p)\times n}$, denoted for T_j, are formed from the vectors t_j, as follows :

- if $\lambda_j \in \Re$, then $T_j = t_j'$;
- if $\lambda_j \in \mathcal{C}$, is considered $\lambda_{j+1} = \lambda_j^*$ and $\begin{cases} T_j = Re\,(t_j') \\ T_{j+1} = Imag\,(t_j') \end{cases}$.

Step 2 : To determine $v_i \in \mathcal{C}^n$ and $w_i \in \mathcal{C}^n$ such that :

$$\begin{bmatrix} A-\lambda_i I & B \\ T & 0 \end{bmatrix}\begin{bmatrix} v_i \\ w_i \end{bmatrix} = 0 \;\forall\; i = n-p+1, \ldots, n \quad (18)$$

In similar form to the previous case, the used matrices V and W for the calculation of K can only be built with real elements. In particular: if $\lambda_i \in \mathcal{C}$, is considered $\lambda_{i+1} = \lambda_i^*$ and $\begin{cases} V_i = Re\,(v_i), & V_{i+1} = Imag\,(v_i) \\ W_i = Re\,(w_i), & W_{i+1} = Imag\,(w_i) \end{cases}$, where v_i and w_i denote the columns of the matrices V and W, respectively .

Remark 1.2: [4] In the step 1, under the observability (detectability) condition it is always possible to build to a matrix T that verifies condition (17) and that, therefore, it guarantees the obtaining of K saw (14). Once certain the matrix T, the step 2 is associated with the joint solution of the equations (9) and (11), or either to (A,B)-invariance of $Ker\,(T)$. This property is associated then to the "zero equation" (18) [2]. To guarantee that the eigenvalues λ_i of step 2 are freely assignable, the system matrix $P(\lambda) = \begin{bmatrix} A-\lambda I & B \\ T & 0 \end{bmatrix}$ of dimension $(2n-p)\times(n+m)$, must have complete rank for row $\forall\lambda$. The algorithm above is based in the fact that under the condition $m+p > n$, the system matrix $P(\lambda)$ it does not have loss of rank for almost all the triples (A, B, T) [10]. Thus the zero equation (18) has solutions for all λ_i. In the cases where it will have the presence of invariant zeros is possible to remake the Step 1 on the search of other solutions for the Sylvester equation (9).

Remark 1.3: In the less restrictive case

$m + p = n$, the system $P(\lambda)$ of dimension $(2n - p) \times (2n - p)$, is an square matrix and almost all the triples (A, B, T) have p invariant zeros finite stable [9]. In this case, the basic procedure can produce to a output feedback matrix that stabilizes the system in closed loop only if the matrix T, found in step 1, generate p stable invariant zeros which should be used to solve the equation (18) [2].

Example 3.1 *: Consider an linear system (1), (2), defined for [7]:*

$$A = \begin{bmatrix} 0 & 1 & 0 & 0 \\ 1 & 1 & 0 & 0 \\ -1 & 0 & 0 & 0 \\ 0 & 0 & 0 & 0 \end{bmatrix} \quad ; \quad B = \begin{bmatrix} 0 & 0 \\ 1 & 0 \\ 0 & 0 \\ 0 & 1 \end{bmatrix}$$

$$C = \begin{bmatrix} 1 & 0 & 0 & 0 \\ 0 & 0 & 1 & 0 \\ 0 & 0 & 0 & 1 \end{bmatrix}$$

The corresponding system is controllable and observable and $m + p = 5 > n$. The eigenvalues to assignment are given for : $\Lambda_T = \{-4\}$ $\cup\, \Lambda_V = \{-3, -2 + 2j, -2 - 2j\}$.
Step 1 : *For $\lambda_1 = -4$, determined T that verifies (17) and such that (A, B, T) not have zeros invariant :*

$$T = [\ -0.3148 \quad 0.0630 \quad -0.2406 \quad -0.2425\ ];$$

Step 2 : *For $\lambda_2 = -3$, $\lambda_3 = -2 + 2j$ and $\lambda_4 = -2 - 2j$, determined V and W using (18) :*

$$V = \begin{bmatrix} 0.0727 & 0.0564 & 0.0594 \\ -0.2182 & -0.2315 & -0.0061 \\ 0.0242 & -0.0008 & 0.0289 \\ -0.1751 & -0.1325 & -0.1074 \end{bmatrix},$$

$$W = \begin{bmatrix} 0.8000 & 0.6504 & -0.5041 \\ 0.5252 & 0.4797 & -0.0502 \end{bmatrix}$$

Step 3 : *Determined G such that $GCV = W$:*

$$G = \begin{bmatrix} -61.0000 & -6.5685 & -30.8197 \\ -19.7741 & -5.6724 & -12.0000 \end{bmatrix}$$

The matrix in loop closed $A_G = A + BGC$ correspondent, whose the eigenvalues are the desired, is :

$$A_G = \begin{bmatrix} 0.0000 & 1.0000 & 0.0000 & 0.0000 \\ -60.0000 & 1.0000 & -6.5685 & -30.8197 \\ -1.0000 & 0.0000 & 0.0000 & 0.0000 \\ -19.7741 & 0.0000 & -5.6724 & -12.0000 \end{bmatrix}.$$

$\triangle$

3.2 Algorithm of Paraskevopoulos

The presented technique to follow is based on the use of a transformation of coordinates, gotten from a decomposition of the matrix C, that it allows to solve the equation (17) saw a system auxiliary of reduced order $n - p$.

This type of decomposition is used in the theory of control mainly for the construction of observers of minimum order [1] [5]. Geometric point of view, it it aims at the construction subspace $\mathcal{V} = Ker\,(T)$ outer stabilizable and the guarantee of the relation $Ker\,(T) \cap Ker\,(C) = \{0\}$.

Consider a base change given for

$$x = [\ P_1 \quad P_2\ ] \begin{bmatrix} x_1 \\ x_2 \end{bmatrix} \qquad (19)$$
$$P_1 \in \Re^{n \times p}, \quad P_2 \in \Re^{n \times n-p}$$

where $P = [\ P_1 \quad P_2\ ]$ is not singular matrix such that:

$$C\,[\ P_1 \quad P_2\ ] = [\ C_1 \quad 0\ ]\ , \qquad (20)$$
$$\text{with} \quad C_1 \in \Re^{p \times p} \quad \text{and} \quad rank(C_1) = p$$

The inverse of the matrix P é denoted for $\bar{P} = \begin{bmatrix} \bar{P}_1' \\ \bar{P}_2' \end{bmatrix}$, with $\bar{P}_1 \in \Re^{n \times p}$, $\bar{P}_2 \in \Re^{n \times n-p}$:
$[\ P_1 \quad P_2\ ] \begin{bmatrix} \bar{P}_1' \\ \bar{P}_2' \end{bmatrix} = I_n$.

In this base, the system in open loop takes the form

$$\begin{bmatrix} \dot{x_1}(t) \\ \dot{x_2}(t) \end{bmatrix} = \begin{bmatrix} A_{11} & A_{12} \\ A_{21} & A_{22} \end{bmatrix} \begin{bmatrix} x_1(t) \\ x_2(t) \end{bmatrix} + \begin{bmatrix} B_1 \\ B_2 \end{bmatrix} u(t)$$
$$y(t) = [\ C_1 \quad 0\ ] \begin{bmatrix} x_1(t) \\ x_2(t) \end{bmatrix} \qquad (21)$$

where, in particular, $A_{12} \in \Re^{p \times n-p}$ and $A_{22} \in \Re^{n-p \times n-p}$.

Lemma 3.1 *If (C, A) is observable, then always exists $T \in \Re^{n-p \times p}$ such that the equation (10) is verified and $Ker\,(T) \cap Ker\,(C) = \{0\}$.*

Proof:
As shown in [5], the observability of the pair (C, A) is equivalent to the observability of the pair (A_{12}, A_{22}) defined from the change base express in (19). They are the matrices $T_2 \in \Re^{(n-p) \times (n-p)}$, with $posto\,(T_2) = n - p$, and $T_1 \in \Re^{(n-p) \times p}$, solutions of Sylvester equations of *order-reduced*

$$T_2 A_{22} - H_T T_2 = -T_1 A_{12}\ , \ \sigma(H_T) \in \mathcal{C}^- \quad (22)$$

where the matrix $H_T \in \Re^{n-p \times n-p}$ is chosen such that $\sigma(H_T) \in \mathcal{C}^-$. Is important to observe that generally it is possible to find T_2 invertible when H_T does not contain the eigenvalues of the matrix A_{22} [1]. Can then, to calculate, $U \in \Re^{n-p \times p}$ as the only solution of:

$$UC_1 = -\left(T_1 A_{11} + T_2 A_{21} - H_T T_1\right) \qquad (23)$$

Jointly, (22) and (23) verify:

$$\left[\begin{array}{cc} T_1 & T_2 \end{array}\right]\left[\begin{array}{cc} A_{11} & A_{12} \\ A_{21} & A_{22} \end{array}\right] - H_T\left[\begin{array}{cc} T_1 & T_2 \end{array}\right] = U\left[\begin{array}{cc} C_1 & 0 \end{array}\right]$$

that, in the original base, it corresponds to Sylvester equation (10). Moreover, as T_2 is invertible, is had:

$$rank\left(\left[\begin{array}{c} T \\ C \end{array}\right] = \left[\begin{array}{cc} T_1 & T_2 \\ C_1 & 0 \end{array}\right]\left[\begin{array}{c} \bar{P}_1' \\ \bar{P}_2' \end{array}\right]\right) = n \Longleftrightarrow Ker\,(T) \cap Ker\,(C) = \{0\}.$$

$\diamond$

The equations (10) and (22) are related to the construction of observers of minimum order [5] [1].

It can, in particular, to associate the eigenvalues of H_T to the eigenvalues of $(A_{22}+L_2A_{12})$ where $L_2 \in \Re^{n-p\times p}$ is such that

$$T_2L_2 = T_1 \tag{24}$$

Thus, substituting (24) in (22) is had

$$T_2(A_{22} + L_2A_{12}) = H_TT_2 \tag{25}$$

or either

$$\sigma(H_T) = \sigma(A_{22} + L_2A_{12}) \in \mathcal{C}$$

Is important to observe that the decomposition $\bar{P}$ used it is not only. In particular, it can computational be gotten through ortogonal transformations, $\bar{P} = P'$ [1] [3].

The Lemma 3.1 can, in particular, to be used to carry through the step 1 Syrmos and Lewis algorithm, presented in the previous section. In this section, it will be used to enunciate the Theorem 2.1 in presented alternative form originally for Paraskevopoulos algorithm in [1].

Theorem 3.1 *Given the system (1), (2),considers a decomposition in the form (21). Either G the output feedback express for* $G = W(CV)^{-1}$. *Then the matrix G verifies* $\sigma(A + BGC) = \sigma(H_V) \dot{\cup} \sigma(H_T)$, *if and only if*

$$\left[\begin{array}{cc} T_1 & T_2 \end{array}\right]\left[\begin{array}{c} \bar{P}_1' \\ \bar{P}_2' \end{array}\right]V = 0 \tag{26}$$

where the matrices $(W \in \Re^{m\times p}, V \in \Re^{n\times p})$ *and* $(T_1 \in \Re^{n-p\times p}, T_2 \in \Re^{n-p\times n-p})$ *satisfy the Sylvester equation (9) and (22),respectively, with* $det\,(CV) \neq 0$.

From the formularization presented in the Theorem 3.1 above, the following procedure is suggested in [1] to get poles assignment when $mp \geq n$.

3.2.1 Procedure for the determination of output feedback matrix

Considering that H_V and H_T are matrices in the diagonal form of Jordan, from (9) can be written W e V in the form

$$W = \left[\begin{array}{cccc} w_1, & w_2, & \ldots, & w_p \end{array}\right]; \tag{27}$$

$$V = \left[\begin{array}{cccc} X^1w_1, & X^2w_2, & \ldots, & X^pw_p \end{array}\right] \tag{28}$$

where

$$X^i = (\lambda_iI - A)^{-1}B, \quad for \quad i = 1, \ldots, p \tag{29}$$

In the same way, from (22) the matrices T_1 and T_2 have the form

$$T_1 = \left[\begin{array}{c} \phi_{p+1}' \\ \phi_{p+2}' \\ \vdots \\ \phi_n' \end{array}\right] \quad and \quad T_2 = \left[\begin{array}{c} \psi_{p+1}' \\ \psi_{p+2}' \\ \vdots \\ \psi_n' \end{array}\right]$$

where ψ_j , $\forall j = p+1, \ldots, n$, can be gotten of:

$$\psi_j' = \phi' A_{12}(\lambda_jI - A_{22})^{-1} \tag{30}$$

From the notation above, the coupling equation (26) can be written in the form of a bilinear system algebraic equations. Thus, substituting (29) and (30) in (26), is had:

$$\phi_j'\left[\begin{array}{cc} I_p & A_{12}[\lambda_jI - A_{22}]^{-1} \end{array}\right]\left[\begin{array}{c} \bar{P}_1' \\ \bar{P}_2' \end{array}\right]X^iw_i = 0 \tag{31}$$

$$for \quad i = 1, , \ldots, p \quad and \quad j = p+1, \ldots, n$$

Solving the equation (31), the parameters are determined for w_i and ϕ_j'. Then, the matrices W and V are defined from the equation (27)and the output feedback matrix G is directly calculated of (14).

From this formularization, the justification to follow is given in [1] for the obtainment of condition less restrictive $mp \geq n$ for arbitrary poles positioning for output feedback: "The equation (27)provides $p(m-1)$ free parameters (from the arbitrary elements of $w_1, w_2, \ldots, w_p$). Additionally the equation (30) provides $(p-1)(n-p)$ free parameters (from the arbitrary elements of $\phi_{p+1}, \phi_{p+2}, \ldots, \phi_n$). On the other hand the equation (31) results in a system of $p(n-p)$ independent equations. Thus for the solution existence, the number of equations must be equal or smaller that the addition of the free parameters. After algebraic manipulations it is gotten condition $mp \geq n$" .

Example 3.2 *: To follow, the procedure of Paraskevopoulos is applied to get the poles assignment for the system defined for A and B, used in the previous example. Is considered in this that only* 2 *states are measurable or either:*

$$C = \begin{bmatrix} 0 & 0 & 1 & 0 \\ 0 & 0 & 0 & 1 \end{bmatrix}$$

The corresponding system is controllable and observable being $mp = 4 = n$, *com* $p = 2$ *e* $m = 2$. *The eigenvalues to assignment are* $\Lambda_V = \{-1, -2\}$ *and* $\Lambda_T = \{-3, -4\}$.

In first place it finds a decomposition

$$P = \begin{bmatrix} 0 & 0 & 1 & 0 \\ 0 & 0 & 0 & 1 \\ 1 & 0 & 0 & 0 \\ 0 & 1 & 0 & 0 \end{bmatrix}$$

using (21) such that:

$$C \begin{bmatrix} P_1 & P_2 \end{bmatrix} = \begin{bmatrix} \bar{C}_1 & 0 \end{bmatrix} = \begin{bmatrix} 1 & 0 & 0 & 0 \\ 0 & 1 & 0 & 0 \end{bmatrix}$$

and is calculated

$$\begin{bmatrix} A_{12} \\ A_{22} \end{bmatrix} = \begin{bmatrix} \bar{P}_1' \\ \bar{P}_2' \end{bmatrix} AP_2 = \begin{bmatrix} 0 & 0 \\ -1 & 0 \\ 0 & 1 \\ 0 & 0 \end{bmatrix}.$$

For $\lambda_1 = -1, \lambda_2 = -2$,*we fix the 2 free parameters in* $\begin{bmatrix} w_1 & w_2 \end{bmatrix} = \begin{bmatrix} 1.0 & 1.0 \\ w_{12} & w_{22} \end{bmatrix}$,*to get* $w_{12} = -2.2$ *and* $w_{22} = 2.8$. *On the other hand for* $\lambda_3 = -3, \lambda_4 = -4$, *we fix the 2 free parameters in* $\begin{bmatrix} \phi_3' \\ \phi_4' \end{bmatrix} = \begin{bmatrix} 1.0000 & \phi_{32} \\ 1.0000 & \phi_{42} \end{bmatrix}$, *to get* $\phi_{32} = -1.6364$ *and* $\phi_{42} = -1.8824$. *In this form the matrices are determined* (W, V) *and* (T_1, T_2, T) *that satisfies the Sylvester equations (9), (22) and (31),respectively with* $det(CV) \neq 0$*:*

$$V = \begin{bmatrix} 0.6 & -0.8 \\ -1.6 & 0.6 \\ 1.6 & -1.2 \\ 0.6 & -0.4 \end{bmatrix} \quad ; \quad W = \begin{bmatrix} 1.0 & 1.0 \\ -2.2 & 2.8 \end{bmatrix}$$

$$T_1 = \begin{bmatrix} 1.0000 & -1.6364 \\ 1.0000 & -1.8824 \end{bmatrix}; T_2 = \begin{bmatrix} -0.5455 & 0.1818 \\ -0.4706 & 0.1176 \end{bmatrix}$$

$$T = \begin{bmatrix} T_1 & T_2 \end{bmatrix} \begin{bmatrix} \bar{P}_1' \\ \bar{P}_2' \end{bmatrix}$$

$$T = \begin{bmatrix} -0.5455 & 0.1818 & 1.0000 & -1.6364 \\ -0.4706 & 0.1176 & 1.0000 & -1.8824 \end{bmatrix}$$

The system (A, B, T) *has as invariant zeros and stable eigenvalues:* $\{-1, -2\}$. *The output feedback matrix correspondent* G *is determined by* $GCV = W$*:*

$$G = \begin{bmatrix} -12.5 & 35.0 \\ -10.0 & 23.0 \end{bmatrix}$$

The matrix in closed loop $A_G = A + BGC$ *correspondent,whose the eigenvalues are the desired , it is:*

$$A_G = \begin{bmatrix} 0.0 & 1.0 & -12.5 & 35.0 \\ 0.0 & 0.0 & 1.0 & 0.0 \\ 0.0 & 0.0 & -10.0 & 24.0 \\ -1.0 & 0.0 & 0.0 & 0.0 \end{bmatrix}.$$

$\triangle$

4 Conclusion

Some base results had been presented in this article that basis the algorithms and theoretical results. The concept of subspace was presented $O.S.$ (C, A, B)-invariant e its relation with the solution of stabilization problem using output feedback , by two coupled Sylvester equations.

Is distinguished the fact of the algorithm of Syrmos modified to allow to the solution of the problem in 2 sequence steps, for systems that verify the condition of Kimura $(m + p > n)$. As the algorithm, is based on the solution of a system of bilinear equations for the attainment of poles assignment, having been able to be applied the systems that verify the condition less restrictive $mp \geq n$.

The character of solution in two steps of the first algorithm still will be explored in the searche future. It is important to point out that this procedure also can solve the stabilization problem in systems that do not verify the Kimura condition, using itself compensating dynamic of order $\nu > n - (m + p)$.

References

[1] A. T Alexandridis and Paraskevopoulos, P. N., A New Approach to Eigenstruture Assignment by Output Feedback, *IEEE Trans. Automatic. Control*, vol. 41, number 7, July, 1996.

[2] E. B. Castelan and J. C. Hennet, Eigenstructure Assignment for State Constrained Linear Continuos Time Systems, *Automatica*, vol. 28, number 3, (1993) 605-611.

[3] E. B. Castelan and J. C. Hennet and E. R. Ll. Villarreal, Quadratic Characterization and Use of Output Stabilizable Subspaces, "Proceedings (CD) of the 8th Mediterranean Conference on Control and Automation", Greece, 2000.

[4] E. B. Castelan and J. C. Hennet and E. R. Ll. Villarreal, Quadratic Characterization and Use of Output Stabilizable Subspaces, *IEEE Trans. Automatic. Control*, vol. 48, number 4, (2003) 654-660.

[5] C. T. Chen, "Linear System Theory ans Design", Holt, Rinehart and Winston, 1996.

[6] L. Dai, "Singular Control System", Springer-Verlag, 1989.

[7] L. R. Fletcher and J. Kautsky and G. K. G. Kolka and N. K. Nichols, Eigenstructure Assingment by Output Feedback in Descriptor Systems, *IEEE Trans. Automatic. Control*, vol. 42, (1985) 1457-1468.

[8] H. Kimura, Pole Assignment by Gain Ouptup Feedback, *IEEE Trans. Automatic. Control*, vol. 20, (1975) 509-516.

[9] V. L. Syrmos and F. L. Lewis, Output Feedback Eigenstructure Assignment Using Two Sylvester Equations, *IEEE Trans. Automatic. Control*, vol. 38, number 3, (1993) 495-499.

[10] V. L. Syrmos and F. L. Lewis, Transmission Zero Assignment using Descriptions, *IEEE Trans. Automatic. Control*, vol. 38, number 7, (1993) 1115-1120.

[11] V. L. Syrmos and F. L. Lewis, Bilinear Formulation for the Output Feedback Problem in Linear System, *IEEE Trans. Automatic. Control*, vol. 39, number 2, (1994) 410-414.

[12] V. L. Syrmos and C. T. Abdallah and P. Dorato and K. Grigoriadis, Static Output Feedback - A Survey *Automatica* , vol 33, number 2, (1997) 125-137.

[13] W. M. Wonahm, "Linear Multivariable Control, a Geometric Approach", Springer-Verlag, 1979.

View publication stats

ResearchGate

See discussions, stats, and author profiles for this publication at: https://www.researchgate.net/publication/280306753

Estabilização de Sistemas Descritores por Realimentação de Saídas via subespaços invariantes

Conference Paper · September 2004

CITATIONS
0

READS
11

2 authors:

E.B. Castelan
Federal University of Santa Catarina
179 PUBLICATIONS **1,883** CITATIONS
SEE PROFILE

Elmer ROLANDO LLANOS Villarreal
Universidade Federal Rural do Semi-Árido - UFERSA
77 PUBLICATIONS **138** CITATIONS
SEE PROFILE

All content following this page was uploaded by Elmer ROLANDO LLANOS Villarreal on 29 May 2019.

The user has requested enhancement of the downloaded file.

ESTABILIZAÇÃO DE SISTEMAS DESCRITORES POR REALIMENTAÇÃO DE SAÍDAS VIA SUBESPAÇOS INVARIANTES

Eugênio B. Castelan*, Elmer R. Llanos Villarreal †

*Departamento de Automação e Sistemas
Universidade Federal de Santa Catarina
88040-900, Florianópolis, SC, Brasil.

†Departamento de Informática
Faculdade de Castelo
29360-000, Castelo, ES, Brasil.

Emails: eugenio@das.ufsc.br, elmerllanos@hotmail.com

Resumo— Considera-se o problema da existência e do cálculo de uma matriz de realimentação de saídas que estabiliza fortemente um sistema descritor linear. Os resultados apresentados baseam-se no conceito de (C, A, E, B)-invariância e de sua caracterização algébrica através de equações acopladas de Sylvester e de equações acopladas de tipo Lyapunov. Apresentam-se algoritmos para o cálculo da matriz de realimentação de saídas, baseados em posicionamento de autoestrutura ou na solução de desigualdades e igualdades matriciais lineares. Os resultados e algoritmos apresentados generalizam resultados anteriores propostos para sistemas lineares clássicos e para classes particulares de sistemas descritores lineares.

Palavras-chave— Sistemas descritores, Realimentação de saídas, Equações de Sylvester, Equações de Lyapunov, LMI/LMEs.

Abstract— We consider the problem of strong stabilization of descriptor systems via output feedback. The proposed results are based on the concept of (C, A, E, B)-invariance and its algebraic characterization by coupled Sylvester equations and coupled Lyapunov-like equations. Based either on eigenstructure assignment techniques and on the solution of linear matrix inequalities and equalities, we propose algorithms for computation of the output feedback matrix for descriptor systems that verify some conditions. The proposed results and algorithms generalize previous works developed for classical linear systems and for particular classes of descriptor systems.

Keywords— Descriptor systems, Output feedback, Sylvester equations, Lyapunov equations, LMI/LMEs.

1 Introdução

Seja um sistema descritor linear e invariante no tempo descrito por:

$$E\dot{x}(t) = Ax(t) + Bu(t) \quad (1)$$
$$y(t) = Cx(t) \quad (2)$$

onde: $x \in \mathcal{X} \sim \Re^n$,$u \in \mathcal{U} \sim \Re^m$, $y \in \mathcal{Y} \sim \Re^p$ e $E \in \Re^{n\times n}$, $posto\,(E) = q < n$; as demais matrizes têm dimensões adequadas com $posto\,(B) = m$ e $posto\,(C) = p$.

O problema a ser tratado consiste em encontrar uma lei de controle do tipo realimentação de saídas

$$u(t) = Ky(t) \ , \ K \in \Re^{m\times p} \quad (3)$$

tal que o sistema em malha fechada

$$E\dot{x}(t) = (A + BKC)x(t) \quad (4)$$

seja regular, assintoticamente estável e livre de impulsões (Varga, 1995). O problema de cálculo de uma realimentação de saídas para o qual essas propriedades em malha fechada são verificadas, é denominado de *estabilização forte* ou, simplesmente, S-estabilização (do inglês "Strong Stabilization").

As três propriedades desejadas podem ser descritas em termos da autoestrutura do sistema em malha fechada (4): (i) a estabilidade assintótica é equivalente a que todos os pólos finitos estejam no semiplano esquerdo; (ii) a ausência dos modos impulsivos é equivalente a ter q pólos finitos em malha fechada; e (iii) a regularidade é garantida se o sistema é livre de impulsões.

A partir da interpretação anterior, condições necessárias e suficientes para a existência de uma realimentação de saídas S-estabilizável podem ser encontradas como um conjunto de equações generalizadas acopladas de Sylvester (Duan, 1999), (Fletcher, 1988). Como no caso de sistemas puramente diferenciais (também chamados de *sistemas normais* (Dai, 1989)), as equações de Sylvester podem ser interpretadas a partir de conceitos da teoria de controle geométrico. Assim, introduz-se a noção de subespaços fortemente $O.S.$ (C, A, E, B)-invariantes a qual é utilizada para a interpretação de alguns resultados. A seguir, mostra-se que equações generalizadas de tipo Lyapunov também podem ser usadas para descrever a (C, A, E, B)-invariância de subespaços e, portanto, para obter um conjunto de condições necessárias e suficientes para a existência de uma realimentação de saídas que S-estabiliza o sistema.

Os resultados citados permitem propor uma extensão para o caso de sistemas descritores dos procedimentos algorítmicos *em dois passos* relatados em (Castelan et al., 2003) para a estabilização de sistemas normais. Diferentemente de resultados propostos anteriormente em (Llanos Villarreal et al., 2000) e (Castelan et al., 2002), nenhuma estrutura particular é requerida das matrizes que definem o sistema descritor em malha aberta. Assim, sob hipóteses de estabilizibilidade e de detectabilidade do sistema (1)-(2), necessárias para

existência de solução do problema, propõe-se algoritmos para estabilização de sistemas descritores que satisfaçam a condição $(m+p) > q$, a qual pode ser considerada uma generalização da conhecida *condição de Kimura* para sistemas normais (Syrmos e Lewis, 1993). Importante salientar o fato que também no caso de sistemas descritores, a solução do primeiro passo do procedimento proposto pode ser associada a um sistema normal de ordem reduzida igual a $(q-p)$, o qual pode ser obtido a partir de uma seqüência de transformações de coordenadas relatadas no presente artigo (Castelan e Gomes da Silva, 2004).

Na seção 2, introduz-se alguns conceitos de controle geométrico associados ao problema tratado. Na terceira seção apresentam-se as condições de existência de solução do problema de S-estabilização, através das equações generalizadas acopladas de Sylvester e de Lyapunov. Baseado nos algoritmos apresentados em (Castelan et al., 2003), propõe-se na seção 4 um algoritmo para resolver o problema de S-estabilização via prosicionamento de autoestrutura. Um algoritmo que utiliza desigualdades e igualdades matriciais lineares (LMI/LMEs) é apresentado na seção 5. Um exemplo ilustrativo e comentários concluem o artigo.

2 Preliminares

Apresentam-se a seguir alguns conceitos de controle geométrico para sistemas descritores (Ozcaldiran e Lewis, 1990) (Castelan et al., 2001), utilizados na seqüência para a interpretação de alguns resultados.

Um subespaço $\mathcal{V} \subset \mathcal{X}$ é (A,E,B)-invariante se existe $F : \mathcal{X} \longrightarrow \mathcal{Y}$ tal que $(A+BF)\mathcal{V} \subset E\mathcal{V}$, ou equivalentemente , $A\mathcal{V} \subset E\mathcal{V} + Im\,(B)$. Dualmente, um subespaço $\mathcal{T} \subset \mathcal{X}$ é (C,A,E)-invariante se existe $L : \mathcal{Y} \longrightarrow \mathcal{X}$ tal que $(A+LC)\mathcal{T} \subset E\mathcal{T}$, ou equivalentemente, $E\mathcal{T} \supset A(\mathcal{T} \cap Ker\,(C))$.

Definição 1 *Um subespaço $\mathcal{V} \subset \mathcal{X}$, de dimensão-$v$, é (C,A,E,B)-invariante se $\mathcal{V}$ é (A,E,B)-invariante e (C,A,E)-invariante.*

As propriedades de estabilizabilidade e detectabilidade podem ser consideradas através das duas definições a seguir:
(i) um subespaço (A,E,B)-invariante $\mathcal{V}$ é (A,E,B)-internamente estabilizável se existe F tal que $(E, A+BF)|\mathcal{V}$ é (assintoticamente) estável;
(ii) um subespaço (C,A,E)-invariante $\mathcal{V}$ é (C,A,E)-externamente detectável se existe L tal que $(E, A+LC)|\mathcal{X}/\mathcal{V}$ é (assintoticamente) estável.

A partir das definições (i) e (ii) tem-se:

Definição 2 *Um subespaço $\mathcal{V}$, de dimensão-v, é $O.S.$ (C,A,E,B)-invariante, se $\mathcal{V}$ é (A,E,B)-internamente estabilizável e (C,A,E)-externamente detectável.*

Observe que um subespaço $\mathcal{V}$ pode ser $O.S.$ (C,A,E,B)-invariante mas o sistema em malha fechada associado ser não regular ou possuir modos impulsivos. Uma definição mais forte que a definição 2 e que permite considerar, em particular, a propriedade de regularizabilidade (Ozcaldiran e Lewis, 1990), segue:

Definição 3 *Um subespaço $\mathcal{V} \subset \mathcal{X}$, de dimensão-$v$, é fortemente $O.S.$ (C,A,E,B)-invariante se ele é $O.S.$ (C,A,E,B)-invariante e $Ker\,E \cap \mathcal{V} = \{0\}$.*

Seja $V \in \Re^{n\times v}$ tal que $Im(V) = \mathcal{V}$. Então a condição $Ker\,E \cap \mathcal{V} = \{0\}$ pode ser equivalentemente substituída por (Ozcaldiran e Lewis, 1990):

$$posto(EV) = v \tag{5}$$

Assumindo que (5) é verificado, a matriz $T \in \Re^{(q-v)\times n}$ é um anulador à esquerda de EV, se $TEV = 0$ e $Ker\,(T) \cap Im\,(E) = \{0\}$. Importante observar que a um subespaço $\mathcal{V} = Im(V)$ fortemente $O.S.$ (C,A,E,B)-invariante pode-se associar um par de equações generalizadas de Sylvester que devem satisfazer, em particular, a condição de acoplamento anterior (Castelan et al., 2001).

3 $O.S.$ (C,A,E,B)-invariância e realimentação de saídas

O resultado a seguir relaciona a existência de uma realimentação de saídas que S-estabiliza o sistema em malha fechada à existência de soluções para duas equaçẽs acopladas de Sylvester e, portanto, ao conceito de subespaços fortemente $O.S.$ (C,A,E,B)-invariantes (Castelan et al., 2001).

Teorema 1 *Existe uma matriz $K \in \Re^{m\times p}$ tal que $\sigma(E, A+BKC) \in \mathcal{C}^-$ e o sistema em malha fechada (4) é regular e livre de impulsões se e somente se as seguintes condições são verificadas para matrizes $(V \in \Re^{n\times v}, H_V \in \Re^{v\times v}, W \in \Re^{m\times v})$, $(T \in \Re^{q-v\times n}, H_T \in \Re^{q-v\times q-v}, U \in \Re^{n-v\times n-v})$ e para algum escalar positivo $v \leq n$:*

$$\begin{aligned}
AV - EVH_V &= -BW, \quad \sigma(H_V) \in \mathcal{C}^- && (6)\\
TA - H_TTE &= -UC, \quad \sigma(H_T) \in \mathcal{C}^- && (7)\\
TEV &= 0 && (8)\\
Ker\,(CV) &\subseteq Ker\,(W) && (9)\\
Ker\,(B'T') &\subseteq Ker\,(U') && (10)
\end{aligned}$$

onde: $posto\,(EV) = posto\,(TE) = q$.

A demonstração proposta em (Castelan et al., 2001) utiliza, fundamentalmente, argumentos de posicionamento de autoestrutura. Em particular, ela leva em consideração que as propriedades desejadas podem ser associadas apenas à estrutura finita do sistema descritor em malha fechada e, portanto, ao subespaço invariante associado aos pólos finitos de (4). Do ponto de vista dos conceitos geométricos anteriormente introduzidos, as equações acopladas de Sylvester (6)-(8) são equivalentes ao fato de $\mathcal{V} = Im\ V$, de dimensão v, ser um subespaço fortemente $O.S.$ (C,A,E,B)-invariante. Portanto, o problema de S-estabilização de sistemas descritores pode ser associado à construção destes subespaços invariantes, como no caso de sistemas normais (Castelan et al., 2003).

Uma caracterização dos subespaços fortemente $O.S.$ (C,A,E,B)- invariantes via estabilidade quadrática pode ser obtida a partir das relações (6)-(8), ao substituirem-se as condições de estabilizabilidade expressas nas equações de Sylvester (6)-(7) pelas duas condições de estabilidade de Lyapunov a seguir (Chen, 1996) :

$$\begin{array}{c}\sigma(H_V)\in\mathcal{C}^- \Longleftrightarrow \exists\ \Pi=\Pi'>0 \text{ tal que}\\ \Pi H_V'+H_V\Pi=-Q_V, \forall\, Q_V=Q_V'>0\end{array} \quad (11)$$

$$\begin{array}{c}\sigma(H_T)\in\mathcal{C}^- \Longleftrightarrow \exists\ \Gamma=\Gamma'>0 \text{ tal que}\\ H_T'\Gamma+\Gamma H_T=-Q_T, \forall\, Q_T=Q_T'>0\end{array} \quad (12)$$

Teorema 2 *: Existe uma matriz $K\in\Re^{m\times p}$ tal que $\sigma(E,A+BKC)\in\mathcal{C}^-$ e o sistema em malha fechada (4) é regular e livre de impulsões, se e somente se as condições seguintes são verificadas para algum escalar positivo $v\leq n$ e para algum par de matrizes $V\in\Re^{n\times v}$ e $T\in\Re^{q-v\times n}$ tais que $TEV=0$, onde posto $(EV)=$ posto $(TE)=q$:*
(i) $\forall\, Q_V=Q_V'>0$, $Q_V\in\Re^{v\times v}$, existem matrizes $P=P'\geq 0$, $P\in\Re^{n\times n}$ e $Y\in\Re^{m\times n}$ tais que

$$APE'+EPA'+BYE'+EY'B'=-EVQ_VV'E' \quad (13)$$

$$V'PV>0\ \ ;\ \ TEPE'T'=0 \quad (14)$$

$$Y=W_\Pi V' \text{ para algum } W_\Pi\in\Re^{m\times v} \quad (15)$$

(ii) $\forall\, Q_T=Q_T'>0$, $Q_T\in\Re^{q-v\times q-v}$, existem matrizes $S=S'\geq 0$, $S\in\Re^{n\times n}$ e $Z\in\Re^{n\times v}$ tais que

$$A'SE+E'SA+C'Z'E+E'ZC=-E'T'Q_TTE \quad (16)$$

$$TST'>0\ \ ;\ \ V'E'SEV=0 \quad (17)$$

$$Z=T'U_\Gamma \text{ para algum } U_\Gamma\in\Re^{q-v\times v} \quad (18)$$

(iii)

$$Ker\,CP\subseteq Ker\,Y \quad (19)$$

$$Ker\,B'S'\subseteq Ker\,Z' \quad (20)$$

A demonstração do resultado acima (Castelan et al., 2001) é tecnicamente similar à demonstração do Teorema *2.1* em (Castelan et al., 2003). Pode-se também resgatar a condição de acoplamento entre as partes (i) e (ii) do Teorema 2 sob a forma:

$$SEP \quad = \quad 0 \quad (21)$$

com $posto\,(SE)=q-posto(EP)$.

Cabe salientar a equivalência entre as relações (13)-(15) e a equação de Sylvester (6) e, de forma similar, a equivalência entre (16)-(18) e (7). Estas equivalências mostram a possibilidade de descrever propriedades geométricas (estruturais) por meio de relações de tipo Lyapunov. Potencialmente, a descrição de tipo Lyapunov permite a extensão de métodos de análise e projeto desenvolvidos a partir das equações de Sylvester, para serem tratados numéricamente através de técnicas de resolução de Desigualdades e Igualdades Matricias Lineares (LMI/LMEs) (Boyd et al., 1994).

4 Aspectos algorítmicos

As caracterizações algébricas dos Teoremas 1 e 2 podem ser usadas para construir subespaços fortemente $O.S.$ (C,A,E,B)-invariantes que permitem o cálculo de realimentações de saídas estabilizantes. Para efeitos algorítimicos, considera-se $v=p$. Então, como no caso de sistemas normais (Castelan et al., 2003), (Syrmos e Lewis, 1993), o cálculo da matriz K pode ser realizado levando-se em conta o requisito de acoplamento e resolvendo-se subsequentemente as equações acopladas de Sylvester ou de Lyapunov generalizadas.

4.1 Extensão do algoritmo de Syrmos-Lewis

Baseado no algoritmo apresentado em (Syrmos e Lewis, 1993),(Castelan et al., 2003), o procedimento básico seguinte foi proposto em (Castelan et al., 2001) para calcular uma realimentação de saídas que estabiliza o sistema em malha fechada, quando $(m+p)>q$. Os autovalores de malha fechada são posicionados arbitrariamente próximos ao conjunto $\Lambda=\Lambda_T\cup\Lambda_V$, onde $\Lambda_T=\{\lambda_1,\ldots,\lambda_{q-p}\}$ e $\Lambda_V=\{\lambda_{q-p+1},\ldots,\lambda_q\}$ são conjuntos simétricos de autovalores pré-especificados. O sistema (E,A,B,C) é considerado fortemente controlável e fortemente detectável (Varga, 1995).

Algoritmo 1

Passo 1: *Escolhe-se $H_T\in\Re^{(q-p)\times(q-p)}$ tal que $\sigma(H_T)=\Lambda_T\in\mathcal{C}^-$ e resolve-se a equação (7) para encontrar $T\in\Re^{(q-p)\times n}$ tal que*

$$posto\left(\left[\begin{array}{c}TE\\ C\end{array}\right]\right)=q \quad (22)$$

Passo 2: *Resolve-se a equação (6) para alguma matriz $H_V\in\Re^{p\times p}$ tal que $\sigma(H_V)=\Lambda_V\in\mathcal{C}^-$, tomando em consideração que V deve verificar a condição de acoplamento (8) e que posto $(EV)=p$ (ou $Ker\,(TE)=Ker\,(E)\oplus Im\,(V)$, onde $\oplus$ representa a soma direta)* [1].

Passo 3: *Por construção, a matriz V deve verificar posto $(CV)=p$ e K pode ser calculada por:*

$$K \quad = \quad W(CV)^{-1} \quad (23)$$

Considerando-se as matrizes H_T e H_V sob a forma de Jordan, os dois primeiros passos podem ser resolvidos utilizando-se técnicas padrão de posicionamento de auto-estrutura como segue. No *Passo 1*, calculam-se $t_j\in\mathcal{C}^n$ e $u_j\in\mathcal{C}^p$, tais que :

$$\left[\begin{array}{cc}t_j' & u_j'\end{array}\right]\left[\begin{array}{c}A-\lambda_jE\\ C\end{array}\right]=0\ \ \forall\ \ j=1,\ldots,q-p \quad (24)$$

As linhas da matriz $T\in\Re^{(q-p)\times n}$, denotadas por T_j, são formadas a partir dos vetores t_j:
se $\lambda_j\in\Re$, então $T_j=t_j'$; se $\lambda_j\in\mathcal{C}$, considera-se $\lambda_{j+1}=\lambda_j^*$ *e* $\left\{\begin{array}{c}T_j=Re\,(t_j')\\ T_{j+1}=Imag\,(t_j')\end{array}\right.$.

Sob a condição que o sistema seja fortemente observável (detectável), é sempre possível construir uma matriz T que verifica a condição (22): uma sistemática baseada na definição de um sistema de ordem reduzida, é mostrada no final da presente seção para a construção de um subespaço externamente detectável cuja matriz T correspondente verifica a condição (22).

No *Passo 2*, determinam-se $v_i\in\mathcal{C}^n$ e $w_i\in\mathcal{C}^n$:

$$\left[\begin{array}{cc}A-\lambda_iE & B\\ TE & 0\end{array}\right]\left[\begin{array}{c}v_i\\ w_i\end{array}\right]=0\ \ \forall\, i=q-p+1,\ldots,q \quad (25)$$

[1] A condição (22) garante, em particular, que $posto\,(TE)=q$

De forma similar ao caso anterior, as matrizes V e W utilizadas para o cálculo de K podem ser construídas somente com elementos reais. Para garantir que os autovalores λ_i do passo 2 sejam livremente alocáveis, o sistema matricial $P(\lambda) = \begin{bmatrix} A-\lambda E & B \\ TE & 0 \end{bmatrix}$ de dimensão $(n+q-p)\times(n+m)$, deve ter posto completo por linhas $\forall\lambda$ e deve-se garantir a possibilidade de encontrar os vetores v_i, a partir de (25), que não pertençam a $Ker\,(E)$. Caso para algum valor particular de $\lambda = \bar{\lambda}$, $posto(P(\bar{\lambda})) < n+q-p$, então $\bar{\lambda}$ deve fazer parte do espectro de H_V (e, portanto, satisfazer $\bar{\lambda} \in \mathcal{C}^-$). Nos casos raros nos quais $P(\lambda)$ não tem posto completo, uma pequena modificação do espectro de autovalores utilizados no Passo 1 e um novo cálculo da matriz T são geralmente suficientes para tornar viável o Passo 2.

4.2 Abordagem via sistema de ordem reduzida

Por hipótese, o sistema representado por (C, A, E) é fortemente detectável, ou, equivalentemente:

$$posto\left(\begin{bmatrix} \lambda E - A \\ C \end{bmatrix}\right) = n\ ,\quad \forall\lambda \text{ finito } \in \bar{\mathcal{C}}^+ \tag{26}$$

$$posto\left(\begin{bmatrix} E \\ L_\infty A \\ C \end{bmatrix}\right) = n\ , \tag{27}$$

onde $L_\infty \in \Re^{n-q\times n}$, com $posto(L_\infty) = n-q$, é tal que $L_\infty E = 0$. Além disso, considera-se que

$$posto\left(\begin{bmatrix} L_\infty A \\ C \end{bmatrix}\right) = n-q+p\ , \tag{28}$$

Na seqüência, as matrizes que descrevem o sistema descritor em malha aberta serão colocadas sob a forma algébrica-diferencial (Dai, 1989):

$$E = \begin{bmatrix} I_q & 0 \\ 0 & 0 \end{bmatrix},\ A = \begin{bmatrix} J_1 & J_2 \\ J_3 & J_4 \end{bmatrix},\ B = \begin{bmatrix} B_1 \\ B_2 \end{bmatrix}\ e\ C = \begin{bmatrix} C_1 & C_2 \end{bmatrix} \tag{29}$$

Proposição 1 *Se (C, A, E) é fortemente detectável, então existe uma matriz $T = \begin{bmatrix} T_1 & T_2 \end{bmatrix} \in \Re^{(q-p)\times n}$, com posto $(TE = \begin{bmatrix} T_1 & 0 \end{bmatrix}) = q-p$, tal que o subespaço $\mathcal{V} = Im \begin{bmatrix} V_1 \\ V_2 \end{bmatrix}$, com $TEV = T_1V_1 = 0$ e $posto(EV = V_1) = p$, é (C, A, E)-externamente detectável e posto $\left(\begin{bmatrix} TE \\ L_\infty A \\ C \end{bmatrix} = \begin{bmatrix} T_1 & 0 \\ J_3 & J_4 \\ C_1 & C_2 \end{bmatrix}\right) = n$.*

A demonstração do resultado anterior baseia-se numa seqüência particular de transformações de coordenadas (veja (Castelan e Gomes da Silva, 2004)) que permite construir soluções para o Passo 1 do Algoritmo 1, como segue:

Algoritmo 2

Passo 1: *Se as matrizes do sistema não estiverem na forma (29), encontre $Q = \begin{bmatrix} Q_1' \\ Q_2' \end{bmatrix} \in \Re^{n\times n}$ e $R = \begin{bmatrix} R_1 & R_2 \end{bmatrix} \in \Re^{n\times n}$ tais que $QER = \begin{bmatrix} I_q & 0 \\ 0 & 0 \end{bmatrix}$, e defina $\begin{bmatrix} J_1 & J_2 \\ J_3 & J_4 \end{bmatrix} = QAR$ e $\begin{bmatrix} C_1 & C_2 \end{bmatrix} = CR$. Senão: $Q = R = I_n$.*

Passo 2: *Encontre uma matriz inversível $\bar{R} = \begin{bmatrix} \bar{R}_1 \\ \bar{R}_2 \end{bmatrix}$, tal que:*

$$\begin{bmatrix} \bar{R}_1 \\ \bar{R}_2 \end{bmatrix}\begin{bmatrix} J_4 \\ C_2 \end{bmatrix} = \begin{bmatrix} \bar{J}_4 \\ 0 \end{bmatrix}\ ,\quad posto(\bar{J}_4) = n-q \tag{30}$$

Considere

$$\begin{bmatrix} \bar{J}_3 \\ \bar{C}_1 \end{bmatrix} = \begin{bmatrix} \bar{R}_1 \\ \bar{R}_2 \end{bmatrix}\begin{bmatrix} J_3 \\ C_1 \end{bmatrix} \tag{31}$$

e defina o sistema auxiliar representado por $(\bar{C}, \bar{A}, \bar{E})$, onde $\bar{E} = \begin{bmatrix} I_q & 0 \\ 0 & 0 \end{bmatrix}$, $\bar{A} = \begin{bmatrix} J_1 & J_2 \\ \bar{J}_3 & \bar{J}_4 \end{bmatrix}$ e $\bar{C} = \begin{bmatrix} \bar{C}_1 & 0 \end{bmatrix}$.

Passo 3: *Encontre $M = \begin{bmatrix} M_1 & M_2 \end{bmatrix} \in \Re^{q\times q}$ tal que*

$$\bar{C}_1 \begin{bmatrix} M_1 & M_2 \end{bmatrix} = \begin{bmatrix} \tilde{C}_1 & 0 \end{bmatrix} \tag{32}$$

$$\tilde{C}_1 \in \Re^{p\times p} \text{de posto completo.}$$

Calcule $\begin{bmatrix} M_3 & M_4 \end{bmatrix} \in \Re^{(n-q)\times q}$ que verifica

$$\bar{J}_4 \begin{bmatrix} M_3 & M_4 \end{bmatrix} = -\bar{J}_3 \begin{bmatrix} M_1 & M_2 \end{bmatrix} \tag{33}$$

Seja $\tilde{M} = \begin{bmatrix} \tilde{M}_1' \\ \tilde{M}_2' \end{bmatrix} \in \Re^{n-q\times n-q}$ a inversa de M, onde $\begin{bmatrix} M_1 & M_2 \end{bmatrix}\begin{bmatrix} \tilde{M}_1' \\ \tilde{M}_2' \end{bmatrix} = I_q$. Defina

$$\tilde{Q} = \begin{bmatrix} \begin{bmatrix} \tilde{M}_1' \\ \tilde{M}_2' \end{bmatrix} & 0 \\ 0 & I_{n-q} \end{bmatrix}\ e\ \tilde{P} = \begin{bmatrix} \begin{bmatrix} M_1 & M_2 \\ M_3 & M_4 \end{bmatrix} & 0 \\ 0 & I_{n-q} \end{bmatrix}$$

para obter o sistema representado por $(\tilde{E}, \tilde{A}, \tilde{C})$:

$$\tilde{E} = \tilde{Q}\bar{E}\tilde{P} = \begin{bmatrix} I_p & 0 & 0 \\ 0 & I_{q-p} & 0 \\ 0 & 0 & 0 \end{bmatrix},\ \tilde{C} = \bar{C}\tilde{P} = \begin{bmatrix} \tilde{C}_1 & 0 & 0 \end{bmatrix}$$

$$\tilde{A} = \tilde{Q}\bar{A}\tilde{P} = \begin{bmatrix} \tilde{J}_{11} & \tilde{J}_{12} & \tilde{J}_{13} \\ \tilde{J}_{21} & \tilde{J}_{22} & \tilde{J}_{23} \\ 0 & 0 & \tilde{J}_{33} \end{bmatrix}\ e\ \begin{array}{l} \tilde{J}_{12} \in \Re^{p\times(q-p)} \\ \tilde{J}_{22} \in \Re^{(q-p)\times(q-p)} \\ \tilde{J}_{33} = \bar{J}_4 \end{array}$$

Passo 4: *Encontre uma solução para a equação de Sylvester de ordem reduzida*

$$\tilde{T}_{12}\tilde{J}_{22} - H_T\tilde{T}_{12} = -\tilde{T}_{11}\tilde{J}_{12}\,,\ \sigma(H_T) = \Lambda_T \in \mathcal{C}^- \tag{34}$$

na qual $H_T \in \Re^{(q-p)\times(q-p)}$, $\tilde{T}_{11} \in \Re^{(q-p)\times p}$ e $\tilde{T}_{12} \in \Re^{(q-p)\times(q-p)}$ deve ser não-singular.

Passo 5: *Calcule*

$$T_1 = \begin{bmatrix} \tilde{T}_{11} & \tilde{T}_{12} \end{bmatrix}\begin{bmatrix} \tilde{M}_1' \\ \tilde{M}_2' \end{bmatrix}$$

Na base original: $TE = \begin{bmatrix} T_1 & 0 \end{bmatrix} Q$.

Observe que a escolha das matrizes Q, R, $\bar{R}$ e M não é única. Então, elas podem ser definidas como matrizes ortogonais, o que contribui para a estabilidade e eficiência numérica da implementação computacional do algoritmo. Finalmente, salientamos que diferentes técnicas podem ser utilizadas para a resolução do Passo 4. Dentre estas, a utilização de posicionamento de autoestrutura ou a resolução de uma equação de tipo Lyapunov associada ao sistema de ordem reduzida, mostrada na seção seguinte.

5 Algoritmo via Equações de Lyapunov

Como em (Castelan et al., 2003), soluções para o Passo 4 do Algoritmo 2 podem ser obtidas a partir de uma desigualdade matricial linear (LMI) associada ao sistema de ordem reduzida representado pelo par $(\tilde{J}_{12}, \tilde{J}_{22})$. Por hipótese, o sistema de ordem reduzida é detectável. Assim, considere matrizes $S_{21} \in \Re^{(q-p)\times p}, S_{22} \in \Re^{(q-p)\times(q-p)}$, com $S_{22} = S_{22}' > 0$, soluções da LMI de ordem reduzida seguinte:

$$\tilde{J}_{22}' S_{22} + S_{22}\tilde{J}_{22} + \tilde{J}_{12}' S_{21}' + S_{21}\tilde{J}_{12} \quad < \quad 0 \qquad (35)$$

Considere a decomposição de Choleski de $S_{22} = S_{22}' > 0$, dada por:

$$S_{22} = \tilde{T}_{12}'\tilde{T}_{12} \qquad (36)$$

na qual $\tilde{T}_{12}$ é inversível, e defina $L_2 \in \Re^{q-p\times p}$ tal que:

$$S_{22}L_2 \quad = \quad S_{21} \qquad (37)$$

A partir de (35) , (37) e (36), obtém-se

$$\tilde{T}_{12}'\tilde{T}_{12}(\tilde{J}_{22} + L_2\tilde{J}_{12}) + (\tilde{J}_{22}' + \tilde{J}_{12}'L_2')\tilde{T}_{12}'\tilde{T}_{12} < 0$$

Por construção, $\sigma(\tilde{J}_{22} + L_2\tilde{J}_{12}) \in \mathcal{C}^-$. Pode-se, então, definir a matriz $H_T \in \Re^{q-p\times q-p}$ a partir da relação de similaridade

$$\tilde{T}_{12}\left(\tilde{J}_{22} + L_2\tilde{J}_{12}\right) = H_T\tilde{T}_{12} \qquad (38)$$

Por construção: $\sigma(H_T) = \sigma\left(\tilde{J}_{22} + L_2\tilde{J}_{12}\right) \in \mathcal{C}^-$. A matriz $\tilde{T}_{11}$ correspondente, que satisfaz (34), verifica

$$\tilde{T}_{11} \quad = \quad \tilde{T}_{12}L_2 \qquad (39)$$

Observação 1 *A partir de (37), (36) e (39), tem-se*

$$\tilde{T}_{12}'\tilde{T}_{11} = \tilde{T}_{12}'\tilde{T}_{12}L_2 = S_{22}L_2 = S_{21} \qquad (40)$$

Então, como $T_1 = \begin{bmatrix} \tilde{T}_{11} & \tilde{T}_{12} \end{bmatrix}\begin{bmatrix} \tilde{M}_1' \\ \tilde{M}_2' \end{bmatrix}$ *e* $\tilde{T}_{12}'$ *é inversível, tem-se:*

$$Ker(T_1) = Ker(\tilde{T}_{12}'T_1) = Ker\left(\begin{bmatrix} S_{21} & S_{22} \end{bmatrix}\begin{bmatrix} \tilde{M}_1' \\ \tilde{M}_2' \end{bmatrix}\right) \qquad (41)$$

Esta relação pode ser utilizada para o cálculo de V *tal que* $TEV = T_1V_1 = 0$

O desenvolvimento anterior mostrou que a solução da LMI (35) implica na solução da equação de Sylvester de ordem reduzida (34). Também é possível mostrar o caminho oposto. Isto implica que não há perda de generalidade de considerar a solução do Passo 4 do Algoritmo 2 via a LMI (35). Relembre que o Algoritmo 2 pode ser utilizado para a realização do Passo 1 do Algoritmo 1. Além disso, sob a condição de acoplamento (8), a equação de Sylvester (6) envolvida no Passo 2 desse primeiro algoritmo é equivalente as relações (13)-(15) do Teorema 2.

Baseado nos resultados e comentário anteriores, o procedimento básico seguinte pode ser usado para calcular a matriz de realimentação de saídas que estabiliza o sistema quando a condição $(m + p) > q$ é satisfeita. Este algoritmo pode ser visto como uma extensão do algoritmo proposto em (Castelan et al., 2003) para a estabilização de sistemas normais e também generaliza resultados anteriores propostos em (Llanos Villarreal et al., 2000), (Castelan et al., 2002).

Algoritmo 3

Passo 1

1.1)Utilizar os Passos 1 a 3 do Algoritmo 2 para encontrar as matrizes $\tilde{J}_{12}$ *e* $\tilde{J}_{22}$.

1.2) Resolver a LMI de ordem reduzida (35) para encontrar S_{12}, $S_{22} = S_{22}' > 0$.

1.3) Calcular $T_1 = \begin{bmatrix} S_{11} & S_{12} \end{bmatrix}\begin{bmatrix} \tilde{M}_1' \\ \tilde{M}_2' \end{bmatrix}$. *Sejam as matrizes* $\mathcal{A} = J_1$, $\mathcal{B} = [-J_2\ 0]$, $\mathcal{C} = \begin{bmatrix} -J_3 \\ -T_1 \end{bmatrix}$ *e* $\mathcal{E} = \begin{bmatrix} -J_4 & 0 \\ 0 & 0 \end{bmatrix}$. *Se* $(\mathcal{A}, \mathcal{B}, \mathcal{C}, \mathcal{E})$ *não tem zeros invariantes, então ir ao* Passo 3*; caso contrário, repetir o* Passo 1 *usando uma nova decomposição de* $\bar{C}_1$.

Passo 2

2.1) Calcular $V = \begin{bmatrix} V_1 \\ V_2 \end{bmatrix}$ *que verifique* $TEV = T_1V_1 = 0$ *e* $posto(CV) = p$.

2.2) Resolver a equação (13), sob as restrições (14) e (15), e encontrar as matrizes P, Y *e* W_Π.

Passo 3 *A matriz de realimentação de saídas verifica:* $KCP = Y \longleftrightarrow KCV\bar{P} = W_\Pi$, *se* $V'V = I_p$.

Observação 2 *No Passo* 2*, objetiva-se resolver as condições (13), (14) e (15), e também calcular* $V = \begin{bmatrix} V_1 \\ V_2 \end{bmatrix}$ *tal que* $TEV = T_1V_1 = 0$ *e* $posto(CV) = posto\left(\begin{bmatrix} C_1 & C_2 \end{bmatrix}\begin{bmatrix} V_1 \\ V_2 \end{bmatrix}\right) = p$. *Como* $V_2 \in \Re^{n-q\times p}$ *é livre:*

se $posto(C_1V_1) = p$, *então considera-se* $V_2 = 0$*;*

se $posto(C_1V_1) < p$, *então* $V_2 \neq 0$ *para garantir que o* $posto(CV)$ *seja completo.*

No presente artigo, a estabilidade assintotica é um dos requerimentos para o sistema em malha-fechada, conjuntamente com a regularidade e a ausência de impulsões. Cabe salientar que os graus de liberdade existentes na abordagem quadrática podem ser exploradas para atingir outros requerimentos, como, por exemplo, posicionamento regional de pólos.

6 Exemplos

Considere o sistema descrito pelas matrizes (Chu et al., 1999):

$$E = \begin{bmatrix} 0.00 & 0.00 & -0.82 & 0.00 & 0.00 \\ 0.00 & 0.00 & 0.00 & 0.00 & 0.00 \\ 0.00 & 0.00 & 0.00 & 0.00 & 0.00 \\ 1.72 & 0.00 & 0.00 & 0.00 & 0.00 \\ 0.00 & 0.00 & 0.00 & 0.00 & 1.00 \end{bmatrix};$$

$$A = \begin{bmatrix} 0.00 & 0.00 & 1.23 & 0.00 & 0.00 \\ 1.10 & 0.00 & 0.00 & 0.00 & 0.00 \\ 0.00 & 1.56 & 0.00 & 0.00 & 1.01 \\ 0.00 & 0.00 & 1.98 & 0.00 & 0.00 \\ 0.00 & 0.00 & 0.00 & 0.00 & 0.00 \end{bmatrix}$$

$$B = \begin{bmatrix} 0.41 & -6.64 & -2.34 \\ 0.00 & 0.00 & 0.45 \\ 0.00 & 0.00 & 0.00 \\ 1.72 & -15.48 & 0.00 \\ 7.00 & 0.00 & -1.00 \end{bmatrix}; \; C = \begin{bmatrix} -1 & 0 & 0 & -1 & 0 \\ 0 & 0 & 0 & 1 & 1 \end{bmatrix}$$

View publication stats

O sistema descritor correspondente é não regular e seus pólos finitos são dados por: $\sigma(E, A) = \{0.0, 0.0, -1.5\}$. O sistema (C, E, A, B) é fortemente controlável e fortemente detectável e, $m + p = 5 > q$. Pode-se então aplicar o Algoritmo 3 como segue.

No Passo 1 determinam-se Q e R tais que $E \longleftarrow QER = \begin{bmatrix} I_3 & 0 \\ 0 & 0 \end{bmatrix}$ e obtém-se:

$$QAR = \begin{bmatrix} 0.0 & 0.00 & 1.15 & 0.00 & 0.0 \\ 0.0 & 0.00 & 0.00 & 0.00 & 0.0 \\ 0.0 & 0.00 & -1.50 & 0.00 & 0.0 \\ -1.1 & 0.00 & 0.00 & 0.00 & 0.0 \\ 0.0 & -1.10 & 0.00 & -1.56 & 0.0 \end{bmatrix},$$

$$QB = \begin{bmatrix} -1.00 & 0.0000 \\ 7.00 & -1.0000 \\ 0.50 & -2.8537 \\ 0.00 & 0.4500 \\ 0.00 & 0.0000 \end{bmatrix}, \; CR = \begin{bmatrix} 1 & 0 \\ 0 & 1 \\ 0 & 0 \\ 0 & 0 \\ 1 & -1 \end{bmatrix}'.$$

A seguir, determinam-se $\begin{bmatrix} \bar{R}_1 \\ \bar{R}_2 \end{bmatrix} = \begin{bmatrix} 0.0000 & 1.0 & 0.0000 & 0.0000 \\ 0.0000 & 1.0 & 0.7071 & -0.7071 \\ 0.7071 & 0.0 & 0.5000 & 0.5000 \\ -0.7071 & 0.0 & 0.5000 & 0.5000 \end{bmatrix}$ e

$$\begin{bmatrix} \bar{J}_3 & \bar{J}_4 \\ \bar{C}_1 & 0 \end{bmatrix} = \begin{bmatrix} 0.0000 & -1.1000 & 0.0 & -1.56 & 0.0000 \\ 0.7071 & -0.7071 & 0.0 & 0.00 & -1.4142 \\ -0.2778 & 0.5000 & 0.0 & 0.00 & 0.0000 \\ 1.2778 & 0.5000 & 0.0 & 0.00 & 0.0000 \end{bmatrix}.$$

Para $\begin{bmatrix} M_1 & M_2 \end{bmatrix} = \begin{bmatrix} -0.4857 & -0.8741 & 0.00 \\ 0.8741 & -0.4857 & 0.00 \\ 0.0000 & 0.0000 & 1.00 \end{bmatrix}$, utiliza-se (33) para obter:

$$\begin{bmatrix} M_3 & M_4 \end{bmatrix} = \begin{bmatrix} -0.6164 & 0.3425 & 0.00 \\ -0.6799 & -0.1942 & 0.00 \end{bmatrix}$$

As matrizes que determinam o sistema de ordem reduzida correspondem a $\begin{bmatrix} \tilde{J}_{12} \\ \tilde{J}_{22} \end{bmatrix} = \begin{bmatrix} -0.5586 \\ -1.0052 \\ -1.5000 \end{bmatrix}$.

Uma solução para o Passo 1.2 é: $\begin{bmatrix} S_{21} & S_{22} \end{bmatrix} = \begin{bmatrix} 0.6213 & 0.3455 & 0.2894 \end{bmatrix}$, a qual resulta no passo 1.3 em: $T_1 = \begin{bmatrix} S_{21} & S_{22} \end{bmatrix} \begin{bmatrix} \bar{M}_1' \\ \bar{M}_2' \end{bmatrix} = \begin{bmatrix} -0.6038 & 0.3753 & 0.2894 \end{bmatrix}$;. Esta solução não tem zeros invariantes. Isto implica no passo 2.1:

$$\begin{bmatrix} V_1 \\ V_2 \end{bmatrix} = \begin{bmatrix} 0.3770 & -0.1032 & 0.9204 & 0.00 & 0.00 \\ 0.4889 & 0.8662 & -0.1032 & 0.00 & 0.00 \end{bmatrix}'.$$

Uma solução factível para o passo 2.2 é :

$$P = \begin{bmatrix} 1906.2914 & 3549.0662 & -625.2525 & -2502.5467 & 0.0 \\ 3549.0662 & 11431.039 & -7419.5297 & -8060.3483 & 0.0 \\ -625.2525 & -7419.5297 & 8317.5769 & 5231.7197 & 0.0 \\ -2502.5467 & -8060.3483 & 5231.7197 & 0.0000 & 0.0 \\ 0.0000 & 0.0000 & 0.0000 & 0.0000 & 0.0 \end{bmatrix}$$

$$W_\Pi = \begin{bmatrix} 2542.4949 & 1003.1718 \\ -545.0746 & 9950.7314 \end{bmatrix}$$

$$Y = \begin{bmatrix} 1449.0571 & 606.61385 & 2236.7134 & 0.0 & 0.0 \\ 4659.8234 & 8675.4952 & -1528.395 & 0.0 & 0.0 \end{bmatrix}$$

A matriz de realimentação de saídas correspondente que estabiliza fortemente o sistema em malha fechada é: $K = \begin{bmatrix} 1.5673 & -0.4335 \\ 2.4444 & 0.0000 \end{bmatrix}$. Os pólos finitos do sistema em malha fechada são: $\sigma(E, A+BKC) = \{-1.1013 \pm 2.2982j \, , -3.8994 \}$, dentre os quais -3.8994 corresponde ao Passo 1.

7 Conclusão

Considerou-se o problema de cálculo da uma matriz de realimentação de saídas que estabiliza fortemente um sistema descritor. Introduziu-se o conceito de (C, A, E, B)-invariância e mostrou-se que os subespaços fortemente (C, A, E, B)-invariantes têm um papel fundamental na estabilização usando realimentação de saídas em sistemas descritores.

Foram apresentados algoritmos para o cálculo da matriz de realimentação de saídas, baseados em técnicas de posicionamento de autoestrutura ou em técnicas para a solução de LMI/LMEs. É importante salientar que o algoritmo de estabilização baseado na solução de Equações de Lyapunov também pode ser adaptado para obter-se posicionamento regional de pólos.

Referências

Boyd, S. P., Ghaoui, L. E., Feron, E. e Balakrishhnan, V. (1994). *Linear Matrix Inequalities in System and Control Theory*, Philadelphia SIAM.

Castelan, E. B., e Silva, A. S., Llanos-Villarreal, E. R. e Tarbouriech, S. (2002). Regional pole placement by output feedback for a class of descriptor systems, *Proc. of the 15th Triennial World Congress of IFAC, (IFAC'02)*, Barcelona - Spain, p. 5 pages.

Castelan, E. B. e Gomes da Silva, V. (2004). On the solution of a sylvester equation appearing in descriptor systems control theory, *scl* p. Aceito para publicação.

Castelan, E. B., Hennet, J.-C. e Llanos Villarreal, E. R. (2003). Quadratic characterization and use of output stabilizable subspaces, *IEEE Trans. Automatic. Control* **48**(4): 654–660.

Castelan, E. B., Llanos Villarreal, E. R. e Tarbouriech, S. (2001). Quadratic characterization and use of output stabilizable subspaces in descriptor systems, *Proceedings (CD) 1st IFAC Symposium on System Structure*, Prague, p. 5.

Chen, C. T. (1996). *Linear System Theory ans Design*, Holt, Rinehart and Winston.

Chu, D. L., Chan, H. C. e Ho, D. W. C. (1999). Necessary and suficient conditions for the output feedback regularization of descriptor systems, *IEEE Trans. Automatic. Control* **44**(2).

Dai, L. (1989). *Singular Control System*, Springer-Verlag.

Duan, G. R. (1999). Eigenstructure assignment in descriptor systems via output feedback: a new complete parametric approach, *Int J. Control* **72**(4): 345–364.

Fletcher, L. R. (1988). Eigenstructure assingment by output feedback in descriptor systems, *IEE Proceedings* **135**(4): 302–308.

Llanos Villarreal, E. R., Castelan, E. B. e Silva, A. S. (2000). Output feedback for stabilization of a class descriptor systems, *Anais do XIII Congresso Brasileiro de Automática*, Florianópolis, Brasil, pp. 423–428.

Ozcaldiran, K. S. e Lewis, F. L. (1990). On the regularizability of singular systems, *IEEE Trans. Automatic. Control* **35**(10): 1156–1160.

Syrmos, V. L. e Lewis, F. L. (1993). Output feedback eigenstructure assignment using two sylvester equations, *IEEE Trans. Automatic. Control* **38**(3): 495–499.

Varga, A. (1995). On stabilization methods of descriptor systems, *scl* **24**: 133–138.

ResearchGate

See discussions, stats, and author profiles for this publication at: https://www.researchgate.net/publication/327468088

Approach For Stabilization by Output Feedback, Invariant Subspaces and Sylvester Equations

Conference Paper · September 2008

CITATIONS
0

READS
23

2 authors, including:

Elmer ROLANDO LLANOS Villarreal
Universidade Federal Rural do Semi-Árido - UFERSA
77 PUBLICATIONS **138** CITATIONS

SEE PROFILE

All content following this page was uploaded by Elmer ROLANDO LLANOS Villarreal on 29 May 2019.

The user has requested enhancement of the downloaded file.

Approach for stabilization by output feedback, invariant subspaces and Sylvester equations

Elmer Rolando Llanos Villarreal *
Departamento de Informática, FANAT,
Universidade do Estado do Rio Grande do Norte,
CEP:59610-090 , Campus Universitário Central, Setor II
BR 110, KM 48, Rua Prof. Antônio Campos, Costa e Silva, Mossoró, RN
E-mail: evillarrea@hotmail.com,

João de Deus Lima
Departamento de Matemática, FANAT,
Universidade do Estado do Rio Grande do Norte,
CEP:59610-090,Campus Universitário Central, Setor II
BR 110, KM 48, Rua Prof. Antônio Campos, Costa e Silva, Mossoró, RN
E-mail: jddeus@uol.com.br

1 Introduction

A system is continuous time when all the variables of the system are known in every moment of time. A control system is called invariant time when its parameters are stationary with respect to time. The representation will be through systems of state equations.

The Sylvester equations play an important role in numerical linear algebra. For example, they arise in the computation of invariant subspaces, in control problems, as linearizations of algebraic Riccati equations, and in the discretization of partial differential equations. For small systems, direct methods are feasible.

This article deals with the problems of stabilization and of regional pole placement by static output feedback in linear continuous-time systems. The results are based on the key notion of (C,A,B)-invariant subspaces which can be characterized through a pair of coupled Sylvester equations. Then, solutions to these equations can be obtained, for systems verifying Kimura's condition ($m + p > n$), into two steps using Syrmos and Lewis's algorithm.

The considered linear time-invariant system are described by :

$$\dot{x}(t) = Ax(t) + Bu(t) \quad (1)$$
$$y(t) = Cx(t) \quad (2)$$

where : $x \in \mathcal{X} \sim \Re^n$, $u \in \mathcal{U} \sim \Re^m$, $y \in \mathcal{Y} \sim \Re^p$.It is also assumed that B is full column-rank , C is full row-rank and that (C, A, B) is stabilizable and detectable. The studied problem is to find a static output feedback control law

$$u(t) = Gy(t) \quad , \quad G \in \Re^{m \times p} \quad (3)$$

such that $\sigma(A + BGC) \in \mathcal{C}^-$, or equivalently, the closed-loop system is asymptotically stable. That is: , where $\sigma(A + BGC) = \{\lambda_1, \lambda_2, \ldots, \lambda_n\}$ is the set of eigenvalues of $A + BGC$.

This presents the basic concepts of theory of geometric control theory that base the approach adopted for the solution of the problem [11], [13]. The coupled Sylvester equation are interpreted on the basis of geometric control theory. Thus, through these equations, the stabilization problem using output feedback can be decomposed in two stages [9]: (i) determination of a (C, A)-outer detectable subspace, and (ii) inner stabilization of this subspace.

In the search of solutions for the stabilization problem they are argued and they presented procedures for the solution of these coupled equations, with emphasis in techniques of eigenstruture assignment [1] [9]. Thus, it is introduced notion of $O.S.$ (C, A, B)-invariant subspace and presented the coupled Sylvester equation. Thus too presented the algorithmic aspects, illustrating them with numerical examples. Some conclusive commentaries finally are presented.

2 Invariant Subspaces and coupled Sylvester Equations

As in [11], some concepts and definitions are used of geometric control theory [13]. It is know that an subespace $\mathcal{V} \subset \mathcal{X}$ is (A, B)-invariant if there exists $F : \mathcal{X} \longrightarrow \mathcal{Y}$ such that $(A + BF)\mathcal{V} \subset \mathcal{V}$, or equivalently , $A\mathcal{V} \subset \mathcal{V} + Im\, B$. For dually an subspace $\mathcal{T} \subset \mathcal{X}$ is (C, A)-invariant if exist $L : \mathcal{Y} \longrightarrow \mathcal{X}$ such that $(A + LC)\mathcal{T} \subset \mathcal{T}$, or equivalently, $\mathcal{T} \supset A(\mathcal{T} \cap Ker\,(C))$.

*Researcher DCR, this work has been supported by FAPERN/CNPq

Definition 2.1 *[11] An subspace $\mathcal{V} \subset \mathcal{X}$, of dimension v , is (C, A, B)-invariant if $\mathcal{V}$ is (A, B)-invariant and (C, A)-invariant.*

Consider $V \in \Re^{v \times v}$ such that $Im(V) = \mathcal{V}$ and consider $T \in \Re^{(n-v)\times v}$ an left annihilator of V, *i.e.* : $Ker(T) = Im(V)$. The definition 2.1 is equivalent an existence of matrices ($H_V \in \Re^{v\times v}$, $W \in \Re^{m\times v}$) and ($H_T \in \Re^{n-v\times n-v}$, $U \in \Re^{(n-v)\times v}$), solutions for the following *coupled Sylvester Equations*:

$$AV - VH_V = -BW \quad (4)$$
$$TA - H_T T = -UC \quad (5)$$
$$TV = 0 \quad (6)$$

An definition 2.1 and the equations (4) , (5) and (6) they have a basic importance in the treatment of the control problem using static output feedback, mainly for Eigenstructure Assignment [9] [11]. The present study it takes in account the properties of stabilizability and detectability, through the two definition to follow:
(i) an subspace (A, B)-invariant $\mathcal{V}$ is (A, B)-inner stabilizable subspace, that is there exist F such that $(A + BF)|\mathcal{V}$ is asymptotically stable; and
(ii) an subspace (C, A)-invariant $\mathcal{V}$ is (C, A)-outer detectable subspace if there exist L such that $(A + LC)|\mathcal{X}/\mathcal{V}$ is asymtotically stable.

Definition 2.2 *[11] An subspace $\mathcal{V}$, of dimension v, is (C, A, B)-invariant output stabilizable subspace , (or simply O.S. (C, A, B)-invariant [1]) if $\mathcal{V}$ is (A, B)-inner stabilizable and (C, A)-outer detectable.*

Thus, a necessary and sufficient condition for the existence $\mathcal{V} = Im(V)$ subspace either *O.S.* (C, A, B)-invariant subspace is that (4), (5) and (6) they are verified with the conditions additional of stability :

$$\sigma(H_V) \in \mathcal{C}^- \quad (7)$$
$$\sigma(H_T) \in \mathcal{C}^- \quad (8)$$

A Theorem to follow it relates the concept of *O.S.* (C, A, B)-invariant subspace to the existence of a law of control of the type static output feedback (3) that it stabilizes the system in closed loop.

Theorem 2.1 *There exists an output feedback matrix $G : \mathcal{Y} \longrightarrow \mathcal{U}$ such that $\sigma(A + BGC) \in \mathcal{C}^-$, if and only if the following conditions are verified for some matrices ($V \in \Re^{n\times v}, H_V \in \Re^{v\times v}, W \in \Re^{m\times v}$), ($T \in \Re^{n-v\times n}, H_T \in \Re^{n-v\times n-v}, U \in \Re^{n-v\times v}$) to some scale positive $v \leq n$:*

$$AV - VH_V = -BW, \text{ with } \sigma(H_V) \in \mathcal{C}^- \quad (9)$$
$$TA - H_T T = -UC, \text{ with } \sigma(H_T) \in \mathcal{C}^- \quad (10)$$
$$TV = 0 \quad (11)$$
$$Ker(CV) \subseteq Ker(W) \quad (12)$$
$$Ker(B'T') \subseteq Ker(U') \quad (13)$$

where: $rank(V) = v$ e $rank(T) = n - v$. $\diamond$

It is important to notice that these results have been presented and explored under different forms in the literature related to the eigenstruture assignment by output feebaback (see [12]). The presented statement corresponds to the statement of the Theorem 3.2 de [11]. As it was seen, the *coupled Sylvester Equations* (9), (10) e (11) describe some geometric properties of subspace $\mathcal{V} = Im(V)$. Under the restriction of imposed stability a matrix H_V, the equation (9) means that the subspace $\mathcal{V} = Im(V)$ must be (A, B)-inner stabilizable subspace; In a dual manner, (10) means that the subspace $Ker(T) = \mathcal{V}$ must be (C, A)-outer detectable subspace. Thus, under the coupling condition (11), is had that the existence of $\mathcal{V} = Ker(T)$ *O.S.* (C, A, B)-invariant subspace,with the conditions you add (12) and (13) is a necessary and suficient condition for the existence solution of the considered problem. Also notices that the conditions (12) and (13) correspond to the existence of a matrix $G \in \Re^{m\times p}$ that it verifies the two following equalities:

$$GCV = W \quad (14)$$
$$TBG = U \quad (15)$$

Is important to observe that guaranteed the existence of solution for the Sylvester equations and that G has been gotten such that (14) (or 15) either verified, the eigenvalues in closed loop are given by:

$$\sigma(A + BGC) = \sigma(H_V) \dot{\cup} \sigma(H_T)$$

3 Algorithmic aspects

The established matrices conditions in the Theorem 2.1 are nonlinear in relation to the matrices variable (V, H_V, W, T, H_T, U). In particular, the terms nonlinear VH_V and $H_T T$ presented in (9) and (10), respectively, can be linear when fixing the matrices H_V and H_T, or equivalent when defining itself the eigenvalues desired for the system in closed loop.

In this section the basic procedure based in two algorithmic techniques of eigenstructure assignment for the attainment a output feedback are presented. The first technique, the algoritm proposed for Syrmos and Lewis in [9]

[1] Output Stabilizable (C,A,B)-invariant [11] [3]

solves the coupled Sylvester equations in two steps and it can directly be applied the systems that verify the condition $m + p > n$, known as condition of Kimura [8]. The second technique, the algorithm proposed for Paraskevopoulos in [1], uses a representation of the system in an adequate base of the state space, to rewrite the coupled Sylvester equations in the form of a set bilinear algebraic equations. In the two techniques, it is assumed that the dimension of $\mathcal{V} = Im\,(V)$ is equal to the number of output p, looking guaranteeing that a matrix $CV \in \Re^{p\times p}$ either invertible and, therefore, that the gain feedback matrix can be found, from (14), under the form $G = W(CV)^{-1}$.

In the sequence, it is considered system represented (C, A, B) is controlable and observable, is this necessary condition for the arbitrary choice of poles to be located in closed loop. This condition can be however to be relaxed for stabilizable and detectabilizable of (C, A, B), what it implies in the use of the non-controlable eigenvalues and non-observable in the spectrum desired for the system in closed loop.

In both the techniques to be presented, are considered that the set of poles desired is denoted by $\Lambda = \{\lambda_1, \ldots, \lambda_{n-p}, \lambda_{n-p+1}, \ldots, \lambda_n\} = \{\Lambda_T, \Lambda_V\}$ where Λ_T and Λ_V are auto-conjugated. These sets are associated the matrices $H_V \in \Re^{p\times p}$ and $H_T \in \Re^{(n-p)\times(n-p)}$ in the following form: $\sigma(H_T) = \Lambda_T = \{\lambda_1, \ldots, \lambda_{n-p}\}$ e $\sigma(H_V) = \Lambda_V = \{\lambda_{n-p+1}, \ldots, \lambda_n\}$. For simplicity, it is considered that the elements of $\Lambda = \sigma(A + BGC)$ are distinct.

3.1 Modified algorithm of Syrmos and Lewis

Based in the express conditions through Theorem 2.1, the following algorithm, considered in [9], generally it leads to a output feedback matrix that stabilizes the system in closed loop when the Kimura's condition $n < m + p$ is verified:

Step 1: It chooses the matrix $H_T \in \Re^{n-p\times n-p}$ such that $\sigma(H_T) = \Lambda_T \in \mathcal{C}^-$ and solve the Sylvester equation (10) for find an matrix $T \in \Re^{n-p\times n}$ such that

$$rank\left(\begin{bmatrix} T \\ C \end{bmatrix}\right) = n \Longleftrightarrow Ker\,T \cap Ker\,C = \{0\} \quad (16)$$

Step 2: Solve the Sylvester equation (9), for some matrix $H_V \in \Re^{p\times p}$ such that $\sigma(H_V) = \Lambda_V \in \mathcal{C}^-$ leading in consideration that the matrix V must verify the coupling condition (11) and that $rank\,(V)$ must be equal p.

Step 3: For construction, the relation (16) guarantees that the rank $(CV) = p$ and the matrix G can be calculated as only solution of (14).

∘

Is presented to follow it some comments with the double objective to show relative aspects to the numerical solution of steps algorithm and to justify them theoretically.

Remark 1.1 : The steps 1 and 2 can be resolved using techniques standards for eigenstructure assignment. Considering the matrices H_T e H_V in the diagonal form of Jordan, the following procedure can be adopted:

Step 1: Find $t_j \in \mathcal{C}^n$ and $u_j \in \mathcal{C}^p$, such that :

$$\begin{bmatrix} t_j' & u_j' \end{bmatrix}\begin{bmatrix} A-\lambda_j I \\ C \end{bmatrix} = 0 \;\forall\; j = 1, \ldots, n-p \quad (17)$$

The row matrix $T \in \Re^{(n-p)\times n}$, denoted for T_j, are formed from the vectors t_j, as follows :

- if $\lambda_j \in \Re$, then $T_j = t_j'$;
- if $\lambda_j \in \mathcal{C}$, is considered $\lambda_{j+1} = \lambda_j^*$ and $\begin{cases} T_j = Re\,(t_j') \\ T_{j+1} = Imag\,(t_j') \end{cases}$.

Step 2 : To determine $v_i \in \mathcal{C}^n$ and $w_i \in \mathcal{C}^n$ such that :

$$\begin{bmatrix} A-\lambda_i I & B \\ T & 0 \end{bmatrix}\begin{bmatrix} v_i \\ w_i \end{bmatrix} = 0 \;\forall\; i = n-p+1, \ldots, n \quad (18)$$

In similar form to the previous case, the used matrices V and W for the calculation of K can only be built with real elements. In particular: if $\lambda_i \in \mathcal{C}$, is considered $\lambda_{i+1} = \lambda_i^*$ and $\begin{cases} V_i = Re\,(v_i), & V_{i+1} = Imag\,(v_i) \\ W_i = Re\,(w_i), & W_{i+1} = Imag\,(w_i) \end{cases}$, where v_i and w_i denote the columns of the matrices V and W, respectively .

Remark 1.2: [4] In the step 1, under the observability (detectability) condition it is always possible to build to a matrix T that verifies condition (17) and that, therefore, it guarantees the obtaining of K saw (14). Once certain the matrix T, the step 2 is associated with the joint solution of the equations (9) and (11), or either to (A,B)-invariance of $Ker\,(T)$. This property is associated then to the "zero equation" (18) [2]. To guarantee that the eigenvalues λ_i of step 2 are freely assignable, the system matrix $P(\lambda) = \begin{bmatrix} A-\lambda I & B \\ T & 0 \end{bmatrix}$ of dimension $(2n-p)\times(n+m)$, must have complete rank for row $\forall\lambda$. The algorithm above is based in the fact that under the condition $m+p > n$, the system matrix $P(\lambda)$ it does not have loss of rank for almost all the triples (A, B, T) [10]. Thus the zero equation (18) has solutions for all λ_i. In the cases where it will have the presence of invariant zeros is possible to remake the Step 1 on the search of other solutions for the Sylvester equation (9).

Remark 1.3: In the less restrictive case

$m + p = n$, the system $P(\lambda)$ of dimension $(2n - p) \times (2n - p)$, is an square matrix and almost all the triples (A, B, T) have p invariant zeros finite stable [9]. In this case, the basic procedure can produce to a output feedback matrix that stabilizes the system in closed loop only if the matrix T, found in step 1, generate p stable invariant zeros which should be used to solve the equation (18) [2].

Example 3.1 *: Consider an linear system (1), (2), defined for [7]:*

$$A = \begin{bmatrix} 0 & 1 & 0 & 0 \\ 1 & 1 & 0 & 0 \\ -1 & 0 & 0 & 0 \\ 0 & 0 & 0 & 0 \end{bmatrix} \quad ; \quad B = \begin{bmatrix} 0 & 0 \\ 1 & 0 \\ 0 & 0 \\ 0 & 1 \end{bmatrix}$$

$$C = \begin{bmatrix} 1 & 0 & 0 & 0 \\ 0 & 0 & 1 & 0 \\ 0 & 0 & 0 & 1 \end{bmatrix}$$

The corresponding system is controllable and observable and $m + p = 5 > n$. The eigenvalues to assignment are given for : $\Lambda_T = \{-4\}$ $\cup\, \Lambda_V = \{-3, -2 + 2j, -2 - 2j\}$.
Step 1 : *For $\lambda_1 = -4$, determined T that verifies (17) and such that (A, B, T) not have zeros invariant :*

$$T = [\ -0.3148 \quad 0.0630 \quad -0.2406 \quad -0.2425\ ];$$

Step 2 : *For $\lambda_2 = -3$, $\lambda_3 = -2 + 2j$ and $\lambda_4 = -2 - 2j$, determined V and W using (18) :*

$$V = \begin{bmatrix} 0.0727 & 0.0564 & 0.0594 \\ -0.2182 & -0.2315 & -0.0061 \\ 0.0242 & -0.0008 & 0.0289 \\ -0.1751 & -0.1325 & -0.1074 \end{bmatrix},$$

$$W = \begin{bmatrix} 0.8000 & 0.6504 & -0.5041 \\ 0.5252 & 0.4797 & -0.0502 \end{bmatrix}$$

Step 3 : *Determined G such that $GCV = W$:*

$$G = \begin{bmatrix} -61.0000 & -6.5685 & -30.8197 \\ -19.7741 & -5.6724 & -12.0000 \end{bmatrix}$$

The matrix in loop closed $A_G = A + BGC$ correspondent, whose the eigenvalues are the desired, is :

$$A_G = \begin{bmatrix} 0.0000 & 1.0000 & 0.0000 & 0.0000 \\ -60.0000 & 1.0000 & -6.5685 & -30.8197 \\ -1.0000 & 0.0000 & 0.0000 & 0.0000 \\ -19.7741 & 0.0000 & -5.6724 & -12.0000 \end{bmatrix}.$$

$\triangle$

3.2 Algorithm of Paraskevopoulos

The presented technique to follow is based on the use of a transformation of coordinates, gotten from a decomposition of the matrix C, that it allows to solve the equation (17) saw a system auxiliary of reduced order $n - p$.

This type of decomposition is used in the theory of control mainly for the construction of observers of minimum order [1] [5]. Geometric point of view, it it aims at the construction subspace $\mathcal{V} = Ker\,(T)$ outer stabilizable and the guarantee of the relation $Ker\,(T) \cap Ker\,(C) = \{0\}$.

Consider a base change given for

$$x = [\ P_1 \quad P_2\ ] \begin{bmatrix} x_1 \\ x_2 \end{bmatrix} \qquad (19)$$
$$P_1 \in \Re^{n \times p}, \quad P_2 \in \Re^{n \times n-p}$$

where $P = [\ P_1 \quad P_2\ ]$ is not singular matrix such that:

$$C\,[\ P_1 \quad P_2\ ] = [\ C_1 \quad 0\ ]\ , \qquad (20)$$
$$\text{with} \quad C_1 \in \Re^{p \times p} \quad \text{and} \quad rank(C_1) = p$$

The inverse of the matrix P é denoted for $\bar{P} = \begin{bmatrix} \bar{P}_1' \\ \bar{P}_2' \end{bmatrix}$, with $\bar{P}_1 \in \Re^{n \times p}$, $\bar{P}_2 \in \Re^{n \times n-p}$:
$[\ P_1 \quad P_2\ ] \begin{bmatrix} \bar{P}_1' \\ \bar{P}_2' \end{bmatrix} = I_n$.

In this base, the system in open loop takes the form

$$\begin{bmatrix} \dot{x_1}(t) \\ \dot{x_2}(t) \end{bmatrix} = \begin{bmatrix} A_{11} & A_{12} \\ A_{21} & A_{22} \end{bmatrix} \begin{bmatrix} x_1(t) \\ x_2(t) \end{bmatrix} + \begin{bmatrix} B_1 \\ B_2 \end{bmatrix} u(t)$$
$$y(t) = [\ C_1 \quad 0\ ] \begin{bmatrix} x_1(t) \\ x_2(t) \end{bmatrix} \qquad (21)$$

where, in particular, $A_{12} \in \Re^{p \times n-p}$ and $A_{22} \in \Re^{n-p \times n-p}$.

Lemma 3.1 *If (C, A) is observable, then always exists $T \in \Re^{n-p \times p}$ such that the equation (10) is verified and $Ker\,(T) \cap Ker\,(C) = \{0\}$.*

Proof:
As shown in [5], the observability of the pair (C, A) is equivalent to the observability of the pair (A_{12}, A_{22}) defined from the change base express in (19). They are the matrices $T_2 \in \Re^{(n-p) \times (n-p)}$, with $posto\,(T_2) = n - p$, and $T_1 \in \Re^{(n-p) \times p}$, solutions of Sylvester equations of *order-reduced*

$$T_2 A_{22} - H_T T_2 = -T_1 A_{12}\ , \ \sigma(H_T) \in \mathcal{C}^- \quad (22)$$

where the matrix $H_T \in \Re^{n-p \times n-p}$ is chosen such that $\sigma(H_T) \in \mathcal{C}^-$. Is important to observe that generally it is possible to find T_2 invertible when H_T does not contain the eigenvalues of the matrix A_{22} [1]. Can then, to calculate, $U \in \Re^{n-p \times p}$ as the only solution of:

$$UC_1 = -\left(T_1 A_{11} + T_2 A_{21} - H_T T_1\right) \qquad (23)$$

Jointly, (22) and (23) verify:

$$\left[\begin{array}{cc} T_1 & T_2 \end{array}\right]\left[\begin{array}{cc} A_{11} & A_{12} \\ A_{21} & A_{22} \end{array}\right] - H_T\left[\begin{array}{cc} T_1 & T_2 \end{array}\right] = U\left[\begin{array}{cc} C_1 & 0 \end{array}\right]$$

that, in the original base, it corresponds to Sylvester equation (10). Moreover, as T_2 is invertible, is had:

$$rank\left(\left[\begin{array}{c} T \\ C \end{array}\right] = \left[\begin{array}{cc} T_1 & T_2 \\ C_1 & 0 \end{array}\right]\left[\begin{array}{c} \bar{P}_1' \\ \bar{P}_2' \end{array}\right]\right) = n \Longleftrightarrow Ker\,(T) \cap Ker\,(C) = \{0\}.$$

$\diamond$

The equations (10) and (22) are related to the construction of observers of minimum order [5] [1].

It can, in particular, to associate the eigenvalues of H_T to the eigenvalues of $(A_{22}+L_2A_{12})$ where $L_2 \in \Re^{n-p\times p}$ is such that

$$T_2L_2 = T_1 \tag{24}$$

Thus, substituting (24) in (22) is had

$$T_2(A_{22} + L_2A_{12}) = H_TT_2 \tag{25}$$

or either

$$\sigma(H_T) = \sigma(A_{22} + L_2A_{12}) \in \mathcal{C}$$

Is important to observe that the decomposition $\bar{P}$ used it is not only. In particular, it can computational be gotten through ortogonal transformations, $\bar{P} = P'$ [1] [3].

The Lemma 3.1 can, in particular, to be used to carry through the step 1 Syrmos and Lewis algorithm, presented in the previous section. In this section, it will be used to enunciate the Theorem 2.1 in presented alternative form originally for Paraskevopoulos algorithm in [1].

Theorem 3.1 *Given the system (1), (2),considers a decomposition in the form (21). Either G the output feedback express for* $G = W(CV)^{-1}$. *Then the matrix G verifies* $\sigma(A + BGC) = \sigma(H_V) \dot{\cup} \sigma(H_T)$, *if and only if*

$$\left[\begin{array}{cc} T_1 & T_2 \end{array}\right]\left[\begin{array}{c} \bar{P}_1' \\ \bar{P}_2' \end{array}\right]V = 0 \tag{26}$$

where the matrices $(W \in \Re^{m\times p}, V \in \Re^{n\times p})$ *and* $(T_1 \in \Re^{n-p\times p}, T_2 \in \Re^{n-p\times n-p})$ *satisfy the Sylvester equation (9) and (22),respectively, with* $det\,(CV) \neq 0$.

From the formularization presented in the Theorem 3.1 above, the following procedure is suggested in [1] to get poles assignment when $mp \geq n$.

3.2.1 Procedure for the determination of output feedback matrix

Considering that H_V and H_T are matrices in the diagonal form of Jordan, from (9) can be written W e V in the form

$$W = \left[\begin{array}{cccc} w_1, & w_2, & \ldots, & w_p \end{array}\right]; \tag{27}$$

$$V = \left[\begin{array}{cccc} X^1w_1, & X^2w_2, & \ldots, & X^pw_p \end{array}\right] \tag{28}$$

where

$$X^i = (\lambda_iI - A)^{-1}B, \quad for \quad i = 1, \ldots, p \tag{29}$$

In the same way, from (22) the matrices T_1 and T_2 have the form

$$T_1 = \left[\begin{array}{c} \phi_{p+1}' \\ \phi_{p+2}' \\ \vdots \\ \phi_n' \end{array}\right] \quad and \quad T_2 = \left[\begin{array}{c} \psi_{p+1}' \\ \psi_{p+2}' \\ \vdots \\ \psi_n' \end{array}\right]$$

where ψ_j , $\forall j = p+1, \ldots, n$, can be gotten of:

$$\psi_j' = \phi' A_{12}(\lambda_jI - A_{22})^{-1} \tag{30}$$

From the notation above, the coupling equation (26) can be written in the form of a bilinear system algebraic equations. Thus, substituting (29) and (30) in (26), is had:

$$\phi_j'\left[\begin{array}{cc} I_p & A_{12}[\lambda_jI - A_{22}]^{-1} \end{array}\right]\left[\begin{array}{c} \bar{P}_1' \\ \bar{P}_2' \end{array}\right]X^iw_i = 0 \tag{31}$$

$$for \quad i = 1, , \ldots, p \quad and \quad j = p+1, \ldots, n$$

Solving the equation (31), the parameters are determined for w_i and ϕ_j'. Then, the matrices W and V are defined from the equation (27)and the output feedback matrix G is directly calculated of (14).

From this formularization, the justification to follow is given in [1] for the obtainment of condition less restrictive $mp \geq n$ for arbitrary poles positioning for output feedback: "The equation (27)provides $p(m-1)$ free parameters (from the arbitrary elements of $w_1, w_2, \ldots, w_p$). Additionally the equation (30) provides $(p-1)(n-p)$ free parameters (from the arbitrary elements of $\phi_{p+1}, \phi_{p+2}, \ldots, \phi_n$). On the other hand the equation (31) results in a system of $p(n-p)$ independent equations. Thus for the solution existence, the number of equations must be equal or smaller that the addition of the free parameters. After algebraic manipulations it is gotten condition $mp \geq n$" .

Example 3.2 *: To follow, the procedure of Paraskevopoulos is applied to get the poles assignment for the system defined for A and B, used in the previous example. Is considered in this that only* 2 *states are measurable or either:*

$$C = \begin{bmatrix} 0 & 0 & 1 & 0 \\ 0 & 0 & 0 & 1 \end{bmatrix}$$

The corresponding system is controllable and observable being $mp = 4 = n$, *com* $p = 2$ *e* $m = 2$. *The eigenvalues to assignment are* $\Lambda_V = \{-1, -2\}$ *and* $\Lambda_T = \{-3, -4\}$.

In first place it finds a decomposition

$$P = \begin{bmatrix} 0 & 0 & 1 & 0 \\ 0 & 0 & 0 & 1 \\ 1 & 0 & 0 & 0 \\ 0 & 1 & 0 & 0 \end{bmatrix}$$

using (21) such that:

$$C \begin{bmatrix} P_1 & P_2 \end{bmatrix} = \begin{bmatrix} \bar{C}_1 & 0 \end{bmatrix} = \begin{bmatrix} 1 & 0 & 0 & 0 \\ 0 & 1 & 0 & 0 \end{bmatrix}$$

and is calculated

$$\begin{bmatrix} A_{12} \\ A_{22} \end{bmatrix} = \begin{bmatrix} \bar{P}_1' \\ \bar{P}_2' \end{bmatrix} AP_2 = \begin{bmatrix} 0 & 0 \\ -1 & 0 \\ 0 & 1 \\ 0 & 0 \end{bmatrix}.$$

For $\lambda_1 = -1, \lambda_2 = -2$,*we fix the 2 free parameters in* $\begin{bmatrix} w_1 & w_2 \end{bmatrix} = \begin{bmatrix} 1.0 & 1.0 \\ w_{12} & w_{22} \end{bmatrix}$,*to get* $w_{12} = -2.2$ *and* $w_{22} = 2.8$. *On the other hand for* $\lambda_3 = -3, \lambda_4 = -4$, *we fix the 2 free parameters in* $\begin{bmatrix} \phi_3' \\ \phi_4' \end{bmatrix} = \begin{bmatrix} 1.0000 & \phi_{32} \\ 1.0000 & \phi_{42} \end{bmatrix}$, *to get* $\phi_{32} = -1.6364$ *and* $\phi_{42} = -1.8824$. *In this form the matrices are determined* (W, V) *and* (T_1, T_2, T) *that satisfies the Sylvester equations (9), (22) and (31),respectively with* $det(CV) \neq 0$*:*

$$V = \begin{bmatrix} 0.6 & -0.8 \\ -1.6 & 0.6 \\ 1.6 & -1.2 \\ 0.6 & -0.4 \end{bmatrix} \quad ; \quad W = \begin{bmatrix} 1.0 & 1.0 \\ -2.2 & 2.8 \end{bmatrix}$$

$$T_1 = \begin{bmatrix} 1.0000 & -1.6364 \\ 1.0000 & -1.8824 \end{bmatrix}; T_2 = \begin{bmatrix} -0.5455 & 0.1818 \\ -0.4706 & 0.1176 \end{bmatrix}$$

$$T = \begin{bmatrix} T_1 & T_2 \end{bmatrix} \begin{bmatrix} \bar{P}_1' \\ \bar{P}_2' \end{bmatrix}$$

$$T = \begin{bmatrix} -0.5455 & 0.1818 & 1.0000 & -1.6364 \\ -0.4706 & 0.1176 & 1.0000 & -1.8824 \end{bmatrix}$$

The system (A, B, T) *has as invariant zeros and stable eigenvalues:* $\{-1, -2\}$. *The output feedback matrix correspondent* G *is determined by* $GCV = W$*:*

$$G = \begin{bmatrix} -12.5 & 35.0 \\ -10.0 & 23.0 \end{bmatrix}$$

The matrix in closed loop $A_G = A + BGC$ *correspondent,whose the eigenvalues are the desired , it is:*

$$A_G = \begin{bmatrix} 0.0 & 1.0 & -12.5 & 35.0 \\ 0.0 & 0.0 & 1.0 & 0.0 \\ 0.0 & 0.0 & -10.0 & 24.0 \\ -1.0 & 0.0 & 0.0 & 0.0 \end{bmatrix}.$$

$\triangle$

4 Conclusion

Some base results had been presented in this article that basis the algorithms and theoretical results. The concept of subspace was presented $O.S.$ (C, A, B)-invariant e its relation with the solution of stabilization problem using output feedback , by two coupled Sylvester equations.

Is distinguished the fact of the algorithm of Syrmos modified to allow to the solution of the problem in 2 sequence steps, for systems that verify the condition of Kimura $(m + p > n)$. As the algorithm, is based on the solution of a system of bilinear equations for the attainment of poles assignment, having been able to be applied the systems that verify the condition less restrictive $mp \geq n$.

The character of solution in two steps of the first algorithm still will be explored in the searche future. It is important to point out that this procedure also can solve the stabilization problem in systems that do not verify the Kimura condition, using itself compensating dynamic of order $\nu > n - (m + p)$.

References

[1] A. T Alexandridis and Paraskevopoulos, P. N., A New Approach to Eigenstruture Assignment by Output Feedback, *IEEE Trans. Automatic. Control*, vol. 41, number 7, July, 1996.

[2] E. B. Castelan and J. C. Hennet, Eigenstructure Assignment for State Constrained Linear Continuos Time Systems, *Automatica*, vol. 28, number 3, (1993) 605-611.

[3] E. B. Castelan and J. C. Hennet and E. R. Ll. Villarreal, Quadratic Characterization and Use of Output Stabilizable Subspaces, "Proceedings (CD) of the 8th Mediterranean Conference on Control and Automation", Greece, 2000.

[4] E. B. Castelan and J. C. Hennet and E. R. Ll. Villarreal, Quadratic Characterization and Use of Output Stabilizable Subspaces, *IEEE Trans. Automatic. Control*, vol. 48, number 4, (2003) 654-660.

[5] C. T. Chen, "Linear System Theory ans Design", Holt, Rinehart and Winston, 1996.

[6] L. Dai, "Singular Control System", Springer-Verlag, 1989.

[7] L. R. Fletcher and J. Kautsky and G. K. G. Kolka and N. K. Nichols, Eigenstructure Assingment by Output Feedback in Descriptor Systems, *IEEE Trans. Automatic. Control*, vol. 42, (1985) 1457-1468.

[8] H. Kimura, Pole Assignment by Gain Ouptup Feedback, *IEEE Trans. Automatic. Control*, vol. 20, (1975) 509-516.

[9] V. L. Syrmos and F. L. Lewis, Output Feedback Eigenstructure Assignment Using Two Sylvester Equations, *IEEE Trans. Automatic. Control*, vol. 38, number 3, (1993) 495-499.

[10] V. L. Syrmos and F. L. Lewis, Transmission Zero Assignment using Descriptions, *IEEE Trans. Automatic. Control*, vol. 38, number 7, (1993) 1115-1120.

[11] V. L. Syrmos and F. L. Lewis, Bilinear Formulation for the Output Feedback Problem in Linear System, *IEEE Trans. Automatic. Control*, vol. 39, number 2, (1994) 410-414.

[12] V. L. Syrmos and C. T. Abdallah and P. Dorato and K. Grigoriadis, Static Output Feedback - A Survey *Automatica* , vol 33, number 2, (1997) 125-137.

[13] W. M. Wonahm, "Linear Multivariable Control, a Geometric Approach", Springer-Verlag, 1979.

View publication stats

ENSINO DAS OPERAÇÕES BÁSICAS NO 9º ANO DO ENSINO FUNDAMENTAL: UMA APLICAÇÃO ATRAVÉS DA RECOMPOSIÇÃO DA APRENDIZAGEM MATEMÁTICA

Rogério da Silva Costa
Professor Efetivo da Secretaria Municipal de Educação de Aracati (SME- Aracati), Aracati, CE.
E-mail: rogerio.costa@aracati.ce.gov.br

Walter Martins Rodrigues
Professor Titular da Universidade Federal Rural do Semi-árido (PROFMAT/UFERSA), Mossoró, RN.
E-mail: walterm@ufersa.edu.br

Elmer Rolando Llanos Villarreal
Professor Associado da Universidade Federal Rural do Semi-árido (PROFMAT/UFERSA), Mossoró, RN.
E-mail: elmerllanos@ufersa.edu.br

Ensino de Matemática

< ENSINO DAS OPERAÇÕES BÁSICAS NO 9º ANO DO ENSINO FUNDAMENTAL >: < uma aplicação através da recomposição da aprendizagem matemática >

Resumo: Esse trabalho traz uma proposta de ensino das operações aritméticas básicas da matemática através da recomposição da aprendizagem em matemática aplicada em uma turma de 9º ano da Escola Domingos Costa Teobaldo no município de Aracati-CE. O objetivo desse trabalho é propor algumas ações a serem compartilhadas entre docentes que atuam no ensino de matemática e enfrentam o desafio da recomposição da aprendizagem que as turmas exigem, pós pandemia da COVID-19. A metodologia utilizada foi de aplicação da proposta de ensino com os alunos do 9º ano da escola, abordada em dezesseis encontros a partir do uso de alguns recursos didáticos. Concluída as ações, apresentam-se resultados significativos no tocante ao fortalecimento da aprendizagem destas operações básicas, e também, resultados de avaliação externa que comprovam um ganho de compreensão e aprendizagem matemática favorável para o aprendizado de habilidades matemáticas mais complexas abordadas na etapa final do ensino fundamental.

Palavras-chave: Recomposição da aprendizagem. Operações básicas. Pandemia da Covid-19.

1. INTRODUÇÃO

A presente pesquisa traz um estudo da educação contextualizada com a realidade social do educando que é um fator muito interessante que veio à tona como uma preocupação educativa necessária no Brasil, principalmente a partir dos trabalhos do ilustre professor Ubiratan D'Ambrosio, no qual afirma que "A Matemática é a única disciplina escolar que é ensinada aproximadamente da mesma maneira (tradicional) e com o mesmo conteúdo para todas as crianças do mundo" (D'AMBROSIO, 1993).

"O saber ensinar não é transferir conhecimento, mas criar as possibilidades para a sua própria produção ou sua construção" (FREIRE, 2011, p. 47). Partindo dessa premissa, as dificuldades de aprendizagem da matemática não incidem somente sobre o aluno, mas, também sobre aquele que ensina.

É de longa data que muitos estudiosos vêm tentando desconstruir a fala de que a matemática é uma disciplina difícil cuja aprendizagem é só para quem nasce com o talento para ela. A discussão em torno dessa crença e o esforço para superá-la têm sido o desafio de muitos professores.

Mesmo com muito empenho, a matemática costuma ser ainda hoje a vilã nas instituições de ensino, pois, como já alertara os Parâmetros Curriculares Nacionais (PCN), é frequente o professor apresentar conteúdos, definições, exemplos, demonstrações para o aluno exercitar pela repetição, pressupondo que a reprodução gere aprendizagem (BRASIL,1998, p. 37).

Com base nesses antecedentes, proponho este trabalho com uma abordagem nas operações aritméticas básicas da matemática numa turma de 9º ano a partir da necessidade de tais operações serem de fundamental importância para o aprendizado de habilidades matemáticas mais complexas na série final do ensino fundamental.

O interesse neste assunto surgiu ao observar o aumento da problemática na aprendizagem matemática dos alunos da Escola Domingos Costa Teobaldo e por dar importância às orientações apresentadas em formações continuadas de Professores do Programa de Aprendizagem na Idade Certa – MAISPAIC sobre a necessidade de mudanças essenciais a serem realizadas para combater essa problemática.

Nesse sentido realizamos um trabalho de pesquisa no mestrado profissional de matemática – PROFMAT, voltado para elaboração da dissertação de mestrado do primeiro autor (COSTA, R. S, 2023). No qual o estudo focou no retorno do ensino presencial após quase dois anos de ensino remoto.

A pandemia intensificou desafios que já existiam na Educação, e agora é necessário articular ações para reordenar e impulsionar as aprendizagens. Antes da covid-19, a Educação pública brasileira já enfrentava graves problemas. Portanto, trata-se de uma situação que é emergencial e requer uma ação rápida, com estratégias para, mais do que recuperar, potencializar a aprendizagem dos estudantes.

De acordo com Santos (2022), na concepção de Sonia Guaraldo, consultora pedagógica e especialista em formação continuada no Instituto Gesto:

O EXCEL COMO FERRAMENTA PARA RESOLUÇÃO DE SISTEMAS DE EQUAÇÕES LINEARES POR ESCALONAMENTO

José Cláudio da Silva
Professor Efetivo da Secretaria Estadual de Educação do Rio grande do Norte (IERN – Campus Maria do Carmo Ferreira), Jardim de Piranhas, RN.
E-mail: josesilva914@educar.rn.gov.br

Walter Martins Rodrigues
Professor Titular da Universidade Federal Rural do Semi-árido (PROFMAT/UFERSA), Mossoró, RN.
E-mail: walterm@ufersa.edu.br

Elmer Rolando Llanos Villarreal
Professor Associado da Universidade Federal Rural do Semi-árido (PROFMAT/UFERSA), Mossoró, RN.
E-mail: elmerllanos@ufersa.edu.br

Ensino de Matemática

O EXCEL COMO FERRAMENTA PARA RESOLUÇÃO DE SISTEMAS DE EQUAÇÕES LINEARES POR ESCALONAMENTO

Resumo: O estudo e a compreensão dos sistemas de equações lineares desempenham um papel fundamental no desenvolvimento das habilidades matemáticas e na resolução de problemas do mundo real. Neste sentido, é importante ressaltar que os estudantes são expostos a conceitos-chave, como a interpretação geométrica de soluções, métodos de resolução algébrica e aplicações em diversas áreas do conhecimento. Dominar esse conteúdo não apenas aprimora a capacidade analítica e de raciocínio lógico, mas também fornece ferramentas essenciais para enfrentar desafios complexos, estimulando a criatividade na resolução de problemas e preparando os alunos para campos profissionais que exigem habilidades em sistemas de equações lineares. Para fortalecer o ensino de sistemas de equações lineares, o presente trabalho apresenta a criação da Calculadora de Sistemas Lineares no Excel (CSLE) e a implementação de uma sequência didática que representam uma abordagem inovadora e prática para enriquecer o ensino desses conceitos. Essa ferramenta proporciona aos alunos uma maneira interativa de explorar e compreender os sistemas de equações lineares, permitindo uma visualização dinâmica das soluções e estimulando o aprendizado ativo. Além disso, a análise de dados sobre a aceitação da CSLE revela percepções valiosos sobre a eficácia dessa abordagem, oferecendo informações sobre a receptividade dos alunos, suas dificuldades e os benefícios percebidos ao utilizar essa ferramenta. Essa iniciativa não só fortalece o entendimento conceitual, mas também possibilita uma avaliação mais ampla e detalhada do processo de aprendizagem, contribuindo para o aprimoramento contínuo das estratégias de ensino-aprendizagem em matemática.
Palavras-chave: Sistemas de equações lineares. Calculadora Excel. Ensino de Matemática.

1. INTRODUÇÃO

A matemática está presente em todas as atividades diárias, proporcionando uma melhor organização e harmonia nas nossas vidas. Ela nos ajuda a entender e resolver problemas, a tomar decisões e a desenvolver habilidades de pensamento crítico. Desde calcular despesas e planejar orçamentos até medir ingredientes para cozinhar ou calcular distâncias em uma viagem, a matemática está sempre presente, nos auxiliando a alcançar uma maior eficiência e precisão em nossas tarefas diárias. Além disso, a matemática também é fundamental em áreas como ciência, tecnologia, engenharia e finanças, desempenhando um papel essencial no avanço da sociedade e no desenvolvimento de novas descobertas e inovações. Nesse sentido, o conhecimento matemático é extremamente relevante, seja para sua aplicação em situações mais básicas, como o método utilizado por povos primitivos que contavam rebanhos utilizando pedras, ossos e nós em cordas, ou em processos mais complexos, como o funcionamento de instrumentos como relógios, termômetros, fornos, calculadoras e computadores, além dos telefones celulares.

O ensino do conteúdo de sistemas de equações lineares no ensino médio desempenha um papel fundamental na formação teórica e prática dos estudantes, preparando-os para adquirir novos conhecimentos em Álgebra. É essencial que a prática de ensino proporcione as condições adequadas para uma compreensão aprofundada dos conceitos matemáticos, a fim de evitar possíveis prejuízos, como a resistência à matéria e a reprovação dos alunos.

Levando em consideração a relevância dos sistemas de equações lineares na vida cotidiana e a conexão desse conhecimento, é fundamental que os educadores assumam um papel ativo no processo de ensino. Como afirmado por Van de Walle (2009, p. 21), “o que os alunos aprendem depende quase que exclusivamente das experiências fornecidas pelos professores em sala de aula”. Diante disso, surge a questão: qual é o papel das tecnologias educacionais no apoio ao ensino e aprendizado de sistemas de equações lineares para alunos do ensino médio com pouco conhecimento prévio? Devido a este questionamento, o objetivo geral desta pesquisa é investigar o papel das tecnologias educacionais no apoio ao ensino e aprendizado de sistemas de equações lineares para alunos do ensino médio (2ª ou 3ª séries), enquanto os objetivos específicos incluem elaborar uma sequência didática, aplicá-la e analisar os resultados obtidos.

A principal contribuição deste trabalho reside na criação e implementação da Calculadora de Sistemas Lineares no Excel (CSLE). Essa ferramenta inovadora, desenvolvida pelo autor deste trabalho, destaca-se como um recurso didático metodológico para o ensino de sistemas de equações lineares no Ensino Médio. Essa calculadora foi desenvolvida com o propósito de proporcionar uma visualização interativa e acessível da

HISTÓRIA DA MATEMÁTICA E ESTRATÉGIAS INTERDISCIPLINARES NO ENSINO DE LOGARITMOS

Walter Martins Rodrigues
Elmer Rolando Llanos Villarreal

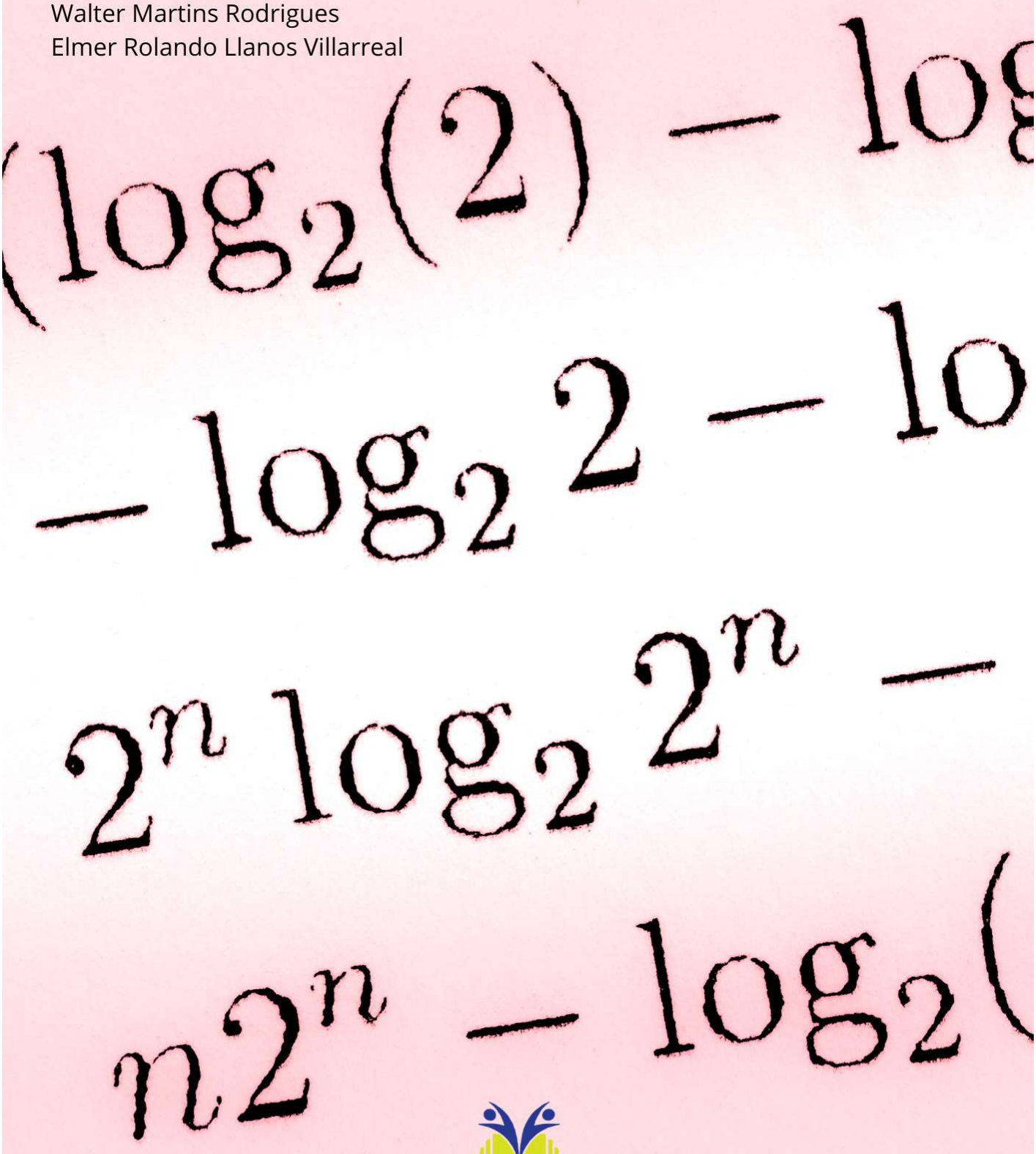

EDITORA CONHECIMENTO LIVRE

Walter Martins Rodrigues
Elmer Rolando Llanos Villarreal

História da Matemática e estratégias interdisciplinares no ensino de Logaritmos

1ª ed.

Piracanjuba-GO
Editora Conhecimento Livre
Piracanjuba-GO

Copyright© 2023 por Editora Conhecimento Livre

1ª ed.

Dados Internacionais de Catalogação na Publicação (CIP)

Rodrigues, Walter Martins
R146H História da Matemática e estratégias interdisciplinares no ensino de Logaritmos / Walter Martins Rodrigues. Elmer Rolando Llanos Villarreal. – Piracanjuba-GO

Editora Conhecimento Livre, 2023

151 f.: il
DOI: 10.37423/2023.edcl809
ISBN: 978-65-5367-388-5
Modo de acesso: World Wide Web
Incluir Bibliografia

1. ensino-contextualizado 2. história-da-matemática 3. ação-interdisciplinar I. Rodrigues, Walter Martins II. Villarreal, Elmer Rolando Llanos III. Título

CDU: 510

https://doi.org/10.37423/2023.edcl809

O conteúdo dos artigos e sua correção ortográfica são de responsabilidade exclusiva dos seus respectivos autores.

EDITORA CONHECIMENTO LIVRE

Corpo Editorial

MSc Edson Ribeiro de Britto de Almeida Junior
MSc Humberto Costa
MSc Thays Merçon
MSc Adalberto Zorzo
MSc Taiane Aparecida Ribeiro Nepomoceno
PHD Willian Douglas Guilherme
MSc Andrea Carla Agnes e Silva Pinto
MSc Walmir Fernandes Pereira
MSc Edisio Alves de Aguiar Junior
MSc Rodrigo Sanchotene Silva
MSc Wesley Pacheco Calixto
MSc Adriano Pereira da Silva
MSc Frederico Celestino Barbosa
MSc Guilherme Fernando Ribeiro
MSc. Plínio Ferreira Pires
MSc Fabricio Vieira Cavalcante
PHD Marcus Fernando da Silva Praxedes
MSc Simone Buchignani Maigret
Dr. Adilson Tadeu Basquerote
Dra. Thays Zigante Furlan
MSc Camila Concato
PHD Miguel Adriano Inácio
MSc Anelisa Mota Gregoleti
PHD Jesus Rodrigues Lemos
MSc Gabriela Cristina Borborema Bozzo
MSc Karine Moreira Gomes Sales
Dr. Saulo Cerqueira de Aguiar Soares
MSc Pedro Panhoca da Silva
MSc Helton Rangel Coutinho Junior
MSc Carlos Augusto Zilli
MSc Euvaldo de Sousa Costa Junior
Dra. Suely Lopes de Azevedo
MSc Francisco Odecio Sales
MSc Ezequiel Martins Ferreira
MSc Eliane Avelina de Azevedo Sampaio

Editora Conhecimento Livre
Piracanjuba-GO
2023

SUMÁRIO

CAPÍTULO 1 5
DA GÊNESE DA INVENÇÃO À FORMULAÇÃO CONCEITUAL DOS LOGARITMOS
Iran Abreu Mendes
Evanildo Costa Soares
DOI 10.37423/231008313

CAPÍTULO 2 37
PROPOSTA DE AÇÃO DIDÁTICA: EXPLORANDO A CONSTRUÇÃO DOS LOGARITMOS
Walter Martins Rodrigues
José Eduardo Colle
William Rodrigues da Silva
Elmer Rolando Llanos Villarreal
DOI 10.37423/231008299

CAPÍTULO 3 57
LOGARITMOS : HISTÓRIA, APLICAÇÕES E VÍDEOS ANIMADOS
Renato Mucciacito
Lúcio Tunes dos Santos
DOI 10.37423/231008279

CAPÍTULO 4 91
LOGARITMOS: HISTÓRIAS DE UM CONCEITO VIVO
Walter Martins Rodrigues
Jackson Jonas da Silva Costa
José Eduardo Colle
William Rodrigues da Silva
DOI 10.37423/231008289

CAPÍTULO 5 111
APLICAÇÕES DA FUNÇÃO LOGARÍTMICA EM TRANSFORMAÇÃO DE DADOS NA ESTATÍSTICA
Walter Martins Rodrigues
Elmer Rolando Llanos Villarreal
Janilson Pinheiro de Assis
Roberto Pequeno de Sousa
Joelma de Assis França
Robson Pequeno de Sousa
Paulo César Ferreira Linhares
DOI 10.37423/230908262

amazon.co.uk Try Prime | Books | Amazon Prime | 30-day free trial
Shop by Department | Your Amazon.co.uk | Today's Deals | Christmas Store | Hello. Sign in Your Account | Try Prime | Your Lists | 0 Basket
Books | Advanced Search | Best Sellers | Top New Releases | Deals in Books | School Books | Textbooks | Children's | Kindle | Audible

one result for **Books** : **"Sâmya Lorena de Medeiros Confessor"** Sort by Relevance

Show results for

Books
Business, Finance & Law (1)

Refine by

Format
Paperback (1)

Language
Portuguese (1)

Delivery Option (What's this?)
prime
Free UK Delivery by Amazon

International Shipping (What's this?)
International Shipping Eligible

Availability
Include Out of Stock

Análise comparativa de controladores MPPT em um sistema fotovoltaico: Comparação entre o método tradicional Perturbação e...

by Sâmya Lorena de Medeiros Confessor and Elmer Rolando Villarreal

Paperback
£28.00 prime
Get it by **Tuesday, Oct 24**
Eligible for FREE UK Delivery

More buying choices
£28.00 (4 used & new offers)

Prime Students get £10 off on £40 spend See Details

Search Feedback

Did you find what you were looking for?

Yes | No

If you need help or have a question for Customer Service, please visit the Help Section.

Your recently viewed items and featured recommendations

See personalised recommendations

Sign in

New customer? Start here.

Back to top

Get to Know Us
Careers
About Us
UK Modern Slavery Statement

Make Money with Us
Sell on Amazon
Sell on Amazon Business
Associates Programme
Fulfilment by Amazon
Advertise Your Products
Independently Publish with Us
Amazon Pay
Become an Amazon Vendor
› See all

Amazon Payment Methods
Amazon Platinum Mastercard
Amazon Money Store
Gift Cards
Amazon Currency Converter
Payment Methods Help
Shop with Points
Top Up Your Account

Let Us Help You
Track Packages or View Orders
Delivery Rates & Policies
Amazon Prime
Returns & Replacements
Manage Your Content and Devices
Amazon Mobile App
Amazon Assistant
Help

amazon
Australia Brazil Canada China France Germany India Italy Japan Mexico Netherlands Spain United States

Amazon Music AbeBooks ACX Amazon BuyVIP

Stream millions
of songs

Amazon Tickets
Music, Theatre
& Comedy

DPReview
Digital
Photography

Kindle Direct Publishing
Indie Digital Publishing
Made Easy

Souq.com
Shop Online in
the Middle East

Books, art
& collectables

Amazon Web Services
Scalable Cloud
Computing Services

Goodreads
Book reviews
& recommendations

Prime Now
2-Hour Delivery
on Everyday Essentials

Warehouse Deals
Deep Discounts
Open-Box Products

Whole Foods Market
We Believe in
Real Food

Audiobook Publishing
Made Easy

Audible
Download
Audio Books

IMDb
Movies, TV
& Celebrities

Shopbop
Designer
Fashion Brands

LOVEFiLM
DVD & Blu-ray
To Rent By Post

The European
Shopping Club

Book Depository
Books With Free
Delivery Worldwide

Junglee.com
Shop Online
in India

Yoyo.com
A Happy Place
To Shop For Toys

Amazon Business
Service for
business customers

Conditions of Use & Sale Privacy Notice Cookies & Internet Advertising © 1996-2017, Amazon.com, Inc. or its affiliates

NEW & INTERESTING FINDS ON AMAZON EXPLORE

amazon Try Prime | Books | Everyday FREE Shipping: Eligible orders over $25

Departments | Your Amazon.com | Today's Deals | EN | Hello. Sign in Account & Lists | Orders | Try Prime | 0 Cart

Books | Advanced Search | New Releases | NEW! Amazon Charts | Best Sellers & More | The New York Times® Best Sellers | Children's Books | Textbooks

1 result for **Books** : **"Elmer Rolando Llanos Villarreal"**

Sort by Relevance

Show results for

Books
Science & Math

Refine by

International Shipping (What's this?)
- Ship to Brazil

Language
- Portuguese

Amazon Prime
- prime

Eligible for Free Shipping
- Free Shipping by Amazon

Condition
New
Used

Availability
- **Include Out of Stock**

Abordagem Geométrica para Estabilização por Realimentação de Saída: Extensão aos Sistemas Descritores (Portuguese Edition) Oc…
by Llanos Villarreal, Elmer Rolando

Paperback
$45.56 ~~$51.00~~ prime
Get it by **Thursday, Oct 19**
FREE Shipping on eligible orders

More Buying Choices
$45.56 (11 used & new offers)

Sponsored Links (What's this?)

1. **Looking for Greek Books? - Online bookshop 200,000 titles** — We ship to all European & Worldwide destinations. Fast and trackable delivery. www.perizitito.com.cy/
2. **Libreria Shalom Books Ny** — Distribuidora libros catolicos visitanos, gran variedad www.shalom**books**ny.com/
3. **Maluco Por Leitura Livros BH - Infantil Juvenil Romances Geek** — Acesse nosso site, e descubra livros fantásticos a preços incríveis. www.malucoporleitura.com.br/

Ad feedback

Search Feedback

Did you find what you were looking for?

Yes | No

If you need help or have a question for Customer Service, please visit the Help Section.

Your recently viewed items and featured recommendations

See personalized recommendations

Sign in

New customer? Start here.

Back to top

Get to Know Us
Careers
About Amazon
Investor Relations
Amazon Devices

Make Money with Us
Sell on Amazon
Sell Your Services on Amazon
Sell on Amazon Business
Sell Your Apps on Amazon
Become an Affiliate
Advertise Your Products
Self-Publish with Us

Amazon Payment Products
Amazon Rewards Visa Signature Cards
Amazon.com Store Card
Amazon.com Corporate Credit Line
Shop with Points
Credit Card Marketplace
Reload Your Balance
Amazon Currency Converter

Let Us Help You
Your Account
Your Orders
Shipping Rates & Policies
Amazon Prime
Returns & Replacements
Manage Your Content and Devices
Amazon Assistant

Become an Amazon Vendor

Help

› See all

amazon

English United States

Amazon Music
Stream millions of songs

Amazon Drive
Cloud storage from Amazon

6pm
Score deals on fashion brands

AbeBooks
Books, art & collectibles

ACX
Audiobook Publishing Made Easy

Alexa
Actionable Analytics for the Web

Amazon Business
Everything For Your Business

AmazonFresh
Groceries & More Right To Your Door

AmazonGlobal
Ship Orders Internationally

Home Services
Handpicked Pros Happiness Guarantee

Amazon Inspire
Digital Educational Resources

Amazon Rapids
Fun stories for kids on the go

Amazon Restaurants
Food delivery from local restaurants

Amazon Video Direct
Video Distribution Made Easy

Amazon Web Services
Scalable Cloud Computing Services

Audible
Download Audio Books

AudiobookStand
Discount Audiobooks on Disc

Book Depository
Books With Free Delivery Worldwide

Box Office Mojo
Find Movie Box Office Data

ComiXology
Thousands of Digital Comics

CreateSpace
Indie Print Publishing Made Easy

DPReview
Digital Photography

East Dane
Designer Men's Fashion

Fabric
Sewing, Quilting & Knitting

Goodreads
Book reviews & recommendations

IMDb
Movies, TV & Celebrities

IMDbPro
Get Info Entertainment Professionals Need

Junglee.com
Shop Online in India

Kindle Direct Publishing
Indie Digital Publishing Made Easy

Prime Now
FREE 2-Hour Delivery on Everyday Items

Prime Photos
Unlimited Photo Storage Free With Prime

Shopbop
Designer Fashion Brands

TenMarks.com
Math Activities for Kids & Schools

Warehouse Deals
Open-Box Discounts

Whispercast
Discover & Distribute Digital Content

Whole Foods Market
America's Healthiest Grocery Store

Withoutabox
Submit to Film Festivals

Woot!
Deals and Shenanigans

Zappos
Shoes & Clothing

Souq.com
Shop Online in the Middle East

Subscribe with Amazon
Discover & try subscription services

Conditions of Use Privacy Notice Interest-Based Ads © 1996-2017, Amazon.com, Inc. or its affiliates

Portal do Docente

UNIVERSIDADE FEDERAL RURAL DO SEMI-ÁRIDO
SISTEMA INTEGRADO DE GESTÃO DE ATIVIDADES ACADÊMICAS

EMITIDO EM 26/08/2024 16:08

DECLARAÇÃO DE ORIENTAÇÃO

Declaramos para os devidos fins que o docente ELMER ROLANDO LLANOS VILLARREAL, matrícula SIAPE de número 1673887, orienta(ou)/coorienta(ou) aluno(s) de STRICTO SENSU, conforme quadro abaixo:

PROGRAMA DE PÓS-GRADUAÇÃO EM ENGENHARIA ELÉTRICA

Nome	Nível	Tipo	Período
REUBER REGIS DE MELO	MESTRADO	Orientador	08/08/2011 a 20/12/2013.
CLAUDIO MARCIO MEDEIROS DE AZEVEDO	MESTRADO	Orientador	14/09/2011 a 29/11/2013.
CARLOS ALBERTO TEIXEIRA JUNIOR	MESTRADO	Orientador	26/09/2012 a 08/10/2014.
CLAYTON ANTONIO DE MIRANDA OLIVEIRA	MESTRADO	Orientador	25/10/2012 a 22/09/2014.

PROGRAMA DE PÓS-GRADUAÇÃO EM MATEMÁTICA

Nome	Nível	Tipo	Período
ANTONIO CARLOS DE QUEIROZ SILVEIRA	MESTRADO	Orientador	04/02/2013 a 12/09/2013.
JOÃO DEHON DE SOUSA	MESTRADO	Orientador	04/02/2013 a 23/09/2013.
JOZILDES VIEIRA LIMA	MESTRADO	Orientador	04/02/2013 a 13/08/2013.

PROGRAMA DE PÓS-GRADUAÇÃO EM ENGENHARIA ELÉTRICA

Nome	Nível	Tipo	Período
SAMEQUE FARIAS CUNHA DE OLIVEIRA	MESTRADO	Orientador	11/03/2013 a 31/03/2015.

PROGRAMA DE PÓS-GRADUAÇÃO EM MATEMÁTICA

Nome	Nível	Tipo	Período
HUGO ARNAUD MENDES	MESTRADO	Orientador	25/04/2013 a 04/05/2016.

PROGRAMA DE PÓS-GRADUAÇÃO EM ENGENHARIA ELÉTRICA

Nome	Nível	Tipo	Período
AUGUSTO CESAR DE SOUSA	MESTRADO	Orientador	20/11/2013 até a presente data.
DANILO DE SANTANA PENA	MESTRADO	Orientador	04/12/2013 a 15/10/2015.

PROGRAMA DE PÓS-GRADUAÇÃO EM MATEMÁTICA

Nome	Nível	Tipo	Período
FRANCISCO RAFAEL DE FREITAS CAVALCANTE	MESTRADO	Orientador	01/03/2014 a 06/09/2016.

PROGRAMA DE PÓS-GRADUAÇÃO EM ENGENHARIA ELÉTRICA

Nome	Nível	Tipo	Período
EDPO RODRIGUES DE MORAIS	MESTRADO	Orientador	25/09/2014 a 29/05/2017.
SAMYA LORENA DE MEDEIROS CONFESSOR	MESTRADO	Orientador	01/10/2014 a 16/12/2014.

PROGRAMA DE PÓS-GRADUAÇÃO EM MATEMÁTICA

Nome	Nível	Tipo	Período
MAYKEL SAMUEL MARINHO CÂMARA	MESTRADO	Orientador	26/06/2017 a 04/07/2018.
ROGÉRIO DA SILVA COSTA	MESTRADO	Orientador	18/10/2022 a 07/08/2023.

Código de Verificação:
26f3f939fa

ATENÇÃO

Para verificar a autenticidade deste documento acesse **https://sigaa.ufersa.edu.br/sigaa/documentos/** e utilize o link *Ensino >> Declaração de Orientação*, informando a Matrícula SIAPE, a data de emissão do documento e o código de verificação.

SIGAA | Superintendência de Tecnologia da Informação e Comunicação

Portal do Docente

Universidade Federal Rural do Semi-Árido
Sistema Integrado de Gestão de Atividades Acadêmicas

Emitido em 04/10/2024 17:51

Pró-Reitoria de Graduação

Declaração de Orientações

Declaramos para os devidos fins que o Docente ELMER ROLANDO LLANOS VILLARREAL, Matrícula SIAPE de número 1673887, atuou nesta instituição nas seguintes orientacoes, em seus respectivos períodos letivos:

2012.2 - AMB0791 - ESTAGIO CUR. SUP. V: SEMINARIO DE DOCENCIA - TCC
2009213535 - JOSE BERNARDO DO NASCIMENTO
2012.1 - AMB1154 - TRABALHO DE CONCLUSAO DE CURSO
2009242514 - YAGO FELIPE DA COSTA
2012.1 - AMB1154 - TRABALHO DE CONCLUSAO DE CURSO
2009242160 - FRANCISCO ALDO DE MORAIS
2015.2 - AMB1154 - TRABALHO DE CONCLUSAO DE CURSO
2013010613 - MAXWELL CAVALCANTE JACOME
2016.1 - AMB1154 - TRABALHO DE CONCLUSAO DE CURSO
2010121881 - RAFAEL HELANO SOARES DE PAIVA
2017.1 - AMB1154 - TRABALHO DE CONCLUSAO DE CURSO
2014020936 - LUIZ FELIPE NUNES DE OLIVEIRA
2017.1 - AMB1154 - TRABALHO DE CONCLUSAO DE CURSO
2014021020 - VALMIR PEREIRA BEZERRA JÚNIOR

MOSSORÓ, 04 de Outubro de 2024

Código de Verificação:
e690ae5476

Para verificar a autenticidade deste documento acesse **https://sigaa.ufersa.edu.br/sigaa/documentos/**, informando a Matrícula do SIAPE, data de emissão do documento e o código de verificação.

SIGAA | Superintendência de Tecnologia da Informação e Comunicação

MINISTÉRIO DA EDUCAÇÃO
UNIVERSIDADE FEDERAL RURAL DO SEMI-ÁRIDO
PRÓ-REITORIA DE PESQUISA E PÓS-GRADUAÇÃ0
Av. Francisco Mota, 572 – C. Postal 137 – Bairro Pres. Costa e Silva – Mossoró – RN – CEP: 59.625-900 - Tel.: (84)3317-8296 – E.mail: proppg@ufersa.edu.br

D E C L A R A Ç Ã O

Declaro, para os fins que se fizerem necessários que, **Elmer Rolando Llanos Villarreal**, professor/pesquisador desta IES, manteve sob sua orientação os discentes listados abaixo:

Aluno	Modalidade	Período
Francisco Aldo de Morais	PIBIC	Agosto/2012 a julho/2013
Yago Felipe da Costa	PICI	Agosto/2012 a fevereiro/2013
Hian de Freitas Macedo		Março/2013 a julho/2013
Nataniel Wontoon Barbosa Lima	PIVIC	Agosto/2012 a julho/2013
Reginaldo Dantas da Silva		
Maria Teresa Targino Macedo Silveira		
Bruna Monallize Duarte Moura		
Hian de Freitas Macedo		
Francisca Joyce dos Santos Bandeira		
Fernanda Ligia dos Santos		
Nataniel Wontoon Barbosa Lima	PIBITI	Setembro/2012 a julho/2013
Francisco Plácido Sting de Paiva		Outubro/2013 a julho/2014
Cauê Coelho Alves	PIBIC	Agosto/2014 a julho/2015
Tiago Mateus Pereira Gonçalves	PICI	
Maxwell Cavalcante Jacomé	PIVIC	
Flavio de Abreu Bezerra Filho	PIBITI	
Natanael Expedito de Carvalho Mendes	PIBIC	Agosto/2015 a julho/2016
Valmir Pereira Bezerra Junior	PICI	
Thiago Ferreira de Carvalho	PIVIC	
Luana Carla de Andrade		
Thiago Dias de Carvalho Quaresma Gama		
Derycly Douglas Eufrásio Galdino		
Maxwell Cavalcante Jácome	PIBITI	Outubro/2015 a julho/2016

Valmir Pereira Bezerra Junior	PIVIC	Agosto/2016 a julho/2017
Natanael Expedito de Carvalho Mendes		
Ciro Simão de Medeiros		
Maxwell Cavalcante Jácome		

Mossoró/RN, 30 de outubro de 2018.

Jean Berg Alves da Silva
Pró-Reitor de Pesquisa e Pós-graduação

UNIVERSIDADE FEDERAL RURAL DO SEMI-ÁRIDO
PRÓ-REITORIA DE PESQUISA E PÓS-GRADUACAO

PROPPG
PRÓ-REITORIA DE PESQUISA E PÓS-GRADUAÇÃO

DECLARAÇÃO

Declaramos que o professor(a) ELMER ROLANDO LLANOS VILLARREAL, mat. 1673887, lotado no DEPARTAMENTO DE CIÊNCIAS NATURAIS, MATEMÁTICA E ESTATÍSTICA, orienta(ou) alunos de Iniciação Científica da Pesquisa "OTIMIZAÇÃO DE ASAS DE MATERIAL COMPÓSITO DE VEÍCULOS AÉREOS NÃO TRIPULADOS USANDO ELEMENTOS FINITOS", conforme quadro abaixo:

Bolsista	Modalidade	Período
MATHEÚS MORAIS FERREIRA GOMES	PIBIC (IC)	01/08/2018 a 31/07/2019

Mossoró, 12 de Outubro de 2024

Liana Holanda Nepomuceno Nobre
Pró-Reitor de Pesquisa

Alexsandra Fernandes Pereira
Pró-Reitor Adjunto de Pesquisa

Para verificar a autenticidade deste documento acesse **https://sigaa.ufersa.edu.br/sigaa/documentos/**, informando data de emissão do documento e o código de verificação.
Código de verificação: **b9666a75ce**
Número do Documento: **611202**

UNIVERSIDADE FEDERAL RURAL DO SEMI-ÁRIDO
PRÓ-REITORIA DE PESQUISA E PÓS-GRADUACAO

DECLARAÇÃO

Declaramos que o professor(a) ELMER ROLANDO LLANOS VILLARREAL, mat. 1673887, lotado no DEPARTAMENTO DE CIÊNCIAS NATURAIS, MATEMÁTICA E ESTATÍSTICA, orienta(ou) alunos de Iniciação Científica da Pesquisa "CONJUNTOS INVARIANTES DE SEGUNDA ORDEM E SUAS APLICAÇÕES", conforme quadro abaixo:

Bolsista	Modalidade	Período
PAULO VICTOR FERNANDES VIEIRA	PIVIC (IC)	02/09/2020 a 02/09/2020
PAULO VICTOR FERNANDES VIEIRA	PICI (IC)	03/03/2021 a 31/08/2021

Mossoró, 12 de Outubro de 2024

Liana Holanda Nepomuceno Nobre
Pró-Reitor de Pesquisa

Alexsandra Fernandes Pereira
Pró-Reitor Adjunto de Pesquisa

Para verificar a autenticidade deste documento acesse **https://sigaa.ufersa.edu.br/sigaa/documentos/**, informando data de emissão do documento e o código de verificação.
Código de verificação: **d3399ad146**
Número do Documento: **611199**

UNIVERSIDADE FEDERAL RURAL DO SEMI-ÁRIDO
PRÓ-REITORIA DE PESQUISA E PÓS-GRADUACAO

DECLARAÇÃO

Declaramos que o professor(a) ELMER ROLANDO LLANOS VILLARREAL, mat. 1673887, lotado no DEPARTAMENTO DE CIÊNCIAS NATURAIS, MATEMÁTICA E ESTATÍSTICA, orienta(ou) alunos de Iniciação Científica da Pesquisa "Controle por Rejeição Ativa de Distúrbios e suas aplicações", conforme quadro abaixo:

Bolsista	Modalidade	Período
JOAO VICTOR DE OLIVEIRA DANTAS	PICI (IC)	09/09/2023 a 31/08/2024
LUCAS DANTAS DA SILVA	A DEFINIR	01/09/2021 a 18/08/2022
NATHAN RODRIGUES DA SILVA	A DEFINIR	02/09/2022 a 22/08/2023

Mossoró, 12 de Outubro de 2024

Liana Holanda Nepomuceno Nobre
Pró-Reitor de Pesquisa

Alexsandra Fernandes Pereira
Pró-Reitor Adjunto de Pesquisa

Para verificar a autenticidade deste documento acesse **https://sigaa.ufersa.edu.br/sigaa/documentos/**, informando data de emissão do documento e o código de verificação.
Código de verificação: **9b44b8d981**
Número do Documento: **611200**

REVIEW CONFIRMATION CERTIFICATE

We are pleased to confirm that

Elmer Rolando Llanos Villarreal

has reviewed 49 papers for the following MDPI journals in the period 2021–2023:

Sensors, Electronics, Sustainability, Processes, Symmetry, Atmosphere, Journal of Marine Science and Engineering, Applied Sciences, Mathematics, Energies, Aerospace, Axioms, Machines

Shu-Kun Lin

Dr. Shu-Kun Lin, Publisher and President
Basel, 15 June 2024

MDPI

MDPI is a publisher of open access, international, academic journals. We rely on active researchers, highly qualified in their field to provide review reports and support the editorial process. The criteria for selection of reviewers include: holding a doctoral degree or having an equivalent amount of research experience; a national or international reputation in the relevant field; and having made a significant contribution to the field, evidenced by peer-reviewed publications.

UNIVERSIDADE FEDERAL RURAL DO SEMI-ÁRIDO
PRÓ-REITORIA DE EXTENSÃO E CULTURA

Certificado

Certificamos que, O(A) PROFESSOR(A) ELMER ROLANDO LLANOS VILLARREAL, SIAPE 1673887, participou do evento de extensão I CONGRESSO DE INOVAÇÃO TECNOLÓGICA DO SEMI-ÁRIDO MOSSORÓ -2016, com carga horária de 80 hora(s), coordenado pelo(a) Professor(a) ELMER ROLANDO LLANOS VILLARREAL, promovido pelo(a) (EXTINTO) - DEPARTAMENTO DE CIÊNCIAS EXATAS E NATURAIS, na função de Coordenador, com 10 hora(s) de atividades desenvolvidas. A atividade foi realizada no período de 22 de Setembro de 2016 a 24 de Setembro de 2016.

Mossoró, 27 de Setembro de 2024

Vania Christina Nascimento Porto

Pró-Reitor de Extensão

Código de verificação: **f777bc26ed**
Número do Documento: **607842**

Para verificar a autenticidade deste documento acesse **https://sigaa.ufersa.edu.br/sigaa/documentos/** e utilize o link *Extensão* >> *Certificado de Participante como Membro da Equipe de Ação de Extensão*, informando o número do documento, data de emissão do documento e o código de verificação.

UNIVERSIDADE FEDERAL RURAL DO SEMI-ÁRIDO
PRÓ-REITORIA DE EXTENSÃO E CULTURA

Certificado

Certificamos que, O(A) PROFESSOR(A) ELMER ROLANDO LLANOS VILLARREAL, SIAPE 1673887, participou do projeto de extensão SEMÍNÁRIOS DE PESQUISA EM MATEMÁTICA, coordenado pelo(a) Professor(a) WALTER MARTINS RODRIGUES, promovido pelo(a) CENTRO DE CIÊNCIAS EXATAS E NATURAIS, na função de Vice-Coordenador, com 38 hora(s) de atividades desenvolvidas. A atividade foi realizada no período de 3 de Agosto de 2017 a 15 de Dezembro de 2017.

Mossoró, 27 de Setembro de 2024

Vania Christina Nascimento Porto

Pró-Reitor de Extensão

Código de verificação: **e91c25fb98**
Número do Documento: **607844**

Para verificar a autenticidade deste documento acesse **https://sigaa.ufersa.edu.br/sigaa/documentos/** e utilize o link *Extensão* >> *Certificado de Participante como Membro da Equipe de Ação de Extensão*, informando o número do documento, data de emissão do documento e o código de verificação.

UNIVERSIDADE FEDERAL RURAL DO SEMI-ÁRIDO
PRÓ-REITORIA DE EXTENSÃO E CULTURA

Certificado

Certificamos que, O(A) PROFESSOR(A) ELMER ROLANDO LLANOS VILLARREAL, SIAPE 1673887, participou do evento de extensão I FÓRUM DE ASSISTÊNCIA ESTUDANTIL DA UNIVERSIDADE FEDERAL RURAL DO SEMI-ÁRIDO - UFERSA, com carga horária de 8 hora(s), coordenado pelo(a) Servidor(a) JÚLIO CÉSAR RODRIGUES DE SOUSA, promovido pelo(a) PRÓ-REITORIA DE ASSUNTOS ESTUDANTIS, na função de Membro, com 4 hora(s) de atividades desenvolvidas. A atividade foi realizada no período de 28 de Agosto de 2017 a 28 de Agosto de 2017.

Mossoró, 27 de Setembro de 2024

Vania Christina Nascimento Porto

Pró-Reitor de Extensão

Código de verificação: **f1e62dcfaa**
Número do Documento: **607843**

Para verificar a autenticidade deste documento acesse **https://sigaa.ufersa.edu.br/sigaa/documentos/** e utilize o link *Extensão* >> *Certificado de Participante como Membro da Equipe de Ação de Extensão*, informando o número do documento, data de emissão do documento e o código de verificação.

UNIVERSIDADE FEDERAL RURAL DO SEMI-ÁRIDO
PRÓ-REITORIA DE EXTENSÃO E CULTURA

Certificado

Certificamos que, O(A) PROFESSOR(A) ELMER ROLANDO LLANOS VILLARREAL, SIAPE 1673887, participou do projeto de extensão DIVULGAÇÃO DE AÇÕES DE ENSINO ASSOCIADAS A TRABALHOS DESENVOLVIDOS NO PROFMAT - UFERSA, coordenado pelo(a) Professor(a) WALTER MARTINS RODRIGUES, promovido pelo(a) DEPARTAMENTO DE CIÊNCIAS NATURAIS, MATEMÁTICA E ESTATÍSTICA, na função de Membro, com 224 hora(s) de atividades desenvolvidas. A atividade foi realizada no período de 1 de Setembro de 2021 a 30 de Setembro de 2022.

Mossoró, 27 de Setembro de 2024

Vania Christina Nascimento Porto

Pró-Reitor de Extensão

Código de verificação: **02bd4704a0**
Número do Documento: **607846**

Para verificar a autenticidade deste documento acesse **https://sigaa.ufersa.edu.br/sigaa/documentos/** e utilize o link *Extensão* >> *Certificado de Participante como Membro da Equipe de Ação de Extensão*, informando o número do documento, data de emissão do documento e o código de verificação.

UNIVERSIDADE FEDERAL RURAL DO SEMI-ÁRIDO
PRÓ-REITORIA DE EXTENSÃO E CULTURA

Certificado

Certificamos que, O(A) PROFESSOR(A) ELMER ROLANDO LLANOS VILLARREAL, SIAPE 1673887, participou do projeto de extensão DIVULGANDO AS AÇÕES DE ENSINO ASSOCIADOS AOS TRABALHOS DESENVOLVIDOS NO PROGRAMA DE MESTRADO PROFISSIONAL EM MATEMÁTICA EM REDE NACIONAL PROFMAT/UFERSA., coordenado pelo(a) Professor(a) ANTONIO RONALDO GOMES GARCIA, promovido pelo(a) DEPARTAMENTO DE CIÊNCIAS NATURAIS, MATEMÁTICA E ESTATÍSTICA, na função de Membro, com 1560 hora(s) de atividades desenvolvidas. A atividade foi realizada no período de 1 de Dezembro de 2021 a 30 de Novembro de 2022.

Mossoró, 27 de Setembro de 2024

Vania Christina Nascimento Porto

Pró-Reitor de Extensão

Código de verificação: **7ee57e53aa**
Número do Documento: **607847**

Para verificar a autenticidade deste documento acesse **https://sigaa.ufersa.edu.br/sigaa/documentos/** e utilize o link *Extensão* >> *Certificado de Participante como Membro da Equipe de Ação de Extensão*, informando o número do documento, data de emissão do documento e o código de verificação.

UNIVERSIDADE FEDERAL RURAL DO SEMI-ÁRIDO
PRÓ-REITORIA DE EXTENSÃO E CULTURA

Certificado

Certificamos que, O(A) PROFESSOR(A) ELMER ROLANDO LLANOS VILLARREAL, SIAPE 1673887, participou do projeto de extensão DIVULGANDO AS AÇÕES DE ENSINO ASSOCIADOS AOS TRABALHOS DESENVOLVIDOS NO PROGRAMA DE MESTRADO PROFISSIONAL EM MATEMÁTICA EM REDE NACIONAL PROFMAT/UFERSA (2023.1)., coordenado pelo(a) Professor(a) ANTONIO RONALDO GOMES GARCIA, promovido pelo(a) DEPARTAMENTO DE CIÊNCIAS NATURAIS, MATEMÁTICA E ESTATÍSTICA, na função de Membro, com 360 hora(s) de atividades desenvolvidas. A atividade foi realizada no período de 24 de Agosto de 2023 a 31 de Dezembro de 2023.

Mossoró, 27 de Setembro de 2024

Vania Christina Nascimento Porto

Pró-Reitor de Extensão

Código de verificação: **c78d1a521e**
Número do Documento: **607845**

Para verificar a autenticidade deste documento acesse **https://sigaa.ufersa.edu.br/sigaa/documentos/** e utilize o link *Extensão* >> *Certificado de Participante como Membro da Equipe de Ação de Extensão*, informando o número do documento, data de emissão do documento e o código de verificação.

ELMER ROLANDO L. VILLARREAL
DEPARTAMENTO DE CIÊNCIAS NATURAIS, MATEMÁTICA E ESTATÍSTICA (11.01.00.08.03)

Semestre atual: **2024.1**

Portal do Docente > Documentos autenticados de Extensão

Atenção:
Os documentos só poderão ser emitidos para Membros da Equipe ativos.
Os Certificados só serão liberados quando a participação do membro da equipe na ação for finalizada.
As Declarações poderão ser emitidas a qualquer tempo para os membros ativos da ação de extensão.
Nos casos de participação como Discente de Extensão os Certificados só serão liberados quando o discente enviar o Relatório Final.

: Visualizar **: Emitir Declaração** **: Emitir Certificado**

Lista de participações como membro de equipe organizadora das Ações de Extensão

2023 - Divulgando as ações de ensino associados aos trabalhos desenvolvidos no Programa de Mestrado Profissional em Matemática em Rede Nacional – PROFMAT/UFERSA (2023.1).

Membro Projeto	Categoria	Função	CH Semanal	Início	Fim
ELMER ROLANDO LLANOS VILLARREAL	DOCENTE	Membro	20 h	24/08/2023	31/12/2023

2021 - Divulgação de Ações de ensino associadas a Trabalhos desenvolvidos no PROFMAT - UFERSA

Membro Projeto	Categoria	Função	CH Semanal	Início	Fim
ELMER ROLANDO LLANOS VILLARREAL	DOCENTE	Membro	4 h	01/09/2021	30/09/2022

2021 - Divulgando as ações de ensino associados aos trabalhos desenvolvidos no Programa de Mestrado Profissional em Matemática em Rede Nacional – PROFMAT/UFERSA.

Membro Projeto	Categoria	Função	CH Semanal	Início	Fim
ELMER ROLANDO LLANOS VILLARREAL	DOCENTE	Membro	30 h	01/12/2021	30/11/2022

2017 - Seminários de Pesquisa em Matemática

Membro Projeto	Categoria	Função	CH Semanal	Início	Fim
ELMER ROLANDO LLANOS VILLARREAL	DOCENTE	Vice-Coordenador	2 h	03/08/2017	15/12/2017

2017 - I Fórum de Assistência Estudantil da Universidade Federal Rural do Semi-Árido - UFERSA

Membro Projeto	Categoria	Função	CH Semanal	Início	Fim		
ELMER ROLANDO LLANOS VILLARREAL	DOCENTE	Membro	4 h	28/08/2017	28/08/2017		

2016 - I Congresso de Inovação tecnológica do Semi-árido– Mossoró -2016

Membro Projeto	Categoria	Função	CH Semanal	Início	Fim		
ELMER ROLANDO LLANOS VILLARREAL	DOCENTE	Coordenador	10 h	22/09/2016	24/09/2016		

Lista de participações como público alvo das Ações de Extensão

EV035-2015 - Programa de Aperfeiçoamento para Professores de Matemática do Ensino Médio - PAPMEM

Participante	Categoria	Participação	Data do Cadastro	Frequência		
ELMER ROLANDO LLANOS VILLARREAL	DISCENTE (UFERSA)	PARTICIPANTE	07/11/2015	100%		

EV220-2019 - 1º Colóquio Potiguar de Matemática – Mossoró-RN

Participante	Categoria	Participação	Data do Cadastro	Frequência		
ELMER ROLANDO LLANOS VILLARREAL	DISCENTE (UFERSA)	PARTICIPANTE	20/12/2019	100%		

EV034-2020 - 1º Ciclo de Palestras do Departamento de Ciências Naturais, Matemática e Estatística

Participante	Categoria	Participação	Data do Cadastro	Frequência		
ELMER ROLANDO LLANOS VILLARREAL	DISCENTE (UFERSA)	PARTICIPANTE	16/05/2020	100%		

Mini Atividade - EV034-2020 - Análise de dados quantitativos

Participante	Categoria	Participação	Data do Cadastro	Frequência		
ELMER ROLANDO LLANOS VILLARREAL	DISCENTE (UFERSA)	PARTICIPANTE	16/05/2020	100%		

Mini Atividade - EV034-2020 - Programa Cientista-Chefe em Educação Básica do Estado do Ceará: Pesquisa e Inovação Pública no Ensino de Matemática

Participante	Categoria	Participação	Data do Cadastro	Frequência		
ELMER ROLANDO LLANOS VILLARREAL	DISCENTE (UFERSA)	PARTICIPANTE	16/05/2020	100%		

Mini Atividade - EV034-2020 - O Terraplanismo e ensino de Ciências

Participante	Categoria	Participação	Data do Cadastro	Frequência
ELMER ROLANDO LLANOS VILLARREAL	DISCENTE (UFERSA)	PARTICIPANTE	16/05/2020	100%

EV097-2020 - II Ciclo de Palestras do Departamento de Ciências Naturais, Matemática e Estatística- Os desafios da pesquisa no ensino de física e matemática.

Participante	Categoria	Participação	Data do Cadastro	Frequência
ELMER ROLANDO LLANOS VILLARREAL	DISCENTE (UFERSA)	PARTICIPANTE	30/09/2020	100%

Mini Atividade - EV097-2020 - CONSTRUTIVISMOS E ABORDAGENS FREIREANAS NO ENSINO DE CIÊNCIAS: UM DESAFIO NO SERTÃO.

Participante	Categoria	Participação	Data do Cadastro	Frequência
ELMER ROLANDO LLANOS VILLARREAL	DISCENTE (UFERSA)	PARTICIPANTE	30/09/2020	0%

Mini Atividade - EV097-2020 - Aprendizagem Baseada em Pesquisa: uma estratégia para desenvolver o ensino da Matemática

Participante	Categoria	Participação	Data do Cadastro	Frequência
ELMER ROLANDO LLANOS VILLARREAL	DISCENTE (UFERSA)	PARTICIPANTE	30/09/2020	0%

Mini Atividade - EV097-2020 - A TEORIA VYGOTSKY E O ENSINO DE CIÊNCIAS

Participante	Categoria	Participação	Data do Cadastro	Frequência
ELMER ROLANDO LLANOS VILLARREAL	DISCENTE (UFERSA)	PARTICIPANTE	30/09/2020	100%

Mini Atividade - EV097-2020 - (RE)PENSANDO A APRENDIZAGEM EM MATEMÁTICA: UM OLHAR SOBRE ALGUMAS PERSPECTIVAS TEÓRICAS

Participante	Categoria	Participação	Data do Cadastro	Frequência
ELMER ROLANDO LLANOS VILLARREAL	DISCENTE (UFERSA)	PARTICIPANTE	30/09/2020	100%

Mini Atividade - EV097-2020 - ENSAIOS DE METODOLOGIA DE PESQUISA E EDUCAÇÃO MATEMÁTICA

Participante	Categoria	Participação	Data do Cadastro	Frequência
ELMER ROLANDO LLANOS VILLARREAL	DISCENTE (UFERSA)	PARTICIPANTE	23/10/2020	100%

Mini Atividade - EV097-2020 - ABORDAGEM CTSA- (Ciência, Tecnologia, Sociedade e Ambiente)

Participante	Categoria	Participação	Data do Cadastro	Frequência

ELMER ROLANDO LLANOS VILLARREAL	DISCENTE (UFERSA)	PARTICIPANTE	28/10/2020	100%

MINI ATIVIDADE - EV097-2020 - O USO DA DIMENSÃO QUANTITATIVA E DA ABORDAGEM QUALITATIVA NA PESQUISA

Participante	Categoria	Participação	Data do Cadastro	Frequência
ELMER ROLANDO LLANOS VILLARREAL	DISCENTE (UFERSA)	PARTICIPANTE	29/10/2020	100%

MINI ATIVIDADE - EV097-2020 - CONHECIMENTO PEDAGÓGICO DO CONTEÚDO: PESQUISAS E APRIMORAMENTOS NECESSÁRIOS

Participante	Categoria	Participação	Data do Cadastro	Frequência
ELMER ROLANDO LLANOS VILLARREAL	DISCENTE (UFERSA)	PARTICIPANTE	04/11/2020	100%

MINI ATIVIDADE - EV097-2020 - ELABORAÇÃO DE ARTIGOS CIENTÍFICOS

Participante	Categoria	Participação	Data do Cadastro	Frequência
ELMER ROLANDO LLANOS VILLARREAL	DISCENTE (UFERSA)	PARTICIPANTE	05/11/2020	100%

EV030-2022 - 1º COLÓQUIO DO DCME

Participante	Categoria	Participação	Data do Cadastro	Frequência
ELMER ROLANDO LLANOS VILLARREAL	DISCENTE (UFERSA)	PARTICIPANTE	05/10/2022	10%

EV045-2023 - 2º COLÓQUIO DO DCME

Participante	Categoria	Participação	Data do Cadastro	Frequência
ELMER ROLANDO LLANOS VILLARREAL	DISCENTE (UFERSA)	PARTICIPANTE	09/05/2023	0%

MINI ATIVIDADE - EV045-2023 - RECOMPOSIÇÃO DA APRENDIZAGEM MATEMÁTICA: UMA ABORDAGEM ATRAVÉS DAS OPERAÇÕES BÁSICAS

Participante	Categoria	Participação	Data do Cadastro	Frequência
ELMER ROLANDO LLANOS VILLARREAL	DISCENTE (UFERSA)	PARTICIPANTE	09/05/2023	100%

MINI ATIVIDADE - EV045-2023 - A NATUREZA CULTURAL DA MATEMÁTICA: UM ESTUDO DE CASO A PARTIR DA OBRA QUATROCENTISTA EX LUDIS RERUM MATHEMATICARUM

Participante	Categoria	Participação	Data do Cadastro	Frequência
ELMER ROLANDO LLANOS VILLARREAL	DISCENTE (UFERSA)	PARTICIPANTE	16/05/2023	100%

EV164-2023 - 1+2+3+4+5+...= -1/12: Os segredos ocultos da matemática

Participante	Categoria	Participação	Data do Cadastro	Frequência		
ELMER ROLANDO LLANOS VILLARREAL	DISCENTE (UFERSA)	PARTICIPANTE	31/08/2023	100%		

EV227-2023 - Primeiro Seminário Temático PROFMAT/UFERSA: (Re)Pensando a Formação de Professores

Participante	Categoria	Participação	Data do Cadastro	Frequência		
ELMER ROLANDO LLANOS VILLARREAL	DISCENTE (UFERSA)	PARTICIPANTE	20/12/2023	75%		

Lista de participações como discente das Ações de Extensão

Usuário atual não participa ou participou como discente de ações de extensão.

Portal do Docente

SIGAA | Superintendência de Tecnologia da Informação e Comunicação - (84) 3317-8210 | Copyright © 2006-2024 - UFRN - sig-prd-sigaa02.ufersa.edu.br.sigaa02 - v4.11.3

ELMER ROLANDO L. VILLARREAL
DEPARTAMENTO DE CIÊNCIAS NATURAIS, MATEMÁTICA E ESTATÍSTICA (11.01.00.08.03)

Semestre atual: **2024.1**

Ensino Pesquisa Extensão Ações de Ensino Convênios Biblioteca Produção Intelectual Ambientes Virtuais Outros

Portal do Docente > Documentos autenticados de Extensão

Atenção:
Os documentos só poderão ser emitidos para Membros da Equipe ativos.
Os Certificados só serão liberados quando a participação do membro da equipe na ação for finalizada.
As Declarações poderão ser emitidas a qualquer tempo para os membros ativos da ação de extensão.
Nos casos de participação como Discente de Extensão os Certificados só serão liberados quando o discente enviar o Relatório Final.

: Visualizar **: Emitir Declaração** **: Emitir Certificado**

Lista de participações como membro de equipe organizadora das Ações de Extensão

2023 - Divulgando as ações de ensino associados aos trabalhos desenvolvidos no Programa de Mestrado Profissional em Matemática em Rede Nacional – PROFMAT/UFERSA (2023.1).

Membro Projeto	Categoria	Função	CH Semanal	Início	Fim
ELMER ROLANDO LLANOS VILLARREAL	DOCENTE	Membro	20 h	24/08/2023	31/12/2023

2021 - Divulgação de Ações de ensino associadas a Trabalhos desenvolvidos no PROFMAT - UFERSA

Membro Projeto	Categoria	Função	CH Semanal	Início	Fim
ELMER ROLANDO LLANOS VILLARREAL	DOCENTE	Membro	4 h	01/09/2021	30/09/2022

2021 - Divulgando as ações de ensino associados aos trabalhos desenvolvidos no Programa de Mestrado Profissional em Matemática em Rede Nacional – PROFMAT/UFERSA.

Membro Projeto	Categoria	Função	CH Semanal	Início	Fim
ELMER ROLANDO LLANOS VILLARREAL	DOCENTE	Membro	30 h	01/12/2021	30/11/2022

2017 - Seminários de Pesquisa em Matemática

Membro Projeto	Categoria	Função	CH Semanal	Início	Fim
ELMER ROLANDO LLANOS VILLARREAL	DOCENTE	Vice-Coordenador	2 h	03/08/2017	15/12/2017

2017 - I Fórum de Assistência Estudantil da Universidade Federal Rural do Semi-Árido - UFERSA

Membro Projeto	Categoria	Função	CH Semanal	Início	Fim
ELMER ROLANDO LLANOS VILLARREAL	DOCENTE	Membro	4 h	28/08/2017	28/08/2017

2016 - I Congresso de Inovação tecnológica do Semi-árido– Mossoró -2016

Membro Projeto	Categoria	Função	CH Semanal	Início	Fim
ELMER ROLANDO LLANOS VILLARREAL	DOCENTE	Coordenador	10 h	22/09/2016	24/09/2016

Lista de participações como público alvo das Ações de Extensão

EV035-2015 - Programa de Aperfeiçoamento para Professores de Matemática do Ensino Médio - PAPMEM

Participante	Categoria	Participação	Data do Cadastro	Frequência
ELMER ROLANDO LLANOS VILLARREAL	DISCENTE (UFERSA)	PARTICIPANTE	07/11/2015	100%

EV220-2019 - 1º Colóquio Potiguar de Matemática – Mossoró-RN

Participante	Categoria	Participação	Data do Cadastro	Frequência
ELMER ROLANDO LLANOS VILLARREAL	DISCENTE (UFERSA)	PARTICIPANTE	20/12/2019	100%

EV034-2020 - 1º Ciclo de Palestras do Departamento de Ciências Naturais, Matemática e Estatística

Participante	Categoria	Participação	Data do Cadastro	Frequência
ELMER ROLANDO LLANOS VILLARREAL	DISCENTE (UFERSA)	PARTICIPANTE	16/05/2020	100%

Mini Atividade - EV034-2020 - Análise de dados quantitativos

Participante	Categoria	Participação	Data do Cadastro	Frequência
ELMER ROLANDO LLANOS VILLARREAL	DISCENTE (UFERSA)	PARTICIPANTE	16/05/2020	100%

Mini Atividade - EV034-2020 - Programa Cientista-Chefe em Educação Básica do Estado do Ceará: Pesquisa e Inovação Pública no Ensino de Matemática

Participante	Categoria	Participação	Data do Cadastro	Frequência
ELMER ROLANDO LLANOS VILLARREAL	DISCENTE (UFERSA)	PARTICIPANTE	16/05/2020	100%

Mini Atividade - EV034-2020 - O Terraplanismo e ensino de Ciências

Participante	Categoria	Participação	Data do Cadastro	Frequência
ELMER ROLANDO LLANOS VILLARREAL	DISCENTE (UFERSA)	PARTICIPANTE	16/05/2020	100%

EV097-2020 - II Ciclo de Palestras do Departamento de Ciências Naturais, Matemática e Estatística- Os desafios da pesquisa no ensino de física e matemática.

Participante	Categoria	Participação	Data do Cadastro	Frequência
ELMER ROLANDO LLANOS VILLARREAL	DISCENTE (UFERSA)	PARTICIPANTE	30/09/2020	100%

Mini Atividade - EV097-2020 - CONSTRUTIVISMOS E ABORDAGENS FREIREANAS NO ENSINO DE CIÊNCIAS: UM DESAFIO NO SERTÃO.

Participante	Categoria	Participação	Data do Cadastro	Frequência
ELMER ROLANDO LLANOS VILLARREAL	DISCENTE (UFERSA)	PARTICIPANTE	30/09/2020	0%

Mini Atividade - EV097-2020 - Aprendizagem Baseada em Pesquisa: uma estratégia para desenvolver o ensino da Matemática

Participante	Categoria	Participação	Data do Cadastro	Frequência
ELMER ROLANDO LLANOS VILLARREAL	DISCENTE (UFERSA)	PARTICIPANTE	30/09/2020	0%

Mini Atividade - EV097-2020 - A TEORIA VYGOTSKY E O ENSINO DE CIÊNCIAS

Participante	Categoria	Participação	Data do Cadastro	Frequência
ELMER ROLANDO LLANOS VILLARREAL	DISCENTE (UFERSA)	PARTICIPANTE	30/09/2020	100%

Mini Atividade - EV097-2020 - (RE)PENSANDO A APRENDIZAGEM EM MATEMÁTICA: UM OLHAR SOBRE ALGUMAS PERSPECTIVAS TEÓRICAS

Participante	Categoria	Participação	Data do Cadastro	Frequência
ELMER ROLANDO LLANOS VILLARREAL	DISCENTE (UFERSA)	PARTICIPANTE	30/09/2020	100%

Mini Atividade - EV097-2020 - ENSAIOS DE METODOLOGIA DE PESQUISA E EDUCAÇÃO MATEMÁTICA

Participante	Categoria	Participação	Data do Cadastro	Frequência
ELMER ROLANDO LLANOS VILLARREAL	DISCENTE (UFERSA)	PARTICIPANTE	23/10/2020	100%

Mini Atividade - EV097-2020 - ABORDAGEM CTSA- (Ciência, Tecnologia, Sociedade e Ambiente)

Participante	Categoria	Participação	Data do Cadastro	Frequência

ELMER ROLANDO LLANOS VILLARREAL	DISCENTE (UFERSA)	PARTICIPANTE	28/10/2020	100%	

MINI ATIVIDADE - EV097-2020 - O USO DA DIMENSÃO QUANTITATIVA E DA ABORDAGEM QUALITATIVA NA PESQUISA

Participante	Categoria	Participação	Data do Cadastro	Frequência	
ELMER ROLANDO LLANOS VILLARREAL	DISCENTE (UFERSA)	PARTICIPANTE	29/10/2020	100%	

MINI ATIVIDADE - EV097-2020 - CONHECIMENTO PEDAGÓGICO DO CONTEÚDO: PESQUISAS E APRIMORAMENTOS NECESSÁRIOS

Participante	Categoria	Participação	Data do Cadastro	Frequência	
ELMER ROLANDO LLANOS VILLARREAL	DISCENTE (UFERSA)	PARTICIPANTE	04/11/2020	100%	

MINI ATIVIDADE - EV097-2020 - ELABORAÇÃO DE ARTIGOS CIENTÍFICOS

Participante	Categoria	Participação	Data do Cadastro	Frequência	
ELMER ROLANDO LLANOS VILLARREAL	DISCENTE (UFERSA)	PARTICIPANTE	05/11/2020	100%	

EV030-2022 - 1º COLÓQUIO DO DCME

Participante	Categoria	Participação	Data do Cadastro	Frequência
ELMER ROLANDO LLANOS VILLARREAL	DISCENTE (UFERSA)	PARTICIPANTE	05/10/2022	10%

EV045-2023 - 2º COLÓQUIO DO DCME

Participante	Categoria	Participação	Data do Cadastro	Frequência
ELMER ROLANDO LLANOS VILLARREAL	DISCENTE (UFERSA)	PARTICIPANTE	09/05/2023	0%

MINI ATIVIDADE - EV045-2023 - RECOMPOSIÇÃO DA APRENDIZAGEM MATEMÁTICA: UMA ABORDAGEM ATRAVÉS DAS OPERAÇÕES BÁSICAS

Participante	Categoria	Participação	Data do Cadastro	Frequência	
ELMER ROLANDO LLANOS VILLARREAL	DISCENTE (UFERSA)	PARTICIPANTE	09/05/2023	100%	

MINI ATIVIDADE - EV045-2023 - A NATUREZA CULTURAL DA MATEMÁTICA: UM ESTUDO DE CASO A PARTIR DA OBRA QUATROCENTISTA EX LUDIS RERUM MATHEMATICARUM

Participante	Categoria	Participação	Data do Cadastro	Frequência	
ELMER ROLANDO LLANOS VILLARREAL	DISCENTE (UFERSA)	PARTICIPANTE	16/05/2023	100%	

EV164-2023 - 1+2+3+4+5+...= -1/12: Os segredos ocultos da matemática

Participante	Categoria	Participação	Data do Cadastro	Frequência
ELMER ROLANDO LLANOS VILLARREAL	DISCENTE (UFERSA)	PARTICIPANTE	31/08/2023	100%

EV227-2023 - Primeiro Seminário Temático PROFMAT/UFERSA: (Re)Pensando a Formação de Professores

Participante	Categoria	Participação	Data do Cadastro	Frequência
ELMER ROLANDO LLANOS VILLARREAL	DISCENTE (UFERSA)	PARTICIPANTE	20/12/2023	75%

Lista de participações como discente das Ações de Extensão

Usuário atual não participa ou participou como discente de ações de extensão.

Portal do Docente

SIGAA | Superintendência de Tecnologia da Informação e Comunicação - (84) 3317-8210 | Copyright © 2006-2024 - UFRN - sig-prd-sigaa02.ufersa.edu.br.sigaa02 - v4.11.3

SERVIÇO PÚBLICO FEDERAL
MINISTÉRIO DA EDUCAÇÃO
UNIVERSIDADE FEDERAL RURAL DO SEMI-ÁRIDO

PORTARIA UFERSA/GAB Nº 935/2009, de 04 de novembro de 2009

O Reitor da **Universidade Federal Rural do Semi-Árido**, no uso de suas atribuições conferidas pelo Decreto de 30 de julho de 2008, publicado no Diário Oficial da União de 31 de julho de 2008,

CONSIDERANDO a DECISÃO CONSUNI/UFERSA Nº 60/2009, de 29 de outubro de 2009;

CONSIDERANDO o que determina o artigo 28, inciso V, do Estatuto da UFERSA,

RESOLVE:

Art. 1º. Nomear os servidores docentes: **Liana Holanda Nepomuceno Nobre, Marcílio Nunes Freire, Marcos Antonio Nóbrega de Souza, Subênia Karine de Medeiros e Ioná Santos Araújo** (Titulares), **Luciana Batista Sales, Augusto Carlos Pavão, Genilson Fernandes de Queiroz, Elmer Rolando Llanos Vilarreal e Jailma Suerda Silva de Lima** (Suplentes), para compor a Comissão Própria de Avaliação – CPA;

Art. 2º. Nomear o servidor técnico-administrativo: **Francimar Honorato dos Santos** (Titular), para compor a Comissão Própria de Avaliação – CPA;

Art. 3º. Nomear os servidores dos campi avançados da UFERSA: **Rita Diana de Freitas Gurgel** (Titular) e **Éder Jofre Marinho Araújo** (Suplente), para compor a Comissão Própria de Avaliação – CPA;

Art. 4º. Nomear os discentes dos cursos de pós-graduação: **Francisco Elvis Ramos de Oliveira** (Titular) e **Fabrícia Nascimento de Oliveira** (Suplente); para compor a Comissão Própria de Avaliação – CPA;

Art. 5º. Nomear os membros das entidades organizadas da comunidade externa à UFERSA: **Almir Mariano de Souza Júnior** (Titular) e **Márcio Azevedo Dias** (Suplente).

Art. 6º. Este Ato entra em vigor a partir desta data.

Josivan Barbosa Menezes Feitoza
Reitor

SERVIÇO PÚBLICO FEDERAL
MINISTÉRIO DA EDUCAÇÃO
UNIVERSIDADE FEDERAL RURAL DO SEMI-ÁRIDO

PORTARIA UFERSA/GAB Nº. 874/2008, de 22 de dezembro de 2008

O Reitor da **Universidade Federal Rural do Semi-Árido**, no uso de suas atribuições conferidas pelo Decreto de 30 de julho de 2008, publicado no Diário Oficial da União de 31 de julho de 2008,

CONSIDERANDO a homologação do concurso público, por meio do edital nº 44/2008, de 11 de dezembro de 2008, publicado no D.O.U. de 16 de dezembro de 2008,

RESOLVE

Art. 1 - Nomear, em caráter efetivo, **Elmer Rolando Llanos Villarreal** para o cargo de Professor Adjunto, nível 1, da Carreira do Magistério Superior, do Quadro Permanente desta Instituição, em regime de Dedicação Exclusiva, nos termos da Lei nº 8.112/90, com as alterações da Lei nº 9.527/97, em vaga decorrente da redistribuição de cargo vago, através da Portaria nº 991/2008, publicada no D.O.U. de 12 de agosto de 2008, código da vaga nº 0873613.

Art. 2 – A posse do servidor, ora nomeado, ocorrerá no prazo de 30 (trinta) dias, contados da publicação deste ato no D.O.U.

Josivan Barbosa Menezes Feitoza
Reitor

MINISTÉRIO DA EDUCAÇÃO
UNIVERSIDADE FEDERAL RURAL DO SEMI-ÁRIDO
GABINETE DA REITORIA

PORTARIA Nº 1.864, DE 4 DE OUTUBRO DE 2023

A REITORA DA UNIVERSIDADE FEDERAL RURAL DO SEMI-ÁRIDO, no uso de suas atribuições conferidas pelo Decreto de 21 de agosto de 2020, publicado na edição extra no Diário Oficial da União de 21 de agosto de 2020, e tendo em vista o que estabelecem os incisos VI e XIX do art. 44 do Estatuto da universidade; o inciso VIII do art. 50, e incisos VI e XIX do art. 58 e do Regimento da Ufersa; a Resolução Consuni/Ufersa nº 10, de 31 de maio de 2017, que regulamenta as eleições para representação docente, discente e técnico-administrativo no Conselho de Curadores - CC e no Conselho de Administração – Consad da Ufersa; a Portaria nº 563, de 15 de setembro de 2021, reconduzida pela Portaria nº 1.536, de 29 de agosto de 2023; o relatório do processo eleitoral da representação docente, enviado ao Gabinete da Reitoria em 4 de outubro de 2023; a Portaria nº 560, de 14 de setembro de 2021, alterada pela Portaria nº 949, de 5 de junho de 2023, reconduzida pela Portaria 1.537, de 29 de agosto de 2023; o relatório do processo eleitoral da representação técnico-administrativa, enviado ao Gabinete da Reitoria em 28 de setembro de 2023, resolve:

Art. 1º Nomear os seguintes servidores docentes para exercer a função de membros do Conselho de Administração – Consad da Ufersa:

I - Membros Títulares:

a) Francisco Edcarlos Alves Leite;

b) Rafael Castelo Guedes Martins;

c) Luís Morão Cabral Ferro; e

d) Elmer Rolando Llanos Villarreal.

Art. 2º Nomear os seguintes servidores técnico-administrativos para exercer a função de membros do Conselho de Administração – Consad da Ufersa:

I - Membros Títulares:

a) Rannah Munay Dantas da Silveira; e

b) Alexandre Miranda Rocha.

Art. 3º Os servidores eleitos cumprirão mandato de 2 (dois) anos, sendo permitida uma recondução, em cumprimento ao § 2º do art. 50 do Regimento da universidade.

Art. 4º Esta Portaria entra em vigor nesta data e seus efeitos retroagem a 28 de setembro de 2023.

LUDIMILLA CARVALHO SERAFIM DE OLIVEIRA:87733161487
Assinado de forma digital por LUDIMILLA CARVALHO SERAFIM DE OLIVEIRA:87733161487
LUDIMILLA CARVALHO SERAFIM DE OLIVEIRA

PORTARIA Nº 1.151, DE 15 DE AGOSTO DE 2024

A REITORA DA UNIVERSIDADE FEDERAL RURAL DO SEMI-ÁRIDO, no uso de suas atribuições conferidas pelo Decreto de 21 de agosto de 2020, publicado na edição extra no Diário Oficial da União de 21 de agosto de 2020, e tendo em vista o que estabelecem os incisos XII e XIX do art. 44 do Estatuto da universidade; os §§ 5º e 6º da Resolução nº 74, de 16 de novembro de 2021 do Consuni da Ufersa; a Portaria nº 199, de 7 de abril de 2022, alterada pelas Portarias nº 363, de 8 de junho de 2022, nº 587, de 28 de setembro de 2022, nº 158, de 15 de fevereiro de 2023 e nº 1.260, de 27 de julho de 2023, retificada pela Portaria nº 1.931, de 11 de outubro de 2023 e prorrogada pela Portaria nº 497, de 15 de abril de 2024; a Portaria nº 711, de 27 de maio de 2024; o Ofício nº 77, de 1º de fevereiro de 2024, da Universidade do Estado do Rio Grande do Norte – Uern; a Resolução nº 21, de 29 de fevereiro de 2024, do Consuni da Ufersa, que trata da homologação do representante externo suplente, para compor a Comissão Permanente de Pessoal Docente – CPPD, resolve:

Art. 1º A Portaria nº 711, de 27 de maio de 2024, passa a vigorar com as seguintes alterações:

"Art. 1º .....

I - Membros Titulares:

a) Jailma Suerda Silva de Lima - CCA;

b) Luciana Vieira de Paiva - CCBS;

c) Yáskara Ygara Menescal Pinto Fernandes - CCEN;

d) Ana Maria Bezerra Lucas - CCSAH;

e) Janaína Cortez de Oliveira - CE;

f) Sileide de Oliveira Ramos - CMA;

g) Wendel Silva Cabral - CMC; e

h) Antônio de Pádua Farias de Souza Filho – CMPF.

II - Membros Suplentes:

a) Josemir de Souza Gonçalves - CCA;

b) Marinalva Oliveira Freitas - CCBS;

c) Elmer Rolando Llanos Villarreal - CCEN;

d) Fernanda Alves Ribeiro - CE;

e) Bruno Coriolano de Almeida Costa - CMC;

f) Reudsmam Rolim de Sousa – CMPF; e

g) Hideraldo Bezerra dos Santos - Representante Externo.

.....

§ 2º O membro da alínea “g”, teve sua homologação através da Resolução nº 21, de 29 de fevereiro de 2024, do Consuni da Ufersa, em cumprimento ao Ofício nº 77, de 1º de fevereiro de 2024, da Universidade do Estado do Rio Grande do Norte – Uern, com encerramento do mandato no dia 28 de fevereiro de 2026.” (NR)

Art. 2º Fica revogado o § 2º do inciso I do art. 1º da Portaria nº 711, de 27 de maio de 2024.

Art. 3º Esta Portaria entra em vigor ,nesta data e seus efeitos retroagem a 27 de maio de 2024.

LUDIMILLA CARVALHO SERAFIM DE OLIVEIRA:87733161487

Assinado de forma digital por LUDIMILLA CARVALHO SERAFIM DE OLIVEIRA:87733161487
Dados: 2024.08.16 15:57:33 -03'00'

LUDIMILLA CARVALHO SERAFIM DE OLIVEIRA

Governo do Estado do Rio Grande do Norte
Secretaria de Estado da Educação e da Cultura – SEEC
UNIVERSIDADE DO ESTADO DO RIO GRANDE DO NORTE – UERN
Comissão Central do Concurso para Docentes – CCD

DECLARAÇÃO

Declaramos para os devidos fins que se fizerem necessários, que **ELMER ROLANDO LLANOS VILLARREAL**, participou, na qualidade de **Membro**, da Banca Examinadora da Área de **Álgebra Linear e Cálculo Integral,** do XV Concurso Público de Provas e Títulos para Docentes, realizado pela Universidade do Estado do Rio Grande do Norte – UERN, no período de 13 a 18 de junho de 2010.

Pelo que firmamos a presente declaração que é a expressão da verdade.

Mossoró-RN, 18 de junho de 2010.

Profa. Sirleyde Dias de Almeida
Presidente da CCD

MINISTÉRIO DA EDUCAÇÃO
UNIVERSIDADE FEDERAL RURAL DO SEMI-ÁRIDO
GABINETE DO REITOR

PORTARIA UFERSA/GAB Nº 1373/2012, de 16 de novembro de 2012

O Reitor da **Universidade Federal Rural do Semi-Árido**, no uso de suas atribuições conferidas pelo Decreto de 14 de junho de 2012, publicado no Diário Oficial da União de 15 de junho de 2012,

CONSIDERANDO o Memorando Eletrônico N° 104/2012 - CPPS, que encaminha os nomes para compor as bancas examinadoras do processo seletivo para Professor Efetivo, conforme Edital n° 46/2012, publicado no DOU de 28/09/2012,

CONSIDERANDO o que determina inciso XI do Artigo 28 do Estatuto da Universidade,

R E S O L V E:

Art. 1º Designar, *ad referendum*, do Conselho Universitário, a Banca Examinadora do Concurso, para preenchimento de vagas de Professor Efetivo, assim constituída:

Disciplina: Estatística – Campus Pau dos Ferros.

Prof. Dr. Geomar Galdino da Silva - UFERSA
Profª. Drª. Elizângela Cabral dos Santos - UFERSA
Prof. Dr. Elmer Rolando Llanos Villarreal - UFERSA

Art. 2º Este Ato entra em vigor a partir desta data.

José de Arimatea de Matos
Reitor

MINISTÉRIO DA EDUCAÇÃO
UNIVERSIDADE FEDERAL RURAL DO SEMI-ÁRIDO
GABINETE DO REITOR

PORTARIA UFERSA/GAB Nº 1373/2012, de 16 de novembro de 2012

O Reitor da **Universidade Federal Rural do Semi-Árido**, no uso de suas atribuições conferidas pelo Decreto de 14 de junho de 2012, publicado no Diário Oficial da União de 15 de junho de 2012,

CONSIDERANDO o Memorando Eletrônico N° 104/2012 - CPPS, que encaminha os nomes para compor as bancas examinadoras do processo seletivo para Professor Efetivo, conforme Edital n° 46/2012, publicado no DOU de 28/09/2012,

CONSIDERANDO o que determina inciso XI do Artigo 28 do Estatuto da Universidade,

R E S O L V E:

Art. 1º Designar, *ad referendum*, do Conselho Universitário, a Banca Examinadora do Concurso, para preenchimento de vagas de Professor Efetivo, assim constituída:

Disciplina: Estatística – Campus Pau dos Ferros.

Prof. Dr. Geomar Galdino da Silva - UFERSA
Profª. Drª. Elizângela Cabral dos Santos - UFERSA
Prof. Dr. Elmer Rolando Llanos Villarreal - UFERSA

Art. 2º Este Ato entra em vigor a partir desta data.

José de Arimatea de Matos
Reitor

BR 110 – km 47 - Bairro Costa e Silva – Caixa Postal 137 – CEP: 59625 - 900 – Mossoró/RN
Fones: (84) 3317-8224 - Fax (84) 3317-8228 - E-mail: gabinete@ufersa.edu.br – www.ufersa.edu.br

MINISTÉRIO DA EDUCAÇÃO
UNIVERSIDADE FEDERAL RURAL DO SEMI-ÁRIDO
GABINETE DO REITOR

PORTARIA UFERSA/GAB Nº 1373/2012, de 16 de novembro de 2012

O Reitor da **Universidade Federal Rural do Semi-Árido**, no uso de suas atribuições conferidas pelo Decreto de 14 de junho de 2012, publicado no Diário Oficial da União de 15 de junho de 2012,

CONSIDERANDO o Memorando Eletrônico N° 104/2012 - CPPS, que encaminha os nomes para compor as bancas examinadoras do processo seletivo para Professor Efetivo, conforme Edital n° 46/2012, publicado no DOU de 28/09/2012,

CONSIDERANDO o que determina inciso XI do Artigo 28 do Estatuto da Universidade,

R E S O L V E:

Art. 1º Designar, *ad referendum*, do Conselho Universitário, a Banca Examinadora do Concurso, para preenchimento de vagas de Professor Efetivo, assim constituída:

Disciplina: Estatística – Campus Pau dos Ferros.

Prof. Dr. Geomar Galdino da Silva - UFERSA
Profª. Drª. Elizângela Cabral dos Santos - UFERSA
Prof. Dr. Elmer Rolando Llanos Villarreal - UFERSA

Art. 2º Este Ato entra em vigor a partir desta data.

José de Arimatea de Matos
Reitor

BR 110 – km 47 - Bairro Costa e Silva – Caixa Postal 137 – CEP: 59625 - 900 – Mossoró/RN
Fones: (84) 3317-8224 - Fax (84) 3317-8228 - E-mail: gabinete@ufersa.edu.br – www.ufersa.edu.br

MINISTÉRIO DA EDUCAÇÃO
UNIVERSIDADE FEDERAL RURAL DO SEMI-ÁRIDO
GABINETE DO REITOR

PORTARIA UFERSA/GAB N.º 0222/2013, de 19 de fevereiro de 2013

O Reitor em exercício da **Universidade Federal Rural do Semi-Árido**, no uso de suas atribuições conferidas pela PORTARIA UFERSA/GAB Nº 0722/2012, de 07 de agosto de 2012, publicada no Diário Oficial da União de 09 de agosto de 2012,

CONSIDERANDO o que determina o inciso XX, artigo 68 do Regimento Geral da UFERSA,

CONSIDERANDO o Memorando Eletrônico Nº 06/2013 – PROAC, de 15 de fevereiro de 2013,

R E S O L V E:

Art. 1º Designar o servidor docente Elmer Rolando Llanos Villareal, professor adjunto III, matrícula SIAPE n.º 1673387 para exercer a função de Assessor Técnico da Pró-Reitoria de Assuntos Comunitários - PROAC, código FG-03.

Art. 2º Este Ato entra em vigor nesta data.

Francisco Odolberto de Araújo
Reitor em exercício

Publique-se, afixando-se no Mural dos Atos Oficiais
19/02/13
Maria Marcia Diogenes Veras
Chefe de Gabinete
CPF: 182.733.784-20

MINISTÉRIO DA EDUCAÇÃO
UNIVERSIDADE FEDERAL RURAL DO SEMI-ÁRIDO
GABINETE DO REITOR

PORTARIA UFERSA/GAB Nº. 1.062/2013, de 17 de julho de 2013

O Reitor em exercício da **Universidade Federal Rural do Semi-Árido**, no uso de suas atribuições conferidas pela PORTARIA UFERSA/GAB Nº 0722/2012, de 07 de agosto de 2012, publicada no Diário Oficial da União de 09 de agosto de 2012,

CONSIDERANDO a solicitação da CPPS, na qual encaminha os nomes para comporem as bancas examinadoras do Processo Seletivo para Professor Substituto, conforme Edital n.° 032/2013;

CONSIDERANDO o que determina o inciso XVIII do Artigo 28 do Estatuto da Universidade,

R E S O L V E:

Art. 1º Designar a Banca Examinadora do Processo Seletivo, para preenchimento de vaga de Professor Substituto - Edital n.º 032/2013, assim constituída:

Disciplina: Cálculo I, Cálculo II, Fundamentos de Matemática, Geometria Analítica, Álgebra Linear – Campus Mossoró:

Prof. Dr. Elmer Rolando Llanos Villarreal – UFERSA (Presidente)
Prof. Msc. Jackson Jonas Silva Costa – UFERSA
Prof. Msc. Paulo César Linhares da Silva – UFERSA
Profª. Msc. Suene Campos Duarte – UFERSA (Suplente)

Art. 2º Este ato entra em vigor a partir desta data.

Francisco Odolberto de Araújo
Reitor em exercício

Av. Francisco Mota, n.º 572, Bairro Costa e Silva – Caixa Postal 137 – CEP: 59.625 - 900 – Mossoró/RN
Fones: (84) 3317-8224 - Fax (84) 3317-8228 - E-mail: gabinete@ufersa.edu.br – www.ufersa.edu.br

MINISTÉRIO DA EDUCAÇÃO
UNIVERSIDADE FEDERAL RURAL DO SEMI-ÁRIDO
GABINETE DO REITOR

PORTARIA UFERSA/GAB Nº. 1.738/2013, de 30 de dezembro de 2013

O Reitor em exercício da **Universidade Federal Rural do Semi-Árido**, no uso de suas atribuições conferidas pela PORTARIA UFERSA/GAB Nº 0722/2012, de 07 de agosto de 2012, publicada no Diário Oficial da União de 09 de agosto de 2012,

CONSIDERANDO o Memorando nº 24/2013, de 18 de dezembro de 2013, da Comissão Própria de Avaliação – CPA;

CONSIDERANDO a PORTARIA UFERSA/GAB Nº 1065/2011, de 23 de dezembro de 2011, que designou membros para compor a Comissão Própria de Avaliação – CPA da UFERSA;

CONSIDERANDO a Decisão CONSUNI/UFERSA N.° 084/2011, de 22 de dezembro de 2011, que homologa as indicações de membros para compor a Comissão Própria de Avaliação – CPA da UFERSA;

CONSIDERANDO o que determina o inciso XVIII, artigo 68 do Regimento Geral da UFERSA,

R E S O L V E:

Art. 1º Prorrogar o prazo determinado pelo Art. 3º da PORTARIA UFERSA/GAB Nº. 1.738/2013, de 30 de dezembro de 2013, para o mandato dos membros da Comissão Própria de Avaliação – CPA da UFERSA.

Art. 2º Permanece inalterada a composição da CPA designada pela PORTARIA UFERSA/GAB Nº. 1.738/2013, de 30 de dezembro de 2013, abaixo detalhada:

a) Representantes docentes do Departamento de Agrotecnologia e Ciências Sociais: Jacqueline Cunha de Vasconcelos Martins (membro titular) e Juliana Rocha Vaez (membro suplente);

b) Representantes docentes do Departamento de Ciências Ambientais e Tecnológicas: Marcílio Nunes Freire (membro titular) e Alexandre José de Oliveira (membro suplente);

c) Representantes docentes do Departamento de Ciências Animais: Inês Xavier Martins (membro titular) e Aracely Rafaelle Fernandes Ricarte (membro suplente);

d) Representantes docentes do Departamento de Ciências Exatas e Naturais: Subênia Karine de Medeiros (membro titular) e Elmer Rolando Llanos Villarreal (membro suplente);

e) Representantes docentes do Departamento de Ciências Vegetais: Maurício Sekiguchi de Godoy (membro titular) e Leandro de Oliveira Furtado de Sousa (membro suplente);

f) Representantes docentes do Campus de Angicos: Rita Diana de Freitas Gurgel (membro titular) e Éder Jofre Marinho Araújo (membro suplente);

g) Representantes docentes do Campus de Caraúbas: Daniel Freitas Freire Martins (membro titular) e André Moreira de Oliveira (membro suplente);

h) Representante dos servidores técnico-administrativos: Mara Raquel de Sousa Freitas, Maria Mércia Salviano de Oliveira e Paulo Cisneiros da Costa Reis (membros titulares); Fernando Henrique Vieira Almeida, Ronaldo Adriano de Almeida e Francisco das Chagas Correia do Nascimento (membros suplentes);

i) Representantes dos discentes dos cursos de graduação: Gleydson Barbosa Gomes e Magnos Luiz Bezerra de Lacerda Filho (membros titulares);

j) Representantes dos discentes dos cursos de pós-graduação: Iriane Teresa de Araújo e Gabriela Semíramis de Sousa Gurgel (membros titulares); Rodrigo Sávio Bessa da Silva e Wesley de Oliveira Santos (membros suplentes);

k) Representantes da sociedade civil organizada: Almir da Silva de Castro e Marilda Maria de Sousa (membros titulares); e Maria José Elias e Raimundo Adolfo de Melo Fernandes (membros suplentes).

Art. 3º O mandato fica prorrogado até 01 de abril de 2014.

Art. 4º Este ato entra em vigor a partir desta data e seus efeitos retroagem a 23 de dezembro de 2013.

Francisco Odolberto de Araújo
Reitor em exercício

MINISTÉRIO DA EDUCAÇÃO
UNIVERSIDADE FEDERAL RURAL DO SEMI-ÁRIDO
GABINETE DO REITOR

PORTARIA UFERSA/GAB Nº. 1.391/2013, de 24 de setembro de 2013

O Reitor em exercício da **Universidade Federal Rural do Semi-Árido**, no uso de suas atribuições conferidas pela PORTARIA UFERSA/GAB Nº 0722/2012, de 07 de agosto de 2012, publicada no Diário Oficial da União de 09 de agosto de 2012,

CONSIDERANDO a RESOLUÇÃO CONSUNI/UFERSA nº 001/2011, de 14 de março de 2011, que cria o Mestrado Profissional em Matemática – PROFMAT, no âmbito da UFERSA;

CONSIDERANDO a solicitação, datada de 20 de setembro de 2013, do Coordenador Local do PROFMAT, de que por exigência da Coordenação Nacional, seja expedido ato destacando os docentes do PROFMAT/UFERSA que lecionaram no semestre 2013.1 e os que estão lecionando no semestre 2013.2;

CONSIDERANDO o que determina o artigo 28, inciso XVIII, do Estatuto da Universidade,

R E S O L V E:

Art. 1º. Distribuir os servidores docentes abaixo relacionados, por disciplinas lecionadas no semestre letivo 2013.1 do Mestrado Profissional em Matemática – PROFMAT, no âmbito da UFERSA:

Antonio Ronaldo Gomes Garcia – (Geometria I e Introdução a Algebra Linear)
Walter Martins Rodrigues – (Matamática Discreta)
Maurício Zuluaga Martinez – (Números e Funções Reais)
Odacir Almeida Neves – (Recursos computacionais no Ensino de Matemática)
Henrique Renno Zanata – (Fundamentos de Cálculo)

Art. 2º. Distribuir os servidores docentes abaixo relacionados, por disciplinas lecionadas no semestre letivo 2013.2 do Mestrado Profissional em Matemática – PROFMAT, no âmbito da UFERSA:

Walter Martins Rodrigues – (Aritmética I)
Valdenize Lopes do Nascimento – (Geometria I)
Santos Demétrio Miranda Borjas – (Álgebra Linear)
Elmer Rolando Llanos Villarreal – (Geometria Analítica)
Maurício Zuluaga Martinez – (Conjunto e Funções Reais)

Art. 3º. Este ato entra em vigor a partir desta data e seus efeitos retroagem a 02 de janeiro de 2013.

Francisco Odolberto de Araújo
Reitor em Exercício

MINISTÉRIO DA EDUCAÇÃO
UNIVERSIDADE FEDERAL RURAL DO SEMI-ÁRIDO
GABINETE DO REITOR

PORTARIA UFERSA/GAB Nº. 1.391/2013, de 24 de setembro de 2013

O Reitor em exercício da **Universidade Federal Rural do Semi-Árido**, no uso de suas atribuições conferidas pela PORTARIA UFERSA/GAB Nº 0722/2012, de 07 de agosto de 2012, publicada no Diário Oficial da União de 09 de agosto de 2012,

CONSIDERANDO a RESOLUÇÃO CONSUNI/UFERSA nº 001/2011, de 14 de março de 2011, que cria o Mestrado Profissional em Matemática – PROFMAT, no âmbito da UFERSA;

CONSIDERANDO a solicitação, datada de 20 de setembro de 2013, do Coordenador Local do PROFMAT, de que por exigência da Coordenação Nacional, seja expedido ato destacando os docentes do PROFMAT/UFERSA que lecionaram no semestre 2013.1 e os que estão lecionando no semestre 2013.2;

CONSIDERANDO o que determina o artigo 28, inciso XVIII, do Estatuto da Universidade,

R E S O L V E:

Art. 1º. Distribuir os servidores docentes abaixo relacionados, por disciplinas lecionadas no semestre letivo 2013.1 do Mestrado Profissional em Matemática – PROFMAT, no âmbito da UFERSA:

Antonio Ronaldo Gomes Garcia – (Geometria I e Introdução a Algebra Linear)
Walter Martins Rodrigues – (Matamática Discreta)
Maurício Zuluaga Martinez – (Números e Funções Reais)
Odacir Almeida Neves – (Recursos computacionais no Ensino de Matemática)
Henrique Renno Zanata – (Fundamentos de Cálculo)

Art. 2º. Distribuir os servidores docentes abaixo relacionados, por disciplinas lecionadas no semestre letivo 2013.2 do Mestrado Profissional em Matemática – PROFMAT, no âmbito da UFERSA:

Walter Martins Rodrigues – (Aritmética I)
Valdenize Lopes do Nascimento – (Geometria I)
Santos Demétrio Miranda Borjas – (Álgebra Linear)
Elmer Rolando Llanos Villarreal – (Geometria Analítica)
Maurício Zuluaga Martinez – (Conjunto e Funções Reais)

Art. 3º. Este ato entra em vigor a partir desta data e seus efeitos retroagem a 02 de janeiro de 2013.

Francisco Odolberto de Araújo
Reitor em Exercício

PORTARIA UFERSA/PROPPG N.º 80/2021, de 16 de novembro de 2021

O Pró-Reitor de Pesquisa e Pós-graduação da Universidade Federal Rural do Semi-Árido, no uso de suas atribuições conferidas pela Portaria UFERSA/GAB Nº 487/2021 de 16 de agosto de 2021, publicada no Diário Oficial da União de 24 de agosto de 2021;

CONSIDERANDO o que determina o artigo 19, inciso III do Regulamento Geral dos Cursos de Pós-Graduação *Stricto Sensu* da UFERSA;

CONSIDERANDO a correspondência eletrônica encaminhada em 11 de novembro de 2021, para o e-mail proppg@ufersa.edu.br, que indica membros para comissão que coordenará o processo de seletivo de discentes para o Programa de Mestrado Profissional em Matemática em Rede Nacional PROFMAT/ UFERSA, para o ano de 2022;

CONSIDERANDO o que determina o artigo 01, inciso VII da Portaria UFERSA/GAB Nº 658/2020, de 04 de novembro de 2020;

R E S O L V E:

Art. 1º Designar a comissão composta pelos (as) membros (as) abaixo relacionados para conduzir o processo seletivo, organização e aplicação da prova, do Programa de Mestrado Profissional em Matemática em Rede Nacional PROFMAT/ UFERSA, para o ano de 2022.

I – Membros titulares:

Prof. Dr. Walter Martins Rodrigues;

Prof. Dr. Antônio Ronaldo Gomes Garcia;

Profª. Drª. Antônia Jocivânia Pinheiro;

Prof. Dr. Odacir Almeida Neves;

Prof. Dr. Elmer Rollando Llanos Villarreal;

Profª. Drª. Mariana de Brito Maia;

II – Membros suplentes:

Prof. Dr. Tony Kleverson Nogueira

Prof. Dr. Paulo Cesar Linhares da Silva

Art. 2º Este ato entra em vigor nesta data e os seus efeitos retroagem a 11 de novembro de 2021.

Glauber Henrique de Sousa Nunes

Prof. Glauber Henrique de Sousa Nunes
Pró-Reitor de Pesquisa e Pós-Graduação

ATA DE DEFESA DE DISSERTAÇÃO DE MESTRADO Nº 03/2023

Aos quatro dias do mês de maio do ano de dois mil e vinte três, às nove horas e sete minutos, no UFERSA, da Universidade Federal Rural do Semi-Árido, sob a presidência da Prof. Dr. Elmer Rolando Llanos Villarreal, reuniu-se a Banca Examinadora de Defesa de Dissertação de Mestrado de autoria de **Rogério da Silva Costa**, aluno do Programa de Pós-Graduação em Matemática em Rede Nacional desta Universidade com o título: **RECOMPOSIÇÃO DA APRENDIZAGEM MATEMÁTICA: UMA ABORDAGEM ATRAVÉS DAS OPERAÇÕES BÁSICAS NO 9º ANO DO ENSINO FUNDAMENTAL.** A Banca Examinadora ficou assim constituída: Prof. Dr. Elmer Rolando Llanos Villarreal, Presidente da Banca e Orientador, Prof. Dr. Walter Martins Rodrigues e Co-orientador, Profa. Dra. Fabiane Regina da Cunha Dantas Araújo, Prof. Dr. Elias das Neves Freire como examinadores. Após declarada aberta a sessão, o Senhor Presidente passou a palavra ao Mestrando para a exposição e a seguir aos examinadores para as devidas análises que se desenvolvem nos termos regimentais. Não foram registradas ocorrências. Concluída a defesa, foram realizadas as arguições e as sugestões feitas foram acatadas. Assim, foi realizada a mudança do título por: **RECOMPOSIÇÃO DA APRENDIZAGEM MATEMÁTICA: UMA ABORDAGEM ATRAVÉS DAS OPERAÇÕES BÁSICAS NA ESCOLA DOMINGOS COSTA TEOBALDO EM ARACATI CEARÁ PÓS PANDEMIA COVID-19.** Em seguida, procedeu-se o julgamento do trabalho pelos membros da Banca Examinadora, que consideraram a dissertação **APROVADA**. O discente tem a ciência de que fará jus ao título de Mestre somente após a entrega definitiva da dissertação com as correções sugeridas pelos membros da banca examinadora em um prazo máximo de 90 (noventa) dias, sendo que esta ata será entregue em até 3 (três) dias após a defesa. E, para constar, eu, *Elmer Rolando Llanos Villarreal*, Presidente da Banca Examinadora, lavrei a presente ata que, após lida e achada conforme, foi assinada por mim e demais membros da Banca Examinadora.

Mossoró, 04 de maio de 2023

Elmer Rolando Llanos Villarreal (21306063850)
Assinado de forma digital por Elmer Rolando Llanos Villarreal (21306063850)
Dados: 2023.05.04 15:15:30 -03'00'

Prof. Dr. Elmer Rolando Llanos Villarreal (UFERSA)

gov.br Documento assinado digitalmente
WALTER MARTINS RODRIGUES
Data: 04/05/2023 15:21:11-0300
Verifique em https://validar.iti.gov.br

Prof. Dr. Walter Martins Rodrigues (UFERSA)

gov.br Documento assinado digitalmente
FABIANE REGINA DA CUNHA DANTAS ARAU
Data: 04/05/2023 19:45:49-0300
Verifique em https://validar.iti.gov.br

Profa. Dra. Fabiane Regina da Cunha Dantas Araújo (UFERSA)

Documento assinado digitalmente
gov.br
ELIAS DAS NEVES FREIRE
Data: 05/05/2023 08:37:29-0300
Verifique em https://validar.iti.gov.br

_____

Prof. Dr. Elias das Neves Freire (IFRN)

Documento assinado digitalmente
gov.br
ROGERIO DA SILVA COSTA
Data: 05/05/2023 09:30:31-0300
Verifique em https://validar.iti.gov.br

_____

Rogério da Silva Costa (discente PROFMAT)

ATA DE DEFESA DE DISSERTAÇÃO DE MESTRADO Nº 05/2023

Ás nove horas e quarenta e cinco minutos, 9h 45min, do dia vinte e oito de junho do ano dois mil e vinte e três, em reunião virtual endereçada pelo link meet meet.google.com/gdz-fxnq-edt , sob a presidência do Prof. Dr. Walter Martins Rodrigues, se reuniu-se a Banca Examinadora de Defesa de Dissertação de Mestrado de autoria de **Francisco José de Souza Silva**, aluno regular do Programa de Pós-Graduação em Matemática (PROFMAT) desta Universidade com o título: CONGRUÊNCIAS MODULARES: A APLICABILIDADE DA TEORIA DOS NÚMEROS NO SUPORTE À RESOLUÇÃO DE PROBLEMAS**.** A Banca Examinadora ficou assim constituída: Prof. Dr. Walter Martins Rodrigues, Presidente da Banca e Orientador do mestrando, Prof. Dr. Elmer Rolando Llanos Villarreal, professor da instituição UFERSA e integrado ao PROFMAT / UFERSA. Prof. Dr. Odirlei Silva Jesus, professor efetivo da Universidade Federal do Rio Grande do Norte, membro externo da banca, esta equipe de examinadores desenvolveu o trabalho avaliativo do trabalho. Após declarada aberta a sessão, o Senhor Presidente passou a palavra ao discente para a exposição e a seguir aos examinadores para as devidas análises que se desenvolveram nos termos regimentais. Após as arguições, as sugestões feitas pela banca, e todas imediatamente acatadas pelo orientador e pelo mestrando Francisco José de Souza Silva. Em seguida, procedeu-se o julgamento do trabalho pelos membros da Banca Examinadora, que consideraram a dissertação **APROVADA**. O discente tem a ciência de que fará jus ao título de Mestre somente após a entrega definitiva da dissertação com as correções sugeridas pelos membros da banca examinadora em um prazo máximo de 90 (noventa) dias, sendo que esta ata será entregue em até 3 (três) dias após a defesa. E, para constar, eu, Walter Martins Rodrigues, Presidente da Banca Examinadora, lavrei a presente ata que, após

lida e achada conforme, foi assinada por mim e demais membros da Banca Examinadora.

Mossoró, 28 de Junho de 2023

Prof. Dr. Walter Martins Rodrigues- Orientador – UFERSA

gov.br
Documento assinado digitalmente
ELMER ROLANDO LLANOS VILLARREAL
Data: 28/06/2023 14:26:55-0300
Verifique em https://validar.iti.gov.br

Prof. Dr. Elmer Rolando Llanos Villarreal – UFERSA

Prof. Dr. Odirlei Silva Jesus - UFRN

Francisco José de Souza Silva (discente) – PROFMAT / UFERSA

ATA DE DEFESA DE DISSERTAÇÃO DE MESTRADO Nº 07/2024

matricula do aluno: 2022100098

Ás oito horas e trinta minutos, 8h 30min, do dia vinte e um de junho do ano de dois mil e vinte e quatro, em reunião virtual endereçada pelo link https://meet.google.com/hcf-wzzu-etf , sob a presidência do Prof. Dr. Walter Martins Rodrigues, se reuniu a Banca Examinadora de Defesa de Dissertação de Mestrado de autoria de **Antônio Neudvam Bandeira Lima**, aluno regular do Programa de Pós-Graduação em Matemática (PROFMAT), desta Universidade, com o título: ANÁLISE E IDENTIFICAÇÃO DE LACUNAS NO APRENDIZADO MATEMÁTICO: UM ESTUDO SOBRE OS CONCEITOS DO ENSINO FUNDAMENTAL II QUE DEMANDAM APRENDIZADO NO ENSINO MÉDIO. A Banca Examinadora ficou assim constituída: do Prof. Dr. Walter Martins Rodrigues, Presidente da Banca e Orientador do mestrando. Prof. Dr. Elmer Rolando LLanos Villarreal, membro interno da Banca, professor da instituição UFERSA e vinculado ao PROFMAT / UFERSA. Prof. Dr. Elias das Neves Freire, professor efetivos do Instituto Federal do Rio Grande do Norte (IFRN / Mossoró - RN), membro externo da Banca. Esta equipe de examinadores desenvolveu o trabalho avaliativo da dissertação de mestrado de Antônio Neudvam Bandeira Lima. Após declarada aberta a sessão, o Senhor Presidente da Banca passou a palavra ao discente para a exposição do trabalho realizado, e a seguir aos examinadores para as devidas análises que se desenvolveram nos termos regimentais. Após as arguições, as sugestões feitas pela Banca Examinadora, todas acatadas pelo Orientador e pelo mestrando Antônio Neudvam Bandeira Lima. Em seguida, procedeu-se o julgamento do trabalho pelo membros da Banca, que consideraram a dissertação **APROVADA.** O discente tem a ciência de que fará jus ao título de Mestre somente após entrega da versão definitiva da Dissertação, com todas correções, sugeridas pela Banca,devidadmente realizadas. O discente dispõe de um prazo de máximo de 90 (noventa) dias para realizar as correções. Ademais, esta ATA será entregue à coordenação em até 3 (três) dias após a defesa . Nada mais havendo a tratar, o Presidente da banca

examinadora deu por encerrado o julgamento que tempor conteúdo o teor desta Ata que, após lida e aprovada, segue assinada por todos os membrosda Banca para fins de produção de seus efeitos legais.

Mossoró, 21 de junho de 2024.

Prof. Dr. Walter Martins Rodrigues - Orientador – UFERSA

Elmer Rolando Llanos Villarreal

Assinado de forma digital por Elmer Rolando Llanos Villarreal
Dados: 2024.06.21 09:53:45 -03'00'

Prof. Dr. Elmer Rolando LLanos Villarreal - UFERSA

Prof. Dr. Elias das Neves Freire – IFRN / Mossoró – RN

Antônio Neudvam Bandeira Lima (Discente) - PROFMAT / UFERSA

DECLARAÇÃO

Declaramos que o Prof. Dr. ELMER ROLANDO LLANOS VILLARREAL, CPF 213.060.638-50, participou como Examinador Externo à Instituição da Comissão Examinadora de Defesa de Tese de Doutorado do(a) pós-graduando(a) FELIPE OLIVEIRA SIMÕES GAMA, intitulada:

DESENVOLVIMENTO DE SISTEMAS DE COMUNICAÇÕES CODIFICADOS POR WAVELETS E BASEADOS NO PADRÃO IEEE 802.15.4 PARA SISTEMAS DE CONTROLE POR REDES DE SENSORES SEM FIO INDUSTRIAL

no PROGRAMA DE PÓS-GRADUAÇÃO EM ENGENHARIA ELÉTRICA E DE COMPUTAÇÃO do CENTRO DE TECNOLOGIA da UNIVERSIDADE FEDERAL DO RIO GRANDE DO NORTE , em sessão pública realizada por videoconferência no dia 24 de Junho de 2021 às 14:00.

Membros da Banca

ANDRES ORTIZ SALAZAR (UFRN - Presidente) - ORIENTADOR
VICENTE ANGELO DE SOUSA JUNIOR (UFRN - Examinador Interno)
LUIZ FELIPE DE QUEIROZ SILVEIRA (UFRN - Examinador Externo ao Programa) - COORIENTADOR
ELMER ROLANDO LLANOS VILLARREAL (UFERSA - Examinador Externo à Instituição)
JEFFERSON DOOLAN FERNANDES (IFRN - Examinador Externo à Instituição)
RODRIGO SOARES SEMENTE (UFERSA - Examinador Externo à Instituição)

Prof(a). Dr. MARCELO AUGUSTO COSTA FERNANDES
Coordenador(a) do PROGRAMA DE PÓS-GRADUAÇÃO EM ENGENHARIA ELÉTRICA E DE COMPUTAÇÃO- UFRN

Número do Documento: 2585544
Código de Verificação: 0634e480fd

ATENÇÃO

Para verificar a autenticidade deste documento acesse **https://sigaa.ufrn.br/sigaa/documentos/** e utilize o link *Ensino >> Declaração de Participação como Membro de Banca de Pós-Graduação Stricto Sensu*, informando o número do documento, a data de emissão e o código de verificação.

SIGAA | Superintendência de Informática - | | Copyright © 2006-2021 - UFRN - sigaa04-producao.info.ufrn.br.sigaa04-producao

Declaração de Membro de Comissão Examinadora

Universidade de Brasília
Secretaria de Administração Acadêmica

Examinador : Elmer Rolando Llanos Villareal

Aluno : Kevin Herman Muraro Gularte
Curso: Engenharia de Sistemas Eletrônicos e de Automação
Grau : Doutor **Nível :** Doutorado

Declaramos, a pedido e para os devidos fins, que o interessado acima identificado participou como Membro Externo da Comissão Examinadora da Defesa de Tese de Kevin Herman Muraro Gularte, matrícula 18/0007220, do curso de Doutorado em Engenharia de Sistemas Eletrônicos e de Automação sob o titulo: "CONTROL OF CHAOTIC AND HYPERCHAOTIC SYSTEMS USING LYAPUNOV STABILITY THEORY", realizada em 10/12/2021, nesta Universidade.

******* Esta declaração só é válida com autenticação da UnB *******

Autenticação

Unidade Emitente	Data	Assinatura/Carimbo
	28/12/2021 7:39:35	

Portal do Coordenador Stricto

UNIVERSIDADE FEDERAL DO RIO GRANDE DO NORTE
SISTEMA INTEGRADO DE GESTÃO DE ATIVIDADES ACADÊMICAS

EMITIDO EM 27/04/2021 11:18

DECLARAÇÃO

Declaramos que o Prof. Dr. ELMER ROLANDO LLANOS VILLARREAL, CPF 213.060.638-50, participou como Examinador Externo à Instituição da Comissão Examinadora de Defesa de Dissertação de Mestrado do(a) pós-graduando(a) RODRIGO DE ANDRADE TEIXEIRA, intitulada:

ANÁLISE DE QUALIDADE DE ENERGIA APLICADA A UM SISTEMA RETIFICADOR TRIFÁSICO PWM UTILIZANDO A TÉCNICA DE CONTROLE DE UM CICLO

no PROGRAMA DE PÓS-GRADUAÇÃO EM ENGENHARIA ELÉTRICA E DE COMPUTAÇÃO do CENTRO DE TECNOLOGIA da UNIVERSIDADE FEDERAL DO RIO GRANDE DO NORTE , em sessão pública realizada no dia 27 de Abril de 2021 às 14:00.

Membros da Banca

ANDRES ORTIZ SALAZAR (UFRN - Presidente) - ORIENTADOR
RICARDO FERREIRA PINHEIRO (UFRN - Examinador Externo ao Programa)
ELMER ROLANDO LLANOS VILLARREAL (UFERSA - Examinador Externo à Instituição)
JOÃO TEIXEIRA DE CARVALHO NETO (IFRN - Examinador Externo à Instituição)

Prof(a). Dr. MARCELO AUGUSTO COSTA FERNANDES
Coordenador(a) do PROGRAMA DE PÓS-GRADUAÇÃO EM ENGENHARIA ELÉTRICA E DE COMPUTAÇÃO- UFRN

Número do Documento: 2426862
Código de Verificação: 1daa0006dd

ATENÇÃO

Para verificar a autenticidade deste documento acesse **https://sigaa.ufrn.br/sigaa/documentos/** e utilize o link *Ensino >> Declaração de Participação como Membro de Banca de Pós-Graduação Stricto Sensu*, informando o número do documento, a data de emissão e o código de verificação.

SIGAA | Superintendência de Informática - | | Copyright © 2006-2021 - UFRN - sigaa08-producao.info.ufrn.br.sigaa08-producao

UFRN
Portal do Coordenador Stricto

UNIVERSIDADE FEDERAL DO RIO GRANDE DO NORTE
SISTEMA INTEGRADO DE GESTÃO DE ATIVIDADES ACADÊMICAS

EMITIDO EM 02/05/2019 11:21

sinfo

DECLARAÇÃO

Declaramos que o Prof. Dr. ELMER ROLANDO LLANOS VILLAREAL, CPF 213.060.638-50, participou como Examinador Externo à Instituição da Comissão Examinadora de Defesa de Tese de Doutorado do(a) pós-graduando(a) GUSTAVO FERNANDES DE LIMA, intitulada:

PROPOSTA DE CONTROLE DE VELOCIDADE DE FERRAMENTA DE INSPEÇÃO DE DUTOS UTILIZANDO VÁLVULA DE DESVIO E MICROELETRÔNICA

no PROGRAMA DE PÓS-GRADUAÇÃO EM CIÊNCIA E ENGENHARIA DE PETRÓLEO do CENTRO DE CIÊNCIAS EXATAS E DA TERRA da UNIVERSIDADE FEDERAL DO RIO GRANDE DO NORTE , em sessão pública realizada no dia 14 de Junho de 2019 às 09:00.

Membros da Banca

ANDRES ORTIZ SALAZAR (UFRN - Presidente) - ORIENTADOR
ANDRÉ LAURINDO MAITELLI (UFRN - Examinador Interno)
ELMER ROLANDO LLANOS VILLAREAL (UFERSA - Examinador Externo à Instituição)
JEFFERSON DOOLAN FERNANDES (IFRN - Examinador Externo à Instituição)
OSCAR GABRIEL FILHO (PETROBRAS - Examinador Externo à Instituição)

Prof(a). Dr. CARLOS ALBERTO MARTINEZ HUITLE
Coordenador(a) do PROGRAMA DE PÓS-GRADUAÇÃO EM CIÊNCIA E ENGENHARIA DE PETRÓLEO- UFRN

Número do Documento: 1468763
Código de Verificação: 55cd1d9803

ATENÇÃO

Para verificar a autenticidade deste documento acesse **https://sigaa.ufrn.br/sigaa/documentos/** e utilize o link *Ensino >> Declaração de Participação como Membro de Banca de Pós-Graduação Stricto Sensu*, informando o número do documento, a data de emissão e o código de verificação.

SIGAA | Superintendência de Informática - (84) 3215-3148 | Copyright © 2006-2019 - UFRN - sigaa08-producao.info.ufrn.br.sigaa08-producao

RELATÓRIO DE EXAME DE QUALIFICAÇÃO DOUTORADO

Universidade de Brasília - UnB
Departamento de Engenharia Mecânica – ENM
Programa de Pós-Graduação em Sistemas Mecatrônicos – PPMEC

1 – Identificação do Aluno

Nome	Matrícula
Willian Arvey Molano Gabalán	16/0160693

Curso
Sistemas Mecatrônicos

2 – Sessão de Defesa

Título:
ESQUEMAS BASEADOS EM CAOS E NA TEORIA DE ESTABILIDADE DE LYAPUNOV PARA A TELECOMUNICAÇÃO SEGURA

3 – Comissão Examinadora

Nome	Função	Assinatura
José Alfredo Ruiz Vargas	Presidente/Orientador	
João Yoshiyuki Ishihara	Membro Externo	
Elmer Rolando Llanos Villarreal	Membro Externo	
Guillermo Alvarez Bestard	Membro Interno	
Jones Yudi Mori Alves da Silva	Membro Interno Suplente	

4 - Resultado

A Comissão Examinadora, em 22/08/2019, após o exame da proposta/relatório de qualificação para o Doutorado (RQD) e argüição do candidato, decidiu:

☒ Pela aprovação do RQD, com revisão de forma, se indicado pela Banca.
☐ Pela reprovação.
☐ Pela reformulação do RQD, indicando o prazo de _____ para nova versão.

Em caso de revisão de forma, indicar abaixo os principais motivos para esta decisão:

Autenticação Presidente da Comissão Examinadora	Autenticação Coordenador do Curso
22/08/2019 Data _____ Assinatura/carimbo	09/09/19 Data _____ Assinatura/carimbo

Prof. Eugênio Libório Feitosa Fortaleza
Coordenador de Pós Gradu
Sistemas Mecatrônicos (PF
Dep. Mecânica – ENM/

UNIVERSIDADE DE BRASÍLIA

PROGRAMA DE PÓS GRADUAÇÃO EM ENGENHARIA ELÉTRICA

Ata Nº: 100

Aos trinta dias do mês de junho do ano de dois mil e vinte e três, instalou-se a banca examinadora de Tese de Doutorado do aluno Juan Carlos González Gómez, matrícula 222110265. A banca examinadora foi composta pelos professores Dr. Guillermo Alvarez Bestard/Membro Interno/FGA - UnB, Dr. João Paulo Javidi da Costa/Membro Externo/Hochschule Hamm-Lippstadt, Dr. Elmer Rolando Llanos Villarreal/Membro Externo/UFERSA, Dr. Bismark Claude Torrico/Membro Externo/UFC (Suplente) e Dr. Jose Alfredo Ruiz Vargas/orientador/presidente/UnB. Por razões pessoais, o Prof. Dr. Guillermo Alvarez Bestard não pôde participar e foi substituído pelo suplente (Prof. Dr. Bismark Claude Torrico). O discente apresentou o trabalho intitulado "SYNCHRONIZATION OF UNDERACTUATED CHAOTIC SYSTEMS WITH APPLICATIONS TO INFORMATION SECURITY".

Concluída a exposição, procedeu-se a arguição do(a) candidato(a), e após as considerações dos examinadores o resultado da avaliação do trabalho foi:

( ) Pela aprovação do trabalho;

(x) Pela aprovação do trabalho, com revisão de forma, indicando o prazo de até 30 dias para apresentação definitiva do trabalho revisado;

( ) Pela reformulação do trabalho, indicando o prazo de (Nº DE MESES) para nova versão;

( ) Pela reprovação do trabalho, conforme as normas vigentes na Universidade de Brasília.

Conforme os Artigos 34, 39 e 40 da Resolução 0080/2021 - CEPE, o(a) candidato(a) não terá o título se não cumprir as exigências acima.

Dr. Guillermo Alvarez Bestard
Examinador Interno

Dr. João Paulo Javidi da Costa
Examinador Externo

Dr. Elmer Rolando Llanos Villarreal
Examinador Externo

Dr. Bismark Claude Torrico
Examinador Externo / Suplente

Dr. Jose Alfredo Ruiz Vargas
Presidente

Juan Carlos González Gómez

(Doutorando)

Documento assinado eletronicamente por **Joao Paulo Javidi da Costa**, **Usuário Externo**, em 17/07/2023, às 17:37, conforme horário oficial de Brasília, com fundamento na Instrução da Reitoria 0003/2016 da Universidade de Brasília.

Documento assinado eletronicamente por **ELMER ROLANDO LLANOS VILLARREAL**, **Usuário Externo**, em 17/07/2023, às 17:48, conforme horário oficial de Brasília, com fundamento na Instrução da Reitoria 0003/2016 da Universidade de Brasília.

A autenticidade deste documento pode ser conferida no site http://sei.unb.br/sei/controlador_externo.php?acao=documento_conferir&id_orgao_acesso_externo=0, informando o código verificador **10019352** e o código CRC **9498CEF3**.

Referência: Processo nº 23106.078397/2023-67 SEI nº 10019352

UNIVERSIDADE DE BRASÍLIA

PROGRAMA DE PÓS GRADUAÇÃO EM ENGENHARIA ELÉTRICA

Ata Nº: 100

Aos vinte e nove dias do mês de junho do ano de dois mil e vinte e três, instalou-se a banca examinadora de Tese de Doutorado do aluno Juan Carlos González Gómez, matrícula 222110265. A banca examinadora foi composta pelos professores Dr(a). Guillermo Alvarez Bestard/Membro Interno/FGA - UnB, Dr(a). João Paulo Javidi da Costa/Membro Externo/Hochschule Hamm-Lippstad, Dr(a). Elmer Rolando Llanos Villarreal/Membro Externo/UFERSA, Dr(a). Bismark Claude Torrico/Membro Externo/UFC (Suplente) e Dr(a). Jose Alfredo Ruiz Vargas/orientador/presidente/UnB. Por razões pessoais, o Prof. Dr. Guillermo Alvarez Bestard não pôde participar e foi substituído pelo suplente (Prof. Dr. Bismark Claude Torrico). O discente apresentou o trabalho intitulado “SYNCHRONIZATION OF UNDERACTUATED CHAOTIC SYSTEMS WITH APPLICATIONS TO INFORMATION SECURITY”.

Concluída a exposição, procedeu-se a arguição do(a) candidato(a), e após as considerações dos examinadores o resultado da avaliação do trabalho foi:

( ) Pela aprovação do trabalho;

(x) Pela aprovação do trabalho, com revisão de forma, indicando o prazo de até 30 dias para apresentação definitiva do trabalho revisado;

( ) Pela reformulação do trabalho, indicando o prazo de (Nº DE MESES) para nova versão;

( ) Pela reprovação do trabalho, conforme as normas vigentes na Universidade de Brasília.

Conforme os Artigos 34, 39 e 40 da Resolução 0080/2021 - CEPE, o(a) candidato(a) não terá o título se não cumprir as exigências acima.

Dr. Guillermo Alvarez Bestard
Examinador Interno

Dr. João Paulo Javidi da Costa
Examinador Externo

Dr. Elmer Rolando Llanos Villarreal
Examinador Externo

Dr. Bismark Claude Torrico

Examinador Externo / Suplente

Dr. Jose Alfredo Ruiz Vargas
Presidente

Juan Carlos González Gómez
(Doutorando)

Documento assinado eletronicamente por **ELMER ROLANDO LLANOS VILLARREAL**, **Usuário Externo**, em 11/07/2023, às 07:51, conforme horário oficial de Brasília, com fundamento na Instrução da Reitoria 0003/2016 da Universidade de Brasília.

A autenticidade deste documento pode ser conferida no site http://sei.unb.br/sei/controlador_externo.php?acao=documento_conferir&id_orgao_acesso_externo=0, informando o código verificador **9985606** e o código CRC **692D443B**.

Referência: Processo nº 23106.078397/2023-67 SEI nº 9985606